biomedicines

Special Issue Reprint

Cardiovascular and Metabolic Disease

New Treatment and Future Directions—the 3rd Edition

Edited by
Alfredo Caturano

mdpi.com/journal/biomedicines

MDPI

Cardiovascular and Metabolic Disease: New Treatment and Future Directions—the 3rd Edition

Cardiovascular and Metabolic Disease: New Treatment and Future Directions—the 3rd Edition

Guest Editor

Alfredo Caturano

MDPI

Basel • Beijing • Wuhan • Barcelona • Belgrade • Novi Sad • Cluj • Manchester

Guest Editor
Alfredo Caturano
Department of Human
Sciences and Promotion of the
Quality of Life
San Raffaele Roma
Open University
Rome
Italy

Editorial Office
MDPI AG
Grosspeteranlage 5
4052 Basel, Switzerland

This is a reprint of the Special Issue, published open access by the journal *Biomedicines* (ISSN 2227-9059), freely accessible at: https://www.mdpi.com/journal/biomedicines/special_issues/YUQVY979VV.

For citation purposes, cite each article independently as indicated on the article page online and as indicated below:

Lastname, A.A.; Lastname, B.B. Article Title. *Journal Name* **Year**, *Volume Number*, Page Range.

ISBN 978-3-7258-7426-2 (Hbk)
ISBN 978-3-7258-7427-9 (PDF)
https://doi.org/10.3390/books978-3-7258-7427-9

© 2026 by the authors. Articles in this reprint are Open Access and distributed under the Creative Commons Attribution (CC BY) license. The reprint as a whole is distributed by MDPI under the terms and conditions of the Creative Commons Attribution-NonCommercial-NoDerivs (CC BY-NC-ND) license (https://creativecommons.org/licenses/by-nc-nd/4.0/).

Contents

About the Editor . . . . . **ix**

Alfredo Caturano
Cardiovascular and Metabolic Disease: New Treatment and Future Directions—The 3rd Edition
Reprinted from: *Biomedicines* **2025**, *13*, 1914, https://doi.org/10.3390/biomedicines13081914 . . **1**

Alexander E. Berezin, Tetiana A. Berezina, Evgen V. Novikov and Oleksandr O. Berezin
Serum Levels of Irisin Are Positively Associated with Improved Cardiac Function in Patients with Heart Failure with Reduced Ejection Fraction
Reprinted from: *Biomedicines* **2025**, *13*, 866, https://doi.org/10.3390/biomedicines13040866 . . . **11**

Irene Martínez-García, Alicia Saz-Lara, Carlos Pascual-Morena, Ana Díez-Fernández, Sara Valladolid-Ayllón, Bruno Bizzozero-Peroni, et al.
Role of Advanced Glycation End Products in Mediating Glycated Haemoglobin and Pulse Wave Velocity in Healthy Adults
Reprinted from: *Biomedicines* **2025**, *13*, 137, https://doi.org/10.3390/biomedicines13010137 . . . **29**

Caitlin P. S. Ellis, Benjamin W. Tero, Christian M. Potts, Kimberly T. Malka, Xuehui Yang, Joshua Hamilton, et al.
Cellular Characteristics and Protein Signatures of Human Adipose Tissues from Donors With or Without Advanced Coronary Artery Disease
Reprinted from: *Biomedicines* **2024**, *12*, 2453, https://doi.org/10.3390/biomedicines12112453 . . **45**

Kareem Awad, Laura Kakkola and Ilkka Julkunen
High Glucose Increases Lactate and Induces the Transforming Growth Factor Beta-Smad 1/5 Atherogenic Pathway in Primary Human Macrophages
Reprinted from: *Biomedicines* **2024**, *12*, 1575, https://doi.org/10.3390/biomedicines12071575 . . **69**

Isabella D. Cooper, Yvoni Kyriakidou, Lucy Petagine, Kurtis Edwards, Adrian Soto-Mota, Kenneth Brookler and Bradley T. Elliott
Ketosis Suppression and Ageing (KetoSAge) Part 2: The Effect of Suppressing Ketosis on Biomarkers Associated with Ageing, HOMA-IR, Leptin, Osteocalcin, and GLP-1, in Healthy Females
Reprinted from: *Biomedicines* **2024**, *12*, 1553, https://doi.org/10.3390/biomedicines12071553 . . **81**

Manjula Nandakumar, Thozhukat Sathyapalan, Stephen L. Atkin and Alexandra E. Butler
Effect of Hypoglycemia and Rebound Hyperglycemia on Proteomic Cardiovascular Risk Biomarkers
Reprinted from: *Biomedicines* **2024**, *12*, 1137, https://doi.org/10.3390/biomedicines12061137 . . **104**

Jazmine A. Eccles-Miller, Tyler D. Johnson and William S. Baldwin
Sexually Dimorphic Effects of CYP2B6 in the Development of Fasting-Mediated Steatosis in Mice: Role of the Oxylipin Products 9-HODE and 9-HOTrE
Reprinted from: *Biomedicines* **2025**, *13*, 295, https://doi.org/10.3390/biomedicines13020295 . . . **112**

Jan Soukop, Ludmila Kazdová, Martina Hüttl, Hana Malínská, Irena Marková, Olena Oliyarnyk, et al.
Beneficial Effect of Fenofibrate in Combination with Silymarin on Parameters of Hereditary Hypertriglyceridemia-Induced Disorders in an Animal Model of Metabolic Syndrome
Reprinted from: *Biomedicines* **2025**, *13*, 212, https://doi.org/10.3390/biomedicines13010212 . . . **141**

Balázs Sági, Tibor Vas, Botond Csiky, Judit Nagy and Tibor József Kovács
Does Metabolic Syndrome and Its Components Have Prognostic Significance for Renal and Cardiovascular Outcomes in IgA Nephropathy?
Reprinted from: *Biomedicines* **2024**, *12*, 1250, https://doi.org/10.3390/biomedicines12061250 . . **162**

Ruike Yan and Yanli Cao
The Safety and Efficacy of Dietary Epigallocatechin Gallate Supplementation for the Management of Obesity and Non-Alcoholic Fatty Liver Disease: Recent Updates
Reprinted from: *Biomedicines* **2025**, *13*, 206, https://doi.org/10.3390/biomedicines13010206 . . . **180**

Ferenc Sztanek, László Imre Tóth, Attila Pető, Marcell Hernyák, Ágnes Diószegi and Mariann Harangi
New Developments in Pharmacological Treatment of Obesity and Type 2 Diabetes—Beyond and within GLP-1 Receptor Agonists
Reprinted from: *Biomedicines* **2024**, *12*, 1320, https://doi.org/10.3390/biomedicines12061320 . . **199**

Salvatore Nesci and Speranza Rubattu
UCP2, a Member of the Mitochondrial Uncoupling Proteins: An Overview from Physiological to Pathological Roles
Reprinted from: *Biomedicines* **2024**, *12*, 1307, https://doi.org/10.3390/biomedicines12061307 . . **220**

Piotr Wańczura, Wiktoria Mytych, Dorota Bartusik-Aebisher, Dawid Leksa, Adrian Truszkiewicz and David Aebisher
Visualization of Atherosclerotic Plaques Paired with Joheksol 350 (Omnipaque)
Reprinted from: *Biomedicines* **2025**, *13*, 399, https://doi.org/10.3390/biomedicines13020399 . . . **234**

Narae Kim, Hui-Jeong Hwang and In-Ho Yang
Assessing Cardiovascular Risk with Coronary Artery Calcium and Carotid Intima-Media Thickness in Patients with Negative Stress Echocardiography
Reprinted from: *Biomedicines* **2024**, *12*, 2151, https://doi.org/10.3390/biomedicines12092151 . . **253**

Jaroslav Chlupac, Jan Frank, David Sedmera, Ondrej Fabian, Zuzana Simunkova, Iveta Mrazova, et al.
External Support of Autologous Internal Jugular Vein Grafts with FRAME Mesh in a Porcine Carotid Artery Model
Reprinted from: *Biomedicines* **2024**, *12*, 1335, https://doi.org/10.3390/biomedicines12061335 . . **263**

Natalia Zdebik, Rafał Poręba and Paweł Gać
Importance of T1-Mapping Sequence in Patients with Hypertrophic Cardiomyopathy without Foci of Non-Ischemic Myocardial Injury in Late Gadolinium Enhancement Sequence
Reprinted from: *Biomedicines* **2024**, *12*, 1330, https://doi.org/10.3390/biomedicines12061330 . . **291**

Robert J. Gil, Adam Kern, Krystian Bojko, Aneta Gziut-Rudkowska, Dobrin Vassilev and Jacek Bil
The Randomized, Multicenter, Open-Label, Controlled POLBOS 3 Trial Comparing Regular Drug-Eluting Stents and the Sirolimus-Eluting BiOSS LIM C Dedicated Coronary Bifurcation Stent: Four-Year Results
Reprinted from: *Biomedicines* **2024**, *12*, 938, https://doi.org/10.3390/biomedicines12050938 . . . **305**

Vaida Šileikienė, Vilma Dženkevičiūtė, Alma Čypienė, Tautvydas Šlapikas, Roma Puronaitė, Jolita Badarienė, et al.
Analysis of Cardiovascular High-Risk Profile in Middle-Aged Lithuanian Men with Arterial Hypertension from 2009 to 2019
Reprinted from: *Biomedicines* **2025**, *13*, 272, https://doi.org/10.3390/biomedicines13020272 . . . **319**

Elke Boxhammer, Matthias Hammerer, Christiana Schernthaner, Erika Prinz, Mathias C. Brandt, Michael Lichtenauer, et al.
The Silent Threat: A Retrospective Cohort Study on the Impact of Prediabetes on ST-Elevation Myocardial Infarction Survival—A Call to Action!
Reprinted from: *Biomedicines* **2024**, *12*, 2223, https://doi.org/10.3390/biomedicines12102223 . . **329**

Mara Volpentesta, Valentino Condoleo, Alberto Panza, Giandomenico Severini, Luca Soraci, Cataldo Rotondo, et al.
Effects of Continuous Positive Airway Pressure Treatment on Vascular Function in a Real-Life Cohort of Elderly Patients with Obstructive Sleep Apnoea Syndrome
Reprinted from: *Biomedicines* **2024**, *12*, 2563, https://doi.org/10.3390/biomedicines12112563 . . **344**

Ramcharan Singh Angom and Naga Malleswara Rao Nakka
Zebrafish as a Model for Cardiovascular and Metabolic Disease: The Future of Precision Medicine
Reprinted from: *Biomedicines* **2024**, *12*, 693, https://doi.org/10.3390/biomedicines12030693 . . . **356**

Yuxin Nie, Liyu Lin, Qiang Yang, Jiachang Hu, Minmin Sun, Fangfang Xiang, et al.
Mitochondrial Dysfunction and Ion Imbalance in a Rat Model of Hemodialysis-Induced Myocardial Stunning
Reprinted from: *Biomedicines* **2024**, *12*, 2402, https://doi.org/10.3390/biomedicines12102402 . . **383**

Alexandra Ioana Popescu, Andreea Luciana Rață, Daliborca Vlad, Cristian Vlad, Roxana Popescu, Ramona Roxana Onofrei, et al.
miRNA in the Diagnosis and Treatment of Critical Limb Ischemia
Reprinted from: *Biomedicines* **2024**, *12*, 2026, https://doi.org/10.3390/biomedicines12092026 . . **395**

Nicholas Pavlatos and Dinesh K. Kalra
The Role of Lipoprotein(a) in Peripheral Artery Disease
Reprinted from: *Biomedicines* **2024**, *12*, 1229, https://doi.org/10.3390/biomedicines12061229 . . **406**

Ekaterina Ogurtsova, Tatiana Arefieva, Anastasiia Filatova, Natalya Radyukhina and Artem Ovchinnikov
Cardiometabolic Phenotype in HFpEF: Insights from Murine Models
Reprinted from: *Biomedicines* **2025**, *13*, 744, https://doi.org/10.3390/biomedicines13030744 . . . **421**

Diana-Aurora Arnautu, Dragos Cozma, Ioan-Radu Lala, Sergiu-Florin Arnautu, Mirela-Cleopatra Tomescu and Minodora Andor
Risk Assessment and Personalized Treatment Options in Inherited Dilated Cardiomyopathies: A Narrative Review
Reprinted from: *Biomedicines* **2024**, *12*, 1643, https://doi.org/10.3390/biomedicines12081643 . . **451**

Nicia I. Profili, Roberto Castelli, Roberto Manetti, Marta C. Sircana, Michela Pagni, Gemma Lisa Sechi, et al.
Sodium–Glucose Cotransporter-2 Inhibitors After Acute Myocardial Infarction
Reprinted from: *Biomedicines* **2025**, *13*, 720, https://doi.org/10.3390/biomedicines13030720 . . . **484**

Vasiliki Katsi, Eleni Manta, Christos Fragoulis and Konstantinos Tsioufis
Weight Loss Therapies and Hypertension Benefits
Reprinted from: *Biomedicines* **2024**, *12*, 2293, https://doi.org/10.3390/biomedicines12102293 . . **497**

Kyosuke Murai, Amir Vasigh, Tamás Alexy, Kálmán Tóth and László Czopf
The Role of Ranolazine in the Treatment of Ventricular Tachycardia and Atrial Fibrillation: A Narrative Review of the Clinical Evidence
Reprinted from: *Biomedicines* **2024**, *12*, 1669, https://doi.org/10.3390/biomedicines12081669 . . **518**

Yotam Kolben, Ittamar Gork, David Peled, Shani Amitay, Peleg Moshel, Nir Goldstein, et al.
Continuous Monitoring of Advanced Hemodynamic Parameters during Hemodialysis Demonstrated Early Variations in Patients Experiencing Intradialytic Hypotension
Reprinted from: *Biomedicines* **2024**, *12*, 1177, https://doi.org/10.3390/biomedicines12061177 . . **529**

Irina Tarasova, Irina Kukhareva, Darya Kupriyanova, Tatjana Temnikova, Evgenia Gorbatovskaya and Olga Trubnikova
Electrical Activity Changes and Neurovascular Unit Markers in the Brains of Patients after Cardiac Surgery: Effects of Multi-Task Cognitive Training
Reprinted from: *Biomedicines* **2024**, *12*, 756, https://doi.org/10.3390/biomedicines12040756 . . . **540**

Gianfranco Piccirillo, Federica Moscucci, Martina Mezzadri, Cristina Caltabiano, Giovanni Cisaria, Guendalina Vizza, et al.
Artificial Intelligence Applied to Electrical and Non-Invasive Hemodynamic Markers in Elderly Decompensated Chronic Heart Failure Patients
Reprinted from: *Biomedicines* **2024**, *12*, 716, https://doi.org/10.3390/biomedicines12040716 . . . **552**

Amilia Aminuddin, Nazirah Samah, Nur Aishah Che Roos, Shawal Faizal Mohamad, Boon Cong Beh, Adila A. Hamid and Azizah Ugusman
Prognostic Value of Lectin-like Oxidized Low-Density Lipoprotein Receptor-1 for Future Cardiovascular Disease Risk and Outcome: A Systematic Review and Meta-Analysis
Reprinted from: *Biomedicines* **2025**, *13*, 444, https://doi.org/10.3390/biomedicines13020444 . . . **566**

Bogdan-Flaviu Buz, Rodica Anamaria Negrean, Florina Caruntu, Tudor Parvanescu, Milena Slovenski, Mirela Cleopatra Tomescu and Diana-Aurora Arnautu
Systematic Review of Left Ventricular Remodeling in Response to Hypoglycemic Medications: Assessing Changes in End-Systolic and End-Diastolic Diameters
Reprinted from: *Biomedicines* **2024**, *12*, 1791, https://doi.org/10.3390/biomedicines12081791 . . **586**

About the Editor

Alfredo Caturano

Alfredo Caturano, MD, PhD, graduated with a degree in Medicine and Surgery from the Second University of Naples (SUN) in 2016. He achieved a Specialization Degree in Internal Medicine in 2021 at the University of Campania "Luigi Vanvitelli". His specialization thesis, concerning the impact of glycemic control on cardiovascular outcomes and mortality in a cohort of patients with type 2 diabetes mellitus in a multifactorial randomized controlled trial, was awarded the 2021 Annapaola Braggio prize by the Italian Society of Diabetology as the best specialization thesis on topics related to insulin resistance. He defended his PhD in Clinical and Experimental Medicine in January 2025, earning the title of Doctor Europaeus. His doctoral thesis focused on the cardiometabolic and hepatic effects of innovative glucose-lowering strategies in patients with type 2 diabetes. Since November 2024, he has served as an Assistant Professor of Internal Medicine at San Raffaele Roma University.

biomedicines

MDPI

Editorial

Cardiovascular and Metabolic Disease: New Treatment and Future Directions—The 3rd Edition

Alfredo Caturano

Department of Human Sciences and Promotion of the Quality of Life, San Raffaele Roma University, 00166 Rome, Italy; alfredo.caturano@uniroma5.it; Tel.: +39-3338616985

1. Introduction

Cardiovascular and metabolic diseases remain the most pressing global health concerns of our time, with a profound impact on both individual lives and healthcare systems [1]. According to recent data, cardiovascular diseases (CVDs) were responsible for nearly 18.6 million deaths globally in 2019, accounting for approximately one-third of all fatalities [2]. This alarming burden is closely intertwined with the global rise in metabolic disorders, most notably diabetes, which affects over 420 million individuals and contributes directly to an additional 1.5 million deaths annually [3]. These conditions rarely occur in isolation and often coexist, forming a dangerous clinical synergy that accelerates disease progression and worsens patient outcomes [4]. This bidirectional link between metabolic dysfunction and cardiovascular disease highlights the importance of a comprehensive, integrated approach to prevention and care [5]. Lifestyle-related risk factors, such as tobacco use, poor nutrition, physical inactivity, and excessive alcohol consumption, continue to play a central role in the onset and progression of both disease groups [6]. However, recent years have also brought significant advancements in therapeutic strategies. Notably, the emergence of sodium–glucose cotransporter-2 inhibitors (SGLT2i) and glucagon-like peptide 1 (GLP-1) receptor agonists has revolutionized the management of both diabetes and heart failure, while evolving interventional techniques are reshaping the clinical landscape [7–9]. This Special Issue brings together some of the most promising scientific insights in this rapidly advancing field.

2. Overview of Published Articles

This Special Issue presents a diverse and methodologically robust collection of 34 scientific articles, including original research, reviews, and experimental studies. addressing the broad and interwoven spectrum of cardiovascular and metabolic diseases. The contributions reflect a multidisciplinary approach that spans from molecular biology to advanced imaging, from novel therapeutic strategies to real-world clinical data. Below, we highlight representative works from this Special Issue, grouped by thematic domain and described individually to reflect their distinct scientific impact.

2.1. Biomarkers and Molecular Mechanisms

Alexander E. Berezin et al. (contribution 1) investigated the predictive role of irisin, a myokine involved in energy homeostasis, in patients with heart failure with reduced ejection fraction (HFrEF). In a prospective study of 313 patients, they demonstrated that higher baseline serum irisin levels were independently associated with improved left ventricular ejection fraction at 3-month follow-up, outperforming even NT-proBNP in

certain predictive models. This study positions irisin as a potential biomarker for cardiac recovery in HFrEF.

Irene Martínez-García et al. (contribution 2) investigated the role of advanced glycation end products (AGEs) in mediating the association between glycated hemoglobin (HbA1c) and aortic pulse wave velocity (a-PWV), an indicator of arterial stiffness, in a cohort of 390 healthy Spanish adults. Using skin autofluorescence (SAF) to measure AGEs, they found that while HbA1c levels were initially associated with increased a-PWV, this effect was largely mediated by SAF. Mediation analysis showed that SAF accounted for over 40% of the relationship, suggesting that AGE accumulation plays a significant role in vascular changes even in healthy individuals.

Caitlin P.S. Ellis et al. (contribution 3) examined protein signatures in perivascular adipose tissue (PVAT) of patients with and without coronary artery disease. Using proteomics and histomorphometric analyses, they identified distinct protein profiles in PVAT related to metabolic signaling, inflammation, and exosome activity. The work provides new insight into adipose tissue heterogeneity and its role in atherogenesis.

Kareem Awad et al. (contribution 4) explored the effects of hyperglycemia on human macrophages and uncovered that high glucose conditions activate the TGF-β1/Smad1/5 signaling pathway, potentially contributing to atherogenic responses. Their findings underscore the role of glucose-induced immune dysregulation in diabetes-related vascular complications.

Isabella D. Cooper et al. (contribution 5) examined the metabolic impact of temporarily suppressing ketosis in a group of healthy, lean, pre-menopausal women who had maintained long-term nutritional ketosis (NK). In a three-phase study, participants transitioned from NK to a 21-day period of suppressed ketosis (SuK) and then returned to NK. During SuK, significant increases were observed in insulin, glucose, HOMA-IR, leptin, and osteocalcin levels, along with reductions in beta-hydroxybutyrate and GLP-1. Importantly, all biomarkers reverted to baseline upon resuming NK, indicating preserved metabolic flexibility. The findings suggest that sustained NK may offer protective effects against hyperinsulinemia without impairing metabolic adaptability.

Manjula Nandakumar et al. (contribution 6) explored the impact of hypoglycemia and subsequent rebound hyperglycemia on cardiovascular risk biomarkers using proteomic profiling. They compared two controlled studies, one involving mild hypoglycemia and the other severe hypoglycemia followed by glucose-induced rebound; selected protein markers were measured in both type 2 diabetes patients and healthy controls. Severe hypoglycemia triggered transient increases in ANGPT1 and DKK1 in controls and suppression of BOC in diabetic participants. Notably, all alterations resolved within one hour, and rebound hyperglycemia did not induce further changes. These results suggest that acute hypoglycemia, rather than glycemic fluctuations, may be the critical driver of short-term cardiovascular risk.

2.2. Cardiometabolic and Endocrine Disorders

Jazmine A. Eccles-Miller et al. (contribution 7) explored the sexually dimorphic role of the enzyme CYP2B6 in fasting-induced hepatic steatosis using humanized transgenic mice. Despite previous links between CYP2B6 and anti-obesity effects, both male and female hCYP2B6-Tg mice developed greater steatosis compared to knockout controls when fasted. While treatment with oxylipins 9-HODE and 9-HOTrE altered serum lipids, especially in females, they did not significantly affect liver fat or gene expression. Females showed greater hepatic lipid retention and broader gene expression changes than males. The study concludes that CYP2B6 contributes to sex-specific susceptibility to steatosis, though oxylipins are not the primary mediators of this effect.

Jan Soukop et al. (contribution 8) evaluated the combined effect of fenofibrate and silymarin in an animal model of hereditary hypertriglyceridemia. While fenofibrate alone

improved lipid metabolism, the addition of silymarin significantly enhanced antioxidant activity and reduced lipoperoxidation in liver and heart tissues. This synergistic effect supports the potential of combining nutraceuticals with conventional therapies in metabolic syndrome.

Balázs Sági et al. (contribution 9) assessed the prognostic impact of metabolic syndrome (MetS) and its components on cardiovascular and renal outcomes in patients with IgA nephropathy (IgAN). In a long-term study involving 145 CKD patients followed for over 15 years, those with MetS experienced significantly higher rates of adverse events, including both renal and cardiovascular endpoints. Key predictors of poor outcomes included dyslipidemia, diabetes, low hemoglobin, and elevated albuminuria. The presence of multiple MetS components further amplified risk. These findings highlight the importance of early metabolic risk assessment and management in improving long-term outcomes for patients with IgAN.

Ruike Yan and Yanli Cao (contribution 10) assessed the safety and efficacy of epigallocatechin gallate (EGCG) supplementation in obesity and non-alcoholic fatty liver disease (NAFLD). The review synthesizes data from human trials, pointing to dose- and time-dependent benefits on metabolic parameters, with a cautionary note regarding hepatotoxicity at higher concentrations.

Ferenc Sztanek et al. (contribution 11) provided a comprehensive review of emerging pharmacological strategies for the treatment of obesity and type 2 diabetes mellitus (T2DM), focusing on the evolving role of incretin-based therapies. While GLP-1 receptor agonists have shown clinical success, their efficacy may be limited by receptor desensitization. The authors highlight novel developments, including oral GLP-1 agonists and next-generation dual and triple receptor agonists, such as GLP-1/GIP and GLP-1/GIP/glucagon combinations, which promise enhanced metabolic effects. By examining cellular signaling and inflammation pathways, the review underscores the expanding therapeutic landscape and the future potential of precision pharmacotherapy in managing obesity and T2DM.

Salvatore Nesci and Speranza Rubattu (contribution 12) presented an in-depth overview of the multifaceted roles of mitochondrial uncoupling protein 2 (UCP2), highlighting its dual physiological and pathological effects. Unlike UCP1, UCP2 does not mediate traditional proton leakage but appears to modulate oxidative phosphorylation through mild uncoupling and the exchange of C4 metabolites. This dual function allows UCP2 to reduce oxidative stress and potentially support healthy aging and cardiovascular protection. However, its activity may also impair mitochondrial ATP production and insulin secretion. The review underscores UCP2's complex and context-dependent bioenergetic impact, which remains incompletely understood.

2.3. Diagnostic Imaging and Interventional Techniques

Piotr Wańczura et al. (contribution 13) proposed a non-destructive method for visualizing atherosclerotic plaques using MRI paired with an iodine-based contrast agent. Their approach allows detailed, volumetric analysis while preserving tissue integrity, offering a promising complement to standard histology in assessing atherosclerotic burden.

Narae Kim et al. (contribution 14) examined the prognostic utility of carotid intima-media thickness and coronary artery calcium scores in patients with negative treadmill stress echocardiography. Both imaging markers independently predicted adverse cardiovascular outcomes, reinforcing their value in refining risk assessment.

Jaroslav Chlupac et al. (contribution 15) tested the FRAME mesh as external support for vein grafts in a porcine carotid model. The mesh significantly improved graft patency and reduced midgraft neo-intimal hyperplasia compared to controls, suggesting a protective role against stenosis in bypass surgery.

Natalia Zdebik et al. (contribution 16) demonstrated that T1-mapping cardiac MRI sequences can reveal elevated extracellular volume (ECV) in patients with hypertrophic cardiomyopathy (HCM) even in the absence of visible injury on late gadolinium enhancement. Their findings suggest T1-mapping offers valuable diagnostic insights into myocardial changes undetectable by conventional imaging.

Robert J. Gil et al. (contribution 17) reported four-year results from the POLBOS 3 trial comparing the BiOSS LIM C dedicated bifurcation stent to standard drug-eluting stents in non-left main coronary bifurcations. While no significant differences in major adverse cardiovascular events were observed, the BiOSS stent showed high implantation success and comparable long-term safety, establishing it as a viable option for complex bifurcation lesions.

2.4. Epidemiology, Population Studies, and Public Health

Vaida Šileikienė et al. (contribution 18) analyzed cardiovascular risk trends in over 52,000 middle-aged Lithuanian men from 2009 to 2019. Despite a decline in hypertension prevalence, nearly half had the condition, with many unaware or untreated. Men with resistant hypertension showed the highest burden of risk factors, particularly obesity, inactivity, and dyslipidemia, underscoring the need for targeted prevention and early intervention strategies.

Elke Boxhammer et al. (contribution 19) explored the impact of prediabetes on survival after ST-elevation myocardial infarction. In a cohort of 725 patients, those with prediabetes had significantly worse three-year survival compared to non-diabetics, with outcomes nearing those of diabetic patients. The findings highlight the need for early recognition and aggressive cardiovascular risk management in individuals with prediabetes.

Mara Volpentesta et al. (contribution 20) assessed the impact of one-year CPAP therapy in elderly patients with obstructive sleep apnea syndrome (OSAS). In a real-life cohort of 469 individuals, CPAP significantly improved respiratory indices, metabolic markers, and vascular function, particularly arterial stiffness and endothelial health. These results support CPAP as a key intervention to mitigate cardiovascular risk in elderly OSAS patients.

Ramcharan Singh Angom et al. (contribution 21) reviewed the advantages of zebrafish as a model for cardiovascular and metabolic diseases. Thanks to their genetic similarity to humans, transparency, and compatibility with gene editing, zebrafish are ideal for studying disease mechanisms, drug screening, and precision medicine. The model's scalability and cost-effectiveness make it a powerful tool for future translational research.

2.5. Translational and Experimental Medicine

Yuxin Nie et al. (contribution 22) explored the mechanisms behind hemodialysis-induced myocardial stunning (HIMS) using a rat model of chronic kidney disease. The study demonstrated that mitochondrial dysfunction and ion imbalances, particularly in potassium and calcium, contribute to HIMS. Activation of mitochondrial ATP-sensitive potassium channels with diazoxide improved both mitochondrial and cardiac function, suggesting a protective strategy against HIMS.

Alexandra Ioana Popescu et al. (contribution 23) investigated the role of microRNAs in patients with chronic limb-threatening ischemia (CLTI), a severe stage of peripheral arterial disease. By analyzing the expression of miR-199a, miR-20a, and miR-30c before and after revascularization, the study highlights their potential as biomarkers for disease monitoring and as future therapeutic targets in the management of critical limb ischemia.

Nicholas Pavlatos and Dinesh K. Kalra (contribution 24) reviewed the role of lipoprotein(a) in peripheral artery disease (PAD), highlighting its pro-atherogenic, pro-inflammatory, and pro-thrombotic properties. Despite its strong causal link to cardiovascu-

lar diseases, lipoprotein(a) remains underrecognized in PAD. The article emphasizes the need for greater clinical awareness and explores emerging therapies aimed at reducing related vascular risks.

Ekaterina Ogurtsova et al. (contribution 25) reviewed murine models used to study the cardiometabolic phenotype of heart failure with preserved ejection fraction (HFpEF), a condition often linked to obesity, type 2 diabetes, and hypertension. The article explores key pathophysiological mechanisms, such as inflammation, oxidative stress, and metabolic dysfunction, offering insights that may guide future therapeutic strategies for this increasingly prevalent and complex condition.

Diana-Aurora Arnautu et al. (contribution 26) provided a narrative review on inherited dilated cardiomyopathies (DCM), emphasizing the growing role of genetic assessment in risk stratification and treatment personalization. The review discusses the complex genotype–phenotype relationships in DCM and highlights how genetic variants influence disease expression, prognosis, and therapeutic response. Tailoring management based on genetic findings is presented as a key step toward more precise and effective care for affected individuals and their families.

3. Therapeutic Innovations and Pharmacological Strategies

Nicia I. Profili et al. (contribution 27) reviewed the emerging role of SGLT2i in patients following acute myocardial infarction. Beyond their glucose-lowering effects, SGLT2i have shown benefits in heart failure management and cardiovascular risk reduction. The article highlights their potential to improve outcomes post-infarction by modulating inflammation, reducing arrhythmias, and supporting ventricular remodeling, especially in patients undergoing percutaneous coronary intervention.

Vasiliki Katsi et al. (contribution 28) reviewed current weight loss therapies and their effects on hypertension. By examining pharmacologic agents, such as GLP-1 receptor agonists, tirzepatide, and combination drugs—as well as bariatric surgery—the article outlines how each intervention influences blood pressure through shared mechanisms such as insulin resistance and neurohormonal dysregulation. The review supports weight loss as a strategic component in hypertension management.

Kyosuke Murai et al. (contribution 29) reviewed clinical evidence on ranolazine, an antianginal agent with notable antiarrhythmic properties. The drug has shown efficacy in reducing ventricular tachycardia episodes and enhancing atrial fibrillation conversion when used alongside agents such as amiodarone. With a favorable safety profile and low proarrhythmic risk, ranolazine emerges as a promising adjunct in arrhythmia management.

Yotam Kolben et al. (contribution 30) assessed the use of wearable technology for real-time hemodynamic monitoring in hemodialysis patients. Their study showed that early and significant drops in blood pressure and other vitals predicted intradialytic hypotension (IDH) episodes. Continuous monitoring proved reliable and may offer a valuable tool for early IDH detection and prevention in clinical practice.

Irina Tarasova et al. (contribution 31) evaluated the impact of multi-task cognitive training (MTT) on brain activity and neurovascular markers in patients after coronary artery bypass surgery. Compared to controls, patients receiving MTT showed improved EEG patterns and favorable shifts in biomarkers such as reduced S100β and increased BDNF. These findings suggest that short-term cognitive training may aid in post-surgical neurocognitive recovery.

Gianfranco Piccirillo et al. (contribution 32) applied artificial intelligence to assess ECG-derived repolarization and non-invasive hemodynamic markers in elderly patients with decompensated chronic heart failure. Higher Tend (Te) intervals were associated with increased mortality, and changes in bioimpedance and repolarization metrics reflected

treatment response. These accessible, non-invasive parameters offer promise for remote monitoring and early detection of clinical deterioration using AI-driven tools.

4. Systematic Reviews and Meta-Analyses

Amilia Aminuddin et al. (contribution 33) conducted a systematic review and meta-analysis to assess the prognostic value of soluble LOX-1 (sLOX-1) in predicting cardiovascular outcomes. Elevated sLOX-1 levels were associated with an increased risk of major adverse cardiovascular and cerebrovascular events in patients with coronary artery disease. While results support its potential as a biomarker, the authors highlight the need for standardized research to confirm its role in clinical risk stratification.

Bogdan-Flaviu Buz et al. (contribution 34) conducted a systematic review evaluating the effects of hypoglycemic medications on left ventricular remodeling in diabetic patients. The analysis revealed that agents such as liraglutide and dapagliflozin significantly improved cardiac function and reduced ventricular dimensions, while others showed minimal impact. These findings suggest that certain glucose-lowering drugs may offer added cardiovascular benefits beyond glycemic control, supporting a more individualized approach in diabetes management.

5. Future Perspectives

Looking ahead, the intersection of cardiovascular and metabolic research is set to benefit from a wave of innovation, fueled by the growth of personalized medicine and precision health [10,11]. Genomic profiling, molecular diagnostics, and individualized risk stratification are opening the door to more targeted and effective interventions, moving beyond a "one-size-fits-all" approach and toward therapies that reflect the unique biology and lifestyle of each patient [12]. The therapeutic frontier is also expanding to include breakthrough technologies such as gene editing, regenerative medicine, and cell-based therapies, offering hope for disease modification and functional restoration in patients with advanced or refractory conditions [13]. At the same time, digital health tools, including wearable sensors, mobile applications, and remote monitoring platforms, are transforming the delivery of care by promoting continuity, accessibility, and patient engagement across geographic and socioeconomic barriers [14–16]. Nonetheless, the full realization of these opportunities requires us to confront enduring challenges. Socioeconomic disparities, unequal access to preventive services, and limited health literacy continue to undermine public health efforts [17]. Future research and policy must work in tandem to close these gaps by promoting early lifestyle interventions, investing in community education, and ensuring that innovation reaches all populations equitably [18]. With a multidisciplinary commitment to both scientific rigor and social responsibility, the future of cardiovascular and metabolic care holds the potential for meaningful, lasting impact.

Funding: This research received no external funding.

Institutional Review Board Statement: The author has reviewed the literature data and has reported results coming from studies approved by local ethics committee.

Informed Consent Statement: Not applicable.

Data Availability Statement: No dataset was generated for the publication of this article.

Conflicts of Interest: The author declares no conflicts of interest.

List of Contributions:

1. Berezin, A.E.; Berezina, T.A.; Novikov, E.V.; Berezin, O.O. Serum Levels of Irisin Are Positively Associated with Improved Cardiac Function in Patients with Heart Failure with Reduced Ejection Fraction. *Biomedicines* **2025**, *13*, 866. https://doi.org/10.3390/biomedicines13040866.
2. Martínez-García, I.; Saz-Lara, A.; Pascual-Morena, C.; Díez-Fernández, A.; Valladolid-Ayllón, S.; Bizzozero-Peroni, B.; Martínez-Cifuentes, Ó.; Rodríguez-Gutiérrez, E.; Cavero-Redondo, I. Role of Advanced Glycation End Products in Mediating Glycated Haemoglobin and Pulse Wave Velocity in Healthy Adults. *Biomedicines* **2025**, *13*, 137. https://doi.org/10.3390/biomedicines13010137.
3. Ellis, C.P.S.; Tero, B.W.; Potts, C.M.; Malka, K.T.; Yang, X.; Hamilton, J.; Vary, C.; Khalil, A.; Liaw, L. Cellular Characteristics and Protein Signatures of Human Adipose Tissues from Donors With or Without Advanced Coronary Artery Disease. *Biomedicines* **2024**, *12*, 2453. https://doi.org/10.3390/biomedicines12112453.
4. Awad, K.; Kakkola, L.; Julkunen, I. High Glucose Increases Lactate and Induces the Transforming Growth Factor Beta-Smad 1/5 Atherogenic Pathway in Primary Human Macrophages. *Biomedicines* **2024**, *12*, 1575. https://doi.org/10.3390/biomedicines12071575.
5. Cooper, I.D.; Kyriakidou, Y.; Petagine, L.; Edwards, K.; Soto-Mota, A.; Brookler, K.; Elliott, B.T. Ketosis Suppression and Ageing (KetoSAge) Part 2: The Effect of Suppressing Ketosis on Biomarkers Associated with Ageing, HOMA-IR, Leptin, Osteocalcin, and GLP-1, in Healthy Females. *Biomedicines* **2024**, *12*, 1553. https://doi.org/10.3390/biomedicines12071553.
6. Nandakumar, M.; Sathyapalan, T.; Atkin, S.L.; Butler, A.E. Effect of Hypoglycemia and Rebound Hyperglycemia on Proteomic Cardiovascular Risk Biomarkers. *Biomedicines* **2024**, *12*, 1137. https://doi.org/10.3390/biomedicines12061137.
7. Eccles-Miller, J.A.; Johnson, T.D.; Baldwin, W.S. Sexually Dimorphic Effects of CYP2B6 in the Development of Fasting-Mediated Steatosis in Mice: Role of the Oxylipin Products 9-HODE and 9-HOTrE. *Biomedicines* **2025**, *13*, 295. https://doi.org/10.3390/biomedicines13020295.
8. Soukop, J.; Kazdová, L.; Hüttl, M.; Malínská, H.; Marková, I.; Oliyarnyk, O.; Miklánková, D.; Gurská, S.; Rácová, Z.; Poruba, M.; et al. Beneficial Effect of Fenofibrate in Combination with Silymarin on Parameters of Hereditary Hypertriglyceridemia-Induced Disorders in an Animal Model of Metabolic Syndrome. *Biomedicines* **2025**, *13*, 212. https://doi.org/10.3390/biomedicines13010212.
9. Sági, B.; Vas, T.; Csiky, B.; Nagy, J.; Kovács, T.J. Does Metabolic Syndrome and Its Components Have Prognostic Significance for Renal and Cardiovascular Outcomes in IgA Nephropathy? *Biomedicines* **2024**, *12*, 1250. https://doi.org/10.3390/biomedicines12061250.
10. Yan, R.; Cao, Y. The Safety and Efficacy of Dietary Epigallocatechin Gallate Supplementation for the Management of Obesity and Non-Alcoholic Fatty Liver Disease: Recent Updates. *Biomedicines* **2025**, *13*, 206. https://doi.org/10.3390/biomedicines13010206.
11. Sztanek, F.; Tóth, L.I.; Pető, A.; Hernyák, M.; Diószegi, Á.; Harangi, M. New Developments in Pharmacological Treatment of Obesity and Type 2 Diabetes—Beyond and within GLP-1 Receptor Agonists. *Biomedicines* **2024**, *12*, 1320. https://doi.org/10.3390/biomedicines12061320.
12. Nesci, S.; Rubattu, S. UCP2, a Member of the Mitochondrial Uncoupling Proteins: An Overview from Physiological to Pathological Roles. *Biomedicines* **2024**, *12*, 1307. https://doi.org/10.3390/biomedicines12061307.
13. Wańczura, P.; Mytych, W.; Bartusik-Aebisher, D.; Leksa, D.; Truszkiewicz, A.; Aebisher, D. Visualization of Atherosclerotic Plaques Paired with Joheksol 350 (Omnipaque). *Biomedicines* **2025**, *13*, 399. https://doi.org/10.3390/biomedicines13020399.
14. Kim, N.; Hwang, H.-J.; Yang, I.-H. Assessing Cardiovascular Risk with Coronary Artery Calcium and Carotid Intima-Media Thickness in Patients with Negative Stress Echocardiography. *Biomedicines* **2024**, *12*, 2151. https://doi.org/10.3390/biomedicines12092151.
15. Chlupac, J.; Frank, J.; Sedmera, D.; Fabian, O.; Simunkova, Z.; Mrazova, I.; Novak, T.; Vanourková, Z.; Benada, O.; Pulda, Z.; et al. External Support of Autologous Internal Jugular Vein Grafts with FRAME Mesh in a Porcine Carotid Artery Model. *Biomedicines* **2024**, *12*, 1335. https://doi.org/10.3390/biomedicines12061335.

16. Zdebik, N.; Poręba, R.; Gać, P. Importance of T1-Mapping Sequence in Patients with Hypertrophic Cardiomyopathy without Foci of Non-Ischemic Myocardial Injury in Late Gadolinium Enhancement Sequence. *Biomedicines* **2024**, *12*, 1330. https://doi.org/10.3390/biomedicines12061330.
17. Gil, R.J.; Kern, A.; Bojko, K.; Gziut-Rudkowska, A.; Vassilev, D.; Bil, J. The Randomized, Multicenter, Open-Label, Controlled POLBOS 3 Trial Comparing Regular Drug-Eluting Stents and the Sirolimus-Eluting BiOSS LIM C Dedicated Coronary Bifurcation Stent: Four-Year Results. *Biomedicines* **2024**, *12*, 938. https://doi.org/10.3390/biomedicines12050938.
18. Šileikienė, V.; Dženkevičiūtė, V.; Čypienė, A.; Šlapikas, T.; Puronaitė, R.; Badarienė, J.; Laucevičius, A.; Butkevičiūtė, E.; Rinkūnienė, E. Analysis of Cardiovascular High-Risk Profile in Middle-Aged Lithuanian Men with Arterial Hypertension from 2009 to 2019. *Biomedicines* **2025**, *13*, 272. https://doi.org/10.3390/biomedicines13020272.
19. Boxhammer, E.; Hammerer, M.; Schernthaner, C.; Prinz, E.; Brandt, M.C.; Lichtenauer, M.; Berezin, A.E.; Wintersteller, W.; Hoppe, U.C.; Kopp, K.L. The Silent Threat: A Retrospective Cohort Study on the Impact of Prediabetes on ST-Elevation Myocardial Infarction Survival—A Call to Action! *Biomedicines* **2024**, *12*, 2223. https://doi.org/10.3390/biomedicines12102223.
20. Volpentesta, M.; Condoleo, V.; Panza, A.; Severini, G.; Soraci, L.; Rotondo, C.; Armentaro, G.; Pelaia, C.; Fiorentino, V.T.; Andreozzi, F.; et al. Effects of Continuous Positive Airway Pressure Treatment on Vascular Function in a Real-Life Cohort of Elderly Patients with Obstructive Sleep Apnoea Syndrome. *Biomedicines* **2024**, *12*, 2563. https://doi.org/10.3390/biomedicines12112563.
21. Angom, R.S.; Nakka, N.M.R. Zebrafish as a Model for Cardiovascular and Metabolic Disease: The Future of Precision Medicine. *Biomedicines* **2024**, *12*, 693. https://doi.org/10.3390/biomedicines12030693.
22. Nie, Y.; Lin, L.; Yang, Q.; Hu, J.; Sun, M.; Xiang, F.; Cao, X.; Yu, J.; Wang, Y.; Teng, J.; et al. Mitochondrial Dysfunction and Ion Imbalance in a Rat Model of Hemodialysis-Induced Myocardial Stunning. *Biomedicines* **2024**, *12*, 2402. https://doi.org/10.3390/biomedicines12102402.
23. Popescu, A.I.; Rață, A.L.; Vlad, D.; Vlad, C.; Popescu, R.; Onofrei, R.R.; Morelli, M.; Pantea, S.; Barac, S. miRNA in the Diagnosis and Treatment of Critical Limb Ischemia. *Biomedicines* **2024**, *12*, 2026. https://doi.org/10.3390/biomedicines12092026.
24. Pavlatos, N.; Kalra, D.K. The Role of Lipoprotein(a) in Peripheral Artery Disease. *Biomedicines* **2024**, *12*, 1229. https://doi.org/10.3390/biomedicines12061229.
25. Ogurtsova, E.; Arefieva, T.; Filatova, A.; Radyukhina, N.; Ovchinnikov, A. Cardiometabolic Phenotype in HFpEF: Insights from Murine Models. *Biomedicines* **2025**, *13*, 744. https://doi.org/10.3390/biomedicines13030744.
26. Arnautu, D.-A.; Cozma, D.; Lala, I.-R.; Arnautu, S.-F.; Tomescu, M.-C.; Andor, M. Risk Assessment and Personalized Treatment Options in Inherited Dilated Cardiomyopathies: A Narrative Review. *Biomedicines* **2024**, *12*, 1643. https://doi.org/10.3390/biomedicines12081643.
27. Profili, N.I.; Castelli, R.; Manetti, R.; Sircana, M.C.; Pagni, M.; Sechi, G.L.; Gidaro, A.; Cossu, C.; Bella, F.; Delitala, A.P. Sodium–Glucose Cotransporter-2 Inhibitors After Acute Myocardial Infarction. *Biomedicines* **2025**, *13*, 720. https://doi.org/10.3390/biomedicines13030720.
28. Katsi, V.; Manta, E.; Fragoulis, C.; Tsioufis, K. Weight Loss Therapies and Hypertension Benefits. *Biomedicines* **2024**, *12*, 2293. https://doi.org/10.3390/biomedicines12102293.
29. Murai, K.; Vasigh, A.; Alexy, T.; Tóth, K.; Czopf, L. The Role of Ranolazine in the Treatment of Ventricular Tachycardia and Atrial Fibrillation: A Narrative Review of the Clinical Evidence. *Biomedicines* **2024**, *12*, 1669. https://doi.org/10.3390/biomedicines12081669.
30. Kolben, Y.; Gork, I.; Peled, D.; Amitay, S.; Moshel, P.; Goldstein, N.; Ben Ishay, A.; Fons, M.; Tabi, M.; Eisenkraft, A.; et al. Continuous Monitoring of Advanced Hemodynamic Parameters during Hemodialysis Demonstrated Early Variations in Patients Experiencing Intradialytic Hypotension. *Biomedicines* **2024**, *12*, 1177. https://doi.org/10.3390/biomedicines12061177.
31. Tarasova, I.; Kukhareva, I.; Kupriyanova, D.; Temnikova, T.; Gorbatovskaya, E.; Trubnikova, O. Electrical Activity Changes and Neurovascular Unit Markers in the Brains of Patients after Cardiac Surgery: Effects of Multi-Task Cognitive Training. *Biomedicines* **2024**, *12*, 756. https://doi.org/10.3390/biomedicines12040756.

32. Piccirillo, G.; Moscucci, F.; Mezzadri, M.; Caltabiano, C.; Cisaria, G.; Vizza, G.; De Santis, V.; Giuffrè, M.; Stefano, S.; Scinicariello, C.; et al. Artificial Intelligence Applied to Electrical and Non-Invasive Hemodynamic Markers in Elderly Decompensated Chronic Heart Failure Patients. *Biomedicines* **2024**, *12*, 716. https://doi.org/10.3390/biomedicines12040716.
33. Aminuddin, A.; Samah, N.; Che Roos, N.A.; Mohamad, S.F.; Beh, B.C.; A. Hamid, A.; Ugusman, A. Prognostic Value of Lectin-like Oxidized Low-Density Lipoprotein Receptor-1 for Future Cardiovascular Disease Risk and Outcome: A Systematic Review and Meta-Analysis. *Biomedicines* **2025**, *13*, 444. https://doi.org/10.3390/biomedicines13020444.
34. Buz, B.-F.; Negrean, R.A.; Caruntu, F.; Parvanescu, T.; Slovenski, M.; Tomescu, M.C.; Arnautu, D.-A. Systematic Review of Left Ventricular Remodeling in Response to Hypoglycemic Medications: Assessing Changes in End-Systolic and End-Diastolic Diameters. *Biomedicines* **2024**, *12*, 1791. https://doi.org/10.3390/biomedicines12081791.

References

1. Dong, X.; Wang, J.; Wang, C.; Wang, B.; Li, G.; Yang, J.; Zou, T. Worldwide Burden of Metabolic Risk-Related Cardiovascular Disease from 1990 to 2021, with Projections to 2050: A Systematic Analysis for the Global Burden of Disease Study 2021. *Diabetes Obes. Metab.* 2025, *Early View*. [CrossRef] [PubMed]
2. Roth, G.A.; Mensah, G.A.; Johnson, C.O.; Addolorato, G.; Ammirati, E.; Baddour, L.M.; Barengo, N.C.; Beaton, A.Z.; Benjamin, E.J.; Benziger, C.P.; et al. Global Burden of Cardiovascular Diseases and Risk Factors, 1990–2019: Update from the GBD 2019 Study. *J. Am. Coll. Cardiol.* **2020**, *76*, 2982–3021. [CrossRef] [PubMed]
3. Saeedi, P.; Petersohn, I.; Salpea, P.; Malanda, B.; Karuranga, S.; Unwin, N.; Colagiuri, S.; Guariguata, L.; Motala, A.A.; Ogurtsova, K.; et al. Global and regional diabetes prevalence estimates for 2019 and projections for 2030 and 2045: Results from the International Diabetes Federation Diabetes Atlas, 9th edition. *Diabetes Res. Clin. Pract.* **2019**, *157*, 107843. [CrossRef] [PubMed]
4. Leon, B.M.; Maddox, T.M. Diabetes and Cardiovascular Disease: Epidemiology, Biological Mechanisms, Treatment Recommendations and Future Research. *World J. Diabetes* **2015**, *6*, 1246–1258. [CrossRef] [PubMed]
5. Wang, Z.; Chen, J.; Zhu, L.; Jiao, S.; Chen, Y.; Sun, Y. Metabolic Disorders and Risk of Cardiovascular Diseases: A Two-Sample Mendelian Randomization Study. *BMC Cardiovasc. Disord.* **2023**, *23*, 529. [CrossRef] [PubMed]
6. Ng, R.; Sutradhar, R.; Yao, Z.; Wodchis, W.P.; Rosella, L.C. Smoking, Drinking, Diet and Physical Activity—Modifiable Lifestyle Risk Factors and Their Associations with Age to First Chronic Disease. *Int. J. Epidemiol.* **2020**, *49*, 113–130. [CrossRef] [PubMed]
7. Nevola, R.; Alfano, M.; Pafundi, P.C.; Brin, C.; Gragnano, F.; Calabrò, P.; Adinolfi, L.E.; Rinaldi, L.; Sasso, F.C.; Caturano, A. Cardiorenal Impact of SGLT-2 Inhibitors: A Conceptual Revolution in the Management of Type 2 Diabetes, Heart Failure and Chronic Kidney Disease. *Rev. Cardiovasc. Med.* **2022**, *23*, 106. [CrossRef] [PubMed]
8. Ferhatbegović, L.; Mršić, D.; Macić-Džanković, A. The Benefits of GLP1 Receptors in Cardiovascular Diseases. *Front. Clin. Diabetes Healthc.* **2023**, *4*, 1293926. [CrossRef] [PubMed]
9. Holmes, D.R., Jr.; Alkhouli, M. Past, Present, and Future of Interventional Cardiology. *J. Am. Coll. Cardiol.* **2020**, *75*, 2738–2743. [CrossRef] [PubMed]
10. Giugni, F.R.; Berry, J.D.; Khera, A.; Shah, A.M.; de Lemos, J.A. Precision Medicine for Cardiovascular Prevention and Population Health: A Bridge Too Far? *Circulation* **2024**, *150*, 1720–1731. [CrossRef] [PubMed]
11. Galiero, R.; Caturano, A.; Vetrano, E.; Monda, M.; Marfella, R.; Sardu, C.; Salvatore, T.; Rinaldi, L.; Sasso, F.C. Precision Medicine in Type 2 Diabetes Mellitus: Utility and Limitations. *Diabetes Metab. Syndr. Obes.* **2023**, *16*, 3669–3689. [CrossRef] [PubMed]
12. Geocadin, R.G. Moving Beyond One-Size-Fits-All Treatment for Patients After Cardiac Arrest. *JAMA Netw. Open* **2020**, *3*, e208809. [CrossRef] [PubMed]
13. Hussen, B.M.; Taheri, M.; Yashooa, R.K.; Abdullah, G.H.; Abdullah, S.R.; Kheder, R.K.; Mustafa, S.A. Revolutionizing Medicine: Recent Developments and Future Prospects in Stem-Cell Therapy. *Int. J. Surg.* **2024**, *110*, 8002–8024. [CrossRef] [PubMed]
14. Liao, Y.; Thompson, C.; Peterson, S.; Mandrola, J.; Beg, M.S. The Future of Wearable Technologies and Remote Monitoring in Health Care. *Am. Soc. Clin. Oncol. Educ. Book* **2019**, *39*, 115–121. [CrossRef] [PubMed]
15. Russo, V.; Bottino, R.; Rago, A.; Papa, A.A.; Liccardo, B.; Proietti, R.; Manna, V.; Golino, P.; D'Onofrio, A.; Nigro, G. The Effect of Sacubitril/Valsartan on Device Detected Arrhythmias and Electrical Parameters among Dilated Cardiomyopathy Patients with Reduced Ejection Fraction and Implantable Cardioverter Defibrillator. *J. Clin. Med.* **2020**, *9*, 1111. [CrossRef] [PubMed]
16. Russo, V.; Rago, A.; Ciardiello, C.; Russo, M.G.; Calabrò, P.; Politano, L.; Nigro, G. The Role of the Atrial Electromechanical Delay in Predicting Atrial Fibrillation in Myotonic Dystrophy Type 1 Patients. *J. Cardiovasc. Electrophysiol.* **2016**, *27*, 65–72. [CrossRef] [PubMed]

17. Schillinger, D. The Intersections Between Social Determinants of Health, Health Literacy, and Health Disparities. *Stud. Health Technol. Inform.* **2020**, *269*, 22–41. [CrossRef] [PubMed]
18. Caturano, A.; Rocco, M.; Tagliaferri, G.; Piacevole, A.; Nilo, D.; Di Lorenzo, G.; Iadicicco, I.; Donnarumma, M.; Galiero, R.; Acierno, C.; et al. Oxidative Stress and Cardiovascular Complications in Type 2 Diabetes: From Pathophysiology to Lifestyle Modifications. *Antioxidants* **2025**, *14*, 72. [CrossRef] [PubMed]

Disclaimer/Publisher's Note: The statements, opinions and data contained in all publications are solely those of the individual author(s) and contributor(s) and not of MDPI and/or the editor(s). MDPI and/or the editor(s) disclaim responsibility for any injury to people or property resulting from any ideas, methods, instructions or products referred to in the content.

biomedicines

MDPI

Article

Serum Levels of Irisin Are Positively Associated with Improved Cardiac Function in Patients with Heart Failure with Reduced Ejection Fraction

Alexander E. Berezin [1,*], Tetiana A. Berezina [2], Evgen V. Novikov [3] and Oleksandr O. Berezin [4]

[1] Division of Cardiology, Department of Internal Medicine II, Paracelsus Medical University, 5020 Salzburg, Austria
[2] VitaCenter, Department of Internal Medicine and Nephrology, 69000 Zaporozhye, Ukraine; talexberezina@gmail.com
[3] Department of Functional Diagnostics, Shupyk National Healthcare University of Ukraine, 04136 Kyiv, Ukraine; doctornovikov@ukr.net
[4] Luzerner Psychiatrie AG, 4915 St. Urban, Switzerland; lunik.mender@gmail.com or oleksandr.berezin@lups.ch
* Correspondence: o.berezin@salk.at or aeberezin@gmail.com

Abstract: Background: The purpose of the study is to investigate a possible predictive value of irisin for improved left ventricular (LV) ejection fraction (EF) in discharged patients with known heart failure with reduced ejection fraction (HFrEF). **Methods**: We included in the study 313 patients who were discharged with HFrEF (at admission, LVEF $\leq$ 40%) and monitored for 3 months. HF with improved LVEF (HFimpEF) was characterized as a >40% increase in LVEF on transthoracic B-mode echocardiography within 3 months of follow-up. Circulating biomarkers including NT-proBNP and irisin were detected at baseline and after 3 months of observation. By the third month, 117 (37.4%) patients had HFimpEF, whereas 196 individuals were categorized as having persistent HFrEF. **Results**: We found that HFimpEF was related to lower LV end-diastolic dimensions and concentrations of NT-proBNP and higher left atrial volume index (LAVI) and irisin concentrations than those with persistent HFrEF. The most balanced cut-offs of irisin and NT-proBNP concentrations (improved LVEF versus non-improved LVEF) were 10.8 ng/mL and 1540 pmol/L, respectively. Multivariate regression analysis showed that atrial fibrillation (odds ratio [OR] = 0.95; p = 0.010), LAVI < 39 mL/m^2 (OR = 1.23; p = 0.001), irisin levels $\geq$ 10.8 ng/mL (OR = 1.73; p = 0.001), and NT-proBNP < 1540 pmol/mL (OR = 1.47; p = 0.001) independently predicted HFimpEF. The discriminative ability of irisin $\geq$ 10.8 ng/mL was better than NT-proBNP < 1540 pmol/mL; the predictive ability of irisin alone was not improved by the combined model (irisin added to NT-proBNP). **Conclusions**: serum irisin $\geq$ 10.8 ng/mL predicted HFimpEF independently of natriuretic peptide in HFrEF patients.

Keywords: heart failure; improved ejection fraction; cardiac function; irisin; natriuretic peptides; biomarkers

1. Introduction

Despite the introduction of new diagnostic, preventive, and treatment options into routine clinical practice, heart failure (HF) remains a condition with unacceptably high mortality rates ranging from 0.2% to 17.7% in the general population [1,2]. Several population-representative studies have shown that one-year mortality from heart failure varied from 4% to 45%, with an average of 33% overall and 24% depending on the presentation of HF

phenotypes, concomitant comorbidities across all adult age groups, and the categorization of left ventricular (LV) ejection fraction (EF) [3,4]. Interestingly, cardiovascular (CV) and HF readmission rates were markedly higher in patients with HF with reduced ejection fraction (HFrEF) and mildly reduced ejection fraction (HFmrEF) compared with those with HF with preserved ejection fraction (HFpEF), whereas the composite endpoint (all-cause mortality, cardiovascular death, and re-hospitalization) was similar in all subgroups [5–7].

With personalized guideline-directed medical therapy (GDMT), a significant proportion of patients with HFrEF show improvement in LVEF (known as HF with improved EF [HFimpEF]) [8]. Improved short and long-term clinical outcomes, including mortality and hospital readmissions, are associated with the recovery of systolic function in patients with HFrEF [9,10]. Despite the presence of several factors as positive predictors of HFimpHF, i.e., female gender, age < 55 years, de novo HF associated with hypertension and atrial fibrillation, sodium–glucose cotransporter-2 (SGLT2) inhibitors, and beta-blockers, and those as negative predictors, such as NYHA class III/IV, anemia, coronary artery disease (CAD), and type 2 diabetes mellitus (T2DM), the role of conventionally used circulating biomarkers in the management of HFimpHF is still not clearly investigated [10,11]. Moreover, the clinical benefit of contemporary management in terms of HFimpHF was present regardless of baseline N-terminal brain natriuretic pro-peptide (NT-proBNP) concentration, while higher NT-proBNP levels were correlated with a greater risk of a poor outcome [12]. However, post-discharge monitoring of NT-proBNP levels showed no clear benefit in predicting re-admission rate or non-HF adverse clinical events but was markedly associated with a lower risk of CV death [13]. Another aspect is the determination of non-HF mortality in HFimpHF after discharge from the hospital because non-cardiac causes accounted for more than 60% of deaths, which are not completely predicted by biomarkers of mechanical stress (NT-proBNP), myocardial damage (high-sensitivity troponin T/I), inflammation (galectin-3, interleukin-6, high-sensitivity C-reactive protein, growth differential factor-15), and fibrosis (soluble suppression of tumorigenicity 2 [sST2]) [14–18]. In addition, the improvement in the systolic function of the LV is associated with a reduction in the levels of serum natriuretic peptides [19]. A significant proportion of these patients frequently determined as having euvolemic status may have low/near-normal NT-proBNP concentrations (<300 pg/mL), which severely limits the ability to discriminate clinical outcomes in HFimpEF, so a large number of these patients may have an underestimated risk of adverse outcomes [20]. In this context, the discovery of new approaches based on circulating biomarkers for predicting HFimpEF could be considered promising.

In previous years, there has been considerable evidence that the intensity of systemic inflammation may be associated with severity and poor prognosis in all HF phenotypes [21,22]. In this context, CV risk factors (age, smoking), metabolic comorbidities (diabetes mellitus, dyslipidemia, obesity, thyroid dysfunction), cardiac cachexia, rheumatic and respiratory diseases, acute and chronic kidney disease (CKD), and altered microbiota contribute to HF occurrence through modulating inadequate immune response, mediating synthesis, and releasing inflammatory mediators, which consequently induce adipose tissue and skeletal muscle dysfunctions and intervene in vascular and cardiac remodeling [23].

Irisin is the membrane-associated component of the fibronectin type III domain-containing 5 protein (FNDC5), which is activated by peroxisome proliferator-activated receptor γ (PPARγ) coactivator-1α (PGC-1α) after stretching in skeletal myocytes [24]. Several forms of physical exercise, i.e., aerobic, anaerobic, and interval training, have been identified as primary causes of increased irisin synthesis and secretion in circulation. In physiological conditions, irisin acts as a regulator of tyrosine residues insulin receptor phosphorylation, which increases the activity of the phosphatidylinositol 3-kinases pathway, thereby attenuating insulin sensitivity, inflammatory response, and cognitive function [25].

FNDC5/irisin stimulates the transcriptional potency RUNX1/2 factors through a focal adhesion kinase-dependent pathway in brain and peripheral tissues including bone and subcutaneous white adipose tissue (WAT) and consequently plays a pivotal role in thermogenesis, energy metabolism, and browning WAT [26,27]. In pathophysiological conditions, irisin is not only produced by skeletal myocytes but also adipocytes, cardiac myocytes, hepatocytes, and astrocytes [28,29]. Irisin prevents ischemia-reperfusion injury and cell necrosis/apoptosis/pyroptosis and protects against autophagy and mitochondrial dysfunction as well as reducing extracellular matrix accumulation, fibrosis, oxidative stress, and inflammation via the AKT/mTOR signaling, ERK1/2, and Sirtuin-1-p53-SLC7A11/GPX4 pathways [30–32]. The biological activities of irisin in physiological and pathophysiological conditions are reported in Figure 1.

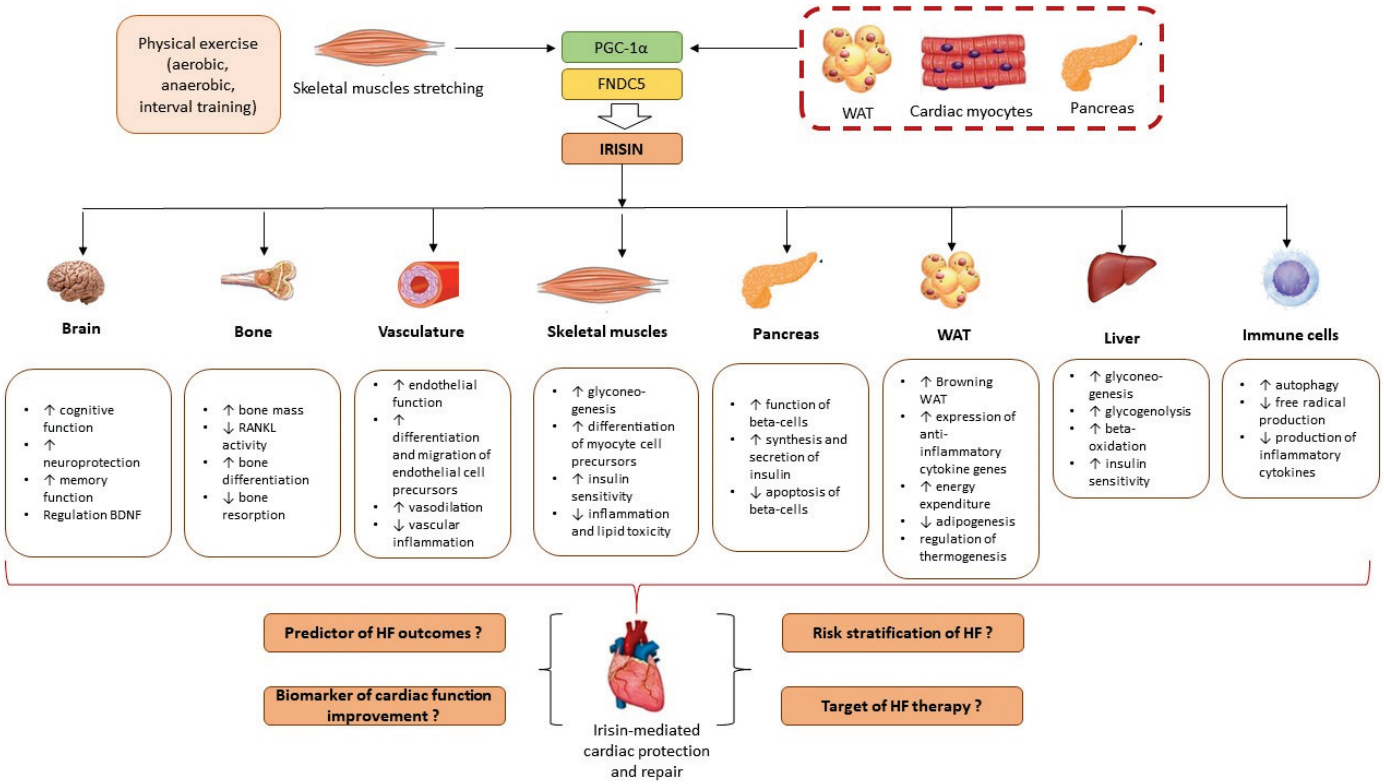


Figure 1. Rationale for investigating irisin in HF patients based on its biological effects. Abbreviations: BDNF, brain-derived neurotrophic factor; HF, heart failure; FNDC5, fibronectin type III domain-containing 5 protein; PGC-1α, peroxisome proliferator-activated receptor γ coactivator-1α; RANKL, receptor activator of nuclear factor -κB ligand; WAT, white adipose tissue; ↑, increase; ↓, decrease.

A decrease in circulating irisin levels was not only associated with cardio- and cerebrovascular conditions and diseases (myocardial infarction, HF, hypertension, atherosclerosis, vascular dementia, stroke), osteoporosis, T2DM, obesity, and CKD but also demonstrated its discriminatory ability for the prognosis of their natural evolution [33–38]. Finally, the predictive potency of irisin concentrations was better than NT-proBNP in HF in patients with metabolic comorbidities, such as obesity and diabetes mellitus [39]. However, the possible role of irisin in predicting functional cardiac recovery in HFrEF patients remains not completely clear. The purpose of the study is to investigate the discriminatory ability of irisin for improved LVEF in discharged individuals with HFrEF.

2. Materials and Methods

2.1. Patient Population and Structure of the Study

We selected 356 in-patients with HFrEF who had hemodynamically stable status with NT-proBNP levels > 300 pmol/mL. Among them, 313 individuals met the inclusion criteria and were consecutively enrolled from October 2020 to November 2024. The subjects were then evaluated during a subsequent inpatient stay at the private hospital "Vita Center" (Zaporozhye, Ukraine), and the inclusion and exclusion criteria, in addition to the study procedures and the determination of clinical outcomes, are outlined in Figure 2. Patients with acute or acutely decompensated HF and HF de novo during hospitalization were not included in the study. However, the main reason for hospitalization was the initiation of optimal GDMT.

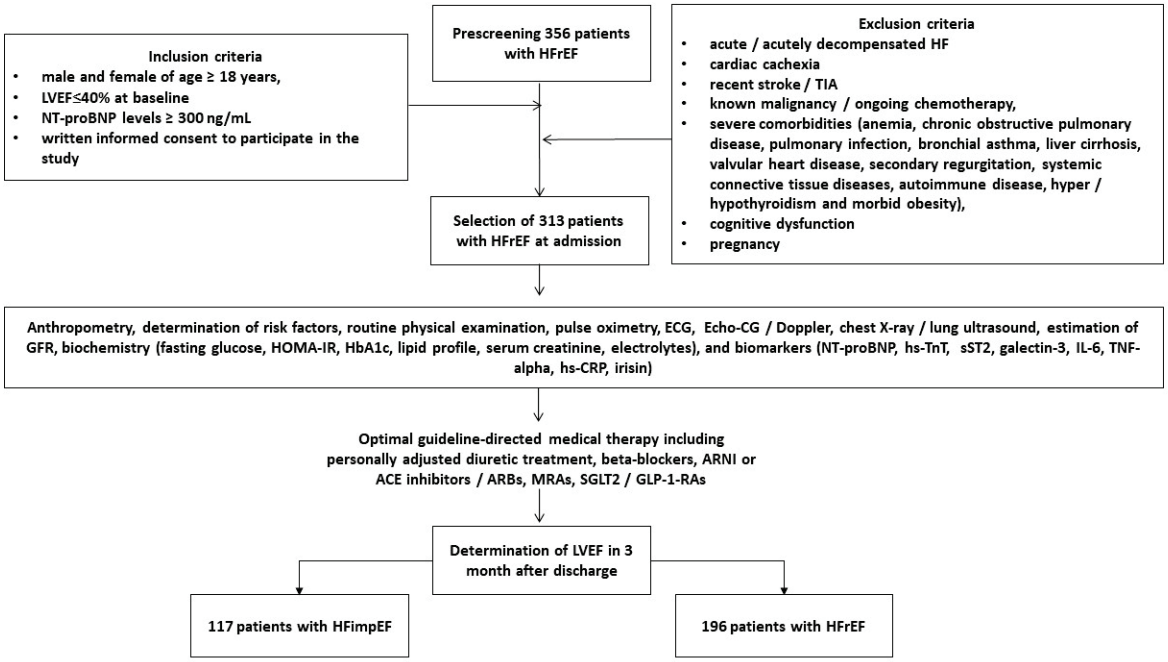


Figure 2. Flow chart of the study design. Abbreviations: ACE, angiotensin-converting enzyme; ARBs, angiotensin-II receptor blockers; ARNI, angiotensin receptor neprilysin inhibitors; Echo-CG, echocardiography; ECG, electrocardiography; GLP-1-RAs, glucagon-like peptide-1 receptor agonists; IL, interleukin; LVEF, left ventricular ejection fraction; hs-CRP, high-sensitivity C-reactive protein; HF, heart failure; HFrEF, heart failure with reduced ejection fraction; HFimpEF, heart failure with improved ejection fraction; MRAs, mineralocorticoid receptor antagonists; NT-proBNP, N-terminal brain natriuretic pro-peptide; TNF-alpha, tumor necrosis factor-alpha; sST2, soluble suppression of tumorigenicity-2; SGLT2, sodium–glucose co-transporter-2; TIA, transient ischemic attack.

All patients were administered optimal GDMT, including personalized doses of diuretics, renin–angiotensin–aldosterone system inhibitors, beta-blockers, sodium–glucose cotransporter 2 (SGLT2) inhibitors, and glucagon-like peptide-1 (GLP-1) receptor agonists. At 3 months post-discharge, patients meeting the criteria for HFimpHF were enrolled in the first cohort (n = 117), whereas those without improvement in LVEF were categorized as having persistent HFrEF and enrolled in the second cohort (n = 196).

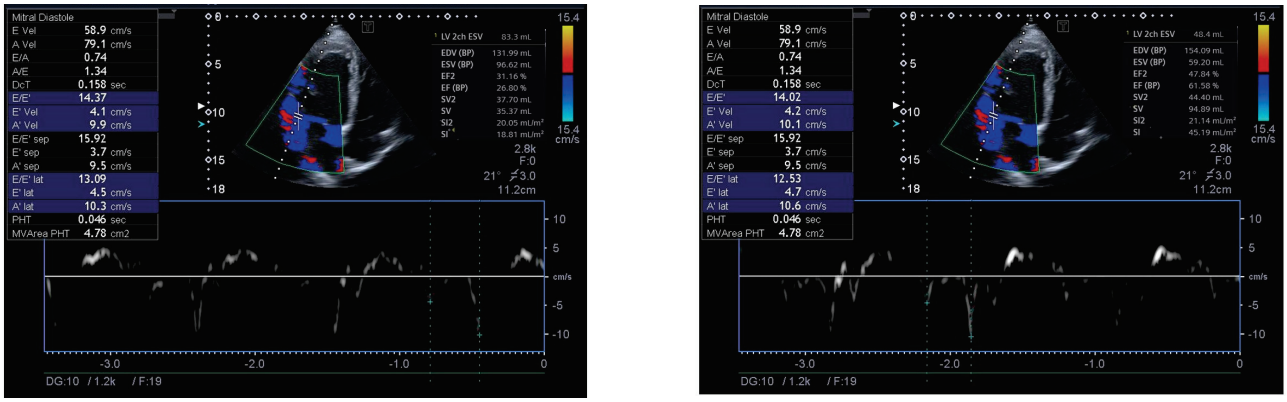
2.2. The Evaluation of Participants' Demographics, Anthropometry Parameters, and Concomitant Diseases/Conditions

The study collected detailed information about the participants' demographics (age, gender) and anthropometry parameters including weight and body mass index (BMI). The evaluation involved an assessment of conventional CV risk factors and concomitant dis-

eases/conditions, such as hypertension, smoking, dyslipidemia, obesity, atrial fibrillation, CAD, T2DM, and CKD.

2.3. Determination of HFimpEF

HFimpEF was defined as an improvement in LVEF from ≤40% at baseline to >40% (with an increase of ≥10%) within 3 months of discharge from the hospital [11]. Figure 3 reports echograms received from the patients with LVEF < 40% at baseline (Figure 3A) and with LVEF > 40% in 3 months (Figure 3B).



(**A**) (**B**)

Figure 3. An example of the determination of HFimpEF in patients with a 3-month interval between investigations. (**A**) Echocardiographic parameters at baseline. (**B**) Echocardiographic parameters in 3 months.

2.4. Echocardiography Examination

Standard B-mode transthoracic echocardiography in apical 2- and 4-chamber views using a GE Healthcare Vivid E95 scanner (General Electric Company, Strandpromenaden 45, 3183 Horten, Norway) was performed by highly qualified assessors in accordance with the 2018 Guideline of the American Society of Echocardiography [40]. This encompassed cardiac dimensions, LV end-diastolic (LVEDV) and end-systolic (LVESV) volumes, left atrial volume index (LAVI), tricuspid annular plane systolic excursion (TAPSE), and LVEF by Simpson's method. Doppler examination was performed to determine the presence of mitral and tricuspid regurgitation and to measure early diastolic mitral blood filling (E) and medial and lateral e' velocities. The averaged medial e' and lateral e' velocities were estimated to obtain E/e'. LV hypertrophy was defined as an LV mass index (LVMI) of ≥95 g/m^2 or ≥115 g/m^2 in women and in men, respectively [40].

2.5. Glomerular Filtration Rate and Insulin Resistance Determination

The CKD-EPI formula was applied to estimate the glomerular filtration rate (eGFR) [41]. The Homeostatic Assessment Model of Insulin Resistance (HOMA-IR) was employed to evaluate insulin resistance [42].

2.6. Circulating Biomarker Evaluation

Peripheral blood samples were obtained via venipuncture and centrifuged at 3000 rpm for a period of 10 min with further storing of harvested serum at a temperature of −70 °C until evaluation.

The routine hematological and biochemical parameters were determined using a Roche P800 analyzer (Basel, Grenzacherstrasse 124, Switzerland) in the Private Medical Center "Vita Centre" (Zaporozhye, Ukraine).

Circulating biomarkers (tumor necrosis factor [TNF]-alpha, high-sensitive C-reactive protein [hs-CRP], high-sensitive troponin T [hs-TnT], NT-proBNP, interleukin [IL]-6, galectin-3, soluble suppression of tumorigenicity-2 [sST2], irisin) were measured in serum samples using ELISA kits (Elabscience, 14780 Memorial Drive, Suite 105, Houston, TX, USA) according to the manufacturer's instructions. Each blood sample was analyzed on two separate occasions, and the mean of these measurements was used for the final evaluation. The coefficient of variability for each marker was found to be less than 10% for both the intra- and inter-assay comparisons.

2.7. Statistics

Statistical analysis of the data was conducted utilizing SPSS Statistics 29 (IBM, 1 Orchard Road, Armonk, NY, USA) and Prism v.10 (GraphPad, 2365 Northside Dr., Ste. 560, San Diego, CA, USA) software. Variables are reported as mean (M) and standard deviation (SD), median (Me), and interquartile range (IQR) or absolute numbers (*n*) and percentages (%) as appropriate. The Anderson–Darling test was employed to verify the data distribution. Continuous variables were compared using the paired t-test or the Mann—-Whitney test, where appropriate, while categorical variables were compared using Fisher's exact test. Univariate logistic regression and backward stepwise multivariate logistic regression were used to identify potential predictors of HFimpEF, with odds ratios (ORs) and 95% confidence intervals (CIs) calculated for each. Factors with a p less than 0.05 in the univariate log regression analysis were included in the multivariate log regression model. For each predictor, the area under the curve (AUC), its confidence interval (CI), sensitivity (Se), and specificity (Sp) were calculated using receiver operating curve (ROC) analysis. The Youden test was used to estimate the cut-off points for serum levels of TNF-alpha, galectin-3, sST2, hs-CRP, irisin, and NT-proBNP. The integrated discrimination indices (IDI) and net reclassification improvement (NRI) were also estimated to assess the discriminatory ability of the predictive models. Comparisons with a p-value of less than 0.05 were considered statistically significant.

3. Results

3.1. Clinical Characteristics, Echocardiographic Parameters and Laboratory Findings

The study included 117 patients with HFimpEF and 196 individuals with persistent HFrEF. The characteristics of the enrolled individuals are presented in Table 1. The mean age of the patients in this study was 69 years, and 58.9% were male. The patients had comorbidity profiles that included smoking (43.1%), obesity (24.0%), dyslipidemia (74.8%), hypertension (56.2%), CAD (51.8%), dilated cardiomyopathy (18.2%), atrial fibrillation (29.7%), CKD 1–3 grades (21.7%), and T2DM (32.6%). Percutaneous coronary intervention was provided to about 31.0% of the patients from the entire group. Along with it, NYHA HF classes II, III, and IV were detected in 23.0%, 58.9%, and 18.1%, respectively. All patients had stable hemodynamics and increased LV diastolic and systolic volumes, as well as an LVEF of less than 40% at baseline. The patients had dyslipidemia, mild increases in HOMA-IR, circulating creatinine, inflammatory biomarkers (hs-CRP, TNF-alpha, IL-6), and indicators of fibrosis (galectin-3 and sST2). The mean serum levels of NT-proBNP and irisin were 1810 pmol/mL and 5.75 ng/mL, respectively. Concomitant medications included RAAS inhibitors, SGLT-2 inhibitors, mineralocorticoid receptor antagonists (MRA), beta-blockers, ivabradine (for those with sinus rhythm and uncontrolled heart rate on beta-blocker therapy), diuretics, statins, and anticoagulants/antiplatelet agents. Patients with concomitant T2DM were treated with a personalized diet, metformin, and/or GLP-1 receptor agonists to reach full control of glycemia.

No significant differences were found between groups in age, gender, BMI, waist circumference, smoking, obesity, dyslipidemia, hypertension, dilated cardiomyopathy, LV hypertrophy, and T2DM. The proportions of current stable CAD, atrial fibrillation, CKD grade 1–3, and PCI history were significantly higher in patients with HFrEF compared to HFimpEF. There were no differences in the presentation of NYHA HF classes between the two patient cohorts.

Patients with HFimpEF had significantly lower LVEDV, LVESV, and LAVI than those with HFrEF. TAPSE, E/e', and LVMI did not differ between the two cohorts. Along with it, eGFR, creatinine, electrolytes, lipid profile, HOMA-IR, fasting glucose, HbA1c, hemoglobin, hematocrit, serum uric acid, hs-CRP, TNF-alpha, IL-6, cTnT, sST2, and galectin-3 were not sufficiently different between cohorts. In contrast, NT-proBNP levels were higher and irisin concentrations were lower in HFimpEF compared with HFrEF. With the exception of anticoagulants, there were no differences in concomitant medications between the cohorts.

Table 1. Baseline general characteristics of eligible patients.

Variables	Entire HF Patient Cohort (*n* = 313)	Patients with HFimpEF (*n* = 117)	Patients with HFrEF (*n* = 196)	*p* Value Between Cohorts
Demographics and anthropometry parameters				
Age, year	69 (61–78)	67 (60–75)	70 (62–81)	0.146
Male gender, *n* (%)	184 (58.9)	68 (58.1)	116 (59.2)	0.146
BMI, kg/m^2	26.2 ± 4.26	25.3 ±3.88	26.9 ± 3.97	0.272
Waist circumference, cm	101 ± 7	99 ± 5	101 ± 8	0.690
Medical history				
Smoking history, *n* (%)	135 (43.1)	48 (41.0)	87 (44.4)	0.642
Abdominal obesity, *n* (%)	75 (24.0)	27 (23.1)	48 (24.5)	0.475
Dyslipidemia, *n* (%)	234 (74.8)	86 (73.5)	148 (75.5)	0.344
Hypertension, *n* (%)	176 (56.2)	66 (56.4)	110 (56.1)	0.871
Stable CAD, *n* (%)	162 (51.8)	57 (48.7)	105 (53.6)	0.046
Dilated cardiomyopathy, *n* (%)	57 (18.2)	20 (17.1)	37 (18.9)	0.242
Atrial fibrillation, *n* (%)	93 (29.7)	28 (23.9)	65 (33.2)	0.048
LVH, *n* (%)	217 (69.3)	81 (69.2)	136 (69.4)	0.844
CKD 1–3 grades, *n* (%)	68 (21.7)	22 (18.8)	46 (23.5)	0.044
T2DM, *n* (%)	102 (32.6)	38 (32.5)	64 (32.7)	0.526
PCI history, *n* (%)	97 (31.0)	42 (35.9)	55 (28.1)	0.048
NYHA functional class, *n* (%)				
II	72 (23.0)	29 (24.8)	43 (21.9)	0.142
III	184 (58.9)	69 (59.0)	115 (58.7)	0.416
IV	57 (18.1)	19 (16.2)	38 (19.4)	0.144
Hemodynamic and echocardiographic parameters				
Systolic BP, mm Hg	127 ± 8	129 ± 8	126 ± 9	0.395
Diastolic BP, mm Hg	68 ± 9	69 ± 7	68 ± 7	0.462
LVEDV, mL	176 (154–197)	178 (155–201)	173 (149–193)	0.274
LVESV, mL	103 (98–106)	99 (95–103)	110 (97–119)	0.022
LVEF, %	41 (34–51)	44 (40–47)	37 (33–39)	0.024
LVMI, g/m^2	148 ± 22	147 ± 19	155 ± 20	0.226
LAVI, mL/m^2	44 (35–54)	42 (36–49)	47 (40–53)	0.046
TAPSE, mm	20 (15–26)	19 (14–24)	22 (15–27)	0.611
E/e', unit	17 ± 7	16 ± 4	17 ± 5	0.355

Table 1. *Cont.*

Variables	Entire HF Patient Cohort (*n* = 313)	Patients with HFimpEF (*n* = 117)	Patients with HFrEF (*n* = 196)	*p* Value Between Cohorts
Laboratory findings				
eGFR, mL/min/1.73 m^2	64 ± 19	65 ± 15	61 ± 13	0.331
K, mmol/L	4.1 (3.3–5.3)	4.3 (3.4–5.5)	4.0 (3.1–5.10)	0.124
Na, mmol/L	139 (128–146)	139 (125–149)	137 (127–145)	0.846
HOMA-IR, units	5.11 ± 2.33	5.05 ± 2.23	5.19± 2.25	0.658
Glucose, mmol/L	4.68 ± 0.57	4.59 ± 0.52	4.70 ± 0.51	0.681
HbA1c, %	5.10 ± 1.99	5.07 ± 1.65	5.11± 1.57	0.560
Hemoglobin, g/L	13.9 (12.6–15.1)	13.8 (12.5–14.7)	14.0 (12.6–15.3)	0.674
Hematocrit, %	38 (34–42)	38 (35–40)	39 (35–43)	0.644
Creatinine, μmol/L	104 ± 10	97 ± 11	106 ± 9	0.128
Serum uric acid, μmol/L	359 ± 85	352 ± 80	360 ± 88	0.672
TC, mmol/L	5.69 ± 0.60	5.61 ± 0.68	5.73 ± 0.66	0.654
HDL-C, mmol/L	1.02 ± 0.10	1.03 ± 0.09	1.02 ± 0.10	0.748
LDL-C, mmol/L	3.60± 0.20	3.50 ± 0.18	3.60± 0.20	0.786
Triglycerides, mmol/L	2.34 ± 0.37	2.30 ± 0.29	2.41 ± 0.27	0.650
hs-CRP, mg/L	5.98 (2.24–9.70)	5.52 (2.12–8.16)	6.11 (2.80–10.56)	0.860
TNF-alpha, pg/mL	3.68 (2.10–5.23)	3.45 (2.03–4.94)	3.81 (2.19–5.21)	0.547
IL-6, ng/mL	2.91 (0.76–4.95)	2.70 (0.67–4.82)	3.20 (0.88–5.61)	0.216
cTnT, ng/mL	0.036 (0.004–0.112)	0.021 (0.001–0.110)	0.048 (0.003–0.120)	0.690
NT-proBNP, pmol/mL	1810 (980–2560)	1330 (870–1580)	2310 (1130–3580)	0.044
sST2, ng/mL	29.40 (13.90–45.70)	27.63 (11.17–41.80)	31.90 (15.82–47.54)	0.844
Galectin-3, ng/mL	27.5 (11.6–53.4)	24.1 (9.8–41.5)	32.7 (10.1–60.3)	0.671
Irisin, ng/mL	5.75 (2.18–9.12)	8.23 (4.26–13.50)	4.37 (1.62–7.17)	0.001
Concomitant medications and devices				
ACE inhibitors, *n* (%)	122 (39.0)	43 (36.8)	79 (40.3)	0.519
ARBs, *n* (%)	39 (12.5)	20 (17.1)	19 (9.7)	0.050
ARNI, *n* (%)	152 (48.7)	54 (46.2)	98 (50.0)	0.538
Beta-blockers, *n* (%)	285 (91.1)	105 (89.7)	180 (91.8)	0.351
Ivabradine, *n* (%)	32(10.2)	10 (8.5)	22 (11.2)	0.271
CCBs, *n* (%)	35 (11.2)	11 (9.4)	24 (12.2)	0.164
MRA, *n* (%)	231 (73.8)	86 (73.5)	145 (74.0)	0.834
Diuretics, *n* (%)	298 (98.2)	112 (95.7)	186 (94.9)	0.877
Antiplatelet agents, *n* (%)	179 (57.2)	69 (59.0)	110 (56.1)	0.048
Anticoagulants, *n* (%)	93 (29.7)	28 (23.9)	65 (33.2)	0.048
Metformin, *n* (%)	97 (31.0)	36 (30.8)	61 (31.1)	0.713
SGLT2 inhibitors, *n* (%)	227 (72.5)	86 (73.5)	141 (71.9)	0.637
GLP-1-RAs, *n* (%)	34 (10.8)	13 (11.1)	21 (10.7)	0.511
Statins, *n* (%)	234 (74.8)	86 (73.5)	148 (75.5)	0.344
RCT, *n* (%)	22 (7.0)	9 (7.7)	13 (6.6)	0.766

Abbreviations: ACE, angiotensin-converting enzyme; ARBs, angiotensin-II receptor blockers; ARNI, angiotensin receptor neprilysin inhibitors; BMI, body mass index; CAD, coronary artery disease; CCBs, calcium channel blockers; CKD, chronic kidney disease; eGFR, estimated glomerular filtration rate; E/e', early diastolic blood filling to longitudinal strain ratio; HDL-C, high-density lipoprotein cholesterol; hs-CRP, high-sensitivity C-reactive protein; GLP-1-RAs, glucagon-like peptide-1 receptor agonists; IL, interleukin; LDL-C, low-density lipoprotein cholesterol; LAVI, left atrial volume index; LVEDV, left ventricular end-diastolic volume; LVESV, left ventricular end-systolic volume; LVEF, left ventricular ejection fraction; LVMI, left ventricle myocardial mass index, LVH, left ventricular hypertrophy; MRA, mineralocorticoid receptor antagonist; RCT, resynchronized therapy; NT-proBNP, N-terminal brain natriuretic pro-peptide; TC, total cholesterol; TNF-alpha, tumor necrosis factor-alpha; sST2, soluble suppression of tumorigenicity-2; SGLT2, sodium-glucose co-transporter-2.

3.2. The Optimal Cut-Offs for Possible Predictors of HFimpEF

To determine the optimal cut-offs for potential predictors of HFimpEF, ROC curve analysis was performed (Table 2). The following factors for further regression analysis have been identified: LAVI < 39 mL/m^2, E/e' < 17; hs-CRP < 6.1 mg/L; TNF-alpha < 3.7 ng/mL; NT-proBNP < 1540 pmol/mL; sST2 < 31 ng/mL, galectin-3 < 28 ng/mL; irisin >10.8 ng/mL) (Table 2). The ROC curves are reported in Figure 4. The AUCs of the biomarkers show a high degree of reliability of the models.

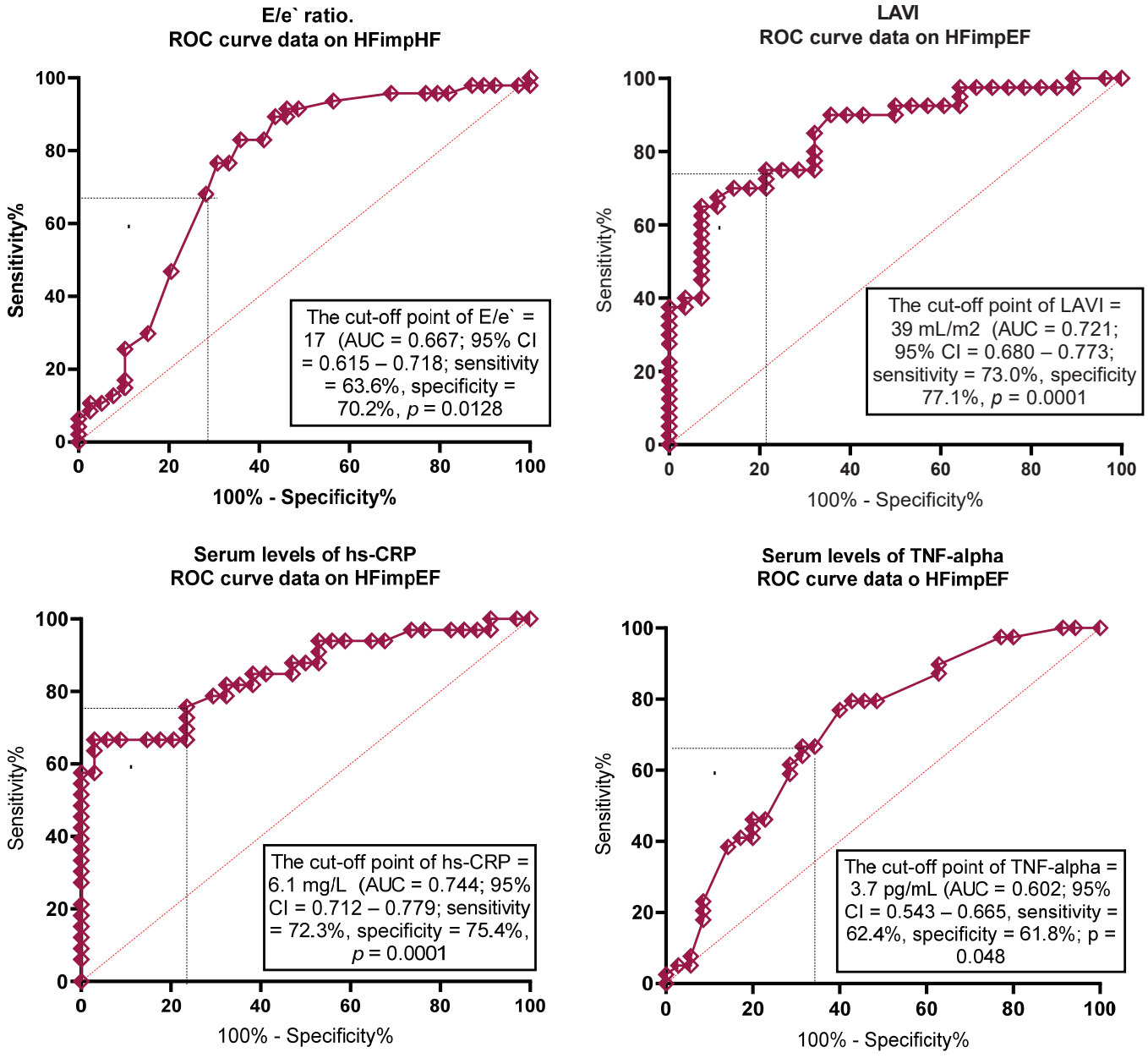


Figure 4. *Cont.*

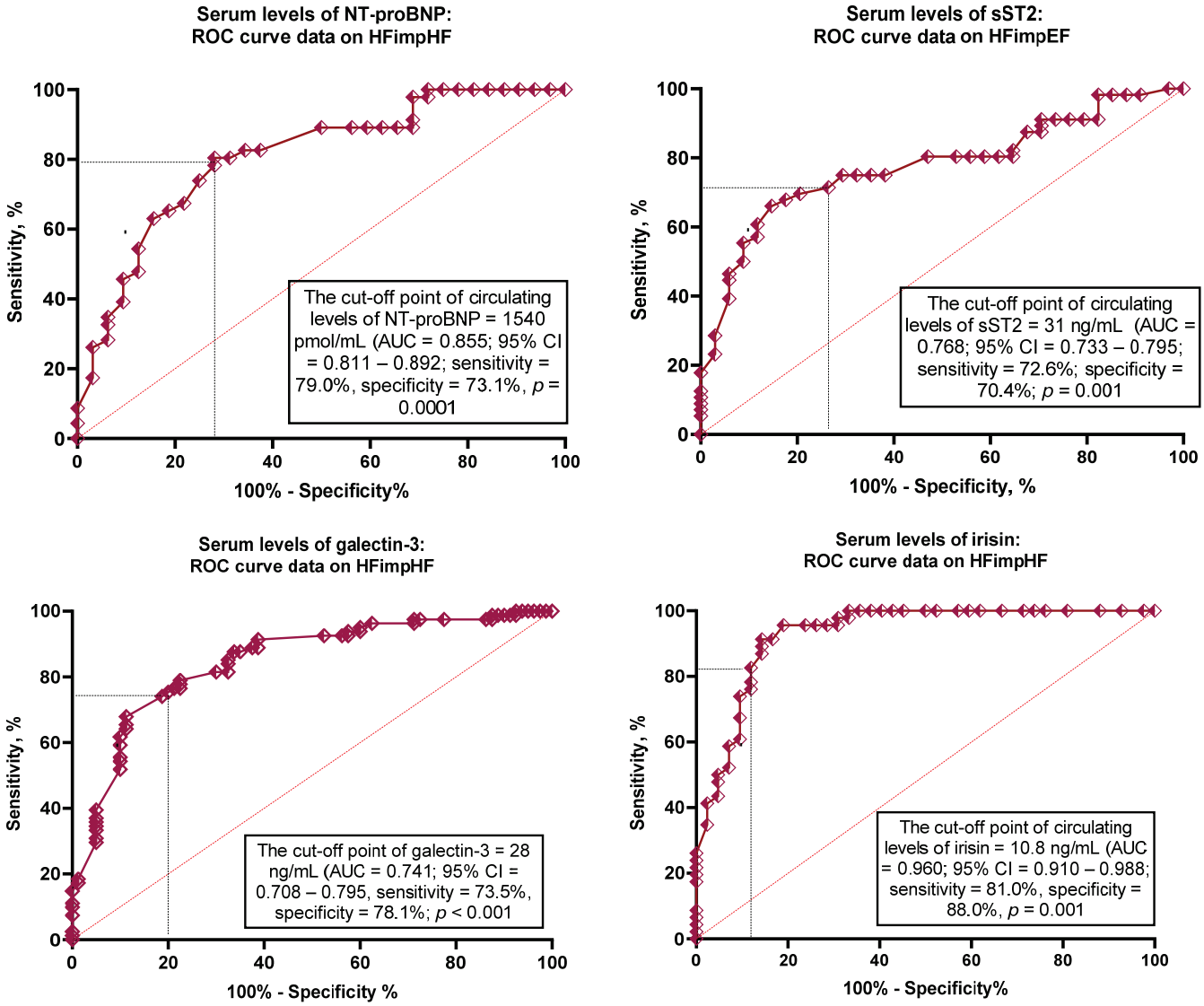


Figure 4. Receiver operating characteristic curves for predictive factors of HFimpHF. Abbreviations: AUC, area under curve; CI, confidence interval; hs-CRP, high-sensitivity C-reactive protein; E/e', early diastolic blood filling to longitudinal strain ratio; LAVI, left atrial volume index; Se, sensitivity; Sp, specificity; NT-proBNP, N-terminal brain natriuretic pro-peptide; sST2, soluble suppression of tumorigenicity-2; TNF-alpha, tumor necrosis factor-alpha.

Table 2. Receiver operating characteristic curve analysis for possible predictive factors of HFimpHF.

Variables	AUC	95% CI	*p*-Value	Cut-Offs	Se, %	Sp, %
LAVI	0.721	0.680–0.773	0.001	39 mL/m^2	73.9	77.1
E/e'	0.667	0.615–0.718	0.001	17	63.6	70.2
hs-CRP	0.744	0.712–0.779	0.001	6.1 mg/L	72.3	75.4
TNF-alpha	0.602	0.543–0.665	0.048	3.7 pg/mL	62.4	61.8
NT-proBNP	0.855	0.811–0.892	0.0001	1540 pmol/mL	79.0	73.1
sST2	0.768	0.733–0.795	0.001	31 ng/mL	72.6	70.4
Galectin-3	0.741	0.708–0.795	0.001	28 ng/mL	73.5	78.1
Irisin	0.960	0.910–0.988	0.0001	10.8 ng/mL	81.0	88.0

Abbreviations: AUC, area under curve; CI, confidence interval; hs-CRP, high-sensitivity C-reactive protein; E/e', early diastolic blood filling to longitudinal strain ratio; LAVI, left atrial volume index; Se, sensitivity; Sp, specificity; NT-proBNP, N-terminal brain natriuretic pro-peptide; sST2, soluble suppression of tumorigenicity-2; TNF-alpha, tumor necrosis factor-alpha.

3.3. Predictive Factors for HFimpEF: Univariate Logistic Regression and Backward Stepwise Multivariate Logistic Regression Models

Univariate logistic regression showed that atrial fibrillation, CKD stages 1–3, LAVI < 39 mL/m^2, E/e' < 17, hs-CRP < 6.1 mg/L, TNF-alpha < 3.7 ng/mL, NT-proBNP < 1540 pmol/mL, sST2 < 31 ng/mL, galectin-3 < 28 ng/mL, and irisin > 10.8 ng/mL were associated with improved LVEF in individuals with HF (Table 3). Backward stepwise multivariate logistic regression revealed that the presence of AF, LAVI < 39 mL/m^2, NT-proBNP < 1540 pmol/mL, and irisin ≥ 10.8 ng/mL were independent predictors for HFimpEF.

Table 3. Predictive factors for HFimpEF: univariate logistic regression and backward stepwise multivariate logistic regression.

Predictive Factors	Univariate Logistic Regression			Backward Stepwise Multivariate Logistic Regression		
	Odds Ratio	95% CI	*p* Value	Odds Ratio	95% CI	*p* Value
T2DM *	0.97	0.91–1.02	0.212		-	
PCI history *	0.95	0.89–1.13	0.437		-	
AF *	0.95	0.91–0.98	0.010	0.95	0.90–0.98	0.010
Stable CAD *	1.02	0.94–1.17	0.380		-	
CKD stages 1–3 *	0.93	0.87–0.99	0.047	0.95	0.89–1.01	0.177
Dilated CMP *	0.96	0.92–1.02	0.422		-	
LAVI < 39 mL/m^2 vs. ≥39 mL/m^2	1.32	1.15–1.56	0.001	1.23	1.11–1.39	0.001
E/e' < 17 vs. ≥17	1.18	1.04–1.35	0.012	1.10	1.00–1.27	0.052
hs-CRP < 6.1 mg/L vs. ≥6.1 mg/L	1.12	1.06–1.20	0.018	1.09	1.00–1.20	0.120
TNF-alpha < 3.7 bg/mL vs. ≥3.7 ng/mL	1.06	1.01–1.12	0.044	1.05	0.99–1.10	0.206
NT-proBNP < 1540 vs. ≥1540 pmol/mL	1.56	1.12–2.15	0.001	1.47	1.11–2.12	0.001
sST2 < 31 ng/mL vs. ≥31 ng/mL	1.24	1.02–1.65	0.048	1.20	1.00–1.68	0.086
Galectin-3 < 28 ng/mL vs. ≥28 ng/mL	1.17	1.01–1.43	0.050	1.12	1.00–1.27	0.064
Irisin ≥ 10.8 ng/mL vs. <10.8 ng/mL	1.75	1.22–4.32	0.001	1.73	1.16–4.18	0.001

Abbreviations: AF, atrial fibrillation; CAD, coronary artery disease; CI, confidence interval; hs-CRP, high-sensitivity C-reactive protein; CKD, chronic kidney disease; LAVI, left atrial volume index; NT-proBNP, N-terminal brain natriuretic pro-peptide; sST2, soluble suppression of tumorigenicity-2; TNF-alpha, tumor necrosis factor-alpha; T2DM, type 2 diabetes mellitus; vs., versus; *, presence versus absent.

3.4. Prediction Model Comparison

Model 1 (NT-proBNP < 1540 pmol/mL) and model 2 (a presence of AF) did not markedly differ from one another in the prediction of HFimpEF, whereas model 3 (LAVI < 39 mL/m^2) was worse than the reference model (Table 4). Model 4 (irisin ≥ 10.8 ng/mL) was significantly better than model 1. Furthermore, the combined model 1 + 4 (NT-proBNP < 1540 pmol/mL + irisin ≥ 10.8 ng/mL) was superior to model 1 alone (NT-proBNP < 1540 pmol/mL) but did not sufficiently increase the discriminatory power of model 4 (irisin ≥ 10.8 ng/mL). Other combined models showed no better benefit for HFimpEF than model 1.

Table 4. The comparisons of predictive models for HFimpEF.

Predictive Models	Dependent Variable: HFimpEF								
	AUC			Net Reclassification Improvement			Integrated Discrimination Indices		
	M	95% CI	*p* Value	M	95% CI	*p* Value	M	95% CI	*p* Value
Model 1 (NT-proBNP < 1540 pmol/mL)	0.855	0.811–0.892	-	Reference		-	Reference		-
Model 2 (presence of AF)	0.820	0.715–0.944	0.427	0.10	0.06–0.15	0.388	0.11	0.05–0.17	0.481
Model 3 (LAVI < 39 mL/m^2)	0.721	0.680–0.773	0.044	0.03	0.01–0.06	0.642	0.06	0.02–0.09	0.552
Model 4 (irisin ≥ 10.8 ng/mL)	0.960	0.910–0.988	0.001	0.36	0.24–0.49	0.001	0.44	0.38–0.52	0.001
Model 1 + model 2	0.848	0.790–0.910	0.066	0.10	0.05–0.17	0.249	0.12	0.06–0.19	0.265
Model 1 + model 3	0.851	0.810–0.912	0.270	0.09	0.03–0.15	0.338	0.11	0.03–0.17	0.286
Model 1 + model 4	0.979	0.932–0.982	0.001	0.38	0.29–0.50	0.001	0.44	0.35–0.54	0.001

Abbreviations: AUC, area under curve; CI, confidence interval; LAVI, left atrial volume index; NT-proBNP, N-terminal brain natriuretic pro-peptide. Note: *p*-value shows a significant difference between variables in terms of Model 1.

4. Discussion

This study has revealed that positive changes in hemodynamics among optimally treated patients with HFimpEF were associated with a decline in serum levels of NT-proBNP and an increase in circulating levels of irisin, whereas the concentrations of conventionally used biomarkers reflecting inflammation (hs-CRP, IL-6, TNF-alpha), fibrosis (galectin-3, sST2), and cardiac damage (hs-TnT) remained comparable between the groups of individuals with HFimpHF and persistent HFrEF. Moreover, serum levels of irisin ≥ 10.8 ng/mL added new predictive information to NT-proBNP for HFimpEF, but the combination of these two biomarkers did not demonstrate its discriminative benefit in comparison with irisin alone.

As HFimpEF relates to a 50% greater reduction in mortality risk and hospitalization compared with HFrEF, promoting improvement in LVEF and predicting a positive response to treatment are both sides of the same coin [43]. Indeed, the prognosis of almost a quarter of patients with HFrEF can be significantly improved in case of sustained improvement in myocardial contractility assessed as LVEF > 40% [43,44]. Notably, recent clinical studies have identified a number of promising positive (NYHA Class II HF, concomitant hypertension, beta-blocker use) and negative (alcohol consumption, dilated cardiomyopathy, serum uric acid) predictors of LVEF improvement [44,45]. However, these studies did not include patients receiving optimal therapy for HFrEF based on four major classes of prognosis-improving drugs. In our study, despite significant comorbidity, all patients received personalized optimal GDMT for HFrEF with any RAAS inhibitor, MRA, beta-blockers, and SGLT2 inhibitors. This resulted in 37.4% of patients in the HFrEF group having a positive response to HF therapy, including a reduction in LVEDV and LVESV, an increase in LVEF, and the control of circulating NT-proBNP (<2000 pmol/mL). These findings support previous evidence of clinical trials and current guideline recommendations for the use of GDMT in patients with HFimpEF [11,46,47].

Another aspect of the study was that atrial fibrillation and CKD were the most significant comorbidities for the prediction of HFimpEF, whereas in some studies and meta-

analyses, not only the abovementioned conditions but also anemia, T2DM, CAD, dyslipidemia, cerebrovascular disease, and hypertension were found to be predictive factors for recovered LVEF [48,49]. However, the signature of comorbidities often depends on the age and gender of the patients. In our study, age was not identified as a negative predictive factor for HFimpEF, probably because related comorbidities also did not show a high association with the recovery of LV contractile function in the short term (about 3 months). It is conceivable that the profile of comorbid factors with plausible predictive values for HFimpEF may change as patient follow-up is extended to one year or even longer.

Nevertheless, the results open one of the most important aspects of the debate around whether NT-proBNP retains its prognostic value in patients with HFimpEF. It has previously been shown that low or near-normal concentrations of NT-proBNP are unlikely to accurately discriminate clinical outcomes in patients with HFpEF [50]. This should not necessarily mean that well-controlled levels of natriuretic peptides lose their importance in HF patients with the recovery of systolic function during guideline-based treatment. However, there is evidence that alternative biomarkers such as irisin can significantly increase the discriminatory potency of NT-proBNP [51]. Our data clearly show that irisin not only adds prognostic information to NT-proBNP but also outperforms NT-proBNP in its ability to predict HFimpEF.

Previous studies have shown that irisin has various influences on key points of the pathogenesis of HF, such as mitochondrial and endothelial dysfunction, vasoconstriction, oxidative stress, immune and inflammatory reactions, metabolic imbalance, skeletal muscle dystrophy, altered energy expenditure, and tissue reparation [29,52,53]. Therefore, low levels of irisin were found to be a negative factor with possible predictive ability for any HF phenotype [54–56]. However, it has remained unclear whether guideline-directed HF therapy is able to modulate serum irisin levels and whether HFimpEF is associated with the restoration of circulating irisin.

First, we have clearly shown that optimal therapy in HFrEF is related to a higher likelihood of improvement in LVEF and that the control of NT-proBNP in HFrEF may be associated with the restoration of irisin levels. It seems particularly valuable that the positive response in the form of improved LVEF with GDMT was not accompanied by significant changes in biomarkers reflecting myocardial injury (hs-TnT), inflammation (hs-CRP, IL-6, TNF-alpha), and fibrosis (sST2, galectin-3). Previously, the possibility of serially measuring these biomarkers to predict response to heart failure therapy and assess the risk of adverse complications has been widely debated. Nevertheless, as observed, no major differences were found between HFimpEF and persistent HFrEF groups at 3 months in our study. This may be partly due to the fact that the study included hemodynamically stable patients who did not require inotropic and mechanical support. It is for these groups of patients with HFrEF and acute or acutely decompensated HF that the predictive role of these biomarkers seems particularly relevant [57]. Although irisin and inflammatory biomarker concentrations are inversely correlated in untreated HFrEF patients or patients with acute HF, this relationship is apparently less pronounced in patients with HFimpEF. In any case, the mechanisms by which irisin may interfere with the recovery of myocardial systolic function need to be studied in detail in the future. Therefore, irisin levels should not only be considered as a plausible predictive biomarker but also as an additional target for the therapy of HF.

5. Clinical Implications

These findings are likely to support the integration of these advances into clinical practice in the future and highlight the need for ongoing clinical research to fully recognize their value to change HFrEF management. The findings of our study possibly open a new approach to predicting the recovery of LV systolic function. Although for most patients with different HF phenotypes, including HFrEF, a decrease in NT-proBNP levels indicates clinical outcomes and a reduced risk of re-hospitalization, it is not clear that a trend toward a decrease in circulating NT-proBNP concentration is associated with the recovery of LVEF and the occurrence of HFimpEF. Moreover, the high variability of serum NT-proBNP, especially pronounced in fluid retention, the progression of CKD, and/or T2DM, may require more frequent repeated measurements of its concentration, which inevitably negatively affects the cost of monitoring. In this context, the measurement of irisin not only improves the prognostic value of single measured NT-proBNP but also reduces the economic burden of predicting HFimpEF. Another important clinical advantage of the new approach is the independence of the predictive value of irisin from the presence of comorbid conditions such as CKD and T2DM. Thus, the creation of a new algorithm for predicting HFimpEF based on the measurement of irisin and NT-proBNP in patients with HFrEF is promising and requires further validation in a study with a larger sample size.

6. Study Limitations

The study includes several limitations. Although only patients receiving optimal GDMT were included in the study, it remains unknown whether the predictive effect of irisin in combination with NT-proBNP in HFimpEF is maintained when treatment is stopped or the doses of the drugs used are reduced. Another limitation is that we did not investigate the predictive value of irisin in individuals with normal or near-normal NT-proBNP concentrations. In addition, the lack of assessment of patients' metabolic and nutritional status and the inclusion of HF patients with GDMT are other limitations of this study. However, we believe that these limitations do not influence the interpretation of the results.

7. Conclusions

We have found that an improvement in LVEF in patients with HFrEF is closely associated with a decisive trend toward the restoration of serum irisin levels and a decrease in NT-proBNP. Serum irisin >10.8 ng/mL has been shown to be independent of NT-proBNP in predicting HFimpEF, while its use in conjunction with NT-proBNP did not sufficiently improve the discriminative value of irisin alone. These findings may see irisin emerge as a valuable biomarker for predicting improved LVEF in HFrEF patients, possibly modifying HF management. A possible algorithm for decision-making based on a comprehensive assessment of biomarker dynamics is presented in Figure 5.

It is likely that monitoring serum NT-proBNP and irisin could help in assessing the risk of HFimpEF destabilization and HFrEF persistence despite GDMT, although this assumption needs to be confirmed in further studies. However, the serial measurement of irisin may be important to personify GDMT in HFrEF or HFimpEF.

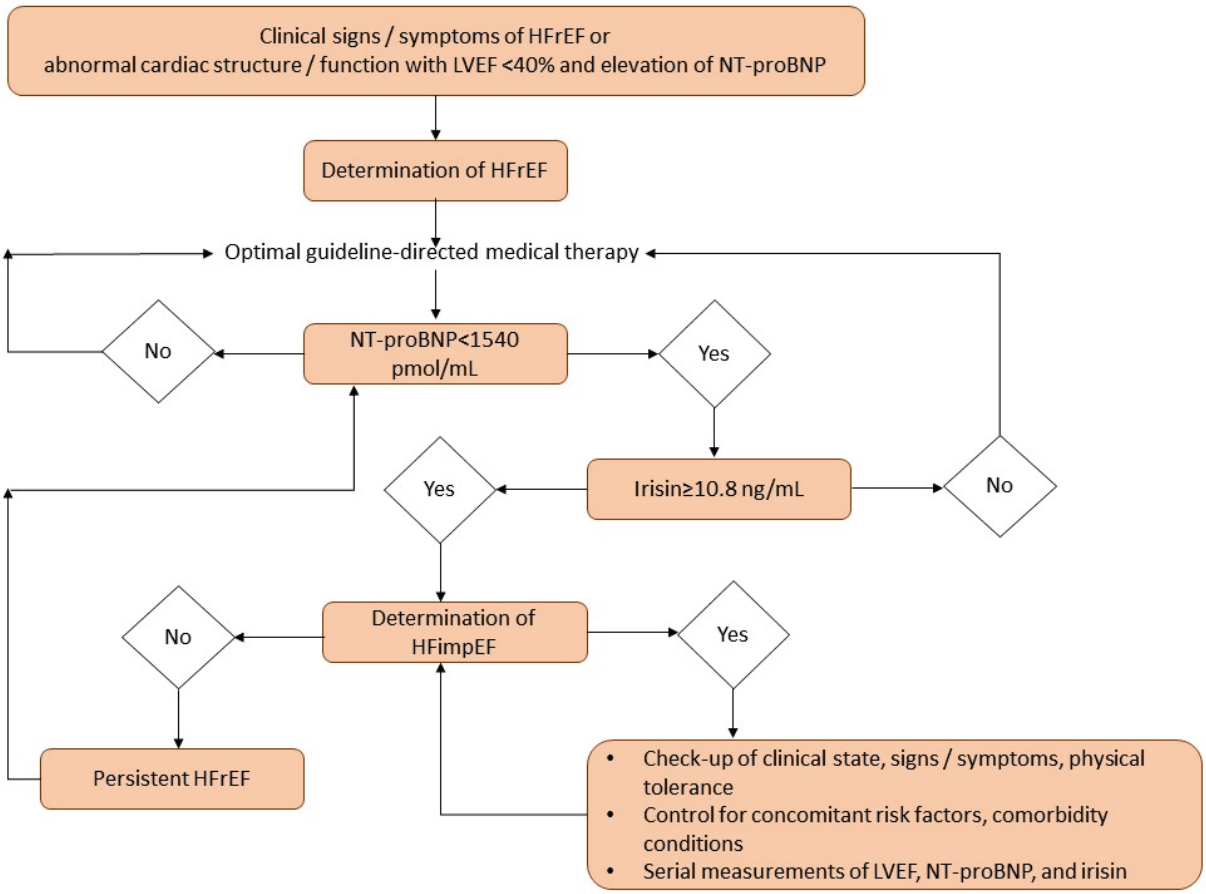


Figure 5. Possible predictive algorithm of HFimpEF with biomarker use. Abbreviation: HFrEF, heart failure with reduced ejection fraction; HFimpEF, heart failure with improved ejection fraction; LVEF, left ventricular ejection fraction; NT-proBNP, N-terminal brain natriuretic pro-peptide.

Author Contributions: Conceptualization, A.E.B.; methodology, A.E.B.; software, A.E.B. and O.O.B.; validation, T.A.B. and A.E.B.; formal analysis, O.O.B., T.A.B., and A.E.B.; investigation, O.O.B. and T.A.B.; resources, T.A.B. and O.O.B.; data curation, A.E.B. and T.A.B.; writing—original draft preparation: T.A.B., O.O.B., E.V.N., and A.E.B.; writing—review and editing, T.A.B., O.O.B., E.V.N., and A.E.B.; visualization, O.O.B., E.V.N., and T.A.B.; supervision, A.E.B.; project administration, T.A.B. and O.O.B. All authors have read and agreed to the published version of the manuscript.

Funding: This research received no external funding.

Institutional Review Board Statement: The study was conducted according to the guidelines of the Declaration of Helsinki and approved by the Institutional Ethics Committee of Zaporozhye Medical Academy of Post-graduate Education (protocol number: 8; date of approval: 10 October 2020).

Informed Consent Statement: Informed consent was received from all individuals involved in the study.

Data Availability Statement: The data presented in this study are available on request from the corresponding author due to privacy restrictions.

Acknowledgments: We thank all patients who gave their consent to participate in the study and all administrative staff and doctors of Private Hospital "Vita-Center" for study assistance.

Conflicts of Interest: Author Oleksandr O. Berezin was employed by Luzerner Psychiatrie AG. The remaining authors declare that the research was conducted in the absence of any commercial or financial relationships that could be construed as a potential conflict of interest.

References

1. Savarese, G.; Becher, P.M.; Lund, L.H.; Seferovic, P.; Rosano, G.M.C.; Coats, A.J.S. Global burden of heart failure: A comprehensive and updated review of epidemiology. *Cardiovasc. Res.* **2023**, *118*, 3272–3287. Erratum in *Cardiovasc. Res.* **2023**, *119*, 1453. https://doi.org/10.1093/cvr/cvad026. [CrossRef] [PubMed]
2. Bozkurt, B.; Ahmad, T.; Alexander, K.M.; Baker, W.L.; Bosak, K.; Breathett, K.; Fonarow, G.C.; Heidenreich, P.; Ho, J.E.; Hsich, E.; et al. Heart Failure Epidemiology and Outcomes Statistics: A Report of the Heart Failure Society of America. *J. Card. Fail.* **2023**, *29*, 1412–1451. [CrossRef]
3. Emmons-Bell, S.; Johnson, C.; Roth, G. Prevalence, incidence and survival of heart failure: A systematic review. *Heart* **2022**, *108*, 1351–1360. [CrossRef]
4. Denfeld, Q.E.; Winters-Stone, K.; Mudd, J.O.; Gelow, J.M.; Kurdi, S.; Lee, C.S. The prevalence of frailty in heart failure: A systematic review and meta-analysis. *Int. J. Cardiol.* **2017**, *236*, 283–289. [CrossRef]
5. Shah, K.S.; Xu, H.; Matsouaka, R.A.; Bhatt, D.L.; Heidenreich, P.A.; Hernandez, A.F.; Devore, A.D.; Yancy, C.W.; Fonarow, G.C. Heart Failure with Preserved, Borderline, and Reduced Ejection Fraction: 5-Year Outcomes. *J. Am. Coll. Cardiol.* **2017**, *70*, 2476–2486. [CrossRef]
6. Chioncel, O.; Lainscak, M.; Seferovic, P.M.; Anker, S.D.; Crespo-Leiro, M.G.; Harjola, V.P.; Parissis, J.; Laroche, C.; Piepoli, M.F.; Fonseca, C.; et al. Epidemiology and one-year outcomes in patients with chronic heart failure and preserved, mid-range and reduced ejection fraction: An analysis of the ESC Heart Failure Long-Term Registry. *Eur. J. Heart Fail.* **2017**, *19*, 1574–1585. [CrossRef]
7. McDowell, K.; Kondo, T.; Talebi, A.; Teh, K.; Bachus, E.; de Boer, R.A.; Campbell, R.T.; Claggett, B.; Desai, A.S.; Docherty, K.F.; et al. Prognostic Models for Mortality and Morbidity in Heart Failure with Preserved Ejection Fraction. *JAMA Cardiol.* **2024**, *9*, 457–465. Erratum in *JAMA Cardiol.* **2024**, *9*, 861. https://doi.org/10.1001/jamacardio.2024.2464. [CrossRef] [PubMed] [PubMed Central]
8. Pensa, A.V.; Khan, S.S.; Shah, R.V.; Wilcox, J.E. Heart failure with improved ejection fraction: Beyond diagnosis to trajectory analysis. *Prog. Cardiovasc. Dis.* **2024**, *82*, 102–112. [CrossRef]
9. Pabon, M.A.; Vaduganathan, M.; Claggett, B.L.; Chatur, S.; Siqueira, S.; Marti-Castellote, P.; de Boer, R.A.; Hernandez, A.F.; Inzucchi, S.E.; Kosiborod, M.N.; et al. In-hospital course of patients with heart failure with improved ejection fraction in the DELIVER trial. *Eur. J. Heart Fail.* **2024**, *26*, 2532–2540. [CrossRef] [PubMed]
10. Park, C.S.; Park, J.J.; Mebazaa, A.; Oh, I.Y.; Park, H.A.; Cho, H.J.; Lee, H.Y.; Kim, K.H.; Yoo, B.S.; Kang, S.M.; et al. Characteristics, Outcomes, and Treatment of Heart Failure with Improved Ejection Fraction. *J. Am. Heart Assoc.* **2019**, *8*, e011077. [CrossRef] [PubMed]
11. McDonagh, T.A.; Metra, M.; Adamo, M.; Gardner, R.S.; Baumbach, A.; Böhm, M.; Burri, H.; Butler, J.; Čelutkienė, J.; Chioncel, O.; et al. 2021 ESC Guidelines for the diagnosis and treatment of acute and chronic heart failure. *Eur. Heart J.* **2021**, *42*, 3599–3726, Erratum in *Eur. Heart J.* **2021**, *42*, 4901. https://doi.org/10.1093/eurheartj/ehab670. [CrossRef]
12. Licordari, R.; Correale, M.; Bonanno, S.; Beltrami, M.; Ciccarelli, M.; Micari, A.; Palazzuoli, A.; Dattilo, G. Beyond Natriuretic Peptides: Unveiling the Power of Emerging Biomarkers in Heart Failure. *Biomolecules* **2024**, *14*, 309. [CrossRef]
13. Pascual-Figal, D.A.; Hernández-Vicente, A.; Pastor-Pérez, F.; Martínez-Sellés, M.; Solé-González, E.; Alvarez-García, J.; García-Pavía, P.; Varela-Román, A.; Sánchez, P.L.; Delgado, J.F.; et al. N-terminal pro-B-type natriuretic peptide post-discharge monitoring in the management of patients with heart failure and preserved ejection fraction—A randomized trial: The NICE study. *Eur. J. Heart Fail.* **2024**, *26*, 776–784. [CrossRef]
14. Mueller, C.; McDonald, K.; de Boer, R.A.; Maisel, A.; Cleland, J.G.F.; Kozhuharov, N.; Coats, A.J.S.; Metra, M.; Mebazaa, A.; Ruschitzka, F.; et al. Heart Failure Association of the European Society of Cardiology practical guidance on the use of natriuretic peptide concentrations. *Eur. J. Heart Fail.* **2019**, *21*, 715–731. [CrossRef]
15. Sciatti, E.; Merlo, A.; Scangiuzzi, C.; Limonta, R.; Gori, M.; D'Elia, E.; Aimo, A.; Vergaro, G.; Emdin, M.; Senni, M. Prognostic Value of sST2 in Heart Failure. *J. Clin. Med.* **2023**, *12*, 3970. [CrossRef]
16. Girerd, N.; Cleland, J.; Anker, S.D.; Byra, W.; Lam, C.S.P.; Lapolice, D.; Mehra, M.R.; van Veldhuisen, D.J.; Bresso, E.; Lamiral, Z.; et al. Inflammation and remodeling pathways and risk of cardiovascular events in patients with ischemic heart failure and reduced ejection fraction. *Sci. Rep.* **2022**, *12*, 8574. [CrossRef]
17. Pellicori, P.; Zhang, J.; Cuthbert, J.; Urbinati, A.; Shah, P.; Kazmi, S.; Clark, A.L.; Cleland, J.G.F. High-sensitivity C-reactive protein in chronic heart failure: Patient characteristics, phenotypes, and mode of death. *Cardiovasc. Res.* **2020**, *116*, 91–100. [CrossRef]
18. Markousis-Mavrogenis, G.; Tromp, J.; Ouwerkerk, W.; Devalaraja, M.; Anker, S.D.; Cleland, J.G.; Dickstein, K.; Filippatos, G.S.; van der Harst, P.; Lang, C.C.; et al. The clinical significance of interleukin-6 in heart failure: Results from the BIOSTAT-CHF study. *Eur. J. Heart Fail.* **2019**, *21*, 965–973. [CrossRef]
19. Verbrugge, F.H.; Omote, K.; Reddy, Y.N.V.; Sorimachi, H.; Obokata, M.; Borlaug, B.A. Heart failure with preserved ejection fraction in patients with normal natriuretic peptide levels is associated with increased morbidity and mortality. *Eur. Heart J.* **2022**, *43*, 1941–1951. [CrossRef]

20. Chen, Y.Y.; Liang, L.; Tian, P.C.; Feng, J.Y.; Huang, L.Y.; Huang, B.P.; Zhao, X.M.; Wu, Y.H.; Wang, J.; Guan, J.Y.; et al. Clinical characteristics and outcomes of patients hospitalized with heart failure with preserved ejection fraction and low NT-proBNP levels. *Medicine* **2023**, *102*, e36351. [CrossRef]
21. Murphy, S.P.; Kakkar, R.; McCarthy, C.P.; Januzzi, J.L., Jr. Inflammation in Heart Failure: JACC State-of-the-Art Review. *J. Am. Coll. Cardiol.* **2020**, *75*, 1324–1340. [CrossRef]
22. Cocco, G.; Jerie, P.; Amiet, P.; Pandolfi, S. Inflammation in Heart Failure: Known knowns and unknown unknowns. *Expert Opin. Pharmacother.* **2017**, *18*, 1225–1233. [CrossRef] [PubMed]
23. Berezin, A.E.; Berezin, A.A. Point-of-care heart failure platform: Where are we now and where are we going to? *Expert Rev. Cardiovasc. Ther.* **2022**, *20*, 419–429. [CrossRef] [PubMed]
24. Liu, S.; Cui, F.; Ning, K.; Wang, Z.; Fu, P.; Wang, D.; Xu, H. Role of irisin in physiology and pathology. *Front. Endocrinol.* **2022**, *13*, 962968. [CrossRef]
25. De Sousa, R.A.L. Exercise-produced irisin effects on brain-related pathological conditions. *Metab. Brain Dis.* **2024**, *39*, 1679–1687. [CrossRef] [PubMed]
26. He, X.; Hua, Y.; Li, Q.; Zhu, W.; Pan, Y.; Yang, Y.; Li, X.; Wu, M.; Wang, J.; Gan, X. FNDC5/irisin facilitates muscle-adipose-bone connectivity through ubiquitination-dependent activation of runt-related transcriptional factors RUNX1/2. *J. Biol. Chem.* **2022**, *298*, 101679. [CrossRef]
27. Hofmann, T.; Elbelt, U.; Stengel, A. Irisin as a muscle-derived hormone stimulating thermogenesis--a critical update. *Peptides* **2014**, *54*, 89–100. [CrossRef]
28. Tomasello, L.; Pitrone, M.; Guarnotta, V.; Giordano, C.; Pizzolanti, G. Irisin: A Possible Marker of Adipose Tissue Dysfunction in Obesity. *Int. J. Mol. Sci.* **2023**, *24*, 12082. [CrossRef]
29. Ho, M.Y.; Wang, C.Y. Role of Irisin in Myocardial Infarction, Heart Failure, and Cardiac Hypertrophy. *Cells* **2021**, *10*, 2103. [CrossRef]
30. Tang, Y.J.; Zhang, Z.; Yan, T.; Chen, K.; Xu, G.F.; Xiong, S.Q.; Wu, D.Q.; Chen, J.; Jose, P.A.; Zeng, C.Y.; et al. Irisin attenuates type 1 diabetic cardiomyopathy by anti-ferroptosis via SIRT1-mediated deacetylation of p53. *Cardiovasc. Diabetol.* **2024**, *23*, 116. [CrossRef]
31. Zhang, X.; Hu, C.; Kong, C.Y.; Song, P.; Wu, H.M.; Xu, S.C.; Yuan, Y.P.; Deng, W.; Ma, Z.G.; Tang, Q.-Z. FNDC5 alleviates oxidative stress and cardiomyocyte apoptosis in doxorubicin-induced cardiotoxicity via activating AKT. *Cell Death Differ.* **2020**, *27*, 540–555. [CrossRef] [PubMed]
32. Li, R.L.; Wu, S.S.; Wu, Y.; Wang, X.X.; Chen, H.Y.; Xin, J.J.; Li, H.; Lan, J.; Xue, K.Y.; Li, X.; et al. Irisin alleviates pressure overload-induced cardiac hypertrophy by inducing protective autophagy via mTOR-independent activation of the AMPK-ULK1 pathway. *J. Mol. Cell Cardiol.* **2018**, *121*, 242–255. [CrossRef] [PubMed]
33. Guo, W.; Zhang, B.; Wang, X. Lower irisin levels in coronary artery disease: A meta-analysis. *Minerva Endocrinol.* **2020**, *45*, 61–69. [CrossRef]
34. Ozturk, D.; Melekoglu, A.; Altinbilek, E.; Calik, M.; Kosem, A.; Kilci, H.; Misirlioglu, N.F.; Uzun, H. Association Between Serum Irisin Levels and ST-Segment Elevation Myocardial Infarction. *Int. J. Gen. Med.* **2023**, *16*, 1355–1362. [CrossRef]
35. Hou, Q.; Song, R.; Zhao, X.; Yang, C.; Feng, Y. Lower circulating irisin levels in type 2 diabetes mellitus patients with chronic complications: A meta-analysis. *Heliyon* **2023**, *9*, e21859. [CrossRef] [PubMed]
36. Wang, P.X.; Fan, Z.J.; Wu, L.Y.; Wang, S.Y.; Zhang, J.L.; Dong, X.T.; Zhang, A.H. Serum irisin levels are negatively associated with blood pressure in dialysis patients. *Hypertens. Res.* **2023**, *46*, 2738–2745. [CrossRef]
37. Yildiz Kopuz, T.N.; Dagdeviren, M.; Fisunoglu, M. Serum irisin levels in newly diagnosed type-II diabetic patients: No association with the overall diet quality but strong association with fruit intake. *Clin. Nutr. ESPEN* **2022**, *49*, 357–364. [CrossRef]
38. Shen, X.; Chen, Y.; Zhang, J.; Yang, M.; Huang, L.; Luo, J.; Xu, L. The association between circulating irisin levels and osteoporosis in women: A systematic review and meta-analysis of observational studies. *Front. Endocrinol.* **2024**, *15*, 1388717. [CrossRef]
39. Berezin, A.E.; Berezin, A.A. Biomarkers in Heart Failure: From Research to Clinical Practice. *Ann. Lab. Med.* **2023**, *43*, 225–236. [CrossRef]
40. Mitchell, C.; Rahko, P.S.; Blauwet, L.A.; Canaday, B.; Finstuen, J.A.; Foster, M.C.; Horton, K.; Ogunyankin, K.O.; Palma, R.A.; Velazquez, E.J. Guidelines for Performing a Comprehensive Transthoracic Echocardiographic Examination in Adults: Recommendations from the American Society of Echocardiography. *J. Am. Soc. Echocardiogr.* **2018**, *32*, 1–64. [CrossRef]
41. Levey, A.S.; Stevens, L.A.; Schmid, C.H.; Zhang, Y.L.; Castro, A.F., 3rd; Feldman, H.I.; Kusek, J.W.; Eggers, P.; Van Lente, F.; Greene, T.; et al. A New Equation to Estimate Glomerular Filtration Rate. *Ann. Intern. Med.* **2009**, *150*, 604–612. [CrossRef] [PubMed]
42. Matthews, D.R.; Hosker, J.P.; Rudenski, A.S.; Naylor, B.A.; Treacher, D.F.; Turner, R.C. Homeostasis model assessment: Insulin resistance and β-cell function from fasting plasma glucose and insulin concentrations in man. *Diabetologia* **1985**, *28*, 412–419. [CrossRef] [PubMed]

43. He, Y.; Ling, Y.; Guo, W.; Li, Q.; Yu, S.; Huang, H.; Zhang, R.; Gong, Z.; Liu, J.; Mo, L.; et al. Prevalence and Prognosis of HFimpEF Developed from Patients With Heart Failure With Reduced Ejection Fraction: Systematic Review and Meta-Analysis. *Front. Cardiovasc. Med.* **2021**, *8*, 757596. [CrossRef]
44. Wu, N.; Lang, X.; Zhang, Y.; Zhao, B.; Zhang, Y. Predictors and Prognostic Factors of Heart Failure with Improved Ejection Fraction. *Rev. Cardiovasc. Med.* **2024**, *25*, 280. [CrossRef] [PubMed]
45. Ho, L.T.; Juang, J.J.; Chen, Y.H.; Chen, Y.S.; Hsu, R.B.; Huang, C.C.; Lee, C.M.; Chien, K.L. Predictors of Left Ventricular Ejection Fraction Improvement in Patients with Early-Stage Heart Failure with Reduced Ejection Fraction. *Acta Cardiol. Sin.* **2023**, *39*, 854–861. [CrossRef]
46. Vardeny, O.; Desai, A.S.; Jhund, P.S.; Fang, J.C.; Claggett, B.; de Boer, R.A.; Hernandez, A.F.; Inzucchi, S.E.; Kosiborod, M.N.; Lam, C.S.P.; et al. Dapagliflozin and Mode of Death in Heart Failure with Improved Ejection Fraction: A Post Hoc Analysis of the DELIVER Trial. *JAMA Cardiol.* **2024**, *9*, 283–289. [CrossRef]
47. Bozkurt, B.; Coats, A.J.S.; Tsutsui, H.; Abdelhamid, C.M.; Adamopoulos, S.; Albert, N.; Anker, S.D.; Atherton, J.; Böhm, M.; Butler, J.; et al. Universal definition and classification of heart failure: A report of the Heart Failure Society of America, Heart Failure Association of the European Society of Cardiology, Japanese Heart Failure Society and Writing Committee of the Universal Definition of Heart Failure: Endorsed by the Canadian Heart Failure Society, Heart Failure Association of India, Cardiac Society of Australia and New Zealand, and Chinese Heart Failure Association. *Eur. J. Heart Fail.* **2021**, *23*, 352–380. [CrossRef]
48. Huang, W.; Nurhafizah, A.; Frederich, A.; Khairunnisa, A.R.; Kezia, C.; Fathoni, M.I.; Samban, S.; Flindy, S. Risk and Protective Factors of Poor Clinical Outcomes in Heart Failure with Improved Ejection Fraction Population: A Systematic Review and Meta-Analysis. *Curr. Cardiol. Rep.* **2025**, *27*, 4. [CrossRef]
49. Pintér, A.; Behon, A.; Veres, B.; Merkel, E.D.; Schwertner, W.R.; Kuthi, L.K.; Masszi, R.; Lakatos, B.K.; Kovács, A.; Becker, D.; et al. The Prognostic Value of Anemia in Patients with Preserved, Mildly Reduced and Recovered Ejection Fraction. *Diagnostics* **2022**, *12*, 517. [CrossRef]
50. Kondo, T.; Campbell, R.; Jhund, P.S.; Anand, I.S.; Carson, P.E.; Lam, C.S.P.; Shah, S.J.; Vaduganathan, M.; Zannad, F.; Zile, M.R.; et al. Low Natriuretic Peptide Levels and Outcomes in Patients with Heart Failure and Preserved Ejection Fraction. *JACC Heart Fail.* **2024**, *12*, 1442–1455. [CrossRef]
51. Berezina, T.A.; Berezin, O.O.; Novikov, E.V.; Lichtenauer, M.; Berezin, A.E. Irisin Predicts Poor Clinical Outcomes in Patients with Heart Failure with Preserved Ejection Fraction and Low Levels of N-Terminal Pro-B-Type Natriuretic Peptide. *Biomolecules* **2024**, *14*, 1615. [CrossRef]
52. Li, J.; Xie, S.; Guo, L.; Jiang, J.; Chen, H. Irisin: Linking metabolism with heart failure. *Am. J. Transl. Res.* **2020**, *12*, 6003–6014. [PubMed] [PubMed Central]
53. Wang, Z.; Chen, K.; Han, Y.; Zhu, H.; Zhou, X.; Tan, T.; Zeng, J.; Zhang, J.; Liu, Y.; Li, Y.; et al. Irisin Protects Heart Against Ischemia-Reperfusion Injury Through a SOD2-Dependent Mitochondria Mechanism. *J. Cardiovasc. Pharmacol.* **2018**, *72*, 259–269. [CrossRef]
54. Silvestrini, A.; Bruno, C.; Vergani, E.; Venuti, A.; Favuzzi, A.M.R.; Guidi, F.; Nicolotti, N.; Meucci, E.; Mordente, A.; Mancini, A. Circulating irisin levels in heart failure with preserved or reduced ejection fraction: A pilot study. *PLoS ONE* **2019**, *14*, e0210320. [CrossRef]
55. Berezin, A.A.; Lichtenauer, M.; Boxhammer, E.; Stöhr, E.; Berezin, A.E. Discriminative Value of Serum Irisin in Prediction of Heart Failure with Different Phenotypes among Patients with Type 2 Diabetes Mellitus. *Cells* **2022**, *11*, 2794. [CrossRef]
56. Berezin, A.A.; Fushtey, I.M.; Pavlov, S.V.; Berezin, A.E. Predictive value of serum irisin for chronic heart failure in patients with type 2 diabetes mellitus. *Mol. Biomed.* **2022**, *3*, 34. [CrossRef]
57. Abubakar, M.; Irfan, U.; Abdelkhalek, A.; Javed, I.; Khokhar, M.I.; Shakil, F.; Raza, S.; Salim, S.S.; Altaf, M.M.; Habib, R.; et al. Comprehensive Quality Analysis of Conventional and Novel Biomarkers in Diagnosing and Predicting Prognosis of Coronary Artery Disease, Acute Coronary Syndrome, and Heart Failure, a Comprehensive Literature Review. *J. Cardiovasc. Transl. Res.* **2024**, *17*, 1258–1285. [CrossRef]

Disclaimer/Publisher's Note: The statements, opinions and data contained in all publications are solely those of the individual author(s) and contributor(s) and not of MDPI and/or the editor(s). MDPI and/or the editor(s) disclaim responsibility for any injury to people or property resulting from any ideas, methods, instructions or products referred to in the content.

biomedicines

MDPI

Article

Role of Advanced Glycation End Products in Mediating Glycated Haemoglobin and Pulse Wave Velocity in Healthy Adults

Irene Martínez-García [1], Alicia Saz-Lara [1,*], Carlos Pascual-Morena [2,3], Ana Díez-Fernández [2], Sara Valladolid-Ayllón [1,4], Bruno Bizzozero-Peroni [2,5], Óscar Martínez-Cifuentes [1,6], Eva Rodríguez-Gutiérrez [2,7] and Iván Cavero-Redondo [1]

1 CarVasCare Research Group, Facultad de Enfermería de Cuenca, Universidad de Castilla-La Mancha, 16071 Cuenca, Spain; irene.mgarcia@uclm.es (I.M.-G.); saravalladolid0@gmail.com (S.V.-A.); osmaci@hotmail.com (Ó.M.-C.); ivan.cavero@uclm.es (I.C.-R.)
2 Health and Social Research Center, Universidad de Castilla-La Mancha, 16071 Cuenca, Spain; carlos.pascual@uclm.es (C.P.-M.); ana.diez@uclm.es (A.D.-F.); bruno.bizzozero@uclm.es (B.B.-P.); eva.rodriguez@uclm.es (E.R.-G.)
3 Facultad de Enfermería de Albacete, Universidad de Castilla-La Mancha, 02006 Albacete, Spain
4 Hospital General Universitario de Elda, 03600 Elda, Spain
5 Higher Institute of Physical Education, Universidad de la República, Rivera 40000, Uruguay
6 Hospital Universitario Mutua Terrassa, 08221 Terrassa, Spain
7 Research Network on Chronicity, Primary Care and Health Promotion (RICAPPS), 16071 Cuenca, Spain
* Correspondence: alicia.delsaz@uclm.es

Abstract: Background/Objectives: Poor metabolic control is associated with increased levels of advanced glycation end products (AGEs), which in turn may lead to increased arterial stiffness. The aim of this study was to estimate the association between glycated haemoglobin A1c (HbA1c) and aortic pulse wave velocity (a-PWV) in healthy subjects and to analyse the mediating effect of AGEs measured by skin autofluorescence (SAF) on this association. **Methods**: HbA1c, a-PWV and SAF were analysed in 390 healthy Spanish subjects from the EVasCu study (42.02 ± 13.14 years, 63.08% females). A directed acyclic graph (DAG) was generated to define the covariates to be included, and the model was confirmed via multiple linear regression analysis. Descriptive and exploratory analyses were performed to investigate the associations between variables. Finally, adjusted and unadjusted mediation analyses were performed to verify the influence of SAF on the main association between HbA1c and a-PWV. **Results**: Multiple linear regression analyses for a-PWV supported the validity of the structure in the DAG. Descriptive and exploratory analyses revealed that when the models were adjusted to include all covariates, the statistical significance of the main association disappeared. Mediation analysis revealed that SAF mediated 35.77% of the effect of HbA1c on a-PWV in the unadjusted model and 42.18% after adjusting for covariates. **Conclusions**: Our study suggests that increases in HbA1c levels are associated with increases in a-PWV and that this relationship is mediated by the SAF score in healthy adults.

Keywords: advanced glycation end products; skin autofluorescence; glycated haemoglobin; pulse wave velocity; arterial stiffness; healthy adults; mediation; cross-sectional

1. Introduction

The prevalence of cardiovascular disease (CVD) has doubled worldwide in the last 20 years, leading to an increased number of deaths and a significant increase in years of life lost, disability-adjusted life years, and years lived with disability [1]. Arterial stiffness is a key biomarker of cardiovascular pathophysiology [2,3] and is influenced by several factors, such as aging and sex [4,5]. In addition, it is affected by impaired glucose metabolism, with persistent hyperglycaemia being one of the causative mechanisms of arterial stiffness, contributing to the subsequent increase in cardiovascular risk (CV risk) [6,7].

Currently, a multitude of validated non-invasive methods are available to measure arterial stiffness, which provide useful biomarkers in the clinical setting [8,9]. Among these, pulse wave velocity (PWV) is regarded as the gold standard for measuring arterial stiffness [9]. In clinical practice, oscillometric assessment of PWV is advocated because of its simplicity, reduced variability and independence from specific distance measurements [10]. In addition, the aortic pulse wave velocity (a-PWV) has been proposed for CV risk assessment because of its high predictive ability for CVD risk [11]. On the other hand, the gold standard for assessing glycaemic control is glycated haemoglobin A1c (HbA1c) [12], which is considered a better glycaemic indicator than fasting plasma glucose [13]. In 2010, the American Diabetes Association proposed it as a diagnostic criterion for diabetes and has maintained it to date, citing its accuracy and stability [14,15].

Several studies have reported a significant association between PWV and HbA1c across different demographic groups, including the Spanish population [13,16,17]. However, important gaps in the understanding of this association remain, as the underlying biological mechanisms are not fully understood. Several pathophysiological pathways associated with HbA1c, such as arterial wall thickness, advanced protein glycation, stress and/or chronic inflammation, influence arterial stiffness [6,18,19]. In particular, advanced protein glycation and the subsequent accumulation of advanced glycation end products (AGEs) may play key mediating roles in this relationship [6], although this interpretation is speculative and needs to be confirmed. AGEs' accumulation has been associated with increased vascular damage [20], in addition to increased AGEs' accumulation in individuals with diabetes as a result of chronic hyperglycaemia and oxidative stress [21,22]. In the pathogenesis of arterial stiffness, protein glycation and AGEs' formation are intermediate steps that may explain the CV risk associated with previous increases in HbA1c in individuals with diabetes [23]. These findings suggest that AGEs' accumulation could be an underlying mechanism determining the relationship between HbA1c and PWV. Skin autofluorescence (SAF) is a non-invasive, rapid and simple technique for the direct measurement of AGEs' accumulation that has been widely validated and reproduced in different populations, including healthy individuals, patients with diabetes and different ethnic groups [20,24,25]. Despite its proven accuracy and efficacy, it is important to consider specific factors that may influence the test results, particularly age, which has been shown to significantly affect SAF measurements [24].

To our knowledge, there are no reports exploring the possible mediating role of SAF in the relationship between HbA1c and a-PWV. Although previous studies have speculated on this possibility [6], research has been limited to exploring bivariate relationships between parameters without considering all three simultaneously [6,17,20,21]. Mediation analysis provides information on the association between two factors, in this case, HbA1c and a-PWV, and the extent to which a third variable, SAF, mediates the main association. Furthermore, the study of this relationship in subjects without diagnosed pathologies could be highly important since it could identify direct and intermediate or mediating factors at an early stage, contributing to improving the design of preventive strategies for cardiovascular health. Because of the need to rationally substantiate the mechanism of

arterial stiffness, this study was conducted with the objective of assessing the associations among the variables HbA1c, a-PWV and SAF, as well as the ability of the SAF to mediate the main association between HbA1c and a-PWV in healthy adults.

2. Materials and Methods

2.1. Study Design

This study is based on data from the cross-sectional EVasCu study in Spain, which was designed to validate a model of early vascular ageing (EVA) as an index of CV risk in healthy adults via confirmatory factor analysis [26]. This study was approved by the Clinical Research Ethics Committee of the Cuenca Health Area (REG: 2022/PI2022) and was conducted according to the standards of the Declaration of Helsinki. This research was conducted following the Guideline for Reporting Mediation Analyses (Supplementary Table S1) and the guidelines for reporting observational studies "Strengthening the Reporting of Observational Studies in Epidemiology (STROBE) Statement" (Supplementary Table S2) [27,28].

2.2. Participants

The sample size was calculated via Epidat software 4.2, which yielded a sample size of 355 healthy participants, an estimated effect of 1, an alpha risk of 0.05 and an absolute precision level of 0.04 to detect a statistically significant result for the Early Vascular Aging Index (EVA Index) [29]. The EVA Index is used to assess vascular health and identify signs of accelerated arterial aging, making it clinically relevant in the early detection of cardiovascular risk factors. The effect size of 1 was determined on the basis of previous studies to ensure that the calculation had sufficient statistical power to allow the study to detect significant differences between individuals. Finally, 390 participants were enrolled, a number that exceeded the sample size originally calculated to allow for potential dropouts or study variability.

The participants volunteered for the study after the project was advertised through various media and social networks. The inclusion criteria were as follows: over 18 years of age, clinically stable for the previous 6 weeks and provided written consent to participate in the study. Subjects enrolled in other trials of any intervention, those receiving pharmacological treatment (such as hypoglycaemic drugs, lipid-lowering drugs, antihypertensive drugs, etc.) or those with a previous diagnosis of CVD (such as diabetes, arterial hypertension, myocardial infarction or stroke) were excluded from the study. The recruitment and measurement period lasted from June 2022 to December 2022 at the Health and Social Research Centre of the University of Castilla-La Mancha.

2.3. Dependent Variable

Arterial stiffness was assessed by a-PWV via the non-invasive oscillometric technique Mobil-O-Graph® (IEM GmbH, Stolberg, Germany). This method has been shown to provide values with an acceptable level of accuracy compared with intra-aortic measurements [30]. The validated ARCSolver algorithm (Austrian Institute of Technology GmbH, Vienna, Austria) was used [31,32]. Measurements were performed in a quiet environment after a five-minute rest period, during which the participant was asked to avoid caffeine, smoking or physical activity for at least 30 min prior to measurement. With the participant seated with their legs uncrossed and feet flat on the floor, a cuff appropriate for the size of the non-dominant arm was placed approximately 2 cm above the elbow. The arterial symbol was placed over the brachial artery, and the pressure tube was passed unbent behind the neck. After entering the patient's age, sex, weight, height and smoking habits into the software, the participant was instructed not to speak during the measurement. The device inflates the cuff and records the oscillations of the brachial pulse wave, providing pulse wave

analysis, along with measurements of brachial blood pressure parameters, central blood pressure, augmentation pressure, the augmentation index, peripheral vascular resistance and cardiac output.

2.4. Independent Variable

Venous blood samples were taken from participants between 8:00 and 9:00 a.m. The participants were instructed to fast overnight, with no food or caloric drinks for 12 h prior to blood extraction. Venipuncture was performed via the antecubital vein of each participant. Blood samples were collected and stored according to established protocols and then sent to the laboratory of the Virgen de La Luz Hospital in Cuenca for subsequent analysis. The samples were handled in a controlled manner to maintain their integrity and obtain accurate laboratory results. HbA1c was determined by high-performance liquid chromatography using the ADAMS A1c analyser HA-8180 V (ARKRAY, Inc., Kyoto, Japan).

2.5. Mediating Variable

AGEs were measured by SAF using the AGE Reader (DiagnOptics TechnologiesBV, Groningen, The Netherlands). As most AGEs are autofluorescent, this device performs an estimation of AGE levels via the SAF [33]. The device emits an excitation light of 300–420 nm, which is directed towards the skin of the forearm. This light excites the fluorescent fractions of the tissue, which then emit a different wavelength. The emitted light is detected by a spectrometer using a specific range where the greatest contribution of fluorescence is derived from AGEs that are bound to collagen, in addition to AGEs that are bound to other proteins and lipids [33]. The approximate measurement time is 20 s. The device performs three measurements on each arm and calculates the mean by obtaining a value for each arm. The mean of the two measurements was calculated for each subject. Measurements were taken on both arms, avoiding skin imperfections such as scars, moles, tattoos and birthmarks, and the resulting average was taken from both arms. The participants were asked not to use any skin creams prior to the measurement to avoid interference with the results [34]. In cases where creams were used, the skin of the forearm was cleaned with soap and water and dried before measurement. In addition, the light in the room was controlled, and a dim room was chosen for all measurements. The amount of light in the room was controlled to avoid interference from any external light source, both natural and artificial. The SAF values are expressed in arbitrary units.

2.6. Potential Confounding Variables: Adjustment of Variables

To identify the minimum sufficient adjustment set (MSAS) for estimating the total effect of HbA1c on a-PWV, a theoretical causal diagram was constructed on the basis of an exhaustive review of the existing scientific literature [3–7,17–24]. A directed acyclic graph (DAG) was subsequently constructed [35] via the online tool DAGitty [36]. The covariates age, sex, smoking status, insulin level, systolic blood pressure (SBP), body mass index (BMI) and socioeconomic status were identified as the MSAS in the model, according to the backdoor criterion [37] (Supplementary Figure S1).

Age, sex and smoking status were collected via self-report questionnaires. For sex, the possible answers were men or women. Smoking status was classified as follows: (i) smoker; (ii) ex-smoker of 0–1 years; (iii) ex-smoker of 1–5 years; (iv) ex-smoker of more than 5 years; and (v) nonsmoker.

Insulin was measured in serum blood samples, which were collected via cubital vein puncture between 8:15 and 9:00 a.m. after at least 12 h of fasting. Blood samples were collected and stored according to established protocols and then sent to the laboratory of the Virgen de La Luz Hospital in Cuenca for subsequent analysis. The samples were processed on the Roche Diagnostics COBAS C711 system (Roche Diagnostics International

Ltd., Rotkreuz, Switzerland), the blood glucose concentration was determined via the hexokinase method, and the fasting insulin concentration was determined via a one-step chemiluminescent microparticle immunoassay via a processing platform consisting of two Abbott Laboratories ARCHITECTi2000SR systems (Abbott Park, IL, USA).

The participants' height and weight were measured twice via a SECA 222 hand-held measuring rod (Seca® GmbH & Co. KG, Hamburg, Germany) and a SECA 869 scale (Seca® GmbH & Co. KG, Hamburg, Germany). The mean of the two measurements was used for analysis. BMI was calculated as kg/m^2.

SBP was measured in a quiet place and after a 5 min rest period using the Omron® M5-I monitor (Omron Healthcare UK Ltd., Buckinghamshire, UK), with a cuff size corresponding to the participant's arm circumference. SBP was measured twice, five minutes apart, and the mean of the two measurements was used for analysis.

Educational level was measured via a self-report questionnaire with 6 response options: (i) unable to read or write; (ii) incomplete primary education; (iii) primary education; (iv) secondary education; (v) professional education/higher education; and (vi) university education. Educational level has been recognised as a socioeconomic determinant of CV risk [38] and was therefore included as a covariate.

In addition, the assessment of CV risk derived from the SAF was considered. The CV risk derived from the SAF classifies risk into 4 levels: no increased CV risk; risk group I: limited increase in CV risk; risk group II: increased CV risk; and risk group III: definite CV risk.

2.7. Statistical Methods

Both statistical (Kolmogorov–Smirnov test) and graphical (normal probability plots) methods were used to examine the fit to a normal distribution for each continuous variable. Sex differences in descriptive data were assessed via Student's *t*-test for continuous descriptive variables and the chi-square test for categorical descriptive variables. The homogeneity of variances was assessed via Levene's test, and scatterplots of the residuals and multicollinearity were generated via variance inflation factors (VIFs).

To evaluate and validate the structure proposed by the DAG, two multiple regression analyses of a-PWV were performed for the unadjusted model and the model adjusted by the MSAS. In addition, local weighted dispersion smoothing (LOESS) regression was performed to assess the association between HbA1c and SAF, considering a CV risk variable provided by the SAF. According to the form of LOESS regression, a subsample excluding subjects classified as risk group III (definite CV risk) was created and identified as potential outliers.

Partial and bivariate Pearson correlation coefficients (MSAS adjusted and unadjusted) were calculated to examine the relationships between HbA1c, a-PWV and SAF. These calculations were performed for the full sample as well as for the subsample without definite CV risk to explore possible differences in the relationships between variables on the basis of participant characteristics.

To explore the variation in a-PWV according to HbA1c exposure levels, HbA1c was categorised into tertiles. Analyses of variance and covariance were subsequently performed for HbA1c tertiles (Model 0), controlling for SAF (Model 1), controlling for MSAS (Model 2) and controlling for MSAS and SAF (Model 3). These analyses were performed both in the full sample and in the subsample by excluding participants identified as having definite CV risk according to SAF risk.

Therefore, mediation analyses were performed via the PROCESS macro for SPSS, version 3.5 [39], with Model 4 selected to assess the possible mediation of SAF in the association between HbA1c and a-PWV, both in the full sample and in the subsample

excluding participants with definite CV risk. In addition, to explore possible sex differences, mediation analyses were conducted separately for men and women. Mediation analyses were performed both with the unadjusted model to assess the direct and indirect relationships between the three variables of interest and with the adjusted MSAS model to ensure more accurate and robust estimates. The purpose was to examine the total effect (c) and the direct effects (a, b, c') to determine the unstandardised regression coefficient and the significance between the independent and dependent variables of the selected model. Similarly, the indirect effect (EI) obtained from the product of the coefficients (a × b) was calculated, showing the change in the a-PWV variable for each unit change in HbA1c that is mediated by the SAF. To test the mediation hypothesis, this macro uses bootstrapping methods as recommended by Preacher and Hayes [40] via a 5000-sample bootstrap resampling procedure. Estimates and confidence intervals (95%) were calculated for the EI, considering the point estimate as the mean when the confidence interval did not contain zero. Finally, the percentage of mediation was calculated by dividing the indirect effect (a × b) by the total effect (c). Following Hayes' recommendation, the concepts of complete mediation and partial mediation were not used in this study [39]. The missing data were not considered in the analyses.

A two-sided statistical significance criterion of $p \leq 0.05$ was used. IBM SPSS 28 software (IBM Corp., Armonk, NY, USA) was used for all the statistical analyses. STATA 15.1 software was used to generate the LOESS scatterplot.

3. Results

The study flowchart is shown in detail in Supplementary Figure S2. A total of 390 healthy adults were included, with a mean age of 42.02 ± 13.14 years, and 63.08% were female. The characteristics of the participants are described in Table 1, which shows the results for the full sample and is stratified by sex.

Table 1. Characteristics of the full sample.

Characteristics	Total (*n* = 390)	Men (*n* = 144)	Women (*n* = 246)	*p*-Value
Age, years				
- Mean Age	42.02 ± 13.14	42.33 ± 12.45	41.84 ± 13.55	0.361
- 18–20 years	13 (3.3)	3 (2.1)	10 (4.1)	
- 20–29 years	77 (19.7)	23 (16.0)	54 (22.0)	
- 30–39 years	56 (14.4)	30 (20.8)	26 (10.6)	
- 40–49 years	116 (29.7)	46 (31.9)	70 (28.5)	
- 50–59 years	100 (25.6)	29 (20.1)	71 (28.9)	
- 60–69 years	25 (6.4)	11 (7.6)	14 (5.7)	
- 70–79 years	3 (0.8)	2 (1.4)	1 (0.4)	0.028 *
Smoking status [1]				
- Smokers	48 (12.4)	14 (9.8)	34 (13.9)	
- Smokers 0–1 years	7 (1.8)	2 (1.4)	5 (2.0)	
- Smokers 1–5 years	13 (3.4)	5 (3.5)	8 (3.3)	
- Smokers >5 years	73 (18.9)	32 (22.4)	41 (16.8)	
- Non-smokers	246 (63.6)	90 (62.9)	156 (63.9)	0.563
Height, cm	167.78 (±0.09)	176.52 (±0.07)	1.63 (±0.06)	<0.001 ***
Weight, kg	70.26 (±14.57)	80.12 (±12.72)	64.48 (±12.33)	<0.001 ***
BMI, kg/m^2				
- Mean BMI	24.87 (4.25)	25.68 (±3.55)	24.39 (±4.54)	0.002 **
- Underweight	11 (2.8)	1 (0.7)	10 (4.1)	
- Normal weight	207 (53.1)	65 (45.1)	142 (57.7)	
- Overweight	122 (31.3)	60 (41.7)	62 (25.2)	
- Obesity	50 (12.8)	18 (12.5)	32 (13.0)	0.003 **

Table 1. *Cont.*

Characteristics	Total (*n* = 390)	Men (*n* = 144)	Women (*n* = 246)	*p*-Value
BP, mmHg [1]				
- SBP (±SD)	116.67 (±15.21)	125.09 (±12.77)	111.77 (±14.37)	<0.001 ***
- DBP (±SD)	70.36 (±10.57)	72.27 (±10.33)	69.24 (±10.58)	0.003 **
a-PWV, m/s	6.34 (±1.35)	6.53 (±1.34)	6.24 (±1.35)	0.019 *
Insulin, mUI/L [1]	8.52 (±6.08)	8.29 (±5.44)	8.65 (±6.43)	0.284
HbA1c, %1				
- Mean HbA1c	5.18 (±0.33)	5.16 (±0.37)	5.19 (±0.31)	0.188
- Low tertile	4.85 (±0.19)	4.80 (±0.24)	4.88 (±0.15)	0.012 *
- Medium tertile	5.17 (±0.07)	5.16 (±0.07)	5.17 (±0.07)	0.229
- High tertile	5.53 (±0.22)	5.55 (±0.28)	5.53 (±0.18)	0.292
Skin autofluorescence, AU [1]				
- Mean AGEs	1.89 (±0.41)	1.91 (±0.46)	1.88 (±0.38)	0.245
- Risk CV 0: No increase	172 (44.6)	62 (43.4)	110 (45.3)	
- Risk CV 1: Limited increase	153 (39.6)	61 (42.7)	92 (37.9)	
- Risk CV 2: Increased	53 (13.7)	17 (11.9)	36 (14.8)	
- Risk CV 3: Very high	8 (2.1)	3 (2.1)	5 (2.1)	0.763
Educational level [1]				
- Unable to read or write	-	-	-	
- Incomplete primary education	-	-	-	
- Primary education	4 (1.0)	1 (0.7)	3 (1.2)	
- Secondary education	45 (11.7)	19 (13.3)	26 (10.7)	
- Professional/Higher education	116 (30.1)	40 (28.0)	76 (31.3)	
- University education	221 (57.3)	83 (58.0)	138 (56.8)	0.773

Observations: Values are the means ± standard deviations, except for age categories, smoking status, BMI categories, risk CV and education level, which are shown as absolute numbers and percentages (%). The *p*-values were calculated via Pearson's chi-square test for categorical variables and the independent samples *t* test for continuous variables, with groups defined by sex (men and women). Statistical significance is indicated by asterisks, where * indicates $p \leq 0.05$, ** indicates $p \leq 0.01$ and *** indicates $p \leq 0.001$. A "[1]" was used to denote variables with missing data for some participants (4 participants lacked information on smoking status, 1 on PA, 7 on insulin levels, 3 on HbA1c, 4 on SAF and 4 on educational level). Abbreviations: a-PWV, aortic pulse wave velocity; AU, arbitrary units; cm: centimetres; BP, blood pressure; CV, cardiovascular; DBP, diastolic blood pressure; HbA1c, glycated haemoglobin; kg, kilograms; m/s: metres per second; mUI/L, milliunits per litre; *p*-value, significance; SD, standard deviation; SBP, systolic blood pressure.

The results of the multiple linear regression analyses for the a-PWV supported the validity of the structure proposed in the DAG (Supplementary Table S3). Significance was observed for all variables except for smoking status, educational level and HbA1c (in the MSAS-adjusted model). All the VIFs were lower than 2, so it was concluded that there was no collinearity between the variables. Both models showed adequate summary statistics (significant ΔF, adequate R2 and Durbin–Watson close to 2), but an improvement in all statistics was observed in the covariate-adjusted model, which improved the model (higher ΔF) and decreased the autocorrelation of the residuals (Durbin–Watson close to 2), with 90% of the variability of the a-PWV in the covariate-adjusted model being explained by the covariates, compared with 30% in the unadjusted model.

Figure 1 shows the association between HbA1c and SAF, considering the CV risk provided by SAF, and reveals that individuals in risk group III had atypical patterns. Consequently, a subsample excluding these individuals was used, and further analyses were performed on this subsample.

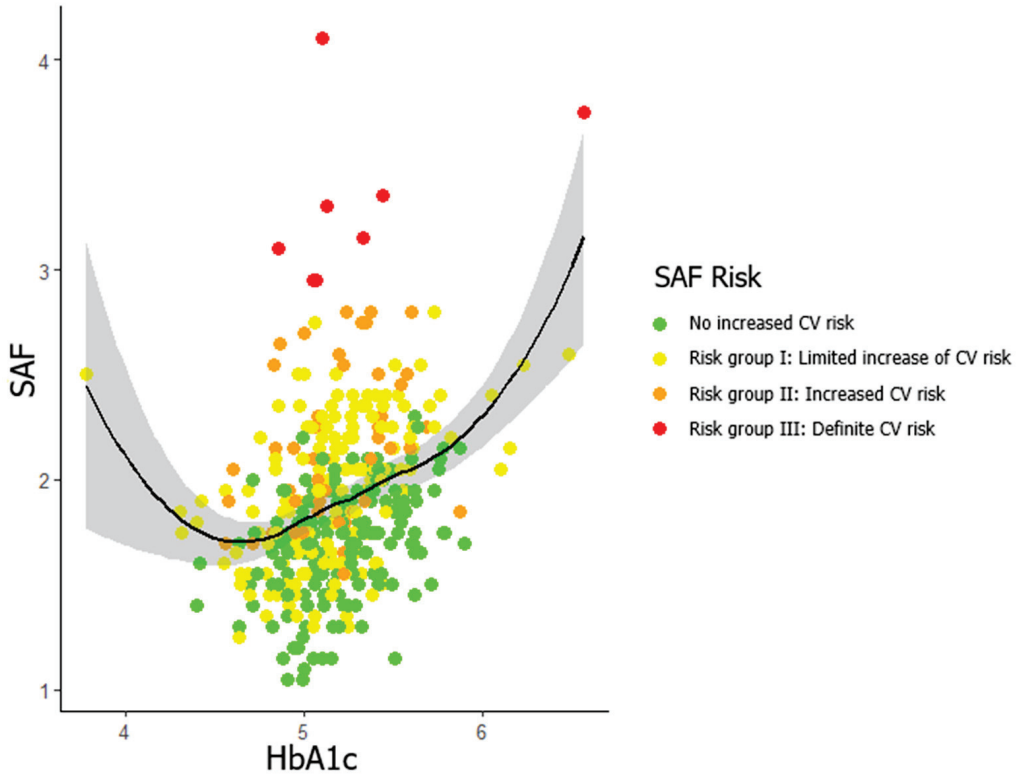


Figure 1. Scatterplot illustrating LOESS regression analysis between skin autofluorescence and HbA1c, including SAF cardiovascular risk. Observations: CV risk, cardiovascular risk; HbA1c, glycated haemoglobin; SAF, skin autofluorescence.

Table 2 shows the bivariate and partial correlation coefficients (r) between HbA1c, SAF and a-PWV for the full sample and the subsample. In unadjusted Model 1, significant associations were found between all model variables ($p < 0.05$). However, in Model 2 adjusted by the MSAS, a loss of significance was found in the main association between HbA1c and a-PWV.

Table 2. Bivariate and partial correlation coefficients (r) between HbA1c, SAF and a-PWV for the full sample and the subsample.

Variables		Model 1			Model 2		
		Sample Size	Bivariate Correlation Coefficients		Sample Size	Partial Correlation Coefficients	
		N/n	Full Sample	Subsample	N/n	Full Sample	Subsample
HbA1c and a-PWV	Total	387/375	0.402 ***	0.388 ***	372/365	0.068	0.046
	Women	245/237	0.446 ***	0.452 ***	236/232	0.107	0.115
	Men	142/138	0.363 ***	0.315 ***	136/133	0.001	−0.079
HbA1c and SAF	Total	383/375	0.310 ***	0.321 ***	372/365	0.139 **	0.156 **
	Women	242/237	0.262 ***	0.319 ***	236/232	0.065	0.111
	Men	141/138	0.373 ***	0.332 ***	136/133	0.236 **	0.236 **
SAF and a-PWV	Total	386/378	0.552 ***	0.555 ***	372/365	0.211 ***	0.176 ***
	Women	243/238	0.494 ***	0.518 ***	236/232	1.172 **	0.124
	Men	143/140	0.640 ***	0.619 ***	136/133	0.285 ***	0.277 **

Observations: The values in bold indicate statistical significance; Model 1: bivariate correlations (r) unadjusted; Model 2: partial correlation (r) adjusted for the minimum sufficient adjustment set provided by the directed acyclic graph, which was corroborated with the multiple regression model for a-PWV (excluding sex in the data provided for men and women); statistical significance is indicated by asterisks, where ** indicates $p \leq 0.01$ and *** indicates $p \leq 0.001$; the subsample was derived from the full sample by excluding participants identified as having definite CV risk according to SAF risk. Abbreviations: a-PWV, aortic pulse wave velocity; HbA1c, glycated haemoglobin; N: sample size for full sample; n: sample size for subsample; SAF, skin autofluorescence.

Table 3 shows the mean differences in the overall a-PWV score by HbA1c tertiles in both the full sample and the subsample, with significant differences in Model 0 (raw data analysis) and Model 1 (controlling for SAF) but disappearing in Model 2 (controlling for MSAS) in Model 3 (controlling for MSAS and SAF).

Table 3. Analysis of variance or covariance of a-PWV by HbA1c categories.

Model for a-PWV		Sample Size	Terciles of HbA1c			*p*-Value
		n	Low (L)	Medium (M)	High (H)	
Full sample	M0	129/129/129	5.805 ± 1.07 ^{M,H}	6.218 ± 1.37 ^{L,H}	7.018 ± 1.31 ^{L,M}	<0.001 ***
	M1	129/127/127	5.805 ± 1.07 ^{H}	6.226 ± 1.38 ^{H}	7.042 ± 1.30 ^{L,M}	<0.001 ***
	M2	127/125/124	5.800 ± 1.07	6.235 ± 1.38	7.023 ± 1.31	0.596
	M3	127/123/122	5.800 ± 1.06	6.244 ± 1.39	7.048 ± 1.30	0.666
Subsample	M0	128/123/124	5803 ± 1.08 ^{M,H}	6196 ± 1.37 ^{L,H}	6989 ± 1.26 ^{L,M}	<0.001 ***
	M1	128/123/124	5803 ± 1.08 ^{H}	6196 ± 1.37 ^{H}	6989 ± 1.26 ^{L,M}	<0.001 ***
	M2	126/120/119	5.798 ± 1.07	6.202 ± 1.38	6.993 ± 1.26	0.617
	M3	126/120/119	5.798 ± 1.07	6.202 ± 1.38	6.993 ± 1.26	0.608

Observations: The subsample was derived from the full sample by excluding participants identified as having definite CV risk according to SAF risk. The data are presented as the means ± standard errors (SEs). Statistical significance is indicated by asterisks, where *** indicates $p \leq 0.001$. Superscript letters indicate statistical significance ($p < 0.05$) between categories for post hoc tests via the Bonferroni comparisons. Abbreviations: a-PWV, aortic pulse wave velocity; HbA1c, glycated haemoglobin, M0: Model 0 (raw data analysis); M1: Model 1 (controlling for SAF); M2: Model 2 (controlling for MSAS); M3: Model 3 (controlling for MSAS and SAF); *p*-value, significance.

On the basis of the above results, mediation analyses were carried out on both the full sample and the subsample, unadjusted and adjusted for MSAS (Figure 2). For the two unadjusted models (Figure 2a,b), significance was found in all the model equations ($p < 0.001$). However, in the adjusted models, we found a weakening of significance in routes a and b compared with the unadjusted models ($p < 0.05$) and a loss of significance in routes c and c′. The percentage of the total mediation effect increased in the adjusted models (full sample: 35.77% to 42.18%; subsample: 39.65% to 58.19%), whereas the indirect effect decreased (full sample: 0.60 to 0.04; subsample: 0.63 to 0.04) but maintained significance.

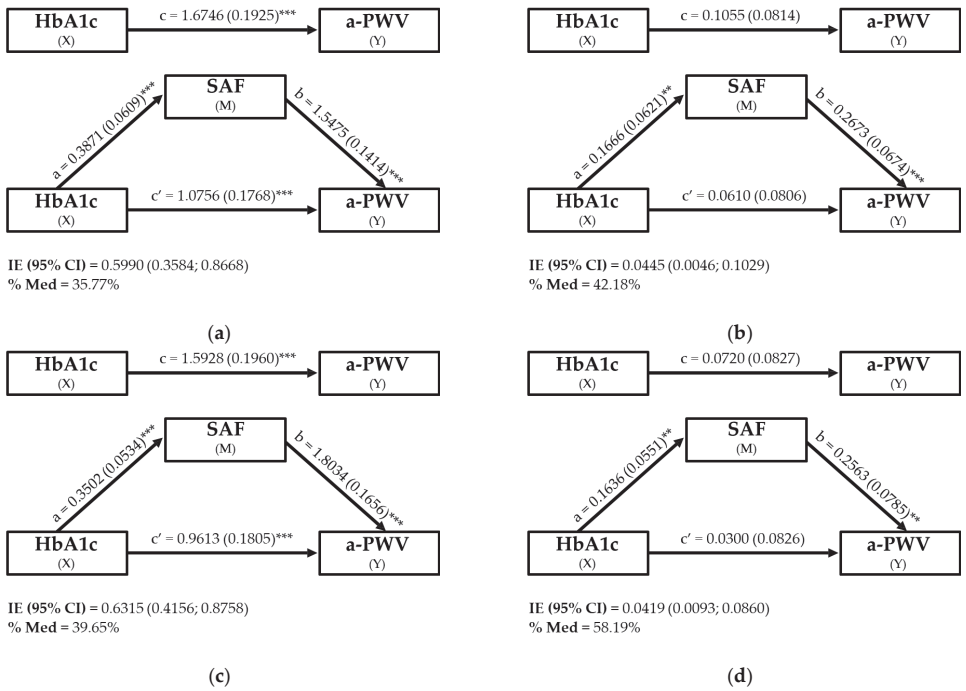


Figure 2. Mediation effects of skin autofluorescence (SAF) on the relationship between HbA1c and a-PWV across four analyses: (**a**) full sample unadjusted,(**b**) subsample unadjusted, (**c**) full sample adjusted for

covariates, (**d**) subsample adjusted for covariates. Observations: The variables in the mediation model were HbA1c (X), SAF (M) and a-PWV (Y). The adjusted model is adjusted by the minimum sufficient adjustment set provided by the directed acyclic graph, which was corroborated with the multiple regression model for a-PWV. The subsample was derived from the full sample by excluding participants identified as having definite CV risk according to SAF risk. The results showed unstandardised beta coefficients and error standards. Statistical significance is indicated by asterisks, where ** indicates $p \leq 0.01$ and *** indicates $p \leq 0.001$. Abbreviations: % Med: mediation percentage; a-PWV, aortic pulse wave velocity; HbA1c, glycated haemoglobin; IE (95% CI): indirect effect (95% confidence interval); IM: mediator variable; SAF, skin autofluorescence; X, independent variable; Y, dependent variable.

Additional analyses by sex are shown in Supplementary Table S4. In the unadjusted models, a higher percentage of mediation was observed in men than in women. In the covariate-adjusted models, the significant indirect effect was lost in women, and no evidence of mediation was found in this group. In contrast, in men, although the percentage of mediation decreased, mediation remained significant.

4. Discussion

To our knowledge, this is the first study to estimate the influence of SAF on the relationship between HbA1c and a-PWV via mediation analysis procedures. Our data support that, in healthy subjects, higher levels of HbA1c are associated with higher levels of SAF and a-PWV. The results of the mediation analysis suggest that SAF explains the association between HbA1c and a-PWV, with a mediation percentage of 35.77% in the full sample. When adjusting for covariates (MSAS), steps c and c' lost statistical significance and increased the percentage of mediation to 42.18% in the full sample. The reduction in the indirect effect in the adjusted model indicates that covariates explain a part of the variability in a-PWV, which was attributed to HbA1c and SAF in the unadjusted model. The increase in the percentage of mediation after adjustment for covariates (MSAS) reinforces the robustness of the model, even in the presence of confounders.

In the subsample excluding participants identified as being at CV risk according to the SAF risk, similar results were found to those of the full sample. When the analyses were stratified by sex, greater mediation was found in men than in women in unadjusted models. However, when covariates were introduced into the model, different results were found in the sample and subsample. Male sex has previously been described as a determinant factor in the development of arterial stiffness [4]; however, the differences found could be due to hormonal, social or behavioural differences not controlled for in the study. Additionally, the differences observed with respect to sex could be a product of statistical noise in smaller subsamples, reducing the statistical power of the analysis. The effect of sex on a-PWV variability was not the largest according to the multiple linear regression (r = 0.115, $p = 0.013$), so its inclusion as a covariate seems to be more appropriate than the analysis stratified by sex. In addition, the covariate-adjusted regression model (including sex in the MSAS) suggested a good model fit, with 90% of the variability in a-PWV being explained by the covariates.

The association between HbA1c and PWV has been described in previous studies [13,16,17], highlighting the importance of metabolic factors in the modulation of arterial stiffness. A previous study reported that the association between HbA1c and PWV was mediated by insulin, with a mediation percentage of 17.9% [17]. Our study extends this knowledge by showing that SAF plays a significant role in the association between HbA1c and a-PWV, even after accounting for possible confounding factors, including insulin. The link between AGEs' accumulation and arterial stiffness has been previously established, suggesting the possible involvement of AGEs' accumulation in the pathophysiology of arterial stiffness [41,42].

AGEs' accumulation induces cross-linking of extracellular matrix proteins, such as collagen and elastin, altering their structure and elasticity and promoting increased oxidative stress and inflammation [43,44]. The resulting cross-links reduce the buffering function of arteries, leading to a subsequent increase in arterial stiffness [45]. The association between AGEs' accumulation and HbA1c is more controversial, with most studies finding a significant association [46–49]. The lack of association between HbA1c and AGEs observed could be explained by the shorter turnover time of HbA1c than that of SAF, as well as individual differences in the management of the hyperglycaemic state and associated oxidative stress [49]. It is possible that SAF correlates better with HbA1c from previous years than with the current HbA1c, as SAF represents longer-term cumulative metabolic control [48]. In healthy subjects, the mediating role of SAF in the relationship between HbA1c and a-PWV may be explained by the initial and progressive nature of the pathophysiological processes. In pathological contexts, the relationship becomes more complex, as the accumulation of AGEs represents not only hyperglycaemia but also increased metabolic load, inflammation and oxidative stress [18,50]. A vicious cycle is thus created in which the accumulation of AGEs, in addition to increasing arterial stiffness, creates a scenario conducive to increased AGEs' formation due to the oxidative stress and inflammation generated [18,51]. Moreover, other additional mechanisms are involved in the pathophysiology of arterial stiffness, generating a multifactorial scenario in which other factors could acquire greater relevance [52].

The results of this study should be interpreted with caution, as some potentially relevant covariates were not included in the analysis, which may affect the generalisability of the findings. Ethnicity and genetic factors may influence SAF [25], but our study consisted of a healthy population of European origin, so the inclusion of this variable was not considered due to the homogeneity of the sample. Previous studies have reported that diet and food preparation may influence some variables, especially AGEs [53–55]. In our study, this information was collected via the Mediterranean Diet Adherence Screener questionnaire [56]; however, there could be recall bias, in addition to the questionnaire's inability to assess in depth the cooking, frequency and quantity of food consumed. The level of physical activity could be another possible confounding factor in the main association [57]. In our study, physical condition was assessed via the International Fitness Scale [58], which is subjective in nature and depends on self-perception when self-reported. Physical activity was also assessed via wearable activity trackers (Xiaomi bands), but the rate of data loss for this variable was significant. These variables were not included in the study as potential confounders, as the DAG plot indicated that they were not included according to the MSAS. In addition, the adjusted model was analysed via multiple linear regression, which revealed that there was no collinearity between the variables and that 90% of the variability in a-PWV was explained by the covariates selected by the DAG (MSAS). This suggests that the selected variables adequately capture the relevant factors for the model.

The results of this study have important clinical and public health implications for the prevention of CVD. The observed association between HbA1c and a-PWV highlights the importance of maintaining optimal glycaemic control in healthy populations as a preventive strategy against the development of atherosclerosis and thus CV risk. In patients with coronary artery disease, the SAF score and a-PWV have previously been proposed as promising markers for risk stratification [59]. Our findings extend this perspective by adding to the evidence suggesting that the SAF may play a key role in the pathophysiology of arterial stiffness and therefore serve as a crucial risk biomarker, even at earlier stages, given its relevance in apparently healthy individuals [41]. This finding is important because the inclusion of SAF as a marker in CV risk prevention and assessment strategies could facilitate the implementation of specific measures to control the AGEs' accumulation and

prevent cardiovascular damage at an early stage before it becomes irreversible. In addition, it could improve primary care in general by facilitating decision making, reducing the burden on the healthcare system and promoting personalised medicine. However, although it is a simple and rapid test, cost–benefit studies are needed to assess its introduction into routine clinical practice.

Some limitations of our study should be recognised. First, the main limitation was the cross-sectional design of the study, as it does not allow for causal inference. Longitudinal and experimental studies are needed to confirm the direction and magnitude of the results and establish the temporal order between the variables. Second, our study included healthy subjects without diagnosed CVDs and of European descent, so the results cannot be extrapolated to other populations. Third, the recruitment method may have influenced the composition of the sample, limiting the representativeness of the study population in relation to the target population. Fourth, some of the participants in our study could have been misclassified as healthy and had previously undiagnosed pathologies. However, to reduce this bias, the analysis was additionally performed on a subsample that excluded individuals at CV risk, and the results were consistent with those of the full sample. Fifth, the limited sample size diminished the ability to clarify the influence of sex on the relationships examined. Sixth, another limitation of our study could be the non-inclusion of confounding variables, such as ethnicity, genetic factors, diet or physical activity, which could bias the model. Finally, in our analysis, SAF was selected as a potential mediator [6]; however, it is necessary to continue studying the role of this variable in the relationship to clarify its possible role, taking into account all the possible confounding variables, especially age and blood pressure, which strongly influence the main model [60].

5. Conclusions

Our study revealed that increases in HbA1c levels are associated with increases in a-PWV and that this relationship is mediated by SAF in healthy adults without preexisting disease. These findings are important from a public health perspective, as better glycaemic control may contribute to improved vascular health. Considering SAF as a biomarker of CV risk could help improve prevention and assessment strategies and promote targeted action before the risk is irreversible, as it would allow the identification of cardiovascular damage at an early stage. However, future longitudinal studies are needed to address this issue, allowing causal relationships to be established while accounting for relevant covariates such as age or blood pressure. Furthermore, a larger sample size would facilitate sex-specific analysis, which could elucidate possible differences or improve the understanding of the role of sex in the relationship studied.

Supplementary Materials: The following supporting information can be downloaded at: https://www.mdpi.com/article/10.3390/biomedicines13010137/s1, Figure S1: Directed acyclic graphs (DAGs) on the causal structure of the relationship between HbA1c (exposure, green) and a-PWV (outcome, blue) and its possible mediating variable, SAF (mediator, blue); Figure S2: Flow chart of the study participants in the current study from the original EVasCu study; Table S1: "Guideline for Reporting Mediation Analyses" checklist for the reporting of mediation analyses of observational studies; Table S2: STROBE Statement. Checklist of items that should be included in reports of cross-sectional studies; Table S3: Results of the multiple linear regression models for the dependent variable (a-PWV), including the full sample: unadjusted model and covariate-adjusted model; Table S4: Mediation effect of SAF on the association between HbA1c and a-PWV, comparing the entire dataset with an additional separate analysis for women and men.

Author Contributions: Conceptualization, I.M.-G., A.S.-L. and I.C.-R.; methodology, I.M.-G.; software, I.M.-G., C.P.-M. and A.D.-F.; formal analysis, I.M.-G. and A.D.-F.; investigation, B.B.-P. and E.R.-G.; data curation, I.M.-G. and C.P.-M.; writing—original draft preparation, I.M.-G.; writing—

review and editing, A.S.-L., C.P.-M., A.D.-F., S.V.-A., B.B.-P., Ó.M.-C., E.R.-G. and I.C.-R.; visualisation, B.B.-P.; supervision, A.S.-L., C.P.-M. and I.C.-R.; project administration, A.S.-L.; funding acquisition, A.S.-L. All authors have read and agreed to the published version of the manuscript.

Funding: This study was funded by the 42nd edition of the Nursing Award of the Pontifical University Comillas and the School of Nursing and Physiotherapy San Juan de Dios. I.M.-G. is supported by a grant from Science, Innovation and University (FPU21/06866). E.R.-G. is supported by a grant from the University of Castilla-La Mancha (2022-UNIVERS-11373). The financiers did not have any role in the design of the study, collection or analysis of the data, or the decision to publish or prepare the manuscript.

Institutional Review Board Statement: The study was conducted in accordance with the Declaration of Helsinki and approved by the Clinical Research Ethics Committee of the Cuenca Health Area (REG: 2022/PI2022).

Informed Consent Statement: Informed consent was obtained from all the subjects involved in the study.

Data Availability Statement: The raw data supporting the conclusions of this article will be made available by the authors, without undue reservation.

Acknowledgments: The researchers would like to express their sincerest gratitude to the project participants for their interest and engagement in the study. They would also like to acknowledge the dedicated health team, comprising nurses, physicians, physiotherapists and specialists in physical activity and sports, whose collaboration was essential for data collection.

Conflicts of Interest: The authors declare no conflicts of interest.

References

1. Roth, G.A.; Mensah, G.A.; Fuster, V. The Global Burden of Cardiovascular Diseases and Risks: A Compass for Global Action. *J. Am. Coll. Cardiol.* **2020**, *76*, 2980–2981. [CrossRef]
2. Vasan, R.S.; Pan, S.; Xanthakis, V.; Beiser, A.; Larson, M.G.; Seshadri, S.; Mitchell, G.F. Arterial Stiffness and Long-Term Risk of Health Outcomes: The Framingham Heart Study. *Hypertension* **2022**, *79*, 1045–1056. [CrossRef]
3. Vlachopoulos, C.; Aznaouridis, K.; Stefanadis, C. Prediction of cardiovascular events and all-cause mortality with arterial stiffness: A systematic review and meta-analysis. *J. Am. Coll. Cardiol.* **2010**, *55*, 1318–1327. [CrossRef]
4. Avolio, A.P.; Kuznetsova, T.; Heyndrickx, G.R.; Kerkhof, P.L.M.; Li, J.K. Arterial Flow, Pulse Pressure and Pulse Wave Velocity in Men and Women at Various Ages. *Adv. Exp. Med. Biol.* **2018**, *1065*, 153–168. [CrossRef]
5. Lu, Y.; Pechlaner, R.; Cai, J.; Yuan, H.; Huang, Z.; Yang, G.; Wang, J.; Chen, Z.; Kiechl, S.; Xu, Q. Trajectories of Age-Related Arterial Stiffness in Chinese Men and Women. *J. Am. Coll. Cardiol.* **2020**, *75*, 870–880. [CrossRef]
6. Rubin, J.; Nambi, V.; Chambless, L.E.; Steffes, M.W.; Juraschek, S.P.; Coresh, J.; Sharrett, A.R.; Selvin, E. Hyperglycemia and arterial stiffness: The Atherosclerosis Risk in the Communities study. *Atherosclerosis* **2012**, *225*, 246–251. [CrossRef]
7. Schram, M.T.; Henry, R.M.; van Dijk, R.A.; Kostense, P.J.; Dekker, J.M.; Nijpels, G.; Heine, R.J.; Bouter, L.M.; Westerhof, N.; Stehouwer, C.D. Increased central artery stiffness in impaired glucose metabolism and type 2 diabetes: The Hoorn Study. *Hypertension* **2004**, *43*, 176–181. [CrossRef]
8. Milan, A.; Zocaro, G.; Leone, D.; Tosello, F.; Buraioli, I.; Schiavone, D.; Veglio, F. Current assessment of pulse wave velocity: Comprehensive review of validation studies. *J. Hypertens.* **2019**, *37*, 1547–1557. [CrossRef]
9. Van Bortel, L.M.; Laurent, S.; Boutouyrie, P.; Chowienczyk, P.; Cruickshank, J.; De Backer, T.; Filipovsky, J.; Huybrechts, S.; Mattace-Raso, F.U.; Protogerou, A.D.; et al. Expert consensus document on the measurement of aortic stiffness in daily practice using carotid-femoral pulse wave velocity. *J. Hypertens.* **2012**, *30*, 445–448. [CrossRef]
10. Cavero-Redondo, I.; Sequí-Domínguez, I.; Saz-Lara, A.; Garcia-Klepzig, J.L.; Lucerón-Lucas-Torres, M.; Martínez-García, I.; Álvarez-Bueno, C.; Martínez-Vizcaíno, V. Concordance among pulse wave velocity assessment methods: A network meta-analysis. *Chin. Med. J.* **2024**, *137*, 2137–2139. [CrossRef]
11. Mitchell, G.F.; Hwang, S.-J.; Vasan, R.S.; Larson, M.; Pencina, M.J.; Hamburg, N.; Vita, J.; Levy, D.; Benjamin, E. Arterial stiffness and cardiovascular events: The Framingham Heart Study. *Circulation* **2010**, *121*, 505–511. [CrossRef]
12. Giugliano, D.; Ceriello, A.; Esposito, K. Glucose metabolism and hyperglycemia. *Am. J. Clin. Nutr.* **2008**, *87*, 217S–222S. [CrossRef]
13. Cavero-Redondo, I.; Martínez-Vizcaíno, V.; Álvarez-Bueno, C.; Recio-Rodríguez, J.I.; Gómez-Marcos, M.Á.; García-Ortiz, L. Relationship between glycaemic levels and arterial stiffness in non-diabetic adults. *Med. Clin.* **2018**, *150*, 56–60. [CrossRef]

14. American Diabetes Association. Standards of medical care in diabetes—2010. *Diabetes Care* **2010**, *33* (Suppl. S1), S11–S61. [CrossRef]
15. American Diabetes Association Professional Practice Committee. 2. Diagnosis and Classification of Diabetes: Standards of Care in Diabetes—2024. *Diabetes Care* **2024**, *47* (Suppl. S1), S20–S42. [CrossRef]
16. Gómez-Sánchez, M.; Patino-Alonso, M.C.; Gómez-Sánchez, L.; Recio-Rodríguez, J.I.; Rodríguez-Sánchez, E.; Maderuelo-Fernández, J.A.; García-Ortiz, L.; Gómez-Marcos, M.A.; EVA Group. Reference values of arterial stiffness parameters and their association with cardiovascular risk factors in the Spanish population. The EVA Study. *Rev. Esp. Cardiol. (Engl. Ed.)* **2020**, *73*, 43–52. [CrossRef]
17. Martagón, A.J.; Fermín-Martínez, C.A.; Antonio-Villa, N.E.; Mehta, R.; Almeda-Valdés, P.; Vargas-Vázquez, A.; Muñoz-Hernández, L.; Gómez-Velasco, D.V.; Elías-López, D.; Galán-Ramírez, G.A.; et al. Arterial Stiffness and HbA1c: Association Mediated by Insulin Resistance in Hispanic Adults. *Int. J. Environ. Res. Public. Health* **2022**, *19*, 11017. [CrossRef]
18. Negre-Salvayre, A.; Salvayre, R.; Augé, N.; Pamplona, R.; Portero-Otín, M. Hyperglycemia and glycation in diabetic complications. *Antioxid. Redox Signal.* **2009**, *11*, 3071–3109. [CrossRef]
19. Liu, J.; Pan, S.; Wang, X.; Liu, Z.; Zhang, Y. Role of advanced glycation end products in diabetic vascular injury: Molecular mechanisms and therapeutic perspectives. *Eur. J. Med. Res.* **2023**, *28*, 553. [CrossRef]
20. Lutgers, H.L.; Graaff, R.; Links, T.P.; Ubink-Veltmaat, L.J.; Bilo, H.J.; Gans, R.O.; Smit, A.J. Skin autofluorescence as a noninvasive marker of vascular damage in patients with type 2 diabetes. *Diabetes Care* **2006**, *29*, 2654–2659. [CrossRef]
21. Monnier, V.M. Nonenzymatic glycosylation, the Maillard reaction and the aging process. *J. Gerontol.* **1990**, *45*, B105–B111. [CrossRef]
22. Dyer, D.G.; A Dunn, J.; Thorpe, S.R.; E Bailie, K.; Lyons, T.J.; McCance, D.R.; Baynes, J.W. Accumulation of Maillard reaction products in skin collagen in diabetes and aging. *J. Clin. Investig.* **1993**, *91*, 2463–2469. [CrossRef]
23. Genuth, S.; Sun, W.; Cleary, P.; Sell, D.R.; Dahms, W.; Malone, J.; Sivitz, W.; Monnier, V.M.; DCCT Skin Collagen Ancillary Study Group. Glycation and carboxymethyllysine levels in skin collagen predict the risk of future 10-year progression of diabetic retinopathy and nephropathy in the diabetes control and complications trial and epidemiology of diabetes interventions and complications participants with type 1 diabetes. *Diabetes* **2005**, *54*, 3103–3111. [CrossRef]
24. Meerwaldt, R.; Links, T.; Graaff, R.; Thorpe, S.R.; Baynes, J.W.; Hartog, J.; Gans, R.; Smit, A. Simple noninvasive measurement of skin autofluorescence. *Ann. N. Y. Acad. Sci.* **2005**, *1043*, 290–298. [CrossRef]
25. Ahmad, M.S.; Kimhofer, T.; Ahmad, S.; AlAma, M.N.; Mosli, H.H.; Hindawi, S.I.; Mook-Kanamori, D.O.; Šebeková, K.; Damanhouri, Z.A.; Holmes, E. Ethnicity and skin autofluorescence-based risk-engines for cardiovascular disease and diabetes mellitus. *PLoS ONE* **2017**, *12*, e0185175. [CrossRef]
26. Saz-Lara, A.; Cavero-Redondo, I.; Pascual-Morena, C.; Martínez-García, I.; Rodríguez-Gutiérrez, E.; Lucerón-Lucas-Torres, M.; Bizzozero-Peroni, B.; Moreno-Herráiz, N.; Martínez-Rodrigo, A. Early vascular aging as an index of cardiovascular risk in healthy adults: Confirmatory factor analysis from the EVasCu study. *Cardiovasc. Diabetol.* **2023**, *22*, 209. [CrossRef]
27. Lee, H.; Cashin, A.G.; Lamb, S.E.; Hopewell, S.; Vansteelandt, S.; VanderWeele, T.J.; MacKinnon, D.P.; Mansell, G.; Collins, G.S.; Golub, R.M.; et al. A Guideline for Reporting Mediation Analyses of Randomized Trials and Observational Studies: The AGReMA Statement. *JAMA* **2021**, *326*, 1045–1056. [CrossRef]
28. Skrivankova, V.W.; Richmond, R.C.; Woolf, B.A.R.; Yarmolinsky, J.; Davies, N.M.; Swanson, S.A.; VanderWeele, T.J.; Higgins, J.P.T.; Timpson, N.J.; Dimou, N.; et al. Strengthening the Reporting of Observational Studies in Epidemiology Using Mendelian Randomization: The STROBE-MR Statement. *JAMA* **2021**, *326*, 1614–1621. [CrossRef]
29. Gomez-Sanchez, M.; Gomez-Sanchez, L.; Patino-Alonso, M.C.; Cunha, P.G.; Recio-Rodriguez, J.I.; Alonso-Dominguez, R.; Sanchez-Aguadero, N.; Rodriguez-Sanchez, E.; Maderuelo-Fernandez, J.A.; Garcia-Ortiz, L.; et al. Vascular aging and its relationship with lifestyles and other risk factors in the general Spanish population: Early Vascular Ageing Study. *J. Hypertens.* **2020**, *38*, 1110–1122. [CrossRef]
30. Hametner, B.; Wassertheurer, S.; Kropf, J.; Mayer, C.; Eber, B.; Weber, T. Oscillometric estimation of aortic pulse wave velocity: Comparison with intra-aortic catheter measurements. *Blood Press. Monit.* **2013**, *18*, 173–176. [CrossRef]
31. Salvadé, I.; Schätti-Stählin, S.; Violetti, E.; Schönholzer, C.; Cereghetti, C.; Zwahlen, H.; Berwert, L.; Burnier, M.; Gabutti, L. A prospective observational study comparing a non-operator dependent automatic PWV analyser to pulse pressure, in assessing arterial stiffness in hemodialysis. *BMC Nephrol.* **2015**, *16*, 62. [CrossRef]
32. Weber, T.; Wassertheurer, S.; Rammer, M.; Maurer, E.; Hametner, B.; Mayer, C.C.; Kropf, J.; Eber, B. Validation of a brachial cuff-based method for estimating central systolic blood pressure. *Hypertension* **2011**, *58*, 825–832. [CrossRef]
33. Meerwaldt, R.; Graaff, R.; Oomen, P.H.N.; Links, T.P.; Jager, J.J.; Alderson, N.L.; Thorpe, S.R.; Baynes, J.W.; Gans, R.O.B.; Smit, A.J. Simple non-invasive assessment of advanced glycation endproduct accumulation. *Diabetologia* **2004**, *47*, 1324–1330. [CrossRef]
34. Noordzij, M.J.; Lefrandt, J.D.; Graaff, R.; Smit, A.J. Dermal factors influencing measurement of skin autofluorescence. *Diabetes Technol. Ther.* **2011**, *13*, 165–170. [CrossRef]

35. Tennant, P.W.G.; Murray, E.J.; Arnold, K.F.; Berrie, L.; Fox, M.P.; Gadd, S.C.; Harrison, W.J.; Keeble, C.; Ranker, L.R.; Textor, J.; et al. Use of directed acyclic graphs (DAGs) to identify confounders in applied health research: Review and recommendations. *Int. J. Epidemiol.* **2021**, *50*, 620–632. [CrossRef]
36. Textor, J.; van der Zander, B.; Gilthorpe, M.S.; Liskiewicz, M.; Ellison, G.T. Robust causal inference using directed acyclic graphs: The R package 'dagitty'. *Int. J. Epidemiol.* **2016**, *45*, 1887–1894. [CrossRef]
37. Cortes, T.R.; Faerstein, E.; Struchiner, C.J. Use of causal diagrams in Epidemiology: Application to a situation with confounding. *Cad. Saude Publica* **2016**, *32*, e00103115. [CrossRef]
38. Kubota, Y.; Heiss, G.; MacLehose, R.F.; Roetker, N.S.; Folsom, A.R. Association of Educational Attainment with Lifetime Risk of Cardiovascular Disease: The Atherosclerosis Risk in Communities Study. *JAMA Intern. Med.* **2017**, *177*, 1165–1172. [CrossRef]
39. Hayes, A.F. *Introduction to Mediation, Moderation, and Conditional Process Analysis: A Regression-Based Approach*, 3rd ed.; Guilford Publications: New York, NY, USA, 2022.
40. Preacher, K.J.; Hayes, A.F. Asymptotic and resampling strategies for assessing and comparing indirect effects in multiple mediator models. *Behav. Res. Methods* **2008**, *40*, 879–891. [CrossRef]
41. van Eupen, M.G.; Schram, M.T.; van Sloten, T.T.; Scheijen, J.; Sep, S.J.; van der Kallen, C.J.; Dagnelie, P.C.; Koster, A.; Schaper, N.; Henry, R.M.; et al. Skin Autofluorescence and Pentosidine Are Associated with Aortic Stiffening: The Maastricht Study. *Hypertension* **2016**, *68*, 956–963. [CrossRef]
42. Birukov, A.; Cuadrat, R.; Polemiti, E.; Eichelmann, F.; Schulze, M.B. Advanced glycation end-products, measured as skin autofluorescence, associate with vascular stiffness in diabetic, pre-diabetic and normoglycemic individuals: A cross-sectional study. *Cardiovasc. Diabetol.* **2021**, *20*, 110. [CrossRef]
43. Semba, R.D.; Nicklett, E.J.; Ferrucci, L. Does accumulation of advanced glycation end products contribute to the aging phenotype. *J. Gerontol. A Biol. Sci. Med. Sci.* **2010**, *65*, 963–975. [CrossRef]
44. Goh, S.Y.; Cooper, M.E. Clinical review: The role of advanced glycation end products in progression and complications of diabetes. *J. Clin. Endocrinol. Metab.* **2008**, *93*, 1143–1152. [CrossRef]
45. Greenwald, S.E. Ageing of the conduit arteries. *J. Pathol.* **2007**, *211*, 157–172. [CrossRef]
46. Hosseini, M.S.; Razavi, Z.; Ehsani, A.H.; Firooz, A.; Afazeli, S. Clinical Significance of Non-invasive Skin Autofluorescence Measurement in Patients with Diabetes: A Systematic Review and Meta-analysis. *EClinicalMedicine* **2021**, *42*, 101194. [CrossRef]
47. Reurean-Pintilei, D.; Stoian, A.P.; Salmen, T.; Stoica, R.-A.; Mititelu-Tartau, L.; Lazăr, S.; Timar, B. Associations between Skin Autofluorescence Levels with Cardiovascular Risk and Diabetes Complications in Patients with Type 2 Diabetes. *Biomedicines* **2024**, *12*, 890. [CrossRef]
48. Noordzij, M.J.; Lefrandt, J.D.; Graaff, R.; Smit, A.J. Skin autofluorescence and glycemic variability. *Diabetes Technol. Ther.* **2010**, *12*, 581–585. [CrossRef]
49. Cho, Y.H.; Craig, M.E.; Januszewski, A.S.; Benitez-Aguirre, P.; Hing, S.; Jenkins, A.J.; Donaghue, K.C. Higher skin autofluorescence in young people with Type 1 diabetes and microvascular complications. *Diabet. Med.* **2017**, *34*, 543–550. [CrossRef]
50. Yamagishi, S.; Matsui, T. Pathologic role of dietary advanced glycation end products in cardiometabolic disorders, and therapeutic intervention. *Nutrition* **2016**, *32*, 157–165. [CrossRef]
51. Ruiz, H.H.; Ramasamy, R.; Schmidt, A.M. Advanced Glycation End Products: Building on the Concept of the "Common Soil" in Metabolic Disease. *Endocrinology* **2020**, *161*, bqz006. [CrossRef]
52. Palombo, C.; Kozakova, M. Arterial stiffness, atherosclerosis and cardiovascular risk: Pathophysiologic mechanisms and emerging clinical indications. *Vascul. Pharmacol.* **2016**, *77*, 1–7. [CrossRef]
53. Jennings, A.; Berendsen, A.M.; De Groot, L.C.P.G.M.; Feskens, E.J.M.; Brzozowska, A.; Sicińska, E.; Pietruszka, B.; Meunier, N.; Caumon, E.; Malpuech-Brugère, C.; et al. Mediterranean-Style Diet Improves Systolic Blood Pressure and Arterial Stiffness in Older Adults. *Hypertension* **2019**, *73*, 578–586. [CrossRef]
54. Vitale, M.; Masulli, M.; Calabrese, I.; Rivellese, A.A.; Bonora, E.; Signorini, S.; Perriello, G.; Squatrito, S.; Buzzetti, R.; Sartore, G.; et al. Impact of a Mediterranean Dietary Pattern and Its Components on Cardiovascular Risk Factors, Glucose Control, and Body Weight in People with Type 2 Diabetes: A Real-Life Study. *Nutrients* **2018**, *10*, 1067. [CrossRef] [PubMed]
55. Sánchez, E.; Betriu, À.; Salas-Salvadó, J.; Pamplona, R.; Barbé, F.; Purroy, F.; Farràs, C.; Fernández, E.; López-Cano, C.; Mizab, C.; et al. Mediterranean diet, physical activity and subcutaneous advanced glycation end-products' accumulation: A cross-sectional analysis in the ILERVAS project. *Eur. J. Nutr.* **2020**, *59*, 1233–1242. [CrossRef]
56. Martínez-González, M.A.; García-Arellano, A.; Toledo, E.; Salas-Salvadó, J.; Buil-Cosiales, P.; Corella, D.; Covas, M.I.; Schröder, H.; Arós, F.; Gómez-Gracia, E.; et al. A 14-item Mediterranean diet assessment tool and obesity indexes among high-risk subjects: The PREDIMED trial. *PLoS ONE* **2012**, *7*, e43134. [CrossRef]
57. Funck, K.L.; Laugesen, E.; Høyem, P.; Fleischer, J.; Cichosz, S.L.; Christiansen, J.S.; Hansen, T.K.; Poulsen, P.L. Low Physical Activity Is Associated with Increased Arterial Stiffness in Patients Recently Diagnosed with Type 2 Diabetes. *Am. J. Hypertens.* **2016**, *29*, 882–888. [CrossRef] [PubMed]

58. Ortega, F.B.; Ruiz, J.R.; España-Romero, V.; Vicente-Rodriguez, G.; Martínez-Gómez, D.; Manios, Y.; Béghin, L.; Molnar, D.; Widhalm, K.; Moreno, L.A.; et al. The International Fitness Scale (IFIS): Usefulness of self-reported fitness in youth. *Int. J. Epidemiol.* **2011**, *40*, 701–711. [CrossRef]
59. Hofmann, B.; Adam, A.-C.; Jacobs, K.; Riemer, M.; Erbs, C.; Bushnaq, H.; Simm, A.; Silber, R.-E.; Santos, A.N. Advanced glycation end product associated skin autofluorescence: A mirror of vascular function. *Exp. Gerontol.* **2013**, *48*, 38–44. [CrossRef]
60. Liang, J.; Zhou, N.; Teng, F.; Zou, C.; Xue, Y.; Yang, M.; Song, H.; Qi, L. Hemoglobin A1c levels and aortic arterial stiffness: The Cardiometabolic Risk in Chinese (CRC) study. *PLoS ONE* **2012**, *7*, e38485. [CrossRef]

Disclaimer/Publisher's Note: The statements, opinions and data contained in all publications are solely those of the individual author(s) and contributor(s) and not of MDPI and/or the editor(s). MDPI and/or the editor(s) disclaim responsibility for any injury to people or property resulting from any ideas, methods, instructions or products referred to in the content.

biomedicines

Article

Cellular Characteristics and Protein Signatures of Human Adipose Tissues from Donors With or Without Advanced Coronary Artery Disease

Caitlin P. S. Ellis [1,2], Benjamin W. Tero [1], Christian M. Potts [1], Kimberly T. Malka [1], Xuehui Yang [1], Joshua Hamilton [2,3], Calvin Vary [1,2], Andre Khalil [2,3] and Lucy Liaw [1,2,*]

[1] MaineHealth Institute for Research, Scarborough, ME 04074, USA; caitlin.stieber@maine.edu (C.P.S.E.); benjamin.tero@mainehealth.org (B.W.T.); christian.potts@mainehealth.org (C.M.P.); kimberly.malka@mainehealth.org (K.T.M.); xuehui.yang@mainehealth.org (X.Y.); calvin.vary@mainehealth.org (C.V.)
[2] Graduate School of Biomedical Science and Engineering, University of Maine, Orono, ME 04469, USA; joshua.hamilton@maine.edu (J.H.); andre.khalil@maine.edu (A.K.)
[3] CompuMAINE Lab, Department of Chemical and Biomedical Engineering, University of Maine, Orono, ME 04469, USA
* Correspondence: lucy.liaw@mainehealth.org; Tel.: +1-207-396-8142

Abstract: Background/Objectives: Perivascular adipose tissue (PVAT) exerts a paracrine effect on blood vessels and our objective was to understand PVAT molecular signatures related to cardiovascular disease. **Methods**: We studied two groups: those undergoing mitral valve repair/replacement (VR, n = 16) and coronary artery bypass graft (CABG, n = 38). VR donors did not have coronary artery disease, whereas CABG donors had advanced coronary artery disease. Clinical and tissue pathologies and proteomics from adipose tissue were assessed. **Results**: Donors undergoing VR had a lower body mass index ($p = 0.01$), HbA1C ($p = 0.0023$), and incidence of diabetes ($p = 0.022$) compared to CABG. VR donors were overall healthier, with higher cardiac function compared to CABG donors, based on ejection fraction. Although adipose histopathology between groups was not markedly different, PVAT had smaller and more adipocytes compared to subcutaneous adipose tissues. These differences were validated by whole specimen automated morphological analysis, and anisotropy analysis showed small (2.8–7.5 μm) and large (22.8–64.4 μm) scale differences between perivascular and subcutaneous adipose tissue from CABG donors, and small scale changes (2.8–7.5 μm) between perivascular and subcutaneous adipose tissue from VR donors. Distinct protein signatures in PVAT and subcutaneous adipose tissue include those involved in secretion, exosomes and vesicles, insulin resistance, and adipocyte identity. Comparing PVAT and subcutaneous adipose tissue from CABG donors, there were 82 significantly different proteins identified with log fold change ≥ 0.3 or ≤ -0.3 ($p < 0.05$). Using this threshold, there were 36 differences when comparing PVAT and subcutaneous adipose tissue from VR donors, 58 differences when comparing PVAT from CABG or VR donors, and 55 when comparing subcutaneous adipose tissue from CABG vs. VR donors. **Conclusions**: Routine histopathology cannot differentiate between PVAT from donors with or without coronary artery disease, but multiscale anisotropy analysis discriminated between these populations. Our mass spectrometry analysis identified a cohort of proteins that distinguish between adipose depots, and are also associated with the presence or absence of coronary artery disease.

Keywords: human adipocyte; perivascular adipose tissue; coronary artery disease; proteomics; metabolism

1. Introduction

Cardiovascular disease (CVD) is the leading cause of death globally [1]. Obesity, diabetes mellitus, and metabolic disease increase the risk of cardiovascular disease [2].

These diseases present a significant strain on the medical system. Adipose tissue, which is comprised of immune cells, nerves, fibroblasts, and vessels, plays a key systemic role in these diseases due to its function as an endocrine and metabolic tissue [3]. We are focused on perivascular adipose tissue (PVAT) within the vascular microenvironment, as paracrine signaling regulates vascular function, and local changes can lead to systemic impacts.

PVAT is contiguous with the blood vessel adventitia and contributes cells and adipokines to the vessel wall [4,5]. In healthy individuals, PVAT secretes factors that decrease smooth muscle cell proliferation and increase relaxation of the smooth muscle, leading to normal lumen diameter and proper blood flow [6]. In the case of metabolic diseases such as obesity and diabetes, PVAT is expanded and altered secretory profiles lead to increased proliferation and contraction of the underlying smooth muscle, leading to a decreased lumen diameter and restricted blood flow [7,8]. Increased blood pressure is a risk factor for other cardiovascular outcomes, such as myocardial infarctions, strokes, and death [9]. We are interested in characterizing PVAT from a variety of donor populations in an attempt to understand and identify the specific factors that lead to the phenotypic change of PVAT.

There are three molecularly and functionally distinct types of adipose tissue—white, brown, and beige. White adipose tissue (WAT) primarily functions as lipid storage, with some endocrine effects [10]. WAT exists adjacent to the skin as subcutaneous (SubQ) fat, in the abdomen as visceral adipose tissue, and in the bone marrow. A recent study has described molecular features of white adipose tissues in mice and humans [11]. The primary function of brown adipose tissue (BAT) is heat production through non-shivering thermogenesis [12]. BAT is found in the interscapular region and the kidneys and expresses thermogenic markers such as UCP1 and GRP75. Activation of BAT has long been a research focus due to its capacity as a glucose sink and its role in insulin sensitivity [13]. In mice, it has been shown that adipose tissues have more brown adipocytes in response to injury, cold, and ß-adrenergic signaling, a process known as beiging [14]. Although morphologically, human PVAT appears like WAT, we are interested in the concept that human PVAT may have thermogenic qualities and can be stimulated to improve cardiovascular function or suppress disease. Indeed, some human adipose tissue, including human epicardial tissue, has been reported to have a beige or brown adipocyte profile [15,16], and we have reported similar evidence for human PVAT [17,18].

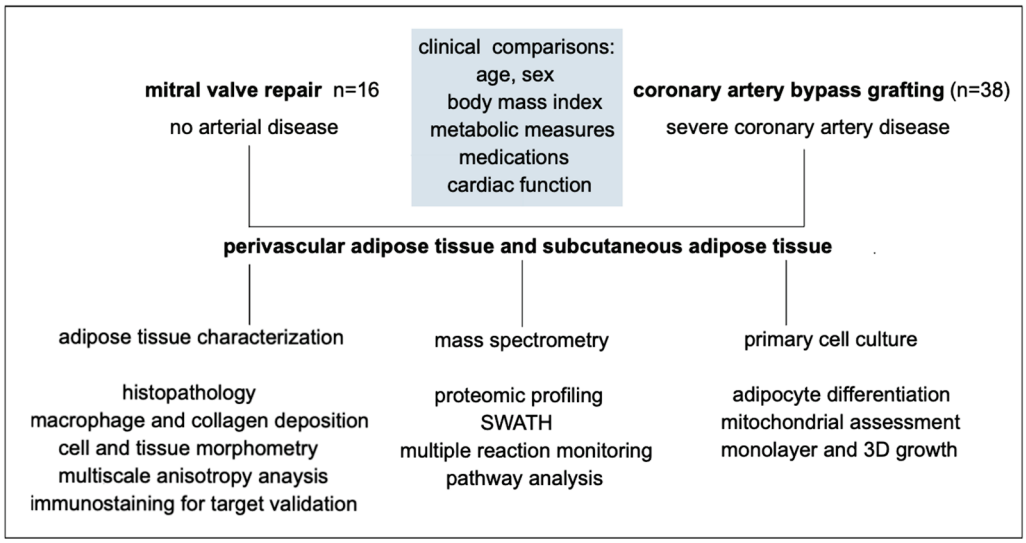
Our study was designed to test the hypothesis that human aortic PVAT associated with advanced coronary artery disease will be molecularly distinct from aortic PVAT from donors without coronary artery disease. Our objective was to define unique proteomic profiles in different adipose depots from the unique donor types studied. Our prediction was that PVAT from donors without atherosclerosis undergoing VR would represent more of a homeostatic phenotype, whereas PVAT from donors in the CABG group would reflect changes associated with metabolic dysfunction correlating with their vascular pathology.

Much of what is known about PVAT was defined in mice and other rodent models [4]. However, PVAT research in humans is rapidly growing. It has been shown that increased PVAT mass corresponds to increased atherosclerosis [19]. With regard to coronary artery disease, adipose tissue overlying the heart (peri-coronary) as well as PVAT adjacent to the aorta may impact coronary disease, in part due to secretion of pro-inflammatory cytokines [20]. Other related pathologies of coronary arteries, including coronary artery spasm has also been linked to PVAT inflammatory state [21]. Additionally, Shi et al. [22] characterized PVAT, subcutaneous, and epicardial adipose tissue in donors from the same cardiovascular disease groups presented here, undergoing VR or CABG surgeries. However, our populations differ demographically, leading to differences in experimental results. Specifically, Shi et al. [22] found no difference in body mass index between their groups and found increased fibrosis in PVAT compared to subcutaneous adipose tissue. We found that CABG donors have a significantly higher body mass index than VR donors and have found no differences in fibrotic tissue between disease and tissue types. Lastly, we have expanded upon this previous work through proteomics techniques to identify unique targets that

distinguish between donor types and adipose tissue locations, and investigated the effect of diabetes in these tissues.

2. Materials and Methods

The overall experimental workflow is shown below:



Sample collection. This work was approved by IRB# 1295440-3 at the MaineHealth Institute for Research. Donors were recruited from two groups undergoing open thoracic surgeries, either coronary artery bypass graft (CABG, n = 38) or mitral valve repair/replacement (VR, n = 16) surgeries. The groups were distinguished by the severity of coronary artery disease, where CABG donors had more atherosclerotic vessels than VR donors (Table 1). Our VR donors did not have diagnosed coronary artery disease, which was distinct from donors requiring CABG surgery due to advanced coronary artery disease. Because of this distinction, the VR group was considered the control group, and our experimental CABG group donors all had coronary artery disease. We documented written consent from tissue donors after sharing information about the research project and the request for collection of tissue that would otherwise be discarded. All samples were deidentified, and research staff had no access to the clinical information, which was maintained by the surgeon. Human perivascular adipose tissue (PVAT) and subcutaneous adipose tissue (SubQ) were collected from donors undergoing coronary artery bypass graft (CABG, n = 38) and mitral valve repair (VR, n = 16) surgeries. SubQ tissue was taken from the incision site and PVAT was collected from ascending aortae. Tissue processing was started within 4 h after collection. Because of the limitation of sample size available, we performed downstream analyses with a representative subset of samples as indicated in figure legends.

Tissue processing. Tissue was processed, as described by Scott et al. [23], and was divided for histology, immunostaining, proteomics, and preadipocyte isolation. The amount of tissue was variable depending on initial sample size, and the order of prioritization was histology/immunostaining, preadipocyte isolation, SWATH, and multiple reaction monitoring proteomics. Samples were processed for paraffin embedding or frozen embedding. For the former, samples were fixed overnight in 10% formalin, washed three times in PBS, and stored in 70% ethanol at 4 °C until processing. Tissue dehydration and paraffin embedding were performed in our Histopathology and Microscopy core facility. Tissue was fixed in 10% formalin overnight, washed three times in PBS, and placed in 70% EtOH at 4 °C. Samples were processed for paraffin embedding and sectioning. Sections were stained with hematoxylin and eosin (H&E), Masson's trichrome stain, imaged at 200x magnification, and analyzed with FIJI 2.9.0 H&E sections were analyzed using the

AdipoSoft 1.6 extension [24]. Immunostaining was analyzed with color deconvolution using the H-dab and Masson's trichrome features in FIJI.

For frozen sections, tissues were fixed in 10% formalin, and fixed tissue samples were incubated in 15% sucrose for 4 to 6 h, and then in 30% sucrose overnight at 4 °C. Samples were embedded in O.C.T compound (SAKURA Finetek, Torrance, CA, USA, cat# 4583) on dry ice, then subjected for cryosection at 7 μm thickness.

For immunofluorescence staining of frozen sections, slides were baked at 60 °C for 2 h, fixed with 10% formalin for 10 min, and then subjected to antigen retrieval using citrate buffer (10 mM citrate buffer containing 0.01% lithium dodecyl sulphate, pH = 6.6) for 5 min. Samples were incubated in 5% goat serum in PBS and 0.1% Triton-X for 1 h at room temperature. Co-immunofluorescence staining was performed by incubation with antibodies against UCP1 (R&D Biosystem, Minneapolis, MN, USA, cat# MAB6158, Lot CCNV0218031, 1:50 (10 μg/mL), Perilipin 1 (Cell Signaling Technology, Danvers, MA, USA, cat# 9349, lot 5, 1:100), Rab27a (Cell Signal Technology, cat# 69295, lot 2, (1.5 μg/mL), and Notch3 (Abcam, Waltham, MA, USA, cat# ab223426, lot 1059086-1 (4.5 μg/mL) at 4 °C overnight, followed by goat FITC-anti-mouse IgG (Vector Laboratories, Newark, CA, USA, cat# FI-2001, lot Y0118, 1:100), Alexa fluor 647-anti-mouse IgG (Invitrogen, Carlsbad, CA, USA, cat# A32728, 1:100), Alexa fluor 647-anti-Rabbit IgG (Molecular Probes, cat# A21244, lot 99E2-1, 1:100), and Alexa fluor 488-anti-Rabbit IgG (Invitrogen, cat# A11008, 1:100. Normal mouse IgG1 or rabbit IgG (Cell Signaling Technology, cat# 5415, lot 10, or cat# 3900, lot 50, respectively), used accordingly for control staining. Nuclei were stained with DAPI. Images were captured using a Leica SP8 confocal microscope.

Samples for preadipocyte isolation were washed in HBSS with 2x antibiotic/antimycotic solution prior to processing. Samples for proteomics were stored frozen at −80 °C prior to processing.

Histological staining and analysis. Tissue sections were stained with H&E or Masson's trichrome stain. Slides were placed in hematoxylin (Richard-Allan Scientific, Kalamazoo, MI, USA, cat# 7231) for 10 min at room temp and washed in tap water until clear. Slides were then placed in 5% acetic acid for 1 min and washed in tap water, followed by Bluing Agent (Richard-Allan cat# 7301) for 2 min and a tap water wash. Slides were placed in 95% EtOH for 1 min, stained in Eosin Y (Richard-Allan cat# 7111) for 2 min and rinsed in two 95% EtOH washes for 30 s each. Tissues were dehydrated in three changes of 100% EtOH, cleared, and mounted with synthetic resin (Permount, Electron Microscopy Sciences, Hatfield, PA, USA).

For Masson's trichrome stain, 40 mL of Bouin's fixative (Newcomer Supply, Middleton, WI, USA, cat# 1020A) was placed in a coplin jar and heated in the microwave for 30 s. Sections were placed in heated solution for 20 min, allowed to cool, and rinsed in running tap water for 10 min. Sections were stained in Weigert's hematoxylin (Richard-Allan cat# 7231) for 10 min. Samples were washed in water for 10 min and stained in Biebrich's scarlet-acid fuchsin (EKI, Joliet, IL, USA, cat# 26905) for 10 min. Samples were washed for 10 min and stained in phosphotungstic/phosphomolybdic (Sigma-Aldrich, St. Louis, MO, USA, cat# MKCT3045) solution for 10 min. Slides were placed in aniline blue solution (Newcomer, cat# 10073C) for 10 min, rinsed in tap water, and placed in 1% acetic acid for 3–5 min. Samples were washed in water for 1 min, 95% EtOH for 1 min, dehydrated, and mounted with synthetic resin.

H&E sections were imaged at 200x and analyzed using the AdipoSoft extension in FIJI. Ten fields of view per sample were imaged and analyzed for adipocyte size, number, and stromal area.

Sliding Window and Anisotropy Analysis (see also Appendix A). H&E sections were imaged on the Keyence BZ-X810 microscope at 20x magnification. Images were then loaded into the scikit-image (ver 0.22.0) library in Python (ver 3.10). Each whole slide image (WSI) underwent a color transformation into hue, saturation, and value from RGB. The saturation channel was made into a black and white binary mask using the Otsu automated thresholding method. This created a tissue mask, in which a bounding box divisible by

1024 was fit to contain the entire mask. The top left corner of the bounding box was used as the top left coordinate to begin the sliding window analysis. The sliding window consisted of 1024 × 1024 pixel subregions from the original RGB WSI and were slid across the image in 256-pixel x-coordinate increments until meeting the right edge of the bounding box. The y-coordinate window was then shifted down a 256-pixel increment and the process continued until reaching the bottom right coordinate of the bounding box.

Each subregion was first color transformed to hue, saturation, value, and the saturation channel used for segmentation of adipocytes. The segmentation began with a 3-pixel Gaussian blur into a Triangle threshold on the saturation channel from the color transformed subregion creating a binary foreground and background image. This resulted in stained material as background and unstained material as foreground, allowing for watershed segmentation of white adipose tissue. Any objects touching the border were removed.

The following thresholds, determined from manual inspections, were used to remove gaps in stromal tissue, vessels, ducts, or low-quality stained adipocytes from the segmentation thereby ensuring inclusion of only whole adipocytes. Any objects with an area larger than 3674 μm (9000 pixels) and smaller than 653.2 μm (1600 pixels) were removed. Objects with areas greater than 10,206 μm, 25,000 pixels, and were highly eccentric (>0.87) were removed as well as any object with a perimeter to area ratio of 0.14 or greater. After all these thresholds, if the area of the subregion was occupied by at least 30% segmented objects, every object's x-centroid, y-centroid, eccentricity, area, perimeter, long-axis, and short-axis were saved into a comma-separated-value (CSV) file to calculate morphometrics. Saved objects whose centroids were within a 12.7 μm (31 pixel) radius of each other were randomly removed until only one remained preventing oversampling of the same adipocyte from the overlapping sliding window analysis. Morphological analysis for area, solidity, circularity, and eccentricity was performed. Subregions that passed all these requirements and had minimal (<20%) overlap with previously saved subregions were also saved as patches for anisotropy analysis.

A custom Python implementation of the 2D Wavelet Transform Modulus Maxima Anisotropy method was used to probe the organization of adipose tissue from these patches at a range of different size scales [25–27]. Critically important observations can be missed when using a computational image analysis tool that only considers a single scale (or a single frequency, if using a Fourier-based method) and the 2D WTMM Anisotropy method overcomes this by acting as a "mathematical microscope" through utilization of continuous wavelet transforms. The method was developed in the context of astrophysics and has since been ported to multiple biological contexts including collagen, soft-tissue in growth, nerves, and most recently, cancer [25–29]. This is the first application of the technique on H&E-stained adipose tissue. The adipocyte morphometrics and anisotropy measurements were calculated and tested using Wilcoxon ranked sum between all four groups (VR PVAT vs. VR SubQ, CABG PVAT vs. CABG SubQ, VR PVAT vs. CABG PVAT, and VR PVAT vs. VR SubQ).

Immunostaining. Sections were deparaffinized and rehydrated. Tissue was outlined with a PapPen, dried, and rinsed in tap water. Antigen retrieval was done as specified for each antibody by the data sheet. The slides were rinsed twice in PBS and twice in TBS-T (Tris buffered saline, pH = 7.6, with 0.05% Tween). Slides were blocked in 2% normal serum blocking buffer (secondary host serum, 1% BSA) for 30 min at room temperature and washed twice in TBS-T. Slides were then blocked with the A/B kit (Vector, Cat.# SP2001) and washed in TBS-T twice. Slides were incubated with primary antibody (MAC1, Abcam, cat.#ab133357) overnight at 4 °C. Slides were washed four times with TBS-T and incubated with secondary antibody diluted in PBS. Slides were washed three times in TBS-T, blocked with endogenous peroxidase with 3% H_2O_2 in PBS, and washed in TBS-T twice. Samples were incubated with ABC amplification reagent (Vector, Cat.# PK6100) and washed in TBST four times. Slides were incubated in working 3,3′-Diaminobenzidine (Sigma, F8764-5G), washed in tap water, dehydrated, cleared, and mounted.

Stromal vascular fraction isolation. The stromal vascular fraction was isolated according to the procedure in Scott et al. 2019 [23]. Briefly, adipose tissues were washed in HBSS with 2x antibiotic/antimycotic solution, digested in collagenase (Millipore, Burlington, MA, USA, cat# 11088815001), spun down at 500× *g* for 8 min, and plated on a gelatin coated plate, typically, a 12 well plate. Cells were incubated in a humidified chamber at 37 °C and 5% CO_2. Cells were fed every four days with growth media (DMEM/F12, 10% FBS, 1x antibiotic/antimycotic) and split at ~95% confluence (1:2, and passage number recorded). Propagated cells were cryopreserved and utilized for downstream characterization.

Lipid Detection. Fixed cells were brought to room temperature and incubated with 1:200 dilution (concentration is proprietary, I called Invitrogen) of LipidTOX 488 (Invitrogen, Cat.# H34475) and 2.5 μg/μL concentration of DAPI (Invitrogen, Cat.# D1306) for 1 h at room temperature. The cells were washed three times in PBS and stored at 4 °C. Cells were brought to room temperature, placed in fresh PBS and imaged on the LI-Cor (Lincoln, NE, USA) Odyssey-M Imager and Keyence (Itasca, IL, USA) BZ-X810 microscope using the 488 cube filter and UV filter. Three full wells per sample were imaged at 20x magnification. Images were quantified using FIJI for intensity of LipidTOX stain per nuclei.

Table 1. The components of adipocyte differentiation media.

Factor	Concentration	Media Type
DMEM/F-12 (50/50) (Corning, Corning, NY, USA, cat# 10-0920-CV)	1x	Induction/maintenance
Heat inactivated-FBS (R&D systems, cat# S11550H)	1x	Induction/maintenance
Antibiotic and antimycotic (Corning, cat# 30-0040-CL)	1x	Induction/maintenance
Insulin (Sigma, cat# 91077C-250 mg)	170 nM	Induction/maintenance
T3 (Sigma, cat# TG397)	2 nM	Induction/maintenance
Rosiglitazone (Sigma, cat# R2408)	1 μM	Induction/maintenance
IBMX (Sigma, cat# R2408)	0.5 mM	Induction
Dexamethasone (Sigma, cat# D4902)	5 μM	Induction
Indomethacin (Sigma, cat# I8280)	125 μM	Induction
TGF-β RI Kinase Inhibitor VI (Cell Signaling, cat# 14775)	5 μM	Induction/maintenance
L-Ascorbic acid 2-phosphate sesquimagnesium salt hydrate (Sigma, cat# A8960)	50 μg/ml	Induction/maintenance

Data visualization and statistical analysis. Anisotropy was visualized using a Python library. Statistical analysis was done with a Wilcox or Mann–Whitney *t*-test. GraphPad Prism (version 10) was used for all other student t-tests and two-way ANOVA analysis, as well as a graphic visualization of quantifiable data.

Mass spectrometry and proteomics analysis. Samples were prepared as described by Rappsilber et al. [30]. Briefly, samples cooled to room temperature, alkylated, and protein precipitated. Pellets were washed in ethanol, centrifuged, and suspended. Digested proteins evaporated and were subjected to solid phase extraction on C18 resin. Purified peptides were eluted into autosampler vials and resuspended in a volume of sample load solvent (5% formic acid (Optima grade, ThermoFisher Scientific, Waltham, MA, USA) and 4% acetonitrile (LC-MS-grade, Honeywell, Morris Plains, NJ, USA) to yield ~1 μg/μL peptides.

Chromatography/Mass spectrometry. Tandem mass spectrometric analysis was performed on an Eksigent NanoLC 425 nano-UPLC System (Sciex, Framingham, MA, USA) in direct-injection mode with a 5 μL sample loop. Fractionation was performed on a reverse-phase nano HPLC column (Acclaim PepMap 100 C18, 75 μm × 150 mm, 3 μm particle, 120 Å pore) held at 45 °C with a flow rate of 350 nL/min.

Analysis was performed in positive ion mode on a TripleToF 5600 quadrupole time-of-flight (QToF) mass spectrometer (Sciex, Framingham, MA, USA). The column eluate was directed to a silica capillary emitter (SilicaTip, 20 μm ID, New Objective, Littleton, MA, USA) maintained at 2500 V. A parent ion scan was acquired, followed by MS/MS analyses of the 50 most-intense ions detected in the parent ion scan. SWATH MS/MS windows of variable widths, 100 in total, were generated using a variable-window calculator (Sciex).

Fragmentation conditions were optimized for ions of a 2+ charge state. SWATH detection parameters were set to a mass range of m/z = 100–1500 with accumulation times of 50 msec in the high-sensitivity mode.

Proteomics Data analysis. Protein identification was performed using Protein Pilot software (Sciex, Version 5.0.2) running the Paragon algorithm. Data were searched against a human proteome database on the Uniprot website. Searches were performed with cysteines modified (iodoacetamide). A target false discovery rate of 0.05 and a thorough ID search effort was selected. A minimum of 95% confidence was used as a threshold for peptide identification. Relative quantification was performed using the SWATH processing microApp in the Sciex PeakView ver 2.2 software. Peak groups were extracted with a 99% peptide confidence threshold and 1% peptide FDR limit. SWATH chromatograms were extracted in 10-min windows with fragment ion mass tolerance set to 75 ppm. Resulting protein quantitative peak areas were further analyzed using MarkerView software (Version 1.3.1, Sciex LLC, Framingham, MA, USA) to compare relative quantities of all detected proteins between samples. Statistical analyses, including *t*-tests and principal component analyses, were completed for data sets using Sciex MarkerView ver 1.3.1 software. Significantly different proteins were determined via *t*-test ($p < 0.05$). In STRING db, a minimum required interaction score of 0.9 was used (highest confidence) and GO terms were sorted based on *p*-value and FDR. Only proteins that were statistically different in levels between comparison groups are listed in the Supplemental Tables. Raw data are in the PRIDE repository under reference number 1-20240423-213918-2242764, accession number PXD051676.

Multiple Reaction Monitoring (MRM) Proteomics. Peptides were prepared as above and subjected to LC/MS and MS/MS fragments (Q1 and Q3 transmission, respectively) (Sciex (Framingham, MA, USA) 6500+ triple quadrupole mass spectrometer). Candidate peptides for MRM detection and quantitation were selected either from primary data acquired by SWATH acquisition using a high resolution quadrupole TripleToF 6600+ system and Eksigent (Dublin, CA, USA) Ekspert 425 liquid chromatograph as described above, or by using the human MRM library on the SRMAtlas utility [31]. For SRMAtlas selection of candidate Sciex QTRAP SRM, Q1 and Q3 ions were chosen from the Human SRMAtlas 2024-01 build, with Target instrument set to QTRAP5500, and y- and b-ions without modifications. Peptides were resolved using a custom hand-made C18 reverse-phase column with a 1.7 µL per minute flow rate and a 10–80% ACN/0.1% FA gradient. MRM was conducted in positive ion mode recommended by SRMAtlas. Results were sorted based on a *p*-value of <0.05, a log fold change of ≤ -0.3 or ≥ 0.3, and visualized using R version 4.3.2.

Immunoblotting. Tissue and cell samples were digested in a RIPA buffer with a protease inhibitor, spun down at 12,800$\times$ *g* for 10 min, and the supernatant was saved. The protein concentration was assessed using the DC protein assay (cat.#) and samples were diluted with a Laemmli buffer. Samples were run on 12% gels at 120 volts until the protein front reached the bottom, transferred using a semidry transfer at 1.5 amps for 30 min, and were blocked in 5% milk in TBS-T for 1 h at room temperature. Samples were placed in a primary antibody (insert table) overnight up to 72 h, washed, and in secondary at 1:1000 for 2 h at room temperature, before digital detection with forte HRP substrate.

Preadipocyte 3D Spheroid Culture and Differentiation. Cells were dissociated using 0.25% trypsin/EDTA (Gibco 65200-056) for 5 minutes, neutralized with growth media and centrifuged at 500$\times$ *g* for 8 min. An amount of 10,000 cells were plated into each well of a 96-well round bottom spheroid plate (NunclonSphera 174925, BioFloat F202003) by diluting to 200,000 cells/mL and adding 50 uL to each well. An additional 50 uL of growth media was added to each well. Cells were incubated for three days to allow spheroid formation. On day three, media was removed around spheres using manual pipetting, 100 uL of induction media (Table 1) was added to cells for differentiation, and growth media was added to control cells. Cells were incubated for three more days, at which point the differentiated cells were changed into maintenance media (Table 1). Regular media changes occurred every Monday and Friday for the duration of the experiment. At ten

days, one batch of differentiated cells with controls were moved into an Eppendorf tube, fixed in 10% Formalin, and washed in PBS, then stored at 4 °C. The rest of the cells were differentiated for a total of eighteen days, before being moved into an Eppendorf tube, fixed with 10% Formalin, washed in PBS, and stored at 4 °C.

Oil Red O Staining of Spheroid Adipocyte Cultures. Spheres were removed from storage Eppendorf tubes into new tubes for staining and were blocked using a solution of 0.2% Triton X-100, 3% BSA, and PBS for 40 min at room temperature. Blocking solution was then removed and the cells were stained in a solution of 2.5µg/µL DAPI (Invitrogen, Cat. # D1306) and a 1:40 dilution of Phalloidin 488 (Invitrogen A12379) in blocking solution for 1 h at room temperature. Spheres were then washed three times in PBS before being stained in a solution of six parts of 50 mg/mL Oil Red O (Sigma Aldrich #O0625) in 6 mL water and four parts water for 2 h at room temperature. Spheres were then washed in a solution of six parts isopropanol and four parts water quickly, before subsequent washing in water until red color was removed. Stained spheres were mounted in water in a glass bottom petri dish and imaged using a Leica SP8 confocal microscope using a 20x magnification objective.

3. Results

3.1. Distinct Clinical and Physiological Features of Patients with Coronary Artery Disease

Adult patients undergoing target surgeries were consented for sample collection; multiple concurrent surgeries led to exclusion. Adipose tissue was taken from two populations, those undergoing mitral valve repair (VR) or coronary artery bypass graft (CABG) surgery. Table 2 summarizes their demographic information (see also Supplemental Table S1). The median age was not different between surgical groups, 66 and 70.5 for VR and CABG, respectively. The proportion of donors on lipid lowering (and anti-hypertension drugs) also did not significantly differ between groups. However, 33.3% of VR patients were on lipid lowering drugs compared to 81.1% of the VR group. Additionally, 56.3% of VR donors are on anti-hypertension drugs, compared to 76.3% of CABG donors. Body mass index (25.26 vs. 29.96), HbA1c (5.45 vs. 5.90), incidence of diabetes (6.25% vs. 36.8%), and donors on anti-diabetic medication (6.25% vs. 37.8%) were all lower in the VR donors compared to CABG donors. CABG donors had more vessels on average that had atherosclerotic legions compared to VR donors. CABG patients also had a lower ejection fraction. Overall, these data indicate that the VR donor group were healthier compared to the CABG donor group.

Table 2. A comparison of donor populations. Lipid-lowering medications include low to high intensity statins such as atorvastatin, rosuvastatin, and simvistatin. Anti-hypertensive medications include linisopril, amlodipine, metoprolol, digoxin, hydrochlorothiazide, torsemide, warfarin, nifedipine, diltiazem, torsemide, acetaminophen, and amiodarone. Additional data are in Supplemental Table S1. ns = not significant.

	VR	CABG	*p* Value
Total sample (female)	16 (5)	38 (3)	
Median age (variance)	66 (14.5)	70.5 (13.5)	ns
Median body mass index (variance)	25.3 (4.9)	30 (8.32)	0.01
Median HbA1c (variance)	5.45 (0.48)	5.9 (1.45)	0.0023
Median # atherosclerotic vessels (variance)	0 (1.1)	3 (2.1)	2.24×10^{-7}
Donors with diabetes	1 (6.3%)	14 (36.8%)	0.022
Donors on anti-diabetic medication	5 (33.3%)	30 (81.1%)	0.022
Donors on lipid lowering drugs	5 (33.3%)	30 (81.1%)	ns
Number on anti-hypertension drugs	9 (56.3%)	29 (76.3%)	ns
Overall ejection fraction			0.043
Ejection fraction > 55%	13 (81.2%)	22 (59.5%)	
Ejection fraction 50–55%	3 (18.8%)	2 (5.4%)	
Ejection fraction 40–50%	0	8 (24.3)	
Ejection fraction 30–40%	0	1 (2.7%)	
Ejection fraction < 30%	0	3 (8.1%)	

3.2. Morphological and Protein Expression Differences in PVAT and SubQ Point to Changes in Adipose Functionality

Given the demographic differences between donor groups, we were interested in assessing differences in their adipose tissue. We examined the histopathology of the tissue by analyzing adipose morphology, tissue fibrosis, and macrophage infiltration (Figure 1A–C). Adipocyte size, number, and stromal area were quantified using AdipoSoft in FIJI. In all three measures, there were no significant differences between conditions (VR vs. CABG). However, within each disease condition, PVAT had more adipocytes that were smaller compared to those in subcutaneous adipose tissue. In the VR group, PVAT had a median of 5.72 adipocytes per 1×10^5 μm^2 compared to 3.26 adipocytes per 1×10^5 μm^2 in VR SubQ. In the CABG group, PVAT had a median of 5.10 adipocytes per 1×10^5 μm^2 compared to 3.16 adipocytes per 1×10^5 μm^2 in subcutaneous adipose tissue.

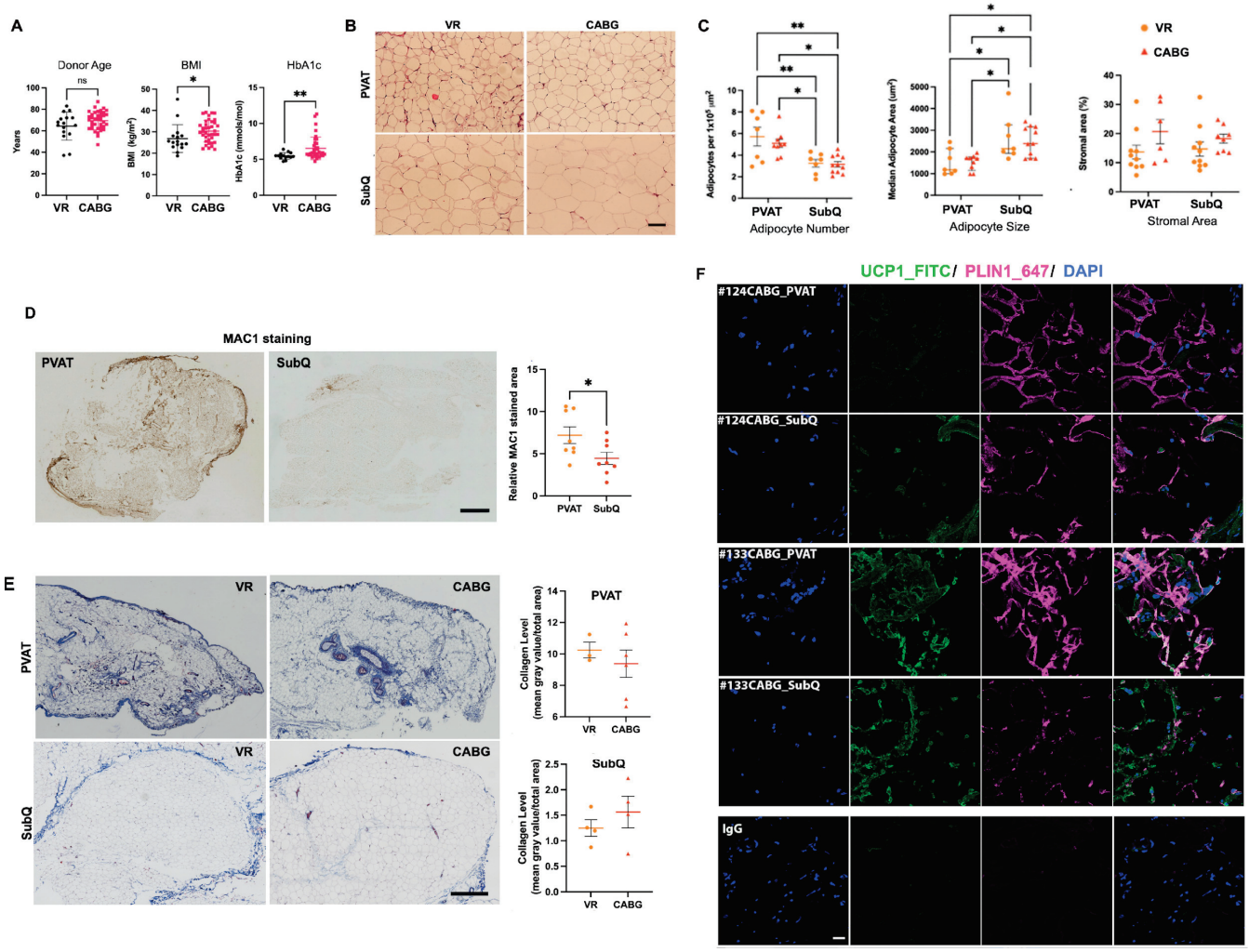


Figure 1. A comparison of PVAT and SubQ between VR and CABG donors. (**A**) While there was no significant difference in age of donors from VR vs. CABG groups, the CABG group had higher body mass indices (BMIs) and circulating HbA1c levels. (**B**) Representative images of adipose tissue sections after hematoxylin/eosin staining for PVAT or subcutaneous adipose (SubQ) from donor groups. Scale bar = 50 μm. (**C**) Morphometric analysis was performed to quantify adipocyte number, size, and stromal area. Adipocytes were smaller in PVAT compared to SubQ regardless of disease incidence. VR PVAT n = 7, VR SubQ n = 7, CABG PVAT n = 9, CABG SubQ n = 11. (**D**) Sections were immunostained to detect MAC1 to quantify macrophages in adipose tissue in CABG PVAT (n = 8) and SubQ (n = 8). Representative images are shown, and quantification indicated higher macrophage presence in CABG PVAT compared to CABG SubQ. Scale bar = 750 μm. (**E**) Sections

were stained with Masson's trichrome stain to identify collagen. There was no detectable difference between CABG and VR PVAT or VR and CABG SubQ. Scale bar = 500 μm. VR PVAT n = 3, CABG PVAT n = 6, VR SubQ n = 4, CABG SubQ n = 4. (**F**) Sections from human adipose tissues from CABG donors were immunostained to detect UCP1 (green) and perilipin1 (PLIN1, pink). Shown is the merge in the right column. The bottom row represents negative control staining with non-immune IgG. Scale bar = 20 μm. * $p < 0.01$, ** $p < 0.001$.

Stroma is the area between adipocytes in the tissue. There were no significant differences between groups in the stromal area and the difference in adipocyte number was fully accounted for by the difference in size. The stromal area was 15.5%, 16.9%, 15.4%, and 16.9% for VR PVAT, CABG PVAT, VR SubQ, and CABG SubQ, respectively. We then analyzed tissue macrophages by immunostaining with MAC1, which is a macrophage marker and indicative of inflammation. There were no significant differences between the donor groups, but there was a significantly higher area of MAC1 stain in the CABG PVAT samples compared to CABG SubQ adipose tissue (Figure 1D). The connective tissue of all four groups was assessed using Masson's trichrome stain (Figure 1E). There were no significant differences in collagen presence between disease types in PVAT or SubQ. PVAT VR had a ratio of mean stained area/total area of 10.24 vs. 9.38 in CABG VR, and VR SubQ had a mean stained area of 1.25 compared to 1.57 in subcutaneous adipose tissue from CABG donors.

We further localized adipocyte markers to human adipose tissue, focusing on perilipin1 (PLIN1), a lipid droplet membrane protein, and UCP1, a marker of thermogenic adipose tissue. Using immunofluorescence, we found that all samples had significant PLIN1 staining in the tissue, as expected. Although more variable, we also did detect UCP1 protein in samples from PVAT and SubQ adipose tissue from our donors. Although we had hypothesized that UCP1 might be more representative in PVAT compared to SubQ, or VR versus CABG tissue, we found variability between subjects with no clear difference between adipose depot and donor type.

3.3. Sliding Window Analysis of Adipocyte Morphology Shows PVAT Adipocytes Have a Smaller Area than SubQ Adipocytes

Histological tissue slides were analyzed using a sliding window analysis to assess adipocyte area, circularity, eccentricity, and solidity. As with the manual subregion selection FIJI analysis, only the adipocyte area was significantly different (VR area $p = 0.008$, CABG area $p = 6.5 \times 10^{-5}$, Figure 2A). Within each disease type, PVAT had smaller adipocytes by area than adipocytes from subcutaneous adipose tissue. This corroborates the manually selected subregions data and confirms that there were no significant differences in adipocyte size, circularity, eccentricity, or solidity between VR and CABG derived tissues.

3.4. The Multiscale Anisotropy Analysis Shows Differences at Both Small (2.8 to 7.5 μm) and Large (22.8 to 64.4 μm) Scales

The anisotropy factor was analyzed to compare the adipose depots (perivascular versus subcutaneous) within VR donors or CABG donors, or the same adipose tissue depot between donor types (VR versus CABG). The anisotropy factor measures structural organization across multiple size scales and can be used to assess changes in tissue and cell organization. Scales smaller than the size of an adipocyte (small) indicate changes in the membrane while scales larger than the adipocytes (large) indicate organizational changes on the cell and tissue level. VR PVAT vs. VR SubQ comparison showed only large scale changes, indicating differences in tissue organization, whereas CABG PVAT vs. CABG SubQ had both small and large scale changes (Figure 2B,C). These data suggest that in CABG patients, changes in the PVAT may represent single adipocyte membranes as well as overall organization. There were no significant differences in anisotropy factors between VR and CABG PVAT or VR and CABG SubQ. The patient-level normalized difference anisotropy plots (Figure 2C) indicated a greater variation at small scales between SubQ and PVAT tissue organization in VR patients when compared to CABG. Overall, this

corroborates the manual subregion FIJI and automated sliding window data confirming that there were limited differences in tissue organization within adipose tissues between disease types.

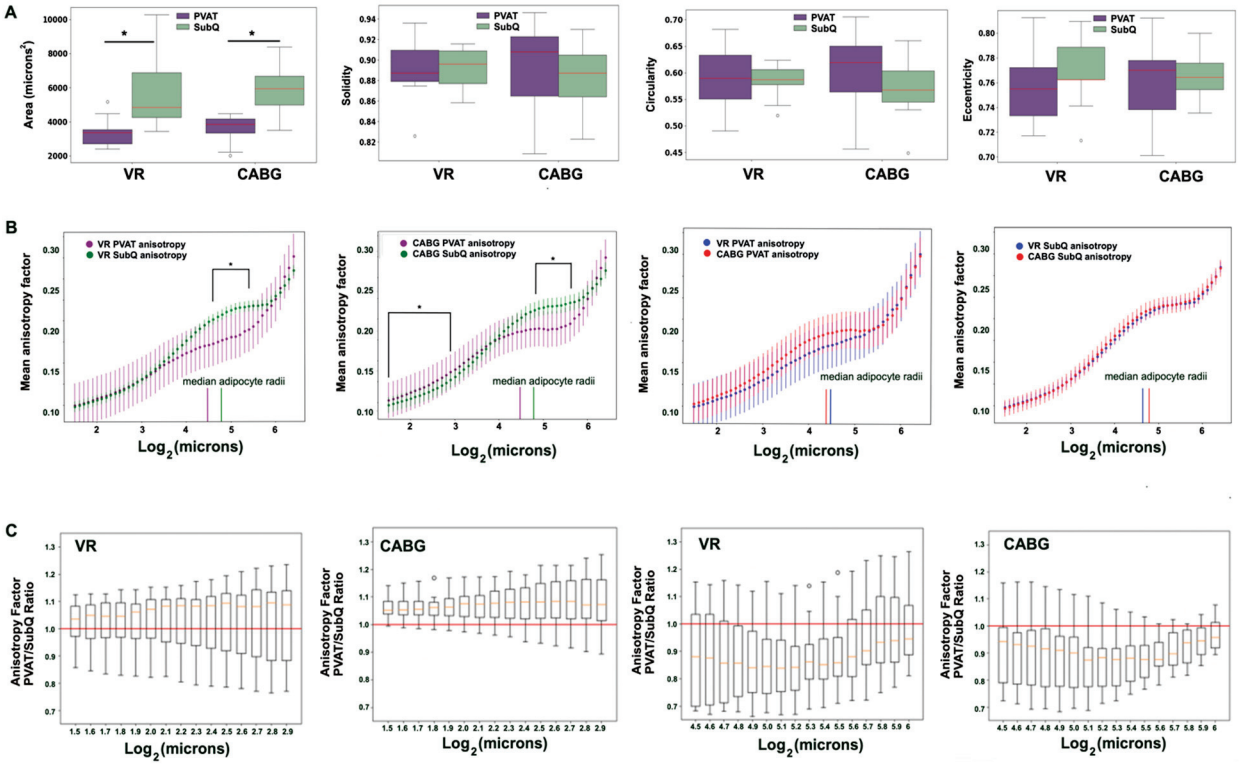


Figure 2. A morphometric and anisotropy analysis of tissues with sliding window segmentation validate FIJI analysis. (**A**) A morphometric analysis of patient adipocytes from the sliding window segmentation analysis where patient median values from all their adipocytes are plotted. Quantified are area, solidity, circularity, and eccentricity. Significance, shown as asterisks, were calculated between patient tissue subtypes and across surgery subtypes using an unpaired Wilcoxon ranked sum test with an α of 0.05. (**B**) Anisotropy Factor plots of patient mean adipose tissue anisotropy factors and standard deviation across 50 wavelet size scales of VR PVAT vs. SubQ, CABG PVAT vs. SubQ, VR PVAT vs. CABG PVAT, and VR SubQ vs. CABG SubQ. All automated sliding window H&E 1024 $\times$ 1024 subregions that passed manual inspection of adipocyte content were used to calculate each of the patients' mean anisotropy factors. Significance, shown as asterisks, were calculated at each wavelet scale using an unpaired Wilcoxon ranked sum test with an α of 0.05. The median adipocyte radii in microns of each category are shown as vertical bars with colors corresponding to the legend. (**C**) Each donor's mean PVAT Anisotropy Factor subtracted from their mean SubQ Anisotropy Factor and divided by their sum is plotted as a boxplot over ranges of statistically significant size scales shown in panel B. Small scale anisotropy ratios are plotted for VR and CABG from 2.8 microns to 7.5 microns. Large scale anisotropy ratios are plotted for VR and CABG from 22.8 microns to 64.4 microns. A horizontal line at 1.0 is shown as red to indicate the location of where the median anisotropy factor from a donor's PVAT tissue is equivalent to the anisotropy factor from their SubQ tissue. * $p < 0.01$.

3.5. Diabetes Does Not Significantly Affect Adipose Tissue Morphology in CABG Patients

Given the high incidence of diabetes in the CABG cohort and the common comorbidity of diabetes and cardiovascular disease, we investigated whether adipose tissue was distinguishable between diabetic and non-diabetic donors (Figure 3). There were no significant differences in adipocyte size, number, or stromal area between PVAT and SubQ regardless of diabetes incidence (Figure 3A,B). PVAT from donors without diabetes averaged 1696 μm^2, with 4.78 adipocytes per 1 $\times$ 10^5 μm^2, and 19.7% stromal area versus

1725 μm^2, 4.81 adipocytes per 1 × 10^5 μm^2, and 13.19% stromal area in PVAT from donors with diabetes. SubQ from donors without diabetes averaged 2650 μm^2, 3.21 adipocytes per 1 × 10^5 μm^2, and 15.96% stromal area versus 2368 μm^2, 3.02 adipocytes per 1 × 10^5 μm^2, and 19.5% stromal area in SubQ from donors with diabetes. There was no difference in the MAC1 stained area (Figure 3C) or the collagen area between non-diabetic and diabetic patients (Figure 3D).

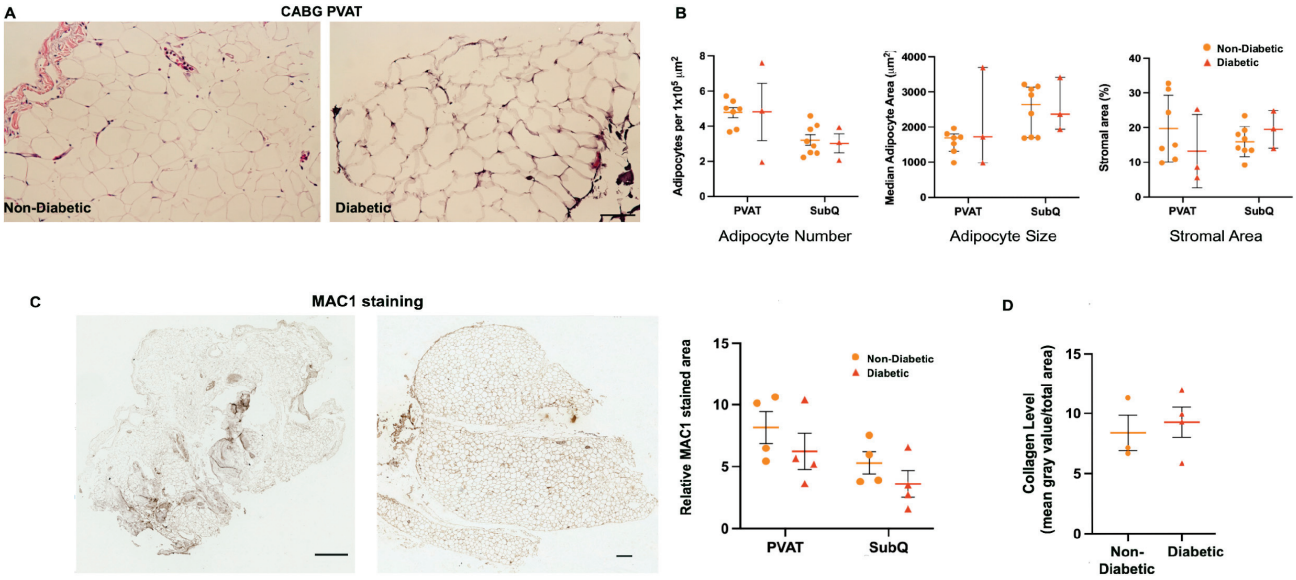


Figure 3. The diabetes status associated with few changes in CABG PVAT and SubQ. (**A**) Hematoxylin/eosin staining, and (**B**) morphometric comparisons of adipocyte size, number, and stromal area in CABG PVAT accounting for diabetes. Non-diabetic PVAT n = 7; diabetic PVAT n = 3; non-diabetic SubQ n = 8; diabetic SubQ n = 3. Scale bar 50 μM. (**C**) The MAC1 immunostaining in CABG and SubQ from donors with and without diabetes of stained area is shown in the graph on the right. Non-diabetic PVAT n = 4; diabetic PVAT n = 4; non-diabetic SubQ n = 4; diabetic SubQ n = 4. Scale bar 250 μm and 50 μm, respectively. Scale bar = 50 μm. (**D**) The quantification of tissue fibrosis using Masson's trichrome Masson in non-diabetic and diabetic PVAT and SubQ. Non-diabetic PVAT n = 3; diabetic PVAT n = 4.

3.6. Proteins Involved in Adipogenesis, Insulin Resistance, and Secretion Are Differentially Expressed Between Donor Groups and Adipose Depots

Given the paracrine signaling function of PVAT, we were interested in differences between the patient groups on a protein scale. SWATH proteomic analysis was done using MS/MS (Figure 4). Principle component analysis (PCA) plots were generated to determine how similar the protein expression of each group was. Based on PCA, all four groups of interest segregate independently and have distinct protein expression (Figure 4A). Proteins of interest that are higher and lower in CABG PVAT/VR PVAT (Figure 4B) and CABG SubQ/VR SubQ (Figure 4C) are labeled in the volcano plots. Proteins involved in adipogenesis, insulin resistance, and secretion are higher in CABG PVAT. Of particular interest are PLIN1, MGLL, and SYUA which are all higher in CABG PVAT compared to VR PVAT. Additionally, PEA15 was higher in subcutaneous adipose tissue from CABG donors compared to VR donors. Perilipin (PLIN1) is a lipid coat protein. The higher the level of PLIN1, the more adipose that is present. PLIN1 being increased in CABG PVAT compared to VR PVAT fits with our hypothesis that PVAT in CABG patients is expanded and has more adipose.

The gene ontology (GO) of cellular component terms were ordered based on the false discovery rate (FDR), strength from STRING, and the observed gene count. Between CABG and VR PVAT, the terms with the highest FDR (indicative of most likely to be a true difference) were extracellular space, extracellular region, extracellular exosome, and vesicle

(Figure 4D). Comparing subcutaneous adipose tissue from CABG and VR donors, the terms with the highest FDR included extracellular exosome, vesicle, extracellular space, and extracellular region (Figure 4E). GO terms for biological process and molecular function were also investigated using STRING, but no differences of note were observed. We then took the proteins classified under the GO terms "extracellular exosome", "vesicle", secretory granule", and "secretory vesicle" and examined significance (*p*-value) and log-fold change for both PVAT (Figure 4F) and subcutaneous adipose tissue (Figure 4G) comparisons. In both heat bar graphs, the darker the color indicates a higher log fold change, while the length of the bar indicates significance. Proteins are sorted from most to least significantly different. Given the involvement of secretory proteins, as well as interest in validating the SWATH proteomics, we used multiple reaction monitoring to assess protein expression.

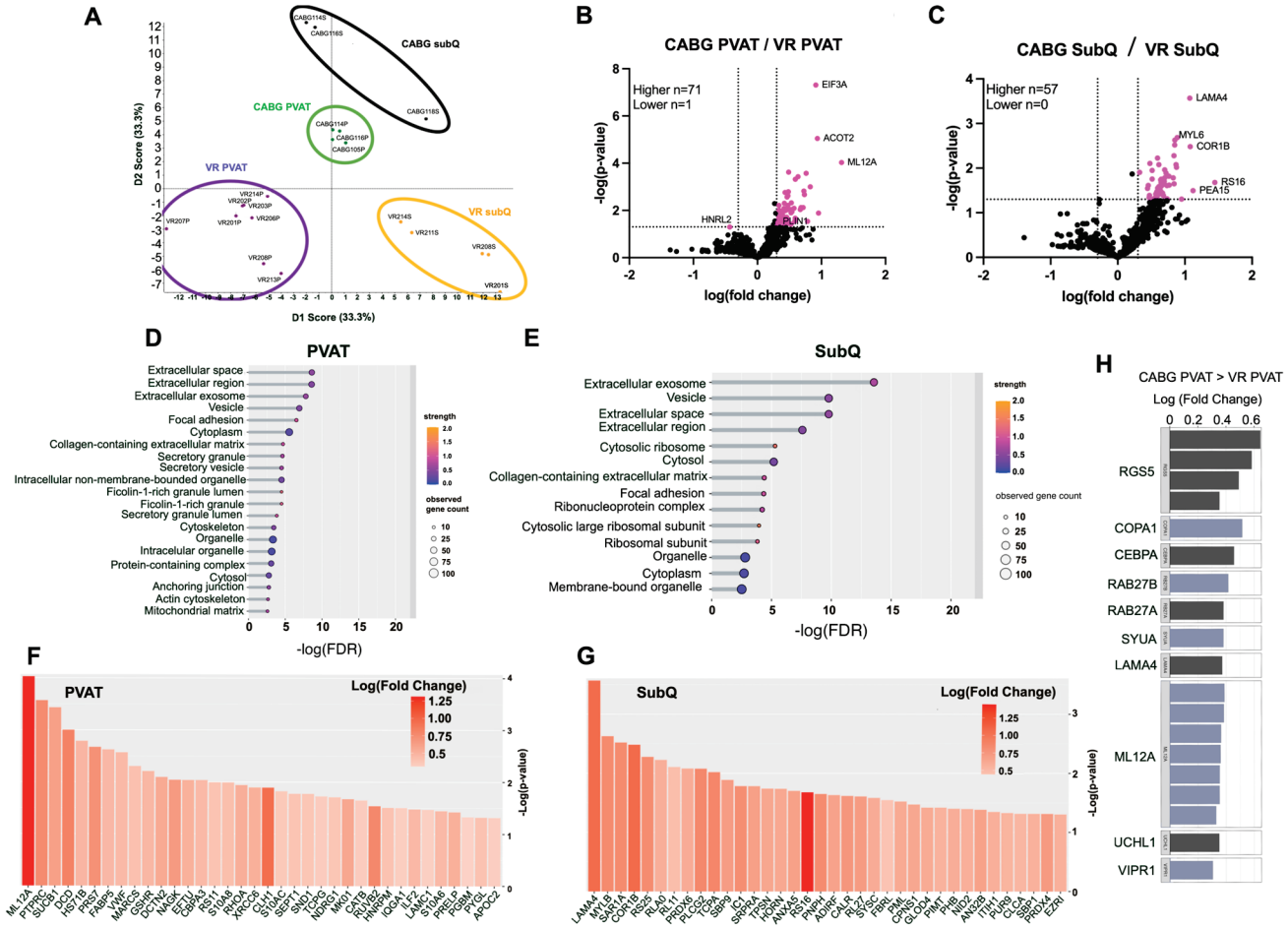


Figure 4. SWATH proteomics reveals differential protein expression in proteins involved in adipogenesis, secretion, and insulin resistance. VR 201 donor had shunt placed ~16 years prior to the VR surgery. (**A**) PCA plot showing differences in 4 SWATH groups: CABG PVAT (n = 4, green), VR PVAT (n = 6, purple), CABG SubQ (n = 3, black), and VR SubQ (n = 5, yellow). (**B**) Volcano plots highlight the proteins of interest that are expressed differently between CABG and VR PVAT. (**C**) Volcano plots highlight the proteins of interest that were significantly differently expressed (pink dots) between CABG and VR SubQ. (**D**) STRING analysis highlighted gene ontology cellular component terms in all differentially expressed proteins between the PVAT. Terms are classified by false discovery rate (FDR), strength (internal STRING measurement), and observed gene count. (**E**) STRING analysis highlighted GO cellular component terms in all differentially expressed proteins between the SubQ groups. Terms were classified by false discovery rate (FDR), strength, and observed gene count. (**F**) Proteins that are classified in gene ontology terms "extracellular space", "extracellular region", "extracellular exosome", and "vesicle" for PVAT were classified by *p*-value and log fold change for CABG PVAT/VR PVAT. (**G**) Proteins that are classified in gene ontology terms "extracellular space",

"extracellular region", "extracellular exosome", and "vesicle" for PVAT, were classified by *p*-value and log fold change for CABG SubQ/VR SubQ. (**H**) MRM targeted proteomics showed log-fold change in proteins of interest that were higher in CABG than VR PVAT. Multiple peaks per peptide is indicative of multiple ions for that peptide.

3.7. Targeted Proteomics for SWATH Validation

Multiple reaction monitoring proteomics were performed on CABG PVAT and SubQ, both non-diabetic and diabetic, and VR PVAT (Figure 4H). Proteins were prioritized based on their identification in the bulk mass spectrometry analyses. Multiple reaction monitoring is a way to select specific peptides of interest out of a library and search for them within a tissue sample [32]. Multiple peptides and multiple ions for each protein can be detected, which often leads to multiple peaks for a single protein, including some that may be upregulated and some downregulated for the same protein, or even the same peptide.

The first goal was to validate the first round of SWATH proteomics. To this end, PLIN1, COL25A1, MYO1B, SYUA, ML12A, and LAMA4 were tested because these proteins were differentially expressed in the first round (Figure 4H). Of note, ML12A was higher in CABG PVAT compared to VR PVAT, where in the original SWATH data it was lower. LAMA4 was detected as higher in in CABG PVAT when compared to VR PVAT. RS16 and PEA15 were not differentially expressed.

In addition to validating the SWATH proteomics, we investigated protein expression of proteins involved in secretion (RAB27A, RAB27B), innervation (PGP9.5), thermogenesis (GRP75 and UCP1), and pericyte markers (VIPR1, RGS5). Using multiple reaction monitoring (Figure 4H), we found that RAB27A and RAB27B are higher in CABG PVAT compared to VR PVAT. This indicates both an increase in secretion and adiposity, which may partially account for the increased PVAT in CABG patients. PGP9.5 (UCHL1) was higher in CABG PVAT than VR PVAT, suggesting that CABG PVAT is more highly innervated than VR PVAT. PGP9.5 was also higher in the perivascular versus subcutaneous adipose depot from CABG donors (Figure 5). There was no difference in thermogenic marker UCP1 or GRP75 expression in PVAT from CABG or VR donors. VIPR1 and RGS5 were both higher in PVAT from CABG donors compared to VR donors, indicating an increased presence of pericytes in these adipose depots. Pericytes are mural cells of capillaries and also regulate insulin secretion in B-islet cells [33].

3.8. Comparison of Adipose Depots Within CABG Donor Groups

The protein expression between the perivascular and subcutaneous adipose depots from CABG donors was compared using proteomics via MS/MS. A total of forty-five proteins were higher in PVAT and two were lower compared to subcutaneous adipose tissue from CABG donors. Proteins of interest are highlighted in Figure 5A. All significantly different proteins were then analyzed using STRING. Top hits included extracellular exosome, vesicle, and secretory granule. This suggested that secretion may be higher in CABG PVAT. Lastly, the proteins in the GO terms "extracellular exosome, vesicle, secretory granule, and secretory vesicle" were examined for log fold change differences (Figure 5C). Overall, most of the secretory proteins were more highly expressed in CABG PVAT, providing further evidence for differences in secretion.

3.9. Analysis of PVAT Protein Profiles of Diabetic vs. Non-Diabetic CABG Donors

Given the high presence of diabetic patients in the CABG cohort, as well as the common comorbidity of diabetes and cardiovascular disease, we investigated whether diabetes was associated with a unique protein signature. In this comparison, PVAT from CABG donors was separated into non-diabetic and diabetic patients (Figure 5). The PCA shows a difference in protein pattern between the non-diabetic and diabetic groups (Figure 5D). A total of ten proteins were higher in the non-diabetic PVAT than the diabetic PVAT and one was lower (Figure 5E). Thus, the proteomic differences between groups were driven by these eleven proteins identified that distinguished between PVAT from

non-diabetic or diabetic donors. UCP1 and PLIN1 were detected in these samples but was not different between groups when analyzed by bulk proteomics. However, in the targeted proteomics (Figure 5F), UCP1 expression was higher in PVAT from diabetic donors. This is potentially indicative of a protective mechanism in the diabetic tissue leading to adipose browning.

SWATH proteomics were validated using multiple reaction monitoring (Figure 5F). We specifically tested QCR9 and HBG2 as they were the lowest and highest differentially expressed proteins based on log fold change in expression. In the multiple reaction monitoring between CABG PVAT from diabetic donors and CABG PVAT from non-diabetic donors, QCR9 was significantly different with a *p*-value of 0.035 and a non-significant log fold change of 0.22. This trend was consistent with the original SWATH proteomics showing lower QCR9 expression in non-diabetic PVAT. HBG2 was also not differentially expressed but given a *p*-value of 0.057 and a log fold change of −0.4; this indicates that HBG2 is lower in non-diabetic PVAT, which also paralleled the SWATH proteomics data. In addition to these changes, protein changes in secretory proteins (RAB27A and RAB27B), a thermogenic protein (UCP1), and pericyte markers (NOTCH3, VIPR1, and RGS5) were investigated. NOTCH3 was higher in diabetic PVAT, but all other proteins were more highly expressed in the non-diabetic PVAT.

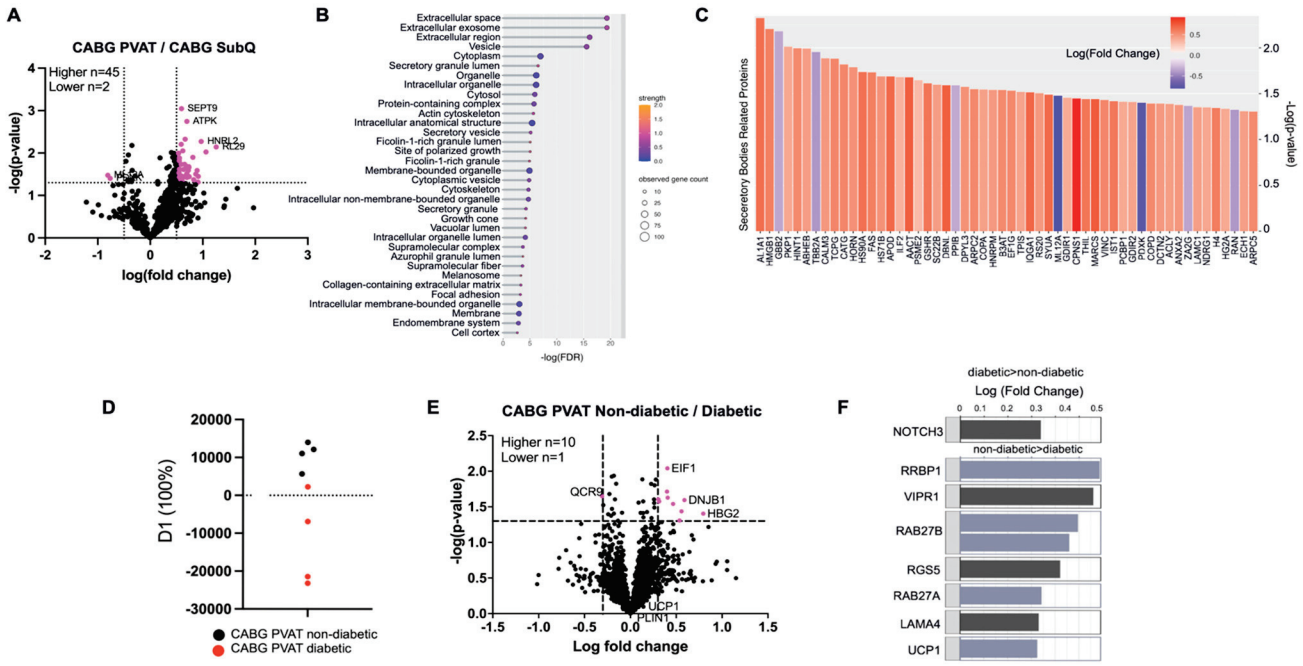


Figure 5. SWATH proteomics of non-diabetic and diabetic CABG PVAT. (**A**) From the first SWATH data set, the volcano plot shows significant protein expression differences (pink dots) between CABG PVAT and SubQ. In this data set, there was a mix of diabetic and non-diabetic samples. (**B**) STRING analysis of proteins differentially expressed between CABG PVAT and SubQ displaying enriched cellular component gene ontology terms. (**C**) Proteins that are classified in gene ontology terms "extracellular space", "extracellular region", "extracellular exosome", and "vesicle" in PVAT/SubQ comparison were classified by *p*-value and log fold change for CABG PVAT/CABG SubQ. (**D**) PCA showed a clear distinction between non-diabetic and diabetic CABG PVAT. (**E**) Volcano plot identified ten proteins higher in non-diabetic than diabetic CABG PVAT. (**F**) Proteins significant in MRM proteomics, displayed by log fold change. Each bar represents an individual ion.

3.10. Localization of RAB27A and NOTCH3 Within Human Adipose Tissue

Immunofluorescence was used to validate protein expression in adipose tissues (Figure 6). RAB27A and NOTCH3 were detected in both perivascular and subcutaneous depots from CABG donors. Because RAB27A is higher in CABG PVAT compared to VR

PVAT (Figure 4H), and higher in diabetic versus non-diabetic CABG PVAT (Figure 5F), we localized it within the tissue. We consistently observed higher levels of RAB27A protein in PVAT compared to subcutaneous adipose from CABG donors, which validates our proteomics result. RAB27A was localized to puncta localized around the nucleus and is expected to be associated with cellular membranes in its trafficking and secretion functions. NOTCH3 was detected in a mural wall of blood vessels and also in cells not associated with vessels. These NOTCH3 cells are of interest, as recent evidence indicates that smooth muscle cells and pericytes populations may comprise a unique adipocyte progenitor population [18]. Further characterization of pericytes in CABG and VR adipose tissue is ongoing.

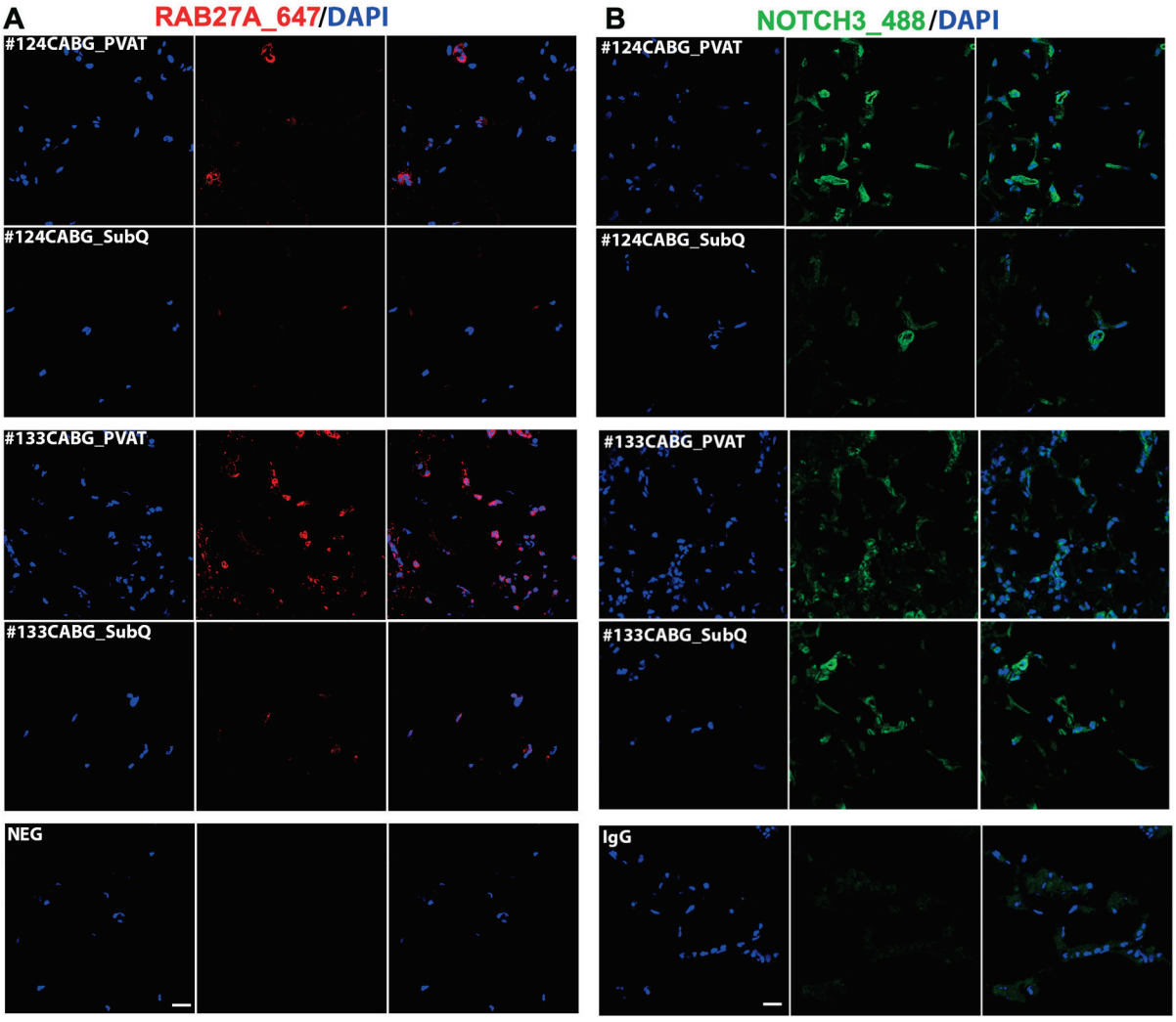


Figure 6. The detection of RAB27A and NOTCH3 in human adipose tissue. Antigens were selected for validation for the proteomics. (**A**) Shown are representative images of immunofluorescence staining in two CABG donor tissues, with matching PVAT or subcutaneous (SubQ) adipose tissue from each donor. The negative control (NEG) was a secondary antibody treatment only. Scale bar = 20 μm. (**B**) The same samples were analyzed for NOTCH3 protein localization. Non-immune IgG staining is shown in the bottom row. Scale bar = 20 μm.

3.11. Differentiation of Human Preadipocytes Is Associated with Elevated Mitochondria

In addition to an analysis of the whole adipose tissue, we isolated cells from the stromal vascular fraction that can be propagated and differentiated into mature lipid laden adipocytes. This model is important because we can manipulate the cells and study pathways of interest, which is not feasible in vivo. This experiment served two important

purposes: (1) to confirm that human preadipocytes can be isolated and differentiated from our donor populations and (2) to confirm expression of protein targets of interest. Primary cultures of these human stromal vascular fraction-derived populations were differentiated using standard conditions. Because of variability in propagating individual human adipose tissue samples, and generally small pieces of PVAT obtained, we performed these experiments on cells derived from subcutaneous adipose tissue. Two independent isolates showed differentiation capacity (Figure 7A), based on cellular lipid accumulation quantified by LipidTOX. Expression of adipocyte markers PLIN1 and PPARG were assessed by immunoblot, and there was some variability in rat and extent of differentiation between donor populations (Figure 7B). RAB27A was also assessed. In two out of three primary cell populations, the RAB27A decreased upon differentiation, which has been shown previously [17]. Undifferentiated and differentiated adipocytes were assessed for mitochondrial presence and activity using MitoTracker (Figure 7C,D). The number of mitochondria increased upon differentiation. Additionally, fission was seen in the differentiated populations.

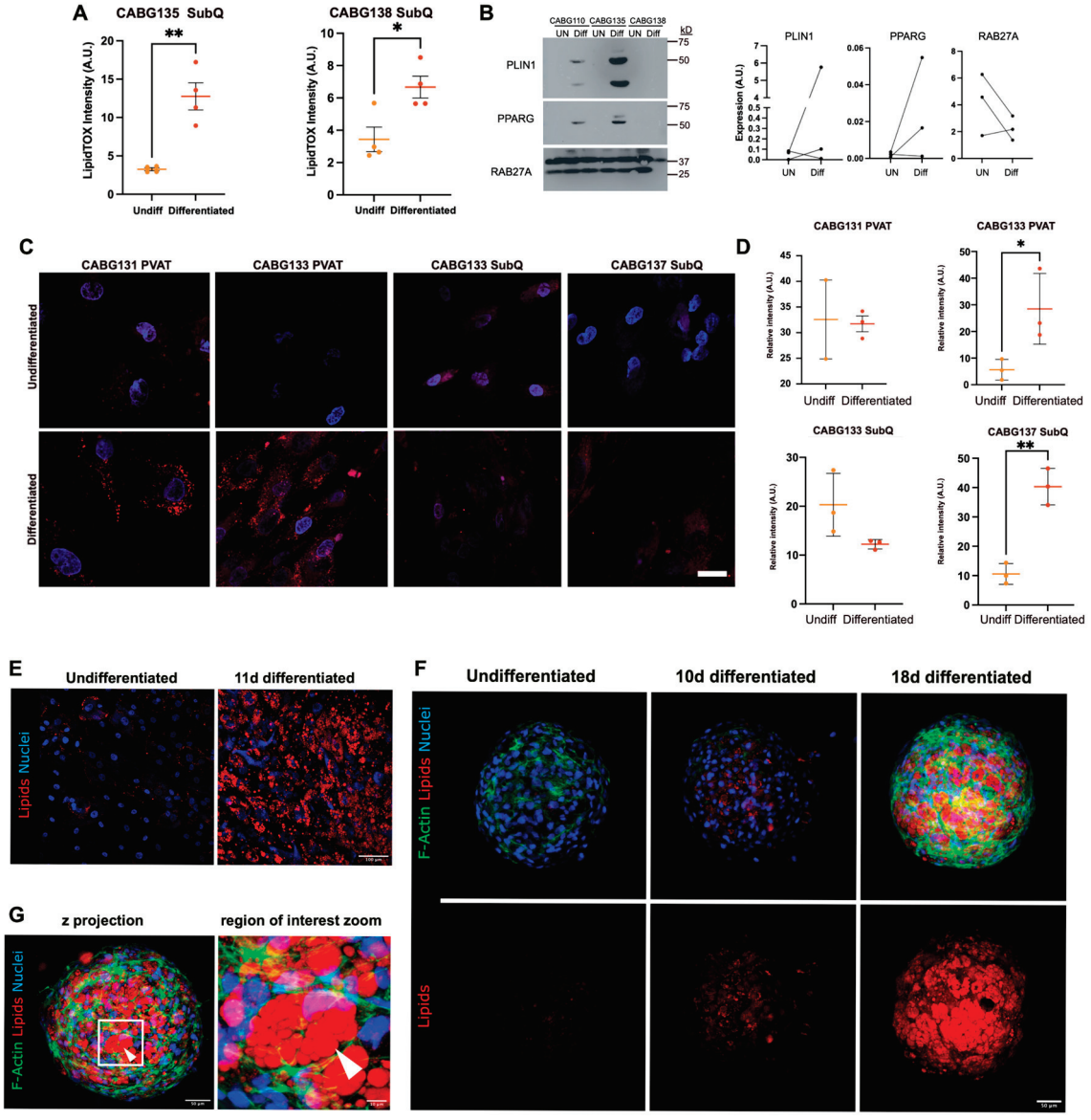


Figure 7. The differentiation of human preadipocytes and impact on mitochondria. Various preadipocyte populations from CABG donors were either left under standard growth conditions or differentiated as described for nine days. (**A**) LipidTOX was used to detect lipids based on fluorescence intensity. (**B**) Immunoblot of PLIN1 (62 kD), PPARG (57, 53 kD), and RAB27A (27 kD)

following differentiation (Diff) compared to undifferentiated (UN) controls. Quantification of the immunoblots are shown in the graphs on the right. (**C**) Mitotracker was used to stain mitochondria as indicated (red) in undifferentiated or differentiated populations. Scale bar = 25 μm. (**D**) Quantification of the mitotracker stain from groups shown in (**C**). *p*-value * $\leq$ 0.05, ** *p*-value $\leq$ 0.01. (**E**) Human PVAT-derived preadipocytes were grown in monolayer culture and differentiated into adipocytes for eleven days. Nuclei were stained with DAPI (blue), and Oil Red O (red) was utilized to detect lipids. (**F**) Human preadipocytes were obtained from PVAT from donors undergoing CABG and grown in 3D spheroid culture as described. Cells were either left undifferentiated in a standard growth medium or differentiated for ten or eighteen days in an adipogenic differentiation medium. Nuclei were stained with DAPI (blue), Oil Red O (red) was utilized to detect lipids, and F-actin was visualized with phalloidin. (**G**) An eighteen-day differentiated spheroid is shown, with a higher magnification region of interest showing the lipid droplets.

4. Discussion

VR donors are metabolically healthier than CABG donors. Samples were collected from both males and females, however the donors were primarily male, consistent with a higher proportion of males undergoing CABG procedures than females [34]. Globally, 30% of CABG patients are female [34,35], while in our cohort, the proportion of females was only 7.9%. Based on the national inpatient database from 2005–2009, between 60 and 65% of mitral valve replacements were performed on females [36,37], while only 31% of our VR cohort was female. Given that diabetes is a risk factor for atherosclerosis [38], it is expected that the patients with severe arterial disease (CABG) are more likely to be diabetic. Additionally, VR donors had a lower BMI than CABG patients and were less likely to be on anti-diabetic medication. Finally, cardiac functional analysis indicated that the VR population had a significantly higher ejection fraction compared to the CABG donors. Collectively, these data indicate the overall better health of VR patients compared to the CABG patients.

Morphological analysis shows limited differences in adipose between donor groups. The only significant differences we found in adipocyte number was in comparison between the perivascular and subcutaneous adipose depots. PVAT has more adipocytes, despite no significant differences in size or stromal area. However, adipocyte size appears to be trending larger in subcutaneous adipose tissue, which fits with the adipocyte size data. The stromal area was not different between groups. This was potentially due to the large size of the adipocytes, leaving a relatively low percentage of stromal area. However, we did find higher levels of MAC1-positive macrophages in perivascular versus subcutaneous adipose tissue from CABG donors, potentially representing a higher inflammatory state. A possible explanation for increased inflammation is the closer proximity of the PVAT to the site of atherosclerosis, as the adipose could be affected by inflammation within the vasculature. Previous studies have shown that increased adipose tissue fibrosis is correlated with increased adiposity and body mass index [39]. However, we detected no differences in tissue fibrosis detected between our donor populations or adipose depots. In our assessment of the association of adipose tissue morphology with diabetes, we did not detect any significant differences. The modest differences observed in the protein signatures based on diabetes status was consistent with this. We believe that the medical management of diabetes may account for the adipose tissue phenotypes being very similar at the morphological and molecular level.

The level of tissue organization differs between PVAT and SubQ. In CABG donors, both perivascular and subcutaneous adipose depots displayed small and large scale changes in anisotropy. Our team has been working on novel applications of computational multiscale approaches to enhance biophysical understanding of disease for biomedical applications. While this approach has been utilized to study human cancer [25], this is a unique application to human adipose tissue. The large scale changes can be interpreted as differences in cellular organization that are undetectable with other analyses. Because this analysis is performed on histological slides and represents primarily data on adipocyte

plasma membranes, we are interested in the concept that the anisotropy measurement reflects differences in plasma membrane structure or function. An important function of adipose tissue is its endocrine function of secretion of paracrine signaling molecules. We are particularly interested in this secretory function of PVAT to underlying blood vessels.

Proteomic analysis shows changes in proteins involved in adipogenesis, insulin resistance, and secretion. Perilipin (PLIN1) is a lipid coat protein that is positively correlated with adipose tissue expansion. In PVAT, our observation that PLIN1 was higher in CABG compared to VR donors was consistent with our hypothesis that adipose tissue expansion is elevated in CABG donors, corresponding to their decreased metabolic health. However, we would also expect there to be an accompanying change in adipocyte size which was not seen. Some attention has focused on the capacity of clinical imaging to monitor adipose tissue expansion or inflammation with relation to metabolic disease or risk for cardiovascular disease, which may provide some context in combination with cellular and molecular studies. Another differentially regulated protein identified to be highest in PVAT from CABG donors was monoglyceride lipase (MGLL), which is involved in the endocannabinoid system and mediates signaling in the brain and peripheral tissues, including adipose [40]. Obesity is associated with higher levels of MGLL expression, and three genes associated with higher BMI are also associated with increased MGLL expression [40,41]. Our result fits what is known about MGLL expression, because CABG patients in our study were more likely to be overweight and obese than VR donors. The effect of MGLL is tissue dependent and has an effect on insulin sensing and glucose tolerance. Given what is known about MGLL function, it could be a potentially interesting target for the controlling of adipogenesis and has implications to insulin sensitivity in diabetes. Another protein that may be controlling insulin sensitivity and was higher in PVAT from CABG donors was alpha synuclein (SYUA). SYUA is often associated with the formation of Lewy bodies in Parkinson's disease (PD), but has recently been shown to be involved in the regulation of insulin sensitivity as well as lipid storage in both mice and humans [42,43]. Low levels of SYUA in humans are associated with insulin resistance, while an increase in SYUA is associated with increased adiposity, in addition to increased insulin sensitivity. Given that SYUA was more highly expressed in CABG PVAT, this is another piece of evidence supporting increased adiposity in CABG PVAT. However, the accompanying implication of increased insulin sensitivity, given the CABG donors higher propensity for insulin resistance, seems to counteract this point.

We identified phosphoprotein enriched in astrocytes 15 (PEA15) in human subcutaneous adipose tissue at higher levels in CABG versus VR donors. This is of interest because PEA15 is involved in type 2 diabetes and is a recently discovered regulator of adipose tissue expansion [44]. In mice, PEA15 null mice have improvements in whole body insulin sensitivity, lower liver weight, and decreased serum triglyceride. As far as we are aware, this work is the first time PEA15 expression has been examined in humans. Our proteomics results suggest that PEA15 has a similar role in insulin sensitivity and adipose tissue expansion seen in mice.

The SWATH proteomics data suggested that secretion may be changed between disease states in both perivascular and subcutaneous adipose tissues. RAB27A and RAB27A are RAS family proteins responsible for trafficking vesicles to the membrane. Boucher et al. showed that human preadipocyte differentiation was inhibited with suppression of RAB27A [17]. Differential expression of these RAB proteins in human adipose depots may reflect changes in protein trafficking and secretion. Interestingly, mutation in *RAB27A* in humans can lead to type II Griscelli syndrome, which is reflected in impaired protein trafficking resulting in hypopigmentation and changes in immune responses [45]. In mice, mutation in *Rab27a* leads to impaired exocytosis of insulin from pancreatic beta cells in response to glucose [46], and we recently discovered that *Rab27a* global null mice have cardiovascular dysfunction in an age- and sex-dependent manner [47]. These results suggest that these pathways may be conserved between mice and humans in regulation of cardiometabolic physiology.

Since we were interested in increased differentiation and adiposity, we are also interested in innervation changes, as it has been previously shown that chemically ablating adipose tissue innervation leads to increased fat pad mass in subcutaneous white adipose [48]. In ob/ob mouse models, there was decreased innervation of both the subcutaneous white adipose depot and the interscapular brown adipose tissue [49]. This study also found that in human white adipose tissue, lower levels of the neural marker PGP9.5 were found in those with a higher body mass index. In our study, the highest level of PGP9.5 was found in the PVAT from CABG donors, who also had the highest body mass index.

Thermogenic markers have long been used as an indicator of the relative health of brown and beige adipose tissue. Human PVAT morphologically resembles white adipose tissue, although it produces UCP1 and other thermogenic markers [17], allowing for use of these markers to determine the degree of beiging in adipose. We hypothesized that PVAT from VR versus CABG donors would be metabolically healthier and thus have higher thermogenic marker expression. However, we found significant and relatively equivalent levels of these proteins in PVAT regardless of donor type, suggesting again that human PVAT maintains thermogenic phenotype.

The increased expression of proteins related to secretion and thermogenesis in non-diabetic PVAT fits with the hypothesis that non-diabetic PVAT has more brown adipocytes than diabetic PVAT. However, we showed that this relationship does not always hold true, and likely represents variations between individuals. Thus, more investigation is needed to accurately determine the effect of these proteins in the adipose.

Overall Conclusions. Human coronary artery disease is highly prevalent, and we utilized the clinical study populations described to assess whether PVAT was molecularly distinguishable in patients with coronary artery atherosclerosis versus those with other types of cardiac pathologies. Our major conclusions are: (1) patients without coronary artery disease have a healthier metabolic and clinical profile, including lower BMI and circulating HbA1c levels, significantly lower diabetes prevalence, and significantly higher cardiac function, as measured by ejection fraction. There was no difference in the age of the donor populations. (2) Adipocytes from human subcutaneous depots are larger than those in PVAT regardless of disease state, and these adipocytes can be distinguished using multiscale anisotropy analysis of histological sections. The significant changes in PVAT and subcutaneous anisotropy factors from CABG donors suggest changes at the single cell membrane level and tissue organization. (3) Major proteomic differences in the adipose depots between donor groups included functional categories such as exosomes, vesicles, extracellular space, and secretory granules/vesicles, supporting changes in the secretory activity of the adipocytes. (4) Human preadipocyte differentiation into lipid-containing adipocytes in vitro is associated with increased mitochondria, and differentiation occurs in monolayer culture as well as 3D spheroid culture. These models can be used further for cell-based assays of human adipocyte function.

Study Limitations. Our study provides novel information about adipose tissue from two types of donors with distinct vascular pathologies, with samples from either subcutaneous or perivascular adipose depots. Starting to define donor-specific and depot-specific molecular markers was the goal of this study. We validated the clinical and molecular differences in PVAT between the donor populations and presented some case studies of the protein targets of interest and the cellular behavior of human primary preadipocyte populations. The limitations of the study are the small amount of PVAT that could be carried on for downstream analysis; not all applications were possible with all samples. We had different levels of success in deriving primary cell cultures from the donor tissues, and this may represent variability in cellular growth rates or survival capacity. In addition, although the donors were clearly distinguished by the CABG group having several coronary artery diseases, and the VR group not having any coronary artery diseases upon surgery, some donors had additional cardiac-related surgeries at the same time as the primary procedure; 34% of the CABG donors and 87.5% of the VR donors had other concomitant cardiac surgeries. Thus, it is possible that other preexisting conditions or

pathologies affected the PVAT from these individuals. Despite these limitations, the ability to study molecular and cellular behavior of primary human adipose tissue is a benefit and will increase translational capacity of research findings.

Supplementary Materials: The following supporting information can be downloaded at: https://www.mdpi.com/article/10.3390/biomedicines12112453/s1, Supplemental proteomics methodology, Supplemental Table S1 (full demographic information), and Supplemental Tables S2–S6, with lists of proteomic differentially regulated proteins between comparison groups.

Author Contributions: The authors have substantially contributed to this research in the following ways. Conceptualization, C.P.S.E., K.T.M., X.Y., C.V. and L.L.; methodology, C.P.S.E., B.W.T., C.M.P., X.Y., J.H., C.V. and A.K.; software, C.M.P., J.H., C.V. and A.K.; validation, C.P.S.E., B.W.T., X.Y., J.H. and C.V.; formal analysis, C.P.S.E., B.W.T., C.M.P., X.Y., J.H., C.V., A.K. and L.L.; investigation, all authors; resources, A.K. and L.L.; data curation, C.M.P. and C.V.; writing—original draft preparation, C.P.S.E. and L.L.; writing—review and editing, all authors; visualization, C.P.S.E., C.M.P., X.Y., J.H., C.V. and A.K.; supervision, K.T.M., X.Y., C.V., A.K. and L.L.; project administration, L.L.; funding acquisition, C.P.S.E. and L.L. All authors have read and agreed to the published version of the manuscript.

Funding: This research was funded by NIH/NHLBI grant F31 HL156320 (C.P.S.E.), NIH/NIGMS grant 1T32GM132006 (Henry and Liaw, PIs), NIH/NHLBI grant R01HL141149 (L.L.), and NIH/NIGMS grant 1P20GM121301 (L.L.).

Institutional Review Board Statement: Protocols for research use of human tissues was reviewed and approved by the Institutional Review Board of MaineHealth Institute for Research (currently active IRB #1295440-3, K.T.M.).

Informed Consent Statement: Informed consent was obtained from all subjects involved in the study to collect tissues that would otherwise be discarded during surgery. Samples were de-identified according to approved protocol IRB #1295440, and laboratory research personnel have no access.

Data Availability Statement: Proteomics raw data are in the PRIDE repository under reference number 1-20240423-213918-2242764, accession number PXD051676. All other raw data are available upon request.

Acknowledgments: The authors would like to thank the Histopathology and Proteomic and Lipidomic Cores at MaineHealth Institute for Research. We are grateful to Armie Mangoba, Qiaozeng Wang, Volkhard Lindner, Carlos Gusti Gartner, and Yulica Santos-Ortega for their experimental support. The authors would also like to thank Young Sun Lee and Alli Roshni for their help analyzing the manually selected morphometry regions.

Conflicts of Interest: The authors declare no conflicts of interest.

Appendix A. Overview of the 2D Wavelet Transform Modulus Maxima Anisotropy Method

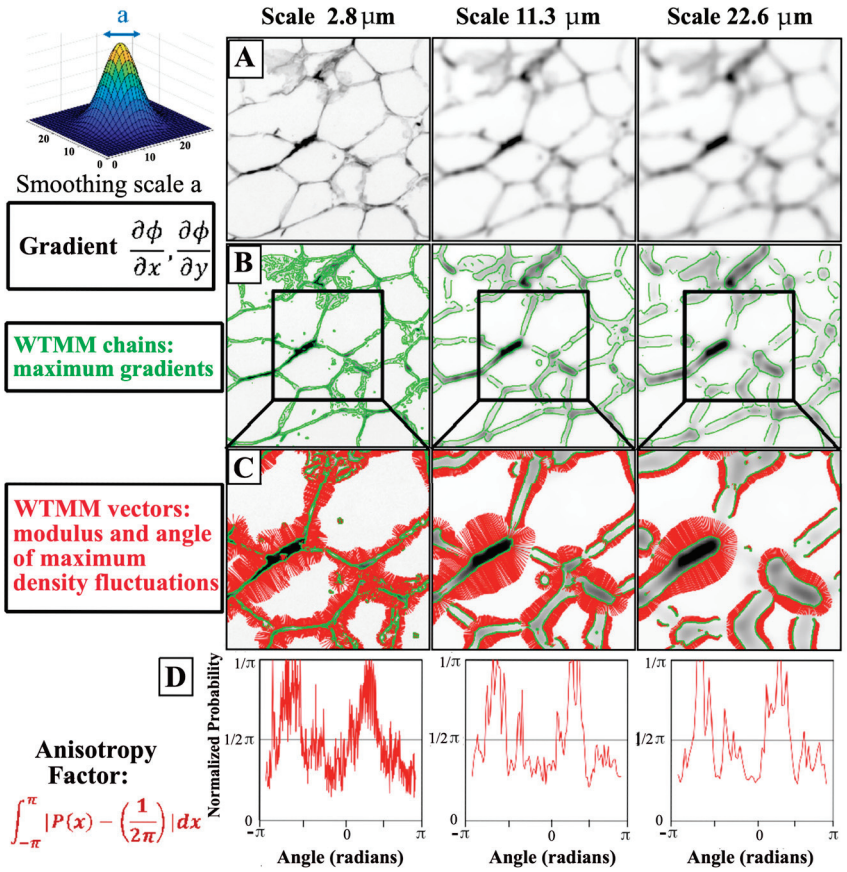


Figure A1. (**A**) A Gaussian wavelet (Φ) convolved with an adipocyte image taken from a PVAT sample at three representative wavelet size scales. (**B**) Maxima chains representing local maximal gradients, i.e., the wavelet-transform modulus maxima (WTMM), at three representative wavelet scales shown in green. (**C**) Magnified inserts from the white outlined area in panel B at three representative wavelet size scales to identify WTMM vectors (red) showing the magnitude and direction of local gradients of the maximum image density fluctuations. (**D**) Probability density functions (PDF), shown in red, of three representative wavelet scales generated from angles of local gradient vectors with the theoretical isotropic $1/2\pi$ line shown in black. The anisotropy factor (see equation in red, where P(X) is the PDF at one scale) is obtained by integrating the difference between each PDF and the theoretical $1/2\pi$ line.

References

1. Tsao, C.W.; Aday, A.W.; Almarzooq, Z.I.; Anderson, C.A.M.; Arora, P.; Avery, C.L.; Baker-Smith, C.M.; Beaton, A.Z.; Boehme, A.K.; Buxton, A.E.; et al. Heart Disease and Stroke Statistics-2023 Update: A Report From the American Heart Association. *Circulation* **2023**, *147*, e93–e621. [CrossRef] [PubMed]
2. Brown, O.I.; Drozd, M.; McGowan, H.; Giannoudi, M.; Conning-Rowland, M.; Gierula, J.; Straw, S.; Wheatcroft, S.B.; Bridge, K.; Roberts, L.D.; et al. Relationship Among Diabetes, Obesity, and Cardiovascular Disease Phenotypes: A UK Biobank Cohort Study. *Diabetes Care* **2023**, *46*, 1531–1540. [CrossRef] [PubMed]
3. Chait, A.; den Hartigh, L.J. Adipose Tissue Distribution, Inflammation and Its Metabolic Consequences, Including Diabetes and Cardiovascular Disease. *Front. Cardiovasc. Med.* **2020**, *7*, 22. [CrossRef]
4. Brown, N.K.; Zhou, Z.; Zhang, J.; Zeng, R.; Wu, J.; Eitzman, D.T.; Chen, Y.E.; Chang, L. Perivascular adipose tissue in vascular function and disease: A review of current research and animal models. *Arterioscler. Thromb. Vasc. Biol.* **2014**, *34*, 1621–1630. [CrossRef]
5. Szasz, T.; Bomfim, G.F.; Webb, R.C. The influence of perivascular adipose tissue on vascular homeostasis. *Vasc. Health Risk Manag.* **2013**, *9*, 105–116. [CrossRef] [PubMed]

6. Saxton, S.N.; Withers, S.B.; Nyvad, J.; Mazur, A.; Matchkov, V.; Heagerty, A.M.; Aalkjær, C. Perivascular Adipose Tissue Contributes to the Modulation of Vascular Tone in vivo. *J. Vasc. Res.* **2019**, *56*, 320–332. [CrossRef]
7. Saxton, S.N.; Clark, B.J.; Withers, S.B.; Eringa, E.C.; Heagerty, A.M. Mechanistic Links Between Obesity, Diabetes, and Blood Pressure: Role of Perivascular Adipose Tissue. *Physiol. Rev.* **2019**, *99*, 1701–1763. [CrossRef]
8. Takaoka, M.; Nagata, D.; Kihara, S.; Shimomura, I.; Kimura, Y.; Tabata, Y.; Saito, Y.; Nagai, R.; Sata, M. Periadventitial adipose tissue plays a critical role in vascular remodeling. *Circ. Res.* **2009**, *105*, 906–911. [CrossRef] [PubMed]
9. Wajngarten, M.; Silva, G.S. Hypertension and Stroke: Update on Treatment. *Eur. Cardiol.* **2019**, *14*, 111–115. [CrossRef]
10. Luong, Q.; Huang, J.; Lee, K.Y. Deciphering White Adipose Tissue Heterogeneity. *Biology* **2019**, *8*, 23. [CrossRef]
11. Emont, M.P.; Jacobs, C.; Essene, A.L.; Pant, D.; Tenen, D.; Colleluori, G.; Di Vincenzo, A.; Jørgensen, A.M.; Dashti, H.; Stefek, A.; et al. A single-cell atlas of human and mouse white adipose tissue. *Nature* **2022**, *603*, 926–933. [CrossRef] [PubMed]
12. Celi, F.S. Human Brown Adipose Tissue Plasticity: Hormonal and Environmental Manipulation. In *Hormones, Metabolism and the Benefits of Exercise*; Spiegelman, B., Ed.; Springer: Cham, Switzerland, 2017; pp. 1–11.
13. Hankir, M.K.; Klingenspor, M. Brown adipocyte glucose metabolism: A heated subject. *EMBO Rep.* **2018**, *19*, e46404. [CrossRef] [PubMed]
14. Adachi, Y.; Ueda, K.; Nomura, S.; Ito, K.; Katoh, M.; Katagiri, M.; Yamada, S.; Hashimoto, M.; Zhai, B.; Numata, G.; et al. Beiging of perivascular adipose tissue regulates its inflammation and vascular remodeling. *Nat. Commun.* **2022**, *13*, 5117. [CrossRef] [PubMed]
15. Sacks, H.S.; Fain, J.N.; Bahouth, S.W.; Ojha, S.; Frontini, A.; Budge, H.; Cinti, S.; Symonds, M.E. Adult Epicardial Fat Exhibits Beige Features. *J. Clin. Endocrinol. Metab.* **2013**, *98*, E1448–E1455. [CrossRef]
16. Gaborit, B.; Venteclef, N.; Ancel, P.; Pelloux, V.; Gariboldi, V.; Leprince, P.; Amour, J.; Hatem, S.N.; Jouve, E.; Dutour, A.; et al. Human epicardial adipose tissue has a specific transcriptomic signature depending on its anatomical peri-atrial, peri-ventricular, or peri-coronary location. *Cardiovasc. Res.* **2015**, *108*, 62–73. [CrossRef]
17. Boucher, J.M.; Robich, M.; Scott, S.S.; Yang, X.; Ryzhova, L.; Turner, J.E.; Pinz, I.; Liaw, L. Rab27a Regulates Human Perivascular Adipose Progenitor Cell Differentiation. *Cardiovasc. Drugs Ther.* **2018**, *32*, 519–530. [CrossRef]
18. Angueira, A.R.; Sakers, A.P.; Holman, C.D.; Cheng, L.; Arbocco, M.N.; Shamsi, F.; Lynes, M.D.; Shrestha, R.; Okada, C.; Batmanov, K.; et al. Defining the lineage of thermogenic perivascular adipose tissue. *Nat. Metab.* **2021**, *3*, 469–484. [CrossRef]
19. Mustu, M.; Gurses, K.M.; Alpaydin, M.S.; Karaarslan, S.; Buyukterzi, M.; Buyukterzi, Z. Periaortic adipose tissue volume is associated with sclerotic changes in the adjacent aortic valve. *Int. J. Cardiovasc. Imaging* **2020**, *36*, 1559–1565. [CrossRef] [PubMed]
20. Lin, A.; Dey, D.; Wong, D.T.L.; Nerlekar, N. Perivascular Adipose Tissue and Coronary Atherosclerosis: From Biology to Imaging Phenotyping. *Curr. Atheroscler. Rep.* **2019**, *21*, 47. [CrossRef]
21. Lin, Z.; Lin, X.; Zhao, X.; Xu, C.; Yu, B.; Shen, Y.; Li, L. Coronary Artery Spasm: Risk Factors, Pathophysiological Mechanisms and Novel Diagnostic Approaches. *Rev. Cardiovasc. Med.* **2022**, *23*, 175. [CrossRef]
22. Shi, K.; Anmin, R.; Cai, J.; Qi, Y.; Han, W.; Li, M.; Zhang, G.; Zhang, S.; Fu, L.; Han, W.; et al. Ascending aortic perivascular adipose tissue inflammation associates with aortic valve disease. *J. Cardiol.* **2022**, *80*, 240–248. [CrossRef] [PubMed]
23. Scott, S.S.; Yang, X.; Robich, M.; Liaw, L.; Boucher, J.M. Differentiation Capacity of Human Aortic Perivascular Adipose Progenitor Cells. *J. Vis. Exp.* **2019**, *145*, e59337. [CrossRef]
24. Galarraga, M.; Campión, J.; Muñoz-Barrutia, A.; Boqué, N.; Moreno, H.; Martínez, J.A.; Milagro, F.; Ortiz-de-Solórzano, C. Adiposoft: Automated software for the analysis of white adipose tissue cellularity in histological sections. *J. Lipid Res.* **2012**, *53*, 2791–2796. [CrossRef] [PubMed]
25. Hamilton, J.; Breggia, A.; Fitzgerald, T.L.; Jones, M.A.; Brooks, P.C.; Tilbury, K.; Khalil, A. Multiscale anisotropy analysis of second-harmonic generation collagen imaging of human pancreatic cancer. *Front. Oncol.* **2022**, *12*, 991850. [CrossRef] [PubMed]
26. Khalil, A.; Joncas, G.; Nekka, F. Morphological Analysis of HI Features I: Metric Space Technique. *Astrophys. J.* **2006**, *601*, 352–364. [CrossRef]
27. Tilbury, K.; Han, X.; Brooks, P.; Khalil, A. Multiscale anisotropy analysis of second-harmonic generation collagen imaging of mouse skin. *J. Biomed. Opt.* **2021**, *26*, 065002. [CrossRef]
28. Khalil, A.; Aponte, C.; Zhang, R.; Davisson, T.; Dickey, I.; Engelman, D.; Hawkins, M.; Mason, M. Image analysis of soft-tissue in-growth and attachment into highly porous alumina ceramic foam metals. *Med. Eng. Phys.* **2009**, *31*, 775–783. [CrossRef]
29. Bailey, E.C.; Alrowaished, S.S.; Kilroy, E.A.; Crooks, E.S.; Drinkert, D.M.; Karunasiri, C.M.; Belanger, J.J.; Khalil, A.; Kelley, J.B.; Henry, C.A. NAD+ improves neuromuscular development in a zebrafish model of FKRP-associated dystroglycanopathy. *Skelet. Muscle* **2019**, *9*, 21. [CrossRef]
30. Rappsilber, J.; Mann, M.; Ishihama, Y. Protocol for micro-purification, enrichment, pre-fractionation and storage of peptides for proteomics using StageTips. *Nat. Protoc.* **2007**, *2*, 1896–1906. [CrossRef]
31. Kusebauch, U.; Campbell, D.S.; Deutsch, E.W.; Chu, C.S.; Spicer, D.A.; Brusniak, M.Y.; Slagel, J.; Sun, Z.; Stevens, J.; Grimes, B.; et al. Human SRMAtlas: A Resource of Targeted Assays to Quantify the Complete Human Proteome. *Cell* **2016**, *166*, 766–778. [CrossRef]
32. Bian, J.; Sze, Y.H.; Tse, D.Y.; To, C.H.; McFadden, S.A.; Lam, C.S.; Li, K.K.; Lam, T.C. SWATH Based Quantitative Proteomics Reveals Significant Lipid Metabolism in Early Myopic Guinea Pig Retina. *Int. J. Mol. Sci.* **2021**, *22*, 4721. [CrossRef] [PubMed]
33. Burganova, G.; Schonblum, A.; Sakhneny, L.; Epshtein, A.; Wald, T.; Tzaig, M.; Landsman, L. Pericytes modulate islet immune cells and insulin secretion through Interleukin-33 production in mice. *Front. Endocrinol.* **2023**, *14*, 1142988. [CrossRef] [PubMed]

34. Matyal, R.; Qureshi, N.Q.; Mufarrih, S.H.; Sharkey, A.; Bose, R.; Chu, L.M.; Liu, D.C.; Senthilnathan, V.; Mahmood, F.; Khabbaz, K.R. Update: Gender differences in CABG outcomes-Have we bridged the gap? *PLoS ONE* **2021**, *16*, e0255170. [CrossRef]
35. Gaudino, M.; Chadow, D.; Rahouma, M.; Soletti, G.J.; Sandner, S.; Perezgrovas-Olaria, R.; Audisio, K.; Cancelli, G.; Bratton, B.A.; Fremes, S.; et al. Operative Outcomes of Women Undergoing Coronary Artery Bypass Surgery in the US, 2011 to 2020. *JAMA Surg.* **2023**, *158*, 494–502. [CrossRef] [PubMed]
36. Vassileva, C.M.; McNeely, C.; Mishkel, G.; Boley, T.; Markwell, S.; Hazelrigg, S. Gender differences in long-term survival of Medicare beneficiaries undergoing mitral valve operations. *Ann. Thorac. Surg.* **2013**, *96*, 1367–1373. [CrossRef]
37. Vassileva, C.M.; Stelle, L.M.; Markwell, S.; Boley, T.; Hazelrigg, S. Sex differences in procedure selection and outcomes of patients undergoing mitral valve surgery. *Heart Surg. Forum* **2011**, *14*, E276–E282. [CrossRef]
38. Leon, B.M.; Maddox, T.M. Diabetes and cardiovascular disease: Epidemiology, biological mechanisms, treatment recommendations and future research. *World J. Diabetes* **2015**, *6*, 1246–1258. [CrossRef]
39. Gliniak, C.M.; Pedersen, L.; Scherer, P.E. Adipose tissue fibrosis: The unwanted houseguest invited by obesity. *J. Endocrinol.* **2023**, *259*, e230180. [CrossRef]
40. Harismendy, O.; Bansal, V.; Bhatia, G.; Nakano, M.; Scott, M.; Wang, X.; Dib, C.; Turlotte, E.; Sipe, J.C.; Murray, S.S.; et al. Population sequencing of two endocannabinoid metabolic genes identifies rare and common regulatory variants associated with extreme obesity and metabolite level. *Genome Biol.* **2010**, *11*, R118. [CrossRef]
41. Matheson, J.; Zhou, X.M.M.; Bourgault, Z.; Le Foll, B. Potential of Fatty Acid Amide Hydrolase (FAAH), Monoacylglycerol Lipase (MAGL), and Diacylglycerol Lipase (DAGL) Enzymes as Targets for Obesity Treatment: A Narrative Review. *Pharmaceuticals* **2021**, *14*, 1316. [CrossRef]
42. Rodriguez-Araujo, G.; Nakagami, H.; Hayashi, H.; Mori, M.; Shiuchi, T.; Minokoshi, Y.; Nakaoka, Y.; Takami, Y.; Komuro, I.; Morishita, R.; et al. Alpha-synuclein elicits glucose uptake and utilization in adipocytes through the Gab1/PI3K/Akt transduction pathway. *Cell. Mol. Life Sci.* **2013**, *70*, 1123–1133. [CrossRef] [PubMed]
43. Rodriguez-Araujo, G.; Nakagami, H.; Takami, Y.; Katsuya, T.; Akasaka, H.; Saitoh, S.; Shimamoto, K.; Morishita, R.; Rakugi, H.; Kaneda, Y. Low alpha-synuclein levels in the blood are associated with insulin resistance. *Sci. Rep.* **2015**, *5*, 12081. [CrossRef] [PubMed]
44. Verschoor, P.J.; Greig, F.H.; Rochford, J.J.; Levate, G.; Delibegovic, M.; Thompson, D.; Leeson-Payne, A.; Dekeryte, R.; Banks, R.; Ramos, J.W.; et al. Phosphoprotein enriched in astrocytes (PEA)-15 is a novel regulator of adipose tissue expansion. *Sci. Rep.* **2021**, *11*, 6949. [CrossRef] [PubMed]
45. Castaño-Jaramillo, L.M.; Lugo-Reyes, S.O.; Cruz Muñoz, M.E.; Scheffler-Mendoza, S.C.; Duran McKinster, C.; Yamazaki-Nakashimada, M.A.; Espinosa-Padilla, S.E.; Saez-de-Ocariz Gutierrez, M.D.M. Diagnostic and therapeutic caveats in Griscelli syndrome. *Scand. J. Immunol.* **2021**, *93*, e13034. [CrossRef]
46. Kasai, K.; Ohara-Imaizumi, M.; Takahashi, N.; Mizutani, S.; Zhao, S.; Kikuta, T.; Kasai, H.; Nagamatsu, S.; Gomi, H.; Izumi, T. Rab27a mediates the tight docking of insulin granules onto the plasma membrane during glucose stimulation. *J. Clin. Investig.* **2005**, *115*, 388–396. [CrossRef]
47. Soucy, A.; Potts, C.; Kaija, A.; Harrington, A.; McGilvrey, M.; Sutphin, G.L.; Korstanje, R.; Tero, B.; Seeker, J.; Pinz, I.; et al. Effects of a Global Rab27a Null Mutation on Murine PVAT and Cardiovascular Function. *Arterioscler. Thromb. Vasc. Biol.* **2024**, *44*, 1601–1616. [CrossRef]
48. Harris, R.B.S. Denervation as a tool for testing sympathetic control of white adipose tissue. *Physiol. Behav.* **2018**, *190*, 3–10. [CrossRef]
49. Blaszkiewicz, M.; Willows, J.W.; Dubois, A.L.; Waible, S.; DiBello, K.; Lyons, L.L.; Johnson, C.P.; Paradie, E.; Banks, N.; Motyl, K.; et al. Neuropathy and neural plasticity in the subcutaneous white adipose depot. *PLoS ONE* **2019**, *14*, e0221766. [CrossRef]

Disclaimer/Publisher's Note: The statements, opinions and data contained in all publications are solely those of the individual author(s) and contributor(s) and not of MDPI and/or the editor(s). MDPI and/or the editor(s) disclaim responsibility for any injury to people or property resulting from any ideas, methods, instructions or products referred to in the content.

biomedicines

MDPI

Article

High Glucose Increases Lactate and Induces the Transforming Growth Factor Beta-Smad 1/5 Atherogenic Pathway in Primary Human Macrophages

Kareem Awad [1,2,3,4,*], Laura Kakkola [1,5] and Ilkka Julkunen [1,5,6]

[1] Institute of Biomedicine, Faculty of Medicine, University of Turku, 20520 Turku, Finland; laura.kakkola@utu.fi (L.K.); ilkka.julkunen@utu.fi (I.J.)
[2] Medical Faculty, Ruprecht-Karls-University of Heidelberg, 69117 Heidelberg, Germany
[3] Academy of Scientific Research & Technology (ASRT-STARS), Cairo 11516, Egypt
[4] Institute of Pharmaceutical and Drug Industries Research, National Research Centre, Giza 12622, Egypt
[5] Clinical Microbiology, Turku University Hospital, 20521 Turku, Finland
[6] InFLAMES Research Flagship, University of Turku, 20014 Turku, Finland
* Correspondence: kareem.awad@web.de or kareem.awad@utu.fi

Abstract: Hundreds of millions of people worldwide are expected to suffer from diabetes mellitus. Diabetes is characterized as a dynamic and heterogeneous disease that requires deeper understanding of the pathophysiology, genetics, and metabolic shaping of this disease and its macro/microvascular complications. Macrophages play an essential role in regulating local immune responses, tissue homeostasis, and disease pathogenesis. Here, we have analyzed transforming growth factor beta 1 (TGFβ1)/Smad signaling in primary human macrophages grown in normal (NG) and high-glucose (HG; +25 mM glucose) conditions. Cell culture lactate concentration and cellular phosphofructokinase (PFK) activity were increased in HG concentrations. High glucose levels in the growth media led to increased macrophage mRNA expression of TGFβ1, and TGFβ-regulated HAMP and PLAUR mRNA levels, while the expression of TGFβ receptor II remained unchanged. Stimulation of cells with TGFβ1 protein lead to Smad2 phosphorylation in both NG and HG conditions, while the phosphorylation of Smad1/5 was detected only in response to TGFβ1 stimulation in HG conditions. The use of the specific Alk1/2 inhibitor dorsomorphin and the Alk5 inhibitor SB431542, respectively, revealed that HG conditions led TGFβ1 to activation of Smad1/5 signaling and its downstream target genes. Thus, high-glucose activates TGFβ1 signaling to the Smad1/5 pathway in primary human macrophages, which may contribute to cellular homeostasis in a harmful manner, priming the tissues for diabetic complications.

Keywords: high glucose; macrophage; TGFβ1; Smad; diabetes; atherosclerosis

1. Introduction

To date, diabetes mellitus accounts more than 500 million cases worldwide and is considered a chronic and heterogeneous group of diseases. Although certain disease mechanisms of diabetes are known, deeper understanding of the pathophysiology, genetics and metabolic disorders contributing to the disease and especially influencing diabetes-related macro/microvascular complications is urgently needed [1].

Macrophages are innate immune cells that reside in many organs and orchestrate various physiological and pathological processes in humans [2–6]. Macrophages are classified into M1 or M2 types based on physiological conditions: infection-induced M1 macrophages protect against pathogens, while cytokine-differentiated M2 macrophages are involved in tissue repair [3–5]. Abnormal function of these immune cells can contribute to chronic inflammation and subsequent pathological consequences including cardiometabolic disorders [3–6]. The function of macrophages is regulated through signaling pathways induced by various extracellular stimuli.

Transforming growth factor-β1 (TGFβ1) is a multifunctional cytokine that, based on environmental or cellular context, leads to a diversity of cellular responses, including cell proliferation, differentiation, migration, apoptosis, and cancer progression [7,8]. TGFβ1 binds to the cytoplasmic serine/threonine kinase domain of type II receptor which assembles a receptor I complex. TGFβ1 binding to its receptor complex leads to phosphorylation of Smad family proteins, which translocate into the nucleus and control gene expression [9,10]. Smad proteins are classified into three groups: receptor-regulated (R-Smad; Smad1, Smad2, Smad3, Smad5, and Smad8/9), inhibitory (I-Smad; Smad6 and Smad7), and common-mediator (Co-Smad; Smad4) [10] Smad proteins. I-Smads can inhibit the activation of R-Smads by competing with R-Smad to bind to its receptor and/or by recruiting specific ubiquitin ligases to the activated receptor complex [9,10].

TGFβ1 has been shown to initiate differential gene expression in immune cells, based on the type of environmental stimuli and expressed Smads, via TGFβ1/Smad2/3 or TGFβ1/Smad1/5 signaling [3]. The balance between Smad1/5- and Smad2/3-dependent signaling, and the expression of inhibitory Smad7, could define the outcome of the effect of TGFβ1 on macrophages, and differential gene expression could lead to either protective or harmful health consequences [3]. The TGFβ1-induced genes that are associated with atherogenesis include HAMP and PLAUR [3].

HAMP is a gene coding for hepcidin that regulates iron hemostasis in macrophages [11]. High hepcidin levels result in iron trapping in macrophages, and retention of iron in macrophages leads to the development of foam cells and plaque formation that enhance atherosclerosis [12–14]. PLAUR is a gene coding for urokinase plasminogen activator surface receptor (uPAR) that is elevated in atherosclerosis and in many cancer types [15–19]. Particularly, increased uPAR modulates monocyte functions and enhances atherogenesis [15,20].

Metabolic events such as high glucose or increased tissue lactate levels have been shown to affect TGFβ1/Smad signaling (reviewed in ref. [21]). Our aim here was to investigate the effect of high glucose on the expression of atherogenic genes via TGFβ1/Smad signaling to provide further knowledge on the possible role of high glucose in the development of atherosclerosis.

2. Materials and Methods

2.1. Primary Human Macrophage Culture

Monocytes were isolated from buffy coat blood products from healthy blood donors, and macrophages were differentiated from monocytes according to a standard procedure [3,22]. Buffy coat preparations were purchased from either the German or Finnish Red Cross Blood Service, Mannheim, Germany or Helsinki, Finland. In brief, peripheral blood mononuclear cells were purified from 13 buffy coat preparations using Ficoll density gradient followed by either $CD14^+$ magnetic cell sorting (Miltenyi Biotech, Bergisch Gladbach, Germany) or by allowing mononuclear cells to adhere to plates (1×10^6 cells per mL; Falcon; Becton Dickinson, Franklin Lakes, NJ, USA) for 1 h in RPMI 1640 medium (Sigma-Aldrich, St. Louis, MO, USA) at +37 °C. Macrophage serum free culture medium (Marcophage-SFM, Thermo Fisher Scientific, Waltham, MA, USA) was supplemented with penicillin/streptomycin, 20 mM HEPES, and 2 mM l-glutamine. Non-adherent cells were removed by washing with cold phosphate-buffered saline (PBS). The adherent monocytes were differentiated into macrophages by growing them in Macrophage-SFM adjusted to levels of normal (~17.5 mM) and high (+25 mM resulting in 42.5 mM) D-glucose (Sigma-Aldrich, USA) before being supplemented with penicillin/streptomycin, 20 mM HEPES, 2 mM l-glutamine, and human recombinant granulocyte macrophage colony-stimulating factor (GM-CSF; 10 ng/mL; Nordic Biosite, Täby, Sweden). The cells were differentiated into macrophages for 7 days with a change of fresh culture medium every 2 days and monitoring of differentiated macrophages via light microscopy. Alternatively, monocytes were differentiated to M2 type macrophages by stimulating with IL-4 (10 ng/mL; Peprotech, London, UK) in X-vivo 10 serum-free medium (Cambrex, Verviers, Belgium) for 6 days. TGF-β1 (TEBU Peprotech, Frankfurt am Main, Germany) was used at a final concentration of 10 ng/mL.

Dexamethasone (Sigma-Aldrich, Munich, Germany) was used at a concentration of 100 nM. Inhibitors of signaling pathways (dorsomorphin or SB431542) and inhibitors of ALK1/2 or ALK5 were used in 1 µM or 5 µM concentrations, respectively. Supernatants of culture media and cell lysates (cells scraped off carefully with rubber cell scratchers into appropriate reagent, see below) were collected and stored at −80 °C until further analysis.

2.2. Lactate Assay

Lactate was assayed colorimetrically in the supernatants of normal and +25 mM glucose culture of 2×10^6 cells using the Abcam lactate assay kit (ab65331, Cambridge, UK) according to the manufacturer's instructions. After 30 min of incubation at room temperature, the lactate concentration was measured using a multi-well plate (VICTOR® Nivo, PerkinElmer, Waltham, MA, USA) reader at 450 nm and calculated using a lactate standard curve.

2.3. Phosphofructokinase (PFK) Assay

PFK1 activity was assayed colorimetrically from cell lysates of macrophages cultured in a normal and +25 mM glucose concentration using the 6-phosphofructokinase activity assay kit from Abcam (ab155898, UK). Cell lysates were prepared by lysing 10^6 cells with the lysis buffer provided in the kit, according to the protocol provided by the manufacturer. PFK activity was measured in the cell lysates using a multi-well plate reader (VICTOR® Nivo, PerkinElmer) at 450 nm at two time points, kinetic T1 (20 min) and T2 (40 min). An NADH standard curve was used to calculate PFK1 activity.

2.4. Quantitative Real-Time Reverse Transcriptase PCR (qRT-PCR)

Total cellular RNA from the macrophages (2×10^6 cells) cultured in normal and +25 mM glucose concentrations was extracted using a PureLink® RNA Mini Kit (Invitrogen, Waltham, MA, USA) according to the protocol of the manufacturer. RNA was quantified with a nano-spectrophotometer (DeNovix, Wilmington, DE, USA). Equal concentrations (100 ng) of RNA were reverse-transcribed into cDNA using the High-Capacity cDNA Reverse Transcription Kit (Thermo Fisher Scientific, USA) according to the manufacturer's protocol. To amplify individual genes, specific primers for TGFβ1, Smad7, HAMP and PLAUR were used (Table 1). RT-qPCR was performed using 100 ng cDNA and PowerTrack SYBR Green Kit (Thermo Fisher Scientific, USA) according to the manufacturer's protocol with Rotor Gene Q PCR machine (Qiagen; Hilden, Germany). The RT-qPCR program was as follows: initial heat activation at 95 °C for 15 min, followed by 40 cycles of denaturation at 94 °C for 15 s, annealing at 52 °C for 30 s, and extension at 72 °C for 30 s. Levels of specific mRNA expression were normalized to mRNA expression levels of GAPDH, and the relative change in gene expression was calculated according to formula $2^{-\Delta\Delta Ct}$.

Table 1. List of primers.

Gene	Primers Forward/Reverse	Accession Number
TGFβ1	TTATTGAGCACCTTGGGCAC	NM_000660.7
	TCTCTGGGCTTGTTTCCTCAC	
Smad7	TTCCTCGGAAGTCAAGAGGCT	NM_005904.4
	CCATCGGGTATCTGGAGTAA	
HAMP	ACAACTTGCAGAGCTGCAAC	NM_021175.4
	GCAGCAGAAAATGCAGATGG	
PLAUR	TGAAGATCACCAGCCTTACC	NM_002659.4
	TGATGAGCCACAGGAAATGC	
GAPDH	GGTGGTCTCCTCTGACTTCAAC	NM_002046.7
	GTTGCTGTAGCCAAATTCGTTG	

2.5. Analysis of the Phosphorylation of Smads Proteins

For the analysis of the phosphorylation of Smads proteins, isolated monocytes were cultured under normal and high glucose concentrations (+25 mM) and differentiated into M2 type macrophages with IL-4 for 6 days. In addition, TGFβ1 receptor expression was induced in the cells with simultaneous incubation with dexamethasone for 6 days [23]. To induce the signaling pathway, TGFβ1 (10 ng/mL) was added for 3 h. Subsequently, 1–3 × 10^6 cells were lysed in 50 µL lysis buffer (50 mM Tris HCl, pH 7.4, 150 mM NaCl, 1 mM EDTA, 5 mM NaF, 1% NP-40, 2 mM $NaVO_3$, 0.25% Na deoxycholate, and 1× Complete protein inhibitors; Roche, Mannheim, Germany). Western blotting (WB) was performed as previously described [12]. Briefly, the samples were separated on a 12% PAGE and transferred to a nitrocellulose membrane. For the detection of proteins, rabbit anti-human Smad2/3 mAb, anti-human Smad1 mAb or anti-human phospho-Smad2 mAb or anti-human phospho-Smad1/5 mAb (Cell Signaling Technology, Danvers, MA, USA) was used in a 1:1000 dilution. As a secondary antibody, HRP-linked anti-rabbit IgG whole A (GE Healthcare, Chicago, IL, USA) was used in a dilution of 1:5000. Chemiluminescence detection was performed using SuperSignal Pico peroxidase substrate (Pierce, Waltham, MA, USA), and exposed to Kodak BioMax light films for 1 to 30 min. Films were developed in an X-ray film processor.

2.6. Flow Cytometry

Cells were scraped carefully from a 6-well plate into 15 mL tubes. The suspension was centrifuged at 300× *g* for 8 min in a swing-out rotor. The supernatant was aspirated, and cells were washed once in 5 mL of 2% BSA in PBS and centrifuged. For staining, the cell pellet was re-suspended in 2% BSA in PBS (approximately 10^6 cells in 100 µL). Then, 5 µL of anti-human TGFβRII phycoerythrin conjugated mouse IgG antibody (R&D systems) or PE conjugated mouse IgG1 K isotype control (BD Bioscience, Franklin Lakes, NJ, USA) was added to the cell suspension (1:60) and incubated on ice for 1 h in the dark. The suspension was centrifuged for 10 min at 200× *g* at +4 °C. Supernatants were discarded, and cells were washed two times with 2% BSA in PBS. After the last centrifugation, the supernatant was aspirated and cell pellets were suspended in 350 µL of 2% BSA in PBS. Staining was analysed using BD FACS Canto II (BD Bioscience, USA).

2.7. Statistical Analysis

Data were analyzed using the Graph Pad Prism software version 8 (La Jolla, San Diego, CA, USA) and Microsoft Excel 2013. Normality was determined by the Shapiro–Wilk test. Data are presented as mean ± SD. Statistical significance was assessed by either a paired Student's *t*-test to compare normal to high-glucose groups from the same donors or by an ordinary one-way ANOVA followed by Tukey's multiple comparisons test to assess significant difference between the donors. A *p*-value of less than 0.05 was considered statistically significant.

3. Results

3.1. Lactate Concentration and Phosphofructokinase Enzyme Activity in Macrophages Cultured under Normal or High Glucose Levels

Macrophages from four donors were grown in normal and in high (+25 mM) glucose, and lactate concentration was measured on day 7 (Figure 1A). When comparing macrophages of the same donor grown in normal glucose to macrophages grown in high glucose, the lactate production in macrophages grown in high glucose was significantly increased (in 3 out of 4 donors). Phosphofructokinase (PFK) activity was measured on day 7 (Figure 1B). According to the PFK activity assay kit, activity was measured at two time points (20 min (T1) and 40 min (T2)). Similarly, the PFK activity was significantly increased after culturing the macrophages in high glucose compared to the normal glucose. The results indicate that the high-glucose environment causes metabolic changes in the macrophages, with increased PFK activity and higher lactate concentrations.

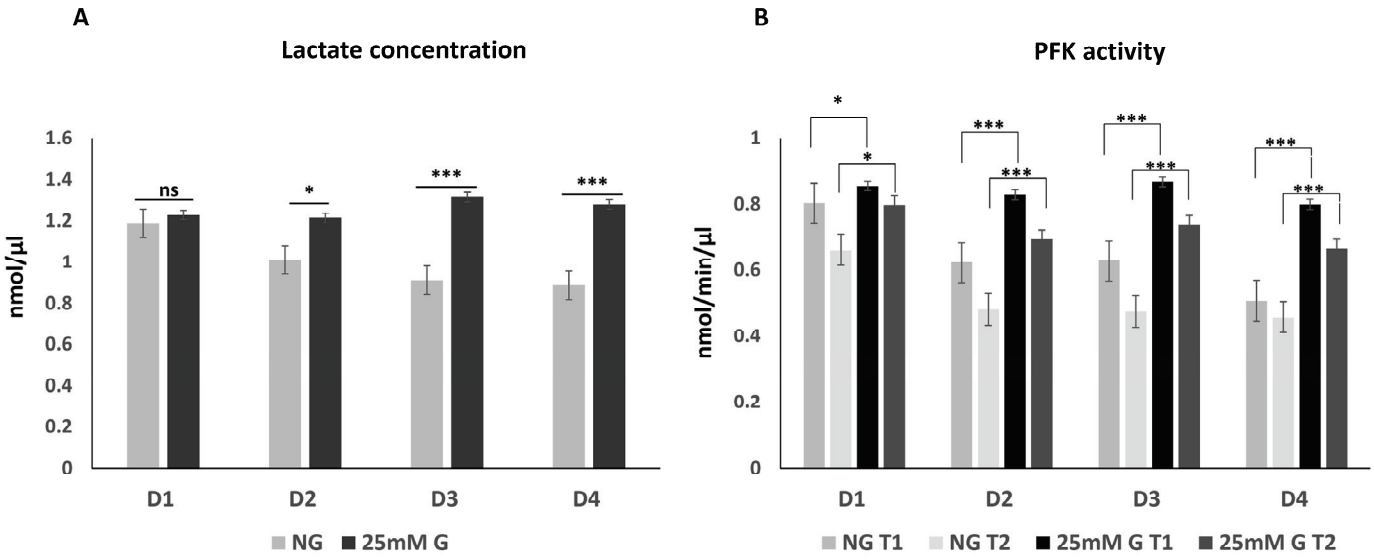


Figure 1. (**A**) Lactate concentration (nmol/µL) and (**B**) phosphofructokinase (PFK) enzyme activity (nmol/min/µL) in culture medium of macrophages from four donors (D1–D4) grown for 7 days in normal (NG) and in high (25 mM) glucose concentrations. Error bars represent the measurement results of duplicates or triplicates, * $p < 0.05$, *** $p < 0.001$).

3.2. The Expression of TGFβ1, Smad7, HAMP, and PLAUR mRNA in Macrophges Cultured under Normal or High-Glucose Conditions

The relative expression of four mRNAs, TGFβ1, Smad7, HAMP and PLAUR, was quantified on day 7 in the macrophages grown in normal and in high (+25 mM) glucose (Figure 2). GAPDH mRNA was used as a reference. The expression of TGFβ1 was significantly increased in high glucose, compared to normal glucose, in macrophages obtained from all four donors (Figure 2A). However, the expression of SMAD7 was significantly decreased in high glucose concentrations. The expression levels of both HAMP (Figure 2B) and PLAUR mRNA (Figure 2C) were significantly increased in high glucose compared to normal glucose in macrophages obtained from all four donors. The results were similar within the donors, although variation in expression levels between the donors was evident.

3.3. TGFβ1/Smad Signaling in Macrophages Cultured under Normal or High Glucose

To analyze the phosphorylation events specific to the TGFβ1 signaling pathway, isolated monocytes were cultured in normal or high-glucose conditions and differentiated into TGFβ1-receptor-expressing macrophages with IL-4 and dexamethasone. The TGFβ1 signaling pathway was activated with TGFβ1, and the cells were analyzed for the phosphorylation of Smad proteins (Figure 3). Smad2 was phosphorylated upon TGFβ1 stimulation in both normal and high-glucose conditions (Figure 3A), while phosphorylation of Smad1/5 was observed only in high-glucose conditions. Of note, variation between the donors was observed with differential intensities of phosphorylated Smads (Table 2, Supplementary Figures S1–S4).

To further analyze the TGFβ1 signaling pathway, specific inhibitors for receptor serine/threonine kinases ALK1/2 and ALK5 (dorsomorphin and SB431542, respectively) were used in high-glucose conditions to inhibit the activation of these receptors in the presence of TGFβ1 (Figure 3B). A specific ALK5 inhibitor, SB431542, (SB, 5 µM) inhibits phosphorylation of both Smad2 and Smad1/5, while the specific ALK1/2 inhibitor, dorsomorphin, inhibits the phosphorylation of Smad1/5 but not that of Smad2. This indicates that TGFβ1-induced phosphorylation of Smad2 requires only the activation of ALK5 receptor, while the phosphorylation of Smad1/5 requires the recruitment of the ALK2 receptor in addition to ALK5.

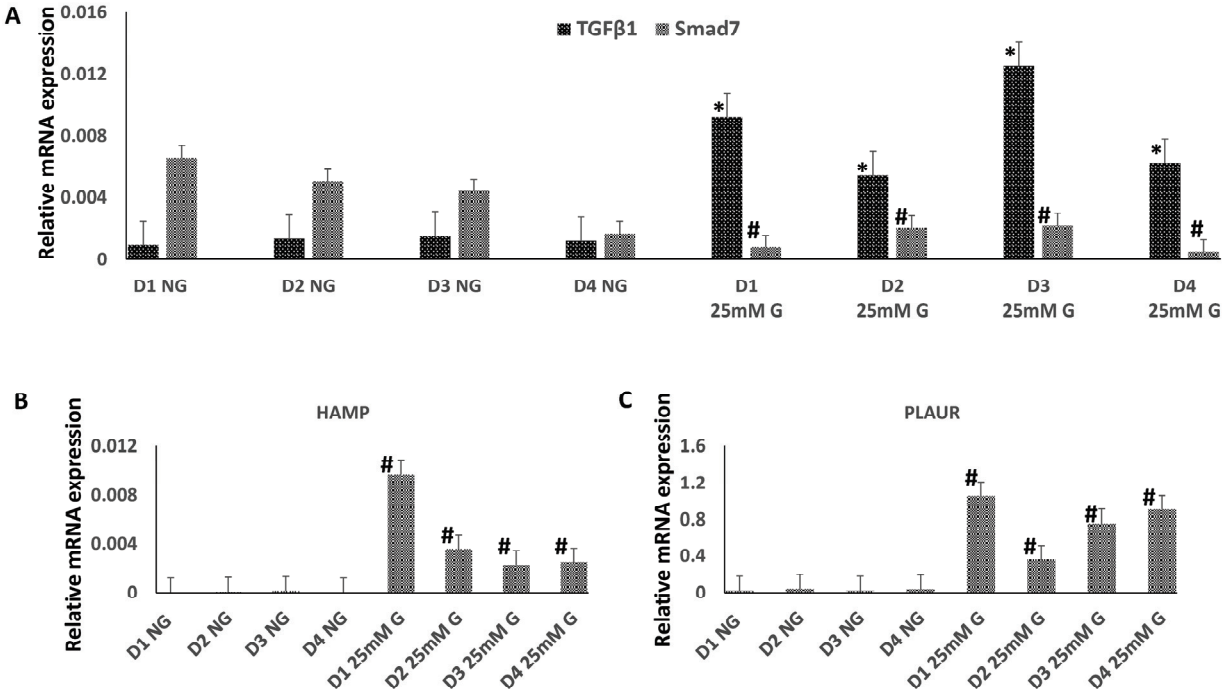


Figure 2. Relative expression levels of (**A**) TGFβ1 and Smad7, (**B**) HAMP, and (**C**) PLAUR mRNAs in the macrophages from four donors (D1–D4) grown in normal (NG) and in high (+25 mM) glucose concentrations. Error bars represent the measurements in duplicates or triplicates, * or # refer to statistical difference $p < 0.05$ between the samples of the same donor in normal glucose (NG) and high glucose (+25 mM) concentrations.

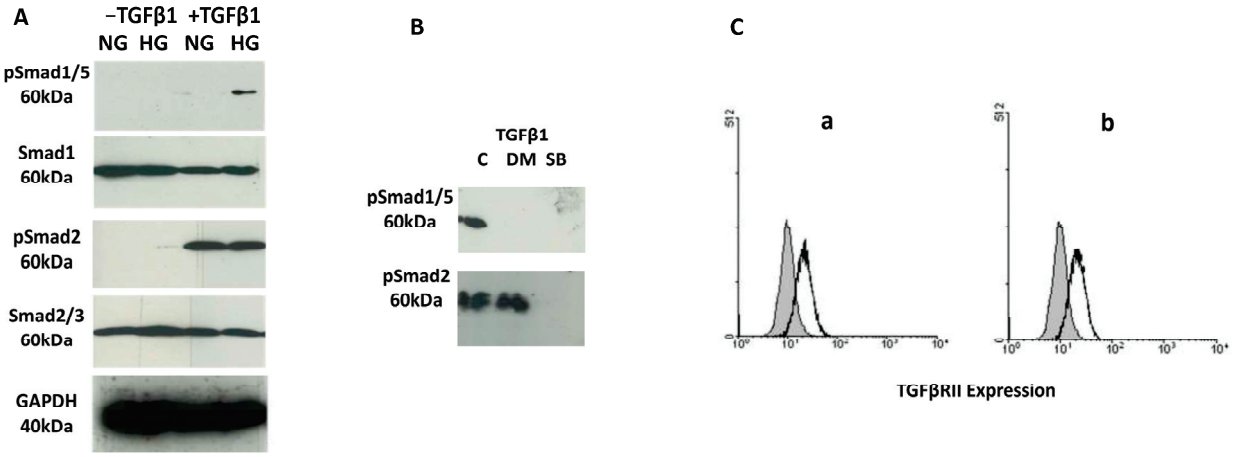


Figure 3. TGFβ1/Smad signaling in macrophages (**A**) cultured under a normal (NG) or high glucose (HG) concentration, and induced with TGFβ1. Phosphorylation of Smad proteins was analyzed with immunoblotting. Phosphorylated Smad1/5 and Smad2 and total Smad1/5 and Smad2/3 proteins were detected. GAPDH was used as a loading control. (**B**) Dorsomorphin (DM), a specific inhibitor of ALK1/2, or SB431542 (SB), a specific inhibitor of ALK5, was added 1 h before TGFβ1 stimulation, and the phosphorylation of Smad proteins in high-glucose conditions was analyzed with immunoblotting. (**C**) FACS analysis of the expression of TGFβRII on the surface of macrophages cultured under normal (a) and high (b)-glucose conditions. ($n = 5$; tests were performed in duplicate).

Table 2. The arbitrary intensity of phosphorylation of Smad2 and Smad1/5 upon stimulation with TGFβ1 in macrophages from seven individual donors. The differences in intensity (i.e., protein expression in immunoblotting) show the differential responses of donors under the same conditions.

Donor	pSmad2	pSmad1/5
1	LG: ++ HG: +++	LG: −− HG: ++
2	LG: ++ HG: ++	LG: −− HG: ++
3	LG: +++ HG: +++	LG: −− HG: +++
4	LG: ++ HG: ++	LG: −− HG: +
5	LG: +++ HG: +++	LG: −− HG: ++
6	LG: +++ HG: +++	LG: −− HG: +
7	LG: +++ HG: −	LG: −− HG: +++

(+++; highest expression, ++; higher expression, +; expressed, −−; not expressed).

To confirm the expression of the TGFβ1 receptor, TGFβRII, on the surface of macrophages, TGFβRII expression was analyzed by FACS on macrophages cultured in normal and high-glucose conditions (Figure 3C). The expression level of TGFβRII was not affected by the increasing glucose concentration. These results indicate that macrophages cultured in normal or high glucose concentrations express equal amounts of TGFβRII, and thus the differential effect of TGFβ1 induction on the phosphorylation of Smad proteins is not dependent on the expression of the receptor but rather on downstream signaling molecules regulated by different glucose concentrations.

4. Discussion

Diabetes mellitus is a disease which may appear with characteristic clinical symptoms like polydipsia, polyuria, weight loss, or ketoacidosis-associated symptoms. The disease may also appear as a non-symptomatic form without its typical clinical symptoms (which are defined as a constant increase in blood glucose levels [24]), meaning that recently, high blood glucose levels have come into question as the only important parameter for defining diabetes. Diabetes mellitus, including type 1 and type 2 diabetes, probably comprises several distinct disorders of the metabolism or post-translational mechanisms, which evidences the need to create novel approaches for understanding the disease and its complications [25]. Late diabetic complications including retinopathy, nephropathy, neuropathy, and other macro/micro vascular complication raises the need to develop in vitro cell culture models to better understand the disease's pathogenesis in different tissues.

In the present work, we cultured human primary macrophages in normal and high-glucose conditions and analyzed cellular responses to high glucose levels. We adjusted normal and high glucose for the cultured macrophage population based on the viability of macrophages to glucose concentrations found in diabetes. There is now evidence that different cell types tolerate specific glucose concentrations in vitro before they show significant changes due to hyperglycemia or abnormal glucose concentration in their growth culture [26,27]. In our cell system, we clearly observed increased gene expression of TGFβ1 and HAMP and PLAUR genes (higher mRNA levels). It is thus likely that constitutively high glucose levels may also enhance the production of TGFβ1 and its downstream target genes HAMP and PLAUR in human primary macrophages. Interestingly, high glucose levels did not regulate TGFβRII expression, suggesting that the effect of high glucose in our experimental system is mediated at the TGFβ signaling level. TGFβ1 is an important

regulator of immune tolerance and homeostasis whose inhibition may contribute to the eradication of cancer and cardiovascular deteriorations [28,29]. TGFβ1 levels have been demonstrated to be increased in experimental atherosclerosis [30], aortic aneurysmal disease [31], atherosclerotic plaques in patients with coronary hearth disease [32], and in monocytes circulating in patients with atrial fibrillation and fibrosis [33].

As TGFβ-activated signaling molecules, Smad proteins consist of two domains, mad homology 1 (MH1) and MH2, which are responsible for DNA binding and protein interactions with other regulatory proteins, respectively [10]. This suggests that various functional domains are responsible for the flexible and differential functions of Smad family proteins. The present work shows that hyperglycemia in human macrophages changes the balance between Smad1/5 and Smad2/3-dependent signaling. This may contribute to the outcome of the effect of TGFβ1 on cardiovascular risks, where Smad1/5 is responsible for the expression of pro-atherogenic genes and Smad2/3 downregulates TGFβ1 functions by upregulating Smad7 expression. Smad7 is known to downregulate signaling by other Smad proteins (10). Interestingly, we saw a great variation in TGFβ1-induced Smad activation among individual blood donors. Even though there was some variation between the donors, the general trend in differentiated macrophages obtained from the monocytes of a total of seven blood donors was very similar. In high-glucose conditions, TGFβ1, HAMP, and PLAUR mRNA expression was increased, and TGFβ1 activated Smad1/5 phosphorylation (in addition to Smad2) suggesting a constant biological phenomenon among all analyzed donors. Thus, this work provides evidence on the cell receptor regulation of this possible Smad1/5–TGFβ1 atherogenic pathway, where inhibition of Alk1/2 but not Alk5 by pharmacological inhibitors may block the activation of the Smad1/5 signaling pathway (Figure 4).

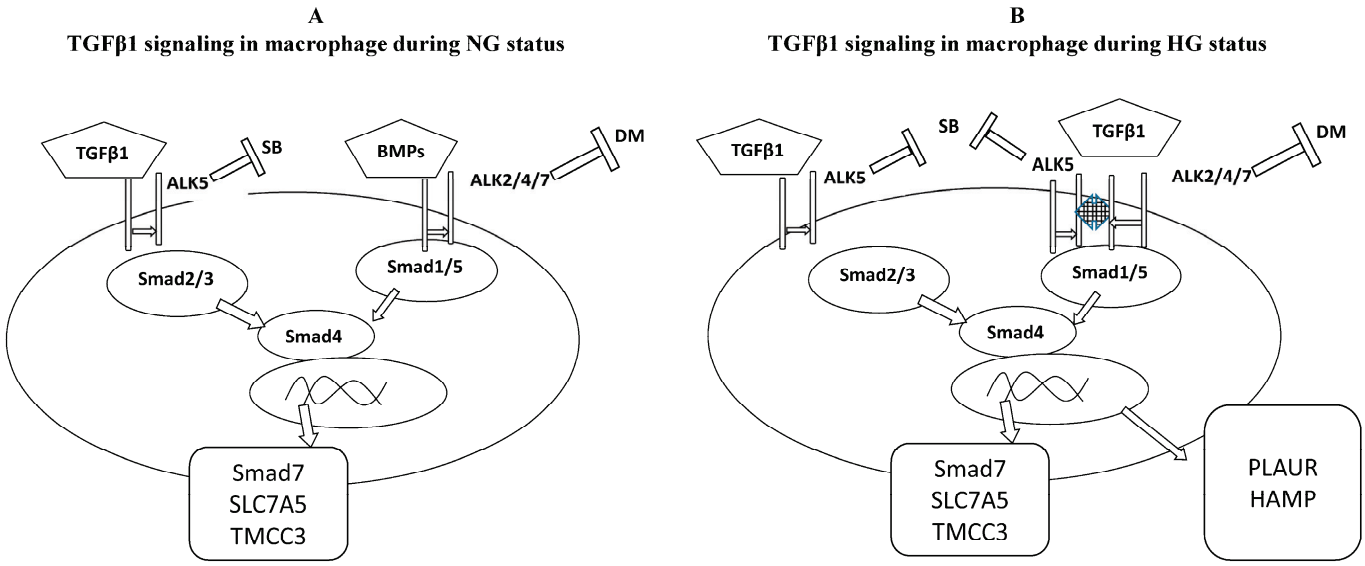


Figure 4. Schematic model of the action of TGFβ1/Smad signaling in human macrophages cultured in normal (NG) vs. high (HG)-glucose conditions. (**A**) Under normal glucose conditions, TGFβ1 binds to a type II receptor which assembles to receptor ALK5, leading to phosphorylation of the Smad2 and 3 proteins. Phosphorylation of Smad1 and 5 proteins occurs through BMPs binding to their specific receptor and recruitment of ALK2. Subsequently, these events lead to TGFβ1- or BMP-induced gene expression, respectively. (**B**) Under high-glucose conditions, TGFβ1 expression increases, and binding of TGFβ1 to a type II receptor leads to activation of both ALK5 and ALK2 receptors, leading to phosphorylation of both Smad2 and 3 as well as Smad1 and 5. Smad1 and 5 activation subsequently leads to differential gene expression, including atherosclerotic genes HAMP and PLAUR. Abbreviations: TGFβ1, transforming growth beta 1; BMPs, bone morphogenic proteins; SB, SB431542; DM, dorsomorphin.

The potentially harmful effects of high glucose levels on the Smad1/5 pathway have been associated with the expression of HAMP and PLAUR genes. Accumulation of iron has been detected in atherosclerotic lesions, particularly in macrophages/foam cells. However, the exact mechanisms explaining the role of hepcidin in atherogenesis and how it induces iron retention in plaque macrophages have never been clearly elucidated [12–14]. In the present study, we provide a possible mechanism for enhanced HAMP expression, i.e., high glucose levels led to enhanced Smad1/5 signaling triggered by increased lactate levels, or a "Warburg"-like status enhanced the expression of HAMP in hyperglycemic macrophages.

Here, we demonstrated increased PLAUR expression in hyperglycemic conditions. PLAUR has been associated with the regulation of uPAR in a mechanism including vascular endothelial growth factor, interfering with the blood–retinal barrier that characterizes the early stages of vascular dysfunction in diabetes [34]. Higher serum uPAR levels were associated with higher mortality beyond traditional risk factors among African Americans with type 2 diabetes mellitus [35]. Higher serum levels of uPAR are also an independent and significant indicator of cardiovascular events in type 1 diabetes [36,37]. Our data and previously published studies suggest that the Smad1/5 PLAUR pathway is a mechanism underlying the association of high glucose levels with risk of cardiovascular events, which may yield new molecular targets for the development new diagnostic/therapeutic strategies.

Our data agree with previous observations that the role of increased lactate levels and PFK activity, which are seen in hyperglycemia, is associated with immunometabolic regulation of TGFβ1 expression and perhaps that of other immunoregulatory molecules [38–40]. A high-glucose environment will activate a genetic cascade that can polarize macrophages toward a specific M1-like phenotype, and this could lead to further tissue damage in diabetic conditions, a phenomenon which is, however, a matter for further investigation [41–43].

In summary, our study provides evidence that high glucose in cultured primary human macrophages increases the lactate concentration and upregulates the expression of TGFβ1 and its downstream HAMP and PLAUR genes. TGFβ1 in high-glucose conditions can also activate Smad 1/5 phosphorylation, likely contributing to enhanced HAMP and PLAUR mRNA expression. Our study may provide a mechanistic explanation for increased glucose levels in primary human cells activating TGFβ1 signaling pathways and thus contributing to pathogenic events in hyperglycemic diseases. This information may be helpful and important in the further development of drugs that can reduce the appearance of severe diabetes-associated disease complications.

5. Conclusions

The present work provides new knowledge on the role of high glucose in activating TGFβ1 signaling to the Smad1/5 pathway in primary human macrophages and presents one possible explanation of the role of HAMP and PLAUR in immune and vascular deteriorations, which are the main complications of diabetes. Moreover, it suggests a possible method of terminating this pathway by designing pharmacological interventions specific to the TGFβ family receptor type.

Supplementary Materials: The following supporting information can be downloaded at: https://www.mdpi.com/article/10.3390/biomedicines12071575/s1, Figures S1–S6: TGFβ1 signaling through Smads in macrophages cultured under NG or HG conditions in analyzed donors under the same experimental conditions.

Author Contributions: Laboratory analyses, K.A.; Funding acquisition, K.A., L.K. and I.J.; Investigation, K.A.; Supervision, L.K. and I.J.; Visualization, L.K. and I.J.; Writing—original draft, K.A.; Review and editing, L.K. and I.J. All authors have read and agreed to the published version of the manuscript.

Funding: This research was funded by the Finnish Government Scholarship Pool number KM-19-11070; the German Egyptian long-term scholarship, Ministry of Higher Education and Research, Egypt, grant number A1190926; and the Egyptian Academy of Scientific Research and Technology (ASRT-STARS) granted to K.A. This study was also supported by the Academy of Finland (grant

number 337530 to I.J. and 339512 to L.K.), the Jane and Aatos Erkko Foundation (grant numbers 3067-84b53 and 5360-cc2fc to I.J.), and the Sigrid Jusélius Foundation (to I.J. and L.K.).

Institutional Review Board Statement: For the period of this study (2013–2023), the law required that BCs were purchased anonymously and that they were not linked to any identifying information of the donor, e.g., name, gender, age, etc. Hence, BC purchases only required the local permission of the Blood Service for the BCs to be used in scientific experiments.

Informed Consent Statement: Not applicable.

Data Availability Statement: All data are available from the corresponding author upon reasonable request. The original contributions presented in this study (blotting/protein analysis) are included in the Supplementary Materials as a minimal dataset necessary for evaluation. Further inquiries can be directed to the corresponding author/s. The numeric data set is presented as figures and included within the manuscript and can be made available by the authors in other forms upon request for presentation protection rights.

Conflicts of Interest: The authors declare no conflicts of interest. The funders had no role in the design of the study; in the collection, analyses, or interpretation of data; in the writing of the manuscript; or in the decision to publish the results.

Abbreviations

TGFβ1	transforming growth factor beta 1
NG	normal glucose
HG	high glucose
PFK	phosphofructokinase
uPAR	urokinase plasminogen activator surface receptor
GM-CSF	granulocyte-MQ colony-stimulating factor
PBS	phosphate-buffered saline

References

1. Ahmad, E.; Lim, S.; Lamptey, R.; Webb, D.R.; Davies, M.J. Type 2 diabetes. *Lancet* **2022**, *400*, 1803–1820. [CrossRef]
2. Motawi, T.K.; Shahin, N.N.; Maghraby, A.S.; Kirschfink, M.; Abd-Elshafy, D.N.; Awad, K.; Bahgat, M.M. H1N1 Infection Reduces Glucose Level in Human U937 Monocytes Culture. *Viral Immunol.* **2020**, *33*, 384–390. [CrossRef]
3. Nurgazieva, D.; Mickley, A.; Moganti, K.; Ming, W.; Ovsyi, I.; Popova, A.; Sachindra; Awad, K.; Wang, N.; Bieback, K.; et al. TGF-β1, but not bone morphogenetic proteins, activates Smad1/5 pathway in primary human macrophages and induces expression of proatherogenic genes. *J. Immunol.* **2015**, *194*, 709–718. [CrossRef]
4. Awad, K.; Maghraby, A.S.; Abd-Elshafy, D.N.; Bahgat, M.M. Carbohydrates metabolic signatures in immune cells: Response to infection. *Front. Immunol.* **2022**, *13*, 912899. [CrossRef]
5. Raggi, F.; Pelassa, S.; Pierobon, D.; Penco, F.; Gattorno, M.; Novelli, F.; Eva, A.; Varesio, L.; Giovarelli, M.; Bosco, M.C. Regulation of Human Macrophage M1-M2 Polarization Balance by Hypoxia and the Triggering Receptor Expressed on Myeloid Cells-1. *Front. Immunol.* **2017**, *8*, 1097. [CrossRef]
6. Wang, L.; Yi, X.; Xiao, X.; Zheng, Q.; Ma, L.; Li, B. Exosomal miR-628-5p from M1 polarized macrophages hinders m6A modification of circFUT8 to suppress hepatocellular carcinoma progression. *Cell. Mol. Biol. Lett.* **2022**, *27*, 106. [CrossRef]
7. Massague, J. TGFbeta signalling in context. *Nat. Rev. Mol. Cell Biol.* **2012**, *13*, 616–630. [CrossRef] [PubMed]
8. Xiao, J.; Huang, J.; Jian, X.; Wang, H.; Lan, H.; Liao, Z.; Gu, R.; Hu, J.; Liao, H. IRE1α arm of unfolded protein response in muscle-specific TGF-β signaling-mediated regulation of muscle cell immunological properties. *Cell. Mol. Biol. Lett.* **2023**, *28*, 15. [CrossRef] [PubMed]
9. David, C.J.; Massagué, J. Contextual determinants of TGFβ action in development, immunity and cancer. *Nat. Rev. Mol. Cell Biol.* **2018**, *19*, 419–435. [CrossRef] [PubMed]
10. Aigner, L.; Bogdahn, U. TGF-beta in neural stem cells and in tumors of the central nervous system. *Cell Tissue Res.* **2008**, *331*, 225–241. [CrossRef] [PubMed]
11. Brissot, P.; Pietrangelo, A.; Adams, P.C.; de Graaff, B.; McLaren, C.E.; Loréal, O. Haemochromatosis. *Nat. Rev. Dis. Primers* **2018**, *4*, 18016. [CrossRef] [PubMed]
12. Fernández-Real, J.M.; Manco, M. Effects of iron overload on chronic metabolic diseases. *Lancet Diabetes Endocrinol.* **2014**, *2*, 513–526. [CrossRef] [PubMed]
13. Xiao, L.; Luo, G.; Guo, X.; Jiang, C.; Zeng, H.; Zhou, F.; Li, Y.; Yu, J.; Yao, P. Macrophage iron retention aggravates atherosclerosis: Evidence for the role of autocrine formation of hepcidin in plaque macrophages. *Biochim. Biophys. Acta Mol. Cell Biol. Lipids* **2020**, *1865*, 158531. [CrossRef] [PubMed]

14. Cai, J.; Zhang, M.; Liu, Y.; Li, H.; Shang, L.; Xu, T.; Chen, Z.; Wang, F.; Qiao, T.; Li, K. Iron accumulation in macrophages promotes the formation of foam cells and development of atherosclerosis. *Cell Biosci.* **2020**, *10*, 137. [CrossRef] [PubMed]
15. Hindy, G.; Hindy, G.; Tyrrell, D.J.; Tyrrell, D.J.; Vasbinder, A.; Vasbinder, A.; Wei, C.; Wei, C.; Presswalla, F.; Presswalla, F.; et al. Increased soluble urokinase plasminogen activator levels modulate monocyte function to promote atherosclerosis. *J. Clin. Investig.* **2022**, *132*, e158788. [CrossRef] [PubMed]
16. Zhang, T.; Wang, B.; Su, F.; Gu, B.; Xiang, L.; Gao, L.; Zheng, P.; Li, X.-M.; Chen, H. TCF7L2 promotes anoikis resistance and metastasis of gastric cancer by transcriptionally activating PLAUR. *Int. J. Biol. Sci.* **2022**, *18*, 4560–4577. [CrossRef] [PubMed]
17. Li, J.; Fan, H.; Zhou, X.; Xiang, Y.; Liu, Y. Prognostic significance and gene co-expression network of plau and plaur in gliomas. *Front. Oncol.* **2022**, *11*, 602321. [CrossRef] [PubMed]
18. Wang, Z.; Wang, K.; Gao, X.; Liu, Z.; Xing, Z. Comprehensive analysis of the importance of PLAUR in the progression and immune microenvironment of renal clear cell carcinoma. *PLoS ONE* **2022**, *17*, e0269595. [CrossRef] [PubMed]
19. Wang, Y.; Sun, Z.; Lu, S.; Zhang, X.; Xiao, C.; Li, T.; Wu, J. Identification of PLAUR-related ceRNA and immune prognostic signature for kidney renal clear cell carcinoma. *Front. Oncol.* **2022**, *12*, 834524. [CrossRef]
20. Goodchild, T.T.; Li, Z.; Lefer, D.J. Soluble urokinase plasminogen activator receptor: From biomarker to active participant in atherosclerosis and cardiovascular disease. *J. Clin. Investig.* **2022**, *132*, e165868. [CrossRef]
21. Liu, H.; Chen, Y.G. The interplay between TGF-β signaling and cell metabolism. *Front. Cell Dev. Biol.* **2022**, *10*, 846723. [CrossRef] [PubMed]
22. Österlund, P.; Jiang, M.; Westenius, V.; Kuivanen, S.; Järvi, R.; Kakkola, L.; Lundberg, R.; Melén, K.; Korva, M.; Županc, T.A.; et al. Asian and African lineage Zika viruses show differential replication and innate immune responses in human dendritic cells and macrophages. *Sci. Rep.* **2019**, *9*, 15710. [CrossRef] [PubMed]
23. Gratchev, A.; Kzhyshkowska, J.; Kannookadan, S.; Ochsenreiter, M.; Popova, A.; Yu, X.; Mamidi, S.; Stonehouse-Usselmann, E.; Muller-Molinet, I.; Gooi, L.; et al. Activation of a TGF-beta-specific multistep gene expression program in mature macrophages requires glucocorticoid-mediated surface expression of TGF-beta receptor II. *J. Immunol.* **2008**, *180*, 6553–6565. [CrossRef] [PubMed]
24. Waldhäusl, W.; Gries, A.; Scherbaum, W. *Diabetes in der Praxis*, 2nd ed.; Springer: Berlin, Germany, 1992; pp. 3–15. ISBN 3-540-58982-1.
25. Nawroth, P. Innovative models for investigation of pathomechanisms leading to late diabetic complications. *Exp. Clin. Endocrinol. Diabetes* **2012**, *120*, 177–178. [CrossRef]
26. Ward, R.; Ergul, A. Relationship of endothelin-1 and NLRP3 inflammasome activation in HT22 hippocampal cells in diabetes. *Life Sci.* **2016**, *159*, 97–103. [CrossRef] [PubMed]
27. Xiong, Y.; Zhou, F.; Liu, Y.; Yi, Z.; Wang, X.; Wu, Y.; Gong, P. 1α,25 Dihydroxyvitamin D3 promotes angiogenesis by alleviating AGEs-induced autophagy. *Arch. Biochem. Biophys.* **2021**, *712*, 109041. [CrossRef] [PubMed]
28. Batlle, E.; Massagué, J. Transforming Growth Factor-β signaling in immunity and cancer. *Immunity* **2019**, *50*, 924–940. [CrossRef]
29. Alrasheed, N.M.; Alammari, R.B.; Alshammari, T.K.; Alamin, M.A.; Alharbi, A.O.; Alonazi, A.S.; Bin Dayel, A.F.; Alrasheed, N.M. α1A Adrenoreceptor blockade attenuates myocardial infarction by modulating the integrin-linked kinase/TGF-β/Smad signaling pathways. *BMC Cardiovasc. Disord.* **2023**, *23*, 153. [CrossRef] [PubMed]
30. Misiakos, E.; Kouraklis, G.; Agapitos, E.; Perrea, D.; Karatzas, G.; Boudoulas, H.; Karayannakos, P. Expression of PDGF-A, TGFb and VCAM-1 during the developmental stages of experimental atherosclerosis. *Eur. Surg. Res.* **2001**, *33*, 264–269. [CrossRef]
31. Saratzis, A.; Bown, M.J. The genetic basis for aortic aneurysmal disease. *Heart* **2014**, *100*, 916–922. [CrossRef]
32. Kukhtina, N.B.; Aref'eva, T.I.; Aref'eva, A.M.; Akchurin, R.S.; Krasnikova, T.L. Expression of chemokines and cytokines in atherosclerotic plaques and internal membrane of the arteries in patients with coronary artery disease. *Ter. Arkh.* **2008**, *80*, 63–69.
33. Heinzmann, D.; Fuß, S.; Ungern-Sternberg, S.V.; Schreieck, J.; Gawaz, M.; Gramlich, M.; Seizer, P. TGFβ is specifically upregulated on circulating CD14++ CD16+ and CD14+ CD16++ monocytes in patients with atrial fibrillation and severe atrial fibrosis. *Cell. Physiol. Biochem.* **2018**, *49*, 226–234. [CrossRef] [PubMed]
34. El-Remessy, A.B.; Behzadian, M.A.; Abou-Mohamed, G.; Franklin, T.; Caldwell, R.W.; Caldwell, R.B. Experimental diabetes causes breakdown of the blood-retina barrier by a mechanism involving tyrosine nitration and increases in expression of vascular endothelial growth factor and urokinase plasminogen activator receptor. *Am. J. Pathol.* **2003**, *162*, 1995–2004. [CrossRef] [PubMed]
35. Hayek, S.S.; Divers, J.; Raad, M.; Xu, J.; Bowden, D.W.; Tracy, M.; Reiser, J.; Freedman, B.I. Predicting mortality in african americans with type 2 diabetes mellitus: Soluble urokinase plasminogen activator receptor, coronary artery calcium, and high-sensitivity c-reactive protein. *J. Am. Heart Assoc.* **2018**, *7*, e008194. [CrossRef]
36. Curovic, V.R.; Theilade, S.; Winther, S.A.; Tofte, N.; Eugen-Olsen, J.; Persson, F.; Hansen, T.W.; Jeppesen, J.; Rossing, P. Soluble urokinase plasminogen activator receptor predicts cardiovascular events, kidney function decline, and mortality in patients with type 1 diabetes. *Diabetes Care* **2019**, *42*, 1112–1119. [CrossRef] [PubMed]
37. Sherif, E.M.; El Maksood, A.A.A.; Youssef, O.I.; Salah El-Din, N.Y.; Khater, O.K.M. Soluble urokinase plasminogen activator receptor in type 1 diabetic children, relation to vascular complications. *J. Diabetes Complicat.* **2019**, *33*, 628–633. [CrossRef] [PubMed]
38. Müller, J.; Radej, J.; Horak, J.; Karvunidis, T.; Valesova, L.; Kriz, M.; Matejovic, M. Lactate: The Fallacy of Oversimplification. *Biomedicines* **2023**, *11*, 3192. [CrossRef] [PubMed]

39. Schumacher, L.; Slimani, R.; Zizmare, L.; Ehlers, J.; Borgmann, F.K.; Fitzgerald, J.C.; Fallier-Becker, P.; Beckmann, A.; Grißmer, A.; Meier, C.; et al. TGF-Beta Modulates the Integrity of the Blood Brain Barrier In Vitro, and Is Associated with Metabolic Alterations in Pericytes. *Biomedicines* **2023**, *11*, 214. [CrossRef] [PubMed]
40. Oliver, M.A.; Davis, X.D.; Bohannon, J.K. TGFbeta macrophage reprogramming: A new dimension of macrophage plasticity. *J. Leukoc. Biol.* **2024**, *115*, 411–414. [CrossRef]
41. Wang, H.; Liu, F.; Zhao, W.; Guo, Y.; Mai, P.; Zhao, S.; Wen, Z.; Su, J.; Li, X.; Wang, Y.; et al. High glucose promotes atherosclerosis by regulating miRNA let7d-5p level. *J. Diabetes Investig.* **2024**, *15*, 711–724. [CrossRef]
42. Sun, H.; Ma, X.; Ma, H.; Li, S.; Xia, Y.; Yao, L.; Wang, Y.; Pang, X.; Zhong, J.; Yao, G.; et al. High glucose levels accelerate atherosclerosis via NLRP3-IL/ MAPK/NF-kappaB-related inflammation pathways. *Biochem. Biophys. Res. Commun.* **2024**, *704*, 149702. [CrossRef] [PubMed]
43. Chen, C.; Cao, J.; Gao, Y.; Xie, X.; Zhao, Z.; Yuan, Q.; He, Y.; Zu, X.; Liu, J. High glucose promotes macrophage M1 polarization through miR-32/Mef2d/cAMP signaling pathway. *Genes Dis.* **2023**, *11*, 539–541. [CrossRef] [PubMed]

Disclaimer/Publisher's Note: The statements, opinions and data contained in all publications are solely those of the individual author(s) and contributor(s) and not of MDPI and/or the editor(s). MDPI and/or the editor(s) disclaim responsibility for any injury to people or property resulting from any ideas, methods, instructions or products referred to in the content.

biomedicines

MDPI

Article

Ketosis Suppression and Ageing (KetoSAge) Part 2: The Effect of Suppressing Ketosis on Biomarkers Associated with Ageing, HOMA-IR, Leptin, Osteocalcin, and GLP-1, in Healthy Females

Isabella D. Cooper [1,*], Yvoni Kyriakidou [1], Lucy Petagine [1], Kurtis Edwards [2], Adrian Soto-Mota [3,4], Kenneth Brookler [5] and Bradley T. Elliott [1]

[1] Ageing Biology and Age-Related Diseases, School of Life Sciences, University of Westminster, 115 New Cavendish Street, London W1W 6UW, UK; y.kyriakidou@westminster.ac.uk (Y.K.); l.petagine@westminster.ac.uk (L.P.); b.elliott@westminster.ac.uk (B.T.E.)
[2] Cancer Biomarkers and Mechanisms Group, School of Life Sciences, University of Westminster, 115 New Cavendish Street, London W1W 6UW, UK; k.edwards3@westminster.ac.uk
[3] Metabolic Diseases Research Unit, National Institute of Medical Sciences and Nutrition Salvador Zubiran, Mexico City 14080, Mexico; adrian.sotom@incmnsz.mx
[4] School of Medicine, Tecnologico de Monterrey, Mexico City 14380, Mexico
[5] Retired former Research Collaborator, Aerospace Medicine and Vestibular Research Laboratory, Mayo Clinic, Scottsdale, AZ 85259, USA; kennethhbrookler@mac.com
* Correspondence: isabella@bellamitochondria.com or i.cooper@westminster.ac.uk

Abstract: Metabolic dysfunctions are among the best documented hallmarks of ageing. Cardiovascular disease, Alzheimer's disease, cancer, type 2 diabetes mellitus, metabolic-dysfunction-associated steatosis liver disease, and fragility fractures are diseases of hyperinsulinaemia that reduce life and healthspan. We studied the effect of suppressing ketosis in 10 lean (BMI 20.5 kg/m^2 ± 1.4), metabolically healthy, pre-menopausal women (age 32.3 ± 8.9 years) maintaining nutritional ketosis (NK) for an average of 3.9 years (± 2.3) who underwent three 21-day phases: nutritional ketosis (NK; P1), suppressed ketosis (SuK; P2), and returned to NK (P3). Ketosis suppression significantly increased insulin, 1.83-fold (p = 0.0006); glucose, 1.17-fold (p = 0.0088); homeostasis model assessment for insulin resistance (HOMA-IR), 2.13-fold (p = 0.0008); leptin, 3.35-fold (p = 0.0010); total osteocalcin, 1.63-fold (p = 0.0138); and uncarboxylated osteocalcin, 1.98-fold (p = 0.0417) and significantly decreased beta-hydroxybutyrate, 13.50-fold (p = 0.0012) and glucagon-like peptide-1 (GLP-1), 2.40-fold (p = 0.0209). Sustained NK showed no adverse health effects and may mitigate hyperinsulinemia. All biomarkers returned to basal P1 levels after removing the intervention for SuK, indicating that metabolic flexibility was maintained with long-term euketonaemia.

Keywords: ageing; cortisol; GLP-1; HOMA-IR; insulin resistance; hyperinsulinaemia; ketosis; leptin; metabolic syndrome; osteocalcin

1. Introduction

Ageing is typically understood in its chronological context, as the length of time that has passed since a person's birth, whereas biological age (BA) is the measure of functional age, often measured in terms of physical and mental performance, as well as morbidities that decrease quality of life and youth-span [1,2]. One-sixth of Europeans are expected to be over 60 years of age by 2030, and 25% of older adults will be above 85 [3], reflecting a chronologically aged population increase. Concurrently, chronic non-communicable diseases promote an earlier decline in BA. Additionally, cardiovascular disease (CVD), Alzheimer's disease (AD), and cancer are the leading causes of morbidity and mortality in

the USA [4], with AD and other dementias being the leading causes for females, followed by CVD, cerebral vascular disease, and cancer in England and Wales [5]. This decline in BA was disturbingly evidenced in an analysis of 8,721 participants from 2009 to 2016 from the National Health and Nutrition Examination Survey (NHANES), showing that the proportion of metabolically unhealthy Americans increased from an already very high level of 80.1% to 87.8% over the span of 7 years, putting the vast majority of the population on the hyperinsulinaemia spectrum [2,6–8]. This increase in a younger BA onset and population proportion (living with morbidity earlier and for longer) is arguably the global pandemic of our time.

The chronic non-communicable diseases AD, CVD, cancer, type 2 diabetes mellitus (T2DM), metabolic syndrome (MetS), metabolic-dysfunction-associated steatotic liver disease (MASLD), and chronic inflammation are the consequence of lifestyle factors that stimulate chronic excess insulin demand and secretion, termed hyperinsulinaemia [2,7–11]. Hyperinsulinaemia is understood to be an ageing metabolo-endocrine state, and can be staged as metabolic phenotypes (MPs) [7,8]. Hyperinsulinaemia, when assessed as fasting insulin above the reference range only, likely does not capture the sub-clinical occult phase of hyperinsulinaemia [1]. We argue that hyperinsulinaemia can be detected before exceeding the population-derived broad reference range, which does not reflect an individual's optimal level of insulin.

A symphony of biomarkers taken together are more sensitive to aid in catching hyperinsulinaemia as early as possible, especially in those with a body mass index (BMI) less than 25 kg/m^2 [1,12–14], thus enabling earlier intervention, preventive care, and minimising the incorrect grouping of research participants, which may lead to increased false negatives in study results. A prospective cohort study from the NHANES, n = 12,563 with median age 45 years (20–85 years), found hyperinsulinaemia to be a greater risk marker for increased mortality compared to BMI [15]. We previously published a report on the effect of suppressing ketosis on ageing- and chronic-disease-associated biomarkers, which included fasting insulin, insulin-like growth factor 1 (IGF-1), glucose, beta-hydroxybutyrate (BHB), gamma-glutaryl transferase (GGT), plasminogen activator inhibitor-1 (PAI-1), monocyte chemotactic protein 1 (MCP-1), and more [7]. Part 2 investigates additional biomarkers strongly associated with morbidity, including homeostasis model assessment for insulin resistance (HOMA-IR), osteocalcin (OCN), leptin, and glucagon-like peptide-1 (GLP-1), which are biomarkers positively and negatively associated with chronic diseases and ageing. We aimed to investigate the effect of long-term sustained nutritional ketosis (NK), also known as euketonaemia, on these biomarkers, and if suppressing ketosis for 21 days would result in any measurable changes, allowing us to understand one lifestyle factor that may meaningfully impact these biomarkers, which could reduce the earlier onset of BA, meaning the potential to enhance youth-span as well as lifespan.

2. Materials and Methods

2.1. Ethics

Ethical approval was obtained by the College of Liberal of Arts and Sciences Research Ethics Committee, University of Westminster, United Kingdom (ETH2122-0634). All procedures were conducted in accordance with the Declaration of Helsinki and UK legislation. Written informed consent was obtained from all participants prior to their participation.

2.2. Participants

Ten healthy pre-menopausal habitually keto-adapted women, classified as metabolic phenotype 1 (MP1) [8], were recruited to take part in this three-phase study named KetoSAge [7]. The participants self-reported their adherence to a lifestyle that sustained NK for $\geq$ 6 months (mean 3.9 $\pm$ 2.3 years), ensuring sufficient time for metabolic adaptations. Ketosis adaptation was proven during a 6-month lead-in period, where the participants were required to take a once-daily capillary BHB reading between 4–6 p.m., before their evening meal, prior to the commencement of the study. This standardised evening mea-

surement was chosen due to it being a more rigorous threshold to pass in order to be judged as sustaining NK over the majority of the 24 h day, in comparison to morning fasted measurements, thus increasing confidence in the participants maintaining NK most of the time. Readings were taken with a Keto-Mojo™ GKI multi-function meter (Keto-Mojo, Napa, CA, USA; [16]). The baseline characteristics of these participants were described in our earlier publication [7].

For the duration of the study, the participants were required to monitor their capillary glucose and ketone BHB concentrations (mmol/L) at four time points throughout the day to ascertain compliance (previously published in Table 3 [7]; herein expressed in rank by concentration in Table 1 in the results section). These time points were between 7:30–9:30 a.m., 11:30 a.m.–13:30 p.m., 15:30–17:30 p.m., and 21:30–23:30 p.m. The participants determined their capillary glucose and BHB using a Keto-Mojo™ GKI multi-function meter. This equipment was selected for its reliability and good diagnostic performance [16].

The exclusion criteria for all participants included smoking, taking any medication, and evidence or history of metabolic syndrome, immunological issues, or CVD. The participants were required to complete a medical history questionnaire to confirm that they were free from all of the above diseases.

2.3. Study Design

The 10 KetoSAge participants took part in an open-labelled, non-randomised crossover trial with three 21-day phases: baseline NK was defined as BHB $\geq$ 0.5 mmol/L (Phase 1; P1) and the suppression of ketosis (SuK) as BHB < 0.3 mmol/L, with dietary carbohydrate reintroduction following the Standard U.K. diet (SUK) Eatwell Guidelines (Phase 2; P2), which recommend consuming a predominance of calories from carbohydrates (e.g., 55% kcal from carbohydrates on a 2000 kcal diet is 275 g/day net carbohydrates). The final phase was the removal of the intervention, returning to NK (Phase 3; P3) (Figure 1). At the end of each of the 21-day study phases, on days 22, 44, and 66, the participants attended the laboratory for one day at 8 a.m. after a 12 h overnight fast to undertake anthropometric measurements and blood sampling. A detailed description of the study design was provided in our previous publication [7]. No participants withdrew from this study.

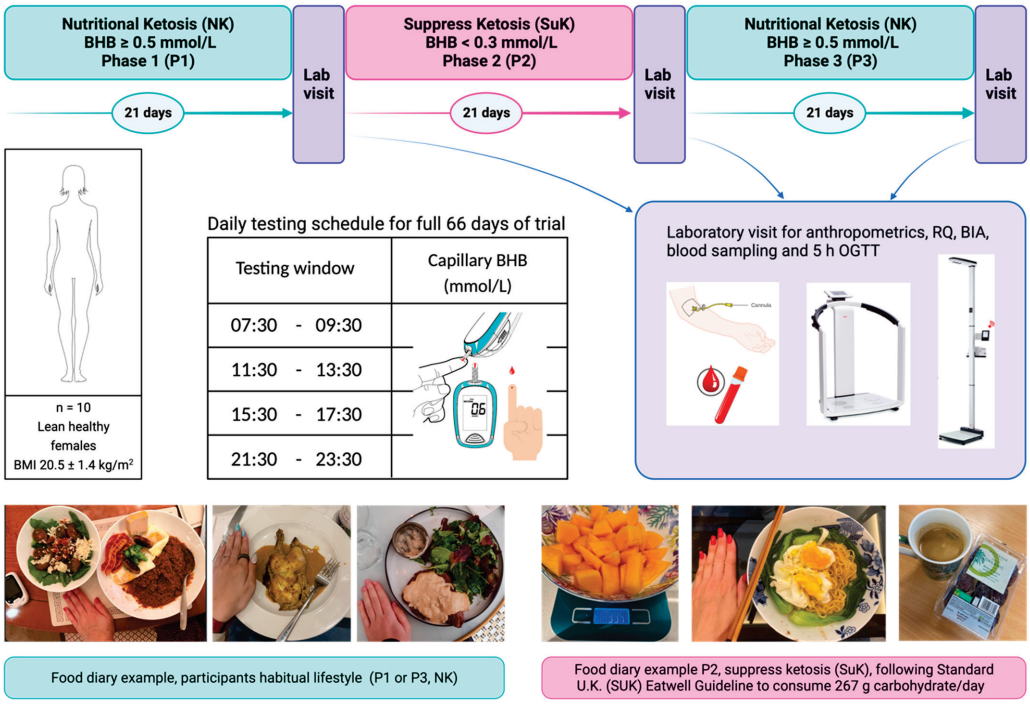


Figure 1. KetoSAge study design. Phase 1 and 3 covered the participants' habitual nutritional ketosis lifestyle. Phase 2 was the interventional phase to suppress ketosis (SuK). Each phase was monitored via finger prick testing of capillary beta-hydroxybutyrate (BHB) concentration (mmol/L). Testing was conducted four times per day, prior to mealtimes, at evenly spaced intervals. At the end of each phase, participants underwent a laboratory testing day for body composition and biochemical tests. Participants were given an oral glucose tolerance test (75 g glucose in 250 mL water) described in our earlier publication [7]. Blood samples were taken at seven time points over 5 hours. Whole blood glucose and BHB were measured sequentially in real time using the Keto-Mojo^{TM} meter, and plasma insulin sensitivity assay was conducted later using ELISA. Body mass index (BMI); oral glucose tolerance test (OGGT); respiratory quotient (RQ).

2.4. Anthropometric Measurements

Upon arrival at the laboratory, height (to the nearest 0.1 cm) was measured using a stadiometer (Marsden HM-250P Leicester Height Measure, Rotherham, UK), and body weight (to the nearest 0.1 kg), waist, and hip circumference measures were obtained with a non-stretch anthropometric circumference measuring tape (Seca® 201, Birmingham, UK) while participants stood upright on both feet. The average value (cm) of three measurements was used for analysis. All measurements were taken from following a 12 h fast wearing standardised clothing.

2.5. Blood Collection and Measurement

Blood was drawn from the antecubital vein into ethylenediaminetetraacetic acid (EDTA) tubes (BD, Oxford, UK) before being centrifuged at 3,857 × *g* for 10 min at 4 °C, as described previously [7]. Plasma was then aliquoted into airtight vials and frozen at −80 °C for batch analysis later.

Samples of blood were immediately sent to SYNLAB Belgium (Alexander Fleming, 3–6220 Heppignies–Company No: 0453.111.546) for the measurement of various markers (see below). Blood was additionally drawn into serum SST^{TM} II Advance tubes with thrombin rapid clot activator and separation gel (BD, Oxford, UK), then left to stand for 30 min at room temperature. Serum tubes were centrifuged (Hettich Zentrifugen, Universal 320 R, Tuttlingen, Germany) at 3,857 × *g* for 10 min at room temperature. Serum samples were aliquoted into cryovial tubes under sterile conditions and stored at −80 °C for later analysis.

2.6. Blood Marker Analysis

Serum insulin was measured via Simple Plex Assay (Ella™, Bio-Techne, Minneapolis, USA). Total osteocalcin (tOCN; DuoSet, R&D Systems, Minneapolis, MN, USA), uncarboxylated osteocalcin (unOCN; BioLegend, San Diego, CA, USA), melatonin, serotonin and serum GLP-1 (Abcam, Cambridge, UK), and leptin (DuoSet, R&D Systems, Minneapolis, MN, USA) were measured by enzyme-linked immunosorbent assay (ELISA) from frozen EDTA plasma or serum samples, according to the manufacturer's instructions. Cortisol was measured externally by SYNALB in the blood samples taken from the KetoSAge participants, as described previously [7]. Glucose concentrations were measured using a Biosen C-Line Clinic Glucose and Lactate analyser (EKF-Diagnostic, GmbH, Barleben, Germany).

2.7. Statistical Analysis

Data were checked for normality using the Shapiro–Wilk test. Different markers measured in the plasma between study phases for the KetoSAge participants were compared using the Friedman test with Dunn's correction for multiple comparisons or repeated measures ANOVA with Tukey's correction for multiple comparisons, depending on the results of the normality tests. Data are presented as mean ± SD. Data were analysed and graphed using GraphPad Prism (Version 9.1.2).

3. Results

3.1. Frequency of Rank-Ordered Capillary BHB Level

Assuming that each test was independent of the other, then the mean of a 21-day testing window had a 25% chance of being the highest. We saw in Phase 1 that 60% of the highest 21-day test window mean BHB concentrations were found in the third test of the day (pre-dinner), with the remaining 40% in the pre-lunch test (Table 1). All biomarkers assessed in this study are presented in below in Table 2.

Table 1. Frequency distribution of beta-hydroxybutyrate (BHB) (the mean of 21 days, BHB concentrations, per test window) expressed in rank, from 1 as the lowest to 4 as the highest concentration. Each participant took 4 tests per day, totalling 840 capillary BHB tests in 10 participants sustaining nutritional ketosis (NK) over 21 consecutive days, in two NK phases (P1 and P3), totalling 1,680 capillary BHB tests. The rank is given to the mean BHB concentration for that test window of 21 days, per phase, per participant. If a participant's test 4 has a rank score of 1, this indicates that the mean BHB concentration for 21 days of tests at bedtime is the lowest of the mean values of all the other test windows.

Phase 1 NK											
Participant	1011	1021	1031	1041	1051	1061	1071	1081	1091	1101	Rank 4 frequency
Test 1 (Wake up)	2	1	2	1	2	1	1	1	1	1	0
Test 2 (Pre-lunch)	3	3	4	3	3	4	4	2	4	2	4
Test 3 (Pre-dinner)	4	4	3	4	4	2	3	4	3	4	6
Test 4 (Bedtime)	1	2	1	2	1	3	2	3	2	3	0
Phase 3 NK											
Participant	1011	1021	1031	1041	1051	1061	1071	1081	1091	1101	Rank 4 frequency
Test 1 (Wake up)	2	1	2	1	2	1	1	1	1	2	0
Test 2 (Pre-lunch)	4	3	4	3	2	3	4	3	3	4	4
Test 3 (Pre-dinner)	3	4	3	4	4	4	3	4	4	3	6
Test 4 (Bedtime)	1	2	1	2	3	2	2	2	2	1	0

Table 2. BMI, fat mass, fasted insulin, glucose, BHB, HOMA-IR, total, carboxylated and uncarboxylated osteocalcin, leptin, cortisol, serotonin, and GLP-1 across all phases in KetoSAge participants. Measurements were taken following each of the study phases: baseline nutritional ketosis (NK), P1; intervention suppress ketosis (SuK), P2; and removal of SuK returning to NK, P3. Measurements were taken at 8 a.m. after a 12 h overnight fast; (n = 10). Values are presented as mean ± SD.

	P1	P2	P3	ANOVA *p* Value	P1 vs. P2	P2 vs. P3	P1 vs. P3
BMI (kg/m^2)	20.52 (±1.39)	21.54 (±1.30)	20.82 (±1.46)	<0.0001	<0.0001	0.0025	0.0197
Fat mass (kg)	14.21 (±2.55)	15.88 (±2.23)	14.78 (±2.20)	<0.0001	0.0008	0.0057	0.1016
Insulin (μIU/mL)	4.95 (±1.24)	9.06 (±2.14)	5.62 (±1.83)	<0.0001	0.0006	0.0027	0.3995
Glucose (mmol/L)	4.36 (±0.53)	5.12 (±0.59)	4.41 (±0.30)	0.0015	0.0088	0.0177	0.9469
BHB (mmol/L)	2.43 (±1.28)	0.18 (±0.13)	2.31 (±0.71)	0.0001	0.0012	<0.0001	0.9854
HOMA-IR	0.97 (±0.32)	2.07 (±0.61)	1.11 (±0.41)	<0.0001	0.0008	0.0013	0.4950
tOCN (ng/mL)	33.84 (±13.66)	55.31 (±29.71)	34.02 (±12.05)	0.0049	0.0138	0.0253	0.9978
cOCN (ng/mL)	31.54 (±12.59)	50.78 (±26.22)	32.02 (±11.13)	0.0040	0.0120	0.0246	0.9840
unOCN (ng/mL)	2.29 (±1.25)	4.54 (±3.79)	2.00 (±1.16)	0.0004	0.0417	0.0010	0.7907
tOCN % (% relative to P1)	100.00	162.36 (±46.53)	109.70 (±40.36)	0.0005	0.0065	0.0094	>0.9999
cOCN % (% relative to P1)	100.00	161.56 (±46.73)	111.52 (±42.90)	0.0007	0.0062	0.0080	0.6836
unOCN % (% relative to P1)	100.00	176.67 (±66.66)	87.11 (±21.43)	0.0028	0.0135	0.0076	0.2476
Leptin (ng/mL)	4.50 (±3.67)	15.08 (±8.00)	4.57 (±3.48)	<0.0001	0.0010	0.0052	>0.9999
Cortisol (ng/mL)	126.20 (±52.67)	112.70 (±58.46)	131.90 (±52.18)	0.4362	>0.9999	0.5391	>0.9999
Serotonin (ng/mL)	21.05 (±22.83)	18.38 (±16.03)	21.77 (±16.80)	0.6013	0.7907	>0.9999	>0.9999
GLP-1 (pg/mL)	1383.18 (±911.36)	576.72 (±452.43)	1471.85 (±1066.75)	0.0075	0.0209	0.0219	>0.9999

Beta-hydroxybutyrate (BHB); body mass index (BMI); carboxylated osteocalcin (cOCN); glucagon like peptide 1 (GLP-1); homeostasis model assessment for insulin resistance (HOMA-IR); total osteocalcin (tOCN); and uncarboxylated osteocalcin (unOCN).

3.2. Suppression of Ketosis is Associated with Increases in HOMA-IR

Following P2, HOMA-IR significantly increased from 0.97 (± 0.32, P1) to 2.07 (± 0.61, P2; p = 0.0008; Figure 2). This trend reversed following P3, where HOMA-IR significantly changed and returned to the participants' baseline levels of 1.12 (± 0.41, P3; p = 0.0013) compared to P2 (Figure 2).

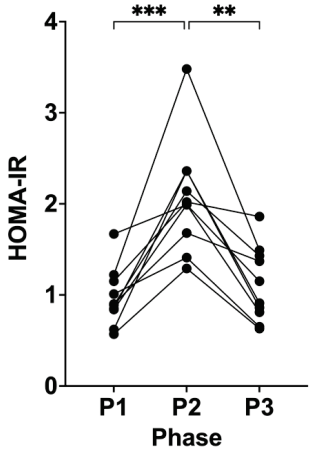


Figure 2. Homeostatic model assessment for insulin resistance (HOMA-IR) across all phases in KetoSAge participants. Fasting serum concentrations of insulin and plasma glucose were measured following each of the study phases: baseline nutritional ketosis (NK), P1; intervention to suppress ketosis (SuK), P2; and removal of SuK returning to NK, P3. Insulin was determined by via Simple Plex Assay (Ella™, Bio-Techne, Minneapolis, USA) and glucose was measured by Biosen C-Line Clinic Glucose and Lactate analyser. HOMA-IR adopts the following formula to index insulin resistance: fasting plasma insulin (uIU/mL) × fasting plasma glucose (mmol/L)/22.5 [1,17,18]. Homeostasis model assessment for insulin resistance (HOMA-IR). Samples were taken at 8 a.m. after a 12 h overnight fast (n = 10). Data were analysed by repeated measures one-way ANOVA. ** $p < 0.01$; and *** $p < 0.001$.

3.3. Suppressing Ketosis Increases all Forms of Osteocalcin

tOCN significantly increased after P1 from 33.84 ng/mL (± 13.66) to 55.31 ng/mL (± 29.71, P2, $p = 0.0138$; Figure 3), and then significantly decreased following the removal of SuK (P3) to 34.02 ng/mL (± 12.05, $p = 0.0253$) compared to P2, returning to similar baseline P1 values. cOCN significantly increased after P1 from 31.54 ng/mL (± 12.59) to 50.8 ng/mL (± 26.2, P2, $p = 0.0120$), then significantly decreased following the removal of SuK in P3 to 32.0 ng/mL (± 11.1, P3, $p = 0.0246$) compared to P2, returning to similar baseline P1 values. unOCN increased after P1 from 2.29 ng/mL (± 1.25) to 4.54 ng/mL (± 3.79, P2, $p = 0.0417$), then decreased following the removal of SuK in P3 to 2.00 ng/mL (± 1.16, $p = 0.0010$) compared to P2, returning to similar baseline P1 values.

We analysed tOCN, cOCN, and unOCN as percentages relative to each participant's own baseline values in P1. tOCN significantly increased after P1 from 100% as the standardised baseline (± 0.00%) to 162.36% (± 46.53%, $p = 0.0065$; Figure 4) relative to P1, then decreased following the removal of SuK in P3 to 109.70% (± 40.36%, P3, $p = 0.0094$), relative to baseline and compared to P2, returning to similar baseline P1 values. cOCN significantly increased after P1 from 100% as the standardised baseline (± 0.00%) to 161.56% (± 46.73%, P2, $p = 0.0062$) relative to P1, then decreased following the removal of SuK in P3 to 111.52% (± 42.90%, P3, $p = 0.0080$), relative to baseline and compared to P2, returning to similar baseline P1 values. unOCN significantly increased after P1 from 100% as the standardised baseline (± 0.00%) to 176.67% (± 66.66%, P2, $p = 0.0135$) relative to P1, then decreased following the removal of SuK in P3 to 87.11% (± 21.43%, P3, $p = 0.0076$), relative to baseline and compared to P2, returning to similar baseline P1 values.

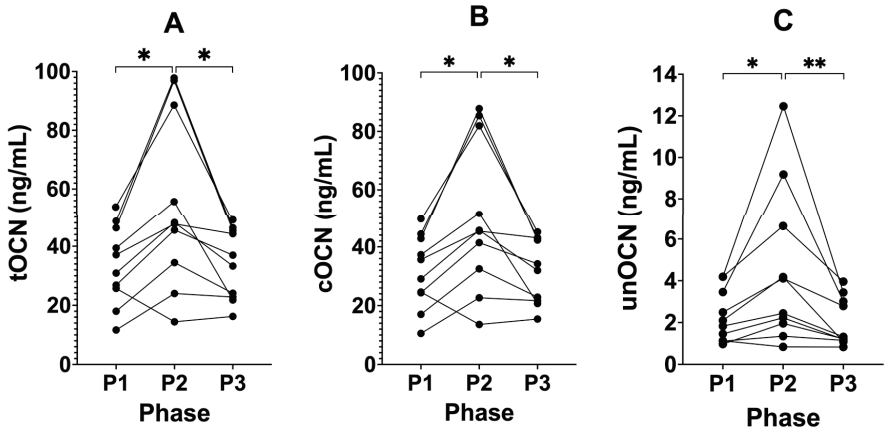


Figure 3. tOCN, cOCN, and unOCN across all phases in KetoSAge participants. Fasting plasma concentrations of (**A**) tOCN, (**B**) cOCN, and (**C**) unOCN were measured following each of the study phases: baseline nutritional ketosis (NK), P1; intervention to suppress ketosis (SuK), P2; and removal of SuK returning to NK, P3; total OCN (tOCN) and uncarboxylated OCN (unOCN) were determined by ELISA and carboxylated OCN (cOCN) was calculated by subtracting unOCN from tOCN. Samples were taken at 8 a.m. after a 12 h overnight fast; (n = 10); tOCN and cOCN data were analysed by repeated measures one-way ANOVA with Tukey's correction for multiple comparisons, unOCN data were analysed using the Friedman test with Dunn's correction for multiple comparisons. * $p < 0.05$ and ** $p < 0.01$.

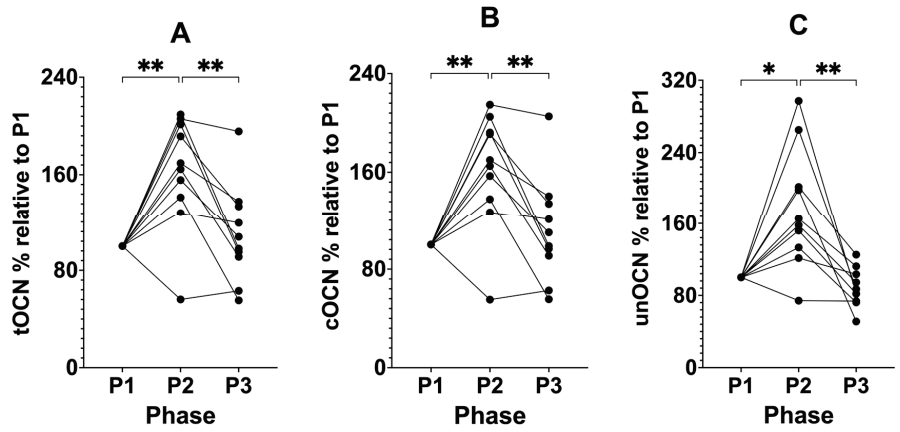


Figure 4. Percentage change from baseline P1 at 100% for tOCN, cOCN, and unOCN across all phases in KetoSAge participants. Fasting plasma concentrations of (**A**) tOCN, (**B**) cOCN, and (**C**) unOCN were measured following each of the study phases: baseline nutritional ketosis (NK), P1; intervention to suppress ketosis (SuK), P2; and removal of SuK returning to NK, P3; total OCN (tOCN) and uncarboxylated OCN (unOCN) were determined by ELISA, carboxylated OCN (cOCN) was calculated by subtracting unOCN from tOCN. Samples were taken at 8 a.m. after a 12 h overnight fast; (n = 10); data were analysed by repeated measures one-way ANOVA with Tukey's correction for multiple comparisons. * $p < 0.05$ and ** $p < 0.01$.

3.4. Suppression of Ketosis is Associated with Increased Leptin

Following P2, leptin significantly increased from 4.50 ng/mL (± 3.67, P1) to 15.08 ng/mL (± 8.00, P2; $p = 0.0010$; Figure 5). This trend reversed following P3, where leptin significantly decreased and returned to the participants' baseline levels of 4.57 ng/mL (± 3.48, P3; $p = 0.0005$) compared to P2.

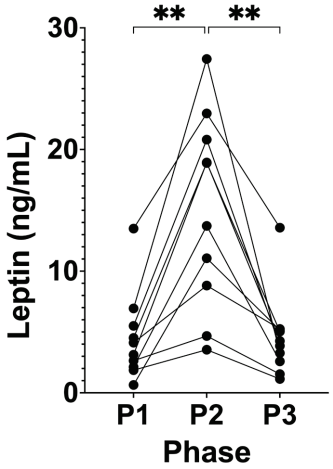


Figure 5. Serum leptin across all phases in KetoSAge participants. Fasting serum concentrations of leptin were measured following each of the study phases: baseline nutritional ketosis (NK), P1; intervention to suppress ketosis (SuK), P2; and removal of SuK returning to NK, P3. Leptin was determined by via ELISA (DuoSet, R&D Systems, Minneapolis, MN, USA). Samples were taken at 8 a.m. after a 12 h overnight fast; (n = 10). Data were analysed by repeated measures one-way ANOVA. ** $p < 0.01$.

3.5. Cortisol Levels Remain at Healthy Low Levels in Long-Term NK, and Serotonin Does Not Significantly Change

Following P2, cortisol did not significantly change after P1, changing from 126.20 ng/mL (± 52.67, P1) to 112.70 ng/mL (± 58.46, P2; $p \geq 0.9999$; Figure 6). Similarly, following P3, there was no significant change compared to P2 at 131.90 ng/mL (± 52.18, P3, $p = 0.5391$). Following P2, plasma serotonin did not significantly change from P1 at 21.05 pmol/L (± 22.83, $p = 0.7907$; Figure 6). With the removal of the intervention for SuK with a return to NK for 21 days at the end of P3, there was no significant change in serotonin compared to P2 at 21.77 pmol/L (± 16.80, P3, $p \geq 0.9999$).

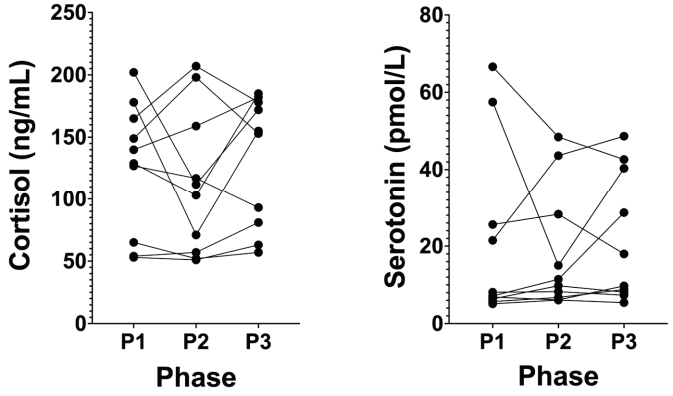


Figure 6. Serum cortisol and serotonin across all phases in KetoSAge participants. Fasting serum concentrations of cortisol and plasma serotonin were measured following each of the study phases: baseline nutritional ketosis (NK), P1; intervention to suppress ketosis (SuK), P2; and removal of SuK returning to NK, P3; cortisol was measured externally by SYNLAB Belgium (Alexander Fleming, 3–6220 Heppignies–Company No: 0453.111.546), serotonin was measured by ELISA (Abcam, Cambridge, UK). Samples were taken at 8 a.m. after a 12 h overnight fast; (n = 10). Data were analysed by Friedman test with Dunn's correction for multiple comparisons.

3.6. Suppression of Ketosis is Associated with Decreased GLP-1

Following P2, active GLP-1 significantly decreased from 1,064.98 pg/mL (± 500.15, P1) to 504.98 pg/mL (± 246.43, P2; $p = 0.0209$; Figure 7). This trend reversed following

P3, where GLP-1 significantly increased and returned to the participants' baseline levels of 1,032.26 pg/mL (± 453.88, P3; $p = 0.0210$) compared to P2.

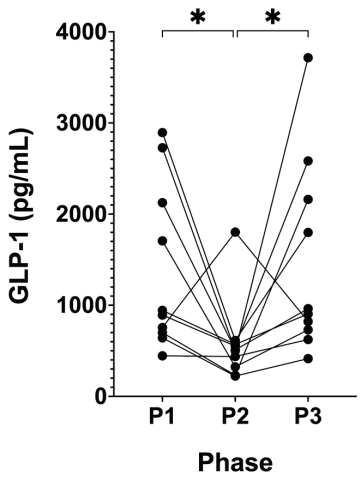


Figure 7. Serum concentrations of active GLP-1 across all phases in KetoSAge participants. Serum concentrations of active GLP-1 were measured following each of the study phases: baseline nutritional ketosis (NK), P1; intervention to suppress ketosis (SuK), P2; and removal of SuK returning to NK, P3. GLP-1 was determined by ELISA (Abcam, Cambridge, UK). Glucagon-like peptide-1 (GLP-1). Samples were taken at 8 a.m. after a 12 h overnight fast; (n = 10). Data were analysed by repeated measures one-way ANOVA. * $p < 0.05$.

4. Discussion

4.1. When to Measure Capillary BHB

The 6-month 4–6 p.m. capillary ketone testing standardised evening measurement as a criterion for eligibility for the trial was chosen due to it being a more rigorous threshold to pass in order to be judged as sustaining NK over the majority of the 24 h day, in comparison to morning fasted measurements, thus increasing the confidence in the participants maintaining NK most of the time. Most people embarking on a ketogenic lifestyle, typically via carbohydrate restriction, time-restricted feeding, or other forms of fasting-mimicking diets, will measure their capillary ketones in the morning, much the same way that morning fasting blood glucose is taken. However, morning ketone readings for hyperinsulinaemic and insulin-resistant individuals will likely produce some measurable levels (potentially up to 0.5 mmol/L) due to an overnight fast. If this was performed on individuals only daily, they could mistakenly then assume that they are successfully maintaining a metabolic state of ketosis. However, if they were to measure their capillary ketones at least 3 to 4 hours after lunch, then this test would capture their breakfast and/or lunch if they had consumed anything, allowing them to truly know if their lifestyle was supportive of maintaining euketonaemia via minimising lifestyle practices that stimulate excess insulin demand, which would inhibit (lower) ketone production.

In our cohort, our participants noted that their pre-lunch and dinner readings were often their highest levels of ketones out of the four times a day tests, with their pre-dinner (4–6 p.m.) reading showing a slightly higher frequency of being greater than their second test of the day (pre-lunch). This informed our participants of how their lifestyle was supporting them in maintaining nutritional levels of ketones ($\geq$ 0.5 mmol/L) throughout the day [7].

4.2. Hypoketonaemia, HOMA-IR, and Fasting Insulin

Throughout the KetoSAge study, the participants maintained healthy fasting glucose levels in all phases, 4.36 mmol/L (± 0.53, P1), 5.12 mmol/L (± 0.59, P2), and 4.41 mmol/L (± 0.30, P3), which are considered to be extremely healthy [17]. HbA1c was not measured in this study, due to the three-phase blood sampling timing that would have resulted in

prior blood sampling affecting the next blood sampling results (P2 affected by P1, and P3 affected by P2). HbA1c is used to assess cumulative glucose exposure, which glycates the haemoglobin (HbA1c) in blood. This provides evidence of average blood glucose levels over the previous two to three months, which is the average half-life of red blood cells [18]. A percentage of glycation damage occurs as a result of hyperglycaemia, which is associated with an increased risk of atherosclerosis, CVD, cerebrovascular disease, all-cause dementia (ACD), and AD. For example, in the AgeCoDe cohort study of 1,342 elderly individuals, a higher HbA1c level was found to be associated with increased ACD and AD. HbA1c $\geq$ 6.5% was associated with an increased risk of ACD by 2.8-fold (p = 0.027) and for AD (p = 0.047). There was an associated 5-fold increased risk of incident ACD (p = 0.001) and a 4.7-fold increased risk of AD (p = 0.004) with HbA1c levels $\geq$ 7% [19]. However, hyperinsulinaemia has been shown to precede hyperglycaemia by up to 24 years [20]. Therefore, there is a weakness when relying on HbA1c to detect earlier disease risk, in that there is a sub-clinical phase (occult stage), during which, a healthy HbA1c value is seen. This is due to an increased insulin concentration that reduces the plasma glucose, whilst the elevated basal insulin still has non-glucose-related signalling effects, such as increasing PI3K and MAPK signalling for growth and division [21–24] and increasing ceramide production, which increases mitochondrial reaction oxygen species generation, therefore increasing oxidative stress in the system [25–27].

An example of how a reduced HbA1c due to more insulin exposure can be less positive for health is found in the ACCORD group randomised controlled trial (RCT) study of 10,251 patients, with a mean age 63 years, who had an 8.1% median HbA1c. All participants were already on exogenous insulin. Half of the group was randomised to a more tailored intensive insulin therapy regimen to achieve a decrease in their HbA1c to 6%, whilst the other group was to follow their standard insulin therapy to target a value of 7.0–7.9%. The three primary outcomes measured in this RCT were non-fatal stroke, non-fatal myocardial infarction, and CVD death. This trial was stopped after 3.5 years due to ethical reasons, as the intervention group receiving the intensive insulin therapy (more insulin) in order to lower their HbA1c by a greater amount had a significantly higher mortality rate [28]. Whilst successfully lowering their HbA1c with more insulin, there was an increase in deaths, indicating that relying on a lower HbA1c may lure physicians and patients into a false sense of security whilst patients are actually exposed to greater insulin levels and, therefore, their subsequent potential harms [2,8,24,27,29–31].

HOMA-IR is recognised as a diagnostic index for insulin resistance, where a higher concentration of fasting insulin to maintain a low fasting glucose results in a higher HOMA-IR value [1]. Insulin resistance is generally accepted as having an HOMA-IR > 2 [32–34], whilst hyperinsulinaemia is considered where the fasting plasma insulin is > 28.8 uIU/mL [8,9,22,35]. Our participants' group mean of fasting insulin levels was 9.06 uIU/mL ($\pm$ 2.13) after 21 days of suppressing ketosis, with the highest individual fasting insulin measuring a value of 11.92 uIU/mL. However, HOMA-IR was able to detect a significant change, where, in both NK phases, our participants' HOMA-IR was at the very healthy levels of 0.97 ($\pm$ 0.32, P1) and 1.11 ($\pm$ 0.41, P3). Conversely, suppressing ketosis managed to significantly double their mean HOMA-IR to 2.07 ($\pm$ 0.61, P2), bringing it into the beginning range of insulin resistance, with one participant having an HOMA-IR of > 3 after suppressing ketosis for 21 days. All participants' HOMA-IR values returned to their healthy baseline values within only 21 days of returning to NK by removing the intervention for SuK via the ingestion of carbohydrates. Given HOMA-IR's strong association and even predictive value in chronic disease risk, it would be of high value to understand how lifestyle may modulate this marker index measured alongside other biomarkers strongly associated with disease risk, such as GGT, IGF-1, MCP-1, and ageing, to provide further confidence and resolution in diagnostics and the more accurate phenotyping/categorisation of patients in studies [7].

In a cross-sectional analysis study of 12,266 participants from the NHANES database, a positive correlation was found between participants' HOMA-IR levels and their BA in US adults [1]. A prospective cohort study of 3,741 asymptomatic employees of Santander Bank

in Madrid, aged between 40–55 years upon recruitment, with no known CVD, investigated the relationship between early insulin resistance, as measured using the HOMA-IR index in normoglycaemic individuals assumed to be at a low risk of atherosclerosis, in addition to the effect of cardiovascular risk factors in individuals with normal HbA1c. The presence and progression of sub-clinical atherosclerosis (SA) were assessed using non-invasive vascular imaging modalities, multiterritorial vascular ultrasound, and coronary arterial calcification (CAC) scans [36]. The study found that HOMA-IR had a direct association with the multiterritorial extent of SA and CACs ($p < 0.001$). In summary, 85.1% of the reference group (HOMA-IR < 2) were free of coronary artery calcium (14% had a CACS of > 0). This proportion of participants with CAC increased as insulin resistance increased, with a HOMA-IR between 2 to 3, the proportion increased to 25.6%, and with a HOMA-IR > 3, the proportion increased further to 39.3%. A bibliometric study of 1,500 publications found HOMA-IR insulin resistance to be strongly associated with cerebral small vessel disease, ischemic stroke incidence, post-stroke depression, and early neurological deterioration in patients who suffered stroke [29].

The 21 days of suppressing ketosis resulted in hypoketonaemia due to insulin's suppressive control of ketogenesis [28]. Whereas P1 and P3 were typified by euketonaemia, along with healthy low insulin and HOMA-IR values. As our cohort was exclusively female, it is imperative to recognise the links between hyperinsulinaemia, metabolic health, and breast cancer [4,30]. In a retrospective case–control study, 80 non-diabetic patients with pre-menopausal and post-menopausal breast tumours were compared to 60 women with normal mammograms as a control. Hyperinsulinaemia and insulin resistance HOMA-IR have been found to be associated with an increased risk of breast cancer in non-diabetic (normoglycaemic) women. Whilst hyperinsulinaemia determined by fasting insulin levels of > 28 uIU/mL may proceed hyperglycaemia for up to 24 years [2,7–9,31], early sub-clinical (occult) hyperinsulinaemia may be considered when there is chronic hypoketonaemia measured between 4–6 p.m. for at least three consecutive days (a longer duration would increase confidence). Measurement at this time of day would reduce the false-positive acceptance of NK compliance from a test result resulting from waking up with ketosis levels (> 0.3 mmol/L) due to an overnight fast [7,32].

In our KetoSAge trial, the chronic suppression of ketosis (P2) intervention resulted in significantly increased fasting insulin levels, which would still be considered as healthy values, yet significantly increased HOMA-IR values into the insulin resistant range. Our participant data show that long-term NK maintains and reduces HOMA-IR to very healthy levels, adding to existing evidence that sustaining a lifestyle that promotes ketosis (minimising insulin demand and secretion) is an effective modality in preventing insulin resistance and its associated diseases, including cancer, CVD, dementia, T2DM, and earlier biological ageing [1,7,9,33–35]. It was very reassuring to see that our participants' HOMA-IR levels returned to their baseline mean value of 1.11 ($\pm$ 0.41, P3) after the removal of carbohydrates, returning to sustained NK, indicating that restricting carbohydrates is a viable and practical method to reduce the risk of insulin-resistance-related morbidities known to affect healthspan and lifespan. Additionally, our data indicate that the effect of 21 days of suppressing ketosis on HOMA-IR, can be reversed by a subsequent period of sustained NK, in individuals who habitually maintain a ketogenic lifestyle.

4.3. Osteocalcin

Human OCN has a molecular weight of 5 kDa, is 49 amino acids long, and is the tenth most abundant protein in the body [37]. It has been shown to have an endocrine function in glucose homeostasis, insulin sensitivity, neurogenesis, cognitive health, and mitochondrial biogenesis [38–43]. The majority of OCN is synthesised by osteoblasts and osteocytes in the bone. Its carboxylated form (cOCN) is both deposited into the bone and released into the system by osteoblasts and osteocytes. unOCN is synthesised and released into the circulation by osteoblasts and osteocytes, as well as resorbed from the bone by osteoclasts [39]. cOCN is required for the correct alignment of hydroxyapatite (HA), which

confers bone its torsion and tensile ductility, giving it resistance to fragility fractures, which is not captured via bone mineral density (BMD) assessment [39,44].

In the KetoSAge trial, all forms of osteocalcin (tOCN, cOCN, and unOCN) significantly increased after 21 days of suppressing ketosis and then decreased back to baseline with the return to ketosis. Interestingly, OCN is synthesised and secreted from adipocytes only during adipogenesis [45]. Weight gain as fat mass occurred during the 21-day intervention phase (P2) to suppress ketosis via the re-introduction of dietary carbohydrates following the SUK Eatwell Guideline recommendations (data previously published in [7]). This may explain the increases in all forms of OCN.

tOCN, cOCN, and unOCN increased from P1 to P2 in all but one participant (ID: 1091). From P2 to P3, tOCN and cOCN decreased in all but one participant, which was the same individual (ID: 1091). Upon further investigation, participant ID: 1091 regularly reported consuming beef bone broth during P1 and P3. Since OCN is the second most abundant protein in bone, it is plausible that this broth may have served as an exogenous source of OCN, thus explaining the increase [38]. Removal of their data in unOCN analysis results in a significant decrease from P2 at 4,691.87 pg/mL (± 3,751.66 pg/mL) to P3 at 1,873.10 pg/mL (± 1,173.00 pg/mL; $p = 0.0489$). Further investigation into the exposure of exogenous OCN from foodstuffs is, therefore, warranted.

An increased HOMA-IR increases coronary atherosclerosis risk; furthermore, insulin resistance has a sub-clinical occult phase potentially detectable via repeated consecutive days blood ketosis and glucose testing (between 4–6 p.m.), where a capillary BHB value of < 0.3 would indicate hypoketonaemia due to occult hyperinsulinaemia. Endothelial progenitor cells (EPCs), which aid in the repair of the vasculature, may also come with vascular calcification, as they have been shown to express OCN genes in insulin-resistant chronic disease conditions such as atherosclerosis [36]. EPCs from 72 patients with coronary atherosclerosis undergoing invasive coronary assessment have been shown to express OCN genes, indicating epigenetic osteogenic transformation [46]. Other studies of patients with hyperinsulinaemia conditions, such as in CVD and chronic kidney disease, have detected vascular smooth muscle cell osteogenic differentiation and aortic valve tissue having an increased expression of sclerostin [39,47–50], corroborating the relationship between chronic increased insulin exposure altering gene expression in the osteogenic profile.

In a study of 2,493 individuals with MetS, plasma OCN levels were found to be inversely correlated with HOMA-IR, fasting insulin and glucose, leptin, and BMI ($p < 0.0010$ for each biomarker) [51]. Interestingly, OCN has been found to be lower in obese people [52,53] and those with T2DM, such as seen in a correlation analysis of 204 patients with T2DM, where an inverse relationship between OCN and HOMA-IR was found [52,54]. With this information, it would be easy to then make the assumption that a higher level of OCN would, therefore, be better. However, our KetoSAge trial showed an opposite pattern, where P1 and P3 had the healthiest low HOMA-IR values and significantly lower OCN (all forms) relative to P2, indicating OCN was positively associated with HOMA-IR in this cohort. Furthermore, as BMI and fat mass increased in P2 [7], so too did all forms of OCN in the present study. In corroboration with Ferron's work [55], OCN increased in P2, where insulin also increased, indicating a potential effect of OCN increasing insulin secretion. However, our trial did not corroborate an increase in sensitising glucose uptake, given that P2 came with a significant increase in fasting blood glucose, although the mean value was still in a healthy range. It is possible that OCN was rescuing the situation, meaning that, if OCN did not increase, perhaps there would have been a greater increase in glycaemia and a trend towards IR. The OCN patterns in MP1 individuals may behave much like free triiodothyronine (T3), where T3 demand increases as mitochondrial reactive oxygen species increase, causing oxidative damage to mitochondrial (mt) oxidative phosphorylation (OXPHOS) proteins and resulting in an increased demand of T3 to upregulate the synthesis of mtOXPHOS electron transport chain proteins. Furthermore, like the pattern seen in our prior work [7,32], we saw a lower T3 when in long-term ketosis and an increase

in T3 after 21 days of suppressing ketosis, likely indicating an increased T3 sensitivity and decreased demand, which may be a similar case to OCN. If we assume that, in a healthy setting, OCN would be synthesised and deposited into the bone and that only a low dose of OCN is steadily released into the circulation, therefore, bone OCN deposition would confer a healthier bone tensile strength, and there may be a potential greater sensitivity to the OCN in the circulation [7,32].

OCN has been shown to stimulate GLP-1 synthesis [56], a pattern that was not corroborated in our trial. However, there may be a difference between endogenous versus oral exposure to OCN. It is interesting that, as OCN significantly increased in P2, GLP-1 conversely decreased, which is an opposite trend to other experiments showing OCN activating GLP-1 synthesis [56,57]. Research into human physiology often investigates pathology and tries to reverse engineer relationships, or very often uses a control group labelled as the "healthy" group, where, in actual fact, they are the "common" group and not necessarily a group reflecting human evolutionary phenotypic living, which is likely to be in a state of ketosis for the majority of each 24 h day [2,8,58]. This would result in a metabolic signature that is different to non-pathology-presenting long-term suppressed ketosis metabolic phenotype 2 (MP2) people [8]. A low OCN concentration in healthy long-term ketosis should not be confused with a low OCN level as seen in obesity, T2DM, CVD, and AD, where these cohorts are also seen to have higher rates of fragility fractures with a normal to high bone mineral density, which is hyperinsulinaemia osteofragilitas and not osteoporosis (Cooper, Brookler and Crofts, 2021 [39]). This indicates poor bone health, with hyper mineralisation as a form of osteocyte fossilisation, rendering them unable to thrive nor survive, nor produce the necessary OCN, not only for the alignment of HA to confer bone tensile strength, but to also to be released into the circulation to play its part in healthy metabolic homeodynamic regulation [39]. In this context, a low plasma OCN concentration is indicative of pathology. It is, therefore, clear that clinicians and researchers need to be aware of understanding biomarkers within the metabolic phenotype profile of each individual, so as not to misdiagnose/categorise according to a single marker out of the patient's metabolic context.

4.4. Leptin Increases with Chronic Suppression of Ketosis a Risk of Hyperleptinaemia

Leptin is an adipokine, synthesised and secreted by white adipocytes, which has a 24 h circadian rhythm [59] and may be a more sensitive marker for hyperinsulinaemia than BMI. In a study of 119 normal-weight 18- to 24-year-old participants with a BMI of < 25, it was found that fasting leptin levels were significantly associated with fasting insulin ($\beta \pm SE = 0.30 \pm 0.06$, $p < 0.001$) and HOMA-IR ($\beta \pm SE = 0.41 \pm 0.20$, $p < 0.001$) [14]. These relationships were independent of age, gender, and total body fat. This indicates that, although leptin increases with obesity, it may be, that which causes obesity or excess body fat, which can exist in normal-BMI individuals, often termed TOFI (thin on the outside, fat on the inside) [60,61], also causes hyperleptinaemia and hyperinsulinaemia. These share a common root cause, and, therefore, explain why we see leptin and insulin rising where obesity may not, or may rise later on, meaning that obesity was not the first mover in causing the rises in these biomarkers associated with chronic metabolic diseases. Chronic excess insulin is the likely root cause, since insulin is so intrinsically linked to the regulation of leptin, and that excess may not be captured by a fasting insulin nor an oral glucose tolerance test (OGTT). Insulin tightly regulates ketogenesis, therefore, many consecutive days of BHB testing between 4–6 p.m. acts as a proxy to understanding individual hyperinsulinaemia, if we accept hyperinsulinaemia to mean "more than is ideal for optimal health" for an individual [28,62]. Our KetoSAge participants' leptin levels were healthily low in their natural habitual ketosis states, at levels classified/categorised as the healthiest in terms of CVD risk [63]. With the 21-day suppression of ketosis, which resulted in a significant increase in fasting insulin, there was a significant increase in fasting leptin too, to levels that re-classify into less healthy ranges associated with poorer health outcome [63]. Returning to ketosis showed a complete return to baseline levels, indicating

how responsive leptin is to dietary carbohydrate-stimulated insulin secretion in long-term habitually keto-adapted females.

The KetoSAge trial participants' weight and fat mass did increase significantly after 21 days of SuK, however, their BMI stayed well within the healthy range. This corroborates the understanding that, although BMI is a good tool for investigating disease risk, there are subsets of people with sub-clinical (occult) conditions that are being pooled into research, which decreases accurate reflections of physiology and pathophysiology in trial findings and data analysis. A BMI of < 25 kg/m^2 is considered as healthy, however, there are subsets of people with a normal BMI who have metabolic diseases and even some with a BMI of > 25 kg/m^2 that may have occult hyperinsulinaemia for many years when their BMI was < 25 kg/m^2 [60,61,64–66]. Boden et al. showed, using a 72 h euglycaemia-hyperinsulinaemia and hyperglycaemic clamp, that prolonged hyperinsulinaemia and not hyperglycaemia increased serum leptin in 28 healthy normal-weight males. Furthermore, high levels of free fatty acids also did not affect leptin release [59]. Whilst this trial intervention for SuK for 21 days resulted in these significant changes, it is thought-provoking to consider if it had lasted months, if not years.

Higher levels of leptin have been shown to be associated with increased frailty in older adults. Fragility fracture rate increases with hyperinsulinaemia [39], which is also associated with ageing, given that the "chronic" in chronic-elevated insulin indicates a long duration of time exposure, which chronological age reflects. In an investigation between leptin levels and incident frailty in 1,573 individuals from the Seniors-ENRICA cohort, aged $\geq$ 60 years and without T2DM [67], those with leptin levels in the highest tertile had a significantly increased risk of frailty (odds ratio [OR]: 2.12; 95% confidence interval [CI]: 1.47–3.06; *p*-trend < 0.001). In a multivariate linear regression analysis, leptin levels were shown to be positively associated with insulin resistance in 398 middle-aged and elderly Taiwanese individuals (β = 0.226, $p < 0.01$) [68]. Leptin has also been shown to be positively associated with atherosclerosis assessed by CAC in a cross-sectional study on 200 participants, aged between 35 and 75 years with T2DM (which is hyperinsulinaemia with hyperglycaemia, with insulin resistance) [63]. Given that the HOMA-IR and progression of early SA-CNIC-Santander study (NCT01410318) showed a significantly increased risk of SA with an increase in HOMA-IR, the KetoSAge trial provides us with valuable information on increasing our knowledge about how to maintain or modulate these biomarkers associated with one of the global leading causes of chronic disease mortality, CVD [36]. Our KetoSAge trial showed lower leptin levels during ketosis, coupled with very low HOMA-IR (no insulin resistance), and the suppression of ketosis increased leptin in lockstep with increasing insulin resistance. The removal of dietary farinaceous carbohydrates to no longer stimulate an increased insulin demand repeatedly showed how responsive these chronic disease biomarkers are to ketosis, the metabolic state that, throughout history, humans likely spent most of their time in.

4.5. Cortisol and Serotonin

The steroid glucocorticoid hormone cortisol is mainly synthesised in the adrenal cortex by the zona fasciculata and, to a much lesser degree, by the thymus, brain, intestine, and skin [69]. Further, cortisol is involved in the regulation of gluconeogenesis and is often considered to be the stress response or related hormone [70]. In 919 participants aged 60–75 years from the Edinburgh Type 2 Diabetes prospective study, elevated fasting plasma cortisol was positively associated with increased ischaemic heart disease [71]. The univariate analysis found an associated increased odds of ischaemic heart disease with cortisol concentrations of > 800 nmol/L (290 ng/mL). The standard reference range for cortisol in plasma is 33–246 ng/mL [72]. Our KetoSAge trial mean fasting serum cortisol levels were within healthy ranges in all phases of the trial, with ketosis phases' mean concentrations of 126.20 ng/mL ($\pm$ 52.67, P1) (348.13 nmol/L) and 131.90 ng/mL ($\pm$ 52.18, P3) (363.90 nmol/L), and after 21 days of SuK (P2), 112.70 ng/mL ($\pm$ 58.46, P2) (310.90 nmol/L). It has been suggested that chronic gluconeogenesis can induce a "fight

or flight" emergency survival process, resulting in chronic elevated cortisol secretion [73]. Interestingly, although there were no significant changes in cortisol in the KetoSAge trial, the overall healthy low levels of cortisol should be noted, which indicated that ketosis via carbohydrate restriction with subsequent reliance on gluconeogenesis for a long period of time did not appear to result in hypercortisolaemia. Furthermore, as the KetoSAge participants were, on average, in long-term ketosis for 3.9 years, their plasma glucose source was predominantly from gluconeogenesis, despite having perfectly healthy cortisol levels. Together, these data strongly negate claims that long-term ketosis gluconeogenesis is a fight or flight emergency survival process.

OCN has been shown to modulate insulin sensitivity and secretion via stimulating β-cell serotonin synthesis and secretion to modulate pancreatic islet α cells [8,39], however, this modulation of serotonin may be intracellular, and its secretory actions act in a paracrine manner within the pancreas and, thus, are undetectable in the blood stream. We did not see significant changes in plasma serotonin in the KetoSAge trial.

4.6. GLP-1

The current "blockbuster" drugs on the market for diabetes and weight loss are classed as GLP-1 agonists. Our participants in long-term NK showed significantly higher levels of GLP-1, whilst suppressing ketosis significantly decreased GLP-1. Lifestyle practices that stimulate chronic excess insulin demand and secretion result in lower GLP-1 levels and, therefore, less GLP-1 receptor (GLP-1R) activation, which is associated with increased insulin resistance, obesity, and T2DM [74]. Interestingly, in a competing risk regression analysis of 462 incident first cancer cases with 2,417 controls, it was found that a higher fasting GLP-1 level was significantly associated with a lower risk of incident first cancer (sub-hazard ratio 0.90; 95% CI 0.82–0.99; $p = 0.022$) [75].

GLP-1 is excreted primarily by ileo-colonic (L) enteroendocrine cells in the distal small bowel and colon [76]. Interestingly, GLP-1 stimulates proinsulin gene expression, resulting in activating the replenishment of insulin stores [77]. GLP-1 activates GLP-1R on pancreatic islet α cells, inhibiting glucagon secretion, resulting in a lowering of plasma glucose independent of insulin [78,79]. We were unable to measure glucagon in our participants' samples due to the low sensitivity of the assays trialled, and potentially as a result of glucagon's rapid degradation ex vivo [80]. However, fasting glucose and insulin were both significantly lower in both NK phases, along with a significantly higher concentration of GLP-1, whilst fasting glucose was significantly higher during the P2 suppression of ketosis with significantly lower GLP-1 levels and higher fasting insulin. This suggests that the lower fasting glucose levels during both NK phases were likely due to the GLP-1 lowering of glucagon, thus resulting in a lower fasting glucose, independent of insulin, and, subsequently, the NK phases having lower fasting insulin values. GLP-1 is an incretin, however, and it enhances insulin secretion in a glucose-dependent manor [81]. Participants' low HOMA-IR values in both NK phases were half those of when suppressing ketosis (P2), meaning they had a significantly greater insulin sensitivity when in ketosis, which would mean that less basal insulin was required to "do the job" of regulating plasma glucose, if one were to ascribe this as the primary role of insulin. However, in the long-term NK state, basal insulin's primary role is not likely to be the regulation of plasma glucose and may instead be the regulation of fat oxidation and ketogenesis, as well as modulating hormones and growth factors [2,7], whilst GLP-1 may regulate basal glucose levels via glucagon.

OCN, more specifically, the uncarboxylated form unOCN, stimulates GLP-1 synthesis via the promiscuous GPRC6A receptor [82]. However, the KetoSAge participants had lower OCN (all forms) in both NK phases with higher GLP-1, indicating that the elevated GLP-1 was not likely to be due to endogenous OCN action. As the incretin effect of GLP-1 is glucose dependent, therefore, elevated basal GLP-1 in long-standing euketonaemia is likely acting on its none-incretin actions, such as the slowing of gastric emptying [83]. This may aid in increasing nutrient uptake during food scarcity periods, or when only consuming one meal a day, to facilitate maximal nutrient absorption which would confer a survival

benefit. The slowing of gastric emptying may assist in extending the time provided for intestinal processing and maximising the absorption of nutrients from the acidic chyme. This may explain the evolutionary purpose of elevated basal GLP-1 levels in humans who likely spent a great amount of time in ketosis and, thus, not exposed to dietary farinaceous nor sucrose-rich foods that would trigger bolus GLP-1 secretion.

Euketonaemia is achievable without fasting through carbohydrate restriction, which results in a fasting-mimicking state. Palmitic-acid-9-hydroxy-stearic-acid (9-PAHSA), a branched fatty acid ester of hydroxy fatty acids (FAHFAs), stimulates GLP-1 secretion. 9-PAHSA is endogenously synthesised and regulated by a fasting state (euketonaemia/NK) and dietary saturated fatty acid consumption [84]. Insulin-resistant people have lower levels of 9-PAHSA in their serum and adipose tissue, and serum 9-PAHSA levels are significantly correlated with insulin sensitivity shown in humans assessed via euglycaemic clamp [84]. FAHFAs are found in the fat of ruminant meat, milk, eggs, fish [85,86], and breast milk, although they are lower in the breast milk of obese lactating mothers [87]. Interestingly, omnivores have significantly higher serum levels of FAHFA than vegetarians/vegans, and in a 1-week over-feeding study in 15 lean males with a BMI < 27, the consumption of saturated fatty acids from whipping cream was shown to increase serum FAFHA [88,89]. All of these foods are common in many ketosis-supportive lifestyles.

The stimulation of basal GLP-1 secretion has been mainly studied in people in suppressed ketosis (hypoketonaemia) states, who are in the lean and overweight categories, or in pathology. It is arguable that stimulators of basal GLP-1 secretion should be studied in healthy long-term sustained NK (euketonaemia) individuals, who may better reflect the metabolic state that humans likely evolved in, where they would have had less frequent meals, with only seasonally available low farinaceous carbohydrate availability, and, thus, would have been naturally in ketosis for a greater number of hours in their 24 h day and overall year [2,7,39,90,91].

Trials administering oral glucose to hypoketonaemic participants have shown dietary glucose-causing bolus-associated GLP-1 secretion [79]. During the NK phases of the KetoSAge trial, the participants did not consume enough carbohydrates to cause the suppression of ketosis, whilst they consumed 267 g of carbohydrate spread over three meals a day during phase 2 to suppress ketosis. As can be seen, basal GLP-1 was significantly higher in the two phases with the least dietary glucose exposure, whilst after the participants had followed the SUK dietary guidelines to habitually consume the equivalent of three OGTTs worth of glucose for 21 days straight, which would be equivalent to 63 OGTTs, the KetoSAge participants' mean basal fasting GLP-1 levels were significantly lower, with higher fasting glucose and insulin. This might be explained by increased GLP-1 clearance in a hypoketonaemia state, via increased DDP-4 enzymatic breakdown or increased renal clearance. Alternatively, euketonaemia may decrease DDP-4 activity, thus reducing GLP-1 clearance [83,92]. This warrants further investigation.

Given that the "blockbuster" drugs for the current treatment for T2DM, and now used for the treatment of obesity to induce weight loss, are GLP-1R agonists [93], it would be beneficial to understand the physiological role of basal GLP-1 in healthy humans in a metabolic state reflective of how we evolved, namely, euketonaemia MP1. The fasting-mimicking-state euketonaemia effectuates weight normalisation, shown to bring back weight homeostasis, meaning that the overweight will lose weight and the underweight will return to a healthier weight, whilst resolving many metabolic and neurological health conditions in the process [94–99].

5. Strengths and Limitations

Our study is a novel investigation of the biomarkers in chronic diseases of ageing in a healthy pre-menopausal female population living in long-term ketosis. OCN and GLP-1 have not been measured in this cohort before. Further work assessing these biomarkers in larger cohorts across different ages and in pathologies should be considered. Due to the low sensitivity of several trialled glucagon assays, we were unable to measure glucagon in

this cohort of participant samples. Further details on strengths and limitations have been previously discussed in detail in our earlier publication [7].

6. Conclusions

Long-term ketosis does not result in chronic elevated cortisol levels, indicating that ketosis is not a chronic stress-inducing nor fight or flight state. Long-term NK, euketonaemia, results in elevated GLP-1 levels that would presumably stimulate GLP-1R, which is associated with maintaining a healthier weight or weight loss and satiety, a method employed by T2DM and weight loss GLP-1R agonists. Long-term sustained euketonaemia results in lower levels of leptin, which is associated with increased satiety sensitivity and healthier metabolic profiles. Whilst OCN is considered to be necessary for insulin secretion, given that we understand that a low level of insulin that does not suppress ketogenesis is a healthy level of insulin, MP1, euketonaemia, presents with lower plasma OCN levels. This likely indicates that the OCN remains in the bone, and would confer greater bone health. This is understood to be corroborated in those with low HOMA-IR values also having a lower risk of fragility fractures, indicating insulin sensitivity and, thus, not being hyperinsulinaemic. Furthermore, the increased plasma OCN seen after suppressing ketosis may be from osteoclast bone resorption, which may, over time, result in the hyper-mineralisation of the bones (increased BMD seen in T2DM and obesity), but also be coupled with an increased brittleness, resulting in increased fragility fractures rate, as seen in obesity and T2DM individuals. Lower OCN levels are found in the healthy euketonaemic state, and are accompanied with lower fasting glucose, insulin, insulin sensitivity HOMA-IR, and leptin and higher GLP- 1. Sustained NK showed no adverse health effects and may mitigate hyperinsulinemia. All biomarkers returned to basal P1 levels after removing the intervention for SuK, indicating that metabolic flexibility is maintained with long-term euketonaemia.

Author Contributions: I.D.C. conceived the hypothesis and study design, wrote the original draft, designed the figures, and reviewed and edited the final manuscript. I.D.C. and Y.K. conducted the trial. I.D.C., Y.K. and L.P. collected and compiled data. I.D.C., Y.K., L.P. and K.E. performed ex vivo bench top assays. I.D.C., Y.K., L.P. and K.E. analysed data. I.D.C. designed tables and graphs. I.D.C., Y.K., L.P., K.E., A.S.-M., K.B. and B.T.E. contributed to writing and reviewed and edited the final manuscript. All authors have read and agreed to the published version of the manuscript.

Funding: This research received no external funding.

Institutional Review Board Statement: The study was conducted in accordance with the Declaration of Helsinki and approved by the College of Liberal of Arts and Sciences Research Ethics Committee, University of Westminster. Ethical approval was obtained by the College of Liberal of Arts and Sciences Research Ethics Committee, University of Westminster, United Kingdom (ETH2122-0634).

Informed Consent Statement: Informed consent was obtained from all subjects involved in the study.

Data Availability Statement: The data presented in this study are available from the corresponding author upon reasonable request.

Acknowledgments: The authors would like to acknowledge the time and dedication of all participants who participated in this study.

Conflicts of Interest: The authors declare no conflicts of interest.

Abbreviations

9-PAHSA	palmitic-acid-9-hydroxy-stearic-acid
ACD	all-cause dementia
AD	Alzheimer's disease
BA	biological ageing
BHB	beta-hydroxybutyrate
BMI	body mass index

CAC	coronary artery calcification
CI	confidence interval
cOCN	carboxylated osteocalcin
CVD	cardiovascular disease
EPC	endothelial progenitor cells
FAHFA	fatty acid ester of hydroxy fatty acids
GGT	gamma-glutamyl transferase
GLP-1	glucagon like peptide-1
GLP-1R	glucagon like peptide-1 receptor
HA	hydroxyapatite
HOMA-IR	homeostatic model assessment for insulin resistance
IGF-1	insulin like growth factor-1
L	ileo-colonic
MASLD	metabolic-dysfunction-associated steatosis liver disease
MCP-1	monocyte chemotactic protein-1
MetS	metabolic syndrome
Mt	mitochondrial
MP	metabolic phenotype
NK	nutritional ketosis
OGTT	oral glucose tolerance test
OR	odds ratio
OXPHOS	oxidative phosphorylation
P1	Phase 1
P2	Phase 2
P3	Phase 3
RCT	randomised control trial
SA	sub-clinical atherosclerosis
SFA	saturated fatty acid
SUK	standard U.K. diet
SuK	suppression of ketosis
TOFI	thin on the outside fat on the inside
T2DM	type 2 diabetes mellitus
T3	triiodothyronine
tOCN	total osteocalcin
unOCN	uncarboxylated osteocalcin

References

1. Yang, H.; Gong, R.; Liu, M.; Deng, Y.; Zheng, X.; Hu, T. HOMA-IR is positively correlated with biological age and advanced aging in the US adult population. *Eur. J. Med. Res.* **2023**, *28*, 470. [CrossRef] [PubMed]
2. Cooper, I.D.; Kyriakidou, Y.; Petagine, L.; Edwards, K.; Elliott, B.T. Bio-hacking better health—Leveraging metabolic biochemistry to maximise healthspan. *Antioxidants* **2023**, *12*, 1749. [CrossRef] [PubMed]
3. UN World Population Ageing 2019: Highlights. Available online: https://www.un.org/en/development/desa/population/publications/pdf/ageing/WorldPopulationAgeing2019-Report.pdf (accessed on 13 September 2023).
4. WHO. Global Health Estimates: Leading Causes of Death. 2019. Available online: https://www.who.int/data/gho/data/themes/mortality-and-global-health-estimates/ghe-leading-causes-of-death (accessed on 13 September 2023).
5. ONS. Death Registration Summary Statistics, England and Wales—Office for National Statistics. ONS Website. 2023. Available online: https://www.ons.gov.uk/peoplepopulationandcommunity/birthsdeathsandmarriages/deaths/articles/deathregistrationsummarystatisticsenglandandwales/2022 (accessed on 14 September 2023).
6. Araújo, J.; Cai, J.; Stevens, J. Prevalence of optimal metabolic ealth in american adults: National health and nutrition examination survey 2009–2016. *Metab. Syndr. Relat. Disord.* **2018**, *17*, 46–52. [CrossRef] [PubMed]
7. Cooper, I.D.; Kyriakidou, Y.; Edwards, K.; Petagine, L.; Seyfried, T.N.; Duraj, T.; Soto-Mota, A.; Scarborough, A.; Jacome, S.L.; Brookler, K.; et al. Ketosis Suppression and Ageing (KetoSAge): The effects of suppressing ketosis in long term keto-adapted non-athletic females. *Int. J. Mol. Sci.* **2023**, *24*, 15621. [CrossRef] [PubMed]
8. Cooper, I.D.; Brookler, K.H.; Kyriakidou, Y.; Elliott, B.T.; Crofts, C.A.P. Metabolic phenotypes and step by step evolution of type 2 diabetes: A new paradigm. *Biomedicines* **2021**, *9*, 800. [CrossRef] [PubMed]

9. Crofts, C.A.P.; Zinn, C.; Wheldon, M.; Schofield, M. Hyperinsulinemia: A unifying theory of chronic disease? *Diabesity* **2015**, *1*, 34. [CrossRef]
10. Petagine, L.; Zariwala, M.G.; Patel, V.B. Non-alcoholic fatty liver disease: Immunological mechanisms and current treatments. *World J. Gastroenterol.* **2023**, *29*, 4831–4850. [CrossRef] [PubMed]
11. Younossi, Z.M.; Rinella, M.E.; Sanyal, A.J.; Harrison, S.A.; Brunt, E.M.; Goodman, Z.; Cohen, D.E.; Loomba, R. From NAFLD to MAFLD: Implications of a Premature Change in Terminology. *Hepatology* **2021**, *73*, 1194–1198. [CrossRef] [PubMed]
12. Salvatore, T.; Galiero, R.; Caturano, A.; Rinaldi, L.; Criscuolo, L.; Di Martino, A.; Albanese, G.; Vetrano, E.; Catalini, C.; Sardu, C.; et al. Current knowledge on the pathophysiology of lean/normal-weight type 2 diabetes. *Int. J. Mol. Sci.* **2022**, *24*, 658. [CrossRef]
13. Nabulsi, A.A.; Folsom, A.R.; Heiss, G.; Weir, S.S.; Chambless, L.E.; Watson, R.L.; Eckfeldt, J.H. Atherosclerosis Risk in Communities Study Investigators Fasting hyperinsulinemia and cardiovascular disease risk factors in nondiabetic adults: Stronger associations in lean versus obese subjects. *Metabolism* **1995**, *44*, 914–922. [CrossRef]
14. Kempf, A.M.; Strother, M.L.; Li, C.; Kaur, H.; Huang, T.T.K. Leptin as a marker of body fat and hyperinsulinemia in college students. *J. Am. Coll. Health* **2006**, *55*, 175–180. [CrossRef]
15. Wiebe, N.; Muntner, P.; Tonelli, M. Associations of body mass index, fasting insulin, and inflammation with mortality: A prospective cohort study. *Int. J. Obes.* **2022**, *46*, 2107–2113. [CrossRef]
16. Moore, A.R.; Holland-Winkler, A.M.; Ansley, J.K.; Boone, E.D.H.; Schulte, M.K.O. Reliability and diagnostic performance of a new blood ketone and glucose meter in humans. *J. Int. Soc. Sports Nutr.* **2021**, *18*, 1–9. [CrossRef]
17. The Emerging Risk Factors Collaboration Diabetes mellitus, fasting glucose, and risk of cause-specific death. *N. Engl. J. Med.* **2011**, *364*, 829–841. [CrossRef]
18. Sherwani, S.I.; Khan, H.A.; Ekhzaimy, A.; Masood, A.; Sakharkar, M.K. Significance of HbA1c test in diagnosis and prognosis of diabetic patients. *Biomark. Insights* **2016**, *11*, 95. [CrossRef]
19. Ramirez, A.; Lange, C.; Kaduszkiewicz, H.; Weyerer, S.; Werle, J.; Pentzek, M.; Fuchs, A.; Riedel-Heller, S.G.; Luck, T.; Mösch, E.; et al. Elevated HbA1c is associated with increased risk of incident dementia in primary care patients. *J. Alzheimers Dis.* **2015**, *44*, 1203–1212. [CrossRef]
20. Crofts, C.; Schofield, G.; Zinn, C.; Wheldon, M.; Kraft, J. Identifying hyperinsulinaemia in the absence of impaired glucose tolerance: An examination of the Kraft database. *Diabetes Res. Clin. Pract.* **2016**, *118*, 50–57. [CrossRef]
21. Goalstone, M.L.; Leitner, J.W.; Wall, K.; Dolgonos, L.; Rother, K.I.; Accili, D.; Draznin, B. Effect of insulin on farnesyltransferase. *J. Biol. Chem.* **1998**, *273*, 23892–23896. [CrossRef]
22. Draznin, B. Mitogenic action of insulin: Friend, foe or "frenemy"? *Diabetologia* **2010**, *53*, 229–233. [CrossRef]
23. Goalstone, M.L.; Draznin, B. What does insulin do to Ras? *Cell. Signal.* **1998**, *10*, 297–301. [CrossRef] [PubMed]
24. Draznin, B. Mechanism of the mitogenic influence of hyperinsulinemia. *Diabetol. Metab. Syndr.* **2011**, *3*, 10. [CrossRef] [PubMed]
25. Hodson, A.E.; Tippetts, T.S.; Bikman, B.T. Insulin treatment increases myocardial ceramide accumulation and disrupts cardiometabolic function. *Cardiovasc. Diabetol.* **2015**, *14*, 153. [CrossRef] [PubMed]
26. Smith, M.E.; Tippetts, T.S.; Brassfield, E.S.; Tucker, B.J.; Ockey, A.; Swensen, A.C.; Anthonymuthu, T.S.; Washburn, T.D.; Kane, D.A.; Prince, J.T.; et al. Mitochondrial fission mediates ceramide-induced metabolic disruption in skeletal muscle. *Biochem. J.* **2013**, *456*, 427–439. [CrossRef] [PubMed]
27. Hansen, M.E.; Tippetts, T.S.; Anderson, M.C.; Holub, Z.E.; Moulton, E.R.; Swensen, A.C.; Prince, J.T.; Bikman, B.T. Insulin increases ceramide synthesis in skeletal muscle. *J. Diabetes Res.* **2014**, *2014*, 765784. [CrossRef] [PubMed]
28. Action to Control Cardiovascular Risk in Diabetes Study Group; Gerstein, H.C.; Miller, M.E.; Byington, R.P.; Goff, D.C., Jr.; Bigger, J.T.; Buse, J.B.; Cushman, W.C.; Genuth, S.; Ismail-Beigi, F.; et al. Effects of intensive glucose lowering in type 2 diabetes. *N. Engl. J. Med.* **2008**, *358*, 2545–2559. [CrossRef]
29. Zhou, X.; Kang, C.; Hu, Y.H.; Wang, X.C. Study on insulin resistance and ischemic cerebrovascular disease: A bibliometric analysis via CiteSpace. *Front. Public Health* **2023**, *11*, 1021378. [CrossRef] [PubMed]
30. Ahmed, S.B.M.; Radwan, N.; Amer, S.; Saheb Sharif-Askari, N.; Mahdami, A.; Samara, K.A.; Halwani, R.; Jelinek, H.F. Assessing the link between diabetic metabolic dysregulation and breast cancer progression. *Int. J. Mol. Sci.* **2023**, *24*, 11816. [CrossRef]
31. Cooper, I.D.; Crofts, C.A.P.; DiNicolantonio, J.J.; Malhotra, A.; Elliott, B.; Kyriakidou, Y.; Brookler, K.H. Relationships between hyperinsulinaemia, magnesium, vitamin D, thrombosis and COVID-19: Rationale for clinical management. *Open Hear.* **2020**, *7*, e001356. [CrossRef]
32. Cooper, I.D.; Sanchez-Pizarro, C.; Norwitz, N.G.; Feldman, D.; Kyriakidou, Y.; Edwards, K.; Petagine, L.; Elliot, B.T.; Soto-Mota, A. Thyroid markers and body composition predict LDL-cholesterol change in lean healthy women on a ketogenic diet: Experimental support for the lipid energy model. *Front. Endocrinol.* **2023**, *14*, 1326768. [CrossRef]
33. Paoli, A.; Rubini, A.; Volek, J.S.; Grimaldi, K.A. Beyond weight loss: A review of the therapeutic uses of very-low-carbohydrate (ketogenic) diets. *Eur. J. Clin. Nutr.* **2013**, *67*, 789–796. [CrossRef]
34. Gershuni, V.M.; Yan, S.L.; Medici, V. Nutritional ketosis for weight management and reversal of metabolic syndrome. *Curr. Nutr. Rep.* **2018**, *7*, 97–106. [CrossRef]
35. Janssen, J.A.M.J.L.; Street, E. Hyperinsulinemia and its pivotal role in aging, obesity, type 2 diabetes, cardiovascular disease and cancer. *Int. J. Mol. Sci.* **2021**, *22*, 7797. [CrossRef] [PubMed]

36. Iglesies-Grau, J.; Garcia-Alvarez, A.; Oliva, B.; Mendieta, G.; García-Lunar, I.; Fuster, J.J.; Devesa, A.; Pérez-Herreras, C.; Fernández-Ortiz, A.; Brugada, R.; et al. Early insulin resistance in normoglycemic low-risk individuals is associated with subclinical atherosclerosis. *Cardiovasc. Diabetol.* **2023**, *22*, 350. [CrossRef] [PubMed]
37. Hauschka, P.V.; Lian, J.B.; Cole, D.E.; Gundberg, C.M. Osteocalcin and matrix Gla protein: Vitamin K-dependent proteins in bone. *Phys. Rev.* **1989**, *69*, 990–1047. [CrossRef] [PubMed]
38. Mizokami, A.; Wang, D.G.; Tanaka, M.; Gao, J.; Takeuchi, H.; Matsui, T.; Hirata, M. An extract from pork bones containing osteocalcin improves glucose metabolism in mice by oral administration. *Biosci. Biotechnol. Biochem.* **2016**, *80*, 2176–2183. [CrossRef] [PubMed]
39. Cooper, I.D.; Brookler, K.H.; Crofts, C.A.P. Rethinking fragility fractures in type 2 diabetes: The link between hyperinsulinaemia and osteofragilitas. *Biomedicines* **2021**, *9*, 1165. [CrossRef] [PubMed]
40. Nakamura, M.; Imaoka, M.; Takeda, M. Interaction of bone and brain: Osteocalcin and cognition. *Int. J. Neurosci.* **2020**, *131*, 1115–1123. [CrossRef] [PubMed]
41. Wang, J.S.; Mazur, C.M.; Wein, M.N. Sclerostin and osteocalcin: Candidate bone-produced hormones. *Front. Endocrinol.* **2021**, *12*, 584147. [CrossRef] [PubMed]
42. Puig, J.; Blasco, G.; Daunis-I-Estadella, J.; Moreno, M.; Molina, X.; Alberich-Bayarri, A.; Xifra, G.; Pedraza, S.; Ricart, W.; Fernández-Aranda, F.; et al. Lower serum osteocalcin concentrations are associated with brain microstructural changes and worse cognitive performance. *Clin. Endocrinol.* **2016**, *84*, 756–763. [CrossRef]
43. Ferron, M.; Lacombe, J. Regulation of energy metabolism by the skeleton: Osteocalcin and beyond. *Arch. Biochem. Biophys.* **2014**, *561*, 137–146. [CrossRef]
44. Dede, A.D.; Tournis, S.; Dontas, I.; Trovas, G. Type 2 diabetes mellitus and fracture risk. *Metabolism* **2014**, *63*, 1480–1490. [CrossRef]
45. Foresta, C.; Strapazzon, G.; De Toni, L.; Gianesello, L.; Calcagno, A.; Pilon, C.; Plebani, M.; Vettor, R. Evidence for osteocalcin production by adipose tissue and its role in human metabolism. *J. Clin. Endocrinol. Metab.* **2010**, *95*, 3502–3506. [CrossRef] [PubMed]
46. Gössl, M.; Mödder, U.I.; Atkinson, E.J.; Lerman, A.; Khosla, S. Osteocalcin expression by circulating endothelial progenitor cells in patients with coronary atherosclerosis. *J. Am. Coll. Cardiol.* **2008**, *52*, 1314. [CrossRef] [PubMed]
47. Zhu, D.; Mackenzie, N.C.W.; Millán, J.L.; Farquharson, C.; MacRae, V.E. The appearance and modulation of osteocyte marker expression during calcification of vascular smooth muscle cells. *PLoS ONE* **2011**, *6*, e19595. [CrossRef] [PubMed]
48. Brandenburg, V.M.; Kramann, R.; Koos, R.; Krüger, T.; Schurgers, L.; Mühlenbruch, G.; Hübner, S.; Gladziwa, U.; Drechsler, C.; Ketteler, M. Relationship between sclerostin and cardiovascular calcification in hemodialysis patients: A cross-sectional study. *BMC Nephrol.* **2013**, *14*, 219. [CrossRef] [PubMed]
49. De Maré, A.; D'haese, P.C.; Verhulst, A. The role of sclerostin in bone and ectopic calcification. *Int. J. Mol. Sci.* **2020**, *21*, 3199. [CrossRef] [PubMed]
50. Tyson, J.; Bundy, K.; Roach, C.; Douglas, H.; Ventura, V.; Segars, M.F.; Schwartz, O.; Simpson, C.L. Mechanisms of the osteogenic switch of smooth muscle cells in vascular calcification: WNT signaling, BMPs, mechanotransduction, and EndMT. *Bioengineering* **2020**, *7*, 88. [CrossRef] [PubMed]
51. Saleem, U.; Mosley, T.H.; Kullo, I.J. Serum osteocalcin is associated with measures of insulin resistance, adipokine levels, and the presence of metabolic syndrome. *Arterioscler. Thromb. Vasc. Biol.* **2010**, *30*, 1474–1478. [CrossRef] [PubMed]
52. Yaylali, Y.T.; Fidan-Yaylali, G.; Dedeoglu, O.; Senol, H. Osteocalcin and epicardial adipose tissue in obesity: New hints for epicardial adipose tissue–bone crosstalk. *Scand. Cardiovasc. J.* **2019**, *53*, 296–298. [CrossRef] [PubMed]
53. Bao, Y.; Xiaojing, M.; Yang, R.; Wang, F.; Hao, Y.; Dou, J.; He, H.; Jia, W. Inverse relationship between serum osteocalcin levels and visceral fat area in chinese men. *J. Clin. Endocrinol. Metab.* **2013**, *98*, 345–351. [CrossRef]
54. Lei, H.; Liu, J.; Wang, W.; Yang, X.; Feng, Z.; Zang, P.; Lu, B.; Shao, J. Association between osteocalcin, a pivotal marker of bone metabolism, and secretory function of islet beta cells and alpha cells in Chinese patients with type 2 diabetes mellitus: An observational study. *Diabetol. Metab. Syndr.* **2022**, *14*, 160. [CrossRef]
55. Ferron, M. Endocrine Functions of Bone. In *Principles of Endocrinology and Hormone Action*; Belfiore, A., LeRoith, D., Eds.; Springer: Cham, Switzerland, 2018; ISBN 978-3-319-44675-2.
56. Mizokami, A.; Yasutake, Y.; Gao, J.; Matsuda, M.; Takahashi, I.; Takeuchi, H.; Hirata, M. Osteocalcin induces release of glucagon-like peptide-1 and thereby stimulates insulin secretion in mice. *PLoS ONE* **2013**, *8*, 57375. [CrossRef]
57. Mizokami, A.; Mukai, S.; Gao, J.; Kawakubo-Yasukochi, T.; Otani, T.; Takeuchi, H.; Jimi, E.; Hirata, M. GLP-1 signaling is required for improvement of glucose tolerance by osteocalcin. *J. Endocrinol.* **2020**, *244*, 285–296. [CrossRef] [PubMed]
58. Ben-Dor, M.; Gopher, A.; Hershkovitz, I.; Barkai, R. Man the fat hunter: The demise of Homo erectus and the emergence of a new Hominin lineage in the middle pleistocene (ca. 400 kyr) Levant. *PLoS ONE* **2011**, *6*, e28689. [CrossRef] [PubMed]
59. Boden, G.; Chen, X.; Kolaczynski, J.W.; Polansky, M. Effects of prolonged hyperinsulinemia on serum leptin in normal human subjects. *J. Clin. Investig.* **1997**, *100*, 1107. [CrossRef] [PubMed]
60. Pluta, W.; Dudzińska, W.; Lubkowska, A. Metabolic obesity in people with normal body weight (MONW)—review of diagnostic criteria. *Int. J. Environ. Res. Public Health* **2022**, *19*, 624. [CrossRef]
61. Ruderman, N.B.; Schneider, S.H.; Berchtold, P. The "metabolically-obese," normal-weight individual. *Am. J. Clin. Nutr.* **1981**, *34*, 1617–1621. [CrossRef] [PubMed]

62. Veech, R.L. The therapeutic implications of ketone bodies: The effects of ketone bodies in pathological conditions: Ketosis, ketogenic diet, redox states, insulin resistance, and mitochondrial metabolism. *Prostaglandins Leukot. Essent. Fat. Acids* **2004**, *70*, 309–319. [CrossRef] [PubMed]
63. Reilly, M.P.; Iqbal, N.; Schutta, M.; Wolfe, M.L.; Scally, M.; Localio, A.R.; Rader, D.J.; Kimmel, S.E. Plasma leptin levels are associated with coronary atherosclerosis in type 2 diabetes. *J. Clin. Endocrinol. Metab.* **2004**, *89*, 3872–3878. [CrossRef]
64. Zdrojewicz, Z.; Popowicz, E.; Szyca, M.; Michalik, T.; Śmieszniak, B. TOFI phenotype-its effect on the occurrence of diabetes. *Pediatr. Endocrinol. Diabetes. Metab.* **2017**, *23*, 96–100. [CrossRef] [PubMed]
65. Ghosh, A.; Abdo, S.; Zhao, S.; Wu, C.-H.; Shi, Y.; Lo, C.-S.; Chenier, I.; Alquier, T.; Filep, J.G.; Ingelfinger, J.R.; et al. Insulin Inhibits Nrf2 Gene Expression via Heterogeneous Nuclear Ribonucleoprotein F/K in Diabetic Mice. *Endocrinology* **2019**, *158*, 903–919. [CrossRef] [PubMed]
66. Ruderman, N.; Chisholm, D.; Pi-Sunyer, X.; Schneider, S. The metabolically obese, normal-weight individual revisited. *Diabetes* **1998**, *47*, 699–713. [CrossRef] [PubMed]
67. Lana, A.; Valdés-Bécares, A.; Buño, A.; Rodríguez-Artalejo, F.; Lopez-Garcia, E. Serum leptin concentration is associated with incident frailty in older adults. *Aging Dis.* **2017**, *8*, 240–249. [CrossRef] [PubMed]
68. Shih, Y.L.; Huang, T.C.; Shih, C.C.; Chen, J.Y. Relationship between leptin and insulin resistance among community-dwelling middle-aged and elderly populations in Taiwan. *J. Clin. Med.* **2022**, *11*, 5357. [CrossRef] [PubMed]
69. Stalder, T.; Kirschbaum, C. Cortisol. In *Encyclopedia of Behavioral Medicine*; Gellman, M.D., Ed.; Springer: Cham, Switzerland, 2020; pp. 561–567. ISBN 978-3-030-39903-0.
70. Yan, Y.X.; Xiao, H.B.; Wang, S.S.; Zhao, J.; He, Y.; Wang, W.; Dong, J. Investigation of the relationship between chronic stress and Insulin resistance in a chinese population. *J. Epidemiol.* **2016**, *26*, 355–360. [CrossRef] [PubMed]
71. Reynolds, R.M.; Labad, J.; Strachan, M.W.J.; Braun, A.; Fowkes, F.G.R.; Lee, A.J.; Frier, B.M.; Seckl, J.R.; Walker, B.R.; Price, J.F. Elevated fasting plasma cortisol is associated with ischaemic heart disease and its risk factors in people with type 2 diabetes: The Edinburgh Type 2 Diabetes Study. *J. Clin. Endocrinol. Metab.* **2010**, *95*, 1602. [CrossRef] [PubMed]
72. Kushnir, M.M.; Neilson, R.; Roberts, W.L.; Rockwood, A.L. Cortisol and cortisone analysis in serum and plasma by atmospheric pressure photoionization tandem mass spectrometry. *Clin. Biochem.* **2004**, *37*, 357–362. [CrossRef] [PubMed]
73. Seal, S.V.; Turner, J.D. The 'Jekyll and Hyde' of gluconeogenesis: Early life adversity, later life stress, and metabolic disturbances. *Int. J. Mol. Sci.* **2021**, *22*, 3344. [CrossRef] [PubMed]
74. Popoviciu, M.S.; Păduraru, L.; Yahya, G.; Metwally, K.; Cavalu, S. Emerging role of GLP-1 agonists in obesity: A comprehensive review of randomised controlled trials. *Int. J. Mol. Sci.* **2023**, *24*, 10449. [CrossRef] [PubMed]
75. Jujić, A.; Godina, C.; Belting, M.; Melander, O.; Juul Holst, J.; Ahlqvist, E.; Gomez, M.F.; Nilsson, P.M.; Jernström, H.; Magnusson, M. Endogenous incretin levels and risk of first incident cancer: A prospective cohort study. *Sci. Rep.* **2023**, *13*, 382. [CrossRef]
76. Drucker, D.J. The biology of incretin hormones. *Cell Metab.* **2006**, *3*, 153–165. [CrossRef]
77. Drucker, D.J.; Philippe, J.; Mojsov, S.; Chick, W.L.; Habener, J.F. Glucagon-like peptide I stimulates insulin gene expression and increases cyclic AMP levels in a rat islet cell line. *Proc. Natl. Acad. Sci. USA* **1987**, *84*, 3434. [CrossRef] [PubMed]
78. Ramracheya, R.; Chapman, C.; Chibalina, M.; Dou, H.; Miranda, C.; González, A.; Moritoh, Y.; Shigeto, M.; Zhang, Q.; Braun, M.; et al. GLP-1 suppresses glucagon secretion in human pancreatic alpha-cells by inhibition of P/Q-type Ca^{2+} channels. *Physiol. Rep.* **2018**, *6*, e13852. [CrossRef] [PubMed]
79. Kreymann, B.; Ghatei, M.A.; Williams, G.; Bloom, S.R. Glucagon-like peptide-1 7-36: A physiological incretin in man. *Lancet* **1987**, *330*, 1300–1304. [CrossRef] [PubMed]
80. Albrechtsen, N.J.W.; Bak, M.J.; Hartmann, B.; Christensen, L.W.; Kuhre, R.E.; Deacon, C.F.; Holst, J.J. Stability of glucagon-like peptide 1 and glucagon in human plasma. *Endocr. Connect.* **2015**, *4*, 50. [CrossRef] [PubMed]
81. Ebou, M.H.; Singh-Estivalet, A.; Launay, J.M.; Callebert, J.; Tronche, F.; Ferré, P.; Gautier, J.F.; Guillemain, G.; Bréant, B.; Blondeau, B.; et al. Glucocorticoids inhibit basal and hormone-induced serotonin synthesis in pancreatic beta cells. *PLoS ONE* **2016**, *11*, 149343. [CrossRef] [PubMed]
82. Pi, M.; Nishimoto, S.K.; Quarles, L.D. GPRC6A: Jack of all metabolism (or master of none). *Mol. Metab.* **2017**, *6*, 185–193. [CrossRef]
83. Müller, T.D.; Finan, B.; Bloom, S.R.; D'Alessio, D.; Drucker, D.J.; Flatt, P.R.; Fritsche, A.; Gribble, F.; Grill, H.J.; Habener, J.F.; et al. Glucagon-like peptide 1 (GLP-1). *Mol. Metab.* **2019**, *30*, 72–130. [CrossRef] [PubMed]
84. Yore, M.M.; Syed, I.; Moraes-Vieira, P.M.; Zhang, T.; Herman, M.A.; Homan, E.A.; Patel, R.T.; Lee, J.; Chen, S.; Peroni, O.D.; et al. Discovery of a class of endogenous mammalian lipids with anti-diabetic and anti-inflammatory effects. *Cell* **2014**, *159*, 318–332. [CrossRef] [PubMed]
85. Manful, C.F.; Pham, T.H.; Wheeler, E.; Nadeem, M.; Adigun, O.A.; Walsh, N.; Thomas, R.H. Assessing the fate of fatty acid esters of hydroxy fatty acids, diglycerides and monoacetyldiacylglycerides in grilled ruminant meats marinated with unfiltered beer-based marinades. *J. Food Drug Anal.* **2022**, *30*, 234. [CrossRef]
86. An, N.; Wang, Y.; He, D.X.; Mei, P.C.; Zhu, Q.F.; Feng, Y.Q. A dataset of branched fatty acid esters of hydroxy fatty acids diversity in foods. *Sci. Data* **2023**, *10*, 790. [CrossRef]
87. Brezinova, M.; Kuda, O.; Hansikova, J.; Rombaldova, M.; Balas, L.; Bardova, K.; Durand, T.; Rossmeisl, M.; Cerna, M.; Stranak, Z.; et al. Levels of palmitic acid ester of hydroxystearic acid (PAHSA) are reduced in the breast milk of obese mothers. *Biochim. Biophys. Acta Mol. Cell Biol. Lipids* **2018**, *1863*, 126–131. [CrossRef] [PubMed]

88. Ott, B.; Skurk, T.; Lagkouvardos, L.; Fischer, S.; Büttner, J.; Lichtenegger, M.; Clavel, T.; Lechner, A.; Rychlik, M.; Haller, D.; et al. Short-term overfeeding with dairy cream does not modify gut permeability, the fecal microbiota, or glucose metabolism in young healthy men. *J. Nutr.* **2018**, *148*, 77–85. [CrossRef] [PubMed]
89. Kellerer, T.; Kleigrewe, K.; Brandl, B.; Hofmann, T.; Hauner, H.; Skurk, T. Fatty acid esters of hydroxy fatty acids (FAHFAs) are associated with diet, BMI, and age. *Front. Nutr.* **2021**, *8*, 691401. [CrossRef] [PubMed]
90. Rollo, F.; Ubaldi, M.; Ermini, L.; Marota, I. Ötzi's last meals: DNA analysis of the intestinal content of the neolithic glacier mummy from the Alps. *Proc. Natl. Acad. Sci. USA* **2002**, *99*, 12594–12599. [CrossRef] [PubMed]
91. Ben-Dor, M.; Sirtoli, R.; Barkai, R. The evolution of the human trophic level during the Pleistocene. *Am. J. Phys. Anthropol.* **2021**, *175*, 27–56. [CrossRef] [PubMed]
92. Meier, J.J.; Nauck, M.A.; Kranz, D.; Holst, J.J.; Deacon, C.F.; Gaeckler, D.; Schmidt, W.E.; Gallwitz, B. Secretion, Degradation, and Elimination of Glucagon-Like Peptide 1 and Gastric Inhibitory Polypeptide in Patients with Chronic Renal Insufficiency and Healthy Control Subjects. *Diabetes* **2004**, *53*, 654–662. [CrossRef] [PubMed]
93. Fareed, A.; Hussain, A. The expanding role of GLP-1: From diabetes management to cancer treatment. *Clin. Med. Insights Endocrinol. Diabetes* **2023**, *16*. [CrossRef] [PubMed]
94. Hallberg, S.J.; McKenzie, A.L.; Williams, P.T.; Bhanpuri, N.H.; Peters, A.L.; Campbell, W.W.; Hazbun, T.L.; Volk, B.M.; McCarter, J.P.; Phinney, S.D.; et al. Effectiveness and safety of a novel care model for the management of type 2 diabetes at 1 Year: An open-label, non-randomized, controlled study. *Diabetes Ther.* **2018**, *9*, 583–612. [CrossRef] [PubMed]
95. Danan, A.; Westman, E.C.; Saslow, L.R.; Ede, G. The ketogenic diet for refractory mental illness: A retrospective analysis of 31 inpatients. *Front. Psychiatry* **2022**, *13*, 951376. [CrossRef]
96. Norwitz, N.G.; Hu, M.T.; Clarke, K. The mechanisms by which the ketone body D-β-hydroxybutyrate may improve the multiple cellular pathologies of Parkinson's disease. *Front. Nutr.* **2019**, *6*, 63. [CrossRef]
97. Kelly, T.; Unwin, D.; Finucane, F. Low-carbohydrate diets in the management of obesity and type 2 diabetes: A review from clinicians using the approach in practice. *Int. J. Environ. Res. Public Health* **2020**, *17*, 2557. [CrossRef] [PubMed]
98. Athinarayanan, S.J.; Adams, R.N.; Hallberg, S.J.; McKenzie, A.L.; Bhanpuri, N.H.; Campbell, W.W.; Volek, J.S.; Phinney, S.D.; McCarter, J.P. Long-term effects of a novel continuous remote care intervention including nutritional ketosis for the management of type 2 diabetes: A 2-year nonrandomized clinical trial. *Front. Endocrinol.* **2019**, *10*, 348. [CrossRef] [PubMed]
99. Norwitz, N.G.; Hurn, M.; Forcen, F.E.; Norwitz, N. Animal-based ketogenic diet puts severe anorexia nervosa into multi-year remission: A case series. *J. Metab. Health* **2023**, *6*, 8. [CrossRef]

Disclaimer/Publisher's Note: The statements, opinions and data contained in all publications are solely those of the individual author(s) and contributor(s) and not of MDPI and/or the editor(s). MDPI and/or the editor(s) disclaim responsibility for any injury to people or property resulting from any ideas, methods, instructions or products referred to in the content.

biomedicines

MDPI

Brief Report

Effect of Hypoglycemia and Rebound Hyperglycemia on Proteomic Cardiovascular Risk Biomarkers

Manjula Nandakumar [1], Thozhukat Sathyapalan [2], Stephen L. Atkin [1,†] and Alexandra E. Butler [1,*,†]

[1] Research Department, Royal College of Surgeons in Ireland, Adliya P.O. Box 15503, Bahrain; mnandakumar@rcsi.com (M.N.); satkin@rcsi.com (S.L.A.)
[2] Academic Endocrinology, Diabetes and Metabolism, Hull York Medical School, Hull HU6 7RU, UK; thozhukat.sathyapalan@hyms.ac.uk
* Correspondence: abutler@rcsi.com or aeb91011@gmail.com; Tel.: +973-66760313
† These authors are senior authors.

Abstract: Introduction: Hypoglycemia has been associated with cardiovascular events, and glucose variability has been suggested to be associated with increased cardiovascular risk. Therefore, in this study, we examined the effect on proteomic cardiovascular risk protein markers of (i) mild iatrogenic hypoglycemia and (ii) severe iatrogenic hypoglycemia followed by rebound hyperglycemia. **Methods**: Two iatrogenic hypoglycemia studies were compared; firstly, mild hypoglycemia in 18 subjects (10 type 2 diabetes (T2D), 8 controls; blood glucose to 2.8 mmoL/L (50 mg/dL) for 1 h), and secondly, severe hypoglycemia in 46 subjects (23 T2D, 23 controls; blood glucose to <2.2 mmoL/L (<40 mg/dL) transiently followed by intravenous glucose reversal giving rebound hyperglycemia). A SOMAscan assay was used to measure 54 of the 92 cardiovascular protein biomarkers that reflect biomarkers involved in inflammation, cellular metabolic processes, cell adhesion, and immune response and complement activation. **Results**: Baseline to euglycemia showed no change in any of the proteins measured in the T2D cohort. With severe hypoglycemia, the study controls showed an increase in Angiopoietin 1 (ANGPT1) ($p < 0.01$) and Dickkopf-1 (DKK1) ($p < 0.01$), but no changes were seen with mild hypoglycemia. In both the mild and severe hypoglycemia studies, at the point of hypoglycemia, T2D subjects showed suppression of Brother of CDO (BOC) ($p < 0.01$). At 1 h post-hypoglycemia, the changes in ANGPT1, DKK1, and BOC had resolved, with no additional protein biomarker changes despite rebound hyperglycemia from 1.8 ± 0.1 to 12.2 ± 2.0 mmol/L. **Conclusions**: Proteomic biomarkers of cardiovascular disease showed changes at hypoglycemia that resolved within 1 h following the hypoglycemic event and with no changes following hyperglycemia rebound, suggesting that any cardiovascular risk increase is due to the hypoglycemia and not due to glucose fluctuation per se.

Keywords: type 2 diabetes; hypoglycemia; glucose variability; cardiovascular markers

1. Introduction

An increased risk of cardiovascular disease is associated with type 2 diabetes [1], and the United Kingdom Prospective Diabetes Study (UKPDS) suggested that tight glycemic control reduced macrovascular complications [2], though subsequent studies did not [3–5]. With intensive glycemic control, all-cause mortality increased in the Action to Control Cardiovascular Risk in Diabetes (ACCORD) study [4], though the cause of the increased deaths remains unclear; however, this has been recently challenged with new modeling techniques, suggesting a protective effect of tight glycemic control [6]. Hypoglycemia is associated with platelet function changes through platelet hyperactivity due to sensitivity to prostacyclin 24 h following the hypoglycemic insult [7] in addition to hypoglycemia-induced platelet activation [8,9] mediated by elevation in adrenaline levels [10,11]. Induced hypoglycemia results in increased inflammatory and oxidative stress markers and metabolic

changes in T2D subjects, and these markers remaining elevated at 24 h may explain some of these platelet-associated changes [12,13].

Glucose variability refers to changes in blood glucose levels occurring within minutes or hours, which can be particularly marked in diabetes [14]. It is recognized that hyperglycemia is associated with diabetes-related complications, which may be prevented by improved glycemic control [15]. Glucose variability has been suggested to be associated with increased cardiovascular risk [16], perhaps through increased oxidative stress [17], though a degree of controversy remains [18]. In a study of normal volunteers injected repeatedly with intravenous glucose to mimic intraday glucose variability (3 times 20 g of glucose intravenously over 5 min at intervals of one hour), acute effects on the cardiovascular risk protein markers bone morphogenetic protein 6 (BMP6); signaling lymphocyte activation molecular family 7 (SLAMF7); a disintegrin and metalloproteinase with a thrombospondin type 1 motif, member 13 (ADAMTS13); interleukin-1 receptor antagonist (IL1RA); pentraxin 3 (PTX3); interleukin 4 receptor alpha (IL-4RA); and lectin-like oxLDL (oxidized low-density lipoprotein) receptor 1 (LOX-1) were reported [19]. What is unclear is whether this is simply due to the increment in the blood glucose or whether it is the increment followed by the decrement that is responsible for the potential adverse cardiovascular risk marker profile and whether this response could be mimicked by a decrease in blood glucose alone. The aim of this study was to measure the panel of cardiovascular risk proteins previously reported for glucose variability [19] in type 2 diabetes (T2D) and control subjects undergoing iatrogenic-induced mild prolonged hypoglycemia versus more acute severe hypoglycemia that was reversed immediately with a glucose rebound leading to marked and rapid hyperglycemia.

2. Material and Methods

Two hypoglycemic study designs were employed using the same hypoglycemic clamp technique, and patient demographics are shown in Table 1. In the first mild hypoglycemic (mild-hypo) study design, a case-control prospective study in Caucasian adult (aged 40–53 years) patients with T2D (n = 10) and nondiabetic control (n = 7) subjects that achieved a blood glucose of 2.8 mmol/L (50 mg/dL), which was maintained for 1 h [12], with blood sampling at baseline and at the end of 1 h of hypoglycemia (prior to reversal); subjects did not have overt symptoms of hypoglycemia. (Ethical approval by Yorkshire and the Humber Research Ethics Committee, registered at www.clinicaltrials.gov (NCT02205996) and performed from November 2011–May 2013).

In the severe hypoglycemic (severe-hypo) study design, a case-control prospective study in Caucasian adult (aged 40–70 years) patients with T2D (n = 23) and nondiabetic control (n = 23) subjects that achieved a blood glucose of $\leq$2.0 mmol/L (36 mg/dL) transiently, which was reversed immediately with intravenous glucose, resulting in a mean rebound blood glucose of 12.2 $\pm$ 2.0 mmol/L (195 $\pm$ 3 mg/dL) at 1 h in T2D subjects post-hypoglycemia but remained within the normal glycemic range in the control subjects. Blood sampling was undertaken at baseline, at normoglycemia (5 mmol/L (90 mg/dL)) in T2D subjects, at the point of hypoglycemia, and at 1 h post-hypoglycemia. All subjects developed hypoglycemic symptoms that were immediately reversed (Ethical approval by the NorthWest-Greater Manchester Research Ethics Committee, trial registration NCT03102801, and performed from March 2017–January 2018). Both the mild-hypo and severe-hypo studies were undertaken in the Diabetes Centre at Hull Royal Infirmary. Written informed consent was provided by all participants.

T2D patients had a diabetes duration <10 years with stable hypertensive, lipid-lowering, and diabetes medication (only metformin as an antidiabetic medication was allowed for study inclusion) for at least 3 months prior; HbA1c levels <10% (86 mmol/mol); and no hypoglycemic unawareness or hypoglycemia history during the prior 3-month period. Age was the only parameter that differed between the two groups, with those in the severe-hypo study being older (Table 1).

For control subjects, diabetes was excluded in all with an oral glucose tolerance test. All subjects had normal renal and hepatic function as assessed by biochemical indices, no history of cancer, or any contraindication to hypoglycemia induction with insulin infusion. Medical history, clinical examination, routine blood tests, and an electrocardiogram were performed on all participants.

Table 1. Demographic and biochemical parameters of control (Ctrl) and type 2 diabetic (T2D) subjects included in study 1 (mild hypoglycemia) and study 2 (severe hypoglycemia). Data are presented as mean ± SD.

	Study 1 Ctrl (*n* = 7)	Study 2 Ctrl (*n* = 23)	*p*-Value	Study 1 T2D (*n* = 10)	Study 2 T2D (*n* = 23)	*p*-Value
Age (years)	47 ± 6	60 ± 10	0.003	46 ± 6	64 ± 8	<0.0001
Sex (M/F)	4M/3F	11M/12F		7M/3F	12M/11F	
BMI (kg/m^2)	29 ± 4	28 ± 3	0.640	36 ± 7	32 ± 4	0.03
Systolic BP (mmHg)	126 ± 15	122 ± 8	0.280	127 ± 20	132 ± 8	0.31
Diastolic BP (mmHg)	75 ± 13	75 ± 6	1.000	75 ± 11	81 ± 7	0.08
Duration of diabetes (years)	N/A	N/A		3.3 ± 2.3	4.5 ± 2.2	0.14
HbA1c (mmol/mol)	33.6 ± 2.9	37.2 ± 2.2	0.004	49 ± 12	51 ± 11	0.62
HbA1c (%)	5.2 ± 0.3	5.6 ± 0.2	0.006	6.6 ± 1.0	6.8 ± 1.0	0.48
Total cholesterol (mmol/L)	5.1 ± 0.8	4.8 ± 0.77	0.230	5.3 ± 0.7	4.2 ± 1.0	0.36
Triglyceride (mmol/L)	1.2 ± 0.5	1.3 ± 0.6	0.540	1.7 ± 0.8	1.7 ± 0.7	0.96
CRP (mg/L)	0.8 ± 0.0	5.1 ± 10.3	0.26	2.8 ± 1.8	3.1 ± 2.9	0.94

BMI—body mass index; BP—blood pressure; HbA1c—glycated hemoglobin; CRP—C-reactive protein; N/A—Not applicable.

For the biochemical markers, blood samples were prepared as previously described [12,20]. Blood samples were separated immediately by centrifugation at 2000× *g* for 15 min at 4 °C, and the aliquots were stored at –80 °C within 30 min of blood collection, until batch analysis. High sensitivity C-reactive protein (hsCRP) was measured using a Synchron systems CRPH reagent kit (Beckman-Coulter, High Wycombe, UK) as per manufacturer's protocol. Fasting plasma glucose (FPG) was measured using a Synchron LX 20 analyzer (Beckman-Coulter) according to the manufacturer's recommended protocol. Total cholesterol, triglycerides, and high-density lipoprotein (HDL) cholesterol levels were measured enzymatically using a Synchron LX20 analyzer (Beckman-Coulter, High Wycombe, UK).

A SOMAscan assay was used to measure 54 of the 92 cardiovascular protein biomarkers previously described [19], which are the biomarkers available on the SOMAscan panel. These reflected biomarkers are involved in inflammation, cellular metabolic processes, cell adhesion, and immune response and complement activation. As previously described [20], the SOMAscan assay was used to quantify proteins utilizing buffers and SOMAmers from the SOMAscan HTS Assay 1.3 K plasma kit (SomaLogic, Boulder, CO, USA) according to manufacturer's instructions [21,22]. Initial relative fluorescent units (RFUs) were obtained from microarray intensity images, normalized, and calibrated using the software pipeline provided by SomaLogic. Statistical analyses were performed on $\log_2$ RFU values using R version 3.5.2 (R Foundation for Statistical Computing, Vienna, Austria), and differential protein expression was analyzed using autonomics and limma [23]. Limma-obtained *p*-values were corrected using the Benjamini–Hochberg method [24].

As this was an explorative study, no calculation of sample size was performed. Data trends were visually evaluated for each parameter and non-parametric tests were applied to data that violated the assumptions of normality when tested using the Kolmogorov–Smirnov test. Comparison between groups was performed at each timepoint using Student's t-test and multiple comparisons were corrected using the false discovery rate. Within-group comparisons of changes between timepoints were compared using Student's t-test. Statistical analysis was undertaken using GraphPad Prism (Version 10.2.0, San Diego, CA, USA).

3. Results

Age was the only parameter that differed between the two groups for both T2D and controls (Table 1). The results of the cardiovascular risk markers for mild-hypo and

severe-hypo are shown in Table 2, and a full list of all markers is shown in Supplementary Table S1.

The markers bone morphogenetic protein 6 (BMP6); signaling lymphocyte activation molecular family 7 (SLAMF7, also known as surface antigen CD319); a thrombospondin type 1 motif, member 13 (ADAMTS13, also known as von Willebrand factor-cleaving protease); and interleukin 1 receptor antagonist (IL1RA), shown to differ in a prior hyperglycemia study [19], were unaffected at the point of induced hypoglycemia in both the hypoglycemia studies, with no additional protein biomarker changes with the rebound hyperglycemia from 1.8 $\pm$ 0.1 to 12.2 $\pm$ 2.0 mmol/L.

In the mild-hypo study, T2D subjects showed an increase in Brother of CDO (BOC) ($p < 0.001$), as was also the case in the severe-hypo study ($p < 0.01$) [19] (Table 2).

In the severe-hypo study, baseline to euglycemia showed no change in any of the proteins measured in the T2D cohort. With severe hypoglycemia, study controls showed an increase in Angiopoietin 1 (ANGPT1) ($p < 0.01$) and Dickkopf-1 (DKK1) ($p < 0.01$), but no changes were seen in controls with mild hypoglycemia. In both the mild and severe hypoglycemia studies, at the point of hypoglycemia, T2D showed a decrease in Brother of CDO (BOC) ($p < 0.01$) (Table 1). At one hour after hypoglycemia, the changes in ANGPT1, DKK1, and BOC had resolved, with only one protein, serine protease 27 (PRSS27), becoming elevated in T2D but not in controls, though this was not significant after FDR.

Table 2. Protein levels at baseline (BL) and hypoglycemia (Hypo) reported as mean ± standard deviation (SD) of relative fluorescent units (RFU) as measured by SOMAscan assay.

Protein	Study1—Ctrl		Study2—Ctrl		Study1—T2D		Study2—T2D	
	Mean ± SD BL vs. Hypo	***p*-Value**	**Mean ± SD BL vs. Hypo**	***p*-Value**	**Mean ± SD BL vs. Hypo**	***p*-Value**	**Mean ± SD BL vs. Hypo**	***p*-Value**
BMP6	BL: 1916 ± 507 Hypo: 2006 ± 205	0.69	BL: 14187 ± 4475 Hypo: 13753 ± 4286	0.73	BL: 5034 ± 9854 Hypo: 5464 ± 9438	0.92	BL: 13729 ± 5119 Hypo: 13054 ± 5144	0.65
SLAMF7	BL: 58124 ± 20707 Hypo: 54791 ± 12294	0.73	BL: 41917 ± 14548 Hypo: 38021 ± 13984	0.35	BL: 73898 ± 26200 Hypo: 70961 ± 27635	0.81	BL: 44153 ± 20302 Hypo: 37646 ± 17153	0.24
ADAMTS13	BL: 4500 ± 1065 Hypo: 4988 ± 1230	0.98	BL: 3921 ± 845 Hypo: 3949 ± 1049	0.92	BL: 5231 ± 1164 Hypo: 5194 ± 1047	0.94	BL: 4080 ± 1062 Hypo: 4118 ± 893	0.89
IL1RA	NA		BL: 5386 ± 3101 Hypo: 5261 ± 3012	0.89	NA		BL: 4971 ± 2477 Hypo: 4490 ± 2118	0.47
BOC	BL: 1541 ± 359 Hypo: 1263 ± 199	0.12	BL: 1618 ± 489 Hypo: 1489 ± 448	0.35	BL: 1565 ± 343 Hypo: 992 ± 311	0.001	BL: 1475.8 ± 355 Hypo: 1216 ± 309	0.01
ANGPT1	BL: 942 ± 494 Hypo: 646 ± 99	0.17	BL: 433 ± 156 Hypo: 815 ± 667	0.01	BL: 766 ± 209 Hypo: 932 ± 598	0.42	BL: 752 ± 610 Hypo: 1007.7 ± 695.0	0.18
DKK1	BL: 15699 ± 6353 Hypo: 11425 ± 3511	0.17	BL: 18152 ± 8054 Hypo: 27728 ± 16313	0.02	BL: 14757 ± 2338 Hypo: 17166 ± 13612	0.59	BL: 28249 ± 17077 Hypo: 34616 ± 16789	0.20

BMP6—bone morphogenetic protein 6; SLAMF7—signaling lymphocytic activation molecule (SLAM) family member 7; ADAMTS13—a disintegrin and metalloproteinase with thrombospondin motif 13; IL1RA—interleukin-1 receptor antagonist protein; BOC—Brother of CDO; ANGPT1—Angiopoietin-1; DKK1—Dickkopf-related protein 1.

4. Discussion

This study suggests that any changes in proteomic cardiovascular risk biomarkers were due to hypoglycemia rather than to fluctuations in glycemic levels per se (as determined by the rebound hyperglycemia following the reversal of the transient severe hypoglycemia in study 2). This study also highlights that any potential increased risk of cardiovascular events due to hypoglycemia is not likely due to changes in the cardiovascular risk markers, as an extensive panel of cardiovascular risk biomarkers was utilized, including those involved in different biological processes which play a role in cardiovascular disease, such as inflammation, cellular metabolic processes, cell adhesion, and immune response and complement activation [19]. This adds further weight to the evidence suggesting that the effect of hypoglycemia on cardiovascular events is through platelet dysfunction via platelet hyperactivity caused by sensitivity to prostacyclin 24 h following the hypoglycemic insult [7] and activation of the sympathetic nervous system leading to hypoglycemia-induced platelet activation [8,9] mediated by an elevation in adrenaline levels [10,11]. In both hypoglycemia studies, only BOC was suppressed at hypoglycemia in T2D, indicating that this protein is likely responsive to hypoglycemia irrespective of its severity though, notably, no change in this protein level was seen in control subjects. BOC is a cell surface receptor that derives its name from the structurally related protein and is related to cell adhesion molecules, is down-regulated by oncogenes, and binds to three Hedgehog ligands [25]. Whilst BOC is not well recognized in diabetes, Hedgehog signaling plays a role in lipid metabolism, insulin sensitivity, inflammatory response, and diabetes-related complications [26], and its deficiency in animal models is associated with the development of neuropathy [27], thus linking it with diabetes-related complication pathogenesis.

This study also suggests that the cardiovascular risk markers BMP6, SLAMF7, ADAMTS13, and IL1RA, shown previously by others to respond to transient elevations in glucose [19], do not respond to a fall in glucose or rebound hyperglycemia in T2D. It is recognized that hyperglycemia is associated with diabetes-related complications and the reduction in mean blood glucose reduces their incidence [15]. This suggests that in the absence of cardiovascular risk protein marker changes consequent upon the reduction in blood glucose, the association of glucose variability with complications may be entirely due to the mean time within hyperglycemia of those glucose excursions, rather than the glucose fluctuations per se.

The strengths of this study include inclusion of T2D subjects having a relatively short disease duration and not on polypharmacy (with no difference in these parameters between studies) and that the same hyperinsulinemic clamp protocol for hypoglycemia was utilized in both studies. Limitations of this study include that the panel previously reported utilized Olink proteomic measurements [19], so it was not identical to the SOMAscan panel; this resulted in the ILRA4, LOX-1, and PTX3 proteins not being included in the SOMAscan panel, so no conclusions can be drawn about them. The relatively small subject numbers in each study cohort, for both T2D and control subjects, is a limitation; however, whilst larger subject numbers may have revealed changes in plasma proteins, there were no trends to suggest that this may be the case. As subjects enrolled in these studies were all Caucasian, these results may not be generalizable to other ethnic populations.

In conclusion, proteomic biomarkers of cardiovascular disease showed changes at hypoglycemia that resolved within 1 h after the hypoglycemic event and with no changes following hyperglycemia rebound, suggesting that any cardiovascular risk increase is due to hypoglycemia and not to glucose fluctuation per se.

Supplementary Materials: The following supporting information can be downloaded at: https://www.mdpi.com/article/10.3390/biomedicines12061137/s1, Table S1: *p* values for all Protein levels at baseline (BL) vs hypoglycemia (Hypo) in T2D and Control in Study1 and Study2.

Author Contributions: Conceptualization, S.L.A. and A.E.B.; methodology, S.L.A. and A.E.B.; formal analysis, M.N. and A.E.B.; investigation, M.N.; data curation, T.S.; writing-original draft preparation, M.N., S.L.A. and A.E.B.; writing-review and editing, M.N., T.S., S.L.A. and A.E.B. All authors have agree to the published version of the manuscript.

Funding: This research received no external funding.

Institutional Review Board Statement: The studies were conducted in accordance with the Declaration of Helsinki, and approved by the following Ethics Committees: Study 1 (mild hypo): Ethical approval by Yorkshire and the Humber Research Ethics Committee, rec number 11/YH/0161, approved November 2011; registered at www.clinicaltrials.gov (NCT02205996) and performed from November 2011–May 2013. Study 2 (deep hypo): Ethical approval by the NorthWest-Greater Manchester Research Ethics Committee, rec number 16/NW/0518, February 2017; trial registration NCT03102801, and performed from March 2017–January 2018).

Informed Consent Statement: Informed consent was obtained from all subjects involved in the study.

Data Availability Statement: All the data for this study will be made available upon reasonable request to the corresponding author.

Conflicts of Interest: The authors declare no conflict of interest.

References

1. Ma, C.X.; Ma, X.N.; Guan, C.H.; Li, Y.D.; Mauricio, D.; Fu, S.B. Cardiovascular disease in type 2 diabetes mellitus: Progress toward personalized management. *Cardiovasc. Diabetol.* **2022**, *21*, 74. [CrossRef] [PubMed]
2. Holman, R.R.; Paul, S.K.; Bethel, M.A.; Matthews, D.R.; Neil, H.A. 10-year follow-up of intensive glucose control in type 2 diabetes. *N. Engl. J. Med.* **2008**, *359*, 1577–1589. [CrossRef] [PubMed]
3. Patel, A.; MacMahon, S.; Chalmers, J.; Neal, B.; Billot, L.; Woodward, M.; Marre, M.; Cooper, M.; Glasziou, P.; Grobbee, D.; et al. Intensive blood glucose control and vascular outcomes in patients with type 2 diabetes. *N. Engl. J. Med.* **2008**, *358*, 2560–2572. [CrossRef] [PubMed]
4. Gerstein, H.C.; Miller, M.E.; Byington, R.P.; Goff, D.C., Jr.; Bigger, J.T.; Buse, J.B.; Cushman, W.C.; Genuth, S.; Ismail-Beigi, F.; Grimm, R.H., Jr.; et al. Effects of intensive glucose lowering in type 2 diabetes. *N. Engl. J. Med.* **2008**, *358*, 2545–2559. [CrossRef] [PubMed]
5. Duckworth, W.; Abraira, C.; Moritz, T.; Reda, D.; Emanuele, N.; Reaven, P.D.; Zieve, F.J.; Marks, J.; Davis, S.N.; Hayward, R.; et al. Glucose control and vascular complications in veterans with type 2 diabetes. *N. Engl. J. Med.* **2009**, *360*, 129–139. [CrossRef] [PubMed]
6. Shakiba, M.; Nazemipour, M.; Mansournia, N.; Mansournia, M.A. Protective effect of intensive glucose lowering therapy on all-cause mortality, adjusted for treatment switching using G-estimation method, the ACCORD trial. *Sci. Rep.* **2023**, *13*, 5833. [CrossRef] [PubMed]
7. Kahal, H.; Aburima, A.; Spurgeon, B.; Wraith, K.S.; Rigby, A.S.; Sathyapalan, T.; Kilpatrick, E.S.; Naseem, K.M.; Atkin, S.L. Platelet function following induced hypoglycaemia in type 2 diabetes. *Diabetes Metab.* **2018**, *44*, 431–436. [CrossRef] [PubMed]
8. Wright, R.J.; Newby, D.E.; Stirling, D.; Ludlam, C.A.; Macdonald, I.A.; Frier, B.M. Effects of acute insulin-induced hypoglycemia on indices of inflammation: Putative mechanism for aggravating vascular disease in diabetes. *Diabetes Care* **2010**, *33*, 1591–1597. [CrossRef]
9. Chow, E.; Iqbal, A.; Walkinshaw, E.; Phoenix, F.; Macdonald, I.A.; Storey, R.F.; Ajjan, R.; Heller, S.R. Prolonged Prothrombotic Effects of Antecedent Hypoglycemia in Individuals With Type 2 Diabetes. *Diabetes Care* **2018**, *41*, 2625–2633. [CrossRef]
10. Moin, A.S.M.; Sathyapalan, T.; Atkin, S.L.; Butler, A.E. The severity and duration of Hypoglycemia affect platelet-derived protein responses in Caucasians. *Cardiovasc. Diabetol.* **2022**, *21*, 202. [CrossRef]
11. Yamamoto, K.; Ito, T.; Nagasato, T.; Shinnakasu, A.; Kurano, M.; Arimura, A.; Arimura, H.; Hashiguchi, H.; Deguchi, T.; Maruyama, I.; et al. Effects of glycemic control and hypoglycemia on Thrombus formation assessed using automated microchip flow chamber system: An exploratory observational study. *Thromb. J.* **2019**, *17*, 17. [CrossRef] [PubMed]
12. Kahal, H.; Halama, A.; Aburima, A.; Bhagwat, A.M.; Butler, A.E.; Graumann, J.; Suhre, K.; Sathyapalan, T.; Atkin, S.L. Effect of induced hypoglycemia on inflammation and oxidative stress in type 2 diabetes and control subjects. *Sci. Rep.* **2020**, *10*, 4750. [CrossRef] [PubMed]
13. Halama, A.; Kahal, H.; Bhagwat, A.M.; Zierer, J.; Sathyapalan, T.; Graumann, J.; Suhre, K.; Atkin, S.L. Metabolic and proteomic signatures of hypoglycaemia in type 2 diabetes. *Diabetes Obes. Metab.* **2018**, *21*, 909–919. [CrossRef] [PubMed]
14. Monnier, L.; Colette, C.; Owens, D.R. The application of simple metrics in the assessment of glycaemic variability. *Diabetes Metab.* **2018**, *44*, 313–319. [CrossRef] [PubMed]
15. Joseph, J.J.; Deedwania, P.; Acharya, T.; Aguilar, D.; Bhatt, D.L.; Chyun, D.A.; Di Palo, K.E.; Golden, S.H.; Sperling, L.S. Comprehensive Management of Cardiovascular Risk Factors for Adults With Type 2 Diabetes: A Scientific Statement From the American Heart Association. *Circulation* **2022**, *145*, e722–e759. [CrossRef] [PubMed]
16. Belli, M.; Bellia, A.; Sergi, D.; Barone, L.; Lauro, D.; Barillà, F. Glucose variability: A new risk factor for cardiovascular disease. *Acta Diabetol.* **2023**, *60*, 1291–1299. [CrossRef] [PubMed]
17. Papachristoforou, E.; Lambadiari, V.; Maratou, E.; Makrilakis, K. Association of Glycemic Indices (Hyperglycemia, Glucose Variability, and Hypoglycemia) with Oxidative Stress and Diabetic Complications. *J. Diabetes Res.* **2020**, *2020*, 7489795. [CrossRef] [PubMed]

18. Alatawi, Z.; Mirghani, H. The Association Between Glycemic Variability and Myocardial Infarction: A Review and Meta-Analysis of Prospective Studies and Randomized Trials. *Cureus* **2020**, *12*, e11556. [CrossRef] [PubMed]
19. Feldbauer, R.; Heinzl, M.W.; Klammer, C.; Resl, M.; Pohlhammer, J.; Rosenberger, K.; Almesberger, V.; Obendorf, F.; Schinagl, L.; Wagner, T.; et al. Effect of repeated bolus and continuous glucose infusion on a panel of circulating biomarkers in healthy volunteers. *PLoS ONE* **2022**, *17*, e0279308. [CrossRef]
20. Moin, A.S.M.; Al-Qaissi, A.; Sathyapalan, T.; Atkin, S.L.; Butler, A.E. Hypoglycaemia in type 2 diabetes exacerbates amyloid-related proteins associated with dementia. *Diabetes Obes. Metab.* **2020**, *23*, 338–349. [CrossRef]
21. Kraemer, S.; Vaught, J.D.; Bock, C.; Gold, L.; Katilius, E.; Keeney, T.R.; Kim, N.; Saccomano, N.A.; Wilcox, S.K.; Zichi, D.; et al. From SOMAmer-based biomarker discovery to diagnostic and clinical applications: A SOMAmer-based, streamlined multiplex proteomic assay. *PLoS ONE* **2011**, *6*, e26332. [CrossRef] [PubMed]
22. Suhre, K.; Arnold, M.; Bhagwat, A.M.; Cotton, R.J.; Engelke, R.; Raffler, J.; Sarwath, H.; Thareja, G.; Wahl, A.; DeLisle, R.K.; et al. Connecting genetic risk to disease end points through the human blood plasma proteome. *Nat. Commun.* **2017**, *8*, 14357. [CrossRef] [PubMed]
23. Ritchie, M.E.; Phipson, B.; Wu, D.; Hu, Y.; Law, C.W.; Shi, W.; Smyth, G.K. limma powers differential expression analyses for RNA-sequencing and microarray studies. *Nucleic Acids Res.* **2015**, *43*, e47. [CrossRef] [PubMed]
24. Benjamini, Y.; Drai, D.; Elmer, G.; Kafkafi, N.; Golani, I. Controlling the false discovery rate in behavior genetics research. *Behav. Brain Res.* **2001**, *125*, 279–284. [CrossRef] [PubMed]
25. Vanderman, K.S.; Tremblay, M.; Zhu, W.; Shimojo, M.; Mienaltowski, M.J.; Coleman, S.J.; MacLeod, J.N. Brother of CDO (BOC) expression in equine articular cartilage. *Osteoarthr. Cartil.* **2011**, *19*, 435–438. [CrossRef] [PubMed]
26. Benchoula, K.; Parhar, I.S.; Wong, E.H. The crosstalk of hedgehog, PI3K and Wnt pathways in diabetes. *Arch. Biochem. Biophys.* **2021**, *698*, 108743. [CrossRef]
27. Chapouly, C.; Yao, Q.; Vandierdonck, S.; Larrieu-Lahargue, F.; Mariani, J.N.; Gadeau, A.P.; Renault, M.A. Impaired Hedgehog signalling-induced endothelial dysfunction is sufficient to induce neuropathy: Implication in diabetes. *Cardiovasc. Res.* **2016**, *109*, 217–227. [CrossRef]

Disclaimer/Publisher's Note: The statements, opinions and data contained in all publications are solely those of the individual author(s) and contributor(s) and not of MDPI and/or the editor(s). MDPI and/or the editor(s) disclaim responsibility for any injury to people or property resulting from any ideas, methods, instructions or products referred to in the content.

biomedicines

MDPI

Article

Sexually Dimorphic Effects of CYP2B6 in the Development of Fasting-Mediated Steatosis in Mice: Role of the Oxylipin Products 9-HODE and 9-HOTrE

Jazmine A. Eccles-Miller, Tyler D. Johnson and William S. Baldwin *

Biological Sciences, Clemson University, Clemson, SC 29634, USA; eccles@clemson.edu (J.A.E.-M.); tdj2@clemson.edu (T.D.J.)
* Correspondence: baldwin@clemson.edu

Abstract: Background: Cytochrome P450 2B6 (CYP2B6) is a sexually dimorphic, anti-obesity CYP enzyme responsible for the metabolism of xeno- and endobiotics, including the metabolism of polyunsaturated fatty acids (PUFAs) into 9-hydroxyoctadecadienoic acid (9-HODE) and 9-hydroxyoctadecatrienoic acid (9-HOTrE). However, humanized CYP2B6 transgenic (hCYP2B6-Tg) mice are sensitive to diet-induced hepatic steatosis despite their resistance to obesity. The purpose of this study was to determine if 9-HODE, 9-HOTrE, or other factors contribute to the sexually dimorphic steatosis observed in hCYP2B6-Tg mice. **Results:** Cyp2b9/10/13-null (Cyp2b-null) mice were injected with either 9-HODE or 9-HOTrE for 2 days and were then subjected to a fasting period of 20 h to induce steatosis. Serum lipids were moderately increased, especially in females, after 9-HODE (triglycerides (TGs), very low-density lipoproteins (VLDLs)) and 9-HOTrE (high-density lipoproteins (HDLs), low-density lipoproteins (LDLs), cholesterol) treatment. No change in hepatic lipids and few changes in hepatic gene expression were observed in mice treated with either oxylipin, suggesting that these oxylipins had minimal to moderate effects. Therefore, to further investigate CYP2B6's role in steatosis, hCYP2B6-Tg and Cyp2b-null mice were subjected to a 20 h fast and compared. Both male and female hCYP2B6-Tg mice exhibited increased steatosis compared to Cyp2b-null mice. Serum cholesterol, triglycerides, HDLs, and VLDLs were increased in hCYP2B6-Tg males. Serum triglycerides and VLDLs were decreased in hCYP2B6-Tg females, suggesting the greater hepatic retention of lipids in females. Hepatic oxylipin profiles revealed eight perturbed oxylipins in female hCYP2B6-Tg mice and only one in males when compared to Cyp2b-null mice. RNA-seq also demonstrated greater effects in females in terms of the number of genes and gene ontology (GO) terms perturbed. There were only a few overlapping GO terms between sexes, and lipid metabolic processes were enriched in hCYP2B6-Tg male mice but were repressed in hCYP2B6-Tg females compared to Cyp2b-nulls. **Conclusions:** hCYP2B6-Tg mice are sensitive to fasting-mediated steatosis in males and females, although the responses are different. In addition, the oxylipins 9-HODE and 9-HOTrE are unlikely to be the primary cause of CYP2B6's pro-steatotic effects.

Keywords: cytochrome P450; oxylipins; steatosis; fasting-induced steatosis; sexually dimorphic

1. Introduction

Obesity is a growing issue worldwide, and the World Health Organization has estimated that nearly 1 in 8 people are obese [1]. Hepatic steatosis is a common comorbidity

with obesity and may lead to metabolic dysfunction, insulin resistance, and type 2 diabetes [2]. The combination of obesity, hepatic steatosis, and extrahepatic dysfunction is referred to as metabolic dysfunction-associated fatty liver disease (MAFLD) [3]. Liver diseases are particularly important to study and understand, given that the liver is responsible for the allocation of nutrients, the metabolism of xenobiotics, and regulating metabolism [4,5].

Recent research demonstrates that the cytochrome P450 2B (CYP2B) family is associated with obesity. Mice express five Cyp2b family members, three of which are highly expressed in the liver and potentially protective from obesity. Cyp2b9/10/13-null (Cyp2b-null) mice experience diet-induced obesity with significant steatosis, with males being much more susceptible than females [6]. Furthermore, CYP2B6 is protective against diet-induced obesity in female transgenic mice expressing the human CYP2B6 gene (hCYP2B6-Tg), with males showing greater steatosis surprisingly coupled with greater glucose resistance, as measured with a glucose tolerance test [7]. Similarly to mice, CYP2B6 is the only human CYP2B family member in which reduced expression is associated with increased body mass index [8].

There are several potential mechanisms by which CYP2B6 could be an anti-obesity enzyme that provides protection against insulin resistance while increasing steatosis [7]. CYP2B6 is a key detoxication enzyme that also metabolizes polyunsaturated fatty acids (PUFAs), steroids, and bile acids [9,10]. The disruption of any of these pathways could increase obesity as increased levels of PUFAs, steroid hormones, and bile acids are associated with obesity [11–13]. CYP2B6 metabolizes PUFAs to a variety of potential signaling molecules called oxylipins [14], most likely under high-fat diet conditions [7,15,16].

For example, CYP2B6 activity is inhibited by several PUFAs such as docosahexaenoic acid (DHA), arachidonic acid (AA), linoleic acid (LA), and α-linolenic acid (ALA) [10]. Each of these PUFAs are also substrates and produce multiple oxylipins with preferential metabolism in the 9- > 13-position. 9-hydroxyoctadecadienoic acid (9-HODE) from LA and 9-hydroxyoctadecatrienoic acid (9-HOTrE) from ALA are two of the most prominently produced oxylipins under high-fat diets in vivo and in vitro conditions, respectively [7]. 9-HODE liver concentrations ranged from approximately 8.3 μM to 6.4 μM in male and female mice, respectively [17]. 9-HOTrE liver concentrations are much lower (0.7–2 nM), presumably due to the difference in LA and ALA concentrations in the diet [7]. Other enzymes may also contribute to the production of these oxylipins. For example, 9-HODE is also produced by cyclooxygenase (COX) and lipoxygenase (LOX) enzymes [18]. Ultimately, oxylipins have a variety of roles, and some may serve as local or endocrine messengers that modulate inflammation, cell growth, pain, differentiation, and energy metabolism, which are therefore of interest in lipid use and obesity.

9-HODE is produced from LA-exposed CYP2B6 baculosomes in vitro, and high-fat diet-treated CYP2B6-Tg mice produced significantly more 9-HODE than high-fat diet-treated Cyp2b-null mice in vivo [7]. 9-HOTrE is preferentially produced more than any other oxylipin from ALA-exposed CYP2B6 baculosomes in vitro; however, 9-HOTrE was not measured in vivo [7]. This was most likely due to the high quantities of LA in the 60% high-fat diet and the relatively low amount of ALA present in the diet, causing LA to outcompete ALA as a substrate [7]. 9-HODE and 9-HOTrE are also of primary interest for CYP2B6-mediated steatotic activity because they increase hepatic lipid accumulation and the expression of genes associated with lipid uptake and synthesis in HepG2 hepatocarcinoma cells [19]. Therefore, we hypothesized that these oxylipins participate in the altered hepatic lipid accumulation observed in hCYP2B6-Tg mice.

The roles of 9-HODE and 9-HOTrE are not well studied. 9-HODE increases lipid accumulation through the activation of peroxisome proliferator-activated receptor (PPAR)

γ2 in murine marrow-derived UAMS-33 cells [20] and also increases lipid uptake in monocytes [21]. 9-HODE also participates in inflammatory pain response signaling through the activation of transient receptor potential vanilloid type 1 (TRPV1) [18]. 9-HODE and 9-HOTrE activated murine and human PPARα; however, only murine PPARγ was activated [7]. There are very few studies on 9-HOTrE action. 9-HOTrE increased lipid accumulation and adipocyte differentiation in murine-derived 3T3-L1 fibroblasts [18], but no mechanism was proposed. Its activation of murine PPARγ may play a role.

Given that 9-HODE and 9-HOTrE are preferentially produced by CYP2B6 and alter hepatic lipid accumulation and gene expression in vitro, we hypothesized that these oxylipins are contributing to the increased steatosis seen in hCYP2B6-Tg mice. Traditional high-fat diet studies are time-consuming and costly, with high-fat diet treatment lasting approximately 10–25 weeks and costing thousands in animal care alone. To avoid long-term treatment with oxylipins, exposure to oxylipins was performed over the course of 2 days, and on the second day of treatment, mice were fasted for 20 h to induce steatosis. Fasting-mediated steatosis has been used successfully in mice to study a variety of pathways related to steatosis, including the involvement of the bile acid receptor (24 h fast) and the role of increased fatty acid oxidation in skeletal muscle (24 h fast) [22,23]. Fasting protocols ranging from 4 to 72 h have been investigated in mice, and hepatic triglyceride accumulation is significantly evident at 16 h [24]; therefore, the 20 h fasting time was chosen based on this 16–24 h range. This presents a unique opportunity to complete short-term exposure to 9-HODE or 9-HOTrE and evaluate their effects on the development of steatosis and its subsequent effects on serum lipids while avoiding expensive long-term treatment. Therefore, to investigate the effects of 9-HODE or 9-HOTrE on the development of steatosis, we performed intraperitoneal injections of either 9-HODE, 9-HOTrE, or a vehicle control in Cyp2b-null mice. To further investigate the role of CYP2B6 in the development of steatosis in vivo and compare the effects of individual oxylipins with CYP2B6 activity in mice, hCYP2B6-Tg mice were also subjected to a 20 h fasting period to investigate the development of steatosis compared to Cyp2b-null mice.

We used a fasting protocol to study the role of CYP2B6, 9-HODE, and 9-HOTrE in steatosis. Cyp2b-null mice were treated with 9-HODE and 9-HOTrE because this model produces lower levels of these oxylipins [7]. We hypothesized that 9-HODE and 9-HOTrE would contribute to fasting-mediated hepatic steatosis and alter the expression of genes involved in lipid metabolism, uptake, and synthesis in a manner similar to hCYP2B6-Tg mice in comparison to Cyp2b-null mice using RNAseq. Similarities observed between 9-HODE/9-HOTrE-treated Cyp2b-null mice compared to hCYP2B6-Tg and Cyp2b-null fasted mice would be interpreted as indicators that 9-HODE/9-HOTrE are a significant reason for the increased steatosis in hCYP2B6-Tg mice. Differences observed between the oxylipin-treated and hCYP2B6-Tg mice would be interpreted as evidence that other factors besides these oxylipins are driving CYP2B6-mediated steatosis.

2. Materials and Methods

2.1. Care and Genotyping of Cyp2b-Null and hCYP2B6-Tg Mice

Animal care and use protocols were approved by Clemson University's Institutional Animal Care and Use Committee (AUP 2019-061). Cyp2b9/10/13-null (Cyp2b-null; C57BL/6J-Del(7Cyp2b10-Cyp2b9)$^{Fatso/mmnc}$, https://www.mmrrc.org/catalog/sds.php?mmrrc_id=50703 (accessed on 17 January 2025)) [25] and humanized CYP2B6-transgenic (hCYP2B6-Tg; 71652; https://www.mmrrc.org/catalog/sds_temp_new.php?mmrrc_id=71652 (accessed on 17 January 2025)) mice on a Cyp2b-null background [26,27], both generated by our lab, are available from the NIH-sponsored Mouse Mutant Resource and Research Centers. DNA was isolated from ear punches to perform genotyping using the

QuantaBio (Beverly, MA, USA) AccuStart II Genotyping kit according to the manufacturer's instructions, as described previously [26].

2.2. Treatment of Cyp2b-Null Mice with 9-HODE or 9-HOTrE

For 9-HODE and 9-HOTrE treatments, both male and female Cyp2b-null 10–12-week-old mice (n = 4–5) were injected with either 9-HODE or 9-HOTrE at 1 mg/kg in saline or with saline alone as a vehicle control once per day for 2 days. Following the day 2 injection, mice were fasted for 20 h and necropsies were performed. The 9-HODE treatment dosage was chosen based on physiologically relevant concentrations of 9-HODE seen in the liver [7], and the 9-HOTrE treatment dosage was chosen to mirror the concentrations of 9-HODE given. Treatment with oxylipins for 2 days was chosen to encompass the 20 h period of fasting, as well as a day's worth of meals to show the potential repression of fasting-mediated steatosis.

2.3. Fasting of Cyp2b-Null and hCYP2B6-Tg Mice

To compare fasting-mediated steatosis between Cyp2b-null and hCYP2B6-Tg mice, 10–12-week-old male and female Cyp2b-null and hCYP2B6-Tg mice (n = 4–5 per sex and genotype) were fasted for 20 h prior to euthanasia and necropsy.

2.4. Necropsy

Mice were weighed prior to euthanasia. Mice were then anesthetized under 3% isoflurane; blood was collected by heart puncture and then they were euthanized by CO_2 asphyxiation, as confirmed by bilateral pneumothorax. Whole blood was collected via heart puncture. Liver was excised, weighed, and cut into several sections for Oil-Red O staining, triglyceride extraction, lipid extraction and analysis, and RNA extractions. Most tissues were snap-frozen in liquid nitrogen for storage at −80 °C.

2.5. Serum Lipid Markers

Blood was incubated at room temperature for 30 min and centrifuged at 6000 rpm for 10 min to isolate serum. Serum was transferred into a new microcentrifuge tube and snap-frozen in liquid nitrogen prior to storage at −80 °C. Aliquots were sent to Baylor College of Medicine's Comparative Pathology lab (Houston, TX, USA) to be evaluated for serum lipids including cholesterol, triglycerides (TGs), high-density lipoproteins (HDLs), low-density lipoproteins (LDLs), and very low-density lipoproteins (VLDLs) with a Beckman–Coulter AU480 analyzer (Beckman Coulter, Brea, CA, USA), according to the manufacturer's instructions (n = 4–5).

2.6. Liver Lipids and Lipidomics

Liver sections from the mice were sent to Baylor College of Medicine's Comparative Pathology laboratory for Oil Red O staining of frozen sections, according to standard procedure [28], to visualize lipids. Several images of Oil Red O-stained sections were taken using Leica Acquire software Version 3.4.7 Build 9121 (Wetzlar, Germany) and evaluated with ImageJ 1.53i (Laboratory for Optical and Computational Instrumentation, Madison, WI, USA) using a previously tested method to quantify the lipid droplet area [26]. A separate section of liver was extracted, and triglycerides were quantified colorimetrically according to the manufacturer's instructions (Cayman Chemical Co., Ann Arbor, MI, USA) at an absorbance rate of 530 nm on a BioTek Synergy H1 hybrid spectrophotometer (US BiotTek Laboratories, Shoreline, WA, USA).

Lipidomic analysis for oxylipins from liver samples was performed by the Emory Integrated Metabolomic and Lipidomic Core (EIMLC) for the analysis of metabolites from AA, LA, ALA, and DHA. Oxidized lipids were selectively extracted from samples by solid-

phase extraction following EIMLC protocols [29]. Oxylipins were extracted and enriched from liver homogenates by solid-phase extraction because of their low abundance. Approximately 50 mg of the liver sample was homogenized, suspended in methanol acidified to a pH of 3.0, placed onto the C18 solid-phase extraction cassette, rinsed with hexane, and eluted with methyl formate using an automated robot (Biotage, Uppsala, Sweden). The enriched oxylipin sample was then analyzed by liquid chromatography–tandem mass spectrometry on a Sciex QTrap5500 (Framingham, MA, USA) using a quantitative multiple reaction monitoring-based method that is highly selective. A Thermo Accucore C18 column (4.6 × 100 mm, 2.6 μm) (Thermo Fisher Scientific, Waltham, MA, USA) provided the chromatographic resolution of the oxylipins using an 18 min stepwise gradient using solvent A as water (with 1 mM ammonium formate) and solvent B as acetonitrile (with 1 mM ammonium formate). The flow rate was 0.5 mL/min at a column temperature of 50 °C, and the gradient worked as follows: 0–0.5 min, 10% A; 0.5–1.0 min, 10% to 50% A; 1.0–2.0 min, 50% A; 2.0–2.1 min, 50% to 75% A; 2.1–5.0 min, 75% A; 5.0–7.0 min, 75% to 85% A; 7.0–13.0 min, 75% A; 13.0–14.0 min, 85% to 10% A; 14.0–18.0 min, 10% A. Ten μL of the extracted sample was injected. Instrumental parameters—collision energy (−70 arbitrary units), declustering potentials (−50 V), electrospray voltage (−4500 V), and temperature (65 °C)—were optimized with synthetic standards and held consistent over the course of analysis. Samples were analyzed in the negative ion mode by using unit mass resolution. Data processing for oxylipins was conducted using Sciex proprietary software Multiquant 1.7.3 (Sciex, Framingham, MA, USA), whereby the area under the curve for each sample was calibrated against external standards for the quantification of analytes in the liver.

2.7. RNA Sequencing (RNAseq)

Total RNA was extracted with Trizol reagent and quantified using a Nanodrop (Thermo Fisher Scientific). Aliquots were sent to Novogene (Sacramento, CA, USA) for library preparation, and mRNA was purified from total RNA using poly-T oligo-attached magnetic beads fragmented to synthesize cDNA from the poly-A tail enrichment. The samples were sequenced with a paired-end 150 NovaSeq 6000 system (Novogene, Sacramento, CA, USA) to an average of 47,782,986 raw reads per sample. Raw reads were processed by Novogene using their in-house perl scripts. Clean reads were then aligned to the murine reference genome (GCF_000001635.25_GRCm38.p6) using Hisat2 v2.0.5, and featureCounts v1.5.0-p3 was used to count the mapped reads. Series GSE282292, containing the RNAseq data, has been uploaded to the gene expression omnibus (GEO).

Differential gene expression analysis was performed by Novogene Inc. with the DESeq2 R package (1.20.0). The *p*-values from DESeq2 were then adjusted using Benjamini and Hochberg's approach to control for false discovery rates. Genes with an adjusted *p*-value < 0.05 were considered differentially expressed genes (DEG) and were used for further analysis. Changes in pathways were determined using the Kyoto Encyclopedia of Genes and Genomes (KEGG) pathway analysis, and differences in gene ontology (GO) were determined with the Database for Annotation, Visualization, and Integrated Discovery (DAVID) [30,31]. Reduce and Visualize Gene Ontology (Revigo) [32] was used to visualize differences in GO terms between the models or after oxylipin treatment.

2.8. Quantitative PCR

qPCR was performed using primers specific for *Gapdh*, *18S*, *Ppp1r3c*, *Lipc*, *Lpin1*, *Igfbp2*, *Plscr4*, *Scd1*, and *Plin4*. Primer sequences (idtDNA, Coralville, IA, USA) and annealing temperatures can be found in Table 1. For qPCR, 1 μL cDNA was mixed with 12.5 μL RT^{2}SYBR Green ROX qPCR Mastermix (Qiagen, Frederick, MD, USA), 9.5 μL molecular biology grade water, 1 μL forward primer, and 1 μL reverse primer, resulting in a final

volume of 25 µL per well. All plates were heated to 95 °C for 1 min, followed by 50 cycles of denaturation at 95 °C for 30 s, annealing for 30 s, and elongation for 45 s at 72 °C, then followed by a melt curve starting at 55 °C for 5 s up to 95 °C for 5 min.

Table 1. Primer sequences and annealing temperatures for qPCR.

Gene	Forward Sequence	Reverse Sequence	Annealing Temp (°C)
Gapdh	CATCACTGCCACCCAGAAGACTG	ATGCCAGTGAGCTTCCCGTTCAG	50
18S	AGTCCCTGCCCTTTGTACACA	CGATCCGAGGGCCTCACTA	56
Ppp1r3c	GCGTTGTGTTTGCTGACTCC	CGGTTGAAGGCTGAGGGAAAT	62.4
Lipc	CTTCCAGCCTGGCTGCCACTT	GCAAGGAGTCAATGAAGAGGTGC	60
Lpin1	TAAACGGAGCCGACACCTTGGA	CCGTTGTCACTGGCTTGTTTGG	60
Igfbp2	CCTCAAGTCAGGCATGAAGGAG	TGGTCCAACTCCTGCTGGCAAG	60
Plscr4	ATCCTGTGACGAATCAGCCTGC	GAGGCTCAACATGCTGAAGAACG	60
Scd1	GCAAGCTCTACACCTGCCTCTT	CGTGCCTTGTAAGTTCTGTGGC	60
Plin4	GCACTAAGGACACGGTGACCAC	GACCACAGACTTGGTAGTGTCC	60

Efficiency was determined using a standard curve consisting of a mix of samples diluted from 1:1 to 1:1024. Protocols were carried out, and fluorescence was measured using a Bio-Rad CFX96 Real-Time System (Bio-Rad, Hercules, CA, USA). Gene expression was normalized to the geometric mean of *Gapdh* and *18S* as housekeeper genes, and changes in gene expression were quantified using the inverted Muller's equation [33,34].

2.9. Hierarchical Clustering

Hierarchical clustering was performed using Morpheus software, available at https://software.broadinstitute.org/morpheus/ (accessed on 1 October 2024), courtesy of the Broad Institute of MIT and Harvard (Cambridge, MA, USA). Data such as RNAseq, oxylipins, serum, and liver lipids for each individual mouse were compiled and inserted into Morpheus to generate a heat map for each genotype or oxylipin treatment group.

2.10. Statistical Analysis and Graph Preparation

Statistical analyses were carried out using GraphPad Prism software 7.0 (San Diego, CA, USA). Significance was determined by unpaired *t*-tests to determine differences between groups. Graphing was performed on GraphPad Prism. Heat maps and hierarchical clustering were performed using Morpheus software (Cambridge, MA, USA). Data used in this manuscript are available in Supplementary Files and GEO—GSE282292.

3. Results and Discussion

3.1. 9-HODE and 9-HOTrE Increase Serum Lipids with Greater Effects in Females than Males

Male and female Cyp2b-null mice were treated with the mouse/human PPARα and mouse PPARγ activators [7], 9-HODE or 9-HOTrE, or a vehicle control at 1 mg/kg/day for 2 days and then fasted for 20 h. No differences in organ weight or gross anatomical differences were found between the control and treated mice (Supplementary Files S1 and S2). However, serum lipid levels increased following oxylipin treatment, with greater sensitivity in female mice than male mice. Female mice treated with 9-HODE displayed increased serum TGs and VLDLs by nearly 40% (Table 2). Females treated with 9-HOTrE displayed increased serum cholesterol, HDLs, and LDLs by 25–36% (Table 3); the three parameters not effected by 9-HODE. In contrast, males treated with 9-HODE displayed only a 26% increase in LDLs, and 9-HOTrE caused no significant changes in serum lipids (Table 3).

Table 2. Serum lipid analysis in Cyp2b-null 9-HODE-treated mice.

Serum Parameter	Control Male	9-HODE Male
Cholesterol (mg/dL)	95.68 ± 4.733	97.23 ± 3.236
Triglycerides (mg/dL)	67.28 ± 2.832	64.75 ± 2.843
HDL (mg/dL)	59.44 ± 2.536	57.79 ± 1.597
LDL (mg/dL)	2.924 ± 0.2501	3.672 ± 0.2044 *
VLDL (mg/dL)	13.36 ± 0.5657	12.95 ± 0.5682
Serum Parameter	**Control Female**	**9-HODE Female**
Cholesterol (mg/dL)	73.08 ± 3.458	75.11 ± 1.789
Triglycerides (mg/dL)	47.5 ± 3.711	66.3 ± 2.012 **
HDL (mg/dL)	43.33 ± 2.105	43.11 ± 1.859
LDL (mg/dL)	3.763 ± 0.4153	4.128 ± 0.3377
VLDL (mg/dL)	9.503 ± 0.7429	13.26 ± 0.4023 **

Data are presented as mean ± SEM. Statistical differences determined by unpaired Student's *t*-tests with GraphPad Prism 7.0. * *p*-value < 0.05, ** *p*-value < 0.01.

Table 3. Serum lipid analysis in Cyp2b-null 9-HOTrE-treated mice.

Serum Parameter	Control Male	9-HOT9-HOTrE Male
Cholesterol (mg/dL)	95.68 ± 4.733	102.4 ± 3.529
Triglycerides (mg/dL)	67.28 ± 2.832	63.23 ± 5.781
HDL (mg/dL)	59.44 ± 2.536	61.2 ± 1.995
LDL (mg/dL)	2.924 ± 0.2501	3.916 ± 0.3611
VLDL (mg/dL)	13.36 ± 0.5657	12.64 ± 1.156
Serum Parameter	**Control Female**	**9-HOTrE Female**
Cholesterol (mg/dL)	61.27 ± 3.395	83.57 ± 3.203 **
Triglycerides (mg/dL)	68.45 ± 5.27	62.1 ± 2.438
HDL (mg/dL)	29.92 ± 0.9884	37.61 ± 1.104 **
LDL (mg/dL)	1.438 ± 0.09801	1.815 ± 0.06538 *
VLDL (mg/dL)	9.503 ± 0.7429	13.26 ± 0.4023 **

Data are presented as mean ± SEM. Statistical differences determined by unpaired Student's *t*-tests with GraphPad Prism 7.0. * *p*-value < 0.05, ** *p*-value < 0.01.

3.2. Oxylipins Did Not Perturb Liver TGs

Neutral lipids from treated mice were measured using a colorimetric assay and confirmed by Oil Red O staining (measures neutral lipids such as cholesterol and TGs), as described in the Materials and Methods (Figure 1). Neither sex showed differences in liver lipid content after 9-HODE or 9-HOTrE treatment in comparison to vehicle-treated controls, indicating that neither 9-HODE nor 9-HOTrE had significant effects on liver steatosis in Cyp2b-null mice. This is surprising given that 9-HODE and 9-HOTrE increased TGs in HepG2 hepatocarcinoma cells in the presence of the monounsaturated fat, oleic acid. However, under normal cell culture conditions, 9-HODE and 9-HOTrE did not increase steatosis [19]. Therefore, it is possible instead that steatosis 9-HODE and 9-HOTrE are inducing the clearance and transport of lipids based on the increase in serum lipids, especially in females (Tables 2 and 3). This suggests the possibility that these oxylipins are increasing lipid production but not steatosis in mice [7,19].

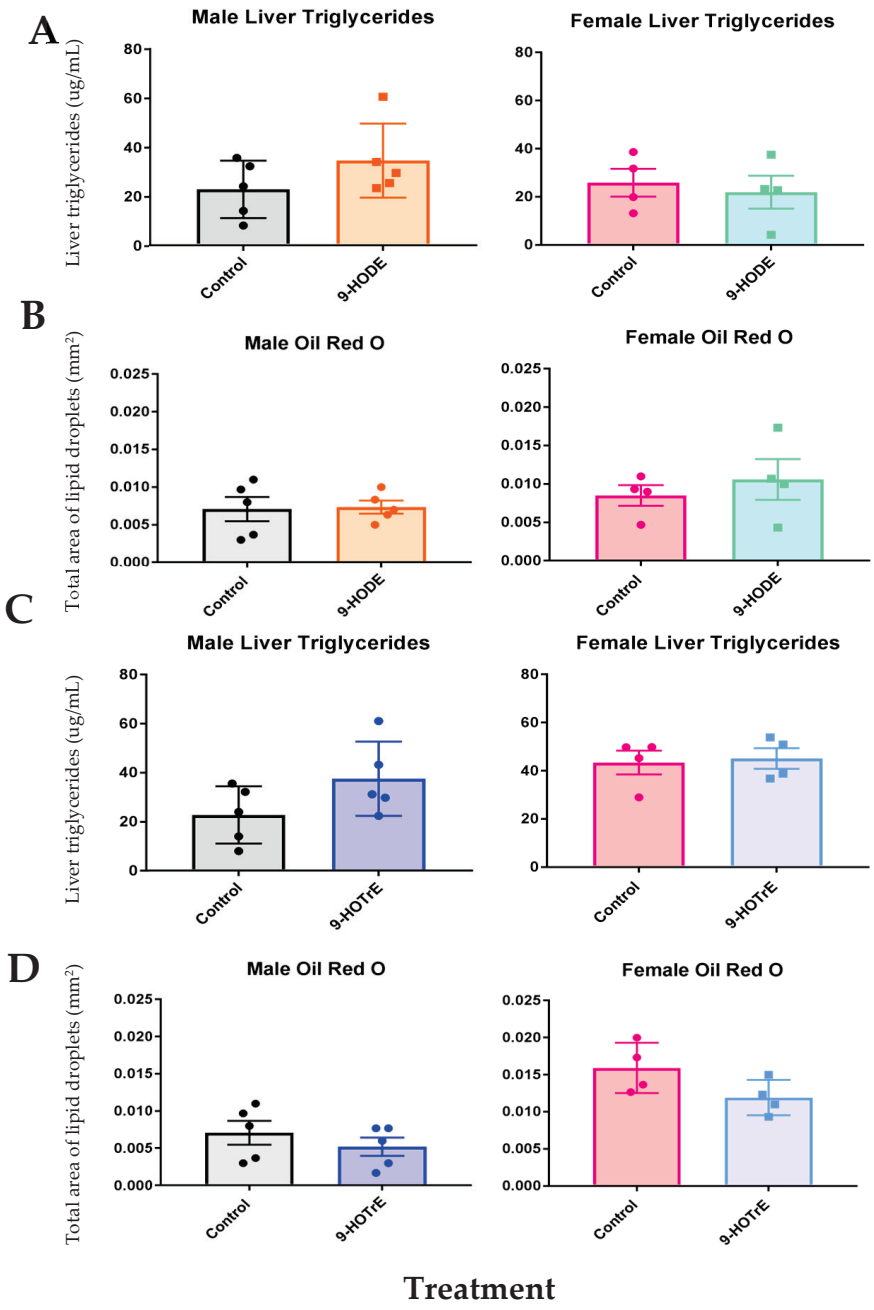


Figure 1. Quantification of liver triglycerides in 9-HODE- and 9-HOTrE-treated mice. (**A**) Quantification of male and female liver triglycerides colorimetrically after 9-HODE treatment. (**B**) Quantification of male and female liver triglycerides via Oil Red O staining of liver sections after 9-HODE treatment. (**C**) Quantification of male and female liver triglycerides colorimetrically after 9-HOTrE treatment. (**D**) Quantification of male and female liver triglycerides via Oil Red O staining of liver sections after 9-HOTrE treatment. Data are presented at mean ± SEM. Statistical significance was determined by unpaired *t*-tests using GraphPad Prism 7.0. No differences were observed.

3.3. Gene Expression Differences with Oxylipin Treatment

RNAseq was performed on liver tissue to estimate the ontologies and pathways altered by 9-HODE (Supplementary File S3) or 9-HOTrE (Supplementary File S4). DEG analysis showed few gene expression changes after the oxylipin treatments. 9-HODE treatment resulted in only twenty-one DEG in males and one DEG in females (Figure 2). Due to the low number of DEG in both sexes, GO term and KEGG pathway analysis showed no significance.

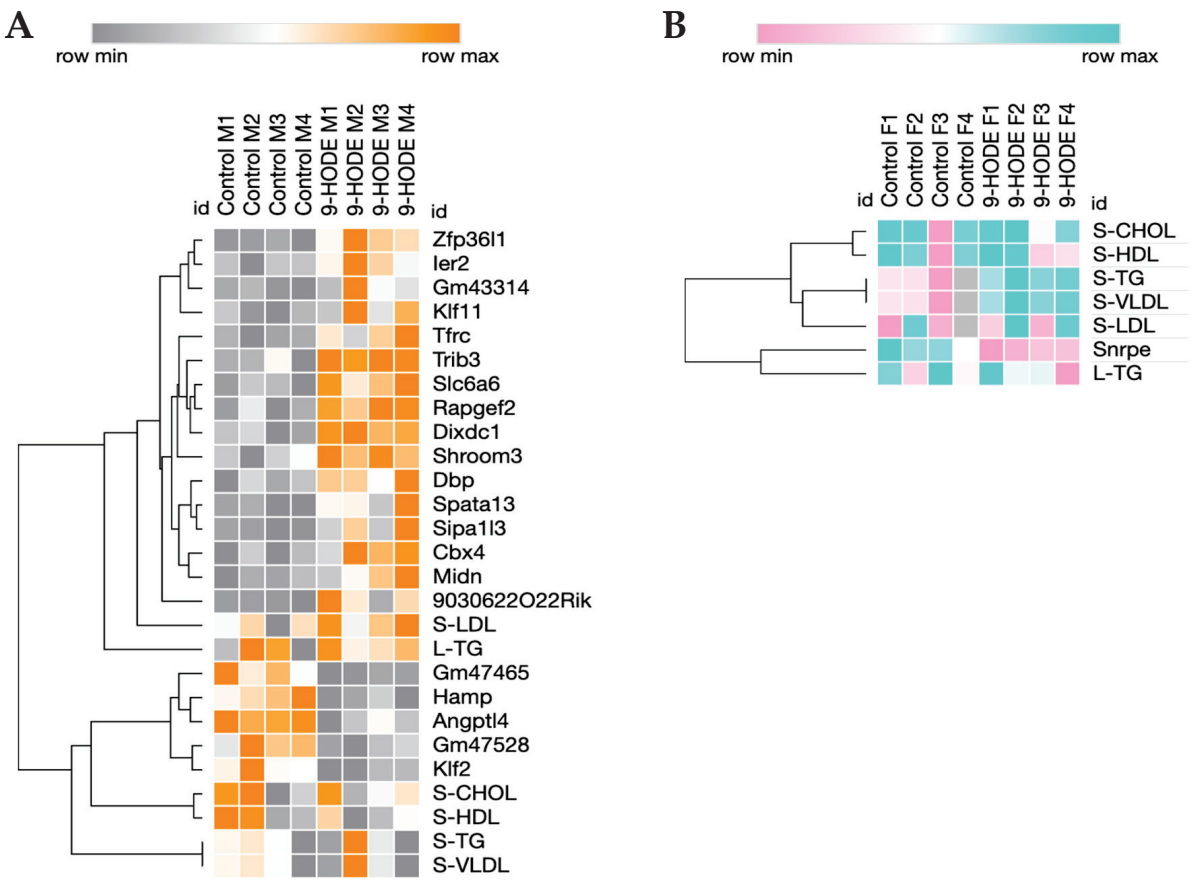


Figure 2. Hierarchical clustering of DEG and serum and liver lipids from male or female mice treated with 9-HODE. (**A**) Clustering of male data showed few associations of DEG with serum or liver lipid content. (**B**) Clustering of female data showed no associations between DEG and lipid content.

Hierarchical clustering showed few but weak associations between DEG and serum/liver lipids in males only (Figure 2). This was expected, with only one serum lipid being significantly altered in the males (LDL) and only one differentially expressed gene in the females following 9-HODE treatment. Interestingly, the genes weakly associated with serum lipids in males, *Angptl4*, *Hamp*, *Klf2*, *Gm47528*, and *Gm47465*, are all involved in lipid processing. For example, Angiopoietin-like 4 (*Angptl4*) inhibits lipoprotein lipase and therefore increases serum TGs [35]. Hepcidin (*Hamp*) is involved in iron regulation and is positively associated with non-alcoholic fatty liver disease (NAFLD) [36]. Kruppel-like factor 2 (*Klf2*) is a transcription factor that represses PPARγ and inhibits adipogenesis [37]. Predicted gene 47528 (*Gm47528*) is increased in hepatic Cpt1a-null male mice after fasting [38], and quantitative trait loci mapping for predicted gene 47465 (*Gm47465*) associates it with blood glucose and obesity [39]. Most of these genes are involved in or are regulated by PPARs and are positively associated with obesity or serum lipids; instead, these genes are repressed by 9-HODE in males as serum TGs and VLDLs go up (Figure 2).

Due to the low number of DEG observed in the liver but the increases observed in serum lipid levels, particularly in females, 9-HODE likely does not lead to any significant liver changes. 9-HODE is produced at high amounts by several enzymes, including the lipoxygenase (LOX) and cyclooxygenase (COX) enzymes, and the additional treatment of 9-HODE to Cyp2b-null mice may have made little difference to the overall 9-HODE concentrations.

9-HOTrE had a greater effect on hepatic gene expression than 9-HODE; however, the DEG analysis still showed few perturbed genes. Male mice treated with 9-HOTrE had 35 DEG and female mice treated with 9-HOTrE had 30 DEG (Figure 3). Due to the low number of DEG, there were no significant KEGG pathways identified. The only significant

GO term identified was the "lipid metabolic process", which was down-regulated in the 9-HOTrE-treated males. Genes of interest within the lipid metabolic process GO term category include fatty acid synthase (*Fasn*), branch chain aminotransferase 2 mitochondrial (*Bcat2*), glycerol-3-phosphate acyltransferase 3 (*Gpat3*), hydroxy-delta-5-steroid dehydrogenase, 3 beta- and steroid delta-isomerase 5 (*Hsd3b5*), sphingosine kinase 2 (*Sphk2*), sulfotransferase family 1D, member 1 (*Sult1d1*), sulfotransferase family 1E, member 1 (*Sult1e1*), and thyroid hormone responsive (*Thrsp*). The hierarchical clustering of male DEG with serum and liver lipids parameters showed no associations between the two sets of data (Figure 3A). However, none of the serum nor hepatic lipids were significantly perturbed (Table 3), making associations with DEG unlikely.

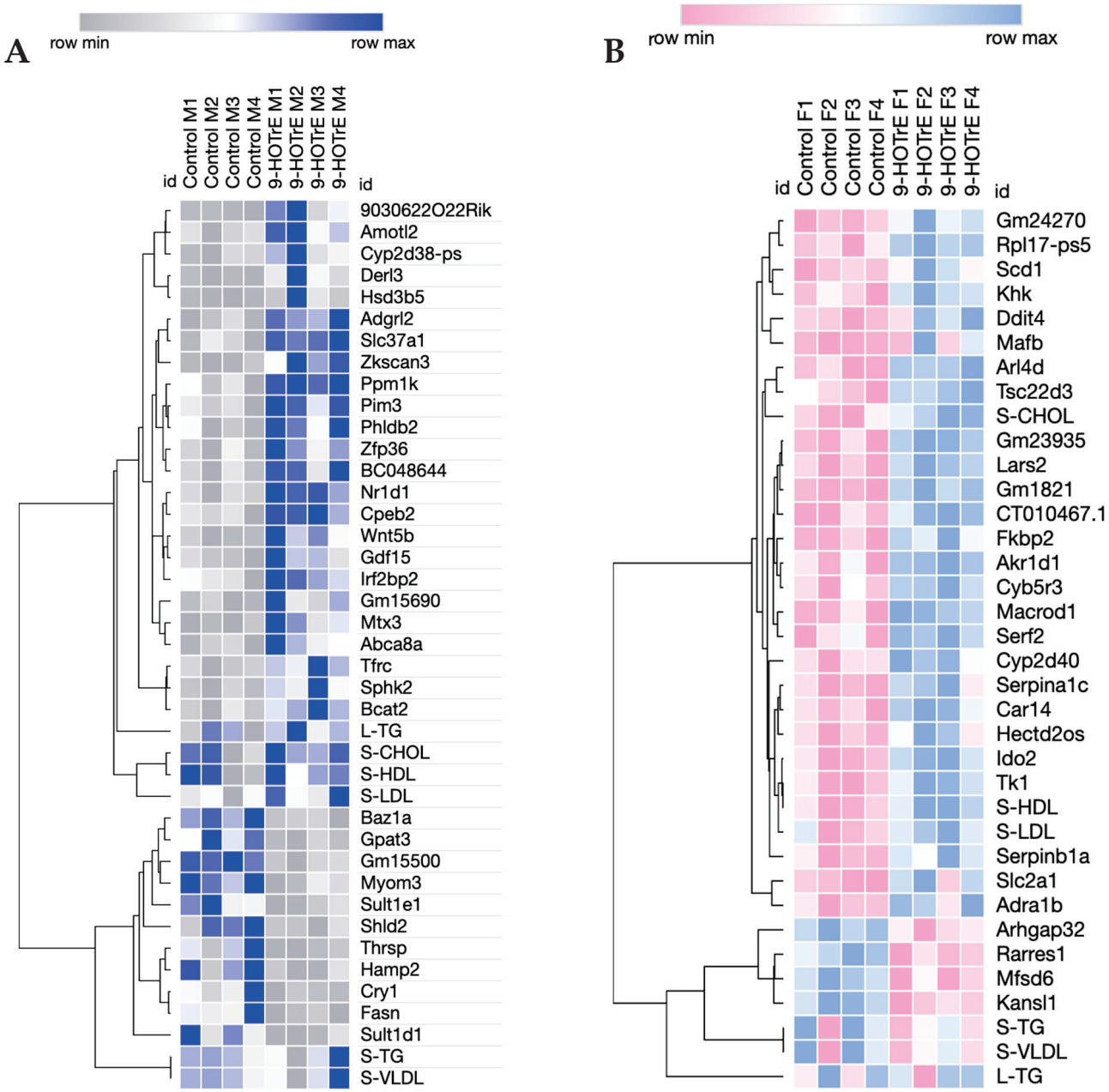


Figure 3. Hierarchical clustering of DEG and serum and liver lipids in male or female mice treated with 9-HOTrE. (**A**) Clustering of male data showed no close associations of gene expression changes and alterations in serum or liver lipids. (**B**) Clustering of female data showed associations between serum HDLs (S-HDLs) and LDLs (S-LDLs) with several genes.

However, the hierarchical clustering of female DEG with serum and liver lipids showed an association between serum HDLs and LDLs with several genes. HDLs, LDLs, and cholesterol were increased by 9-HOTrE in females (Table 3). Genes that cluster with HDLs and LDLs include thymidine kinase 1 (*Tk1*), indoleamine 2,3-dioxygenase 2 (*Ido2*), carbonic anhydrase 14 (*Car14*), and serine (or cysteine) peptidase inhibitor clade a member 1c and clade b member 1a (*Serpina1c* and *Serpinb1a*). *Tk1* is an enzyme involved in the biosynthesis of dTTP for DNA replication and has been implicated in the progression of hepatocellular carcinoma [40]. *Ido2* is involved in the metabolism of tryptophan and is associated with inflammation in the liver [41]. *Car14* is predicted to be involved in one-carbon metabolism and has recently been shown to participate in the biliary bicarbonate buffering system, and Car14-knockout mice show greater liver damage compared to their wildtype counterparts following the ligation of the common bile duct [42]. *Serpina1c* and *Serpinb1a* are both implicated in inflammatory pathways within the liver [43,44]. Cholesterol directly clustered with the Glucocorticoid-Induced Leucine Zipper Protein (*Tsc22d3*), which is stimulated by glucocorticoids and acts as an anti-inflammatory signal [45], and ADP-ribosylation factor 4D (*Arl4d*), which buffers HDL cholesterol levels [46]. Gene expression changes coupled with increases in serum cholesterol, HDLs, and LDLs suggest that 9-HOTrE could increase hepatic inflammation in female mice. Overall, 9-HOTrE had a greater effect than 9-HODE, and this suggests that the lipid type we ingest (n-6 vs. n-3) is crucial in CYP2B6's physiological actions.

Other genes such as *Cyb5r3*, *Macrod1*, *Serf2*, *Akr1d1*, *Fkbp2*, *Lars2*, and *Cyp2d40* also clustered with the greater clade associated with LDLs and HDLs. Several of these genes are associated with mitochondrial function or lipid metabolism (fatty acid, bile acid, and steroids) as well as NAFLD progression. These genes include leucyl-tRNA synthetase 2 (*Lars2*, mitochondrial protein production) [47], aldo-keto reductase family 1, member D1 (*Akr1d1*, bile acid and steroid metabolism) [48], cytochrome P450 family 2, subfamily d, polypeptide 40 (*Cyp2d40*, steroid and cholesterol metabolism) [49], mono-ADP Ribosylhydrolase 1 (*Macrod1*, enhances steroid function at receptor) [50], and cytochrome.

B5 Reductase 3 (*Cyb5r3*, fatty acid and cholesterol desaturation and elongation) [51]. *Cyb5r3* represses the benefits of caloric restriction [52]. Other genes perturbed by 9-HOTrE in female mice that are related to energy metabolism include stearoyl-CoA desaturase 1 (*Scd1*, fatty and cholesterol metabolism) [53] and ketohexokinase (*Khk*, metabolizes fructose) [54].

Overall, 9-HOTrE treatment in females led to the increased expression of genes involved in energy metabolism and inflammation, and some of the inflammatory genes clustered with HDLs and LDLs (Figure 3 and Table 3). In addition, serum cholesterol clustered with an increase in *Tsc22d3* (Table 3 and Figure 3). In summary, alterations in serum lipids levels with 9-HODE or 9-HOTrE treatment coupled with few gene expression changes in the liver may not be the only organ or primary organ affected by 9-HODE and 9-HOTrE.

3.4. Changes in Gross Anatomy and Serum Lipids Between hCYP2B6-Tg and Cyp2b-Null Mice Are Sexually Dimorphic

9-HODE and 9-HOTrE are some of the most highly perturbed oxylipins by CYP2B6 metabolism [7]. However, they had moderate to minimal effects on hepatic steatosis and gene expression. Therefore, we went back to our Cyp2b-null and hCYP2B6-Tg mice to confirm that hCYP2B6-Tg mice are sensitive to fasting-mediated hepatic steatosis (not just diet-induced), determine if oxylipins are associated with fasting-mediated steatosis, and compare the gene expression effects of 9-HODE and 9-HOTrE to the effects of adding CYP2B6 to the liver.

Male and female Cyp2b-null and hCYP2B6-Tg mice were fasted for 20 h, and body weight, organ weights, and serum and liver lipids measured. Female hCYP2B6-Tg mice weighed significantly less at the outset of the study compared to their Cyp2b-null counterparts, but saw no difference in organ weight between groups, leading to an increase in the liver-to-body weight ratio by 8.84% (Supplementary File S1). Male hCYP2B6-Tg mice had a significant increase in liver weight by 9.29%, but no other significant changes in gross anatomy were observed (Supplementary File S2).

Serum lipid analysis revealed strong sexually dimorphic differences between male and female hCYP2B6-Tg mice. Male hCYP2B6-Tg mice were highly sensitive to a 20 h fasting period, where they exhibited an increase in serum cholesterol, triglycerides (TGs), HDLs, and VLDLs compared to Cyp2b-null mice (Table 4). In contrast, female hCYP2B6-Tg mice exhibited a decrease in serum triglycerides and VLDLs compared to Cyp2b-null mice (Table 4). In summary, the presence of human CYP2B6 altered serum lipids with a strong sexually dimorphic response, where males show greater serum lipids and females lower serum TGs and VLDLs.

Table 4. Serum lipids analysis of Cyp2b-null and hCYP2B6-Tg mice.

Serum Parameter	Cyp2-Null Male	hCYP2B6-Tg Male
Cholesterol (mg/dL)	104.1 ± 2.863	117.1 ± 2.289 *
Triglycerides (mg/dL)	82.18 ± 4.017	132 ± 6.781 ***
HDL (mg/dL)	54.54 ± 1.709	62.77 ± 1.331 *
LDL (mg/dL)	2.938 ± 0.1074	3.305 ± 0.6967
VLDL (mg/dL)	16.44 ± 0.8024	26.4 ± 1.356 ***
Serum Parameter	**Cyp2-Null Female**	**hCYP2B6-Tg Female**
Cholesterol (mg/dL)	74.5 ± 1.829	77.64 ± 4.385
Triglycerides (mg/dL)	95.96 ± 4.5	67.18 ± 5.404 **
HDL (mg/dL)	37.76 ± 0.8123	38.55 ± 1.162
LDL (mg/dL)	4.736 ± 0.2744	4.72 ± 0.8014
VLDL (mg/dL)	19.19 ± 0.8999	13.44 ± 1.08 **

Data are presented as mean ± SEM. Statistical differences determined by unpaired *t*-tests using GraphPad Prism 7.0. * *p*-value < 0.05, ** *p*-value < 0.01, *** *p*-value < 0.001.

3.5. Liver TG Difference Between hCYP2B6-Tg and Cyp2b-Null Mice

Liver lipids were analyzed using a colorimetric TG assay and verified with Oil Red O staining and quantification. hCYP2B6-Tg mice exhibited increased liver TG content compared to Cyp2b-null mice in both sexes (Figure 4A). Oil Red O staining and quantification confirmed a significant increase in TGs in females (Figure 4B,C). Males exhibited a similar trend with both the colorimetric assay and Oil Red O staining; however, only the colorimetric assay was significant (Figure 4). The increased release of lipids from the liver into the serum in males may explain the lack of statistical significance in Oil Red O measurements coupled with increased serum lipids.

Females showed a significant increase in lipid colorimetric and Oil Red O staining coupled with reduced serum lipids, indicating the preferential retention of lipids in the liver. Males have greater serum and liver lipid levels although liver TG levels may be somewhat muted. Overall, these data suggest a sexually dimorphic response in which they have lower serum lipids because of liver lipid retention. RNAseq was performed in part to determine the potential mechanisms leading to increased retention.

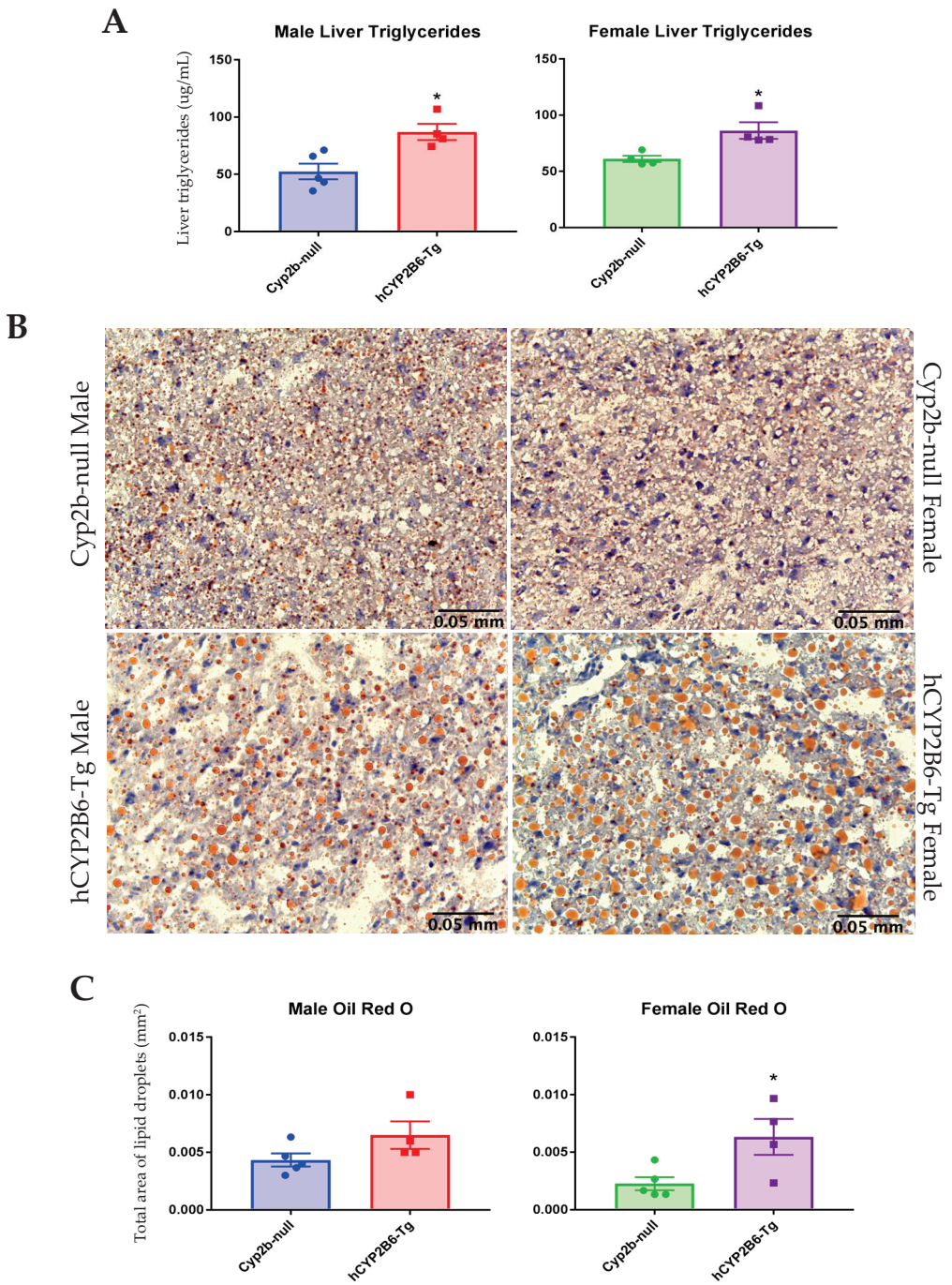


Figure 4. Increased hepatic triglyceride content in hCYP2B6-Tg mice. (**A**) Both male and female hCYP2B6-Tg mice show a significant increase in liver triglycerides measured colorimetrically. Quantification (**C**) of Oil Red-O-stained histological sections of liver (**B**) showed significance only in female hCYP2B6-Tg mice. Data are represented as mean ± SEM. Statistical significance determined by unpaired *t*-tests on GraphPad Prism 7.0. * p-value < 0.05.

3.6. Gene Expression Differences Between hCYP2B6-Tg and Cyp2b-Null Mice

RNAseq was performed on liver tissues to evaluate differences in gene expression between Cyp2b-null and hCYP2B6-Tg mice and provide insight on CYP2B6-mediated hepatic steatosis. Analysis of differentially expressed genes (DEG) showed a total of 807 DEG between Cyp2b-null and hCYP2B6-Tg males and 1224 DEG between Cyp2b-null and hCYP2B6-Tg females (Table 5). Earlier studies demonstrated that these mouse models have similar liver gene expression profiles under normal diet/control conditions [27], indicating that they respond differently under fasting or dietary stress conditions. In addition,

152 DEG were shared between sexes, 96 of these genes were dysregulated similarly by each sex, and 56 genes were dysregulated but in an opposing manner (Table 5). Both the Cyp2b-null and hCYP2B6-Tg mice responded vigorously to fasting based on hepatic steatosis and gene expression changes. Furthermore, a clear sexually dimorphic response occurred under fasting conditions in hCYP2B6-Tg mice, highlighting the importance of CYP2B6 expression differences in males and females and how it may influence lipid homeostasis. A full list of DEG and GO/KEGG analysis can be found (Supplementary Files S5–S9).

Table 5. DEG counts comparing transcriptome of Cyp2b-null vs. hCYP2B6-Tg mice.

Comparison	Total DEG	Enriched in hCYP2B6-Tg Mice	Enriched in Cyp2b-Null Mice
Male Cyp2b-null vs. Male hCYP2B6-Tg	807	414	393
Female Cyp2b-null vs. Female hCYP2B6-Tg	1224	623	601
Males and Females SHARED	152	58	38

n = 4. Differential genes determined by read counts from gene expression level analysis, followed by model dependent p-value estimation and FDR (adjusted p-value) value estimation based on multiple hypothesis testing.

3.7. Gene Expression Changes Evaluated via qPCR

To confirm the data previously elucidated by the RNA sequencing data above, qPCR was performed to confirm specific DEG involved in lipid utilization by RNAseq. Protein phosphatase 1 regulatory subunit 3C (*Ppp1r3c*), insulin-like growth factor binding protein 2 (*Igfbp2*), and phospholipid scramblase 4 (*Plscr4*) were not differentially expressed in female mice by RNAseq, only in males. qPCR confirmed significant expression changes in five of the seven genes evaluated in male mice and three of the four genes differentially expressed by RNAseq in female mice (Table 6). All of the DEG by RNAseq trended in the same direction as the qPCR data, except Perilipin 4 (*Plin4*) in females. Overall, RNAseq and qPCR showed very similar results.

Table 6. RNA sequencing and qPCR data for DEG in Cyp2b-null vs. hCYP2B6-Tg mice.

	Males—Fold Change		Females—Fold Change	
Gene	**RNAseq**	**qPCR**	**RNAseq**	**qPCR**
Ppp1r3c	−1.044 **	−0.639 *	−0.696	0.101
Lipc	0.556 ***	0.143	−0.725 ***	−0.704 *
Lpin1	1.117 **	1.294	1.528 ***	1.550 **
Igfbp2	0.760 *	0.616 *	−0.496	−0.668
Plscr4	−0.669 *	−0.893 **	0.505	0.268
Scd1	−1.390 ***	−1.471 ***	−1.253 *	−0.934 ***
Plin4	−0.775 *	−1.618 ***	−0.736 *	0.110

Data expressed as log2 fold change compared to Cyp2b-null. Significance determined by read counts from gene expression level analysis, followed by model dependent p-value estimation and FDR (adjusted p-value) value estimation based on multiple hypothesis testing. Significance determined by unpaired t-tests with GraphPad Prism 7.0 for qPCR. * p-value < 0.05, ** p-value < 0.01, *** p-value < 0.001.

The genes analyzed by qPCR are associated with processes involving lipid metabolism, homeostasis, and transport, except for *Igfbp2*, which mediates insulin-like growth factor (IGF) activity and half-life [55]. *Ppp1r3c* strongly up-regulates glycogen synthesis in hepatocytes [56]. Lipin-1 (*Lpin1*) and *Plscr4* are involved with lipid transport and mobilization [57], and hepatic lipase (*Lipc*) catalyzes the formation of the serum carrier molecule and LDL cholesterol via the production of hepatic lipase [58]. *Scd1* codes for the stearoyl-CoA desaturase enzyme that produces monounsaturated fatty acids from saturated fats [59], and *Plin4* encodes for a lipid-coating protein that protects lipid droplets from endogenous lipases [60]. These data verify the RNAseq data and confirm sexually dimorphic changes in gene expression.

3.8. GO Term and KEGG Pathway Analysis of Cyp2b-Null vs. Hcyp2b6-Tg DEG

Gene ontology (GO) was performed and Revigo was used to visualize changes in GO terms in the "biological processes" category. Male hCYP2B6-Tg mice displayed a variety of enriched GO terms related to lipid and steroid metabolism (Figure 5A); terms enriched in male Cyp2b-null mice included those related to cell cycle and circadian rhythm (Figure 5B). GO terms enriched in female hCYP2B6-Tg mice included the circadian regulation of gene expression as well as several terms related to proteins, such as response to unfolded protein, protein catabolic process, and protein phosphorylation (Figure 5C). Terms enriched in female Cyp2b-null mice included lipid metabolic process, cholesterol metabolic process, and steroid metabolic process (Figure 5D). Genes involved in lipid and steroid metabolic processes responded in opposing directions in the male and female hCYP2B6-Tg mice: enriched in male hCYP2B6-Tg mice and conversely enriched in female Cyp2b-null mice (Figure 5). Given the increase in hepatic steatosis in the female hCYP2B6-Tg mice, the enrichment of lipid, cholesterol, steroid, and fatty acid metabolic processes as the top four enriched terms in Cyp2b-null mice may help explain the reduced steatosis as an adaptive response.

Interestingly, GO term analysis of shared up- and down-regulated genes by sex, excluding genes dysregulated in a contradicting manner, showed the lipid metabolic process as an enriched term in hCYP2B6-Tg mice. Other terms enriched in hCYP2B6-Tg mice include the regulation of transcription from RNA pol II promoter, response to unfolded protein, and response to ER stress (Figure 6). Sex-shared GO terms enriched in Cyp2b-null mice include circadian rhythm and the negative regulation of cyclin-dependent protein serine/threonine kinase activity (Figure 6). Supplementary Files S5–S9 found in Mendeley Data (https://data.mendeley.com/datasets/wnvkz8f7ft/1 (accessed on 31 December 2024)), which provides a full list of GO terms with corresponding Revigo figures.

DEG analysis was also used to perform KEGG pathway analysis to determine the pathways affected by dysregulated genes. KEGG pathways enriched in male hCYP2B6-Tg mice include protein processing in endoplasmic reticulum, steroid hormone biosynthesis, complement and coagulation cascades, and the metabolic pathway (Supplementary File S5). Pathways enriched in male Cyp2b-null mice included Hippo signaling pathways, hepatocellular carcinoma, breast cancer, and AGE-RAGE signaling pathway diabetic complications (Supplementary File S6).

Pathways enriched in female hCYP2B6-Tg mice included phosphatidylinositol signaling pathway, prostate cancer, inositol phosphate metabolism, and oxidative phosphorylation (Supplementary File S7). Pathways enriched in female Cyp2b-null mice included chemical carcinogenesis–DNA adducts, drug metabolism, other enzymes, steroid hormone biosynthesis, the biosynthesis of cofactors, and peroxisome (Supplementary File S8).

In summary, hCYP2B6-Tg mice showed large changes in gene expression compared to Cyp2b-null mice, and many of these changes were sexually dimorphic. Female mice were more sensitive to fasting, as they showed a greater number of DEG (Table 5). The enrichment of GO terms associated with lipid metabolism was sexually dimorphic, as male hCYP2B6-Tg mice showed the enrichment of terms related to lipid metabolism and female Cyp2b-null mice often showed the enrichment of similar terms (Figure 5). When evaluating shared DEG between sexes, the GO term "lipid metabolic process" was enriched in hCYP2B6-Tg mice (Figure 6), showing that both sexes did experience alterations in gene expression related to lipid metabolism, but male hCYP2B6-Tg mice had a greater number of genes associated with this term. Female hCYP2B6-Tg mice showed a greater number of terms related to proteins, suggesting that males experience more changes in lipid metabolism in the liver under fasting conditions and that females experience greater changes in protein function and metabolism under fasting conditions. A ranked list of GO

and KEGG terms enriched in either hCYP2B6-Tg or Cyp2b-null male and female mice is provided in Supplementary Files S5–S9.

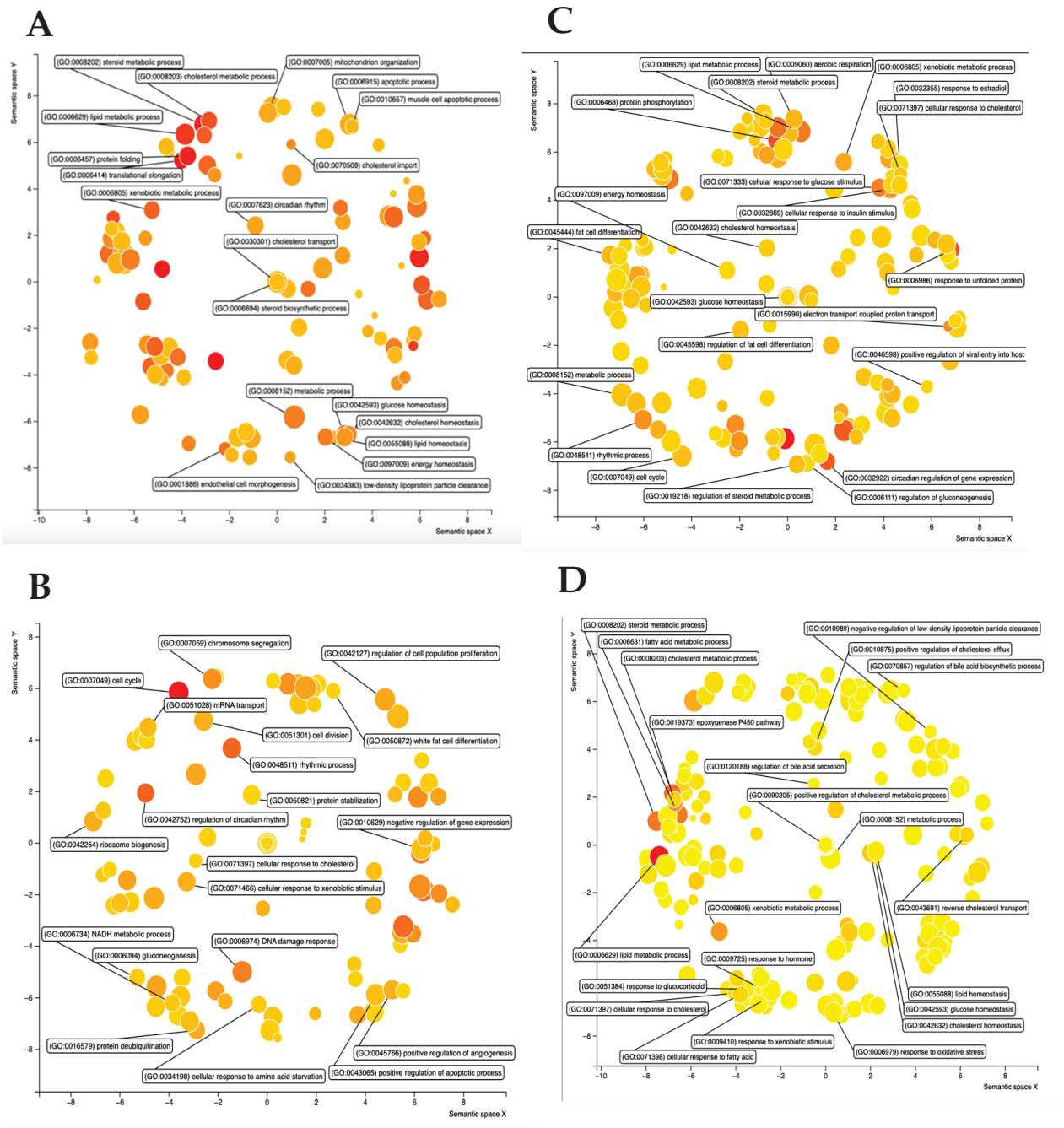


Figure 5. Gene ontology (GO) terms in the Biological Processes category enriched in either hCYP2B6-Tg mice or Cyp2b-null mice. (**A**) GO terms enriched in hCYP2B6-Tg male mice. (**B**) GO terms enriched in Cyp2b-null male mice. (**C**) GO terms enriched in hCYP2B6-Tg female mice. (**D**) GO terms enriched in Cyp2b-null female mice. GO terms were included if they had an FDR (adjusted *p*-value) of <0.05. Larger dots indicating greater number of genes and darker colors (reds) indicates greater statistical significance.

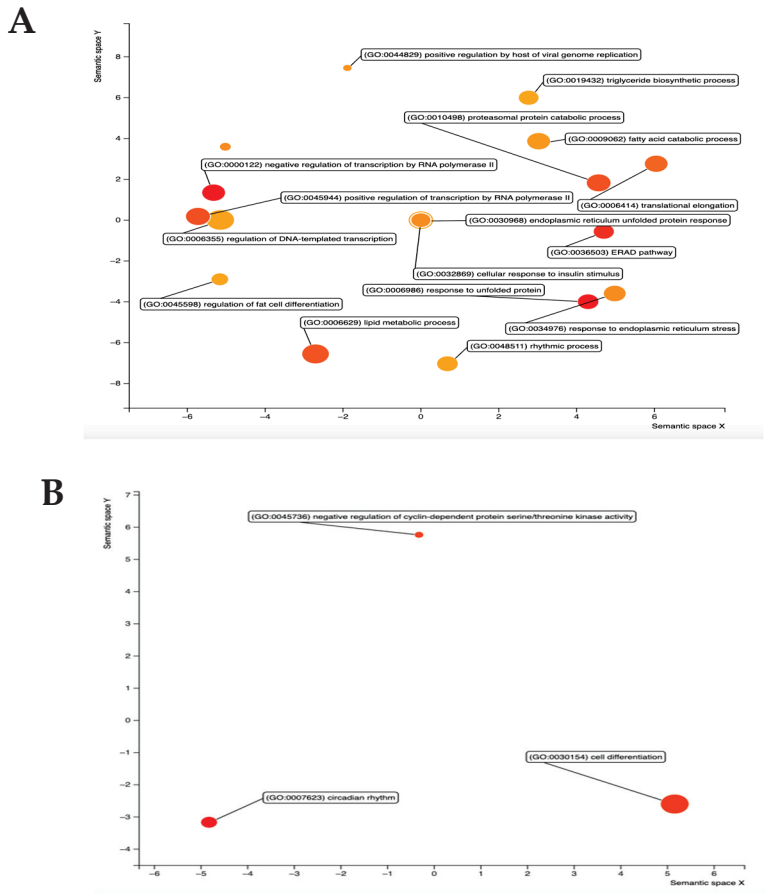


Figure 6. Visualization of GO terms shared between male and female DEG analysis. Significant DEG were used to generate GO term lists across sexes that were not dysregulated in an opposing manner. (**A**) GO terms enriched in hCYP2B6-Tg mice. (**B**) GO terms enriched in Cyp2b-null mice. Shared GO terms were identified within these lists then visualized using Revigo. GO terms included have a *p*-value of <0.05. Larger dots indicating greater number of genes and darker colors (reds) indicates greater statistical significance.

3.9. Oxylipin Profile Changes Between hCYP2B6-Tg and Cyp2b-Null Mice

Oxylipins were quantified using selective solid-phase extraction and analyzed by liquid chromatography–mass spectrometry to determine differences between genotypes. 14,15-epoxyeicosa-5,8,11-trienoic acid (14(15)-EET) was the only oxylipin increased in male hCYP2B6-Tg mice (Figure 7A), and this AA-derived oxylipin was also increased in females (Figure 7B). Female hCYP2B6-Tg also had several other oxylipins with increased liver concentrations, including 9-hydroperoxyoctadecadienoic acid (9(S)-HpODE), 13-hydroperoxyoctadecadienoic acid (13(S)-HpODE), docosahexaenoyl ethanolamide (DHEA), linoleoyl ethanolamide (LEA), 12(13)epoxy-9Z-octadecenoic acid (12(13)-EpOME), palmitoyl ethanolamide, and alpha-linolenoyl ethanolamide (Figure 7B). 9-HpODE and 13-HpODE are precursors to 9-HODE and 13-HODE [14]. 12(13)-EpOME and 14(15)-EET are also produced by CYP2B6 in vitro and in vivo [7], and both oxylipins were increased in female hCYP2B6-Tg mice (Figure 7B). 14,15-EET has several established functions, including suppressing mitochondrial apoptosis during ischemic injury and several established functions within pulmonary endothelial cells [14]. Some of these oxylipins, such as 9-HpODE, 13-HpODE, and 12(13)-EpOME, are associated with oxidative stress [14].

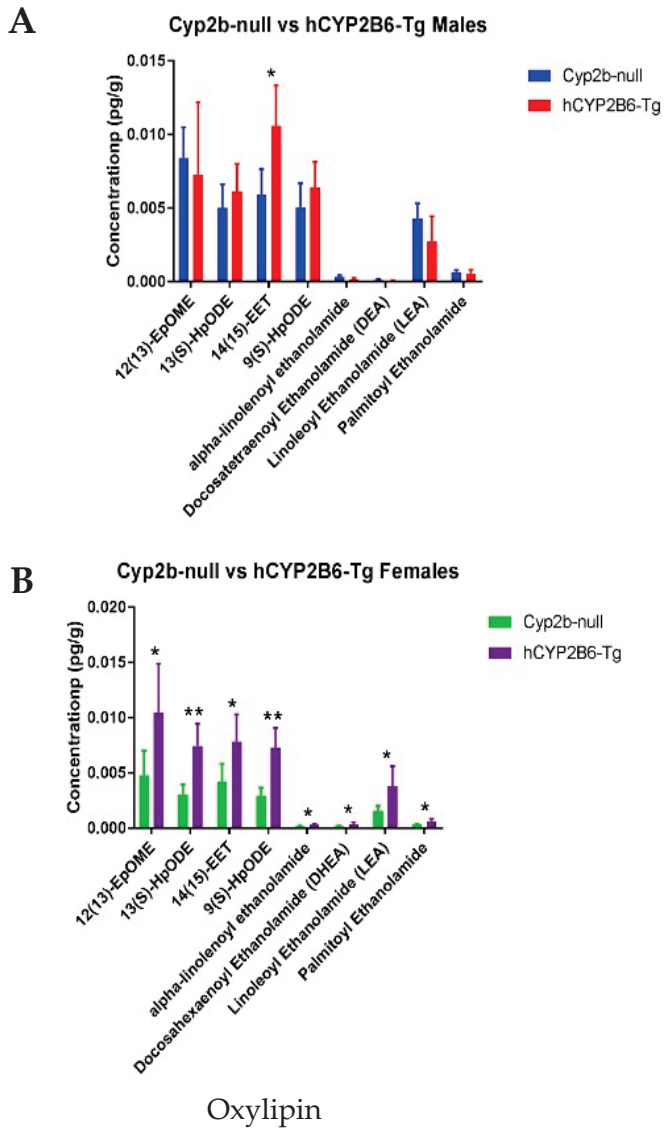


Figure 7. Oxylipin profiles in Cyp2b-null vs. gCYP2B6-Tg mice. (**A**) Profiles showed increased concentrations of only one oxylipin in livers of hCYP2B6-Tg male mice. (**B**) Profiles showed increased concentrations of eight oxylipins in livers of in hCYP2B6-Tg female mice. Multiple *t*-tests. Mean ± SEM. * p value < 0.05, ** p value < 0.01.

14(15)-EET (AA metabolite) and 12(13)-EpOME (LA metabolite) are produced by CYP enzymes [14], and both are produced by CYP2B6 [7]. 9(S)-HpODE and 13(S)-HpODE (LA metabolites) can be produced by both the LOX and CYP enzymes [14,61], and they are also produced by CYP2B6 [7]. DHEA (DHA metabolite), LEA (LA metabolite), palmitoyl ethanolamide (palmitic acid metabolite), and alpha-linolenoyl ethanolamide (ALA metabolite) are members of a group of compounds referred to as N-acylethanolamines (NAEs) that are produced via the N-acylphosphatidylethanolamine (NAPE) pathway [62]. NAEs are lipid derivatives involved in signaling for satiety, mitochondrial energetics, stress, and a variety of other pathways [63,64]. The association of NAEs with metabolic diseases such as obesity and steatosis has drawn greater attention in recent years, with many of these metabolites showing anti-obesity effects [65–67]. Recent research has shown that fasting for periods between 3 and 24 h results in an increased level of NAEs in the liver and may be a response to oxidative stress and cross-talk between the brain and liver during periods of glucose deprivation [68], but the exact mechanism of this response is still under investigation.

3.10. Hierarchical Clustering of DEG with Oxylipins

Hierarchical clustering was performed to compare DEG to oxylipins and serum lipids. In males, few DEG and lipids co-clustered; however, DEG that did cluster with lipids are crucial in fatty acid oxidation. For example, serum LDLs clustered with Regulator of G protein Signaling 16 (*Rgs16*), which inhibits fatty acid oxidation in hepatocytes [69] by enhancing GTPase activity and repressing signal transduction (Figure 8). Serum TGs and VLDLs clustered with acyl-CoA dehydrogenase member 12 (*Acad12*), mitochondrially encoded tRNA asparagine (*Mt-Tn*), and mitochondrially encoded tRNA cysteine (*Mt-Tc*), and also, to a lesser extent, with mitochondrially encoded tRNA leucine (*Mt-Tl1*), ribonuclease 4 (*Rnase4*), and *BC024386*. *Acad12* is homologous to ACAD10 in humans, an enzyme that assists with fatty acid b-oxidation in the mitochondria [70]. *Mt-Tn*, *Mt-Tc*, and *Mt-Tl1* function as tRNAs [71]. *BC024386* translationally represses *Nlrp6* [72], an inflammasome gene expressed in the intestine and liver, which is important in repressing metabolic disease progression [73]. These data suggest that β-oxidation is disrupted along with increased TGs and VLDLs.

In females, the drop serum TGs and VLDLs clustered with reduced actin gamma 1 (*Actg1*), histone compatibility 2, class II antigen E beta (*H2-Eb1*), and histone compatibility 2, class II antigen A alpha (*H2-Aa*) (Figure 8). *Actg1* is involved in the synthesis of actin for the cytoskeleton, and increased expression has been associated with increased fibrosis [74,75]. Both *H2-Eb1* and *H2-Aa* are involved in antigen sensing [76,77]. Greater liver triglycerides in females were associated with a gene of unknown function, *Fam214a*, interleukin-1 receptor type 1 (*IL1r1*), and influenza virus NS1A binding protein (*Ivns1abp*) which encodes the Nd1 actin binding protein. All three of these genes have previously been associated with NAFLD [78–81], and two (*Il1r1*, *Fam214a*) are associated with inflammation. Thus, increased liver triglycerides were associated with NAFLD, increased inflammation, and reduced serum triglycerides with reduced antigen sensing genes.

In females, there are 17 genes in the larger clade associated with the oxylipins 9(S)-HpODE, 13(S)-HpODE, and 14(15)-EET (Figure 8); other differentially produced oxylipins were not closely associated with DEG. Of these seventeen genes, five are associated with fatty acid metabolic processes via GO term analysis. These include *Fmo2*, *Cyp7a1*, *Apoa4*, *Treh*, and *Lpin1* (Figure 8). 9(S)-HpODE and 13(S)-HpODE clustered with several genes, including *Cyp7a1*, involved in cholesterol and bile acid synthesis. *Cyp7a1* is protective against NAFLD and inflammation through the increased activation of FXR [82], and this gene was enriched in hCYP2B6-Tg female mice despite these mice experiencing increased steatosis (Supplementary File S6). Flavin containing dimethylaniline monoxygenase 2 (*Fmo2*) is a xenobiotic metabolizing enzyme inversely associated with NAFLD. The increased expression of *Fmo2* is associated with repressed Srebf1 activation and protection against steatosis [83]. This gene was enriched in hCYP2B6-Tg female mice despite increased steatosis (Supplementary File S6). *Apoa4* is involved in lipid transport and LDL oxidation, and increased expression is associated with reduced gluconeogenesis and protection against liver steatosis [84,85]. Trehalose (*Treh*) is an enzyme associated with cortisol or high-sugar diet-induced NAFLD [86]. *Lpin1* is involved in the synthesis of triglycerides and can act as a co-activator of both PPARα and γ, further influencing lipid metabolic pathways [87]. These associations indicate that CYP2B6, through the production of oxylipins, alters fatty acid homeostasis in the liver, although both genes associated and inversely associated with steatosis were increased in hCYP2B6-Tg mice.

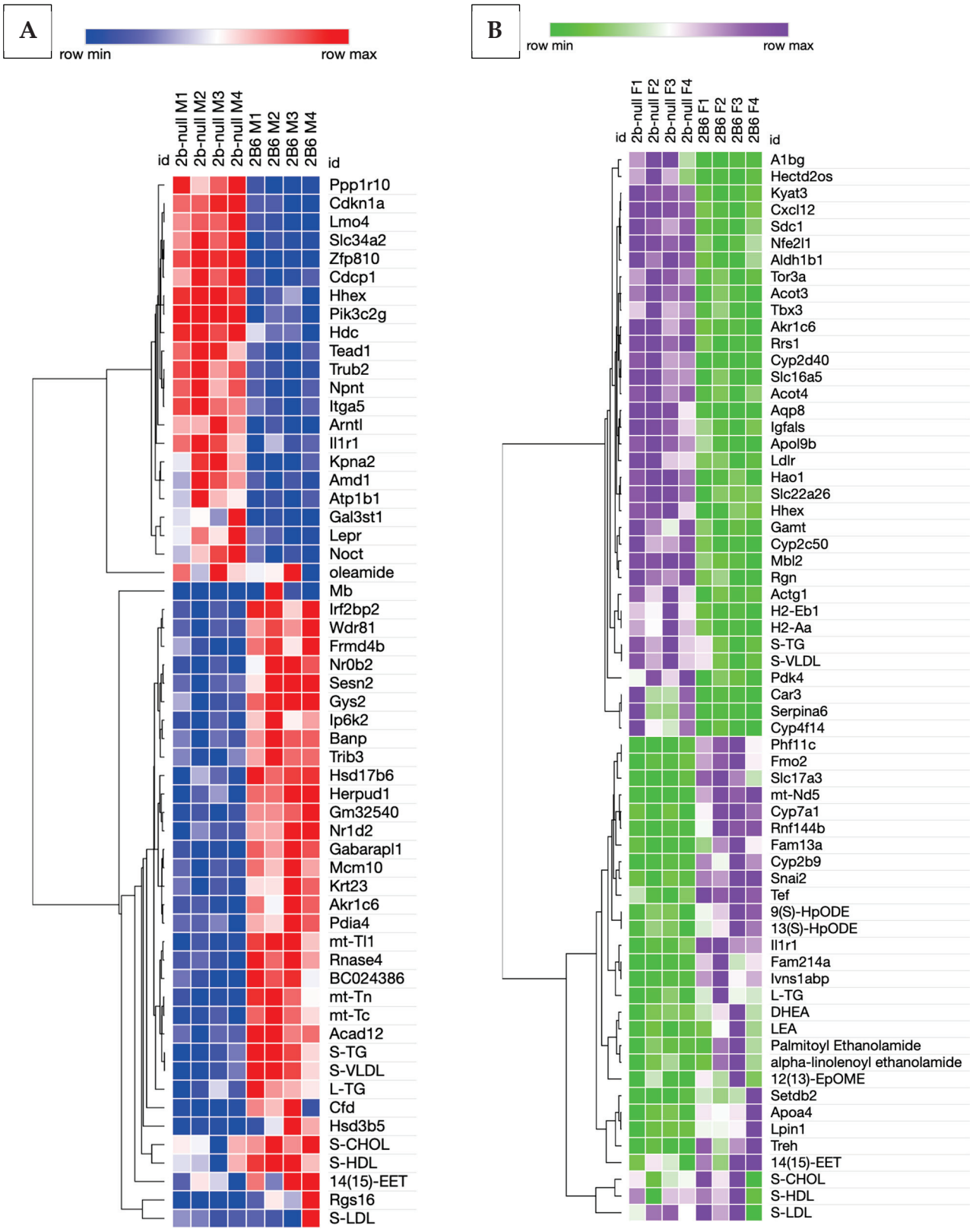


Figure 8. Hierarchical clustering of DEG, oxylipins, serum, and liver lipids. (**A**) Hierarchical clustering of differential gene expression data and oxylipins/lipids in male Cyp2b-null and hCYP2B6-Tg mice showed minimal co-clustering. (**B**) Hierarchical clustering of differential gene expression data and oxylipins/lipids comparing female Cyp2b-null and hCYP2B6-Tg mice showed that some oxylipins and serum lipids clustered with DEG.

Other genes that clustered closely with these oxylipins in females include a transcription factor involved in epithelial–mesenchymal transition (snail family transcriptional repressor 2 (*Snai2*)—protects from liver fibrosis) [88], a factor involved in thyroid-stimulating hormone (Thyrotroph embryonic factor (*Tef*)), a ubiquitin-protein transferase (Ring Finger Protein 144B (*Rnf144b*)), a mitochondrial NADH dehydrogenase (mitochondrially encoded NADH dehydrogenase 5 (*Mt-Nd5*); part of complex 1), a histone methyltransferase (SET Domain Bifurcated Histone Lysine Methyltransferase 2 (*Setdb2*)), and a GTPase protein (Family With Sequence Similarity 13 Member A (*Fam13a*)), which represses AMPK activity and is associated with fatty liver disease. Fam13a-null mice are resistant to high-fat diet induced obesity and NAFLD [89]. *Setdb2* has been purposely down-regulated (it is increased in hCYP2B6-Tg mice) to reduce NAFLD [90]. Interestingly, of the eight genes associated with NAFLD, four are closely associated with 14(15)-EET, and all four are associated with NAFLD.

The only oxylipin that was differentially produced in male hCYP2B6-Tg mice was 14(15)-EET. It clustered somewhat similarly to increased serum HDLs and cholesterol; however, there were no genes closely clustered to 14(15)-EET. Previous research showed 14(15)-EET is associated with HFD-induced steatosis in hCYP2B6-Tg mice [7]. However, other research indicates 14(15)-EET is inversely associated with NAFLD and non-alcoholic steatohepatitis (NASH) [91]. Further investigation of 14(15)-EET is needed to determine the importance of this metabolite.

Male and female hCYP2B6-Tg mice had different responses to fasting. Male hCYP2B6-Tg mice showed a significant increase in serum cholesterol, triglycerides, HDLs, and VLDLs compared to Cyp2b-null mice, and female hCYP2B6-Tg mice showed a decrease in serum triglycerides and VLDLs compared to Cyp2b-null mice (Table 3). Both male and female hCYP2B6-Tg mice showed increased steatosis compared to Cyp2b-null mice, and female mice showed a stronger steatotic response and more DEG than male mice (Figure 4), possibly due to the decreased serum lipid load. DEG varied significantly between sexes, with only 18.8% of total DEG between genotypes in males and 12.4% of DEG between genotypes in female mice being shared between sexes. Upon further evaluation of the shared genes, these 152 DEG were often dysregulated in a different direction between sexes. Additionally, 36.8% of these 152 genes showed dysregulation in different directions when comparing sexes, further emphasizing the sexual dimorphism of the liver, especially in hCYP2B6-Tg mice, a gene that is female-predominant [92].

These very different and sometimes contradictory transcriptomic responses between male and female mice emphasize the importance of evaluating steatotic responses in both sexes. CYP2B6 is sexually dimorphic [92], and the receptors primarily responsible for the regulation of CYP2B6 are also sexually dimorphic. The constitutive androstane receptor (CAR) is the strongest regulator of CYP2B6, and CAR regulation is part of a complex network that is sexually dimorphic. CAR is regulated by the hepatocyte nuclear factor 4 alpha (HNF4α), which in turn is regulated by the signal transducer and activator of transcription 5 a and b (STAT5A and STAT5B) via temporal patterns of growth hormone release from the pituitary, which differ in males and females [93]. CAR activity is also repressed by androgens [94,95], leading to the greater expression of genes regulated by CAR in females than males. Forkhead box protein A2 (FOXA2) also participates in the regulation of CYP2B6, and FOXA2 and STAT5B regulate a number of energy-related genes in male mice [96], further driving sexual dimorphism. Interestingly, CAR's expression is circadian and many of the circadian rhythm genes, including GH-regulated igf-1, are sexually dimorphic [97]. We have previously demonstrated that hCYP2B6-Tg mice show sexually dimorphic responses to a high-fat diet as related to steatosis and obesity [7]; therefore, it was expected that some degree of sexual dimorphism would be present in the

results of this study investigating fasting-mediated steatosis due to the upstream regulation of CYP2B6 and previously observed sex-influenced differences.

Transcriptomic analysis revealed that male Cyp2b-null mice were more sensitive to changes in circadian rhythm and cell cycle than male hCYP2B6-Tg mice. Female Cyp2b-null mice did not experience the same disruption of these processes. Instead, female hCYP2B6-Tg mice were more sensitive to changes in circadian rhythm. Female Cyp2b-null showed the enrichment of genes and processes involved in cholesterol, steroid, and fatty acid metabolism. Opposingly, hCYP2B6-Tg male mice showed the enrichment of genes and processes involved in cholesterol, steroid, and fatty acid metabolism. hCYP2B-Tg female mice showed the enrichment of processes related to protein phosphorylation and folding, xenobiotic response, and glucose and insulin responses, while several of these processes were enriched in male Cyp2b-null mice. These examples demonstrate the sex differences between the male and female mice when fasting and may indicate differences in the transport, synthesis, and metabolism of fatty acids that explain differences in serum lipids (Table 3).

For example, genes involved in lipid synthesis that are enriched in hCYP2B6-Tg males include *Lpin1* [98] and *Lpin2* [99]. Genes involved in lipid synthesis that are enriched in female hCYP2B6-Tg mice, including all three members of the lipin family (*Lpin1*, *Lpin2*, and *Lpin3*) [98–100], include diacylglycerol kinase Eta (*Dgkh*) [101], acetoacetyl-CoA synthetase (*Aacs*) [102], and acetyl-Coenzyme A carboxylase alpha (*Acaca*) [103]. Genes involved in lipid transport showed sexually dimorphic changes. Male hCYP2B6-Tg mice showed the enrichment of genes related to lipid transport, including kallikrein B1 (*Klkb1*) involved in HDL-mediated cholesterol efflux [104] and the D site of the albumin promoter binding protein (*Dbp*), which is crucial for fatty acid transport in the blood via its function in the transport protein albumin [105]. Female Cyp2b-null mice showed the enrichment of genes related to lipid transport, including several apolipoproteins associated with or predicted to be associated with HDLs and VLDLs (*Apom*, *Apol9a*, *Apol9b*) [106]. This provides a possible explanation for the increase in serum lipids seen in male hCYP2B6-Tg mice and the decrease in serum lipids seen in female hCYP2B6-Tg mice (Table 4). Genes involved in lipid metabolism enriched in male Cyp2b-null mice include carboxylesterase 1D (*Ces1d*) [107], glycerophosphodiester phosphodiesterase 1 (*Gde1*) [108], and *Scd1* [109]. Genes involved in lipid and fatty acid metabolism enriched in Cyp2b-null female mice include three of the five members of the acyl-CoA synthetase long-chain family member (*Acsl1*, *Acsl3*, and *Acsl5*) [110] and *Scd1* [109].

While this study identifies transcriptomic changes related to steatosis and CYP2B6 in vivo using transgenic mouse models, as well as physiological differences seen between Cyp2b-null and hCYP2B6-Tg mice by evaluations of lipidomics and serum and liver lipids, there are limitations. RNA expression does not always directly equate to protein expression or activity. However, this paper provides physiological outcomes, comparisons between the models and the two oxylipins produced by CYP2B6, and possible mechanisms to investigate more thoroughly for future studies on the interplay between toxicology, diet, and metabolic disease. Furthermore, other tissues may contribute to hepatic steatosis due to their misuse of fats. This study focused on the liver and serum, as that is where CYP2B6 is primarily expressed. In future studies, investigation of other tissues such as adipose and skeletal muscle may be warranted to further understand the whole-body response.

Fasting-induced steatosis has been used for a variety of applications [23,24,111] and proved useful in this study evaluating genotype and sex differences between Cyp2b-null and hCYP2B6Tg mice. Fasting-induced steatosis is also a much faster and cheaper option for studying fatty liver disease than diet-induced obese models. In this study, hCYP2B6-Tg mice experienced increased steatosis compared to Cyp2b-null mice, indicating that a 20 h

fasting period is sufficient to observe substantial differences in steatosis. Substantial sexual dimorphism was also observed, and therefore, fasting-induced steatosis could be useful for understanding the differences in the metabolic response of the liver between males and females in genetic, diet-induced, and toxicology models.

4. Conclusions

CYP2B6 is a sexually dimorphic gene with greater expression in females [83]. Two of the metabolites synthesized by CYP2B6, 9-HODE from LA and 9-HOTrE from ALA, did not show significant effects on the livers of treated mice. Serum lipids were typically only affected in males. In general, 9-HOTrE, 9-HODE, and Cyp2b-null vs. hCYP2B6-Tg mice all showed sexually dimorphic effects (Figure 9). Female mice experienced a stronger steatotic response and a greater number of differentially expressed genes; male mice experienced greater changes in serum lipids coupled with less severe steatosis. Male hCYP2B6-Tg mice appear to show increased lipid metabolism and export compared to females, which were more likely to retain fats within the liver, leading to decreased serum lipids and greater steatosis. Female mice also showed more changes in their oxylipin profile than male mice, as female mice had increased concentrations of eight oxylipins, whereas male mice had only one. Overall, this study demonstrated that a 20 h fast can induce significant steatosis in hCYP2B6-Tg mice, CYP2B6 in vivo elicits a strong sexually dimorphic response in lipid metabolism and liver steatosis which affects females more than males, and the oxylipins 9-HODE and 9-HOTrE are only a minor part of CYP2B6's effects, leaving other oxylipins or lipid metabolites that most likely mediate its anti-obesity and steatotic effects.

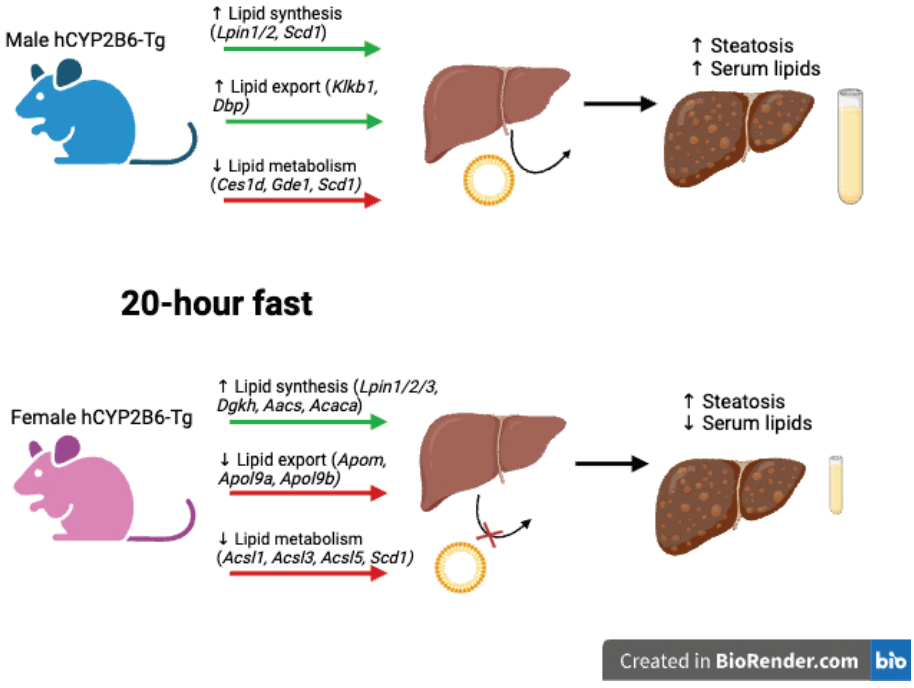


Figure 9. Summary of proposed sexually dimorphic lipid metabolic alterations caused by CYP2B6 in fasting-mediated steatosis. Comparisons of Cyp2b-null to hCYP2B6-Tg mice after a 20 h period of fasting indicated that male hCYP2B6-Tg mice appear to increase lipid synthesis in the liver and transport of lipids out of the liver while decreasing lipid metabolism, leading to increased steatosis and increased serum lipids. Female hCYP2B6-Tg mice in comparison to Cyp2b-null mice appear to increase lipid synthesis in the liver but decrease lipid metabolism and transport of lipids out of the liver, leading to increased steatosis but decreased serum lipids. Example genes are provided over the green (up-regulated pathways) and red arrows (down-regulated pathways). Figure created using BioRender.com.

Supplementary Materials: The following supporting information can be downloaded at https://www.mdpi.com/article/10.3390/biomedicines13020295/s1, Supplementary File S1: Raw data for each biological replicate, including liver triglycerides, serum lipids, and gross anatomy (organ and total body weight). Supplementary File S2: Gross anatomy analysis to determine differences between gross anatomy of oxylipin-treated or untreated mice or Cyp2b-null and hCYP2B6-Tg mice. Supplementary File S3: RNA sequencing data analysis for 9-HODE treated Cyp2b-null mice. Supplementary File S4: RNA sequencing analysis for 9-HOTrE treated Cyp2b-null mice. Supplementary File S5: RNA sequencing data analysis for genes enriched in hCYP2B6-Tg male mice compared to Cyp2b-null male mice. Supplementary File S6: RNA sequencing data analysis for genes enriched in Cyp2b-null male mice compared to hCYP2B6-Tg male mice. Supplementary File S7: RNA sequencing data analysis for genes enriched in hCYP2B6-Tg female mice compared to Cyp2b-null female mice. Supplementary File S8: RNA sequencing data analysis for genes enriched in Cyp2b-null female mice compared to hCYP2B6-Tg female mice. Supplementary File S9: Shared DEG between male and female analysis for Cyp2b-null and hCYP2B6-Tg mice.

Author Contributions: Conceptualization, J.A.E.-M. and W.S.B.; methodology, J.A.E.-M. and W.S.B.; validation, J.A.E.-M., W.S.B. and T.D.J.; formal analysis, J.A.E.-M., W.S.B. and T.D.J.; Investigation, J.A.E.-M., W.S.B. and T.D.J.; resources, W.S.B.; data curation, J.A.E.-M. and W.S.B.; writing—original draft preparation, J.A.E.-M., W.S.B. and T.D.J.; writing—review and editing, W.S.B.; visualization, J.A.E.-M., W.S.B. and T.D.J.; supervision, W.S.B. project administration, W.S.B.; funding acquisition, W.S.B. All authors have read and agreed to the published version of the manuscript.

Funding: This research was primarily funded by the National Institutes of Environmental Health Sciences (NIEHS) grant R15ES017321 to W.S.B. and supplemented with a program award to Clemson University from the National Institute of General Medical Sciences (NIGMS), P20GM121342.

Institutional Review Board Statement: The animal study protocol was approved by the Institutional Animal Care and Use Committee of Clemson University (AUP 2019-061 approved 30 August 2019).

Informed Consent Statement: Not applicable.

Data Availability Statement: All data is available upon request. Supplementary Files containing quantitative data presented in this manuscript can be found in GEO (GSE282292) and *Mendeley Data*: Eccles-Miller, Jazmine; Johnson, Tyler; Baldwin, William (2024), "Sexually dimorphic effects of CYP2B6 in the development of fasting-mediated steatosis in mice: Role of the oxylipin products 9-HODE and 9-HOTrE", Mendeley Data, V1, doi: 10.17632/wnvkz8f7ft.1—https://data.mendeley.com/datasets/wnvkz8f7ft/1 (accessed on 31 December 2024). In addition, pictures of all slides are available upon request.

Acknowledgments: The authors would like to thank Melissa Heintz for her help breeding and maintaining the mouse colonies and performing necropsies.

Conflicts of Interest: The authors declare no conflicts of interest.

References

1. World Health Organization: Obesity and Overweight. Available online: https://www.who.int/news-room/fact-sheets/detail/obesity-and-overweight (accessed on 1 March 2024).
2. Vanni, E.; Bugianesi, E.; Kotronen, A.; De Minicis, S.; Yki-Järvinen, H.; Svegliati-Baroni, G. From the metabolic syndrome to NAFLD or vice versa? *Dig. Liver Dis.* **2010**, *42*, 320–330. [CrossRef] [PubMed]
3. Saltiel, A.R.; Olefsky, J.M. Inflammatory mechanisms linking obesity and metabolic disease. *J. Clin. Investig.* **2017**, *127*, 1–4. [CrossRef]
4. Huggett, Z.J.; Smith, A.; De Vivo, N.; Gomez, D.; Jethwa, P.; Brameld, J.M.; Bennett, A.; Salter, A.M. A Comparison of Primary Human Hepatocytes and Hepatoma Cell Lines to Model the Effects of Fatty Acids, Fructose and Glucose on Liver Cell Lipid Accumulation. *Nutrients* **2022**, *15*, 40. [CrossRef] [PubMed]
5. Merrell, M.D.; Cherrington, N.J. Drug metabolism alterations in nonalcoholic fatty liver disease. *Drug Metab. Rev.* **2011**, *43*, 317–334. [CrossRef] [PubMed]

6. Heintz, M.M.; McRee, R.; Kumar, R.; Baldwin, W.S. Gender differences in diet-induced steatotic disease in Cyp2b-null mice. *PLoS ONE* **2020**, *15*, e0229896. [CrossRef]
7. Heintz, M.M.; Eccles, J.A.; Olack, E.M.; Maner-Smith, K.M.; Ortlund, E.A.; Baldwin, W.S. Human CYP2B6 produces oxylipins from polyunsaturated fatty acids and reduces diet-induced obesity. *PLoS ONE* **2022**, *17*, e0277053. [CrossRef]
8. Krogstad, V.; Peric, A.; Robertsen, I.; Kringen, M.K.; Wegler, C.; Angeles, P.C.; Hjelmesæth, J.; Karlsson, C.; Andersson, S.; Artursson, P.; et al. A Comparative Analysis of Cytochrome P450 Activities in Paired Liver and Small Intestinal Samples from Patients with Obesity. *Drug Metab. Dispos.* **2020**, *48*, 8–17. [CrossRef]
9. Mo, S.L.; Liu, Y.H.; Duan, W.; Wei, M.Q.; Kanwar, J.R.; Zhou, S.F. Substrate specificity, regulation, and polymorphism of human cytochrome P450 2B6. *Curr. Drug Metab.* **2009**, *10*, 730–753. [CrossRef]
10. Olack, E.M.; Heintz, M.M.; Baldwin, W.S. Dataset of endo- and xenobiotic inhibition of CYP2B6: Comparison to CYP3A4. *Data Brief* **2022**, *41*, 108013. [CrossRef]
11. Li, J.; Lai, H.; Chen, S.; Zhu, H.; Lai, S. Interaction of sex steroid hormones and obesity on insulin resistance and type 2 diabetes in men: The Third National Health and Nutrition Examination Survey. *J. Diabetes Complicat.* **2017**, *31*, 318–327. [CrossRef]
12. Wabitsch, M.; Hauner, H.; Heinze, E.; Böckmann, A.; Benz, R.; Mayer, H.; Teller, W. Body fat distribution and steroid hormone concentrations in obese adolescent girls before and after weight reduction. *J. Clin. Endocrinol. Metab.* **1995**, *80*, 3469–3475. [PubMed]
13. Kim, J.; Li, Y.; Watkins, B.A. Fat to treat fat: Emerging relationship between dietary PUFA, endocannabinoids, and obesity. *Prostaglandins Other Lipid Mediat.* **2013**, *104–105*, 32–41. [CrossRef] [PubMed]
14. Eccles, J.A.; Baldwin, W.S. Detoxification Cytochrome P450s (CYPs) in Families 1-3 Produce Functional Oxylipins from Polyunsaturated Fatty Acids. *Cells* **2022**, *12*, 82. [CrossRef] [PubMed]
15. Damiri, B.; Baldwin, W.S. Cyp2b-Knockdown Mice Poorly Metabolize Corn Oil and Are Age-Dependent Obese. *Lipids* **2018**, *53*, 871–884. [CrossRef]
16. Finn, R.D.; Henderson, C.J.; Scott, C.L.; Wolf, C.R. Unsaturated fatty acid regulation of cytochrome P450 expression via a CAR-dependent pathway. *Biochem. J.* **2009**, *417*, 43–54. [CrossRef]
17. Williams, L.A.; Hamilton, M.C.; Edin, M.L.; Lih, F.B.; Eccles-Miller, J.A.; Tharayil, N.; Leonard, E.; Baldwin, W.S. Increased Perfluorooctanesulfonate (PFOS) Toxicity and Accumulation Is Associated with Perturbed Prostaglandin Metabolism and Increased Organic Anion Transport Protein (OATP) Expression. *Toxics* **2024**, *12*, 106. [CrossRef]
18. Wedel, S.; Osthues, T.; Zimmer, B.; Angioni, C.; Geisslinger, G.; Sisignano, M. Oxidized linoleic acid metabolites maintain mechanical and thermal hypersensitivity during sub-chronic inflammatory pain. *Biochem. Pharmacol.* **2022**, *198*, 114953. [CrossRef]
19. Evans, W.A.; Eccles-Miller, J.A.; Anderson, E.; Farrell, H.; Baldwin, W.S. 9-HODE and 9-HOTrE alter mitochondrial metabolism, increase triglycerides, and perturb fatty acid uptake and synthesis associated gene expression in HepG2 cells. *Prostaglandins Leukot. Essent. Fat. Acids* **2024**, *202*, 102635. [CrossRef]
20. Zahradka, P.; Neumann, S.; Aukema, H.M.; Taylor, C.G. Adipocyte lipid storage and adipokine production are modulated by lipoxygenase-derived oxylipins generated from 18-carbon fatty acids. *Int. J. Biochem. Cell Biol.* **2017**, *88*, 23–30. [CrossRef]
21. Vangaveti, V.; Shashidhar, V.; Collier, F.; Hodge, J.; Rush, C.; Malabu, U.; Baune, B.; Kennedy, R.L. 9- and 13-HODE regulate fatty acid binding protein-4 in human macrophages, but does not involve HODE/GPR132 axis in PPAR-γ regulation of FABP4. *Ther. Adv. Endocrinol. Metab.* **2018**, *9*, 137–150. [CrossRef]
22. Donepudi, A.C.; Boehme, S.; Li, F.; Chiang, J.Y. G-protein-coupled bile acid receptor plays a key role in bile acid metabolism and fasting-induced hepatic steatosis in mice. *Hepatology* **2017**, *65*, 813–827. [CrossRef] [PubMed]
23. Guan, H.P.; Goldstein, J.L.; Brown, M.S.; Liang, G. Accelerated fatty acid oxidation in muscle averts fasting-induced hepatic steatosis in SJL/J mice. *J. Biol. Chem.* **2009**, *284*, 24644–24652. [CrossRef] [PubMed]
24. Heijboer, A.C.; Donga, E.; Voshol, P.J.; Dang, Z.-C.; Havekes, L.M.; Romijn, J.A.; Corssmit, E.P.M. Sixteen hours of fasting differentially affects hepatic and muscle insulin sensitivity in mice. *J. Lipid Res.* **2005**, *46*, 582–588. [CrossRef] [PubMed]
25. Heintz, M.M.; Kumar, R.; Rutledge, M.M.; Baldwin, W.S. Cyp2b-null male mice are susceptible to diet-induced obesity and perturbations in lipid homeostasis. *J. Nutr. Biochem.* **2019**, *70*, 125–137. [CrossRef]
26. Hamilton, M.C.; Heintz, M.M.; Pfohl, M.; Marques, E.; Ford, L.; Slitt, A.L.; Baldwin, W.S. Increased toxicity and retention of perflourooctane sulfonate (PFOS) in humanized CYP2B6-Transgenic mice compared to Cyp2b-null mice is relieved by a high-fat diet (HFD). *Food Chem. Toxicol.* **2021**, *152*, 112175. [CrossRef]
27. Wei, Y.; Wu, H.; Li, L.; Liu, Z.; Zhou, X.; Zhang, Q.Y.; Weng, Y.; D'Agostino, J.; Ling, G.; Zhang, X.; et al. Generation and characterization of a CYP2A13/2B6/2F1-transgenic mouse model. *Drug Metab. Dispos.* **2012**, *40*, 1144–1150. [CrossRef]
28. Ramírez-Zacarías, J.L.; Castro-Muñozledo, F.; Kuri-Harcuch, W. Quantitation of adipose conversion and triglycerides by staining intracytoplasmic lipids with oil red O. *Histochemistry* **1992**, *97*, 493–497. [CrossRef]

29. Naudin, C.R.; Maner-Smith, K.; Owens, J.A.; Wynn, G.M.; Robinson, B.S.; Matthews, J.D.; Reedy, A.R.; Luo, L.; Wolfarth, A.A.; Darby, T.M.; et al. Lactococcus lactis Subspecies cremoris Elicits Protection Against Metabolic Changes Induced by a Western-Style Diet. *Gastroenterology* **2020**, *159*, 639–651.e635. [CrossRef]
30. Huang, D.W.; Sherman, B.T.; Lempicki, R.A. Systematic and integrative analysis of large gene lists using DAVID bioinformatics resources. *Nat. Protoc.* **2009**, *4*, 44–57. [CrossRef]
31. Sherman, B.T.; Hao, M.; Qiu, J.; Jiao, X.; Baseler, M.W.; Lane, H.C.; Imamichi, T.; Chang, W. DAVID: A web server for functional enrichment analysis and functional annotation of gene lists (2021 update). *Nucleic Acids Res.* **2022**, *50*, W216–W221. [CrossRef]
32. Supek, F.; Bošnjak, M.; Škunca, N.; Šmuc, T. REVIGO summarizes and visualizes long lists of gene ontology terms. *PLoS ONE* **2011**, *6*, e21800. [CrossRef] [PubMed]
33. Roling, J.A.; Bain, L.J.; Baldwin, W.S. Differential gene expression in mummichogs (Fundulus heteroclitus) following treatment with pyrene: Comparison to a creosote contaminated site. *Mar. Environ. Res.* **2004**, *57*, 377–395. [CrossRef] [PubMed]
34. Muller, P.Y.; Janovjak, H.; Miserez, A.R.; Dobbie, Z. Processing of gene expression data generated by quantitative real-time RT-PCR. *Biotechniques* **2002**, *33*, 514.
35. Singh, A.K.; Chaube, B.; Zhang, X.; Sun, J.; Citrin, K.M.; Canfrán-Duque, A.; Aryal, B.; Rotllan, N.; Varela, L.; Lee, R.G.; et al. Hepatocyte-specific suppression of ANGPTL4 improves obesity-associated diabetes and mitigates atherosclerosis in mice. *J. Clin. Investig.* **2021**, *131*, e140989. [CrossRef]
36. Senates, E.; Yilmaz, Y.; Colak, Y.; Ozturk, O.; Altunoz, M.E.; Kurt, R.; Ozkara, S.; Aksaray, S.; Tuncer, I.; Ovunc, A.O. Serum levels of hepcidin in patients with biopsy-proven nonalcoholic fatty liver disease. *Metab. Syndr. Relat. Disord.* **2011**, *9*, 287–290. [CrossRef]
37. Wu, Z.; Wang, S. Role of kruppel-like transcription factors in adipogenesis. *Dev. Biol.* **2013**, *373*, 235–243. [CrossRef]
38. Zelows, M.M.; Cady, C.; Dharanipragada, N.; Mead, A.E.; Kipp, Z.A.; Bates, E.A.; Varadharajan, V.; Banerjee, R.; Park, S.H.; Shelman, N.R.; et al. Loss of carnitine palmitoyltransferase 1a reduces docosahexaenoic acid-containing phospholipids and drives sexually dimorphic liver disease in mice. *Mol. Metab.* **2023**, *78*, 101815. [CrossRef]
39. Su, Z.; Korstanje, R.; Tsaih, S.W.; Paigen, B. Candidate genes for obesity revealed from a C57BL/6J x 129S1/SvImJ intercross. *Int J. Obes.* **2008**, *32*, 1180–1189. [CrossRef]
40. Cai, Q.; Zhu, M.; Duan, J.; Wang, H.; Chen, J.; Xiao, Y.; Wang, Y.; Wang, J.; Yu, X.; Yang, H. Comprehensive Analysis of Immune-Related Prognosis of TK1 in Hepatocellular Carcinoma. *Front. Oncol.* **2021**, *11*, 786873. [CrossRef]
41. Hoshi, M.; Osawa, Y.; Nakamoto, K.; Morita, N.; Yamamoto, Y.; Ando, T.; Tashita, C.; Nabeshima, T.; Saito, K. Kynurenine produced by indoleamine 2,3-dioxygenase 2 exacerbates acute liver injury by carbon tetrachloride in mice. *Toxicology* **2020**, *438*, 152458. [CrossRef]
42. Zhou, Z.; Qian, J.; Kini, A.; Riederer, B.; Römermann, D.; Gros, G.; Seidler, U. Loss of luminal carbonic anhydrase XIV results in decreased biliary bicarbonate output, liver fibrosis, and cholangiocyte proliferation in mice. *Pflug. Arch.* **2022**, *474*, 529–539. [CrossRef] [PubMed]
43. Meghadri, S.H.; Martinez-Delgado, B.; Ostermann, L.; Gomez-Mariano, G.; Perez-Luz, S.; Tumpara, S.; Wrenger, S.; DeLuca, D.S.; Maus, U.A.; Welte, T.; et al. Loss of Serpina1 in Mice Leads to Altered Gene Expression in Inflammatory and Metabolic Pathways. *Int. J. Mol. Sci.* **2022**, *23*, 10425. [CrossRef] [PubMed]
44. Choi, Y.J.; Kim, S.; Choi, Y.; Nielsen, T.B.; Yan, J.; Lu, A.; Ruan, J.; Lee, H.-R.; Wu, H.; Spellberg, B.; et al. SERPINB1-mediated checkpoint of inflammatory caspase activation. *Nat. Immunol.* **2019**, *20*, 276–287. [CrossRef] [PubMed]
45. Demir, S.; Wolff, G.; Wieder, A.; Maida, A.; Bühler, L.; Brune, M.; Hautzinger, O.; Feuchtinger, A.; Poth, T.; Szendroedi, J.; et al. TSC22D4 interacts with Akt1 to regulate glucose metabolism. *Sci. Adv.* **2022**, *8*, eabo5555. [CrossRef]
46. Li, R.H.; Churchill, G.A. Epistasis contributes to the genetic buffering of plasma HDL cholesterol in mice. *Physiol. Genom.* **2010**, *42a*, 228–234. [CrossRef]
47. López-Soldado, I.; Torres, A.G.; Ventura, R.; Martínez-Ruiz, I.; Díaz-Ramos, A.; Planet, E.; Cooper, D.; Pazderska, A.; Wanic, K.; O'Hanlon, D.; et al. Decreased expression of mitochondrial aminoacyl-tRNA synthetases causes downregulation of OXPHOS subunits in type 2 diabetic muscle. *Redox Biol.* **2023**, *61*, 102630. [CrossRef]
48. Nikolaou, N.; Gathercole, L.L.; Marchand, L.; Althari, S.; Dempster, N.J.; Green, C.J.; van de Bunt, M.; McNeil, C.; Arvaniti, A.; Hughes, B.A.; et al. AKR1D1 is a novel regulator of metabolic phenotype in human hepatocytes and is dysregulated in non-alcoholic fatty liver disease. *Metabolism* **2019**, *99*, 67–80. [CrossRef]
49. Ning, M.; Jeong, H. High-Fat Diet Feeding Alters Expression of Hepatic Drug-Metabolizing Enzymes in Mice. *Drug Metab. Dispos.* **2017**, *45*, 707–711. [CrossRef]
50. Ahmed, S.; Bott, D.; Gomez, A.; Tamblyn, L.; Rasheed, A.; Cho, T.; MacPherson, L.; Sugamori, K.S.; Yang, Y.; Grant, D.M.; et al. Loss of the Mono-ADP-ribosyltransferase, Tiparp, Increases Sensitivity to Dioxin-induced Steatohepatitis and Lethality. *J. Biol. Chem.* **2015**, *290*, 16824–16840. [CrossRef]
51. Sánchez-Mendoza, L.M.; Pérez-Sánchez, C.; García-Caballero, C.; Pérez-Rodríguez, M.; Calero-Rodríguez, P.; Vellón-García, B.; Moreno, J.A.; Burón, M.I.; de Cabo, R.; González-Reyes, J.A.; et al. CYB5R3 overexpression exhibits sexual dimorphism:

Mitochondrial and metabolic adaptations in transgenic female mice during calorie restriction. *Free Radic. Biol. Med.* **2024**, *223*, 69–86. [CrossRef]
52. Rodríguez-López, S.; López-Bellón, S.; González-Reyes, J.A.; Burón, M.I.; de Cabo, R.; Villalba, J.M. Mitochondrial adaptations in liver and skeletal muscle to pro-longevity nutritional and genetic interventions: The crosstalk between calorie restriction and CYB5R3 overexpression in transgenic mice. *Geroscience* **2020**, *42*, 977–994. [CrossRef] [PubMed]
53. Jeyakumar, S.M.; Vajreswari, A. Stearoyl-CoA desaturase 1: A potential target for non-alcoholic fatty liver disease?-perspective on emerging experimental evidence. *World J. Hepatol.* **2022**, *14*, 168–179. [CrossRef] [PubMed]
54. Kazierad, D.J.; Chidsey, K.; Somayaji, V.R.; Bergman, A.J.; Birnbaum, M.J.; Calle, R.A. Inhibition of ketohexokinase in adults with NAFLD reduces liver fat and inflammatory markers: A randomized phase 2 trial. *Med* **2021**, *2*, 800–813.e803. [CrossRef]
55. Boughanem, H.; Yubero-Serrano, E.M.; López-Miranda, J.; Tinahones, F.J.; Macias-Gonzalez, M. Potential Role of Insulin Growth-Factor-Binding Protein 2 as Therapeutic Target for Obesity-Related Insulin Resistance. *Int. J. Mol. Sci.* **2021**, *22*, 1133. [CrossRef] [PubMed]
56. Ruchti, E.; Roach, P.J.; DePaoli-Roach, A.A.; Magistretti, P.J.; Allaman, I. Protein targeting to glycogen is a master regulator of glycogen synthesis in astrocytes. *IBRO Rep.* **2016**, *1*, 46–53. [CrossRef]
57. Reue, K. The role of lipin 1 in adipogenesis and lipid metabolism. *Novartis Found. Symp.* **2007**, *286*, 58–68; discussion 68–71, 162–163, 196–203.
58. Chatterjee, C.; Sparks, D.L. Hepatic lipase, high density lipoproteins, and hypertriglyceridemia. *Am. J. Pathol.* **2011**, *178*, 1429–1433. [CrossRef]
59. Mori, H.; Peterson, S.K.; Simmermon, R.C.; Overmyer, K.A.; Nishii, A.; Paulsson, E.; Li, Z.; Jen, A.; Uranga, R.M.; Maung, J.N.; et al. Scd1 and monounsaturated lipids are required for autophagy and survival of adipocytes. *Mol. Metab.* **2024**, *83*, 101916. [CrossRef]
60. Sztalryd, C.; Brasaemle, D.L. The perilipin family of lipid droplet proteins: Gatekeepers of intracellular lipolysis. *Biochim. Biophys. Acta Mol. Cell Biol. Lipids* **2017**, *1862*, 1221–1232. [CrossRef]
61. Soldo, B.; Šprung, M.; Mušac, G.; Pavela-Vrančić, M.; Ljubenkov, I. Evaluation of Olive Fruit Lipoxygenase Extraction Protocols on 9- and 13-Z,E-HPODE Formation. *Molecules* **2016**, *21*, 506. [CrossRef]
62. Balvers, M.G.J.; Verhoeckx, K.C.M.; Plastina, P.; Wortelboer, H.M.; Meijerink, J.; Witkamp, R.F. Docosahexaenoic acid and eicosapentaenoic acid are converted by 3T3-L1 adipocytes to N-acyl ethanolamines with anti-inflammatory properties. *Biochim. Biophys. Acta (BBA)—Mol. Cell Biol. Lipids* **2010**, *1801*, 1107–1114. [CrossRef] [PubMed]
63. Jones, P.J.; Lin, L.; Gillingham, L.G.; Yang, H.; Omar, J.M. Modulation of plasma N-acylethanolamine levels and physiological parameters by dietary fatty acid composition in humans. *J. Lipid Res.* **2014**, *55*, 2655–2664. [CrossRef] [PubMed]
64. Wasilewski, M.; Więckowski, M.R.; Dymkowska, D.; Wojtczak, L. Effects of N-acylethanolamines on mitochondrial energetics and permeability transition. *Biochim. Biophys. Acta (BBA)—Bioenerg.* **2004**, *1657*, 151–163. [CrossRef] [PubMed]
65. Everard, A.; Plovier, H.; Rastelli, M.; Van Hul, M.; de Wouters d'Oplinter, A.; Geurts, L.; Druart, C.; Robine, S.; Delzenne, N.M.; Muccioli, G.G.; et al. Intestinal epithelial N-acylphosphatidylethanolamine phospholipase D links dietary fat to metabolic adaptations in obesity and steatosis. *Nat. Commun.* **2019**, *10*, 457. [CrossRef]
66. Mock, E.D.; Gagestein, B.; van der Stelt, M. Anandamide and other N-acylethanolamines: A class of signaling lipids with therapeutic opportunities. *Progress Lipid Res.* **2023**, *89*, 101194. [CrossRef]
67. Tovar, R.; Gavito, A.L.; Vargas, A.; Soverchia, L.; Hernandez-Folgado, L.; Jagerovic, N.; Baixeras, E.; Ciccocioppo, R.; Rodríguez de Fonseca, F.; Decara, J. Palmitoleoylethanolamide Is an Efficient Anti-Obesity Endogenous Compound: Comparison with Oleylethanolamide in Diet-Induced Obesity. *Nutrients* **2021**, *13*, 2589. [CrossRef]
68. Shao, Y.; Fu, Z.; Wang, Y.; Yang, Z.; Lin, Y.; Li, S.; Cheng, C.; Wei, M.; Liu, Z.; Xu, G.; et al. A metabolome atlas of mouse brain on the global metabolic signature dynamics following short-term fasting. *Signal Transduct. Target. Ther.* **2023**, *8*, 334. [CrossRef]
69. Pashkov, V.; Huang, J.; Parameswara, V.K.; Kedzierski, W.; Kurrasch, D.M.; Tall, G.G.; Esser, V.; Gerard, R.D.; Uyeda, K.; Towle, H.C.; et al. Regulator of G protein signaling (RGS16) inhibits hepatic fatty acid oxidation in a carbohydrate response element-binding protein (ChREBP)-dependent manner. *J. Biol. Chem.* **2011**, *286*, 15116–15125. [CrossRef]
70. Goetzman, E.S. Advances in the Understanding and Treatment of Mitochondrial Fatty Acid Oxidation Disorders. *Curr. Genet. Med. Rep.* **2017**, *5*, 132–142. [CrossRef]
71. Jiang, P.; Ling, Y.; Zhu, T.; Luo, X.; Tao, Y.; Meng, F.; Cheng, W.; Ji, Y. Mitochondrial tRNA mutations in Chinese Children with Tic Disorders. *Biosci. Rep.* **2020**, *40*, BSR20201856. [CrossRef]
72. Bracey, N.A.; Platnich, J.M.; Lau, A.; Chung, H.; Hyndman, M.E.; MacDonald, J.A.; Chun, J.; Beck, P.L.; Girardin, S.E.; Gordon, P.M.; et al. Tissue-selective alternate promoters guide NLRP6 expression. *Life Sci. Alliance* **2021**, *4*, e202000897. [CrossRef] [PubMed]
73. Ghimire, L.; Paudel, S.; Jin, L.; Jeyaseelan, S. The NLRP6 inflammasome in health and disease. *Mucosal Immunol.* **2020**, *13*, 388–398. [CrossRef] [PubMed]

74. Spano, D.; Cimmino, F.; Capasso, M.; D'Angelo, F.; Zambrano, N.; Terracciano, L.; Iolascon, A. Changes of the Hepatic Proteome in Hepatitis B-Infected Mouse Model at Early Stages of Fibrosis. *J. Proteome Res.* **2008**, *7*, 2642–2653. [CrossRef] [PubMed]
75. Shi, Z.; Rockey, D.C. Upregulation of the actin cytoskeleton via myocardin leads to increased expression of type 1 collagen. *Lab. Investig.* **2017**, *97*, 1412–1426. [CrossRef]
76. Monzón-Casanova, E.; Rudolf, R.; Starick, L.; Müller, I.; Söllner, C.; Müller, N.; Westphal, N.; Miyoshi-Akiyama, T.; Uchiyama, T.; Berberich, I.; et al. The Forgotten: Identification and Functional Characterization of MHC Class II Molecules H2-Eb2 and RT1-Db2. *J. Immunol.* **2016**, *196*, 988–999. [CrossRef]
77. Logunova, N.; Kapina, M.; Kondratieva, E.; Apt, A. The H2-A Class II molecule α/β-chain cis-mismatch severely affects cell surface expression, selection of conventional CD4(+) T cells and protection against TB infection. *Front. Immunol.* **2023**, *14*, 1183614. [CrossRef]
78. Liao, S.; He, H.; Zeng, Y.; Yang, L.; Liu, Z.; An, Z.; Zhang, M. A nomogram for predicting metabolic steatohepatitis: The combination of NAMPT, RALGDS, GADD45B, FOSL2, RTP3, and RASD1. *Open Med.* **2021**, *16*, 773–785. [CrossRef]
79. Hilsabeck, T.A.U.; Liu-Bryan, R.; Guo, T.; Wilson, K.A.; Bose, N.; Raftery, D.; Beck, J.N.; Lang, S.; Jin, K.; Nelson, C.S.; et al. A fly GWAS for purine metabolites identifies human FAM214 homolog medusa, which acts in a conserved manner to enhance hyperuricemia-driven pathologies by modulating purine metabolism and the inflammatory response. *Geroscience* **2022**, *44*, 2195–2211. [CrossRef]
80. Gehrke, N.; Hofmann, L.J.; Straub, B.K.; Rühle, F.; Waisman, A.; Galle, P.R.; Schattenberg, J.M. Hepatic interleukin-1 receptor type 1 signalling regulates insulin sensitivity in the early phases of nonalcoholic fatty liver disease. *Clin. Transl. Med.* **2022**, *12*, e1048. [CrossRef]
81. Kovi, R.C.; Bhusari, S.; Mav, D.; Shah, R.R.; Ton, T.V.; Hoenerhoff, M.J.; Sills, R.C.; Pandiri, A.R. Genome-wide promoter DNA methylation profiling of hepatocellular carcinomas arising either spontaneously or due to chronic exposure to Ginkgo biloba extract (GBE) in B6C3F1/N mice. *Arch. Toxicol.* **2019**, *93*, 2219–2235. [CrossRef]
82. Liu, H.; Pathak, P.; Boehme, S.; Chiang, J.L. Cholesterol 7α-hydroxylase protects the liver from inflammation and fibrosis by maintaining cholesterol homeostasis. *J. Lipid Res.* **2016**, *57*, 1831–1844. [CrossRef] [PubMed]
83. Ke, C.; Xiao, C.; Li, J.; Wu, X.; Zhang, Y.; Chen, Y.; Sheng, S.; Fu, Z.; Wang, L.; Ni, C.; et al. FMO2 ameliorates nonalcoholic fatty liver disease by suppressing ER-to-Golgi transport of SREBP1. *Hepatology* **2025**, *81*, 181–197. [CrossRef] [PubMed]
84. Qu, J.; Ko, C.W.; Tso, P.; Bhargava, A. Apolipoprotein A-IV: A Multifunctional Protein Involved in Protection against Atherosclerosis and Diabetes. *Cells* **2019**, *8*, 319. [CrossRef] [PubMed]
85. Cheng, C.; Liu, X.H.; He, J.; Gao, J.; Zhou, J.T.; Fan, J.N.; Jin, X.; Zhang, J.; Chang, L.; Xiong, Z.; et al. Apolipoprotein A4 Restricts Diet-Induced Hepatic Steatosis via SREBF1-Mediated Lipogenesis and Enhances IRS-PI3K-Akt Signaling. *Mol. Nutr. Food Res.* **2022**, *66*, e2101034. [CrossRef] [PubMed]
86. Xiang, L.; Jiao, Y.; Qian, Y.; Li, Y.; Mao, F.; Lu, Y. Comparison of hepatic gene expression profiles between three mouse models of Nonalcoholic Fatty Liver Disease. *Genes Dis.* **2022**, *9*, 201–215. [CrossRef]
87. Meijer, I.A.; Sasarman, F.; Maftei, C.; Rossignol, E.; Vanasse, M.; Major, P.; Mitchell, G.A.; Brunel-Guitton, C. LPIN1 deficiency with severe recurrent rhabdomyolysis and persistent elevation of creatine kinase levels due to chromosome 2 maternal isodisomy. *Mol. Genet. Metab. Rep.* **2015**, *5*, 85–88. [CrossRef]
88. Wang, P.; Kang, Q.; Wu, W.S.; Rui, L. Hepatic Snai1 and Snai2 promote liver regeneration and suppress liver fibrosis in mice. *Cell Rep.* **2024**, *43*, 113875. [CrossRef]
89. Lin, X.; Liou, Y.H.; Li, Y.; Gong, L.; Li, Y.; Hao, Y.; Pham, B.; Xu, S.; Jiang, Z.; Li, L.; et al. FAM13A Represses AMPK Activity and Regulates Hepatic Glucose and Lipid Metabolism. *iScience* **2020**, *23*, 100928. [CrossRef]
90. Yu, T.; Wang, L.; Cheng, Y.; Zhang, Y.; Zhu, J.; Zhang, G.; Hu, S. Downregulation of Setdb2 promotes alternative activation of macrophages via the PI3K/Akt pathway to attenuate NAFLD after sleeve gastrectomy. *Biochem. Biophys. Res. Commun.* **2024**, *726*, 150264. [CrossRef]
91. Arvind, A.; Osganian, S.A.; Sjoquist, J.A.; Corey, K.E.; Simon, T.G. Epoxygenase-Derived Epoxyeicosatrienoic Acid Mediators Are Associated With Nonalcoholic Fatty Liver Disease, Nonalcoholic Steatohepatitis, and Fibrosis. *Gastroenterology* **2020**, *159*, 2232–2234.e2234. [CrossRef]
92. Lamba, V.; Lamba, J.; Yasuda, K.; Strom, S.; Davila, J.; Hancock, M.L.; Fackenthal, J.D.; Rogan, P.K.; Ring, B.; Wrighton, S.A.; et al. Hepatic CYP2B6 expression: Gender and ethnic differences and relationship to CYP2B6 genotype and CAR (constitutive androstane receptor) expression. *J. Pharmacol. Exp. Ther.* **2003**, *307*, 906–922. [CrossRef]
93. Wiwi, C.A.; Gupte, M.; Waxman, D.J. Sexually Dimorphic P450 Gene Expression in Liver-Specific Hepatocyte Nuclear Factor 4α-Deficient Mice. *Mol. Endocrinol.* **2004**, *18*, 1975–1987. [CrossRef] [PubMed]
94. Baldwin, W.S.; Roling, J.A. A concentration addition model for the activation of the constitutive androstane receptor by xenobiotic mixtures. *Toxicol. Sci.* **2009**, *107*, 93–105. [CrossRef] [PubMed]
95. Forman, B.M.; Tzameli, I.; Choi, H.-S.; Chen, J.; Simha, D.; Seol, W.; Evans, R.M.; Moore, D.D. Androstane metabolites bind to and deactivate the nuclear receptor CAR-β. *Nature* **1998**, *395*, 612–615. [CrossRef]

96. Waxman, D.J.; Holloway, M.G. Sex Differences in the Expression of Hepatic Drug Metabolizing Enzymes. *Mol. Pharmacol.* **2009**, *76*, 215–228. [CrossRef]
97. Astafev, A.A.; Patel, S.A.; Kondratov, R.V. Calorie restriction effects on circadian rhythms in gene expression are sex dependent. *Sci. Rep.* **2017**, *7*, 9716. [CrossRef]
98. Csaki, L.S.; Dwyer, J.R.; Li, X.; Nguyen, M.H.K.; Dewald, J.; Brindley, D.N.; Lusis, A.J.; Yoshinaga, Y.; de Jong, P.; Fong, L.; et al. Lipin-1 and lipin-3 together determine adiposity in vivo. *Mol. Metab.* **2014**, *3*, 145–154. [CrossRef]
99. Gropler, M.C.; Harris, T.E.; Hall, A.M.; Wolins, N.E.; Gross, R.W.; Han, X.; Chen, Z.; Finck, B.N. Lipin 2 is a liver-enriched phosphatidate phosphohydrolase enzyme that is dynamically regulated by fasting and obesity in mice. *J. Biol. Chem.* **2009**, *284*, 6763–6772. [CrossRef]
100. Finck, B.N.; Gropler, M.C.; Chen, Z.; Leone, T.C.; Croce, M.A.; Harris, T.E.; Lawrence, J.C.; Kelly, D.P. Lipin 1 is an inducible amplifier of the hepatic PGC-1α/PPARα regulatory pathway. *Cell Metab.* **2006**, *4*, 199–210. [CrossRef]
101. Massart, J.; Zierath, J.R. Role of Diacylglycerol Kinases in Glucose and Energy Homeostasis. *Trends Endocrinol. Metab.* **2019**, *30*, 603–617. [CrossRef]
102. Bergstrom, J.D. The lipogenic enzyme acetoacetyl-CoA synthetase and ketone body utilization for denovo lipid synthesis, a review. *J. Lipid Res.* **2023**, *64*, 100407. [CrossRef] [PubMed]
103. Goedeke, L.; Bates, J.; Vatner, D.F.; Perry, R.J.; Wang, T.; Ramirez, R.; Li, L.; Ellis, M.W.; Zhang, D.; Wong, K.E.; et al. Acetyl-CoA Carboxylase Inhibition Reverses NAFLD and Hepatic Insulin Resistance but Promotes Hypertriglyceridemia in Rodents. *Hepatology* **2018**, *68*, 2197–2211. [CrossRef] [PubMed]
104. Schachtl-Riess, J.F.; Schönherr, S.; Lamina, C.; Forer, L.; Coassin, S.; Streiter, G.; Kheirkhah, A.; Li, Y.; Meiselbach, H.; Di Maio, S.; et al. KLKB1 and CLSTN2 are associated with HDL-mediated cholesterol efflux capacity in a genome-wide association study. *Atherosclerosis* **2023**, *368*, 1–11. [CrossRef] [PubMed]
105. Bouillon, R.; Schuit, F.; Antonio, L.; Rastinejad, F. Vitamin D Binding Protein: A Historic Overview. *Front. Endocrinol.* **2019**, *10*, 910. [CrossRef] [PubMed]
106. Borup, A.; Christensen, P.M.; Nielsen, L.B.; Christoffersen, C. Apolipoprotein M in lipid metabolism and cardiometabolic diseases. *Curr. Opin. Lipidol.* **2015**, *26*, 48–55. [CrossRef]
107. Bahitham, W.; Watts, R.; Nelson, R.; Lian, J.; Lehner, R. Liver-specific expression of carboxylesterase 1g/esterase-x reduces hepatic steatosis, counteracts dyslipidemia and improves insulin signaling. *Biochim. Biophys. Acta* **2016**, *1861*, 482–490. [CrossRef]
108. Cheng, Y.; Zhou, W.; El Sheery, N.I.; Peters, C.; Li, M.; Wang, X.; Huang, J. Characterization of the Arabidopsis glycerophosphodiester phosphodiesterase (GDPD) family reveals a role of the plastid-localized AtGDPD1 in maintaining cellular phosphate homeostasis under phosphate starvation. *Plant J.* **2011**, *66*, 781–795. [CrossRef]
109. Chu, K.; Miyazaki, M.; Man, W.C.; Ntambi, J.M. Stearoyl-coenzyme A desaturase 1 deficiency protects against hypertriglyceridemia and increases plasma high-density lipoprotein cholesterol induced by liver X receptor activation. *Mol. Cell Biol.* **2006**, *26*, 6786–6798. [CrossRef]
110. Yan, S.; Yang, X.F.; Liu, H.L.; Fu, N.; Ouyang, Y.; Qing, K. Long-chain acyl-CoA synthetase in fatty acid metabolism involved in liver and other diseases: An update. *World J. Gastroenterol.* **2015**, *21*, 3492–3498. [CrossRef]
111. Kwanten, W.J.; Vandewynckel, Y.P.; Martinet, W.; De Winter, B.Y.; Michielsen, P.P.; Van Hoof, V.O.; Driessen, A.; Timmermans, J.P.; Bedossa, P.; Van Vlierberghe, H.; et al. Hepatocellular autophagy modulates the unfolded protein response and fasting-induced steatosis in mice. *Am. J. Physiol. Gastrointest. Liver Physiol.* **2016**, *311*, G599–G609. [CrossRef]

Disclaimer/Publisher's Note: The statements, opinions and data contained in all publications are solely those of the individual author(s) and contributor(s) and not of MDPI and/or the editor(s). MDPI and/or the editor(s) disclaim responsibility for any injury to people or property resulting from any ideas, methods, instructions or products referred to in the content.

biomedicines

MDPI

Article

Beneficial Effect of Fenofibrate in Combination with Silymarin on Parameters of Hereditary Hypertriglyceridemia-Induced Disorders in an Animal Model of Metabolic Syndrome

Jan Soukop [1], Ludmila Kazdová [2], Martina Hüttl [2], Hana Malínská [2], Irena Marková [2], Olena Oliyarnyk [2], Denisa Miklánková [2], Soňa Gurská [3], Zuzana Rácová [1], Martin Poruba [1,*] and Rostislav Večeřa [1,*]

[1] Department of Pharmacology, Faculty of Medicine and Dentistry, Palacky University Olomouc, 77515 Olomouc, Czech Republic; jan.soukop01@upol.cz (J.S.)
[2] Centre for Experimental Medicine, Institute for Clinical and Experimental Medicine, 14021 Prague, Czech Republic
[3] Institute of Molecular and Translational Medicine, Faculty of Medicine and Dentistry, Palacky University Olomouc, 77515 Olomouc, Czech Republic
* Correspondence: martin.poruba@upol.cz (M.P.); rostislav.vecera@upol.cz (R.V.)

Abstract: Background: Hypertriglyceridemia has serious health risks such as cardiovascular disease, type 2 diabetes mellitus, nephropathy, and others. Fenofibrate is an effective hypolipidemic drug, but its benefits for ameliorating disorders associated with hypertriglyceridemia failed to be proven in clinical trials. **Methods:** To search for possible causes of this situation and possibilities of their favorable influence, we tested the effect of FF monotherapy and the combination of fenofibrate with silymarin on metabolic disorders in a unique model of hereditary hypertriglyceridemic rats (HHTg). **Results:** Fenofibrate treatment (100 mg/kg BW/day for four weeks) significantly decreased serum levels of triglyceride, (−77%) and free fatty acids (−29%), the hepatic accumulation of triglycerides, and the expression of genes encoding transcription factors involved in lipid metabolism (Srebf2, Nr1h4. Rxrα, and Slco1a1). In contrast, the hypertriglyceridemia-induced ectopic storage of lipids in muscles, the heart, and kidneys reduced glucose utilization in muscles and was not affected. In addition, fenofibrate reduced the activity of the antioxidant system, including Nrf2 expression (−35%) and increased lipoperoxidation in the liver and, to a lesser extent, in the kidneys and heart. Adding silymarin (micronized form, 600 mg/kg BW/day) to fenofibrate therapy increased the synthesis of glycogen in muscles, (+36%) and reduced hyperinsulinemia (−34%). In the liver, it increased the activity of the antioxidant system, including PON-1 activity and Nrf2 expression, and reduced the formation of lipoperoxides. The beneficial effect of combination therapy on the parameters of oxidative stress and lipoperoxidation was also observed, to a lesser extent, in the heart and kidneys. **Conclusions:** Our results suggest the potential beneficial use of the combination of FF with SLM in the treatment of hypertriglyceridemia-induced metabolic disorders.

Keywords: fenofibrate; silymarin; triglycerides; metabolic syndrome; oxidative stress; insulin resistance; glycogen synthesis; reesterification of fatty acids

1. Introduction

Epidemiological studies show that hypertriglyceridemia is increasingly prevalent worldwide, reaching 10% to 25% in the adult population [1,2]. The cause of elevated triglyceride levels may have a genetic background, but most often, it is a combination of polygenic predisposition and unhealthy lifestyle factors, such as nutritional habits, a

lack of exercise, and obesity [3,4]. Hypertriglyceridemia also carries serious health risks. Multiple epidemiological studies report associations between cardiovascular disease and circulating triglycerides carried in chylomicrons and very-low density lipoproteins (VLDL), collectively termed triglyceride-rich lipoproteins, (TRL) [5]. There is increasing evidence that TRLs are actually more atherogenic than low-density lipoprotein (LDL), and they increase vascular inflammation and promote atherosclerosis [6–8].

Another serious complication of hypertriglyceridemia is the increased ectopic triglyceride deposition in non-adipose tissues. Elevated lipid accumulation is associated with a variety of complications: In the liver, it leads to steatosis and insulin resistance [9]; in the heart, it can induce lipotoxic cardiomyopathy [10]. Increased triglycerides in muscles are associated with muscle insulin resistance, which contributes to the development of metabolic syndrome [11]. In the kidneys, it can cause nephropathy [12]. For this reason, lowering plasma TG is a therapeutic goal to reduce the risk of cardiovascular and other diseases.

Fibrates are one of the most commonly used drugs for hypertriglyceridemia treatment. Their hypolipidemic activity occurs predominantly through peroxisome proliferator-activated receptor alpha (PPARα) activation, which regulates intracellular lipid metabolism through direct transcriptional control of the genes involved in peroxisomal and mitochondrial β-oxidation, fatty acid transport, lipoprotein lipase activation, and triglyceride catabolism [13,14].

Fenofibrate (FF) is a representative of the fibrate drugs that has been the most commonly used in recent years in clinical practice and its effects have also been extensively studied in a number of clinical trials. However, several randomized controlled trials showed that despite a decrease in blood triglyceride levels of approximately 26%, there was no significant decrease in cardiovascular events [15–17]. Fenofibrate therapy also did not reduce disorders involved in the development of metabolic syndrome and its complications [18,19]. Moreover, adverse effects of fibrate therapy, such as liver and kidney injury, especially in the presence of high levels of human C-reactive protein (CRP), have been observed [20–22]. Adverse side effects associated with renal events and the risk of venous thromboembolism have also been found after treatment with pemafibrate, a new PPARα-selective drug [23]. Research efforts are, therefore, focused on finding additional compounds with the potential to increase the efficacy and mitigate the adverse effects induced by FF therapy.

One such compound, which is a suitable supplement to this type of hypolipidemic therapy, is silymarin (SLM), a standardized polyphenolic extract from the milk thistle (Silybum marianum). According to current knowledge and our own published results, SLM has hepatoprotective, cardioprotective, antioxidant, antidiabetic, and anti-inflammatory effects due to the modulation of various transcription factors, antioxidant enzymes, receptors, and signaling pathways [24–27].

The hepatoprotective properties of SLM have been utilized in the treatment of conditions such as hepatic steatosis, amatoxin poisoning, and transplantation complications [28,29]. In earlier research, we found that SLM decreased plasma VLDL cholesterol levels, increased the activity of superoxide dismutase (SOD) and glutathione levels (GSH), and reduced the production of lipid peroxides in the liver of rats fed a high-sucrose diet [24]. The therapeutic effects of SLM are limited by its low absorption from the gastrointestinal tract and rapid excretion. However, using micronized extracts increased its bioavailability and in rats with metabolic syndrome, it had more pronounced effects on the increase in HDL cholesterol and improved glucose metabolism compared to the standard extract [25,26].

We hypothesized that the combined therapy of FF with SLM could reduce disorders associated with hypertriglyceridemia such as ectopic lipid accumulation, insulin resistance,

oxidative stress, and inflammation in tissues. Previous studies have focused mainly on the effects of FF and SLM monotherapy on lipid metabolism disorders. In the pathogenesis of CVD and T2DM, not only does hypertriglyceridemia play a key role, but so do its lipotoxic mechanisms, such as ectopic triglyceride accumulation, insulin resistance, inflammation, and oxidative stress. We, therefore, hypothesize that the addition of SLM, which has proven antioxidative, anti-inflammatory, and antifibrotic properties, could favorably affect the disorders induced by current or even previously persistent hypertriglyceridemia in HHTg rats. The therapeutic effects of combined therapy of FF and SLM on disorders associated with the lipotoxicity of hypertriglyceridemia have not yet been investigated and there is insufficient evidence of their interaction.

To study the therapeutic effects of FF and its combination with SLM, we used a unique model of hereditary hypertriglyceridemic rats (HHTg). This strain of rats was selected for basal and sucrose-stimulated blood triglyceride levels and mimics the most common cause of hypertriglyceridemia in humans, which is, as mentioned, a combination of genetic and lifestyle factors. HHTg rats exhibit most symptoms associated with metabolic syndrome in humans: hypertriglyceridemia, liver steatosis, muscle lipid accumulation, muscle and adipose tissue insulin resistance, hyperinsulinemia, impaired glucose tolerance, higher serum CRP, and mildly elevated blood pressure. This rat strain is an accepted model of metabolic syndrome [30–32], which is not associated with excessive obesity or fat intake.

In this study, we investigated the effect of FF monotherapy and the combined therapy of FF with SLM on metabolic disorders caused by genetically determined hypertriglyceridemia such as ectopic lipid accumulation, impaired glucose utilization in muscle and adipose tissue, oxidative stress in the liver, heart, and kidneys, chronic inflammation, and the expression of genes involved in lipid metabolism. The therapeutic effects of FF with SLM have not yet been tested and there are no data on their mutual interaction.

2. Materials and Methods

2.1. Animals and Diets

All animal experiments were carried out using 4-month-old male hereditary hypertriglyceridemic (HHTg) rats, provided by the Institute for Clinical and Experimental Medicine (Prague, Czech Republic). This strain of rats was selected from Wistar rats based on a higher sensitivity to sucrose-induced triglyceride formation. HHTg rats are characterized by a higher synthesis of triglycerides in the liver, their increased concentrations in circulation and ectopic accumulation in the liver, muscle, and kidneys. As mentioned in the introduction, other disorders associated with the metabolic syndrome were also demonstrated, such as the resistance of muscle and adipose tissue to the action of insulin, hyperinsulinemia, impaired glucose tolerance, oxidative stress in tissues, and the activation of inflammatory parameters. Detailed characteristics of this rat strain are described [30,32–34].

The rats (n = 19) were maintained in a 12 h/12 h light–dark cycle at a temperature of 22–25 °C with free access to food and water. They were fed a standard laboratory diet without supplementation (control group, n = 6) or supplemented with micronized FF in a dose of 100 mg/kg of body weight per day (FF, n = 6) or supplemented with the same dose of FF in a combination with micronized silymarin in a dose of 600 mg/kg body weight per day (FF + SLM, n = 7) for 4 weeks. The reason for using the micronized form of SLM is the knowledge of the low bioavailability of standardized extracts caused by low absorption from the gastrointestinal tract and rapid excretion from the body. We previously found that the micronized form of SLM or its component silybin caused the highest increase in HDL cholesterol levels and the greatest decreased glycemia and insulinemia in the animal model of metabolic syndrome compared to standard or phytosome forms [26]. The dose and form

of SLM used were chosen based on our previous experimental data [22,24]. The standard laboratory diet contained 23% protein, 43% starch, 7% fat, 5% fiber, and 1% vitamin and mineral mixture (Bonagro, Blazovice, Czech Republic). The doses of FF and SLM were chosen according to the doses reported in the literature and according to our previous studies [22,26]. Micronized FF (Fenofix®, Teva Pharmaceuticals, Prague, Czech Republic) was purchased from Ingers Industrial Solutions (Brno, Czech Republic). Micronized SLM was purchased from Favea (Koprivnice, Czech Republic). Daily food intake was measured throughout the duration of the experiment. At the end of the study, the rats were decapitated in a postprandial state and their blood serum and tissues were collected for ex vivo incubation, final biochemical analyzes, or gene expression determination.

All experiments were performed in agreement with the Animal Protection Law of the Czech Republic (501/2020), which complies with the European Community Council recommendations for the use of laboratory animals (86/609/ECC), and approved by the Ethics Committee of the Institute for Clinical and Experimental Medicine, Prague.

2.2. Biochemical Analysis

The serum concentration of triglycerides, glucose, and total cholesterol was measured using commercially available kits (Erba-Lachema, Brno, Czech Republic). Non-esterified fatty acid (NEFA) concentrations were determined using an acyl-CoA oxidase-based colorimetric kit (F. Hoffmann-La Roche AG, Basel, Switzerland). Glycerol was measured by kit from Merck (Darmstadt, Germany). Serum insulin concentration was determined using a Rat Insulin ELISA kit from Mercodia (Uppsala, Sweden), HMW adiponectin using ELISA kit from MyBioSource (San Diego, CA, USA), and C-reactive protein concentration using a Rat CRP ELISA kit from Alpha Diagnostics (San Antonio, TX, USA). Serum IL-6 was determined using rat ELISA kits (BioSource International, Inc., Camarillo, CA, USA), and rat MCP-1 by ELISA kits (Instant ELISA eBioscience, Thermo Fisher Scientific, Waltham, MA, USA). AST and ALT enzyme activities were measured spectrophotometrically by routine methods using a kit from Roche.

2.3. Oxidative Stress Parameters

The activities of superoxide dismutase (SOD), glutathione peroxidase (GSH-Px), glutathione reductase (GR), and glutathione transferase (GST) were analyzed using Assay kits (Cayman Chemical Company, Ann Arbor, MI, USA). Catalase activity determination was based on the ability of H_2O_2 to form a color complex with ammonium molybdate ($(NH_4)_6Mo_7O_{24}$) detected spectrophotometrically. The concentration of conjugated dienes was determined by extraction with a mixture of heptane and the level was analyzed by the reaction with thiobarbituric acid according to Malinska et al. [34]. Paraoxonase-1 (PON-1) activity was determined according to the rate of hydrolysis of paraoxon to p-nitrophenol [35].

2.4. Analysis of Triglyceride Concentrations in Tissues

A determination of the concentration of triglycerides in the liver and skeletal muscle was performed using extraction in a mixture of chloroform and methanol. Subsequently, a solution of 2% potassium dihydrogen phosphate (KH_2PO_4) was added. After extraction, the organic phase was taken and evaporated under nitrogen gas. The resulting pellet was dissolved in isopropyl alcohol and then, the concentration of triglycerides and cholesterol was measured by an enzymatic assay (Erba-Lachema, Brno, Czech Republic).

2.5. Lipolysis in Abdominal Adipose Tissue

The measurement of lipolysis in adipose tissue was carried out as described before [36]. Briefly, distal parts of epididymal adipose tissue were incubated in Krebs-Ringer phosphate buffer with 3% of bovine serum albumin (fraction V) at 37 °C for 2 h and the non-esterified

fatty acids (NEFA) and glycerol concentrations in the medium were measured using the kit described.

2.6. Glucose Utilization in Muscle

Basal and insulin-stimulated glycogen synthesis and glucose oxidation were determined ex vivo in isolated muscle by measuring the incorporation of ^{14}C-U glucose into glycogen and CO_2 as described previously [37]. Briefly, diaphragmatic muscles were incubated for 2 h in 95% O_2 + 5% CO_2 in Krebs-Ringer bicarbonate buffer, pH 7.4, containing 0.1 μCi/mL of ^{14}C-U glucose, 5 mmol/L of unlabelled glucose, and 2.5 mg/mL of bovine serum albumin (Merck, Prague, Czech Republic), with or without 250 μU/mL insulin. After the incubation, glycogen was extracted from the tissue and counted for radioactivity. To determine glucose oxidation, 0.3 mL of hyamine hydroxide (Perkin Elmer, Waltham, MA, USA) was injected into the central compartment of the incubation vial and 0.3 mL of 5 M H_2SO_4 was added to liberate CO_2. After the incubation for 45 min, when the trapping took place, the hyamine hydroxide was quantitatively transferred to the vial containing scintillation fluid for measuring of $^{14}CO_2$ radioactivity.

2.7. Glucose Utilization in Adipose Tissue

Glucose utilization in adipose tissue was determined ex vivo by measuring the incorporation of ^{14}C-U-glucose into adipose tissue lipids, as described previously [38]. Briefly, distal parts of epididymal adipose tissue were incubated for 2 h in the same buffer as described above for muscles, in the presence (250 IU/mL) or absence of insulin in incubation media. After the incubation, the estimation of ^{14}C-glucose incorporation into neutral lipids was carried out. The pieces of tissues were homogenized, and lipids were extracted (chloroform–methanol 2:1) at 4 °C for 16 h, then, KH_2PO_4 was added, an aliquot was evaporated and reconstituted in scintillation liquid, and the radioactivity was measured by scintillation counting.

2.8. Gene Expression Assay

For the total mRNA isolation, we used the RNeasy Mini Kit (Qiagen, Valencia, CA, USA). We used the amount of 1 μg of mRNA for cDNA synthesis using a Transcriptor High Fidelity cDNA synthesis kit (F. Hoffmann-La Roche AG, Basel, Switzerland). For the determination, we used TaqMan Gene Expression Assays probes (Thermo Fisher Scientific, Waltham, MA, USA) containing target primers and a sequence-specific probe optimized for the best functional performance. Commercially available primers purchased from the same corporation were used to determine the mRNA of, Srebf1, Srebf2, Nr1h4, Nr1h3, Rxr, Pparα, and Slco1a1. The real-time PCR was performed on 1536-well plates using acoustic liquid handler Echo 550 (Labcyte, Dublin, Ireland) and LightCycler 1536 Instrument (F. Hoffmann-La Roche AG, Basel, Switzerland). We performed the measurements in six parallels. Reverse transcription and quantitative real-time PCR analyses for expression of the Nrf2 gene in the liver were carried out using the TaqMan RNA-to-CTTM 1-Step Kit and the TaqMan Gene Expression Assay (Applied Biosystems, Foster City, CA, USA) and analyzed via the ViiA^{TM} 7 Real-Time PCR System (Applied Biosystems, Foster City, CA, USA). The results were evaluated by the $^{\Delta\Delta}$Ct method, and all results were normalized and related to the Hprt1 gene (Thermo Fisher Scientific, Waltham, MA, USA).

2.9. Statistical Analysis

The data are expressed as means ± standard error of the mean (SEM). All the data were analyzed using Statistica software (ver. 12.0, 2013, TIBCO Software, Palo Alto, CA, USA). The normality of the data was tested using the Shapiro–Wilk test. We used one-way

analyses of variance (ANOVA) at the significance level of $p < 0.05$ followed by the post hoc Bonferroni to avoid false-positive results.

3. Results

3.1. Effect of Fenofibrate Alone and Fenofibrate in Combination with Silymarin on Body Weight and Metabolic Parameters

As shown in Figure 1, treatment with FF alone reduced the body weight of the rats by 11% ($p < 0.01$) compared to the control group (Figure 1A). The amount of abdominal adipose tissue assessed by epididymal (Figure 1B) and perirenal (Figure 1C) fat pad weight was reduced after FF treatment by 18% and 31%, respectively (both $p < 0.01$), while food intake was not affected by FF. FF treatment reduced serum concentrations of triglycerides by 77% ($p < 0.001$; Figure 1D) and non-esterified fatty acids (NEFA) by 29% ($p < 0.05$; Figure 1E) compared to the untreated control. On the other hand, serum concentrations of glucose (Figure 1F), insulin (Figure 1G), alanine (Figure 1H), and aspartate (Figure 1I) aminotransferases, as well as adiponectin (Figure 1J), were not affected by FF monotherapy.

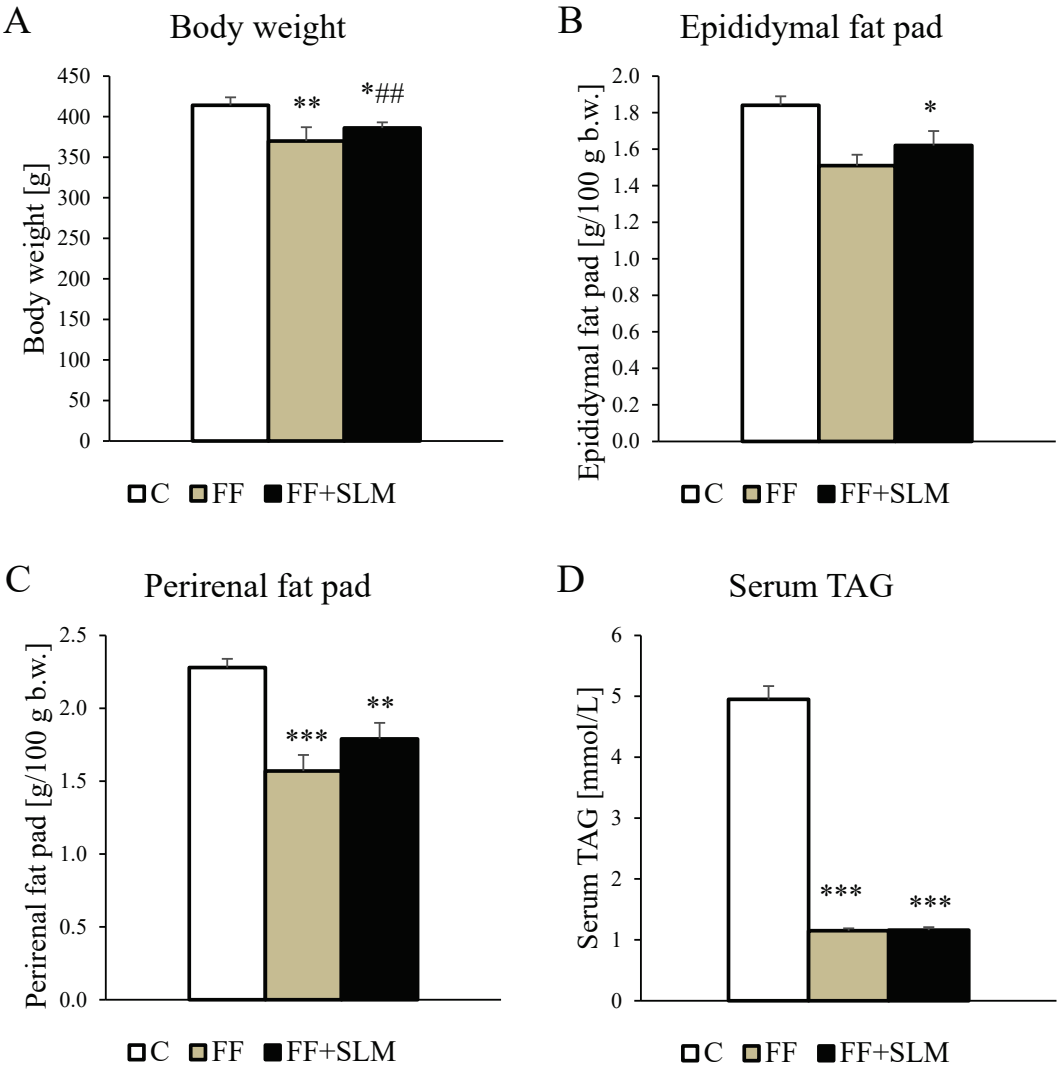


Figure 1. *Cont.*

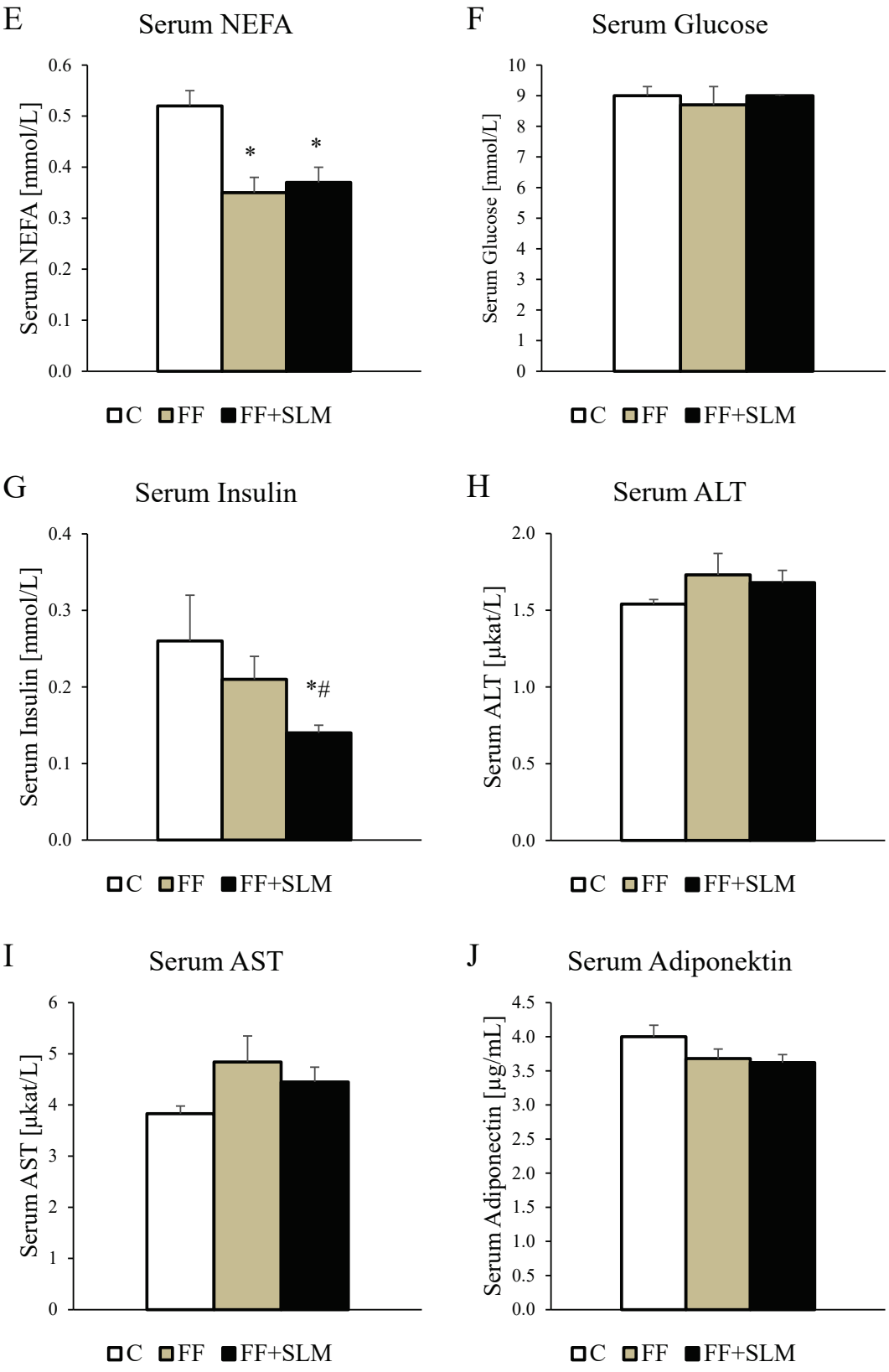


Figure 1. Effects of FF alone and FF in combination with SLM on body weight (**A**) and metabolic parameters (**B**–**J**) in HHTg rats. Data are expressed as mean ± SEM; n = 6–7 animals per group. Abbreviations: C—control; FF—fenofibrate; FF + SLM—fenofibrate + silymarin; NEFA—non-esterified fatty acids. Statistically significant differences: * $p < 0.05$; ** $p < 0.01$; *** $p < 0.001$ denote significance versus the control; # $p < 0.05$; ## $p < 0.01$ denote significance versus the FF group.

FF combined with SLM reduced body weight by 7% ($p < 0.01$; Figure 1A) and unexpectedly increased food intake by 12%, which led to a milder reduction of epididymal (−12% Figure 1B) and perirenal (−21% Figure 1C) fat pad weight (both $p < 0.05$) compared to untreated groups. Combined FF therapy with SLM affected serum concentrations of triglycerides, NEFA, and glucose (Figure 1D–F) as much as FF monotherapy.

The addition of SLM to FF therapy resulted in a significant reduction in serum insulin concentration of 34% ($p < 0.05$; Figure 1G) compared with FF therapy alone.

3.2. Effect of Fenofibrate Alone and in Combination with Silymarin on Lipid Metabolism

Furthermore, we monitored whether FF alone and in combination with SLM would influence the hypertriglyceridemia-associated ectopic accumulation of lipids in tissues (Figure 2). A moderate decrease in soleus muscle triglycerides of 23% in the group treated with FF did not reach statistical significance. Hepatic triglyceride levels were significantly reduced in FF- (−67%; $p < 0.01$) and FF + SLM (−65%; $p < 0.01$)-treated rats in comparison to the controls. The concentration of triglycerides in the kidneys was not affected by FF or FF + SLM treatment.

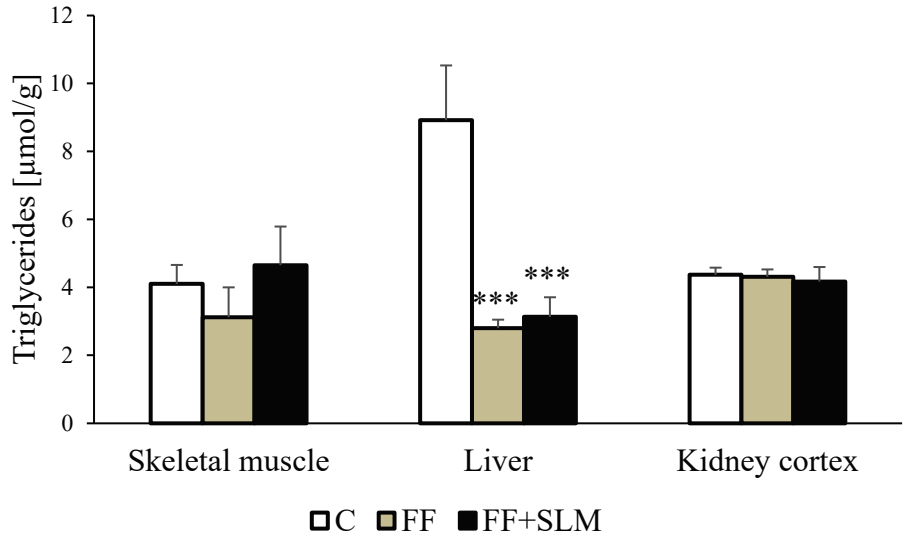


Figure 2. Ectopic accumulation of triglycerides in tissues of HHTg rats treated with FF alone and FF with combination with SLM. Data are expressed as means ± SEM; n = 6–7 animals per group. Abbreviations: C—control; FF—fenofibrate; SLM—silymarin. Statistically significant differences: *** denotes $p < 0.001$ significance versus control.

We further analyzed whether changes in the concentration of lipids in the blood and tissues were associated with fatty acids released from adipose tissue (Figure 3). We found that FF increased the release of NEFA (+28%; $p < 0.05$) and glycerol (+62%; $p < 0.01$) from abdominal adipose tissue. It is known that a certain percentage of fatty acids after release from adipose tissue is re-esterified and returned to the tissue. We found that the re-esterification of fatty acids into triglycerides, as measured by the NEFA/glycerol ratio, was reduced in FF-treated animals (−22%; $p < 0.05$) and in FF + SLM-treated rats (−17%; NS). Reduced re-esterification of released fatty acids from adipose tissue may be one of the mechanisms involved in the reduced amount of visceral adipose tissue in FF-treated rats.

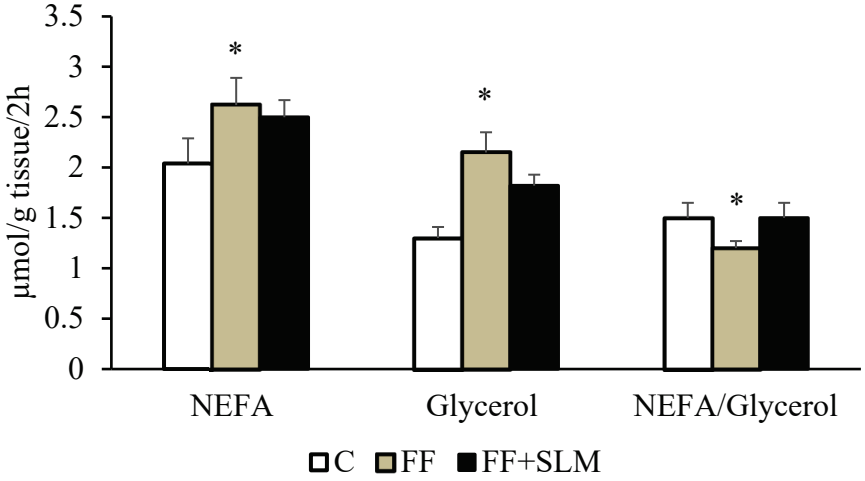


Figure 3. Effect of FF alone and in combination with SLM on adrenaline-stimulated lipolysis in epididymal adipose tissue of HHTg rats. Data are expressed as means ± SEM; n = 6–7 animals per group. Abbreviations: C—control; FF—fenofibrate; FF + SLM—fenofibrate + silymarin; NEFA—non-esterified fatty acids. Statistically significant differences: * $p < 0.05$; denotes significance versus control.

3.3. Effects of Fenofibrate Alone and in Combination with Silymarin on Glucose Metabolism and Insulin Sensitivity

Although elevated postprandial glycemia levels in HHTg rats were not affected by FF treatment alone or the combination of FF with SLM, insulin concentrations were significantly reduced by this therapy (Figure 1F, G). This suggests that glucose utilization in muscle tissue for glycogen synthesis, which represents the majority of postprandial glucose disposal [39], may be affected. Therefore, we measured the effect of FF and FF + SLM treatment on ^{14}C-U-glucose incorporation for glycogen synthesis and for oxidation in skeletal muscle.

As shown in Figure 4A, FF treatment significantly decreased basal incorporation of glucose into glycogen (−39%; $p < 0.05$). This adverse effect was partially alleviated by the combination of FF + SLM (+36%, FF + SLM vs. FF; $p < 0.05$). An interesting finding was the increased glucose oxidation in muscle tissue observed in FF- (+50%; $p < 0.05$) and FF + SLM (+40%; $p < 0.05$)-treated groups compared to untreated controls (Figure 4B).

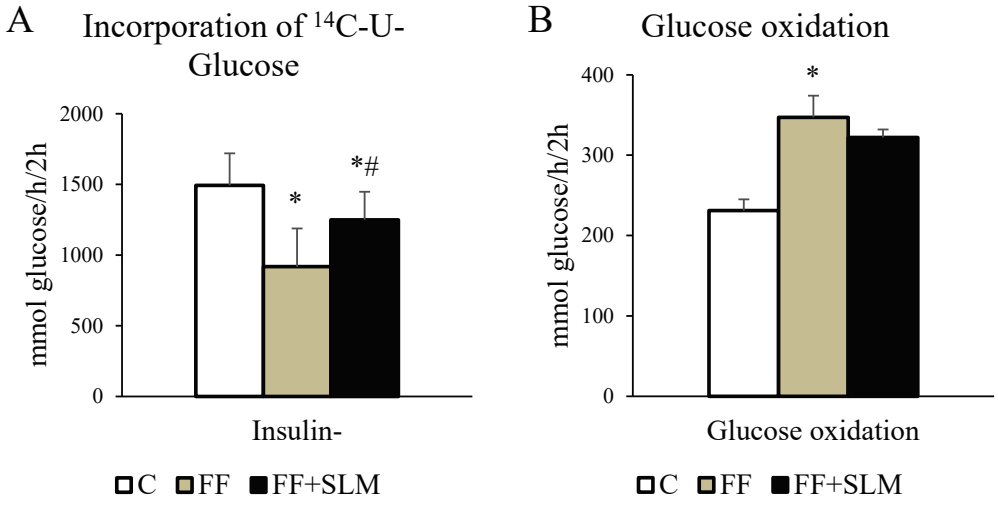


Figure 4. Effect of FF alone and in combination with SLM on basal and insulin-stimulated incorporation of ^{14}C-U-Glucose into glycogen (**A**) and into CO_2 (**B**) in muscle of HHTg rats. Data are expressed as means ± SEM; n = 6–7 animals per group. Abbreviations: C—control; FF—fenofibrate; FF + SLM—fenofibrate + silymarin. Statistically significant differences: * $p < 0.05$ denotes significance versus the control; # $p < 0.05$ denotes significance versus the FF group.

To investigate further the effects of FF on glucose utilization in tissues, we analyzed the basal and insulin-stimulated glucose incorporation into lipids in epididymal adipose tissue (Figure 5). Contrary to our expectations, treatment with FF alone and FF in combination with SLM resulted in a similar increase in basal glucose incorporation into lipids of 30% (both $p < 0.05$) and insulin-stimulated lipid synthesis of 22% and 17% (both NS) compared to the untreated control group.

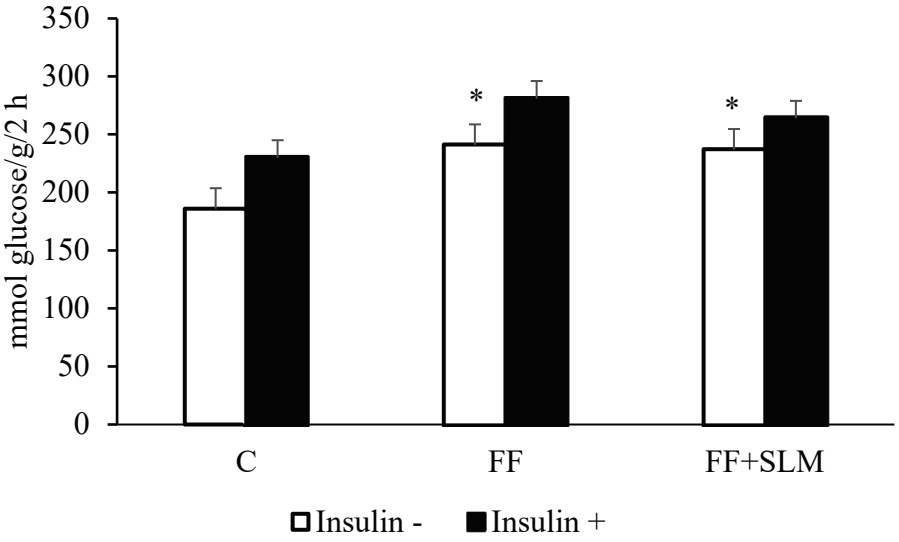


Figure 5. Effect of FF alone and in combination with SLM on basal and insulin-stimulated incorporation of ^{14}C-U-Glucose into in epididymal adipose tissue of HHTg rats. Data are expressed as mean ± SEM; n = 6–7 animals per group. Abbreviations: C—control; FF—fenofibrate; FF + SLM—fenofibrate + silymarin. Statistically significant differences: * $p < 0.05$; denotes significance versus untreated control.

3.4. Effect of Fenofibrate Monotherapy and Combination with Silymarin on Oxidative Stress and Inflammation—Related Parameters

Oxidative stress is a key mediator of cellular damage and inflammation and may contribute to the formation of lipotoxic peroxides, which are involved in the development of the disorders associated with hypertriglyceridemia. We assessed the effect of FF alone and in combination with SLM on hypertriglyceridemia-related oxidative stress in tissues by measuring the activities of antioxidative enzymes, glutathione, and lipoperoxidation products, conjugated dienes, and TBARS. As shown in Table 1, in the liver, FF treatment reduced the expression of Nrf2, an important transcription factor that controls the expression of several genes of antioxidant enzymes. FF therapy also decreased the activity of PON-1 and SOD, and despite the slightly increased activity of GST and catalase, led to increased formation of lipoperoxidation products. Interestingly, the addition of SLM to FF therapy reduced the negative effect of FF as suggested by increasing the activity of SOD, CAT, glutathione-dependent enzymes, and PON-1. Our results further showed that glutathione may play a role in the mechanism of the beneficial effect of SLM on oxidative stress. FF in combination with SLM increased the concentration of the oxidized form of glutathione—GSSG—and the GSH/GSSG ratio, suggesting that it could positively affect the activity of glutathione-dependent enzymes. Further evidence for the positive effect of SLM on oxidative stress was partial to the elimination of FF-induced lipoperoxidation as shown by a reduced TBARS concentration in HHTg rats treated with FF + SLM compared to rats treated with FF alone.

Table 1. Oxidative stress parameters in the liver of HHTg rats treated with fenofibrate alone and FF in combination with silymarin.

Parameter	Control	FF	FF + SLM
Antioxidant system			
Nrf2 expression ($^{\Delta\Delta}$Ct)	1.04 ± 0.32	0.68 ± 0.07 *	0.80 ± 0.06
PON-1 (μM/min/mg prot)	6.07 ± 0.67	4.34 ± 0.74 **	6.48 ± 0.98 ##
SOD (U/mgprot)	0.124 ± 0.015	0.107 ± 0.008 *	0.132 ± 0.017 ##
CAT (mM H_2O_2/min/mg prot)	1341 ± 213	1848 ± 359 *	1951 ± 431 *
GSH-Px (μM NADPH/min/mgprot)	307 ± 32	301 ± 48	330 ± 62
GR (μM NADPH/min/mg prot)	122 ± 19	136 ± 35	132 ± 22
GST (nM CDNB/min/mg prot)	154 ± 25	194 ± 33 *	226 ± 31 *
GSH (μM/mg prot)	42.47 ± 4.97	39.97 ± 1.40	43.84 ± 11.47
GSSG (μM/mg prot)	3.89 ± 0.46	3.51 ± 0.38	2.93 ± 1.04 *#
GSH/GSSG ratio	11.20 ± 2.56	11.73 ± 1.35	15.37 ± 1.06 *#
Lipoperoxidation products			
Conjugated dienes (nM/mgprot)	31.5 ± 5.8	38.0 ± 6.7	38.4 ± 5.9 *
TBARS (nM/mg prot)	1.69 ± 0.44	2.14 ± 0.25 *	1.37 ± 0.32 ##

Data are expressed as means ± SEM; n = 6–7 animals per group. Abbreviations: FF—fenofibrate; FF + SLM—fenofibrate + silymarin; Nrf2—nuclear factor erythroid 2-related factor 2; PON-1—paraoxonase-1; SOD—superoxide dismutase; CAT—catalase; GSH-Px—glutathione peroxidase; GR—glutathione reductase; GST—glutathione transferase; GSH—reduced form of glutathione; GSSG—oxidized form of glutathione; TBARS—thiobarbituric reactive substances. Statistically significant differences: * $p < 0.05$; ** $p < 0.01$ denotes significance versus control; # $p < 0.05$; ## $p < 0.01$ denotes significance versus FF.

In the heart, FF treatment only increased glutathione reductase activity and the production of the initial products of lipid peroxidation, conjugated dienes. Combined treatment with FF + SLM increased the activity of glutathione dependent enzymes—GSH-Px, GR, and GST—and reduced the formation of the final products of lipoperoxidation by 21% ($p < 0.05$) compared to FF-treated rats (Table 2).

Table 2. Oxidative stress parameters in the heart of HHTg rats treated with fenofibrate alone and with combination with silymarin.

Parameter	Control	FF	FF + SLM
Antioxidant system			
SOD (U/mg prot)	0.071 ± 0.011	0.069 ± 0.009	0.065 ± 0.008
GSH-Px (μM NADPH/min/mg prot)	128 ± 11	120 ± 13	162 ± 10 *#
GR (μM NADPH/min/mg prot)	42 ± 4	55 ± 4 *	55 ± 1.8 *
GST (nM CDNB/min/mg prot)	31 ± 3	36 ± 5	46 ± 4 *
CAT (mM H_2O_2/min/mg prot)	486 ± 38	521 ± 39	510 ± 35
GSH (μM/mg prot)	17 ± 1.3	18.4 ± 0.9	18.6 ± 1.1
Lipoperoxidation products			
Conjugated dienes (nM/mg prot)	31.5 ± 5.8	38.0 ± 6.7 *	38.4 ± 5.9 *
TBARS (nM/mg prot)	0.57 ± 0.03	0.59 ± 0.03 *	0.47 ± 0.05 #

Data are expressed as means ± SEM; n = 6–7 animals per group. Abbreviations identical to those in Table 2. Statistically significant differences: * $p < 0.05$ denotes significance versus control; # $p < 0.05$ denotes significance versus FF.

In the kidney cortex, FF therapy led to a slight increase in the activity of antioxidant enzymes GR and GST and to an increase in the production of lipoperoxidation products—conjugated dienes (+70%, $p < 0.05$) and TBARS (+27%, $p < 0.05$)—compared with untreated control. SLM in combination with FF increased GSH-Px activity and reduced the FF-induced increase in conjugated dienes concentration (Table 3).

Table 3. Oxidative stress parameters in the kidney cortex of HHTg rats treated with fenofibrate alone and with combination with silymarin.

Parameter	Control	FF	FF + SLM
Antioxidant system			
SOD (U/mgprot)	0.039 ± 0.004	0.043 ± 0.05	0.057 ± 0.06 *
GSH-Px (μM NADPH/min/mg prot)	111 ± 9	95 ± 7	142 ± 12 #
GR (μM NADPH/min/mg prot)	44 ± 9	53 ± 3 *	40 ± 3 #
GST (nM CDNB/min/mg prot)	56 ± 4	78 ± 4 *	77 ± 7 *
CAT (mM H_2O_2/min/mg prot)	600 ± 39	576 ± 19	601 ± 62
GSH (μM/mg prot)	22.9 ± 1.4	24.0 ± 1.6	18.8 ± 1.6
Lipoperoxidation products			
Conjugated dienes (nM/mg prot)	19.7 ± 1.5	38.0 ± 2.6 *	21.9 ± 2.6 #
TBARS (nM/mg prot)	0.52 ± 0.02	0.66 ± 0.05 *	0.58 ± 0.04

Data are expressed as means ± SEM; n = 6–7 animals per group. Abbreviations identical to those in Table 2. Statistically significant differences: * $p < 0.05$ denotes significance versus control; # $p < 0.05$ denotes significance versus FF.

Oxidative stress appears to be an important mechanism underlying the progression of chronic inflammation and, therefore, we tested the effect of FF and its combination with SLM on serum levels of inflammatory markers. As shown in Table 4, serum concentrations of MCP-1, a chemokine with a pivotal role in the regulation of inflammatory processes by migration and infiltration of monocytes/macrophages, were significantly reduced by FF treatment, while FF in combination with SLM increased concentrations. On the other hand, the FF and FF + SLM treatment had no significant effect on the serum concentrations of inflammatory biomarkers, IL-6 and CRP.

Table 4. Effects of FF alone and in combination with SLM on serum inflammation parameters.

Parameter	Control	FF	FF + SLM
MCP-1 (ng/mL)	3.36 ± 0.85	1.96 ± 0.31 **	2.38 ± 0.58 #
IL-6 (pg/mL)	125 ± 34	105 ± 46	97 ± 45
CRP (μg/mL)	324 ± 39	287 ± 78	279 ± 40

Data are expressed as means ± SEM; n = 6–7 animals per group. Abbreviations: FF—fenofibrate; FF + SLM—fenofibrate + silymarin; protein; MCP-1—monocyte chemoattractant protein-1; IL-6—interleukin 6; CRP—C reactive protein. Statistically significant differences: ** $p < 0.01$ denotes significance versus control; # $p < 0.05$ denotes significance versus FF.

3.5. Effects of Fenofibrate Monotherapy and Combination with Silymarin on Gene Expression

To search for the mechanisms responsible for the effects of FF in combination with SLM on lipid metabolism, the expression of genes in the liver was analyzed. Sterol regulatory element binding proteins (SREBPs) are transcription factors that regulate genes involved in cholesterol, fatty acid, and triglyceride synthesis. The gene expression of Srebf1 was not affected by experimental therapy (Figure 6A) but Srebf2 gene expression was decreased in rats treated with FF (−42%; $p < 0.01$) or FF + SLM (−50%; $p < 0.01$) compared to control animals (Figure 6B). The question of whether the effects of SLM are mediated by the activation of PPARα has not yet been clarified. The results shown in Figure 6C show that while PPARα expression was stimulated by FF (+60%; $p < 0.05$), SLM did not affect expression. This is consistent with the fact that FF improves dyslipidemia by mediating PPARα.

There was no difference between groups in the gene expression of Nr1h3 encoding liver X receptor alpha (LXRα) (Figure 6D). In contrast, FF alone and in combination with SLM suppressed Nr1h4 gene expression (−59%; $p < 0.01$), encoding farnesoid X receptor (Figure 6E). The gene expression of retinoid X receptor α (Rxrα) was slightly decreased in

rats treated with FF alone and in combination with SLM compared with untreated controls (Figure 6F). Further results showed that FF alone (−42%; $p < 0.01$) and in combination with SLM (−57%; $p < 0.01$) reduced the expression of the Slco1a1, a bile acid uptake transporter gene (Figure 6G).

Next, we analyzed the relative expression of transcription factor Nrf2, which is a regulator of multiple genes involved in protection against oxidative stress. We found (Figure 6H) that FF significantly decreased expression in comparison with untreated controls (−35%; $p < 0.05$), and the addition of SLM to FF therapy partially decreased this negative impact (+18%; $p = 0.28$) compared with FF alone treatment. It can be summarized that treatment with SLM alone did not affect the expression of the analyzed genes compared to the untreated control group. In contrast, FF therapy increased the expression of PPARα and downregulated the gene expression of Srebf2, Nr1h4, Rxrα, Slco1a1, and Nrf2. Combining FF therapy with SLM, despite a slight increase in Nrf2 expression, did not affect the changes in the expression of genes involved in lipid metabolism induced by FF therapy alone.

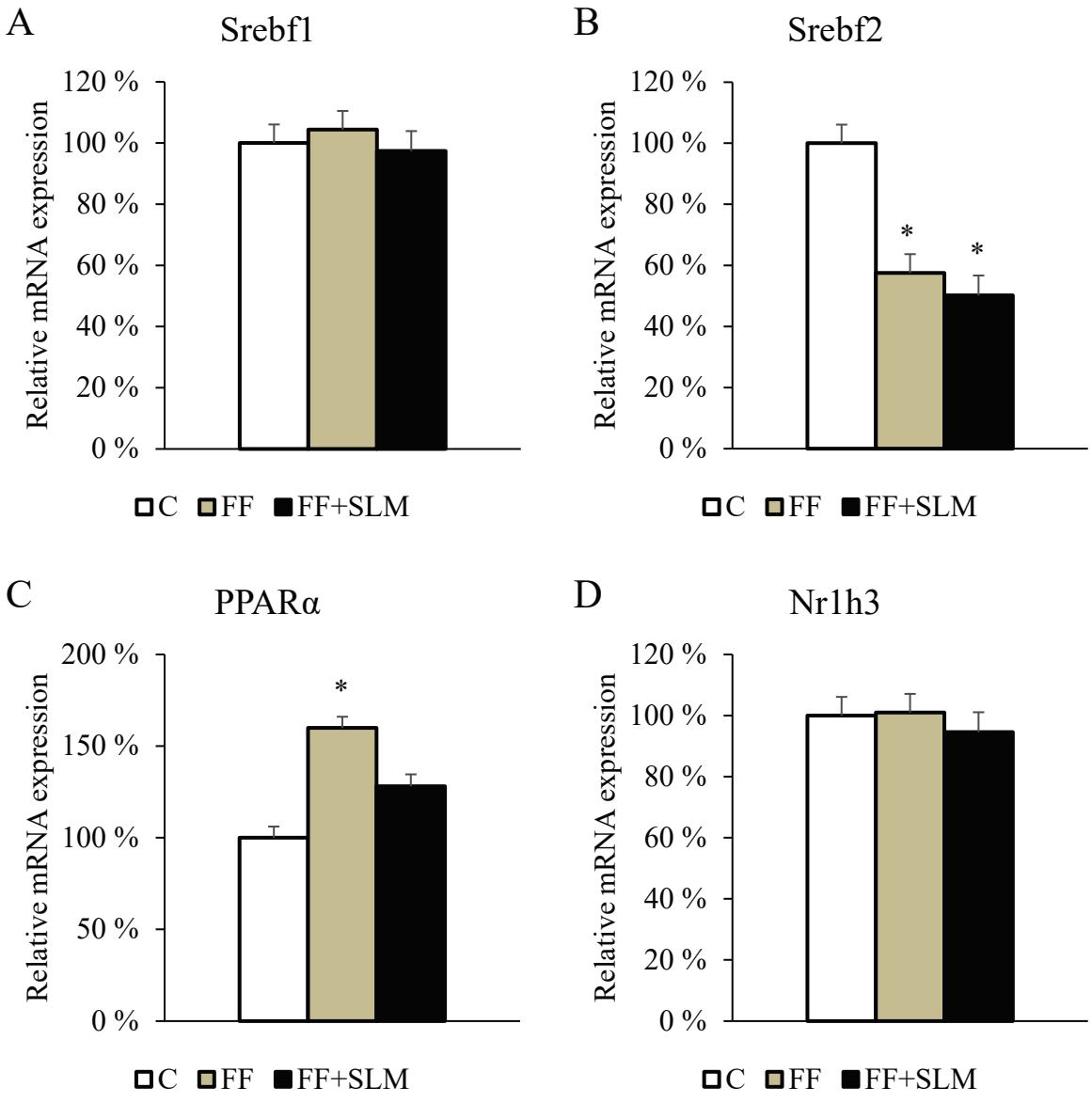


Figure 6. *Cont.*

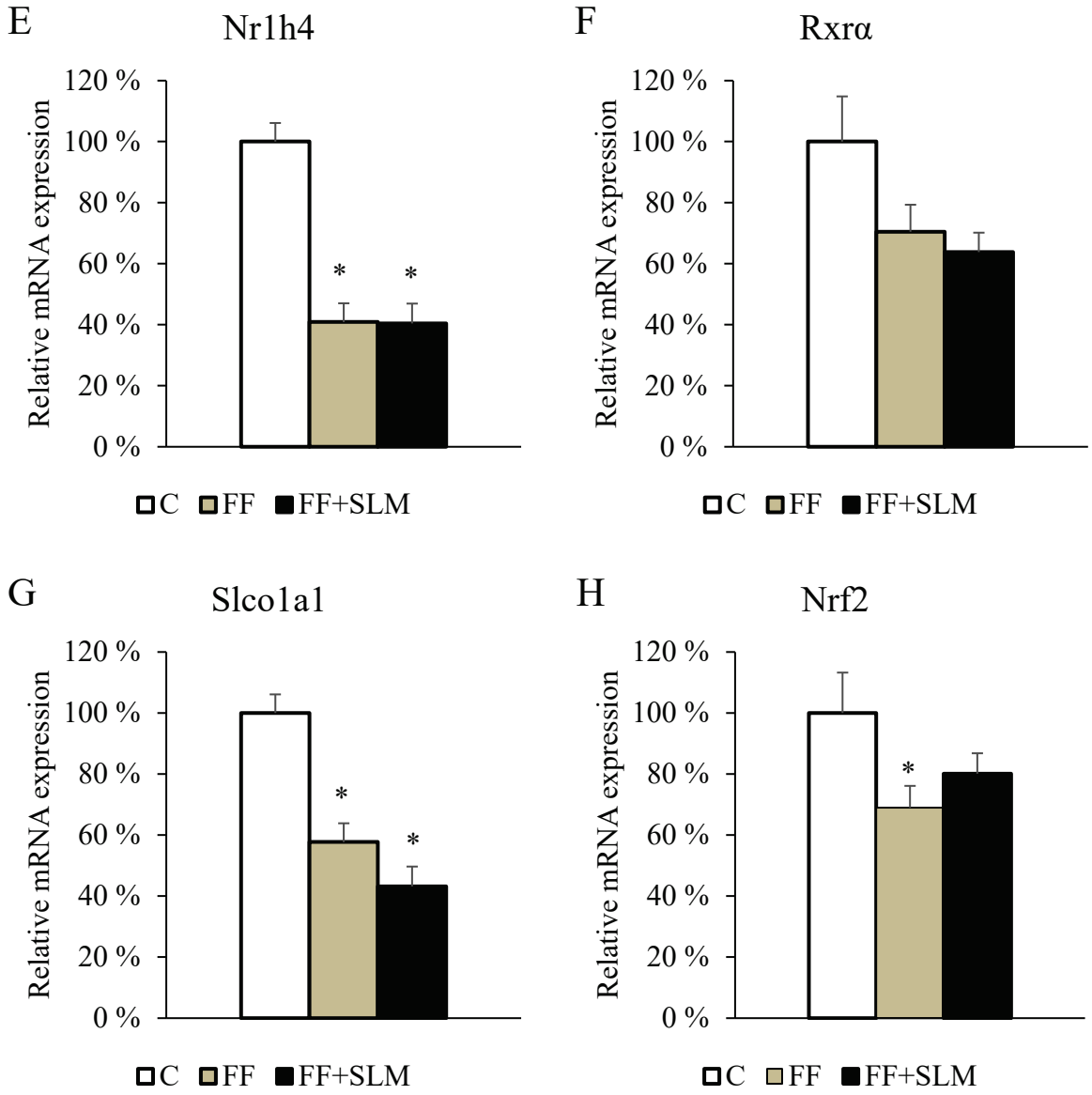


Figure 6. Relative mRNA expression of selected genes involved in lipid metabolism in the liver of HHTg rats treated with FF and combination of FF + SLM compared to untreated HHTg control rats. Data are expressed as means ± SEM; n = 6–7 animals per group. Abbreviations: C—control; FF—fenofibrate; FF + SLM—fenofibrate + silymarin. Statistically significant differences: * $p < 0.05$ denotes significance versus the control group.

4. Discussion

One of the most commonly used drugs for the treatment of hypertriglyceridemia is fenofibrate. This effectively decreases blood triglycerides, including atherogenic chylomicron and very low-density lipoprotein remnants [40]. In contrast, in well-controlled clinical trials, neither fenofibrate nor pemafibrate reduced cardiovascular disease [15–17]. The beneficial effect of lowering triglycerides on the risk of developing metabolic syndrome has also not been clearly proven [41,42]. Moreover, in some studies, fibrate treatment is associated with an increased risk of liver damage and renal dysfunction [20–22]. The underlying causes and preventive measures for their elimination remain unclear.

In this study, we investigated the effect of FF monotherapy on metabolic disorders caused by genetically determined hypertriglyceridemia. We further tested whether it is

possible to alleviate some adverse effects of FF by combining the therapy of FF with that of SLM, which exhibits antioxidant, anti-inflammatory, and cardioprotective properties [27].

The study was conducted on a unique strain of rats with genetically determined hypertriglyceridemia exhibiting skeletal muscle and liver steatosis, insulin resistance, mild hypertension, and oxidative stress in tissues. This model is currently well established for the study of the pathogenesis and treatment of hypertriglyceridemia and its consequences [30,32,34,38]. In addition, metabolic disorders in HHTg rats resemble a situation comparable to human conditions, where genetic predisposition is the main cause of the hypertriglyceridemia.

Our results showed that in HHTg rats, FF treatment reduced the levels of serum triglycerides, NEFA, and triglyceride accumulation in the liver, which is consistent with the known effects of FF. FF treatment reduced visceral fat depots in HHTg rats as assessed by epididymal and perirenal fat pad weights. The number of triglycerides in adipose tissue is determined by the intake of fatty acids from circulating lipoproteins, de novo synthesis of fatty acids in adipose tissue, and/or release of fatty acids from stored triglycerides in adipocytes. Detailed analysis showed that that FF treatment reduced lipid accumulation in adipose tissue not only by the increased release of fatty acids from adipose tissue but also by the newly observed reduced re-esterification of fatty acids to triglycerides, which is a necessary step before being stored in adipocytes (Figure 3).

The data from this study provide innovative information about the effect of FF on the mechanisms that may contribute to the fact that the hypotriglyceridemic effect of FF does not reduce the risk of CVD and insulin resistance. These include the findings that FF therapy decreased fatty acids re-esterification and their reduced storage as triglycerides in adipose tissue, which may lead to their increased ectopic storage (outside adipose tissue) even in the presence of lower circulating triglyceride levels. This disorder may also result in reduced glucose utilization for muscle glycogen synthesis, which represents the majority of postprandial glucose disposal and contributes to insulin resistance.

Increased accumulation of triglycerides and their intermediates, diacylglycerols and ceramides, in non-adipose tissues is one of the most serious complications associated with hypertriglyceridemia. Increased lipid accumulation in muscle is connected to muscle insulin resistance [43]; in the liver, it leads to insulin resistance [39]; in the kidney, it can cause nephropathy [44]; and in the heart and blood vessels, it can result in reduced ventricular compliance and an increased risk of atherosclerosis [45,46]. Despite these facts, intramuscular lipids are rarely analyzed in studies. Our results showing the inability of FF to reduce ectopic triglyceride storage in muscle in hereditary hypertriglyceridemia are inconsistent with the results in high-fat-fed animal models, in which clofibrate, gemfibrozil, and WY14643 reduced muscle triglycerides [47]. Reduced intramuscular lipid accumulation has also been observed in high-fat-diet-induced obesity in mice treated with FF [48]. In contrast, in clinical studies, FF administration did not affect muscle triglyceride accumulation [18,19], similar to our study. Further studies should verify whether the observed differences between diet and genetically induced obesity can explain the differences in resistance to lipid-lowering therapy.

Our study showed that another mechanism that may influence the inability of FF to reduce glucose metabolism disorders in hypertriglyceridemia is the observed reduced glucose incorporation into muscle glycogen in FF treated rats. The significance of this finding is of primary importance because reduced glycogen synthesis in muscles is the underlying cause of insulin resistance. Reports to date investigating the effects of fenofibrate on insulin resistance are equivocal. While improved insulin sensitivity with fibrate treatment has been generally observed in rodent models [47], it has been virtually never observed in human

studies [18,19]. Our findings in HHTg rats are similar to those in humans, where FF did not affect muscle triglyceride concentration [18].

Our results suggest that the reason for the reduced utilization of glucose for glycogen synthesis may be the increased utilization for the oxidation of glucose in muscle as an energy substrate at lower levels of circulating fatty acids.

Oxidative stress and inflammation are considered key mechanisms in the progression of hypertriglyceridemia to insulin resistance, diabetes, and cardiovascular complications [48], but the findings on the effect of FF on oxidative stress in metabolic syndrome and diabetes remain unclear. It has been found that FF treatment can reduce, not affect or even aggravate, oxidative stress [22,49,50]. In this study, we show new findings about the effect of FF therapy on increased oxidative stress in tissues in genetically determined hypertriglyceridemia. HHTg rats treated with FF alone showed increased oxidative stress in the liver, kidney cortex, and, to a small extent, also in the heart. In the liver, FF therapy reduced the activity of SOD and PON-1, and elevated concentrations of lipid peroxidation products. The effect of FF on the decrease in PON-1 activity is an important new finding that could contribute to explaining the inability of FF to reduce cardiovascular disorders. This enzyme hydrolyses oxidized lipids and protects microvascular complications caused by oxidative stress, and its decreased activity has been associated with an increase in the incidence of cardiovascular disease [51,52]. These changes in the antioxidant system were associated with a markedly reduced expression of transcription factor Nrf2, a crucial regulator of the cellular defense against oxidative stress.

Oxidative stress is associated with the induction of inflammation processes. We found that in HHTg rats, FF therapy only reduced serum MCP-1 concentrations, while CRP and IL-6 levels were not affected.

To search for the mechanisms responsible for the lipid-lowering effects of FF, we analyzed the hepatic mRNA expression of genes encoding transcription factors involved in lipid metabolism. FF treatment markedly increased the gene expression of PPARα, which is consistent with the known fact that FF exerts lipid-lowering effects through the upregulation of the transcription factor PPARα that regulates genes involved in fatty acid uptake, as well as their metabolism, and increased lipid oxidation [53]. In contrast, FF downregulated the expression of Nr1h4 encoding farnesoid X receptor, Rxrα, and Slco1a1, a bile acid uptake transporter gene.

Oxidative stress is associated with the induction of inflammation processes. We found that in HHTg rats, FF therapy only reduced serum MCP-1 concentrations, while CRP and IL-6 levels were not affected.

In this study, we provide new findings showing that the addition of SLM to FF therapy alleviates the adverse effects of FF on some metabolic parameters that could reduce the effectiveness of FF in influencing the risks of cardiovascular diseases and insulin resistance. A significant finding was that SLM alleviated the FF-induced adverse effect on muscle glucose utilization for glycogen synthesis (Figure 2). Given that skeletal muscle is the main tissue responsible for tissue glucose utilization and insulin action, and is, therefore, considered a major site for the development of insulin resistance and type 2 diabetes, this finding is important. The beneficial effect of SLM on insulin resistance has also been observed in a clinical trial [54]. A consequence of the positive effect of SLM on glycogen synthesis may be a reduced postprandial insulin level in rats treated with FF in combination with SLM (Table 1).

Another beneficial effect of SLM was the reduction in oxidative stress, especially in the liver, but also in the myocardium and kidneys, as shown by the reduced activity of the antioxidant system and the increased formation of lipid peroxidation products, conjugated dienes, and TBARS. The beneficial effect of SLM on hepatic PON-1 activity is an important

new finding because this enzyme hydrolyses oxidized lipids and protects microvascular complications caused by oxidative stress, and its decreased activity has been associated with an increase in the incidence of cardiovascular disease [51,52]. The beneficial effect of SLM on oxidative stress may be related to the antioxidant activity, which may be a consequence of direct free radical scavenging, a reduced production of reactive oxygen substances in mitochondria, and an increase in antioxidant defense via nuclear transcription factor Nrf2, a crucial regulator of the cellular defense against oxidative stress [55–57]. Our results show that a marked decrease in Nrf2 expression in FF-treated rats can be attenuated by SLM therapy, although the increase was not statistically significant.

Our study is limited by the small number of animals in the groups (n = 6–7). Since HHTg rats are bred in a brother x sister system, variances between animals are minimized.

5. Conclusions

Our results show that in a model of genetically determined hypertriglyceridemia, FF monotherapy effectively reduces serum concentrations of triglycerides, NEFA, in the liver and reduced the accumulation of triglycerides and the expression of genes encoding transcription factors involved in lipid metabolism. The results provide new findings that the FF-induced reduction of visceral adipose tissue is a consequence of not only reduced lipolysis but also of the reduced re-esterification of fatty acids and their deposition in adipose tissue. New findings that could partially explain the failure of FF therapy to reduce insulin resistance and cardiovascular disorders are reduced glucose utilization in muscle tissue for glycogen synthesis, and lowered activity of the antioxidant system associated with increased lipid peroxidation in the liver and, to a lesser extent, in heart and kidneys, where ectopic triglyceride accumulation was not reduced by FF. Adding SLM to FF therapy increased the utilization of glucose in muscles, and reduced hyperinsulinemia, which indicates improvement in insulin resistance. In line with the known hepatoprotective effects of SLM, its beneficial effect on lipid metabolism and the antioxidant system was most evident in the liver and less so in the heart and kidneys. Our findings should be the basis for verification in clinical studies. Also, the search for other options to increase the effectiveness of FF therapy by combining it with substances with antioxidant and anti-inflammatory effects to increase the effectiveness of FF therapy in reducing the risk of cardiovascular disorders and type 2 diabetes should be the subject of further studies. Given the suggested differences in the effectiveness of hypolipidemic therapy between dietary and genetically induced hypertriglyceridemia, these differences should be analyzed in more detail.

Author Contributions: J.S., R.V., M.P., Z.R. and L.K. designed the experiments, analyzed the data, and participated in the writing of the manuscript; H.M., M.H., O.O., I.M., D.M., S.G. and Z.R. performed the experiments, analyzed the data, and reviewed the manuscript. All authors have read and agreed to the published version of the manuscript.

Funding: This study was supported by grant IGA_LF_2024_006 of the Internal Grant Agency of Palacky University Olomouc, a grant from the Czech Science Foundation and by the Ministry of Health of the Czech Republic under its program for the conceptual development of research organizations (Institute for Clinical and Experimental Medicine–IKEM, IN 00023001).

Institutional Review Board Statement: The animal study protocol was approved by the Ethics Committee of the Ministry of Health of the Czech Republic and IKEM's Ethics Committee (Protocol Number: 28/2016).

Informed Consent Statement: Not applicable.

Data Availability Statement: Data is contained within the article.

Conflicts of Interest: The authors declare no conflicts of interest.

Abbreviations

The following abbreviations are used in this manuscript:

CAT	Catalase
CRP	C-reactive protein
FF	Fenofibrate
FXRα	Farnesoid X receptor
GR	Glutathione reductase
GSH	Glutathione
GSH-Px	Glutathione peroxidase
GSSG	Oxidized form of glutathione
HDL	High-density lipoproteins
HHTg	Hereditary hypertriglyceridemic rat
HMW	High molecular weight
Hprt1	Hypoxanthine phosphoribosyltransferase 1
IL-6	Interleukin 6
LDL	Low-density lipoprotein
LXRα	Liver X receptor alpha
MCP-1	Monocyte chemoattractant protein
NEFA	Non-esterified fatty acid
Nr1h3	Nuclear receptor subfamily 1, group H, member 3
Nr1h4	Nuclear receptor subfamily 1, group H, member 4
Nrf2	Nuclear factor erythroid 2-related factor 2
PON-1	Paraoxonase-1
PPARα	Peroxisome proliferator-activated receptor alpha
Rxrα	Retinoid X receptor alpha
Slco1a1	Solute carrier organic anion transporter 1a1
SLM	Silymarin
SOD	Superoxide dismutase
Srebf1	Sterol regulatory element-binding protein 1
Srebf2	Sterol regulatory element-binding protein 2
TAG	Triglyceride
TBAR	Thiobarbituric reactive substances
TRL	Triglyceride-rich lipoproteins
VLDL	Very-low-density lipoproteins
$^{\Delta\Delta}$Ct	Double Delta Ct

References

1. Aggarwal, R.; Bhatt, D.L.; Rodriguez, F.; Yeh, R.W.; Wadhera, R.K. Trends in Lipid Concentrations and Lipid Control Among US Adults, 2007–2018. *JAMA* **2022**, *328*, 737–745. [CrossRef] [PubMed]
2. Fan, W.; Philip, S.; Granowitz, C.; Toth, P.P.; Wong, N.D. Hypertriglyceridemia in Statin-Treated US Adults: The National Health and Nutrition Examination Survey. *J. Clin. Lipidol.* **2019**, *13*, 100–108. [CrossRef] [PubMed]
3. Dron, J.S.; Wang, J.; Cao, H.; McIntyre, A.D.; Iacocca, M.A.; Menard, J.R.; Movsesyan, I.; Malloy, M.J.; Pullinger, C.R.; Kane, J.P.; et al. Severe Hypertriglyceridemia Is Primarily Polygenic. *J. Clin. Lipidol.* **2019**, *13*, 80–88. [CrossRef]
4. Hegele, R.A.; Ginsberg, H.N.; Chapman, M.J.; Nordestgaard, B.G.; Kuivenhoven, J.A.; Averna, M.; Borén, J.; Bruckert, E.; Catapano, A.L.; Descamps, O.S.; et al. The Polygenic Nature of Hypertriglyceridaemia: Implications for Definition, Diagnosis, and Management. *Lancet Diabetes Endocrinol.* **2013**, *2*, 655. [CrossRef]
5. Duran, E.K.; Pradhan, A.D. Triglyceride-Rich Lipoprotein Remnants and Cardiovascular Disease. *Clin. Chem.* **2021**, *67*, 183–196. [CrossRef]
6. Tybjærg-Hansen, A.; Nordestgaard, B.G.; Christoffersen, M. Triglyceride-Rich Remnant Lipoproteins Are More Atherogenic than LDL per Particle: Is This Important? *Eur. Heart J.* **2023**, *44*, 4196–4198. [CrossRef]

7. Raposeiras-Roubin, S.; Rosselló, X.; Oliva, B.; Fernández-Friera, L.; Mendiguren, J.M.; Andrés, V.; Bueno, H.; Sanz, J.; Martínez de Vega, V.; Abu-Assi, E.; et al. Triglycerides and Residual Atherosclerotic Risk. *J. Am. Coll. Cardiol.* **2021**, *77*, 3031–3041. [CrossRef]
8. Peng, X.; Wu, H. Inflammatory Links Between Hypertriglyceridemia and Atherogenesis. *Curr. Atheroscler. Rep.* **2022**, *24*, 297–306. [CrossRef]
9. Wu, X.; Wang, Y.; Jia, Y.; Liu, J.; Wang, G. Risk Factors for Nonalcoholic Fatty Liver Disease with Different Insulin Resistance in a Nonobese Chinese Population. *J. Diabetes Res.* **2022**, *2022*, 9060405. [CrossRef]
10. Nakamura, M.; Sadoshima, J. Cardiomyopathy in Obesity, Insulin Resistance and Diabetes. *J. Physiol.* **2020**, *598*, 2977–2993. [CrossRef]
11. Samuel, V.T.; Shulman, G.I. The Pathogenesis of Insulin Resistance: Integrating Signaling Pathways and Substrate Flux. *J. Clin. Investig.* **2016**, *126*, 12–22. [CrossRef] [PubMed]
12. Pontremoli, R.; Desideri, G.; Arca, M.; Temporelli, P.L.; Perrone, V.; Dovizio, M.; Borghi, C.; Esposti, L.D. Hypertriglyceridemia Is Associated with Decline of Estimated Glomerular Filtration Rate and Risk of End-Stage Kidney Disease in a Real-Word Italian Cohort: Evidence from the TG-RENAL Study. *Eur. J. Intern. Med.* **2023**, *111*, 90–96. [CrossRef] [PubMed]
13. McCullough, P.A.; Ahmed, A.B.; Zughaib, M.T.; Glanz, E.D.; Di Loreto, M.J. Treatment of Hypertriglyceridemia with Fibric Acid Derivatives: Impact on Lipid Subfractions and Translation into a Reduction in Cardiovascular Events. *Rev. Cardiovasc. Med.* **2011**, *12*, 173–185. [CrossRef]
14. Yu, X.H.; Zheng, X.L.; Tang, C.K. Peroxisome Proliferator-Activated Receptor α in Lipid Metabolism and Atherosclerosis. *Adv. Clin. Chem.* **2015**, *71*, 171–203. [CrossRef]
15. Keech, A.; Simes, R.J.; Barter, P.; Best, J.; Scott, R.; Taskinen, M.R.; Forder, P.; Pillai, A.; Davis, T.; Glasziou, P.; et al. Effects of Long-Term Fenofibrate Therapy on Cardiovascular Events in 9795 People with Type 2 Diabetes Mellitus (the FIELD Study): Randomised Controlled Trial. *Lancet* **2005**, *366*, 1849–1861. [CrossRef]
16. Ginsberg, H.N.; Elam, M.B.; Lovato, L.C.; Crouse, J.R., III; Leiter, L.A.; Linz, P.; Friede-wald, W.T.; Buse, J.B.; Gerstein, H.C.; Probst-field, J.; et al. Effects of Combination Lipid Therapy in Type 2 Diabetes Mellitus. *N. Engl. J. Med.* **2010**, *362*, 1563–1574. [CrossRef]
17. Das Pradhan, A.; Glynn, R.J.; Fruchart, J.-C.; MacFadyen, J.G.; Zaharris, E.S.; Everett, B.M.; Campbell, S.E.; Oshima, R.; Amarenco, P.; Blom, D.J.; et al. Triglyceride Lowering with Pemafibrate to Reduce Cardiovascular Risk. *N. Engl. J. Med.* **2022**, *387*, 1923–1934. [CrossRef]
18. Perreault, L.; Bergman, B.C.; Hunerdosse, D.M.; Howard, D.J.; Eckel, R.H. Fenofibrate Administration Does Not Affect Muscle Triglyceride Concentration or Insulin Sensitivity in Humans. *Metabolism* **2011**, *60*, 1107–1114. [CrossRef]
19. Belfort, R.; Berria, R.; Cornell, J.; Cusi, K. Fenofibrate Reduces Systemic Inflammation Markers Independent of Its Effects on Lipid and Glucose Metabolism in Patients with the Metabolic Syndrome. *J. Clin. Endocrinol. Metab.* **2010**, *95*, 829–836. [CrossRef]
20. Kostapanos, M.S.; Florentin, M.; Elisaf, M.S. Fenofibrate and the Kidney: An Overview. *Eur. J. Clin. Investig.* **2013**, *43*, 522–531. [CrossRef]
21. Ahmad, J.; Odin, J.A.; Hayashi, P.H.; Chalasani, N.; Fontana, R.J.; Barnhart, H.; Cirulli, E.T.; Kleiner, D.E.; Hoofnagle, J.H. Identification and Characterization of Fenofibrate-Induced Liver Injury. *Dig. Dis. Sci.* **2017**, *62*, 3596–3604. [CrossRef] [PubMed]
22. Škop, V.; Trnovská, J.; Oliyarnyk, O.; Marková, I.; Malínská, H.; Kazdová, L.; Zídek, V.; Landa, V.; Mlejnek, P.; Šimáková, M.; et al. Hepatotoxic Effects of Fenofibrate in Spontaneously Hypertensive Rats Expressing Human C-Reactive Protein. *Physiol. Res.* **2016**, *65*, 891–899. [CrossRef] [PubMed]
23. Miller, M. Pemafibrate and Other Triglyceride-Lowering Therapies to Reduce Risk of Cardiovascular and Metabolic Disease. *Curr. Opin. Cardiol.* **2024**, *39*, 286–291. [CrossRef] [PubMed]
24. Škottová, N.; Kazdová, L.; Oliyarnyk, O.; Večeřa, R.; Sobolová, L.; Ulrichová, J. Phenolics-Rich Extracts from *Silybum marianum* and *Prunella vulgaris* Reduce a High-Sucrose Diet Induced Oxidative Stress in Hereditary Hypertriglyceridemic Rats. *Pharmacol. Res.* **2004**, *50*, 123–130. [CrossRef]
25. Tajmohammadi, A.; Razavi, B.M.; Hosseinzadeh, H. *Silybum marianum* (Milk Thistle) and Its Main Constituent, Silymarin, as a Potential Therapeutic Plant in Metabolic Syndrome: A Review. *Phytother. Res.* **2018**, *32*, 1933–1949. [CrossRef]
26. Poruba, M.; Kazdová, L.; Oliyarnyk, O.; Malinská, H.; Matusková, Z.; Tozzi Di Angelo, I.; Skop, V.; Vecera, R. Improvement Bioavailability of Silymarin Ameliorates Severe Dyslipidemia Associated with Metabolic Syndrome. *Xenobiotica* **2015**, *45*, 751–756. [CrossRef]
27. Wadhwa, K.; Pahwa, R.; Kumar, M.; Kumar, S.; Sharma, P.C.; Singh, G.; Verma, R.; Mittal, V.; Singh, I.; Kaushik, D.; et al. Mechanistic Insights into the Pharmacological Significance of Silymarin. *Molecules* **2022**, *27*, 5327. [CrossRef]
28. Mengs, U.; Torsten Pohl, R.-; Mitchell, T. Legalon® SIL: The Antidote of Choice in Patients with Acute Hepatotoxicity from Amatoxin Poisoning. *Curr. Pharm. Biotechnol.* **2012**, *13*, 1964–1970. [CrossRef]
29. Ferenci, P.; Beinhardt, S. Silibinin: An Old Drug in the High Tech Era of Liver Transplantation. *J. Hepatol.* **2013**, *58*, 409–411. [CrossRef]

30. Vrána, A.; Kazdová, L. The Hereditary Hypertriglyceridemic Nonobese Rat: An Experimental Model of Human Hypertriglyceridemia. *Transplant. Proc.* **1990**, *22*, 2579.
31. Kazdová, L.; Žák, A.; Vrána, A. Increased Lipoprotein Oxidability and Aortic Lipid Peroxidation in an Experimental Model of Insulin Resistance Syndromea. *Ann. N. Y Acad. Sci.* **1997**, *827*, 521–525. [CrossRef] [PubMed]
32. Zicha, J.; Pecháňová, O.; Čačányiová, S.; Cebová, M.; Kristek, F.; Török, J.; Šimko, F.; Dobešová, Z.; Kuneš, J. Hereditary Hypertriglyceridemic Rat: A Suitable Model of Cardiovascular Disease and Metabolic Syndrome? *Physiol. Res.* **2006**, *55*, 49–63. [CrossRef] [PubMed]
33. Markova, I.; Miklankova, D.; Hüttl, M.; Kacer, P.; Skibova, J.; Kucera, J.; Sedlacek, R.; Kacerova, T.; Kazdova, L.; Malinska, H. The Effect of Lipotoxicity on Renal Dysfunction in a Nonobese Rat Model of Metabolic Syndrome: A Urinary Proteomic Approach. *J. Diabetes Res.* **2019**, *2019*, 8712979. [CrossRef] [PubMed]
34. Malinska, H.; Hüttl, M.; Oliyarnyk, O.; Bratova, M.; Kazdova, L. Conjugated Linoleic Acid Reduces Visceral and Ectopic Lipid Accumulation and Insulin Resistance in Chronic Severe Hypertriacylglycerolemia. *Nutrition* **2015**, *31*, 1045–1051. [CrossRef] [PubMed]
35. Malínská, H.; Oliyarnyk, O.; Hubová, M.; Zídek, V.; Landa, V.; Šimáková, M.; Mlejnek, P.; Kazdová, L.; Kurtz, T.W.; Pravenec, M. Increased Liver Oxidative Stress and Altered PUFA Metabolism Precede Development of Non-Alcoholic Steatohepatitis in SREBP-1a Transgenic Spontaneously Hypertensive Rats with Genetic Predisposition to Hepatic Steatosis. *Mol. Cell Biochem.* **2010**, *335*, 119–125. [CrossRef]
36. Pravenec, M.; Kazdová, L.; Maxová, M.; Zídek, V.; Mlejnek, P.; Šimáková, M.; Kurtz, T.W. Long-Term Pioglitazone Treatment Enhances Lipolysis in Rat Adipose Tissue. *Int. J. Obes.* **2008**, *32*, 1848–1853. [CrossRef]
37. Pravenec, M.; Kazdová, L.; Landa, V.; Zídek, V.; Mlejnek, P.; Jansa, P.; Wang, J.; Qi, N.; Kurtz, T.W. Transgenic and Recombinant Resistin Impair Skeletal Muscle Glucose Metabolism in the Spontaneously Hypertensive Rat. *J. Biol. Chem.* **2003**, *278*, 45209–45215. [CrossRef]
38. Qi, N.; Kazdova, L.; Zidek, V.; Landa, V.; Kren, V.; Pershadsingh, H.A.; St. Lezin, E.; Abumrad, N.A.; Pravenec, M.; Kurtz, T.W. Pharmacogenetic Evidence That Cd36Is a Key Determinant of the Metabolic Effects of Pioglitazone. *J. Biol. Chem.* **2002**, *277*, 48501–48507. [CrossRef]
39. Ramnanan, C.J.; Edgerton, D.S.; Rivera, N.; Irimia-Dominguez, J.; Farmer, B.; Neal, D.W.; Lautz, M.; Donahue, E.P.; Meyer, C.M.; Roach, P.J.; et al. Molecular Characterization of Insulin-Mediated Suppression of Hepatic Glucose Production in Vivo. *Diabetes* **2010**, *59*, 1302–1311. [CrossRef]
40. Canfora, I.; Pierno, S. Hypertriglyceridemia Therapy: Past, Present and Future Perspectives. *Int. J. Mol. Sci.* **2024**, *25*, 9727. [CrossRef]
41. Anderlová, K.; Doležalová, R.; Housová, J.; Bošanská, L.; Haluzíková, D.; Křemen, J.; Škrha, J.; Haluzík, M. Influence of PPAR-Alpha Agonist Fenofibrate on Insulin Sensitivity and Selected Adipose Tissue-Derived Hormones in Obese Women with Type 2 Diabetes. *Physiol. Res.* **2007**, *56*, 579–586. [CrossRef] [PubMed]
42. Abbasi, F.; Chen, Y.D.I.; Farin, H.M.F.; Lamendola, C.; Reaven, G.M. Comparison of Three Treatment Approaches to Decreasing Cardiovascular Disease Risk in Nondiabetic Insulin-Resistant Dyslipidemic Subjects. *Am. J. Cardiol.* **2008**, *102*, 64–69. [CrossRef] [PubMed]
43. Borén, J.; Taskinen, M.R.; Olofsson, S.O.; Levin, M. Ectopic Lipid Storage and Insulin Resistance: A Harmful Relationship. *J. Intern. Med.* **2013**, *274*, 25–40. [CrossRef] [PubMed]
44. Gröne, E.F.; Walli, A.K.; Gröne, H.J.; Miller, B.; Seidel, D. The Role of Lipids in Nephrosclerosis and Glomerulosclerosis. *Atherosclerosis* **1994**, *107*, 1–13. [CrossRef]
45. Saric, M.; Kronzon, I. Aortic Atherosclerosis and Embolic Events. *Curr. Cardiol. Rep.* **2012**, *14*, 342–349. [CrossRef]
46. Sarma, S.; Carrick-Ranson, G.; Fujimoto, N.; Adams-Huet, B.; Bhella, P.S.; Hastings, J.L.; Shafer, K.M.; Shibata, S.; Boyd, K.; Palmer, D.; et al. Effects of Age and Aerobic Fitness on Myocardial Lipid Content. *Circ. Cardiovasc. Imaging* **2013**, *6*, 1048–1055. [CrossRef]
47. Lee, H.J.; Choi, S.S.; Park, M.K.; An, Y.J.; Seo, S.Y.; Kim, M.C.; Hong, S.H.; Hwang, T.H.; Kang, D.Y.; Garber, A.J.; et al. Fenofibrate Lowers Abdominal and Skeletal Adiposity and Improves Insulin Sensitivity in OLETF Rats. *Biochem. Biophys. Res. Commun.* **2002**, *296*, 293–299. [CrossRef]
48. Włodarski, A.; Strycharz, J.; Wróblewski, A.; Kasznicki, J.; Drzewoski, J.; Śliwińska, A. The Role of MicroRNAs in Metabolic Syndrome-Related Oxidative Stress. *Int. J. Mol. Sci.* **2020**, *21*, 6902. [CrossRef]
49. Olukman, M.; Sezer, E.D.; Ülker, S.; Szmen, E.Y.; Çnar, G.M. Fenofibrate Treatment Enhances Antioxidant Status and Attenuates Endothelial Dysfunction in Streptozotocin-Induced Diabetic Rats. *Exp. Diabetes Res.* **2010**, *2010*, 828531. [CrossRef]
50. Abd El-Haleim, E.A.; Bahgat, A.K.; Saleh, S. Resveratrol and Fenofibrate Ameliorate Fructose-Induced Nonalcoholic Steatohepatitis by Modulation of Genes Expression. *World J. Gastroenterol.* **2016**, *22*, 2931–2948. [CrossRef]
51. Shunmoogam, N.; Naidoo, P.; Chilton, R. Paraoxonase (PON)-1: A Brief Overview on Genetics, Structure, Polymorphisms and Clinical Relevance. *Vasc. Health Risk Manag.* **2018**, *14*, 137–143. [CrossRef] [PubMed]

52. Kowalska, K.; Socha, E.; Milnerowicz, H. Review: The Role of Paraoxonase in Cardiovascular Diseases. *Ann. Clin. Lab. Sci.* **2015**, *45*, 226–233. [PubMed]
53. Montagner, A.; Polizzi, A.; Fouché, E.; Ducheix, S.; Lippi, Y.; Lasserre, F.; Barquissau, V.; Régnier, M.; Lukowicz, C.; Benhamed, F.; et al. Liver PPARα Is Crucial for Whole-Body Fatty Acid Homeostasis and Is Protective against NAFLD. *Gut* **2016**, *65*, 1202–1214. [CrossRef]
54. MacDonald-Ramos, K.; Michán, L.; Martínez-Ibarra, A.; Cerbón, M. Silymarin Is an Ally against Insulin Resistance: A Review. *Ann. Hepatol.* **2021**, *23*, 100255. [CrossRef]
55. Gillessen, A.; Schmidt, H.H.J. Silymarin as Supportive Treatment in Liver Diseases: A Narrative Review. *Adv. Ther.* **2020**, *37*, 1279–1301. [CrossRef]
56. Surai, P.F. Silymarin as a Natural Antioxidant: An Overview of the Current Evidence and Perspectives. *Antioxidants* **2015**, *4*, 204–247. [CrossRef]
57. Bellavite, P.; Fazio, S.; Affuso, F. A Descriptive Review of the Action Mechanisms of Berberine, Quercetin and Silymarin on Insulin Resistance/Hyperinsulinemia and Cardiovascular Prevention. *Molecules* **2023**, *28*, 4491. [CrossRef]

Disclaimer/Publisher's Note: The statements, opinions and data contained in all publications are solely those of the individual author(s) and contributor(s) and not of MDPI and/or the editor(s). MDPI and/or the editor(s) disclaim responsibility for any injury to people or property resulting from any ideas, methods, instructions or products referred to in the content.

biomedicines

MDPI

Article

Does Metabolic Syndrome and Its Components Have Prognostic Significance for Renal and Cardiovascular Outcomes in IgA Nephropathy?

Balázs Sági [1,2], Tibor Vas [1], Botond Csiky [1,2], Judit Nagy [1] and Tibor József Kovács [1,*]

[1] Medical School, Clinical Center, 2nd Department of Internal Medicine and Nephrology, Diabetes Center, University of Pécs, 7624 Pécs, Hungary; balazs.sagidr28@gmail.com (B.S.); vas.tibor@pte.hu (T.V.); botond.csiky@gmail.com (B.C.); judit.nagy@aok.pte.hu (J.N.)

[2] Triton Life Dialysis Center, 7624 Pécs, Hungary

* Correspondence: kovacs.tibor.jozsef@pte.hu; Tel.: +36-72-536-053 or +36-20-9952579

Abstract: Background: Patients with IgA nephropathy (IgAN), a chronic kidney disease (CKD), are significantly more likely to have cardiovascular (CV) mortality and morbidity than the general population. The occurrence of metabolic syndrome (MetS) and metabolic risk factors are independent risk factors for CV disease and renal progression. The purpose of this study was to determine how metabolic characteristics in a homogeneous population of CKD patients relate to prognosis. Methods: A total of 145 patients with CKD stages 1–4 diagnosed with IgA nephropathy (92 men and 53 women, aged 54.7 ± 13 years) were examined and monitored for a median of 190 months. All-cause mortality and any CV event, such as stroke, myocardial infarction, revascularization (CV), end-stage renal disease, and renal replacement therapy (renal), have been included in the composite endpoints (CV and renal). Results: Patients with MetS had significantly more primary endpoint events (23/65 patients vs. 15/60 patients, $p < 0.001$) compared to the non-MetS group. The MetS group had a statistically significant increase in both primary renal and CV endpoints (18/65 vs. 10/60, $p = 0.001$), and in CV endpoint events (7/65 vs. 6/60, $p = 0.029$) among the secondary endpoints (CV and renal separately). Based on Cox regression analysis, the main endpoint independent predictors of survival were dyslipidemia, eGFR, hemoglobin, urine albuminuria, and diabetes mellitus. Independent predictors of secondary renal endpoints were dyslipidemia, hemoglobin, urine albumin, and eGFR. Predictors of secondary cardiovascular endpoints were gender, BMI, and diabetes. When Kaplan–Meier curves were analyzed at the combined endpoints (CV and renal) or each endpoint independently, significant differences were seen between MetS and non-MetS. With more MetS components, the primary endpoint rate increased significantly (MetS comp. 0 vs. MetS comp. 2+, primary endpoints, $p = 0.012$). Conclusions: Our results show that the metabolic profile has a prognostic role not only for renal endpoints but also for CV endpoints in IgAN. BMI, hyperuricemia, hypertension, and diabetes have a predictive value for the prognosis of IgA nephropathy.

Keywords: chronic kidney disease; IgA nephropathy; renal function; metabolic syndrome; arterial stiffness

1. Introduction

Cardiovascular (CV) morbidity and mortality in patients with chronic kidney disease (CKD) is many times higher than in the general population [1,2], and in primary glomerular diseases such as IgA nephropathy (IgAN), the absolute risk of cardiovascular disease (CVD) is roughly 2.5 times higher than in the population without any kidney diseases [3]. The classification of CVD risk in these individuals may be improved by taking into account eGFR, proteinuria, the type of glomerular disease [3], and the patient's metabolic profile. Moderate and severe CKDs are independent risk factors for cardiovascular disease [4]. IgA nephropathy is the most common primary glomerular disease worldwide and is a relatively

common cause of end-stage kidney disease (ESKD) [5,6]. Long-term observational studies have shown that IgAN causes ESKD in 40% of patients within 20 years after diagnosis [7,8]. The clinical presentation is usually nephritic syndrome and hematuria with variable degrees of proteinuria. Pathologically, IgAN is defined by polymeric IgA1 being deposited in the glomerulus, primarily in the mesangium; mesangial hypercellularity and mesangial matrix expansion are also present, along with various degrees of interstitial fibrosis and glomerulosclerosis. The degree of glomerulosclerosis and tubulointerstitial fibrosis in renal pathology, the presence of hypertension and excessive proteinuria, and a marked decline in glomerular filtration rate (GFR) at the time of renal biopsy are all considered adverse prognostic indications [9,10].

Although research on MetS's independent relationship with the onset and progression of CKD has been increasingly studied, the results are inconsistent. According to a population-based study, patients with non-diabetic early-stage CKD (stages 1–3) are the only ones whose MetS has a substantial effect on the progression of CKD; patients with non-diabetic late-stage and diabetic CKD are not affected [11]. Independent of diabetes grades, a different investigation found a substantial correlation between CKD and components of MetS [12]. Furthermore, despite a positive and considerable risk of estimated glomerular filtration rate (eGFR) decline, a previous cohort study found no correlation between MetS and incident CKD [13]. Several meta-analyses have been conducted to settle these disputes. According to a prior meta-analysis involving 11 cohort studies, MetS may promote the onset of CKD [14].

MetS and its components are putative risk factors for albuminuria and proteinuria, according to a different meta-analysis of 57 studies [15]. Previous meta-analyses, however, have solely comprised research on individuals without CKD. There have not been any meta-analyses conducted to look into the relationship between ESKD and renal events like eGFR decline and MetS and its components.

Apart from the aforementioned established risk factors, new research has also linked the advancement in the progression of IgAN to other cardiovascular risk factors, including hypertriglyceridemia, hyperuricemia, excessive body weight, and smoking [16,17]. However, there are limited data about the prevalence of metabolic syndrome and the metabolic profile association between metabolic syndrome (MetS) and renal and cardiovascular (CV) outcomes in IgAN patients. More focus is being placed on identifying and treating the modifiable risk factors that can stop or slow down the deterioration of renal function.

Earlier cross-sectional studies have also demonstrated a link between MetS and CKD [18,19]. Kurella et al. conducted only one longitudinal investigation [20], demonstrating a significantly increased risk of incident CKD in non-diabetic adults with MetS. However, in our study, we investigated the effects of MetS and metabolic profiles on the outcomes of IgAN. We explored metabolic syndrome components (hypertension, diabetes, obesity, dyslipidemia, hyperuricemia) separately and whether they have an impact on renal and CV outcomes.

2. Materials and Methods

We included 145 renal biopsy-proven IgAN patients in our follow-up study to our earlier 2013 investigation, and we analyzed their data prospectively (Figure 1A,B). The study procedure was approved by the University of Pécs Regional Research Ethics Committee, and all participants provided written consent for its completion.

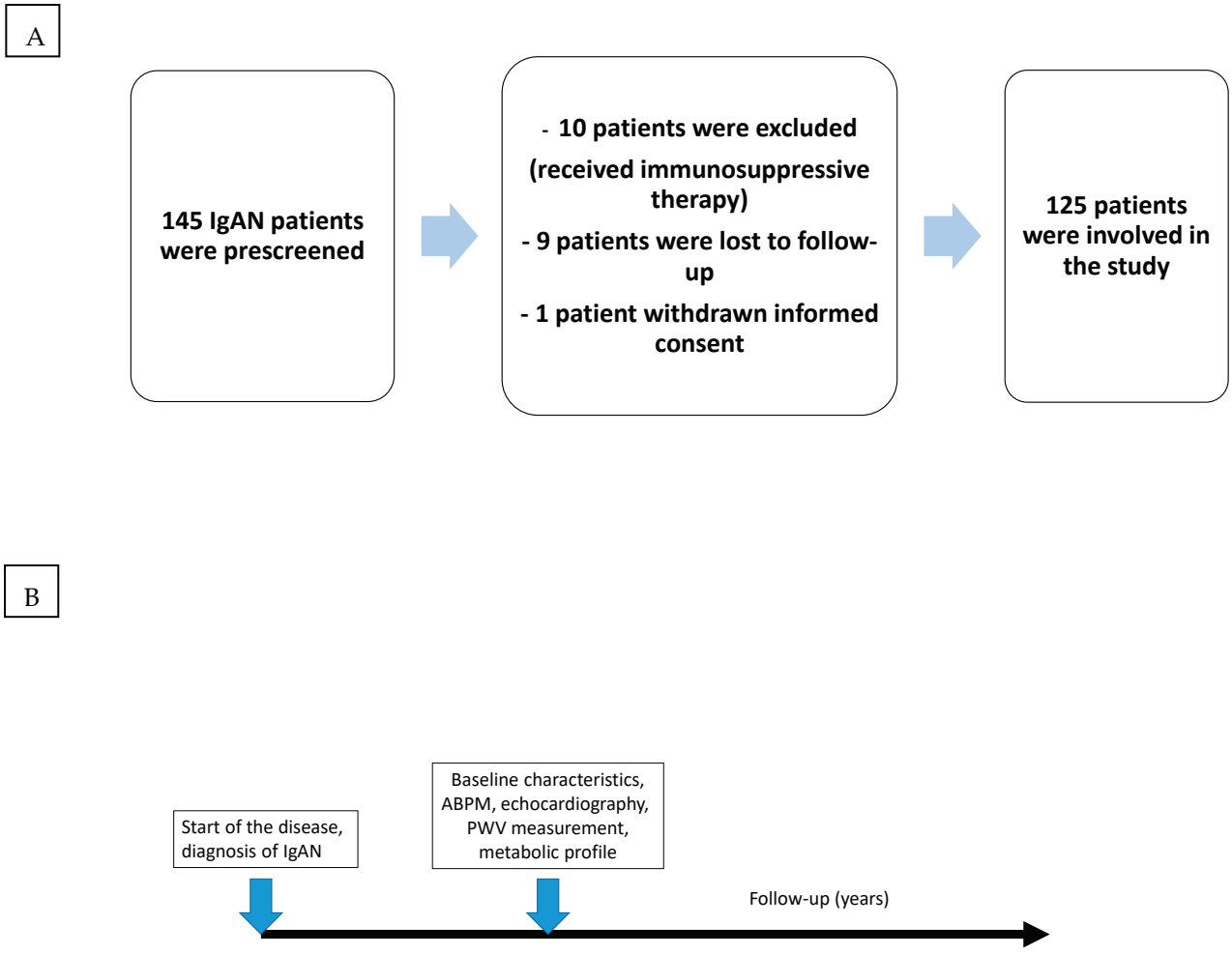


Figure 1. A flow chart of recruited patients (**A**), and a flow chart of the present study's process (**B**).

The inclusion criteria for this study were confirmed IgAN and being over the age of 18. The exclusion criteria were previous or current immunosuppressive treatment (due to the modifying effects of the metabolic components) and severe comorbidities (such as malignancies that required active treatment or acute infection).

Metabolic syndrome (MetS) was defined as the NCEP ATP III (National Cholesterol Education Program Adult Treatment Panel III) criterion, which necessitates any three of the following five criteria: waist circumference (>102 cm in males, >90 cm in females) or BMI > 27 kg/m^2, fasting glucose $\geq$ 5.6 mmol/L, triglyceride $\geq$ 1.7 mmol/L, HDL cholesterol <1.0 mmol/L in males and <1.3 in females, and systolic/diastolic blood pressure >130/85 mmHg.

An echocardiography examination was performed at the beginning of patient enrollment, and information about classic CV risk factors such as smoking, lipid abnormalities, obesity, diabetes, hypertension, and antihypertensive medications (ACEI/ARB, BB, and CCB) was also recorded. The obesity inclusion criterion was a BMI over 27 kg/m^2. The CKD-EPI formula was used to estimate renal function (eGFR, mL/min, 1.73 m^2). A 24 h blood pressure monitor was used, provided by ABPM (Meditech, Budapest, Hungary) devices, to determine the patient's 24 h average systolic and diastolic blood pressure, pulse pressure, and diurnal index. At the start of the study, arterial stiffness and pulse wave velocity (PWV) were measured by a SphygmoCor System (AtCor Medical, Sydney, Australia). During these visits, medical events that had occurred since the previous visit were recorded, the patient's physical status was examined, and detailed laboratory tests were performed. Blood pressure values were determined from the average of three measurements taken after

10 min of rest. Serum parameters were determined by implementing routine, standardized laboratory methods.

2.1. Endpoint Definition

The primary composite endpoints were all-cause mortality and any CV event, such as stroke, myocardial infarction, or revascularization. Secondary cardiovascular (CV) endpoints were any CV event, such as stroke, myocardial infarction, or any revascularization. Secondary renal endpoints were reaching end-stage renal disease and starting renal replacement therapy. We collected these data prospectively.

2.2. Statistical Analysis

Statistical analyses were performed using SPSS 21.0 software (SPSS, Inc., Chicago, IL, USA). A comparison of clinical and laboratory parameters was made using Student's *t*-test and ANOVA, as appropriate. The mean SD was used to express data from a normal distribution. Correlations between continuous variables were evaluated with linear regression using the Pearson test, and for categorical variables, the Spearman correlation test was used. The survival rates of the two groups were examined by using the Mantel-Cox log-rank test. The effect of metabolic syndrome components on survival was evaluated by using Cox regression analysis. Values of $p < 0.05$ were considered statistically significant.

3. Results

This study included 145 patients, but 20 patients were excluded: 10 patients due to immunosuppressive therapy, 9 patients lost before follow-up, and 1 patient who withdrew informed consent; so, in total, 125 patients' data were investigated. The average age was 53.0 ± 12.7 years, and 92 were male. The median follow-up time was 190 ± 170 months. Patients were divided into two groups based on MetS presence or absence. Baseline clinical data are shown in Table 1. There were significant differences between the two groups in systolic blood pressure, pulse pressure, systolic diurnal rhythm, diastolic dysfunction, BMI, pre-diabetes (impaired fasting glucose: IFG; impaired glucose tolerance: IGT), eGFR, PWV, HDL cholesterol, TG, and uric acid, but not in age or gender. The distribution of metabolic parameters in the MetS presence and MetS absence groups is summarized in Table 2.

Table 1. Baseline clinical data of IgAN patients.

Clinical Data (n = 125)	Met sy − (n = 60)	Met sy + (n = 65)	*p*
Man/woman (n/%)	36/24 (60/40)	46/19 (71/29)	0.079
Age (year) (mean and 25–75th percentiles)	53.2 (43.0–63.0)	55.4 (44.0–64.0)	0.109
Average systolic BP (Hgmm) (mean and 25–75th percentiles)	123.5 (115.0–129.25)	127.4 (117.3–131.2)	0.002 *
Average diastolic BP (Hgmm)	73 ± 9.6	75.7 ± 9.5	0.231
24 h pulse pressure (Hgmm) (mean and 25–75th percentiles)	49.35 (43.0–54.0)	53.10 (44.5–56.5)	0.012 *
Diurnal index systolic (%)	10.92 ± 5.08	8.36 ± 7.72	0.020 *
Abdominal circumference in males (cm)	100.2 ± 4.2	112.1 ± 6.5	0.030 *
Abdominal circumference in females (cm)	90.1 ± 5.7	94.4 ± 7.3	0.023 *
Metabolic Parameters			
Hypertension (n,%)	41 (68)	53 (81)	0.118
BMI (kg/m^2) (mean and 25–75th percentiles)	26.5 (22.9–29.7)	28.6 (23.4–30.1)	0.001 *
Dyslipidemia (n,%)	24 (40)	34 (52)	0.137
Diabetes (n, %)	9 (15)	21 (32)	0.087
IFG and IGT (n/%)	2 (3)	10 (15)	0.025 *

Table 1. *Cont.*

Clinical Data (n = 125)	Met sy − (n = 60)	Met sy + (n = 65)	*p*
Overweighted (n/%)	3 (5)	5 (8)	0.098
Obesity (n/%)	2 (3)	32 (49)	0.001 *
Visceral obesity (n/%)	2 (3)	28 (43)	0.001 *
eGFR (mL/min)	94.6 ± 29.3	78.9 ± 37.9	0.005 *
eGFR < 60 mL/min (n/%)	2 (3)	4 (6)	0.086
Duration of kidney disease (year)	10.2 ± 9.7	8.8 ± 9.1	0.101
Smoking (n, %)	7 (12)	11(17)	0.156
Therapy			
ACEI/ARB (n, %)	46 (77)	60 (92)	0.079
BB (n, %)	12 (20)	19 (29)	0.178
Statin (n, %)	16 (27)	22 (34)	0.164
CCB (n, %)	9 (15)	19 (29)	0.082
Echocardiographic Parameters			
LVEF (%) (mean and 25–75th percentiles)	62.8 (59.0–66.5)	63.5 (60.1–66.7)	0.211
LVMI (g/m^2)	103.53 ± 15.95	109.21 ± 21.25	0.123
LVEDD (cm)	6.05 ± 6.29	5.57 ± 5.13	0.173
DD (n/%)	7 (11)	17 (26)	<0.001 *
E/A	1.18 ± 0.32	0.93 ± 0.30	<0.001 *
Arterial Stiffness			
cfPWV (m/s) (mean and 25–75th percentiles)	9.97 (8.48–11.35)	11.34 (10.1–12.2)	0.003 *
Laboratory Results			
Hb (g/dL)	13.9 ± 1.6	13.6 ± 1.7	0.245
AU (mg/day) (mean and 25–75th percentiles)	457.48 (65.0–700.0)	558.34 (75.1–789.1)	0.078
UA (μmol/L)	303 ± 97.4	342 ± 84.9	0.009 *
Total cholesterol (mmol/L) (mean and 25–75th percentiles)	4.97 (4.28–5.51)	4.79 (4.35–5.41)	0.124
HDL cholesterol (mmol/L) (mean and 25–75th percentiles)	1.27 (1.03–1.44)	1.21 (1.0–1.38)	0.029 *
TG (mmol/L) (mean and 25–75th percentiles)	1.72 (0.93–2.04)	1.99 (0.99–2.34)	0.012 *
Hypercholesterinemia (n/%)	9 (15)	21 (32)	0.04 *
Hypertriglyceridemia (n/%)	5 (8)	52 (80)	0.001 *
Earlier CV Disease			
Heart failure	0 (0)	1(1)	0.176
Stroke	0 (0)	1 (1)	0.187
CAD	1 (2)	3 (5)	0.087
COPD	0 (0)	1 (1)	0.139

* = $p < 0.05$. BP: blood pressure; BMI: body mass index; IFG: impaired fasting glucose; IGT: impaired glucose tolerance; eGFR: estimated glomerular filtration rate; ACEI: angiotensin-converting enzyme inhibitor; ARB: angiotensin receptor blocker; BB: beta blocker; CCB: calcium channel blocker; CAD: coronary artery disease; LVEF: left ventricle ejection fraction; LVMI: left ventricle mass index; LVEDD: left ventricular end-diastolic diameter; DD: diastolic dysfunction; E/A: early and late mitral inflow; cfPWV: carotid–femoral pulse wave velocity; Hb: hemoglobin; AU: albuminuria; UA: uric acid; HDL cholesterol: high-density lipoprotein cholesterol; TG: triglyceride; CAD: coronary artery disease; COPD: chronic pulmonary obstructive disease.

Table 2. Distribution of metabolic parameters in MetS − and MetS + groups.

	HT (n/%)	IFG/ IGT (n/%)	DM (n/%)	Obesity (n/%)	Triglyceride (n/%)	HDL Cholesterol (n/%)	Number of Positive Parameters/ Patients (average/n)
MetS + (n = 65)	53 (82)	10 (15)	21 (32)	32 (49)	52 (80)	33 (51)	201 (3.09)
MetS − (n = 60)	41 (68)	2 (3)	9 (15)	2 (3)	5 (8)	15(25)	74 (1.23)

HT: hypertension; IFG: impaired fasting glucose; IGT: impaired glucose tolerance; DM: diabetes mellitus; MetS: metabolic syndrome; HDL: high-density lipoprotein.

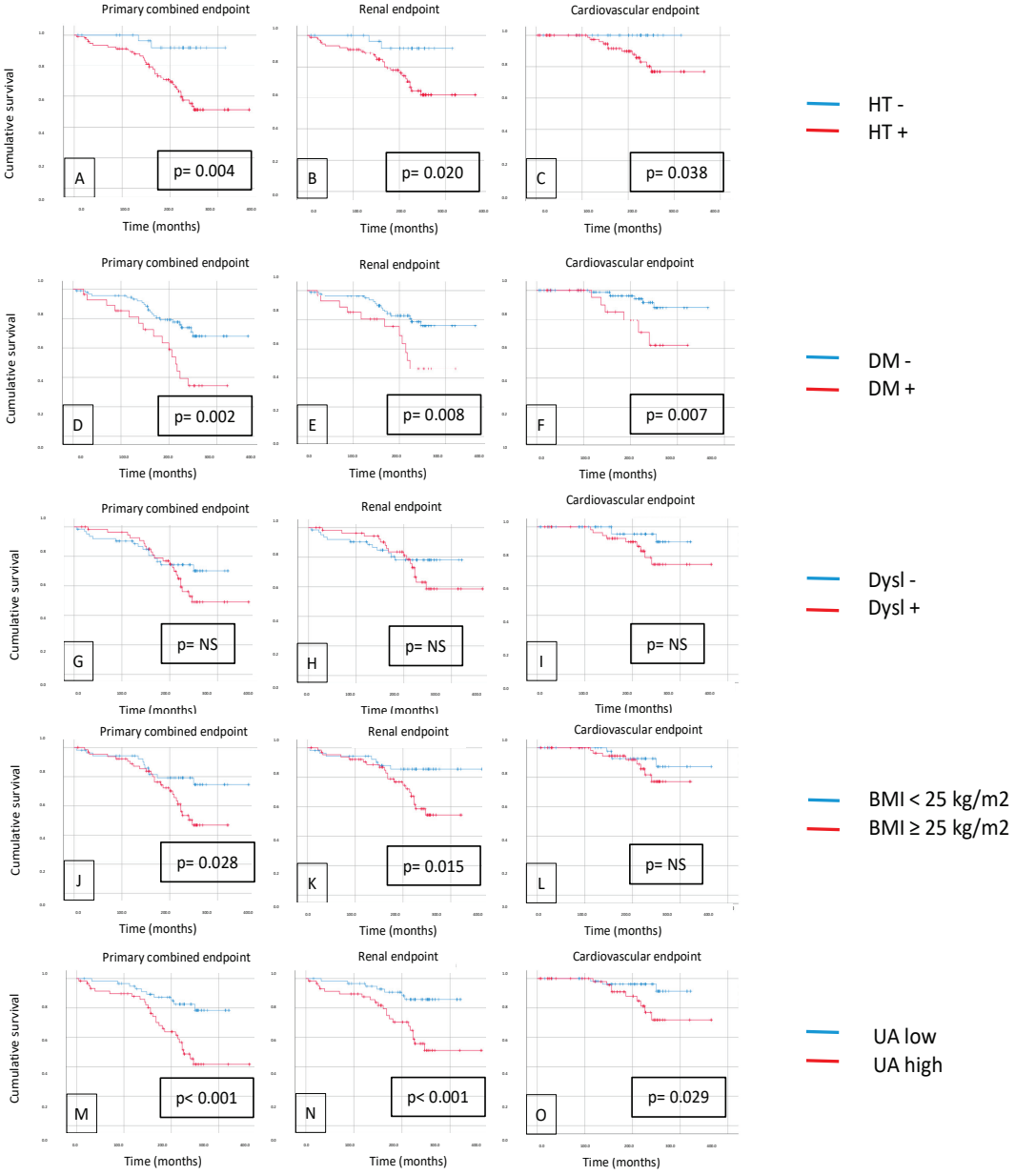
Primary combined endpoint and secondary renal and CV endpoint event rates are presented in Table 3 in cases of the presence of MetS components and MetS combined with PWV.

Table 3. Primary combined endpoint and secondary renal and CV endpoint event rates.

Parameters	Primary Combined Endpoint Rate (n/%)	Secondary Renal Endpoint Rate (n/%)	Secondary CV Endpoint Rate (n/%)
HT− (n = 30)	2 (7)	2 (7)	0 (0)
HT+ (n = 95)	36 (38)	26 (27)	13 (14)
DM− (n = 95)	22 (23)	17 (18)	6 (6)
DM+ (n = 30)	16 (53)	11 (37)	7 (23)
Dyslipidemia− (n = 67)	16 (24)	12 (18)	4 (6)
Dyslipidemia+ (n = 58)	22 (38)	16 (27)	9 (15)
BMI low (n = 57)	11 (19)	7 (12)	4 (7)
BMI high (n = 68)	27 (40)	21 (31)	9 (13)
UA low (n = 65)	11 (17)	7 (11)	4 (6)
UA high (n = 60)	27 (45)	21 (35)	9 (15)
MetS− (n = 60)	15 (25)	10 (17)	6 (10)
MetS+ (n = 65)	23 (35)	18 (27)	7 (11)
MetS component 0 (n = 35)	1 (3)	1 (3)	0 (0)
MetS component 1 (n = 22)	8 (36)	9 (41)	3 (13)
MetS components 2+ (n = 68)	29 (42)	18 (26)	10 (15)
PWV < 10 m/s and MetS− (n = 61)	9 (15)	8 (13)	1 (2)
PWV > 10 m/s and MetS+ (n = 38)	13 (34)	9 (23)	5 (13)
PWV < 10 m/s and MetS− (n = 10)	6 (60)	4 (40)	3 (30)
PWV > 10 m/s and MetS+ (n = 16)	10 (62)	7 (44)	4 (25)

HT: hypertension; DM: diabetes mellitus; BMI: body mass index; UA: uric acid; MetS: metabolic syndrome; PWV: pulse valve velocity.

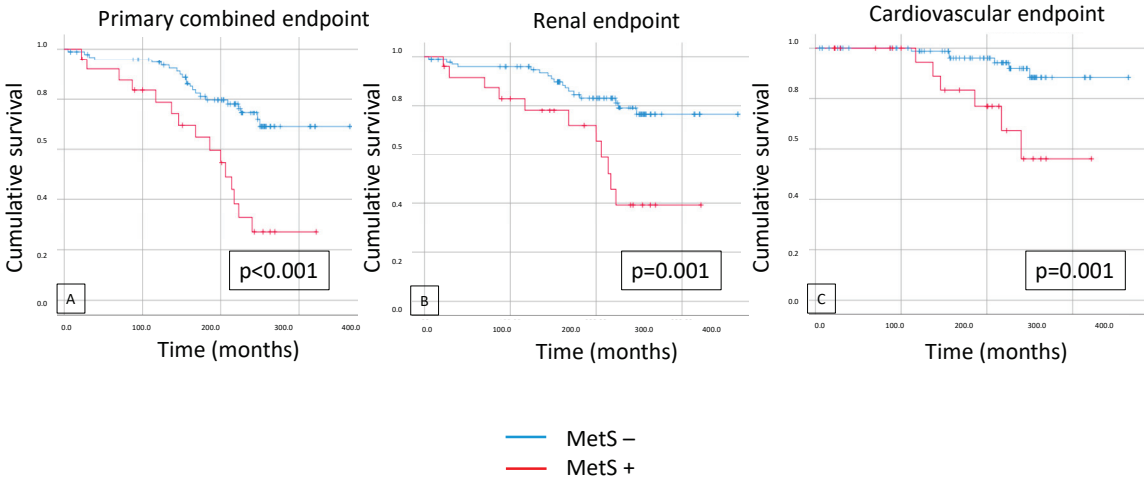
When we investigated MetS components (HT, DM, BMI, dyslipidemia), the K-M curves showed significantly worse survival in cases of hypertension (primary endpoint: $p = 0.004$, secondary renal endpoint: $p = 0.020$, secondary CV endpoint: $p = 0.0038$), diabetes mellitus ($p = 0.002$, $p = 0.008$, $p = 0.007$), and a higher BMI (cut-off 25 kg/m^2) ($p = 0.028$, $p = 0.015$, p = NS) in both primary and secondary endpoints. Surprisingly, there was a non-significant difference in the primary and secondary outcomes in the case of dyslipidemia, but we found significant differences in the case of hyperuricemia (cut-off 360 μmol/L) ($p < 0.001$, $p < 0.001$, $p = 0.029$) (see Figure 2).



HT: hypertension; DM: diabetes mellitus; Dysl: dyslipidemia; BMI: body mass index; UA: uric acid.

Figure 2. The Kaplan–Meier curves demonstrate the following primary endpoints: primary combined (**A**), renal (**B**), and cardiovascular (**C**) endpoints in patients with or without hypertension; primary combined (**D**), renal (**E**), and cardiovascular (**F**) endpoints in patients with diabetes; primary combined (**G**), renal (**H**), and cardiovascular (**I**) endpoints in patients with dyslipidemia; primary combined (**J**), renal (**K**), and cardiovascular (**L**) endpoints in patients with a BMI of 25 kg/m^2; primary combined (**M**), renal (**N**), and cardiovascular (**O**) endpoints in patients with and without hyperuricemia.

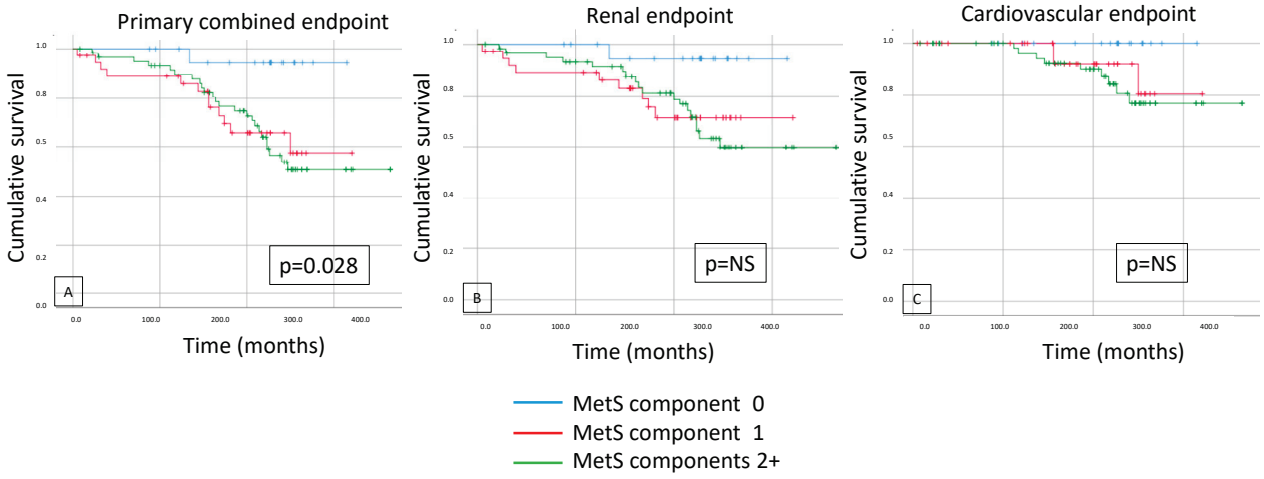
There were significant differences in survival on the K-M curves in the case of the primary combined endpoint ($p < 0.001$) and the secondary renal ($p = 0.001$) and cardiovascular endpoints ($p = 0.001$) when we compared the IgAN patients with and without MetS (Figure 3).



MetS: metabolic syndrome.

Figure 3. Kaplan–Meier curves show primary combined (**A**), renal (**B**), and cardiovascular (**C**) endpoints in cases of patients with and without metabolic syndrome.

There was a significant difference in survival only in the primary endpoint when we compared the patients with MetS components (0 vs. 1. vs. 2+); the secondary endpoints were not significantly different (p = 0.028) (Figure 4).



MetS: metabolic syndrome.

Figure 4. Assuming metabolic syndrome components are detected, the Kaplan–Meier curves show the primary combined (**A**), renal (**B**), and cardiovascular (**C**) outcomes (0 vs. 1 vs. 2+).

When we combined arterial stiffness, PWV (<10 m/s vs. ≥10 m/s), and MetS presence or absence in the survival examination, there was a significant difference between the low-PWV group without MetS compared to the high-PWV group with MetS. All endpoints, the primary combined endpoint (p = 0.001) and both secondary endpoints (renal and cardiovascular) (p = 0.008; p = 0.005), were significant (Figure 5).

Multivariate analyses were performed on the clinical data, metabolic parameters, echocardiographic parameters, and laboratory results. The significant factors in the competitive risk model were gender (OR = 4.333, p = 0.001), age (OR = 2.906, p = 0.026), dyslipi-

demia (OR = 3.474, $p = 0.034$), hypertension (OR = 5.806, $p = 0.018$), diabetes (OR = 1.912, $p = 0.011$), BMI (OR = 2.205, $p = 0.021$), eGFR (OR = 3.187, $p = 0.021$), hemoglobin (OR = 2.237, $p = 0.029$), albuminuria (OR = 2.568, $p = 0.013$), and uric acid level (OR = 1.837, $p = 0.021$) (Table 4).

Table 4. Multivariate analyses on clinical data, metabolic parameters, echocardiographic parameters, and laboratory results in competitive risk model.

Clinical Data (n = 125)	OR	CI (95%)	*p*
Gender	4.333	3.973–4.761	0.001 *
Age	2.906	2.198–3.214	0.026 *
Average systolic BP	0.800	0.290–0.993	0.354
Average diastolic BP	0.576	0.119–0.626	0.615
24 h pulse pressure	0.737	0.174–0.947	0.535
Diurnal index systolic	0.559	0.283–0.874	0.693
Metabolic Parameters			
HT	5.806	5.301–6.455	0.018 *
DM	1.912	1.808–2.178	0.011 *
BMI	2.205	1.913–2.742	0.021 *
Dyslipidemia	3.474	2.237–4.546	0.034 *
IFG and IGT	0.564	0.118–0.922	0.787
Overweighted	0.479	0.340–0.941	0.109
Obesity	0.367	0.204–0.530	0.607
eGFR	3.187	2.455–4.366	0.021 *
Duration of kidney disease	0.718	0.387–0.972	0.284
Smoking	0.341	0.327–0.823	0.499
Echocardiographic Parameters			
LVEF	0.635	0.602–0.968	0.526
LVMI	0.460	0.068–0.691	0.772
LVEDD	0.508	0.285–0.952	0.293
Laboratory Results			
Hb	2.237	2.151–2.486	0.029 *
AU	2.568	1.933–3.653	0.013 *
UA	1.837	1.735–1.952	0.021 *
Total cholesterol	0.903	0.450–0.937	0604
HDL cholesterol	0.476	0.045–0.846	0.997
TG	0.806	0.463–0.944	0.143

* = $p < 0.05$. BP: blood pressure; HT: hypertension; DM: diabetes mellitus; BMI: body mass index; IFG: impaired fasting glucose; IGT: impaired glucose tolerance; eGFR: estimated glomerular filtration rate; LVEF: left ventricle ejection fraction; LVMI: left ventricle mass index; LVEDD: left ventricular end-diastolic diameter; Hb: hemoglobin; AU: albuminuria; UA: uric acid; HDL cholesterol: high-density lipoprotein cholesterol; TG: triglyceride.

The primary endpoint independent predictors of survival were dyslipidemia, eGFR, hemoglobin, urine albuminuria, and diabetes mellitus, as determined by using Cox regression analysis. The secondary renal endpoint independent predictors were dyslipidemia, hemoglobin, urine albuminuria, and eGFR. The secondary cardiovascular endpoint predictors were gender, BMI, and diabetes (Table 5).

Table 5. Cox regression for primary and secondary renal and cardiovascular endpoints.

	B	*p*	Exp(B)	95% CI for Exp(B) Lower	95% CI for Exp(B) Upper
Primary combined endpoint					
Gender	−0.898	0.078	0.408	0.150	1.104
Age	0.027	0.093	1.028	0.995	1.061
Dyslipidemia	1.144	0.034 *	3.140	1.091	9.042
HT	−0.774	0.363	0.461	0.087	2.447
DM	−0.964	0.031 *	0.381	0.159	0.914
BMI	0.014	0.787	1.014	0.916	1.123
eGFR	−0.021	0.010 *	0.980	0.964	0.995
Hb	−0.344	0.006 *	0.709	0.555	0.905
AU	0.001	0.001 *	1.001	1.001	1.002
UA	0.004	0.083	1.004	0.999	1.009
Secondary renal endpoint					
Gender	−0.492	0.416	0.611	0.186	2.003
Age	0.021	0.234	1.021	0.986	1.058
Dyslipidemia	1.964	0.003 *	7.130	1.931	26.328
HT	−0.743	0.430	0.476	0.075	3.011
DM	−0.568	0.285	0.567	0.200	1.605
BMI	0.087	0.151	1.091	0.969	1.228
eGFR	−0.030	0.004 *	0.971	0.951	0.991
Hb	−0.493	0.002 *	0.611	0.444	0.841
AU	0.002	0.001 *	1.002	1.001	1.002
UA	0.005	0.119	1.005	0.999	1.011
Secondary CV endpoint					
Gender	−2.632	0.029 *	0.072	0.007	0.759
Age	0.072	0.095	1.075	0.987	1.170
Dyslipidemia	0.571	0.531	1.771	0.296	10.581
HT	−11.318	0.961	0.001	0.001	126.263
DM	−2.240	0.002 *	0.106	0.025	0.454
BMI	−0.231	0.029 *	0.794	0.646	0.976
eGFR	−0.002	0.874	0.998	0.969	1.027
Hb	−0.260	0.192	0.771	0.521	1.140
AU	0.001	0.744	1.000	0.999	1.001
UA	0.002	0.542	1.002	0.995	1.010

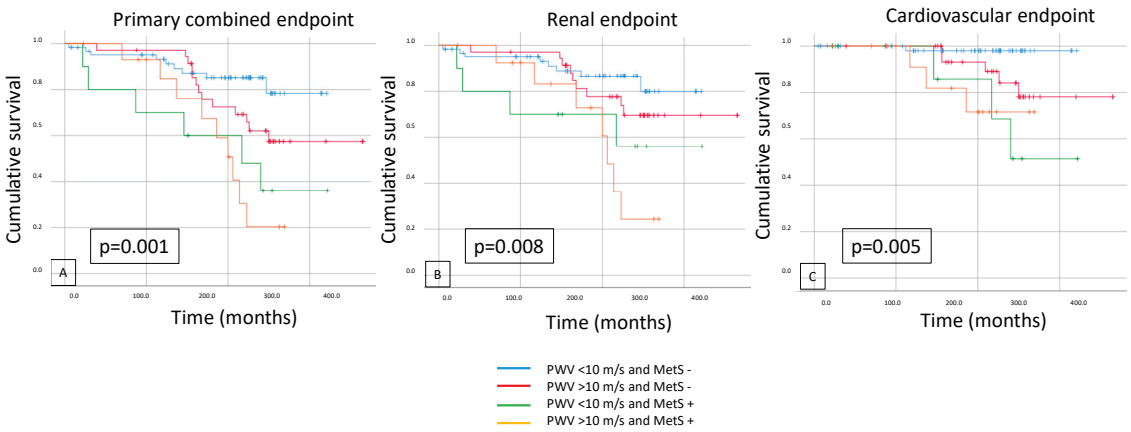
* = $p < 0.05$. HT: hypertension; DM: diabetes mellitus; BMI: body mass index; eGFR: estimated glomerular filtration rate; Hb: hemoglobin; AU: albuminuria; UA: uric acid.

Cox regression analysis adjusted for MetS components showed that the primary endpoint and the secondary renal endpoint independent predictors were uric acid and diabetes (Table 6).

Table 6. Cox proportional hazard ratios of the metabolic syndrome parameters for the primary and secondary endpoints (adjusted for metabolic syndrome components).

	B	*p*	Exp(B)	95% CI for Exp(B) Lower	95% CI for Exp(B) Upper
Primary endpoint					
Dyslipidemia	−0.008	0.981	0.992	0.493	1.995
HT	−1.249	0.102	0.287	0.064	1.279
DM	−0.800	0.051	0.449	0.201	1.002
BMI	−0.013	0.743	0.987	0.913	1.067
UA	0.006	0.002 *	1.006	1.002	1.009
Secondary renal endpoint					
Dyslipidemia	0.114	0.777	1.121	0.508	2.475
HT	−0.828	0.290	0.437	0.094	2.024
DM	−0.549	0.258	0.578	0.223	1.496
BMI	0.040	0.357	1.041	0.955	1.135
UA	0.006	0.003 *	1.006	1.002	1.010
Secondary CV endpoint					
Dyslipidemia	−0.728	0.254	0.483	0.138	1.687
HT	−12.342	0.971	0.001	0.001	8.049
DM	−1.840	0.005 *	0.159	0.044	0.567
BMI	−0.128	0.077	0.880	0.763	1.014
UA	0.004	0.150	1.004	0.998	1.010

* = $p < 0.05$. HT: hypertension, DM: diabetes mellitus, BMI: body mass index, and UA: uric acid.



PWV: pulse wave velocity; MetS: metabolic syndrome.

Figure 5. Kaplan–Meier curves show primary combined (**A**), renal (**B**), and cardiovascular (**C**) endpoints in cases of low or high PWV (<10 m/s vs. ≥10 m/s) and metabolic syndrome presence or absence (Met sy − vs. Met sy +).

4. Discussion

In the present study, we demonstrated that metabolic syndrome and its components, especially hypertension, diabetes, obesity, and hyperuricemia, were significantly associated with the primary combined endpoint (renal plus CV) and the secondary renal and car-

diovascular outcomes, but dyslipidemia was not, in a relatively small number of patients, which are counterbalanced by the long follow-up. Due to the variability in serum lipids, one measurement had no impact on CV or renal endpoints. MetS development with increased pulse wave velocity (PWV) showed a worse renal and CV prognosis.

Survival curves stratified by MetS status (at least three factors from the above-mentioned ones) showed significant differences in the association with the various endpoints in a longer follow-up.

The key objective of the MetS diagnosis criteria was to identify the population most at risk of developing cardiovascular diseases [21,22]. In today's world, it is undeniable that individuals with MetS have a markedly increased risk of developing both CVD and CKD [14,23–26]. The majority of the observational studies covered in these articles discovered a strong correlation between MetS and CKD. Nevertheless, as most of the research was cross-sectional, it was unable to identify whether MetS is linked to long-term changes in renal function or to demonstrate a cause-and-effect relationship between the decline in kidney function and MetS.

In our earlier research, we found a strong correlation between MetS and the progressive loss of kidney function, except for ESKD, which may have an impact on the progression of the earliest stages of IgAN [23]. The present data support these observations, and not only the renal endpoints but also the CV endpoints are affected by the presence of MetS in IgAN.

Lee et al. found that MetS had an impact on CKD progression only in early-stage CKD patients in their short follow-up (average 10.6 months) study [11]. The short follow-up may be the reason that the impact of MetS was not observed among late-stage and diabetic CKD patients. In the present study, we had more than ten times longer follow-up, clearly demonstrating the effect of MetS on the primary combined (CV plus renal) and secondary renal endpoints, despite the lower number of cases.

The other important difference was that the proportion of diabetic patients was higher (in Lee et al.'s study, 53% vs. 24%), and our patients were homogenous for CKD.

The two main causes of CKD worldwide, diabetes and hypertension, are among the elements of MetS that have been extensively studied and reported. Regarding the connection between diabetes and IgAN, Fliser et al. [27] reported that patients with IgAN or ADPKD who have incipient chronic renal disease already exhibit insulin resistance and hyperinsulinemia. These early changes may be worsened by other MetS factors.

At the start of the patient follow-up in our current investigation, 30 patients, or 24% of the total, had diabetes mellitus (see Table 1), which is nearly double the prevalence of DM in the whole population. It is recognized that in patients with diabetes, IgAN may also be the only renal abnormality or that it may superimpose on diabetic nephropathy. Because IgA1 immune complexes or aggregates can be more easily deposited in diabetic patients' glomeruli due to metabolic changes, intraglomerular hypertension, and hyperfiltration, the relationship between IgAN and diabetes may not be a coincidence. Moreover, type 2 diabetes is frequently associated with malformations of the IgA immune system [28].

Common in CKD patients, hypertension is a predictor of cardiovascular morbidity and mortality, the same as it is in the general population. A U-shaped relationship has been shown between blood pressure and mortality. Early mortality is predicted not only by high blood pressure but also by low mean systolic and diastolic blood pressure [29]. The progression of IgAN is more severe when hypertension is present [30]. It was therefore not surprising that among the MetS parameters examined in our investigation, hypertension had the highest impact on the prognosis of IgAN, consistent with our previous recommendation that IgAN patients require strict blood pressure control [31].

Numerous epidemiological studies have linked obesity to an increased risk of developing CKD and ESKD [32–34]. Regardless of the existence of diabetes or hypertension, obesity, as measured by an elevated BMI, was linked to ESKD and reduced renal function in the populations under investigation. Losing weight slows the advancement of chronic kidney disease [35]. Obesity was found to be a predictive factor for both the development

of ESKD and hypertension in IgAN patients. Obese patients also exhibit glomerular enlargement and ultrastructural modification of the glomerular basement membrane, which are well-documented phenomena [27,36,37]. The present study and our former observation are also able to confirm this [23].

Observational studies and meta-analyses have shown dyslipidemia, namely, atherogenic dyslipidemia (high triglyceride and low HDL cholesterol), to be an independent risk factor for the onset and course of chronic kidney disease (CKD) [38,39]. Dyslipidemia was an important, significant factor according to Cox regression analysis in the primary combined endpoints and secondary renal endpoints (see Table 3). The lower number of secondary CV endpoints may explain the non-significant connection between secondary CV endpoints and dyslipidemia.

Moreover, the progressive deterioration of renal function may increase oxidative stress and inflammation, which may trigger several metabolic changes, including hypertriglyceridemia, diabetes, and insulin resistance. These changes have the potential to create vicious cycles. In the study of Syrjänen et al. [16], elevated triglyceride levels were associated with progressive IgAN. Our long-term follow-up also supports these findings (see Table 3).

According to recent epidemiologic and experimental data, hyperuricemia may play a part in IgAN as well as serving as a risk factor for the onset and progression of renal illness and a marker of decreased kidney function [40,41].

In addition to being linked to renal tissue inflammation in patients with IgAN, serum uric acid may also have another role in the development of tubulointerstitial lesions [42]. In the Jerusalem Lipid Research Clinic cohort trial, serum uric acid was a long-term predictor of acute kidney injury and CKD. This was not dependent on GFR [43], based on a follow-up of 2449 patients. Our results were very similar in a homogenous but lower number of patient groups with long follow-ups.

Previous meta-analyses have indicated that individuals with MetS have a higher chance of developing chronic kidney disease (CKD), as evidenced by albuminuria or proteinuria [15] and a reduction in eGFR [14,44]. The results of previous research that examined the role of MetS and its components in the risk of developing renal disease in addition to incident CKD are inconsistent. The significant role that MetS plays in the evolution of CKD was highlighted by a large prospective cohort study conducted across the United States. This demonstrated that people with MetS had a two-fold increased risk of developing ESKD compared to people without the condition [45].

On the other hand, an African American study's secondary analysis showed that MetS is not directly linked to the advancement of CKD. The relationship between it and CKD acceleration is complicated by other variables [46].

Li et al.'s meta-analysis provided evidence for a strong correlation between MetS and the acceleration of renal failure, indicating that MetS may be a separate predictor of disease progression from acute CKD [47]. In both industrialized and developing nations, diabetes and hypertension are the main causes of both CKD and ESKD [48]. However, their study indicated that the risk was highest for increased blood pressure and lowest for IFG. Similar results were observed among our IgAN patients (see Table 5). A few investigations have confirmed the link between increased blood pressure and renal insufficiency [49,50]. The present study's risk estimate is consistent with earlier meta-analyses [44], which found a positive correlation between high blood pressure and poor kidney function, with an odds ratio (RR) of 1.37 (1.29–1.46).

Conversely, prior research examining the correlation between glycemic status and renal disease has produced contradictory results. According to a recent meta-analysis, the risk of CKD was found to be slightly enhanced by pre-diabetes (RR = 1.11, 95% CI 1.02–1.21), which includes IFG (IGT), and elevated glycated hemoglobin A1c [51]. In the non-diabetic group, IFG was not causally linked to the development of CKD, according to a Mendelian randomization study [52]. This difference may be due to the unique characteristics of the study participants. Individuals with diabetes at baseline or during follow-up may

have been included in studies addressing IFG as part of MetS, whereas individuals with IGT may not have been included. Therefore, depending on different glycemic exposures, the link between IFG and renal impairment may change. Therefore, it is important to consider MetS when interpreting the risk estimations. IFG is not usually reported by itself; rather, it is thought to be the outcome of intricate interactions between several MetS components [53], especially in individuals with chronic kidney disease (CKD) who are more likely to have prior cardiovascular disease, diabetes, hypertension, and abnormal lipid metabolism [54,55]. This may also explain the inconsistency in our results.

In an individual-level meta-analysis of 5.5 million people in 39 general population cohorts, BMI values of 30, 35, and 40 kg/m^2 were associated with an elevated risk of eGFR drop $\geq$40% by 18%, 69%, and 102%, respectively [34]. When comparing patients with and without baseline CKD, the relationship was quite similar.

Studies on dyslipidemia and renal dysfunction have looked at different phases of chronic kidney disease. A cohort study found that among individuals without chronic kidney disease (CKD), increased TG was a risk factor contributing to the observed link between MetS and deterioration in renal function [56]. The data from a different investigation revealed that while high TG levels had no or inverse relationships with time to end-stage renal disease (ESKD) in CKD stages 4–5, they were linked to a higher incidence of CKD and a faster deterioration in renal function in non-CKD and CKD stage 3 [57]. In a different study, there was also no significant link found between TG and HDL cholesterol levels and the development of renal replacement therapy and rapid renal progression in CKD stages 3–5 [58].

The consequences of hyperlipidemia in patients with advanced chronic kidney disease (CKD), especially those with end-stage renal disease (ESKD), may be obscured by the presence of more potent conventional CVD risk factors.

Our results allow nephrologists to concentrate on the initial phases of chronic kidney disease (CKD), perhaps resulting in the early implementation of therapies for metabolic disorders, like dietary changes or medication. Furthermore, prior research has shown that the distribution of fat, namely, the amount in the abdomen rather than overall obesity, is a significant factor in poor renal outcomes [59]. However, the current study did not perform a subgroup analysis based on fat distribution. There was a significantly higher abdominal circumference in males ($p = 0.030$) and females ($p = 0.023$) in the MetS group compared to the non-MetS group.

Lin et al. demonstrated that blood pressure is the most important component of MetS for renal outcomes in CKD 1–4 stage patients. The MetS group had a higher risk for renal outcomes and all-cause mortality (HR: 1.62 and 1.43) [60], and our results also confirm this (see Table 4).

We demonstrated in our previous study that arterial stiffness had predictive value for renal and CV prognosis in autosomal polycystic kidney disease [61], and the etiology of the kidney disease did not similarly alter the vascular function of different CKD groups. Blood pressure was an independent risk factor for PWV [62]. Arterial stiffness was associated with GFR and left ventricular hypertrophy (LVH) in IgAN [63]. In this study, we could demonstrate that if we combined MetS with an arterial stiffness parameter (PWV), the renal and cardiovascular risk prediction would be more pronounced. Vascular stiffness measurements could help nephrologists with further risk assessment.

In our other earlier study, we found an association between LVH and eGFR in IgAN. There was a strong correlation between the left ventricular mass index (LVMI) and renal function in a homogenous immunocomplex-mediated CKD population of IgAN patients. An independent predictor of the LVMI was the initial stage of renal function. Renal composite endpoints and CV were higher when the LVMI was higher. An independent predictor of ESKD and CV events may be a higher LVMI. An increased LVMI should draw attention to CKD patients who require closer monitoring, referral for additional CV testing, and maximal renal and heart protection since they have a higher risk of cardiovascular and

renal disease at an early stage of the disease (II–IV) [64]. In our current study, there was no significant difference in the LVMI between the MetS and non-MetS groups.

5. Limitations of this Study

Firstly, this study has a relatively small sample size and a small endpoint event rate, but this is a medium-term follow-up study conducted at a single center. Secondly, this cohort provides the basis for the cut-off value and the single baseline measurement. It might not be suitable for other racial and ethnic groups as a result. Thirdly, residual confounding effects from lifting style, drugs that alter CV risk, and comorbidity might introduce bias into prospective analyses. For this reason, larger sample sizes and more prospective research are required. Fourth, there were more men than women in this study, which could have influenced the findings.

6. Conclusions

In conclusion, our study proved that despite the lower number of cases, but longer prospective follow-up, the importance of metabolic changes at the start of IgAN have an important impact on the outcome. Therefore, risk stratification of IgAN patients is very helpful in identifying high-risk individuals, especially when the metabolic profile is combined with an increased arterial stiffness evaluation for additional risk. Further, multicenter, randomized clinical trials with a large number of patients are warranted to confirm our results.

Our results also confirm that complex metabolic risk reduction therapy is necessary in all IgAN patients, especially in high-risk groups, which contains ACEI/ARB, statins, uric acid-lowering agents in cases of lower GFR (<60 mL/min) and proteinuria, as well as today's SGLT-2-inhibitors [65,66].

Author Contributions: B.S.: conceived and designed the study, collected the clinical data, and drafted and approved the manuscript. B.C.: identified the study plot and contributed to the interpretation and drafting approval of the manuscript. T.V.: identified the study plot, identified the classification of biopsies, performed statistical analyses, and reviewed and approved the manuscript. J.N.: drafted an application to the committee of ethics, organized the database, and reviewed and approved the manuscript. T.J.K.: revised the manuscript. All authors have read and agreed to the published version of the manuscript.

Funding: This research received no external funding.

Institutional Review Board Statement: This study was approved by the University of Pécs Clinical Center Regional Research Ethical Committee (Reference No. 3170/2008). Informed consent was obtained from all subjects involved in this study. This study was conducted according to the Declaration of Helsinki.

Informed Consent Statement: Not applicable.

Data Availability Statement: The data underlying this article cannot be shared publicly due to Hungarian regulations and the privacy of individuals who participated in this study. The data could be shared upon reasonable request to the corresponding author if accepted by the Regional Committee for Medical and Health Research Ethics and local data protection officials.

Acknowledgments: The authors give special thanks to Ilona Varga Sámikné for their help with data collection.

Conflicts of Interest: The authors declare no conflicts of interest.

Abbreviations

ACEI/ARB	angiotensin-converting enzyme inhibitor/angiotensin receptor blocker
ADPKD	autosomal dominant polycystic kidney disease
AU	albuminuria
BB	beta blocker
BMI	body mass index
BP	blood pressure
CAD	coronary artery disease
CCB	calcium channel blocker
CKD	chronic kidney disease
COPD	chronic pulmonary obstructive disease
CV	cardiovascular
CVD	cardiovascular disease
DD	diastolic dysfunction
DM	diabetes mellitus
E/A	early and late mitral inflow
eGFR	estimated glomerular filtration rate
ESKD	end-stage kidney disease
Hb	hemoglobin
HDL	high-density lipoprotein
HT	hypertension
IFG	impaired fasting glucose
IgAN	immunoglobulin-A nephropathy
IGT	impaired glucose tolerance
LVEF	left ventricle ejection fraction
LVEDD	left ventricular end-diastolic diameter
LVH	left ventricular hypertrophy
LVMI	left ventricular mass index
MetS	metabolic syndrome
NCEP	ATP III National Cholesterol Education Program Adult Treatment Panel III
cfPWV	carotid–femoral pulse wave velocity
SGLT-2-inhibitor	sodium–glucose transporter-2-inhibitor
TG	triglyceride
UA	uric acid

References

1. Jha, V.; Garcia-Garcia, G.; Iseki, K.; Li, Z.; Naicker, S.; Plattner, B.; Saran, R.; Wang, A.Y.; Yang, C.W. Chronic kidney disease: Global dimension and perspectives. *Lancet* **2013**, *382*, 260–272. [CrossRef]
2. Gansevoort, R.T.; Correa-Rotter, R.; Hemmelgarn, B.R.; Jafar, T.H.; Heerspink, H.J.; Mann, J.F.; Matsushita, K.; Wen, C.P. Chronic kidney disease and cardiovascular risk: Epidemiology, mechanisms, and prevention. *Lancet* **2013**, *382*, 339–352. [CrossRef]
3. Canney, M.; Gunning, H.M.; Zheng, Y.; Rose, C.; Jauhal, A.; Hur, S.A.; Sahota, A.; Reich, H.N.; Barbour, S.J. Risk of Cardiovascular Events in Individuals with Primary Glomerular Diseases. *Am. J. Kidney Dis.* **2022**, *80*, 740–750. [CrossRef]
4. Ortiz, A.; Wanner, C.; Gansevoort, R. Chronic kidney disease as cardiovascular risk factor in routine clinical practice: A position statement by the Council of the European Renal Association. *Eur. J. Prev. Cardiol.* **2022**, *29*, 2211–2215. [CrossRef]
5. Kwon, C.S.; Daniele, P.; Forsythe, A.; Ngai, C. A Systematic Literature Review of the Epidemiology, Health-Related Quality of Life Impact, and Economic Burden of Immunoglobulin A Nephropathy. *J. Health Econ. Outcomes Res.* **2021**, *8*, 36–45. [CrossRef]
6. Schena, F.P.; Pesce, F. Epidemiology and ancestral difference. In *Recent Advances in IgA Nephropathy*; Lai, K.N., Ed.; World Scientific Publishing Co.: Hackensack, NJ, USA, 2009; pp. 9–20.
7. Berthoux, C.B.; Mohey, H. Clinical course of primary IgA nephropathy. In *Recent Advances in IgA Nephropathy*; Lai, K.N., Ed.; World Scientific Publishing Co.: Hackensack, NJ, USA, 2009; pp. 107–120.
8. Floege, J.; Feehally, J. IgA nephropathy: Recent developments. *J. Am. Soc. Nephrol.* **2000**, *11*, 2395–2403. [CrossRef]
9. Barrat, J.; Feehally, J. IgA nephropathy. *J. Am. Soc. Nephrol.* **2005**, *16*, 2088–2097. [CrossRef]
10. Bonnet, F.; Deprele, C.; Sassolas, A.; Moulin, P.; Berthezène, F.; Berthoux, F. Excessive body weight as a new independent risk factor for clinical and pathological progression in primary IgA nephritis. *Am. J. Kidney Dis.* **2001**, *37*, 720–727. [CrossRef]
11. Lee, C.-C.; Sun, C.; Wu, I.-W.; Wang, S.-Y.; Wu, M.-S. Metabolic syndrome loses its predictive power in late-stage chronic kidney disease progression—A paradoxical phenomenon. *Clin. Nephrol.* **2011**, *75*, 141–149. [CrossRef]
12. Wang, Y.; Sun, B.; Sheng, L.T.; Pan, X.F.; Zhou, Y.; Zhu, J.; Li, X.; Yang, K.; Guo, K.; Zhang, X.; et al. Association between weight status, metabolic syndrome, and chronic kidney disease among middle-aged and elderly Chinese. *Nutr. Metab. Cardiovasc. Dis.* **2020**, *30*, 2017–2026. [CrossRef]

13. Li, Y.; Xie, D.; Qin, X.; Tang, G.; Xing, H.; Li, Z.; Xu, X.; Xu, X.; Hou, F. Metabolic syndrome, but not insulin resistance, is associated with an increased risk of renal function decline. *Clin. Nutr.* **2015**, *34*, 269–275. [CrossRef]
14. Thomas, G.; Sehgal, A.R.; Kashyap, S.R.; Srinivas, T.R.; Kirwan, J.P.; Navaneethan, S.D. Metabolic Syndrome and Kidney Disease: A Systematic Review and Meta-analysis. *Clin. J. Am. Soc. Nephrol.* **2011**, *6*, 2364–2373. [CrossRef]
15. Rashidbeygi, E.; Safabakhsh, M.; Aghdam, S.D.; Mohammed, S.H.; Alizadeh, S. Metabolic syndrome and its components are related to a higher risk for albuminuria and proteinuria: Evidence from a meta-analysis on 10,603,067 subjects from 57 studies. *Diabetes Metab. Syndr. Clin. Res. Rev.* **2019**, *13*, 830–843. [CrossRef]
16. Syrjänen, J.; Mustonen, J.; Pasternack, A. Hypertriglyceridaemia and hyperuricemia are risk factors for progression of IgA nephropathy. *Nephrol. Dial. Transplant.* **2000**, *15*, 34–42. [CrossRef]
17. Yamamoto, R.; Nagasawa, Y.; Shoji, T.; Iwatani, H.; Hamano, T.; Kawada, N.; Inoue, K.; Uehata, T.; Kaneko, T.; Okada, N.; et al. Cigarette smoking and progression of IgA nephropathy. *Am. J. Kidney Dis.* **2010**, *56*, 313–324. [CrossRef]
18. Lakka, H.-M.; Laaksonen, D.E.; Lakka, T.A.; Niskanen, L.K.; Kumpusalo, E.; Tuomilehto, J.; Salonen, J.T. The metabolic syndrome and total and cardiovascular disease mortality in middle-aged men. *JAMA* **2002**, *288*, 2709–2716. [CrossRef]
19. Chen, J.; Muntner, P.; Hamm, L.L.; Jones, D.W.; Batuman, V.; Fonseca, V.; Whelton, P.K.; He, J. The metabolic syndrome and chronic kidney disease in US adults. *Ann. Intern. Med.* **2004**, *140*, 167–174. [CrossRef]
20. Kurella, M.; Lo, J.C.; Chertow, G.M. Metabolic syndrome and the risk for chronic kidney disease among nondiabetic adults. *J. Am. Soc. Nephrol.* **2005**, *16*, 2134–2140. [CrossRef]
21. Grundy, S.M.; Cleeman, J.I.; Daniels, S.R.; Donato, K.A.; Eckel, R.H.; Franklin, B.A.; Gordon, D.J.; Krauss, R.M.; Savage, P.J.; Smith, S.C., Jr.; et al. Diagnosis and management of the metabolic syndrome: American Heart Association/National Heart, Lung, and Blood Institute scientific statement. *Circulation* **2005**, *112*, 2735–2752. [CrossRef]
22. Reaven, G. Metabolic syndrome: Pathophysiology and implications for management of cardiovascular disease. *Circulation* **2002**, *106*, 286–292. [CrossRef]
23. Kovács, T.; Vas, T.; Kovesdy, C.P.; Késõi, I.; Sági, B.; Wittmann, I.; Nagy, J. Metabolic syndrome and other cardiovascular risk factors associated with the progression of IgA nephropathy. *Clin. Kidney J.* **2013**, *6*, 395–401. [CrossRef]
24. Lastra, G.; Manrique, C.; McFarlane, S.I.; Sowers, J.R. Cardiometabolic syndrome and chronic kidney disease. *Curr. Diabetes Rep.* **2006**, *6*, 207–212. [CrossRef]
25. Natali, A.; Pucci, G.; Boldrini, B.; Schillaci, G. Metabolic syndrome: At the crossroads of cardiorenal risk. *J. Nephrol.* **2009**, *22*, 29–38.
26. Zoccali, C. Overweight, obesity and metabolic alterations in chronic kidney disease. *Contrib. Soc. Biol. Med. Sci. MASA* **2009**, *30*, 17–31.
27. Fliser, D.; Pacini, G.; Engelleiter, R.; Kautzky-Willer, A.; Prager, R.; Franek, E.; Ritz, E. Insulin resistance and hyperinsulinemia are already present in patients with incipient renal disease. *Kidney Int.* **1998**, *53*, 1343–1347. [CrossRef]
28. Ștefan, G.; Zugravu, A.; Stancu, S. Mortality in IgA Nephropathy: A Long-Term Follow-Up of an Eastern European Cohort. *Medicina* **2024**, *60*, 247. [CrossRef]
29. Nagy, J.; Kovacs, T. Special clinical syndromes. In *Recent Advances in IgA Nephropathy*; Lai, K.N., Ed.; World Scientific Publishing Co.: Hackensack, NJ, USA, 2009; pp. 121–138.
30. Kovesdy, C.P.; Trivedi, B.K.; Kalantar-Zadeh, K.; Anderson, J.E. Association of low blood pressure with increased mortality in patients with moderate to severe chronic kidney disease. *Nephrol. Dial. Transplant.* **2006**, *21*, 1257–1262. [CrossRef]
31. Nagy, J.; Kovács, T.; Wittmann, I. Renal protection in IgA nephropathy requires strict blood pressure control. *Nephrol. Dial. Transplant.* **2005**, *20*, 1533–1539. [CrossRef]
32. Kwan, B.C.H.; Murtaugh, M.A.; Beddhu, S. Associations of body size with metabolic syndrome and mortality in moderate chronic kidney disease. *Clin. J. Am. Nephrol.* **2007**, *2*, 992–998. [CrossRef]
33. Kopple, J.D.; Feroze, U. The effect of obesity on chronic kidney disease. *J. Ren. Nutr.* **2011**, *21*, 66–71. [CrossRef]
34. Hsu, C.-Y.; McCulloch, C.E.; Iribarren, C.; Darbinian, J.; Go, A.S. Body mass index and risk for end-stage renal disease. *Ann. Intern. Med.* **2006**, *144*, 21–28. [CrossRef]
35. Madero, M.; Sarnak, M.J.; Wang, X.; Sceppa, C.C.; Greene, T.; Beck, G.J.; Kusek, J.W.; Collins, A.J.; Levey, A.S.; Menon, V. Body mass index and mortality in CKD. *Am. J. Kidney Dis.* **2007**, *3*, 404–411. [CrossRef]
36. Tanaka, M.; Yamada, S.; Iwasaki, Y.; Sugishita, T.; Yonemoto, S.; Tsukamoto, T.; Fukui, S.; Takasu, K.; Muso, E. Impact of obesity on IgA nephropathy: Comparative ultrastructural study between obese and non-obese patients. *Nephron Clin. Pract.* **2009**, *112*, 71–78. [CrossRef]
37. Shimamoto, M.; Ohsawa, I.; Suzuki, H.; Hisada, A.; Nagamachi, S.; Honda, D.; Inoshita, H.; Shimizu, Y.; Horikoshi, S.; Tomino, Y. Impact of Body Mass Index on Progression of IgA Nephropathy Among Japanese Patients. *J. Clin. Lab. Anal.* **2015**, *29*, 353–360. [CrossRef]
38. Muntner, P.; Coresh, J.; Smith, J.C.; Eckfeldt, J.; Klag, M.J. Plasma lipids and risk of developing renal dysfunction: The atherosclerosis risk in community study. *Kidney Int.* **2000**, *58*, 293–301. [CrossRef]
39. Fried, F.; Orchard, T.J.; Kasiske, B.L. Effect of lipid reduction on the progression of renal disease: A meta-analysis. *Kidney Int.* **2001**, *59*, 260–269. [CrossRef]
40. Feig, I.D. Uric acid: A novel mediator and marker of risk in chronic kidney disease. *Curr. Opin. Nephrol. Hypertens.* **2009**, *18*, 526–530. [CrossRef]
41. Obermayr, R.P.; Temml, C.; Gutjahr, G.; Knechtelsdorfer, M.; Oberbauer, R.; Klauser-Braun, R. Elevated uric acid increases the risk for kidney disease. *J. Am. Soc. Nephrol.* **2008**, *19*, 2407–2413. [CrossRef]

42. Myllymäki, J.; Honkanen, T.; Syrjänen, J.; Helin, H.; Rantala, I.; Pasternack, A.; Mustonen, J. Uric acid correlates with the severity of histopathological parameters in IgA nephropathy. *Nephrol. Dial. Transplant.* **2005**, *20*, 89–95. [CrossRef]
43. Ben-Dov, I.Z.; Kark, J.D. Serum uric acid is a GFR-independent long-term predictor of acute and chronic renal insufficiency: The Jerusalem Lipid Research Clinic cohort study. *Nephrol. Dial. Transplant.* **2011**, *26*, 2558–2566. [CrossRef]
44. Alizadeh, S.; Ahmadi, M.; Nejad, B.G.; Djazayeri, A.; Shab-Bidar, S. Metabolic syndrome and its components are associated with increased chronic kidney disease risk: Evidence from a meta-analysis on 11 109 003 participants from 66 studies. *Int. J. Clin. Pract.* **2018**, *72*, e13201. [CrossRef]
45. Panwar, B.; Hanks, L.J.; Tanner, R.M.; Muntner, P.; Kramer, H.; McClellan, W.M.; Warnock, D.G.; Judd, S.E.; Gutiérrez, O.M. Obesity, metabolic health, and the risk of end-stage renal disease. *Kidney Int.* **2015**, *87*, 1216–1222. [CrossRef]
46. Lea, J.; Cheek, D.; Thornley-Brown, D.; Appel, L.; Agodoa, L.; Contreras, G.; Gassman, J.; Lash, J.; Miller, E.R., 3rd; Randall, O.; et al. Metabolic Syndrome, Proteinuria, and the Risk of Progressive CKD in Hypertensive African Americans. *Am. J. Kidney Dis.* **2008**, *51*, 732–740. [CrossRef]
47. Li, X.; Liang, Q.; Zhong, J.; Gan, L.; Zuo, L. The Effect of Metabolic Syndrome and Its Individual Components on Renal Function: A Meta-Analysis. *J. Clin. Med.* **2023**, *12*, 1614. [CrossRef]
48. Drawz, P.; Rahman, M. Chronic Kidney Disease. *Ann. Intern. Med.* **2015**, *162*, ITC1–ITC16. [CrossRef]
49. Kim, H.W.; Park, J.T.; Joo, Y.S.; Kang, S.C.; Lee, J.Y.; Lee, S.; Chang, T.I.; Kang, E.W.; Ryu, D.-R.; Yoo, T.H. Systolic blood pressure and chronic kidney disease progression in patients with primary glomerular disease. *J. Nephrol.* **2021**, *34*, 1057–1067. [CrossRef]
50. Wang, M.; Xia, M.; Yang, H.; Zhang, D.; Zhao, Y.; He, Y.; Liu, J.; Zhang, L.; Yin, C.; Bai, Y. Interaction effect of blood glucose and pressure on the risk of chronic kidney disease: A population-based prospective cohort study. *Endocrine* **2022**, *77*, 252–261. [CrossRef]
51. Echouffo-Tcheugui, J.B.; Narayan, K.M.V.; Weisman, D.; Golden, S.H.; Jaar, B.G. Association between prediabetes and risk of chronic kidney disease: A systematic review and meta-analysis. *Diabet. Med.* **2016**, *33*, 1615–1624. [CrossRef]
52. Kim, H.; Park, S.; Kwon, S.H.; Jeon, J.S.; Han, D.C.; Noh, H. Impaired fasting glucose and development of chronic kidney disease in non-diabetic population: A Mendelian randomization study. *BMJ Open Diabetes Res. Care* **2020**, *8*, e001395. [CrossRef]
53. Swiecicka-Klama, A.; Połtyn-Zaradna, K.; Szuba, A.; Zato'nska, K. The Natural Course of Impaired Fasting Glucose. *Adv. Exp. Med. Biol.* **2021**, *1324*, 41–50.
54. Barbour, S.; Er, L.; Djurdjev, O.; Karim, M.; Levin, A. The prevalence of hematologic and metabolic abnormalities during chronic kidney disease stages in different ethnic groups. *Kidney Int.* **2008**, *74*, 108–114. [CrossRef]
55. Jankowski, J.; Floege, J.; Fliser, D.; Böhm, M.; Marx, N. Cardiovascular Disease in Chronic Kidney Disease: Pathophysiological Insights and Therapeutic Options. *Circulation* **2021**, *143*, 1157–1172. [CrossRef]
56. Hager, M.R.; Narla, A.D.; Tannock, L.R. Dyslipidemia in patients with chronic kidney disease. *Rev. Endocr. Metab. Disord.* **2017**, *18*, 29–40. [CrossRef]
57. Stefansson, V.T.; Schei, J.; Solbu, M.D.; Jenssen, T.G.; Melsom, T.; Eriksen, B.O. Metabolic syndrome but not obesity measures are risk factors for accelerated age-related glomerular filtration rate decline in the general population. *Kidney Int.* **2018**, *93*, 1183–1190. [CrossRef]
58. Soohoo, M.; Hashemi, L.; Hsiung, J.-T.; Moradi, H.; Budoff, M.J.; Kovesdy, C.P.; Kalantar-Zadeh, K.; Streja, E. Association of Serum Triglycerides and Renal Outcomes among 1.6 Million US Veterans. *Nephron* **2022**, *146*, 457–468. [CrossRef]
59. Rahman, M.; Yang, W.; Akkina, S.; Alper, A.; Anderson, A.H.; Appel, L.J.; He, J.; Raj, D.S.; Schelling, J.; Strauss, L.; et al. Relation of Serum Lipids and Lipoproteins with Progression of CKD: The CRIC study. *Clin. J. Am. Soc. Nephrol.* **2014**, *9*, 1190–1198. [CrossRef]
60. Lin, H.Y.; Chang, L.; Niu, S.; Kuo, I.; Yen, C.; Shen, F.; Chen, P.; Chang, J.; Hung, C. High risk of renal outcome of metabolic syndrome independent of diabetes in patients with CKD stage 1-4: The ICKD database. *Diabetes Metab. Res. Rev.* **2023**, *39*, e3618. [CrossRef]
61. Sági, B.; Késői, I.; Késői, B.; Vas, T.; Csiky, B.; Kovács, T.; Nagy, J. Arterial stiffness may predict renal and cardiovascular prognosis in autosomal-dominant polycystic kidney disease. *Physiol. Int.* **2018**, *105*, 145–156. [CrossRef]
62. Késoi, I.; Sági, B.; Tóth, O.I.; Vas, T.; Fazekas, A.; Kovács, T.; Pintér, T.; Wittmann, I.; Nagy, J. Different effect of IgA nephropathy and polycystic kidney disease on arterial stiffness. *Kidney Blood Press. Res.* **2011**, *34*, 158–166. [CrossRef]
63. Sági, B.; Késői, I.; Vas, T.; Csiky, B.; Nagy, J.; Kovács, T.J. Relationship between arterial stiffness, left ventricular diastolic function, and renal function in chronic kidney disease. *BMC Nephrol.* **2023**, *24*, 261. [CrossRef]
64. Sági, B.; Késői, I.; Vas, T.; Csiky, B.; Nagy, J.; Kovács, T.J. Left ventricular myocardial mass index associated with cardiovascular and renal prognosis in IgA nephropathy. *BMC Nephrol.* **2022**, *23*, 285. [CrossRef]
65. Anders, H.J.; Peired, A.J.; Romagnani, P. SGLT2 inhibition requires reconsideration of fundamental paradigms in chronic kidney disease, 'diabetic nephropathy', IgA nephropathy and podocytopathies with FSGS lesions. *Nephrol. Dial. Transplant.* **2022**, *37*, 1609–1615. [CrossRef]
66. Caster, D.J.; Lafayette, R.A. The Treatment of Primary IgA Nephropathy: Change, Change, Change. *Am. J. Kidney Dis.* **2024**, *83*, 229–240. [CrossRef]

Disclaimer/Publisher's Note: The statements, opinions and data contained in all publications are solely those of the individual author(s) and contributor(s) and not of MDPI and/or the editor(s). MDPI and/or the editor(s) disclaim responsibility for any injury to people or property resulting from any ideas, methods, instructions or products referred to in the content.

biomedicines

MDPI

Review

The Safety and Efficacy of Dietary Epigallocatechin Gallate Supplementation for the Management of Obesity and Non-Alcoholic Fatty Liver Disease: Recent Updates

Ruike Yan and Yanli Cao *

Department of Endocrinology and Metabolism, Institute of Endocrinology, NHC Key Laboratory of Diagnosis and Treatment of Thyroid Diseases, The First Affiliated Hospital of China Medical University, Shenyang 110001, China; yanruike0130@163.com

* Correspondence: vanilla421@163.com

Abstract: Epigallocatechin gallate (EGCG) is the predominant bioactive catechin in green tea, and it has been ascribed a range of beneficial health effects. Current increases in obesity and non-alcoholic fatty liver disease (NAFLD) rates represent a persistent and burdensome threat to global public health. While many clinical studies have demonstrated that EGCG is associated with positive effects on various health parameters, including metabolic biomarkers, waist circumference, and body weight when consumed by individuals affected by obesity and NAFLD, there are also some reports suggesting that it may entail some degree of hepatotoxicity. The present review provides a comprehensive summary of the extant clinical findings pertaining to the safety and effectiveness of EGCG in managing obesity and NAFLD, with a particular focus on how treatment duration and dose level affect the bioactivity of this compound.

Keywords: epigallocatechin gallate; obesity; non-alcoholic fatty liver disease; metabolic disease

1. Introduction

Obesity is a serious and growing threat to global public health and human longevity [1]. Based on recent statistics, the prevalence of obesity among women globally has risen from 8.8% (8.5–9.1%) in 1990 to 18.5% (17.9–19.1%) in 2022, with a corresponding increase from 4.8% (4.6–5.0%) to 14.0% (13.4–14.6%) among men [2]. Treating obesity is a costly process, and healthcare costs tend to rise in parallel with increasing body mass index (BMI) values. By 2035, the global costs associated with managing excessive weight and obesity are forecast to reach USD 4.32 trillion [3,4]. In addition to shortening the life expectancy of affected individuals, obesity also increases the risk of cardiovascular disease and diabetes [5,6]. Rising obesity rates are also closely associated with rising non-alcoholic fatty liver disease (NAFLD) incidence rates, with a 3.5-fold greater likelihood of NAFLD among obese individuals relative to individuals of normal body weight (RR = 3.53, 95% CI 2.48 to 5.03, $p < 0.001$) [7]. The prevalence of NAFLD is rising to epidemic proportions, with patients exhibiting a range of phenotypes along a spectrum from simple steatosis to non-alcoholic steatohepatitis (NASH), which can lead to cirrhosis and hepatocellular carcinoma [8]. In 2022, NAFLD was estimated to affect 32–34% of the global population [9].

While obesity is associated with a wide range of health risks, achieving weight loss and maintaining any reductions in body weight remains extremely difficult [10]. Myriad approaches are used to treat obesity, including dietary modifications, lifestyle changes,

behavioral therapy, nutritional supplementation, pharmacologic treatment, and, if appropriate, surgery [11]. The low adherence rates for dietary modification, lifestyle adjustment, and behavioral intervention-focused approaches to managing obesity tend to yield low rates of success. While pharmacologic and surgical interventions can be effective, they are also costly and expose patients to the potential for adverse events [12]. It has been proposed that nutritional supplementation may represent a safer yet effective approach to managing obesity, providing patients with the opportunity to lose weight and restore metabolic health with fewer side effects relative to surgery or pharmacologic treatment. Much like obesity, there are few effective options available for the treatment of NAFLD and NASH, making the management of this disease challenging [13]. Rezdiffra, the first globally authorized treatment for NASH, was approved by the US FDA in 2024 [14]. While efficacious, this drug is associated with the potential for nausea, diarrhea, and other adverse events, and its utilization is also contraindicated in certain patient populations. The therapeutic efficacy of Rezdiffra treatment is also limited, with only ~30% of patients presenting with improved NASH symptoms [15]. Under current clinical guidelines, phase 3 clinical trials have been authorized for biopsy-confirmed NASH patients [16], involving trials focused on the therapeutic effects of vitamin E [17], pioglitazone [17,18], Selonsertib [19], obeticholic acid [20], Cenicriviroc [21], and Elafibranor [22]. In line with the fact that NAFLD has been linked with metabolic syndrome, exercise, dietary changes, and other lifestyle modifications can reduce hepatic fat levels and limit hepatic fibrosis. Most patients still face difficulties sustaining weight loss, and a majority of these individuals are unable to maintain the associated lifestyle changes over extended periods [23–25]. There is therefore a pressing need to define reliable approaches to treating NAFLD and initiating these interventions at early time points to more effectively slow or prevent progression to NASH.

Green tea is rich in bioactive compounds and remains an extremely popular beverage globally, especially in Asian countries. It is rich in vitamins, carbohydrates, minerals, pigments, proteins, polyphenols, and caffeine, all of which have been proposed to contribute to the health-promoting properties of this beverage [26]. Green tea-derived polyphenols, particularly catechins, are believed to mediate its therapeutic anti-inflammatory, antioxidant, and metabolic effects, as demonstrated in a series of published clinical studies [27–29]. Epigallocatechin gallate (EGCG) is highly bioactive and represents the predominant catechin in green tea, making up 20–30% of green tea leaves by dry weight [30]. EGCG presents with a plethora of beneficial effects, such as antioxidant, anticancer, and anti-inflammatory properties [31–33]. As a common plant-derived compound, EGCG can be obtained cost-effectively and it is generally recognized as safe [34]. In recent years, an increasing body of research has demonstrated its ability to support weight reduction and retard NAFLD progression. Animal studies have demonstrated that EGCG can significantly reduce body weight in mice fed a high-fat diet and positively influence their lipid profile, including triglyceride, cholesterol, high-density lipoprotein cholesterol (HDL-C), and low-density lipoprotein cholesterol (LDL-C) levels [35]. In high-fat diet-induced obese rats, EGCG improved serum glucose levels, mitigated inflammation, and reduced oxidative stress associated with aging [36]. Furthermore, EGCG has been shown to enhance liver health by reducing hepatic fat accumulation, oxidative damage, and inflammatory responses in high-fat-fed rats [37]. Clinical studies also suggest that EGCG can aid in weight reduction and metabolic improvement in obese patients while slowing the progression of NAFLD [38–40]. Variability in dosage, intervention duration, and study outcomes has been noted in existing research. Clinical studies investigating EGCG intervention for obesity and NAFLD have utilized daily doses ranging from 150 mg to 900 mg. However, studies have suggested that EGCG may pose risks to liver health, with potential concerns related to dosage. Currently, there is a limited number of comprehensive reviews summarizing the clinical evidence for

EGCG in the treatment of NAFLD. The determination of safe and effective dosages, as well as the therapeutic potential of EGCG for managing obesity and NAFLD, remain important areas for further investigation.

Considering the association between obesity and NAFLD, this review aims to summarize the current evidence on the utilization of green tea extracts, specifically EGCG, in the management of obesity or NAFLD. It seeks to evaluate the therapeutic efficacy and safety of EGCG across different dosages and intervention durations.

2. EGCG: A Brief Overview

EGCG has a core structure consisting of four rings that are the primary site of its bioactivity owing primarily to reactive phenolic hydroxyl groups present on its core rings [41]. The reported therapeutic effects of EGCG include antitumor, anti-mutagenic, anti-inflammatory, and antioxidant activities, and it has also been linked to reductions in body weight and visceral fat levels [33,42–45].

2.1. Sources of EGCG

EGCG is primarily isolated from green tea, wherein it comprises ~40% of the total catechins [46]. Smaller amounts of EGCG can also be isolated from black tea, white tea, and oolong tea, while trace amounts are present in certain beans, nuts, and fruits including berries, plums, and apples [33,47,48].

2.2. Potential Biological Effects of EGCG in the Treatment of Obesity and NAFLD

EGCG can reduce lipogenesis by activating Adenosine Monophosphate-Activated Protein Kinase (AMPK). For example, Santana et al. found that after 8 weeks, compared to high-fat diet + EGCG-fed mice, high-fat diet + placebo-fed mice showed increased body weight. Additionally, when compared to the control diet + placebo group, the control diet + EGCG group showed a 16% reduction in body weight and a 32% decrease in serum triglyceride levels. Compared to the control diet + placebo group, the control diet + EGCG group exhibited increased phosphorylation of AMPK and hormone-sensitive lipase in both epididymal and retroperitoneal adipose tissues. Furthermore, increased phosphorylation of acetyl-CoA carboxylase was observed in both types of adipose tissues [49]. In vitro studies have shown that EGCG activates AMPK and reduces lipid accumulation in *HepG2* cells. Activation of AMPK shifted some free fatty acids (FFAs) toward oxidation, away from lipid and triglyceride storage, and suppressed hepatic gluconeogenesis [50]. These findings suggest that EGCG may alleviate body weight and delay NAFLD progression by promoting fat breakdown and reducing lipid accumulation. Lee et al. reported that in the epididymal white adipose tissue of mice fed EGCG, there was a significant reduction in the mRNA expression of adipogenic genes, including *peroxisome proliferator-activated receptor-gamma* (*PPAR-γ*), *CCAAT enhancer-binding protein-alpha* (*C/EBP-α*), *sterol regulatory element-binding protein-1c* (*SREBP-1c*), *adipocyte fatty acid-binding protein* (*aP2*), *lipoprotein lipase* (*LPL*), and *fatty acid synthase* (*FAS*). In contrast, the mRNA levels of *carnitine palmitoyltransferase-1* (*CPT-1*), *uncoupling protein 2* (*UCP2*), and *lipolytic genes like hormone-sensitive lipase* (*HSL*) and *adipose triglyceride lipase* (*ATGL*) were significantly elevated [51]. This suggests that EGCG's effects on weight reduction are mediated by multiple genes. In addition to reducing body weight by promoting fat breakdown and decreasing fat synthesis, EGCG can also affect the gastrointestinal absorption of lipids and proteins. For example, in a study with mice, EGCG dose-dependently reduced food digestibility and increased fecal excretion. With a 13C-triglyceride-enriched diet, EGCG supplementation increased the 13C levels in the feces. Moreover, the study also found that EGCG could downregulate genes related to hepatic fat synthesis, including *Acetyl-CoA carboxylase* (ACC), *FAS*, and

Stearoyl-CoA desaturase 1 (*SCD1*) [52]. Studies have shown that EGCG can increase the lipid content in the feces of mice, which is related to its effect on pancreatic lipase [53]. EGCG can reduce liver weight and triglyceride levels in high-fat-fed mice, decreasing lipid accumulation in hepatocytes [54]. Additionally, Santamarina et al. found that EGCG seems to enhance mitochondrial complex chain activity, thereby increasing lipid oxidation and preventing liver fat degeneration [55]. EGCG can also improve the expression of inflammatory mediators in liver adipose tissue. Yuan et al. found that EGCG significantly reduced the levels of NF-κB protein in the liver of rats fed a high-fat diet [36], which may help prevent the progression of simple fatty liver to NASH. EGCG can also modulate the gut microbiota. EGCG significantly increased the abundance of *Dubosiella* and *Akkermansia* in mice fed a high-fat diet, which is crucial for alleviating obesity [56]. Overall, EGCG treatment for obesity and NAFLD primarily exerts its effects by reducing lipogenesis, promoting lipolysis, inhibiting lipid absorption, and alleviating inflammatory responses.

2.3. EGCG Absorption and Bioavailability

EGCG absorption primarily occurs in the jejunum and ileum wherein it diffuses across the epithelium without any concomitant hydrolysis or decoupling [57]. Despite its advantageous health effects, EGCG and other catechins are associated with drawbacks that include poor stability [58]. Indeed, when incubated for 1 h in simulated intestinal fluid (pH 7.4), roughly 80% of EGCG is degraded. Studies of ileal fluid samples collected 24 h after administering green tea extract (200 mg) yielded catechin recovery rates between 39% and 48% of the ingested amount [59]. The recovery rate for EGCG is comparatively high at ~60% [60].

In both humans and rats, EGCG oral bioavailability has been found to be fairly low at just 0.1–0.3% [61]. This poor availability is attributed to the presence of polyphenolic hydroxyl groups within EGCG that are subject to reactions that include methylation, sulfonation, glucuronidation, and cysteine conjugation [62].

3. Clinical Overview of the Effects of EGCG on Obesity and NAFLD

3.1. The Impact of Supplemental EGCG Intake on Overweight and Obese Individuals

3.1.1. Body Weight and Glycolipid Metabolism Responses to Low- or Medium-Dose EGCG

Table 1 shows an overview of clinical studies published to date in which researchers have examined the impacts of EGCG on overweight and obese individuals. An investigation by Kovacs et al. found that daily intake of green tea extract (323 mg/day of EGCG, 104 mg/day of caffeine) for three months had no significant effect on body weight [63]. A further study similarly determined that daily EGCG intake (300 mg/day) for three months failed to positively impact the body weight, fat metabolism, fat content, or energy balance of premenopausal obese women [38]. Despite the negative findings in both studies, the majority of the studies reviewed here still suggest that supplementation with low doses of EGCG over a three-month period can yield beneficial effects.

For example, Zhang et al. studied the impact of EGCG on blood lipid levels and hepatic function among males who were overweight or obese, administering green tea extract (150 mg/day of EGCG) or placebo control to 24 subjects for 12 weeks. They determined that participants receiving green tea extract exhibited markedly reduced LDL-C and total cholesterol (TC) levels relative to placebo controls at the end of this period [64]. Sulibursk a et al. further found that supplemental EGCG capsule intake (208 mg/day) for three months significantly decreased the body weights, waist circumferences, and LDL-C, TC, and triglyceride (TG) levels of obese participants [65]. Bogdanski et al. found that the daily intake of green tea extract capsules (208 mg/day of EGCG) for three months was associated with markedly reduced TC, LDL-C, and TG levels together with increased

HDL-C levels relative to placebo in hypertensive obese patients. These changes also coincided with decreases in blood sugar, insulin, and fasting glucose levels, as well as improved insulin resistance, significantly decreased TNF-α and CRP levels, and the overall augmentation of patient antioxidant status [66]. The above study demonstrated that supplementation with EGCG for approximately three months can significantly improve lipid levels in overweight and obese individuals. This effect is attributed to EGCG's ability to enhance lipid metabolism. Animal studies have shown that EGCG increases the expression of proteins such as fatty acid binding protein-1 (FABP1), long-chain acyl-CoA synthetase 1 (ACSL1), and carnitine palmitoyltransferase II (CPT2), which promote fatty acid transport and oxidation. Additionally, EGCG reduces the expression of acetyl-CoA carboxylase (ACC1) and fatty acid synthase (FAS), both of which are involved in fatty acid synthesis [36].

It was also found that the intake of a mixture of green tea and caffeine (EGCG, 270 mg/day; caffeine, 150 mg/day) for three months by participants who were overweight or moderately obese led to reduced body weights, waist circumferences, body fat, and respiratory quotients (RQs), while also increasing energy expenditure at rest [67]. In their randomized controlled trial enrolling overweight postmenopausal women with class I obesity, Rondanelli et al. found that the administration of a tea extract (300 mg/day, containing $\geq$13% EGCG) for 60 days resulted in significant reductions in CRP and insulin levels, enhanced fat oxidation, improved waist circumference, and enhanced resting energy expenditure relative to placebo control [68]. These two studies demonstrated that EGCG supplementation increased resting energy expenditure in overweight and obese participants, with a significant impact on anthropometric measurements. It has been reported that EGCG promotes fat oxidation (FOX) and weight loss by enhancing resting energy expenditure and reducing RQ. Additionally, this meta-analysis also indicated that EGCG supplementation led to a reduction in waist circumference [69]. Together, the above results suggest that the supplemental intake of EGCG at doses of 150–300 mg/day by obese individuals for approximately 3 months may help improve lipid levels and lower fasting blood glucose, and might improve anthropometric measurements.

Basu et al. found that obese individuals who drank four cups of green tea (440 mg/day of EGCG) or took two green tea extract capsules (460 mg/day of EGCG) per day for 8 weeks exhibited significant reductions in body weight and BMI. In these same individuals, EGCG intake led to pronounced reductions in circulating levels of the oxidative stress markers malondialdehyde (MDA) and hydroxynonenal (HNE), consistent with the mitigation of systemic lipid peroxidation [70]. Alves Ferreira et al. determined that the daily supplemental intake of 1 g of green tea extract (560 mg/day of total polyphenols) for 12 weeks by overweight women without diabetes markedly improved fasting blood glucose and lipid profiles, outperforming daily metformin treatment (1 g/day) [71]. Quinhoneiro et al. determined that when women with class III obesity consumed supplemental EGCG (450 mg/day) for 8 weeks, the *UCP3* gene associated with enhanced energy expenditure and reduced fat accumulation was upregulated. Even with these changes at the molecular level, however, the body weight of study participants was not significantly impacted by EGCG treatment [72]. Studies have shown that EGCG can reduce body weight in mice fed a high-fat diet by upregulating *UCP3* mRNA levels [73]. The study only observed an upregulation of *UCP3* levels without resulting in weight loss, possibly due to insufficient observation duration. Relatively few studies have thus explored the influence of supplemental EGCG doses in the 400–600 mg/day range on obesity, and differences in follow-up durations and analyzed outcomes are evident across these studies. At a high level, the evidence that is available suggests that EGCG exhibits antioxidant activity, can reduce levels of blood sugar, and may enhance energy expenditure.

3.1.2. The Responses of Body Weight and Glycolipid Metabolism to High-Dose EGCG Treatment

Expanding on the above results, there have also been several studies specifically examining the impact of high-dose EGCG intake on obese individuals. In their study of 115 women with central obesity, Chen et al., for example, administered 856.8 mg/day of EGCG to a subset of these participants and observed markedly lower body weights, BMI values, and waist circumferences among EGCG-treated individuals relative to those in the placebo control group [74]. In contrast, Brown et al. found that the daily supplemental intake of 800 mg/day of EGCG for eight weeks failed to impact the glucose tolerance, insulin secretion, or insulin sensitivity of overweight/obese men relative to placebo controls, although it did reduce levels of diastolic blood pressure [75]. Dostal et al. reported significantly lower insulin levels among obese postmenopausal women with baseline fasting insulin levels $\geq$ 10 μIU/mL following high-dose EGCG treatment (843 mg/day) relative to placebo control. Study participants with homozygosity for a high-activity (G/G) variant of the *catechol-O-methyltransferase* (*COMT*) gene also presented with markedly lower adiponectin levels relative to individuals with the low-activity (A/A) genotype [76]. In a separate report, however, Dostal failed to observe any improvements in plasma leptin, ghrelin, or adiponectin levels among overweight postmenopausal women following daily EGCG treatment (834 mg/day) for 11–12 months [77]. Dostal et al. similarly found that the daily supplemental consumption of EGCG from green tea (843 mg/day) for 12 months had no impact on satiety, leptin, adiponectin, or ghrelin levels among postmenopausal women [78]. Huang et al. conducted a study of 36 overweight or obese women with elevated levels of LDL-C who were given 856.8 mg/day of ECGC for six weeks. Relative to placebo treatment, EGCG consumption led to markedly decreased LDL-C levels together with significantly elevated leptin levels [79]. Nicoletti et al. demonstrated that the daily supplemental intake of EGCG (901.4 mg/day) by severely obese women for 8 weeks resulted in the upregulation of *rapamycin-insensitive companion of mTOR* (*RICTOR*) and *hypoxia inducible factor 1 alpha* (*HIF1-α*), whereas *phosphoinositide-3-kinase* (*PI3K*) expression was unaffected. In the same study, EGCG also failed to reduce the weight of enrolled participants [80]. A randomized controlled trial indicated that, compared to the low dose (200 mg/day), a high dose (600 mg/day) of EGCG did not increase fat oxidation [81]. The effect of EGCG on body weight or metabolism may not necessarily be better with higher doses. The majority of these reports also suggest that EGCG supplementation is insufficient to reduce body weight, BMI, or other body measurements among obese subjects, even when administered at high doses. Moreover, high doses of EGCG may pose a risk of liver damage, which will be discussed in Section 4.

3.1.3. The Synergistic Effects of EGCG and Other Polyphenols

Several studies to date have investigated possible combinatory or synergistic interactions between EGCG and other polyphenols in overweight or obese individuals. For instance, Most et al. noted no significant changes in overall body fat, energy expenditure, or plasma metabolite profiles following the supplemental intake of 282 mg of EGCG and 80 mg of resveratrol for three months [82]. This same combined polyphenol regimen, however, lowered the levels of factors involved in pathways linked to inflammation, immunity, and energy metabolism when suppressing apoptotic activity [83]. Supplemental EGCG and resveratrol intake among overweight or obese males has also been shown to be associated with significant decreases in *Bacteroidetes* and *Faecalibacterium prausnitzii* abundance within the gut microbiome. Baseline *Bacteroidetes* abundance was also demonstrated to predict increases in fat oxidation among these male participants in response to combined polyphenol supplementation, whereas these responses were absent among female participants [84].

Together, these results suggest that a 3-month supplemental EGCG and resveratrol treatment course can alter metabolic parameters and the composition of the gut microbiome in obese males, although these effects may be gender-specific. This information is crucial as it lays the foundation for further exploration of whether combining EGCG with other polyphenols could yield better results than using EGCG alone as a monotherapy.

3.1.4. The Synergistic Effects of EGCG and Exercise

In their study exploring the potential additive benefits of green tea extract on exercise-induced bodily changes, Bagheri et al. separated 30 overweight women into three groups, including a placebo-treated group with no exercise training, a placebo-treated group that underwent endurance training, and a green tea extract-treated group that underwent endurance training. Participants in the lattermost group took 500 mg of green tea extract (15 mg caffeine, 45% EGCG) daily. Following an 8-week intervention period, markedly higher levels of adiponectin together with decreased high-sensitivity CRP (hs-CRP) in endurance training + green tea extract participants relative to the two other study groups, whereas IL-6 and irisin levels were comparable across groups [85]. Intriguingly, the administration of this same interventional approach to obese middle-aged men revealed that the combination of endurance training and green tea extract intake significantly reduced IL-6 levels and significantly reduced irisin levels, whereas TNF-α levels were unaffected by such treatment in either study [86]. These results suggest that there may be gender-specific effects on the EGCG treatment of obese patient populations. Hill et al. also demonstrated that daily EGCG supplementation (300 mg) together with regular exercise for 12 weeks led to marked reductions in blood glucose and resting heart rate levels compared to placebo combined with exercise, without any concomitant changes in body weights, waist circumferences, waist-to-hip ratios, total body fat, or abdominal fat [87]. More rigorous studies are needed to investigate the potential synergistic effects of combining EGCG with exercise.

Table 1. Clinical studies of the effects of epigallocatechin gallate (EGCG) on overweight and obese individuals.

Author	Country	Patients	Age	Dose, Intervention Period	Control	Outcomes
Mielgo-Ayuso et al. [38].	Spain	Obese pre-menopausal women.	19–49 years	Received a tablet of EGCG at 300 mg daily for 3 months (n = 43).	Placebo (n = 40)	Did not affect body weight, fat mass, energy and fat metabolism, homeostasis assessment model for insulin resistance, total cholesterol, LDL-cholesterol, triglycerides, and liver function markers
Kovacs et al. [63]	The Netherlands	Overweight and moderately obese subjects.	18–60 years	Received green tea extracts tablets containing 323 mg EGCG and 104 mg caffeine dailyfor 3 months (n = 51).	Placebo (n = 53)	Did not significantly affect weight gain in subjects on a very-low-energy diet intervention.
Zhang et al. [64].	China	Overweight and obese men.	42.5 years	Received 300 mg green tea extract containing 95% EGCG per day and four 60-min-sessions/week for 12 weeks (n = 12).	Placebo and four 60-min-sessions/week (n = 12).	Reduced the level of LDL-C, aspartate aminotransferase, HDL-C, and TC.

Table 1. *Cont.*

Author	Country	Patients	Age	Dose, Intervention Period	Control	Outcomes
Suliburska et al. [65].	Poland	Obese subjects	30–60 years	Received a capsule containing 379 mg green tea extract containing 208 mg EGCG for 3 months (n = 23)	Placebo (n = 23)	Reduced body mass index, waist circumference, and levels of total cholesterol, LDL-cholesterol, and triglyceride, while enhancing total antioxidant level and zinc concentration in serum.
Bogdanski et al. [66].	Poland	Obese and hypertension subjects	30–60 years	Received a capsule containing 208 mg EGCG for 3 months (n = 28)	Placebo (n = 28)	Reduced blood pressures, fasting serum glucose, insulin levels, insulin resistance, Serum tumor necrosis factor α, C-reactive protein, the total and low-density lipoprotein cholesterol, and triglycerides; increased total antioxidant status and high-density lipoprotein cholesterol.
Westerterp-Plantenga et al. [67].	The Netherlands	Overweight and moderately obese subjects.	18–60 years	Received a green tea-caffeine mixture (270 mg EGCG + 150 mg caffeine per day) for 3 months (n = 38).	Placebo (n = 38)	Reduced body weight, waist, respiratory quotient, and body fat, while increasing resting energy expenditure.
Rondanelli et al. [68].	Italy	Overweight post-menopausal and class I obese women.	60.57 years	Received 300 mg Greenselect® Phytosome® containing more than 13% EGCG per day for 60 days. (n = 14)	Placebo (n = 14)	Reduced the level of the respiratory quotient, insulin, HOMA, the resting energy expenditure, waist circumference and CRP. Increased % fat oxidation.
Basu et al. [70].	United States	Obesity and metabolic syndrome subjects	25–63 years	Received green tea 4 cups per day containing 440 mg EGCG (n = 13), or green tea extract 2 capsules per day containing 460 mg EGCG and 4 cups of water (n = 10) for 8 weeks	Receive 4 cups of water per day for 8 weeks (n = 12)	Both treatments reduced body weight and body mass index. Green tea beverages showed a decreasing trend in LDL-cholesterol and LDL/HDL-cholesterol ratio versus controls. Green tea beverage also significantly decreased malondialdehyde (MDA) and hydroxynonenal (HNE) levels

Table 1. *Cont.*

Author	Country	Patients	Age	Dose, Intervention Period	Control	Outcomes
Alves Ferreir et al. [71]	Brazil	Overweight without diabetes women.	20–45 years	Receive 1000 mg green tea extract containing 560 mg polyphenols (n = 32), receive 1000 mg metformin (n = 28), receive 1000 mg green tea extract containing 560 mg polyphenols and 1000 mg metformin (n = 31) for 12 weeks.	Receive 1000 mg cellulose (n = 29)	The group received 1000 mg green tea extract were reduced the level of fasting glucose, total cholesterol and LDL-c.
Quinhoneiro et al. [72].	Brazil	Women with obesity grade III.	34.5 years	Receive 450 mg EGCG per day for 8 weeks (n = 11).	No intervention (n = 10).	Upregulated the *UCP3* gene but did not promote weight loss. Did not alter the expression of *UCP1*, *PLIN1*, *PPARG2* and *ADRB3*.
Chen et al. [74].	Taiwan, China	Central obesity women.	44 years	Received a tablet of EGCG at 856.8 mg daily for 12 weeks. (n = 39)	Placebo (n = 38)	Promoted weight loss, reduced waist circumference, and a consistent decrease in total cholesterol and LDL-cholesterol.
Brown et al. [75].	United Kingdom	Overweight or obese male subjects	40–65 years	Receive 800 mg EGCG per day for 8 weeks. (n = 46)	Placebo (n = 42)	Did not affect insulin sensitivity, insulin secretion or glucose tolerance but did reduce diastolic blood pressure
Dostal et al. [76].	United States	Overweight and obese postmenopausal women.	61 years	Receive green tea extract containing EGCG at 843 mg daily for 12 months. (n = 117)	Placebo (n = 120)	Did not change energy intake, body weight, BMI, or waist circumference. No differences were seen in circulating leptin, ghrelin, adiponectin, or glucose concentrations at month 12. Did not affect post-prandial responses of leptin, ghrelin, adiponectin, and satiety.
Dostal et al. [77].	United States	Overweight and obese postmenopausal-women.	61 years	Receive green tea extract containing EGCG at 843 mg daily for 11–12 months (n = 30).	Placebo (n = 30).	Did not affect post-prandial responses of leptin, ghrelin, adiponectin, and satiety, though it may be involved in the post-meal insulinemic response.

Table 1. *Cont.*

Author	Country	Patients	Age	Dose, Intervention Period	Control	Outcomes
Dostal et al. [78]	United States	Overweight and obese postmenopausal women.	50–70 years	Receive green tea extract containing EGCG at 843 mg daily for 12 months. (n = 61)	Placebo (n = 60)	Did not affect adiposity or improve bone mineral density. No changes were seen in circulating leptin, ghrelin, adiponectin, or insulin concentrations. *COMT* genotype did not modify the effect of GTE on any variable.
Huang et al. [79].	Taiwan, China	Obese and high level of LDL-C women.	53.1 years	Receive 856.8 mg EGCG per day for 6 weeks, after 14 days of washout period, switched to placebo for 6 weeks (n = 36).	Receive placebo for 6 weeks, after 14 days of washout period, switched to 856.8 mg EGCG per day for 6 weeks (n = 37).	Reduced the level of serum LDL-C and increased the level of leptin.
Nicoletti et al. [80].	Brazil	Women with severe obesity.	35.1 years	Received 901.4 mg EGCG per day for 8 weeks (n = 11).	-	Upregulated the *RICTOR* and *HIF1-α* expression, however, did not modify *PI3K* expression. Did not change body weight, BMI and fat mass.
Most et al. [82].	The Netherlands	Overweight and obese subjects.	38 ± 2 years	Received a tablet of EGCG at 282 mg and resveratrol at 80 mg day for 12 weeks (n = 18)	Placebo (n = 20)	Did not significantly affect plasma metabolic profile, whole-body fat mass or energy expenditure.
Most et al. [83].	The Netherlands	Overweight and obese subjects.	36 years	Received a tablet of EGCG at 282 mg and resveratrol at 80 mg day for 12 weeks. (n = 11)	Placebo (n = 14)	Reduced the expression of pathways related to energy metabolism, oxidative stress, inflammation, and immune defense. Also, blocking cell circle and apoptosis.
Most et al. [84].	The Netherlands	Overweight and obese subjects.	37.8 ± 1.6 years	Received a tablet of EGCG at 282 mg and resveratrol at 80 mg day for 12 weeks. (n = 18)	Placebo (n = 19)	Reduced bacteroidetes and tended to decrease Faecalibacterium prausnitzii in men but not in women. Moreover, baseline Bacteroidetes abundance was predictive for the combination treatment-induced increase in fat oxidation in men but not in women.

Table 1. *Cont.*

Author	Country	Patients	Age	Dose, Intervention Period	Control	Outcomes
Bagheri et al. [85].	Iran	Overweight women.	38.36 years	Received 500 mg green tea extract containing 45% EGCG per day and endurance training for 8 weeks (n = 10).	Endurance training + placebo (n = 10); no exercise + placebo (n = 10).	The reduction of values including body weight, body index, waist to hip ratio, adiponectin, hs-CRP and body fat percentage in the endurance training and green tea group was significantly higher than endurance training and placebo group interventions. Increased the level of adiponectin.
Bagheri et al. [86]	Iran	Overweight middle-aged males.	40–50 years	Received 500 mg green tea extract containing 45% EGCG per day and endurance training for 8 weeks (n = 5).	Endurance training + placebo (n = 5); no exercise + placebo (n = 5).	The reduction of values including body weight, body index, body fat percentage (BFP), visceral fat area, IL-6 and hs-CRP in the endurance training and green tea group was significantly higher than endurance training and placebo group interventions. Increased the level of adiponectin.
Hill et al. [87]	Australia	Overweight/obese post-menopausal women	45–70 years	Receive 300 mg EGCG per day and regular aerobic exercise for 12 weeks (n = 19)	Receive placebo and regular aerobic exercise (n = 19)	Reduced heart rate and plasma glucose.

3.2. The Impact of Supplemental EGCG Intake on NAFLD

To date, there have been relatively few studies focused on the effects of EGCG in NAFLD, with searches of the PubMed and Web of Science databases returning just four relevant clinical studies (Table 2). Akata et al. performed a 12-week randomized controlled trial wherein 17 individuals with NAFLD were randomly assigned to consume green tea beverages with different catechin doses. Relative to individuals in the placebo control group (0 mg catechins/700 mL) and those receiving low catechin doses (200 mg/700 mL), patients in the high-dose group (1080 mg/700 mL) presented with significant reductions in body fat levels, serum ALT levels, urinary 8-prostaglandin excretion, and liver–spleen computed tomography (CT) attenuation ratios [88]. High-dose catechin intake may thus reduce hepatic adiposity, inflammation, and oxidative stress in individuals with NAFLD. Pezeshki et al. examined the impact of green tea extract consumption on the serum ALT, AST, and ALP levels in 80 NAFLD patients assigned at random to the green tea extract (500 mg/day, 31.429% EGCG) or placebo control. Following a 12-week intervention period, markedly lower serum AST and ALT concentrations were observed in participants receiving green tea extract relative to baseline, while both groups exhibited reductions in serum ALP levels. No comparisons in these values between the groups were performed on completion of the study, however [89]. Hussian et al. similarly treated 80 NAFLD patients

with either 500 mg green tea extract capsules (31.429% EGCG) or placebo control twice per day for 12 weeks. Relative to placebo treatment, green tea extract intake was associated with significantly reduced body weight and BMI values, lower serum ALT, AST, hs-CRP, and lipid levels, and enhanced insulin resistance. Ultrasonography also revealed a 67.5% reduction in fatty liver indications after consumption of green tea extract, relative to just 25% in the placebo group [90]. However, a meta-analysis showed that the effect of EGCG on liver enzymes depends on the individual's health status. In patients with NAFLD, EGCG tends to moderately reduce liver enzyme levels, while in healthy individuals, it may lead to a slight increase [91]. Future studies should take this into account when selecting participants. The most recent report that focused on how EGCG affects NAFLD patients was a randomized controlled trial performed by Yang et al. in which 15 NAFLD patients were enrolled, and outcomes were compared between baseline and the end of a 24-week daily EGCG (300 mg/day) supplementation period. Relative to baseline, these treated patients exhibited significant reductions in hepatic fat content, waist circumference, waist-to-hip ratio, and serum cholesterol together with increased serum HDL-C [40]. The study also indicates that EGCG may improve the progression of NAFLD by reducing serum dipeptidyl peptidase 4 (DPP4) levels. Elevated levels of DPP4 in the liver promote the occurrence and progression of NAFLD. Liver-specific DPP4 knock-in mice exhibit increased weight, higher adiposity, hepatic steatosis, liver injury, adipose inflammation, and elevated cholesterol levels [92].

Table 2. Clinical studies of epigallocatechin gallate (EGCG) and its impact on NAFLD.

Author	Country	Patients	Average Age	Dose, Intervention Period	Control	Outcomes
Yang et al. [40].	China	NAFLD	38.53 years	Receive 300 mg EGCG per day for 24 weeks. (n = 15)	-	Reduced the liver fat content, waist measurement, waist-to-hip ratio, the level of TC, and increased the level of HDL-C.
Sakata et al. [88].	Japen	NAFLD	20–70 years	Received 700 mL green tea per day for 12 weeks respectively containing 1080 mg/700 mL (n = 7) or 200 mg/700 mL (n = 5) catechins.	Placebo (n = 5)	Reduced body fat content, liver–spleen CT attenuation ratio, serum ALT level and urinary 8-prostaglandin excretion.
Pezeshki et al. [89].	Iran	NAFLD	20–50 years	Receive green tea extract 500 mg containing 31.429% EGCG per day for 12 weeks. (n = 40)	Placebo (n = 40)	Reduced the level of serum AST and ALT.
Hussian et al. [90].	Pakistan	NAFLD	25 years	Receive 2 capsules green tea extract 500 mg containing 31.429% EGCG per day for 12 weeks. (n = 40)	Placebo (n = 40)	Reduced weight, BMI, HOMA-IR, the level of serum ALT, AST, hs-CRP, LDL-C, TC and TG. Increased the level of HDL-C and adiponectin. Caused a 67.5% regression of fatty liver changes on ultrasound as compared to placebo which is 25% only.

4. The Safety of EGCG

While there are many potentially beneficial effects associated with dietary EGCG supplementation, at high doses it may be associated with certain health risks. Notably,

there have been several case reports detailing instances of liver damage linked to green tea extract intake (Table 3). For instance, Patel et al. reported a 16-year-old male from Spain who had been taking the Applied Nutrition® Green Tea Fat Burner supplement containing an EGCG dose of 400 mg/day in an effort to lose weight for 60 days before being hospitalized. While the patient had lost 56 pounds over this period, he was ultimately admitted to the hospital for acute liver injury and potential liver failure. On admission, laboratory testing revealed abnormal findings, while liver histology exhibited diffuse portal and lobular mixed inflammatory cell infiltration, together with evidence of acute and chronic inflammatory activity, hepatocellular necrosis, and cholestasis. As these histological findings were consistent with prior reports of green tea extract-related toxicity, following the exclusion of other potential causes, the hepatic damage in this case was proposed to be attributable to the green tea fat burner supplement [93]. Surapaneni et al. described another case in which a patient suffered from green tea extract-induced acute liver injury. On admission, this patient presented with abnormal liver function test results, and severe scleral icterus was evident on examination of the abdomen. The patient's BMI was 24.4, their abdomen was soft and not tender, and they did not exhibit any evidence of obesity. No significant abnormalities were detected via abdominal ultrasonography, but magnetic resonance cholangiopancreatography (MRCP) exhibited edema around the distal common bile duct, without apparent stenosis. Two days following admission, the patient developed more severe nausea and vomiting. Further investigation revealed that the patient consumed a green tea extract-containing over-the-counter nutritional supplement (Vital Stem) daily for 1 month before hospitalization. After other possible causes of acute liver injury had been excluded, the green tea extract was considered the most likely cause of the severe hepatic necrosis observed in this case [94]. Gavrić et al. described two cases of acute liver injury among patients consuming dietary supplements containing green tea extract for the purposes of weight loss [95]. Grajecki et al. reported a case of a patient who received a high dose of a GET mixture 72 and 48 h prior to admission and developed jaundice 24 h prior to admission. A physical examination revealed slight liver enlargement with abdominal pain. After excluding other causes, the GET mixture was considered to be the main cause of liver injury in patients [96]. Weinstein et al. described the case of a patient harboring the *α-1 antitrypsin* MZ phenotype who suffered from liver injury, focal necrosis, and parenchymal loss after consuming 4 Slim Quick™ capsules (containing 540 mg EGCG overall) per day [97].

Table 3. Cases of liver toxicity caused by EGCG.

Author	Country	Age (Years)	AST	ALT	ALP	GGT	Total Serum Bilirubin (mg/dL)	Direct Serum Bilirubin (mg/dL)	Unconjugated Bilirubin (mg/dL)
Patel et al. [93].	United States	16	2106 (U/L)	2984 (U/L)	186 (U/L)	78 (U/L)	-	-	1.9
Surapaneni et al. [94].	United States	50	1657 (U/L)	1170 (U/L)	113 (U/L)	-	38	32	-
Gavrić et al. [95].	The Republic of Slovenia	51	14,588 (U/L)	12,882 (U/L)	162 (U/L)	110 (U/L)	-	-	-
Gavrić et al. [95].	The Republic of Slovenia	57	1652 (U/L)	3385 (U/L)	242 (U/L)	262 (U/L)	9.1	-	-
Grajecki et al. [96].	Germany	24	2647 (U/L)	3863 (U/L)	57 (U/L)	21 (U/L)	2.1	-	0.7
Weinstein et al. [97].	United States	24	2320 (IU/L)	2615 (IU/L)	200 (IU/L)	-	4.0	-	-

After reviewing the data of 38 interventional studies of EGCG, the European Food Safety Authority's Panel on Food Additives and Nutrient Sources Added to Food determined that exposure to high doses of EGCG (≥800 mg/day) for extended periods (≥4 weeks) may lead to elevated serum ALT and AST levels in some individuals [98]. A 1-year study of 500 subjects found that 5.1% of these participants experienced moderate-to-severe hepatic dysfunction following daily EGCG intake (843 mg/day), for an odds ratio of 7.0 (95% CI: 2.4–20.3, $p = 0.0002$) [99,100]. Acosta et al. determined that the *uridine 5′-diphospho-glucuronosyltransferase 1A4* (*UGT1A4*) genotype may be significantly related to the risk of increases in serum transaminase levels that are clinically relevant in postmenopausal women following high-dose EGCG supplementation (843 mg/day) [101].

5. Summary and Future Perspectives

In conclusion, there is a need for additional studies aimed at clarifying the therapeutic value of EGCG as a treatment for obesity and NAFLD. Based on the available data, the supplemental intake of 150–300 mg/day of EGCG for roughly 12 weeks may help normalize blood lipid and glucose levels in individuals who are obese. The influence of such supplementation on other metabolic parameters such as blood pressure, insulin resistance, and body measurements, however, has not been consistent across studies. Indeed, ongoing debate persists regarding the value of low-dose EGCG (150–300 mg/day) as a means of improving the metabolic status of obese individuals alone or in combination with exercise or other polyphenols. Additional long-term clinical studies will be vital to clarify how EGCG impacts obesity-associated metabolic parameters, particularly given the potential for variations across genotypes and as a function of gender.

In NAFLD patients, there is only relatively weak evidence suggesting the potential beneficial effects of EGCG on hepatic fat and aminotransferase levels, with these results primarily coming from inconsistent, small-scale studies that lack corresponding large-scale validation. High-quality studies will be crucial to definitively establish the impact of EGCG on hepatic fat levels and metabolic outcomes in patients with NAFLD, while also seeking to improve the bioavailability of this compound such that the administered dose levels can be reduced.

Despite the promise of EGCG as a mediator of beneficial health outcomes, some concerns also persist that its use at high doses may lead to hepatotoxicity, particularly at doses exceeding 400 mg/day. As EGCG sensitivity may also be influenced by individual genetics, additional research should be conducted to clarify EGCG tolerability and safety in patients with different genetic profiles.

In summary, while the evidence regarding the health benefits of EGCG as a treatment for obesity or NAFLD remains inconclusive, it continues to hold promise as a tool to combat these disorders. Additional long-term, large-scale studies will ultimately be required to fully clarify the biological activity and therapeutic utility of EGCG in these and other clinical settings.

Author Contributions: R.Y.: literature search and original draft; Y.C.: final approval of the manuscript. All authors have read and agreed to the published version of the manuscript.

Funding: This study was supported by the National Natural Science Foundation of China (Project No. 81970750) and the Xingliao Program of Excellence-Young Medical Masters Project (YXMJ-QN-01) of Liaoning Provincial Health Commission.

Conflicts of Interest: The authors of this review have no conflicts of interest.

References

1. Perdomo, C.M.; Cohen, R.V.; Sumithran, P.; Clément, K.; Frühbeck, G. Contemporary Medical, Device, and Surgical Therapies for Obesity in Adults. *Lancet* **2023**, *401*, 1116–1130. [CrossRef] [PubMed]
2. Worldwide Trends in Underweight and Obesity from 1990 to 2022: A Pooled Analysis of 3663 Population-Representative Studies with 222 Million Children, Adolescents, and Adults. *Lancet* **2024**, *403*, 1027–1050. [CrossRef] [PubMed]
3. Mahase, E. Global Cost of Overweight and Obesity Will Hit $4.32tn a Year by 2035, Report Warns. *BMJ* **2023**, *380*, 523. [CrossRef] [PubMed]
4. Cawley, J.; Meyerhoefer, C. The Medical Care Costs of Obesity: An Instrumental Variables Approach. *J. Health Econ.* **2012**, *31*, 219–230. [CrossRef]
5. Piché, M.E.; Tchernof, A.; Després, J.P. Obesity Phenotypes, Diabetes, and Cardiovascular Diseases. *Circ. Res.* **2020**, *126*, 1477–1500. [CrossRef]
6. Bhaskaran, K.; Dos-Santos-Silva, I.; Leon, D.A.; Douglas, I.J.; Smeeth, L. Association of BMI with Overall and Cause-Specific Mortality: A Population-Based Cohort Study of 3·6 Million Adults in the UK. *Lancet Diabetes Endocrinol.* **2018**, *6*, 944–953. [CrossRef]
7. White, D.L.; Kanwal, F.; El-Serag, H.B. Association between Nonalcoholic Fatty Liver Disease and Risk for Hepatocellular Cancer, Based on Systematic Review. *Clin. Gastroenterol. Hepatol.* **2012**, *10*, 1342–1359.e2. [CrossRef]
8. Feng, G.; Valenti, L.; Wong, V.W.-S.; Fouad, Y.M.; Yilmaz, Y.; Kim, W.; Sebastiani, G.; Younossi, Z.M.; Hernandez-Gea, V.; Zheng, M.-H. Recompensation in Cirrhosis: Unravelling the Evolving Natural History of Nonalcoholic Fatty Liver Disease. *Nat. Rev. Gastroenterol. Hepatol.* **2024**, *21*, 46–56. [CrossRef]
9. Li, L.; Liu, D.W.; Yan, H.Y.; Wang, Z.Y.; Zhao, S.H.; Wang, B. Obesity Is an Independent Risk Factor for Non-Alcoholic Fatty Liver Disease: Evidence from a Meta-Analysis of 21 Cohort Studies. *Obes. Rev.* **2016**, *17*, 510–519. [CrossRef]
10. van Baak, M.A.; Mariman, E.C.M. Obesity-Induced and Weight-Loss-Induced Physiological Factors Affecting Weight Regain. *Nat. Rev. Endocrinol.* **2023**, *19*, 655–670. [CrossRef]
11. Bray, G.A.; Frühbeck, G.; Ryan, D.H.; Wilding, J.P. Management of Obesity. *Lancet* **2016**, *387*, 1947–1956. [CrossRef] [PubMed]
12. Tan, H.S.; Habib, A.S. Obesity in Women: Anaesthetic Implications for Peri-Operative and Peripartum Management. *Anaesthesia* **2021**, *76* (Suppl. S4), 108–117. [CrossRef] [PubMed]
13. Riazi, K.; Azhari, H.; Charette, J.H.; Underwood, F.E.; King, J.A.; Afshar, E.E.; Swain, M.G.; Congly, S.E.; Kaplan, G.G.; Shaheen, A.A. The Prevalence and Incidence of NAFLD Worldwide: A Systematic Review and Meta-Analysis. *Lancet Gastroenterol. Hepatol.* **2022**, *7*, 851–861. [CrossRef] [PubMed]
14. FDA Approves First Treatment for Patients with Liver Scarring Due to Fatty Liver Disease. Available online: https://www.fda.gov/news-events/press-announcements/fda-approves-first-treatment-patients-liver-scarring-due-fatty-liver-disease (accessed on 30 June 2024).
15. Harrison, S.A.; Bedossa, P.; Guy, C.D.; Schattenberg, J.M.; Loomba, R.; Taub, R.; Labriola, D.; Moussa, S.E.; Neff, G.W.; Rinella, M.E.; et al. A Phase 3, Randomized, Controlled Trial of Resmetirom in NASH with Liver Fibrosis. *N. Engl. J. Med.* **2024**, *390*, 497–509. [CrossRef]
16. The Diagnosis and Management of Nonalcoholic Fatty Liver Disease: Practice Guidance from the American Association for the Study of Liver Diseases. *Clin. Liver Dis.* **2018**, *11*, 81. [CrossRef]
17. Chitturi, S.; Wong, V.W.; Chan, W.K.; Wong, G.L.; Wong, S.K.; Sollano, J.; Ni, Y.H.; Liu, C.J.; Lin, Y.C.; Lesmana, L.A.; et al. The Asia-Pacific Working Party on Non-Alcoholic Fatty Liver Disease Guidelines 2017-Part 2: Management and Special Groups. *J. Gastroenterol. Hepatol.* **2018**, *33*, 86–98. [CrossRef]
18. European Association for the Study of the Liver (EASL); European Association for the Study of Diabetes (EASD); European Association for the Study of Obesity (EASO). EASL-EASD-EASO Clinical Practice Guidelines for the Management of Non-Alcoholic Fatty Liver Disease. *Diabetologia* **2016**, *59*, 1121–1140. [CrossRef]
19. Harrison, S.A.; Wong, V.W.; Okanoue, T.; Bzowej, N.; Vuppalanchi, R.; Younes, Z.; Kohli, A.; Sarin, S.; Caldwell, S.H.; Alkhouri, N.; et al. Selonsertib for Patients with Bridging Fibrosis or Compensated Cirrhosis Due to NASH: Results from Randomized Phase III STELLAR Trials. *J. Hepatol.* **2020**, *73*, 26–39. [CrossRef]
20. Younossi, Z.M.; Ratziu, V.; Loomba, R.; Rinella, M.; Anstee, Q.M.; Goodman, Z.; Bedossa, P.; Geier, A.; Beckebaum, S.; Newsome, P.N.; et al. Obeticholic Acid for the Treatment of Non-Alcoholic Steatohepatitis: Interim Analysis from a Multicentre, Randomised, Placebo-Controlled Phase 3 Trial. *Lancet* **2019**, *394*, 2184–2196. [CrossRef]
21. Anstee, Q.M.; Neuschwander-Tetri, B.A.; Wong, V.W.; Abdelmalek, M.F.; Younossi, Z.M.; Yuan, J.; Pecoraro, M.L.; Seyedkazemi, S.; Fischer, L.; Bedossa, P.; et al. Cenicriviroc for the Treatment of Liver Fibrosis in Adults with Nonalcoholic Steatohepatitis: AURORA Phase 3 Study Design. *Contemp. Clin. Trials* **2020**, *89*, 105922. [CrossRef]
22. Westerouen Van Meeteren, M.J.; Drenth, J.P.H.; Tjwa, E.T.T.L. Elafibranor: A Potential Drug for the Treatment of Nonalcoholic Steatohepatitis (NASH). *Expert Opin. Investig. Drugs* **2020**, *29*, 117–123. [CrossRef] [PubMed]

23. Vilar-Gomez, E.; Martinez-Perez, Y.; Calzadilla-Bertot, L.; Torres-Gonzalez, A.; Gra-Oramas, B.; Gonzalez-Fabian, L.; Friedman, S.L.; Diago, M.; Romero-Gomez, M. Weight Loss Through Lifestyle Modification Significantly Reduces Features of Nonalcoholic Steatohepatitis. *Gastroenterology* **2015**, *149*, 367–378.e5. [CrossRef] [PubMed]
24. Wong, V.W.; Chan, R.S.; Wong, G.L.; Cheung, B.H.; Chu, W.C.; Yeung, D.K.; Chim, A.M.; Lai, J.W.; Li, L.S.; Sea, M.M.; et al. Community-Based Lifestyle Modification Programme for Non-Alcoholic Fatty Liver Disease: A Randomized Controlled Trial. *J. Hepatol.* **2013**, *59*, 536–542. [CrossRef] [PubMed]
25. Younossi, Z.M.; Zelber-Sagi, S.; Henry, L.; Gerber, L.H. Lifestyle Interventions in Nonalcoholic Fatty Liver Disease. *Nat. Rev. Gastroenterol. Hepatol.* **2023**, *20*, 708–722. [CrossRef]
26. Narotzki, B.; Reznick, A.Z.; Aizenbud, D.; Levy, Y. Green Tea: A Promising Natural Product in Oral Health. *Arch. Oral Biol.* **2012**, *57*, 429–435. [CrossRef]
27. Williamson, G.; Sheedy, K. Effects of Polyphenols on Insulin Resistance. *Nutrients* **2020**, *12*, 3135. [CrossRef]
28. Mahjabeen, W.; Khan, D.A.; Mirza, S.A. Role of Resveratrol Supplementation in Regulation of Glucose Hemostasis, Inflammation and Oxidative Stress in Patients with Diabetes Mellitus Type 2: A Randomized, Placebo-Controlled Trial. *Complement. Ther. Med.* **2022**, *66*, 102819. [CrossRef]
29. Hassan, S.; Shah, M.; Malik, M.O.; Ehtesham, E.; Habib, S.H.; Rauf, B. Treatment with Combined Resveratrol and Myoinositol Ameliorates Endocrine, Metabolic Alterations and Perceived Stress Response in Women with PCOS: A Double-Blind Randomized Clinical Trial. *Endocrine* **2023**, *79*, 208–220. [CrossRef]
30. Musial, C.; Kuban-Jankowska, A.; Gorska-Ponikowska, M. Beneficial Properties of Green Tea Catechins. *Int. J. Mol. Sci.* **2020**, *21*, 1744. [CrossRef]
31. He, Z.; Luo, H.; Wang, Z.; Chen, D.; Feng, Q.; Cao, X. Injectable and Tissue Adhesive EGCG-Laden Hyaluronic Acid Hydrogel Depot for Treating Oxidative Stress and Inflammation. *Carbohydr. Polym.* **2023**, *299*, 120180. [CrossRef]
32. Yu, Q.; Sun, H.; Zhang, L.; Jiang, L.; Liang, L.; Yu, C.; Dong, X.; Guo, B.; Qiu, Y.; Li, J.; et al. A Zwitterionic Hydrogel with Anti-Oxidative and Anti-Inflammatory Properties for the Prevention of Peritoneal Adhesion by Inhibiting Mesothelial-Mesenchymal Transition. *Adv. Healthc. Mater.* **2023**, *12*, e2301696. [CrossRef] [PubMed]
33. Aggarwal, V.; Tuli, H.S.; Tania, M.; Srivastava, S.; Ritzer, E.E.; Pandey, A.; Aggarwal, D.; Barwal, T.S.; Jain, A.; Kaur, G.; et al. Molecular Mechanisms of Action of Epigallocatechin Gallate in Cancer: Recent Trends and Advancement. *Semin. Cancer Biol.* **2022**, *80*, 256–275. [CrossRef]
34. Singh, B.N.; Shankar, S.; Srivastava, R.K. Green Tea Catechin, Epigallocatechin-3-Gallate (EGCG): Mechanisms, Perspectives and Clinical Applications. *Biochem. Pharmacol.* **2011**, *82*, 1807–1821. [CrossRef] [PubMed]
35. Li, F.; Gao, C.; Yan, P.; Zhang, M.; Wang, Y.; Hu, Y.; Wu, X.; Wang, X.; Sheng, J. EGCG Reduces Obesity and White Adipose Tissue Gain Partly Through AMPK Activation in Mice. *Front. Pharmacol.* **2018**, *9*, 1366. [CrossRef] [PubMed]
36. Yuan, H.; Li, Y.; Ling, F.; Guan, Y.; Zhang, D.; Zhu, Q.; Liu, J.; Wu, Y.; Niu, Y. The Phytochemical Epigallocatechin Gallate Prolongs the Lifespan by Improving Lipid Metabolism, Reducing Inflammation and Oxidative Stress in High-Fat Diet-Fed Obese Rats. *Aging Cell* **2020**, *19*, e13199. [CrossRef]
37. Zuo, G.; Chen, M.; Zuo, Y.; Liu, F.; Yang, Y.; Li, J.; Zhou, X.; Li, M.; Huang, J.-A.; Liu, Z.; et al. Tea Polyphenol Epigallocatechin Gallate Protects Against Nonalcoholic Fatty Liver Disease and Associated Endotoxemia in Rats via Modulating Gut Microbiota Dysbiosis and Alleviating Intestinal Barrier Dysfunction and Related Inflammation. *J. Agric. Food Chem.* **2024**, *72*, 9067–9086. [CrossRef]
38. Mielgo-Ayuso, J.; Barrenechea, L.; Alcorta, P.; Larrarte, E.; Margareto, J.; Labayen, I. Effects of Dietary Supplementation with Epigallocatechin-3-Gallate on Weight Loss, Energy Homeostasis, Cardiometabolic Risk Factors and Liver Function in Obese Women: Randomised, Double-Blind, Placebo-Controlled Clinical Trial. *Br. J. Nutr.* **2014**, *111*, 1263–1271. [CrossRef]
39. Nogueira, L.P.; Nogueira Neto, J.F.; Klein, M.R.; Sanjuliani, A.F. Short-Term Effects of Green Tea on Blood Pressure, Endothelial Function, and Metabolic Profile in Obese Prehypertensive Women: A Crossover Randomized Clinical Trial. *J. Am. Coll. Nutr.* **2017**, *36*, 108–115. [CrossRef]
40. Yang, M.; Yan, R.; Sha, R.; Wang, X.; Zhou, S.; Li, B.; Zheng, Q.; Cao, Y. Epigallocatechin Gallate Alleviates Non-Alcoholic Fatty Liver Disease through the Inhibition of the Expression and Activity of Dipeptide Kinase 4. *Clin. Nutr.* **2024**, *43*, 1769–1780. [CrossRef]
41. Dai, W.; Ruan, C.; Zhang, Y.; Wang, J.; Han, J.; Shao, Z.; Sun, Y.; Liang, J. Bioavailability Enhancement of EGCG by Structural Modification and Nano-Delivery: A Review. *J. Funct. Foods* **2020**, *65*, 103732. [CrossRef]
42. Ye, J.; Li, Q.; Zhang, Y.; Su, Q.; Feng, Z.; Huang, P.; Zhang, C.; Zhai, Y.; Wang, W. ROS Scavenging and Immunoregulative EGCG@Cerium Complex Loaded in Antibacterial Polyethylene Glycol-Chitosan Hydrogel Dressing for Skin Wound Healing. *Acta Biomater.* **2023**, *166*, 155–166. [CrossRef] [PubMed]
43. Huang, L.; Wang, X.; Zheng, Y.; Lang, D.; Wang, J.; Yan, S.; Chen, Y. EGCG-NPs Inhibition *HO-1*-Mediated Reprogram Iron Metabolism against Ferroptosis after Subarachnoid Hemorrhage. *Redox Biol.* **2024**, *70*, 103075. [CrossRef] [PubMed]

44. Braegelmann, C.; Niebel, D.; Ferring-Schmitt, S.; Fetter, T.; Landsberg, J.; Hölzel, M.; Effern, M.; Glodde, N.; Steinbuch, S.; Bieber, T.; et al. Epigallocatechin-3-Gallate Exhibits Anti-Inflammatory Effects in a Human Interface Dermatitis Model-Implications for Therapy. *J. Eur. Acad. Dermatol. Venereol.* **2022**, *36*, 144–153. [CrossRef] [PubMed]
45. Ou, K.; Zhang, Q.; Xi, F.; Ni, H.; Lu, J.; Lyu, X.; Wang, C.; Li, Q.; Wang, Q. Prenatal EGCG Consumption Impacts Hepatic Glycogen Synthesis and Lipid Metabolism in Adult Mice. *Int. J. Biol. Macromol.* **2024**, *260*, 129491. [CrossRef]
46. Evageliou, V.; Panagopoulou, E.; Mandala, I. Encapsulation of EGCG and Esterified EGCG Derivatives in Double Emulsions Containing Whey Protein Isolate, Bacterial Cellulose and Salt. *Food Chem.* **2019**, *281*, 171–177. [CrossRef]
47. Darvesh, A.S.; Bishayee, A. Chemopreventive and Therapeutic Potential of Tea Polyphenols in Hepatocellular Cancer. *Nutr. Cancer-Int. J.* **2013**, *65*, 329–344. [CrossRef]
48. Sinha, D.; Biswas, J.; Nabavi, S.M.; Bishayee, A. Tea Phytochemicals for Breast Cancer Prevention and Intervention: From Bench to Bedside and Beyond. *Semin. Cancer Biol.* **2017**, *46*, 33–54. [CrossRef]
49. Santana, A.; Santamarina, A.; Souza, G.; Mennitti, L.; Okuda, M.; Venancio, D.; Seelaender, M.; do Nascimento, C.O.; Ribeiro, E.; Lira, F.; et al. Decaffeinated Green Tea Extract Rich in Epigallocatechin-3-Gallate Improves Insulin Resistance and Metabolic Profiles in Normolipidic Diet--but Not High-Fat Diet-Fed Mice. *J. Nutr. Biochem.* **2015**, *26*, 893–902. [CrossRef]
50. Liu, Z.; Li, Q.; Huang, J.; Liang, Q.; Yan, Y.; Lin, H.; Xiao, W.; Lin, Y.; Zhang, S.; Tan, B.; et al. Proteomic Analysis of the Inhibitory Effect of Epigallocatechin Gallate on Lipid Accumulation in Human *HepG2* Cells. *Proteome Sci.* **2013**, *11*, 32. [CrossRef]
51. Lee, M.-S.; Kim, C.-T.; Kim, Y. Green Tea (-)-Epigallocatechin-3-Gallate Reduces Body Weight with Regulation of Multiple Genes Expression in Adipose Tissue of Diet-Induced Obese Mice. *Ann. Nutr. Metab.* **2009**, *54*, 151–157. [CrossRef]
52. Friedrich, M.; Petzke, K.J.; Raederstorff, D.; Wolfram, S.; Klaus, S. Acute Effects of Epigallocatechin Gallate from Green Tea on Oxidation and Tissue Incorporation of Dietary Lipids in Mice Fed a High-Fat Diet. *Int. J. Obes.* **2012**, *36*, 735–743. [CrossRef] [PubMed]
53. Grove, K.A.; Sae-tan, S.; Kennett, M.J.; Lambert, J.D. (-)-Epigallocatechin-3-Gallate Inhibits Pancreatic Lipase and Reduces Body Weight Gain in High Fat-Fed Obese Mice. *Obesity* **2012**, *20*, 2311–2313. [CrossRef] [PubMed]
54. Bose, M.; Lambert, J.D.; Ju, J.; Reuhl, K.R.; Shapses, S.A.; Yang, C.S. The Major Green Tea Polyphenol, (-)-Epigallocatechin-3-Gallate, Inhibits Obesity, Metabolic Syndrome, and Fatty Liver Disease in High-Fat-Fed Mice. *J. Nutr.* **2008**, *138*, 1677–1683. [CrossRef] [PubMed]
55. Santamarina, A.B.; Carvalho-Silva, M.; Gomes, L.M.; Okuda, M.H.; Santana, A.A.; Streck, E.L.; Seelaender, M.; do Nascimento, C.M.O.; Ribeiro, E.B.; Lira, F.S.; et al. Decaffeinated Green Tea Extract Rich in Epigallocatechin-3-Gallate Prevents Fatty Liver Disease by Increased Activities of Mitochondrial Respiratory Chain Complexes in Diet-Induced Obesity Mice. *J. Nutr. Biochem.* **2015**, *26*, 1348–1356. [CrossRef] [PubMed]
56. Ma, H.; Wang, Y.; Wei, J.; Wang, X.; Yang, H.; Wang, S. Stabilization of Hypoxia-Inducible Factor 1α and Regulation of Specific Gut Microbes by EGCG Contribute to the Alleviation of Ileal Barrier Disorder and Obesity. *Food Funct.* **2024**, *15*, 9983–9994. [CrossRef]
57. Zhang, L.; Zheng, Y.; Chow, M.S.; Zuo, Z. Investigation of Intestinal Absorption and Disposition of Green Tea Catechins by Caco-2 Monolayer Model. *Int. J. Pharm.* **2004**, *287*, 1–12. [CrossRef]
58. Alam, M.; Ali, S.; Ashraf, G.M.; Bilgrami, A.L.; Yadav, D.K.; Hassan, M.I. Epigallocatechin 3-Gallate: From Green Tea to Cancer Therapeutics. *Food Chem.* **2022**, *379*, 132135. [CrossRef]
59. Zhu, T.; Li, M.; Zhu, M.; Liu, X.; Huang, K.; Li, W.; Wang, S.-X.; Yin, Y.; Li, P. Epigallocatechin-3-Gallate Alleviates Type 2 Diabetes Mellitus via β-Cell Function Improvement and Insulin Resistance Reduction. *Iran. J. Basic Med. Sci.* **2022**, *25*, 483–488. [CrossRef]
60. Auger, C.; Mullen, W.; Hara, Y.; Crozier, A. Bioavailability of Polyphenon E Flavan-3-Ols in Humans with an Ileostomy. *J. Nutr.* **2008**, *138*, 1535s–1542s. [CrossRef]
61. Kuriyama, S.; Hozawa, A.; Ohmori, K.; Shimazu, T.; Matsui, T.; Ebihara, S.; Awata, S.; Nagatomi, R.; Arai, H.; Tsuji, I. Green Tea Consumption and Cognitive Function: A Cross-Sectional Study from the Tsurugaya Project 1. *Am. J. Clin. Nutr.* **2006**, *83*, 355–361. [CrossRef]
62. Feng, W.Y. Metabolism of Green Tea Catechins: An Overview. *Curr. Drug Metab.* **2006**, *7*, 755–809. [CrossRef] [PubMed]
63. Kovacs, E.M.; Lejeune, M.P.; Nijs, I.; Westerterp-Plantenga, M.S. Effects of Green Tea on Weight Maintenance after Body-Weight Loss. *Br. J. Nutr.* **2004**, *91*, 431–437. [CrossRef] [PubMed]
64. Zhang, T.; Li, N.; Chen, S.I.; Hou, Z.; Saito, A. Effects of Green Tea Extract Combined with Brisk Walking on Lipid Profiles and the Liver Function in Overweight and Obese Men: A Randomized, Double-Blinded, Placebo-Control Trial. *An. Acad. Bras. Cienc.* **2020**, *92*, e20191594. [CrossRef] [PubMed]
65. Suliburska, J.; Bogdanski, P.; Szulinska, M.; Stepien, M.; Pupek-Musialik, D.; Jablecka, A. Effects of Green Tea Supplementation on Elements, Total Antioxidants, Lipids, and Glucose Values in the Serum of Obese Patients. *Biol. Trace Elem. Res.* **2012**, *149*, 315–322. [CrossRef]

66. Bogdanski, P.; Suliburska, J.; Szulinska, M.; Stepien, M.; Pupek-Musialik, D.; Jablecka, A. Green Tea Extract Reduces Blood Pressure, Inflammatory Biomarkers, and Oxidative Stress and Improves Parameters Associated with Insulin Resistance in Obese, Hypertensive Patients. *Nutr. Res.* **2012**, *32*, 421–427. [CrossRef]
67. Westerterp-Plantenga, M.S.; Lejeune, M.P.; Kovacs, E.M. Body Weight Loss and Weight Maintenance in Relation to Habitual Caffeine Intake and Green Tea Supplementation. *Obes. Res.* **2005**, *13*, 1195–1204. [CrossRef]
68. Rondanelli, M.; Gasparri, C.; Perna, S.; Petrangolini, G.; Allegrini, P.; Fazia, T.; Bernardinelli, L.; Cavioni, A.; Mansueto, F.; Oberto, L.; et al. A 60-Day Green Tea Extract Supplementation Counteracts the Dysfunction of Adipose Tissue in Overweight Post-Menopausal and Class I Obese Women. *Nutrients* **2022**, *14*, 5209. [CrossRef]
69. Kapoor, M.P.; Sugita, M.; Fukuzawa, Y.; Okubo, T. Physiological Effects of Epigallocatechin-3-Gallate (EGCG) on Energy Expenditure for Prospective Fat Oxidation in Humans: A Systematic Review and Meta-Analysis. *J. Nutr. Biochem.* **2017**, *43*, 1–10. [CrossRef]
70. Basu, A.; Sanchez, K.; Leyva, M.J.; Wu, M.; Betts, N.M.; Aston, C.E.; Lyons, T.J. Green Tea Supplementation Affects Body Weight, Lipids, and Lipid Peroxidation in Obese Subjects with Metabolic Syndrome. *J. Am. Coll. Nutr.* **2010**, *29*, 31–40. [CrossRef]
71. Alves Ferreira, M.; Oliveira Gomes, A.P.; Guimarães de Moraes, A.P.; Ferreira Stringhini, M.L.; Mota, J.F.; Siqueira Guedes Coelho, A.; Borges Botelho, P. Green Tea Extract Outperforms Metformin in Lipid Profile and Glycaemic Control in Overweight Women: A Double-Blind, Placebo-Controlled, Randomized Trial. *Clin. Nutr. ESPEN* **2017**, *22*, 1–6. [CrossRef]
72. Quinhoneiro, D.C.G.; Nicoletti, C.F.; Pinhel, M.A.S.; Noronha, N.Y.; Braga, C.B.M.; Oliveira, B.A.P.; Cortes-Oliveira, C.; Oliveira, W.P.; Salgado Junior, W.; Marchini, J.S.; et al. Green Tea Supplementation Upregulates *Uncoupling Protein 3* Expression in Severe Obese Women Adipose Tissue but Does Not Promote Weight Loss. *Int. J. Food Sci. Nutr.* **2018**, *69*, 995–1002. [CrossRef] [PubMed]
73. Sae-Tan, S.; Grove, K.A.; Kennett, M.J.; Lambert, J.D. (-)-Epigallocatechin-3-Gallate Increases the Expression of Genes Related to Fat Oxidation in the Skeletal Muscle of High Fat-Fed Mice. *Food Funct.* **2011**, *2*, 111–116. [CrossRef] [PubMed]
74. Chen, I.J.; Liu, C.Y.; Chiu, J.P.; Hsu, C.H. Therapeutic Effect of High-Dose Green Tea Extract on Weight Reduction: A Randomized, Double-Blind, Placebo-Controlled Clinical Trial. *Clin. Nutr.* **2016**, *35*, 592–599. [CrossRef]
75. Brown, A.L.; Lane, J.; Coverly, J.; Stocks, J.; Jackson, S.; Stephen, A.; Bluck, L.; Coward, A.; Hendrickx, H. Effects of Dietary Supplementation with the Green Tea Polyphenol Epigallocatechin-3-Gallate on Insulin Resistance and Associated Metabolic Risk Factors: Randomized Controlled Trial. *Br. J. Nutr.* **2009**, *101*, 886–894. [CrossRef]
76. Dostal, A.M.; Samavat, H.; Espejo, L.; Arikawa, A.Y.; Stendell-Hollis, N.R.; Kurzer, M.S. Green Tea Extract and Catechol-O-Methyltransferase Genotype Modify Fasting Serum Insulin and Plasma Adiponectin Concentrations in a Randomized Controlled Trial of Overweight and Obese Postmenopausal Women. *J. Nutr.* **2016**, *146*, 38–45. [CrossRef]
77. Dostal, A.M.; Arikawa, A.; Espejo, L.; Bedell, S.; Kurzer, M.S.; Stendell-Hollis, N.R. Green Tea Extract and *Catechol-O-Methyltransferase* Genotype Modify the Post-Prandial Serum Insulin Response in a Randomised Trial of Overweight and Obese Post-Menopausal Women. *J. Hum. Nutr. Diet.* **2017**, *30*, 166–176. [CrossRef]
78. Dostal, A.M.; Arikawa, A.; Espejo, L.; Kurzer, M.S. Long-Term Supplementation of Green Tea Extract Does Not Modify Adiposity or Bone Mineral Density in a Randomized Trial of Overweight and Obese Postmenopausal Women. *J. Nutr.* **2016**, *146*, 256–264. [CrossRef]
79. Huang, L.H.; Liu, C.Y.; Wang, L.Y.; Huang, C.J.; Hsu, C.H. Effects of Green Tea Extract on Overweight and Obese Women with High Levels of Low Density-Lipoprotein-Cholesterol (LDL-C): A Randomised, Double-Blind, and Cross-over Placebo-Controlled Clinical Trial. *BMC Complement. Altern. Med.* **2018**, *18*, 294. [CrossRef]
80. Nicoletti, C.F.; Delfino, H.B.P.; Pinhel, M.; Noronha, N.Y.; Pinhanelli, V.C.; Quinhoneiro, D.C.G.; de Oliveira, B.A.P.; Marchini, J.S.; Nonino, C.B. Impact of Green Tea Epigallocatechin-3-Gallate on *HIF1-α* and *mTORC2* Expression in Obese Women: Anti-Cancer and Anti-Obesity Effects? *Nutr. Hosp.* **2019**, *36*, 315–320. [CrossRef]
81. Thielecke, F.; Rahn, G.; Böhnke, J.; Adams, F.; Birkenfeld, A.L.; Jordan, J.; Boschmann, M. Epigallocatechin-3-Gallate and Postprandial Fat Oxidation in Overweight/Obese Male Volunteers: A Pilot Study. *Eur. J. Clin. Nutr.* **2010**, *64*, 704–713. [CrossRef]
82. Most, J.; Timmers, S.; Warnke, I.; Jocken, J.W.; van Boekschoten, M.; de Groot, P.; Bendik, I.; Schrauwen, P.; Goossens, G.H.; Blaak, E.E. Combined Epigallocatechin-3-Gallate and Resveratrol Supplementation for 12 Wk Increases Mitochondrial Capacity and Fat Oxidation, but Not Insulin Sensitivity, in Obese Humans: A Randomized Controlled Trial. *Am. J. Clin. Nutr.* **2016**, *104*, 215–227. [CrossRef] [PubMed]
83. Most, J.; Warnke, I.; Boekschoten, M.V.; Jocken, J.W.E.; de Groot, P.; Friedel, A.; Bendik, I.; Goossens, G.H.; Blaak, E.E. The Effects of Polyphenol Supplementation on Adipose Tissue Morphology and Gene Expression in Overweight and Obese Humans. *Adipocyte* **2018**, *7*, 190–196. [CrossRef] [PubMed]
84. Most, J.; Penders, J.; Lucchesi, M.; Goossens, G.H.; Blaak, E.E. Gut Microbiota Composition in Relation to the Metabolic Response to 12-Week Combined Polyphenol Supplementation in Overweight Men and Women. *Eur. J. Clin. Nutr.* **2017**, *71*, 1040–1045. [CrossRef]

85. Bagheri, R.; Rashidlamir, A.; Ashtary-Larky, D.; Wong, A.; Alipour, M.; Motevalli, M.S.; Chebbi, A.; Laher, I.; Zouhal, H. Does Green Tea Extract Enhance the Anti-Inflammatory Effects of Exercise on Fat Loss? *Br. J. Clin. Pharmacol.* **2020**, *86*, 753–762. [CrossRef]
86. Bagheri, R.; Rashidlamir, A.; Ashtary-Larky, D.; Wong, A.; Grubbs, B.; Motevalli, M.S.; Baker, J.S.; Laher, I.; Zouhal, H. Effects of Green Tea Extract Supplementation and Endurance Training on Irisin, pro-Inflammatory Cytokines, and Adiponectin Concentrations in Overweight Middle-Aged Men. *Eur. J. Appl. Physiol.* **2020**, *120*, 915–923. [CrossRef]
87. Hill, A.M.; Coates, A.M.; Buckley, J.D.; Ross, R.; Thielecke, F.; Howe, P.R. Can EGCG Reduce Abdominal Fat in Obese Subjects? *J. Am. Coll. Nutr.* **2007**, *26*, 396s–402s. [CrossRef]
88. Sakata, R.; Nakamura, T.; Torimura, T.; Ueno, T.; Sata, M. Green Tea with High-Density Catechins Improves Liver Function and Fat Infiltration in Non-Alcoholic Fatty Liver Disease (NAFLD) Patients: A Double-Blind Placebo-Controlled Study. *Int. J. Mol. Med.* **2013**, *32*, 989–994. [CrossRef]
89. Pezeshki, A.; Safi, S.; Feizi, A.; Askari, G.; Karami, F. The Effect of Green Tea Extract Supplementation on Liver Enzymes in Patients with Nonalcoholic Fatty Liver Disease. *Int. J. Prev. Med.* **2016**, *7*, 28. [CrossRef]
90. Hussain, M.; Habib Ur, R.; Akhtar, L. Therapeutic Benefits of Green Tea Extract on Various Parameters in Non-Alcoholic Fatty Liver Disease Patients. *Pak. J. Med. Sci.* **2017**, *33*, 931–936. [CrossRef]
91. Tang, G.; Xu, Y.; Zhang, C.; Wang, N.; Li, H.; Feng, Y. Green Tea and Epigallocatechin Gallate (EGCG) for the Management of Nonalcoholic Fatty Liver Diseases (NAFLD): Insights into the Role of Oxidative Stress and Antioxidant Mechanism. *Antioxidants* **2021**, *10*, 1076. [CrossRef]
92. Baumeier, C.; Schlüter, L.; Saussenthaler, S.; Laeger, T.; Rödiger, M.; Alaze, S.A.; Fritsche, L.; Häring, H.-U.; Stefan, N.; Fritsche, A.; et al. Elevated Hepatic DPP4 Activity Promotes Insulin Resistance and Non-Alcoholic Fatty Liver Disease. *Mol. Metab.* **2017**, *6*, 1254–1263. [CrossRef] [PubMed]
93. Patel, S.S.; Beer, S.; Kearney, D.L.; Phillips, G.; Carter, B.A. Green Tea Extract: A Potential Cause of Acute Liver Failure. *World J. Gastroenterol.* **2013**, *19*, 5174–5177. [CrossRef] [PubMed]
94. Surapaneni, B.K.; Le, M.; Jakobovits, J.; Vinayek, R.; Dutta, S. A Case of Acute Severe Hepatotoxicity and Mild Constriction of Common Bile Duct Associated With Ingestion of Green Tea Extract: A Clinical Challenge. *Clin. Med. Insights Gastroenterol.* **2018**, *11*, 1179552218779970. [CrossRef] [PubMed]
95. Gavrić, A.; Ribnikar, M.; Šmid, L.; Luzar, B.; Štabuc, B. Fat Burner-Induced Acute Liver Injury: Case Series of Four Patients. *Nutrition* **2018**, *47*, 110–114. [CrossRef] [PubMed]
96. Grajecki, D.; Ogica, A.; Boenisch, O.; Hübener, P.; Kluge, S. Green Tea Extract-Associated Acute Liver Injury: Case Report and Review. *Clin. Liver Dis.* **2022**, *20*, 181–187. [CrossRef]
97. Weinstein, D.H.; Twaddell, W.S.; Raufman, J.P.; Philosophe, B.; Mindikoglu, A.L. SlimQuick^{TM}—Associated Hepatotoxicity in a Woman with Alpha-1 Antitrypsin Heterozygosity. *World J. Hepatol.* **2012**, *4*, 154–157. [CrossRef]
98. Younes, M.; Aggett, P.; Aguilar, F.; Crebelli, R.; Dusemund, B.; Filipič, M.; Frutos, M.J.; Galtier, P.; Gott, D.; Gundert-Remy, U.; et al. Scientific Opinion on the Safety of Green Tea Catechins. *EFSA J.* **2018**, *16*, e05239. [CrossRef]
99. Dostal, A.M.; Samavat, H.; Bedell, S.; Torkelson, C.; Wang, R.; Swenson, K.; Le, C.; Wu, A.H.; Ursin, G.; Yuan, J.M.; et al. The Safety of Green Tea Extract Supplementation in Postmenopausal Women at Risk for Breast Cancer: Results of the Minnesota Green Tea Trial. *Food Chem. Toxicol.* **2015**, *83*, 26–35. [CrossRef]
100. Yu, Z.; Samavat, H.; Dostal, A.M.; Wang, R.; Torkelson, C.J.; Yang, C.S.; Butler, L.M.; Kensler, T.W.; Wu, A.H.; Kurzer, M.S.; et al. Effect of Green Tea Supplements on Liver Enzyme Elevation: Results from a Randomized Intervention Study in the United States. *Cancer Prev. Res.* **2017**, *10*, 571–579. [CrossRef]
101. Acosta, L.; Byham-Gray, L.; Kurzer, M.; Samavat, H. Hepatotoxicity with High-Dose Green Tea Extract: Effect of *Catechol-O-Methyltransferase* and *Uridine 5′-Diphospho-Glucuronosyltransferase 1A4* Genotypes. *J. Diet. Suppl.* **2023**, *20*, 850–869. [CrossRef]

Disclaimer/Publisher's Note: The statements, opinions and data contained in all publications are solely those of the individual author(s) and contributor(s) and not of MDPI and/or the editor(s). MDPI and/or the editor(s) disclaim responsibility for any injury to people or property resulting from any ideas, methods, instructions or products referred to in the content.

biomedicines

MDPI

Review

New Developments in Pharmacological Treatment of Obesity and Type 2 Diabetes—Beyond and within GLP-1 Receptor Agonists

Ferenc Sztanek [1,*], László Imre Tóth [1], Attila Pető [1,2], Marcell Hernyák [1,3], Ágnes Diószegi [1] and Mariann Harangi [1,4,5]

[1] Division of Metabolism, Department of Internal Medicine, Faculty of Medicine, University of Debrecen, H-4032 Debrecen, Hungary
[2] Third Department of Internal Medicine, Semmelweis Hospital of Borsod-Abauj-Zemplen County Central Hospital and University Teaching Hospital, H-3529 Miskolc, Hungary
[3] Doctoral School of Health Sciences, University of Debrecen, H-4032 Debrecen, Hungary
[4] Institute of Health Studies, Faculty of Health Sciences, University of Debrecen, H-4032 Debrecen, Hungary
[5] ELKH-UD Vascular Pathophysiology Research Group 11003, University of Debrecen, H-4032 Debrecen, Hungary
* Correspondence: sztanek@belklinika.com

Abstract: Guidelines for the management of obesity and type 2 diabetes (T2DM) emphasize the importance of lifestyle changes, including a reduced-calorie diet and increased physical activity. However, for many people, these changes can be difficult to maintain over the long term. Medication options are already available to treat obesity, which can help reduce appetite and/or reduce caloric intake. Incretin-based peptides exert their effect through G-protein-coupled receptors, the receptors for glucagon-like peptide-1 (GLP-1) and glucose-dependent insulinotropic polypeptide (GIP), and glucagon peptide hormones are important regulators of insulin secretion and energy metabolism. Understanding the role of intercellular signaling pathways and inflammatory processes is essential for the development of effective pharmacological agents in obesity. GLP-1 receptor agonists have been successfully used, but it is assumed that their effectiveness may be limited by desensitization and downregulation of the target receptor. A growing number of new agents acting on incretin hormones are becoming available for everyday clinical practice, including oral GLP-1 receptor agonists, the dual GLP-1/GIP receptor agonist tirzepatide, and other dual and triple GLP-1/GIP/glucagon receptor agonists, which may show further significant therapeutic potential. This narrative review summarizes the therapeutic effects of different incretin hormones and presents future prospects in the treatment of T2DM and obesity.

Keywords: G-protein-coupled receptors; GLP-1 receptor agonist; GIP receptor agonist; glucagon receptor agonist; obesity; type 2 diabetes

1. Introduction

The prevalence of diabetes and obesity has been rising globally, posing significant public health challenges. According to an analysis of global data, adult obesity rates have more than doubled in women and nearly tripled in men. In 2022, a total of 879 million adults worldwide were living with obesity. Obesity is responsible for approximately 43% of all cases of type 2 diabetes, with rates as high as 80–85% in some populations [1]. Obesity not only increases the risk of developing type 2 diabetes but also exacerbates complications and related comorbidities, such as cardiovascular disease, cancer, and osteoarthritis, while decreasing life expectancy and increasing health care costs. Significant and sustainable weight loss can be beneficial in the development of type 2 diabetes (T2DM) and related complications, as well as in the occurrence of cardiovascular events [2]. Lifestyle changes,

such as appropriate diet and regular exercise, are key to weight loss and optimizing adipose tissue metabolism. Pharmacological options are already available for the treatment of obesity, which can help reduce appetite and/or calorie intake [3]. Understanding the role of intercellular signaling pathways and inflammatory processes occurring in adipose tissue is essential for the development of effective pharmacological agents in the complex mechanism of obesity. A therapeutic approach based on innovation and the discovery of mechanisms of action offers promising opportunities for a deeper understanding of the connections between obesity and T2DM, which may lead to the development of new therapeutic options in addition to lifestyle changes [4].

Guidelines for the management of obesity and T2DM emphasize the importance of lifestyle changes, including a reduced-calorie diet and increased physical activity. A weight loss of at least 5% can delay the onset of T2DM and reduce the occurrence of cardiovascular diseases, while long-term sustained weight loss of 10–15% can even induce T2DM remission and provide numerous other health benefits [3,4]. However, achieving and maintaining significant weight loss is particularly challenging in patients with T2DM. Additionally, rapid weight loss may improve insulin sensitivity, which can lead to further weight loss plateau and repeated weight regain [5]. Therefore, the addition of pharmacological therapies with properties that promote weight loss and reduce blood glucose levels represents a desirable approach in the management of obesity and T2DM [2]. In this regard, several incretin-based peptide therapies have emerged: once-weekly subcutaneous injections of glucagon-like peptide-1 (GLP-1) receptor agonist semaglutide, available also as a once-daily tablet, and the dual agonist tirzepatide, which interacts with both GLP-1 and glucose-dependent insulinotropic polypeptide (GIP) receptors, also administered as a once-weekly subcutaneous injection. Clinical trials concluded in the past decades have confirmed that GLP-1 receptor agonists have proven effective in the management of T2DM, and some formulations are now also used in higher doses for the treatment of obesity [6].

The development of incretin-based therapy for T2DM began in the 1990s, with the widespread use of daily short-acting injectable GLP-1 receptor agonists and oral dipeptidyl peptidase-4 inhibitors occurring in the 2000s. In the following decade, long-acting subcutaneous or daily oral GLP-1 receptor agonists administered weekly emerged [7]. In recent years, new formulations have been developed, and dual and/or triple GLP-1/GIP/glucagon receptor agonists have shown promise in the treatment of T2DM [8]. Figure 1 schematically depicts the incretin-based agents that are currently used in everyday medical practice or that are currently under clinical development [9].

Significant progress has been made in recent years in the development and clinical application of new incretin-based peptide therapies for the treatment of obesity and T2DM. The purpose of this narrative review is to summarize the therapeutic effects of various incretin hormones and to present future prospects in the treatment of T2DM and obesity. In addition, our aim is to briefly review recent pharmacological treatments for obesity and type 2 diabetes and summarize the latest results from clinical trials. We obtained the data for this review from PubMed, Scopus, Web of Science, and ClinicalTrials.gov, using the following keywords: “obesity”, “type 2 diabetes”, “new drug treatment”, “recent developments”, “clinical studies”, “G-protein-coupled receptor”, “glucagon-like peptide-1 receptor agonists”, “glucose-dependent insulinotropic polypeptide receptor agonist”, “glucagon receptor agonist”, “dual agonist”, and “triple agonist”.

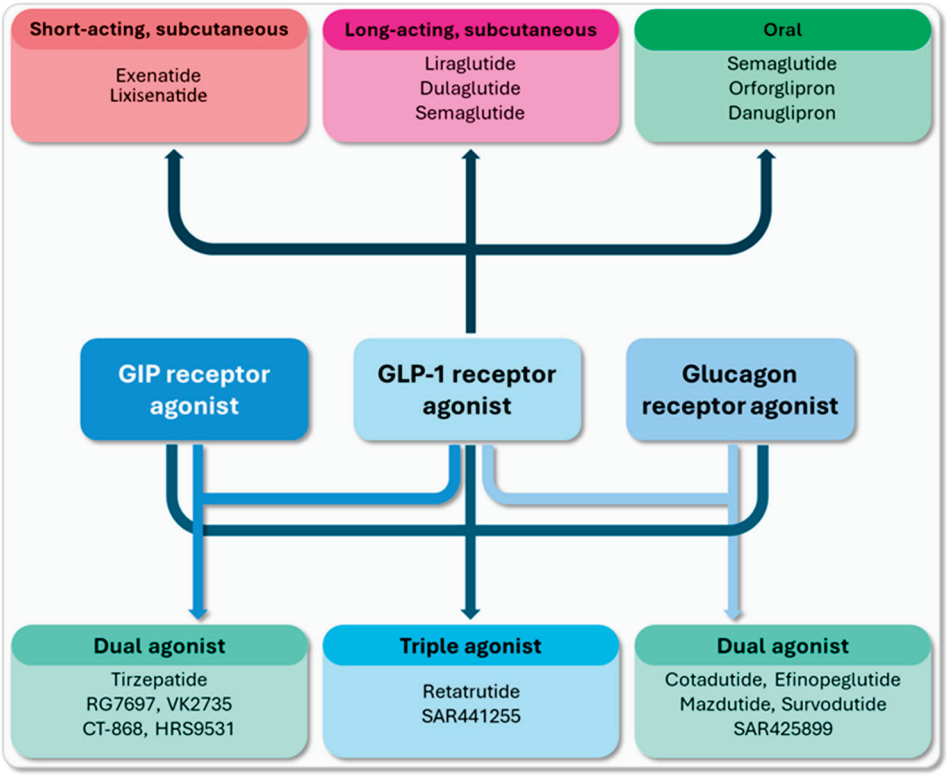


Figure 1. The incretin-based agents that are currently used in everyday medical practice or that are currently under clinical development [9].

2. The Importance of Inflammatory Processes and Oxidative Stress in Adipose Tissue

White adipose tissue possesses highly complex functions, with its primary role lying in energy storage. The function of white adipose tissue is often impaired in obese and diabetic individuals, resulting in adipocyte hypertrophy, pathological fat accumulation, and ectopic fat deposition, which can lead to the development of metabolic and cardiovascular diseases. Obesity is associated with increased insulin secretion, leading to insulin resistance and ultimately beta-cell failure, thereby promoting the development of T2DM [10].

Numerous inflammatory mediators are produced in adipose tissue, significantly contributing to the development of chronic inflammatory conditions [11] (Figure 2). One of the main characteristics in white adipose tissue is an increase in the number of macrophages, which also participate in the development of insulin resistance [12]. Among obese individuals, it is possible for the phenotype of macrophages to change, indicating the dominance of proinflammatory M1-polarized macrophages over M2 macrophages involved in anti-inflammatory and reparative mechanisms. This suggests a change in the innate immune system in obesity [13]. Due to chronic inflammation, the secretion profile of adipokines in white adipose tissue also shifts, increasing the production of proinflammatory factors such as tumor necrosis factor-alpha (TNFα), interleukin-1 (IL-1), interleukin-6 (IL-6), interleukin-8 (IL-8), and leptin, while decreasing the secretion of anti-inflammatory interleukin-10 (IL-10) and adiponectin. M1-polarized macrophages enhance the development of abnormal lipid profiles and insulin resistance, regardless of the inflammatory mediators in adipose tissue. Ultimately, persistent inflammation occurs in dysfunctional adipose tissue due to hypoxia, fibrosis, and mitochondrial dysfunction, leading to systemic inflammation, progression of atherosclerosis, and the development of T2DM and cardiovascular diseases [14].

Obesity and associated insulin resistance are accompanied by increased oxidative stress in endothelial cells, during which the production of reactive oxygen species (ROS) surpasses the capacity of antioxidant factors to balance them. As a result, signaling pathways are modified, and the lipid, protein, and DNA content of cells is damaged. The

superoxide anion, with high reactivity, binds and inactivates the physiological function of endothelial nitric oxide synthase (eNOS), leading to the production of peroxynitrite instead of NO. Peroxynitrite is a potent oxidizing agent that can cause lipid peroxidation, protein tyrosine nitration, DNA damage, and cell death. Additionally, peroxynitrite oxidizes tetrahydrobiopterin, an essential cofactor for eNOS, rendering it biologically inactive and unable to catalyze endothelial NO synthesis [15]. Consequently, eNOS catalyzes the production of further superoxide radicals instead of NO. Beyond other intracellular signaling and metabolic changes, the inactivation of eNOS is a key factor in the relationship between oxidative stress and pathological functional changes in the endothelium. In diabetes, chronic hyperglycemia, acute fluctuations in blood glucose levels, and insulin resistance all contribute to increased oxidative stress and, therefore, to the development of endothelial dysfunction [16].

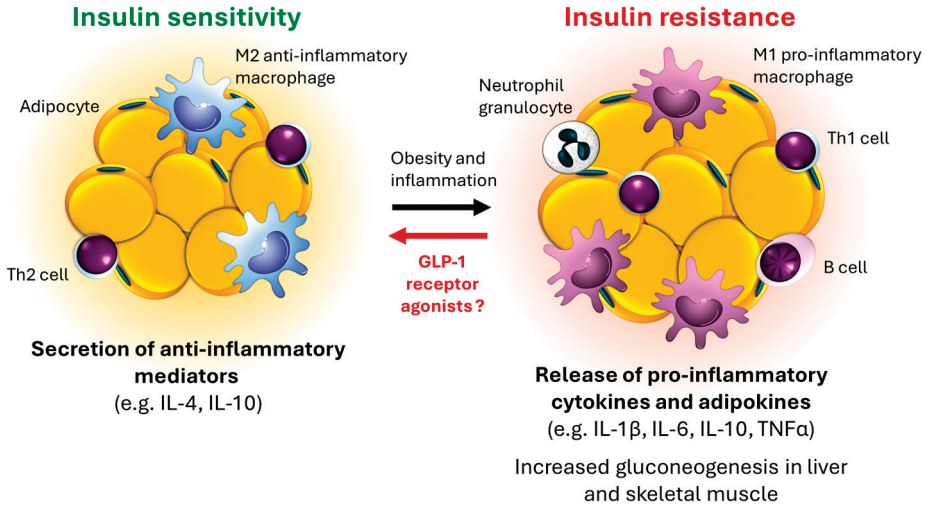


Figure 2. Inflammatory mediators in adipose tissue, contributing to the development of chronic inflammatory conditions [11]. GLP-1: glucagon-like peptide-1; TNF-α: tumor necrosis factor-alpha; Th1cell: T-helper 1; Th2 cell: T-helper 2 cell; IL-1β: interleukin-1β; IL-4: interleukin-4; IL-6: interleukin-6; IL-10: interleukin-10.

GLP-1 receptor agonists may potentially reduce inflammation and oxidative stress in adipose tissue by affecting the expression of cytokines, chemokines, and macrophage infiltration, with prolonged GLP-1 action potentially alleviating obesity-related adipose tissue inflammation while enhancing the expression of anti-inflammatory genes [17,18] (Figure 2).

3. The Importance of G-Protein-Coupled Receptors in Obesity and T2DM

Incretin-based peptides exert their cellular effects through G-protein-coupled receptors, which have become important therapeutic targets in the treatment of obesity and T2DM in recent years. However, the exact mechanism underlying G-protein-coupled receptors/G-protein specificity remains ambiguous and warrants further investigation [19]. G-protein-coupled receptors constitute the largest family of membrane proteins, and ligand binding can lead to activation of multiple intracellular pathways, including G proteins, beta-arrestins, and other non-G-protein-regulated signaling pathways, such as mitogen-activated protein kinase phosphorylation [20] (Figure 3). Molecules that bind directly to G-protein-coupled receptors can be either orthosteric (binding to the same pocket as the natural ligand) or allosteric (binding to a different pocket). Allosteric modulators can cooperatively interact with the natural orthosteric ligand, thereby enhancing or attenuating receptor signaling. Beta-arrestins contribute to a reduction in the response to receptor agonism through internalization of the specific G-protein-coupled receptor [21]. Presumably, the effect of native GLP-1 on the GLP-1 receptor evenly activates various signaling

pathways. However, certain agonists of activated G-protein-coupled receptors can promote the activation of a subset of signaling pathways, resulting in "ligand bias" associated with unique cellular responses. Deviation from the typical effect profile of a certain receptor type is termed "biased agonism". Certain biased agonists of the GLP-1 receptor may more strongly facilitate G-protein activation than recruitment of beta-arrestins [22]. However, it is possible that bias towards G-protein signaling may stem more from reduced activation of G-protein-coupled receptor kinases than inhibition of binding to beta-arrestins, while other studies have shown that certain β2AR ligands prefer beta-arrestin signaling over G-protein activation [23,24]. Beta-arrestin-dependent seven-transmembrane receptor signaling includes beta-arrestins, which function as multifunctional proteins regulating receptor desensitization, endocytosis, and ubiquitination while modulating G-protein signaling and promoting activation of alternative intracellular pathways. G-protein-based GLP-1 agonists appear to achieve significant weight and blood sugar-reducing effects, in part through reduced beta-arrestin recruitment, thereby avoiding receptor desensitization and downregulation [25]. β-arrestins intracellularly exert an inhibitory effect on signaling pathways mediated by G-protein-coupled receptors; concurrently, they possess the capability to regulate cellular functions independently of G proteins, such as through interaction with peroxisome proliferator-activated receptor-γ [26]. It appears that both G-protein signal activation and the beta-arrestin pathway may facilitate weight loss by inhibiting adipogenesis and inflammatory response [23,27]. Different intracellular cellular responses following binding to G-protein-coupled receptors may also explain the different efficacy of different peptide-based therapies (Figure 3).

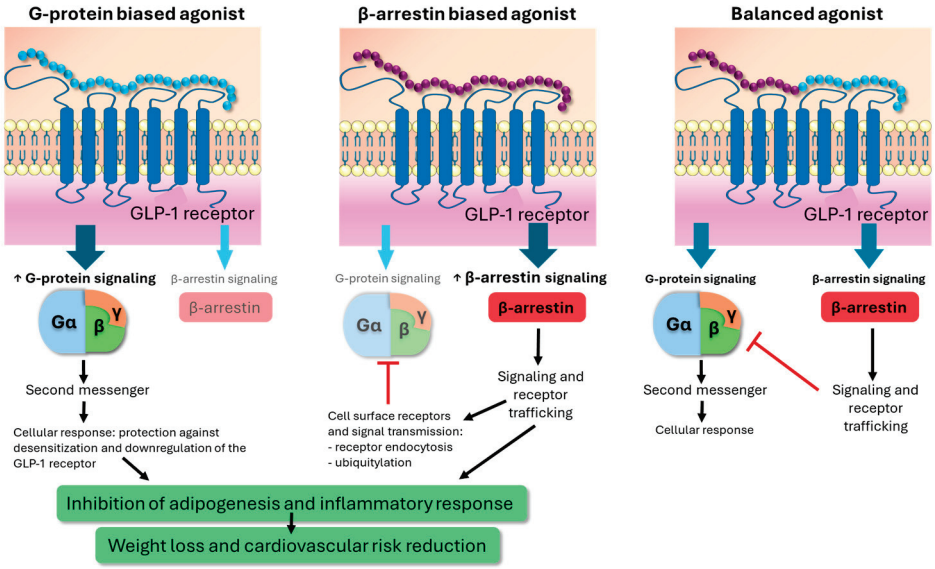


Figure 3. Activation of intracellular pathways by G-protein-coupled receptors and ligand binding, including G proteins, beta-arrestins, and other non-G-protein-regulated signaling pathways [20]. GLP-1: glucagon-like peptide-1.

GLP-1, GIP, and glucagon receptors belong to class B G-protein-coupled receptors within the secretin receptor family. Their activation involves G protein (Gαs), leading to increased insulin secretion in beta cells via cyclic adenosine monophosphate (cAMP) production, but they also activate the beta-arrestin pathway, which impedes G-protein signaling. Each receptor undergoes agonist-induced endocytosis to varying degrees, thus fine-tuning spatial and temporal modulation of intracellular signaling and hormonal response [28]. During biased agonism, the balance between receptor recruitment, activation of intracellular signaling, and subsequent receptor trafficking may be ligand specific. There are numerous examples of biased agonism at the GLP-1 receptor, including both natural and pharmacological orthosteric agonists. Biased GLP-1 receptor agonists derived from

exendin-4 result in prolonged insulin secretion by reducing GLP-1 receptor desensitization and endocytosis, as well as mitigating GLP-1 receptor downregulation [29]. The dual GLP-1/GIP receptor agonist tirzepatide exhibits unbalanced dual agonism at GLP-1 and GIP receptors, but with significantly lower affinity for the GLP-1 receptor and much milder cAMP activation [30].

GLP-1, GIP, and glucagon receptors are present on pancreatic beta cells, and their physiological or pharmacological activation leads to significant metabolic effects [9] (Figure 4). Activation of all three receptors enhances glucose-stimulated insulin secretion, but they differ in their effects on fasting and postprandial blood glucose levels, gluconeogenesis, and lipogenesis, while their common effects include increased energy expenditure and enhanced satiety for weight loss [31]. GLP-1 receptor agonists moderate fasting and postprandial blood glucose levels and, beyond their weight-reducing effects, have demonstrated anti-atherogenic protection in terms of cardiovascular diseases [32,33]. In the case of GIP analogs, beyond effective blood sugar reduction, they have also shown effects on food intake and weight loss, especially when combined with GLP-1 receptor agonists. However, the effects of GIP on fatty acid metabolism, atherosclerosis, adipose tissue metabolic activity, and energy expenditure remain unclear [33]. Despite glucagon's blood sugar-increasing effect, glucagon receptor activation moderates food intake, enhances fatty acid breakdown, and increases energy expenditure, supporting the rational use of glucagon in combination with other incretin hormones in the treatment of obesity and T2DM [34].

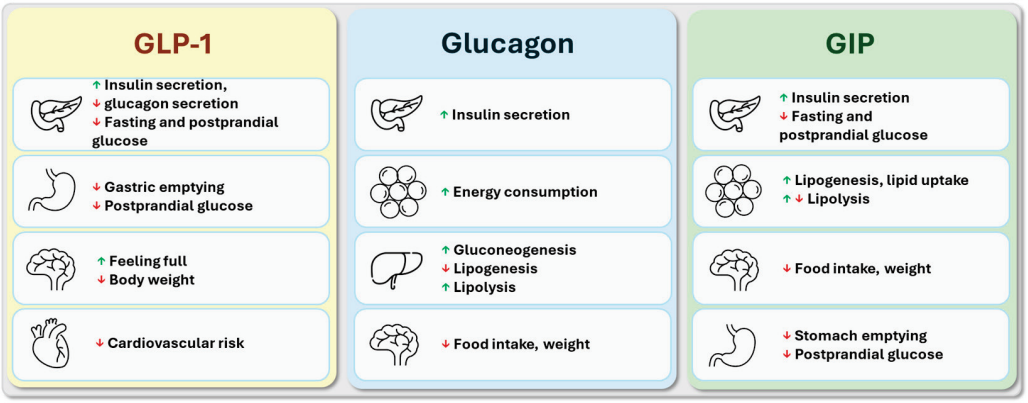


Figure 4. The main effects of glucagon-like peptide-1 (GLP-1), glucose-dependent insulinotropic polypeptide (GIP), and glucagon [9].

3.1. The Main Effects of Glucagon-like Peptide-1

Glucagon-like peptide-1 hormone (GLP-1) is produced in the L cells of the small intestine following meals and stimulates insulin secretion in a glucose-dependent manner. Its action activates the GLP-1 receptor, a glycoprotein receptor belonging to the family of G-protein-coupled receptors with seven transmembrane helices [35]. Activation of GLP-1 receptors leads to the formation of cAMP from adenosine triphosphate (ATP). cAMP activates protein kinase A, resulting in closure of ATP-sensitive potassium channels and depolarization of beta cells, leading to the opening of voltage-gated calcium channels on the cell membrane and exocytosis of insulin-containing granules released from the endoplasmic reticulum due to calcium release [36]. Additionally, experimental studies suggest that activation of GLP-1 receptors inhibits beta-cell apoptosis [37]. Metabolic effects mediated by GLP-1 include increased glucose uptake and glycogen production in skeletal muscle, as well as inhibition of gluconeogenesis in the liver [38] (Figure 4). Due to its positive chronotropic and inotropic effects on cardiac muscle cells, GLP-1 slightly increases the heart rate, which is counteracted by the favorable effect of incretin hormones on left ventricular diastolic dysfunction, common in T2DM [39,40]. GLP-1 inhibits glucagon secretion in alpha cells, slows gastric emptying, reduces appetite, and increases satiety through GLP-1 receptors in the hypothalamus in the central nervous system. In cardiovascular

protection, the anti-atherogenic, anti-inflammatory effect on the vascular wall and inhibition of macrophage activation play a significant role [18,41]. Animal models have shown that GLP-1 can increase energy expenditure and regulate heat production and conversion from white adipose tissue to brown adipose tissue in obese mice [42], although human data on this effect are not yet convincing [18,43]. The weight-reducing effect achieved with GLP-1 receptor agonists may alleviate cardiac insulin resistance in obese and overweight individuals. Reduced insulin resistance may be linked to decreased ejection fraction in individuals with T2DM [44] and in non-diabetic obese patients [45]. These effects may partially contribute to the cardioprotective effects of agents targeting the incretin axis, particularly in the context of heart failure. Furthermore, GLP-1 receptor agonists have been demonstrated to exert a protective effect on the microvascular compartment of the myocardium [46,47]. Substantial evidence also supports the beneficial effects of the GLP-1 hormone on epicardial adipose tissue [48] and in the treatment of metabolic-associated fatty liver disease (MAFLD—formerly known as non-alcoholic fatty liver disease) [49]. Overall, the main effects of GLP-1 include reducing fasting and postprandial blood glucose levels, weight loss, and confirmed anti-atherogenic protection against cardiovascular diseases.

3.2. The Main Effects of Glucose-Dependent Insulinotropic Polypeptide

Glucose-dependent insulinotropic polypeptide (GIP) is produced from K cells in the mucosa of the small intestine and exerts its effects through a receptor coupled to a G protein. The glucose-dependent insulin-releasing effect of GIP, like GLP-1, is impaired in T2DM, but combining them may further improve beta-cell function and insulin secretion [50] (Figure 4). Similar to GLP-1, GIP also inhibits beta-cell apoptosis in the pancreas, thereby improving its survival during T2DM progression [51]. GIP also stimulates bone formation by inhibiting osteoclast apoptosis [52]. The precise effects of GIP on lipid metabolism are currently unclear; some studies suggest it may increase lipid uptake in adipose tissue and decrease lipolysis [53,54], while others suggest GIP may have lipolytic activity, as adipose tissue from transgenic mice overexpressing GIP has been found to be resistant to high-fat feeding [55,56]. It is hypothesized that by enhancing lipid-buffering capacity and insulin sensitivity in white adipose tissue postprandially, GIP may prevent ectopic fat deposition between tissues and muscles [57]. Activation of GIP receptors improved blood glucose levels in obese mouse models without altering body weight or fat tissue quantity [58], and activation of GIP receptors in the hypothalamus reduced food intake as well [59]. Whole-genome association studies have shown associations between different activity levels of human GIP receptor variants and the degree of obesity [60]. The anti-inflammatory effect of GIP on atherosclerosis is not clear from preclinical studies; therefore, the role of GIP in the atherosclerosis process seems to be controversial at the moment. In cell cultures, the administration of GIP may exert both anti-atherogenic effects (increased nitric oxide and adiponectin concentration, decreased endothelin-1 levels, reduced oxidative stress, decreased migration and proliferation of fibroblast cells) and pro-atherogenic effects (decreased adiponectin levels, increased endothelin-1 and osteopontin levels) [61]. In another study, high-dose administration of GIP reduced macrophage translocation into the vessel wall, thereby reducing foam cell formation, decreasing matrix metallopeptidase-9 activity and interleukin-6 secretion, and ultimately reducing the size of atherosclerotic plaques [62]. In summary, besides effectively reducing blood sugar levels, GIP analog treatment has also been shown to affect food intake and weight loss, especially when combined with GLP-1 receptor agonists. However, the detailed effects of GIP on lipid metabolism, atherosclerosis, metabolic activity of adipose tissue, and energy expenditure are still unclear.

3.3. The Main Effects of Glucagon

Glucagon is released from pancreatic α-cells through cleavage of its precursor, proglucagon. In maintaining blood glucose levels, glucagon responds to low glucose levels by increasing gluconeogenesis and glycogenolysis in the liver (Figure 4). In T2DM,

the inhibition of glucagon secretion in response to serum glucose levels is impaired, leading to sustained hyperglycemia due to prolonged hormone action [63]. Similar to GLP-1 and GIP, glucagon stimulates beta cells; however, it acts differently on alpha cells: While GLP-1 continuously inhibits glucagon secretion, GIP stimulates glucagon secretion under normal blood sugar and hypoglycemic conditions, but not during hyperglycemia. This physiological effect may mitigate postprandial hyperglycemia and provide protection against the adverse effects of persistently high blood sugar levels [64]. Glucagon exerts its effects through the glucagon receptor, which is also a seven-transmembrane receptor coupled to G proteins. Glucagon receptors are primarily present in liver cells but can also be found in the central nervous system, kidneys, digestive system, and pancreas [65]. In addition to its blood glucose-increasing effect, glucagon activates fat breakdown and inhibits lipogenesis in the liver, reducing concentrations of non-esterified fatty acids and triacylglycerol, and moderating triglyceride content in liver cells in animal experiments [66]. Based on these findings, activation of the glucagon receptor may have a favorable effect on the development and treatment of MAFLD, commonly seen in T2DM. Glucagon receptors are also expressed in pancreatic beta cells, showing significant amino acid homology with incretin receptors and promoting insulin secretion. Glucagon enhances the feeling of satiety and exerts an anorexigenic effect by crossing the blood–brain barrier and acting on the hypothalamus [67]. In animal models, glucagon stimulates energy expenditure through activation of brown adipose tissue [68], although the significance of this effect has not been confirmed by human data [69]. In summary, despite its blood glucose-increasing effect, glucagon moderates food intake, enhances fatty acid breakdown, and increases energy expenditure. These properties support the rational use of glucagon in combination with other incretin hormones in the treatment of T2DM.

4. Peptide-Based Therapies in the Treatment of Obesity

The GLP-1 receptor agonist liraglutide at a high dose (administered as a single daily injection of 3 mg subcutaneously) has been approved as an adjunctive medication for weight loss achieved through a low-calorie diet and physical activity in adults with obesity or overweight-related comorbidities, as well as for the treatment of obese children and adolescents aged 12 years or older [70]. Previous large randomized clinical trials have demonstrated that a 3 mg dose of liraglutide can result in an average weight loss of 5.6 kg over nearly one year in overweight or obese individuals without diabetes [71]. The results achieved with high-dose liraglutide have encouraged further development of peptide therapies for the management of obesity and overweight. Recent significant clinical trials evaluating the efficacy of weight loss are summarized in Figures 5 and 6.

The STEP clinical trials collectively provide valuable information about semaglutide's safety, efficacy, and impact on weight loss and cardiovascular outcomes in various patient populations. The STEP trials have evaluated the effects of once-weekly subcutaneous administration of the GLP-1 receptor agonist semaglutide at a dose of 2.4 mg [72] (Figure 5). Generally, approximately 15% weight loss was observed in overweight and obese, non-diabetic adults across various treatment periods, lasting up to 2 years (from STEP-1 to STEP-6, STEP-8) [72–79]. Similar efficacy was achieved with once-weekly subcutaneous injections of 2.4 mg semaglutide in the STEP Teens trial among adolescents aged 12–18 years [80], as well as with high-dose oral administration of 50 mg semaglutide in overweight and obese, non-diabetic adults (OASIS-1) [81] (Figure 6). In the STEP-2 trial, a smaller but significant 9.6% weight loss was observed with weekly subcutaneous administration of 2.4 mg semaglutide in obese patients with T2DM [73]. In the 52-week STEP-HFpEF study, besides significant weight reduction in obese patients with heart failure with preserved ejection fraction treated with once-weekly subcutaneous 2.4 mg semaglutide, a decrease in heart failure symptoms (fatigue, dyspnea, and edema) and improvement in physical performance were observed [82]. In the SELECT trial, over an average of 40 weeks of follow-up, a 20% reduction in the occurrence of the three-point composite cardiovascular endpoint (cardiovascular death, nonfatal myocardial

infarction, and nonfatal stroke) was found in overweight and obese, non-diabetic adults with once-weekly subcutaneous semaglutide (2.4 mg) [83].

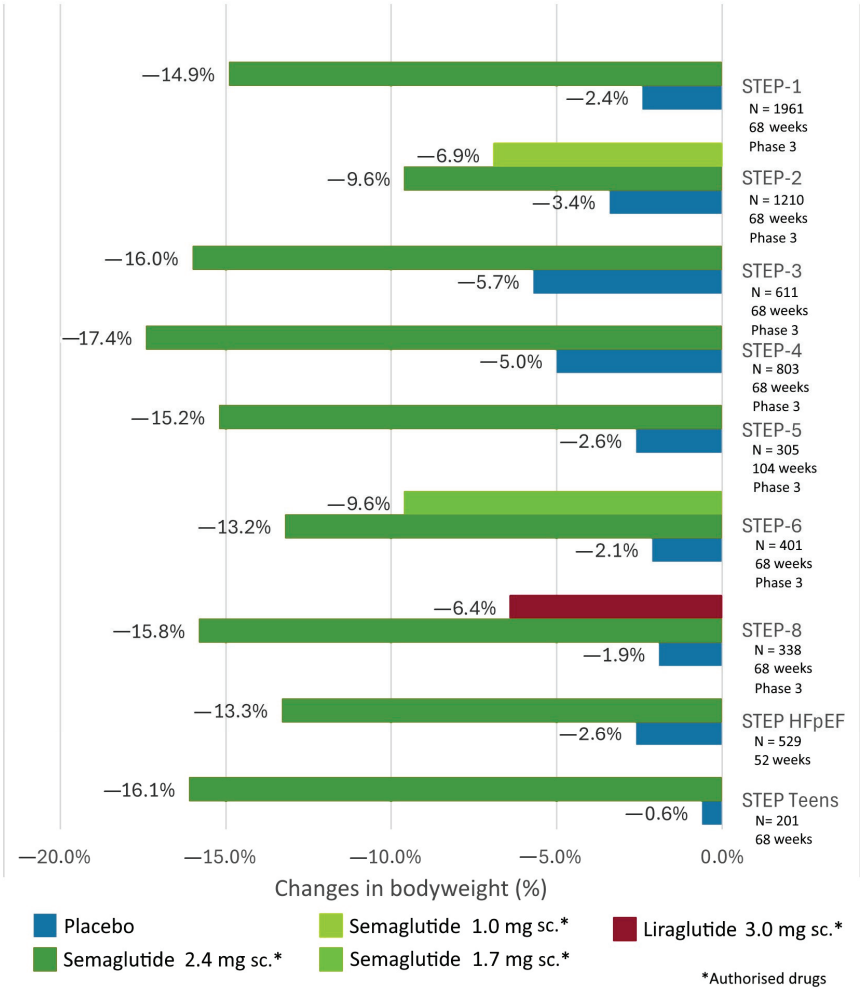


Figure 5. Clinical trials of subcutaneous semaglutide in overweight and obese individuals to evaluate weight loss efficacy (STEP 1–6, STEP-8, STEP Teens, STEP HFpEF).

In clinical trials with high-dose semaglutide, nausea and vomiting were the most common side effects, which were associated with delayed gastric emptying and occurred in approximately 40% of participants in the studies. These side effects were generally mild to moderate in severity and resolved after 1–3 months of treatment, leading to treatment discontinuation in less than 5% of cases. Initial gastrointestinal side effects were observed in approximately 80% of participants taking high-dose oral semaglutide (50 mg once daily), but like with subcutaneous weekly 2.4 mg semaglutide, their severity decreased over time [81]. Currently, high-dose subcutaneous semaglutide (2.4 mg once weekly) is approved in the United States and Europe for the treatment of obesity and overweight as an adjunct to a calorie-restricted diet and increased physical activity. Further data are needed for regulatory approval as part of the ongoing OASIS trial program evaluation.

The design of the SURMOUNT clinical trials of experiments with the dual GLP-1 and GIP receptor agonist tirzepatide bears many similarities to the STEP program (Figure 6). The SURMOUNT trials have demonstrated tirzepatide glucose-lowering efficacy, weight loss efficacy, and cardiovascular safety in various patient populations. In the SURMOUNT-1 and -3 studies, tirzepatide administered at a high dose of 15 mg subcutaneously once weekly resulted in approximately a 20% reduction in body weight in overweight and obese, non-diabetic adults, even after up to 2 years of treatment [84,85]. Weight loss was slightly lower, at 14.7%, in overweight and obese patients with T2DM in the SURMOUNT-2

study [86]. To minimize gastrointestinal side effects, the tirzepatide dose was gradually increased in all SURMOUNT clinical trials, starting at 2.5 mg and escalating by 2.5 mg every 4 weeks until reaching the maintenance dose required. Initial gastrointestinal side effects were reported by approximately 30% of participants, which were generally mild to moderate in severity and significantly diminished during sustained treatment achieved through dose titration, resulting in a discontinuation rate of less than 8% [87]. Several large, randomized clinical trials are currently underway in the SURMOUNT program, aiming to determine the effectiveness of tirzepatide in promoting weight loss in overweight and obese children, individuals with obstructive sleep apnea, and those with heart failure with preserved ejection fraction [88]. A longer-term study, SURPASS-CVOT, is ongoing to evaluate the effect of tirzepatide on major cardiovascular events in overweight and obese adults, with an expected completion date of October 2024 [88]. Tirzepatide has been approved by the United States Food and Drug Administration (FDA) and the European Medicines Agency (EMA) for the treatment of weight in obese and overweight individuals.

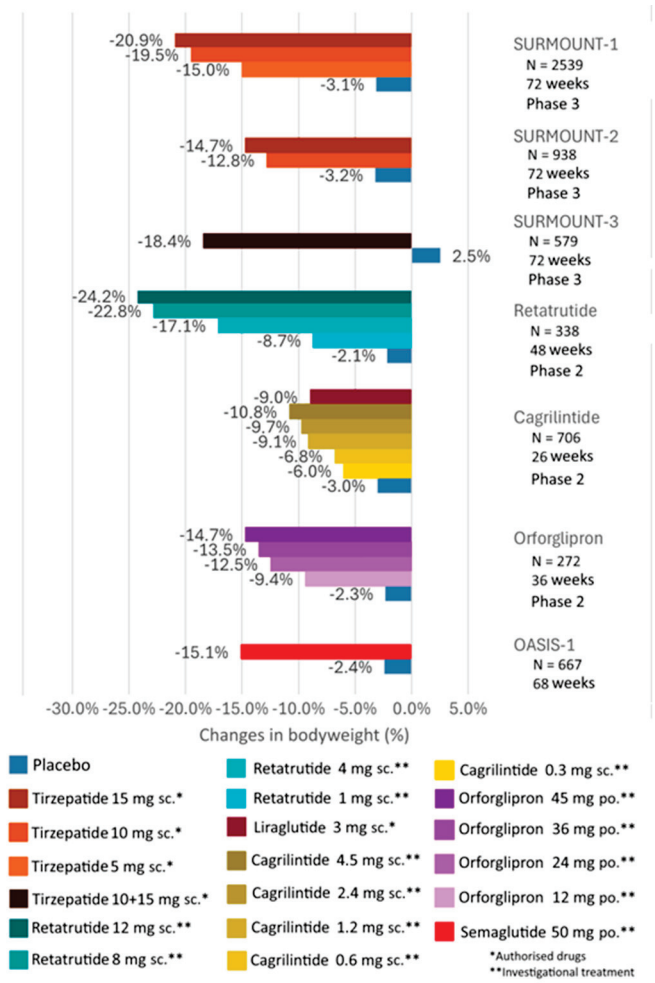


Figure 6. Clinical trials of subcutaneous tirzepatide (SURMOUNT-1, -2 and -3 trials), retatrutide and cagrilintide, and oral semaglutide and orforglipron in overweight and obese subjects to evaluate weight reduction efficacy.

High-dose semaglutide and tirzepatide have been extensively studied for their efficacy in weight management and glycemic control. However, their use can be associated with several side effects, which are important to consider during clinical application. Gastrointestinal symptoms such as nausea, vomiting, diarrhea, or constipation were the most common side effects, observed at a significantly higher incidence in patients receiving high-dose semaglutide or tirzepatide compared to comparators. These side effects are usually mild to moderate in

severity and tend to be temporary. The use of semaglutide and tirzepatide may increase the risk of biliary disorders such as cholelithiasis, a risk similar to that of other GLP-1 receptor agonists, and therefore patients should be monitored during clinical use [89,90]. There is concern about the potential risk of pancreatitis and pancreatic and thyroid cancers with the use of GLP-1 receptor agonists. However, the incidence of these conditions is low, and definitive conclusions cannot be drawn at this time. In clinical trials, severe hypoglycemia, acute pancreatitis, gallstones, and cholecystitis occurred rarely and were observed only in a few cases during the use of high-dose semaglutide and tirzepatide [89,90].

5. Peptide-Based Therapies in the Treatment of Obesity and Type 2 Diabetes

5.1. Dual GIP/GLP-1 Receptor Agonists

The first GIP/GLP-1 receptor co-agonist was discovered in 2013, exhibiting significantly more pronounced glucose-lowering and insulin-releasing efficacy than selective GLP-1 receptor agonists in obese and leptin receptor-deficient mouse models, as well as in humans [91]. Further development of GIP/GLP-1 receptor co-agonists followed these results, with tirzepatide becoming the most widely studied representative of this drug class. Tirzepatide binds more strongly to the GIP receptor than to the GLP-1 receptor; in receptor-binding studies, tirzepatide's affinity was comparable to the native hormone's affinity for the GIP receptor, while it was approximately five times weaker than native GLP-1's affinity for the receptor [92]. However, binding to the GLP-1 receptor also seems significant in tirzepatide's cell surface receptor mechanism, as tirzepatide had no effect on body weight, food intake, fasting insulin levels, skeletal muscle, subcutaneous adipose tissue endogenous glucose production, or insulin-stimulated glucose uptake in GLP-1 receptor non-expressing knockout mice [93].

The US and European drug regulatory agencies approved tirzepatide for the treatment of T2DM in 2022. As part of the SURPASS program, phase III trials were conducted to evaluate the therapeutic efficacy (glycemic control and weight reduction), safety, and tolerability of tirzepatide in patients with T2DM [94,95]. Tirzepatide treatment was administered in three doses (5 mg, 10 mg, or 15 mg weekly subcutaneously), starting with a 2.5 mg weekly dose, then titrated up every 4 weeks. These studies show that tirzepatide significantly reduced fasting blood glucose and HbA1c levels not only compared to placebo but also compared to degludec and glargine insulins or semaglutide. The change in HbA1c ranged from −1.87% to −2.59% for various doses of tirzepatide compared to placebo, −1.86% for weekly 1 mg semaglutide in the SURPASS-2 trial, −1.34% for degludec insulin in the SURPASS-3 trial, and −1.44% for glargine insulin in the SURPASS-4 trial [94–96] (Figure 7). Additionally, tirzepatide significantly reduced weight in obese T2DM patients in a dose-dependent manner; by weeks 40–52 of the trials, the 5 mg dose of tirzepatide resulted in a weight loss of 6.2–7.8 kg, the 10 mg dose led to a weight loss of 7.8–10.7 kg, and the 15 mg dose caused a weight loss of 9.5–12.9 kg [96]. Currently, several dual GIP/GLP-1 receptor agonists are under clinical development, among which tirzepatide was approved in the United States and Europe in 2022 for the treatment of T2DM.

5.2. Dual Glucagon/GLP-1 Receptor Agonists

Glucagon alters lipid metabolism and energy expenditure favorably while also reducing appetite and food intake, making it an attractive option for the treatment of T2DM and obesity, especially when combined with the insulinotropic effects of GLP-1. The first monomolecular glucagon receptor/GLP-1 receptor co-agonist was discovered in 2009, and its weekly administration significantly improved carbohydrate metabolism and reduced weight in obese mice fed a high-calorie diet during preclinical studies [97]. In recent years, two glucagon receptor/GLP-1 receptor co-agonists underwent phase II clinical trials in human experiments, namely, SAR425899 and cotadutide [98,99]. Further development of SAR425899 was eventually halted during human trials. Cotadutide effectively lowered blood sugar levels and reduced weight in obese individuals and T2DM patients, increased insulin secretion, delayed gastric emptying, with the most common side effects being gastrointestinal symptoms (nausea

and vomiting), which were dose-dependent [99,100]. A multicenter study evaluated the effects of subcutaneously administered cotadutide in 834 participants in daily doses of 100 µg, 200 µg, and 300 µg compared with placebo and 1.8 mg liraglutide daily [101]. The study lasted for 54 weeks and assessed liver abnormalities and metabolic parameters in overweight and obese T2DM patients. Every dose of cotadutide and liraglutide significantly reduced HbA1c levels compared to placebo (change in HbA1c—cotadutide 100 µg: −1.03%; 200 µg: −1.16%; 300 µg: −1.19%, liraglutide 1.8 mg: −1.17%); however, there was no significant difference in HbA1c reduction between cotadutide and liraglutide. The highest dose of cotadutide resulted in a significantly greater reduction in weight compared to liraglutide and placebo (change in weight—cotadutide 100 µg: −3.7 kg; 200 µg: −3.22 kg; 300 µg: −5.02 kg, liraglutide 1.8 mg: −3.33 kg). Higher doses of cotadutide also showed more significant improvement in liver enzyme levels and parameters indicative of liver fibrosis compared to liraglutide [101]. Based on the favorable results, the effects of cotadutide are primarily planned to be extended towards the treatment of MAFLD. A comparison of the HbA1c and weight-reducing effects of cotadutide with various doses of dulaglutide, liraglutide, and semaglutide currently in clinical use is shown in Figure 3 [102].

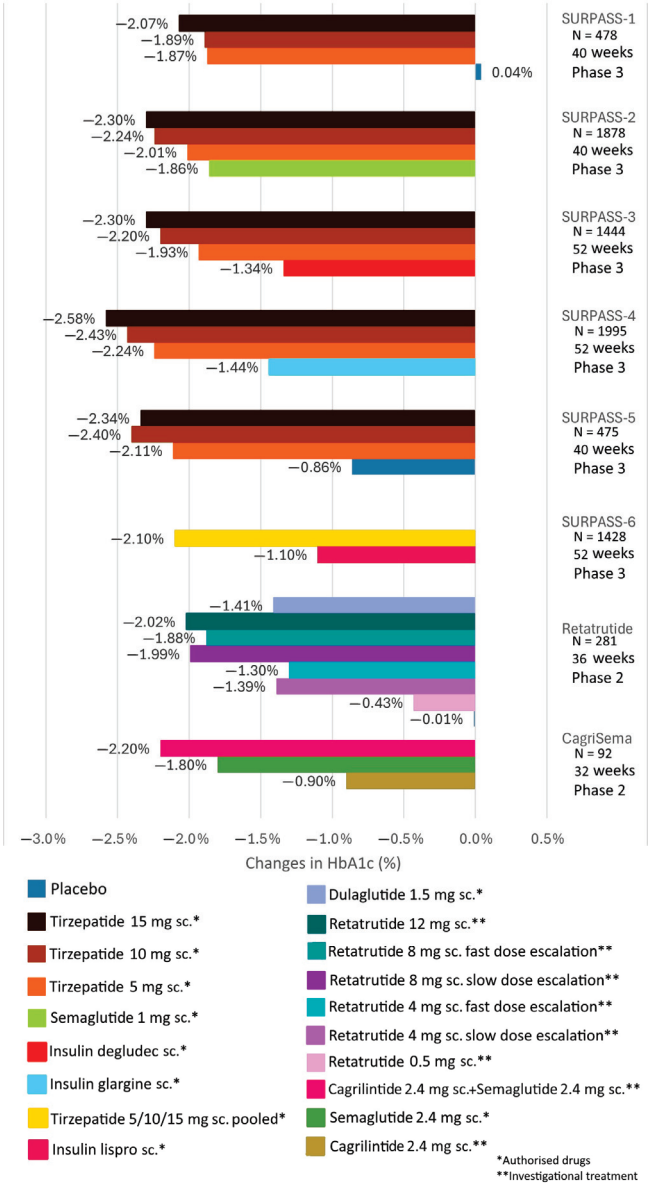


Figure 7. Clinical trials of subcutaneous tirzepatide, retatrutide, and cagrilintide/semaglutide in type 2 diabetic subjects to evaluate HbA1c reduction efficacy.

5.3. Triple GIP/GLP-1/Glucagon Receptor Agonists

The significant results of clinical trials with dual receptor agonists have stimulated the development of new combination approaches in the treatment of T2DM and obesity. The synergistic metabolic benefits of pharmacological modulation of GLP-1, GIP, and glucagon receptors were first demonstrated in 2015. Triple agonism of GLP-1, GIP, and glucagon resulted in greater weight loss and reduction in blood glucose levels in obese mice compared to monoagonists and dual GLP-1/GIP receptor agonists [31]. A triple receptor agonist, known as SAR441255, dose-dependently reduced weight by up to 25% after 4 weeks of treatment. When administered subcutaneously, SAR441255 at the two highest test doses (80 μg and 150 μg) normalized fasting blood glucose levels within the first hour of treatment in overweight individuals, with the highest dose being well tolerated and the most common treatment-related side effects being gastrointestinal complaints [103]. New triple receptor agonists with longer duration of action have been developed, allowing for once-weekly dosing. In a recent study, these novel, long-acting triple receptor agonist formulations more effectively and successfully reduced weight in obese mouse models compared to semaglutide, tirzepatide, dual GLP-1/glucagon receptor agonists, or short-acting triple receptor agonists, and their use did not entail increased risk of hypoglycemia [104]. In a recent phase I study, retatrutide, a triple glucagon/GIP/GLP-1 receptor agonist, significantly reduced body weight and improved glycemic control, exhibiting a safety and tolerability profile similar to other incretin formulations in study participants, and body weight continued to decrease steadily after a single dose until the end of the study [105] (Figure 6). Retatrutide has also been subjected to human trials in patients with T2DM, showing significant reductions in body weight and HbA1c by the end of the 12th week compared to baseline values [106] (Figure 7). Whether triple receptor agonists will surpass the clinical outcomes of GLP-1/GIP receptor agonists will be determined by further investigations in the future.

6. Studies with Other Weight-Loss Medications

Orforglipron is an orally administered, non-peptide GLP-1 receptor agonist that can be taken once daily. However, it binds differently to the GLP-1 receptor compared to native GLP-1, thereby inducing G-protein activation rather than beta-arrestin recruitment [107]. It is being investigated for the treatment of obesity and T2DM and could represent a competitive alternative to oral semaglutide, as its less burdensome administration does not require fasting. In T2DM patients, the average change in HbA1c was −2.1% with a dose of 45 mg of orforglipron (compared to dulaglutide and placebo), and nearly half of the participants achieved more than a 10% reduction in body weight in a 26-week phase 2 trial [108]. In obese, non-diabetic individuals, orforglipron administration for 36 weeks in a phase 2 trial, ranging from 12 mg to 45 mg doses, resulted in dose-dependent weight loss of up to 14.7%, accompanied by improvements in cardiometabolic risk factors [109] (Figure 6).

Danuglipron is another orally administered, non-peptide GLP-1 receptor agonist oriented towards G-protein [110]. In a phase 2 study in T2DM patients over 16 weeks, the highest dose of danuglipron administered twice daily (120 mg) resulted in an average HbA1c reduction of 1.2%, with an average weight loss of 4.2 kg [111]. A recently completed phase 2 trial in obese and non-diabetic individuals revealed, according to a press release, that danuglipron at doses ranging from 40 to 200 mg twice daily resulted in a 11.7% weight loss after 32 weeks of treatment compared to placebo. However, the rate of discontinuation due to adverse events (gastrointestinal side effects) exceeded 50% in each dosage group compared to placebo [112].

Several potential formulations for obesity treatment are currently undergoing clinical trials. The triple GLP-1/GIP/glucagon receptor agonist retatrutide (administered once weekly as 12 mg subcutaneous injections) achieved a 24% weight loss in a 48-week study involving overweight and obese individuals [113]. Several unimolecular dual or triple agonist proteins are also currently being studied, including those based on the action of the oxyntomodulin hormone, such as survodutide, pemvidutide, and mazdutide, which

show promising weight-reducing effects [114]. The dual GLP-1/glucagon receptor agonist cotadutide and the triple GLP-1/GIP/glucagon receptor agonist efpeglenatide are being studied for the treatment of MAFLD [101]. The appetite-suppressing effect of pancreatic peptide YY (peptide tyrosine tyrosine) is well known, and initial clinical studies are underway with long-acting YY peptide analogs as monotherapy and in combination with GLP-1 receptor agonists for obesity treatment [115].

The amylin analog pramlintide, used in the United States as a prandial adjunct to insulin therapy, delays gastric emptying, improves postprandial blood sugar levels, and reduces weight [116]. A long-acting amylin analog similar to pramlintide, cagrilintide, administered parenterally once weekly at the highest dose of 4.5 mg, induced a significant 10.8% weight loss [117] (Figure 6). According to results from a recently published 32-week phase 2 trial, combined therapy with weekly parenteral administration of 2.4 mg cagrilintide and 2.4 mg semaglutide (CagriSema) reduced body weight by an average of 15.6% and HbA1c by an average of 2.2% in patients with T2DM compared to baseline [118] (Figure 7). Phase 3 trials with CagriSema combination therapy, part of the REDEFINE program, are evaluating its efficacy in weight loss and cardiovascular safety in patients with T2DM and overweight/obese, non-diabetic individuals [119]. The completion of the trials is expected in 2026 and 2027. Clinical trials have recently been initiated for obesity treatment with other long-acting amylin analogs and a dual amylin/calcitonin receptor agonist [120,121].

Further investigations are underway regarding protein-based approaches relying on other hormonal effects for effective weight loss; however, it currently appears that the potential clinical benefits of these are moderate. The appetite-suppressing effect of leptin analogs rapidly diminishes with the development of leptin resistance; thus, the use of metreleptin is limited to cases of congenital or acquired leptin deficiency [122]. Direct activation of the melanocortin-4 receptor in the hypothalamus with melanocortin-4 receptor agonist setmelanotide resulted in significant weight loss in small clinical studies conducted in severely obese individuals with pro-opiomelanocortin deficiency or other rare congenital conditions affecting the melanocortin-4 signaling pathway [123]. While inhibition of the appetite-stimulating (orexigenic) hormone ghrelin may seem an attractive therapeutic target, studies targeting ghrelin receptor inhibition have not reported sufficient efficacy to encourage further clinical development [124].

7. Limitations and Future Perspectives of Peptide-Based Therapy

Peptide-based therapies are emerging as promising treatments for diabetes and obesity due to their ability to effectively regulate glucose metabolism and body weight. However, the development and clinical application of these therapies will continue to face numerous challenges that must be addressed to optimize their efficacy and safety [125,126]. The process from peptide design and testing to the creation of a fully characterized therapeutic product is complex and fraught with challenges. Stability and degradation issues may arise during the development of peptide-based therapies, as peptides often have poor stability and are prone to rapid degradation, limiting their therapeutic potential. Immunological issues must also be considered; novel peptide structures can trigger immune responses, leading to potential immunological complications. Optimizing administration methods and ensuring targeted delivery to specific tissues remain significant obstacles. There is a risk of inducing severe hypoglycemia due to excessive lowering of blood sugar levels. Targeting multiple receptors with hybrid and chimeric peptides holds significant potential, but further research is needed to confirm their efficacy and safety. Targeting central and peripheral peptidergic systems, such as the central nervous system and the gastrointestinal tract, offers opportunities but also presents several challenges for clinical application and efficacy. Future research would focus on overcoming these barriers to fully realize the therapeutic benefits of peptides in the treatment of these conditions [125,126].

8. Conclusions

Obesity represents a serious public health issue, characterized as a chronic inflammatory condition closely associated with insulin resistance, T2DM, and an increased risk of cardiovascular diseases. Pharmacological treatment for obesity has seen dynamic development in recent years, with ongoing research focusing on the long-term clinical efficacy and safety of the employed formulations. These studies will further elucidate their role in the management of obesity and its related complications in the coming years.

Long-acting GLP-1 receptor agonists are widely applicable in the treatment of T2DM, known not only for their favorable effects on glycemic control and weight but also for significantly reducing the risk of cardiovascular diseases associated with atherosclerosis. GLP-1 receptor agonists have proven effective in the treatment of obesity and MAFLD alongside T2DM. Moreover, an increasing number of new and innovative formulations based on the mechanism of action of incretin hormones are becoming available for everyday clinical practice, including oral GLP-1 receptor agonists, the dual GLP-1/GIP receptor agonist tirzepatide, and other dual and triple GLP-1/GIP/glucagon receptor agonists, which may demonstrate further significant therapeutic potential. The dual GLP-1/GIP receptor agonist tirzepatide has already received approval in the United States and Europe, with the introduction of other dual receptor agonists expected soon. These novel agents may open further possibilities for future diabetes therapies in a personalized manner. For dual and triple GLP-1/GIP/glucagon receptor agonist formulations, as with efficacy, it is also warranted to assess safety through cardiovascular outcome trials.

Author Contributions: Conceptualization, F.S.; data curation, L.I.T., M.H. (Marcell Hernyák) and A.P.; writing—original draft preparation, F.S.; writing—review and editing, Á.D. and M.H. (Mariann Harangi); visualization, M.H. (Mariann Harangi) and L.I.T.; supervision, M.H. (Mariann Harangi); funding acquisition, M.H. (Mariann Harangi). All authors have read and agreed to the published version of the manuscript.

Funding: This research was funded by the National Research, Development and Innovation Office (NKFIH, grant number: K142273). Project no. TKP2021-EGA-18 has been implemented with the support provided by the Ministry of Innovation and Technology of Hungary from the National Research, Development and Innovation Fund, financed under the TKP2021-EGA funding scheme. The research group is supported by the Eötvös Loránd Research Network (11003).

Institutional Review Board Statement: Not applicable.

Informed Consent Statement: Not applicable.

Data Availability Statement: All data generated or analyzed during this study are included in this published article.

Conflicts of Interest: The authors declare no conflicts of interest.

References

1. NCD Risk Factor Collaboration (NCD-RisC). Worldwide trends in underweight and obesity from 1990 to 2022: A pooled analysis of 3663 population-representative studies with 222 million children, adolescents, and adults. *Lancet* **2024**, *403*, 1027–1050. [CrossRef] [PubMed]
2. Lingvay, I.; Sumithran, P.; Cohen, R.V.; le Roux, C.W. Obesity management as a primary treatment goal for type 2 diabetes: Time to reframe the conversation. *Lancet* **2022**, *399*, 394–405. [CrossRef] [PubMed]
3. Davies, M.J.; Aroda, V.R.; Collins, B.S.; Gabbay, R.A.; Green, J.; Maruthur, N.M.; Rosas, S.E.; Del Prato, S.; Mathieu, C.; Mingrone, G.; et al. Management of hyperglycaemia in type 2 diabetes, 2022. A consensus report by the American Diabetes Association (ADA) and the European Association for the Study of Diabetes (EASD). *Diabetologia* **2022**, *65*, 1925–1966. [CrossRef] [PubMed]
4. Cornier, M.A. A review of current guidelines for the treatment of obesity. *Am. J. Manag. Care* **2022**, *28*, S288–S296. [CrossRef] [PubMed]
5. Evert, A.B.; Franz, M.J. Why Weight Loss Maintenance Is Difficult. *Diabetes Spectr.* **2017**, *30*, 153–156. [CrossRef] [PubMed]
6. Holst, J.J. Treatment of Type 2 Diabetes and Obesity on the Basis of the Incretin System: The 2021 Banting Medal for Scientific Achievement Award Lecture. *Diabetes* **2021**, *70*, 2468–2475. [CrossRef] [PubMed]
7. Nauck, M.A.; Meier, J.J. MANAGEMENT OF ENDOCRINE DISEASE: Are all GLP-1 agonists equal in the treatment of type 2 diabetes? *Eur. J. Endocrinol.* **2019**, *181*, R211–R234. [CrossRef] [PubMed]

8. Bradley, C.L.; McMillin, S.M.; Hwang, A.Y.; Sherrill, C.H. Tirzepatide, the Newest Medication for Type 2 Diabetes: A Review of the Literature and Implications for Clinical Practice. *Ann. Pharmacother.* **2023**, *57*, 822–836. [CrossRef] [PubMed]
9. Tschöp, M.; Nogueiras, R.; Ahrén, B. Gut hormone-based pharmacology: Novel formulations and future possibilities for metabolic disease therapy. *Diabetologia* **2023**, *66*, 1796–1808. [CrossRef]
10. Iacobini, C.; Pugliese, G.; Blasetti Fantauzzi, C.; Federici, M.; Menini, S. Metabolically healthy versus metabolically unhealthy obesity. *Metabolism* **2019**, *92*, 51–60. [CrossRef]
11. Riddy, D.M.; Delerive, P.; Summers, R.J.; Sexton, P.M.; Langmead, C.J. G Protein-Coupled Receptors Targeting Insulin Resistance, Obesity, and Type 2 Diabetes Mellitus. *Pharmacol. Rev.* **2018**, *70*, 39–67. [CrossRef] [PubMed]
12. Wu, H.; Ballantyne, C.M. Metabolic Inflammation and Insulin Resistance in Obesity. *Circ. Res.* **2020**, *126*, 1549–1564. [CrossRef] [PubMed]
13. Xu, X.; Grijalva, A.; Skowronski, A.; van Eijk, M.; Serlie, M.J.; Ferrante, A.W. Obesity activates a program of lysosomal-dependent lipid metabolism in adipose tissue macrophages independently of classic activation. *Cell Metab.* **2013**, *18*, 816–830. [CrossRef] [PubMed]
14. Kusminski, C.M.; Bickel, P.E.; Scherer, P.E. Targeting adipose tissue in the treatment of obesity-associated diabetes. *Nat. Rev. Drug Discov.* **2016**, *15*, 639–660. [CrossRef] [PubMed]
15. Caturano, A.; D'Angelo, M.; Mormone, A.; Russo, V.; Mollica, M.P.; Salvatore, T.; Galiero, R.; Rinaldi, L.; Vetrano, E.; Marfella, R.; et al. Oxidative Stress in Type 2 Diabetes: Impacts from Pathogenesis to Lifestyle Modifications. *Curr. Issues Mol. Biol.* **2023**, *45*, 6651–6666. [CrossRef] [PubMed]
16. Meza, C.A.; La Favor, J.D.; Kim, D.H.; Hickner, R.C. Endothelial Dysfunction: Is There a Hyperglycemia-Induced Imbalance of NOX and NOS? *Int. J. Mol. Sci.* **2019**, *20*, 3775. [CrossRef] [PubMed]
17. Lee, Y.S.; Park, M.S.; Choung, J.S.; Kim, S.S.; Oh, H.H.; Choi, C.S.; Ha, S.Y.; Kang, Y.; Kim, Y.; Jun, H.S. Glucagon-like peptide-1 inhibits adipose tissue macrophage infiltration and inflammation in an obese mouse model of diabetes. *Diabetologia* **2012**, *55*, 2456–2468. [CrossRef] [PubMed]
18. Müller, T.D.; Finan, B.; Bloom, S.R.; D'Alessio, D.; Drucker, D.J.; Flatt, P.R.; Fritsche, A.; Gribble, F.; Grill, H.J.; Habener, J.F.; et al. Glucagon-like peptide 1 (GLP-1). *Mol. Metab.* **2019**, *30*, 72–130. [CrossRef] [PubMed]
19. Ryan, D.H. Next Generation Antiobesity Medications: Setmelanotide, Semaglutide, Tirzepatide and Bimagrumab: What do They Mean for Clinical Practice? *J. Obes. Metab. Syndr.* **2021**, *30*, 196–208. [CrossRef]
20. Sriram, K.; Insel, P.A. G Protein-Coupled Receptors as Targets for Approved Drugs: How Many Targets and How Many Drugs? *Mol. Pharmacol.* **2018**, *93*, 251–258. [CrossRef]
21. Lefkowitz, R.J.; Rajagopal, K.; Whalen, E.J. New roles for beta-arrestins in cell signaling: Not just for seven-transmembrane receptors. *Mol. Cell* **2006**, *24*, 643–652. [CrossRef]
22. Shukla, A.K.; Xiao, K.; Lefkowitz, R.J. Emerging paradigms of β-arrestin-dependent seven transmembrane receptor signaling. *Trends Biochem. Sci.* **2011**, *36*, 457–469. [CrossRef]
23. Smith, J.S.; Rajagopal, S. The β-Arrestins: Multifunctional Regulators of G Protein-coupled Receptors. *J. Biol. Chem.* **2016**, *291*, 8969–8977. [CrossRef]
24. Reiter, E.; Lefkowitz, R.J. GRKs and beta-arrestins: Roles in receptor silencing, trafficking and signaling. *Trends Endocrinol. Metab.* **2006**, *17*, 159–165. [CrossRef]
25. Sonoda, N.; Imamura, T.; Yoshizaki, T.; Babendure, J.L.; Lu, J.C.; Olefsky, J.M. Beta-Arrestin-1 mediates glucagon-like peptide-1 signaling to insulin secretion in cultured pancreatic beta cells. *Proc. Natl. Acad. Sci. USA* **2008**, *105*, 6614–6619. [CrossRef]
26. Pydi, S.P.; Barella, L.F.; Meister, J.; Wess, J. Key Metabolic Functions of β-Arrestins: Studies with Novel Mouse Models. *Trends Endocrinol. Metab.* **2021**, *32*, 118–129. [CrossRef]
27. Zhuang, L.N.; Hu, W.X.; Xin, S.M.; Zhao, J.; Pei, G. Beta-arrestin-1 protein represses adipogenesis and inflammatory responses through its interaction with peroxisome proliferator-activated receptor-gamma (PPARgamma). *J. Biol. Chem.* **2011**, *286*, 28403–28413. [CrossRef]
28. Roed, S.N.; Wismann, P.; Underwood, C.R.; Kulahin, N.; Iversen, H.; Cappelen, K.A.; Schäffer, L.; Lehtonen, J.; Hecksher-Soerensen, J.; Secher, A.; et al. Real-time trafficking and signaling of the glucagon-like peptide-1 receptor. *Mol. Cell Endocrinol.* **2014**, *382*, 938–949. [CrossRef]
29. Fang, Z.; Chen, S.; Pickford, P.; Broichhagen, J.; Hodson, D.J.; Corrêa, I.R.; Kumar, S.; Görlitz, F.; Dunsby, C.; French, P.M.W.; et al. The Influence of Peptide Context on Signaling and Trafficking of Glucagon-like Peptide-1 Receptor Biased Agonists. *ACS Pharmacol. Transl. Sci.* **2020**, *3*, 345–360. [CrossRef]
30. Willard, F.S.; Douros, J.D.; Gabe, M.B.; Showalter, A.D.; Wainscott, D.B.; Suter, T.M.; Capozzi, M.E.; van der Velden, W.J.; Stutsman, C.; Cardona, G.R.; et al. Tirzepatide is an imbalanced and biased dual GIP and GLP-1 receptor agonist. *JCI Insight* **2020**, *5*, 140532. [CrossRef]
31. Finan, B.; Yang, B.; Ottaway, N.; Smiley, D.L.; Ma, T.; Clemmensen, C.; Chabenne, J.; Zhang, L.; Habegger, K.M.; Fischer, K.; et al. A rationally designed monomeric peptide triagonist corrects obesity and diabetes in rodents. *Nat. Med.* **2015**, *21*, 27–36. [CrossRef]
32. Wilbon, S.S.; Kolonin, M.G. GLP1 Receptor Agonists-Effects beyond Obesity and Diabetes. *Cells* **2023**, *13*, 65. [CrossRef]
33. Nauck, M.A.; Meier, J.J. The incretin effect in healthy individuals and those with type 2 diabetes: Physiology, pathophysiology, and response to therapeutic interventions. *Lancet Diabetes Endocrinol.* **2016**, *4*, 525–536. [CrossRef]

34. Tan, T.M.; Field, B.C.; McCullough, K.A.; Troke, R.C.; Chambers, E.S.; Salem, V.; Gonzalez Maffe, J.; Baynes, K.C.; De Silva, A.; Viardot, A.; et al. Coadministration of glucagon-like peptide-1 during glucagon infusion in humans results in increased energy expenditure and amelioration of hyperglycemia. *Diabetes* **2013**, *62*, 1131–1138. [CrossRef]
35. Graaf, C.; Donnelly, D.; Wootten, D.; Lau, J.; Sexton, P.M.; Miller, L.J.; Ahn, J.M.; Liao, J.; Fletcher, M.M.; Yang, D.; et al. Glucagon-Like Peptide-1 and Its Class B G Protein-Coupled Receptors: A Long March to Therapeutic Successes. *Pharmacol. Rev.* **2016**, *68*, 954–1013. [CrossRef]
36. Drucker, D.J. GLP-1 physiology informs the pharmacotherapy of obesity. *Mol. Metab.* **2022**, *57*, 101351. [CrossRef]
37. González, N.; Acitores, A.; Sancho, V.; Valverde, I.; Villanueva-Peñacarrillo, M.L. Effect of GLP-1 on glucose transport and its cell signalling in human myocytes. *Regul. Pept.* **2005**, *126*, 203–211. [CrossRef]
38. Lee, Y.S.; Shin, S.; Shigihara, T.; Hahm, E.; Liu, M.J.; Han, J.; Yoon, J.W.; Jun, H.S. Glucagon-like peptide-1 gene therapy in obese diabetic mice results in long-term cure of diabetes by improving insulin sensitivity and reducing hepatic gluconeogenesis. *Diabetes* **2007**, *56*, 1671–1679. [CrossRef]
39. Kim, C.H.; Hwang, I.C.; Choi, H.M.; Ahn, C.H.; Yoon, Y.E.; Cho, G.Y. Differential cardiovascular and renal benefits of SGLT2 inhibitors and GLP1 receptor agonists in patients with type 2 diabetes mellitus. *Int. J. Cardiol.* **2022**, *364*, 104–111. [CrossRef]
40. Drucker, D.J. Mechanisms of Action and Therapeutic Application of Glucagon-like Peptide-1. *Cell Metab.* **2018**, *27*, 740–756. [CrossRef]
41. Sabouret, P.; Bocchino, P.P.; Angelini, F.; D'Ascenzo, F.; Galati, G.; Fysekidis, M.; DE Ferrari, G.M.; Fischman, D.L.; Bhatt, D.L.; Biondi-Zoccai, G. Comparing benefits from sodium-glucose cotransporter-2 inhibitors and glucagon-like peptide-1 receptor agonists in randomized clinical trials: A network meta-analysis. *Minerva Cardiol. Angiol.* **2023**, *71*, 199–207. [CrossRef]
42. Cannon, B.; Nedergaard, J. Nonshivering thermogenesis and its adequate measurement in metabolic studies. *J. Exp. Biol.* **2011**, *214*, 242–253. [CrossRef]
43. Vergès, B.; Bonnard, C.; Renard, E. Beyond glucose lowering: Glucagon-like peptide-1 receptor agonists, body weight and the cardiovascular system. *Diabetes Metab.* **2011**, *37*, 477–488. [CrossRef]
44. Sasso, F.C.; Carbonara, O.; Cozzolino, D.; Rambaldi, P.; Mansi, L.; Torella, D.; Gentile, S.; Turco, S.; Torella, R.; Salvatore, T. Effects of insulin-glucose infusion on left ventricular function at rest and during dynamic exercise in healthy subjects and noninsulin dependent diabetic patients: A radionuclide ventriculographic study. *J. Am. Coll. Cardiol.* **2000**, *36*, 219–226. [CrossRef]
45. Sasso, F.C.; Carbonara, O.; Nasti, R.; Marfella, R.; Esposito, K.; Rambaldi, P.; Mansi, L.; Salvatore, T.; Torella, R.; Cozzolino, D. Effects of insulin on left ventricular function during dynamic exercise in overweight and obese subjects. *Eur. Heart J.* **2005**, *26*, 1205–1212. [CrossRef]
46. Dadwani, R.S.; Wan, W.; Skandari, M.R.; Huang, E.S. Expected Health Benefits of SGLT-2 Inhibitors and GLP-1 Receptor Agonists in Older Adults. *MDM Policy Pract.* **2023**, *8*, 23814683231187566. [CrossRef]
47. Salvatore, T.; Galiero, R.; Caturano, A.; Vetrano, E.; Loffredo, G.; Rinaldi, L.; Catalini, C.; Gjeloshi, K.; Albanese, G.; Di Martino, A.; et al. Coronary Microvascular Dysfunction in Diabetes Mellitus: Pathogenetic Mechanisms and Potential Therapeutic Options. *Biomedicines* **2022**, *10*, 2274. [CrossRef]
48. Salvatore, T.; Galiero, R.; Caturano, A.; Vetrano, E.; Rinaldi, L.; Coviello, F.; Di Martino, A.; Albanese, G.; Colantuoni, S.; Medicamento, G.; et al. Dysregulated Epicardial Adipose Tissue as a Risk Factor and Potential Therapeutic Target of Heart Failure with Preserved Ejection Fraction in Diabetes. *Biomolecules* **2022**, *12*, 176. [CrossRef]
49. Nevola, R.; Epifani, R.; Imbriani, S.; Tortorella, G.; Aprea, C.; Galiero, R.; Rinaldi, L.; Marfella, R.; Sasso, F.C. GLP-1 Receptor Agonists in Non-Alcoholic Fatty Liver Disease: Current Evidence and Future Perspectives. *Int. J. Mol. Sci.* **2023**, *24*, 1703. [CrossRef]
50. Müller, T.D.; Finan, B.; Clemmensen, C.; DiMarchi, R.D.; Tschöp, M.H. The New Biology and Pharmacology of Glucagon. *Physiol. Rev.* **2017**, *97*, 721–766. [CrossRef]
51. Campbell, J.E.; Ussher, J.R.; Mulvihill, E.E.; Kolic, J.; Baggio, L.L.; Cao, X.; Liu, Y.; Lamont, B.J.; Morii, T.; Streutker, C.J.; et al. TCF1 links GIPR signaling to the control of beta cell function and survival. *Nat. Med.* **2016**, *22*, 84–90. [CrossRef] [PubMed]
52. Tsukiyama, K.; Yamada, Y.; Yamada, C.; Harada, N.; Kawasaki, Y.; Ogura, M.; Bessho, K.; Li, M.; Amizuka, N.; Sato, M.; et al. Gastric inhibitory polypeptide as an endogenous factor promoting new bone formation after food ingestion. *Mol. Endocrinol.* **2006**, *20*, 1644–1651. [CrossRef]
53. Miyawaki, K.; Yamada, Y.; Ban, N.; Ihara, Y.; Tsukiyama, K.; Zhou, H.; Fujimoto, S.; Oku, A.; Tsuda, K.; Toyokuni, S.; et al. Inhibition of gastric inhibitory polypeptide signaling prevents obesity. *Nat. Med.* **2002**, *8*, 738–742. [CrossRef] [PubMed]
54. Althage, M.C.; Ford, E.L.; Wang, S.; Tso, P.; Polonsky, K.S.; Wice, B.M. Targeted ablation of glucose-dependent insulinotropic polypeptide-producing cells in transgenic mice reduces obesity and insulin resistance induced by a high fat diet. *J. Biol. Chem.* **2008**, *283*, 18365–18376. [CrossRef] [PubMed]
55. Holst, J.J.; Windeløv, J.A.; Boer, G.A.; Pedersen, J.; Svendsen, B.; Christensen, M.; Torekov, S.; Asmar, M.; Hartmann, B.; Nissen, A. Searching for the physiological role of glucose-dependent insulinotropic polypeptide. *J. Diabetes Investig.* **2016**, *7* (Suppl. 1), 8–12. [CrossRef]
56. Kim, S.J.; Nian, C.; Karunakaran, S.; Clee, S.M.; Isales, C.M.; McIntosh, C.H. GIP-overexpressing mice demonstrate reduced diet-induced obesity and steatosis, and improved glucose homeostasis. *PLoS ONE* **2012**, *7*, e40156. [CrossRef] [PubMed]
57. Samms, R.J.; Coghlan, M.P.; Sloop, K.W. How May GIP Enhance the Therapeutic Efficacy of GLP-1? *Trends Endocrinol. Metab.* **2020**, *31*, 410–421. [CrossRef] [PubMed]

58. Martin, C.M.; Irwin, N.; Flatt, P.R.; Gault, V.A. A novel acylated form of (d-Ala(2))GIP with improved antidiabetic potential, lacking effect on body fat stores. *Biochim. Biophys. Acta* **2013**, *1830*, 3407–3413. [CrossRef]
59. Adriaenssens, A.E.; Biggs, E.K.; Darwish, T.; Tadross, J.; Sukthankar, T.; Girish, M.; Polex-Wolf, J.; Lam, B.Y.; Zvetkova, I.; Pan, W.; et al. Glucose-Dependent Insulinotropic Polypeptide Receptor-Expressing Cells in the Hypothalamus Regulate Food Intake. *Cell Metab.* **2019**, *30*, 987–996.e986. [CrossRef]
60. Killion, E.A.; Lu, S.C.; Fort, M.; Yamada, Y.; Véniant, M.M.; Lloyd, D.J. Glucose-Dependent Insulinotropic Polypeptide Receptor Therapies for the Treatment of Obesity, Do Agonists = Antagonists? *Endocr. Rev.* **2020**, *41*, 1–21. [CrossRef]
61. Mori, Y.; Matsui, T.; Hirano, T.; Yamagishi, S.I. GIP as a Potential Therapeutic Target for Atherosclerotic Cardiovascular Disease—A Systematic Review. *Int. J. Mol. Sci.* **2020**, *21*, 1509. [CrossRef]
62. Jonik, S.; Marchel, M.; Grabowski, M.; Opolski, G.; Mazurek, T. Gastrointestinal Incretins-Glucose-Dependent Insulinotropic Polypeptide (GIP) and Glucagon-like Peptide-1 (GLP-1) beyond Pleiotropic Physiological Effects Are Involved in Pathophysiology of Atherosclerosis and Coronary Artery Disease-State of the Art. *Biology* **2022**, *11*, 288. [CrossRef] [PubMed]
63. Caruso, I.; Marrano, N.; Biondi, G.; Genchi, V.A.; D'Oria, R.; Sorice, G.P.; Perrini, S.; Cignarelli, A.; Natalicchio, A.; Laviola, L.; et al. Glucagon in type 2 diabetes: Friend or foe? *Diabetes Metab. Res. Rev.* **2023**, *39*, e3609. [CrossRef] [PubMed]
64. Christensen, M.B.; Gasbjerg, L.S.; Heimbürger, S.M.; Stensen, S.; Vilsbøll, T.; Knop, F.K. GIP's involvement in the pathophysiology of type 2 diabetes. *Peptides* **2020**, *125*, 170178. [CrossRef] [PubMed]
65. Scheen, A.J.; Lefèbvre, P.J. Glucagon, from past to present: A century of intensive research and controversies. *Lancet Diabetes Endocrinol.* **2023**, *11*, 129–138. [CrossRef] [PubMed]
66. Longuet, C.; Sinclair, E.M.; Maida, A.; Baggio, L.L.; Maziarz, M.; Charron, M.J.; Drucker, D.J. The glucagon receptor is required for the adaptive metabolic response to fasting. *Cell Metab.* **2008**, *8*, 359–371. [CrossRef] [PubMed]
67. Quiñones, M.; Al-Massadi, O.; Gallego, R.; Fernø, J.; Diéguez, C.; López, M.; Nogueiras, R. Hypothalamic CaMKKβ mediates glucagon anorectic effect and its diet-induced resistance. *Mol. Metab.* **2015**, *4*, 961–970. [CrossRef] [PubMed]
68. Kleinert, M.; Sachs, S.; Habegger, K.M.; Hofmann, S.M.; Müller, T.D. Glucagon Regulation of Energy Expenditure. *Int. J. Mol. Sci.* **2019**, *20*, 5407. [CrossRef] [PubMed]
69. Whytock, K.L.; Carnero, E.A.; Vega, R.B.; Tillner, J.; Bock, C.; Chivukula, K.; Yi, F.; Meyer, C.; Smith, S.R.; Sparks, L.M. Prolonged Glucagon Infusion Does Not Affect Energy Expenditure in Individuals with Overweight/Obesity: A Randomized Trial. *Obesity* **2021**, *29*, 1003–1013. [CrossRef] [PubMed]
70. Committee, A.D.A.P.P. 8. Obesity and Weight Management for the Prevention and Treatment of Type 2 Diabetes: Standards of Care in Diabetes-2024. *Diabetes Care* **2024**, *47*, S145–S157. [CrossRef]
71. Pi-Sunyer, X.; Astrup, A.; Fujioka, K.; Greenway, F.; Halpern, A.; Krempf, M.; Lau, D.C.; le Roux, C.W.; Violante Ortiz, R.; Jensen, C.B.; et al. A Randomized, Controlled Trial of 3.0 mg of Liraglutide in Weight Management. *N. Engl. J. Med.* **2015**, *373*, 11–22. [CrossRef] [PubMed]
72. Wilding, J.P.H.; Batterham, R.L.; Calanna, S.; Davies, M.; Van Gaal, L.F.; Lingvay, I.; McGowan, B.M.; Rosenstock, J.; Tran, M.T.D.; Wadden, T.A.; et al. Once-Weekly Semaglutide in Adults with Overweight or Obesity. *N. Engl. J. Med.* **2021**, *384*, 989–1002. [CrossRef] [PubMed]
73. Davies, M.; Færch, L.; Jeppesen, O.K.; Pakseresht, A.; Pedersen, S.D.; Perreault, L.; Rosenstock, J.; Shimomura, I.; Viljoen, A.; Wadden, T.A.; et al. Semaglutide 2·4 mg once a week in adults with overweight or obesity, and type 2 diabetes (STEP 2): A randomised, double-blind, double-dummy, placebo-controlled, phase 3 trial. *Lancet* **2021**, *397*, 971–984. [CrossRef] [PubMed]
74. Wadden, T.A.; Bailey, T.S.; Billings, L.K.; Davies, M.; Frias, J.P.; Koroleva, A.; Lingvay, I.; O'Neil, P.M.; Rubino, D.M.; Skovgaard, D.; et al. Effect of Subcutaneous Semaglutide vs Placebo as an Adjunct to Intensive Behavioral Therapy on Body Weight in Adults With Overweight or Obesity: The STEP 3 Randomized Clinical Trial. *JAMA* **2021**, *325*, 1403–1413. [CrossRef] [PubMed]
75. Rubino, D.; Abrahamsson, N.; Davies, M.; Hesse, D.; Greenway, F.L.; Jensen, C.; Lingvay, I.; Mosenzon, O.; Rosenstock, J.; Rubio, M.A.; et al. Effect of Continued Weekly Subcutaneous Semaglutide vs Placebo on Weight Loss Maintenance in Adults With Overweight or Obesity: The STEP 4 Randomized Clinical Trial. *JAMA* **2021**, *325*, 1414–1425. [CrossRef] [PubMed]
76. Garvey, W.T.; Batterham, R.L.; Bhatta, M.; Buscemi, S.; Christensen, L.N.; Frias, J.P.; Jódar, E.; Kandler, K.; Rigas, G.; Wadden, T.A.; et al. Two-year effects of semaglutide in adults with overweight or obesity: The STEP 5 trial. *Nat. Med.* **2022**, *28*, 2083–2091. [CrossRef] [PubMed]
77. Kadowaki, T.; Isendahl, J.; Khalid, U.; Lee, S.Y.; Nishida, T.; Ogawa, W.; Tobe, K.; Yamauchi, T.; Lim, S.; STEP 6 Investigators. Semaglutide once a week in adults with overweight or obesity, with or without type 2 diabetes in an east Asian population (STEP 6): A randomised, double-blind, double-dummy, placebo-controlled, phase 3a trial. *Lancet Diabetes Endocrinol.* **2022**, *10*, 193–206. [CrossRef] [PubMed]
78. Rubino, D.M.; Greenway, F.L.; Khalid, U.; O'Neil, P.M.; Rosenstock, J.; Sørrig, R.; Wadden, T.A.; Wizert, A.; Garvey, W.T.; Investigators, S. Effect of Weekly Subcutaneous Semaglutide vs Daily Liraglutide on Body Weight in Adults With Overweight or Obesity Without Diabetes: The STEP 8 Randomized Clinical Trial. *JAMA* **2022**, *327*, 138–150. [CrossRef]
79. Bergmann, N.C.; Davies, M.J.; Lingvay, I.; Knop, F.K. Semaglutide for the treatment of overweight and obesity: A review. *Diabetes Obes. Metab.* **2023**, *25*, 18–35. [CrossRef]
80. Weghuber, D.; Barrett, T.; Barrientos-Pérez, M.; Gies, I.; Hesse, D.; Jeppesen, O.K.; Kelly, A.S.; Mastrandrea, L.D.; Sørrig, R.; Arslanian, S.; et al. Once-Weekly Semaglutide in Adolescents with Obesity. *N. Engl. J. Med.* **2022**, *387*, 2245–2257. [CrossRef]

81. Knop, F.K.; Aroda, V.R.; do Vale, R.D.; Holst-Hansen, T.; Laursen, P.N.; Rosenstock, J.; Rubino, D.M.; Garvey, W.T.; Investigators, O. Oral semaglutide 50 mg taken once per day in adults with overweight or obesity (OASIS 1): A randomised, double-blind, placebo-controlled, phase 3 trial. *Lancet* **2023**, *402*, 705–719. [CrossRef] [PubMed]
82. Kosiborod, M.N.; Abildstrøm, S.Z.; Borlaug, B.A.; Butler, J.; Rasmussen, S.; Davies, M.; Hovingh, G.K.; Kitzman, D.W.; Lindegaard, M.L.; Møller, D.V.; et al. Semaglutide in Patients with Heart Failure with Preserved Ejection Fraction and Obesity. *N. Engl. J. Med.* **2023**, *389*, 1069–1084. [CrossRef] [PubMed]
83. Lincoff, A.M.; Brown-Frandsen, K.; Colhoun, H.M.; Deanfield, J.; Emerson, S.S.; Esbjerg, S.; Hardt-Lindberg, S.; Hovingh, G.K.; Kahn, S.E.; Kushner, R.F.; et al. Semaglutide and Cardiovascular Outcomes in Obesity without Diabetes. *N. Engl. J. Med.* **2023**, *389*, 2221–2232. [CrossRef] [PubMed]
84. Jastreboff, A.M.; Aronne, L.J.; Ahmad, N.N.; Wharton, S.; Connery, L.; Alves, B.; Kiyosue, A.; Zhang, S.; Liu, B.; Bunck, M.C.; et al. Tirzepatide Once Weekly for the Treatment of Obesity. *N. Engl. J. Med.* **2022**, *387*, 205–216. [CrossRef] [PubMed]
85. Wadden, T.A.; Chao, A.M.; Machineni, S.; Kushner, R.; Ard, J.; Srivastava, G.; Halpern, B.; Zhang, S.; Chen, J.; Bunck, M.C.; et al. Tirzepatide after intensive lifestyle intervention in adults with overweight or obesity: The SURMOUNT-3 phase 3 trial. *Nat. Med.* **2023**, *29*, 2909–2918. [CrossRef] [PubMed]
86. Garvey, W.T.; Frias, J.P.; Jastreboff, A.M.; le Roux, C.W.; Sattar, N.; Aizenberg, D.; Mao, H.; Zhang, S.; Ahmad, N.N.; Bunck, M.C.; et al. Tirzepatide once weekly for the treatment of obesity in people with type 2 diabetes (SURMOUNT-2): A double-blind, randomised, multicentre, placebo-controlled, phase 3 trial. *Lancet* **2023**, *402*, 613–626. [CrossRef] [PubMed]
87. Gorgojo-Martínez, J.J.; Mezquita-Raya, P.; Carretero-Gómez, J.; Castro, A.; Cebrián-Cuenca, A.; de Torres-Sánchez, A.; García-de-Lucas, M.D.; Núñez, J.; Obaya, J.C.; Soler, M.J.; et al. Clinical Recommendations to Manage Gastrointestinal Adverse Events in Patients Treated with Glp-1 Receptor Agonists: A Multidisciplinary Expert Consensus. *J. Clin. Med.* **2022**, *12*, 145. [CrossRef] [PubMed]
88. McDermid, E. A Quick Guide to the SURPASS and SURMOUNT Trials. Available online: https://diabetes.medicinematters.com/en-GB/tirzepatide/type-2-diabetes/a-quick-guide-to-the-surpass-and-surmount-trials/18478154 (accessed on 27 March 2024).
89. Bradley, C.L.; McMillin, S.M.; Hwang, A.Y.; Sherrill, C.H. High-Dose Once-Weekly Semaglutide: A New Option for Obesity Management. *Ann. Pharmacother.* **2022**, *56*, 941–950. [CrossRef] [PubMed]
90. Mishra, R.; Raj, R.; Elshimy, G.; Zapata, I.; Kannan, L.; Majety, P.; Edem, D.; Correa, R. Adverse Events Related to Tirzepatide. *J. Endocr. Soc.* **2023**, *7*, bvad016. [CrossRef]
91. Finan, B.; Ma, T.; Ottaway, N.; Müller, T.D.; Habegger, K.M.; Heppner, K.M.; Kirchner, H.; Holland, J.; Hembree, J.; Raver, C.; et al. Unimolecular dual incretins maximize metabolic benefits in rodents, monkeys, and humans. *Sci. Transl. Med.* **2013**, *5*, 209ra151. [CrossRef]
92. Coskun, T.; Sloop, K.W.; Loghin, C.; Alsina-Fernandez, J.; Urva, S.; Bokvist, K.B.; Cui, X.; Briere, D.A.; Cabrera, O.; Roell, W.C.; et al. LY3298176, a novel dual GIP and GLP-1 receptor agonist for the treatment of type 2 diabetes mellitus: From discovery to clinical proof of concept. *Mol. Metab.* **2018**, *18*, 3–14. [CrossRef]
93. Samms, R.J.; Christe, M.E.; Collins, K.A.; Pirro, V.; Droz, B.A.; Holland, A.K.; Friedrich, J.L.; Wojnicki, S.; Konkol, D.L.; Cosgrove, R.; et al. GIPR agonism mediates weight-independent insulin sensitization by tirzepatide in obese mice. *J. Clin. Investig.* **2021**, *12*, 131. [CrossRef]
94. Nauck, M.A.; D'Alessio, D.A. Tirzepatide, a dual GIP/GLP-1 receptor co-agonist for the treatment of type 2 diabetes with unmatched effectiveness regrading glycaemic control and body weight reduction. *Cardiovasc. Diabetol.* **2022**, *21*, 169. [CrossRef]
95. Sinha, R.; Papamargaritis, D.; Sargeant, J.A.; Davies, M.J. Efficacy and Safety of Tirzepatide in Type 2 Diabetes and Obesity Management. *J. Obes. Metab. Syndr.* **2023**, *32*, 25–45. [CrossRef]
96. De Block, C.; Bailey, C.; Wysham, C.; Hemmingway, A.; Allen, S.E.; Peleshok, J. Tirzepatide for the treatment of adults with type 2 diabetes: An endocrine perspective. *Diabetes Obes. Metab.* **2023**, *25*, 3–17. [CrossRef] [PubMed]
97. Pocai, A.; Carrington, P.E.; Adams, J.R.; Wright, M.; Eiermann, G.; Zhu, L.; Du, X.; Petrov, A.; Lassman, M.E.; Jiang, G.; et al. Glucagon-like peptide 1/glucagon receptor dual agonism reverses obesity in mice. *Diabetes* **2009**, *58*, 2258–2266. [CrossRef]
98. Corbin, K.D.; Carnero, E.A.; Allerton, T.D.; Tillner, J.; Bock, C.P.; Luyet, P.P.; Göbel, B.; Hall, K.D.; Parsons, S.A.; Ravussin, E.; et al. Glucagon-like peptide-1/glucagon receptor agonism associates with reduced metabolic adaptation and higher fat oxidation: A randomized trial. *Obesity* **2023**, *31*, 350–362. [CrossRef] [PubMed]
99. Ambery, P.; Parker, V.E.; Stumvoll, M.; Posch, M.G.; Heise, T.; Plum-Moerschel, L.; Tsai, L.F.; Robertson, D.; Jain, M.; Petrone, M.; et al. MEDI0382, a GLP-1 and glucagon receptor dual agonist, in obese or overweight patients with type 2 diabetes: A randomised, controlled, double-blind, ascending dose and phase 2a study. *Lancet* **2018**, *391*, 2607–2618. [CrossRef] [PubMed]
100. Parker, V.E.R.; Robertson, D.; Wang, T.; Hornigold, D.C.; Petrone, M.; Cooper, A.T.; Posch, M.G.; Heise, T.; Plum-Moerschel, L.; Schlichthaar, H.; et al. Efficacy, Safety, and Mechanistic Insights of Cotadutide, a Dual Receptor Glucagon-Like Peptide-1 and Glucagon Agonist. *J. Clin. Endocrinol. Metab.* **2020**, *105*, 803–820. [CrossRef]
101. Nahra, R.; Wang, T.; Gadde, K.M.; Oscarsson, J.; Stumvoll, M.; Jermutus, L.; Hirshberg, B.; Ambery, P. Effects of Cotadutide on Metabolic and Hepatic Parameters in Adults With Overweight or Obesity and Type 2 Diabetes: A 54-Week Randomized Phase 2b Study. *Diabetes Care* **2021**, *44*, 1433–1442. [CrossRef]
102. De Block, C.E.M.; Dirinck, E.; Verhaegen, A.; Van Gaal, L.F. Efficacy and safety of high-dose glucagon-like peptide-1, glucagon-like peptide-1/glucose-dependent insulinotropic peptide, and glucagon-like peptide-1/glucagon receptor agonists in type 2 diabetes. *Diabetes Obes. Metab.* **2022**, *24*, 788–805. [CrossRef]

103. Bossart, M.; Wagner, M.; Elvert, R.; Evers, A.; Hübschle, T.; Kloeckener, T.; Lorenz, K.; Moessinger, C.; Eriksson, O.; Velikyan, I.; et al. Effects on weight loss and glycemic control with SAR441255, a potent unimolecular peptide GLP-1/GIP/GCG receptor triagonist. *Cell Metab.* **2022**, *34*, 59–74.e10. [CrossRef]
104. Knerr, P.J.; Mowery, S.A.; Douros, J.D.; Premdjee, B.; Hjøllund, K.R.; He, Y.; Kruse Hansen, A.M.; Olsen, A.K.; Perez-Tilve, D.; DiMarchi, R.D.; et al. Next generation GLP-1/GIP/glucagon triple agonists normalize body weight in obese mice. *Mol. Metab.* **2022**, *63*, 101533. [CrossRef]
105. Coskun, T.; Urva, S.; Roell, W.C.; Qu, H.; Loghin, C.; Moyers, J.S.; O'Farrell, L.S.; Briere, D.A.; Sloop, K.W.; Thomas, M.K.; et al. LY3437943, a novel triple glucagon, GIP, and GLP-1 receptor agonist for glycemic control and weight loss: From discovery to clinical proof of concept. *Cell Metab.* **2022**, *34*, 1234–1247.e1239. [CrossRef]
106. Urva, S.; Coskun, T.; Loh, M.T.; Du, Y.; Thomas, M.K.; Gurbuz, S.; Haupt, A.; Benson, C.T.; Hernandez-Illas, M.; D'Alessio, D.A.; et al. LY3437943, a novel triple GIP, GLP-1, and glucagon receptor agonist in people with type 2 diabetes: A phase 1b, multicentre, double-blind, placebo-controlled, randomised, multiple-ascending dose trial. *Lancet* **2022**, *400*, 1869–1881. [CrossRef]
107. Kawai, T.; Sun, B.; Yoshino, H.; Feng, D.; Suzuki, Y.; Fukazawa, M.; Nagao, S.; Wainscott, D.B.; Showalter, A.D.; Droz, B.A.; et al. Structural basis for GLP-1 receptor activation by LY3502970, an orally active nonpeptide agonist. *Proc. Natl. Acad. Sci. USA* **2020**, *117*, 29959–29967. [CrossRef]
108. Frias, J.P.; Hsia, S.; Eyde, S.; Liu, R.; Ma, X.; Konig, M.; Kazda, C.; Mather, K.J.; Haupt, A.; Pratt, E.; et al. Efficacy and safety of oral orforglipron in patients with type 2 diabetes: A multicentre, randomised, dose-response, phase 2 study. *Lancet* **2023**, *402*, 472–483. [CrossRef]
109. Wharton, S.; Blevins, T.; Connery, L.; Rosenstock, J.; Raha, S.; Liu, R.; Ma, X.; Mather, K.J.; Haupt, A.; Robins, D.; et al. Daily Oral GLP-1 Receptor Agonist Orforglipron for Adults with Obesity. *N. Engl. J. Med.* **2023**, *389*, 877–888. [CrossRef]
110. Griffith, D.A.; Edmonds, D.J.; Fortin, J.P.; Kalgutkar, A.S.; Kuzmiski, J.B.; Loria, P.M.; Saxena, A.R.; Bagley, S.W.; Buckeridge, C.; Curto, J.M.; et al. A Small-Molecule Oral Agonist of the Human Glucagon-like Peptide-1 Receptor. *J. Med. Chem.* **2022**, *65*, 8208–8226. [CrossRef]
111. Saxena, A.R.; Frias, J.P.; Brown, L.S.; Gorman, D.N.; Vasas, S.; Tsamandouras, N.; Birnbaum, M.J. Efficacy and Safety of Oral Small Molecule Glucagon-Like Peptide 1 Receptor Agonist Danuglipron for Glycemic Control Among Patients With Type 2 Diabetes: A Randomized Clinical Trial. *JAMA Netw. Open* **2023**, *6*, e2314493. [CrossRef]
112. Pfizer Inc. Pfizer Announces Topline Phase 2b Results of Oral GLP-1R Agonist, Danuglipron, in Adults with Obesity. Available online: https://www.pfizer.com/news/press-release/press-release-detail/pfizer-announces-topline-phase-2b-results-oral-glp-1r (accessed on 27 March 2024).
113. Jastreboff, A.M.; Kaplan, L.M.; Frías, J.P.; Wu, Q.; Du, Y.; Gurbuz, S.; Coskun, T.; Haupt, A.; Milicevic, Z.; Hartman, M.L.; et al. Triple-Hormone-Receptor Agonist Retatrutide for Obesity—A Phase 2 Trial. *N. Engl. J. Med.* **2023**, *389*, 514–526. [CrossRef]
114. Müller, T.D.; Blüher, M.; Tschöp, M.H.; DiMarchi, R.D. Anti-obesity drug discovery: Advances and challenges. *Nat. Rev. Drug Discov.* **2022**, *21*, 201–223. [CrossRef]
115. Lafferty, R.A.; Flatt, P.R.; Irwin, N. Established and emerging roles peptide YY (PYY) and exploitation in obesity-diabetes. *Curr. Opin. Endocrinol. Diabetes Obes.* **2021**, *28*, 253–261. [CrossRef]
116. Qiao, Y.C.; Ling, W.; Pan, Y.H.; Chen, Y.L.; Zhou, D.; Huang, Y.M.; Zhang, X.X.; Zhao, H.L. Efficacy and safety of pramlintide injection adjunct to insulin therapy in patients with type 1 diabetes mellitus: A systematic review and meta-analysis. *Oncotarget* **2017**, *8*, 66504–66515. [CrossRef]
117. Lau, D.C.W.; Erichsen, L.; Francisco, A.M.; Satylganova, A.; le Roux, C.W.; McGowan, B.; Pedersen, S.D.; Pietiläinen, K.H.; Rubino, D.; Batterham, R.L. Once-weekly cagrilintide for weight management in people with overweight and obesity: A multicentre, randomised, double-blind, placebo-controlled and active-controlled, dose-finding phase 2 trial. *Lancet* **2021**, *398*, 2160–2172. [CrossRef]
118. Frias, J.P.; Deenadayalan, S.; Erichsen, L.; Knop, F.K.; Lingvay, I.; Macura, S.; Mathieu, C.; Pedersen, S.D.; Davies, M. Efficacy and safety of co-administered once-weekly cagrilintide 2·4 mg with once-weekly semaglutide 2·4 mg in type 2 diabetes: A multicentre, randomised, double-blind, active-controlled, phase 2 trial. *Lancet* **2023**, *402*, 720–730. [CrossRef]
119. Melson, E.; Ashraf, U.; Papamargaritis, D.; Davies, M.J. What is the pipeline for future medications for obesity? *Int. J. Obes.* **2024**, 1–19. [CrossRef]
120. Sonne, N.; Karsdal, M.A.; Henriksen, K. Mono and dual agonists of the amylin, calcitonin, and CGRP receptors and their potential in metabolic diseases. *Mol. Metab.* **2021**, *46*, 101109. [CrossRef]
121. Mathiesen, D.S.; Bagger, J.I.; Knop, F.K. Long-acting amylin analogues for the management of obesity. *Curr. Opin. Endocrinol. Diabetes Obes.* **2022**, *29*, 183–190. [CrossRef]
122. Adamski, K.; Cook, K.; Gupta, D.; Morris, E.; Tuttle, E.; Carr, E.; Cremasco, F.; Cochran, E.; Brown, R.J. Effects of metreleptin in patients with lipodystrophy with and without baseline concomitant medication use. *Curr. Med. Res. Opin.* **2021**, *37*, 1881–1889. [CrossRef]
123. Trapp, C.M.; Censani, M. Setmelanotide: A promising advancement for pediatric patients with rare forms of genetic obesity. *Curr. Opin. Endocrinol. Diabetes Obes.* **2023**, *30*, 136–140. [CrossRef]
124. Altabas, V.; Zjačić-Rotkvić, V. Anti-ghrelin antibodies in appetite suppression: Recent advances in obesity pharmacotherapy. *Immunotargets Ther.* **2015**, *4*, 123–130. [CrossRef]

125. Bailey, C.J. Glucose-lowering therapies in type 2 diabetes: Opportunities and challenges for peptides. *Peptides* **2018**, *100*, 9–17. [CrossRef]
126. Casey, R.; Adelfio, A.; Connolly, M.; Wall, A.; Holyer, I.; Khaldi, N. Discovery through Machine Learning and Preclinical Validation of Novel Anti-Diabetic Peptides. *Biomedicines* **2021**, *9*, 276. [CrossRef]

Disclaimer/Publisher's Note: The statements, opinions and data contained in all publications are solely those of the individual author(s) and contributor(s) and not of MDPI and/or the editor(s). MDPI and/or the editor(s) disclaim responsibility for any injury to people or property resulting from any ideas, methods, instructions or products referred to in the content.

biomedicines

MDPI

Review

UCP2, a Member of the Mitochondrial Uncoupling Proteins: An Overview from Physiological to Pathological Roles

Salvatore Nesci [1] and Speranza Rubattu [2,3,*]

[1] Department of Veterinary Medical Sciences, Alma Mater Studiorum University of Bologna, 40064 Ozzano Emilia, Italy; salvatore.nesci@unibo.it
[2] Department of Clinical and Molecular Medicine, School of Medicine and Psychology, "Sapienza" University of Rome, 00189 Rome, Italy
[3] IRCCS Neuromed, 86077 Pozzilli, Italy
* Correspondence: speranzadonatella.rubattu@uniroma1.it

Abstract: UCP2 is an uncoupling protein homolog to UCP1. Unlike UCP1, which participates in non-shivering thermogenesis by uncoupling oxidative phosphorylation (OXPHOS), UCP2 does not perform a canonical H^+ leak, consuming the protonmotive force (Δp) through the inner mitochondrial membrane. The UCP2 biological role is elusive. It can counteract oxidative stress, acting with a "mild uncoupling" process to reduce ROS production, and, in fact, UCP2 activities are related to inflammatory processes, triggering pathological conditions. However, the Δp dissipation by UCP2 activity reduces the mitochondrial ATP production and rewires the bioenergetic metabolism of the cells. In all likelihood, UCP2 works as a carrier of metabolites with four carbon atoms (C4), reversing the anaerobic glycolysis-dependent catabolism to OXPHOS. Indeed, UCP2 can perform catalysis in dual mode: mild uncoupling of OXPHOS and metabolite C4 exchange of mitochondria. In vivo, the UCP2 features in the biology of mitochondria promote healthy ageing, increased lifespan, and can assure cerebro- and cardiovascular protection. However, the pathological conditions responsible for insulin secretion suppression are dependent on UCP2 activity. On balance, the uncertain biochemical mechanisms dependent on UCP2 do not allow us to depict the protective role in mitochondrial bioenergetics.

Keywords: bioenergetics; mitochondria; H^+ leak; UCP2; oxidative phosphorylation; cardiovascular diseases

1. Introduction

The energy transduction mechanism in mitochondria performs the conversion of the chemical potential of substrate oxidation in protonmotive force (Δp) to drive ADP phosphorylation. Mitochondrial respiratory complexes exploit the redox potential of NADH- or $FADH_2$-linked reducing equivalents, working as H^+ pumps, and establish the Δp through the inner mitochondrial membrane (IMM). The Δp dissipated by F_1F_O-ATPase is transformed in the energy chemical bond with ADP phosphorylation to ATP [1]. The energy conversion in this mitochondrial chemiosmotic H^+ circuit is fulfilled in the oxidative phosphorylation (OXPHOS) system. Therefore, the efficiency of the process relies on the capacity of coupling oxygen consumption to ADP phosphorylation. Otherwise, pathological or physiological conditions can hinder OXPHOS [2,3]. In particular, the Δp de-coupled from ATP synthesis might be affected by specific proteins in the IMM, impairing the OXPHOS [4] via different mechanisms of energy consumption.

2. The Uncoupling of OXPHOS

Uncoupling protein-1 (UCP1) is the protein responsible for producing heat in the mitochondria of brown adipose tissue. Working as a proton carrier, UCP1 catalyzes an H^+ leak, consuming the Δp built at the expense of the energy of substrates oxidized on respiration.

This physiological uncoupling of UCP1 can mediate adaptive non-shivering thermogenesis, increasing the energy expenditure [5,6]. The H^+ transport mediated by UCP1 needs free fatty acids, whereas it is inhibited by nucleotides such as GTP [7]. The physiological differences between thermogenesis supported by UCP1 and UCP1-independent thermogenesis, through ATP-consuming futile cycle in mitochondria or between multiple subcellular compartments, consist of Δp dissipation with two different mitochondrial mechanisms of uncoupling, without ATP production or coupling with ATP expenditure, respectively [4,8]. In the latter bioenergetic phenomenon, the Δp is dissipated by F_1F_O-ATPase as in the normal function of OXPHOS, but the synthesized ATP is not used in cellular processes [9]. Indeed, in the mitochondrial creatine-dependent ATP/ADP substrate cycling, the phosphocreatine (PCr)/creatine (Cr) kinase system hydrolyzes the mitochondrial ATP to ADP, and the Cr is phosphorylated to PCr. Then, tissue-nonspecific alkaline phosphatase hydrolyses PCr to initiate a futile cycle of Cr phosphorylation and dephosphorylation by consuming ATP [10] (Figure 1A). Noteworthy are the energy-dissipating mechanisms of ATP-consuming cycles that connect multiple subcellular compartments and/or tissues. Indeed, the calcium cycle causes ineffective ATP consumption, which is responsible for energy dissipation. The endoplasmic reticulum (ER) of beige adipocytes promotes the efflux of Ca^{2+} in response to cold exposure driven by norepinephrine-mediated stimulation of ryanodine receptor 2 (RyR2) activity on ER. The accumulation of cytosolic Ca^{2+} stimulates its uptake by the sarcoendoplasmic reticulum Ca^{2+}, known as SERCA, which mediates calcium cycling, sustained by ATP synthetized in mitochondria. Ca^{2+} exported in the cytosol by RyR2 is imported into the ER by the Ca^{2+}-ATPase activity of SERCA. This ATP-dependent futile cycle is a thermogenic mechanism used by beige adipocytes expressing a high level of F_1F_O-ATPase to produce heat, dissipating the Δp and regulating glucose homeostasis [11]. Moreover, the glycerol *de novo* synthesis by glyceroneogenesis and coenzyme A addition to free fatty acids, which are necessary for promoting the triglyceride re-esterification in adipose tissue, causes a futile ATP consumption by the lipid cycle of fatty acids storage and triacylglycerols degradation [9].

Other proteins and biophysical conditions can cause H^+ leak across the IMM [4]. Indeed, together with UCP1, the adenine nucleotide translocase (ANT), also called ADP/ATP transporter (AAC), can mediate fatty acid-dependent H^+ transport [12] using lipid molecules as co-factors to support the translocation of protons. One of the primary physiological sources of free fatty acid production might rely on the activity of phospholipase A2 [13], which could be responsible for ANT-dependent H^+ leak. In general, UCP1 expressed in brown/beige adipose tissue is responsible for H^+ leak, whereas this inducible H^+ conductance across the IMM depends on ANT in all other tissues. The primary common features of H^+ leak mediated by ANT and UCP1 are fatty acid-activated and purine nucleotide negative-regulated [14] (Figure 1B). However, a known non-inducible "basal H^+ leak" across the lipid bilayer, due to non-specific IMM permeability to H^+, violates Ohm's Law, exponentially increasing at high values of membrane potential [4,15] (Figure 1C).

It could be interesting to consider the transhydrogenation of electrons transferred by nicotinamide nucleotide transhydrogenase (NNT) from NADH to reduce $NADP^+$ to NADPH [16]. The Δp dissipated by NNT-mediated H^+ translocation generates NADPH in an energy-consumed mechanism not linked to thermogenesis. However, the NNT uncoupling of mitochondrial respiration from ATP synthesis sustains the antioxidant defence and sirtuin actions of mitochondria [17].

Other UCPs proteins, i.e., uncoupling protein-2 (UCP2) and uncoupling protein-3 (UCP3), might have physiological roles different from the obvious thermogenic functions explained above and attained through the respiratory uncoupling phenomenon. Oxidative stress and lipotoxicity in mitochondria inducing metabolic diseases and energy unbalance of metabolic process [2] could be counteracted by UCP activity. UCP2 is identified in a variety of organs, the kidney in particular, whereas UCP3 is primarily encountered in skeletal muscle. However, the story of the putative new uncoupling proteins, UCP2 and UCP3, is a little more complicated [18]. Indeed, there are two hypotheses: either they

work as functional protonophoric homologues of UCP1 or the proteins are conventional metabolite transporters. Similar to UCP1, the photonophoric regulatory mechanism of UCP2 and UCP3 might rely on high sensitivity to fatty acid activation and inhibition exerted by purine nucleotide. The physiological role of the UCP1-like mechanism has led to the concept of "mild uncoupling" not related to thermogenesis but as a protective mechanism against oxidative stress [18,19].

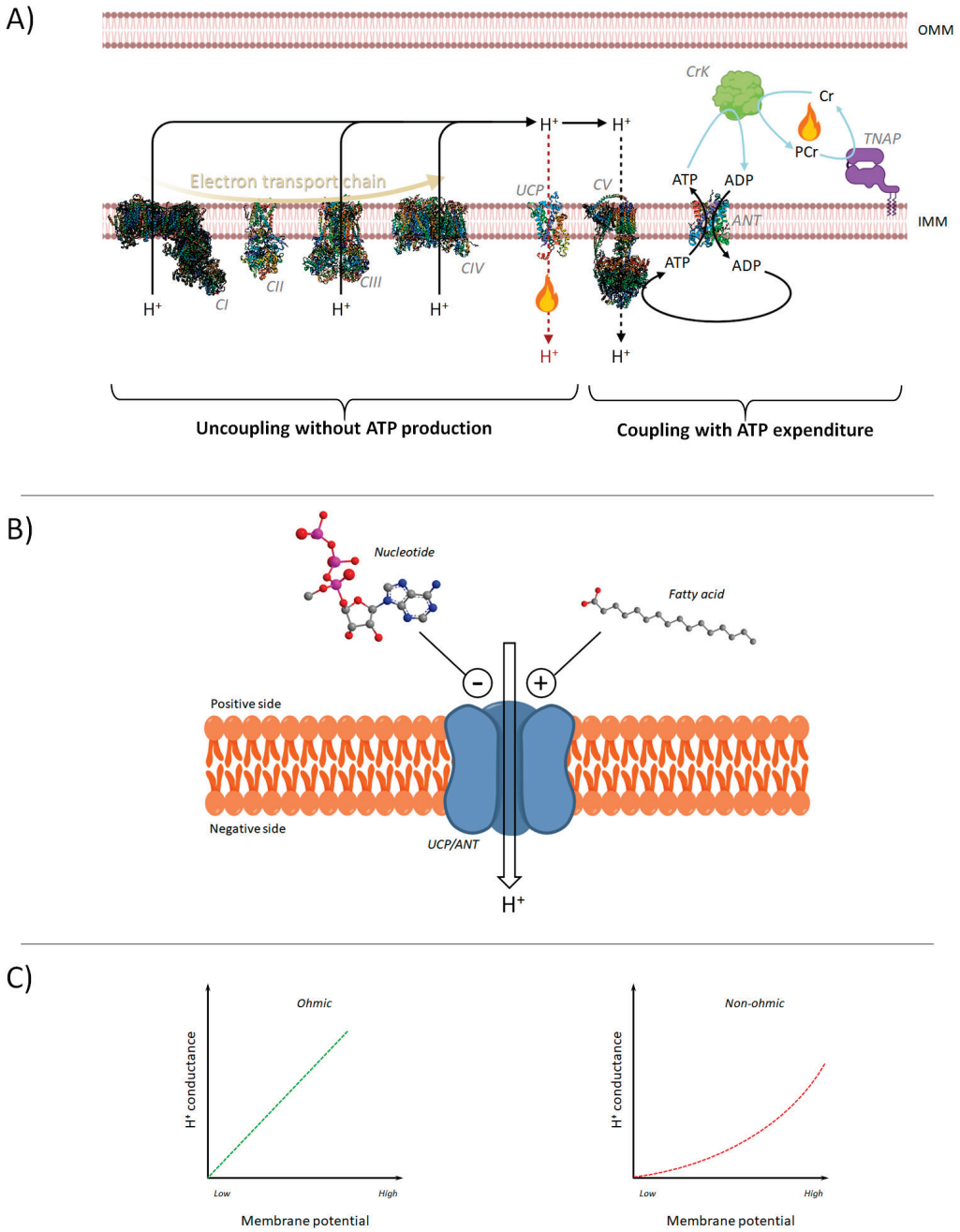


Figure 1. Mitochondrial bioenergetic features. (**A**) Schematic representation of protonmotive force by uncoupling driven by UCP or ATP-dependent futile cycle. CI, CII, CIII, and CIV identify the respiratory complexes, whereas CV is the F_1F_O-ATPase. ANT, adenine nucleotide translocase; CrK, creatine kinase, TNAP, tissue-nonspecific alkaline phosphatase; IMM and OMM, inner and outer mitochondrial membrane, respectively. (**B**) Positive and negative regulation of H^+ leak by carrier. (**C**) Relationship of H^+ conductance vs. membrane potential for ohmic (on the **right**) and non-ohmic (on the **left**) circuits.

In the absence of nucleotides, UCP3 catalyzes remarkable GDP-sensitive and superoxide-stimulated protonophoric activity. The mild uncoupling promoted by UCP3 is superoxide-dependent and plays an important role in controlling ROS production. However, superoxide does not directly activate UCP3, but it acts indirectly through the hydroxynonenal (HNE) generated with lipid peroxidation [20]. Alternative suggestions for the functions of uncoupling proteins consider pyruvate and amino acid metabolism [21,22].

In this review, the multifaceted role of UCP2 in physiological and pathological conditions will be considered in light of increasing evidence of the protein function(s) and the elucidation of the underlying mechanisms in mitochondria bioenergetics.

3. UCP2: A Possible Multifunctional Mitochondrial Carrier

UCP2 participates in various physiological and pathological processes, but its biological role is still elusive (Table 1). The UCP2 biochemical and physiological functions can cover the role of protecting cells from oxidative stress; increasing antitumor immunity in the tumour microenvironment to limit cancer development; regulating tumour progression through changes in glycolytic, oxidative, and calcium metabolism [23]; defending target organs in cardiovascular diseases such as hypertension [24]. Rising ionic leaks in the IMM are known as mitochondrial respiration dissociated from ATP synthesis, leading to uncoupling. UCP2 can affect the OXPHOS system by decreasing the membrane potential [25]. However, the H^+ leak associated with UCP2 could be related to a thermogenic phenotype of UCP1 generated from the uncoupling of OXPHOS [26]. The UCP2 activity is increased in the presence of ROS in a manner dependent on fatty acid oxidation. As a result, the UCP2 acts to revert ROS production by decreasing the membrane potential of mitochondria through a mechanism of H^+ leak that could be different from UCP1. Indeed, essential histidine residues of UCP1 supporting the protonophore kinetics of the enzyme are absent in UCP2 [27].

Table 1. Deleterious vs. beneficial roles of UCP2 in different pathological conditions.

Diseases	UCP2 Effect on Health (−) Deleterious/(+) Beneficial	References
Atherogenesis	+	[28]
Melanoma	+	[29]
Cholangiocarcinoma	−	[30]
Lung adenocarcinoma	−	[31]
T-cell acute lymphoblastic leukemia	−	[32]
Colorectal cancer	+	[33]
Cerebral ischemic injury	−	[34]
Septic acute kidney injury	+	[35]
Hypertension	+	[36]
Cerebrovascular and ischemic heart disease	−	[37]
Congenital hyperinsulinism	+	[38]
Obesity and diabetes	+	[39,40]

The UCP2 aids mitochondrial functions by constraining excessive ROS production with the "mild uncoupling" process. Otherwise, it can cause an unbalance in mitochondrial ATP production by increasing the ADP/ATP ratio. In particular, H^+ leak catalyzed by UCP2, bypassing the F_1F_O-ATPase, reduces the cellular ATP content in pancreatic β cells. The decrease in insulin secretion is related to the decline in exocytosis of insulin vesicles in glucose-stimulated insulin secretion conditions. The molecular mechanism is explained by the polarization of the plasma membrane with the ATP-gated K^+ channel opened under a low level of ATP, which, in turn, closes the voltage-gated Ca^{2+} channel. The missing energetic signalling of mitochondrial ATP production, eluded by UCP2 activity, blocks the translocation of insulin granules and release [41].

Insulin resistance develops from chronic inflammation of lipids in adipose tissue, particularly in patients with metabolic syndrome or in obese subjects [42]. The altered microenvironment of adipose tissue causes customised metabolic reprogramming, which promotes tissue inflammation. UCP2 deficiency dramatically enhances glycolysis and oxidative respiration in the setting of obesity-induced adipose tissue inflammation and insulin resistance. However, UCP2 activity does not perform an important role in shaping macrophage activation in adipose tissue of diabetes associated with insulin resistance [43]. Thus, in inflammatory or autoimmune diseases, UCP2 can control macrophage activation by modulating the production of mitochondrial ROS [44].

A reduction in the UCP2 mRNA level was found to be related to a consequent increase in ROS generation. Thus an increase in the UCP2 mRNA level was associated with reduced ROS production [45]. Indeed, UCP2 deletion increased macrophage formation of ROS, highlighting the hypothesis that UCP2 could be triggered by superoxide, providing negative feedback to limit oxidative damage [18]. The UCP2 function linked to cellular metabolism affects the redox state and the oxidative stress of the cells. Interestingly, in this context, UCP2 plays a role in chronic inflammation associated with related disorders of atherogenesis and low-density lipoprotein oxidation as a consequence of obesity [46]. Atherogenesis triggered by inflamed endothelial cells is controlled by stress-dependent regulation of UCP2 expression by Krüppel-like factor 2. Increased UCP2 levels produce a mechanosensitive action, which leads to decreased inflammation. In this condition, a reduced Western diet-induced atherosclerosis and less-disturbed flow-associated atherosclerosis are observed [28]. The role of UCP2 as a regulator of mitochondrial ROS production is corroborated by results in the presence of nucleotide GDP that blocks the UCP2 activity, causing mitochondrial membrane polarization and ROS production [46].

Mild uncoupling of OXPHOS, reducing mitochondrial ROS production, avoids mitochondrial dysfunction. The products of lipid oxidative stress, e.g., HNE, *trans*-retinoic acid, *trans*-retinal, and other reactive 2-alkenal groups, lead to the uncoupling of mitochondria, stimulating the UCPs. In kidney mitochondria, ROS production-induced ROS release [47] is decreased by UCP2. However, GDP-sensitive ROS released under HNE conditions is partially hampered [48].

Hepatocytes can accumulate fatty acids, and liver lipotoxicity induces metabolic-associated fatty liver disease (MAFLD). UCP1 is not present in any liver cell type. Conversely, UCP2 is expressed in Kupffer cell-specific macrophages of the liver [49]. Immunomodulation of the MAFLD linked to the inflammatory response in macrophage mitochondria could be related to the development of fibrosis, which triggers steatohepatitis or dangerous conditions of cirrhosis and hepatocarcinoma [50].

Moreover, in cancer, UCP2 could allow for ROS accumulation during the initial phase of tumour growth. Indeed, controlled elevated levels of ROS promote tumour growth by acquiring oncogene mutations and activating pro-tumour metabolic signals related to the depletion of antioxidant systems [51]. ROS control in tumour cells could be restrained by UCP2. UCP2 deficiency might promote tumour cells that are less likely to metastasize. Therefore, UCP2 as a metabolic sensor can reprogram the tumour metabolism of cells, with metabolites exported by UCP2 reversing the Warburg effect to oxidative phosphorylation. The decrease in glycolysis-dependent metabolism can reduce the tumorigenic capacity of cells [29]. However, there is evidence suggesting that UCP2 involvement in cancer cell glycolytic metabolism has a poor prognosis on tumour growth, relying on a different energy metabolism [30]. In particular, UCP2 can be involved in two events related to the Warburg effect, promoting metabolic adaptations of cancer cells. UCP2 can reduce the redox pressure on the mitochondrial respiration by exporting metabolites of tricarboxylic acid cycle (TCA) and, as a consequence, prevent ROS generation; stimulate glutamine oxidation as an energetic fuel [31]. Depending on whether tumor metabolism is oxidative or glycolytic, the transporter role of UCP2 in cancer may have a distinct effect on the development of cancer [32,33].

By considering the regulatory role of ROS production in mitochondria, alternative suggestions on functional features of UCP2 have included glutathione transport as a mechanism for resistance to cerebral ischemic injury. UCP2 mRNA is massively induced after three days post-ischemia, which provides a decreased resistance to cerebral ischemia due to an increased oxidative injury and downed cerebral neuronal antioxidant condition. Therefore, the elimination of ROS might be accomplished with glutathione in the reduced state in the matrix [34]. UCP2 may perform other functions related to cellular metabolism. Genetic loss of UCP2 induces the stimulation of glucose metabolism. By promoting a shift from sugar to fatty acids metabolism, UCP2 transports the fatty acids out of mitochondria, hindering oxidation [52].

Together with glucose, glutamine is an essential oxidative fuel in immune and proliferative cells, and both are preferentially consumed by fast-growth cells to the detriment of mitochondrial sources of energy [53]. The absence of UCP2 is associated with decreased glutaminolysis in mitochondria [54].

The dual mode work of UCP2 might consider the uncoupling mechanism responsible for ROS regulation or substrate exchange transport that might deplete the mitochondria of intermediate compounds of the TCA. In both cases, UCP2 can repress ATP-producing reactions, driving mitochondria towards the non-phosphorylating state. As a consequence, a cellular adaptation to a reduced substrate or oxygen supply is induced. In particular, under ischemic conditions, the adenine nucleotide pool decreases, whereas succinate accumulates in mitochondria [55]. After reperfusion, the excess of succinate is oxidized, sustaining the hyperpolarization of IMM by canonical electron transfer through complex III and complex IV to oxygen and maintaining the reduced coenzyme Q pool. The latter, sustained by the membrane potential, drives the reverse electron transfer at complex I to produce ROS responsible for the ischemia–reperfusion (IR) injury. Protection against IR injury is obtained with rotenone or malonate, which block the oxidation of coenzyme Q and succinate at complex I and complex II sites, respectively [56,57]; by mild uncoupling dissipating the Δp [58]. As a result, UCP2 activity could establish cellular conditions of resistance to pathological situations [59].

In a contest of promotion of healthy ageing and increased lifespan, the cell metabolism might be boosted by a UCP2-dependent longevity activity. The maintenance of fatty acid oxidation and restriction of subsequent oxidative damage related to lipid catabolism allow for to maintenance of the mitochondrial oxidative capacity and biogenesis [60]. The involvement of UCP2 functions in the maintenance of mitochondrial activity, exploiting the control of oxidative stress in physiological or pathological conditions, can affect the immune response and inflammation, thus characterizing the septic acute kidney injury [35]. ROS production causes mitochondrial dysfunction and, in turn, the oxidation of mitochondrial DNA (mtDNA). Damaged mtDNA is cleaved and exported out mitochondria through the mitochondrial permeability transition pore, an ion non-selective membrane pore involved in a wide range of mitochondrial dysfunction events, triggering regulated cell death, and the voltage-dependent anion channel. These two different pores are placed on the inner and outer mitochondrial membrane, respectively. The mtDNA released in the cytosol acts as a DAMP (damage-associated molecular pattern) molecule, activating the inflammasome and the cGAS-STING complex responsible for proinflammatory molecules, such as interleukin-1β and interleukin-18 and interferon signalling [61,62]. Thus, the antioxidant activities of UCP2 can revert the renal injury aggravated by lipopolysaccharide (LPS), counteracting the inflammation, macrophage infiltration, and the mitochondrial dysfunction linked to oxidative stress [35].

In addition to the protection against ROS formation, the physiological functions of UCP2 have been revised to include obesity protection and thermogenic involvement in the fever response. In the latter case, LPS stimulation, which induces fever, causes a remarkable increase in the mRNA and protein levels of UCP2 in different tissues, including the lung [63], brain [64], and liver [65,66].

An increasing amount of evidence, as detailed below, suggests that UCP2 should be classified as a mitochondrial transporter rather than an uncoupling protein.

4. Mitochondrial Respiration and the Role of UCP2 as Uncoupling Protein or Metabolite Carrier

UCP2 expression under conditions of stimulated fatty acid metabolism may be related to an as yet unidentified role in the metabolism of lipid molecules. Indeed, UCP2 is a *bona fide* uncoupling protein that decouples the OXPHOS, but it should rather be considered as a mitochondrial metabolite carrier [52]. Since UCP2 is present in fish, it is possible to speculate that this carrier is not directly associated with homeothermia, endothermia, non-shivering thermogenesis, or high mammalian basal metabolic rate [67]. We can assert that the H^+ leak activity of UCP2 is a "relief valve" for the polarized IMM (Figure 2) to avoid the formation of superoxide anion in conditions in which the mitochondrial electron carriers of the respiratory chain are in a reduced state [4,68].

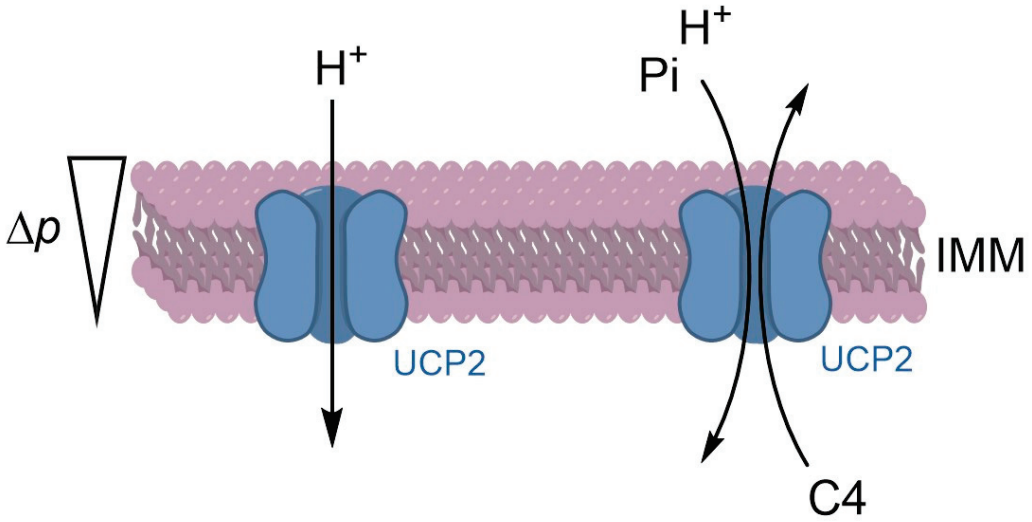


Figure 2. Proposed mechanism of uncoupling protein-2 (UCP2)-mediated transport activity. The mild uncoupling by H^+ leak acting as a relief valve on polarized IMM is depicted on the left. UCP2 transport of C4 metabolites is shown on the right. Δ*p*, proton motive force; C4, metabolites with four carbon atoms; Pi, inorganic phosphate; IMM, inner mitochondrial membrane.

UCP2 is not present in all organisms alive today, even if it is evolutionarily ancient. It is considered a member of the larger family of mitochondrial anion carrier proteins identified as SLC25. The transporters of this family ensure the supply of ions, important metabolic intermediates, and coenzymes to mitochondria. UCP2 might facilitate the transfer of anions from the negative to the positive side of IMM and the return transfer of H^+ from the positive to the negative side of IMM [69]. Considering the high homology between UCP1 and UCP2, researchers initially focused on the similar mitochondrial membrane uncoupling of OXPHOS. These assumptions are also consistent with the results of Rial et al., who argue that purine nucleotides, palmitic acid, and retinoic acid do not influence the respiratory rate of UCP2-overexpressing yeast mitochondria under standard conditions (pH 6.8) [70]. In contrast, they discovered that an increase in pH is positively regulated by retinoids, increasing mitochondrial respiration. It has been shown that pHs ranging from 6.8 to 7.5 and retinoic acid are two parameters that can increase the uncoupling activity of UCP2 [70]. Indeed, the first study on UCP2 KO mice showed that UCP2 has no uncoupling function at physiological levels since the deletion of UCP2 does not change spleen mitochondrial respiration [71].

The uptake of Ca^{2+} in mitochondria is performed by macromolecular complexes that consist of the pore-forming mitochondrial Ca^{2+} uniporter (MCU) protein, the essential MCU regulator (EMRE), the mitochondrial Ca^{2+} uptake 1 (MICU1), and MICU2 in the intermem-

brane space [72]. Methylation of Arg_{455} of MICU1 by protein arginine methyl transferase 1 (PRMT1) is a post-translational modification that desensitizes the mitochondrial Ca^{2+} uniporter complex for Ca^{2+}, decreasing the uptake of the divalent cation. In various age-related diseases, such as cancer, neurodegenerative, and metabolic/cardiovascular disorders, the PRMT1 activity increases, impairing mitochondrial Ca^{2+} homeostasis [73]. UCP2 binds primarily to the methylated MICU1, restoring Ca^{2+} sensitivity and mitochondrial Ca^{2+} uptake. Therefore, under situations of enhanced PRMT1 activity, UCP2 is described as a sensitizer of Ca^{2+} uniport in mitochondria, acting as a unique regulator of methylated MICU1 [74].

UCP2 can regulate the substrate oxidation in mitochondria, supporting the transport of metabolites with four carbon atoms (C4) and playing a role in reprogramming metabolic pathways. The metabolic switch from fatty acid oxidation to glucose metabolism is supported in $UCP2^{-/-}$ proliferating cells [75]. The transport mechanism of UCP2 is catalyzed by an exchange of cytosolic phosphate inorganic (Pi) for intramitochondrial C4 metabolites. The antiport mechanism of Pi/C4 is conducted by the H^+ uptake in cotransport with Pi. In other words, Pi and H^+ are uptaken in the matrix, whereas the C4 is moved out of mitochondria (Figure 2). The H^+-assisted mechanism is driven by IMM membrane potential (negative inside) and pH gradient (acidic outside) of energized mitochondria [54].

However, the exchange mechanism of the carrier can explain the bioenergetic role of UCP2 for the mild uncoupling, the metabolic reprogramming under different physiological or pathological conditions as well as the tissue-specific distribution and the common presence in endotherms and in the ectotherm kingdom, where thermogenesis is absent. Indeed, oxalacetate is a C4 compound in mitochondria exported outside by UCP2. The TCA cycle starts with the citrate synthesis, driven by the condensation reaction of acetyl-CoA to oxaloacetate. The availability of the latter limits the cycle reactions of the pathway. The UCP2 catalyzing the oxalacetate transport decreases the production of NADH and $FADH_2$ in the TCA cycle, limiting the electron flux and lowering the redox pressure on the mitochondrial respiration. As a consequence, the attenuation of mitochondrial respiration reduces the ATP synthesis by F_1F_O-ATPase and the ROS generation [54]. These conditions stimulate aerobic glycolysis, hindering mitochondrial glucose oxidation [76]. In β cells, the oxalacetate transport by UCP2 can explain the restraint of insulin secretion, caused by the increased ADP/ATP ratio and lactate release [77].

Glutaminolysis is an anaplerotic pathway used to fuel the TCA cycle in proliferating cells [53]. The glutamine transformation restores oxaloacetate for continued TCA cycle function (anaplerosis) required for rapid synthesis of macromolecules, including lipids, proteins, and nucleotides [78], skipping the OXPHOS in the metabolic adaptations required for cell proliferation. UCP2 expression is stimulated by glutamine, and the flux of glutaminolysis decreases in the absence of a carrier [79]. Moreover, the UCP2-mediated export of C4 compounds can promote the Warburg effect by shifting glucose utilization from respiration to anabolic reactions for macromolecule synthesis. Thus, UCP2 is implicated in two Warburg effect-related events: the utilization of glutamine as an energetic fuel and the export of TCA cycle C4 metabolites from mitochondria for macromolecule biosynthesis [31]. Indeed, UCP2 silencing in human lung adenocarcinoma cell line A549, which is actively proliferating, lowers basal respiration. The inhibition of F_1F_O-ATPase synthesis of ATP is not compensated by an increase in glycolysis. Thus, the tumour cells might rely on reduced cellular ATP demand, insensitive to an impaired bioenergetic metabolism, but it depends on a metabolic adaptation of proliferating cells supported by C4-metabolite transported by UCP2 [31].

Therefore, the role of UCP2 as a metabolic sensor contributes to lipid metabolism regulation by supporting a switch from carbohydrate to lipid metabolism. In the absence of UCP2, pyruvate accumulation in the matrix could provide an adequate supply to the TCA cycle that inhibits the fatty acids and glutamine oxidation [80]. However, the role of efflux of pyruvate is physiologically linked with UCP2 tissue localization and expression.

5. Pathogenetic Role of UCP2 Deficiency in Animal Models and Humans

The cytoprotective effects of UCP2 were extended to animal and human tissues/organs in both physiological and pathological conditions. Since UCP2 supports fatty acid oxidation and mainly limits oxidative damage, allowing for a regular mitochondrial oxidative capacity and mitochondrial biogenesis, it can promote healthy ageing and increased lifespan. The metabolic hypothesis of UCP2-dependent longevity was proven in transgene and *knock-out* mice models: UCP2 transgene revealed an extended lifespan, whereas mice deficient in UCP2 showed a significantly shorter lifespan [81]. A decrease in UCP2 was reported in isolated cardiomyocytes from old mice compared to young ones [82] and also in cardiac tissue-derived stem-like cells (CTSCs). In the latter experimental condition, UCP2 was highly expressed in CTSCs from the neonatal heart. In contrast, UCP2 was reduced in aged CTSCs, shifting energy metabolism to OXPHOS, thus reducing cellular proliferation and survival [83]. In line with this evidence, it was recently demonstrated that UCP2-KO mice kept under moderate hypoxia showed a more pronounced decline in cardiac function compared to *wild-type* (*wt*) mice. In addition, cardiomyocyte cell cycle activity was reduced, while fibrosis and DNA damage were significantly increased in UCP2KO compared with *wt* under hypoxia. The results support a role for mitochondrial UCP2 as an oxygen sensor, regulating cardiomyocyte cell cycle activity, acetyl-CoA levels, and histone acetylation in response to moderate hypoxia [84]. In a different animal model, the spontaneously hypertensive rat showing a higher predisposition to target organ damage development (SHRSP), an age-related decrease in UCP2 expression, was found in the heart, kidney, and microglia compared to its strictly related control, the stroke-resistant SHR (SHRSR) [36].

However, a protective effect of UCP2 has been reported in both cerebrovascular and ischemic heart disease. UCP2 protects the heart from IR injury, being upregulated in this condition along with increased autophagy stimulation [37]. Two experimental models of stroke revealed the neuroprotective effect of UCP2: the MCAO mouse [85] and the SHRSP [86]. The experience gained with SHRSP investigation strongly supported a deleterious consequence of a stroke-promoting diet on UCP2 expression in the brain of SHRSP vs. SHRSR. The decrease in UCP2 induced by the high-salt diet, which is mediated by microRNA-503, involved an impaired mitochondrial function with increased ROS accumulation. In this context, the significant therapeutic effect of a few approaches able to stimulate UCP2 expression, fenofibrate and a *Brassica oleracea sprout* extract, was revealed [86]. An intriguing interplay between salt loading, ROS, UCP2, and autophagy was later discovered [87]. In humans, UCP2 and UCP5 expression was significantly increased in brain ischemic lesions compared to the intact area. This evidence could be interpreted as an adaptive protective response to the ischemic insult [88].

UCP2 is involved in obesity and diabetes mellitus, mainly through its ability to suppress insulin secretion [6,39]. On the other hand, UCP2 downregulation favoured insulin secretion and obesity [39]. Although UCP2 is a mitochondrial protein that inhibits insulin secretion from β cells, it is unaffected by excessive glucosamine exposure, in both pancreatic islets and the β-cell line [89]. Instead, genipin, an inhibitor of UCP2, can reduce the expression of UCP2, limiting the amount of glucose that can be transferred to cells and lowering the production of advanced glycation end products (AGEs) and receptor for AGEs [90]. UCP2 mutations are associated with human diseases, highlighting an important role for mitochondria in congenital hyperisulinism [38]. In a rat model of metabolic syndrome, the increase in UCP2 in the liver serves as a mechanism of protection toward oxidative stress [9,91]. Accordingly, UCP2 stimulation through a dietary intervention in this model improved lipid metabolism and mitochondrial function along with an increase in UCP2 expression in several tissues [10,92]. Since UCP2 influences ROS generation, cell metabolism and proliferation, apoptosis and autophagy, its role was also explored in cancer and tumour drug sensitivity. As a result, a controversial role of UCP2 has been reported in these conditions [93].

Although a clear pathogenic effect of UCP2 has not been demonstrated yet in human diseases, an interesting variant of the human gene (-866G>A SNP), with the A allele being

associated with increased UCP2 expression and decreased ROS accumulation, was shown to associate with obesity and diabetes in several populations [40].

6. Conclusions

Based on the available experimental evidence, UCP2 emerges as a mitochondrial protein able to exert important modulatory effects in both physiology and pathology in several organs and apparatuses. It is even expected that the modulation of UCP2 expression may serve as a suitable pharmacological strategy to treat common human diseases. However, the unsolved biochemical mechanism of the enzymatic catalysis of UCP2 makes it difficult to attribute a definite cellular role. Recent evidence argues that UCP2 is a C4 metabolite rather than an uncoupling carrier. The elucidation of this arcane phenomenon could explain the physiological or pathological behaviour of UCP2 in mitochondrial bioenergetics.

Author Contributions: Conceptualization, S.N. and S.R.; validation, S.N. and S.R.; writing—original draft preparation, S.N. and S.R.; writing—review and editing, S.N. and S.R.; visualization, S.N.; supervision, S.R.; funding acquisition, S.R. All authors have read and agreed to the published version of the manuscript.

Funding: This work was partially funded by the Italian Ministry of Health (Ricerca Corrente) to S.R., by Progetto PRIN 2022 (from the Italian Ministry of Instruction, University and Research, no. 2022E75TWB) to S.R. and S.N. The research leading to these results has also received funding from the European Union-NextGenerationEU through the Italian Ministry of University and Research under PNRR–M4C2-I1.3 Project PE_00000019 "HEAL ITALIA" to S.R., CUP B53C22004000006. The views and opinions expressed are those of the authors only and do not necessarily reflect those of the European Union or the European Commission. Neither the European Union nor the European Commission can be held responsible for them.

Institutional Review Board Statement: Not applicable.

Informed Consent Statement: Not applicable.

Conflicts of Interest: The authors declare no conflicts of interest.

References

1. Saraste, M. Oxidative Phosphorylation at the Fin de Siècle. *Science* **1999**, *283*, 1488–1493. [CrossRef]
2. Ricquier, D.; Bouillaud, F. Mitochondrial Uncoupling Proteins: From Mitochondria to the Regulation of Energy Balance. *J. Physiol.* **2000**, *529 Pt 1*, 3–10. [CrossRef]
3. Nesci, S.; Trombetti, F.; Pagliarani, A.; Ventrella, V.; Algieri, C.; Tioli, G.; Lenaz, G. Molecular and Supramolecular Structure of the Mitochondrial Oxidative Phosphorylation System: Implications for Pathology. *Life* **2021**, *11*, 242. [CrossRef]
4. Nesci, S. Proton Leak through the UCPs and ANT Carriers and beyond: A Breath for the Electron Transport Chain. *Biochimie* **2023**, *214*, 77–85. [CrossRef]
5. Nicholls, D.G.; Rial, E. A History of the First Uncoupling Protein, UCP1. *J. Bioenerg. Biomembr.* **1999**, *31*, 399–406. [CrossRef]
6. Nedergaard, J.; Golozoubova, V.; Matthias, A.; Asadi, A.; Jacobsson, A.; Cannon, B. UCP1: The Only Protein Able to Mediate Adaptive Non-Shivering Thermogenesis and Metabolic Inefficiency. *Biochim. Biophys. Acta* **2001**, *1504*, 82–106. [CrossRef]
7. González-Barroso, M.M.; Fleury, C.; Bouillaud, F.; Nicholls, D.G.; Rial, E. The Uncoupling Protein UCP1 Does Not Increase the Proton Conductance of the Inner Mitochondrial Membrane by Functioning as a Fatty Acid Anion Transporter. *J. Biol. Chem.* **1998**, *273*, 15528–15532. [CrossRef]
8. Kazak, L.; Chouchani, E.T.; Jedrychowski, M.P.; Erickson, B.K.; Shinoda, K.; Cohen, P.; Vetrivelan, R.; Lu, G.Z.; Laznik-Bogoslavski, D.; Hasenfuss, S.C.; et al. A Creatine-Driven Substrate Cycle Enhances Energy Expenditure and Thermogenesis in Beige Fat. *Cell* **2015**, *163*, 643–655. [CrossRef]
9. Brownstein, A.J.; Veliova, M.; Acin-Perez, R.; Liesa, M.; Shirihai, O.S. ATP-Consuming Futile Cycles as Energy Dissipating Mechanisms to Counteract Obesity. *Rev. Endocr. Metab. Disord.* **2022**, *23*, 121–131. [CrossRef]
10. Sun, Y.; Rahbani, J.F.; Jedrychowski, M.P.; Riley, C.L.; Vidoni, S.; Bogoslavski, D.; Hu, B.; Dumesic, P.A.; Zeng, X.; Wang, A.B.; et al. Mitochondrial TNAP Controls Thermogenesis by Hydrolysis of Phosphocreatine. *Nature* **2021**, *593*, 580–585. [CrossRef]
11. Ikeda, K.; Kang, Q.; Yoneshiro, T.; Camporez, J.P.; Maki, H.; Homma, M.; Shinoda, K.; Chen, Y.; Lu, X.; Maretich, P.; et al. UCP1-Independent Signaling Involving SERCA2b-Mediated Calcium Cycling Regulates Beige Fat Thermogenesis and Systemic Glucose Homeostasis. *Nat. Med.* **2017**, *23*, 1454–1465. [CrossRef]
12. Bertholet, A.M.; Chouchani, E.T.; Kazak, L.; Angelin, A.; Fedorenko, A.; Long, J.Z.; Vidoni, S.; Garrity, R.; Cho, J.; Terada, N.; et al. H+ Transport Is an Integral Function of the Mitochondrial ADP/ATP Carrier. *Nature* **2019**, *571*, 515–520. [CrossRef]

13. Fedorenko, A.; Lishko, P.V.; Kirichok, Y. Mechanism of Fatty-Acid-Dependent UCP1 Uncoupling in Brown Fat Mitochondria. *Cell* **2012**, *151*, 400–413. [CrossRef]
14. Bertholet, A.M.; Natale, A.M.; Bisignano, P.; Suzuki, J.; Fedorenko, A.; Hamilton, J.; Brustovetsky, T.; Kazak, L.; Garrity, R.; Chouchani, E.T.; et al. Mitochondrial Uncouplers Induce Proton Leak by Activating AAC and UCP1. *Nature* **2022**, *606*, 180–187. [CrossRef]
15. Jastroch, M.; Divakaruni, A.S.; Mookerjee, S.; Treberg, J.R.; Brand, M.D. Mitochondrial Proton and Electron Leaks. *Essays Biochem.* **2010**, *47*, 53–67. [CrossRef]
16. Kampjut, D.; Sazanov, L.A. Structure and Mechanism of Mitochondrial Proton-Translocating Transhydrogenase. *Nature* **2019**, *573*, 291–295. [CrossRef]
17. Nesci, S.; Trombetti, F.; Pagliarani, A. Nicotinamide Nucleotide Transhydrogenase as a Sensor of Mitochondrial Biology. *Trends Cell Biol.* **2020**, *30*, 1–3. [CrossRef]
18. Nicholls, D.G. Mitochondrial Proton Leaks and Uncoupling Proteins. *Biochim. Biophys. Acta Bioenerg.* **2021**, *1862*, 148428. [CrossRef]
19. Korshunov, S.S.; Skulachev, V.P.; Starkov, A.A. High Protonic Potential Actuates a Mechanism of Production of Reactive Oxygen Species in Mitochondria. *FEBS Lett.* **1997**, *416*, 15–18. [CrossRef]
20. Echtay, K.S.; Pakay, J.L.; Esteves, T.C.; Brand, M.D. Hydroxynonenal and Uncoupling Proteins: A Model for Protection against Oxidative Damage. *BioFactors* **2005**, *24*, 119–130. [CrossRef]
21. Mozo, J.; Ferry, G.; Studeny, A.; Pecqueur, C.; Rodriguez, M.; Boutin, J.A.; Bouillaud, F. Expression of UCP3 in CHO Cells Does Not Cause Uncoupling, but Controls Mitochondrial Activity in the Presence of Glucose. *Biochem. J.* **2006**, *393*, 431–439. [CrossRef] [PubMed]
22. Aguer, C.; Piccolo, B.D.; Fiehn, O.; Adams, S.H.; Harper, M. A Novel Amino Acid and Metabolomics Signature in Mice Overexpressing Muscle Uncoupling Protein 3. *FASEB J.* **2017**, *31*, 814–827. [CrossRef] [PubMed]
23. Luby, A.; Alves-Guerra, M.-C. UCP2 as a Cancer Target through Energy Metabolism and Oxidative Stress Control. *Int. J. Mol. Sci.* **2022**, *23*, 15077. [CrossRef] [PubMed]
24. Di Castro, S.; Scarpino, S.; Marchitti, S.; Bianchi, F.; Stanzione, R.; Cotugno, M.; Sironi, L.; Gelosa, P.; Duranti, E.; Ruco, L.; et al. Differential Modulation of Uncoupling Protein 2 in Kidneys of Stroke-Prone Spontaneously Hypertensive Rats Under High-Salt/Low-Potassium Diet. *Hypertension* **2013**, *61*, 534–541. [CrossRef] [PubMed]
25. Jabůrek, M.; Varecha, M.; Gimeno, R.E.; Dembski, M.; Jezek, P.; Zhang, M.; Burn, P.; Tartaglia, L.A.; Garlid, K.D. Transport Function and Regulation of Mitochondrial Uncoupling Proteins 2 and 3. *J. Biol. Chem.* **1999**, *274*, 26003–26007. [CrossRef] [PubMed]
26. Conti, B.; Sanchez-Alavez, M.; Winsky-Sommerer, R.; Morale, M.C.; Lucero, J.; Brownell, S.; Fabre, V.; Huitron-Resendiz, S.; Henriksen, S.; Zorrilla, E.P.; et al. Transgenic Mice with a Reduced Core Body Temperature Have an Increased Life Span. *Science* **2006**, *314*, 825–828. [CrossRef] [PubMed]
27. Bienengraeber, M.; Echtay, K.S.; Klingenberg, M. H+ Transport by Uncoupling Protein (UCP-1) Is Dependent on a Histidine Pair, Absent in UCP-2 and UCP-3. *Biochemistry* **1998**, *37*, 3–8. [CrossRef] [PubMed]
28. Luo, J.-Y.; Cheng, C.K.; He, L.; Pu, Y.; Zhang, Y.; Lin, X.; Xu, A.; Lau, C.W.; Tian, X.Y.; Ma, R.C.W.; et al. Endothelial UCP2 Is a Mechanosensitive Suppressor of Atherosclerosis. *Circ. Res.* **2022**, *131*, 424–441. [CrossRef] [PubMed]
29. Esteves, P.; Pecqueur, C.; Ransy, C.; Esnous, C.; Lenoir, V.; Bouillaud, F.; Bulteau, A.-L.; Lombès, A.; Prip-Buus, C.; Ricquier, D.; et al. Mitochondrial Retrograde Signaling Mediated by UCP2 Inhibits Cancer Cell Proliferation and Tumorigenesis. *Cancer Res.* **2014**, *74*, 3971–3982. [CrossRef]
30. Yu, J.; Shi, L.; Shen, X.; Zhao, Y. UCP2 Regulates Cholangiocarcinoma Cell Plasticity via Mitochondria-to-AMPK Signals. *Biochem. Pharmacol.* **2019**, *166*, 174–184. [CrossRef]
31. Segalés, J.; Sánchez-Martín, C.; Pujol-Morcillo, A.; Martín-Ruiz, M.; De Los Santos, P.; Lobato-Alonso, D.; Oliver, E.; Rial, E. Role of UCP2 in the Energy Metabolism of the Cancer Cell Line A549. *Int. J. Mol. Sci.* **2023**, *24*, 8123. [CrossRef] [PubMed]
32. Sancerni, T.; Renoult, O.; Luby, A.; Caradeuc, C.; Lenoir, V.; Croyal, M.; Ransy, C.; Aguilar, E.; Postic, C.; Bertho, G.; et al. UCP2 Silencing Restrains Leukemia Cell Proliferation through Glutamine Metabolic Remodeling. *Front. Immunol.* **2022**, *13*, 960226. [CrossRef] [PubMed]
33. Aguilar, E.; Esteves, P.; Sancerni, T.; Lenoir, V.; Aparicio, T.; Bouillaud, F.; Dentin, R.; Prip-Buus, C.; Ricquier, D.; Pecqueur, C.; et al. UCP2 Deficiency Increases Colon Tumorigenesis by Promoting Lipid Synthesis and Depleting NADPH for Antioxidant Defenses. *Cell Rep.* **2019**, *28*, 2306–2316.e5. [CrossRef] [PubMed]
34. De Bilbao, F.; Arsenijevic, D.; Vallet, P.; Hjelle, O.P.; Ottersen, O.P.; Bouras, C.; Raffin, Y.; Abou, K.; Langhans, W.; Collins, S.; et al. Resistance to Cerebral Ischemic Injury in UCP2 Knockout Mice: Evidence for a Role of UCP2 as a Regulator of Mitochondrial Glutathione Levels. *J. Neurochem.* **2004**, *89*, 1283–1292. [CrossRef] [PubMed]
35. Ding, Y.; Zheng, Y.; Huang, J.; Peng, W.; Chen, X.; Kang, X.; Zeng, Q. UCP2 Ameliorates Mitochondrial Dysfunction, Inflammation, and Oxidative Stress in Lipopolysaccharide-Induced Acute Kidney Injury. *Int. Immunopharmacol.* **2019**, *71*, 336–349. [CrossRef] [PubMed]
36. Rubattu, S.; Bianchi, F.; Busceti, C.L.; Cotugno, M.; Stanzione, R.; Marchitti, S.; Di Castro, S.; Madonna, M.; Nicoletti, F.; Volpe, M. Differential Modulation of AMPK/PPARα/UCP2 Axis in Relation to Hypertension and Aging in the Brain, Kidneys and Heart of Two Closely Related Spontaneously Hypertensive Rat Strains. *Oncotarget* **2015**, *6*, 18800–18818. [CrossRef] [PubMed]

37. Wu, H.; Ye, M.; Liu, D.; Yang, J.; Ding, J.-W.; Zhang, J.; Wang, X.-A.; Dong, W.-S.; Fan, Z.-X.; Yang, J. UCP2 Protect the Heart from Myocardial Ischemia/Reperfusion Injury via Induction of Mitochondrial Autophagy. *J. Cell. Biochem.* **2019**, *120*, 15455–15466. [CrossRef]
38. González-Barroso, M.M.; Giurgea, I.; Bouillaud, F.; Anedda, A.; Bellanné-Chantelot, C.; Hubert, L.; de Keyzer, Y.; de Lonlay, P.; Ricquier, D. Mutations in UCP2 in Congenital Hyperinsulinism Reveal a Role for Regulation of Insulin Secretion. *PLoS ONE* **2008**, *3*, e3850. [CrossRef] [PubMed]
39. Zhang, C.Y.; Baffy, G.; Perret, P.; Krauss, S.; Peroni, O.; Grujic, D.; Hagen, T.; Vidal-Puig, A.J.; Boss, O.; Kim, Y.B.; et al. Uncoupling Protein-2 Negatively Regulates Insulin Secretion and Is a Major Link between Obesity, Beta Cell Dysfunction, and Type 2 Diabetes. *Cell* **2001**, *105*, 745–755. [CrossRef] [PubMed]
40. Stanzione, R.; Cotugno, M.; Forte, M.; Bianchi, F.; Marchitti, S.; Palomba, N.P.; Esposito, T.; Zanda, B.; Sanna, A.; Rubattu, S. Role of Uncoupling Protein 2 Gene Polymorphisms on the Risk of Ischemic Stroke in a Sardinian Population. *Life* **2022**, *12*, 721. [CrossRef]
41. Chan, C.B.; De Leo, D.; Joseph, J.W.; McQuaid, T.S.; Ha, X.F.; Xu, F.; Tsushima, R.G.; Pennefather, P.S.; Salapatek, A.M.; Wheeler, M.B. Increased Uncoupling Protein-2 Levels in Beta-Cells Are Associated with Impaired Glucose-Stimulated Insulin Secretion: Mechanism of Action. *Diabetes* **2001**, *50*, 1302–1310. [CrossRef] [PubMed]
42. Guilherme, A.; Virbasius, J.V.; Puri, V.; Czech, M.P. Adipocyte Dysfunctions Linking Obesity to Insulin Resistance and Type 2 Diabetes. *Nat. Rev. Mol. Cell Biol.* **2008**, *9*, 367–377. [CrossRef]
43. van Dierendonck, X.A.M.H.; Sancerni, T.; Alves-Guerra, M.-C.; Stienstra, R. The Role of Uncoupling Protein 2 in Macrophages and Its Impact on Obesity-Induced Adipose Tissue Inflammation and Insulin Resistance. *J. Biol. Chem.* **2020**, *295*, 17535–17548. [CrossRef]
44. Emre, Y.; Hurtaud, C.; Karaca, M.; Nubel, T.; Zavala, F.; Ricquier, D. Role of Uncoupling Protein UCP2 in Cell-Mediated Immunity: How Macrophage-Mediated Insulitis Is Accelerated in a Model of Autoimmune Diabetes. *Proc. Natl. Acad. Sci. USA* **2007**, *104*, 19085–19090. [CrossRef]
45. Arsenijevic, D.; Onuma, H.; Pecqueur, C.; Raimbault, S.; Manning, B.S.; Miroux, B.; Couplan, E.; Alves-Guerra, M.-C.; Goubern, M.; Surwit, R.; et al. Disruption of the Uncoupling Protein-2 Gene in Mice Reveals a Role in Immunity and Reactive Oxygen Species Production. *Nat. Genet.* **2000**, *26*, 435–439. [CrossRef]
46. Nègre-Salvayre, A.; Hirtz, C.; Carrera, G.; Cazenave, R.; Troly, M.; Salvayre, R.; Pénicaud, L.; Casteilla, L. A Role for Uncoupling Protein-2 as a Regulator of Mitochondrial Hydrogen Peroxide Generation. *FASEB J.* **1997**, *11*, 809–815. [CrossRef]
47. Zorov, D.B.; Juhaszova, M.; Sollott, S.J. Mitochondrial Reactive Oxygen Species (ROS) and ROS-Induced ROS Release. *Physiol. Rev.* **2014**, *94*, 909–950. [CrossRef]
48. Echtay, K.S.; Esteves, T.C.; Pakay, J.L.; Jekabsons, M.B.; Lambert, A.J.; Portero-Otín, M.; Pamplona, R.; Vidal-Puig, A.J.; Wang, S.; Roebuck, S.J.; et al. A Signalling Role for 4-Hydroxy-2-Nonenal in Regulation of Mitochondrial Uncoupling. *EMBO J.* **2003**, *22*, 4103–4110. [CrossRef] [PubMed]
49. Larrouy, D.; Laharrague, P.; Carrera, G.; Viguerie-Bascands, N.; Levi-Meyrueis, C.; Fleury, C.; Pecqueur, C.; Nibbelink, M.; André, M.; Casteilla, L.; et al. Kupffer Cells Are a Dominant Site of Uncoupling Protein 2 Expression in Rat Liver. *Biochem. Biophys. Res. Commun.* **1997**, *235*, 760–764. [CrossRef] [PubMed]
50. Myint, M.; Oppedisano, F.; De Giorgi, V.; Kim, B.-M.; Marincola, F.M.; Alter, H.J.; Nesci, S. Inflammatory Signaling in NASH Driven by Hepatocyte Mitochondrial Dysfunctions. *J. Transl. Med.* **2023**, *21*, 757. [CrossRef]
51. Cheung, E.C.; Vousden, K.H. The Role of ROS in Tumour Development and Progression. *Nat. Rev. Cancer* **2022**, *22*, 280–297. [CrossRef] [PubMed]
52. Nedergaard, J.; Cannon, B. The "Novel" "uncoupling" Proteins UCP2 and UCP3: What Do They Really Do? Pros and Cons for Suggested Functions. *Exp. Physiol.* **2003**, *88*, 65–84. [CrossRef] [PubMed]
53. Nesci, S. Glucose and Glutamine in the Mitochondrial Oxidative Metabolism of Stem Cells. *Mitochondrion* **2017**, *35*, 11–12. [CrossRef] [PubMed]
54. Vozza, A.; Parisi, G.; De Leonardis, F.; Lasorsa, F.M.; Castegna, A.; Amorese, D.; Marmo, R.; Calcagnile, V.M.; Palmieri, L.; Ricquier, D.; et al. UCP2 Transports C4 Metabolites out of Mitochondria, Regulating Glucose and Glutamine Oxidation. *Proc. Natl. Acad. Sci. USA* **2014**, *111*, 960–965. [CrossRef] [PubMed]
55. Chouchani, E.T.; Pell, V.R.; Gaude, E.; Aksentijević, D.; Sundier, S.Y.; Robb, E.L.; Logan, A.; Nadtochiy, S.M.; Ord, E.N.J.; Smith, A.C.; et al. Ischaemic Accumulation of Succinate Controls Reperfusion Injury through Mitochondrial ROS. *Nature* **2014**, *515*, 431–435. [CrossRef] [PubMed]
56. Chouchani, E.T.; Methner, C.; Nadtochiy, S.M.; Logan, A.; Pell, V.R.; Ding, S.; James, A.M.; Cochemé, H.M.; Reinhold, J.; Lilley, K.S.; et al. Cardioprotection by S-Nitrosation of a Cysteine Switch on Mitochondrial Complex I. *Nat. Med.* **2013**, *19*, 753–759. [CrossRef] [PubMed]
57. Wojtovich, A.P.; Smith, C.O.; Haynes, C.M.; Nehrke, K.W.; Brookes, P.S. Physiological Consequences of Complex II Inhibition for Aging, Disease, and the mKATP Channel. *Biochim. Biophys. Acta* **2013**, *1827*, 598–611. [CrossRef] [PubMed]
58. Brennan, J.P.; Southworth, R.; Medina, R.A.; Davidson, S.M.; Duchen, M.R.; Shattock, M.J. Mitochondrial Uncoupling, with Low Concentration FCCP, Induces ROS-Dependent Cardioprotection Independent of KATP Channel Activation. *Cardiovasc. Res.* **2006**, *72*, 313–321. [CrossRef]

59. Bouillaud, F.; Alves-Guerra, M.-C.; Ricquier, D. UCPs, at the Interface between Bioenergetics and Metabolism. *Biochim. Biophys. Acta* **2016**, *1863*, 2443–2456. [CrossRef]
60. Andrews, Z.B. Uncoupling Protein-2 and the Potential Link between Metabolism and Longevity. *Curr. Aging Sci.* **2010**, *3*, 102–112. [CrossRef]
61. Xian, H.; Watari, K.; Sanchez-Lopez, E.; Offenberger, J.; Onyuru, J.; Sampath, H.; Ying, W.; Hoffman, H.M.; Shadel, G.S.; Karin, M. Oxidized DNA Fragments Exit Mitochondria via mPTP- and VDAC-Dependent Channels to Activate NLRP3 Inflammasome and Interferon Signaling. *Immunity* **2022**, *55*, 1370–1385.e8. [CrossRef] [PubMed]
62. Nesci, S.; Spagnoletta, A.; Oppedisano, F. Inflammation, Mitochondria and Natural Compounds Together in the Circle of Trust. *Int. J. Mol. Sci.* **2023**, *24*, 6106. [CrossRef] [PubMed]
63. Pecqueur, C.; Alves-Guerra, M.C.; Gelly, C.; Levi-Meyrueis, C.; Couplan, E.; Collins, S.; Ricquier, D.; Bouillaud, F.; Miroux, B. Uncoupling Protein 2, in Vivo Distribution, Induction upon Oxidative Stress, and Evidence for Translational Regulation. *J. Biol. Chem.* **2001**, *276*, 8705–8712. [CrossRef] [PubMed]
64. Busquets, S.; Alvarez, B.; Van Royen, M.; Figueras, M.T.; López-Soriano, F.J.; Argilés, J.M. Increased Uncoupling Protein-2 Gene Expression in Brain of Lipopolysaccharide-Injected Mice: Role of Tumour Necrosis Factor-Alpha? *Biochim. Biophys. Acta* **2001**, *1499*, 249–256. [CrossRef] [PubMed]
65. Cortez-Pinto, H.; Yang, S.Q.; Lin, H.Z.; Costa, S.; Hwang, C.S.; Lane, M.D.; Bagby, G.; Diehl, A.M. Bacterial Lipopolysaccharide Induces Uncoupling Protein-2 Expression in Hepatocytes by a Tumor Necrosis Factor-Alpha-Dependent Mechanism. *Biochem. Biophys. Res. Commun.* **1998**, *251*, 313–319. [CrossRef] [PubMed]
66. Faggioni, R.; Shigenaga, J.; Moser, A.; Feingold, K.R.; Grunfeld, C. Induction of UCP2 Gene Expression by LPS: A Potential Mechanism for Increased Thermogenesis during Infection. *Biochem. Biophys. Res. Commun.* **1998**, *244*, 75–78. [CrossRef] [PubMed]
67. Stuart, J.A.; Harper, J.A.; Brindle, K.M.; Brand, M.D. Uncoupling Protein 2 from Carp and Zebrafish, Ectothermic Vertebrates. *Biochim. Biophys. Acta* **1999**, *1413*, 50–54. [CrossRef] [PubMed]
68. Klingenberg, M. UCP1—A Sophisticated Energy Valve. *Biochimie* **2017**, *134*, 19–27. [CrossRef] [PubMed]
69. Ruprecht, J.J.; Kunji, E.R.S. The SLC25 Mitochondrial Carrier Family: Structure and Mechanism. *Trends Biochem. Sci.* **2019**, *45*, 244–258. [CrossRef]
70. Rial, E. Retinoids Activate Proton Transport by the Uncoupling Proteins UCP1 and UCP2. *EMBO J.* **1999**, *18*, 5827–5833. [CrossRef]
71. Couplan, E.; del Mar Gonzalez-Barroso, M.; Alves-Guerra, M.C.; Ricquier, D.; Goubern, M.; Bouillaud, F. No Evidence for a Basal, Retinoic, or Superoxide-Induced Uncoupling Activity of the Uncoupling Protein 2 Present in Spleen or Lung Mitochondria. *J. Biol. Chem.* **2002**, *277*, 26268–26275. [CrossRef] [PubMed]
72. Kamer, K.J.; Mootha, V.K. The Molecular Era of the Mitochondrial Calcium Uniporter. *Nat. Rev. Mol. Cell Biol.* **2015**, *16*, 545–553. [CrossRef]
73. Koshenov, Z.; Oflaz, F.E.; Hirtl, M.; Bachkoenig, O.A.; Rost, R.; Osibow, K.; Gottschalk, B.; Madreiter-Sokolowski, C.T.; Waldeck-Weiermair, M.; Malli, R.; et al. The Contribution of Uncoupling Protein 2 to Mitochondrial Ca^{2+} Homeostasis in Health and Disease—A Short Revisit. *Mitochondrion* **2020**, *55*, 164–173. [CrossRef] [PubMed]
74. Madreiter-Sokolowski, C.T.; Klec, C.; Parichatikanond, W.; Stryeck, S.; Gottschalk, B.; Pulido, S.; Rost, R.; Eroglu, E.; Hofmann, N.A.; Bondarenko, A.I.; et al. PRMT1-Mediated Methylation of MICU1 Determines the UCP2/3 Dependency of Mitochondrial Ca^{2+} Uptake in Immortalized Cells. *Nat. Commun.* **2016**, *7*, 12897. [CrossRef] [PubMed]
75. Pecqueur, C.; Bui, T.; Gelly, C.; Hauchard, J.; Barbot, C.; Bouillaud, F.; Ricquier, D.; Miroux, B.; Thompson, C.B. Uncoupling Protein-2 Controls Proliferation by Promoting Fatty Acid Oxidation and Limiting Glycolysis-Derived Pyruvate Utilization. *FASEB J.* **2008**, *22*, 9–18. [CrossRef] [PubMed]
76. Zhang, J.; Khvorostov, I.; Hong, J.S.; Oktay, Y.; Vergnes, L.; Nuebel, E.; Wahjudi, P.N.; Setoguchi, K.; Wang, G.; Do, A.; et al. UCP2 Regulates Energy Metabolism and Differentiation Potential of Human Pluripotent Stem Cells: UCP2 Regulates hPSC Metabolism and Differentiation. *EMBO J.* **2011**, *30*, 4860–4873. [CrossRef] [PubMed]
77. De Souza, C.T.; Araújo, E.P.; Stoppiglia, L.F.; Pauli, J.R.; Ropelle, E.; Rocco, S.A.; Marin, R.M.; Franchini, K.G.; Carvalheira, J.B.; Saad, M.J.; et al. Inhibition of UCP2 Expression Reverses Diet-Induced Diabetes Mellitus by Effects on Both Insulin Secretion and Action. *FASEB J.* **2007**, *21*, 1153–1163. [CrossRef]
78. DeBerardinis, R.J.; Mancuso, A.; Daikhin, E.; Nissim, I.; Yudkoff, M.; Wehrli, S.; Thompson, C.B. Beyond Aerobic Glycolysis: Transformed Cells Can Engage in Glutamine Metabolism That Exceeds the Requirement for Protein and Nucleotide Synthesis. *Proc. Natl. Acad. Sci. USA* **2007**, *104*, 19345–19350. [CrossRef]
79. Hurtaud, C.; Gelly, C.; Chen, Z.; Lévi-Meyrueis, C.; Bouillaud, F. Glutamine Stimulates Translation of Uncoupling Protein 2mRNA. *Cell. Mol. Life Sci.* **2007**, *64*, 1853–1860. [CrossRef] [PubMed]
80. Pecqueur, C.; Alves-Guerra, C.; Ricquier, D.; Bouillaud, F. UCP2, a Metabolic Sensor Coupling Glucose Oxidation to Mitochondrial Metabolism? *IUBMB Life* **2009**, *61*, 762–767. [CrossRef]
81. Hirose, M.; Schilf, P.; Lange, F.; Mayer, J.; Reichart, G.; Maity, P.; Jöhren, O.; Schwaninger, M.; Scharffetter-Kochanek, K.; Sina, C.; et al. Uncoupling Protein 2 Protects Mice from Aging. *Mitochondrion* **2016**, *30*, 42–50. [CrossRef] [PubMed]
82. Zhang, Y.; Mi, S.-L.; Hu, N.; Doser, T.A.; Sun, A.; Ge, J.; Ren, J. Mitochondrial Aldehyde Dehydrogenase 2 Accentuates Aging-Induced Cardiac Remodeling and Contractile Dysfunction: Role of AMPK, Sirt1, and Mitochondrial Function. *Free Radic. Biol. Med.* **2014**, *71*, 208–220. [CrossRef]

83. Kurian, J.; Yuko, A.E.; Kasatkin, N.; Rigaud, V.O.C.; Busch, K.; Harlamova, D.; Wagner, M.; Recchia, F.A.; Wang, H.; Mohsin, S.; et al. Uncoupling Protein 2-Mediated Metabolic Adaptations Define Cardiac Cell Function in the Heart during Transition from Young to Old Age. *Stem Cells Transl. Med.* **2021**, *10*, 144–156. [CrossRef]
84. Rigaud, V.O.; Zarka, C.; Kurian, J.; Harlamova, D.; Elia, A.; Kasatkin, N.; Johnson, J.; Behanan, M.; Kraus, L.; Pepper, H.; et al. UCP2 Modulates Cardiomyocyte Cell Cycle Activity, Acetyl-CoA, and Histone Acetylation in Response to Moderate Hypoxia. *JCI Insight* **2022**, *7*, e155475. [CrossRef]
85. Mattiasson, G.; Shamloo, M.; Gido, G.; Mathi, K.; Tomasevic, G.; Yi, S.; Warden, C.H.; Castilho, R.F.; Melcher, T.; Gonzalez-Zulueta, M.; et al. Uncoupling Protein-2 Prevents Neuronal Death and Diminishes Brain Dysfunction after Stroke and Brain Trauma. *Nat. Med.* **2003**, *9*, 1062–1068. [CrossRef] [PubMed]
86. Rubattu, S.; Stanzione, R.; Bianchi, F.; Cotugno, M.; Forte, M.; Della Ragione, F.; Fioriniello, S.; D'Esposito, M.; Marchitti, S.; Madonna, M.; et al. Reduced Brain UCP2 Expression Mediated by microRNA-503 Contributes to Increased Stroke Susceptibility in the High-Salt Fed Stroke-Prone Spontaneously Hypertensive Rat. *Cell Death Dis.* **2017**, *8*, e2891. [CrossRef]
87. Forte, M.; Bianchi, F.; Cotugno, M.; Marchitti, S.; Stanzione, R.; Maglione, V.; Sciarretta, S.; Valenti, V.; Carnevale, R.; Versaci, F.; et al. An Interplay between UCP2 and ROS Protects Cells from High-Salt-Induced Injury through Autophagy Stimulation. *Cell Death Dis.* **2021**, *12*, 919. [CrossRef] [PubMed]
88. Nakase, T.; Yoshida, Y.; Nagata, K. Amplified Expression of Uncoupling Proteins in Human Brain Ischemic Lesions. *Neuropathology* **2007**, *27*, 442–447. [CrossRef] [PubMed]
89. Anello, M.; Spampinato, D.; Piro, S.; Purrello, F.; Rabuazzo, A.M. Glucosamine-Induced Alterations of Mitochondrial Function in Pancreatic Beta-Cells: Possible Role of Protein Glycosylation. *Am. J. Physiol. Endocrinol. Metab.* **2004**, *287*, E602–E608. [CrossRef]
90. Sun, K.; Chen, Y.; Zheng, S.; Wan, W.; Hu, K. Genipin Ameliorates Diabetic Retinopathy via the HIF-1α and AGEs-RAGE Pathways. *Phytomedicine* **2024**, *129*, 155596. [CrossRef]
91. Ruiz-Ramírez, A.; Chávez-Salgado, M.; Peñeda-Flores, J.A.; Zapata, E.; Masso, F.; El-Hafidi, M. High-Sucrose Diet Increases ROS Generation, FFA Accumulation, UCP2 Level, and Proton Leak in Liver Mitochondria. *Am. J. Physiol. Endocrinol. Metab.* **2011**, *301*, E1198–E1207. [CrossRef] [PubMed]
92. Wei, D.; Zheng, N.; Zheng, L.; Wang, L.; Song, L.; Sun, L. Shexiang Baoxin Pill Corrects Metabolic Disorders in a Rat Model of Metabolic Syndrome by Targeting Mitochondria. *Front. Pharmacol.* **2018**, *9*, 137. [CrossRef] [PubMed]
93. Li, J.; Jiang, R.; Cong, X.; Zhao, Y. UCP2 Gene Polymorphisms in Obesity and Diabetes, and the Role of UCP2 in Cancer. *FEBS Lett.* **2019**, *593*, 2525–2534. [CrossRef] [PubMed]

Disclaimer/Publisher's Note: The statements, opinions and data contained in all publications are solely those of the individual author(s) and contributor(s) and not of MDPI and/or the editor(s). MDPI and/or the editor(s) disclaim responsibility for any injury to people or property resulting from any ideas, methods, instructions or products referred to in the content.

biomedicines

MDPI

Article

Visualization of Atherosclerotic Plaques Paired with Joheksol 350 (Omnipaque)

Piotr Wańczura [1,*], Wiktoria Mytych [2], Dorota Bartusik-Aebisher [3], Dawid Leksa [4], Adrian Truszkiewicz [5] and David Aebisher [5,*]

[1] Department of Cardiology, Medical College of Sciences, The Rzeszów University, 35-310 Rzeszów, Poland
[2] English Division Science Club, Medical College, The Rzeszów University, 35-310 Rzeszów, Poland; wiktoriamytych@gmail.com
[3] Department of Biochemistry and General Chemistry, Medical College, The Rzeszów University, 35-310 Rzeszów, Poland; dbartusikaebisher@ur.edu.pl
[4] Rzeszów Center for Vascular and Endovascular Surgery, 35-310 Rzeszów, Poland; dleksa@gmail.com
[5] Department of Photomedicine and Physical Chemistry, Medical College, The Rzeszów University, 35-310 Rzeszów, Poland; atruszkiewicz@ur.edu.pl
* Correspondence: p.wanczura@poczta.fm (P.W.); daebisher@ur.edu.pl (D.A.)

Abstract: Background: Cardiovascular disease is one of the leading causes of death around the globe. Atherosclerosis, a chronic inflammatory blood vessel disease that takes years to develop, is its primary cause. Instability and further plaque buildup are caused by chronic inflammation, which creates the conditions for possible rupture. The visualization of arterial lesions in situ can enhance understanding of atherosclerosis progression and potentially improve experimental therapies. Conventional histology methods for assessing atherosclerotic lesions are robust but are destructive and may prevent further tissue analysis. **Objectives:** The objective of the current study was to evaluate a novel, nondestructive method for the visualization and characterization of atherosclerotic lesions. **Methods and Results:** Thus, we tested the hypothesis that MRI paired with an iodine-based radiopaque stain would effectively characterize atherosclerotic plaques in a manner comparable to routine histology while maintaining sample integrity and providing whole-volume data.

Keywords: visualization; atherosclerotic plaques; MRI; iodine; atherosclerosis

1. Introduction

One of the leading causes of death around the globe is cardiovascular disease. Atherosclerosis, a chronic inflammatory blood artery disease that takes years to develop, is its primary cause [1,2]. It can be asymptomatic at first, which can make identification challenging [3]. Atherosclerosis causes the artery lumen to narrow as it advances, raising the risk of heart attacks, strokes, and other severe health issues. A stroke is a medical emergency in which the brain's blood supply is cut off, leading to damage or death of brain cells. Fatty deposits in the arteries can cause atherosclerosis, which narrows or stops blood flow. This may cause the brain to receive less oxygen, which could lead to a stroke [4]. Furthermore, although it was often believed to be a disease that only affected the elderly, younger individuals are increasingly becoming affected as well [5]. Approximately 80% of deadly coronary thromboses are caused by ruptured atherosclerotic plaques. Men are more frequently impacted than women. It has been proposed that the disease develops because of both environmental and genetic causes [6,7]. Atherosclerosis is characterized by the development of so-called atherosclerotic plaques in the artery walls. Over time, this process leads to structural alterations that obstruct blood flow [8]. Hypertension,

diabetes, hypercholesterolemia, obesity, and smoking are important contributors to the development of atherosclerotic plaques. Environmental pollution, sleep problems, and physical inactivity also have an impact on the development of atherosclerotic lesions [9–11]. In its 2022 statement, the European Atherosclerosis Society noted that elevated levels of lipoprotein(a) are particularly significant in the development of atherosclerosis and have been found to be a contributing factor to the disease [12]. Extensive studies have been conducted for many years to determine the precise mechanism of atherosclerotic lesions or the pathophysiology of atherosclerosis [13]. The alterations that lead to the development of plaques start with the inflammatory process. Fatty and fibrous debris is deposited in the artery walls because of an interaction between risk factors and arterial wall cells [14,15]. Lesions develop and vessel walls harden over time, which can totally stop blood flow [16]. Both invasive and non-invasive techniques are used to diagnose atherosclerosis to gauge the disease's severity and potential for consequences. Computed tomography (CT), nuclear scanning, magnetic resonance imaging (MRI), blood biomarkers, and stress tests to measure coronary blood flow are examples of non-invasive diagnostics [17,18]. For several reasons, investigating T_1 and T_2 relaxation times in atherosclerosis is novel and highlights their potential as predictive and diagnostic instruments in cardiovascular disease. Researchers can now obtain far more specific information regarding tissue composition thanks to recent developments in MRI techniques (Figure 1), sophisticated pulse sequences, and enhanced spatial and temporal resolution [19]. These developments make it possible to measure the T_1 and T_2 relaxation durations in plaques and the arterial wall with greater sensitivity and accuracy. To evaluate the microstructural heterogeneity of atherosclerotic plaques and correlate changes in relaxation time with underlying tissue properties like inflammation, calcification, or lipid content, high-resolution imaging is very important [20,21]. Current research is starting to concentrate on the relationship between plaque components and T_1 and T_2 relaxation times. Researchers are starting to create more accurate non-invasive methods to evaluate plaque vulnerability by linking T_1 and T_2 times to certain plaque components. This could help detect plaques at risk of rupture before clinical events take place. The non-invasive visualization of atherosclerotic plaques and their components has become a cornerstone of modern cardiovascular medicine. However, imaging soft tissues, especially the vascular walls and atherosclerotic lesions, can be challenging due to the inherent low contrast between soft tissues. In this context, optical coherence tomography (OCT) offers a promising alternative to traditional imaging modalities, providing high-resolution, cross-sectional images of arterial structures without the need for extensive contrast agents or staining procedures [22–25]. OCT operates based on light scattering rather than radiation, enabling it to provide detailed tissue analysis at the microscopic level and making it an invaluable tool in the assessment of atherosclerosis. In the context of atherosclerosis, OCT has proven particularly useful in imaging the arterial wall and the components of atherosclerotic plaques, such as fibrous tissue, lipid cores, calcifications, and the fibrous cap [26–28]. Unlike CT, OCT offers much higher resolution, typically in the range of 10–20 microns, allowing for precise imaging of plaque morphology, a key factor in determining plaque stability and the risk of rupture [29,30]. However, OCT also faces some limitations, particularly in its ability to visualize deep tissue structures and certain plaque components. The primary challenge with OCT lies in the low intrinsic contrast of soft tissues, like the issues encountered in CT imaging [31,32]. While OCT is excellent for visualizing the microstructure of the vessel wall, it can struggle to distinguish different soft tissue components within the plaque. To overcome this limitation, OCT may utilize contrast agents that enhance the visibility of specific tissue structures, providing additional information about plaque composition and vulnerability [33,34]. Optical coherence tomography contrasts differ from those used in CT or MRI, as they often involve the use

of exogenous agents designed to enhance tissue contrast through scattering rather than relying on density differences as in radiographic imaging. Several types of contrast agents have been developed specifically for OCT [35,36]. Fluorescent and micron-sized particles are often designed to target specific plaque components, such as macrophages, to identify regions of inflammation. For example, fluorescent nanoparticles that bind to inflammatory markers in the plaque can provide detailed insights into the cellular composition of the lesion [37,38]. Intravenous dye-based agents, such as indocyanine green (ICG), are sometimes used in OCT to enhance the imaging of endothelial cells and blood vessels. Although these dyes are more commonly used in ophthalmic OCT, their potential in cardiovascular imaging is still under exploration [39,40]. The use of molecularly targeted contrast agents that specifically bind to atherosclerotic plaques is an emerging field. These agents could enhance the detection of vulnerable plaques by targeting macrophages or oxidized LDL, which are markers associated with inflammation and plaque instability [41]. The advantage of using contrast agents in OCT is their ability to enhance the contrast of specific tissue types, such as the fibrous cap or lipid-rich necrotic core, improving the accuracy of plaque characterization. This approach helps distinguish between stable and unstable plaques, which is critical for risk stratification in patients with coronary artery disease [42,43]. OCT offers detailed imaging of atherosclerotic plaques, revealing key structural features that contribute to plaque stability. The ability to assess these features in real time is crucial for identifying plaques that may be at risk of rupture and subsequent thrombotic events [44]. The fibrous cap is the outer layer of an atherosclerotic plaque and plays a crucial role in determining plaque stability. A thin or ruptured fibrous cap is a hallmark of vulnerable plaques, which are more likely to rupture and cause an acute coronary event [45,46]. OCT allows for the precise measurement of fibrous cap thickness and the assessment of its integrity, making it one of the most important features in plaque vulnerability assessment [47]. The lipid-rich necrotic core is another important component of atherosclerotic plaques, and its size and composition can influence plaque stability. On OCT, the lipid core typically appears as a hypointense region (dark area), while the fibrous cap appears hyperintense (bright). Changes in the size or composition of the lipid core can be indicative of plaque progression or destabilization [48–50]. OCT is also capable of visualizing calcifications, which are often present in advanced stages of atherosclerosis. These calcified areas appear as bright spots on OCT images due to their high scattering properties. Calcifications are important for assessing plaque stability, as they may contribute to plaque rigidity and reduce the likelihood of rupture [51].



Figure 1. An example of MRI equipment for setup of atherosclerosis plaque imaging.

The current study set out to assess a new, nondestructive technique for atherosclerotic lesion MR imaging with Omnipaque 350; we also present the optical coherence tomography results.

2. Materials and Methods

2.1. Materials

During experiments presented in this paper, all samples were placed in Eppendorf® 0030 000.919 tubes (Sigma Aldrich, Warsaw, Poland). We used Joheksol 350 (Omnipaque 350 mg I/mL) produced by General Electric HealthCare (Munchen, Germany). For the preparation of a suitable concentration of Omnipaque solution, we used the AquaB Duo reverse osmosis system manufactured by Fresenius Medical Care in Singapore. Shortly after samples were collected, MRI acquisition experiments were performed with a 1.5 Tesla OPTIMA 360MR manufactured by General Electric HealthCare Munchen, manufactured in Munchen, Germany. In this research, we used a balance from Ohaus PX224 (Geifensee, Switzerland). The room temperature during all performed experiments was 18 °C.

2.2. Methods

2.2.1. Plaque Tissue Sample Preparation for MRI Measurement

Tissue samples of arteries with atherosclerotic lesions were collected by endarterectomies from 7 patients (5 male and 2 female). Patients qualified for endarterectomy were in the age range of 69–81 years and had experienced an episode of ischemic stroke. The inclusion criteria for the study plaque analysis were a history of ischemic stroke due to critical carotid artery stenosis and qualification for surgical treatment by endarterectomy. The exclusion criteria were the following: other than normal sinus rhythm, for example, history of atrial fibrillation/flutter as a possible reason for ischemic stroke, and qualification for other than a surgical way of carotid artery stenosis treatment. The significance of carotid artery stenosis must have been confirmed by angio CT (computed tomography). Samples were excised from the carotid artery, which had previously been image-diagnosed and finally qualified for removal. All bioethical consents presented in this research were performed according to Bioethical Certificate no 43/2024/B issued by the Bioethics Committee of the Rzeszow Regional Medical Chamber.

Fourteen samples (two from one patient; the number of patients was seven) were evaluated. Only plaques from patients undergoing surgical endarterectomies due to ischemic stroke were qualified for further assessment (Table 1). The history of supraventricular arrythmias as atrial fibrillations and low ejection fraction due to myocardial infarction were excluded from the study pool in order to concentrate only on ischemic stroke due to significant/critical carotid artery stenosis. The history of ischemic stroke must have been confirmed based on available medical records, including CT scan assessments. The diagnostic tool was the Philips AFFINITI 50 ultrasound machine with a C6-2, S4-2, L12-4 transducer. The patients were operated on at the Department of Vascular Surgery of the Polish-American Heart Clinics PAKS IX in Rzeszów. Each patient was informed in detail about ischemic stroke resulting from carotid artery stenosis. All patients were informed about both the benefits and complications associated with the procedure, to which they gave written consent. Patients included in the study were all Caucasians. All patients were diagnosed with hemodynamically significant stenosis of the right or left carotid artery. Before the procedure, patients received acetylsalicylic acid and statins according to the recommendations for endarterectomy procedures.

The collected samples were placed in test tubes with physiological saline, which were then subjected to in vitro testing. The samples were measured with and without the Omnipaque 350 contrast. Omnipaque 350 was administrated according to the procedure

below. The collected atherosclerotic lesions had weights of 0.2354 g, 0.4393 g, 0.2747 g, 0.412 g, 0.3368 g, 0.1991 g, 0.5710 g, 0.442 g, 0.312 g, 0.389 g, 0.258 g, 0.483 g, 0.294 g, and 0.304 g. The samples (Figure 2) were measured by Ohaus PX224 (Geifensee, Switzerland).

Table 1. Study group characteristics.

Disease or Case	n/N (%)
Age, year (mean, range)	76 (69–81)
Male/female gender	5/2
Cardiovascular risk factors	
Hypertension	7/7 (100%)
Diabetes mellitus	5/7 (71.4%)
Dyslipidemia	7/7 (100%)
Smoking history	5/7 (71.4%)
Chronic kidney disease	3/7 (42.8%)
Cardiovascular comorbidities	
Previous myocardial infarction	2/7 (28.6%)
Previous percutaneous coronary intervention	5/7 (71.4%)
Previous coronary artery bypass surgery	1/7 (14.3%)
History of stroke	7/7 (100%)
Normal sinus rythm	7/7 (100%)
Medications	
Statin	7/7 (100%)
Beta-blocker (B-blocker)	6/7 (85.7%)
Aspirin (ASA)	7/7 (100%)
Clopidogrel	2/7 (28.6%)
ACE inhibitors (ACE-i)	5/7 (71.4%)
Angiotensin II receptor blockers (ARB)	1/7 (14.3%)
SGLT2 inhibitors (Flozin)	2/7 (28.6%)

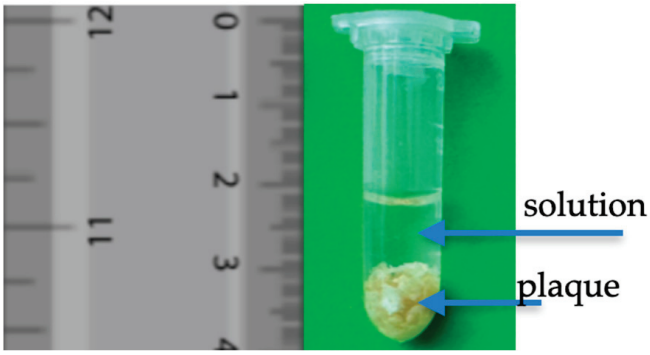


Figure 2. An example of the setup of an atherosclerosis plaque in an Eppendorf tube in a 1.6 mL solution.

In brief, a concentration of 4 µL Omnipaque 350 mg I/mL manufactured by General Electric HealthCare (Munchen, Germany) (Figure 3) was applied to the atherosclerotic plaques. From the predecessor's protocol, the preferred in vivo dose in humans for the external carotid artery is 6–9 mL, and for the internal carotid artery is 8–10 mL. Omnipaque 350 contrast was added to the test samples to study the possible absorption of Omnipaque 350 and its possible visible effect on T_1 and T_2 relaxation times. A 24 h incubation time was used to allow Omnipaque 350 contrast to penetrate and accumulate. Extended incubation allows iodine molecules to perfuse the atherosclerotic plaque and enhance better signal intensity on MRI images, allowing a more detailed visualization of the plaque. The concentration used in the study was calculated from a clinical dose provided by the contrast manufacturer, as mentioned above. Samples were immersed in 1.6 mL of distilled water + 4 µL of Omnipaque 350. In our laboratory, water for the preparation of stock solutions from commercially obtained

Omnipaque 350 was purified using an AquaB Duo reverse osmosis system from Fresenius Medical Care, Singapore.

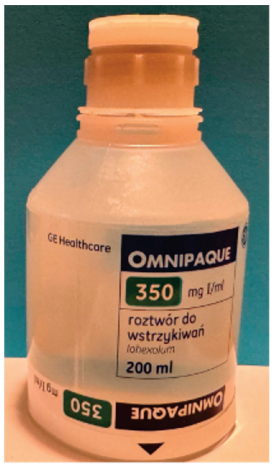


Figure 3. Joheksol 350 (Omnipaque 350 mg I/mL) manufactured by General Electric HealthCare (Munchen, Germany) [52].

2.2.2. MRI Examination

The samples were left in Omnipaque 350 mg I/mL solution for 24 h at room temperature. After 24 h, the samples were subjected to magnetic resonance imaging (MRI). The study was designed to determine longitudinal (T_1) and transverse (T_2) relaxation times. It was performed using a clinical magnetic resonance system—OPTIMA 360M R prod. GEHC (Milwaukee, WI, USA) (Figure 4). The system used for the study had a 1.5T superconducting magnet. The device used software version SV23. For the test, a coil was used that allowed for flexibility, allowing it to better fit the test items, which are the test tubes used. This approach allowed the imaging capabilities of the system to be maximized. The study was performed using standard echo sequences. As a result of image acquisition, material was obtained for further processing, because of which the numerical values of T_1 and T_2 times and the distribution of these times in the test space were obtained. In addition, the distribution of the R2 coefficient was obtained, which illustrates the accuracy of fitting the approximating exponential function to the numerical data.



Figure 4. MR imaging.

By progressively increasing the duration, the repetition time-TR was evaluated for the T_1 measurements in the 50–15,000 ms range. In all, twelve trials were conducted. From the following range of values—all measured in milliseconds—the TR time value was

progressively chosen: 50; 100; 200; 300; 500; 1000; 1500; 2000; 3000; 5000; 10,000; and 15,000. Every stage of the MRI examination was conducted using the same technical settings. The field of view (FOV) was 6 cm × 6 cm, the scan matrix was 256 × 256 pixels, the section thickness was 1 mm, the spacing was 0.5 mm, and NEX = 2. Three milliseconds was the constant echo-TE time. The MR images of the tested samples and their parameters were obtained by manipulating the TR-time settings to obtain the fast spin-echo (FSE) sequence. SNR is increased and examination time is decreased with fast spin-echo (FSE) imaging. The following steps made up the test protocol for figuring out the T_1 relaxation time: system calibration; recognition sequence, which involves finding an object in three planes (frontal, sagittal, transverse, and 3-plane); and coronal sequence (T_1) of the fast spin-echo—FSE (with varying repetition time-TR) values. Various spin-echo (TE) periods were employed to measure the relaxation time T_2. With the same scanning parameters, 12 steps with varying TE times (from 1 ms to 250 ms) were employed. The echo time ranged from 11.8 to 300 ms (11.8, 20, 42, 68, 85, 102, 130, 160, 200, 230, and 250 ms), but the repetition time remained constant at 10,000 ms. The repetition time in this setup remained constant at 15 × 103 ms. The T_2 FSE frontal sequence, not the T_1 FSE, was the third stage in the measurement process, whereas the subsequent phases were the same as for the T_1 relaxation time (system calibration and recognition sequence). Both pre-Omnipaque 350 and post-Omnipaque 350 tissues underwent MR scanning. A signal intensity versus time curve fitting model might then be used to calculate the T_1 values pixel-by-pixel. A signal intensity versus echo time curve fitting mode might then be used to calculate the T_2 values pixel-by-pixel.

2.2.3. Optical Coherence Tomography

Intravascular optical coherence tomography allows for the accurate analysis of the composition of atherosclerotic plaque in individual sections. The study involves spiral scanning of a vessel with a beam of homogeneous light with a wavelength corresponding to near-infrared and analyzing the spectrum of the reflected light. Since the frequency of electromagnetic waves is many times higher than that of ultrasound, the resolution of images generated by this technique is also much higher. The smallest element identified as a single point is only 10 μm in size, which is sufficient for the precise imaging of atherosclerotic plaques, including the measurement of the thickness of the surface fibrous layer. OCT allows for a vivid view of the atherosclerotic plaque and the identification of unstable lesions.

2.2.4. Statistical Analysis

For each sample of atherosclerotic plaque used in this study, a two-way ANOVA test was performed to test for the simultaneous effects of time after treatment on the outcome variables. Statistical significance was defined as $p < 0.05$. All MRI data are reported as mean ± SD. The data were analyzed using Statistica 13.1 software (StatSoft Polska Sp.z o.o., Krakow, Poland).

3. Results

Table 1 presents the characteristics of the study group. The number of cases (n) and total number of patients (N) are provided for each category.

3.1. MRI Results

In this study, we analyzed the effect of Omnipaque 350 administration on the T_1 and T_2 relaxation times of human atherosclerotic plaques, with a particular focus on the alterations in the spatial distribution and concentration of the contrast agent within the plaques. The average T_1 and T_2 relaxation times for each experimental step are summarized in Table 2, which serves as a basis for understanding the dynamics of water content and Omnipaque

350 distribution within the plaques. Figure 5 illustrates typical T_1 and T_2 relaxation time distributions in human plaques, obtained before and 48 h after the administration of Omnipaque 350, respectively.

Table 2. The average of T_1 and T_2 relaxation times on each step of the experiment: before Omnipaque 350 implementation and 1 h and 48 h after Omnipaque 350 implementation. Significant variables p-value < 0.05 are highlighted with a star *.

Mean ± SD		
Relaxation Time	**T_1 [ms]**	**T_2 [ms]**
Before Omnipaque 350 implementation	1231 ± 12 *	63 ± 23 *
1 h after	673 ± 24 *	45 ± 6 *
48 h after	460 ± 45 *	33 ± 4 *

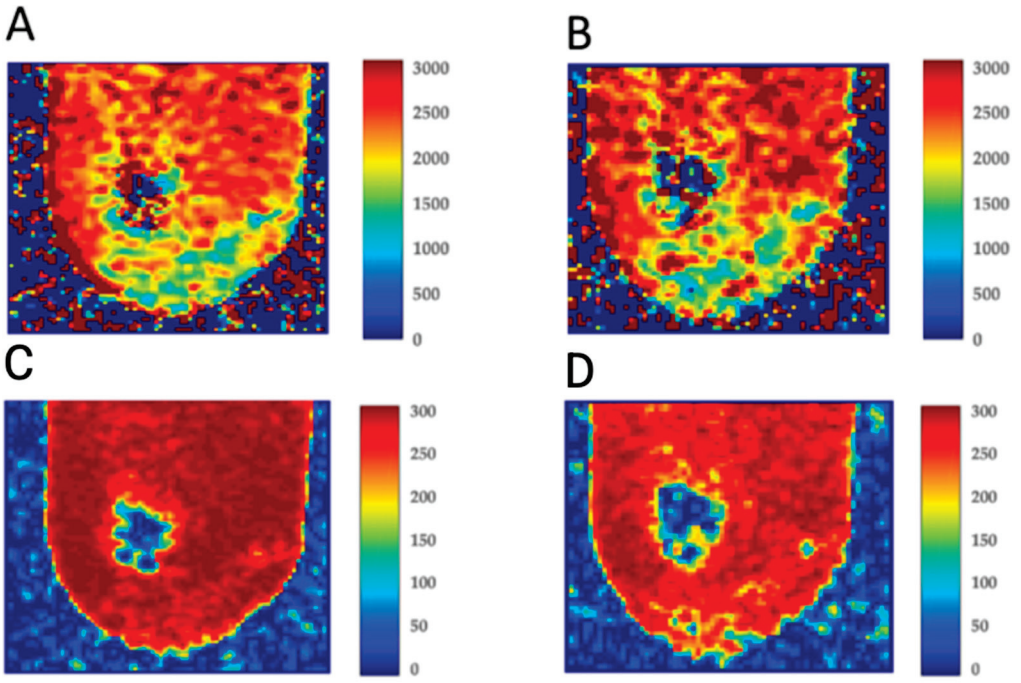


Figure 5. T_1 and T_2 distribution in human plaques. (**A**) T_1 before Omnipaque 350 administration; (**B**) T_1 48 h after Omnipaque 350 administration; (**C**) T_2 before Omnipaque 350 administration; (**D**) T_2 48 h after Omnipaque 350 administration.

The qualitative differences in T_1 and T_2 values highlight the impact of Omnipaque 350 on the biochemical and biophysical properties of atherosclerotic plaques. Specifically, the MRI data indicate that the distribution of the contrast agent in plaques alters both T_1 and T_2 relaxation times, reflecting significant changes in the tissue's water content and the presence of the contrast agent. Before contrast administration, the plaques exhibited higher T_1 and T_2 values, indicative of higher water content and less restricted molecular motion. This is consistent with the characteristics of atherosclerotic plaques, which typically contain substantial amounts of water in their extracellular matrix. Following the administration of Omnipaque 350, significant changes in both T_1 and T_2 relaxation times were observed, which can be attributed to the higher concentration of Omnipaque 350 within the plaques. The contrast agent's presence is known to affect proton relaxation, primarily by altering the local magnetic field interactions in water molecules, leading to faster relaxation times in the presence of Omnipaque. As expected, following the equilibration period of 48 h, the Omnipaque 350 concentration within the plaques was notably higher, as evidenced by the marked reduction in T_1 and T_2 relaxation times when compared to pre-contrast

values. The spatial distribution of Omnipaque 350 within the plaques was further assessed, revealing a distinct pattern. In regions with higher Omnipaque 350 accumulation, there was a corresponding decrease in T_1 and T_2 relaxation times, suggesting a localized reduction in water content and an increase in the concentration of the contrast agent. This finding is consistent with the known behavior of contrast agents in biological tissues, where their presence often leads to a reduction in water proton relaxation times due to their paramagnetic properties. Interestingly, the plaques demonstrated a more heterogeneous distribution of Omnipaque 350 after 48 h, with some areas showing significantly lower relaxation times than others. This heterogeneity could be indicative of varying degrees of plaque composition, such as lipid content, fibrous tissue, and necrotic core, all of which can influence the way contrast agents distribute within the plaque. The altered relaxation times are reflective of changes in the molecular environment within the plaques, where areas with higher concentrations of Omnipaque 350 tend to show faster relaxation times, and areas with higher water content, which retain less contrast agent, exhibit slower relaxation times. Both T_1 and T_2 relaxation times provide valuable insights into the tissue composition, especially regarding water content (Table 3). Longer T_1 and T_2 times are generally associated with higher water content and less restricted molecular motion, whereas shorter times indicate a lower water content and more restricted motion, often due to the presence of macromolecules or contrast agents like Omnipaque 350. The significantly longer T_1 and T_2 relaxation times observed in the control plaques suggest that they retained a higher water content compared to the treated plaques, which had absorbed the contrast agent and exhibited a reduction in water content as a result. This decrease in relaxation times following Omnipaque 350 administration is likely due to the contrast agent's effect on the plaques' structural and chemical composition. The presence of Omnipaque 350 leads to a reduction in the molecular freedom of water molecules within the plaque, which is reflected in the shortened T_1 and T_2 values. These changes are important because they offer insight into the potential of contrast agents like Omnipaque 350 to influence plaque characteristics, which may have implications for both diagnostic and therapeutic strategies in cardiovascular disease. The results of this study underscore the sensitivity of T_1 and T_2 relaxation times to changes in plaque composition and the distribution of contrast agents. The marked reductions in T_1 and T_2 times following Omnipaque 350 administration provide compelling evidence of its uptake by atherosclerotic plaques, resulting in a decrease in water content and an alteration in tissue characteristics. These findings have significant implications for the non-invasive imaging of atherosclerotic plaques, as changes in MRI-derived parameters such as T_1 and T_2 relaxation times can serve as biomarkers for plaque composition and the effectiveness of contrast agents in enhancing plaque visualization. Future studies may further investigate the relationship between these MRI parameters and the histopathological features of plaques, as well as explore the potential of Omnipaque 350 and other contrast agents in monitoring plaque stability and the risk of rupture.

Table 3. Values of T_1 and T_2 relaxation times of Atherosclerotic Plaque Samples. Significant variables p-value < 0.05 are highlighted with a star *.

Atherosclerotic Plaque Samples (n = 14) Before Omnipaque 350 Implementation			**Atherosclerotic Plaque Samples (n = 14) 1 h After Omnipaque 350 Implementation**		**Atherosclerotic Plaque Samples (n = 14) 24 h After Omnipaque 350 Implementation**	
No.	**T_1 [ms]**	**T_2 [ms]**	**T_1 [ms]**	**T_2 [ms]**	**T_1 [ms]**	**T_2 [ms]**
1	1163	58	674	45	461	33
2	1271	54	675	47	455	32
3	989	76	679	43	472	28

Table 3. *Cont.*

Atherosclerotic Plaque Samples (n = 14) Before Omnipaque 350 Implementation			Atherosclerotic Plaque Samples (n = 14) 1 h After Omnipaque 350 Implementation		Atherosclerotic Plaque Samples (n = 14) 24 h After Omnipaque 350 Implementation	
No.	**T_1 [ms]**	**T_2 [ms]**	**T_1 [ms]**	**T_2 [ms]**	**T_1 [ms]**	**T_2 [ms]**
4	1234	79	585	45	467	31
5	1263	67	684	47	460	29
6	1370	68	673	51	467	35
7	1191	45	677	43	457	28
8	1278	67	679	40	467	35
9	1324	64	698	44	435	38
10	1297	65	701	45	460	45
11	1298	67	785	45	474	27
12	1341	57	654	41	449	33
13	989	56	658	48	469	34
14	1239	64	662	47	464	34
Mean ± SD	1231 ± 12 *	63 ± 23 *	673 ± 24 *	45 ± 6 *	460 ± 45 *	33 ± 4 *

In this study, we observed significant differences in the median T_1 and T_2 relaxation times of plaques before and after the administration of Omnipaque 350, a contrast agent. Our findings indicate that Omnipaque 350 influences the relaxation times in a manner that is dependent on its penetration depth in the plaque. In human plaques, both T_1 and T_2 relaxation times typically decreased as the contrast agent infiltrated deeper into the plaque. These changes reflect underlying alterations in the plaque's biochemical composition. The reduction in relaxation times suggests that Omnipaque 350 may be altering the water content, the tissue microstructure, or the molecular environment within the plaque, which, in turn, could modify the signal intensity observed on MRI scans. A key observation from this study was the discrepancy between T_1 and T_2 relaxation times measured at two different time points: 1 h and 48 h post-Omnipaque 350 administration. This temporal variation in the relaxation times may reflect ongoing physiological processes, such as the redistribution or washout of the contrast agent, or more complex tissue responses to contrast medium infiltration. These differences are not simply technical or artifact-driven but are statistically significant, indicating that they likely represent true biochemical differences within the plaque tissue. The contrasting patterns observed between T_1 and T_2 values could also suggest differential effects of Omnipaque 350 on the plaque's lipid-rich core versus the fibrous cap, highlighting the heterogeneous nature of plaque structure and its response to contrast enhancement. Furthermore, the changes in T_1 and T_2 relaxation times that we observed are not merely an artifact of contrast administration but are indicative of alterations in the fundamental tissue properties of human plaques. This suggests that MRI, when combined with contrast agents like Omnipaque 350, can provide a more detailed and nuanced characterization of plaque composition, structure, and stability. Such information is critical for assessing the risk of plaque rupture, which is a major cause of acute cardiovascular events. The ability to non-invasively monitor plaque progression and composition using MRI could thus have significant implications for clinical practice, aiding in the risk stratification of patients with atherosclerosis and potentially guiding therapeutic decisions. Our results encourage further investigation into the use of MRI, with particular attention to contrast agents like Omnipaque 350, in the assessment of human plaques. Future studies should explore the relationship between T_1 and T_2 relaxation times

and the specific histopathological features of plaques to better understand the underlying mechanisms driving plaque vulnerability. Additionally, a more comprehensive study design that incorporates a larger cohort of patients and a longer follow-up period would help validate the clinical utility of MRI as a tool for monitoring plaque stability and progression in atherosclerotic disease.

3.2. Imaging of Coronary Artery In Vivo

To investigate the changes in the left main coronary artery (LMCA) during coronary angioplasty, optical coherence tomography (OCT) technology was used to capture detailed imaging at various stages of treatment. The imaging process is illustrated in Figure 6. Left main before treatment (Figure 6A): this image shows the left main coronary artery before any interventions, with no measurements provided. The OCT probe is centered in the middle, surrounded by the initial segment of the left coronary artery. In the upper section of the image, a transverse view is presented, while the lower section shows a longitudinal view of the artery. Left main with measurements (Figure 6B): a marked stenosis is present in the left main coronary artery, with a yellow outline highlighting the artery's borders. The minimal lumen area (MLA) is measured at 1.4–3.5 mm^2, indicating the presence of significant narrowing. Left main after intracoronary lithotripsy without measurements (Figure 6C): the image immediately after intracoronary lithotripsy therapy, showing a noticeable increase in the minimum lumen area to 5.2 mm^2. This demonstrates the successful expansion of the artery following the procedure. Left main after intracoronary lithotripsy with measurements (Figure 6D): after lithotripsy, the image shows the calcium deposits within the artery. The deposits are clearly fragmented, indicating successful microfracturing by the lithotripsy procedure. Left main after drug-eluting stent (DES) placement (Figure 6E): a magnified view of the left main coronary artery shows the stent placed in the vessel with the visible deployment and expansion of the stent struts, which are outlined by a yellow circle. Left main after stenting with measurements (Figure 6F): following stent implantation, the OCT image shows well-expanded stent struts and a properly dilated vessel. This section illustrates the final angiographic result post-stenting. OCT imaging effectively captured the stages of coronary angioplasty, from pre-treatment conditions to post-stent implantation. The imaging clearly highlights the treatment process, including the lithotripsy procedure's role in fragmenting calcium deposits and the success of the stent in restoring the vessel lumen and achieving optimal angiographic results.

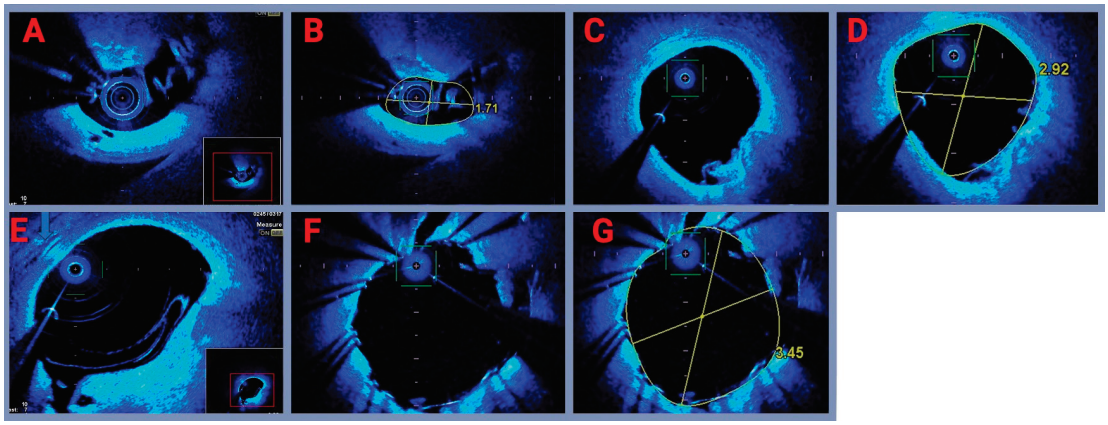


Figure 6. OCT assessment of coronary artery plaque in vivo before and after intravascular lithotripsy from one of the patients (IVL). (**A**,**B**) Critical LM stenosis with transactional area measurement; (**C**,**D**) IVL results with transactional area measurement; (**E**) calcium tissue defragmented by IVL; (**F**,**G**) final result after stent implantation with transactional area measurement.

4. Discussion

MRI is the most used modality for the non-invasive detection of changes in solid and liquid biological samples. In this study, specific MRI parameters, such as T_1 and T_2 measurements, have been correlated with the tissue changes associated with tissue contrast administration. The MRI-measured parameters T_1 and T_2 have been shown to respond to Omnipaque 350 implementation and changes in hydration, respectively.

The identification of an atherosclerotic plaque and its structure is crucial for successful treatment. Raising different parameters of plaque detection may play an important role in choosing the most effective diagnostic and therapeutic method. In the presented study, the average of the T_1 and T_2 relaxation times on the carotid atherosclerotic plaque are analyzed in correlation with the usage of one of the most popular invasive radiology iodine contrast solutions (Omnipaque 350). The implementation of the aforementioned contrast resulted in a decrease in the T_1 and T_2 relaxation times in the observed periods 1 h and 48 h after Omnipaque 350 implementation (T_1 slope from 1231 ms to 460 ms, T_2 slope from 63 ms to 33 ms). The obtained changes suggest that MRI assessment after the usage of iodine contrast may deliver additional information about atherosclerotic plaque distribution and differentiation toward more effective, conservative, pharmacological treatment of soft plaques versus more calcified plaques resistant to pharmacology—mostly sclerotic or calcified plaques. The structure of atherosclerosis could be visualized in the invasive procedure as well. OCT is a diagnostic procedure with the highest spectral resolution; however, it requires artery catheterization with intraarterial iodine contrast delivery. The plaque burden, deposits of calcium before and after debulking procedures such as rotational or orbital atherectomy, plaque dissections, and finally, the apposition of stent struts after artery stenting may deliver additional information for minimalizing the risk of early restenosis or intrastent thrombosis. In the presented study, the typical usages of OCT in intravascular plaque treatment are presented with excellent results for final stent apposition. The results of our experimental work underline the further investigations that are still needed in atherosclerotic plaque structure to obtain the most effective multidisciplinary approach in multilevel atherosclerosis, including invasive and aggressive pharmacological modifications.

The main treatment for atherosclerosis combines lifestyle changes, medications, and potential procedures or surgeries to manage plaque buildup in arteries, reduce cardiovascular risks, and improve blood flow. Lifestyle modifications are essential for slowing atherosclerosis progression. A diet low in saturated fats, cholesterol, and refined sugars; regular exercise; weight management; and smoking cessation help reduce blood pressure, lower LDL (bad) cholesterol, and improve overall cardiovascular health [53,54]. Medications are often prescribed to manage risk factors, such as statins to lower cholesterol, antihypertensive drugs to control blood pressure, and antiplatelet agents like aspirin to reduce blood clot risk. In patients with diabetes, drugs to regulate blood sugar are also critical [55,56]. For severe atherosclerosis where blood flow is significantly obstructed, procedures like angioplasty or surgical interventions may be necessary. Angioplasty involves inserting a balloon or stent to widen narrowed arteries [57,58]. Coronary artery bypass grafting creates new pathways around blocked arteries to restore blood flow [59]. Another procedure, endarterectomy, is used to directly remove atherosclerotic plaques from larger arteries, such as the carotid artery, to prevent strokes. In an endarterectomy, the surgeon carefully excises the plaque from within the artery, reducing the risk of future blockages [60,61]. These treatments, combined, address symptoms and complications of atherosclerosis, prevent further plaque buildup, and improve patient outcomes, particularly when paired with ongoing lifestyle and medical management. T_1 time and T_2 time imaging sequences are the most useful MRI techniques for determining the properties of atherosclerotic plaques. Predicting the likelihood of plaque rupture and subsequent

thrombotic events requires complementing information regarding the tissue composition and stability of the plaques, which these sequences offer. The way MRI functions is by identifying the body's protons' magnetic characteristics [62,63]. These protons' behavior in a magnetic field, which is utilized to create images, is influenced by the tissue's characteristics, such as its fat and water content. By varying the timing of radiofrequency pulses, the MRI signal can be altered, producing several image types based on the pulses' timing. The various components that make up atherosclerotic plaques are heterogeneous and can be seen differently with T_1 and T_2 MRI [64]. Understanding plaque composition and forecasting plaque stability depend on the capacity to differentiate between various plaque components. The outermost layer of atherosclerotic plaques, known as the fibrous cap, is essential to the integrity of the plaque. While a weak or ruptured fibrous cap is a major sign of plaque fragility, a thick, unbroken fibrous cap is typically linked to stable plaques. Due to its high collagen concentration and comparatively low water content, the fibrous cap looks hyperintense (bright) on T_1 imaging. T_2 scans, on the other hand, can occasionally display a more intricate structure of the fibrous cap, especially in cases of severe inflammation or edema [65]. Another important element of atherosclerotic plaques is the lipid core, which is linked to plaque instability. Due to its relatively low water content, the lipid-rich necrotic core may look hypointense (black) on T_1 imaging. The lipid core may appear hyperintense (bright) on T_2 imaging, particularly when there is a high water content or when the plaque contains inflammatory activities. Calcifications, or regions of mineral deposition inside the plaque, are frequently seen in atherosclerotic plaques [66,67]. Because calcified regions have very little water content and do not generate a strong MRI signal, they look hypointense (black) on both T_1 and T_2 imaging. Since calcification may indicate an advanced state of atherosclerosis, its detection is crucial. T_1 and T_2 MRI are helpful for determining the general size and volume of plaques, as well as for defining their constituent parts [68]. Determining the degree of atherosclerosis and forecasting the likelihood of unfavorable cardiovascular events require this knowledge. The volume of plaque constituents (such as the lipid core, fibrous tissue, and calcifications), as well as the total plaque size, can be measured using both T_1 and T_2 sequences. This can assist medical professionals in determining the extent of artery stenosis and forecasting the risk of plaque rupture. T_1 and T_2 MRI measurements of the ratio of fibrous tissue to lipid core size have been shown in studies to be a useful indicator for plaque vulnerability [69,70]. MRI can be used to characterize plaque, track the development of atherosclerosis over time, and evaluate the results of therapies meant to lessen plaque burden or increase plaque stability. Changes in plaque volume and composition over time can be monitored using T_1 and T_2 MRI. Plaque stabilization may be indicated by an increase in fibrous tissue or a decrease in the lipid-rich necrotic core, whereas plaque destabilization may be suggested by an increase in inflammation or bleeding [71,72]. Additionally, MRI can be used to evaluate the effectiveness of therapeutic therapies, including lifestyle changes, anti-inflammatory medications, and statin therapy. T_1 and T_2 imaging can be used to track changes in plaque composition, such as a decrease in lipid core volume or an increase in fibrous tissue, to evaluate the effectiveness of treatment. MRI has limits in terms of resolution and penetration despite its many benefits, including non-invasiveness and superior soft tissue contrast [73,74]. However, T_1 and T_2 MRI will remain crucial for the diagnosis, tracking, and treatment of atherosclerosis due to continuous improvements in MRI technology and image processing, which will ultimately enhance cardiovascular risk assessment and patient outcomes [75]. OCT creates detailed images using light waves rather than sound waves, but it works on the same principles as ultrasound. To create photographs, infrared light is emitted into tissues, and the reflected light is measured. OCT offers a far more detailed image than other imaging modalities, like intravascular ultrasonography, because

of its strong penetration of infrared light, which enables it to examine arterial wall features with micron-level resolution (10–20 microns) [76]. OCT is frequently used for retinal imaging in ophthalmology, but it has also found important uses in cardiology, especially in the evaluation of coronary artery disease and atherosclerosis. This technology is a vital tool for identifying and describing atherosclerotic plaques because it makes it possible to see the artery wall at the microscopic level [77]. Even at the level of specific components like the fibrous cap, lipid core, and calcifications, OCT's capacity to generate high-resolution images—typically ranging from 10 to 20 microns—allows for the thorough evaluation of plaque morphology. Plaques with big lipid cores, fragile plaques with thin fibrous crowns, and stable fibrous plaques can all be distinguished using OCT. The risk of rupture and thrombosis varies for these kinds of plaques [78]. One important factor influencing the stability of an atherosclerotic plaque is its fibrous cap. An increased risk of acute events and plaque rupture is linked to a thin or ruptured fibrous cap. OCT is very useful for determining the thickness and integrity of the fibrous cap, which is crucial for estimating the risk of plaque rupture. A thorough examination of the makeup of a plaque is made possible by OCT's ability to distinguish between distinct elements of the plaque, including the lipid-rich necrotic core, fibrous tissue, and calcifications. This can assist in locating susceptible plaques that have a higher risk of causing unfavorable cardiovascular events [79]. OCT can also be used in the long-term evaluation of atherosclerosis, assisting medical professionals in tracking the disease's development and the effectiveness of interventional therapies, such as balloon angioplasty or stenting, lifestyle changes, and statins. The early detection of any decline in plaque stability is made possible by the capacity of repeated OCT imaging to monitor changes in plaque size, shape, and composition over time [80]. OCT can be used to validate the expansion and location of the stent, evaluate the existence of any residual plaque or dissection, and evaluate the success of stent insertion following an interventional treatment, such as percutaneous coronary intervention. The propensity of vulnerable or high-risk plaques to rupture, resulting in thrombus formation and acute coronary events like myocardial infarction (MI), is one of their defining characteristics [81]. One of the main objectives of atherosclerosis imaging is to identify susceptible plaques, and OCT has shown itself to be especially effective in this regard. It has been demonstrated that OCT is quite successful in precisely recognizing these traits, which is essential for early intervention to avert disastrous consequences. OCT has drawbacks, including limited tissue penetration and high cost, although it offers substantial benefits in plaque characterization, particularly when evaluating fibrous cap integrity and plaque composition [82]. However, OCT has a lot of potential to help with atherosclerosis diagnosis, management, and treatment, especially when it comes to spotting fragile plaques that are likely to burst. OCT technology is expected to play a bigger part in clinical cardiology as it develops further, providing even more potent instruments for the early identification and treatment of cardiovascular disorders.

Limitations

The presented results are based on 14 plaques taken from seven patients during surgical endarterectomy due to significant/critical carotid artery stenosis. The number of patients in the study pool may limit the final results, regardless of inclusion criteria, for atherosclerotic plaques in carotid arteries leading to ischemic stroke. Patients with a history of supraventricular arrythmias, such as atrial fibrillations and low ejection fraction due to myocardial infarction, were excluded from the study pool in order to concentrate only on ischemic stroke due to significant/critical carotid artery stenosis. The selection of the contrast agent (Joheksol) Omnipaque was intentional due to the size of the medium particle and its wide availability and use in interventional radiology.

It is critical to acknowledge the study's limitations, especially regarding sample size, as these could impact how broadly the findings can be applied. Stronger findings might have been obtained with a larger sample. Furthermore, there was little study of related factors, and a more thorough investigation of possible confounders might have produced more complex findings. Lastly, the study only looked at atherosclerosis in carotid arteries; a more thorough understanding of cardiovascular disorders would be possible if a wider range of lesion types were considered. However, we wanted to show that T_1 and T_2 relaxation durations might be used to research atherosclerosis. Since MRI imaging does not cause harm to human health, it is a very useful study that may be carried out repeatedly without waiting periods.

5. Conclusions

The average of T_1 and T_2 relaxation times before and after Joheksol (Omnipaque 350) implementation may be helpful in recognizing the most favorable features of atherosclerotic plaques before scheduled PDT therapy. Further experimental research in animal models may deliver an evaluation of the effectiveness of possible therapy.

In summary, OCT and MRI together provide valuable compositional and morphological information related to changes in articular cartilage at the early stages of osteoarthritic degradation. Together, these techniques provide a powerful complementary approach that results in a comprehensive picture of molecular and biophysical changes in atherosclerotic plaques.

Author Contributions: Conceptualization, P.W., W.M., D.B.-A., D.L., A.T., and D.A.; methodology, P.W., W.M., D.B.-A., D.L., A.T., and D.A.; validation, P.W., W.M., D.B.-A., D.L., A.T., and D.A.; formal analysis, P.W., W.M., D.B.-A., D.L., A.T., and D.A.; resources, P.W., W.M., D.B.-A., D.L., A.T., and D.A.; writing—original draft preparation, P.W., W.M., D.B.-A., D.L., A.T., and D.A.; writing—review and editing, P.W., W.M., D.B.-A., D.L., A.T., and D.A.; visualization, P.W., W.M., D.B.-A., D.L., A.T., and D.A.; supervision, P.W. and D.A. All authors have read and agreed to the published version of the manuscript.

Funding: This research received no external funding.

Institutional Review Board Statement: The study was performed according to Bioethical Certificate no 43/2024/B issued by the Bioethics Committee of the Rzeszow Regional Medical Chamber on 09.09.2024.

Informed Consent Statement: Not applicable.

Data Availability Statement: The original contributions presented in this study are included in the article. Further inquiries can be directed to the corresponding authors.

Conflicts of Interest: The authors declare no conflicts of interest.

Abbreviations

The following abbreviations are used in this manuscript:

CT	Computed tomography
MRI	Magnetic resonance imaging
OCT	Optical coherence tomography
ms	Milliseconds

References

1. Demina, E.P.; Miroshnikova, V.V.; Schwarzman, A.L. Role of the ABC transporters A1 and G1, key reverse cholesterol transport proteins, in atherosclerosis. *Mol. Biol.* **2016**, *50*, 223–230. (In Russian) [CrossRef]
2. Luthi, A.J.; Patel, P.C.; Ko, C.H.; Mutharasan, R.K.; Mirkin, C.A.; Thaxton, C.S. Nanotechnology for synthetic high-density lipoproteins. *Trends Mol. Med.* **2010**, *16*, 553–560. [CrossRef] [PubMed]
3. Leaphart, D.; Waring, A.; Suranyi, P.; Fernandes, V. Call a Spade a Spade: Missed Diagnosis of Apical Hypertrophic Cardiomyopathy. *Am. J. Med. Sci.* **2019**, *358*, 299–303. [CrossRef] [PubMed]

4. Zhou, F.; Li, K.; Yang, K. Adipose-Derived Stem Cell Exosomes and Related microRNAs in Atherosclerotic Cardiovascular Disease. *J. Cardiovasc. Transl. Res.* **2023**, *16*, 453–462. [CrossRef]
5. Almohtasib, Y.; Fancher, A.J.; Sawalha, K. Emerging Trends in Atherosclerosis: Time to Address Atherosclerosis From a Younger Age. *Cureus* **2024**, *16*, e56635. [CrossRef]
6. Arbab-Zadeh, A.; Nakano, M.; Virmani, R.; Fuster, V. Acute coronary events. *Circulation* **2012**, *125*, 1147–1156. [CrossRef] [PubMed]
7. Luca, A.C.; David, S.G.; David, A.G.; Țarcă, V.; Pădureț, I.A.; Mîndru, D.E.; Roșu, S.T.; Roșu, E.V.; Adumitrăchioaiei, H.; Bernic, J.; et al. Atherosclerosis from Newborn to Adult-Epidemiology, Pathological Aspects, and Risk Factors. *Life* **2023**, *13*, 2056. [CrossRef] [PubMed]
8. Jebari-Benslaiman, S.; Galicia-García, U.; Larrea-Sebal, A.; Olaetxea, J.R.; Alloza, I.; Vandenbroeck, K.; Benito-Vicente, A.; Martín, C. Pathophysiology of Atherosclerosis. *Int. J. Mol. Sci.* **2022**, *23*, 3346. [CrossRef] [PubMed]
9. Gusev, E.; Sarapultsev, A. Atherosclerosis and Inflammation: Insights from the Theory of General Pathological Processes. *Int. J. Mol. Sci.* **2023**, *24*, 7910. [CrossRef]
10. Sharifi-Rad, J.; Rodrigues, C.F.; Sharopov, F.; Docea, A.O.; Can Karaca, A.; Sharifi-Rad, M.; Kahveci Karıncaoglu, D.; Gülseren, G.; Şenol, E.; Demircan, E.; et al. Diet, Lifestyle and Cardiovascular Diseases: Linking Pathophysiology to Cardioprotective Effects of Natural Bioactive Compounds. *Int. J. Environ. Res. Public Health* **2020**, *17*, 2326. [CrossRef] [PubMed]
11. Ziółkiewicz, A.; Kasprzak-Drozd, K.; Rusinek, R.; Markut-Miotła, E.; Oniszczuk, A. The Influence of Polyphenols on Atherosclerosis Development. *Int. J. Mol. Sci.* **2023**, *24*, 7146. [CrossRef] [PubMed]
12. Kronenberg, F.; Mora, S.; Stroes, E.S.G.; Ference, B.A.; Arsenault, B.J.; Berglund, L.; Dweck, M.R.; Koschinsky, M.; Lambert, G.; Mach, F.; et al. Lipoprotein(a) in atherosclerotic cardiovascular disease and aortic stenosis: A European Atherosclerosis Society consensus statement. *Eur. Heart J.* **2022**, *43*, 3925–3946. [CrossRef] [PubMed]
13. Singh, R.B.; Mengi, S.A.; Xu, Y.J.; Arneja, A.S.; Dhalla, N.S. Pathogenesis of atherosclerosis: A multifactorial process. *Exp. Clin. Cardiol.* **2002**, *7*, 40–53.
14. Rafieian-Kopaei, M.; Setorki, M.; Doudi, M.; Baradaran, A.; Nasri, H. Atherosclerosis: Process, indicators, risk factors and new hopes. *Int. J. Prev. Med.* **2014**, *5*, 927–946.
15. Madaudo, C.; Coppola, G.; Parlati, A.L.M.; Corrado, E. Discovering Inflammation in Atherosclerosis: Insights from Pathogenic Pathways to Clinical Practice. *Int. J. Mol. Sci.* **2024**, *25*, 6016. [CrossRef] [PubMed]
16. Lusis, A.J. Atherosclerosis. *Nature* **2000**, *407*, 233–241. [CrossRef] [PubMed]
17. Poznyak, A.V.; Sukhorukov, V.N.; Eremin, I.I.; Nadelyaeva, I.I.; Orekhov, A.N. Diagnostics of atherosclerosis: Overview of the existing methods. *Front. Cardiovasc. Med.* **2023**, *10*, 1134097. [CrossRef]
18. Verjans, J.W.; Jaffer, F.A. Biological imaging of atherosclerosis: Moving beyond anatomy. *J. Cardiovasc. Transl. Res.* **2013**, *6*, 681–694. [CrossRef] [PubMed]
19. Peng, K.J.; Huang, Y.S.; An, L.N.; Han, X.Q.; Zhang, J.G.; Wang, Q.L.; Sun, J.; Wang, S.R. Effect of ozone produced from antibody-catalyzed water oxidation on pathogenesis of atherosclerosis. *Acta Biochim. Biophys. Sin.* **2006**, *38*, 417–422. [CrossRef] [PubMed]
20. Vinegoni, C.; Botnaru, I.; Aikawa, E.; Calfon, M.A.; Iwamoto, Y.; Folco, E.J.; Ntziachristos, V.; Weissleder, R.; Libby, P.; Jaffer, F.A. Indocyanine green enables near-infrared fluorescence imaging of lipid-rich, inflamed atherosclerotic plaques. *Sci. Transl. Med.* **2011**, *3*, 84ra45. [CrossRef] [PubMed] [PubMed Central]
21. Khalafi, S.; Botero Fonnegra, C.; Reyes, A.; Hui, V.W. Developments in the Use of Indocyanine Green (ICG) Fluorescence in Colorectal Surgery. *J. Clin. Med.* **2024**, *13*, 4003. [CrossRef] [PubMed] [PubMed Central]
22. Daghem, M.; Bing, R.; Fayad, Z.A.; Dweck, M.R. Noninvasive Imaging to Assess Atherosclerotic Plaque Composition and Disease Activity: Coronary and Carotid Applications. *JACC Cardiovasc. Imaging* **2020**, *13*, 1055–1068. [CrossRef] [PubMed] [PubMed Central]
23. Shishikura, D. Noninvasive imaging modalities to visualize atherosclerotic plaques. *Cardiovasc. Diagn. Ther.* **2016**, *6*, 340–353. [CrossRef] [PubMed] [PubMed Central]
24. Fujimoto, J.G.; Pitris, C.; Boppart, S.A.; Brezinski, M.E. Optical coherence tomography: An emerging technology for biomedical imaging and optical biopsy. *Neoplasia* **2000**, *2*, 9–25. [CrossRef] [PubMed] [PubMed Central]
25. Spaide, R.F.; Fujimoto, J.G.; Waheed, N.K.; Sadda, S.R.; Staurenghi, G. Optical coherence tomography angiography. *Prog. Retin. Eye Res.* **2018**, *64*, 1–55. [CrossRef] [PubMed] [PubMed Central]
26. Araki, M.; Park, S.J.; Dauerman, H.L.; Uemura, S.; Kim, J.S.; Di Mario, C.; Johnson, T.W.; Guagliumi, G.; Kastrati, A.; Joner, M.; et al. Optical coherence tomography in coronary atherosclerosis assessment and intervention. *Nat. Rev. Cardiol.* **2022**, *19*, 684–703, Erratum in: *Nat. Rev. Cardiol.* **2024**, *21*, 348. https://doi.org/10.1038/s41569-023-00982-z. [CrossRef] [PubMed] [PubMed Central]
27. Coletta, J.; Suzuki, N.; Nascimento, B.R.; Bezerra, H.G.; Rosenthal, N.; Guagliumi, G.; Rollins, A.M.; Costa, M.A. Use of optical coherence tomography for accurate characterization of atherosclerosis. *Arq. Bras. Cardiol.* **2010**, *94*, 250–254, In Portuguese version pp. 268-272 and in Spanish version pp. 254-259. [CrossRef] [PubMed]

28. He, C.; Li, Z.; Wang, J.; Huang, Y.; Yin, Y.; Li, Z. Atherosclerotic Plaque Tissue Characterization: An OCT-Based Machine Learning Algorithm With *ex vivo* Validation. *Front. Bioeng. Biotechnol.* **2020**, *8*, 749. [CrossRef] [PubMed] [PubMed Central]
29. Cao, J.J.; Shen, L.; Nguyen, J.; Rapelje, K.; Porter, C.; Shlofmitz, E.; Jeremias, A.; Cohen, D.J.; Ali, Z.A.; Shlofmitz, R. Accuracy and limitation of plaque detection by coronary CTA: A section-to-section comparison with optical coherence tomography. *Sci. Rep.* **2023**, *13*, 11845. [CrossRef] [PubMed] [PubMed Central]
30. Pang, W.; Yuan, C.; Zhong, T.; Huang, X.; Pan, Y.; Qu, J.; Nie, L.; Zhou, Y.; Lai, P. Diagnostic and therapeutic optical imaging in cardiovascular diseases. *iScience* **2024**, *27*, 111216. [CrossRef] [PubMed] [PubMed Central]
31. Popescu, D.P.; Choo-Smith, L.P.; Flueraru, C.; Mao, Y.; Chang, S.; Disano, J.; Sherif, S.; Sowa, M.G. Optical coherence tomography: Fundamental principles, instrumental designs and biomedical applications. *Biophys. Rev.* **2011**, *3*, 155. [CrossRef] [PubMed] [PubMed Central]
32. Matcher, S.J. Practical aspects of OCT imaging in tissue engineering. *Methods Mol. Biol.* **2011**, *695*, 261–280. [CrossRef] [PubMed]
33. Wang, J.; Yuan, S.; Qi, J.; Zhang, Q.; Ji, Z. Advantages and prospects of optical coherence tomography in interventional therapy of coronary heart disease (Review). *Exp. Ther. Med.* **2022**, *23*, 255. [CrossRef] [PubMed] [PubMed Central]
34. Terashima, M.; Kaneda, H.; Suzuki, T. The role of optical coherence tomography in coronary intervention. *Korean J. Intern. Med.* **2012**, *27*, 1–12. [CrossRef] [PubMed] [PubMed Central]
35. Wang, A.; Qi, W.; Gao, T.; Tang, X. Molecular Contrast Optical Coherence Tomography and Its Applications in Medicine. *Int. J. Mol. Sci.* **2022**, *23*, 3038. [CrossRef] [PubMed] [PubMed Central]
36. Pierce, M.C.; Javier, D.J.; Richards-Kortum, R. Optical contrast agents and imaging systems for detection and diagnosis of cancer. *Int. J. Cancer* **2008**, *123*, 1979–1990. [CrossRef] [PubMed] [PubMed Central]
37. Chen, W.; Schilperoort, M.; Cao, Y.; Shi, J.; Tabas, I.; Tao, W. Macrophage-targeted nanomedicine for the diagnosis and treatment of atherosclerosis. *Nat. Rev. Cardiol.* **2022**, *19*, 228–249. [CrossRef] [PubMed] [PubMed Central]
38. Bagalkot, V.; Badgeley, M.A.; Kampfrath, T.; Deiuliis, J.A.; Rajagopalan, S.; Maiseyeu, A. Hybrid nanoparticles improve targeting to inflammatory macrophages through phagocytic signals. *J. Control Release* **2015**, *217*, 243–255. [CrossRef] [PubMed] [PubMed Central]
39. Wei, X.; Runnels, J.M.; Lin, C.P. Selective uptake of indocyanine green by reticulocytes in circulation. *Investig. Ophthalmol. Vis. Sci.* **2003**, *44*, 4489–4496. [CrossRef] [PubMed] [PubMed Central]
40. Alander, J.T.; Kaartinen, I.; Laakso, A.; Pätilä, T.; Spillmann, T.; Tuchin, V.V.; Venermo, M.; Välisuo, P. A review of indocyanine green fluorescent imaging in surgery. *Int. J. Biomed. Imaging* **2012**, *2012*, 940585. [CrossRef] [PubMed] [PubMed Central]
41. Langer, H.F.; Haubner, R.; Pichler, B.J.; Gawaz, M. Radionuclide imaging: A molecular key to the atherosclerotic plaque. *J. Am. Coll. Cardiol.* **2008**, *52*, 1–12. [CrossRef] [PubMed] [PubMed Central]
42. Varga-Szemes, A.; Maurovich-Horvat, P.; Schoepf, U.J.; Zsarnoczay, E.; Pelberg, R.; Stone, G.W.; Budoff, M.J. Computed Tomography Assessment of Coronary Atherosclerosis: From Threshold-Based Evaluation to Histologically Validated Plaque Quantification. *J. Thorac. Imaging* **2023**, *38*, 226–234. [CrossRef] [PubMed] [PubMed Central]
43. Goel, S.; Miller, A.; Agarwal, C.; Zakin, E.; Acholonu, M.; Gidwani, U.; Sharma, A.; Kulbak, G.; Shani, J.; Chen, O. Imaging Modalities to Identity Inflammation in an Atherosclerotic Plaque. *Radiol. Res. Pract.* **2015**, *2015*, 410967. [CrossRef] [PubMed] [PubMed Central]
44. Fernández-Alvarez, V.; Linares-Sánchez, M.; Suárez, C.; López, F.; Guntinas-Lichius, O.; Mäkitie, A.A.; Bradley, P.J.; Ferlito, A. Novel Imaging-Based Biomarkers for Identifying Carotid Plaque Vulnerability. *Biomolecules* **2023**, *13*, 1236. [CrossRef] [PubMed] [PubMed Central]
45. Alonso-Herranz, L.; Albarrán-Juárez, J.; Bentzon, J.F. Mechanisms of fibrous cap formation in atherosclerosis. *Front. Cardiovasc. Med.* **2023**, *10*, 1254114. [CrossRef] [PubMed] [PubMed Central]
46. Stefanadis, C.; Antoniou, C.K.; Tsiachris, D.; Pietri, P. Coronary Atherosclerotic Vulnerable Plaque: Current Perspectives. *J. Am. Heart Assoc.* **2017**, *6*, e005543. [CrossRef] [PubMed] [PubMed Central]
47. Chamié, D.; Wang, Z.; Bezerra, H.; Rollins, A.M.; Costa, M.A. Optical Coherence Tomography and Fibrous Cap Characterization. *Curr. Cardiovasc. Imaging Rep.* **2011**, *4*, 276–283. [CrossRef] [PubMed] [PubMed Central]
48. Toutouzas, K.; Karanasos, A.; Tousoulis, D. Optical Coherence Tomography For the Detection of the Vulnerable Plaque. *Eur. Cardiol.* **2016**, *11*, 90–95. [CrossRef] [PubMed] [PubMed Central]
49. Lee, Y.K.; Kwak, H.S.; Chung, G.H.; Hwang, S.B. Lipid-Rich Necrotic Core of Basilar Artery Atherosclerotic Plaque: Contrast-Enhanced Black Blood Imaging on Vessel Wall Imaging. *Diagnostics* **2019**, *9*, 69. [CrossRef] [PubMed] [PubMed Central]
50. Xia, J.; Yin, A.; Li, Z.; Liu, X.; Peng, X.; Xie, N. Quantitative Analysis of Lipid-Rich Necrotic Core in Carotid Atherosclerotic Plaques by In Vivo Magnetic Resonance Imaging and Clinical Outcomes. *Med. Sci. Monit.* **2017**, *23*, 2745–2750. [CrossRef] [PubMed] [PubMed Central]
51. Onea, H.L.; Olinic, M.; Lazar, F.L.; Homorodean, C.; Ober, M.C.; Spinu, M.; Achim, A.; Tataru, D.A.; Olinic, D.M. A Review Paper on Optical Coherence Tomography Evaluation of Coronary Calcification Pattern: Is It Relevant Today? *J. Cardiovasc. Dev. Dis.* **2024**, *11*, 231. [CrossRef] [PubMed] [PubMed Central]

52. Summary of Product Characteristics for CONTRAPAQUE 350. Available online: http://www.efda.gov.et/wp-content/uploads/2023/08/Iohexol-Injection-USP-350-mg-I-mL-CONTRAPAQUE-350-UNIQUE-PHARMACEUTICAL-LABORATORIES.pdf (accessed on 22 December 2024).
53. Ghodeshwar, G.K.; Dube, A.; Khobragade, D. Impact of Lifestyle Modifications on Cardiovascular Health: A Narrative Review. *Cureus* **2023**, *15*, e42616. [CrossRef] [PubMed]
54. Rippe, J.M. Lifestyle Strategies for Risk Factor Reduction, Prevention, and Treatment of Cardiovascular Disease. *Am. J. Lifestyle Med.* **2018**, *13*, 204–212. [CrossRef]
55. Sizar, O.; Khare, S.; Patel, P.; Talati, R. Statin Medications. In *StatPearls*; StatPearls Publishing: Treasure Island, FL, USA, 2024.
56. Yachmaneni, A., Jr.; Jajoo, S.; Mahakalkar, C.; Kshirsagar, S.; Dhole, S. A Comprehensive Review of the Vascular Consequences of Diabetes in the Lower Extremities: Current Approaches to Management and Evaluation of Clinical Outcomes. *Cureus* **2023**, *15*, e47525. [CrossRef] [PubMed]
57. Chhabra, L.; Zain, M.A.; Siddiqui, W.J. Angioplasty. In *StatPearls*; StatPearls Publishing: Treasure Island, FL, USA, 2024.
58. Jongsma, H.; Bekken, J.; Ayez, N.; Hoogewerf, C.J.; Van Weel, V.; Fioole, B. Angioplasty versus stenting for iliac artery lesions. *Cochrane Database Syst. Rev.* **2020**, *12*, CD007561. [PubMed]
59. Harris, R.; Croce, B.; Tian, D.H. Coronary artery bypass grafting. *Ann. Cardiothorac. Surg.* **2013**, *2*, 579.
60. DaCosta, M.; Tadi, P.; Surowiec, S.M. Carotid Endarterectomy. In *StatPearls*; StatPearls Publishing: Treasure Island, FL, USA, 2024.
61. Rerkasem, A.; Orrapin, S.; Howard, D.P.; Rerkasem, K. Carotid endarterectomy for symptomatic carotid stenosis. *Cochrane Database Syst. Rev.* **2020**, *9*, CD001081.
62. Tarkin, J.M.; Dweck, M.R.; Evans, N.R.; Takx, R.A.; Brown, A.J.; Tawakol, A.; Fayad, Z.A.; Rudd, J.H. Imaging Atherosclerosis. *Circ. Res.* **2016**, *118*, 750–769. [CrossRef] [PubMed] [PubMed Central]
63. Truong, M.; Lennartsson, F.; Bibic, A.; Sundius, L.; Persson, A.; Siemund, R.; In't Zandt, R.; Goncalves, I.; Wassélius, J. Classifications of atherosclerotic plaque components with T_1 and T2* mapping in 11.7 T MRI. *Eur. J. Radiol. Open* **2021**, *8*, 100323. [CrossRef] [PubMed] [PubMed Central]
64. Berger, A. Magnetic resonance imaging. *BMJ* **2002**, *324*, 35. [CrossRef] [PubMed] [PubMed Central]
65. Babaniamansour, P.; Mohammadi, M.; Babaniamansour, S.; Aliniagerdroudbari, E. The Relation between Atherosclerosis Plaque Composition and Plaque Rupture. *J. Med. Signals Sens.* **2020**, *10*, 267–273. [CrossRef] [PubMed] [PubMed Central]
66. Benson, J.C.; Saba, L.; Bathla, G.; Brinjikji, W.; Nardi, V.; Lanzino, G. MR Imaging of Carotid Artery Atherosclerosis: Updated Evidence on High-Risk Plaque Features and Emerging Trends. *AJNR Am. J. Neuroradiol.* **2023**, *44*, 880–888. [CrossRef] [PubMed] [PubMed Central]
67. Dong, L.; Kerwin, W.S.; Ferguson, M.S.; Li, R.; Wang, J.; Chen, H.; Canton, G.; Hatsukami, T.S.; Yuan, C. Cardiovascular magnetic resonance in carotid atherosclerotic disease. *J. Cardiovasc. Magn. Reson.* **2009**, *11*, 53. [CrossRef] [PubMed] [PubMed Central]
68. Wu, Z.; Mittal, S.; Kish, K.; Yu, Y.; Hu, J.; Haacke, E.M. Identification of calcification with MRI using susceptibility-weighted imaging: A case study. *J. Magn. Reson. Imaging* **2009**, *29*, 177–182. [CrossRef] [PubMed] [PubMed Central]
69. Mushenkova, N.V.; Summerhill, V.I.; Zhang, D.; Romanenko, E.B.; Grechko, A.V.; Orekhov, A.N. Current Advances in the Diagnostic Imaging of Atherosclerosis: Insights into the Pathophysiology of Vulnerable Plaque. *Int. J. Mol. Sci.* **2020**, *21*, 2992. [CrossRef] [PubMed] [PubMed Central]
70. Saba, L.; Loewe, C.; Weikert, T.; Williams, M.C.; Galea, N.; Budde, R.P.J.; Vliegenthart, R.; Velthuis, B.K.; Francone, M.; Bremerich, J.; et al. State-of-the-art CT and MR imaging and assessment of atherosclerotic carotid artery disease: Standardization of scanning protocols and measurements-a consensus document by the European Society of Cardiovascular Radiology (ESCR). *Eur. Radiol.* **2023**, *33*, 1063–1087, Erratum in: *Eur. Radiol.* **2023**, *33*, 1497–1498. https://doi.org/10.1007/s00330-022-09246-9. [CrossRef] [PubMed] [PubMed Central]
71. Kramer, C.M.; Anderson, J.D. MRI of atherosclerosis: Diagnosis and monitoring therapy. *Expert. Rev. Cardiovasc. Ther.* **2007**, *5*, 69–80. [CrossRef] [PubMed] [PubMed Central]
72. Andelovic, K.; Winter, P.; Jakob, P.M.; Bauer, W.R.; Herold, V.; Zernecke, A. Evaluation of Plaque Characteristics and Inflammation Using Magnetic Resonance Imaging. *Biomedicines* **2021**, *9*, 185. [CrossRef] [PubMed] [PubMed Central]
73. Zhou, P.; Wang, Y.; Sun, J.; Yu, Y.; Mossa-Basha, M.; Zhu, C. Assessment of Therapeutic Response to Statin Therapy in Patients With Intracranial or Extracranial Carotid Atherosclerosis by Vessel Wall MRI: A Systematic Review and Updated Meta-Analysis. *Front. Cardiovasc. Med.* **2021**, *8*, 742935. [CrossRef] [PubMed] [PubMed Central]
74. Huang, J.; Liu, C.; Jiao, S.; Chen, Y.; Xu, L.; Gong, T.; Zhu, C.; Song, Y. Application of high-resolution MRI in evaluating statin efficacy on symptomatic intracranial atherosclerosis. *Eur. Radiol.* **2025**, *35*, 441–452. [CrossRef] [PubMed]
75. Counseller, Q.; Aboelkassem, Y. Recent technologies in cardiac imaging. *Front. Med. Technol.* **2023**, *4*, 984492. [CrossRef] [PubMed] [PubMed Central]
76. Jung, W.; Boppart, S.A. Optical coherence tomography for rapid tissue screening and directed histological sectioning. *Anal. Cell Pathol.* **2012**, *35*, 129–143. [CrossRef] [PubMed] [PubMed Central]

77. Viscusi, M.M.; La Porta, Y.; Migliaro, G.; Gargano, G.M.; Nusca, A.; Gatto, L.; Budassi, S.; Paolucci, L.; Mangiacapra, F.; Ricottini, E.; et al. Current Applications and New Perspectives in Optical Coherence Tomography (OCT) Coronary Atherosclerotic Plaque Assessment: From PCI Optimization to Pharmacological Treatment Guidance. *Photonics* **2023**, *10*, 158. [CrossRef]
78. Jang, I.K.; Tearney, G.J.; MacNeill, B.; Takano, M.; Moselewski, F.; Iftima, N.; Shishkov, M.; Houser, S.; Aretz, H.T.; Halpern, E.F.; et al. In vivo characterization of coronary atherosclerotic plaque by use of optical coherence tomography. *Circulation* **2005**, *111*, 1551–1555. [CrossRef] [PubMed] [PubMed Central]
79. Sinclair, H.; Bourantas, C.; Bagnall, A.; Mintz, G.S.; Kunadian, V. OCT for the identification of vulnerable plaque in acute coronary syndrome. *JACC Cardiovasc. Imaging* **2015**, *8*, 198–209. [CrossRef] [PubMed]
80. Huang, J.; Yang, F.; Gutiérrez-Chico, J.L.; Xu, T.; Wu, J.; Wang, L.; Lv, R.; Lai, Y.; Liu, X.; Onuma, Y.; et al. Optical Coherence Tomography-Derived Changes in Plaque Structural Stress Over the Cardiac Cycle: A New Method for Plaque Biomechanical Assessment. *Front. Cardiovasc. Med.* **2021**, *8*, 715995. [CrossRef] [PubMed] [PubMed Central]
81. Longobardo, L.; Mattesini, A.; Valente, S.; Di Mario, C. OCT-guided Percutaneous Coronary Intervention in Bifurcation Lesions. *Interv. Cardiol.* **2019**, *14*, 5–9. [CrossRef] [PubMed] [PubMed Central]
82. Tearney, G.J.; Jang, I.K.; Bouma, B.E. Optical coherence tomography for imaging the vulnerable plaque. *J. Biomed. Opt.* **2006**, *11*, 021002. [CrossRef] [PubMed] [PubMed Central]

Disclaimer/Publisher's Note: The statements, opinions and data contained in all publications are solely those of the individual author(s) and contributor(s) and not of MDPI and/or the editor(s). MDPI and/or the editor(s) disclaim responsibility for any injury to people or property resulting from any ideas, methods, instructions or products referred to in the content.

biomedicines

MDPI

Article

Assessing Cardiovascular Risk with Coronary Artery Calcium and Carotid Intima-Media Thickness in Patients with Negative Stress Echocardiography

Narae Kim, Hui-Jeong Hwang and In-Ho Yang *

Department of Cardiology, Kyung Hee University College of Medicine, Kyung Hee University Hospital at Gangdong, Seoul 05278, Republic of Korea; knr802@naver.com (N.K.); neonic7749@hanmail.net (H.-J.H.)
* Correspondence: seventi4@hanmail.net; Tel.: +82-2-440-6948

Abstract: Background: The role of treadmill stress echocardiography (TSE) in symptomatic patients may be limited. We evaluated whether carotid intima-media thickness (cIMT) and coronary artery calcium (CAC) scores can predict cardiovascular (CV) outcomes in patients with negative TSE. **Methods**: Patients who had negative TSE and measured cIMT or CAC scoring were enrolled and followed up. The primary CV outcome was defined as a composite of acute coronary syndrome, coronary revascularization, heart failure, stroke, and CV death. **Results**: Overall, 1095 patients participated. The median follow-up duration was 5.8 years. Patients with increased cIMT and CAC scores experienced a high incidence of primary CV outcomes (normal vs. increased group on cIMT and CAC scoring: 4.4% vs. 20.0% and 0.4% vs. 25.0%, respectively, $p < 0.001$). In the Cox proportional hazard model, increased cIMT and CAC scores were associated with increased primary CV outcomes (adjusted hazard ratio [95% confidence interval], *p*-value for increased cIMT and increased CAC scores = 2.939 [1.241–6.960], $p = 0.014$ and 45.192 [5.497–371.505], $p < 0.001$, respectively). **Conclusions**: Patients with increased cIMT and CAC scores have poor CV outcomes even though they have negative TSE results, and therefore, they should be carefully monitored.

Keywords: treadmill echocardiography; coronary artery calcium score; carotid intima-media thickness; cardiovascular outcomes

1. Introduction

According to the World Health Organization, cardiovascular disease (CVD) stands as the most common cause of mortality worldwide, claiming more than 18 million lives annually, which accounts for one-third of all global deaths [1]. CVD is closely related to the progression of atherosclerosis. Thus, early detection of significant atherosclerosis before it progresses to CVD is important. However, current treatment guidelines consider factors such as age, sex, race, smoking, and underlying diseases for CVD risk estimation without factoring in the presence or absence of atherosclerosis in imaging [2].

Treadmill stress echocardiography (TSE) is a useful test for diagnosing coronary artery disease (CAD) [3]; the prognosis for patients with negative TSE is usually considered to be good [4]. Nonetheless, TSE has inherent limitations as a functional study, particularly that it cannot differentiate subclinical atherosclerotic diseases from normal coronary arteries [5]. Furthermore, acute coronary syndrome does not necessarily result from significant chronic luminal narrowing; however, it may be provoked by spasm, plaque rupture, and thrombus [6].

Carotid intima-media thickness (cIMT) is a marker for the early stages of atherosclerosis [7]. cIMT can predict CV risk, and some studies suggest increased cIMT is associated with CVD in patients with inconclusive treadmill test results [7–11]. However, unlike carotid plaques, which have independent predictive value for CV risk, the relative importance of cIMT on CV risk is still controversial [7]. In several studies, adding cIMT did

not improve CV risk stratification [7,12]. In addition, data on patients with symptomatic negative TSE are scarce.

Carotid intima-media thickness (cIMT) is a marker for the early stages of atherosclerosis [7]. Some studies suggest increased cIMT is associated with CVD in patients with inconclusive treadmill test results [7–11]. However, unlike carotid plaques, which have independent predictive value for CV risk, the relative importance of cIMT on CV risk is still controversial [7]. In several studies, adding cIMT did not improve CV risk stratification [7,12]. In addition, data on patients with symptomatic negative TSE are scarce.

Coronary artery calcium (CAC) scoring is a test to quantify morphological abnormalities of atherosclerosis [5,9]. An increased CAC score is related to CV risk, and recent guidelines on dyslipidemia recommend that a CAC score can be considered for CV risk assessment and treatment [2,13]. In the 2019 European Society of Cardiology/European Atherosclerosis Society (ESC/EAS) guidelines for the management of dyslipidemias, the CV risk increases when the CAC score is $\geq$100 [2]. The 2018 American Heart Association/American College of Cardiology (AHA/ACC) guideline on the management of blood cholesterol recommends the use of statins in patients with a CAC score of $\geq$100, or a score of 1–99 over 55 years of age [13]. In addition, some studies combined the treadmill test and CAC score to predict CV risk, and previous studies showed that the CAC score had an additional predictive role in patients with positive TSE [14,15]. However, their clinical implications have not been established in symptomatic patients with negative TSE.

Among studies on the relationship between cIMT or CAC score and CV outcome, data combined with the treadmill test for symptomatic patients are insufficient. In this study, we conducted a study on symptomatic patients with a negative TSE. We aimed to evaluate whether increased cIMT and CAC scores can predict CV outcomes in patients with chest pain but with negative TSE.

2. Materials and Methods

2.1. Patient Population

We recruited patients who had angina symptoms and underwent TSE between November 2006 and August 2021 at our hospital (Kyung Hee University Hospital at Gangdong, Seoul, Republic of Korea). Among them, patients who underwent cIMT or CAC scoring tests within 7 days were enrolled (Figure 1). Patients with positive TSE findings were excluded. Patients aged < 20 years with regional wall motion abnormalities, previous history of percutaneous coronary intervention or coronary artery bypass grafting, valvular heart diseases of greater than moderate grade, significant cardiomyopathy such as heart failure, and severe systemic diseases such as chronic obstructive pulmonary disease, hepatic failure, and end-stage renal disease were also excluded. Informed consent was acquired verbally during the telephone interview. This study received the approval of the hospital Ethics Committee (KHNMC 202211011).

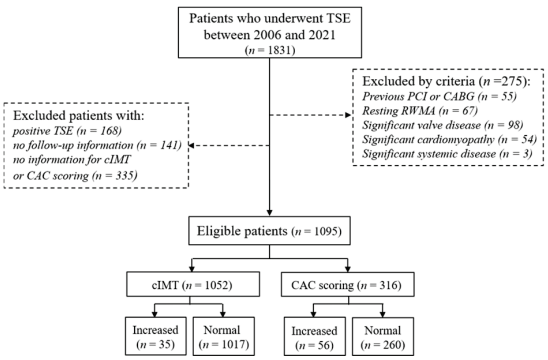


Figure 1. Study population. TSE, treadmill stress echocardiography; cIMT, carotid intima-media thickness; CAC, coronary artery calcium; PCI, percutaneous coronary intervention; CABG, coronary artery bypass graft; RWMA, regional wall motion abnormality.

2.2. Treadmill Stress Echocardiography

TSE was performed using the standard Bruce protocol with symptom-limited exercise interruption. Tests were performed while monitoring 12-lead electrocardiography, blood pressure, and heart rate. Baseline echocardiography was taken at the left decubitus position before exercise and left ventricular wall motion was compared with postexercise echocardiography at the left decubitus position. A normal unchanged echocardiographic result signified a negative TSE. Angina was defined as chest pain or dyspnea developed during exercise.

2.3. Carotid Artery Ultrasound

A carotid artery ultrasound was concomitantly performed during echocardiography before exercise. The cIMT was measured at both common carotid arteries in the supine position using a high-resolution B-mode ultrasound system (iE33 Ultrasound with Linear Array Transducer, Philips, San Jose, CA, USA) according to a standardized protocol; it was obtained in the posterior wall of the common carotid artery 1 cm below the carotid artery bifurcation in the longitudinal view. The mean cIMT was calculated as a mean value of bilateral cIMT and was defined to be increased when the mean cIMT was >0.90 mm. All measurements were performed by experienced operators blinded to the patient's information.

2.4. Coronary Artery Calcium Scoring

The CAC scores were measured with a 64-slice multi-detector computed tomography (CT) system (Brilliance 64 CT, Philips Medical System, Cleveland, OH, USA). CT was performed with a total voltage of 120 kV, an effective current of 800 mAs, a gentle rotation time of 200 ms, and a 64 $\times$ 0.625 mm slice configuration setting. The CAC score was measured through Agatston scoring, which was defined to be increased when the CAC score was measured above 75. A detailed rationale will be provided in the discussion.

2.5. Follow-Up and Cardiovascular Outcomes

Patients were divided into both groups according to cIMT and CAC scoring: (1) increased (>0.9 mm) vs. normal ($\leq$0.9 mm) groups on cIMT; (2) increased (>75) vs. normal ($\leq$75) groups on CAC scores. Acute coronary syndrome, coronary revascularization, stroke, heart failure, and CV death were evaluated as CV outcomes. The primary outcome was the composite of CV outcomes. Clinical characteristics, TSE results, and follow-up data for CV outcomes were acquired through medical records and telephone interviews.

2.6. Statistical Analysis

Statistical analysis was performed with SPSS version 13.0. Continuous variables were expressed as mean $\pm$ standard deviation (or median value [25th percentile; 75th percentile] for variables with skewed data). The categorical variable was demonstrated as a percentage of the group. Student's *t*-test (or the Mann–Whitney test for variables with skewed data) was used to compare continuous variables in the two groups. χ^2-test (or Fisher's exact test for cell counts < 5) was used to compare categorical variables. The cutoff value of the CAC score was determined as a value with high sensitivity and specificity using the receiver operating characteristic (ROC) curve. Incidence rates for the primary outcomes in increased cIMT and CAC groups were compared with those in normal groups using Kaplan–Meier curves and log-rank tests. Univariable and multivariable Cox proportional hazard models were used to evaluate whether increased cIMT and CAC scores are predictors of CV outcome. Values of $p < 0.05$ were considered statistically significant.

3. Results

A total of 1095 patients with negative TSE were eligible and enrolled (Figure 1). Among them, patients who underwent cIMT and CAC scoring tests were 1052 and 316, respectively. The median follow-up time was 5.8 (2.4; 8.3) years. Patients with increased cIMT were older and had higher body mass index (BMI), hypertension, diabetes, and dyslipidemia and took more antiplatelet agents, angiotensin-converting enzyme inhibitor (ACEI)/angiotensin

receptor blocker (ARB), and statins (Table 1). Patients with increased CAC scores were older, had a higher incidence of hypertension and dyslipidemia, and took more antiplatelet agents, ACEI/ARBs, and statins (Table 1). The mean cIMT was 0.62 ± 0.11 mm in the normal group and 0.98 ± 0.07 mm in the increased group; the CAC score was 0 (0; 5.2) in the normal group and 180.8 (118.15; 410.1) in the increased group (Table 2). The primary outcome was higher in increased cIMT (4.4% in the normal group vs. 20.0% in the increased group, $p < 0.001$) and CAC (0.4% in the normal group vs. 25.0% in the increased group, $p < 0.001$) groups (Table 2).

Table 1. Baseline characteristics.

	cIMT Group			**CAC Scoring Group**		
	Normal (n = 1017)	**Increased (n = 35)**	***p*-Value**	**Normal (n = 260)**	**Increased (n = 56)**	***p*-Value**
Clinical Characteristics						
Age, years	56.0 ± 9.7	62.5 ± 8.6	<0.001	55.7 ± 9.8	62.1 ± 10.1	<0.001
Male, n (%)	544 (53.5)	20 (57.1)	0.670	138 (53.1)	34 (60.7)	0.298
BMI, kg/m^2	24.9 ± 3.2	26.2 ± 3.3	0.019	24.8 ± 3.1	25.3 ± 3.6	0.243
Smoking, n (%)	199 (19.7)	7 (20.0)	0.965	46 (17.8)	10 (18.2)	0.951
Hypertension, n (%)	402 (39.5)	21 (60.0)	0.015	90 (34.6)	32 (57.1)	0.002
Diabetes, n (%)	213 (20.9)	15 (42.9)	0.002	27 (10.4)	10 (17.9)	0.115
Dyslipidemia, n (%)	506 (49.8)	35 (77.1)	0.001	129 (49.6)	41 (73.2)	0.001
Medications, n (%)						
Antiplatelet agents	202 (19.9)	14 (40.0)	0.004	58 (22.3)	26 (46.4)	<0.001
ACEI/ARBs	202 (19.9)	15 (42.9)	0.001	38 (14.6)	19 (33.9)	0.001
BBs	93 (9.1)	4 (11.4)	0.646	29 (11.2)	5 (8.9)	0.626
Statins	337 (33.1)	19 (54.3)	0.009	80 (30.8)	30 (53.6)	0.001
TSE data						
SBP, mmHg	115.6 ± 14.9	124.5 ± 19.6	0.012	115.0 ± 15.0	120.0 ± 16.9	0.028
DBP, mmHg	67.7 ± 10.6	71.1 ± 14.9	0.192	67.1 ± 11.3	69.6 ± 14.7	0.158
HR, mmHg	70.8 ± 11.4	67.0 ± 8.4	0.014	70.2 ± 11.8	68.7 ± 9.1	0.289
Target HR, %	98.5 ± 9.8	95.9 ± 12.4	0.126	98.5 ± 8.8	95.3 ± 12.4	0.075
METs	11.5 ± 2.1	10.4 ± 2.3	0.004	11.6 ± 2.2	11.0 ± 2.5	0.084
Angina during test, n (%)	514 (52.3)	16 (47.1)	0.544	124 (48.1)	20 (37.7)	0.170

cIMT, carotid intima-media thickness; CAC, coronary artery calcium; BMI, body mass index; ACEI/ARB, renin-angiotensin-converting enzyme inhibitor/angiotensin receptor blocker; BB, beta blocker; TSE, treadmill stress echocardiography; SBP, systolic blood pressure; DBP, diastolic blood pressure; HR, heart rate; MET, metabolic equivalent of tasks.

Table 2. Atherosclerotic markers and cardiovascular outcomes.

	cIMT Group			**CAC Scoring Group**		
	Normal (n = 1017)	**Increased (n = 35)**	***p*-Value**	**Normal (n = 260)**	**Increased (n = 56)**	***p*-Value**
Atherosclerotic Markers						
Mean cIMT, mm	0.62 ± 0.11	0.98 ± 0.07	<0.001	–		
CAC score		–		0 [0; 5.2]	180.8 [118.15; 410.1]	<0.001
CV outcomes, n (%)	45 (4.4)	7 (20.0)	<0.001	1 (0.4)	14 (25.0)	<0.001
ACS	3 (0.3)	1 (2.9%)	0.016	0	1 (1.8)	0.031
PCI	34 (3.5)	5 (14.7)	0.001	0	13 (23.2)	<0.001
Stroke	7 (0.7)	1 (2.9)	0.151	1 (0.4)	0	0.642
Death	1 (0.1)	0	0.853	0	0	–

cIMT, carotid intima-media thickness; CAC, coronary artery calcium; CV, cardiovascular; ACS, acute coronary syndrome; PCI, percutaneous coronary intervention.

On comparing the cumulative incidence of the primary outcome in the cIMT-increased group and the cIMT-normal group using a Kaplan–Meier plot, significantly more CV outcomes occurred in the cIMT-increased group than in the cIMT-normal group ($p < 0.001$, Figure 2). Similarly, the occurrence of the primary outcome was higher in the CAC-increased group ($p < 0.001$, Figure 2).

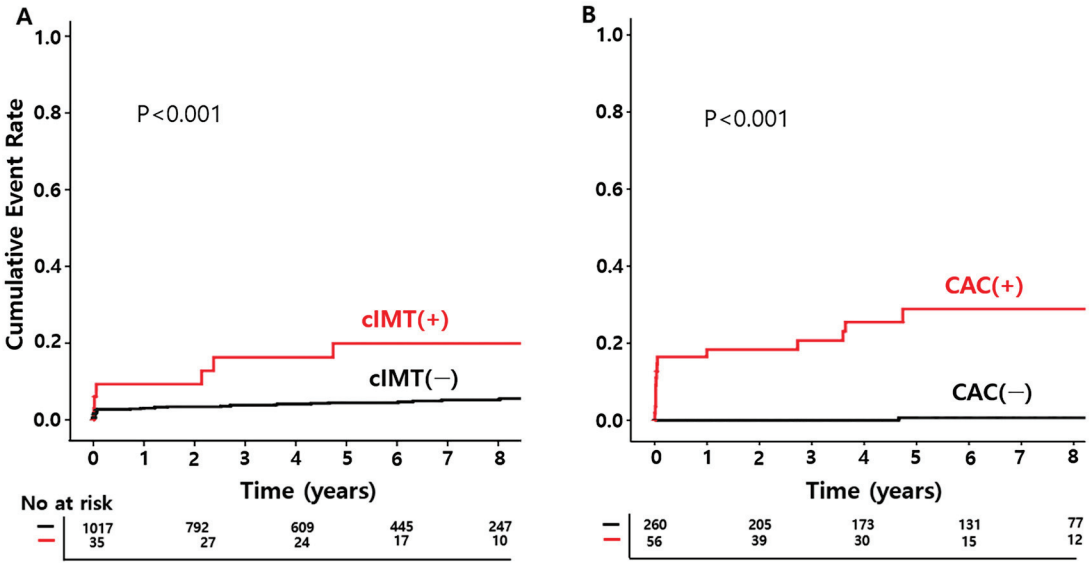


Figure 2. The cumulative incidence of the primary outcomes: A. cIMT, B, CAC scoring. cIMT, carotid intima-media thickness; CAC, coronary artery calcium score; (−), normal group; (+), increased group.

Most CV outcomes occurred within 3 months of examination, and except for one stroke, all early events were due to coronary revascularization. Most cases of coronary revascularization (39/50) had been carried out within 1 year after the TSE test. The coronary angiographic findings of these patients showed most patients had intermediate lesions (50–90%) in the mid or distal coronary artery or lesions in branch arteries such as the obtuse marginal artery (OM) (Table S1).

In univariable analysis of the Cox proportional hazard model, the primary outcomes were high in older persons, male, patients with hypertension and diabetes, high systolic and diastolic blood pressures, low heart rate and target heart rate, and patients with angina during the test, and increased cIMT and CAC score (Tables 3 and S2). In multivariable analysis of the Cox proportional hazard model, age, sex, history of hypertension and diabetes, blood pressure, heart rate, target heart rate, and angina during the TSE test were adjusted. Increased cIMT and CAC scores were independent predictors of the occurrence of the primary outcome (hazard ratio [HR] = 2.939, 95% confidence interval [95%CI] = 1.241–6.960, $p = 0.014$ in the cIMT group; HR = 45.192, 95% CI = 5.497–371.505, $p < 0.001$ in the CAC group).

Table 3. Univariable and multivariable predictors of the primary cardiovascular outcomes.

	Univariable		**Multivariable**			
			cIMT		**CAC**	
	HR (95% CI)	***p*-Value**	**HR (95% CI)**	***p*-Value**	**HR (95% CI)**	***p*-Value**
Clinical Characteristics						
Age	1.064 (1.036–1.093)	<0.001	1.068 (1.029–1.108)	<0.001	1.082 (0.997–1.175)	0.060
Male	2.181 (1.282–3.711)	0.004	2.372(1.250–4.501)	0.008	5.682(1.127–28.650)	0.035
BMI	1.036 (0.971–1.105)	0.285				
Smoking	1.352 (0.779–2.348)	0.284				
Hypertension	1.921 (1.184–3.115)	0.008	0.837 (0.451–1.550)	0.571	1.800 (0.524–6.187)	0.351

Table 3. *Cont.*

	Univariable		Multivariable			
			cIMT		CAC	
	HR (95% CI)	***p*-Value**	**HR (95% CI)**	***p*-Value**	**HR (95% CI)**	***p*-Value**
Diabetes	1.832 (1.106–3.034)	0.019	0.749 (0.364–1.542)	0.433	2.726 (0.689–10.785)	0.153
Dyslipidemia	1.085 (0.672–1.752)	0.739				
TSE data						
SBP	1.028 (1.013–1.043)	<0.001	1.023 (1.000–1.046)	0.045	1.040 (1.001–1.081)	0.045
DBP	1.033 (1.012–1.054)	0.002	1.026 (0.996–1.058)	0.093	1.028 (0.981–1.077)	0.253
Heart rate	0.968 (0.947–0.990)	0.005	0.959 (0.930–0.989)	0.009	0.998 (0.931–1.069)	0.946
Target heart rate, %	0.969 (0.947–0.991)	0.007	0.969 (0.943–0.995)	0.020	0.972 (0.909–1.038)	0.396
METs	0.914(0.824–1.014)	0.089				
Angina during test	1.717 (1.017–2.898)	0.043	1.741 (0.940–3.225)	0.078	1.081 (0.276–4.228)	0.911
Atherosclerotic markers						
Increased cIMT	4.772 (2.151–10.586)	<0.001	2.939 (1.241–6.960)	0.014	–	
Increased CAC	72.917 (9.578–555.097)	<0.001	–		45.192(5.497–371.505)	<0.001

cIMT, carotid intima-media thickness; CAC, coronary artery calcium; HR, hazard ratio; CI, confidence interval; BMI, body mass index; TSE, treadmill stress echocardiography; SBP, systolic blood pressure; DBP, diastolic blood pressure; METs, metabolic equivalent of tasks.

4. Discussion

We evaluated the relevance of increased cIMT and CAC scores in predicting CV outcomes among patients presenting with angina symptoms but with negative TSE tests. Our findings suggest that increased cIMT and CAC scores may serve as useful markers for predicting CV outcomes even in symptomatic patients with negative TSE results. The key findings from this study are as follows: First, compared to the normal group, patients with increased cIMT or CAC scores are older, have a higher BMI, and have underlying diseases. Second, patients with increased cIMT or CAC scores exhibit a significantly increased incidence of CV outcome. Third, in patients with angina with negative TSE test results, increased cIMT and CAC scores are independent risk factors for the occurrence of CV outcomes.

Patients with increased cIMT or CAC scores can be considered to have atherosclerosis. Age, obesity, and underlying CV diseases are well-known risk factors for atherosclerosis. This study also demonstrated that the group with an increased cIMT or CAC score was older, had a higher BMI, and possessed underlying CV diseases compared to the normal group. Patients with increased cIMT or CAC scores took more antiplatelets, ACEi/ARB, and statins. This is because patients with atherosclerosis had underlying CV diseases rather than the progression of atherosclerosis occurring despite taking medications. On the other hand, some diseases are strongly related to CV risk. Myeloproliferative neoplasms are diseases associated with high CV risk by increasing thrombotic risk and worsening CV complications due to genetic mutations and chronic inflammation [16]. Rheumatic diseases such as systemic lupus erythematosus or rheumatoid arthritis are well known to increase CV risk by inducing a prothrombotic state due to an inflammatory response. [17,18]. This study excluded patients with such severe systemic disease to prevent bias.

The cutoff value of cIMT and CAC score in this study was determined based on previous data. Setting a cutoff value for cIMT is very controversial, and the normal range for cIMT varies with age [7]. However, according to the 2023 ESH guidelines for the management of arterial hypertension, cIMT above 0.90 mm is considered abnormal [7]. Based on the guidelines, when the mean cIMT exceeded 0.90 mm, it was classified as increased in this study. As for the CAC score, recent guidelines have indicated that CV risk

is elevated regardless of other factors when the CAC score is ≥100 [2,13]. Previous studies have often set the cutoff value of the CAC score at 100 [19]. However, existing studies have suggested that a CAC score of zero holds significance in symptomatic patients [20]. Considering these studies, we set the cutoff value of the CAC score to 75 through the ROC curve analysis (Figure S1).

Despite the varied data regarding the diagnostic accuracy of TSE, the recent EVAREST observational study [21] reported a high accuracy rate of 95%. This suggests that patients with negative TSE results are likely to be without CAD. However, issues with the diagnostic accuracy of TSE may have affected the results because most CV outcomes in this study occurred within a short period after the TSE test. The primary reasons for early coronary angiography after the TSE test were abnormal findings on coronary CT angiography or myocardial single photon emission CT. Most coronary angiographic findings for early events showed intermediate lesions in the distal portion of the coronary artery or lesions in branch arteries (Table S1). The ischemic burden due to these lesions was not significant, and it is presumed that these patients had negative results in the TSE test. Therefore, the increase in CV outcomes in patients with increased atherosclerotic markers suggests that increased cIMT and CAC scores may help predict CVD in symptomatic patients even if TSE is negative.

In this study, the increased cIMT was identified as an independent predictor of CV outcomes. Some studies have suggested that cIMT does not have an independent effect on CV risk, and current guidelines do not recommend routine use of carotid imaging [7,12,13]. However, a recent meta-analysis suggested that reducing the progression of cIMT using antihypertensive, lipid-lowering, and antidiabetic drugs reduced the risk of CV outcome [22]. The mean value of cIMT measured in the common carotid artery was related to CV risk, and medication for the progression of cIMT was associated with reduced CV risk [22]. A recent meta-study found that a 1-standard deviation increase in cIMT measured in the common carotid artery was associated with CVD events (HR = 1.28, 95% CI = 1.19–1.37) [23]. Several studies demonstrated that the younger the patients or the thicker the cIMT, the stronger the correlation between cIMT and CV risk [23,24]. A recent small prospective study showed that cIMT and CV risk were related in Asians [25]. However, studies conducted in patients who had negative findings on treadmill tests are scarce, and some of the studies that included such patients did not have a sufficient sample size [8,26]. This study supplements these insufficient data. Therefore, patients with increased cIMT should be managed carefully even when they have negative TSE results.

Regarding the relationship between CAC scores and CVD risk, CAC scoring is recommended when risk estimation for CV diseases is uncertain [14]. A recent meta-analysis demonstrated that patients with CAC had increased all-cause mortality (pooled relative risk [RR] 2.13, 95% CI 1.57–2.90, $p = 0.004$) and CV events (pooled RR 2.91, 95% CI 2.26–3.93, $p < 0.001$) compared to patients without CAC [27]. The addition of the CAC score to the transitional risk factor significantly improved CVD prediction in middle-aged and older patients [28]. Risk classification using the CAC score helps with clinical management, especially in patients with a low clinical likelihood of CAD. [29]. However, previous studies have demonstrated the utility of the CAC score in asymptomatic patients [16]. The value of the CAC score in symptomatic patients is less known [22–25]. In a recent study conducted on patients with stable chest pain, those without CAC had a lower CV risk (HR = 0.08, 95% CI = 0.02–0.30, $p < 0.001$), but the treadmill test was not performed [30]. Combining the treadmill test and CAC scores in low-risk patients, with or without symptoms, helps predict long-term clinical outcomes [31]. Another study suggested that the CAC score is helpful for CVD prediction in symptomatic patients with treadmill-equivocal results [14]. However, the value of the CAC score for symptomatic patients with negative TSE findings has not been studied. This study suggests that an increased CAC score is associated with increased CV outcomes and can be a predictive marker for CV outcomes in symptomatic patients with negative TSE results.

This study is distinctive in that it was conducted on patients with negative TSE but with angina symptoms. Compared to previous studies, the significance of this study is as follows: First, in TSE-negative patients with angina symptoms, atherosclerosis is related to CV outcomes, and atherosclerosis can be assessed by cIMT or CAC scores. Second, an increase in cIMT or CAC scores can be an independent risk factor for CV outcomes in symptomatic patients with negative TSE findings.

Limitation

There are several limitations in this study. The first limitation is the small sample size. In particular, the number of patients undergoing CAC scoring was small due to various factors, including cost, use of contrast medium, and domestic insurance coverage. Moreover, CAC scoring was conducted only in patients with negative TSE findings; therefore, the CAC score was extremely skewed, resulting in a wide CI for HR. Nevertheless, we demonstrated the value of the CAC score, and its clinical implication was considerable.

Second, the study was conducted at a single center, which limits the generalizability. Follow-up studies using diverse and large samples are needed.

Third, the follow-up median time is only 5.8 years. This is because many patients recently participated in the study. Short follow-up time may cause errors in predicting prognosis. Future studies, including continuous follow-up, are necessary.

5. Conclusions

In this study, the increased cIMT and CAC scores were associated with increased CV events in symptomatic patients with negative TSE findings. The cIMT and CAC scores are markers for evaluating atherosclerosis, and patients with atherosclerosis are likely to have a higher CV risk than patients without atherosclerosis. However, because the increase in cIMT or CAC scores indicates the early stages of atherosclerosis, it was controversial whether these abnormalities affect CV outcomes. By selecting symptomatic patients with negative TSE, this study highlights that the presence or absence of atherosclerosis may be a useful indicator for predicting CV events in symptomatic patients without prominent ischemia. This study demonstrated that the increased cIMT and CAC scores in symptomatic patients with negative TSE may be a risk factor for CV events. If additional evidence is available, active lipid-lowering therapy and antihypertensive therapy may be considered for these patients in the future. In conclusion, although TSE-negative, symptomatic patients with increased cIMT or CAC scores should be carefully managed and closely monitored. Prospective studies with various and larger sample sizes will be needed in the future to establish radiological atherosclerosis as an independent risk factor for CVD.

Supplementary Materials: The following supporting information can be downloaded at: https://www.mdpi.com/article/10.3390/biomedicines12092151/s1, Table S1: Coronary angiography in patients with coronary artery disease; Table S2: Primary cardiovascular outcomes for absolute value of atherosclerotic markers; Figure S1: The cutoff value of coronary artery calcium score.

Author Contributions: N.K. contributed to manuscript writing and editing and data collection. H.-J.H. helped with manuscript editing and conceptualization. I.-H.Y. contributed to manuscript editing, data collection, and supervision. All authors have read and agreed to the published version of the manuscript.

Funding: This research received no external funding.

Institutional Review Board Statement: The study was conducted in accordance with the Declaration of Helsinki and approved by the Ethics Committee of Kyung Hee University Hospital at Gangdong (KHNMC 202003063).

Informed Consent Statement: Patient consent was waived due to the study was retrospective and the risk to the patients was extremely low.

Data Availability Statement: The raw data supporting the conclusions of this article will be made available by the authors on request.

Conflicts of Interest: The authors declare no conflict of interest.

References

1. Buettner, R.; Schunter, M. Efficient machine learning based detection of heart disease. In Proceedings of the 2019 IEEE International Conference on E-health Networking, Application & Services (HealthCom), Bogota, Colombia, 14–16 October 2019; pp. 1–6.
2. Mach, F.; Baigent, C.; Catapano, A.L.; Koskinas, K.C.; Casula, M.; Badimon, L.; Chapman, M.J.; De Backer, G.G.; Delgado, V.; Ference, B.A.; et al. 2019 ESC/EAS Guidelines for the management of dyslipidaemias: Lipid modification to reduce cardiovascular risk. *Eur. Heart J.* **2020**, *41*, 111–188. [CrossRef] [PubMed]
3. Fihn, S.D.; Blankenship, J.C.; Alexander, K.P.; Bittl, J.A.; Byrne, J.G.; Fletcher, B.J.; Fonarow, G.C.; Lange, R.A.; Levine, G.N.; Maddox, T.M.; et al. 2014 ACC/AHA/AATS/PCNA/SCAI/STS focused update of the guideline for the diagnosis and management of patients with stable ischemic heart disease: A report of the American College of Cardiology/American Heart Association Task Force on Practice Guidelines, and the American Association for Thoracic Surgery, Preventive Cardiovascular Nurses Association, Society for Cardiovascular Angiography and Interventions, and Society of Thoracic Surgeons. *Circulation* **2014**, *130*, 1749–1767. [CrossRef] [PubMed]
4. McCully, R.B.; Roger, V.L.; Mahoney, D.W.; Karon, B.L.; Oh, J.K.; Miller, F.A., Jr.; Seward, J.B.; Pellikka, P.A. Outcome after normal exercise echocardiography and predictors of subsequent cardiac events: Follow-up of 1,325 patients. *J. Am. Coll. Cardiol.* **1998**, *31*, 144–149. [CrossRef] [PubMed]
5. Knuuti, J.; Wijns, W.; Saraste, A.; Capodanno, D.; Barbato, E.; Funck-Brentano, C.; Prescott, E.; Storey, R.F.; Deaton, C.; Cuisset, T.; et al. 2019 ESC Guidelines for the diagnosis and management of chronic coronary syndromes. *Eur. Heart J.* **2020**, *41*, 407–477. [CrossRef] [PubMed]
6. Mohamed, H.A. Negative exercise stress test Does it mean anything? *Libyan J. Med.* **2007**, *2*, 103–105. [CrossRef]
7. Mancia, G.; Kreutz, R.; Brunstrom, M.; Burnier, M.; Grassi, G.; Januszewicz, A.; Muiesan, M.L.; Tsioufis, K.; Agabiti-Rosei, E.; Algharably, E.A.E.; et al. 2023 ESH Guidelines for the management of arterial hypertension The Task Force for the management of arterial hypertension of the European Society of Hypertension: Endorsed by the International Society of Hypertension (ISH) and the European Renal Association (ERA). *J. Hypertens.* **2023**, *41*, 1874–2071. [CrossRef]
8. Karabay, C.Y.; Kocabay, G.; Guler, A.; Kalayci, A.; Akgun, T.; Kirma, C. The clinical usefulness of carotid ultrasonography in patients with an inconclusive exercise treadmill stress test result. *J. Cardiol.* **2014**, *64*, 70–74. [CrossRef]
9. Holaj, R.; Spacil, J.; Petrasek, J.; Malik, J.; Haas, T.; Aschermann, M. Intima-media thickness of the common carotid artery is the significant predictor of angiographically proven coronary artery disease. *Can. J. Cardiol.* **2003**, *19*, 670–676.
10. Calmarza, P.; Trejo, J.M.; Lapresta, C.; Lopez, P. Lack of association between carotid intima-media thickness and apolipoprotein (a) isoforms in a sample of Spanish general population. *J. Cardiol.* **2013**, *61*, 372–377. [CrossRef]
11. Bernard, S.; Serusclat, A.; Targe, F.; Charriere, S.; Roth, O.; Beaune, J.; Berthezene, F.; Moulin, P. Incremental predictive value of carotid ultrasonography in the assessment of coronary risk in a cohort of asymptomatic type 2 diabetic subjects. *Diabetes Care* **2005**, *28*, 1158–1162. [CrossRef]
12. Den Ruijter, H.M.; Peters, S.A.; Anderson, T.J.; Britton, A.R.; Dekker, J.M.; Eijkemans, M.J.; Engstrom, G.; Evans, G.W.; de Graaf, J.; Grobbee, D.E.; et al. Common carotid intima-media thickness measurements in cardiovascular risk prediction: A meta-analysis. *JAMA* **2012**, *308*, 796–803. [CrossRef] [PubMed]
13. Grundy, S.M.; Stone, N.J.; Bailey, A.L.; Beam, C.; Birtcher, K.K.; Blumenthal, R.S.; Braun, L.T.; de Ferranti, S.; Faiella-Tommasino, J.; Forman, D.E.; et al. 2018 AHA/ACC/AACVPR/AAPA/ABC/ACPM/ADA/AGS/APhA/ASPC/NLA/PCNA Guideline on the Management of Blood Cholesterol: A Report of the American College of Cardiology/American Heart Association Task Force on Clinical Practice Guidelines. *J. Am. Coll. Cardiol.* **2019**, *73*, e285–e350. [CrossRef] [PubMed]
14. Huang, W.; Huang, Z.; Koh, N.S.Y.; Ho, J.S.; Chua, T.S.J.; Tan, S.Y. Adding coronary calcium score to exercise treadmill test: An alternative to refine coronary artery disease risk stratification in patients with intermediate risk chest pain. *Glob. Heart* **2020**, *15*, 22. [CrossRef] [PubMed]
15. Grossman, C.; Ehrlich, S.; Shemesh, J.; Koren-Morag, N.; Grossman, E. Coronary artery calcium and exercise electrocardiogram as predictors of coronary events in asymptomatic adults. *Am. J. Cardiol.* **2015**, *115*, 745–750. [CrossRef]
16. Todor, S.B.; Ichim, C.; Boicean, A.; Mihaila, R.G. Cardiovascular Risk in Philadelphia-Negative Myeloproliferative Neoplasms: Mechanisms and Implications-A Narrative Review. *Curr. Issues Mol. Biol.* **2024**, *46*, 8407–8423. [CrossRef]
17. Bezuidenhout, J.A.; Venter, C.; Roberts, T.J.; Tarr, G.; Kell, D.B.; Pretorius, E. Detection of Citrullinated Fibrin in Plasma Clots of Rheumatoid Arthritis Patients and Its Relation to Altered Structural Clot Properties, Disease-Related Inflammation and Prothrombotic Tendency. *Front. Immunol.* **2020**, *11*, 577523. [CrossRef]
18. Turk, S.M.; Cansu, D.U.; Teke, H.U.; Kasifoglu, T.; Meltem Akay, O.; Bilgin, M.; Korkmaz, C. Can we predict thrombotic tendency in rheumatoid arthritis? A thromboelastographic analysis (with ROTEM). *Clin. Rheumatol.* **2018**, *37*, 2341–2349. [CrossRef]
19. Chua, A.; Blankstein, R.; Ko, B. Coronary artery calcium in primary prevention. *Aust. J. Gen. Pract.* **2020**, *49*, 464–469. [CrossRef]
20. Neves, P.O.; Andrade, J.; Monção, H. Coronary artery calcium score: Current status. *Radiol. Bras.* **2017**, *50*, 182–189. [CrossRef]
21. Woodward, W.; Dockerill, C.; McCourt, A.; Upton, R.; O'Driscoll, J.; Balkhausen, K.; Chandrasekaran, B.; Firoozan, S.; Kardos, A.; Wong, K.; et al. Real-world performance and accuracy of stress echocardiography: The EVAREST observational multi-centre study. *Eur. Heart J. Cardiovasc. Imaging* **2022**, *23*, 689–698. [CrossRef]

22. Willeit, P.; Tschiderer, L.; Allara, E.; Reuber, K.; Seekircher, L.; Gao, L.; Liao, X.; Lonn, E.; Gerstein, H.C.; Yusuf, S.; et al. Carotid Intima-Media Thickness Progression as Surrogate Marker for Cardiovascular Risk: Meta-Analysis of 119 Clinical Trials Involving 100 667 Patients. *Circulation* **2020**, *142*, 621–642. [CrossRef] [PubMed]
23. Ling, Y.; Wan, Y.; Barinas-Mitchell, E.; Fujiyoshi, A.; Cui, H.; Maimaiti, A.; Xu, R.; Li, J.; Suo, C.; Zaid, M. Varying Definitions of Carotid Intima-Media Thickness and Future Cardiovascular Disease: A Systematic Review and Meta-Analysis. *J. Am. Heart Assoc.* **2023**, *12*, e031217. [CrossRef] [PubMed]
24. Ge, J.; Jing, F.; Ji, R.; Tian, A.; Su, X.; Li, W.; He, G.; Pu, B.; Lei, L.; Lu, J.; et al. Age-Related Trends in the Predictive Value of Carotid Intima-Media Thickness for Cardiovascular Death: A Prospective Population-Based Cohort Study. *J. Am. Heart Assoc.* **2023**, *12*, e029656. [CrossRef] [PubMed]
25. Sekar, A.; Amir, A.P.; Seeni Mohamed, A.M.; Natarajan, P. Decoding Cardiovascular Health: Carotid Intima-Media Thickness and Its Association With Coronary Artery Disease in the Indian Population. *Cureus* **2024**, *16*, e55836. [CrossRef]
26. Kanwar, M.; Rosman, H.S.; Fozo, P.K.; Fahmy, S.; Vikraman, N.; Gardin, J.M.; Bess, R.L.; Cohen, G.I. Usefulness of carotid ultrasound to improve the ability of stress testing to predict coronary artery disease. *Am. J. Cardiol.* **2007**, *99*, 1196–1200. [CrossRef]
27. Osborne-Grinter, M.; Ali, A.; Williams, M.C. Prevalence and clinical implications of coronary artery calcium scoring on non-gated thoracic computed tomography: A systematic review and meta-analysis. *Eur. Radiol.* **2024**, *34*, 4459–4474. [CrossRef]
28. Khan, S.S.; Post, W.S.; Guo, X.; Tan, J.; Zhu, F.; Bos, D.; Sedaghati-Khayat, B.; van Rooij, J.; Aday, A.; Allen, N.B.; et al. Coronary Artery Calcium Score and Polygenic Risk Score for the Prediction of Coronary Heart Disease Events. *JAMA* **2023**, *329*, 1768–1777. [CrossRef]
29. Brix, G.S.; Rasmussen, L.D.; Rohde, P.D.; Schmidt, S.E.; Nyegaard, M.; Douglas, P.S.; Newby, D.E.; Williams, M.C.; Foldyna, B.; Knuuti, J.; et al. Calcium Scoring Improves Clinical Management in Patients With Low Clinical Likelihood of Coronary Artery Disease. *JACC Cardiovasc. Imaging* **2024**, *17*, 625–639. [CrossRef]
30. Biavati, F.; Saba, L.; Boussoussou, M.; Kofoed, K.F.; Benedek, T.; Donnelly, P.; Rodriguez-Palomares, J.; Erglis, A.; Stechovsky, C.; Sakalyte, G.; et al. Coronary Artery Calcium Score Predicts Major Adverse Cardiovascular Events in Stable Chest Pain. *Radiology* **2024**, *310*, e231557. [CrossRef]
31. Chang, S.M.; Nabi, F.; Xu, J.; Pratt, C.M.; Mahmarian, A.C.; Frias, M.E.; Mahmarian, J.J. Value of CACS compared with ETT and myocardial perfusion imaging for predicting long-term cardiac outcome in asymptomatic and symptomatic patients at low risk for coronary disease: Clinical implications in a multimodality imaging world. *JACC Cardiovasc. Imaging* **2015**, *8*, 134–144. [CrossRef]

Disclaimer/Publisher's Note: The statements, opinions and data contained in all publications are solely those of the individual author(s) and contributor(s) and not of MDPI and/or the editor(s). MDPI and/or the editor(s) disclaim responsibility for any injury to people or property resulting from any ideas, methods, instructions or products referred to in the content.

biomedicines

MDPI

Article

External Support of Autologous Internal Jugular Vein Grafts with FRAME Mesh in a Porcine Carotid Artery Model

Jaroslav Chlupac [1,2,*], Jan Frank [1], David Sedmera [3], Ondrej Fabian [4,5], Zuzana Simunkova [6], Iveta Mrazova [6], Tomas Novak [1], Zdenka Vanourková [6], Oldrich Benada [7], Zdenek Pulda [8], Theodor Adla [8], Martin Kveton [4,9], Alena Lodererova [4], Ludek Voska [4], Jan Pirk [10] and Jiri Fronek [1,2,11]

1 Transplantation Surgery Department, Institute for Clinical and Experimental Medicine (IKEM), Videnska 1958/9, 140 21 Prague, Czech Republic; jan.frank@ikem.cz (J.F.); tomas.novak@lfmotol.cuni.cz (T.N.); jiri.fronek@ikem.cz (J.F.)
2 Department of Anatomy, Second Faculty of Medicine, Charles University, V Uvalu 84, 150 06 Prague, Czech Republic
3 Institute of Anatomy, First Faculty of Medicine, Charles University, U Nemocnice 3, Praha 2, 128 00 Prague, Czech Republic; david.sedmera@lf1.cuni.cz
4 Clinical and Transplant Pathology Centre, Institute for Clinical and Experimental Medicine (IKEM), Videnska 1958/9, 140 21 Prague, Czech Republic; ondrej.fabian@ikem.cz (O.F.); martin.kveton@ikem.cz (M.K.); alena.lodererova@ikem.cz (A.L.); ludek.voska@ikem.cz (L.V.)
5 Department of Pathology and Molecular Medicine, Third Faculty of Medicine, Charles University, and Thomayer University Hospital, Ruska 87, 100 00 Prague, Czech Republic
6 Experimental Medicine Centre, Institute for Clinical and Experimental Medicine (IKEM), Videnska 1958/9, 140 21 Prague, Czech Republic; zuzana.simunkova@ikem.cz (Z.S.); iveta.mrazova@ikem.cz (I.M.); zdenka.vanourkova@ikem.cz (Z.V.)
7 Laboratory of Molecular Structure Characterization, Institute of Microbiology of the Czech Academy of Sciences, Vídeňská 1083, 142 00 Prague, Czech Republic; benada@biomed.cas.cz
8 Department of Imaging Methods, Institute for Clinical and Experimental Medicine (IKEM), Videnska 1958/9, 140 21 Prague, Czech Republic; zdpu@seznam.cz (Z.P.); theodor.adla@ikem.cz (T.A.)
9 Third Faculty of Medicine, Charles University, Ruska 87, 100 00 Prague, Czech Republic
10 Cardiovascular Surgery Department, Institute for Clinical and Experimental Medicine (IKEM), Videnska 1958/9, 140 21 Prague, Czech Republic; jan.pirk@ikem.cz
11 First Surgical Clinic, First Faculty of Medicine, Charles University, U Nemocnice 499/2, 128 08 Prague, Czech Republic
* Correspondence: jaroslav.chlupac@ikem.cz

Abstract: Background: Autologous vein grafts are widely used for bypass procedures in cardiovascular surgery. However, these grafts are susceptible to failure due to vein graft disease. Our study aimed to evaluate the impact of the latest-generation FRAME external support on vein graft remodeling in a preclinical model. Methods: We performed autologous internal jugular vein interposition grafting in porcine carotid arteries for one month. Four grafts were supported with a FRAME mesh, while seven unsupported grafts served as controls. The conduits were examined through flowmetry, angiography, macroscopy, and microscopy. Results: The one-month patency rate of FRAME-supported grafts was 100% (4/4), whereas that of unsupported controls was 43% (3/7, Log-rank $p = 0.071$). On explant angiography, FRAME grafts exhibited significantly more areas with no or mild stenosis (9/12) compared to control grafts (3/21, $p = 0.0009$). Blood flow at explantation was higher in the FRAME grafts (145 ± 51 mL/min) than in the controls (46 ± 85 mL/min, $p = 0.066$). Area and thickness of neo-intimal hyperplasia (NIH) at proximal anastomoses were similar for the FRAME and the control groups: 5.79 ± 1.38 versus 6.94 ± 1.10 mm^2, respectively ($p = 0.558$) and 480 ± 95 vs. 587 ± 52 $\mu m^2/\mu m$, respectively ($p = 0.401$). However, in the midgraft portions, the NIH area and thickness were significantly lower in the FRAME group than in the control group: 3.73 ± 0.64 vs. 6.27 ± 0.64 mm^2, respectively ($p = 0.022$) and 258 ± 49 vs. 518 ± 36 $\mu m^2/\mu m$, respectively ($p = 0.0002$). Conclusions: In our porcine model, the external mesh FRAME improved the patency of vein-to-carotid artery grafts and protected them from stenosis, particularly in the mid regions. The midgraft neo-intimal hyperplasia was two-fold thinner in the meshed grafts than in the controls.

Keywords: blood vessel prosthesis; autologous vein graft; external stent; carotid artery; pig

1. Introduction

Cardiovascular disease is a leading cause of morbidity and mortality worldwide. Bypass grafting is a widely used surgical technique to treat atherosclerotic occlusive or aneurysmal disease [1]. Autologous arterial conduits, such as the internal thoracic artery or the radial artery, are considered the most durable grafts for cardiac bypass procedures. These arterial grafts exhibit an excellent 10-year patency rate of 90% [2]; however, their use is constrained by limited availability.

Autologous saphenous vein graft (SVG) is the most frequently utilized conduit for coronary (CABG) and peripheral artery bypass grafting (PABG). The saphenous vein is a superficial, non-essential vein that can be harvested from the patient's leg(s). It is then implanted as a small-caliber ($\leq$6 mm) arterial bypass or substitution on the heart or extremities. However, the key limitation is a high failure rate due to vein graft disease (VGD). The patency rate of SVGs drops to 50% by 10 years in both cardiac and peripheral bypass applications [1,3].

The VGD occurs because the vein, originally situated in a low-flow and low-pressure venous environment, undergoes a harvest injury and is then transplanted into the arterial circulation, which has high-flow and high-pressure conditions. These conditions increase shear stress and wall tension on the graft, leading to compensatory graft dilation and wall thickening, a process known as neo-intimal hyperplasia (NIH). NIH is characterized by the proliferation and migration of vascular smooth muscle cells (VSMCs) from the media to denuded and dysfunctional intima accompanied by the deposition of extracellular matrix. NIH comes along as diffuse wall thickening and/or focal lumen irregularities causing flow disturbances. NIH further predisposes the graft to thrombosis and accelerated atherosclerosis [3]. Such negative remodeling may result in vessel stenosis and occlusion. Early graft failures within one month post surgery are attributed to technical factors, inadequate conduit quality, poor run-off, and acute thrombosis. NIH is a primary cause of mid-term failures occurring from 1 month onward to 1–2 years postoperatively. Graft atherosclerosis is responsible for late events [4].

Currently, the only proven methods to prevent VGD involve the "no-touch" vein harvesting technique [5], lipid-lowering therapies, and antiplatelet agents [1]. Several other strategies have been explored to combat VGD, including modified surgical techniques, preservation solutions, topical ex vivo pretreatments, pharmacological interventions, gene manipulations, and external stenting [1,4].

The VGD is considered biomechanical in nature [6], justifying the use of external stents as an outer layer that protects vein grafts in arterial circulation [6]. External mesh devices influence venous wall remodeling post-arterial grafting in several ways. They reduce wall tension and prevent non-uniform dilation, thereby improving lumen uniformity and flow patterns. Furthermore, these supports facilitate adventitial neovascularization and redirect VSMC migration outwards through a reverse chemotactic gradient [7]. These actions mitigate wall thickening and suppress the formation of NIH and the development of graft atherosclerosis.

External stenting has shown considerable promise in preclinical [3,8] and, to some extent, in clinical studies [9,10] (for a review, see [6,11,12]). Most clinical trials have been conducted on CABG surgery [13]; however, reports on PABG surgery are limited [14,15].

The aim of our in vivo animal study was to investigate the effect of a current-generation FRAME external support device, which is intended for peripheral vascular surgery, on patency and neointima formation of autologous internal jugular vein interposition grafts that were implanted in porcine carotid arteries. Four weeks after implantation, we found that supported grafts had lower occlusion and stenosis rates than their control unsupported counterparts.

2. Materials and Methods

2.1. Surgery

2.1.1. Implantation

Our porcine animal model with respect to carotid artery implantations has previously been described; these descriptions would include anesthesia and surgical considerations [16]. With regards to the handling of the pigs, we implemented standard means of general anesthesia (GA), analgesia, and peri-operative care. The average weight of the female domestic pigs (*sus scrofa domesticus*) at implantation was 42 $\pm$ 4 kg.

We carried out operative bilateral common carotid artery exposure with two neck incisions under sterile conditions in a supine position. Using the no-touch technique (albeit not exclusively), the internal jugular vein (IJV), which is anatomically located along the carotid artery, was carefully retrieved and gently flushed with (and stored in) warm heparinized saline. In order to identify and suture potential leaks, we applied routine gentle surgical distension with a cannula and a syringe (without pressure monitoring).

The vein was harvested unilaterally from the right side in Pigs 1 and 2 and divided into two halves, i.e., one graft each for the right and left side. In Pigs 3 and 4, the veins were retrieved bilaterally and implanted in carotid arteries on the ipsilateral sides. We consider bilateral retrieval of the IJV safe and well tolerated in swine since blood outflow from the head may be secured via external jugular veins much larger (8–9 mm) than the retrieved internal jugulars (4–4.5 mm) [17]. In addition, the diameter of the IJV grafts matched that of the carotid arteries.

We also implanted autologous IJV grafts in right-sided carotids and autologous IJV patch grafts in left-sided carotids in three additional pigs in another experiment (Pigs 5–7). We shared the right-sided implants as controls in the current study to reduce the number of animals within the 3R principle (reduction, replacement, and refinement).

After full heparinization (200 IU/kg initially plus redosing according to activated clotting time), a ~2–3 cm-long segment of the cross-clamped common carotid artery was resected and replaced with an autologous vein interposition graft, which was implanted under optical magnification using end-to-end anastomoses with a running polypropylene 7/0 suture. The tubular FRAME mesh was threaded over the vein grafts upon completion of the proximal anastomosis and prior to suturing the distal anastomosis. The grafts were oriented in a reversed fashion due to valves enabling one-way blood flow in veins. The implanted grafts eventually needed to be longer than the excised carotid segments due to physiological retraction of the proximal and distal arterial stumps. Finally, the incisions were closed in layers, and the animals were allowed to recover. Each animal was given 100 mg of aspirin one day prior to surgery and thereafter received the same dose daily.

The FRAME device was purchased from Vascular Graft Solutions (VGS, Tel Aviv, Israel; locally traded by CARDION Ltd., Brno, Czech Republic). This is a flexible, kink-resistant, braided, metal (chromium-cobalt alloy) external mesh support apparatus used for vein grafts in peripheral (i.e., non-cardiac) bypass and reconstruction procedures. The device features axial plasticity as well as radial elasticity and is supposed to mitigate the pathological remodeling of vein grafts. Product models A, B, C, and D are intended for vein graft diameters of 3.5–4.5 mm, 4.6–5.5 mm, 5.6–6.5 mm, and 6.6–8.0 mm, respectively [18]. Throughout our study, we used the model B diameter based on intraoperative calibration. Additionally, the company produces two other devices (not utilized in our study): the FRAME FR device intended for support of arteriovenous fistulas for hemodialysis access; and the VEST device used for coronary artery vein bypass grafts. No fixation of the external stents is required. Our procedure is presented in Figure 1.

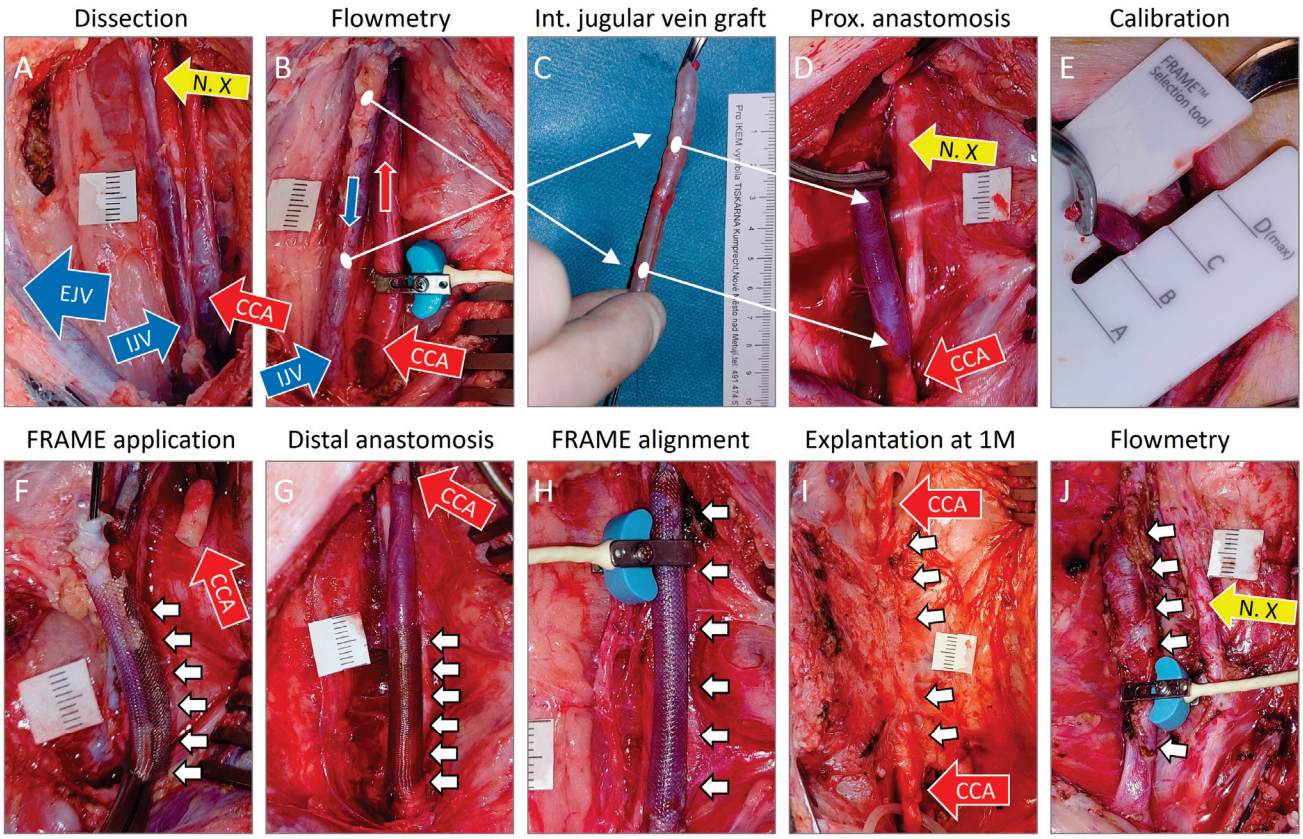


Figure 1. Implantation of a FRAME-supported internal jugular vein interposition graft in a porcine carotid artery. (**A**)—Dissection of a common carotid artery (CCA, red arrow) and an internal jugular vein (IJV, smaller blue arrow). A larger external jugular vein was also visible (EJV, larger blue arrow). N. X—vagal nerve, tenth cranial nerve, yellow arrow. (**B**)—A flowmetry probe was placed around the native carotid artery to measure blood flow volume prior to graft implantation. (**C**)—Retrieved reversed internal jugular vein graft. (**D**)—Completion of proximal anastomosis in an end-to-end fashion (red arrow). (**E**)—Calibration and selection of FRAME mesh diameter on a pressurized vein graft. (**F**)—Application of the FRAME mesh (white arrows) over a non-pressurized vein graft. The distal stump of the carotid artery is visible (red arrow). (**G**)—Completion of distal anastomosis in an end-to-end fashion (red arrow). The FRAME device was pushed proximally (white arrows). (**H**)—Alignment of the FRAME mesh (white arrows) over the entire graft. A flowmetry probe was placed around the FRAME-supported vein graft to measure blood flow volume immediately after implantation. (**I**)—Dissection of the graft from postoperative fibrous adhesions (white arrows) during the explantation procedure carried out one month (M) post implantation. The adjacent native carotid artery was encircled with rubber loops placed proximally and distally to the graft location (red arrows). (**J**)—Flowmetry at explantation on a surgically exposed graft.

In Pig 1, we deployed the FRAME support mesh over the vein grafts bilaterally, i.e., both on the right and left sides. In Pig 2, we implanted bare unsupported vein grafts bilaterally as controls. In Pigs 3 and 4, the FRAME support device was applied on the right-sided grafts, while the left sides comprised unsupported control grafts. In this manner, Pigs 3 and 4 served as their own controls. A list of all implanted grafts is presented in Table 1. The mean graft length was somewhat greater in the FRAME group (4.6 ± 0.8 cm) than in the control group (3.8 ± 1.1 cm); however, the difference was not statistically significant ($p = 0.227$).

Table 1. List of FRAME-supported and control internal jugular vein interposition grafts implanted in porcine carotid arteries. Beveling refers to anastomosis beveling.

		Right Carotid Artery				Left Carotid Artery			
	Protocol #	**Group**	**Graft**	**Beveling**	**Length (cm)**	**Group**	**Graft**	**Beveling**	**Length (cm)**
Pig 1	50	FRAME	IJV right	No	5.0	FRAME	IJV right	No	3.5
Pig 2	56	Control	IJV right	Yes	4.0	Control	IJV right	Yes	2.5
Pig 3	60	FRAME	IJV right	Yes	5.0	Control	IJV left	Yes	5.0
Pig 4	61	FRAME	IJV right	Yes	5.0	Control	IJV left	Yes	5.0
Pig 5	20	Control	IJV right	No	2.5	N/A			
Pig 6	29	Control	IJV right	No	4.0	N/A			
Pig 7	48	Control	IJV left	No	4.0	N/A			
			FRAME		Control				
Mean ± SD			4.6 ± 0.8 cm (n = 4)		3.8 ± 1.1 cm (n = 7)			n.s. $p = 0.227$	

IJV—internal jugular vein, N/A—not applicable SD—standard deviation, n.s.—non-significant, #—number.

2.1.2. Flowmetry

Blood flow volume was measured using a flow probe (Transonic, ADInstruments, Oxford, UK) in the following manners and times periods: (1) on the surgically exposed native artery during the implantation procedure prior to grafting; (2) during the implantation procedure immediately after vein grafting; and (3) during the explantation procedure (one month post implantation) immediately after angiography, when the graft was dissected from postoperative adhesions. Before carrying out flow measurements, we bathed the wounds in warm saline for 10–20 min in an attempt to relax the graft spasm brought on by surgical manipulation. The highest measured flow rate was taken into account. We are aware that flowmetry is burdened by interindividual variability and may be influenced by vasospasm (see flow values before and after implantations in the Results Section 3.1.2. Flowmetry). Therefore, a more precise and gold-standard evaluation of patency is through angiograms of undissected vessels.

2.1.3. Angiography

After a period of 1 month, i.e., 28 days, the pigs underwent angiographic examination and graft explantation under a second GA. The average body weight of the animals at explantation was 58 ± 5 kg. Selective carotid angiography (X-ray mobile C-arm Ziehm Vision FD, Ziehm Imaging, Ltd., Nuremberg, Germany) with an iodinated contrast agent (Optiray, Guerbet, Princeton, NJ, USA) was carried out using the femoral artery access according to the Seldinger technique. Each graft was arbitrarily divided into three portions: proximal anastomosis, mid-graft, and distal anastomosis; this amounted to a total of 12 areas (4 grafts × 3 portions) in the FRAME and 21 areas (7 grafts × 3 portions) in the control group. The degree of eventual stenosis in each graft area was calculated according to the North American Symptomatic Carotid Endarterectomy Trial (NASCET) formula, i.e., $[1 - (G/C)] \times 100$, wherein G represents the diameter of the investigated graft portion and C represents the diameter of the adjacent native carotid artery [19]. We carried out anterior-posterior, right lateral, and left lateral projections at an angle of 30°. Therefore, narrowing (expressed as percentage) was calculated as a mean of these three values. A narrowing of ≤40%, 41–60%, and >60% were considered mild, moderate, and severe cases of stenosis, respectively.

2.1.4. Explantation

Immediately following the angiographic examinations, we carefully dissected the implants, carried out flowmetry measurements on exposed grafts, and explanted them along with parts of native carotid arteries. Heparin was not administered during the explantation procedure. The retrieved samples were gently flushed with warm saline,

cross-sectioned at equidistant points along the entire graft, and photographed. The animals were then euthanized with an overdose of thiopental and potassium.

2.2. Macroscopic Examinations

All cross-section photo-macrographs were zoomed-in and examined for the development of luminal neo-intima. We used QuPath open-source software (version 0.3.0) to analyze macrograph images [20]. Average NIH thickness ($\mu m^2/\mu m$) was calculated as the NIH area (μm^2) divided by the presumed (original) lumen circumference (μm) [19]. The mean values were calculated from all sections of each graft within a specific group. We used this formula uniformly with all possible NIH events: circular, semicircular (i.e., not covering the entire lumen circumference), and even with total graft occlusions (Figure 2). We observed NIH in all cases, with the exception of the left-sided midgraft in Pig 1; we therefore took a zero value into account in this case.

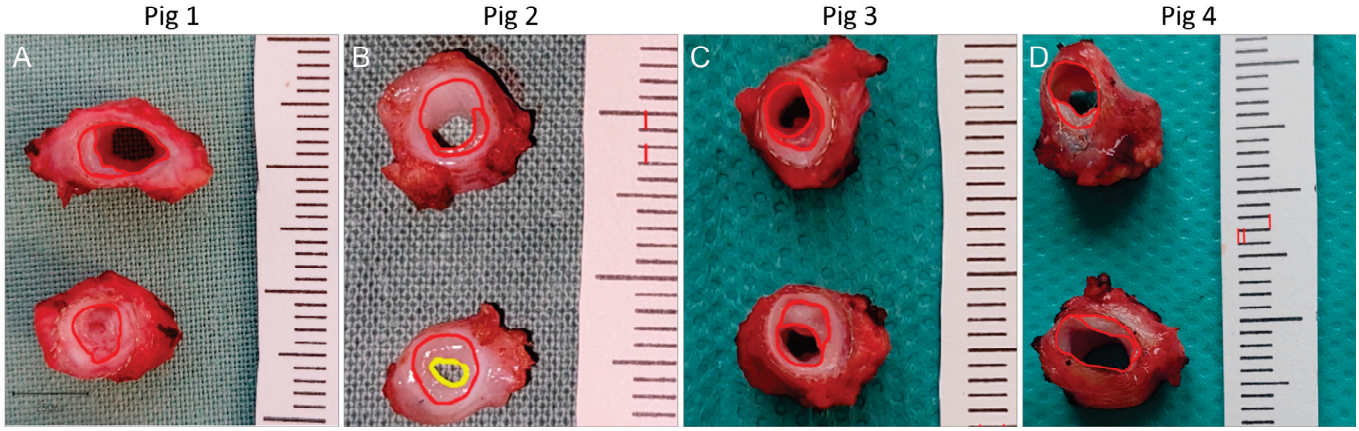


Figure 2. Measurement of neo-intimal hyperplasia (NIH) area and thickness using zoomed macrographs of cross-sectioned explants in Pigs 1, 2, 3, and 4 ((**A**), (**B**), (**C**), and (**D**), respectively). Average NIH thickness ($\mu m^2/\mu m$) was calculated as the NIH area (μm^2) divided by the original lumen circumference (μm).

Near occlusion and total graft occlusions that occurred in the control group can induce atrophy, i.e., shrinkage of the graft diameter. As such, the NIH area divided by the original lumen circumference may give lower values. Despite this, the outcomes regarding NIH formation were more favorable in the FRAME group than in the control group. In contrast, other studies did not include occluded grafts in their analysis [21].

NIH values were calculated separately for proximal anastomoses and midgraft sections. Sufficient NIH measurements for distal anastomoses could not be acquired due to technical reasons: three of the four distal anastomoses in the FRAME group and two in the control group were not cross-sectioned but rather cut open longitudinally, which impeded analysis more so than with the other graft portions. Distal anastomotic regions, however, were evaluated angiographically.

We could not process the supported grafts for histological examinations because of the adhering FRAME mesh. The presence of any metal material precludes common histological sectioning. The required technology and equipment, which include methyl-methacrylate resin embedding as well as appropriate tungsten carbide blade for cutting [7,22], were not available to us [23].

We are aware of the potential inaccuracy in measuring NIH parameters using macrographs as opposed to histological images, which produce more precise measurements. Similar inaccuracies, however, were most likely present for the FRAME and control groups. That is why we considered detailed macroscopic image analysis sufficient for group comparisons. Moreover, digital analysis of macroscopic images has been reported in previous studies [22].

2.3. Microscopical Examinations

2.3.1. Histology and Immunohistochemistry

The cross-sectioned control samples (without FRAME metal support) were emersion fixed with 4% formaldehyde (48 h), embedded in paraffin, cut into 4–5 μm thick sections, mounted on glass slides, dried and stained with hematoxylin and eosin (Merck & Co., Inc., Kenilworth, NJ, USA) and Weigert van Gieson and Resorcin-fuchsin for elastic fibers (proprietary method). We carried out immunostaining for the expression of alpha-smooth muscle actin (primary antibody: REF: 202M, Cell Marque Corp., a part of MilliporeSigma, Rocklin, CA, USA; secondary antibody: provided as part of the UltraView Universal DAB Detection Kit, REF: 760–500, Ventana Medical Systems, Inc., Roche Group, Tucson, AZ, USA), endothelial marker CD31 (primary antibody: REF: NB100-2284, Novus Biologicals, LLC, Centennial, CO, USA; secondary antibody: REF: BA-1000, Vector Laboratories, Inc., Burlingame, CA, USA), and endothelial marker ERG (primary antibody: REF: 434R, Cell Marque Corp., a part of MilliporeSigma, Rocklin, CA, USA; secondary antibody: provided as part of the OptiView DAB IHC Detection Kit, REF: 760–700, Ventana Medical Systems, Inc., Roche Group, Tucson, AZ, USA). The slides were viewed and scanned with an Olympus VS110-S5 Slide Scanner (Olympus, Hamburg, Germany).

We used QuPath open-source software (version 0.3.0) for digital pathology image analysis [20] and measured NIH area and thickness in multiple midgraft histological sections of the control grafts. The NIH thickness was calculated in a manner identical to that of the macrograph method, i.e., the NIH area divided by the original lumen circumference. These parameters can be measured precisely using histology images: the NIH area was defined as any neo-tissue luminal from internal elastic lamina, and the presumed (original) lumen circumference was delineated by this internal elastic lamina. The neo-tissue abluminal from external elastic lamina was termed neo-adventitia.

2.3.2. Macro Photography

Macro photographs were taken under an Olympus SZX125 dissecting microscope using, a 1.0× objective, and DP 74 CCD camera (Olympus, Japan).

2.3.3. Confocal Microscopy

Confocal imaging was performed following whole mount staining, as described recently [24], with anti-von Willebrand factor antibody (1:50, Sigma #3520, Sigma-Aldrich, Saint Louis, MO, USA), detected with Cy5 secondary antibody (Jackson ImmunoResearch, Cambridgeshire, UK) to label the endothelial cells. The instrument used was an Olympus BX61 upright microscope fitted with an Olympus Fluoview FV1000 confocal system (Olympus, Hamburg, Germany). The stained specimens underwent clearing in CUBIC for 24 h, as described in references [25,26], and were then pinned to the bottom of a deep Sylgard-coated Petri dish for imaging. Imaging utilized a 2× 0.14 NA dry and a 10× 0.6 NA multi-immersion objectives with appropriate excitation and emission settings. A 25× 1.0 NA multi-immersion objective was used for high-power views, allowing for up to 1 μm z-resolution.

2.3.4. Scanning Electron Microscopy (SEM)

SEM was carried out using an established protocol [27]. The fixed samples underwent extensive washing in phosphate-buffered saline (1× PBS, pH 7.2) and were postfixed in a buffered solution of 1% OsO_4 for one hour at room temperature. Following another round of extensive washing with 1× PBS, the samples were dehydrated in a graded series of alcohols (25%, 50%, 70%, 80%, 96%, 100%, and 100%) and subsequently dried in a K850 Critical Point Dryer (Quorum Technologies Ltd., Ringmer, UK). The dried samples were then mounted onto standard aluminum SEM stubs and sputter-coated with a 3 nm layer of platinum using a high-resolution Q150T Turbo-Pumped Sputter Coater (Quorum Technologies Ltd., Ringmer, UK). For the final analysis, the samples were examined under

an FEI Nova NanoSEM 450 scanning electron microscope (FEI, Brno, Czech Republic) employing an SED detector at a voltage of 5 kV.

2.4. Statistical Analysis

Continuous variables with normal distribution were expressed as mean and standard deviation (SD). NIH values are expressed as the mean and standard error of the mean (SE). A two-tailed Student's *t*-test was used to compare two data sets, while a one-way analysis of variance (ANOVA, Newman–Keuls test) was implemented for three data sets, and finally, the log-rank (Mantel-Cox) test was used for survival (patency) analysis. Categorical variables were presented as positive and negative observations (expressed as percentages) and compared using a two-tailed Fisher's exact test. Data were computed in Microsoft Excel (version 2108) spreadsheets. We utilized GraphPad Prism software (version 5.03, 2009) for statistical evaluations. A p-value of ≤ 0.05 was considered statistically significant.

3. Results

3.1. Surgery

3.1.1. Implantation

The mean surgery time was 152 ± 28 min. There were no significant peri-operative or post-operative adverse events. The mean carotid artery clamping time was 40 ± 8 min in the FRAME group and 33 ± 6 min in the control group ($p = 0.116$). The slightly longer time for the FRAME group was statistically non-significant (n.s.), which indicates favorable and swift surgical handling when deploying the FRAME device. Intra-operative views of implanted constructs, pre-explant angiograms, and macrographs of cross-sections explanted at 1 month post implantation are shown in Figure 3. Views of the additional three control grafts are shown in Figure 4.

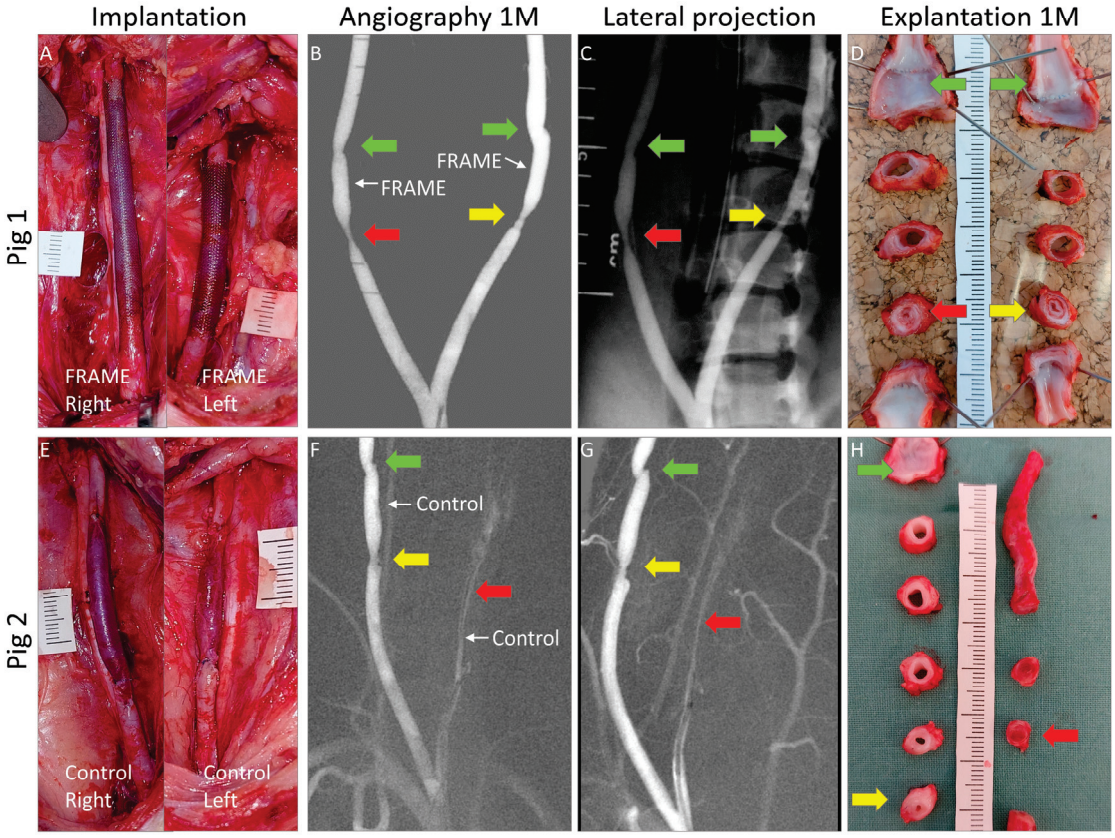


Figure 3. *Cont.*

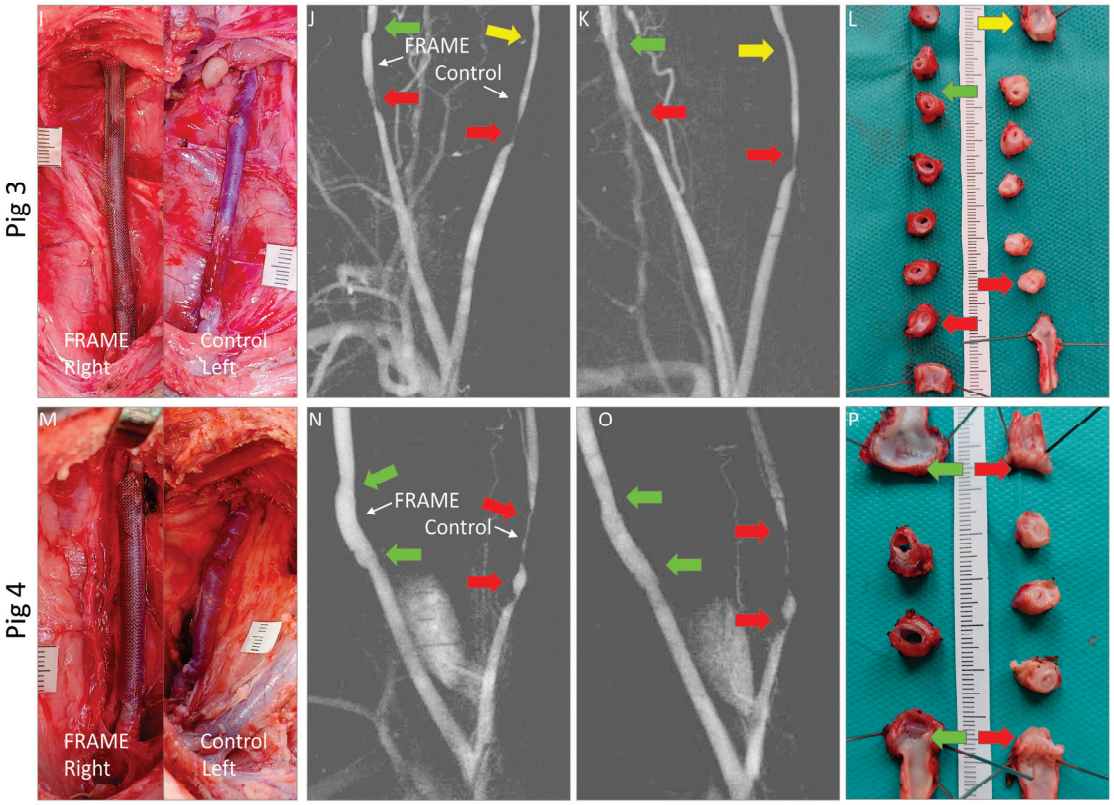


Figure 3. Implantation, pre-explantation angiography, and explantation of autologous internal jugular vein interposition grafts in porcine carotid arteries of Pigs 1 (**A**–**D**), 2 (**E**–**H**), 3 (**I**–**L**), and 4 (**M**–**P**). We implanted grafts supported with FRAME mesh as well as unsupported grafts as controls. Macroscopic views of the grafts after declamping and hemostasis during implantations are shown in the left-hand column. Selective carotid angiograms performed from femoral access at 1 month (1 M) post implantation are shown in the middle two columns (anterior-posterior and lateral projections). Gross appearances of cross-sectioned explants at 1 M are presented in the right-hand column. Proximal and distal anastomoses are marked with arrows; green indicates no or mild stenosis (≤40%), yellow moderate (41–60%), and red severe stenosis (>60%) or occlusion.

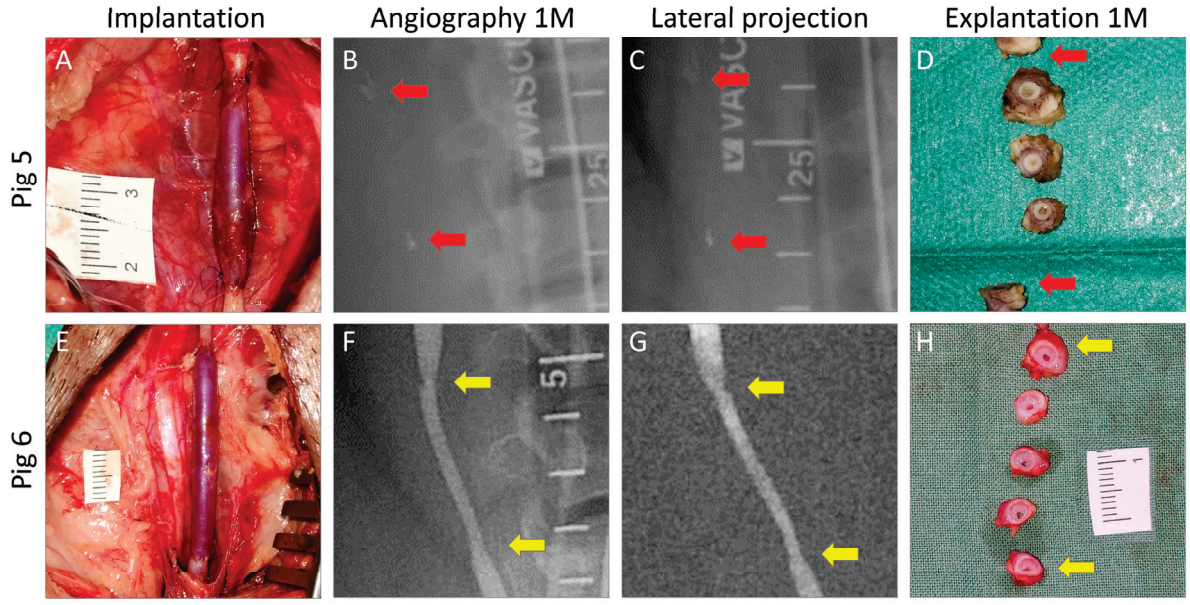


Figure 4. *Cont.*

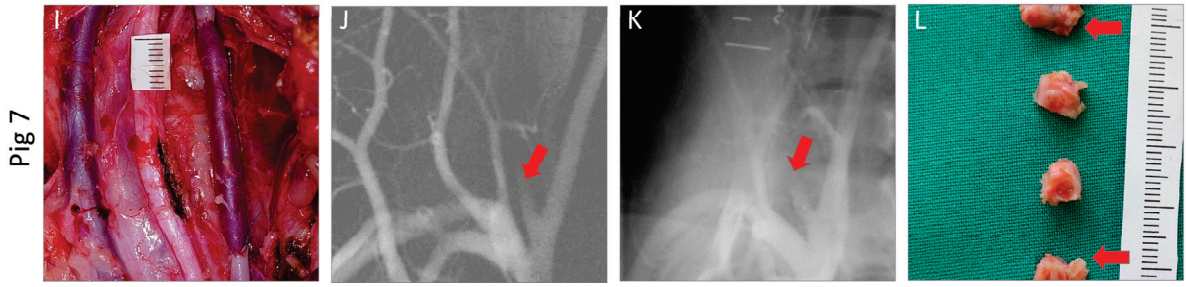


Figure 4. Implantation, pre-explantation angiography, and explantation of autologous internal jugular vein grafts in porcine carotid arteries of Pigs 5 (**A**–**D**), 6 (**E**–**H**), and 7 (**I**–**L**). We implanted interposition grafts to the right-sided carotids and patch grafts to the left-sided carotids. We utilized the right-sided implants as controls to reduce the numbers of experimental animals. Macroscopic views of the grafts after declamping and hemostasis during implantations are shown in the left-hand column. Selective carotid angiograms performed from femoral access at 1 month (1 M) post implantation are shown in the middle two columns (anterior-posterior and lateral projections). Gross appearances of cross-sectioned explants at 1 M are presented in the right-hand column. Proximal and distal anastomoses are marked with arrows; green indicates no or mild stenosis (≤40%), yellow moderate (41–60%), and red severe stenosis (>60%) or occlusion. (**B**,**C**)—red arrows point at metal clips, which indicate boundaries of the occluded grafts. (**J**,**K**)—red arrows point at proximal stumps of occluded carotid arteries.

3.1.2. Flowmetry

Flowmetry results and mean arterial pressures (MAPs) at three time points: native carotid artery before graft implantation, after graft implantation, and explantation at one month (i.e., after 28 days), are presented in Table 2. In the FRAME group, mean blood flow dropped insignificantly after implantation, most likely due to vasospasms and graft placement per se. Differences between the three time points were not significant. At explantation, flow in the right-sided graft in Pig 1 was markedly lower than in the three remaining FRAME-supported grafts, indicating more significant stenosis in proximal anastomosis consistent with the angiograms. Flow in the remaining three FRAME-supported grafts was normal.

In the control group, mean blood flow after graft implantation dropped significantly, most likely also due to vasospasms, graft placement per se, as well as lower, albeit non-significant MAP. The mean flow at explantation dropped markedly, which was statistically significant in contrast to the values prior to implantation. Neither the FRAME group nor the control group exhibited any differences between MAPs.

There were no statistically significant differences in mean flows nor in the MAPs between the FRAME and control groups at any time point. The flow at explantation in the control group was zero in four out of the seven grafts due to graft occlusions and as low as 22 mL/min in the left-sided graft in Pig 3, indicating a failing graft. Flow in the stenotic right-sided graft in Pig 6 was subnormal. The only graft with sufficient flow in the control group was the right-sided graft in Pig 2. Flowmetry results at explantation were, therefore, generally better in the FRAME group, although narrowly missing statistical significance ($p = 0.066$) due to high variations (Figure 5).

Table 2. Flowmetry results in FRAME-supported and control groups of autologous internal jugular vein interposition graft in porcine carotid arteries at three time points: native carotid artery prior to implantation, after graft implantation, and at explantation (1 month post implantation).

FRAME	**Pre-Implantation**		**Post-Implantation**		**Explantation 1 M**	
	Blood Flow (mL/min)	**MAP (mmHg)**	**Blood Flow (mL/min)**	**MAP (mmHg)**	**Blood Flow (mL/min)**	**MAP (mmHg)**
Pig 1 right	85	67	100	72	85	67
Pig 1 left	185	77	220	84	185	77
Pig 3 right	120	76	95	76	120	76
Pig 4 right	190	69	250	67	190	69
Mean ± SD	228 ± 51	73 ± 8	166 ± 80	75 ± 7	145 ± 51	72 ± 5
ANOVA $p = 0.208$	n.s.		n.s.		n.s.	
ANOVA $p = 0.845$		n.s.		n.s.		n.s.
Control						
Pig 2 right	160	65	95	56	230	67
Pig 2 left	450	65	60	58	0	70
Pig 3 left	310	88	190	71	22	80
Pig 4 left	320	77	130	68	0	73
Pig 5 right	400	66	20	60	0	82
Pig 6 right	160	56	75	51	70	74
Pig 7 right	270	68	90	89	0	80
Mean ± SD	296 ± 110	69 ± 10	94 ± 54	65 ± 13	46 ± 85	75 ± 6
ANOVA $p = 0.0001$			* vs. Pre-impl.		* vs. Pre-impl.	
ANOVA $p = 0.177$		n.s.		n.s.		n.s.
FRAME vs. Control	$p = 0.280$	$p = 0.601$	$p = 0.107$	$p = 0.186$	$p = 0.066$	$p = 0.419$

MAP—mean arterial pressure, SD—standard deviation, M—month, n.s.—non-significant, vs. versus, * statistically significant difference.

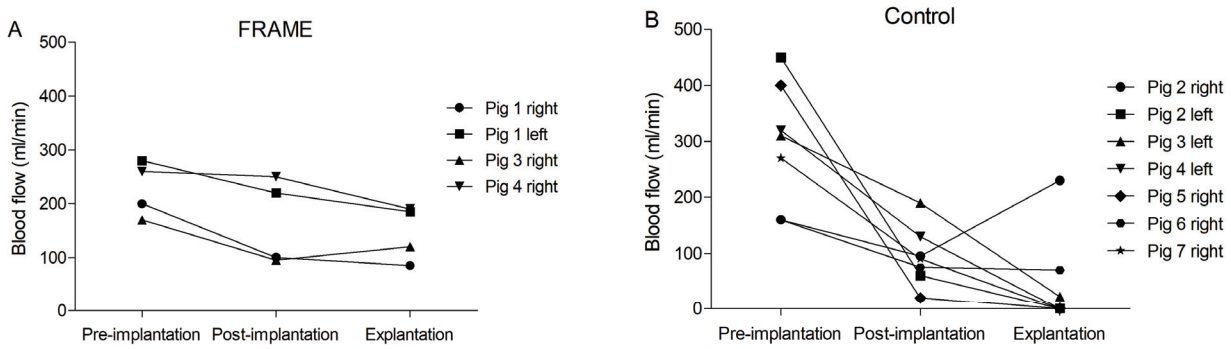


Figure 5. Flowmetry results in (**A**) FRAME-supported and (**B**) control groups of autologous internal jugular vein interposition grafts in porcine carotid arteries at three time points: native carotid artery prior to graft implantation, after graft implantation, and at explantation (1 month post implantation). See Table 2 for exact numbers and statistics.

3.1.3. Angiography

Angiography results in the form of a heat map are summarized in Table 3. They closely correlate with flowmetry results from Table 2 and Figure 5. The correlation is shown in Figure 6A; the percentage of angiographic patency was inversely proportional to the percentage of the most severe angiographic stenosis in each graft listed in Table 3. The left-sided graft in Pig 4 appeared near occluded on the angiogram; however, we considered this graft completely occluded given the zero flow reading.

Table 3. Quantitative angiography results in a tabular heat map. Degrees of stenosis in proximal anastomoses, graft body, and distal anastomoses are given as means from three measurements (anterior-posterior, right lateral, and left lateral (30° angles) projections), calculated according to the North American Symptomatic Carotid Endarterectomy Trial (NASCET) formula (see Methods). Green color indicates no or mild stenosis (≤40%), while yellow and red indicate moderate (41–60%) and severe stenosis/occlusion (>60%), respectively. We considered the left-sided graft in Pig 4 occluded based on zero flow reading. There are significantly more green areas in the FRAME group (9/12) than in the control group (3/21, $p = 0.0009$).

FRAME	Proximal Anastomosis	Graft Body	Distal Anastomosis
Pig 1 right	Severe stenosis 68%	No stenosis *	Mild stenosis 36%
Pig 1 left	Moderate stenosis 60%	No stenosis	Mild stenosis 14%
Pig 3 right	Severe stenosis 66%	No stenosis *	Mild stenosis 40%
Pig 4 right	Mild stenosis 37%	No stenosis *	Mild stenosis 11%
Control			
Pig 2 right	Moderate stenosis 56%	No stenosis	Mild stenosis 29%
Pig 2 left	Occlusion	Occlusion	Occlusion
Pig 3 left	Severe stenosis 76%	Mild long stenosis 25%	Medium stenosis 41%
Pig 4 left	Severe stenosis 73%	Long near occlusion 84%	Near occlusion 83%
Pig 5 right	Occlusion	Occlusion	Occlusion
Pig 6 right	Moderate stenosis 47%	Moderate long stenosis 40%	Moderate stenosis 52%
Pig 7 right	Occlusion	Occlusion	Occlusion

* Mild eccentric semicircular non-stenotic neo-intimal hyperplasia on cross-sections.

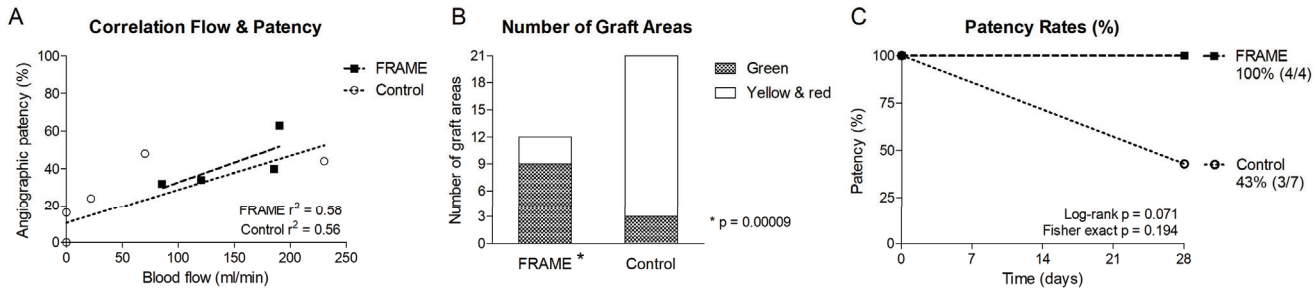


Figure 6. (**A**)—Correlation between blood flow and angiographic patency of FRAME-supported and control autologous internal jugular vein interposition grafts in porcine carotid arteries one month post implantation. (**B**)—Numbers of green versus yellow and red areas in the heat map from Table 3. Green indicates no or mild stenosis (≤40%), while yellow and red indicate moderate (41–60%) and severe stenosis/occlusion (>60%), respectively. Each graft was divided into three sections: proximal anastomosis, midgraft, and distal anastomosis. This provided a total of 12 areas in the FRAME group and 21 in the control group. There are significantly more green areas in the FRAME group (9/12, $p = 0.0009$) than in the control group (3/21). (**C**)—Patency rates in the FRAME-supported and control groups. The graph is a schematic representation of patency rates at one month, i.e., 28 days post implantation, since we do not know the exact times of graft occlusions, i.e., drops of the curve in the control group. The one-month patency rate was 100% (4/4) for the FRAME and 43% (3/7) for the control group. The difference fell just short of statistical significance (Log-rank $p = 0.071$, Fisher exact $p = 0.194$), most likely due to the low number of grafts.

Nine out of twelve areas in the FRAME group were green, whereas only three out of twenty-one areas in the control group were green (Figure 6B), which indicates significantly more favorable angiographic results in the FRAME group ($p = 0.0009$). The one-month patency rate of FRAME-supported grafts was 100% (4/4), while that of unsupported control grafts was 43% (3/7) (Figure 6C). However, the obvious difference in patency rates

narrowly missed statistical significance (Log-rank $p = 0.071$, Fisher exact $p = 0.194$), which was most likely due to the low number of grafts.

3.1.4. Explantation and Macroscopical Examinations

Average NIH area and thickness values calculated from macrograph analysis are given in Table 4 and in Figure 7. The NIH was less pronounced in FRAME-supported than in control grafts, albeit non-significantly in proximal anastomoses. However, in midgraft sections, the difference was statistically significant; this was also the case when proximal anastomosis and midgraft portions were calculated together, which gave an overview of the majority of the grafts. Mild eccentric semicircular non-stenosing NIH was observed in midgraft portions in three of the four FRAME-supported grafts. This type of NIH was not visible on angiograms. Notably, there was no NIH whatsoever in the left-sided midgraft of Pig 1 (Figure 3D).

Table 4. Area and thickness of neo-intimal hyperplasia (NIH) in FRAME-supported and control internal jugular vein interposition grafts in porcine carotid arteries at one month post implantation. Data are presented as means ± standard errors of NIH area and thickness computed from a digital analysis of macrographs of serial cross-sections along the grafts. Thickness was calculated as the NIH area divided by the original lumen circumference.

Neointimal Area (mm^2)	**Proximal Anastomosis**	**Midgraft**	**Prox. Anastomosis and Midgraft**
Control	6.94 ± 1.10	6.27 ± 0.64	6.38 ± 0.56
FRAME	5.79 ± 1.34	3.73 ± 0.64	4.53 ± 0.68
Reduction (%)	16.6%	40.5%	29%
t-test	n.s. $p = 0.558$	* $p = 0.022$	* $p = 0.044$
Neointimal Thickness ($\mu m^2/\mu m$)			
Control	587 ± 52	518 ± 36	530 ± 32
FRAME	480 ± 95	258 ± 49	344 ± 53
Reduction (%)	18.2%	50.2%	35.1%
t-test	n.s. $p = 0.401$	* $p = 0.0002$	* $p = 0.002$

n.s.—non-significant, * significant.

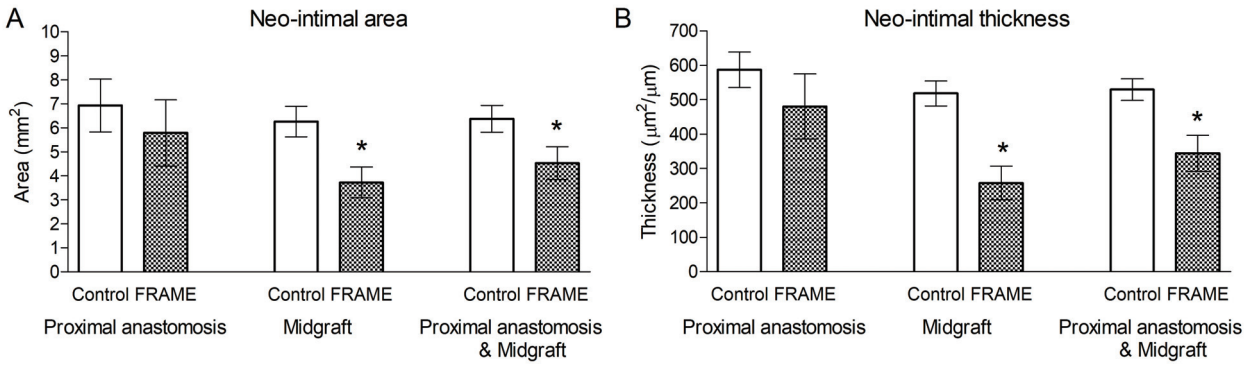


Figure 7. (**A**) Area and (**B**) thickness of neo-intimal hyperplasia (NIH) in FRAME-supported and control internal jugular vein interposition grafts in porcine carotid arteries at one month post implantation. Data are given as means ± standard errors of NIH area and thickness computed from a digital analysis of macrographs of serial cross-sections along the grafts. Thickness was calculated as NIH area divided by the original lumen circumference. The asterisks (*) indicate statistical significance between FRAME and control groups.

We were unable to measure NIH in distal anastomoses due to technical issues. There were, however, no significant angiographic stenoses in the distal anastomoses of the FRAME group, which was in contrast to the control group (Figure 3 and Table 3). This is

further indication of the overall more favorable outcomes provided by the FRAME support in terms of protection against NIH development.

3.2. Microscopical Examinations

3.2.1. Histology and Immunohistochemistry

Histology and immunostaining examinations of the unsupported control grafts are shown in Figure 8. The seven samples were lined up according to degree of pathological remodeling and vein graft lesions, i.e., patent, mildly stenotic, severely stenotic, or totally occluded. The micrographs correlate with angiography and flowmetry examinations. Four of the seven grafts became occluded (Pigs 2 left, 4 left, 5 right, and 7 right), two remained patent but developed substantial neointima (Pigs 3 left and 6 right), and only the right-sided graft in Pig 2 was wide open with insignificant NIH. Detailed microscopical examinations are shown in Figure 9. Endothelial coverage was visible in the patent grafts.

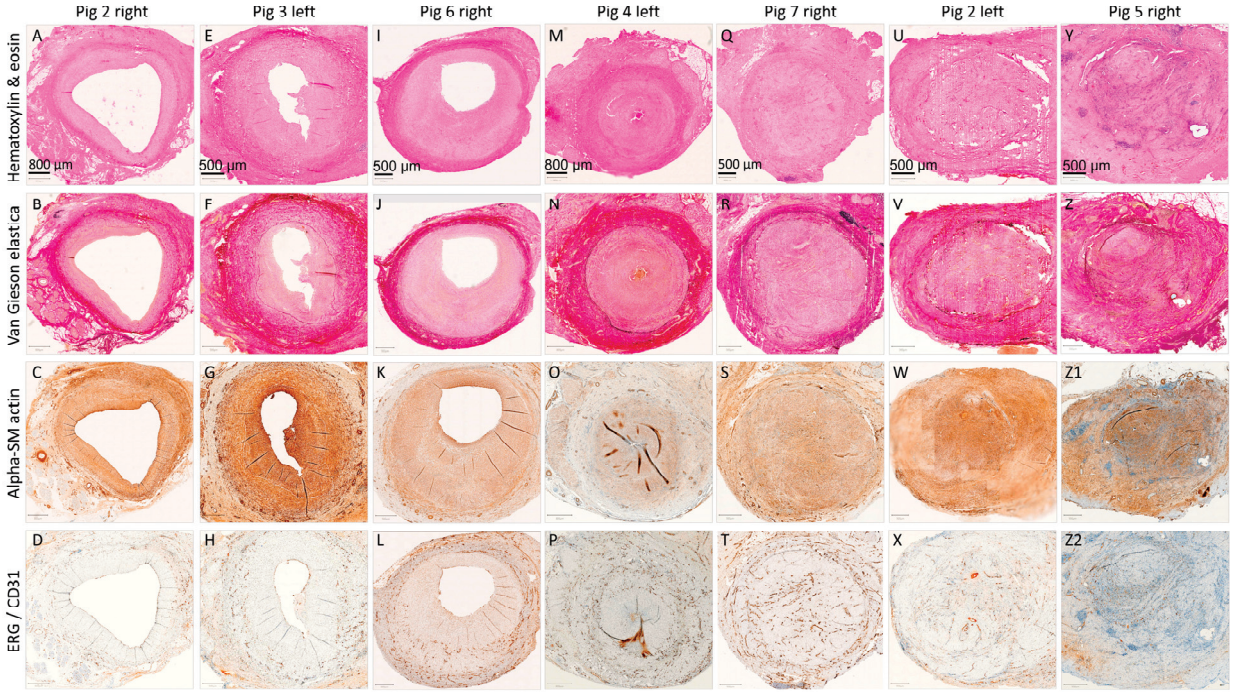


Figure 8. Microscopical examinations of autologous internal jugular vein interposition grafts in porcine carotid arteries at one month post implantation (control group). Representative cross-sections of the midgraft regions are shown in Pigs 2 (**A**–**D** and **U**–**X**), 3 (**E**–**H**), 4 (**M**–**P**), 5 (**Y**–**Z2**), 6 (**I**–**L**), and 7 (**Q**–**T**). The seven control samples are ordered from left to right according to degree of pathological remodeling and vein graft lesions, i.e., patent, mildly stenotic, severely stenotic, or totally occluded (see Figure 9 for more details). We performed histological staining with hematoxylin and eosin and Weigert van Gieson and Resorcin-fuchsin (elastica), as well as immunohistochemistry of alpha-smooth muscle (SM) actin and endothelial markers ERG (**D**,**L**,**P**,**X**) or CD31 (**H**,**T**,**Z2**). Magnification was 20×.

The control midgrafts, calculated from histological sections, had a mean NIH area and thickness of 4.73 ± 0.58 mm^2 and 458 ± 45 $\mu m^2/\mu m$, respectively. These values were 25% (area) and 12% (thickness) lower than those calculated from the zoomed-in photomacrographs (6.27 ± 0.64 mm^2 and 518 ± 36 $\mu m^2/\mu m$, respectively), most likely as a consequence of tissue shrinkage during histological processing. Zilla et al. presented a similar fixation-related tissue shrinkage of 9.9% ± 3.9% [28]. We could not directly compare histological NIH values between the FRAME and control groups since we were unable to conduct histological examinations of the FRAME-supported grafts (see Materials and Methods). However, the mean NIH thickness in the FRAME midgrafts (258 ± 49 $\mu m^2/\mu m$)

was still significantly lower than that in the control grafts, even when utilizing two different methods of measurement: macroscopic in FRAME and histological (i.e., shrank) in control (p = 0.0062). It is noteworthy that other research studies have acquired and compared vascular dimensions from two different measurement methods, e.g., ultrasound and the morphometry of pressure-fixed samples [28].

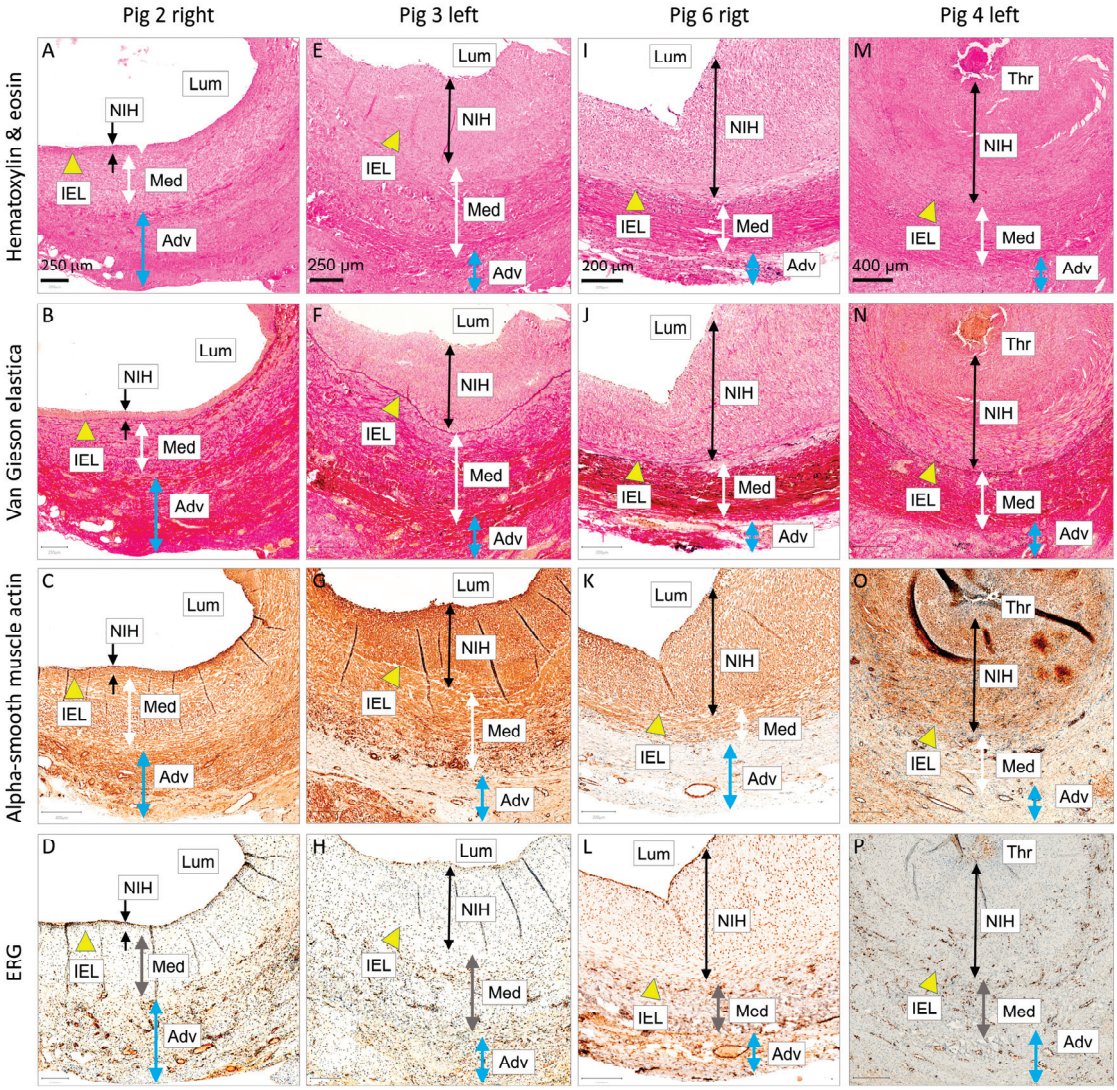


Figure 9. Detailed microscopical examinations of autologous internal jugular vein interposition grafts in porcine carotid arteries at one month post implantation (control group). Representative cross-sections of the midgraft regions are shown. (**A**–**D**) shows a patent graft with minimal neointimal hyperplasia (NIH), (**E**–**H**) shows a patent graft with moderate NIH, (**I**–**L**) shows a patent graft with severe NIH, and (**M**–**P**) shows a graft occluded with substantial NIH and a thrombus. We performed histological staining with hematoxylin and eosin and Weigert van Gieson and Resorcin-fuchsin (elastica), as well as immunohistochemistry of alpha-smooth muscle actin and the endothelial nuclear marker ERG. Magnification was 20×. Abbreviations: Lum—lumen, NIH—neo-intimal hyperplasia, Med—tunica media, Adv—tunica adventitia (neo-adventitia), IEL—internal elastic lamina, and Thr—thrombus.

3.2.2. Confocal Microscopy and Scanning Electron Microscopy (SEM)

The macrograph and corresponding confocal micrograph of the midgraft section of the left-sided FRAME-supported graft of Pig 1 are presented in Figure 10. The graft was wide open, and there was literally no neointimal formation. Due to the graft wall being

extremely delicate, the mesh contours were visible throughout its entirety. The lumen was smooth and lined with endothelial cells.

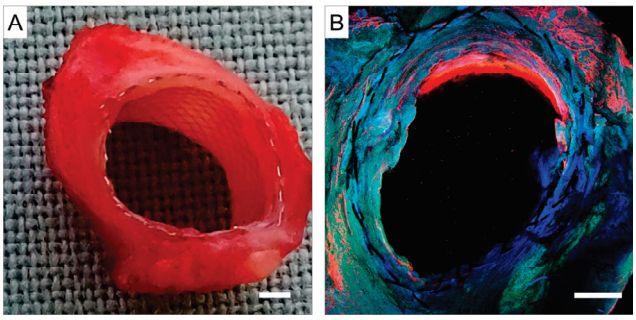


Figure 10. Pig 1—Representative photographs of the left-sided midgraft section at explantation (one month post implantation). (**A**)—Photo-macrograph, scale bar = 1 mm. The graft is patent, and the FRAME mesh is visible from the inside. (**B**)—Photo-micrograph, confocal microscopy, scale bar = 1 mm. The graft lumen is lined with endothelial cells (red color). Red represents staining for von Willebrand factor; blue represents 4′,6-diamidino-2-phenylindole (DAPI) counterstain for cell nuclei; and green is autofluorescence (confocal microscope Olympus Fluoview FV1000).

Macrographs, confocal micrographs, macrographs taken with a microscope, and SEM micrographs of the right-sided FRAME-supported grafts and left-sided bare control grafts from the same animal are shown in Figure 11. Semicircular NIH regions that brought about mild stenosis (Pig 3) and no stenosis (Pig 4) were visible in the lumen of the FRAME-supported grafts. Conversely, NIH in the form of severe circular stenosis (Pig 3) and near occlusion (Pig 4) was found in the control grafts. All grafts were lined with endothelium.

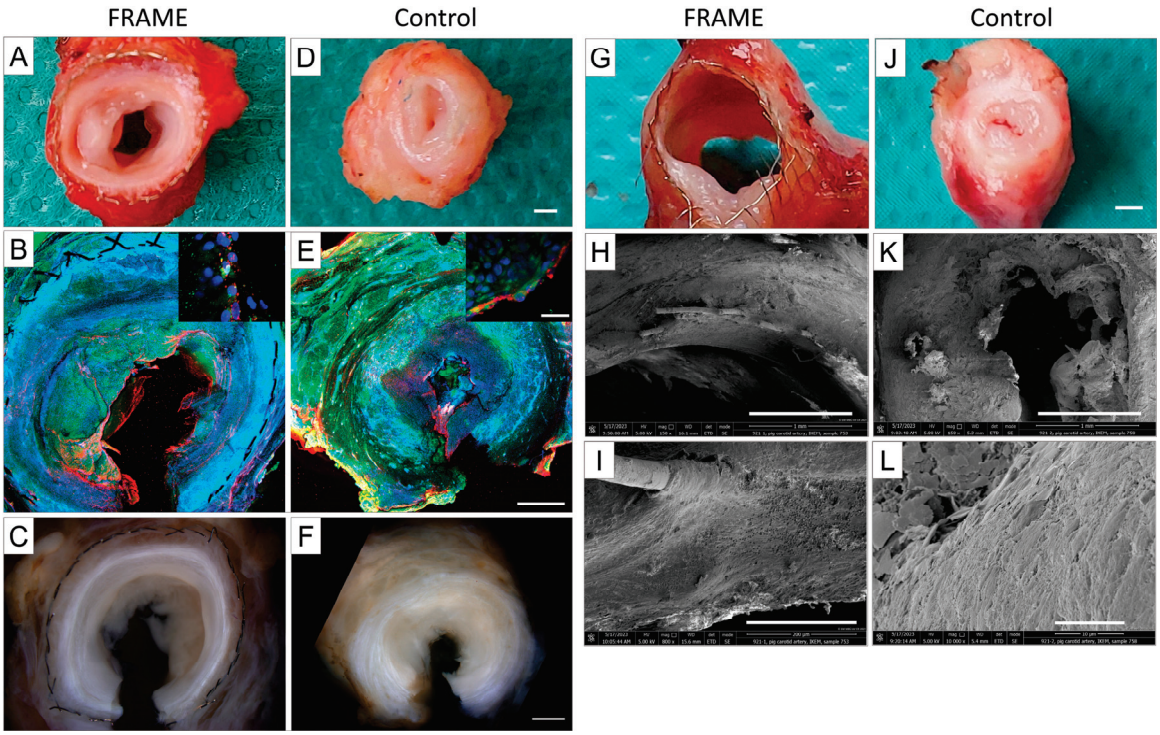


Figure 11. Pig 3 and Pig 4 (representative photographs at explantation, i.e., one month post implantation); (**A**–**F**), left two columns: representative photographs of proximal graft sections of Pig 3. First column (**A**–**C**): right-sided FRAME-supported graft; semicircular neo-intimal hyperplasia (NIH) causing mild stenosis is visible in the lumen. Second column (**D**–**F**): left-sided unsupported control

graft; circular NIH causing severe stenosis is found in the lumen. (**A**,**D**)—photo-macrographs, scale bar = 1 mm. (**B**,**E**)—confocal micrographs, magnification 2×, scale bar = 1 mm; insets: high-power views, magnification 25×, scale bar = 50 μm. Both grafts possess endothelial cells in the lumen. Red represents staining for von Willebrand factor; blue represents 4′,6-diamidino-2-phenylindole (DAPI) counterstain for cell nuclei; and green is autofluorescence (confocal microscope Olympus Fluoview FV1000). (**C**,**F**)—macrographs from a dissecting microscope, scale bar = 1 mm. (**G**–**L**), right two columns: representative photographs of midgraft sections of Pig 4. Third column (**G**–**I**): right-sided FRAME-supported graft; semicircular NIH (no stenosis) is visible in the lumen. Fourth column (**J**–**L**): left-sided unsupported control graft; circular NIH (near occlusion) is visible in the lumen. (**G**,**J**)—photo-macrographs, scale bar = 1 mm. (**H**,**I**,**K**,**L**)—scanning electron microscopy, (**H**,**K**): scale bars = 1 mm, (**I**): scale bar = 200 μm, and (**L**): scale bar = 10 μm; FEI Nova NanoSEM 450 scanning electron microscope.

4. Discussion

In our in vivo animal study, we demonstrated the beneficial effects of external support on porcine autologous vein-to-carotid artery interposition grafts. Specifically, we observed improvements in patency rates and a reduction in the formation of neointimal hyperplasia compared to control group without support. Our novel findings include (1) confirming the efficacy of the latest generation external FRAME stenting device in preventing adverse remodeling in the midgraft regions of veins, and (2) utilizing a specific model involving internal jugular vein grafts interposed into the carotid artery circulation in pigs. The beneficial effect was less pronounced at the proximal anastomoses.

4.1. Animal Model

A recent systematic review (2023) on large animal models of vein graft hyperplasia [8] identified five studies that utilized porcine internal jugular veins as vascular graft in carotid arteries [29–33]. Additionally, we have found one more [34]. All these studies investigated the mechanisms or treatments of vein graft disease but did not involve the use of an external stenting device. The sole study that explored the use of peri-vascular wrap on porcine IJVs was conducted in vitro in a perfusion system [35]. The in vivo study designs and vein graft patency rates, in comparison to our study, are presented in Table 5. The studies employing interposition end-to-end grafting do not mention anastomosis beveling [29,31,34], with one exception that explicitly reported the absence of beveling [33]. Additionally, most studies have omitted details regarding intraoperative graft storage solutions [30–33]. In the gene manipulation studies, the vein grafts were specifically rinsed in the gene transfection solutions [29,34].

The published patency rates of porcine internal jugular vein-to-carotid artery grafts varied from 37.5% to 100% at various time points. One-month patency rate of the control grafts in our series was 42.9% (3/7). In analogy to our study, Quint et al. achieved a one-month-patency rate of 37.5% (3/8) in an end-to-side bypass model [32].

In comparison, several large series of pig distended saphenous vein-to-carotid artery interposition grafting demonstrated patency rates of, e.g., 60% (15/25) at one month [36] and 64% (16/25) at 22 ± 2 (range 5–37) days [37]. Interestingly, grafts made with un-distended veins harvested with a "no-touch" technique had significantly better patency rates of 89% (8/9) [21], 96% (24/25) at 16 ± 2 (range 7 to 36) days [37], or even remarkable rates of 100% (9/9) at 4 weeks [38]. Our inferior patency of the control grafts may possibly be explained by using other graft types (jugular vs. saphenous veins) [37], not strictly applying the "no-touch" harvesting technique [36], and using different animal subspecies [34].

Table 5. Published studies using the internal jugular vein-to-carotid artery model in pigs. The conventional vein graft harvest involves a technique as opposed to a no-touch technique.

Study	Objective	Animal Model	Graft Harvest	Configuration	Heparin	Antiplatelet	Period	Patency
Chen et al. 1994 [29]	Vein graft gene transfer (iNOS)	Farm pig	N/R, prob. conventional	Interposition end-to-end	300 IU/kg	Aspirin 150 mg (3 ds bef.)	3 ds	100% (8/8)
Kibbe et al., 2001 [34]	Vein graft gene transfer (VCAM)	Domestic pig	N/R, prob. conventional	Interposition end-to-end	100 IU/kg	N/R	21 ds	100% (8/8)
Bartels et al., 2003 [30]	Vein graft brachytherapy, control group	Hyperchol. Landrace pig	N/R, prob. conventional	Bypass end-to-side	N/R	Aspirin 100 mg (post-op.)	4 wks	87.5% (14/16)
Jevon et al., 2011 [31]	Vein graft disease study	Inbred Landrace pig	N/R, prob. conventional	Interposition end-to-end	1000 IU/kg	N/R	4 wks	100% (4/4)
Quint et al., 2011 [32]	Tissue engineering, control group	Yorkshire pig	N/R, prob. conventional	Bypass end-to-side	100 IU/kg	Aspirin 5 mg/kg + clopidogrel 1 mg/kg, (1 d bef.)	30 ds	37.5% (3/8)
Thim et al., 2012 [33]	Vein graft disease study	Hyperchol. minipig	Conventional, no distension	Interposition end-to-end not beveled	Yes, dose N/R	Aspirin 150 mg (post-op)	12–14 wks	88.9% (8/9)
Our study	External stenting, control group	Domestic pig	Conventional, gentle distension	Interposition end-to-end	200 IU/kg	Aspirin 100 mg (1 d bef.)	4 wks	42.9% (3/7)

Abbreviations: before surgery and post-operatively (bef.), day (d), days (ds), hypercholesterolemic (hyperchol.), inducible nitric oxide synthase (iNOS), not reported (N/R), post-operatively (post-op.), probably (prob.), vascular cell adhesion molecule (VCAM), weeks (wks).

In the majority of our FRAME midgrafts, mild semicircular eccentric not stenotic NIH was found, analogous to other studies [22]. This type of NIH, however, was not visible on angiograms and may thus be regarded as clinically insignificant. On the contrary, control midgrafts displayed NIH and negative remodeling ranging from stenotic lesions to total occlusions. Notably, there was no intimal thickening at all in the left-sided FRAME-supported midgraft in Pig 1. The contralateral right-sided graft was also supported with FRAME and developed only mild lesions. By contrast, no adverse remodeling either was found in the right-sided control graft in Pig 2. Here, the contralateral graft was also unsupported and became occluded. This occlusion, however, might have been related to technical factors or poor vein quality (insufficient diameter). It seems that FRAME functioned fully protectively in one particular animal while the support was not needed in another particular one. It has been postulated that some vein grafts adapt better to arterial conditions while others undergo progressive negative remodeling [28,39]. In humans, possible individual genetic predisposition to vein graft disease has been reported; polymorphism in the p27Kip1 gene was associated with improved peripheral vein graft patency [40].

4.2. Anastomosis Considerations

Instructions for Use (IFU) advise covering the entire graft with the FRAME mesh and positioning it as close as 2 mm to the anastomotic sites. In our experiment, the mesh extended a few millimeters beyond the anastomoses, as shown in Figures 1 and 3. This extension is feasible in end-to-end anastomosis within interposition grafting, unlike the end-to-side anastomosis commonly used in bypass grafting. Specifically, coronary artery procedures exclusively use end-to-side bypass grafting, while both end-to-side and end-to-end configurations are employed in peripheral vascular reconstructions, including surgery on extremity arteries. In their clinical series on replacing popliteal artery aneurysms, Ciftci et al. (2021) adhered to the IFU guidelines [15]. Conversely, several experimental studies, including ours, have placed the mesh over the anastomotic regions [7,21,41,42].

Notably, anastomotic lesions in our study emerged irrespective of the FRAME device's use, with stenoses developing more frequently at proximal than at distal anastomoses in both FRAME and control groups. Consequently, we believe that extending the mesh over the end-to-end anastomoses in our experimental setup did not adversely affect the outcomes. We further hypothesize that this placement may even offer additional protection, particularly in distal anastomoses.

From a technical standpoint, the stent should initially permit unrestricted graft expansion in response to arterial pressure. Additionally, a close fit of the external stent along the vein graft is crucial for its effective function. The stent is supposed to be designed highly porous and become incorporated into the neo-adventitia, as disruption of the adventitia can lead to vessel wall hypoxia [38]. However, the anastomotic site is generally more susceptible to NIH development due to surgical trauma from stitches, graft/artery compliance and diameter mismatches [3], and increased platelet aggregation [34]

In analogy to our findings, Zilla et al. (2011) observed manifold thicker NIH in anastomotic regions compared to midgraft regions, possibly attributed to pannus overgrowth from adjacent arteries, with this disparity being notably more pronounced in proximal anastomoses [43]. Conversely, other studies have focused solely on NIH formation in midgraft regions [22,28].

4.3. Existing Preclinical Data

Parsonnet et al. proposed using external support for vein grafts for the first time in 1963. They applied a knitted polypropylene tube stent over the external jugular vein to carotid artery interpose grafts in dogs to prevent dilation for up to 63 days [44]. External stents made of various nonabsorbable and absorbable, loose-fitting and tight-fitting, polymeric and metal materials (polyethylene terephthalate—Dacron, polytetrafluoroethylene—PTFE, polyethylene, polypropylene, polyester, polygalactin, polydioxan, braided or knitted nitinol, chrome-cobalt alloy) have been further tested as a treatment for vein graft disease in several animal models (murine, leporine, canine, porcine, ovine), anatomical positions (carotid, femoral, and coronary), and observational periods (usually from 4 weeks to up to 6 months); for reviews, see [6,11]. For instance, a PTFE wrap around jugular vein grafts interposed in common carotid arteries significantly reduced wall thickness, cross-sectional area, and formation of foam cells in both normocholesterolemic and hypercholesterolemic rabbits for 8 weeks [45].

Large animal models, however, have predominated, owing to vessel dimensions similar to man. In an ovine model, Ramachandra et al. (2022) implanted four external jugular-to-carotid artery grafts that were externally wrapped with a biodegradable, braided Vicril-Rapide scaffold. All of the wrapped grafts remained patent at four months; meanwhile, of the four control grafts, one developed an aneurysm, one exhibited severe stenosis, and two remained patent with no signs of stenosis [41].

The research group of Angelini et al. showed numerous short-term and long-term beneficial effects of polyester and polygalactin external stents on suppression of neointimal hyperplasia and early atherosclerotic events in a model of pig saphenous vein-to-carotid artery interposition grafting [21,38,46–51].

The group of Zilla et al. demonstrated positive effects of braided and knitted nitinol stents on various vessel dimensions in saphenous veins implanted as femoral interposition or coronary bypass grafts in nonhuman primates—senescent Chacma baboons [22,28,42,43,52–54] whose anatomy and vascular healing responses are closest to man [55]. They even showed that extreme constriction led to almost absent neointima formation in femoral grafts [53]. Based on different flow hemodynamics, shear stress patterns, and target artery-to-graft caliber mismatch degrees, they found distinctly more intimal hyperplasia in coronary than in femoral vein grafts [28]. Thus, the inhibitory effect of nitinol stenting on neointimal tissue formation was still significant in coronary but less pronounced than in infra-inguinal femoral grafts using the same baboon model [22]. Notwithstanding, they declared that milder coronary artery/saphenous vein graft diameter

mismatch in humans would make the effect of mesh likely to be more pronounced when clinically used [22].

Preclinical testing showed considerable promise; nonetheless, due to a range of technical or methodological issues, none of the external support frameworks were adopted into routine surgical procedures [56].

Similar types of external stents as those in our study have been evaluated in the following two preclinical studies in sheep. Ben-gal et al. (2013) proved the Fluent external stent device (braided cobalt-chromium-nickel-molybdenum-iron alloy, VGS, Tel Aviv, Israel) to be efficacious in reducing saphenous vein graft irregularity and intimal hyperplasia and improving graft patency rate in an ovine case-controlled model (n = 10) of cardiac revascularization over a period of 12 weeks [56]. Following this successful animal study, a clinical randomized controlled trial was initiated (Venous External Stenting Trial, VEST Trial). Nitecki et al. (2017) evaluated a novel braided cobalt-chromium external support for peripheral, i.e., extra-cardiac, vascular reconstructions (FRAME, VGS, Tel Aviv, Israel) in an ovine model (n = 6) of saphenous vein-to-carotid artery bilateral, case-controlled interposition grafting. All six supported and six unsupported grafts remained patent at 12–14 weeks. The diameter of supported veins was unchanged, as opposed to unsupported grafts that significantly dilated, elicited greater lumen irregularity (as shown by the angiographic coefficient of variance), and also developed significantly more intimal hyperplasia [7].

4.4. Existing Clinical Data

4.4.1. Coronary Artery Bypass Grafting

First-generation external stents have given disappointing results, e.g., in 2007 with the Extent device (Vascutek, Ltd., Inchinnan, Scotland) that was a knitted Dacron tube reinforced with polytetrafluoroethylene ribs [57]. In 2015, studies with eSVS mesh (nitinol knit, Kipsbay Medical, Inc., Minneapolis, USA) also reported discouraging outcomes [58,59]. Nevertheless, new technologies have emerged, and new trials have been conducted.

Current-generation VEST external support is a cobalt-chrome braid with axial plasticity and radial elasticity. It is manufactured by the same company as FRAME (VGS Ltd., Tel Aviv, Israel); however, VEST is intended for use in heart bypass surgery. In 2015, Taggart et al. first reported a positive effect of VEST on suppressing NIH one year after CABG [60]. A recently published (2023) meta-analysis of three randomized controlled trials (the VEST I trial [60], the VEST III trial [61], and the VEST Pivotal trial [62]) performed between 2011 and 2020, including 437 patients, summarized the current available evidence [9]. Each patient received one stented and one or more non-stented control bypass grafts to obtain a within-patient comparison. VEST did not seem to reduce the incidence of graft failure at short-term follow-up of 1–2 years, although it was associated with significant attenuation of graft nonuniformity or ectasia (as assessed by angiography) and significant reduction of intimal hyperplasia area or thickness (as assessed by intravascular ultrasound). Thus, all risk factors for the development of vein graft atherosclerosis were attenuated. A follow-up of 4.5 years ("the VEST IV trial") has been reported in 21 patients from the VEST I trial; external stenting significantly reduced diffuse intimal hyperplasia and the development of lumen irregularities; however, graft failure rates were still comparable between stented and non-stented groups [63]. Other meta-analyses [64,65] and a review [13] have reported similar conclusions. Larger trials with longer follow-ups are warranted to determine whether the positive remodeling effects might translate into clinical benefits [6,9].

4.4.2. Peripheral Vascular Surgery

External reinforcements have been used for decades to cover varicose veins used as grafts in peripheral (i.e., extra-cardiac) vascular surgery, most commonly in the lower extremities, thus preventing the development of both graft aneurysm and stenosis. Neointimal hyperplasia is actually more commonly formed in dilated grafts [66,67]. In a prospective multicenter study involving 50 patients and using polyester (polyethylene terephthalate, PET) mesh (ProVena, BBraun, Aesculap, Melsungen, Germany), an acceptable 6-month

primary patency rate of 82.3% was achieved with no occurrence of device infection. The indications for infra-inguinal bypass in this study included critical limb ischemia, severe claudication, or popliteal aneurysm. The use of external scaffolding was indicated for varicosity or ectasia of the vein graft or the use of spliced vein grafts with segments of widely differing diameters [66]. In another study involving 21 patients undergoing infra-inguinal bypass surgery with suboptimal, i.e., varicose vein grafts covered with ProVena mesh, the primary patency at 24 months was 57.1%, similar to that of unmeshed, i.e., normal-quality bypass grafts (63.8%). No mesh infection was noted. The authors recommended the use of external mesh in young patients with a long-term bypass patency expectancy to prevent graft dilation [67]. Noteworthily, ProVena mesh is no longer manufactured.

The purpose of external stenting, however, extends to preventing the mid and long-term development of neointimal hyperplasia in grafts of sufficient quality, i.e., non-varicose venous grafts as well [56]. Reports on the use of current-generation external support for normal vein grafts in peripheral vascular surgery are scarce.

Ciftci et al. (2021) performed open surgical repair of popliteal artery aneurysms using FRAME-supported saphenous vein grafts in 12 patients. Eleven subjects received a bypass, and one subject received an interposition graft (mean length 22 $\pm$ 5 cm, mean diameter 5 $\pm$ 1 mm). Three of the twelve procedures were emergent due to acute limb ischemia. At a mean follow-up of 12 months (range, 7–17 months), the primary patency rate was 100%, there was no change in graft diameters or in the coefficient of variance, and there were no graft revisions, reinterventions, or deep infections. The authors emphasized the potential benefit of using the external stent in patients with aneurysmal arterial disease, as they tend to develop vein graft aneurysms as well [15].

Vigliotti et al. (2022) reported a case of an autologous saphenous vein graft (40–45 cm in length) covered with a FRAME external support to prevent compression in an extra-anatomical position as an axillary-brachial artery bypass around the infected shoulder area. One-year patency was confirmed by a Duplex scan [14].

Vein bypass grafts for lower extremity peripheral arterial occlusive disease are typically longer (40–60 cm) than their coronary counterparts (15 cm) [9] The possible problem with maintaining close contact or conformity along the entire length of the graft may elicit the risk of unprotected segments [43,54]. Furthermore, given the longer grafts' exposure to bending and the presence of irregular segments that would be excised in coronary grafts, a mildly worse clinical performance of externally stented long infra-inguinal bypass grafts may be encountered [28].

4.4.3. Arterio-Venous Fistulas (AVFs) for Hemodialysis Access

Autologous AVFs for hemodialysis are prone to develop high flow rates and/or aneurysmal dilation. Volume overload correlates with adverse cardiac remodeling in these end-stage kidney failure patients. Steal syndrome and limb ischemia can also occur. Aneurysmorhaphy, with or without external reinforcement, is the surgical treatment method of choice. ProVena mesh has been utilized for external stenting to prevent recurrent high flow after an aneurysmorhaphy procedure [68,69]; however, the results of a randomized AVAH trial are still awaited. Chemla et al. (2016) placed VasQ (Laminate Medical Technologies, Tel Aviv, Israel) metal external support device to improve flow and reduce NIH at the anastomotic site in 20 patients undergoing a brachiocephalic fistula. They reported device safety with high unassisted maturation and patency rates [70].

Matoussevitch et al. (2021) reconstructed and supported 43 high-flow and/or aneurysmal upper arm fistulas in 42 hemodialysis patients using an external stent FRAME FR (VGS). The stent is designed to cover at least 4 cm of the reconstructed fistula and is not intended to cover the cannulation area. Recurrence of high flow (i.e., $\geq$1500 mL/min) occurred in 16% and 25% of the patients at 6 and 12 months, respectively, while primary patency rates were 86% and 70%, respectively. Only three patients (9%) experienced flow rates exceeding 2000 mL/min and underwent surgical revision to address the recurrent high flow [71]. In contrast, the banding technique is associated with a 52% 12-month-recurrence rate [72].

The authors concluded that the novel external stenting technique is a safe and effective method for reducing and stabilizing flow rates up to 1 year post-operatively. Additionally, their initial learning curve should be considered.

In contrast, Kuemmerli et al. (2020) applied the FRAME device already during the creation of a brachial-basilic upper arm transposition AVF to prevent possible vein dilation. The shunt showed a plateauing flow volume 3 months post-procedurally, illustrating the safety and feasibility of this intervention [73].

4.5. Limitations

Our study has several limitations. First, the number of grafts supported with the FRAME device was limited (n = 4), which likely contributed to the marginally significant differences in patency rates and blood flows between groups. The control group had a slightly higher number of grafts (n = 7); however, their mean blood flow post-implantation was significantly lower than that in native carotid arteries. This drop in flow volume was insignificant in the FRAME-supported grafts. The low post-implantation flow is typically attributed to vasospasm of the adjacent carotid artery as long as technical errors are excluded. Nonetheless, we can speculate that the quality or diameter of the control grafts (Pig 2 left and Pig 5 right in particular) could have been suboptimal, potentially compromising their outcomes.

Second, we lack data on graft patency rates and the extent of NIH beyond one month. In a pig model, maximal NIH thickness has been observed at one month, but it can continue to increase over a six-month period [3].

Next, our use of end-to-end interposition grafting, while common in animal models for its simplicity and reproducibility, differs from the more frequent use of end-to-side bypass grafting in actual clinical practice. Angelini et al. reported similar turbulent flow in proximal anastomoses but significantly less turbulent flow in midpoints and distal anastomoses in porcine end-to-end vein-to-artery grafting compared to end-to-side bypass grafting [37]. It is important to note that variations in the angle of beveling in our end-to-end anastomoses occurred (see Table 1) despite all implantations being performed by a single surgeon (J. Ch.).

We acknowledge that our model of internal jugular vein-to-artery grafting may have somewhat less clinical relevance compared to conventional models using saphenous vein grafts, such as those in pigs [46,51], sheep [7,56], or baboons [22,42], since the saphenous vein is commonly used in clinical practice. However, saphenous veins exhibit physiological differences in bipeds and other species, which can limit the applicability of various experimental models [74]. Furthermore, jugular veins engrafted in carotid arteries have previously been utilized in research on vein graft disease in mice [75], rabbits [76,77], and pigs [29–34]. These grafts have also been used in studies involving external stenting in animal models (excluding pigs), namely rabbits [45,78,79], dogs [44,80], and sheep [41,81]. Interestingly, Angelini et al. (1990) initially used IJVs as experimental grafts in pig carotid arteries but had to abandon them due to their larger diameters and early ruptures, opting instead for saphenous veins [37]. We speculate that they utilized external rather than internal jugular veins [17]. In contrast, we did not encounter such adverse events, and IJVs were well-matched in diameter with porcine carotid arteries [17,34].

Further, our methodology, which involves placing explanted specimens in warm saline followed by formaldehyde immersion fixation, may have resulted in natural recoil of non-pressurized vessels, potentially leading to tissue analysis in a slightly shrunken state. Most studies have used (perfusion) fixation at arterial pressures, such as 80 mmHg [37], 100 mmHg [38,56], or even systolic 120 mmHg [7,28] to better preserve in vivo dimensions, while others did not [82]. Our group comparisons, however, remain valid, as all samples underwent identical processing. Though speculative, the presence of the healed metal mesh may have provided some protection against sample shrinkage, or conversely, the mesh itself could have exerted a recoil force [22].

We focused exclusively on measuring neo-intimal parameters, in contrast to other studies that also assessed parameters of the medial layer [34,56], the intima-medial thickness [34,38,61], and the adventitia [43]. It is noteworthy that, unlike neointima formation, the preservation of functional smooth muscle mass in the medial layer is a desired outcome when applying an external mesh [43].

Then, only two of our animals (Pigs 3 and 4) received both stented and non-stented grafts as part of a within-subject control strategy. This approach, employed in both preclinical [7,21,51,56] and clinical trials [9], eliminates subject-related factors that might otherwise influence the extent of vein graft disease. In these two animals, however, the right vs. left carotid artery was not randomized for the application of the tested device as opposed to other studies [7,56]. Furthermore, the vein grafts for the right and left sides were specifically taken from their respective sides, thus avoiding the use of vein segments with similar quality from the same vein for implantation. This approach may have influenced the vein remodeling process following implantation [7].

After that, we chose to use female pigs exclusively due to their docile nature and slower weight gain over the study period compared to male pigs. As a result, our experimental findings should not be generalized to both sexes. It is worth noting that many prior studies did not specify the sex of their experimental animals [22,38,43,48].

Finally, it is essential to recognize that our findings pertain to grafts of shorter lengths placed in healthy juvenile animals. These results cannot be directly extrapolated to clinical scenarios involving longer grafts in elderly patients with cardiovascular diseases [55].

4.6. Clinical Implications and Future Directions

The results of our study do not have a straightforward clinical impact as the FRAME mesh has already received approval for clinical use in peripheral vascular surgery [18]. However, our study demonstrated the efficacy of FRAME support in our specific animal model, i.e., porcine internal jugular vein-to-carotid artery interposition grafting. Additionally, the study provided us with valuable experience in handling the device before proceeding to clinical use.

Many questions regarding the optimal mesh material, porosity, potential degradation kinetics, and design (such as loose-fitting vs. constrictive, permanent vs. bioabsorbable, or braided vs. knitted) remain unanswered [11,43]. Nonetheless, metal meshes are known to elicit hardly any inflammatory reaction [7,43] and offer protection to vein grafts not only against over-distention and neointima formation [7] but also against external compression and deformation [43].

It is crucial to emphasize that external stenting is not intended to prevent short-term graft failures but rather to mitigate neointimal hyperplasia and superimposed atherosclerosis in the long term [62]. Vein graft failure is a complex issue with multiple contributing factors, and no single treatment is likely to provide a complete solution [11]. Factors such as graft selection, meticulous surgical techniques for vein harvesting, manipulation, preservation, grafting configuration, and anastomosing, along with optimal medical therapy, remain essential for graft function and cannot be replaced by a device-oriented approach [83]. Notably, despite being an innovative and simple device, the mesh incurs additional costs in bypass procedures [84].

Possible future directions may involve combining external support with other interventions for vein graft disease, such as pharmacological treatment [3], gene delivery [85,86], or tissue-engineered vascular grafts.

5. Conclusions

In our preclinical model, using an external mesh FRAME enhanced the patency rate of porcine autologous internal jugular vein-to-carotid artery interposition grafts at one month. Upon explant angiography, grafts supported by the FRAME exhibited significantly fewer stenotic areas compared to unsupported grafts. The formation of neointimal hyperplasia was substantially reduced in the FRAME-stented grafts, particularly in the mid portions.

Notably, the thickness of the midgraft neointima in the FRAME-supported grafts was half that of their non-supported counterparts.

Author Contributions: Conceptualization, J.C. and J.F. (Jan Frank); methodology, J.C. and D.S.; validation, J.C.; formal analysis, J.C.; investigation, J.C., J.F. (Jan Frank), D.S., O.F., Z.S., I.M., T.N., Z.V., O.B., Z.P., M.K. and A.L.; resources, J.C.; data curation, J.C.; writing—original draft preparation, J.C.; writing—review and editing, J.C., D.S., O.F., Z.S., O.B., T.A., M.K., A.L., L.V. and J.P.; visualization, J.C.; supervision, T.A., L.V., J.P. and J.F. (Jiri Fronek); project administration, J.C. and Z.S.; funding acquisition, J.C. and J.P. All authors have read and agreed to the published version of the manuscript.

Funding: This research was supported by the Ministry of Health of the Czech Republic, grant nr. NV19-02-00068, all rights reserved; and by the National Institute for Research of Metabolic and Cardiovascular Diseases (Programme EXCELES, ID Project No. LX22NPO5104)—Funded by the European Union—Next Generation EU.

Institutional Review Board Statement: The animal study protocol was approved by the Institutional Review Board of the Institute for Clinical and Experimental Medicine, Prague, Czech Republic (protocol code: 406; date of approval: 4 February 2021) and the Ministry of Health of the Czech Republic (protocol code: MZDR 5871/2021-4/OVZ, PID: MZDRX01EFSFL, 14/2021; date of approval: 12 February 2021).

Informed Consent Statement: Not applicable.

Data Availability Statement: The original contributions presented in the study are included in the article; further inquiries can be directed to the corresponding author.

Acknowledgments: The authors are grateful for access to the electron microscopy facility of IMIC, which was supported by the Czech Academy of Sciences (RVO CZ61388971). We are grateful to Michal Bures for animal care and Milan Zapletal for assistance with angiography. We wish to thank Brian Kavalir for his proofreading services.

Conflicts of Interest: The authors declare no conflicts of interest.

References

1. de Vries, M.R.; Simons, K.H.; Jukema, J.W.; Braun, J.; Quax, P.H. Vein graft failure: From pathophysiology to clinical outcomes. *Nat. Rev. Cardiol.* **2016**, *13*, 451–470. [CrossRef] [PubMed]
2. Martínez-González, B.; Reyes-Hernández, C.G.; Quiroga-Garza, A.; Rodríguez-Rodríguez, V.E.; Esparza-Hernández, C.N.; Elizondo-Omaña, R.E.; Guzmán-López, S. Conduits Used in Coronary Artery Bypass Grafting: A Review of Morphological Studies. *Ann. Thorac. Cardiovasc. Surg.* **2017**, *23*, 55–65. [CrossRef] [PubMed]
3. Thomas, A.C. Animal models for studying vein graft failure and therapeutic interventions. *Curr. Opin. Pharmacol.* **2012**, *12*, 121–126. [CrossRef] [PubMed]
4. Guida, G.; Ward, A.O.; Bruno, V.D.; George, S.J.; Caputo, M.; Angelini, G.D.; Zakkar, M. Saphenous vein graft disease, pathophysiology, prevention, and treatment. A review of the literature. *J. Card. Surg.* **2020**, *35*, 1314–1321. [CrossRef] [PubMed]
5. Samano, N.; Geijer, H.; Liden, M.; Fremes, S.; Bodin, L.; Souza, D. The no-touch saphenous vein for coronary artery bypass grafting maintains a patency, after 16 years, comparable to the left internal thoracic artery: A randomized trial. *J. Thorac. Cardiovasc. Surg.* **2015**, *150*, 880–888. [CrossRef] [PubMed]
6. Weltert, L.P.; Wolf, L.G.; Garufi, L.; Scaffa, R.; Salica, A.; Ricci, A.; Irace, F.G.; Fusca, S.; D'Aleo, S.; Chirichilli, I.; et al. External Stents for Vein Grafts in Coronary Artery Bypass Grafting: Targeting Intimal Hyperplasia. *Surg. Technol. Int.* **2020**, *35*, 197–201. [PubMed]
7. Nitecki, S.; Yosef, L.; Tozzi, M.; Shofti, R. Inhibition of vein graft remodeling and neo-intimal formation using a cobalt chrome external support. *Arch. Clin. Exp. Surg.* **2018**, *7*, 108–115. [CrossRef]
8. Fashina, O.; Abbasciano, R.G.; McQueen, L.W.; Ladak, S.; George, S.J.; Suleiman, S.; Punjabi, P.P.; Angelini, G.D.; Zakkar, M. Large animal model of vein grafts intimal hyperplasia: A systematic review. *Perfusion* **2023**, *38*, 894–930. [CrossRef] [PubMed]
9. Gemelli, M.; Gallo, M.; Addonizio, M.; Pahwa, S.; Van den Eynde, J.; Trivedi, J.; Slaughter, M.S.; Gerosa, G. Venous External Support in Coronary Artery Bypass Surgery: A Systematic Review and Meta-Analysis. *Curr. Probl. Cardiol.* **2023**, *48*, 101687. [CrossRef]
10. Emmert, M.Y.; Bonatti, J.; Caliskan, E.; Gaudino, M.; Grabenwöger, M.; Grapow, M.T.; Heinisch, P.P.; Kieser-Prieur, T.; Kim, K.-B.; Kiss, A.; et al. Consensus statement—Graft treatment in cardiovascular bypass graft surgery. *Front. Cardiovasc. Med.* **2024**, *11*, 1285685. [CrossRef]
11. Hu, J.; Wan, S. External support in preventing vein graft failure. *Asian Cardiovasc. Thorac. Ann.* **2012**, *20*, 615–622. [CrossRef] [PubMed]

12. Goldstein, D.J. Device profile of the VEST for external support of SVG Coronary artery bypass grafting: Historical development, current status, and future directions. *Expert Rev. Med. Devices* **2021**, *18*, 921–931. [CrossRef] [PubMed]
13. Soletti, G.J.; Dell'Aquila, M.; Harik, L.; Cancelli, G.; Alzghari, T.; Perezgrovas-Olaria, R.; Dimagli, A.; An, K.R.; Leith, J.; Rossi, C.S.; et al. The VEST External Support for Saphenous Vein Grafts in Coronary Surgery: A Review of Randomized Clinical Trials. *J. Cardiovasc. Dev. Dis.* **2023**, *10*, 453. [CrossRef] [PubMed]
14. Vigliotti, R.C.; Montelione, N.; Franceschi, F.; Franceschini, E.; Zardi, E.; Spinelli, F.; Stilo, F. Externally Supported Extra-anatomical Venous Bypass to Treat Upper Limb Ischemia with Shoulder Prosthetic Infection. *Ann. Vasc. Surg.* **2020**, *69*, 453.e5–453.e10. [CrossRef] [PubMed]
15. Ciftci, Ü.; Marti, R.; Fahrni, J.; Gähwiler, R.; Thalhammer, C.; Gürke, L.; Isaak, A. External stenting and disease progression in vein grafts 1 year after open surgical repair of popliteal artery aneurysm. *J. Vasc. Surg.* **2021**, *74*, 521–527. [CrossRef] [PubMed]
16. Chlupac, J.; Matejka, R.; Konarik, M.; Novotny, R.; Simunkova, Z.; Mrazova, I.; Fabian, O.; Zapletal, M.; Pulda, Z.; Lipensky, J.F.; et al. Vascular Remodeling of Clinically Used Patches and Decellularized Pericardial Matrices Recellularized with Autologous or Allogeneic Cells in a Porcine Carotid Artery Model. *Int. J. Mol. Sci.* **2022**, *23*, 3310. [CrossRef] [PubMed]
17. Góes, A.M.O.; Chaves, R.H.F.; Furlaneto, I.P.; Rodrigues, E.M.; de Albuquerque, F.B.A.; Smit, J.H.A.; de Oliveira, C.P.; Abib, S.C.V. Comparative angiotomographic study of swine vascular anatomy: Contributions to research and training models in vascular and endovascular surgery. *J. Vasc. Bras.* **2021**, *20*, e20200086. [CrossRef] [PubMed]
18. FRAME TM. External Support for Peripheral Vascular Reconstructions. Available online: https://www.cardion.cz/file/1466/lb461-rev02-frame-product-page.pdf (accessed on 27 July 2023).
19. Mrowczynski, W.; Mugnai, D.; de Valence, S.; Tille, J.C.; Khabiri, E.; Cikirikcioglu, M.; Moller, M.; Walpoth, B.H. Porcine carotid artery replacement with biodegradable electrospun poly-e-caprolactone vascular prosthesis. *J. Vasc. Surg.* **2014**, *59*, 210–219. [CrossRef]
20. Bankhead, P.; Loughrey, M.B.; Fernández, J.A.; Dombrowski, Y.; McArt, D.G.; Dunne, P.D.; McQuaid, S.; Gray, R.T.; Murray, L.J.; Coleman, H.G.; et al. QuPath: Open source software for digital pathology image analysis. *Sci. Rep.* **2017**, *7*, 16878. [CrossRef]
21. Angelini, G.D.; Lloyd, C.; Bush, R.; Johnson, J.; Newby, A.C. An external, oversized, porous polyester stent reduces vein graft neointima formation, cholesterol concentration, and vascular cell adhesion molecule 1 expression in cholesterol-fed pigs. *J. Thorac. Cardiovasc. Surg.* **2002**, *124*, 950–956. [CrossRef]
22. Moodley, L.; Franz, T.; Human, P.; Wolf, M.F.; Bezuidenhout, D.; Scherman, J.; Zilla, P. Protective constriction of coronary vein grafts with knitted nitinol. *Eur. J. Cardio Thorac. Surg.* **2013**, *44*, 64–71. [CrossRef] [PubMed]
23. Rippstein, P.; Black, M.K.; Boivin, M.; Veinot, J.P.; Ma, X.; Chen, Y.X.; Human, P.; Zilla, P.; O'Brien, E.R. Comparison of processing and sectioning methodologies for arteries containing metallic stents. *J. Histochem. Cytochem.* **2006**, *54*, 673–681. [CrossRef] [PubMed]
24. Honetschlägerová, Z.; Husková, Z.; Kikerlová, S.; Sadowski, J.; Kompanowska-Jezierska, E.; Táborský, M.; Vaňourková, Z.; Kujal, P.; Červenka, L. Renal sympathetic denervation improves pressure-natriuresis relationship in cardiorenal syndrome: Insight from studies with Ren-2 transgenic hypertensive rats with volume overload induced using aorto-caval fistula. *Hypertens. Res.* **2024**, *47*, 998–1016. [CrossRef] [PubMed]
25. Kolesová, H.; Bartoš, M.; Hsieh, W.C.; Olejníčková, V.; Sedmera, D. Novel approaches to study coronary vasculature development in mice. *Dev. Dyn.* **2018**, *247*, 1018–1027. [CrossRef] [PubMed]
26. Kolesová, H.; Čapek, M.; Radochová, B.; Janáček, J.; Sedmera, D. Comparison of different tissue clearing methods and 3D imaging techniques for visualization of GFP-expressing mouse embryos and embryonic hearts. *Histochem. Cell Biol.* **2016**, *146*, 141–152. [CrossRef] [PubMed]
27. Sochman, J.; Peregrin, J.H.; Pavcnik, D.; Uchida, B.T.; Timmermans, H.A.; Sedmera, D.; Benada, O.; Kofronova, O.; Keller, F.S.; Rosch, J. Reverse endoventricular artificial obturator in tricuspid valve position. Experimental feasibility research study. *Physiol. Res.* **2014**, *63*, 157–165. [CrossRef] [PubMed]
28. Zilla, P.; Moodley, L.; Scherman, J.; Krynauw, H.; Kortsmit, J.; Human, P.; Wolf, M.F.; Franz, T. Remodeling leads to distinctly more intimal hyperplasia in coronary than in infrainguinal vein grafts. *J. Vasc. Surg.* **2012**, *55*, 1734–1741. [CrossRef] [PubMed]
29. Chen, S.J.; Wilson, J.M.; Muller, D.W. Adenovirus-mediated gene transfer of soluble vascular cell adhesion molecule to porcine interposition vein grafts. *Circulation* **1994**, *89*, 1922–1928. [CrossRef] [PubMed]
30. Bartels, C.; Erasmi, A.; Sayk, F.; Eggers, R.; Dendorfer, A.; Feyerabend, T.; Eichler, W.; Sievers, H.H. Prophylactic gamma radiation of unaffected vein grafts failed to prevent vein graft disease in a chronic hypercholesterolemic porcine model. *Eur. J. Cardiothorac. Surg.* **2003**, *24*, 92–97. [CrossRef]
31. Jevon, M.; Ansari, T.I.; Finch, J.; Zakkar, M.; Evans, P.C.; Shurey, S.; Sibbons, P.D.; Hornick, P.; Haskard, D.O.; Dorling, A. Smooth muscle cells in porcine vein graft intimal hyperplasia are derived from the local vessel wall. *Cardiovasc. Pathol.* **2011**, *20*, e91–e94. [CrossRef]
32. Quint, C.; Kondo, Y.; Manson, R.J.; Lawson, J.H.; Dardik, A.; Niklason, L.E. Decellularized tissue-engineered blood vessel as an arterial conduit. *Proc. Natl. Acad. Sci. USA* **2011**, *108*, 9214–9219. [CrossRef] [PubMed]
33. Thim, T.; Hagensen, M.K.; Hørlyck, A.; Drouet, L.; Paaske, W.P.; Bøtker, H.E.; Falk, E. Oversized vein grafts develop advanced atherosclerosis in hypercholesterolemic minipigs. *BMC Cardiovasc. Disord.* **2012**, *12*, 24. [CrossRef]

34. Kibbe, M.R.; Tzeng, E.; Gleixner, S.L.; Watkins, S.C.; Kovesdi, I.; Lizonova, A.; Makaroun, M.S.; Billiar, T.R.; Rhee, R.Y. Adenovirus-mediated gene transfer of human inducible nitric oxide synthase in porcine vein grafts inhibits intimal hyperplasia. *J. Vasc. Surg.* **2001**, *34*, 156–165. [CrossRef] [PubMed]
35. El-Kurdi, M.S.; Hong, Y.; Stankus, J.J.; Soletti, L.; Wagner, W.R.; Vorp, D.A. Transient elastic support for vein grafts using a constricting microfibrillar polymer wrap. *Biomaterials* **2008**, *29*, 3213–3220. [CrossRef]
36. Angelini, G.D.; Bryan, A.J.; Williams, H.M.; Soyombo, A.A.; Williams, A.; Tovey, J.; Newby, A.C. Time-course of medial and intimal thickening in pig venous arterial grafts: Relationship to endothelial injury and cholesterol accumulation. *J. Thorac. Cardiovasc. Surg.* **1992**, *103*, 1093–1103. [CrossRef]
37. Angelini, G.D.; Bryan, A.J.; Williams, H.M.; Morgan, R.; Newby, A.C. Distention promotes platelet and leukocyte adhesion and reduces short-term patency in pig arteriovenous bypass grafts. *J. Thorac. Cardiovasc. Surg.* **1990**, *99*, 433–439. [CrossRef] [PubMed]
38. Angelini, G.D.; Izzat, M.B.; Bryan, A.J.; Newby, A.C. External stenting reduces early medial and neointimal thickening in a pig model of arteriovenous bypass grafting. *J. Thorac. Cardiovasc. Surg.* **1996**, *112*, 79–84. [CrossRef]
39. Isaji, T.; Hashimoto, T.; Yamamoto, K.; Santana, J.M.; Yatsula, B.; Hu, H.; Bai, H.; Jianming, G.; Kudze, T.; Nishibe, T.; et al. Improving the Outcome of Vein Grafts: Should Vascular Surgeons Turn Veins into Arteries? *Ann. Vasc. Dis.* **2017**, *10*, 8–16. [CrossRef] [PubMed]
40. Conte, M.S.; Owens, C.D.; Belkin, M.; Creager, M.A.; Edwards, K.L.; Gasper, W.J.; Kenagy, R.D.; LeBoeuf, R.C.; Sobel, M.; Clowes, A. A single nucleotide polymorphism in the p27(Kip1) gene is associated with primary patency of lower extremity vein bypass grafts. *J. Vasc. Surg.* **2013**, *57*, 1179–1185.E2. [CrossRef]
41. Ramachandra, A.B.; Wang, H.; Wnorowski, A.; Schwarz, E.L.; Pickering, J.; Heiler, J.C.; Lucian, H.J.; Hironaka, C.E.; Tran, N.A.; Liu, Y.; et al. Biodegradable external wrapping promotes favorable adaptation in an ovine vein graft model. *Acta Biomater.* **2022**, *151*, 414–425. [CrossRef]
42. Zilla, P.; Human, P.; Wolf, M.; Lichtenberg, W.; Rafiee, N.; Bezuidenhout, D.; Samodien, N.; Schmidt, C.; Franz, T. Constrictive external nitinol meshes inhibit vein graft intimal hyperplasia in nonhuman primates. *J. Thorac. Cardiovasc. Surg.* **2008**, *136*, 717–725. [CrossRef] [PubMed]
43. Zilla, P.; Moodley, L.; Wolf, M.F.; Bezuidenhout, D.; Sirry, M.S.; Rafiee, N.; Lichtenberg, W.; Black, M.; Franz, T. Knitted nitinol represents a new generation of constrictive external vein graft meshes. *J. Vasc. Surg.* **2011**, *54*, 1439–1450. [CrossRef] [PubMed]
44. Parsonnet, V.; Lari, A.A.; Shah, I.H. New Stent For Support of Veins in Arterial GRAFTS. *Arch. Surg.* **1963**, *87*, 696–702. [CrossRef] [PubMed]
45. Batellier, J.; Wassef, M.; Merval, R.; Duriez, M.; Tedgui, A. Protection from atherosclerosis in vein grafts by a rigid external support. *Arterioscler. Thromb.* **1993**, *13*, 379–384. [CrossRef] [PubMed]
46. Izzat, M.B.; Mehta, D.; Bryan, A.J.; Reeves, B.; Newby, A.C.; Angelini, G.D. Influence of external stent size on early medial and neointimal thickening in a pig model of saphenous vein bypass grafting. *Circulation* **1996**, *94*, 1741–1745. [CrossRef]
47. Jeremy, J.Y.; Dashwood, M.R.; Mehta, D.; Izzat, M.B.; Shukla, N.; Angelini, G.D. Nitric oxide, prostacyclin and cyclic nucleotide formation in externally stented porcine vein grafts. *Atherosclerosis* **1998**, *141*, 297–305. [CrossRef] [PubMed]
48. Mehta, D.; George, S.J.; Jeremy, J.Y.; Izzat, M.B.; Southgate, K.M.; Bryan, A.J.; Newby, A.C.; Angelini, G.D. External stenting reduces long-term medial and neointimal thickening and platelet derived growth factor expression in a pig model of arteriovenous bypass grafting. *Nat. Med.* **1998**, *4*, 235–239. [CrossRef] [PubMed]
49. Caro, C.; Jeremy, J.; Watkins, N.; Bulbulia, R.; Angelini, G.; Smith, F.; Wan, S.; Yim, A.; Sherwin, S.; Peiró, J.; et al. The geometry of unstented and stented pig common carotid artery bypass grafts. *Biorheology* **2002**, *39*, 507–512. [PubMed]
50. Jeremy, J.Y.; Bulbulia, R.; Johnson, J.L.; Gadsdon, P.; Vijayan, V.; Shukla, N.; Smith, F.C.; Angelini, G.D. A bioabsorbable (polyglactin), nonrestrictive, external sheath inhibits porcine saphenous vein graft thickening. *J. Thorac. Cardiovasc. Surg.* **2004**, *127*, 1766–1772. [CrossRef]
51. Vijayan, V.; Shukla, N.; Johnson, J.L.; Gadsdon, P.; Angelini, G.D.; Smith, F.C.; Baird, R.; Jeremy, J.Y. Long-term reduction of medial and intimal thickening in porcine saphenous vein grafts with a polyglactin biodegradable external sheath. *J. Vasc. Surg.* **2004**, *40*, 1011–1019. [CrossRef]
52. Human, P.; Franz, T.; Scherman, J.; Moodley, L.; Zilla, P. Dimensional analysis of human saphenous vein grafts: Implications for external mesh support. *J. Thorac. Cardiovasc. Surg.* **2009**, *137*, 1101–1108. [CrossRef] [PubMed]
53. Zilla, P.; Wolf, M.; Rafiee, N.; Moodley, L.; Bezuidenhout, D.; Black, M.; Human, P.; Franz, T. Utilization of shape memory in external vein-graft meshes allows extreme diameter constriction for suppressing intimal hyperplasia: A non-human primate study. *J. Vasc. Surg.* **2009**, *49*, 1532–1542. [CrossRef] [PubMed]
54. Franz, T.; Human, P.; Dobner, S.; Reddy, B.D.; Black, M.; Ilsley, H.; Wolf, M.F.; Bezuidenhout, D.; Moodley, L.; Zilla, P. Tailored sizes of constrictive external vein meshes for coronary artery bypass surgery. *Biomaterials* **2010**, *31*, 9301–9309. [CrossRef] [PubMed]
55. Zilla, P.; Bezuidenhout, D.; Human, P. Prosthetic vascular grafts: Wrong models, wrong questions and no healing. *Biomaterials* **2007**, *28*, 5009–5027. [CrossRef] [PubMed]
56. Ben-Gal, Y.; Taggart, D.P.; Williams, M.R.; Orion, E.; Uretzky, G.; Shofti, R.; Banai, S.; Yosef, L.; Bolotin, G. Expandable external support device to improve Saphenous Vein Graft Patency after CABG. *J. Cardiothorac. Surg.* **2013**, *8*, 122. [CrossRef] [PubMed]
57. Murphy, G.J.; Newby, A.C.; Jeremy, J.Y.; Baumbach, A.; Angelini, G.D. A randomized trial of an external Dacron sheath for the prevention of vein graft disease: The Extent study. *J. Thorac. Cardiovasc. Surg.* **2007**, *134*, 504–505. [CrossRef] [PubMed]

58. Emery, R.W.; Solien, E.; Klima, U. Clinical Evaluation of the eSVS Mesh: First-In-Man Trial Outcomes. *ASAIO J.* **2015**, *61*, 178–183. [CrossRef] [PubMed]
59. Inderbitzin, D.T.; Bremerich, J.; Matt, P.; Grapow, M.T.; Eckstein, F.S.; Reuthebuch, O. One-year patency control and risk analysis of eSVS®-mesh-supported coronary saphenous vein grafts. *J. Cardiothorac. Surg.* **2015**, *10*, 108. [CrossRef]
60. Taggart, D.P.; Ben Gal, Y.; Lees, B.; Patel, N.; Webb, C.; Rehman, S.M.; Desouza, A.; Yadav, R.; De Robertis, F.; Dalby, M.; et al. A Randomized Trial of External Stenting for Saphenous Vein Grafts in Coronary Artery Bypass Grafting. *Ann. Thorac. Surg.* **2015**, *99*, 2039–2045. [CrossRef]
61. Taggart, D.P.; Gavrilov, Y.; Krasopoulos, G.; Rajakaruna, C.; Zacharias, J.; De Silva, R.; Channon, K.M.; Gehrig, T.; Donovan, T.J.; Friedrich, I.; et al. External stenting and disease progression in saphenous vein grafts two years after coronary artery bypass grafting: A multicenter randomized trial. *J. Thorac. Cardiovasc. Surg.* **2022**, *164*, 1532–1541.e2. [CrossRef]
62. Goldstein, D.J.; Puskas, J.D.; Alexander, J.H.; Chang, H.L.; Gammie, J.S.; Marks, M.E.; Iribarne, A.; Vengrenyuk, Y.; Raymond, S.; Taylor, B.S.; et al. External Support for Saphenous Vein Grafts in Coronary Artery Bypass Surgery: A Randomized Clinical Trial. *JAMA Cardiol.* **2022**, *7*, 808–816. [CrossRef] [PubMed]
63. Taggart, D.P.; Webb, C.M.; Desouza, A.; Yadav, R.; Channon, K.M.; De Robertis, F.; Di Mario, C. Long-term performance of an external stent for saphenous vein grafts: The VEST IV trial. *J. Cardiothorac. Surg.* **2018**, *13*, 117. [CrossRef] [PubMed]
64. Chen, H.; Wang, Z.; Si, K.; Wu, X.; Ni, H.; Tang, Y.; Liu, W.; Wang, Z. External stenting for saphenous vein grafts in coronary artery bypass grafting: A meta-analysis. *Eur. J. Clin. Investig.* **2023**, *53*, e14046. [CrossRef]
65. Soletti, G.J.; Dimagli, A.; Harik, L.; Cancelli, G.; Perezgrovas-Olaria, R.; Alzghari, T.; Dell'Aquila, M.; Leith, J.; Castagnini, S.; Lau, C.; et al. External Stenting for Saphenous Vein Grafts in Coronary Surgery: A Systematic Review and Meta-Analysis. *J. Clin. Med.* **2023**, *12*, 7395. [CrossRef] [PubMed]
66. Arvela, E.; Kauhanen, P.; Albäck, A.; Lepäntalo, M.; Neufang, A.; Adili, F.; Schmitz-Rixen, T. Initial Experience with a New Method of External Polyester Scaffolding for Infrainguinal Vein Grafts. *Eur. J. Vasc. Endovasc. Surg.* **2009**, *38*, 456–462. [CrossRef]
67. Carella, G.S.; Stilo, F.; Benedetto, F.; David, A.; Risitano, D.C.; Buemi, M.; Spinelli, F. Femoro-Distal Bypass with Varicose Veins Covered by Prosthetic Mesh. *J. Surg. Res.* **2011**, *168*, e189–e194. [CrossRef]
68. Berard, X.; Brizzi, V.; Mayeux, S.; Sassoust, G.; Biscay, D.; Ducasse, E.; Bordenave, L.; Corpataux, J.M.; Midy, D. Salvage Treatment for Venous Aneurysm Complicating Vascular Access Arteriovenous Fistula: Use of an Exoprosthesis to Reinforce the Vein after Aneurysmorrhaphy. *Eur. J. Vasc. Endovasc. Surg.* **2010**, *40*, 100–106. [CrossRef]
69. Rokošný, S.; Baláž, P.; Wohlfahrt, P.; Palouš, D.; Janoušek, L. Reinforced Aneurysmorrhaphy for True Aneurysmal Haemodialysis Vascular Access. *Eur. J. Vasc. Endovasc. Surg.* **2014**, *47*, 444–450. [CrossRef] [PubMed]
70. Chemla, E.; Velazquez, C.C.; D'Abate, F.; Ramachandran, V.; Maytham, G. Arteriovenous fistula construction with the VasQ™ external support device: A pilot study. *J. Vasc. Access* **2016**, *17*, 243–248. [CrossRef]
71. Matoussevitch, V.; Kalmykov, E.; Shahverdyan, R. Novel external stenting for reconstruction of high flow arteriovenous fistula. *J. Vasc. Access* **2022**, *23*, 864–870. [CrossRef]
72. Vaes, R.H.; Wouda, R.; van Loon, M.; van Hoek, F.; Tordoir, J.H.; Scheltinga, M.R. Effectiveness of surgical banding for high flow in brachial artery-based hemodialysis vascular access. *J. Vasc. Surg.* **2015**, *61*, 762–766. [CrossRef] [PubMed]
73. Kuemmerli, C.; Habrina, D.; Puchner, S.; Laminger, F.; Werzowa, J.; Roka, S. Primary External Stenting of an Autogenous Brachial-Basilic Upper Arm Transposition. *Ann. Vasc. Surg.* **2020**, *65*, 288.e1–288.e4. [CrossRef] [PubMed]
74. Dashwood, M.R.; Loesch, A. The saphenous vein as a bypass conduit: The potential role of vascular nerves in graft performance. *Curr. Vasc. Pharmacol.* **2009**, *7*, 47–57. [CrossRef]
75. Cooley, B.C. Murine Model of Neointimal Formation and Stenosis in Vein Grafts. *Arterioscler. Thromb. Vasc. Biol.* **2004**, *24*, 1180–1185. [CrossRef]
76. Zwolak, R.M.; Adams, M.C.; Clowes, A.W. Kinetics of vein graft hyperplasia: Association with tangential stress. *J. Vasc. Surg.* **1987**, *5*, 126–136. [CrossRef] [PubMed]
77. Wong, A.P.; Nili, N.; Jackson, Z.S.; Qiang, B.; Leong-Poi, H.; Jaffe, R.; Raanani, E.; Connelly, P.W.; Sparkes, J.D.; Strauss, B.H. Expansive remodeling in venous bypass grafts: Novel implications for vein graft disease. *Atherosclerosis* **2008**, *196*, 580–589. [CrossRef]
78. Tian, X.D.; Zhou, N.K.; Li, B.J.; Xiao, C.S.; Liu, X.; Liang, C.Y.; Zhang, T.; Gao, C.Q. Effects and mechanisms of non-restrictive external stent for prevention of vein graft restenosis in a rabbit model. *Chin. Med. J.* **2010**, *123*, 2400–2404. [PubMed]
79. You, Q.; Duan, L.; Wang, F.; Du, X.; Xiao, M. Characterization of the inhibition of vein graft intimal hyperplasia by a biodegradable vascular stent. *Cell Biochem. Biophys.* **2011**, *59*, 99–107. [CrossRef]
80. Karayannacos, P.E.; Hostetler, J.R.; Bond, M.G.; Kakos, G.S.; Williams, R.A.; Kilman, J.W.; Vasko, J.S. Late failure in vein grafts: Mediating factors in subendothelial fibromuscular hyperplasia. *Ann. Surg.* **1978**, *187*, 183–188. [CrossRef]
81. Barra, J.A.; Volant, A.; Leroy, J.P.; Braesco, J.; Airiau, J.; Boschat, J.; Blanc, J.J.; Penther, P. Constrictive perivenous mesh prosthesis for preservation of vein integrity. Experimental results and application for coronary bypass grafting. *J. Thorac. Cardiovasc. Surg.* **1986**, *92*, 330–336. [CrossRef]
82. Goldstein, R.L.; McCormack, M.C.; Mallidi, S.; Runyan, G.; Randolph, M.A.; Austen, W.G., Jr.; Redmond, R.W. Photochemical Tissue Passivation of Arteriovenous Grafts Prevents Long-Term Development of Intimal Hyperplasia in a Swine Model. *J. Surg. Res.* **2020**, *253*, 280–287. [CrossRef] [PubMed]

83. Nantsios, A.; Vo, T.X.; Ruel, M. Commentary: External stenting of saphenous vein grafts-reinVESTing to achieve best returns in coronary artery bypass grafting. *J. Thorac. Cardiovasc. Surg.* **2022**, *164*, 1542–1543. [CrossRef] [PubMed]
84. Zwischenberger, B.A.; Gaudino, M. Commentary: A device solution for the saphenous vein graft's infamous foible? *J. Thorac. Cardiovasc. Surg.* **2022**, *164*, 1543–1545. [CrossRef] [PubMed]
85. Conte, M.S.; Bandyk, D.F.; Clowes, A.W.; Moneta, G.L.; Seely, L.; Lorenz, T.J.; Namini, H.; Hamdan, A.D.; Roddy, S.P.; Belkin, M.; et al. Results of PREVENT III: A multicenter, randomized trial of edifoligide for the prevention of vein graft failure in lower extremity bypass surgery. *J. Vasc. Surg.* **2006**, *43*, 742–751; discussion 751. [CrossRef] [PubMed]
86. Alexander, J.H.; Hafley, G.; Harrington, R.A.; Peterson, E.D.; Ferguson, T.B., Jr.; Lorenz, T.J.; Goyal, A.; Gibson, M.; Mack, M.J.; Gennevois, D.; et al. Efficacy and safety of edifoligide, an E2F transcription factor decoy, for prevention of vein graft failure following coronary artery bypass graft surgery: PREVENT IV: A randomized controlled trial. *JAMA* **2005**, *294*, 2446–2454. [CrossRef]

Disclaimer/Publisher's Note: The statements, opinions and data contained in all publications are solely those of the individual author(s) and contributor(s) and not of MDPI and/or the editor(s). MDPI and/or the editor(s) disclaim responsibility for any injury to people or property resulting from any ideas, methods, instructions or products referred to in the content.

biomedicines

MDPI

Article

Importance of T1-Mapping Sequence in Patients with Hypertrophic Cardiomyopathy without Foci of Non-Ischemic Myocardial Injury in Late Gadolinium Enhancement Sequence

Natalia Zdebik [1], Rafał Poręba [1,2] and Paweł Gać [1,3,*]

[1] Centre for Diagnostic Imaging, 4th Military Hospital, 50-981 Wroclaw, Poland
[2] Department of Internal Medicine, Occupational Diseases, Hypertension and Clinical Oncology, Wroclaw Medical University, 50-556 Wroclaw, Poland
[3] Department of Population Health, Division of Environmental Health and Occupational Medicine, Wroclaw Medical University, 50-345 Wroclaw, Poland
* Correspondence: pawelgac@interia.pl

Abstract: Background: The aim of this study was to assess the importance of T1-mapping sequences in the diagnosis of hypertrophic cardiomyopathy (HCM) in patients without foci of non-ischemic myocardial injury in classic cardiac magnetic resonance (CMR) sequences. Methods: Two groups were compared: 28 patients with HCM, without any foci of myocardial injury in the late gadolinium enhancement (LGE) sequence (HCM group), and 28 patients without cardiomyopathy (CON group). Classic CMR sequences and T1-mapping sequences were performed. The following parameters were assessed: T1 time of the whole left ventricular myocardium, T1 time of myocardium in the basal, middle and apical layers of the left ventricle, and T1 time in individual segments of the left ventricular myocardium. Myocardial extracellular volume (ECV) was assessed similarly. Results: ECV was significantly higher in the HCM group than in the CON group, for the whole left ventricular myocardium, for the basal and apical layers of the left ventricle, and for segments 1–3, 8, and 13–16 of the left ventricle. Regression analysis showed that a higher left-ventricular mass index (LVMI), a higher body mass index and older age are factors independently associated with a higher ECV of the whole myocardium but only in the group with LVMI $\geq$ 131.84 g/m^2. Conclusion: In patients with HCM without foci of non-ischemic myocardial injury, higher ECV values of the left ventricular myocardium are observed.

Keywords: cardiac magnetic resonance; extracellular volume; hypertrophic cardiomyopathy

1. Introduction

Hypertrophic cardiomyopathy (HCM), with a prevalence of 1:500 in the general population, is a relatively common autosomal-dominant inherited monogenic disorder. HCM is characterized by left ventricular (LV) hypertrophy, which is most often asymmetric. Histologically, left ventricular hypertrophy is associated with the disruption of the myocardial fiber system, coronary microcirculation dysfunction, and myocardial replacement fibrosis. Myocardial fibrosis in HCM is a poor prognostic factor [1,2]. Myocardial hypertrophy most often affects the interventricular septum. However, any segment of the myocardium may also be hypertrophied [1].

Left ventricular wall thickness is 15 mm or more according to the European Society of Cardiology guidelines (the average is 21 mm) but may demonstrate massive thickness (30 to 50 mm) in some cases [3]. However, normal dimensions may occur in gene carriers [4].

Clinical symptoms encompass cardiac-related symptoms like dyspnea, chest pain, palpitations and syncope, or asymptomatic signs like a heart murmur or an abnormal electrocardiogram [5,6]. The most common cardiovascular events in patients with HCM include sudden cardiac death (51%), heart failure (36%), and stroke (13%) [6,7].

Clinically, hypertrophic cardiomyopathy is diagnosed based on a confirmation of myocardial hypertrophy of the non-enlarged LV using diagnostic imaging, correlating with anamnesis data [4]. The basic diagnostic imaging method in the assessment of HCM is echocardiography due to its good availability and low costs. The routine use of cardiac magnetic resonance (CMR) in the management of HCM patients has recently become the standard [8].

Late gadolinium enhancement (LGE) is a reference standard for the non-invasive imaging of myocardial scar and focal fibrosis. Typically, in hypertrophic cardiomyopathy, foci of non-ischemic myocardial injury (intramural or subepicardial LGE foci) are found. Topographically, they most often occur first in hypertrophied segments of the myocardium of the left ventricle, as well as in RV–LV insertion points. The occurrence of LGE foci in patients with hypertrophic cardiomyopathy is an unfavorable prognostic factor [9]. Gadolinium contrast media cannot cross intact sarcolemma membranes [6]. LGE sequences can detect only regional myocardial fibrosis [10].

T1 mapping measures the longitudinal or spin-lattice relaxation time [2,9]. Gadolinium-based contrast agents are distributed throughout the extracellular space and shorten T1 relaxation times of the myocardium proportional to the local concentration for gadolinium. Pre- and post-contrast T1-mapping techniques are used to quantify myocardial extracellular volume (ECV). HCM patients have significantly shorter post-contrast myocardial T1 times compared to healthy controls due to myocardial elevated diffuse fibrosis [2,11].

Native T1 values are a composite signal of myocytes and extracellular volume that decrease in fat or iron deposition in the myocardium while increasing with edema, amyloid deposition, and fibrosis. Studies proved that native (non-contrast) T1 mapping can differentiate myocardial abnormality of hypertrophic cardiomyopathy from healthy myocardium [12]. T1-mapping sequences can also be used in the differential diagnosis of myocardial accumulation diseases, e.g., in patients with amyloidosis. In AL amyloidosis, due to the predominant myocardial edema, very high values of myocardial T1 time and moderately high ECV values are observed. However, in ATTR amyloidosis, which is dominated by amyloid deposition in the myocardium, very high ECV values are observed with moderately high myocardial T1 times [13]. T1-mapping sequences may also be useful in monitoring the course of the disease. T1-mapping sequences enable the quantitative measurement of the absolute T1 time of the myocardium. Therefore, it is possible to compare the values of the measured T1 time and ECV between subsequent acquisitions and assess the dynamics of changes occurring in the myocardium [13].

T1-mapping imaging is currently used in cardiac magnetic resonance (CMR) protocols in clinical practice. However, most scientific evidence regarding the usefulness of T1 mapping concerns patients with foci of non-ischemic myocardial damage in the LGE sequence. There is less scientific evidence regarding the importance of T1-mapping sequences in patients without myocardial damage in the LGE sequence.

The aim of this study was to assess the importance of T1-mapping sequences in the diagnosis of hypertrophic cardiomyopathy in patients in whom no signs of focal myocardial injury were found using classic CMR imaging sequences.

2. Materials and Methods

2.1. Study Group

The study was conducted in accordance with the Declaration of Helsinki and approved by the Ethics Committee of Wroclaw Medical University (protocol code KB-414/2021). Informed consent was obtained from all subjects involved in the study.

The study protocol included estimating the required size of the study group, qualifying patients to the group with hypertrophic cardiomyopathy without LGE foci (HCM group) based on the assumed inclusion and exclusion criteria, and selecting patients for the control group (CON group).

The size of the study group was estimated based on the sample size calculator. The following evaluation conditions were assumed in the calculator: estimated fraction size 5%,

significance level 0.05, population size 2,800,000, and permissible error 10%. The minimum required size of the study group was estimated at 19 patients.

The criteria for inclusion in the HCM group were age >18 years, diagnosis of hypertrophic cardiomyopathy based on the diagnostic procedure (wall thickness >15 mm or septal to lateral wall thickness ratio >1.3 or apical to basal wall thickness ratio $\geq$1.3 to 1.5 in apical HCM), and consent to participate in the study. The criteria for exclusion from the study in the initially recruited HCM group were the presence of non-ischemic myocardial injury (LGE foci) on cardiac magnetic resonance imaging, other causes of hypertrophic left ventricular morphotype in CMR (amyloidosis, sarcoidosis, athlete's heart, hypertensive cardiomyopathy, aortic stenosis, third degree obesity, systemic diseases), lack of hypertrophic left ventricular morphotype in CMR, insufficient technical quality of the examination CMR, and incidentally diagnosed ischemic heart disease with ischemic myocardial injury in CMR. Based on the inclusion criteria, a group of 69 patients was included in the study, and 41 patients were excluded from the study group.

The CON group was recruited from healthy volunteers with similar anthropometric parameters (same gender, age $\pm$3 years, BMI $\pm$2 kg/m^2). The health status of the volunteers was verified based on interviews, physical examinations, echocardiography and the analysis of the results of cardiac magnetic resonance performed in the project.

Finally, 2 groups of subjects were compared: 28 patients with hypertrophic cardiomyopathy, without any foci of myocardial injury in the late gadolinium enhancement (LGE) sequence (HCM group; mean age 52.17 $\pm$ 6.35 years), and 28 patients without cardiomyopathy (CON group; mean age 51.76 $\pm$ 6.49 years). Basic clinical information about the study group is summarized in Table 1.

Table 1. Clinical characteristics of the study groups.

	HCM Group (n = 28)	**CON Group (n = 28)**	p [c]
age [years] [a]	52.17 $\pm$ 1.32	51.76 $\pm$ 1.19	-
gender [b]			
men	57.1	57.1	1.00
women	42.9	42.9	1.00
height [cm] [a]	167.25 $\pm$ 1.54	169.00 $\pm$ 1.72	-
weight [kg] [a]	71.14 $\pm$ 2.03	73.32 $\pm$ 2.17	-
BMI [kg/m^2] [a]	25.34 $\pm$ 0.71	25.66 $\pm$ 0.39	-
overweight/obesity [b]			
normal body mass	57.1	50.0	0.59
overweight	28.6	39.3	0.40
obesity	14.3	10.7	0.68
coexistence of cardiovascular risk factors [b]			
arterial hypertension	28.6	32.1	0.77
type 2 diabetes	10.7	17.8	0.45
smoking	39.3	42.8	0.79

a—quantitative variable expressed as mean $\pm$ standard error of mean, b—categorical variable expressed as percentage, c—in the case of categorical variables, the p-value for the chi-square test; and in the case of quantitative variables, p-value for each response variable $p < 0.05$ and the Wilks Lambda value of the one-way MANOVA analysis (Wilks Lambda = 0.938, $p = 0.506$) and for the contrast between CON—control, HCM—hypertrophic cardiomyopathy, BMI—body mass index.

2.2. Cardiac Magnetic Resonance

First, 1.5 Tesla cardiac magnetic resonance (CMR) imaging was performed using the Magnetom Aera device (Siemens Healthcare, Forchheim, Germany). All CMR was performed using the same examination protocol. This protocol consisted of a steady-state slow precession CINE sequence, a short tau inversion recovery (STIR) sequence, a native T1-mapping sequence, a late gadolinium enhancement (LGE) sequence, and a T1-mapping C+ sequence. T1-mapping C+ sequences were performed 5 min and 20 min after intravenous bolus injections of gadobutrol (Gadovist, Bayer Healthcare, Leverkusen, Germany), at

a dose of 0.2 mmol/kg body weight. Medis Suite MR 4 software (Medis, Leiden, The Netherlands) was used to evaluate the post-processing of CMR images. Examples of CMR images obtained for a patient from the HCM group are shown in Figure 1, and the same can be seen for a patient from the CON group in Figure 2.

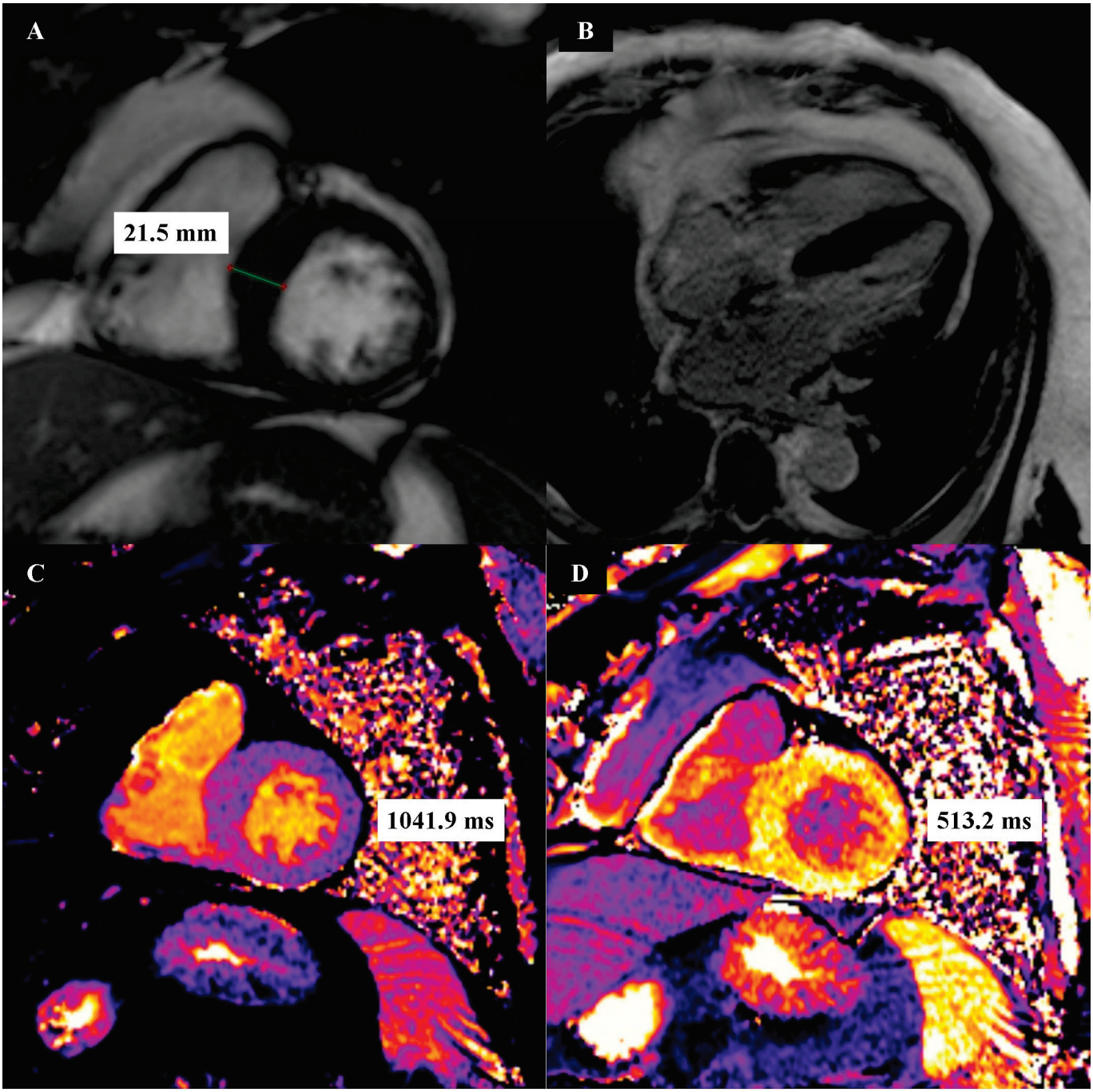


Figure 1. Example CINE (**A**), late gadolinium enhancement (**B**), native T1 mapping (**C**) and post-contrast T1 mapping (**D**) images in patients from the hypertrophic cardiomyopathy group.

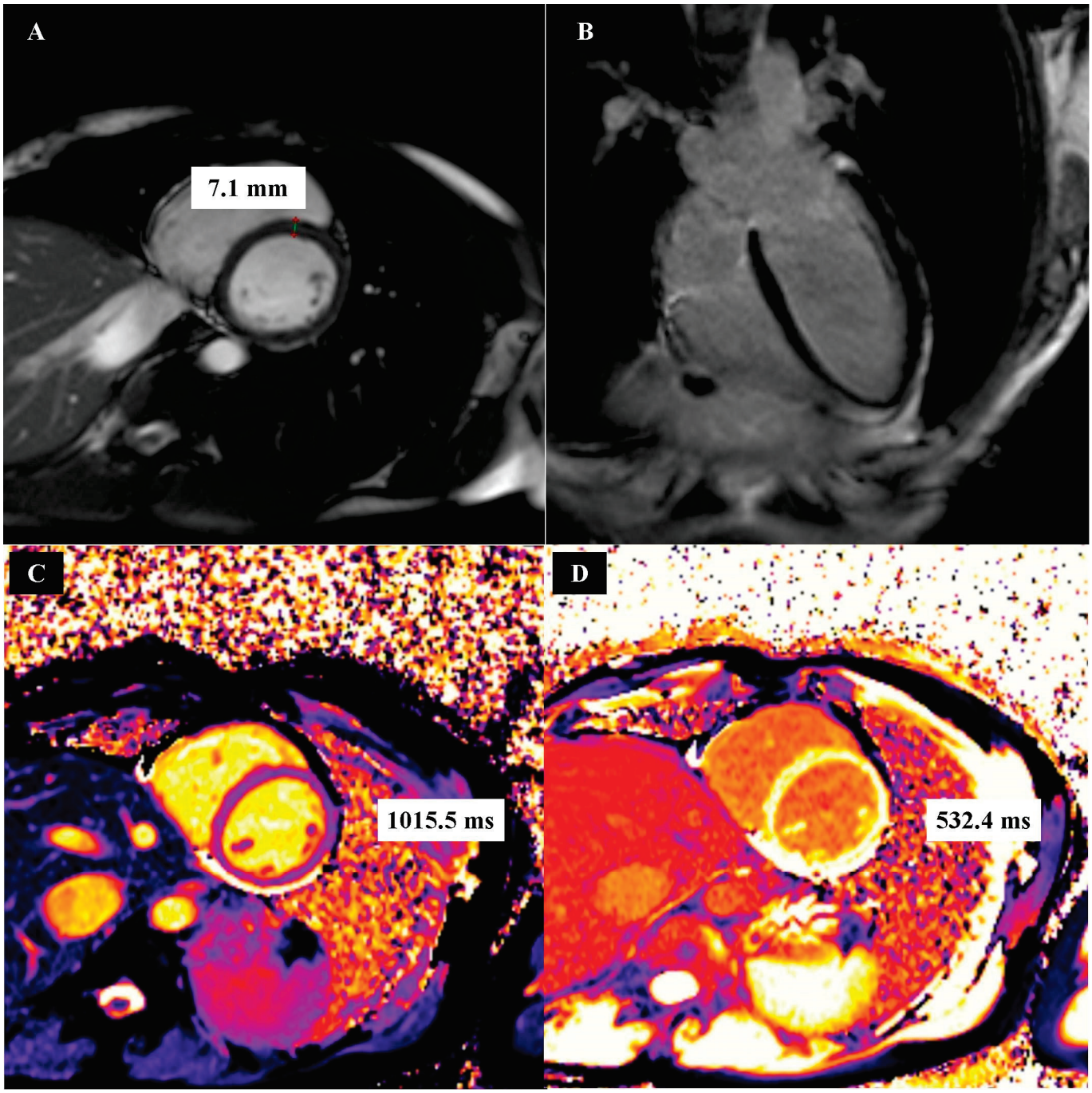


Figure 2. Example CINE (**A**), late gadolinium enhancement (**B**), native T1 mapping (**C**) and post-contrast T1 mapping (**D**) images in patients from the control group.

CINE sequences were obtained in the left ventricular short axis and long axis in two-chamber, three-chamber, and four-chamber views. The following linear and planimetric measurements of the cardiac chambers were conducted based on CINE sequence images: right atrial area (RAA), left atrial area (LAA), left ventricular end-diastolic diameter (LVEDD), left ventricular end-systolic diameter (LVESD), anterior interventricular septal diastolic diameter (aIVSDD), posterior wall diastolic diameter (PWDD) and maximum left ventricular myocardial diastolic diameter (maxLVMDD).

CINE sequence images were also used to measure left ventricular functional parameters. End-diastolic and end-systolic volumes (EDV and ESV) were estimated using the volumetric method. EDV and ESV values were calculated as the sum of the left ventricular

area in successive short-axis image layers multiplied by the slice thickness in the left ventricular end-diastolic and end-systolic phases, respectively. The difference between EDV and ESV values was the stroke volume (SV), and the percentage ratio of SV to EDV was the ejection fraction (EF). All left ventricular functional parameters were expressed as values indexed by body surface area (BSA). In addition, the left ventricular mass (LVM) and left ventricular mass index (LVMI) were estimated.

In the STIR sequence, the occurrence of foci of left ventricular oedema was assessed, and in the LGE sequence, the occurrence of foci of left ventricular myocardial injury was assessed.

In addition to classical sequences, T1-mapping sequences were performed. The following parameters were assessed: T1 time of the whole left ventricular myocardium (T1 whole myocardium), T1 time of the myocardium in the basal (T1 basal), middle (T1 middle) and apical (T1 apical) layers of the left ventricle, and T1 time in individual segments of the left ventricular myocardium. The T1 time for the whole left ventricular myocardium is the average of the T1 time of all myocardium voxels. The T1 time for each of the left ventricular myocardial layers is the average of all voxels in each of these layers. The T1 time for each of the 16 left ventricular myocardial segments is the average of all voxels in each of these segments. Myocardial extracellular volume (ECV) was assessed similarly. Hematocrit for ECV calculation was determined in the range of 0–48 h before the study.

Details of the CMR protocol are presented in the center's previous publication [14].

2.3. Statistical Analysis

Dell Statistica (data analysis software system), version 13 (Dell Inc., Tulsa, OK, USA), was used for statistical calculations. Quantitative variables were presented as arithmetic means ± standard error of mean. Due to the high probability of type II statistical errors, quantitative variables were compared using one-way MANOVA. In the first stage, it was assessed whether there was a contrast in any of the assessed variables, obtaining the value of the Wilks Lambda statistic with the appropriate p-value. In the case of the statistical significance of the Wilks Lambda statistic, the impact of the contrast of the compared factor (HCM vs. CON) was estimated for each of the analyzed variables. Qualitative variables were presented as percentages. Percentage distributions of qualitative variables were compared using the maximum likelihood chi-square test. Correlation analysis and regression analysis were used to assess the relationship between variables. In the case of quantitative variables with a normal distribution, Pearson's r correlation coefficients were determined. In the case of quantitative variables with a distribution other than normal, Spearman's r coefficients were determined. Results at the $p < 0.05$ level were considered statistically significant.

3. Results

In CINE sequences of the HCM group compared to the CON group, the anterior interventricular septal diastolic diameter and posterior wall diastolic diameter were significantly higher. The maximum left ventricular myocardial diastolic diameter, left ventricular mass and left ventricular mass index were also statistically significantly higher in the HCM group than in the CON group. In the HCM group, thickening of the basal segments of the interventricular septum and the anterior wall of the left ventricle; thickening of the middle segments of the interventricular septum; thickening of the apical segments of the interventricular septum, inferior and lateral walls of the left ventricle; and apex thickening occurred significantly more often in the HCM group than in the CON group, as seen in Table 2.

Table 2. Standard cardiac magnetic resonance parameters in the study groups.

	HCM Group (n = 28)	**CON Group (n = 28)**	p [c]
cardiac cavities dimensions			
LAA [cm^2] [a]	22.17 ± 1.38	23.42 ± 0.73	-
RAA [cm^2] [a]	20.63 ± 0.67	21.74 ± 0.58	-
LVEDD [mm] [a]	59.76 ± 2.64	57.86 ± 1.66	-
LVESD [mm] [a]	30.49 ± 2.42	33.13 ± 2.21	-
aIVSDD [mm] [a]	15.59 ± 0.69	8.47 ± 0.69	0.01
PWDD [mm] [a]	11.68 ± 0.53	6.96 ± 0.46	0.01
maxLVMDD [mm] [a]	19.16 ± 0.67	9.14 ± 0.25	0.01
LVM [g] [a]	215.86 ± 6.39	135.83 ± 7.10	0.01
LVMI [g/m^2] [a]	137.49 ± 3.57	71.13 ± 4.72	0.01
thickening of the left ventricular myocardium [b]			
interventricular septum basal segments	64.3	0.0	0.01
interventricular septum middle segments	60.7	0.0	0.01
interventricular septum apical segments	35.7	0.0	0.01
anterior wall basal segments	46.4	0.0	0.01
anterior wall middle segments	17.8	0.0	0.06
anterior wall apical segments	7.1	0.0	0.15
inferior wall basal segments	3.6	0.0	0.31
inferior wall middle segments	7.1	0.0	0.15
inferior wall apical segments	25.0	0.0	0.01
lateral wall basal segments	10.7	0.0	0.07
lateral wall middle segments	10.7	0.0	0.07
lateral wall apical segments	28.6	0.0	0.01
apex	35.7	0.0	0.01
left ventricular systolic function			
EDV/BSA [ml/m^2] [a]	96.18 ± 4.76	95.47 ± 3.60	-
ESV/BSA [ml/m^2] [a]	30.57 ± 2.32	30.18 ± 2.17	-
SV/BSA [ml/m^2] [a]	62.74 ± 2.13	61.48 ± 2.12	-
EF [%] [a]	67.15 ± 1.50	66.96 ± 1.12	-
LVSD [b]	0.0	0.0	1.00
left ventricular morphology			
edema foci [b]	0.0	0.0	1.00
LGE foci [b]	0.0	0.0	1.00

a—quantitative variable expressed as mean ± standard error of mean, b—categorical variable expressed as percentage, c—in the case of categorical variables, the p-value for the chi-square test; and in the case of quantitative variables, p-value for each response variable $p < 0.05$ and the Wilks Lambda value of the one-way MANOVA analysis (Wilks Lambda = 0.075, $p < 0.01$) and for the contrast between CON—control, HCM—hypertrophic cardiomyopathy, aIVSDD—anterior interventricular septal diastolic diameter, BSA—body surface area, EDV—end-diastolic volume, EF—ejection fraction, ESV—end-systolic volume, LAA—left atrial area, LGE—late gadolinium enhancement, LVEDD—left ventricular end-diastolic diameter, LVESD—left ventricular end-systolic diameter, LVM—left ventricular mass, LVMI—left ventricular mass index, LVSD—left ventricular systolic dysfunction, maxLVMDD—maximum left ventricular myocardial diastolic diameter, PWDD—posterior wall diastolic diameter, RAA—right atrial area, SV—stroke volume.

There was no difference in the left ventricular ejection fraction between the HCM and CON groups. Left ventricular systolic dysfunction was not observed in both study groups, as seen in Table 2.

In the classical sequences of the structural assessment of the LV myocardium, i.e., in the STIR and LGE sequences, which resulted from the inclusion and exclusion criteria, no statistically significant differences were observed either, as shown in Table 2.

Myocardial T1 times did not differentiate the studied groups. No differences were observed in the mean values of the T1 time of the whole myocardium, the mean values of the T1 time of the subsequent layers of the left ventricle—the basal, middle and apical layers, or the mean values of the T1 times of each of the 16 left ventricular myocardial segments (Table 3).

Table 3. Myocardial T1 times in the cardiac magnetic resonance T1-mapping sequence in the study groups.

	HCM Group (n = 28)	**CON Group (n = 28)**	p [b]
whole myocardium [ms] [a]	1038.15 ± 2.98	1031.56 ± 3.65	-
basal layer [ms] [a]	1042.56 ± 3.68	1035.84 ± 4.02	-
middle layer [ms] [a]	1031.11 ± 3.66	1025.17 ± 4.26	-
apical layer [ms] [a]	1048.64 ± 3.00	1040.97 ± 4.49	-
segment 1 [ms] [a]	1040.59 ± 4.62	1034.61 ± 4.83	-
segment 2 [ms] [a]	1048.48 ± 4.38	1039.42 ± 4.18	-
segment 3 [ms] [a]	1050.03 ± 4.15	1041.58 ± 3.82	-
segment 4 [ms] [a]	1040.28 ± 4.07	1042.65 ± 3.43	-
segment 5 [ms] [a]	1037.15 ± 3.96	1037.02 ± 2.99	-
segment 6 [ms] [a]	1039.12 ± 4.66	1030.62 ± 3.61	-
segment 7 [ms] [a]	1027.59 ± 3.36	1022.49 ± 3.98	-
segment 8 [ms] [a]	1039.15 ± 3.79	1032.15 ± 3.84	-
segment 9 [ms] [a]	1029.13 ± 3.76	1027.58 ± 2.77	-
segment 10 [ms] [a]	1030.87 ± 3.61	1025.78 ± 3.79	-
segment 11 [ms] [a]	1034.18 ± 3.79	1026.29 ± 3.77	-
segment 12 [ms] [a]	1031.84 ± 3.05	1024.42 ± 3.01	-
segment 13 [ms] [a]	1048.69 ± 3.98	1039.15 ± 3.41	-
segment 14 [ms] [a]	1049.19 ± 3.74	1040.01 ± 3.59	-
segment 15 [ms] [a]	1050.24 ± 3.14	1041.03 ± 3.37	-
segment 16 [ms] [a]	1048.12 ± 3.36	1041.59 ± 4.97	-

a—quantitative variable expressed as mean ± standard error of mean, b—p-value for each response variable $p < 0.05$ and the Wilks Lambda value of the one-way MANOVA analysis (Wilks Lambda = 0.947, $p = 0.589$) and for the contrast between CON—control, HCM—hypertrophic cardiomyopathy.

However, the study groups differed in the extracellular volume of the myocardium. In the HCM group, compared to the CON group, the ECV values of the whole myocardium, the ECV values of the basal and apical ECV, and the values of ECV segments 1–3, 8, and 13–16 were statistically significantly higher, as seen in Table 4, Figure 3.

Table 4. Extracellular volume (ECV) in the cardiac magnetic resonance T1-mapping sequence in the study groups.

	HCM Group (n = 28)	**CON Group (n = 28)**	p [b]
whole myocardium [%] [a]	30.23 ± 0.84	25.08 ± 0.36	0.01
basal layer [%] [a]	32.14 ± 0.91	26.04 ± 0.73	0.01
middle layer [%] [a]	28.36 ± 0.80	26.62 ± 0.84	-
apical layer [%] [a]	31.72 ± 0.51	24.20 ± 0.59	0.01
segment 1 [%] [a]	35.08 ± 0.69	26.28 ± 0.61	0.01
segment 2 [%] [a]	34.33 ± 0.78	26.56 ± 0.64	0.01
segment 3 [%] [a]	33.87 ± 0.53	25.81 ± 0.70	0.01
segment 4 [%] [a]	29.08 ± 0.75	25.58 ± 0.63	-
segment 5 [%] [a]	28.86 ± 0.84	25.66 ± 0.72	-
segment 6 [%] [a]	29.30 ± 0.59	25.90 ± 0.58	-
segment 7 [%] [a]	27.63 ± 0.56	26.78 ± 0.53	-
segment 8 [%] [a]	32.17 ± 0.69	26.60 ± 0.63	0.01
segment 9 [%] [a]	28.48 ± 0.73	26.86 ± 0.63	-
segment 10 [%] [a]	28.17 ± 0.82	26.02 ± 0.54	-
segment 11 [%] [a]	27.44 ± 0.85	26.77 ± 0.78	-
segment 12 [%] [a]	26.39 ± 0.74	26.76 ± 0.42	-
segment 13 [%] [a]	31.41 ± 0.61	24.03 ± 0.97	0.01
segment 14 [%] [a]	32.33 ± 0.68	24.97 ± 0.68	0.01
segment 15 [%] [a]	31.40 ± 0.49	23.94 ± 0.48	0.01
segment 16 [%] [a]	31.76 ± 0.70	24.05 ± 0.61	0.01

a—quantitative variable expressed as mean ± standard error of mean, b—p-value for each response variable $p < 0.05$ and the Wilks Lambda value of the one-way MANOVA analysis (Wilks Lambda = 0.034, $p < 0.01$) and for the contrast between CON—control, HCM—hypertrophic cardiomyopathy.

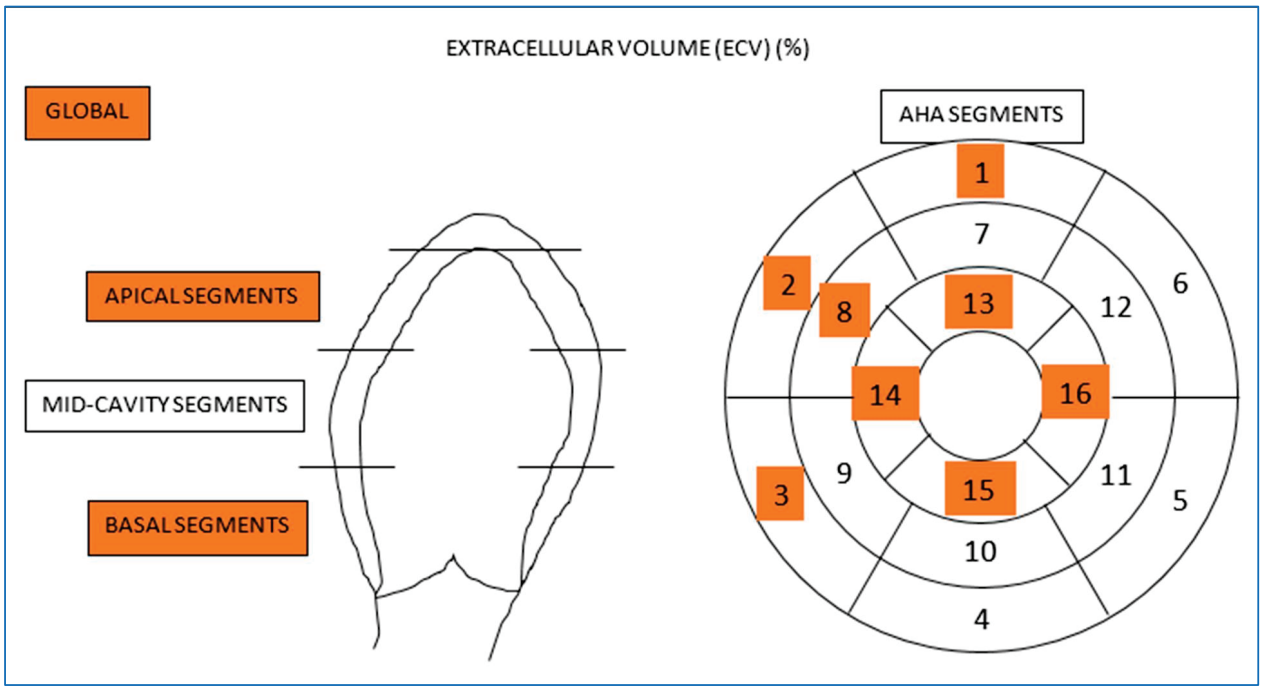


Figure 3. Location of significantly higher extracellular volume values in the left ventricular myocardium in patients with hypertrophic cardiomyopathy without foci of myocardial injury in the late gadolinium enhancement sequence. Statistically significant differences regarding the entire myocardium, myocardial layers and myocardial segments are marked in orange. AHA—American Heart Association.

The performed correlation analysis showed no linear relationship between left ventricular myocardial thickness (aIVSDD, PWDD, maxLVMDD) and T1 times and extracellular volumes of the left ventricle myocardium. There were also no significant linear relationships between left ventricular mass (LVM, LVMI) and myocardial T1 times and ECV in the T1-mapping sequence (Table 5).

Table 5. The results of the correlation analysis between standard left ventricular evaluation parameters and T1-mapping sequence parameters in cardiac magnetic resonance in the study group.

	Whole Myocardium T1 Time [ms]		**Whole Myocardium ECV [%]**	
	r	***p***	**r**	***p***
LVEDD [mm]	0.05	0.84	0.11	0.73
LVESD [mm]	0.07	0.82	0.03	0.94
aIVSDD [mm]	0.17	0.59	0.17	0.59
PWDD [mm]	0.15	0.61	0.18	0.54
maxLVMDD [mm]	0.21	0.22	0.23	0.24
LVM [g]	0.19	0.54	0.19	0.34
LVMI [g/m^2]	0.21	0.22	0.20	0.22
EDV/BSA [ml/m^2]	0.14	0.71	0.16	0.49
ESV/BSA [ml/m^2]	0.02	0.97	0.10	0.56
SV/BSA [ml/m^2]	0.05	0.84	0.14	0.71
EF [%]	−0.03	0.94	−0.06	0.84

aIVSDD—anterior interventricular septal diastolic diameter, BSA—body surface area, EDV—end-diastolic volume, ECV—extracellular volume, EF—ejection fraction, ESV—end-systolic volume, LVEDD—left ventricular end-diastolic diameter, LVESD—left ventricular end-systolic diameter, LVM—left ventricular mass, LVMI—left ventricular mass index, maxLVMDD—maximum left ventricular myocardial diastolic diameter, PWDD—posterior wall diastolic diameter, SV—stroke volume.

Based on the multivariate segmental linear regression analysis with a break-through point carried out for the entire study group, the following relationship model was obtained:

- For LVMI < 131.84 g/m^2: whole myocardium ECV = 15.528 + 0.025 LVMI + 0.259 BMI + 0.124 age ($p > 0.05$).
- For LVMI $\geq$ 131.84 g/m^2: whole myocardium ECV = 24.025 + 0.038 LVMI + 0.271 BMI + 0.139 age ($p < 0.05$).

The obtained model indicates that in the study group, a higher LVMI, higher BMI and older age are factors independently associated with higher extracellular volume values of the whole myocardium but only in the group of patients with LVMI $\geq$ 131.84 g/m^2. At lower LVMI values, the relationship between the LVMI and ECV of the whole myocardium becomes statistically insignificant (Table 6).

Table 6. Results of estimation for the final model obtained using multivariate regression analysis.

Model for Whole Myocardium ECV [%]			
	Intercept	**Lvmi [g/m^2]**	**Age [Years]**
regression coefficient for LVMI < 131.84 g/m^2	15.528	0.025	0.124
p	0.01	0.27	0.04
p of model for LVMI < 131.84 g/m^2	0.19		
regression coefficient for LVMI $\geq$ 131.84 g/m^2	24.025	0.038	0.139
p	0.01	0.04	0.03
p of model for LVMI $\geq$ 131.84 g/m^2	0.04		
p of whole model	0.03		
determination coefficient (R2)	77.12%		

BMI—body mass index, ECV—extracellular volume, LVMI—left ventricular mass index.

4. Discussion

HCM is characterized by the excessive thickening of the ventricular myocardium, particularly the basal interventricular septum subjacent to the aortic valve [5,15]. Cardiac hypertrophy may be occasionally restricted to other myocardial regions [3]. In our study, the end-diastolic thickness of the anterior part of the interventricular septum and the end-diastolic thickness of the posterior wall of the left ventricle were significantly higher in the HCM group compared to the CON group. Also, the left ventricular mass index was significantly higher in the HCM group than in the CON group. However, increased left ventricular mass is not a requirement for establishing a clinical diagnosis of hypertrophic cardiomyopathy. According to some studies, the LV mass index was normal in approximately 20% of patients with a specific HCM phenotype [16]. In the study group, a higher LVMI, higher BMI and older age were factors independently associated with higher ECV values of the whole myocardium but only in the group of patients with LVMI $\geq$ 131.84 g/m^2 (at lower LVMI values, the relationship between the LVMI and ECV of the whole myocardium becomes statistically insignificant). The LVMI is a recognized independent predictor of adverse cardiovascular events in patients with HCM, such as mortality, need for heart transplantation, and the occurrence of malignant ventricular arrhythmia [17]. ECV is a biomarker of diffuse interstitial fibrosis. It has been postulated that extracellular volume and the LVMI did not correlate with each other [18].

Left ventricular systolic function is characteristically normal to hyperdynamic in patients with hypertrophic cardiomyopathy, which was proved in this study, because both groups did not differ in left ventricular ejection fraction [3]. However, previous studies suggested that 4–9% of patients develop systolic dysfunction, defined by an LV ejection fraction (LVEF) < 50%. This complication of disease has previously been termed end-stage or burnt-out HCM and is typically accompanied by diffuse myocardial fibrosis (although left ventricular wall thinning and cavity enlargement may also be present) [19]. The left ventricle in hypertrophic cardiomyopathy usually has a normal end-diastolic volume and a reduced end-systolic volume [3]. In this study, groups did not differ in left ventricular

end-systolic and end-diastolic diameter. The studied groups also did not differ in right and left atrium surface area in four-chamber projection. Left atrial volume is often increased in patients with hypertrophic cardiomyopathy and is a known predictor of the development of atrial fibrillation and heart failure [3]. An increased left atrial volume in HCM is associated with greater hypertrophy, more diastolic dysfunction, and higher filling pressures. From a clinical point of view, left atrial anteroposterior diameter is a well-known marker of HCM severity [20].

The non-invasive assessment of diffuse interstitial fibrosis is of interest in terms of better risk stratification in HCM patients [21].

The presence of late gadolinium enhancement in cardiac MRI in hypertrophic cardiomyopathy reflects irreversible myocardial injury and is a significant prognostic factor in the prediction of severe cardiac complications [7,22]. Extensive LGE (15% of LV mass) can identify HCM patients with increased risk for sudden cardiac death and progressive heart failure [21]. In our study, there were no patients with focal myocardial damage on the LGE sequence. According to available studies, higher ECV values are observed in HCM patients with focal LV myocardial damage in the LGE sequence. It is indicated that ECV changes in HCM patients without LGE foci may be more subtle [23]. Approximately half of patients with HCM have no LGE on MRI [7], which indicates that this technique cannot be the only one used to diagnose cardiac lesions in HCM patients.

Native T1 mapping is one of the most rapidly developing fields in cardiac magnetic resonance and is of particular benefit in diffuse or early myocardial diseases, where traditional CMR methods such as LGE might fail. The technique is advantageous in patients with renal dysfunction and severe allergic reactions because it precludes the injection of a contrast medium [12,22]. Cardiac myocytes in HCM are hypertrophied, disorganized, and separated by areas of interstitial fibrosis at a cellular level. Native T1 is a composite signal of both the cellular and extracellular components of the myocardium, and because of that, it does not differentiate cellular hypertrophy from diffuse fibrosis. ECV is a more specific assessment of the extracellular matrix alone and therefore a measure of interstitial fibrosis [10]. The ECV values of the whole LV myocardium, ECV of the LV basal layers, ECV of the middle LV layers, ECV of the LV apical layers, and ECV values in LV segments 1–3, 8 and 13–16 were significantly higher in our study in patients with hypertrophic cardiomyopathy than in the control group. It should be emphasized that this indicates diffuse myocardial fibrosis in HCM patients without LGE foci, which is difficult to demonstrate using CMR sequences other than T1-mapping sequences. There were no statistically significant differences in T1 times between the studied groups in segmental analysis covering the entire LV myocardium. Native T1 time increases with aging, interstitial edema secondary to infarction with associated cellular destruction, and enlarged interstitial space from fibrosis [10]. In previous studies, myocardial T1 native time was elevated in patients with hypertrophic cardiomyopathy regardless of the presence or absence of LGE, but T1 values in segments with LGE were significantly higher than those measured in segments without LGE [20]. In one of the studies, patients were 10 years older than the controls, which potentially contributed to this difference [21]. In our study, both groups had a similar mean age.

Native T1 time can be prolonged in many other myocardial pathologies (acute coronary syndromes, myocardial infarction, myocarditis, amyloidosis) and other diseases (increased intracellular water volume in diabetic adults with normal ECV values) [24]. Therefore, specific T1 time thresholds for the detection of pathologies within the myocardium will be able to improve differential diagnosis in the future [22]. These factors, recognized at the molecular level, may have contributed to the differences in T1 native time in previous studies between the HCM and control groups.

In one of the previous studies, T1 time was calculated by one-point sampling mid-cavity segments of the interventricular septum, while whole-heart T1 mapping should be recommended for the accurate assessment of myocardial T1 abnormality in patients with HCM. The single-slice approach might miss a substantial number of segments with

elevated native T1 time in patients with HCM. Further multicenter studies are needed to determine the importance of native T1 mapping in HCM patients [21].

Concluding from the T1 native time and other parameters compared in both groups in this study (no changes in left ventricular ejection fraction or left atrial dimensions; no difference in left ventricular end-systolic and end-diastolic diameter; no focal injury in LGE; higher myocardial ECV values), myocardial fibrosis was present and diffuse but not advanced.

Patients with hypertrophic cardiomyopathy in our studied group had an early form of the disease and subtle changes in cardiac tissue (disseminated myocardial fibrosis), which could be detected due to increased ECV values assessed in the T1-mapping sequence.

In view of the eternal aspirations of medicine to detect lesions as early as possible, preferably with the help of non-invasive techniques, the T1-mapping sequence is future-proof, allowing us to provide a group of HCM patients with better risk stratification and care and finally improve their long-term prognosis. In the era of clinical trials of oral anti-fibrotic agents (e.g., pirfenidone), the prompt diagnosis of hypertrophic cardiomyopathy may contribute to receiving a life-extending therapy. Similarly, quick diagnosis of ATTR amyloidosis and the initiation of treatment with patisiran may be crucial for the prognosis of patients with this type of accumulative disease [25].

The main limitation of this study is the lack of a final confirmation of hypertrophic cardiomyopathy in the examined patients. Myocardial biopsy was not performed in the examined patients. The diagnosis was made based on the entire clinical picture and imaging tests considering other causes of the hypertrophic left ventricular morphotype in the differential diagnosis. All patients in whom amyloidosis, sarcoidosis, athlete's heart, hypertensive cardiomyopathy, aortic stenosis, third degree obesity, and systemic diseases were considered to be the probable cause of left ventricular hypertrophy were excluded from the study.

5. Conclusions

In patients with hypertrophic cardiomyopathy in whom no foci of injury in the left ventricular myocardium were detected in classic CMR sequences, higher ECV values of the left ventricular myocardium were observed.

Advanced left ventricular hypertrophy in patients with hypertrophic cardiomyopathy without myocardium focal injury in the LGE sequence increases the ECV value.

Author Contributions: Conceptualization, P.G.; Funding acquisition, P.G.; Investigation, N.Z. and P.G.; Methodology, P.G.; Resources, N.Z.; Software, P.G.; Supervision, R.P. and P.G.; Writing—original draft, N.Z.; Writing—review & editing, R.P. and P.G. All authors have read and agreed to the published version of the manuscript.

Funding: Wroclaw Medical University, SUBZ.E264.24.033.

Institutional Review Board Statement: The study was conducted according to the guidelines of the Declaration of Helsinki and approved by the Ethics Committee of Wroclaw Medical University (protocol code KB-414/2021, date of approval 20 April 2021).

Informed Consent Statement: Informed consent was obtained from all subjects involved in the study.

Data Availability Statement: The data presented in this study are available on request from the corresponding author.

Conflicts of Interest: The authors declare that there are no conflicts of interest regarding the publication of this paper. Preliminary research results were presented at the EuroCMR 2021—18th Annual Meeting on CMR of the EACVI, Online congress 6–8 May 2021. The abstract was published in the conference materials [26]: Gać Paweł et al. "T1-Mapping and Extracellular Volume in Patients with Hypertrophic Cardiomyopathy without Focal Myocardial Injury in Late Gadolinium Enhancement Sequence". *European Heart Journal-Cardiovascular Imaging*, 22, suppl. 2, 2021, s. ii167, https://doi.org/10.1093/ehjci/jeab090.115.

References

1. Hindieh, W.; Chan, R.; Rakowski, H. Complementary Role of Echocardiography and Cardiac Magnetic Resonance in Hypertrophic Cardiomyopathy. *Curr. Cardiol. Rep.* **2017**, *19*, 81. [CrossRef] [PubMed]
2. Ellims, A.H.; Iles, L.M.; Ling, L.-H.; Hare, J.L.; Kaye, D.M.; Taylor, A.J. Diffuse myocardial fibrosis in hypertrophic cardiomyopathy can be identified by cardiovascular magnetic resonance, and is associated with left ventricular diastolic dysfunction. *J. Cardiovasc. Magn. Reson.* **2012**, *14*, 70–76. [CrossRef] [PubMed] [PubMed Central]
3. Marian, A.J.; Braunwald, E. Hypertrophic Cardiomyopathy: Genetics, Pathogenesis, Clinical Manifestations, Diagnosis, and Therapy. *Circ. Res.* **2017**, *121*, 749–770. [CrossRef] [PubMed] [PubMed Central]
4. Maron, B.J. Clinical Course and Management of Hypertrophic Cardiomyopathy. *N. Engl. J. Med.* **2018**, *379*, 655–668. [CrossRef] [PubMed]
5. van Driel, B.; Nijenkamp, L.; Huurman, R.; Michels, M.; van der Velden, J. Sex differences in hypertrophic cardiomyopathy: New insights. *Curr. Opin. Cardiol.* **2019**, *34*, 254–259. [CrossRef] [PubMed]
6. Kim, R.J.; Judd, R.M. Gadolinium-enhanced magnetic resonance imaging in hypertrophic cardiomyopathy: In vivo imaging of the pathologic substrate for premature cardiac death? *J. Am. Coll. Cardiol.* **2003**, *41*, 1568–1572. [CrossRef] [PubMed]
7. Xu, J.; Zhuang, B.; Sirajuddin, A.; Li, S.; Huang, J.; Yin, G.; Song, L.; Jiang, Y.; Zhao, S.; Lu, M. MRI T1 Mapping in Hypertrophic Cardiomyopathy: Evaluation in Patients without Late Gadolinium Enhancement and Hemodynamic Obstruction. *Radiology* **2020**, *294*, 275–286. [CrossRef] [PubMed]
8. Bull, S.; White, S.K.; Piechnik, S.K.; Flett, A.S.; Ferreira, V.M.; Loudon, M.; Francis, J.M.; Karamitsos, T.D.; Prendergast, B.D.; Robson, M.D.; et al. Human non-contrast T1 values and correlation with histology in diffuse fibrosis. *Heart* **2013**, *99*, 932–937. [CrossRef] [PubMed] [PubMed Central]
9. Haaf, P.; Garg, P.; Messroghli, D.R.; Broadbent, D.A.; Greenwood, J.P.; Plein, S. Cardiac T1 Mapping and Extracellular Volume (ECV) in clinical practice: A comprehensive review. *J. Cardiovasc. Magn. Reson.* **2016**, *18*, 89. [CrossRef] [PubMed] [PubMed Central]
10. Fries, R.C.; Kadotani, S.; Keating, S.C.J.; Stack, J.P. Cardiac extracellular volume fraction in cats with preclinical hypertrophic cardiomyopathy. *J. Vet. Intern. Med.* **2021**, *35*, 812–822. [CrossRef] [PubMed] [PubMed Central]
11. van Ooij, P.; Allen, B.D.; Contaldi, C.; Garcia, J.; Collins, J.; Carr, J.; Choudhury, L.; Bonow, R.O.; Barker, A.J.; Markl, M. 4D flow MRI and T1 -Mapping: Assessment of altered cardiac hemodynamics and extracellular volume fraction in hypertrophic cardiomyopathy. *J. Magn. Reson. Imaging* **2016**, *43*, 107–114. [CrossRef] [PubMed] [PubMed Central]
12. Hamdy, A.; Kitagawa, K.; Ishida, M.; Sakuma, H. Native Myocardial T1 Mapping, Are We There Yet? *Int. Heart J.* **2016**, *57*, 400–407. [CrossRef] [PubMed]
13. Baggiano, A.; Del Torto, A.; Guglielmo, M.; Muscogiuri, G.; Fusini, L.; Babbaro, M.; Collevecchio, A.; Mollace, R.; Scafuri, S.; Mushtaq, S.; et al. Role of CMR Mapping Techniques in Cardiac Hypertrophic Phenotype. *Diagnostics* **2020**, *10*, 770. [CrossRef] [PubMed]
14. Tański, W.; Gać, P.; Chachaj, A.; Sobieszczańska, M.; Poręba, R.; Szuba, A. Selected clinical parameters and changes in cardiac morphology and function assessed by magnetic resonance imaging in patients with rheumatoid arthritis and ankylosing spondylitis without clinically apparent heart disease. *Clin. Rheumatol.* **2021**, *40*, 4701–4711. [CrossRef] [PubMed]
15. Semsarian, C.; French, J.; Trent, R.J.; Richmond, D.R.; Jeremy, R.W. The natural history of left ventricular wall thickening in hypertrophic cardiomyopathy. *Aust. N. Z. J. Med.* **1997**, *27*, 51–58. [CrossRef] [PubMed]
16. Olivotto, I.; Maron, M.S.; Autore, C.; Lesser, J.R.; Rega, L.; Casolo, G.; De Santis, M.; Quarta, G.; Nistri, S.; Cecchi, F.; et al. Assessment and significance of left ventricular mass by cardiovascular magnetic resonance in hypertrophic cardiomyopathy. *J. Am. Coll. Cardiol.* **2008**, *52*, 559–566. [CrossRef] [PubMed]
17. Dohy, Z.; Szabo, L.; Toth, A.; Czimbalmos, C.; Horvath, R.; Horvath, V.; Suhai, F.I.; Geller, L.; Merkely, B.; Vago, H. Prognostic significance of cardiac magnetic resonance-based markers in patients with hypertrophic cardiomyopathy. *Int. J. Cardiovasc. Imaging* **2021**, *37*, 2027–2036. [CrossRef] [PubMed] [PubMed Central]
18. Maanja, M.; Wieslander, B.; Schlegel, T.T.; Bacharova, L.; Abu Daya, H.; Fridman, Y.; Wong, T.C.; Schelbert, E.B.; Ugander, M. Diffuse Myocardial Fibrosis Reduces Electrocardiographic Voltage Measures of Left Ventricular Hypertrophy Independent of Left Ventricular Mass. *J. Am. Heart Assoc.* **2017**, *6*, e003795. [CrossRef] [PubMed] [PubMed Central]
19. Marstrand, P.; Han, L.; Day, S.M.; Olivotto, I.; Ashley, E.A.; Michels, M.; Pereira, A.C.; Wittekind, S.G.; Helms, A.; Saberi, S.; et al. Hypertrophic Cardiomyopathy with Left Ventricular Systolic Dysfunction: Insights from the SHaRe Registry. *Circulation* **2020**, *141*, 1371–1383. [CrossRef] [PubMed]
20. Limongelli, G.; Fioretti, V.; Di Maio, M.; Verrengia, M.; Rubino, M.; Gravino, R.; Masarone, D.; D'Andrea, A.; Ciampi, Q.; Picano, E.; et al. Left Atrial Volume during Stress Is Associated with Increased Risk of Arrhythmias in Patients with Hypertrophic Cardiomyopathy. *J. Cardiovasc. Echography* **2019**, *29*, 1–6. [CrossRef] [PubMed] [PubMed Central]
21. Kato, S.; Nakamori, S.; Bellm, S.; Jang, J.; Basha, T.; Maron, M.; Manning, W.J.; Nezafat, R. Myocardial Native T1 Time in Patients with Hypertrophic Cardiomyopathy. *Am. J. Cardiol.* **2016**, *118*, 1057–1062. [CrossRef] [PubMed]
22. Małek, Ł.A.; Werys, K.; Kłopotowski, M.; Śpiewak, M.; Miłosz-Wieczorek, B.; Mazurkiewicz, Ł.; Petryka-Mazurkiewicz, J.; Marczak, M.; Witkowski, A. Native T1-mapping for non-contrast assessment of myocardial fibrosis in patients with hypertrophic cardiomyopathy--comparison with late enhancement quantification. *Magn. Reson. Imaging* **2015**, *33*, 718–724. [CrossRef] [PubMed]

23. Shang, Y.; Zhang, X.; Zhou, X.; Wang, J. Extracellular volume fraction measurements derived from the longitudinal relaxation of blood-based synthetic hematocrit may lead to clinical errors in 3 T cardiovascular magnetic resonance. *J. Cardiovasc. Magn. Reson.* **2018**, *20*, 56. [CrossRef] [PubMed] [PubMed Central]
24. Lam, B.; Stromp, T.A.; Hui, Z.; Vandsburger, M. Myocardial native-T1 times are elevated as a function of hypertrophy, HbA1c, and heart rate in diabetic adults without diffuse fibrosis. *Magn. Reson. Imaging* **2019**, *61*, 83–89. [CrossRef] [PubMed] [PubMed Central]
25. Di Stefano, V.; Fava, A.; Gentile, L.; Guaraldi, P.; Leonardi, L.; Poli, L.; Tagliapietra, M.; Vastola, M.; Fanara, S.; Ferrero, B.; et al. Italian Real-Life Experience of Patients with Hereditary Transthyretin Amyloidosis Treated with Patisiran. *Pharmgenom. Pers. Med.* **2022**, *15*, 499–514. [CrossRef] [PubMed]
26. Gac, P.; Kedzierski, B.; Truszkiewicz, K.; Poreba, R. T1-mapping and extracellular volume in patients with hypertrophic cardiomyopathy without focal myocardial injury in late gadolinium enhancement sequence. *Eur. Heart J. Cardiovasc. Imaging* **2021**, *22* (Suppl. S2), jeab090.115. [CrossRef]

Disclaimer/Publisher's Note: The statements, opinions and data contained in all publications are solely those of the individual author(s) and contributor(s) and not of MDPI and/or the editor(s). MDPI and/or the editor(s) disclaim responsibility for any injury to people or property resulting from any ideas, methods, instructions or products referred to in the content.

biomedicines

Article

The Randomized, Multicenter, Open-Label, Controlled POLBOS 3 Trial Comparing Regular Drug-Eluting Stents and the Sirolimus-Eluting BiOSS LIM C Dedicated Coronary Bifurcation Stent: Four-Year Results

Robert J. Gil [1], Adam Kern [2], Krystian Bojko [2], Aneta Gziut-Rudkowska [1], Dobrin Vassilev [3] and Jacek Bil [4,*]

[1] Department of Cardiology, State Medical Institute of the Ministry of Interior and Administration, 02-507 Warsaw, Poland; robert.gil@cskmswia.gov.pl (R.J.G.); aneta.gziut@cskmswia.gov.pl (A.G.-R.)
[2] Department of Cardiology and Internal Medicine, School of Medicine, Collegium Medicum, University of Warmia and Mazury, 10-719 Olsztyn, Poland; adam.kern@uwm.edu.pl (A.K.); krystian.bojko@uwm.edu.pl (K.B.)
[3] Medica Cor University Hospital, University of Ruse, 7017 Ruse, Bulgaria; dobrinv@gmail.com
[4] Department of Invasive Cardiology, Centre of Postgraduate Medical Education, 01-826 Warsaw, Poland
* Correspondence: jacek.bil@cmkp.edu.pl; Tel.: +48-47-722-11-00

Abstract: This multicenter, randomized study aimed to compare the sirolimus-eluting BiOSS LIM C dedicated coronary bifurcation stent with second-generation -limus drug-eluting stents (rDESs) in the treatment of non-left main (non-LM) coronary bifurcation. The deployment of a single stent in the main vessel–main branch across a side branch was the default strategy in all patients. The primary endpoint was the rate of major cardiovascular events (cardiac death, myocardial infarction, and target lesion revascularization) at 48 months. We enrolled 230 patients, allocating 116 patients to the BiOSS LIM C group and 114 patients to the rDES group. Most procedures were elective (BiOSS vs. rDES: 48.3% vs. 59.6%, $p = 0.09$) and performed in bifurcations within the left anterior descending/diagonal branch (BiOSS vs. rDES: 51.7% vs. 61.4%, $p = 0.15$). At 48 months, there were no statistically significant differences between the BiOSS and rDES groups in terms of major adverse cardiovascular events (MACE), cardiac death, myocardial infarction (MI), or target lesion revascularization (TLR) as follows: MACEs—18.1% vs. 14.9%, HR 1.36, 95% CI 0.62–2.22, and $p = 0.33$; cardiac death—4.3% vs. 3.5%, HR 1.23, 95% CI 0.33–4.56, and $p = 0.75$; MI—2.6% vs. 3.5%, HR 0.73, 95% CI 0.17–3.23, and $p = 0.68$; and TLR—11.2% vs. 7.9%, HR 1.66, 95% CI 0.75–3.71, and $p = 0.21$. The implantation success rate of the BiOSS LIM C stent was very high, and the cumulative MACE rates were promising. The POLBOS 3 trial sets an important benchmark for treating non-LM coronary bifurcations (ClinicalTrials.gov NCT03548272).

Keywords: non-LM bifurcation; percutaneous coronary intervention; high-risk PCI; long-term data

1. Introduction

Advancements in various technologies employed in percutaneous coronary intervention (PCI) have prompted greater efforts to address increasingly complex coronary lesions, encompassing even intricate coronary bifurcations. Among the most demanding types of complex lesions, coronary bifurcations present significant challenges. It is noted that complex lesions, including bifurcations, are linked to poorer immediate and long-term results compared to simpler lesions [1–3].

The heightened risk associated with coronary bifurcation lesions has sparked ongoing discussion regarding their management; when is it imperative to address the side branch (SB) alongside the main vessel (MV)? Two approaches are prominent: the provisional stent placement strategy, in which the focus is on treating the MV initially and intervening in the SB only if it faces imminent closure or closure occurs, and the dedicated two-stent strategy

which, conversely, entails planning for the simultaneous treatment of both the MV and SB from the very beginning [4–6].

All things considered, there still might be a place for dedicated bifurcation stents. One such stent is the BiOSS (Bifurcation Optimization Stent System, Balton, Poland), which has been investigated for over 15 years. The initial BiOSS stent was bare metal (stainless steel), but it was soon followed by the introduction of a paclitaxel-eluting variant known as the BiOSS Expert stent (CE Mark 2010). Subsequently, in 2012, the sirolimus-eluting BiOSS LIM stent was developed. Results obtained from registries, clinical randomized trials such as POLBOS 1 and POLBOS 2, as well as everyday clinical practice were deemed satisfactory. However, room for improvement remained [7–9]. Relatively large neointimal growths associated with thick struts (120 μm) were a reason to design a cobalt–chromium sirolimus-eluting version—the BiOSS LIM C stent [10].

After both successful preclinical testing and a first-in-human study of the BiOSS LIM C stent, a randomized study (POLBOS 3) was designed [11–13].

This study aimed to compare the BiOSS LIM C with - second-generation -limus drug-eluting stents (regular DESs and rDESs) in the treatment of non-left main (non-LM) coronary bifurcation. This study was designed to include five hundred eighteen patients with symptomatic stable coronary artery disease or NSTE-ACS who qualified for PCI in non-LM coronary bifurcation [14]. However, due to the outbreak of the COVID-19 pandemic and an extremely low enrolment rate, the decision was made to stop the study at 230 patients. Here, we present our 4-year clinical results.

2. Materials and Methods

2.1. Device

The BiOSS LIM C stent is a dedicated bifurcation stent crafted from a cobalt–chromium alloy with a strut thickness of 70 μm. It releases sirolimus (1.3 μg/mm^2) from a biodegradable coating in a process lasting around 8 weeks. This stent comprises two distinct parts with varying diameters; it is wider proximally and smaller distally. The proximal segment is always shorter than the distal one (45% vs. 55%, respectively). The ratio of the diameters of the proximal part (ranging from 3.0 to 5.0 mm) and the distal part (ranging from 2.5 to 4.0 mm) varies between 1.15 and 1.3, ensuring physiological compatibility and optimal flow dynamics. A middle zone of 2.0 to 2.4 mm accommodates two connecting struts to facilitate an opening for the SB. BiOSS stents are available in three lengths: 16, 19, and 24 mm (Figure 1) [11].

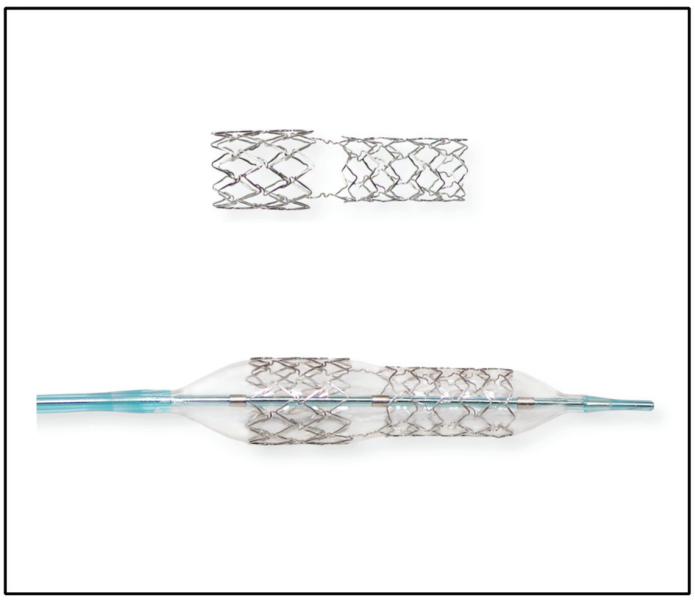


Figure 1. BiOSS LIM C structure.

2.2. Study Population and Study Design

This was a multicenter (two centers in Poland) randomized, controlled study that enrolled patients between 2018 and 2020. Patients were enrolled if an informed consent form was signed and all inclusion criteria and no exclusion criteria were met. The inclusion and exclusion criteria are provided in Table 1 [14].

Table 1. Inclusion and exclusion criteria.

Inclusion Criteria	Exclusion Criteria
1. The subject is at least 18 years of age. 2. The subject is able to verbally confirm their understanding of the risks and benefits of receiving PCI for bifurcation lesions, and they or their legally authorized representative provide written informed consent prior to any study-related procedure. 3. The target main branch lesion(s) is located in a native coronary artery and has a diameter measuring $\geq$2.5 mm and $\leq$4.5 mm. The target side branch lesion(s) located in a native coronary artery with a diameter of $\geq$2.0 mm. 4. The target lesion(s) is amenable for PCI with balloon angioplasty of the side branch.	1. Non-cardiac comorbidities are present with a life expectancy < 1 year or may result in protocol non-compliance (per the site investigator's medical judgment). 2. Subjects who refuse to give informed consent. 3. Subjects with an LVEF < 30%. 4. Subjects with a moderate or severe degree of valvular heart disease or primary cardiomyopathy. 5. Patients with distal left main stenosis. 6. Bifurcation lesions requiring the two-stent technique a priori.

PCI—percutaneous coronary intervention; LVEF—left ventricular ejection fraction.

Patients were randomized 1:1 to a BiOSS LIM C stent group versus a regular DES (rDES) group. The following rDESs were used: Xience (Abbott Laboratories, Warsaw, Poland), Resolute Onyx (Medtronic Poland, Warsaw, Poland), Orsiro (Biotronik Polska, Poznan, Poland), Synergy (Boston Scientific Polska, Warsaw, Poland), and Promus Elite (Boston Scientific). This study's protocol was compliant with SPIRIT guidelines [15]. An independent Ethics Committee approved the study protocol (No. 14/2018) (ClinicalTrials.gov NCT03548272).

2.3. Study Methodology

The study procedure was described in detail earlier [14]. In short, single-stent deployment in the MV-MB across the SB was the default strategy (provisional T-stenting, PTS) in all patients. We defined the MB as the part of the MV below the emergence of the SB. Bifurcation lesions were assessed according to the Medina classification, using an index of 1 for stenosis greater than 50% and 0 for no stenosis (as per a visual estimation) [16]. There was no restriction regarding lesion length in patient selection. If required, an additional stent could be implanted. A stent in an SB was allowed only if there was proximal residual stenosis greater than 70% after balloon dilatation and/or significant flow impairment after MV—MV stenting and/or a flow-limiting dissection.

The implantation protocol for bifurcation was as follows:

1. Wiring the MB and SB;
2. MV-MB predilatation according to the operator's decision (with a balloon–MB diameter ratio close to 1:1);
3. SB predilatation according to the operator's decision (only with a small balloon);
4. Stent implantation (with inflation for at least 20 s);
5. Use of the proximal optimization technique (POT);
6. SB postdilatation or SB stent implantation if required;
7. A final kissing balloon inflation at the operator's discretion (mandatory only if the two-stent technique was applied);
8. A final use of the proximal optimization technique (re-POT).

For patients diagnosed with acute coronary syndrome (ACS), a loading dose of ticagrelor (180 mg) or clopidogrel (600 mg) was administered, with the option of an loading dose of additional acetylsalicylic acid (ASA) if necessary (300 mg). Prior to the planned

procedures, all patients received ASA (75 mg/24 h) and clopidogrel (75 mg/24 h) starting seventy-two hours before percutaneous coronary intervention (PCI). PCI procedures were conducted using standard protocols via either radial or femoral access, utilizing 6 or 7 Fr guiding catheters. Following arterial sheath insertion, each patient received unfractionated heparin (100 IU/kg), with additional boluses administered to maintain an activated clotting time > 250 s. Dual antiplatelet therapy (75 mg q.d. ASA and 75 mg q.d. of clopidogrel or 90 mg b.i.d. of ticagrelor) was prescribed for 12 months.

Patients underwent evaluations of their troponin I (TnI), creatine kinase (CK), and CK-MB levels before the procedure and at 6 and 24 h post procedure. An assessment of periprocedural myocardial infarction (type 4a) was conducted following the criteria outlined in the fourth universal definition, with patients diagnosed with non-ST-segment-elevation myocardial infarction (NSTEMI) excluded from this evaluation [17].

2.4. Follow-Up

Follow-up visits were performed at 30 days, 6 months, 12 months, 24 months, 36 months, and 48 months. At the clinical follow-up visit, clinical status (including angina symptoms according to the Canadian Cardiovascular Society classification), adverse events according to the protocol, hospitalization, and medication intake were evaluated.

2.5. Endpoints

The primary endpoint was the rate of major cardiovascular events (cardiac death, myocardial infarction, and target lesion revascularization) at 48 months. The secondary endpoints were as follows: all-cause death; cardiovascular death—all deaths considered cardiovascular death if not proved otherwise; myocardial infarction; target lesion revascularization; and stent thrombosis at 12 and 48 months.

An independent Clinical Event Committee was created by three cardiologists who were otherwise not involved in the study. Each clinical event was adjudicated independently and blindly by two members of the Committee. In case of a disagreement, the third member was involved, and a joint agreement was reached.

2.6. Statistics

The original sample size calculation was as follows: assuming a noninferiority margin (delta) of 8%, a total sample size of 518 patients (with a drop-out rate of 5%), 259 patients per group, were calculated to be necessary (type I error: 0.05; type II error: 0.2; statistical power: 80%).

Descriptive statistics are shown as mean values with standard deviation values, minimum values, median values with an interquartile range, and maximum values for continuous variables; categorical variables are presented as counts and percentages. Pearson's Chi-squared test or Fisher's exact test were used to compare categorical variables between the 2 subgroups (BiOSS and rDES patients). We applied Fisher's exact test if at least one of the subgroups had a count = 0. Wilcoxon's rank-sum test was performed to compare continuous variables between the 2 subgroups (BiOSS and rDES patients). A p-value < 0.05 was judged statistically significant.

Kaplan–Meier estimators with 95% confidence intervals (CIs) were used to compare 48-month survival curves for various endpoints between the 2 subgroups (BiOSS and rDES patients). If a particular endpoint occurred for a given patient more than once in a 48-month follow-up period, then survival time was treated as the time until the first occurrence of this event. Notably, when considering MACEs (which represent a composite endpoint), the survival time was defined as the period leading up to the occurrence of the first event among the following: all-cause death, cardiac death, MI, or TLR.

Univariable and multivariable Cox regression analyses (utilizing the Cox proportional hazards model) were conducted to assess differences in survival rates among the groups. The multivariable Cox regression model was selected through stepwise selection, employing a backward elimination algorithm with a significance threshold set at 0.1. The outcomes,

including the hazard ratio (HR) and the corresponding 95% confidence intervals for the HR, were subsequently reported.

Statistical analyses were performed using GraphPad Prism 10 for mac OS software (Sonoma 14.4.1).

3. Results

3.1. Baseline Vharacteristics

Out of 297 screened patients, we enrolled 230 patients, sorting 116 patients into the BiOSS LIM C group and 114 patients into the rDES group (Figure 2). The mean ages of the patients in the BiOSS and rDES groups were 62.7 ± 10.6 and 65.8 ± 8.4 years old (p = 0.01), respectively. Patients in the rDES group had higher rates of prior MI (47.4% vs. 31.9%, p = 0.02) and prior CABG (10.5% vs. 2.6%, p = 0.02). Most procedures were performed as elective PCIs (BiOSS vs. rDES: 48.3% vs. 59.6%, p = 0.09) and were performed in bifurcations within the LAD/diagonal branch (BiOSS vs. rDES: 51.7% vs. 61.4%, p = 0.15). Numerically, true bifurcations were more frequent in the BiOSS group (66.4% vs. 56.1%, p = 0.13) (Table 2).

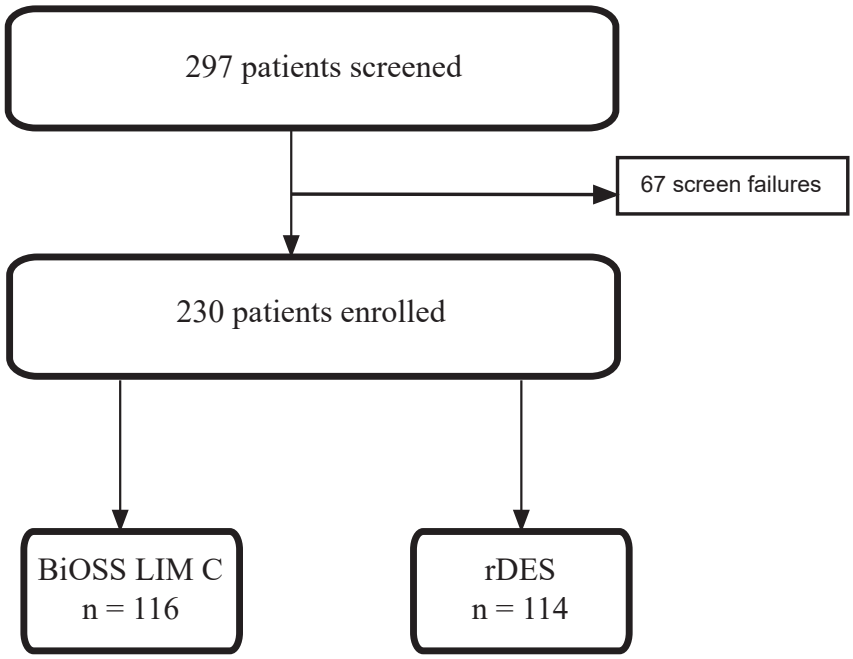


Figure 2. Study flow chart. rDES—regular drug-eluting stent.

Table 2. Baseline characteristics.

Parameter	Total Population N = 230 (%)	BiOSS Group n = 116 (%)	rDES Group n = 114 (%)
Age [years]	64.3 ± 9.6	62.7 ± 10.6	65.8 ± 8.4 *
Women	45 (19.6)	22 (19)	23 (20.2)
Hypertension	183 (79.6)	97 (83.6)	86 (75.4)
Hypercholesterolemia	230 (100)	116 (100)	114 (100)
Diabetes type 2	80 (34.8)	38 (32.8)	42 (36.8)
Prior myocardial infarction	91 (39.6)	37 (31.9)	54 (47.4) *
Prior PCI	114 (49.6)	50 (43.1)	64 (56.1)

Table 2. *Cont.*

Parameter		Total Population N = 230 (%)	BiOSS Group n = 116 (%)	rDES Group n = 114 (%)
Coronary artery bypass grafting		15 (6.5)	3 (2.6)	12 (10.5) *
Peripheral artery disease		15 (6.5)	5 (4.3)	10 (8.8)
Chronic kidney disease		28 (12.2)	10 (8.6)	18 (15.8)
History of smoking		79 (34.3)	35 (30.2)	44 (38.6)
Clinical indication for PCI				
	Planned PCI	124 (53.9)	56 (48.3)	68 (59.6)
	Unstable angina	34 (14.8)	22 (19)	12 (10.5)
	NSTEMI	41 (17.8)	29 (25)	12 (10.5)
	STEMI	31 (13.5)	9 (7.8)	22 (19.4)
Lesion location				
	LAD	130 (56.5)	60 (51.7)	70 (61.4)
	LCx	58 (25.2)	22 (18.9)	36 (31.6)
	RCA	42 (18.3)	34 (29.3)	8 (7.0)
SYNTAX score		22.8 ± 3.7	23.1 ± 3.9	22.5 ± 4.1
Medina classification				
	1.1.1.	131 (56.9)	73 (62.9)	58 (50.9)
	1.0.1.	6 (2.6)	4 (3.4)	2 (1.8)
	0.1.1.	4 (1.7)	0	4 (3.5)
	1.0.0.	12 (5.2)	0	12 (10.5)
	0.1.0.	6 (2.6)	6 (5.2)	0
	1.1.0.	71 (30.9)	33 (28.4)	38 (33.3)
True bifurcation	1.1.1./1.0.1./0.1.1.	141 (61.3)	77 (66.4)	64 (56.1)

* $p < 0.05$; LAD—left anterior descending artery; LCx—left circumflex artery; NSTEMI—non-ST-elevation myocardial infarction; PCI—percutaneous coronary intervention; RCA—right coronary artery; rDES—regular drug-eluting stent; STEMI—ST-elevation myocardial infarction.

3.2. Procedure Characteristics

The successful device implantation rate was 100% in both groups. MV predilating was performed in almost all cases (BiOSS vs. rDES: 98.3% vs. 94.7%, $p = 0.17$), and SB predilating was performed in less than 40% in both groups (BiOSS vs. rDES: 37.9% vs. 38.6%, $p = 0.99$). Stents in the BiOSS group had larger proximal diameters (3.36 ± 0.32 mm vs. 3.07 ± 0.40 mm, $p < 0.01$) and were shorter (19.5 ± 3.6 mm vs. 22.1 ± 6.3 mm, $p < 0.01$). The use of the proximal optimization technique was much lower in the BiOSS group (20.7% vs. 47.4%, $p < 0.01$). Stents implanted in SBs were comparable (BiOSS vs. rDES: 21.6% vs. 17.5%, $p = 0.62$) (Table 3).

Table 3. Procedural characteristics.

Parameter	Total Population N = 230 (%)	BiOSS Group n = 116 (%)	rDES Group n = 114 (%)
Successful implantation	230 (100)	116 (100)	114 (100)
Main vessel predilatation	222 (96.5)	114 (98.3)	108 (94.7)
Side branch predilatation	88 (38.3)	44 (37.9)	44 (38.6)
Predilation of both branches	34 (14.8)	8 (6.9)	26 (22.8) *

Table 3. *Cont.*

Parameter	Total Population N = 230 (%)	BiOSS Group n = 116 (%)	rDES Group n = 114 (%)
Nominal stent diameter in main vessel [mm]	3.22 ± 0.34	3.36 ± 0.32	3.07 ± 0.40 *
Nominal stent diameter in main branch [mm]	-	2.73 ± 0.31	-
Nominal stent length [mm]	20.8 ± 4.8	19.5 ± 3.6	22.1 ± 6.3 *
Side branch postdilatation	52 (22.6)	28 (24.1)	24 (21.1)
Proximal optimization technique	78 (33.9)	24 (20.7)	54 (47.4) *
Final kissing balloon technique	60 (26.1)	28 (24.1)	32 (28.1)
Stent in a side branch	45 (19.6)	25 (21.6)	20 (17.5)
Dissection requiring an additional stent in a main vessel—main branch	5 (2.2)	3 (2.6)	2 (1.8)
Fluoroscopy time [min]	12.8 ± 5.9	13.14 ± 5.6	12.5 ± 7.3
Contrast volume [mL]	196.8 ± 70.2	203.8 ± 78.7	189.6 ± 71.9
Vascular access femoral/radial	0/100%	0/100%	0/100%
Guiding catheter 6F/7F	100%/0	100%/0	100%/0

* $p < 0.05$; rDES—regular drug-eluting stent.

3.3. Clinical Outcomes

We obtained data from all patients in both groups. Detailed data on MACE, death, cardiac death, MI, and TLR rates are provided in Table 4 and Figure 3. At 48 months, there were no statistically significant differences between the BiOSS and rDES groups in terms of MACE, cardiac death, MI, or TLR. There were no stent thrombosis cases in any of the groups. In detail, the results were as follows for BiOSS vs. rDES: MACEs—18.1% vs. 14.9%, HR 1.36, 95% CI 0.62–2.22, and $p = 0.33$; cardiac death—4.3% vs. 3.5%, HR 1.23, 95% CI 0.33–4.56, and $p = 0.75$, MI (2.6% vs. 3.5%, HR 0.73, 95% CI 0.17–3.23, and $p = 0.68$; and TLR—11.2% vs. 7.9%, HR 1.66, 95% CI 0.75–3.71, and $p = 0.21$. All MACE cases were reported as serious adverse events.

Table 4. Forty-eight-month outcomes.

Outcome	1 Year	2 Years	3 Years	4 Years
		BiOSS LIM C		
MACE	10 (8.6)	14 (12.1)	18 (15.5)	21 (18.1)
Death	3 (2.6)	4 (3.4)	6 (5.2)	8 (6.7)
Cardiac death	2 (1.7)	3 (2.6)	4 (3.4)	5 (4.3)
MI	1 (0.9)	2 (1.7)	2 (1.7)	3 (2.6)
TLR	7 (6.0)	9 (7.8)	12 (10.3)	13 (11.2)
		rDES		
MACE	9 (7.9)	9 (7.9)	12 (10.5)	17 (14.9)
Death	4 (3.5)	4 (3.5)	5 (4.4)	6 (5.2)
Cardiac death	2 (1.8)	2 (1.8)	2 (1.8)	4 (3.5)
MI	2 (1.8)	2 (1.8)	3 (2.6)	4 (3.5)
TLR	5 (4.4)	5 (4.4)	7 (6.1)	9 (7.9)

rDES—regular drug-eluting stent; MACE—major adverse cardiovascular event; MI—myocardial infarction; TLR—target lesion revascularization.

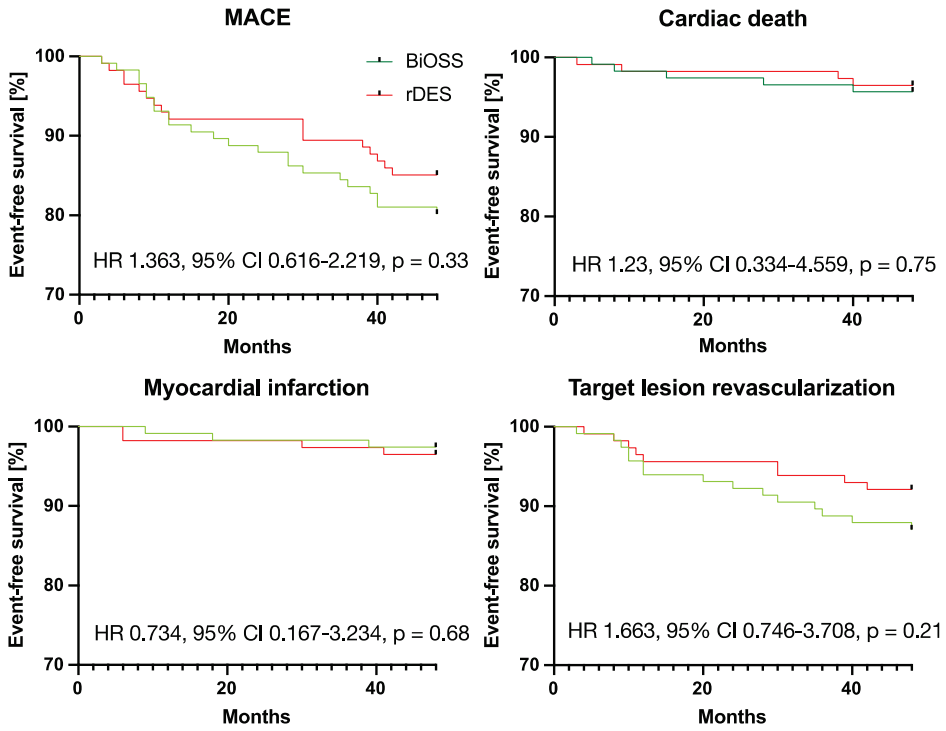


Figure 3. Kaplan–Meier curves showing 48-month outcomes. MACE—major adverse cardiovascular event.

3.4. Predictors of MACE and TLR

To identify the potential predictors of MACE and TLR in the study population, we initially performed a univariable analysis (Supplementary Tables S1 and S2); here, we present only multivariable analyses for MACE (Table 5) and TLR (Table 6) for the BiOSS and rDES subgroups.

Table 5. Multivariable logistic regression for MACE.

Parameter	Multivariable Analysis	
	HR (95% CI)	***p*-Value**
BIOSS		
Female vs. male	0.43 (0.29–0.88)	0.02
NSTEMI/UA	1.60 (1.13–3.99)	0.03
Prior myocardial infarction	2.21 (1.44–4.67)	0.02
True bifurcation	1.34 (1.09–3.03)	0.01
Main vessel predilatation	1.89 (1.56–4.04)	0.02
rDES		
Female vs. male	0.31 (0.19–0.44)	0.01
NSTEMI/UA	2.13 (1.44–3.09)	0.04
Prior myocardial infarction	2.53 (1.89–7.04)	0.02
True bifurcation	2.44 (1.09–5.90)	<0.01
Diabetes	1.98 (1.34–5.12)	0.02
Proximal optimization technique	0.23 (0.14–0.43)	<0.01

MACE—major cardiovascular adverse event; NSTEMI—non-ST-elevation myocardial infarction; UA—unstable angina; CI—confidence interval; HR—hazard ratio.

Table 6. Multivariable logistic regression for TLR.

Parameter	Multivariable Analysis	
	HR (95% CI)	***p*-Value**
BiOSS		
Prior myocardial infarction	3.78 (2.43–11.01)	<0.01
True bifurcation	1.23 (1.13–3.23)	0.01
Main vessel predilatation	1.09 (1.02–2.99)	0.04
rDES		
Prior myocardial infarction	4.22 (1.78–10.09)	<0.01
True bifurcation	2.87 (1.67–7.02)	<0.01
Diabetes	2.33 (1.56–5.33)	0.02
Proximal optimization technique	0.23 (0.05–0.49)	0.01

CI—confidence interval; HR—hazard ratio; TLR—target lesion revascularization.

In the case of the BiOSS group, the MACE rate was lower in women (HR 0.43). PCI in NSTEMI/UA (HR 1.60), PCI within true bifurcations (HR 1.34), MV predilatation (HR 1.89), and prior MI (HR 2.21) were predictors associated with higher MACE rates. In the rDES group, diabetes (HR 1.98) and the POT (HR 0.23) were identified as additional important predicting factors.

In the case of the BIOSS group, PCI within true bifurcations (HR 3.78), MV predilatation (HR 1.09), and true bifurcations (HR 1.23) were predictors associated with higher TLR rates. In the rDES group, diabetes (HR 2.33) and the POT (HR 0.23) were identified as additional important predicting factors.

4. Discussion

Here, we present the 4-year results of a randomized controlled study in which coronary bifurcations were treated. The success rate of the implantation of the BiOSS LIM C stent was very high. The cumulative rates of MACEs were comparable between the BiOSS LIM C and rDES groups. Therefore, the POLBOS 3 trial sets an important benchmark for treating non-LM coronary bifurcations. Nevertheless, because of an inadequate sample size (premature study termination), it was not possible to confirm or refute the non-inferiority of BiOSS to rDES stents.

Gasior et al. analyzed overexpansion capabilities and thrombogenicity at the SB ostium after stent implantation in an in vitro bifurcation model. The authors used four DES: BiOSS LIM C and three rDESs (Xience Sierra, Ultimaster, and Biomime) [12]. Interestingly, when conducting confocal microscopy, the thrombus area was the smallest in the BiOSS LIM C and statistically significant when compared with Biomime stents (Bioss LIM C vs. Biomime: 0.21 mm^2 vs. 4.80 mm^2, $p < 0.01$). Also, areas with a high shear rate (>1000 s^{-1}) and the maximum shear rate were numerically an in vivo study (pigs), in which BiOSS LIM C and Orsiro stents yielded similar results [11]. After 28 days, optical coherence tomography (OCT) verified the patency of all stents without any evidence of thrombus formation. A morphometric analysis revealed no discernible variances between the groups in terms of stent diameter ($p = 0.141$), neointima area ($p = 0.247$), percentage of area stenosis ($p = 0.293$), or percentage of diameter stenosis ($p = 0.069$). Additionally, no notable variations were observed between the groups in terms of their histopathology scores. Across all groups, injury and inflammation scores remained low (mean grade < 1).

In comparison with previous studies on the BiOSS stent (POLBOS 1 and POLBOS 2), the results were better. In the current study, the results were as follows for BiOSS vs. the rDESs: MACEs (18.1% vs. 14.9%, $p = 0.33$), cardiac death (4.3% vs. 3.5%, $p = 0.75$), MI (2.6% vs. 3.5%, $p = 0.68$), and TLR (11.2% vs. 7.9%, $p = 0.21$). The 4-year clinical outcomes following POLBOS 1 and POLBOS 2 were a bit worse. At 48 months, the MACE rate was

19.8% in the BiOSS group and 18.8% in the rDES group (p = 0.64), whereas the TLR rates were 15.3% and 12.1%, respectively (p = 0.34) [18].

The results of POLBOS 3 are quite comparable to those observed in the first-in-human study with the BiOSS LIM C [13]. Similarly, the device success rate was 100%. However, the rDES was deployed in the SB at a lower incidence. At 12 months, the MACE rate was 9.5% (our current study: 8.6%), and clinically driven TLR was 6.3% (our current study: 6.0%). It is worth stressing that in the current study, the rate of POT was lower (20.7% vs. 53.7%). This is against current recommendations; however, it might be associated with the BiOSS structure [4,19]. Also, POT rates below 40% can be observed in other studies [20–24].

In the EPIC3-BIOSS prospective study, 124 patients in whom the BiOSS LIM C stent was deployed were enrolled [25]. The stent was successfully deployed in 97.6% of patients, and in 14.5% of cases, a double-stenting technique was used. True bifurcations were present in 47.2% of cases, and the POT was performed in 26.6% of cases. At 12 months, the MI rate was 2.72%, the TLR rate was 5.4%, and the stent thrombosis rate was 0.9%. The rates were comparable to those in our study, and in our study, we included more true bifurcation cases.

A new registry with BiOSS LIM C was recently published—IBIOSS [26]. Interestingly, only patients with true bifurcations were included. Although 207 patients were enrolled, 1.1.1. bifurcations comprised only 30.9% (in our paper: 62.9%). The double-stenting technique was used in 9.3% of cases, and the POT was used in 11.7% of cases. At a mean follow-up of 24.1 $\pm$ 19.5 months, the MACE rate was 11.1% (in our study: 12.2%), the TLR rate was 2.9%, and the MI rate was 2.9%.

The data obtained in POLBOS 3 are similar to those observed in the literature. Among the entire cohort of patients in the LEADERS trial, those who underwent percutaneous coronary interventions for bifurcation lesions exhibited the following 5-year outcomes: a MACE rate of 35.3%, a cardiac death rate of 8.5%, an MI rate of 11.9%, and a TLR rate of 14.9% [27]. Furthermore, upon examining data from other dedicated bifurcation stents, the long-term data (over 3 years) of the Axxess stent revealed a MACE rate of 19.5%, a cardiac death rate of 2.0%, an MI rate of 7.4%, and a clinically driven TLR rate of 10.1% [28]. Findings from a separate cohort demonstrated even more favorable outcomes for the Axxess stent at 5 years [29]. At 2 years, the extended data for Tryton revealed a MACE rate of 23.8%, a cardiac death rate of 4.4%, an MI rate of 10.2%, and a TLR rate of 9.2% [30]. For Stentys, at 5 years, the incidence of target vessel failure was 22.8%, with a notably high rate of stent thrombosis at 4.5%. [31]. Also, Riku et al. recently showed that late TLR cases continued over 10 years at a rate of 2.4%/year in a complex PCI group and 1.1%/year in a noncomplex PCI group [32].

In our study, we identified the following factors predicting of MACEs and TLR. In the case of the BiOSS group, the MACE rate was lower in women (HR 0.43). PCIs in NSTEMI/UA (HR 1.60), PCIs within true bifurcations (HR 1.34), MV predilatation (HR 1.89), and prior MI (HR 2.21) were predictors associated with higher MACE rates. In the rDES group, diabetes (HR 1.98) and the use of the POT (HR 0.23) were identified as additional important predicting factors. In the case of the BIOSS group, PCIs within true bifurcations (HR 3.78), MV predilatation (HR 1.09), and true bifurcations (HR 1.23) were predictors associated with higher TLR rates. In the rDES group, diabetes (HR 2.33) and the POT (HR 0.23) were identified as additional important predicting factors. It is worth stressing that the POT was a predicting factor in the rDES group and not in the BiOSS group. This may be associated with the BiOSS stent's structure. They are in agreement with other studies. Within the Milan and New Tokyo (MITO) Registry, calcification, true bifurcation, and insulin-dependent diabetes were identified as independent predictors of in-stent restenosis within MB [33]. In another research study, the primary factors influencing MACE rates were identified as the utilization of a two-stent technique and the presence of diabetes [34]. Chen et al. similarly verified the correlation between two-stent deployment and increased MACE rates. The researchers proposed that among the various two-stent techniques, the double-kissing (DK) crush yielded the most advantageous results [35].

In the end, it is rightful to raise the issue of using provisional T-stenting vs. two-stent techniques. Fujisaki et al. conducted a meta-analysis comprising 13 randomized controlled trials (RCTs) that compared provisional with dedicated bifurcation stent placements employing various PCI techniques [36]. A notable aspect of their study is the incorporation of RCTs primarily or exclusively utilizing second-generation drug-eluting stents. Previous meta-analyses on bifurcation PCIs encompassed studies employing bare metal stents or first-generation drug-eluting stents which are now considered outdated. We concur that utilizing contemporary data is preferable for gaining insights into future approaches in this field. This meta-analysis reinforced several key findings. Firstly, advancements in newer-generation stents, alongside improved guidewires, support catheters, adjunctive therapies, and imaging modalities, have resulted in enhanced two-stent strategies for managing coronary bifurcation lesions [3]. Secondly, among complex lesion subsets, the DK crush technique emerges as superior to alternative approaches [6,37]. Lastly, while a dedicated two-stent strategy appears more effective than a provisional strategy in treating complex bifurcations, the superiority of a two-stent strategy in "noncomplex" bifurcations remains uncertain [38,39]. Also, smaller bifurcations (non-LM bifurcations), as our study shows, can be safely treated with a provisional stenting technique. Interestingly, Jones et al. showed promising results with provisional bifurcation stenting and sirolimus-eluting balloon use in the SB [40].

Study Limitations

The POLBOS 3 study has several limitations that should be acknowledged. First, the study was prematurely terminated, and the initial sample size calculations were not applicable. Using various stent types and drugs within the control group presents a limitation, although this approach aimed to mimic real-world clinical scenarios. The predetermined randomization scheme might have influenced investigators' decisions to enroll patients based on specific angiographic characteristics. Moreover, disparities in final kissing balloon/POT strategies between the two study groups (randomization in the rDES group versus operator discretion in the BiOSS group) could have impacted the outcomes as well.

5. Conclusions

The implantation success rate of the BiOSS LIM C stent was very high, and cumulative rates of MACEs were comparable between the BiOSS LIM C and rDES groups, although the study population was underpowered due to premature study termination. These results show the function of dedicated bifurcation stents, especially when a proper deployment protocol is applied.

Supplementary Materials: The following supporting information can be downloaded at https://www.mdpi.com/article/10.3390/biomedicines12050938/s1, Table S1: Univariable Cox regression for MACEs; Table S2: Univariable Cox regression for TLR.

Author Contributions: Conceptualization, R.J.G., D.V. and J.B.; methodology, R.J.G. and J.B.; investigation, A.K., K.B., A.G.-R., R.J.G. and J.B.; data curation, J.B. and R.J.G.; writing—original draft preparation, J.B.; writing—review and editing, A.K.; supervision, R.J.G. and D.V. All authors have read and agreed to the published version of the manuscript.

Funding: This research received no external funding.

Institutional Review Board Statement: This study was conducted in accordance with the Declaration of Helsinki and approved by the Independent Ethics Committee of the Central Clinical Hospital of the Ministry of Interior and Administration in Warsaw (No. 14/2018 of 14 April 2018).

Informed Consent Statement: Informed consent was obtained from all subjects involved in the study.

Data Availability Statement: Data are available from the corresponding author upon request.

Conflicts of Interest: The authors declare no conflicts of interest.

References

1. Mohamed, M.O.; Polad, J.; Hildick-Smith, D.; Bizeau, O.; Baisebenov, R.K.; Roffi, M.; Iniguez-Romo, A.; Chevalier, B.; von Birgelen, C.; Roguin, A.; et al. Impact of coronary lesion complexity in percutaneous coronary intervention: One-year outcomes from the large, multicentre e-Ultimaster registry. *EuroIntervention* **2020**, *16*, 603–612. [CrossRef] [PubMed]
2. Rus, M.; Filimon, G.C.; Ardelean, A.I. T and Small Protrusion (TAP) Technique in Bifurcations: Coronary Artery Disease in Acute Myocardial Infarction Patients after COVID-19 Pneumonia. *Biomedicines* **2023**, *11*, 2255. [CrossRef] [PubMed]
3. Lee, J.H.; Youn, Y.J.; Jeon, H.S.; Lee, J.W.; Ahn, S.G.; Yoon, J.; Gwon, H.C.; Song, Y.B.; Choi, K.H.; Kim, H.S.; et al. Transradial Versus Transfemoral Access for Bifurcation Percutaneous Coronary Intervention Using Second-Generation Drug-Eluting Stent. *J. Korean Med. Sci.* **2024**, *39*, e111. [CrossRef] [PubMed]
4. Lassen, J.F.; Albiero, R.; Johnson, T.W.; Burzotta, F.; Lefevre, T.; Iles, T.L.; Pan, M.; Banning, A.P.; Chatzizisis, Y.S.; Ferenc, M.; et al. Treatment of coronary bifurcation lesions, part II: Implanting two stents. The 16th expert consensus document of the European Bifurcation Club. *EuroIntervention* **2022**, *18*, 457–470. [CrossRef] [PubMed]
5. Albiero, R.; Burzotta, F.; Lassen, J.F.; Lefevre, T.; Banning, A.P.; Chatzizisis, Y.S.; Johnson, T.W.; Ferenc, M.; Pan, M.; Daremont, O.; et al. Treatment of coronary bifurcation lesions, part I: Implanting the first stent in the provisional pathway. The 16th expert consensus document of the European Bifurcation Club. *EuroIntervention* **2022**, *18*, e362–e376. [CrossRef] [PubMed]
6. Uzun, F.; Guner, A.; Demirci, G.; Ciloglu, K.; Uysal, H.; Cizgici, A.Y.; Bulut, U.; Kahraman, S.; Agus, H.Z.; Gokce, K.; et al. Comparison of long-term outcomes of double kissing crush versus T and minimal protrusion techniques in complex bifurcation lesions: The EVOLUTE-CRUSH II registry. *Catheter. Cardiovasc. Interv.* **2024**, *103*, 511–522. [CrossRef] [PubMed]
7. Gil, R.J.; Bil, J.; Grundeken, M.J.; Kern, A.; Inigo Garcia, L.A.; Vassilev, D.; Pawlowski, T.; Formuszewicz, R.; Dobrzycki, S.; Wykrzykowska, J.J.; et al. Regular drug-eluting stents versus the dedicated coronary bifurcation sirolimus-eluting BiOSS LIM(R) stent: The randomised, multicentre, open-label, controlled POLBOS II trial. *EuroIntervention* **2016**, *12*, e1404–e1412. [CrossRef] [PubMed]
8. Gil, R.J.; Bil, J.; Dzavik, V.; Vassilev, D.; Kern, A.; Formuszewicz, R.; Zalewska-Adamiec, M.; Dobrzycki, S. Regular Drug-Eluting Stent vs Dedicated Coronary Bifurcation BiOSS Expert Stent: Multicenter Open-Label Randomized Controlled POLBOS I Trial. *Can. J. Cardiol.* **2015**, *31*, 671–678. [CrossRef]
9. Gil, R.J.; Kern, A.; Formuszewicz, R.; Inigo Garcia, L.A.; Dobrzycki, S.; Vassilev, D.; Bil, J. 6-year results of BiOSS stents in coronary bifurcation treatment. *Eur. J. Clin. Investig.* **2021**, *51*, e13555. [CrossRef]
10. Kozlik, M.; Harpula, J.; Chuchra, P.J.; Nowak, M.; Wojakowski, W.; Gasior, P. Drug-Eluting Stents: Technical and Clinical Progress. *Biomimetics* **2023**, *8*, 72. [CrossRef]
11. Bil, J.; Gil, R.J.; Pawlowski, T.; Milewski, K.P. Assessment of vascular response to BiOSS LIM C((R)) stents vs Orsiro((R)) stents in the porcine coronary artery model. *Cardiovasc. Ther.* **2017**, *35*, e12267. [CrossRef]
12. Gasior, P.; Lu, S.; Ng, C.K.J.; Toong, W.Y.D.; Wong, E.H.P.; Foin, N.; Kedhi, E.; Wojakowski, W.; Ang, H.Y. Comparison of overexpansion capabilities and thrombogenicity at the side branch ostia after implantation of four different drug eluting stents. *Sci. Rep.* **2020**, *10*, 20791. [CrossRef]
13. Gil, R.J.; Kern, A.; Pawlowski, T.; Bil, J. Twelve-month clinical results from the new cobalt-chromium sirolimus-eluting dedicated bifurcation stent BiOSS LIM C Registry. *Arch. Med. Sci.* **2023**, *19*, 324–330. [CrossRef]
14. Gil, R.J.; Pawlowski, T.; Legutko, J.; Lesiak, M.; Witkowski, A.; Gasior, M.; Kern, A.; Bil, J. Rationale and design of the randomized, multicenter, open-label, controlled POLBOS 3 trial aimed to compare regular drug-eluting stents versus the dedicated coronary bifurcation sirolimus-eluting BiOSS LIM C stent. *Medicine* **2019**, *98*, e15106. [CrossRef] [PubMed]
15. Chan, A.W.; Tetzlaff, J.M.; Altman, D.G.; Laupacis, A.; Gotzsche, P.C.; Krleza-Jeric, K.; Hrobjartsson, A.; Mann, H.; Dickersin, K.; Berlin, J.A.; et al. SPIRIT 2013 statement: Defining standard protocol items for clinical trials. *Ann. Intern. Med.* **2013**, *158*, 200–207. [CrossRef]
16. Medina, A.; Suarez de Lezo, J.; Pan, M. A new classification of coronary bifurcation lesions. *Rev. Esp. Cardiol.* **2006**, *59*, 183. [CrossRef]
17. Thygesen, K.; Alpert, J.S.; Jaffe, A.S.; Chaitman, B.R.; Bax, J.J.; Morrow, D.A.; White, H.D.; The Executive Group on behalf of the Joint European Society of Cardiology (ESC)/American College of Cardiology (ACC)/American Heart Association (AHA)/World Heart Federation (WHF) Task Force for the Universal Definition of Myocardial Infarction. Fourth Universal Definition of Myocardial Infarction (2018). *Circulation* **2018**, *138*, e618–e651. [CrossRef] [PubMed]
18. Gil, R.J.; Bil, J.; Kern, A.; Ingio Garcia, L.A.; Formuszewicz, R.; Dobrzycki, S.; Vassilev, D.; Segiet, A. Regular drug-eluting stents versus dedicated bifurcation drug-eluting BiOSS stents for coronary bifurcation treatment: Four-year results of the randomised POLBOS I and POLBOS II clinical trials. *EuroIntervention* **2020**, *15*, 1460–1463. [CrossRef] [PubMed]
19. Pan, M.; Lassen, J.F.; Burzotta, F.; Ojeda, S.; Albiero, R.; Lefevre, T.; Hildick-Smith, D.; Johnson, T.W.; Chieffo, A.; Banning, A.P.; et al. The 17th expert consensus document of the European Bifurcation Club—Techniques to preserve access to the side branch during stepwise provisional stenting. *EuroIntervention* **2023**, *19*, 26–36. [CrossRef]
20. Doolub, G.; Iannaccone, M.; Rab, T.; Routledge, H.; Aminian, A.; Chevalier, B.; Hildick-Smith, D.; Jacobs, L.; Kobo, O.; Roguin, A.; et al. Sex-based treatment and outcomes for coronary bifurcation stenting: A report from the e-ULTIMASTER registry. *Catheter. Cardiovasc. Interv.* **2023**, *102*, 430–439. [CrossRef]

21. Giustino, G.; Sharma, S.K.; Kini, A. Systematic Proximal Optimization Technique During Bifurcation Stenting: Where Is the Evidence? *JACC Cardiovasc. Interv.* **2024**, *17*, 801–806. [CrossRef]
22. Derimay, F.; Aminian, A.; Lattuca, B.; Souteyrand, G.; Maillard, L.; Alvain, S.; Cayla, G.; Motreff, P.; Bochaton, T.; Hayek, A.; et al. One year results of coronary bifurcation revascularization with the re-POT provisional sequential technique. The CABRIOLET registry. *Int. J. Cardiol.* **2024**, *397*, 131632. [CrossRef]
23. Laraichi, Z.; Faraj, R.; Fellat, N. The POT-PUFF Sign: A New Angiographic Indicator of Stent Malapposition During Proximal Optimization Therapy. *Cureus* **2023**, *15*, e43552. [CrossRef] [PubMed]
24. Cetinkal, G.; Balaban Kocas, B.; Keskin, K.; Kilci, H.; Ser, O.S.; Kilickesmez, K. Comparison of Sequential POT-Side-POT and Kissing Balloon Techniquesin Patientswith Coronary Bifurcation Lesions Treatedwith Single-Stent Strategy; Which One is Simple and Safe? Propensity Score Analysis. *Anatol. J. Cardiol.* **2022**, *26*, 559–566. [CrossRef]
25. del Blanco, B.; Lara, J.; Rama Merchan, J.; Carballo Garrido, J.; Palazuelos Molinero, J.; Bullones Ramírez, J.; Sandoval, J.; Rumoroso Cuevas, J.; Calle Perez, G.; Nofrerías, E.; et al. EPIC03-BIOSS observational prospective study. Performance analysis of the BIOSS LIM C dedicated stent in coronary bifurcation lesion angioplasty. *REC Interv. Cardiol.* **2022**, *4*, 294–303. [CrossRef]
26. Briguori, C.; Capodanno, D.; Contarini, M.; Donahue, M.E.; Evola, S.; Garro, N.; Greco, F.; Murè, P.; Nicosia, A.; Migliore, G.; et al. Acute and long-term results of percutaneous coronary intervention of bifurcation lesions with the dedicated Bioss Lim C stent: The Italian BIfurcation Observational Spontaneous Study (IBIOSS). *Minerva Med.* **2024**. [CrossRef] [PubMed]
27. Grundeken, M.J.; Wykrzykowska, J.J.; Ishibashi, Y.; Garg, S.; de Vries, T.; Garcia-Garcia, H.M.; Onuma, Y.; de Winter, R.J.; Buszman, P.; Linke, A.; et al. First generation versus second generation drug-eluting stents for the treatment of bifurcations: 5-year follow-up of the LEADERS all-comers randomized trial. *Catheter. Cardiovasc. Interv.* **2016**, *87*, E248–E260. [CrossRef]
28. Buysschaert, I.; Dubois, C.L.; Dens, J.; Ormiston, J.; Worthley, S.; McClean, D.; Ottervanger, J.P.; Meredith, I.; Uren, N.; Wijns, W.; et al. Three-year clinical results of the Axxess Biolimus A9 eluting bifurcation stent system: The DIVERGE study. *EuroIntervention* **2013**, *9*, 573–581. [CrossRef]
29. Bennett, J.; Adriaenssens, T.; McCutcheon, K.; Dens, J.; Desmet, W.; Sinnaeve, P.; Vrolix, M.; Dubois, C. 5-Year clinical follow-up of the COBRA (complex coronary bifurcation lesions: Randomized comparison of a strategy using a dedicated self-expanding biolimus A9-eluting stent vs. a culotte strategy using everolimus-eluting stents) study. *Catheter. Cardiovasc. Interv.* **2018**, *92*, E375–E380. [CrossRef]
30. Grundeken, M.J.; Kraak, R.P.; Baan, J., Jr.; Arkenbout, E.K.; Piek, J.J.; Vis, M.M.; Henriques, J.P.; Koch, K.T.; Tijssen, J.G.; de Winter, R.J.; et al. First report on long-term clinical results after treatment of coronary bifurcation lesions with the Tryton dedicated bifurcation stent. *Catheter. Cardiovasc. Interv.* **2014**, *84*, 759–765. [CrossRef]
31. Lu, H.; Bekker, R.J.; Grundeken, M.J.; Woudstra, P.; Wykrzykowska, J.J.; Tijssen, J.G.P.; de Winter, R.J.; Koch, K.T. Five-year clinical follow-up of the STENTYS self-apposing stent in complex coronary anatomy: A single-centre experience with report of specific angiographic indications. *Neth. Heart. J.* **2018**, *26*, 263–271. [CrossRef]
32. Riku, S.; Suzuki, S.; Yokoi, T.; Sakaguchi, T.; Yamamoto, T.; Jinno, Y.; Tanaka, A.; Ishii, H.; Inden, Y.; Murohara, T. Very long-term clinical outcomes after percutaneous coronary intervention for complex vs non-complex lesions: 10-year outcomes following sirolimus-eluting stent implantation. *Nagoya J. Med. Sci.* **2022**, *84*, 352–365. [CrossRef]
33. Takagi, K.; Ielasi, A.; Basavarajaiah, S.; Chieffo, A.; Shannon, J.; Godino, C.; Hasegawa, T.; Naganuma, T.; Fujino, Y.; Latib, A.; et al. The impact of main branch restenosis on long term mortality following drug-eluting stent implantation in patients with de novo unprotected distal left main bifurcation coronary lesions: The Milan and New-Tokyo (MITO) Registry. *Catheter. Cardiovasc. Interv.* **2014**, *84*, 341–348. [CrossRef]
34. De la Torre Hernandez, J.M.; Alfonso, F.; Sanchez Recalde, A.; Jimenez Navarro, M.F.; Perez de Prado, A.; Hernandez, F.; Abdul-Jawad Altisent, O.; Roura, G.; Garcia Camarero, T.; Elizaga, J.; et al. Comparison of paclitaxel-eluting stents (Taxus) and everolimus-eluting stents (Xience) in left main coronary artery disease with 3 years follow-up (from the ESTROFA-LM registry). *Am. J. Cardiol.* **2013**, *111*, 676–683. [CrossRef] [PubMed]
35. Chen, S.L.; Zhang, Y.; Xu, B.; Ye, F.; Zhang, J.; Tian, N.; Liu, Z.; Qian, X.; Ding, S.; Li, F.; et al. Five-year clinical follow-up of unprotected left main bifurcation lesion stenting: One-stent versus two-stent techniques versus double-kissing crush technique. *EuroIntervention* **2012**, *8*, 803–814. [CrossRef] [PubMed]
36. Fujisaki, T.; Kuno, T.; Numasawa, Y.; Takagi, H.; Briasoulis, A.; Kwan, T.; Latib, A.; Tamis-Holland, J.; Bangalore, S. Provisional or 2-Stent Technique for Bifurcation Lesions in the Second-Generation Drug-Eluting Stent Era. *J. Soc. Cardiovasc. Angiogr. Interv.* **2022**, *1*, 100410. [CrossRef]
37. Nikolakopoulos, I.; Vemmou, E.; Karacsonyi, J.; Azzalini, L.; Bergmark, B.A.; Chatzizisis, Y.S.; Hall, A.B.; Wollmuth, J.; Croce, K.; Jneid, H.; et al. Practice Patterns in the Interventional Treatment of Coronary Bifurcation Lesions: A Global Survey. *J. Invasive Cardiol.* **2022**, *34*, E43–E48.
38. Ungureanu, C.; Natalis, A.; Cocoi, M.; Dumitrascu, S.; Noterdaeme, T.; Gach, O.; Jossart, A.; Soetens, R.; Colletti, G. The impact of the bifurcation angle for the Nano-Crush two-stent coronary bifurcation technique on long-term outcomes in a real-world clinical population. *Cardiovasc. Revasc. Med.* 2024; *in press*. [CrossRef]

39. Gupta, A.; Shrivastava, A.; Chhikara, S.; Mamas, M.A.; Vijayvergiya, R.; Swamy, A.; Mahesh, N.K.; Singh, N.; Bajaj, N.; Singh, B.; et al. Optical Coherence Tomography Predictors of SIde Branch REstenosis after unprotected Left Main bifurcation angioplasty using double kissing crush technique (OP-SIBRE LM Study). *Catheter. Cardiovasc. Interv.* **2024**, *103*, 51–60. [CrossRef]
40. Jones, J.; Mouyis, K.; Tyrlis, A.; Rathod, K.S.; Guttmann, O.; Wragg, A.; O'Mahony, C.; Mathur, A.; Baumbach, A.; Jones, D.A. An observational study assessing the use of Sirolimus-eluting balloons for side-branch treatment in the provisional stenting of coronary bifurcations. *Am. Heart J. Plus* **2023**, *30*, 100301. [CrossRef]

Disclaimer/Publisher's Note: The statements, opinions and data contained in all publications are solely those of the individual author(s) and contributor(s) and not of MDPI and/or the editor(s). MDPI and/or the editor(s) disclaim responsibility for any injury to people or property resulting from any ideas, methods, instructions or products referred to in the content.

biomedicines

MDPI

Article

Analysis of Cardiovascular High-Risk Profile in Middle-Aged Lithuanian Men with Arterial Hypertension from 2009 to 2019

Vaida Šileikienė [1], Vilma Dženkevičiūtė [1], Alma Čypienė [1,2], Tautvydas Šlapikas [1,*], Roma Puronaitė [3], Jolita Badarienė [1], Aleksandras Laucevičius [1], Eglė Butkevičiūtė [4] and Egidija Rinkūnienė [1]

[1] Clinic of Cardiac and Vascular Diseases, Faculty of Medicine, Vilnius University, Ciurlionio str. 21, LT-03101 Vilnius, Lithuania
[2] State Research Institute Centre for Innovation and Medicine, Santariskiu str. 5, LT-03101 Vilnius, Lithuania
[3] Clinic Department of Information Systems, Centre of Informatics and Development, Sauletekio str. 9, LT-10222 Vilnius, Lithuania
[4] Department of Software Engineering, Faculty of Informatics, Kaunas University of Technology, Studentu str. 50, LT-51368 Kaunas, Lithuania
* Correspondence: tautvydas.slapikas@gmail.com

Abstract: Objective: The prevalence of arterial hypertension in adult men is 34% worldwide and 52% in Lithuania. This paper aims to provide an overview of the prevalence trends of arterial hypertension and its clinical forms in middle-aged Lithuanian men and to assess the risk profiles of the different groups. **Methods**: This retrospective research study collected data from 52,012 Lithuanian male patients. The study population consisted of men aged 40–55 who participated in the Lithuanian High Cardiovascular Risk Program between 2009 and 2019. **Results**: Of the 52,012 participants, 47.2% (n = 24,531) were men with arterial hypertension. The prevalence of arterial hypertension in Lithuanian men decreased between 2009 and 2019 ($p < 0.001$). Before the study visit, 12.6% (n = 6583) of men were unaware of their diagnosis, and 8.8% (n = 4555) of diagnosed cases were untreated. In addition, 2.6% (n = 1334) of the men had resistant arterial hypertension. Significant differences in most general characteristics were found between the groups with arterial hypertension. Waist circumference increased from 92.8 ± 10.7 cm in men without arterial hypertension to 109 ± 13.3 cm and in men with resistant arterial hypertension ($p < 0.001$), and mean triglyceride levels increased from 1.55 ± 1.22 mmol/L to 2.32 ± 1.82 mmol/L in these groups ($p < 0.001$). Obesity (63.6%), unhealthy diet (74.7%), physical inactivity (62.9%), and diabetes (25.2%) were more common in the group with resistant arterial hypertension than in all other groups ($p < 0.001$). Meanwhile, dyslipidaemia was the most common risk factor in all groups (from 83.2% in men without arterial hypertension to 92.6% in men with resistant hypertension). **Conclusions**: Almost half of middle-aged men had arterial hypertension, with prevalence decreasing from 2009 to 2019. Significant changes in cardiometabolic characteristics were observed in newly diagnosed cases of arterial hypertension. These changes are even more notable in men with resistant hypertension compared to a non-resistant form. Most cardiovascular risk factors were most prevalent in over 50% of resistant hypertension cases, with dyslipidaemia being the most common risk factor in the entire male sample.

Keywords: arterial hypertension; primary prevention; cardiovascular risk factors

1. Introduction

Cardiovascular disease is the most common cause of death worldwide, causing around 17.9 million deaths each year. According to the World Health Organization, four out of

five cardiovascular-related deaths are due to heart attacks and strokes, with one-third of these occurring in people under the age of 70 [1]. In Lithuania, almost 50% of all deaths are attributed to cardiovascular events [2]. These mortality rates could be significantly reduced by early detection and effective treatment of cardiovascular risk factors such as dyslipidaemia, elevated blood glucose levels, and smoking. This is particularly important for the most prevalent modifiable cardiovascular risk factor, arterial hypertension, which is often referred to as the "silent killer", affecting more than 1.3 billion adults worldwide [3].

High blood pressure is closely associated with an increased risk of stroke, heart failure, coronary heart disease, ischemic heart disease, and kidney failure. The risk is exceptionally high in people who develop arterial hypertension before the age of 45 [4]. Although arterial hypertension is rarely an isolated disease, it is often associated with other risk factors, including genetic, gender, age, and environmental factors. It is also closely related to several cardiovascular risk factors such as metabolic syndrome, diabetes, smoking, poor dietary habits, obesity, alcohol and tobacco consumption, and physical inactivity [5].

Globally, the prevalence of arterial hypertension in adult men is 34%, while in Lithuania it reaches 52% [3,6]. Among men with hypertension, only 49% are diagnosed, 38% receive treatment, and only 18% have their blood pressure successfully controlled [3]. Alarmingly, 51% of men with arterial hypertension are unaware of their condition, a figure that is 10% higher than in the female population [3].

It is estimated that increasing the rate of successfully treated hypertension to 50% between 2023 and 2050 could prevent 76 million deaths worldwide [6]. However, progress towards achieving the stated goal is hampered by numerous factors. The high prevalence of other cardiovascular risk factors in men with arterial hypertension and the lack of awareness of their diagnosis are just a few examples. Addressing these challenges through comprehensive treatment strategies is critical to improving men's cardiovascular health and the whole population's health.

The aim of this study is to provide an overview of the prevalence trends of arterial hypertension and its clinical forms in middle-aged Lithuanian men and to evaluate the cardiovascular risk profiles of different groups.

2. Materials and Methods

2.1. Study Design and Population

This retrospective study analysed the data of 52,012 Lithuanian male patients aged 40–55 who participated in the Lithuanian High Cardiovascular Risk Primary Prevention Programme (LitHiR) between 2009 and 2019. The programme, active since 2006, involves approximately 91.6% of all primary healthcare centres in Lithuania.

Patients were screened for cardiovascular risk factors, including lifestyle habits (physical activity, diet, smoking), cardiovascular history (personal and family) and anthropometric measurements (height, weight, waist circumference, body mass index (BMI), blood pressure, and heart rate). Additional investigations included blood tests to measure glucose, total cholesterol (TC), high-density lipoprotein (HDL) and low-density lipoprotein (LDL) cholesterol, and triglycerides to determine the prevalence of metabolic syndrome in high-risk patients.

Blood pressure was measured on the dominant arm at heart level after the patient had been sitting for at least five minutes. Physicians were advised to obtain three measurements and use the average.

Arterial hypertension was diagnosed if systolic blood pressure was $\geq$140 mmHg and diastolic blood pressure was $\geq$90 mmHg or if hypertension had been previously documented. Newly diagnosed arterial hypertension referred to cases identified during screening that did not have a documented diagnosis before participation in the primary

prevention programme. Previously diagnosed but untreated arterial hypertension referred to patients with documented hypertension but without prescribed treatment. Resistant arterial hypertension was defined as uncontrolled blood pressure (>140/90 mmHg) despite the use of three different classes of antihypertensive medication, including diuretics. Non-resistant arterial hypertension referred to medically treated instances that do not meet the criteria for resistant hypertension.

Abdominal obesity was assessed by waist circumference. The correct place to measure your waist is halfway between your lowest rib and the top of your hipbone. This is roughly in line with your belly button. Abdominal obesity was defined as a waist circumference greater than 102 cm in men.

Dyslipidaemia was diagnosed if one or more blood lipid values were outside the normal range: total cholesterol > 5 mmol/L, LDL cholesterol > 3 mmol/L, HDL cholesterol < 1 mmol/L, or triglycerides > 1.7 mmol/L.

Based on the data collected, patients were divided into five groups according to their arterial hypertension status, and the prevalence of cardiovascular risk factors within each group was analysed:

- Men without arterial hypertension;
- Men with undiagnosed arterial hypertension;
- Men with diagnosed but untreated arterial hypertension;
- Men with non-resistant arterial hypertension;
- Men with resistant arterial hypertension.

2.2. Statistical Methods

Continuous variables were expressed as mean ± standard deviation (±SD). ANOVA or the non-parametric Kruskal–Wallis test was used to compare these variables between the different forms of hypertension, followed by pairwise comparisons using either the *t*-test or the non-parametric Mann–Whitney *U* test as appropriate. Categorical variables were presented as absolute frequencies (*n*) and percentages (%), with differences between groups assessed using the χ^2 test or Fisher's exact test. Trends in the prevalence of different clinical forms of arterial hypertension from 2009 to 2019 were analysed using the Cochran–Armitage test for trends (also known as the χ^2 test for trends). A significance level of $p < 0.05$ was set for all statistical tests. The analysis was performed with the statistical software "R" (version 4.4.1), while the tables and graphs for visualisation and presentation of the data were created with "Microsoft Word for Microsoft 365".

3. Results

3.1. Prevalence of the Different Clinical Forms of Arterial Hypertension in Men from 2009 to 2019

A total of 52,012 men were examined between 2009 and 2019 as part of the prevention program. Of these, 52.8% (n = 27,481) had no diagnosis of arterial hypertension. In 12.6% (n = 6583) of cases, arterial hypertension was detected during screening, while 8.8% (n = 4555) had been previously diagnosed but did not receive treatment. In addition, 23.2% (n = 12,059) of cases were diagnosed and responded to treatment, with 2.6% (n = 1334) of participants having resistant arterial hypertension (Figure 1). The overall prevalence of arterial hypertension in male participants was 47.2%, and 74.6% of these patients, excluding newly diagnosed cases, were on treatment. Of the treated cases, 9.96% developed resistant arterial hypertension.

There was a stable and significant increase in the proportion of men without arterial hypertension, rising from 48.7% in 2009 to 54.8% in 2019 ($p < 0.001$). From 2018, there was also a notable decrease in untreated cases of diagnosed arterial hypertension and an increase in non-resistant forms ($p < 0.001$) (Figure 2, Table S1).

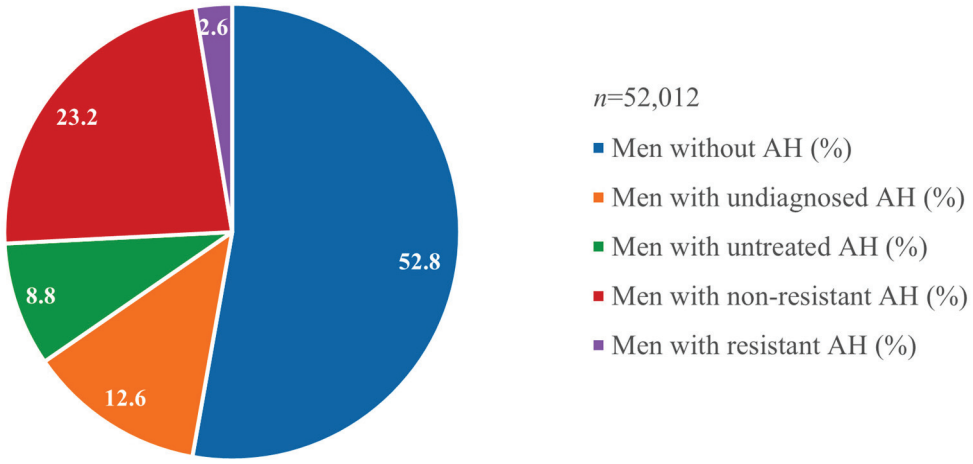


Figure 1. Prevalence of the different clinical forms of arterial hypertension in men.

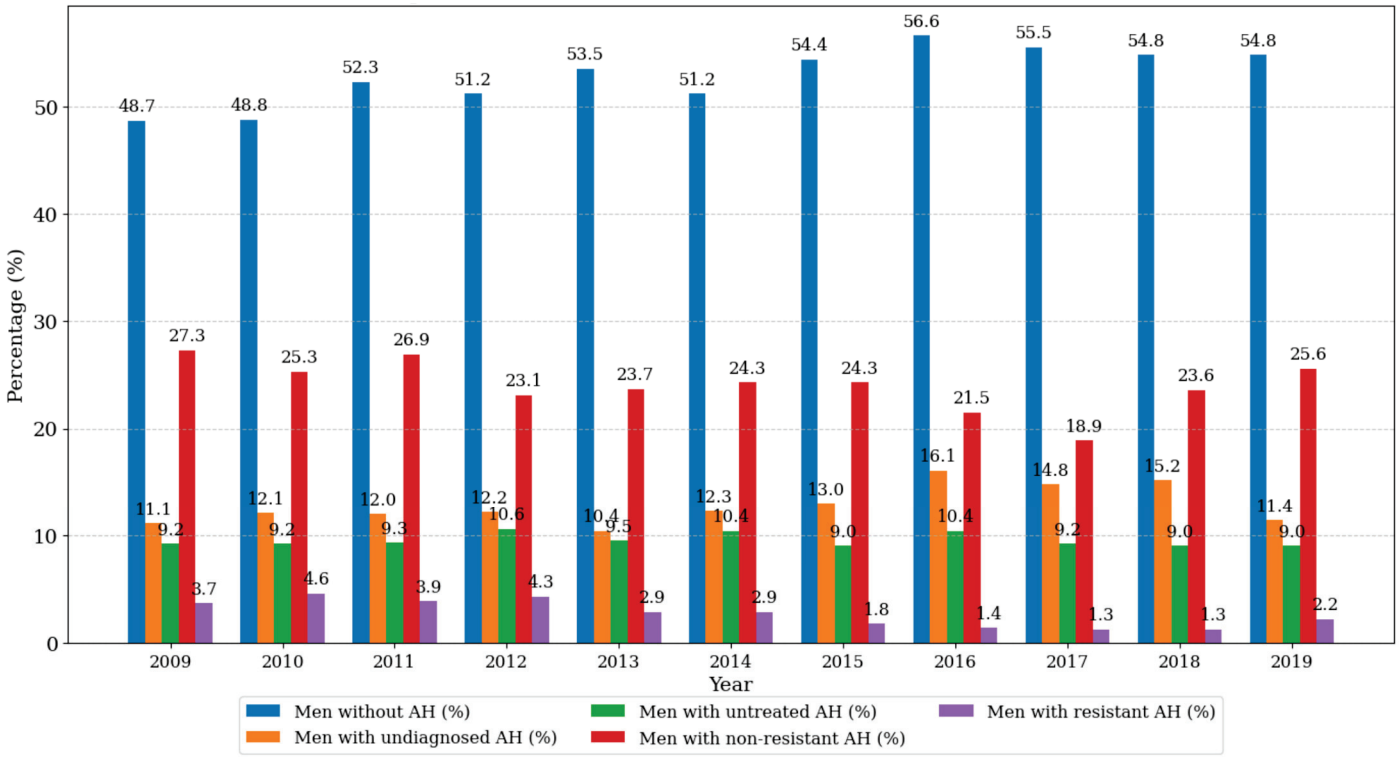


Figure 2. Prevalence of the different clinical forms of arterial hypertension in men in 2009–2019, $p < 0.001$.

3.2. General Characteristics in Men

The lowest mean age was observed in men without arterial hypertension, at 46.2 ± 4.43 years, while the highest mean age was among men with resistant arterial hypertension, at 48.4 ± 4.19. Men without arterial hypertension had the lowest mean arterial pressure, of 123/77.7 ± 7.24/5.46 mmHg, whereas men with resistant arterial hypertension had the highest mean arterial pressure, at 151/92.4 ± 17.1/10.4 mmHg.

Significant changes in general characteristics were observed between different arterial hypertension groups. The lowest average BMI was recorded in men without arterial hypertension, at 26.4 ± 3.87 kg/m^2, with BMI increasing progressively across different arterial hypertension groups ($p < 0.001$). A notable increase in BMI was observed between men with non-resistant arterial hypertension, at 30.3 ± 5.07 kg/m^2, and those with resistant arterial hypertension, at 32.8 ± 5.57 kg/m^2, respectively ($p < 0.001$). Similar trends were

seen in waist measurements, where the mean waist size increased from 92.8 ± 10.7 cm in men without arterial hypertension to 97.1 ± 11.4 cm in men with newly diagnosed arterial hypertension ($p < 0.001$). Comparing men with treatment-responsive and resistant arterial hypertension, waist measurements increased from 103.7 ± 12.9 cm to 109 ± 13.3 cm ($p < 0.001$).

Mean glucose levels also significantly increased from 5.38 ± 1.01 mmol/L in men without arterial hypertension to 6.12 ± 1.74 mmol/L in men with resistant arterial hypertension ($p < 0.001$). Mean triglyceride levels increase from 1.55 ± 1.22 mmol/L in men without arterial hypertension to 2.32 ± 1.82 mmol/L in those with resistant arterial hypertension ($p < 0.001$). Differences in mean LDL cholesterol levels in most groups with arterial hypertension were insignificant ($p > 0.05$). Meanwhile, changes in HDL cholesterol were insignificant comparing only groups with newly diagnosed and untreated arterial hypertension cases ($p = 0.464$) (Figure 3, Table S2).

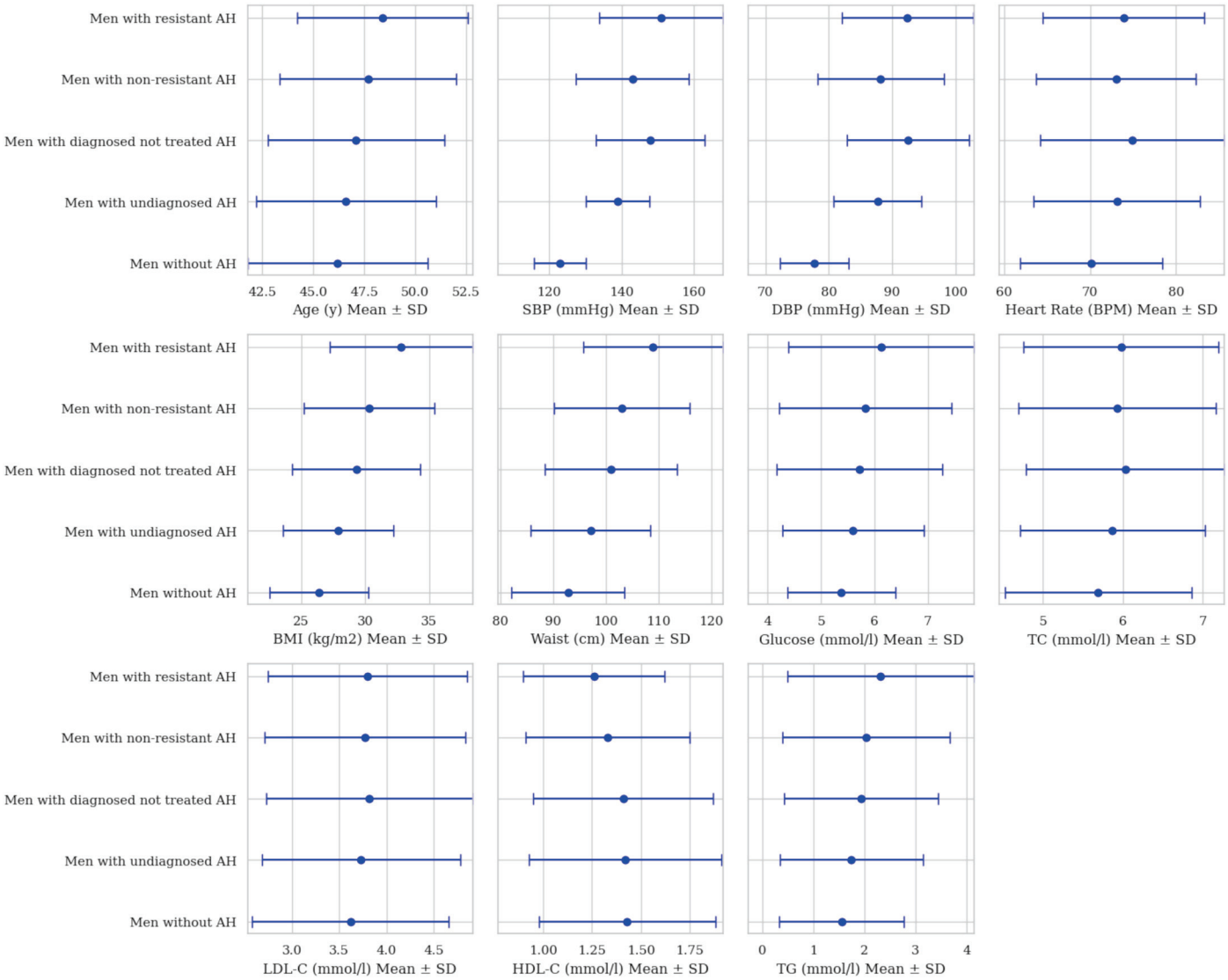


Figure 3. General characteristics in men with and without arterial hypertension. Abbreviations: SBP—systolic blood pressure; DBP—diastolic blood pressure, BPM—beats per minute, BMI—body mass index, TC—total cholesterol, LDL-C—low-density lipoprotein cholesterol, HDL-C—high-density lipoprotein cholesterol, TG—triglycerides.

3.3. Cardiovascular Risk Factors in Men with and Without Arterial Hypertension

The highest prevalence of almost all cardiovascular risk factors was observed in men with resistant arterial hypertension, including decreased HDL cholesterol (47.1%), increased triglyceride levels (56.8%), insufficient physical activity (63.6%), unhealthy dietary habits (74.9%), and a high prevalence of obesity (66.8%) and diabetes (25.9%). The most remarkable differences in the prevalence of risk factors were found between men without arterial hypertension and those with resistant arterial hypertension. For example, 15.9% of men without arterial hypertension were obese compared with 66.8% of men with resistant arterial hypertension ($p < 0.001$). Elevated triglyceride levels were found in 28.5% of men without arterial hypertension, while 56.8% of men with resistant arterial hypertension had hypertriglyceridaemia ($p < 0.001$).

Dyslipidaemia was the most common risk factor in all participants. It affected 87.7% of men without arterial hypertension; and this increased to 95.5% in men with resistant arterial hypertension. The prevalence of diabetes was 6.29% in men without arterial hypertension but increased significantly in men with arterial hypertension: it was 16.0% in men with untreated arterial hypertension and 25.9% in men with resistant arterial hypertension ($p < 0.001$).

Lifestyle risk factors were also common in the study groups. In the men without arterial hypertension, the prevalence of poor dietary habits was 57.6%, smoking was 39.8%, and lack of physical activity was 39.5%. The prevalence of most risk factors increased significantly when comparing men without arterial hypertension to those with various forms of arterial hypertension ($p < 0.001$). The highest rates of smoking were observed in men with newly diagnosed arterial hypertension and untreated cases of arterial hypertension (43.0% and 44.8%, respectively, $p = 0.064$) (Figure 4, Table S3).

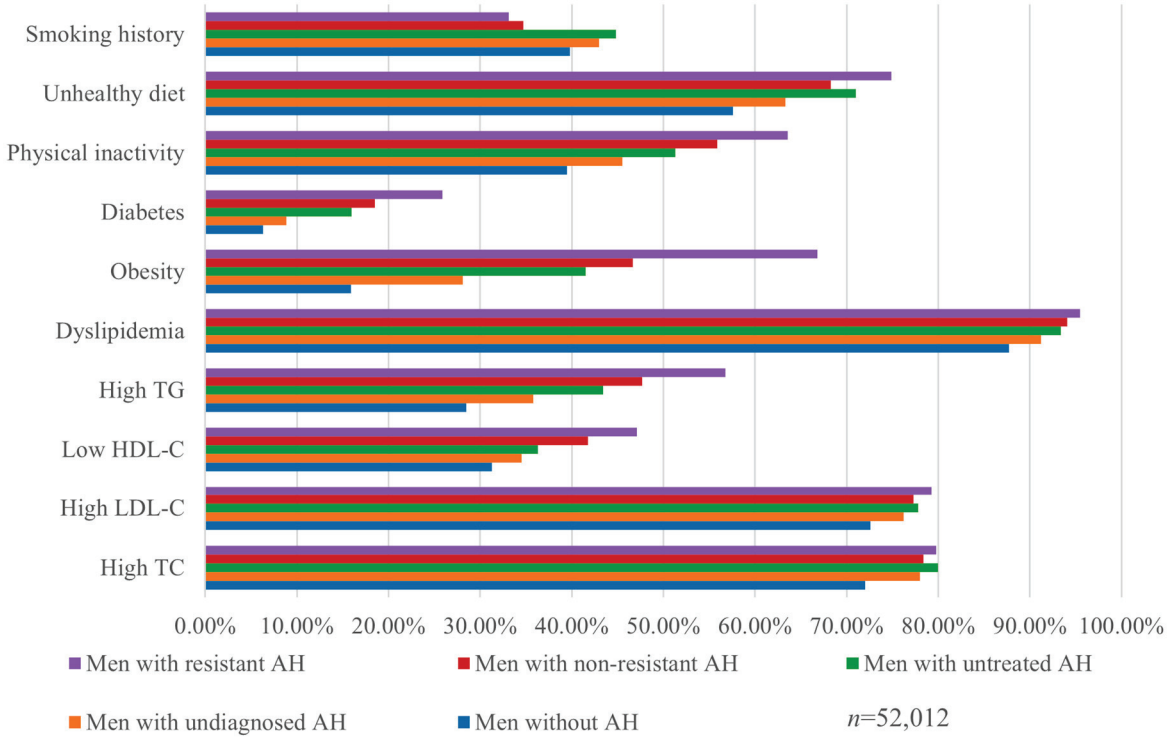


Figure 4. Cardiovascular risk factors in men with and without arterial hypertension. Abbreviations: TG—triglycerides, HDL-C—high-density lipoprotein cholesterol, LDL-C—low-density lipoprotein cholesterol, TC—total cholesterol.

4. Discussion

Worldwide, the prevalence of arterial hypertension in 2019 was 32% for women and 34% for men aged 30–79 years [3]. Canada reported some of the lowest rates, with 20% of women and 24% of men affected. In contrast, Central and Eastern European countries such as Poland (55%), Lithuania (54%), Latvia (49%), and the Czech Republic (49%) were among the nations with the highest prevalence of hypertension in men, well above the global average of 34% [3].

In Canada, the prevalence of arterial hypertension in men was 23.6% in 2013, an increase compared to previous years, although awareness and treatment outcomes have improved over the same period [7]. The low prevalence may be surprising, as it seems to be more challenging to access care in Canada than in Lithuania. In 2016, 93% of Canadians reported access to care, while only 1.5% of Lithuanians faced challenges while seeking care in 2019 [8,9]. Between 2007 and 2015, 39.2% of Canadian men reported not getting enough exercise, 77.5% had poor dietary habits, 69.5% were obese, and 26.9% were smokers [10]. In 2018–2019, 56.7% of men over the age of 40 were diagnosed with dyslipidaemia [11]. While smoking rates and physical inactivity declined by 2018, rates of obesity, diabetes, and hypertension have continued to rise since 2001 [12]. These findings may suggest a notable association between dyslipidaemia and arterial hypertension. While self-reported lifestyle habits among Canadian men are broadly similar to those of Lithuanian men, the lower prevalence of dyslipidaemia in Canada should be considered as one of several factors contributing to lower prevalence of arterial hypertension in the Canadian population.

Despite cultural and health differences, Central Eastern European countries, including the Baltics, face similar challenges in terms of cardiovascular risk factors. The LIPIDOGRAM2015 study in Poland, which analysed data from 5034 male patients in primary care, found that 65% of men had hypertension, 88% had dyslipidaemia, and 13% had diabetes. Abdominal obesity was prevalent in 73% of men, and 59% had a history of smoking [13]. A study from the Czech Republic found that 43% of middle-aged men suffered from arterial hypertension, with 8% unaware of their diagnosis. Diabetes was diagnosed in 11% of both men and women. Dyslipidaemia was the most common risk factor, affecting 39% of men. The study also found a significant association between arterial hypertension and other cardiovascular risk factors, including diabetes and dyslipidaemia [14]. In Latvia, 2016 men were interviewed about their cardiovascular risk factors, and 976 men underwent physical examinations as part of a two-part cross-sectional study conducted in 2019–2020. Self-reported rates of hypertension and high cholesterol were 15.9% and 15.4%, respectively, while 40.4% of participants were current smokers [15]. However, objective testing revealed that 40.3% of men had arterial hypertension, 63.1% had LDL cholesterol levels of 3 mmol/L or more, and 60.7% had elevated triglyceride levels [15]. These findings highlight the worrying underestimation of personal health risks that could significantly impact the prevalence and management of cardiovascular disease in men.

This study found that 46.8% of middle-aged men in Lithuania suffered from arterial hypertension. Remarkably, 26.7% of these men were newly diagnosed with arterial hypertension during screening, suggesting that a significant proportion of participants were previously unaware of their cardiovascular health status. Of those with arterial hypertension, 7 out of 10 were receiving treatment, while a quarter of previously diagnosed men were not receiving treatment for AH. Of all treated cases, 11.7% were classified as treatment-resistant. Despite the high overall prevalence, the study observed a decline in arterial hypertension over the decade, with a marked increase in treated cases and a decrease in untreated cases, particularly from 2018 onwards.

Dyslipidaemia was the most prevalent cardiovascular risk factor in all groups of middle-aged men in Lithuania, alongside elevated cholesterol levels and self-reported

poor dietary habits. The highest prevalence of elevated triglycerides, insufficient physical activity, and other risk factors was found in men with resistant arterial hypertension, except for smoking. Smoking was more common in men without arterial hypertension or those with untreated hypertension. The most significant differences between men without arterial hypertension and men with resistant arterial hypertension were observed in the prevalence of obesity, elevated triglyceride levels, and the presence of diabetes.

The cardiovascular risk factors are typically classified as modifiable or non-modifiable. This study focuses on the prevalence of modifiable factors, including dyslipidaemia, diabetes, obesity, and lifestyle habits such as physical inactivity, poor dietary habits, and smoking. Arterial hypertension itself is considered a modifiable risk factor for other cardiovascular diseases. However, the aforementioned risk factors play a crucial role in the pathology and aetiology of arterial hypertension. A linear relationship between sodium intake and high blood pressure has been established in multiple studies, with salt reduction proving effective in lowering blood pressure among salt-sensitive individuals [16–18]. Physical activity is another well-documented determinant of arterial hypertension, with moderate levels of physical activity shown to reduce the risk of hypertension by 6% [19]. Furthermore, a healthy diet and regular physical activity are vital for preventing diabetes and dyslipidaemia, which are considered as significant contributors to the development of arterial hypertension [20–22]. Therefore, the mentioned factors should always be addressed both as preventative and management measures for cardiovascular diseases and cardiometabolic disorders such as diabetes, dyslipidaemia, and arterial hypertension.

Limitations

This study focuses exclusively on men aged 40–55 years, as the LitHiR primary prevention programme includes men at this age because they are at the highest risk of developing cardiovascular disease. The inclusion criteria for cases of resistant arterial hypertension did not take into account pseudo-resistant or secondary arterial hypertension; thus, caution is advised when interpreting these results. In addition, this study did not consider psychosocial, socioeconomic, and other risk factors nor was there an objective assessment of physical activity, diet, and smoking habits, as these were based solely on self-reported data. As previously mentioned in the discussion, self-reported data should be interpreted cautiously due to potential biases, including underestimating personal health issues and harmful lifestyle habits. Moreover, without objective measurements of these behaviours (e.g., using physical activity trackers or dietary assessments), it is difficult to verify the accuracy of the self-reported data, which limits the accuracy of the study's conclusions. Therefore, caution should be exercised when interpreting the association between self-reported lifestyle factors and cardiovascular health in this sample. Finally, as the study focuses exclusively on middle-aged men, the results may not be generalizable to other demographic groups, including women or younger people. They may not fully represent the wider Lithuanian population.

5. Conclusions

The study highlights the prevalence of arterial hypertension and its trends in middle-aged Lithuanians, as well as the profile of concomitant cardiovascular risk factors in different case groups. According to the results, almost half of middle-aged men (49.8%) suffered from arterial hypertension, with the prevalence decreasing by 6% in the period 2009–2019. However, more than 10% of middle-aged Lithuanian men were unaware of their AH diagnosis, and a quarter of diagnosed cases were untreated. In addition, worrying changes in cardiometabolic characteristics were observed in the newly diagnosed cases of arterial hypertension. These changes were even more pronounced in men with resistant

hypertension compared to a non-resistant form. Significant metabolic changes, such as changes in waist circumference, BMI, glucose, and lipid levels, were observed in men with and without AH. Most cardiovascular risk factors, such as unhealthy diet, physical inactivity, obesity, dyslipidaemia, and high low-density lipoprotein cholesterol and total cholesterol levels, were most prevalent in over 50% of resistant hypertension cases, with dyslipidaemia being the most common risk factor in the entire male sample.

Supplementary Materials: The following supporting information can be downloaded at: https://www.mdpi.com/article/10.3390/biomedicines13020272/s1, Table S1: Prevalence of the different clinical forms of arterial hypertension in men in 2009–2019; Table S2: General characteristics in men with and without arterial hypertension; Table S3: Cardiovascular risk factors in men with and without arterial hypertension.

Author Contributions: Conceptualization, V.Š. and A.L.; methodology, V.Š., A.L. and E.R.; formal analysis, R.P. and E.B.; writing—original draft preparation, V.Š. and T.Š.; writing—review and editing, V.Š., V.D., A.Č., T.Š., A.L. and E.R.; visualization, R.P. and E.B.; supervision, A.L. and E.R.; project administration, J.B., A.L. and E.R. All authors have read and agreed to the published version of the manuscript.

Funding: This research received no external funding.

Institutional Review Board Statement: The study protocol was approved by the Regional Ethics Committee for Biomedical Research in Vilnius (reference number 158200-15-816-329). As stated in the protocol submitted to the Regional Biomedical Research Ethics Committee, it was not possible to obtain written informed consent from each patient.

Informed Consent Statement: Not applicable.

Data Availability Statement: The datasets used and analysed during the current study are available from the corresponding author upon reasonable request.

Conflicts of Interest: The authors declare no conflicts of interest.

Abbreviations

The following abbreviations are used in this manuscript:

SBP	Systolic blood pressure
DBP	Diastolic blood pressure
BPM	Beats per minute
BMI	Body mass index
TC	Total cholesterol
LDL-C	Low-density lipoprotein cholesterol
HDL-C	High-density lipoprotein cholesterol
TG	Triglycerides
AH	Arterial hypertension

References

1. Cardiovascular Diseases (CVDs) [Internet]. Available online: https://www.who.int/news-room/fact-sheets/detail/cardiovascular-diseases-(cvds) (accessed on 28 April 2024).
2. OECD [Internet]. 2023. Lithuania: Country Health Profile 2023. Available online: https://www.oecd.org/en/publications/lithuania-country-health-profile-2023_5ed683c8-en.html (accessed on 8 January 2025).
3. NCD Risk Factor Collaboration (NCD-RisC). Worldwide trends in hypertension prevalence and progress in treatment and control from 1990 to 2019: A pooled analysis of 1201 population-representative studies with 104 million participants. *Lancet Lond. Engl.* **2021**, *398*, 957–980. [CrossRef] [PubMed]
4. Wang, C.; Yuan, Y.; Zheng, M.; Pan, A.; Wang, M.; Zhao, M.; Li, Y.; Yao, S.; Chen, S.; Wu, S.; et al. Association of Age of Onset of Hypertension with Cardiovascular Diseases and Mortality. *J. Am. Coll. Cardiol.* **2020**, *75*, 2921–2930. [CrossRef] [PubMed]

5. Williams, B.; Mancia, G.; Spiering, W.; Agabiti Rosei, E.; Azizi, M.; Burnier, M.; Clement, D.L.; Coca, A.; De Simone, G.; Dominiczak, A.; et al. 2018 ESC/ESH Guidelines for the management of arterial hypertension: The Task Force for the management of arterial hypertension of the European Society of Cardiology (ESC) and the European Society of Hypertension (ESH). *Eur. Heart J.* **2018**, *39*, 3021–3104. [CrossRef] [PubMed]
6. Global Report on Hypertension: The Race Against a Silent Killer [Internet]. Available online: https://www.who.int/publications-detail-redirect/9789240081062 (accessed on 22 April 2024).
7. Padwal, R.S.; Bienek, A.; McAlister, F.A.; Campbell, N.R.C. Epidemiology of Hypertension in Canada: An Update. *Can. J. Cardiol.* **2016**, *32*, 687–694. [CrossRef] [PubMed]
8. Canadian Institute for Health Information. International Survey Shows Canada Lags Behind Peer Countries in Access to Primary Health Care [Internet]. Available online: https://www.cihi.ca/en/international-survey-shows-canada-lags-behind-peer-countries-in-access-to-primary-health-care#ref1 (accessed on 8 January 2025).
9. OECD [Internet]. 2019. Lithuania: Country Health Profile 2019. Available online: https://www.oecd.org/en/publications/lithuania-country-health-profile-2019_35913deb-en.html (accessed on 8 January 2025).
10. Leung, A.; Bushnik, T.; Hennessy, D.; McAlister, F.; Manuel, D. Risk factors for hypertension in Canada. *Health Rep.* **2019**, *30*, 3–13.
11. Spohn, O.; Morkem, R.; Singer, A.G.; Barber, D. Prevalence and management of dyslipidemia in primary care practices in Canada. *Can. Fam. Physician* **2024**, *70*, 187–196. [CrossRef] [PubMed]
12. Chen, K.Y.A.; Eddeen, A.B.; Bennett, C.; Yusuf, W.; Hennessey, D.; Barnes, J.D.; Manuel, D.G. Trends in Cardiovascular Risk Factors in Canada: Variation by Migration and Temporal Factors, 2001-2018. *CJC Open* **2024**, *6*, 951–958. Available online: https://www.sciencedirect.com/science/article/pii/S2589790X24001768 (accessed on 9 May 2024). [CrossRef] [PubMed]
13. Jóźwiak, J.J.; Studziński, K.; Tomasik, T.; Windak, A.; Mastej, M.; Catapano, A.L.; Ray, K.K.; Mikhailidis, D.P.; Toth, P.P.; Howard, G.; et al. The prevalence of cardiovascular risk factors and cardiovascular disease among primary care patients in Poland: Results from the LIPIDOGRAM2015 study. *Atheroscler. Suppl.* **2020**, *42*, e15–e24. [CrossRef] [PubMed]
14. Chmelík, Z.; Vaclová, M.; Lánská, V.; Laštůvka, J.; Vrablík, M. Analysis of incidence and prevalence of cardiovascular risk factors and evaluation of their control in epidemiological survey in the Czech Republic. *Cent. Eur. J. Public Health* **2020**, *28*, 114–119. [CrossRef] [PubMed]
15. Erglis, A.; Bajare, I.; Jegere, S.; Mintale, I.; Barzdins, J.; Luguzis, A.; Apinis, P.; Caksa, A.; Gavare, I.; Dzerve, V. Comparative Analysis of the Most Important Cardiovascular Risk Factors Based on Cross-Sectional Studies in the Population of Latvia. *Medicina* **2022**, *58*, 643. [CrossRef]
16. Pinto, I.C.; Martins, D. Prevalence and risk factors of arterial hypertension: A literature review. *J. Cardiovasc. Med. Ther.* **2017**, *1*, 1–7.
17. Filippini, T.; Malavolti, M.; Whelton, P.K.; Naska, A.; Orsini, N.; Vinceti, M. Blood Pressure Effects of Sodium Reduction. *Circulation* **2021**, *143*, 1542–1567. [CrossRef] [PubMed]
18. Grillo, A.; Salvi, L.; Coruzzi, P.; Salvi, P.; Parati, G. Sodium Intake and Hypertension. *Nutrients* **2019**, *11*, 1970. [CrossRef] [PubMed]
19. Liu, X.; Zhang, D.; Liu, Y.; Sun, X.; Han, C.; Wang, B.; Ren, Y.; Zhou, J.; Zhao, Y.; Shi, Y.; et al. Dose–Response Association Between Physical Activity and Incident Hypertension. *Hypertension* **2017**, *69*, 813–820. [CrossRef] [PubMed]
20. Agarwala, A.; Petersen, K.S.; Jafari, F.; Kris-Etherton, P.M. Dietary management of dyslipidemia and the impact of dietary patterns on lipid disorders. *Prog. Cardiovasc. Dis.* **2022**, *75*, 49–58. [CrossRef] [PubMed]
21. Scher-Nemirovsky, E.A.; Ruiz-Manco, D.; Mendivil, C.O. Impacto del ejercicio sobre el metabolismo de los lípidos y la dislipidemia. *Rev. Nutr. Clínica Metab.* **2019**, *2*, 26–36. [CrossRef]
22. Zahalka, S.J.; Abushamat, L.A.; Scalzo, R.L.; Reusch, J.E.B. The Role of Exercise in Diabetes. In *Endotext [Internet]*; Feingold, K.R., Anawalt, B., Blackman, M.R., Boyce, A., Chrousos, G., Corpas, E., de Herder, W.W., Dhatariya, K., Dungan, K., Hofland, J., et al., Eds.; MDText.com, Inc.: South Dartmouth, MA, USA, 2000. Available online: http://www.ncbi.nlm.nih.gov/books/NBK549946/ (accessed on 11 January 2025).

Disclaimer/Publisher's Note: The statements, opinions and data contained in all publications are solely those of the individual author(s) and contributor(s) and not of MDPI and/or the editor(s). MDPI and/or the editor(s) disclaim responsibility for any injury to people or property resulting from any ideas, methods, instructions or products referred to in the content.

biomedicines

MDPI

Article

The Silent Threat: A Retrospective Cohort Study on the Impact of Prediabetes on ST-Elevation Myocardial Infarction Survival—A Call to Action!

Elke Boxhammer †, Matthias Hammerer †, Christiana Schernthaner, Erika Prinz, Mathias C. Brandt, Michael Lichtenauer, Alexander E. Berezin, Wilfried Wintersteller, Uta C. Hoppe [1] and Kristen L. Kopp *

Department of Internal Medicine II, Division of Cardiology, Paracelsus Medical University of Salzburg, 5020 Salzburg, Austria

* Correspondence: k.kopp@salk.at

† These authors contributed equally to this work.

Abstract: Background: Prediabetes is frequently underdiagnosed and undertreated, yet it poses significant cardiovascular risks. This study investigates the impact of prediabetes on short- and long-term survival outcomes in patients who experienced ST-elevation myocardial infarction (STEMI). **Methods:** In this retrospective, single-center cohort study, we evaluated 725 STEMI patients stratified into non-diabetic, prediabetic, and diabetic groups based on HbA1c levels at presentation. A Kaplan–Meier survival analysis was employed to compare long-term outcomes over a three-year follow-up period. Cardiovascular risk factors, including hypertension and dyslipidemia, were analyzed across the groups. The discriminatory power of HbA1c for predicting all-cause mortality was assessed using an Area Under the Receiver Operating Characteristic (AUROC) analysis. **Results**: Of the 725 patients, 407 (56.1%) were non-diabetic, 184 (25.4%) were prediabetic, and 134 (18.5%) were diabetic. Prediabetic patients exhibited significant additional cardiovascular risk factors, such as arterial hypertension (67.4%) and dyslipidemia (78.3%), with prevalence rates between those of non-diabetic and diabetic patients. The Kaplan–Meier analysis revealed that at a three-year follow-up, prediabetic patients faced a survival disadvantage, with a significant decrease in survival rates compared to non-diabetic patients (log-rank $p = 0.016$); their survival outcomes approached those of diabetic patients ($p = 0.125$). The AUROC analysis demonstrated that HbA1c was a significant predictor of short- and long-term mortality, with a cut-off value of 5.75% and an Area Under the Curve (AUC) of 0.580–0.617 (95% CI: 0.458–0.721), indicating a moderate ability to predict survival in patients with STEMI. **Conclusions:** Prediabetes significantly worsens survival outcomes following STEMI, nearly approaching the risk level of diabetes. Integrating rigorous cardiovascular risk management strategies for prediabetic individuals, including lifestyle interventions and potentially pharmacological treatments, could prevent the progression to diabetes and mitigate associated cardiovascular risks.

Keywords: cardiovascular disease; diabetes; glycemic status; prediabetes; STEMI

1. Introduction

Acute ST-segment elevation myocardial infarction (STEMI) stands as a formidable medical emergency, demanding swift intervention and comprehensive management. Despite advancements in acute care, long-term prognosis remains a challenge, particularly in patients with underlying metabolic disorders [1,2]. Among these, prediabetes emerges as a critical, yet often underappreciated, factor influencing survival outcomes [3,4].

Prediabetes, which is defined by impaired fasting glucose or impaired glucose tolerance, represents an intermediate metabolic state with blood glucose levels elevated above normal but not high enough to be classified as diabetes. This condition is alarmingly

prevalent, with significant implications for cardiovascular health [5]. The pathophysiological mechanisms linking prediabetes to adverse cardiac events are multifaceted, involving insulin resistance, subclinical inflammation, endothelial dysfunction, and accelerated atherogenesis [6].

The current literature highlights a compelling connection between prediabetes and increased cardiovascular risk, comparable to that observed in overt diabetes [7]. Patients with prediabetes are at a higher risk of progressing to diabetes and experiencing cardiovascular events, including STEMI. Importantly, evidence suggests that prediabetic individuals who survive a STEMI face a significantly elevated long-term risk of mortality and recurrent cardiac events compared to normoglycemic patients [8].

The prognostic importance of prediabetes in the context of STEMI is underscored by several key studies. Research has demonstrated that even modest elevations in glycemic indices, such as hemoglobin A1c (HbA1c), are associated with worse outcomes post-STEMI. This highlights the insidious impact of prediabetes on myocardial recovery and long-term survival, necessitating the early identification and aggressive management of this at-risk population [9].

In clinical practice, the challenge lies in recognizing prediabetes as a potent risk factor and integrating it into risk stratification models for STEMI patients. Traditional risk assessments often overlook the subtle yet significant influence of prediabetic states, potentially leading to suboptimal management strategies [10].

Incorporating glycemic parameters such as HbA1c into predictive models may enhance the precision of risk stratification, enabling tailored therapeutic approaches that address the unique metabolic vulnerabilities of prediabetic patients. Therefore, our study aims to bridge this gap by providing robust evidence on the impact of prediabetes on survival following STEMI. By analyzing a large cohort and employing rigorous statistical methods, we seek to elucidate the prognostic significance of prediabetes. This endeavor not only advances our understanding of the interplay between glycemic status and cardiovascular outcomes but also paves the way for personalized intervention strategies designed to improve long-term survival in STEMI patients.

2. Materials and Methods

2.1. Study Population

For this retrospective study, all patients (n = 964) presenting with STEMI at a single large tertiary center in Salzburg, Austria, between 1 January 2018, and 31 December 2020, were screened. Eligible participants were STEMI patients aged 18 years or older, with documented cardiovascular risk factors and available baseline HbA1c values obtained during their initial hospitalization for STEMI (n = 725). Patients lacking HbA1c or with conservative treatment (without receiving a percutaneous coronary intervention) were excluded from this study.

The primary endpoint for this study was overall mortality within a three-year follow-up period. To determine outcomes, we established clear criteria for classifying mortality, which included reviewing medical records and death certificates. Additionally, we monitored and recorded cardiovascular events, defining them based on clinical guidelines and patient follow-up data. This thorough approach ensured an accurate assessment of survival rates and provided a comprehensive understanding of the long-term outcomes in this patient cohort.

To estimate the required sample size for this study, we utilized G*Power 3.1: (University of Duesseldorf, Duesseldorf, Germany) for an a priori analysis. The calculations indicated that each group should consist of 105 participants to ensure adequate statistical power. This estimation was based on an expected effect size of 0.5, an alpha level set at 0.05, and a target power of 0.95, with an equal distribution of participants across the study groups.

2.2. Ethics Declaration

This study was approved by the State of Salzburg Ethics Commission (EK-Nr. 1038/2021). All data handling complied with the Declaration of Helsinki principles and Good Clinical Practice (ICH-GCP) guidelines.

2.3. Data Extraction

Information was collected from the ORBIS electronic medical records system (Agfa-ORBIS; Agfa HealthCare GmbH, Mortsel, Belgium, Version 08043301.04110DACHL) and the medical archiving system (Krankengeschichtsarchiv, Uniklinikum Salzburg, Softworx by Andreas Schwab TM, 2008, Salzburg, Austria) at the University Clinic Salzburg in Austria. This data included patient charts, as well as reports from admissions, discharges, and laboratory results throughout the course of treatment. Subsequently, patient data were pseudo-anonymized and compiled into an Excel ((2016). Microsoft Excel, Redmond, WA, USA) database for analysis.

2.4. Laboratory Chemical Examinations

All laboratory values were analyzed at the University Institute for Medical-Chemical Laboratory Diagnostics at University Hospital Salzburg. HbA1c levels were measured using high-performance liquid chromatography (HPLC), which is a standard and precise method for quantifying the percentage distribution of glycosylated hemoglobin. The intra- and inter-assay coefficients of variation for all kits were found to be less than 10%. This method allows for accurate assessment of average blood glucose levels over the preceding 2–3 months. The Friedewald formula was used to calculate plasma low-density lipoprotein cholesterol (LDL-C) concentration when triglyceride levels were below 275 mg/dL. For higher triglyceride levels, the LDL particle number was assessed using the c702 module of the Roche Cobas® 8000 analyzer (Roche Diagnostics, Mannheim, Germany), adhering to the manufacturer's guidelines for measuring LDL-C levels.

2.5. Clinical Criteria of STEMI

STEMI was diagnosed based on guidelines set by the European Society of Cardiology (ESC) [11].

2.6. Categorization of Glycemic Status

Patients were categorized into three groups based on their glycemic status using the following two-step approach:

Step 1: Medical History Review

Initially, a comprehensive medical history review (anamnesis) was conducted for each patient to determine if they had a prior diagnosis of diabetes and how it was managed (diet only, oral medication, or insulin). If a patient was identified as having pre-existing diabetes, they were categorized as diabetics regardless of their current HbA1c levels.

Step 2: HbA1c Measurement

For patients without a prior diabetes diagnosis, HbA1c levels were measured and used to classify them according to the following criteria:

Non-diabetic: HbA1c $< 5.7\%$;

Prediabetic: HbA1c 5.7–6.4%;

Diabetic (new diagnosis): HbA1c $\geq 6.5\%$.

Therefore, the diagnosis of non-diabetic and prediabetic patients was based solely on the measured HbA1c at the time of the STEMI event, whereas patients with a prior diagnosis of diabetes were categorized based on their medical history, independent of their current HbA1c levels [12].

2.7. Comorbidity Identification

Obesity, chronic kidney disease (CKD), heart failure, hypertension, and dyslipidemia were defined and evaluated according to current clinical guidelines [13–16]. The conventional CKD-EPI formula was used to estimate the glomerular filtration rate (eGFR).

2.8. Statistical Analyses

Statistical analyses and data visualization were performed using SPSS Version 25 (IBM SPSS Statistics, Armonk, New York, NY, USA). The Kolmogorov–Smirnov–Lilliefors test was employed to evaluate the normality of variable distributions. Metrics exhibiting normal distribution were reported as mean ± standard deviation (SD) and analyzed using an unpaired Student's *t*-test. For metrics not following a normal distribution, data were presented as the median and interquartile range (IQR), with statistical comparisons made using the Mann–Whitney U test. Categorical variables were expressed as frequencies and percentages, with comparisons conducted using the chi-square test. Kaplan–Meier survival curves and corresponding log-rank tests were performed for both short- and long-term survival. Further analyses included calculating the area under the receiver operating characteristic (AUROC) curves for the studied HbA1c values in relation to short-term (up to 6 months) and long-term survival (up to 3 years). This also involved determining cut-off values with corresponding sensitivity, specificity, and the Youden index (YI). In this study, we utilized various *p*-values to compare the survival rates among different glycemic groups. The *p*_general value represents the overall comparison among all three groups (non-diabetic, prediabetic, and diabetic). The *p** value denotes the comparison between non-diabetic and prediabetic patients. The *p*** value signifies the comparison between non-diabetic and diabetic patients, while the *p**** value represents the comparison between prediabetic and diabetic patients. A *p*-value of $\leq$0.05 was determined as statistical significance.

3. Results

3.1. Study Population—No Diabetes, Prediabetes, and Diabetes

The study population comprised 725 patients presenting with STEMI at a single, large tertiary care center in Salzburg, Austria. These patients were systematically categorized based on their diabetes status. Initially, we screened for a history of diabetes. Of the total, 107 patients (14.8%) had a prior diabetes diagnosis. We reviewed their medical history to determine the nature of their diabetes management, identifying whether they controlled their condition through diet (n = 14, 13.1%), oral medication (n = 62, 57.9%), or insulin ± oral medication (n = 31, 29.0%). Patients falling into these categories were classified as having pre-diagnosed diabetes, regardless of their HbA1c levels.

For the remaining 618 patients (85.2%) without a known history of diabetes, we assessed their HbA1c levels to determine their glycemic status at the time of the STEMI event. Based on the HbA1c values, patients were categorized into three groups. Those with HbA1c levels below 5.7% (n = 407, 65.9%) were classified as non-diabetic, those with HbA1c levels between 5.7% and 6.4% (n = 184, 29.8%) were considered prediabetic, and those with HbA1c levels equal to or greater than 6.5% (n = 27, 4.4%) were identified as having newly diagnosed diabetes. This detailed categorization is visualized in Figure 1.

3.2. Baseline Characteristics

In this study, we analyzed the baseline characteristics (Table 1) of the following three groups: no diabetes, prediabetes, and diabetes. A demographic analysis revealed no significant gender differences among the groups. However, age distribution indicated that non-diabetic patients were generally younger, with a higher percentage under 50 years compared to their prediabetic and diabetic counterparts, with significant differences between non-diabetic and diabetic patients ($p^{**} < 0.001$) and non-diabetic and prediabetic patients ($p^{*} = 0.045$). The comparison between prediabetic and diabetic patients also showed significant differences ($p^{***} = 0.013$).

Table 1. Baseline characteristics of study cohort.

.	No Diabetes	Prediabetes	Diabetes	*p**	*p***	*p****
			***n* (%)**			
Number	407 (56.1)	184 (25.4)	134 (18.5)	-	-	-
Gender (Male)	301 (74.0)	130 (70.7)	100 (74.6)	0.403	0.878	0.434
Age						
<50 years	60 (14.7)	13 (7.1)	11 (8.2)	**0.009**	0.052	0.703
50–69 years	228 (56.0)	107 (58.2)	71 (53.0)	0.628	0.540	0.359
70–79 years	89 (21.9)	40 (21.7)	37 (27.6)	0.972	0.172	0.227
≥ 80 years	30 (7.4)	24 (13.0)	15 (11.2)	**0.027**	0.165	0.620
CVRF						
Arterial Hypertension	261 (64.1)	124 (67.4)	111 (82.8)	0.441	**<0.001**	**0.002**
Dyslipidemia	287 (70.5)	144 (78.3)	93 (69.4)	**0.050**	0.807	0.073
Smoking	256 (62.9)	113 (61.4)	74 (55.2)	0.730	0.114	0.268
BMI						
<20.0 kg/m^2	9 (2.2)	6 (3.3)	5 (3.7)	0.448	0.320	0.802
20.0–24.9 kg/m^2	137 (33.7)	47 (25.6)	19 (14.2)	**0.049**	**<0.001**	**0.013**
25.0–29.9 kg/m^2	194 (47.6)	74 (40.2)	58 (43.3)	0.096	0.352	0.628
30.0–34.9 kg/m^2	50 (12.3)	46 (25.0)	37 (27.6)	**<0.001**	**<0.001**	0.575
35.0–39.9 kg/m^2	17 (4.2)	10 (5.4)	13 (9.7)	0.491	**0.013**	0.137
>40.0 kg/m^2	0 (0.0)	1 (0.5)	2 (1.5)	0.136	**0.013**	0.380
STEMI Characteristics						
CHD–1 vessel	178 (43.7)	70 (38.0)	43 (32.1)	0.194	**0.017**	0.273
CHD–2 vessels	104 (25.6)	68 (37.0)	32 (23.9)	**0.005**	0.699	**0.013**
CHD–3 vessels	125 (30.7)	46 (25.0)	59 (44.0)	0.156	**0.005**	**<0.001**
CPR	55 (13.5)	16 (8.7)	18 (13.4)	0.095	0.981	0.177
Cardiogenic shock	62 (15.2)	18 (9.8)	28 (20.9)	0.073	0.127	**0.005**
Fibrinolysis	8 (2.0)	3 (1.6)	1 (0.7)	0.780	0.338	0.485
DES implantation	387 (95.1)	172 (93.4)	121 (90.3)	0.237	**0.028**	0.564
CABG indication	17 (4.2)	6 (3.3)	7 (5.2)	0.594	0.598	0.375
In-hospital death	8 (2.0)	7 (3.8)	10 (7.5)	0.188	**0.002**	0.152
Previous Disease						
MI	32 (7.9)	30 (16.3)	21 (15.7)	0.188	**0.008**	0.879
PCI or CABG	41 (10.1)	33 (17.9)	29 (21.6)	**0.002**	**0.001**	0.410
Heart Failure	12 (2.9)	11 (6.0)	14 (10.4)	**0.008**	**<0.001**	0.138
Renal Failure	28 (6.9)	18 (9.8)	31 (23.1)	0.078	**<0.001**	**0.001**
AF	14 (3.4)	11 (6.0)	11 (8.2)	0.223	**0.023**	0.439
Cancer	36 (8.8)	18 (9.8)	7 (5.2)	0.156	0.367	0.299
			mean ± SD			
Age (years)	61.9 ± 12.2	64.7 ± 11.8	65.7 ± 10.9	**0.010**	**0.002**	0.464
BMI (kg/m^2)	26.5 ± 3.9	27.9 ± 5.4	29.1 ± 4.8	**0.002**	**<0.001**	**0.044**
LVEF (%)	43.9 ± 8.9	42.5 ± 9.5	41.6 ± 11.3	0.086	**0.031**	0.427
			median ± IQR			
Laboratory Values						
TC (mg/dL)	185.0 ± 63.5	186.0 ± 64.0	168.0 ± 63.5	0.949	**<0.001**	**0.001**
HDL (mg/dL)	50.0 ± 18.0	48.0 ± 21.0	41.5 ± 19.3	0.057	**<0.001**	**0.002**
Non-HDL (mg/dL)	134.0 ± 61.5	133.0 ± 65.0	126.0 ± 60.8	0.513	**0.024**	**0.014**
LDL (mg/dL)	111.0 ± 57.5	111.0 ± 60.0	93.0 ± 55.0	0.814	**<0.001**	**<0.001**
Triglycerides (mg/dL)	103.0 ± 69.0	112.0 ± 81.0	143.5 ± 108.3	0.078	**<0.001**	**<0.001**
Troponin T max (ng/L)	3504.0 ± 5347.0	3417.0 ± 4919.0	3220.0 ± 6415.0	0.974	0.847	0.848
Creatinkinase max (U/L)	1475.0 ± 2252.5	1298.0 ± 2154.0	1426.0 ± 2080.0	0.841	0.515	0.664
HbA1c (%)	5.4 ± 0.3	5.8 ± 0.3	7.3 ± 1.6	**<0.001**	**<0.001**	**<0.001**

*p** No diabetes vs. prediabetes; *p*** no diabetes vs. diabetes; *p*** prediabetes vs. diabetes; CVRF: cardiovascular risk factors; BMI: body mass index; STEMI: ST-segment elevation myocardial infarction; CHD: coronary heart disease; CPR: cardiopulmonary resuscitatio; DES: drug eluting stent, CABG: coronary artery bypass graft; MI: myocardial infarction; PCI: percutaneous coronary intervention; AF: atrial fibrillation; LVEF: left ventricular ejection fraction; TC: total cholesterol; HDL: high-density lipoprotein; LDL: low-density lipoprotein.

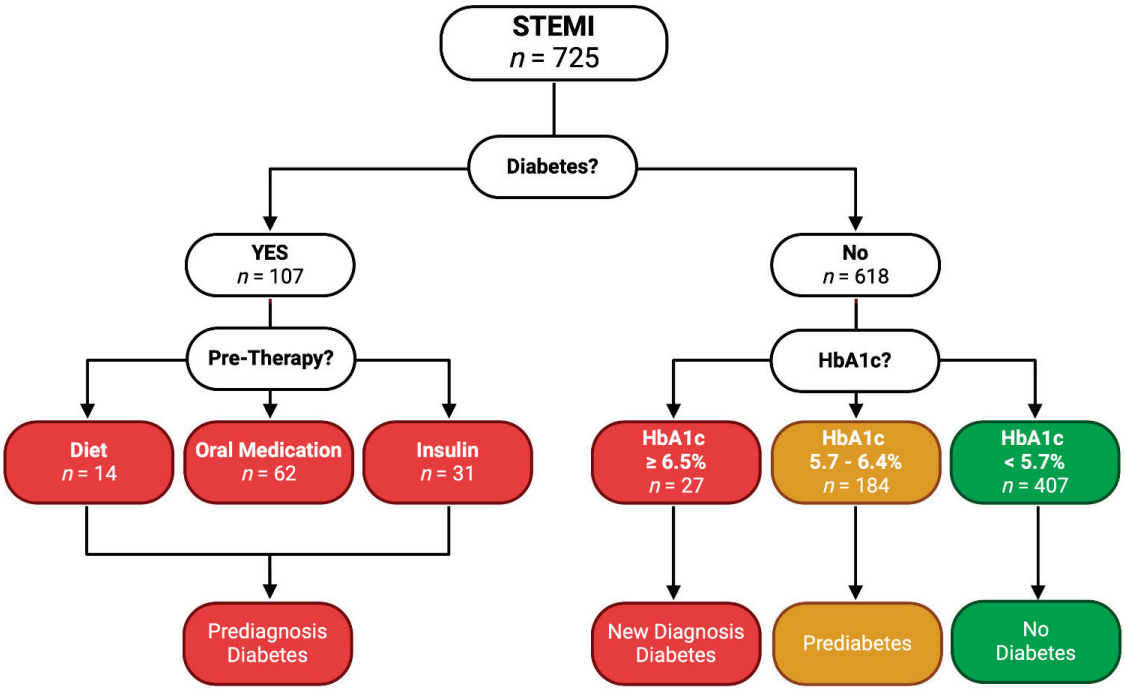


Figure 1. Flowchart of study design.

Cardiovascular risk factors showed notable variations. Arterial hypertension was more prevalent in the diabetic group (82.8%) compared to non-diabetic (64.1%, $p^{**} < 0.001$) and prediabetic (67.4%, $p^{*} = 0.034$) patients, with a significant difference also observed between prediabetic and diabetic patients ($p^{***} = 0.021$). Dyslipidemia was most common in the prediabetic group (78.3%), and smoking rates were relatively similar across all groups, though slightly lower in the diabetic group (55.2%).

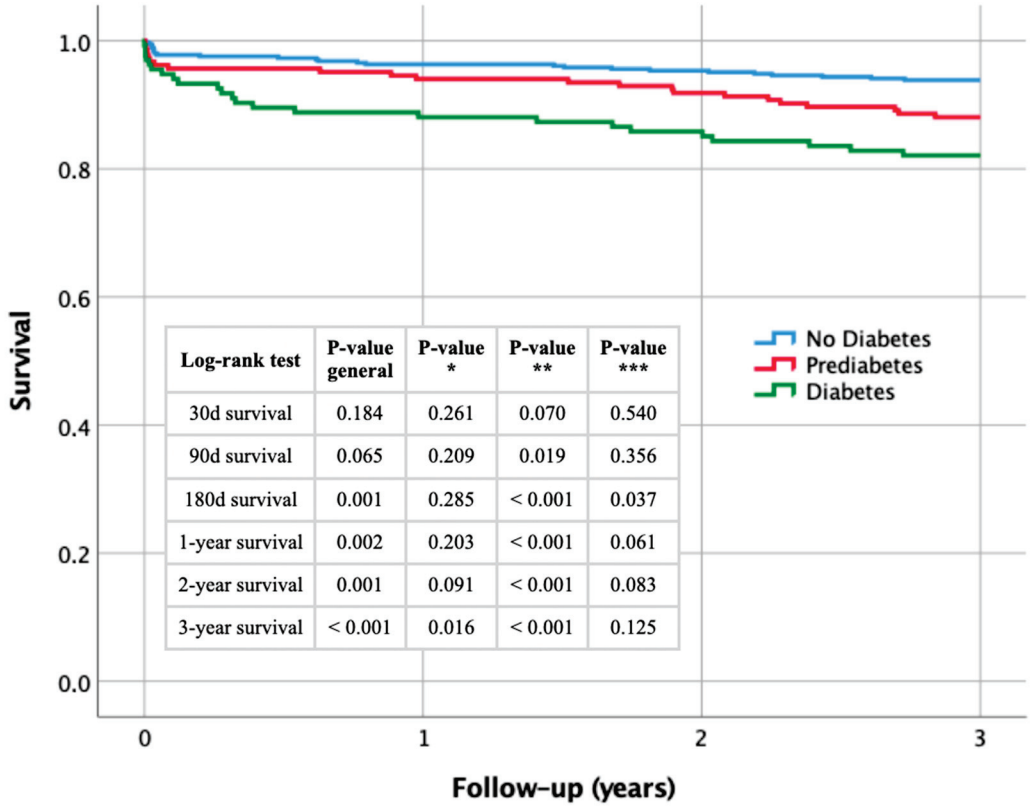
A body mass index (BMI) analysis highlighted significant differences, with diabetic patients having higher BMI values. The prevalence of obesity (BMI $\geq$ 30 kg/m^2) was particularly pronounced in the diabetic group, with 27.6% having a BMI in the 30.0–34.9 kg/m^2 range and 9.7% in the 35.0–39.9 kg/m^2 range.

Regarding STEMI characteristics, diabetic patients exhibited a higher incidence of three-vessel disease (44.0%) compared to non-diabetic (30.7%, $p^{**} < 0.001$) and prediabetic (25.0%, $p^{*} = 0.015$) patients. Cardiogenic shock was also more common in the diabetic group (20.9%). Laboratory values further illustrated significant variations, particularly in glycemic control markers. Lipid profiles indicated lower high-density lipoprotein cholesterol (HDL) and higher triglyceride levels in diabetic patients.

3.3. Kaplan–Meier Curves—No Diabetes, Prediabetes, and Diabetes

Figure 2 presents Kaplan–Meier survival curves for the study population stratified by glycemic status (non-diabetic, prediabetic, and diabetic) over a three-year period following STEMI. Survival rates were analyzed at 30 days, 90 days, 180 days, 1 year, 2 years, and 3 years.

At 30 days, survival rates did not significantly differ between the groups (log-rank $p = 0.184$). By 90 days, survival rates showed a trend toward significance (log-rank $p = 0.065$), with a significant difference between non-diabetic and diabetic patients ($p^{**} = 0.019$). At 180 days, differences became more pronounced (log-rank $p = 0.001$), with significant disparities between non-diabetic and diabetic ($p^{**} < 0.001$) and prediabetic and diabetic patients ($p^{***} = 0.037$).



Log-rank test	P-value general	P-value *	P-value **	P-value ***
30d survival	0.184	0.261	0.070	0.540
90d survival	0.065	0.209	0.019	0.356
180d survival	0.001	0.285	< 0.001	0.037
1-year survival	0.002	0.203	< 0.001	0.061
2-year survival	0.001	0.091	< 0.001	0.083
3-year survival	< 0.001	0.016	< 0.001	0.125

Number at Risk	0 days	30 days	90 days	180 days	1 years	2 years	3 years
No Diabetes	407	398	397	396	392	388	382
Prediabetes	184	177	176	176	173	169	162
Diabetes	134	127	125	120	118	115	110
Overall	725	702	698	692	683	672	654

Figure 2. Kaplan–Meier survival analysis with corresponding numbers at risk and log-rank tests for detection of short- and long-term mortality regarding glycemic status in STEMI patients. *p** No diabetes vs. prediabetes; *p*** no diabetes vs. diabetes; *p**** prediabetes vs. diabetes.

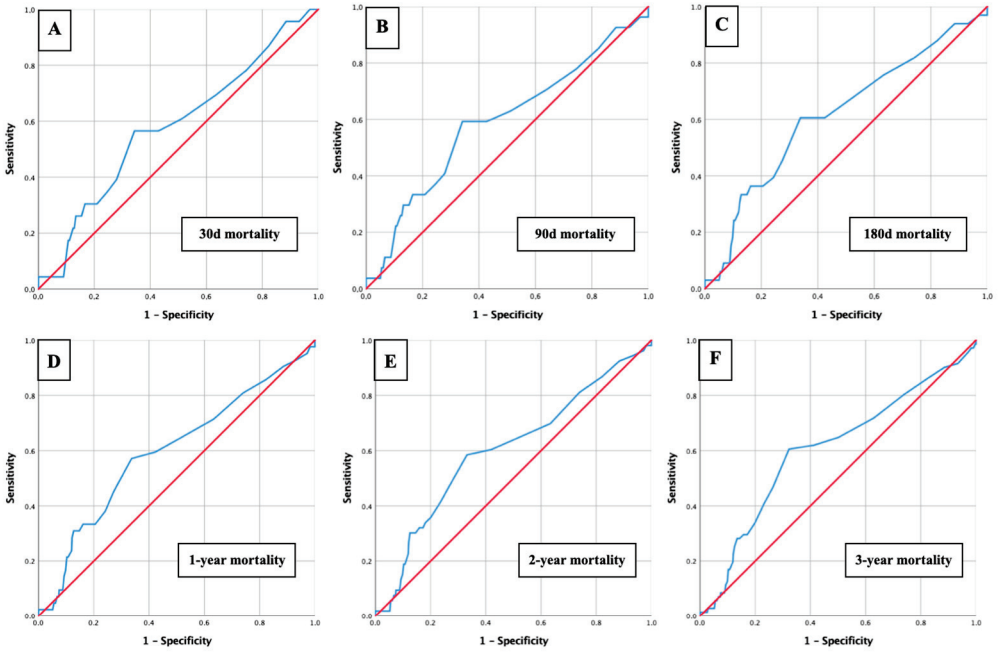
A one-year survival analysis showed significant differences (log-rank $p = 0.002$), mainly between non-diabetic and diabetic patients ($p^{**} < 0.001$), with prediabetic vs. diabetic comparisons nearing significance ($p^{***} = 0.061$). At two years, significant differences persisted (log-rank $p = 0.001$), with notable differences between non-diabetic and diabetic ($p^{**} < 0.001$), and prediabetic and diabetic patients ($p^{***} = 0.083$).

At three years, survival rates diverged significantly (log-rank $p < 0.001$), highlighting the impact of diabetes on long-term survival. The non-diabetic vs. diabetic ($p^{**} < 0.001$) and prediabetic vs. diabetic ($p^{***} = 0.125$) comparisons underscored the risk. The non-diabetic vs. prediabetic comparison also became significant ($p^{*} = 0.016$), indicating substantial long-term risks for prediabetic patients.

3.4. AUROC Analysis of HbA1c for Predicting Mortality

Figure 3 illustrates the AUROC analysis for HbA1c as a predictor of mortality at various time intervals, as follows: 30 days, 90 days, 180 days, 1 year, 2 years, and 3 years post-STEMI. The analysis shows that HbA1c has a moderate predictive power for mortality, with AUROC values improving slightly over longer follow-up periods. A HbA1c cut-off value of 5.75%, and therefore prediabetic glycemic status, was consistently identified as relevant across all time frames, demonstrating sensitivities between 57 and 61% and

specificities between 66 and 68%. This highlights the utility of HbA1c in identifying patients at increased risk of mortality following STEMI.



	Value	Prediction	AUC	95%CI	P-value	Cut-off	Sensitivity	Specificity	Youden Index
A	HbA1c (%)	30d mortality	0.580	0.458 — 0.701	0.193	5.75	0.57	0.66	0.22
B	HbA1c (%)	90d mortality	0.590	0.472 — 0.709	0.112	5.75	0.59	0.66	0.25
C	HbA1c (%)	180d mortality	0.617	0.514 — 0.721	0.023	5.75	0.61	0.66	0.27
D	HbA1c (%)	1-year mortality	0.597	0.503 — 0.691	0.035	5.75	0.57	0.66	0.23
E	HbA1c (%)	2-year mortality	0.603	0.519 — 0.687	0.012	5.75	0.59	0.67	0.25
F	HbA1c (%)	3-year mortality	0.603	0.530 — 0.677	0.004	5.75	0.61	0.68	0.28

Figure 3. Area Under the Receiver Operating Characteristic (AUROC) analysis of HbA1c with corresponding cut-off values, sensitivity, specificity, and Youden index for short- and long-term mortality in patients with STEMI (Panel (**A**): 30d mortality; Panel (**B**): 90d mortality; Panel (**C**): 180d mortality; Panel (**D**): 1-year mortality; Panel (**E**): 2-year mortali-ty; Panel (**F**): 3-year mortality).

3.5. Study Population—No Diabetes, Prediabetes, and Diabetes with Further Cardiovascular Risk Factors

Figure 4 presents a comprehensive flowchart that illustrates the distribution of 725 patients diagnosed with STEMI, categorized by their glycemic status and associated comorbid conditions.

Among the total number of STEMI patients classified as having no diabetes, 64.1% (n = 261) suffered from hypertension, with 59.4% (n = 155) of these hypertensive patients receiving pretreatment. Additionally, 62.9% (n = 256) were smokers. Furthermore, 70.5% (n = 287) of non-diabetic patients had dyslipidemia, and 15.7% (n = 45) of these dyslipidemic patients were pretreated.

Within the prediabetic subgroup, 67.4% (n = 124) exhibited hypertension, and 62.9% (n = 78) of those hypertensive patients had been pretreated. With respect to smoking, 61.4% (n = 113) of prediabetic patients were smokers. Regarding dyslipidemia, 78.3% (n = 144) of prediabetic patients had this condition and 24.3% (n = 35) were pretreated.

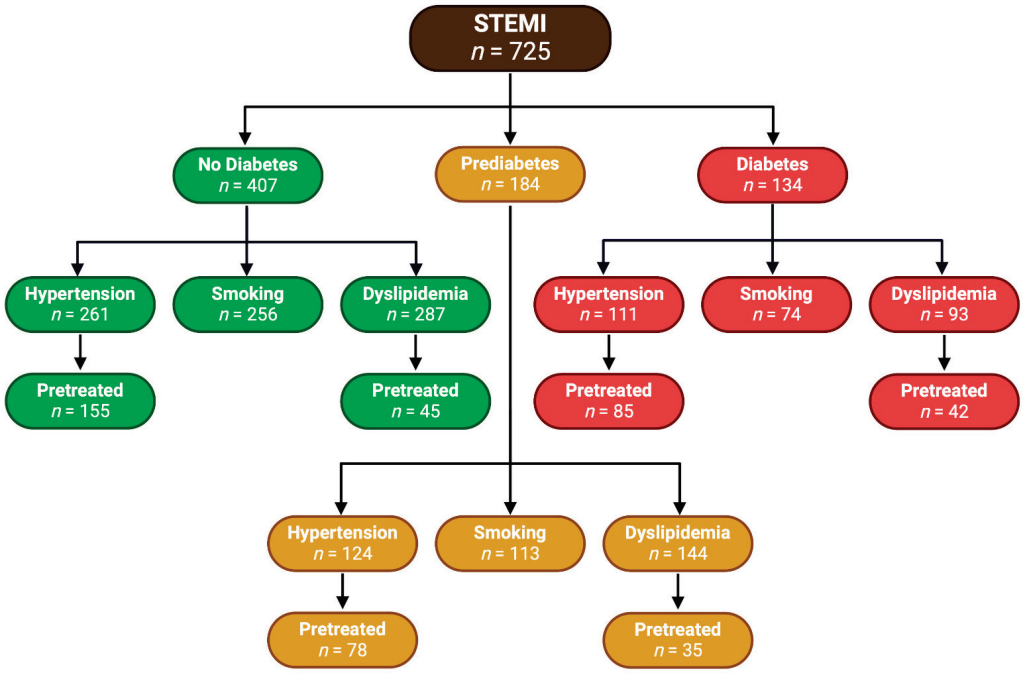


Figure 4. Glycemic status and further cardiovascular risk factor distribution of study cohort.

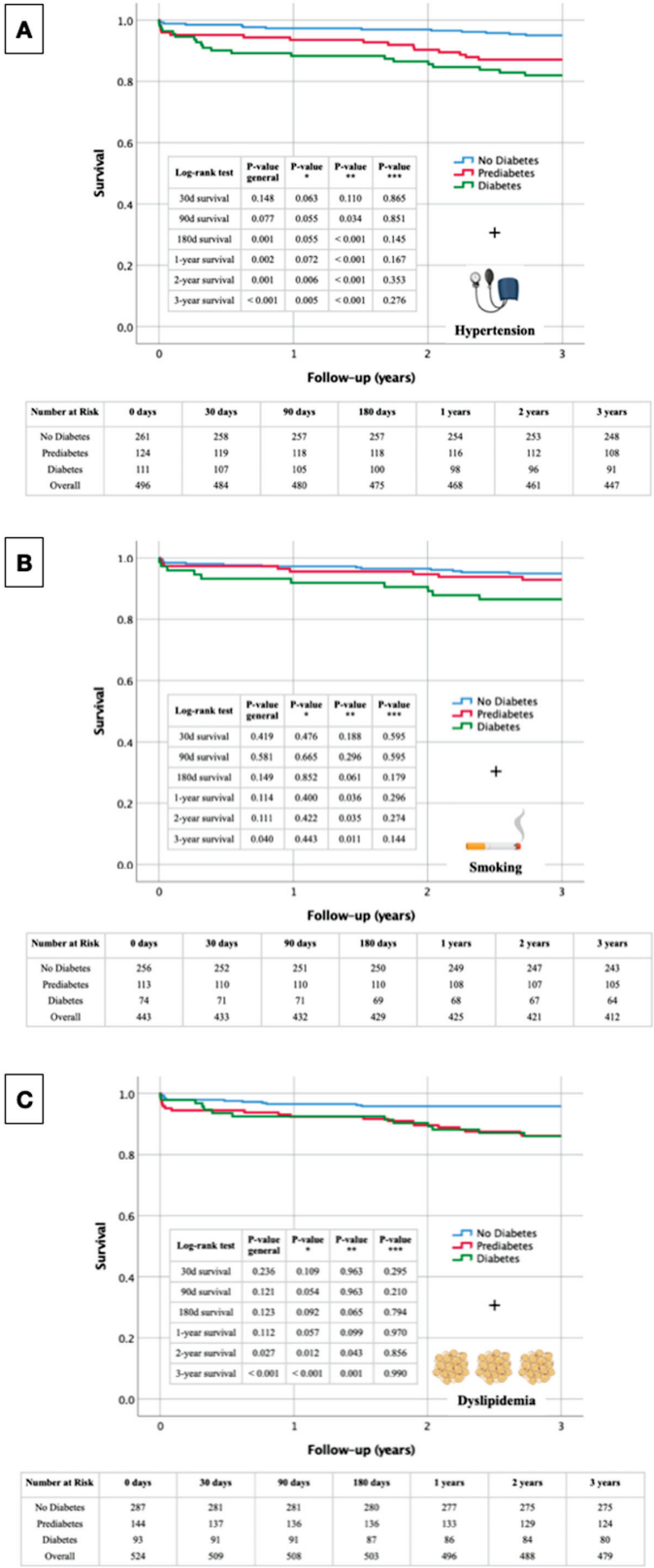
The diabetic group included 82.8% (n = 111) of patients with hypertension, with 76.6% (n = 85) of these hypertensive patients being pretreated. Additionally, 54.8% (n = 74) were smokers. Regarding dyslipidemia, 69.4% (n = 93) of diabetic patients were affected, with 45.2% (n = 42) being pretreated.

3.6. Kaplan–Meier Curves—No Diabetes, Prediabetes, and Diabetes with Further Cardiovascular Risk Factors

The following Kaplan–Meier survival curves presented in Figure 5 illustrate the overall survival of STEMI patients, stratified by glycemic status (no diabetes, prediabetes, and diabetes) in conjunction with the presence of arterial hypertension (Figure 5A), smoking (Figure 5B), and dyslipidemia (Figure 5C). Key survival probabilities with respective p-values at specific time points (30 days, 90 days, 180 days, 1 year, 2 years, and 3 years) highlight the significance of differences in survival among the groups. Each figure also includes a tabular overview of the numbers at risk at these specific time points, providing a comprehensive view of the patient population throughout the study period.

3.6.1. Glycemic Status + Arterial Hypertension

The Kaplan–Meier survival curve in Figure 5A shows significant differences in survival rates among non-diabetic, prediabetic, and diabetic STEMI patients over three years, with arterial hypertension as a stratifying factor. At 30 days, survival differences were not significant overall (p_general = 0.148), although a trend toward lower survival in diabetic patients was observed (p^* = 0.063). By 90 days, differences approached significance (p_general = 0.077), with significantly lower survival in diabetic patients compared to non-diabetic patients (p^{**} = 0.034). At 180 days, significant differences were evident (p_general = 0.001), particularly between non-diabetic and diabetic patients (p^{**} < 0.001). A one-year survival analysis revealed significant disparities (p_general = 0.002), with diabetic patients showing worse outcomes (p^{**} < 0.001). By two years, the differences remained significant (p_general = 0.001), with poorer survival in diabetic patients compared to non-diabetic (p^{**} < 0.001) and prediabetic patients (p^* = 0.006). At three years, the survival disparities were highly significant (p_general < 0.001), with diabetic patients continuing to show the lowest survival rates (p^{**} < 0.001) and significant differences observed between non-diabetic and prediabetic patients (p^* = 0.005).



Log-rank test	P-value general	P-value *	P-value **	P-value ***
30d survival	0.148	0.063	0.110	0.865
90d survival	0.077	0.055	0.034	0.851
180d survival	0.001	0.055	< 0.001	0.145
1-year survival	0.002	0.072	< 0.001	0.167
2-year survival	0.001	0.006	< 0.001	0.353
3-year survival	< 0.001	0.005	< 0.001	0.276

Number at Risk	0 days	30 days	90 days	180 days	1 years	2 years	3 years
No Diabetes	261	258	257	257	254	253	248
Prediabetes	124	119	118	118	116	112	108
Diabetes	111	107	105	100	98	96	91
Overall	496	484	480	475	468	461	447

Log-rank test	P-value general	P-value *	P-value **	P-value ***
30d survival	0.419	0.476	0.188	0.595
90d survival	0.581	0.665	0.296	0.595
180d survival	0.149	0.852	0.061	0.179
1-year survival	0.114	0.400	0.036	0.296
2-year survival	0.111	0.422	0.035	0.274
3-year survival	0.040	0.443	0.011	0.144

Number at Risk	0 days	30 days	90 days	180 days	1 years	2 years	3 years
No Diabetes	256	252	251	250	249	247	243
Prediabetes	113	110	110	110	108	107	105
Diabetes	74	71	71	69	68	67	64
Overall	443	433	432	429	425	421	412

Log-rank test	P-value general	P-value *	P-value **	P-value ***
30d survival	0.236	0.109	0.963	0.295
90d survival	0.121	0.054	0.963	0.210
180d survival	0.123	0.092	0.065	0.794
1-year survival	0.112	0.057	0.099	0.970
2-year survival	0.027	0.012	0.043	0.856
3-year survival	< 0.001	< 0.001	0.001	0.990

Number at Risk	0 days	30 days	90 days	180 days	1 years	2 years	3 years
No Diabetes	287	281	281	280	277	275	275
Prediabetes	144	137	136	136	133	129	124
Diabetes	93	91	91	87	86	84	80
Overall	524	509	508	503	496	488	479

Figure 5. Kaplan–Meier survival analysis with corresponding numbers at risk and log-rank tests for detection of short- and long-term mortality regarding glycemic status and several cardiovascular risk factors in STEMI patients (Panel (**A**): Glycemic status and arterial hypertension; Panel (**B**): Glycemic status and smoking; Panel (**C**): Glycemic status and dyslipidemia). *p** No diabetes vs. prediabetes; *p*** no diabetes vs. diabetes; *p**** prediabetes vs. diabetes.

3.6.2. Glycemic Status + Smoking

The Kaplan–Meier survival curves for STEMI patients show significant differences based on glycemic status and smoking over three years (Figure 5B). At 30 days, no significant survival differences were observed (p_general = 0.419). By 90 days, the survival differences remained non-significant overall (p_general = 0.581). At 180 days, the differences approached significance (p_general = 0.149), with a notable trend between non-diabetic and diabetic patients (p^{**} = 0.061). A one-year analysis showed significant differences, with diabetic patients having worse survival compared to non-diabetic patients (p^{**} = 0.036). Two-year survival differences remained significant between non-diabetic and diabetic patients (p^{**} = 0.035), with overall differences nearing significance (p_general = 0.111). By three years, significant survival disparities were observed (p_general = 0.040), especially between non-diabetic and diabetic patients (p^{**} = 0.011).

3.6.3. Glycemic Status + Dyslipidemia

The Kaplan–Meier survival curves for STEMI patients, stratified by glycemic status and dyslipidemia, reveal significant differences in survival rates over three years (Figure 5C). At 30 days, survival differences were not significant (p_general = 0.236), with non-significant comparisons between the different groups. By 90 days, overall survival differences remained non-significant (p_general = 0.121), although the difference between non-diabetic and prediabetic patients approached significance (p^{*} = 0.054). At 180 days, the survival differences approached significance overall (p_general = 0.123), again with a notable trend between non-diabetic and diabetic patients (p^{**} = 0.065). A one-year survival analysis indicated a trend toward significant differences (p_general = 0.112), particularly between non-diabetic and prediabetic patients (p^{*} = 0.057). By two years, significant survival differences emerged overall (p_general = 0.027), with significant differences between non-diabetic and prediabetic patients (p^{*} = 0.012) and non-diabetic and diabetic patients (p^{**} = 0.043). At three years, survival disparities were highly significant (p_general < 0.001), especially between non-diabetic and prediabetic patients (p^{*} < 0.001) and non-diabetic and diabetic patients (p^{**} = 0.001).

4. Discussion

4.1. The Overlooked Risk in Prediabetic Patients

This study highlights the following critical and often overlooked aspect of cardiovascular care on long-term survival following acute STEMI: the substantial risk faced by prediabetic patients, a group that is frequently underdiagnosed and undertreated. Our findings reveal that prediabetic individuals presenting with STEMI exhibit survival outcomes that are markedly worse than those of their non-diabetic counterparts and, in some cases, approach the poor outcomes observed in diabetic patients. This raises the following urgent question for the medical community: are we doing enough for prediabetic patients?

4.2. Baseline Characteristics and Cardiovascular Risk

The baseline characteristics of our cohort underscore the increasing prevalence of dysglycemia among patients with cardiovascular disease. Prediabetic patients, while not yet reaching the glycemic thresholds for a diabetes diagnosis, exhibited significant cardiovascular risk factors, such as arterial hypertension and dyslipidemia [17], and are medically underserved [18]. These risk factors were present at levels intermediate between those observed in non-diabetic and diabetic patients, suggesting a continuum of risk that starts well before the onset of overt diabetes [19,20].

4.3. Kaplan–Meier Survival Analysis: A Wake-Up Call

The Kaplan–Meier survival curves vividly illustrate the neglected plight of prediabetic patients. While the immediate post-STEMI survival (30 days) was comparable across all groups, as also described in Tian et al. [21], the divergence in survival rates became pronounced with longer follow-ups. By 90 days and 180 days, prediabetic patients began to

show significantly worse survival outcomes, and this trend continued to worsen over one, two, and three years. By the three-year mark, prediabetic patients faced a survival disadvantage nearly as severe as that faced by diabetic patients, particularly when considering the compounded effects of other cardiovascular risk factors, such as arterial hypertension and dyslipidemia. These findings are consistent with those of Xu et al. [17,22], who also reported that prediabetes was associated with worse long-term outcomes in young patients $\leq$ 45 years of age with acute coronary syndrome. Another point worth discussing is the proportion of STEMI patients with complete revascularization. Unfortunately, it is not possible to assess the contribution of this factor to the survival rate of prediabetic patients compared to diabetic patients.

4.4. Better Management of Diabetes and Cardiovascular Risk Factors (Before or after STEMI)

This study also highlights the importance of better management of diabetes, particularly concerning additional cardiovascular risk factors, such as hypertension and dyslipidemia, as risk-based atherosclerotic cardiovascular disease (ASCVD) prevention deficits were observed in patients with diabetes and prediabetes at the time of presentation for STEMI. The effective treatment of diabetes, including optimal control of blood pressure and lipid levels, has been shown to significantly reduce cardiovascular events and improve survival outcomes [17,23]. This comprehensive approach to managing diabetes could serve as a model for treating prediabetic patients, addressing not only glycemic control but also the broader spectrum of cardiovascular risk factors. By adopting a holistic approach that addresses these additional risk factors, healthcare providers can significantly enhance patient outcomes and reduce the burden of cardiovascular disease in both prediabetic and diabetic populations.

4.5. The Imperative for Change: Treating Prediabetes

Our findings compel a re-evaluation of current clinical practices and treatment guidelines. The data clearly indicate that prediabetic patients are not merely in a transitional state but are at a critical juncture, at which early intervention could significantly alter their cardiovascular outcomes. Currently, the standard of care predominantly focuses on the treatment and management of diabetes, with prediabetic patients often receiving minimal intervention. Indeed, the ESC Guidelines for the Management of Hyperlipidemia, for example, recognized diabetes mellitus I and II patients as those at high or very high risk for fatal 10-year cardiovascular disease (CVD), depending on the constellation of further risk factors, including hypertension, hyperlipidemia, smoking status, and duration of diabetes; however, prediabetes is not yet found in higher risk categories [16,24]. This oversight places prediabetic patients at a disproportionate risk, as evidenced by their survival rates in this study. Similar concerns were highlighted by Kim et al. [25], who found that prediabetic patients with STEMI and multivessel disease had worse clinical outcomes compared to non-diabetic patients, underscoring the need for more aggressive management in this population.

4.6. A Call to Action: Revolutionizing Prediabetes Management

The evidence presented necessitates a paradigm shift in how we approach prediabetes. It is imperative that we extend rigorous cardiovascular risk management strategies to prediabetic patients, similar to those employed for diabetic patients [26]. This includes aggressive monitoring (HbA1c, fasting glucose, oral glucose tolerance test), lifestyle interventions, and, potentially, pharmacological treatments aimed at controlling glycemic levels, blood pressure, and lipid profiles. The integration of prediabetic management into routine cardiovascular care could be transformative, while there are controversial findings regarding the inconclusive impact of the agents, which are widely used in prediabetes/diabetes mellitus type II, i.e., Sodium-glucose cotransporter 2 (SGLT-2) inhibitors, on the clinical course of STEMI [27]. The proactive treatment of prediabetes has the potential to prevent the progression to diabetes and mitigate the associated cardiovascular risks [28]. The estab-

lishment of comprehensive prediabetes management programs could reduce the incidence of STEMI and improve long-term survival outcomes for this vulnerable population.

5. Limitation

This study has several limitations that must be considered when interpreting the results.

Firstly, the single-center retrospective design may limit the generalizability of our findings to other populations and healthcare settings.

Secondly, the classification of glycemic status was based on a single HbA1c measurement, which may not capture fluctuations in glycemic control over time. Current guidelines recommend conducting more than one test to confirm the diagnosis, and using only a single measurement may lead to misclassification, thereby impacting this study's validity. Misclassification can obscure the true prevalence of prediabetes and its associated risks, potentially skewing the results and conclusions drawn.

Thirdly, potential confounding factors, such as variations in treatment regimens and patient adherence to medication and lifestyle modifications, were not addressed during the follow-up period. Yet, we did not evaluate the impact of several confounding factors, such as atrial fibrillation and the severity of atherosclerosis, left ventricular hypertrophy (LVH), and heart failure and its phenotypes, which had been previously defined as powerful predictors for all-cause and cardiovascular (CV) mortality in STEMI, on the risk of the STEMI-related outcomes.

Fourthly, the follow-up period, although extending to three years, may still be insufficient to fully capture the long-term impact of prediabetes on survival outcomes post-STEMI. Future multi-center studies with longer follow-up periods and more comprehensive assessments of glycemic control and cardiovascular risk factors are warranted to validate and extend our findings for post-STEMI patients, as well as other patient populations, in secondary and primary cardiovascular prevention.

6. Conclusions

In conclusion, this study highlights the critical need to reconsider our approach to cardiovascular risk management by prioritizing prediabetic patients. The significant survival disparities identified through a Kaplan–Meier analysis underscore the importance of early intervention in prediabetic individuals with STEMI. While the findings suggest that treating prediabetes with comparable seriousness to diabetes may be associated with improved patient outcomes, further validation through more robust data analysis is necessary to substantiate these claims.

To optimize care, we propose exploring multi-marker strategies (HbA1c, fasting glucose, oral glucose tolerance test) that could enhance the predictive value of interventions. Additionally, a more comprehensive discussion on the value of HbA1c as a predictive measure for mortality is warranted, particularly in light of its moderate predictive power observed in the AUROC analysis.

As we move forward, it is crucial to evolve our clinical practices to ensure that prediabetic STEMI patients receive the comprehensive management they require, ultimately recognizing them as a high-risk group deserving of focused attention.

Author Contributions: Conceptualization E.B. and K.L.K.; statistical analysis E.B.; writing—original draft preparation E.B. and K.L.K.; writing—review and editing A.E.B., M.L., M.H. and U.C.H.; data collection E.B. and K.L.K.; implementation of interventions C.S., E.P., M.C.B., W.W., M.H. and U.C.H.; project administration M.L., U.C.H. and K.L.K.; language correction K.L.K. All authors have read and agreed to the published version of the manuscript.

Funding: This research received no external funding.

Institutional Review Board Statement: This study was conducted in accordance with the Declaration of Helsinki and approved by the State of Salzburg Ethics Commission (EK-Nr. 1038/2021), approval on the 13 April 2021.

Informed Consent Statement: Patient consent was waived due to the retrospective nature of the study design.

Data Availability Statement: The raw data supporting the conclusions of this article will be made available by the authors on request.

Acknowledgments: The graphical abstract, Figure 1, and Figure 4 were created with BioRender.com. Selected artwork shown in Figure 5 was also developed using BioRender.com.

Conflicts of Interest: The authors declare that the research was conducted in the absence of any commercial or financial relationships that could be constructed as a potential conflict of interest.

References

1. Elendu, C.; Amaechi, D.C.; Elendu, T.C.; Omeludike, E.K.; Alakwe-Ojimba, C.E.; Obidigbo, B.; Akpovona, O.L.M.; Sucari, Y.P.O.; Saggi, S.K.; Dang, K.; et al. Comprehensive review of ST-segment elevation myocardial infarction: Understanding pathophysiology, diagnostic strategies, and current treatment approaches. *Medicine* **2023**, *102*, e35687. [CrossRef] [PubMed]
2. Gao, J.; Wang, Y.; Yang, Y.N.; Wu, X.Y.; Cui, Y.; Zou, Z.H.; Cui, Z.; Liu, Y. Impact of Metabolic Syndrome and Its Components on Clinical Severity and Long-Term Prognosis in Patients with Premature Myocardial Infarction. *Front. Endocrinol.* **2022**, *13*, 920470. [CrossRef] [PubMed]
3. Chatzianagnostou, K.; Guiducci, L.; Paradossi, U.; De Caterina, A.R.; Mazzone, A.; Berti, S.; Vassalle, C. The Role of Prediabetes as a Predictive Factor for the Outcomes in Patients with STEMI. Which Is the Right Range of Glycated Hemoglobin to Adopt in This Setting? *Appl. Sci.* **2021**, *11*, 5518. [CrossRef]
4. Mata Marín, L.A.; Schmucker, J.; Fach, A.; Osteresch, R.; Rühle, S.; Garstka, D.; Eitel, I.; Hambrecht, R.; Wienbergen, H. Prevalence and clinical characteristics of prediabetes and diabetes mellitus in young patients with ST-segment elevation myocardial infarction. *Clin. Res. Cardiol.* **2021**, *110*, 1647–1658. [CrossRef]
5. Bansal, N. Prediabetes diagnosis and treatment: A review. *World J. Diabetes* **2015**, *6*, 296–303. [CrossRef] [PubMed]
6. Brannick, B.; Dagogo-Jack, S. Prediabetes and Cardiovascular Disease: Pathophysiology and Interventions for Prevention and Risk Reduction. *Endocrinol. Metab. Clin. N. Am.* **2018**, *47*, 33–50. [CrossRef]
7. Mutie, P.M.; Pomares-Millan, H.; Atabaki-Pasdar, N.; Jordan, N.; Adams, R.; Daly, N.L.; Tajes, J.F.; Giordano, G.N.; Franks, P.W. An investigation of causal relationships between prediabetes and vascular complications. *Nat. Commun.* **2020**, *11*, 4592; Erratum in *Nat. Commun.* **2021**, *12*, 202. [CrossRef] [PubMed]
8. Mando, R.; Waheed, M.; Michel, A.; Karabon, P.; Halalau, A. Prediabetes as a risk factor for major adverse cardiovascular events. *Ann. Med.* **2021**, *53*, 2090–2098. [CrossRef]
9. Zhang, J.; Du, Y.; Hu, C.; Liu, Y.; Liu, J.; Gao, A.; Zhao, Y.; Zhou, Y. Elevated Glycated Albumin in Serum Is Associated with Adverse Cardiac Outcomes in Patients with Acute Coronary Syndrome Who Underwent Revascularization Therapy. *J. Atheroscler. Thromb.* **2022**, *29*, 482–491. [CrossRef]
10. Alvarez, S.; Coffey, R.; Mathias, P.M.; Algotar, A.M. Prediabetes. In *StatPearls*; StatPearls Publishing: Treasure Island, FL, USA, 2023.
11. Byrne, R.A.; Rossello, X.; Coughlan, J.J.; Barbato, E.; Berry, C.; Chieffo, A.; Claeys, M.J.; Dan, G.-A.; Dweck, M.R.; Galbraith, M.; et al. 2023 ESC Guidelines for the management of acute coronary syndromes. *Eur. Heart J.* **2023**, *44*, 3720–3826; Erratum in *Eur. Heart J.* **2024**, *45*, 1145. [CrossRef] [PubMed]
12. American Diabetes Association Professional Practice Committee. 2. Classification and Diagnosis of Diabetes: Standards of Medical Care in Diabetes-2022. *Diabetes Care* **2022**, *45*, S17–S38. [CrossRef] [PubMed]
13. Lameire, N.H.; Levin, A.; Kellum, J.A.; Cheung, M.; Jadoul, M.; Winkelmayer, W.C.; Stevens, P.E.; Caskey, F.J.; Farmer, C.K.; Fuentes, A.F.; et al. Harmonizing acute and chronic kidney disease definition and classification: Report of a Kidney Disease: Improving Global Outcomes (KDIGO) Consensus Conference. *Kidney Int.* **2021**, *100*, 516–526. [CrossRef] [PubMed]
14. McDonagh, T.A.; Metra, M.; Adamo, M.; Gardner, R.S.; Baumbach, A.; Böhm, M.; Burri, H.; Butler, J.; Čelutkienė, J.; Chioncel, O.; et al. 2021 ESC Guidelines for the diagnosis and treatment of acute and chronic heart failure. *Eur. Heart J.* **2021**, *42*, 3599–3726, Erratum in *Eur. Heart J.* **2021**, *42*, 4901. [CrossRef] [PubMed]
15. Mancia, G.; Kreutz, R.; Brunström, M.; Burnier, M.; Grassi, G.; Januszewicz, A.; Muiesan, M.L.; Tsioufis, K.; Agabiti-Rosei, E.; Algharably, E.A.E.; et al. 2023 ESH Guidelines for the management of arterial hypertension The Task Force for the management of arterial hypertension of the European Society of Hypertension: Endorsed by the International Society of Hypertension (ISH) and the European Renal Association (ERA). *J. Hypertens.* **2023**, *41*, 1874–2071, Erratum in *J. Hypertens.* **2024**, *42*, 194.
16. Mach, F.; Baigent, C.; Catapano, A.L.; Koskinas, K.C.; Casula, M.; Badimon, L.; Chapman, M.J.; De Backer, G.G.; Delgado, V.; A Ference, B.; et al. 2019 ESC/EAS Guidelines for the management of dyslipidaemias: Lipid modification to reduce cardiovascular risk. *Eur. Heart J.* **2020**, *41*, 111–188, Erratum in *Eur. Heart J.* **2020**, *41*, 4255. [CrossRef] [PubMed]
17. Kalyani, R.R.; Everett, B.M.; Perreault, L.; Michos, E.D. Heart Disease and Diabetes. In *Diabetes in America*; Lawrence, J.M., Casagrande, S.S., Herman, W.H., Wexler, D.J., Cefalu, W.T., Eds.; National Institute of Diabetes and Digestive and Kidney Diseases (NIDDK): Bethesda, MD, USA, 2023.

18. Ostrominski, J.W.; Vaduganathan, M.; Girish, M.P.; Gupta, P.; Hendrickson, M.J.; Qamar, A.; Arora, S.; Pandey, A.; Bansal, A.; Batra, V.; et al. Missed Opportunities for Screening and Management of Dysglycemia among Patients Presenting with Acute Myocardial Infarction in North India: The Prospective NORIN STEMI Registry. *Glob. Hear.* **2022**, *17*, 54. [CrossRef] [PubMed]
19. Nanavaty, D.; Green, R.; Sanghvi, A.; Sinha, R.; Singh, S.; Mishra, T.; Devarakonda, P.; Bell, K.; Rodriguez, C.A.; Gambhir, K.; et al. Prediabetes is an incremental risk factor for adverse cardiac events: A nationwide analysis. *Atheroscler. Plus* **2023**, *54*, 22–26. [CrossRef] [PubMed]
20. Cai, X.; Zhang, Y.; Li, M.; Wu, J.H.; Mai, L.; Li, J.; Yang, Y.; Hu, Y.; Huang, Y. Association between prediabetes and risk of all cause mortality and cardiovascular disease: Updated meta-analysis. *BMJ* **2020**, *370*, m2297. [CrossRef]
21. Tian, L.; Zhu, J.; Liu, L.; Liang, Y.; Li, J.; Yang, Y. Prediabetes and short-term outcomes in nondiabetic patients after acute ST-elevation myocardial infarction. *Cardiology.* **2014**, *127*, 55–61. [CrossRef] [PubMed]
22. Xu, R.; Wang, C.; Lang, J.; Wu, J.; Hu, Y.; Wang, T.; Zhang, J.; Cong, H.; Wang, L. Prediabetes is Associated with Worse Long-Term Outcomes in Young Patients with Acute Coronary Syndrome. *Diabetes Metab. Syndr. Obes.* **2023**, *16*, 3213–3222. [CrossRef]
23. Joseph, J.J.; Deedwania, P.; Acharya, T.; Aguilar, D.; Bhatt, D.L.; Chyun, D.A.; Di Palo, K.E.; Golden, S.H.; Sperling, L.S. Comprehensive Management of Cardiovascular Risk Factors for Adults With Type 2 Diabetes: A Scientific Statement From the American Heart Association. *Circulation* **2022**, *145*, e722–e759. [CrossRef] [PubMed]
24. Catapano, A.L.; Graham, I.; De Backer, G.; Wiklund, O.; Chapman, M.J.; Drexel, H.; Hoes, A.W.; Jennings, C.S.; Landmesser, U.; Pedersen, T.R.; et al. 2016 ESC/EAS Guidelines for the Management of Dyslipidaemias. *Eur. Heart J.* **2016**, *37*, 2999–3058. [CrossRef]
25. Kim, Y.H.; Her, A.Y.; Jeong, M.H.; Kim, B.K.; Hong, S.J.; Kim, S.; Ahn, C.-M.; Kim, J.-S.; Ko, Y.-G.; Choi, D.; et al. Two-Year Clinical Outcomes Between Prediabetic and Diabetic Patients With STEMI and Multivessel Disease Who Underwent Successful PCI Using Drug-Eluting Stents. *Angiology* **2021**, *72*, 50–61. [CrossRef]
26. Færch, K.; Vistisen, D.; Johansen, N.B.; Jørgensen, M.E. Cardiovascular risk stratification and management in pre-diabetes. *Curr. Diabetes Rep.* **2014**, *14*, 493. [CrossRef] [PubMed]
27. von Lewinski, D.; Kolesnik, E.; Tripolt, N.J.; Pferschy, P.N.; Bendedikt, M.; Wallner, M.; Alber, H.; Berger, R.; Lichtenauer, M.; Saely, C.H.; et al. Empagliflozin in acute myocardial infarction: The EMMY trial. *Eur. Heart J.* **2022**, *43*, 4421–4432. [CrossRef]
28. Lizarzaburu-Robles, J.C.; Herman, W.H.; Garro-Mendiola, A.; Galdón Sanz-Pastor, A.; Lorenzo, O. Prediabetes and Cardiometabolic Risk: The Need for Improved Diagnostic Strategies and Treatment to Prevent Diabetes and Cardiovascular Disease. *Biomedicines* **2024**, *12*, 363. [CrossRef] [PubMed]

Disclaimer/Publisher's Note: The statements, opinions and data contained in all publications are solely those of the individual author(s) and contributor(s) and not of MDPI and/or the editor(s). MDPI and/or the editor(s) disclaim responsibility for any injury to people or property resulting from any ideas, methods, instructions or products referred to in the content.

biomedicines

Article

Effects of Continuous Positive Airway Pressure Treatment on Vascular Function in a Real-Life Cohort of Elderly Patients with Obstructive Sleep Apnoea Syndrome

Mara Volpentesta [1,†], Valentino Condoleo [2,†], Alberto Panza [3], Giandomenico Severini [3,*], Luca Soraci [1], Cataldo Rotondo [4], Giuseppe Armentaro [2], Corrado Pelaia [3], Vanessa Teresa Fiorentino [3], Francesco Andreozzi [3], Giorgio Sesti [5], Andrea Corsonello [1,6,‡] and Angela Sciacqua [2,3,‡]

[1] Unit of Geriatric Medicine, IRCCS INRCA, 87100 Cosenza, Italy; mara.volpentesta@yahoo.it (M.V.); l.soraci@inrca.it (L.S.); a.corsonello@inrca.it (A.C.)
[2] Geriatrics Division, University Hospital "R. Dulbecco", 88100 Catanzaro, Italy; condoleovalentino@gmail.com (V.C.); giuseppearmentaro91@gmail.com (G.A.); sciacqua@unicz.it (A.S.)
[3] Department of Medical and Surgical Sciences, University Magna Graecia of Catanzaro, 88100 Catanzaro, Italy; albertopanza94@libero.it (A.P.); pelaia.corrado@gmail.com (C.P.); vanessa.fiorentino@unicz.it (V.T.F.); andreozzif@unicz.it (F.A.)
[4] Coordinamento Medico legale, Istituto Nazionale della Previdenza Sociale, 88100 Catanzaro, Italy; crotondo63@gmail.com
[5] Department of Clinical and Molecular Medicine, University of Rome-Sapienza, 00185 Rome, Italy; giorgio.sesti@uniroma1.it
[6] Department of Pharmacy, Health and Nutritional Sciences, University of Calabria, 87100 Rende, Italy
* Correspondence: giandomenicoseverini@gmail.com
† Equally contributed as first author.
‡ Equally contributed as last author.

Abstract: Background: Obstructive sleep apnoea syndrome (OSAS) is an independent risk factor for cardiovascular morbidity and mortality and has a detrimental effect on vascular function, in particular on arterial stiffness and endothelial function. Continuous positive airway pressure (CPAP) is the gold-standard therapy for OSAS and its effects on arterial stiffness and endothelial function have been demonstrated in non-elderly patients. Objectives: The objective of this study was to evaluate the effect of one year of CPAP treatment on arterial stiffness, through assessment of carotid–femoral pulse wave velocity (cf-PWV), and on endothelial function, through the reactive hyperaemia index (RHi), in a real-life cohort of elderly patients with moderate-to-severe OSAS and several comorbidities. Methods: In this nonrandomised prospective study, we enrolled 469 consecutive elderly patients affected by moderate-to-severe OSAS distributed in two groups: CPAP-treated (n = 225) and untreated patients (n = 244). Results: At one-year follow-up, in the treated group emerged an important improvement in poligraphics (AHI, ODI, TC90, mean SpO_2%), laboratory (HOMA index, eGFR, hs-CRP) and vascular function parameters: cf-PWV. The stepwise multivariate linear regression demonstrated a significant correlation between the delta of the polygraph parameters and the delta of PWV and RHi. Conclusions: Our study confirmed the favourable effects of CPAP therapy in a cohort of elderly patients affected by OSAS and several comorbidities on sleep respiratory parameters and vascular function; early diagnosis and treatment with CPAP might be beneficial to delay or prevent the occurrence of cardiovascular events in these groups of patients.

Keywords: CPAP; elderly; OSAS; arterial stiffness; endothelial dysfunction

1. Introduction

Obstructive sleep apnoea syndrome (OSAS) consists of repetitive episodes of upper airway (UA) collapse that cause complete (apnoea) or partial (hypopnoea) intermittent airflow obstruction during sleep. The estimated prevalence of OSAS is approximately

5–15% in the general population and affecting up to 33.3% of elderly people in the eighth decade of life and 39.5% in the ninth decade; but risk factors, symptoms and natural history differ from those in middle-aged patients [1–4]. OSAS is considered an independent risk factor for cardiovascular disease. UA collapse leads to chronic intermittent hypoxemia (CIH), hypercapnia, intrathoracic pressure fluctuations and sleep fragmentation that, in turn, increase oxidative stress and systemic inflammation and cause sympathetic and renin–angiotensin–aldosterone system (RAAS) hyperactivity [5]. These pathogenic mechanisms are believed to induce arterial stiffness augmentation and endothelial dysfunction, which are early vascular damage markers associated with increased cardiovascular risk [6,7]. Further, it is widely accepted that age is a major determinant of increased arterial stiffness and endothelial dysfunction [8,9]. Prior research has indicated a correlation between obstructive sleep apnoea syndrome (OSAS) and a reduction in arterial stiffness, irrespective of alterations in blood pressure. Furthermore, in a cohort of elderly patients with sleep breathing disorders, a notable correlation was observed between blood pressure/pulse rate and endothelial function parameters. In younger patients, CPAP therapy demonstrated a favourable impact on endothelial function [10]. In light of these observations, the aim of this study was to evaluate the effects of one year of CPAP treatment on arterial stiffness, as measured by carotid–femoral pulse wave velocity (cf-PWV), and on endothelial function, as determined by the reactive hyperaemia index (RHi), in a cohort of elderly patients affected by moderate-to-severe OSAS and several comorbidities, not included in previous studies.

2. Materials and Methods

2.1. Study Population

The present study, which was prospective, observational and not randomised, enrolled 469 consecutive patients aged $\geq$ 65 years affected by moderate or severe OSAS who had several comorbidities and were referring to the Geriatric Division of the University "Magna Graecia" in Catanzaro from October 2012 to September 2023, in the Catanzaro Metabolic Risk Factors (CATAMERI) Study. Inclusion criteria were the following: patients aged $\geq$ 65 years, able to give written consent and affected by moderate or severe OSAS with or without respiratory failure, with indications to nocturnal CPAP, eventually enriched with oxygen therapy. Exclusion criteria were the presence of central or mixed apnoea syndrome, severe dementia or Alzheimer's disease, prior ischemic or haemorrhagic major stroke, psychiatric comorbidities or drug therapies that may affect respiratory function or sleep and common contraindications to nocturnal CPAP, recent facial or upper airways/aesophagogastric surgery, anatomical alterations or facial trauma and difficulty in swallowing, detected by medical history. At the time of enrolment and after one year, patients underwent clinical interview, physical examination, sero-haematological exams, overnight polygraphy and instrumental determination of vascular function. The Epworth sleepiness scale (ESS) questionnaire was administered to all participants at diagnosis and after one year. At baseline, patients underwent an ear, nose and throat (ENT) visit to evaluate Mallampati score and exclude surgical indications. After preliminary evaluations, patients started nocturnal CPAP titration using a ResMed Airsense 10 Autoset (Resmed, Sydney, Australia) in auto-CPAP mode with default minimum–maximum pressure settings at 4–20 cm H_2O. Humidification and choice of interface were made on an individualised patient basis. Patients who well adapted to therapy and reached a mean use time $\geq$ 4 h/night were assigned to the group of CPAP-treated patients (n = 225), while patients who interrupted titration early, did not adapt well or chose to receive best support care were included in the untreated group (n = 244). BSC was provided through advice on sleep hygiene and weight loss, as appropriate to each patient. Medical appointments were scheduled for all patients at 1 year after diagnosis to ensure the same number of medical visits in all patients (with or without CPAP). Evaluation of adherence to CPAP therapy was objectively assessed by reading the device's smart card from the start of treatment to the end of the follow-up. Patients were classified as being adherent if the average cumulative compliance was $\geq$4 h/day.

2.2. Laboratory Determinants

All laboratory measurements were carried out on peripheral blood samples after at least 12 h of fasting. Glycaemia was determined by the glucose oxidase method (glucose analyser, Beckman Coulter, Milan, Italy). Creatinine levels were measured using the Jaffé method. The estimation of glomerular filtration rate (eGFR) was based on the new CKD-EPI (Chronic Kidney Disease Epidemiology Collaboration) equation [11]. Serum uric acid (UA) levels were assessed using the URICASE/POD method (Boehringer Mannheim, Mannheim, Germany). Serum levels of high-sensitivity C-reactive protein (hs-CRP) were measured by an immune-turbidimetric method automated system (Cardio Phase hs-CRP, Milan, Italy). In addition, glycated haemoglobin (HbA1c) was measured by high-performance liquid chromatography certified by the national glycohaemoglobin standardisation program (NGSP) and using an automatic analyser (Adams HA-8160 HbA1c analyser, Menarini, Italy). Analytical determinations were taken using an automatic particle counter (Siemens Healthcare Diagnostics, ADVIA 120/2120 Haematology System, Milan, Italy) to measure haemoglobin, haematocrit and white blood cell count. Plasma concentrations of insulin were determined by chemi-luminescence test (Roche Diagnostics, Mannheim, Germany). Insulin resistance was determined by the homeostasis model assessment (HOMA) index [12].

2.3. OSAS Diagnosis

OSAS diagnosis was made after one-night polygraphy that included recordings of nasal flow, chest and abdomen movements and oxygen saturation. The report was analysed with dedicated software by two expert operators blinded to patients' characteristics, according to 2017 American Academy of Sleep Medicine (AASM) guidelines [13]. Referring to the number of apnoea plus hypopnea events per hour of sleep (AHI, e/h), OSAS was defined as moderate with AHI between 15 and 29.9/h and severe when $\geq$30/h. We also evaluated the average nocturnal saturation (mean SpO_2, %), the oxygen desaturation index (ODI, e/h) corresponding to the number of episodes of desaturation > 3% per hour of sleep and the percentage time of saturation <90% (TC90, %). A value of TC90 > 30% allows the diagnosis of nocturnal respiratory failure (NRF).

2.4. Vascular Function Parameters Measurement

Arterial stiffness measurements were obtained by a validated system (SphygmocorTM; AtCor Medical, Sydney, Australia) that employs high-fidelity applanation tonometry (Millar) and appropriate computer software for the analysis of pressure waves (SphygmocorTM), as previously reported. Aortic PWV was determined by setting the distance between the surface markings of the mandibular angle, the sternal notch and the femoral artery as the path length between the carotid and femoral arteries (L) and measuring the time of propagation (DT) of the pressure waveform through this segment (L/DT) [14]. Endothelial function was assessed using EndoPAT (Itamar Medical, Caesarea, Israel), a non-invasive device based on the plethysmography method that uses the peripheral response to reactive hyperaemia to evaluate endothelial function. The device records endothelium-mediated changes in the digital pulse waveform known as the PAT (peripheral arterial tone) signal, measured through a special finger probe on the index finger of the two hands; after that, hyperaemia was induced by occluding blood flow through the brachial artery for 5 min using an inflatable cuff on one hand. The amplitude of the induced hyperaemia is used to calculate RHi [15].

2.5. Statistical Analysis

Continuous data were expressed as mean $\pm$ standard deviation (SD) or as the median and interquartile range when appropriate. Normally distributed data were analysed using *t*-test for paired data, while not normally distributed data were analysed by the Mann–Whitney test. Subsequently, in the group of CPAP-treated patients, a simple linear regression model was built with the delta (Δ, i.e., changes) between follow-up and baseline in PWV and in RHi as the dependent variable and Δ of the other clinical variables

considered to be major as independent variables. Therefore, changes in the variables that significantly correlated with changes in the dependent variable were entered into a stepwise multivariate linear regression model. Statistical analysis was carried out using the SPSS V20.0 program for Windows (SPSS Inc., Chicago, IL, USA).

3. Results

From an initial cohort of 621 patients, 12 were excluded because they did not sign the informed consent, 14 because they were affected by dementia, 9 because they had contraindications to CPAP, and 63 because they had central or mixed apnoea syndrome (Figure 1).

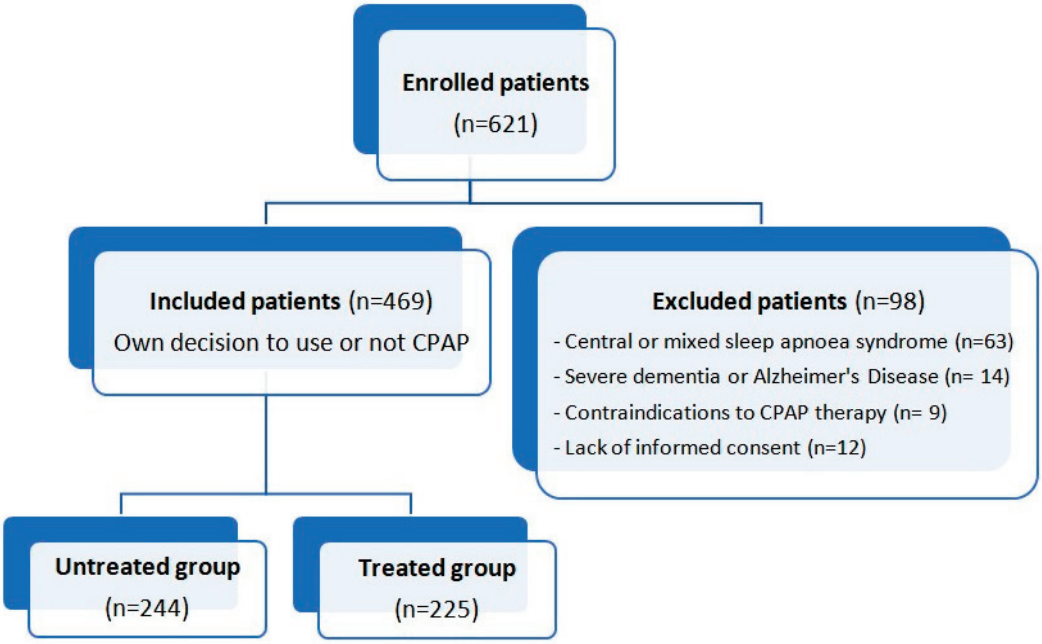


Figure 1. Flowchart of the recruitment process of the study.

The final cohort included 469 patients, 70.4% men and 29.6% women, with a median age of 74.8 ± 5 years. In particular, 47.9% were affected by moderate OSAS while 52% by severe OSAS and 28.1% were complicated by NRF. In the population, 77.8% were affected by arterial hypertension, 55.2% of patients suffered from type 2 diabetes mellitus, 44.1% from chronic kidney disease (eGFR <60 mL/min/1.73 m^2), 12.6% from chronic heart failure (CHF), 22.6% from ischemic heart disease (IHD) and 36% from chronic obstructive pulmonary disease (COPD) or asthma. At baseline, statistically significant differences only emerged between the two studied groups for smoking habit and dyslipidaemia (Table 1).

Table 1. Comparison of comorbidities and pharmacotherapy of the study population between treated and untreated groups.

	Whole Population (*n* = 469)	**Untreated Group (*n* = 244)**	**Treated Group (*n* = 225)**	***p* ***
Smokers, *n* (%)	85 (18.1)	59 (24.2)	26 (11.5)	0.0004
Hypertension, *n* (%)	365 (77.8)	186 (76.2)	179 (79.6)	0.386
Dyslipidaemia, *n* (%)	328 (69.9)	157 (64.3)	171 (76)	0.006
Carotid ATS, *n* (%)	239 (50.9)	127 (52)	112 (49.8)	0.623
Type 2 DM, *n* (%)	259 (55.2)	129 (52.8)	130 (57.8)	0.285
HF, *n* (%)	59 (12.6)	30 (12.3)	29 (12.9)	0.846
CAD, *n* (%)	106 (22.6)	53 (21.7)	53 (23.6)	0.635

Table 1. *Cont.*

	Whole Population (*n* = 469)	Untreated Group (*n* = 244)	Treated Group (*n* = 225)	*p* *
AF, *n* (%)	331 (70.6)	172 (70.5)	159 (70.7)	0.966
TIA/minor stroke, *n* (%)	95 (20.3)	53 (21.7)	42 (18.7)	0.410
CKD (eGFR < 60 mL/min/1.73 m^2), *n* (%)	207 (44.1)	113 (46.3)	94 (41.8)	0.323
COPD/asthma, *n* (%)	169 (36)	84 (34.4)	85 (37.8)	0.450
NAFLD, *n* (%)	85 (18.1)	44 (18)	41 (18.2)	0.957
ACEi/ARB, *n* (%)	312 (66.5)	155 (63.9)	156 (69.3)	0.215
ARNI, *n* (%)	34 (7.2)	19 (7.8)	15 (6.7)	0.640
SGLT2-i, *n* (%)	157 (33.4)	76 (31.1)	81 (36.0)	0.265
GLP1-RA, *n* (%)	107 (22.8)	55 (22.5)	52 (23.1)	0.883
Metformin, *n* (%)	199 (42.4)	98 (40.2)	101 (44.9)	0.300
DOAC, *n* (%)	313 (66.7)	165 (67.6)	148 (65.8)	0.671
VKA, *n* (%)	18 (3.8)	7 (2.9)	11 (4.9)	0.255
B-blocker, *n* (%)	228 (72.0)	178 (72.9)	160 (71.1)	0.657
Statin, *n* (%)	222 (47.3)	104 (42.6)	118 (52.4)	0.033
PCSK9-i, *n* (%)	88 (18.8)	42 (17.2)	46 (20.4)	0.370
Anti-PLT, *n* (%)	136 (28.9)	71 (29.0)	65 (28.9)	0.960
Diuretic, *n (%)*	235 (50.1)	121(49.6)	114 (50.7)	0.815
MRA, *n* (%)	107 (22.8)	59 (24.0)	51 (22.8)	0.556
LAMA, *n* (%)	35 (7.5)	15 (6.1)	20 (8.9)	0.259
LAMA/LABA, *n* (%)	77 (16.4)	41 (16.8)	36 (16.0)	0.814
LAMA/LABA/ICS, *n* (%)	56 (11.9)	28 (11.5)	28 (12.4)	0.746

* performed by chi square test. Abbreviations: ATS, atherosclerosis; DM, diabetes mellitus; HF, heart failure; CAD, coronary artery disease; AF, atrial fibrillation; TIA, transient ischemic attack; CKD, chronic kidney disease; COPD, chronic obstructive pulmonary disease; NAFLD, non-alcoholic fatty liver disease; ACEi, angiotensin-converting enzyme inhibitor; ARB, angiotensin receptor blocker; ARNI, angiotensin receptor neprilysin inhibitors; SGLT2i, sodium/glucose cotransporter 2 inhibitor; GLP1-RA, GLP-1 receptor agonist; DOAC, direct oral anticoagulant; VKA, vitamin K antagonist; PCSK9-i, PCSK9 inhibitor; MRA, mineralocorticoid receptor antagonist; LAMA, long-acting muscarinic antagonist; LABA, long-acting beta agonist; ICS, inhaled corticosteroid.

After seven days of CPAP titration, only 47.9% adapted to CPAP and chose to continue therapy and best support care (BSC) (*n* = 225); the remaining patients entered the untreated group and received BSC (*n* = 244). Finally, treated patients presented significantly higher Mallampati scores (2.9 ± 0.9 vs. 2.4 ± 1.0 in untreated group, $p = 0.0001$). Only 20% of treated patients needed oxygen supplementation. In the untreated group, the mean AHI was 36.7 ± 15.5/h versus 37.5 ± 17.7/h in the treated group, $p = 0.576$ (Table 2).

Table 2. Comparison of baseline characteristics between treated and untreated group.

	Whole Population (*n* = 469)	Untreated Group (*n* = 244)	Treated Group (*n* = 225)	*p*
Age, years	74.8 ± 5	74.6 ± 4.3	75.0 ± 5.6	0.284
Gender (males), *n* (%)	330 (70.4)	174 (71.3)	156 (69.3)	0.639
CHA_2DS_2Vasc, score	3.8 ± 1.4	3.8 ± 1.3	3.9 ± 1.4	0.309
HAS-BLEED, score	2.8 ± 1.0	2.9 ± 0.9	2.6 ± 1.1	0.001
BMI, kg/m^2	32.4 ± 6.2	32.2 ± 6.0	32.5 ± 6.3	0.673
ESS, score	10.6 ± 4.4	10.9 ± 4.7	10.4 ± 4.7	0.274
AHI, e/h	36.9 ± 16.1	36.7 ± 15.5	37.5 ± 17.7	0.576
TC 90, %	11.2 (3.0–32.7)	9.6 (2.9–32.6)	12.6 (3.4–34.4)	0.537
ODI, e/h	33.6 ± 15.9	32.3 ± 13.2	34.5 ± 18.3	0.084
Mean SpO_2, %	91.8 ±3.2	92.0 ± 2.9	91.5 ± 3.4	0.065
Night-time HR, bpm	68.0 ± 12.3	69.0 ± 11.9	66.9 ± 12.5	0.056
SBP, mmHg	137.0 ± 13.5	137.4 ± 13.0	136.7 ± 14.0	0.572
DBP, mmHg	78.3 ± 10.0	78.3 ± 9.9	78.4 ± 10.0	0.917
Day-time HR, bpm	69.8 ± 10.9	69.6 ± 10.3	69.9 ± 11.6	0.792
HOMAi, score	4.9 ± 3.1	5.1 ± 3.1	4.6 ± 3.1	0.080

Table 2. *Cont.*

	Whole Population (*n* = 469)	**Untreated Group (*n* = 244)**	**Treated Group (*n* = 225)**	***p***
HbA1c, %	6.9 ± 1.3	6.8 ± 1.0	6.9 ± 1.5	0.209
LDL-C, mg/dL	117.9 ± 33.9	119.8 ± 34.2	115.8 ± 33.6	0.208
TGRs, mg/dL	126.1 ± 53.2	129.6 ± 57.9	122.4 ± 47.3	0.144
Creatinine, mg/dL	1.1 ± 0.3	1.2 ± 0.3	1.1 ± 0.3	0.008
eGFR, ml/min/1.73 m^2	62.7 ± 17.5	61.2 ± 17.9	64.4 ± 16.9	0.048
Uric acid, mg/dL	6.7 ± 1.4	6.8 ± 1.3	6.7 ± 1.5	0.264
HCT, %	42.9 ± 5.3	43.1 ± 5.4	42.6 ± 5.3	0.312
Hb, g/dL	13.7 ± 1.7	13.7 ± 1.7	13.7 ± 1.7	0.977
PLTs, u/µL	248.1 ± 80.2	252.0 ± 81.8	243.4 ± 78.3	0.267
hs-CRP, mg/L	3.9 ± 3.4	3.7 ± 3.6	3.7 ± 5.2	0.874
Mallampati, score	2.6 ± 1.0	2.4 ± 1.0	2.9 ± 0.9	0.0001

In the CPAP group, after one-year follow-up, there was an important improvement in respiratory, some laboratory and vascular function parameters. No differences emerged in BMI, probably because the untreated group strictly followed life-style advice established in BSC. No statistically significant differences emerged between the two groups among vascular function parameters at baseline (Table 3); after one year of treatment with CPAP, a significant improvement was obtained in all considered parameters, in particular, in PWV (−1.0 (−1.7/−0.8) vs. −1.6 (−2.1/−1.3) m/s, $p < 0.0001$) and RHi (0.4 (0.3/0.5) vs. 0.6 (0.5/0.7), $p < 0.0001$) (Table 4) (Figure 2).

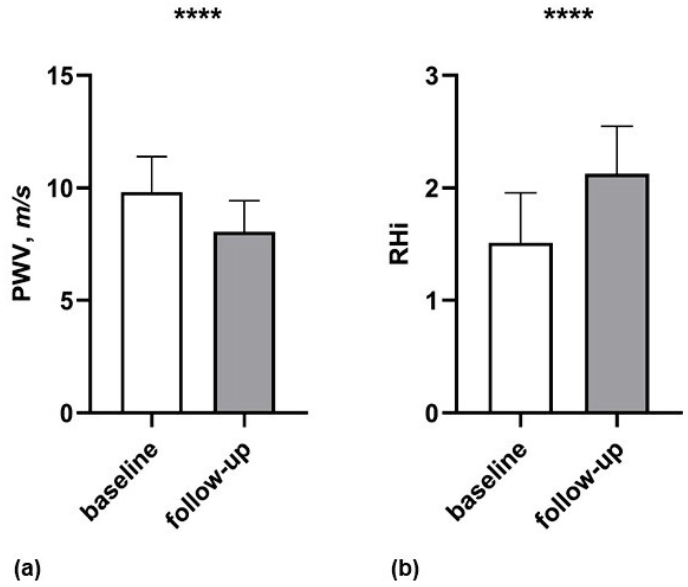
Table 3. Comparison of vascular function parameters at baseline between treated and untreated group.

	Whole Population (*n* = 469)	**Untreated Group (*n* = 244)**	**Treated Group (*n* = 225)**	***p***
IMT dx, mm	1.02 ± 0.2	1.03 ± 0.2	1.02 ± 0.2	0.423
IMT sn, mm	1.02 ± 0.2	1.02 ± 0.2	1.02 ± 0.1	0.671
ABI dx	1.02 ± 0.2	1.03 ± 0.2	1.0 ± 0.2	0.374
ABI sn	1.04 ± 0.2	1.04 ± 0.2	1.04 ± 0.2	0.857
AI, %	40.2 ± 9.2	40.4 ± 9.6	39.9 ± 8.9	0.531
PP, mmHg	42 ± 13.3	42.1 ± 13.4	42.1 ± 13.5	0.955
PWV, m/s	9.8 ±1.7	9.7 ± 1.7	9.8 ± 1.6	0.556
AP, mmHg	29.8 ± 9.3	30.2 ± 9.7	29.4 ± 8.9	0.342
c-SBP, mmHg	109.0 ± 16.6	109.5 ± 15.5	109.1 ± 15.7	0.953
c-DBP, mmHg	62.6 ± 9.9	62.5 ± 10.5	62.6 ± 9.4	0.917
RHi, score	1.5 ± 0.4	1.6 ±0.4	1.5 ± 0.4	0.218

Table 4. Vascular function parameters at baseline and follow-up of the study population.

	Baseline	**Follow-Up**	***p***
AI, %	40.2 ± 9.2	36.2 ± 8.1	0.0001
PP, mmHg	42.1 ± 13.3	38.3 ± 12.3	0.0001
PWV, m/s	9.8 ±1.7	8.2 ± 1.5	0.0001
AP, mmHg	29.8 ± 9.3	27.4 ± 8.7	0.0001
c-SBP, mmHg	109.1 ± 16.6	103.8 ± 15.2	0.0001
c-DBP, mmHg	62.6 ± 9.9	60.4 ± 9.7	0.0001
RHi	1.5 ± 0.4	2.1 ± 0.4	0.0001

Abbreviations: PWV, pulse wave velocity; AI, augmentation index; PP, pulse pressure; AP, augmentation pressure; c-SBP, central systolic blood pressure; c-DBP, diastolic blood pressure; RHi, reactive hyperaemia index.



Data are mean ± SD. ****p < 0.0001 vs. baseline.

Figure 2. Changes in vascular parameters, (**a**) PWV, (**b**) RHi in treated group between baseline and follow-up.

A comparison of the changes in polygraphic parameters between the two groups revealed a significant difference between the CPAP therapy and the control groups (Table 5). In the treated group, linear regression analysis revealed a statistically significant relationship between ΔPWV and ΔRHi and the major considered clinical variables (Table 6).

Table 5. Changes in major parameters between baseline and follow-up according to CPAP use.

	Untreated Group (*n* = 244)	**Treated Group (*n* = 225)**	*p* *
Λ BMI, kg/m^2	−0.7 (−1.2/−0.3)	−0.7 (−1.6/−0.4)	0.081
Λ ESS, score	−6.3 (−9.0/−2.0)	−7.2 (−9.0/−4.0)	0.014
Λ AHI, e/h	−3.8 (−3.8/6.8)	−26.3 (−34.7/−16.4)	0.0001
Λ TC 90, %	−4.9 (−13.3/−1.2)	−10.2 (−25/−2.0)	0.0001
Λ ODI, e/h	−3.40 (−4.2/6.4)	−23.7 (−37.4/−13.5)	0.0001
Λ mean SpO_2, %	3 (1.0/3.0)	3 (1.0/5.0)	0.001
Λ HOMAi, score	−1.1 (−2.4/−0.8)	−1.4 (−2.2/−0.6)	0.009
Λ eGFR, mL/min/1.73 m^2	−6.0 (−8.2/−2.8)	6.4 (3/11.7)	0.0001
Λ uric acid, mg/dL	−0.4 (−1.3/−0.1)	−0.5 (−1.3/−0.2)	0.126
Λ HCT, %	−0.3 (1.7/1.2)	−0.3 (−2.0/1.2)	0.818
Λ hs-CRP, mg/L	−0.4 (−1.2/0.2)	−1.4 (−2.2/−0.5)	0.0001
Λ PWV, m/s	−1.0 (−1.7/−0.8)	−1.6 (−2.1/−1.3)	0.0001
Λ RHi, score	0.4 (0.3/0.5)	0.6 (0.5/0.7)	0.0001

* Performed by Mann–Whitney test. Abbreviations: BMI, body mass index; ESS, Epworth sleepiness scale; AHI, number of episodes of apnoea and hypopnoea/h; TC90, % of time with spO_2 < 90%; ODI, number of episodes of desaturation > 3%/h; HOMAi, homeostatic model assessment index; e-GFR, estimated glomerular filtration rate (CKD-EPI); HCT, haematocrit; hs-CRP, high-sensitivity CRP; PWV, pulse wave velocity; RHi, reactive hyperaemia index.

Table 6. Simple linear regression analysis between Δpwv and Δrhi and δ of other covariates in the treated group.

	Δ PWV (r/p)	**Δ RHi (r/p)**
Δ BMI, g/m^2	0.032/0.479	−0.021/0.664
Δ ESS, *score*	0.029/0.524	−0.097/0.047
Δ AHI, e/h	0.344/0.0001	−0.251/0.0001
Δ TC 90, %	0.048/0.379	−0.103/0.007
Δ ODI, e/h	0.253/0.0001	−0.248/0.0001
Δ mean SpO_2, %	−0.043/0.491	0.023/0.727
Δ HOMAi, score	0.010/0.857	−0.021/0.727
ΔeGFR, ml/min/1.73 m^2	−0.095/0.005	0.037/0.480
Δ uric acid, mg/dL	0.193/0.0001	−0.309/0.0001
Δ HCT, %	0.070/0.124	−0.098/0.041
Δ hs-CRP, mg/L	0.211/0.0001	−0.143/0.012

Abbreviations: BMI, body mass index; ESS, Epworth sleepiness scale; AHI, number of episodes of apnoea and hypopnoea/h; TC90, % of time with spO_2 < 90%; ODI, number of episodes of desaturation > 3%/h; HOMA index, homeostatic model assessment index; e-GFR, estimated glomerular filtration rate; HCT, haematocrit; hs-CRP, high-sensitivity CRP; PWV, pulse wave velocity; RHi, reactive hyperaemia index.

By using Δ PWV as a dependent variable, PWV changes were significantly associated with variations in AHI, ODI, eGFR, uric acid and hs-CRP. Variations in PWV correlated significantly and directly with changes in poligraphic parameters, uric acid and hs-CPR and inversely with eGFR changes. The same parameters, except for eGFR and with contributions of ESS, TC 90 and haematocrit (HCT) changes, were significantly associated with Δ RHi. Variations in RHi correlated significantly and inversely with poligraphic parameters, ESS score, uric acid, hs-CRP and HCT changes. Furthermore, variables that showed a significant correlation with changes in Λ PWV and Λ RHi were included in a stepwise multivariate linear regression model to identify the independent predictors of these variations. We observed that changes in AHI, ODI, hs-CRP, uric acid and eGFR contributed, respectively, to 35.8%, 10.4%, 5.5%, 2.5% and 1.2% of the variability in PWV, with the whole model accounting for 55.4% of PWV variations (Table 7). On the other side, considering RHi variations, we observed that changes in uric acid, AHI, ODI, hs-CRP, ESS score, HCT and TC90 contributed, respectively, to 27.0%, 13.0%, 7.0%, 2.0%, 1.0%, 0.7%, and 0.2% of the variability, with the whole model accounting for 50.9% of RHi variations.

Table 7. Stepwise multivariate linear regression analysis between Δpwv and Δrhi as dependent variable, and δ of different covariates.

Δ of PWV as Dependent Variable				**Δ of RHi as Dependent Variable**			
	R^2 Partial (%)	**R^2 Total (%)**	***p***		**R^2 Partial (%)**	**R^2 Total (%)**	***p***
Δ AHI, e/h	35.8	35.8	0.0001	Δ uric acid, mg/dL	27.0	27.0	0.0001
Δ ODI, e/h	10.4	46.2	0.0001	Δ AHI, e/h	13.0	40.0	0.0001
Δ hs-PCR, mg/L	5.5	51.7	0.0001	Δ ODI, e/h	7.0	47.0	0.0001
Δ uric acid, mg/dL	2.5	54.2	0.0001	Δ hs-PCR, mg/L	2.0	49.0	0.004
Δ eGFR, mL/min/1.73 m^2	1.2	55.4	0.009	Δ ESS, score	1.0	50.0	0.028
----	----	----	----	Δ HCT, %	0.7	50.7	0.043
----	----	----	----	Δ TC 90, %	0.2	50.9	0.048

Abbreviations: AHI, number of episodes of apnoea and hypopnoea/h; ODI, number of episodes of desaturation > 3%/h; hs-CRP, high-sensitivity CRP; eGFR, estimated glomerular filtration rate; ESS, Epworth sleepiness scale; HCT, haematocrit; TC90, % of time with spO_2 < 90%.

4. Discussion

In a real-life cohort of elderly patients affected by moderate-to-severe OSAS and other important comorbidities, we observed that CPAP treatment with a compliance

$\geq$ 4 h/night significantly improved vascular function parameters, in particular PWV and RHi, after one year of treatment. According to previous studies, we confirmed the positive effect of CPAP on poligraphic parameters (AHI, ODI, TC90, mean SpO_2), renal function (eGFR), systemic inflammation (hs-CPR) and metabolic status (HOMA index and uric acid) [16–18]. In our population, baseline characteristics of PWV and RHi did not significantly differ between the two studied groups, but at follow-up, statistically significant differences emerged. These findings are a result of the known effects of CPAP, which corrects sleep-related respiratory events and associated CIH, reduces the mechanical stress on the vasculature caused by pressure fluctuations during apnoea and interferes with the mechanism involved in the pathogenesis of AS and endothelial dysfunction. A statistically significant association was found between improved PWV and reduced respiratory apnoea events (AHI and ODI), metabolic parameters (uric acid), improved renal function (eGFR) and inflammatory markers (hs-CRP) in the treated group. More specifically, simple and multivariate linear regression analysis showed that improvements in AHI and ODI largely explained the variation in PWV, and reductions in uric acid, AHI and ODI correlated with the changes in RHi after one year of treatment with CPAP. The reduction in AHI and ODI explained 46.2% of PWV changes and the reduction in uric acid, AHI and ODI explained 47% of RHi variations. It is widely accepted that uric acid, eGFR and hs-CPR are the main determinants of arterial stiffness and endothelial dysfunction [19–21]. The reported reduction in uric acid and hs-CPR due to the effect of CPAP on CIH contributed to the improvement of both PWV and RHi by further reduction in oxidative stress, inflammation and insulin resistance. Uric acid has been established as a major predictor of PWV in a cohort of hypertensive patients, supporting a synergistic action between uric acid and HOMA index in inducing subclinical vascular damage, and the role of insulin resistance as a mediator by which uric acid increases AS. The mechanisms by which this occurs have been identified through experimental studies. They involve interference with insulin signalling, IGF-1 levels, and the activation of inflammatory processes and systems such as RAAS and the sympathetic system. These mechanisms promote oxidative stress and endothelial dysfunction [22–24]. However, in contrast with this evidence, in our study, changes in HOMA index did not significantly correlate with changes in PWV. In a previous study we conducted on obese patients affected by moderate or severe OSAS with normal renal function, CPAP therapy significantly improved eGFR after a follow-up of 6 months, and the main determinant of eGFR variations were the reductions in AHI and TC90; so in our study, the improvement in renal function in the CPAP-treated group represented one of the determinants of PWV variations. This finding supports the hypothesis that CKD and OSAS share common pathogenic mechanisms, including oxidative stress, metabolic alterations and sympathetic activity, and that resolution of respiratory events and CIH improve endothelial glomerular function [25–27]. A pathogenic role in renal function decline is also played by arterial stiffness; mineral metabolism disturbances, vascular calcifications, formation of advanced glycation end-products (AGEs) and acute and chronic volume overload occurring in ESRD and CKD patients have been proposed as the main pathogenic mechanisms linking arterial stiffness to renal disease. Changes in ESS score, TC90 and HCT were involved in j variations in RHi. The underlying pathogenic mechanism of sleepiness in OSAS includes CIH and repetitive arousals that result in sleep fragmentation and changes in neurons and the brain circuit involving noradrenergic and dopaminergic neurotransmission in wake-promoting regions of the brain [27]. In particular, sleep fragmentation itself may adversely affect endothelial function and CPAP stops this mechanism, improving both sleepiness and endothelial function [28]. Several studies have also found a significant association between variations in endothelial function and TC90. For instance, a study conducted in elderly patients found that brachial artery baseline diameter and flow-mediated dilation correlated more with TC90 than AHI, which confirms the pathogenic role of hypoxemia/re-oxygenation cycles [13]. The effects of HCT variations are probably due to the higher level of oxygenation reached with CPAP. The novelty of our study is that we considered a numerous group of elderly patients affected by

several comorbidities as in real life. Moreover, our study population at baseline complained of mild sleepiness (ESS score < 16), but contrary to what emerged from other studies on AS, the positive impact of treatment was already evident [29]. Patients in the CPAP-treated group had a good compliance to therapy, not always reached in other studies. Finally, the follow-up was longer than other studies reported, confirming the persistence of positive effects after one-year follow-up.

Limitations

The principal limitation of this study is its single-centred and nonrandomised design, which did not eliminate the potential for bias in participant selection. Furthermore, the inclusion of a matched control group would have been beneficial. Another limitation is the use of one-night polysomnography to make a diagnosis, which did not include electroencephalogram (EEG) recordings and did not allow for the study of the contribution of arousal, respiratory effort-related arousal (RERA), and fragmentation of sleep architecture. Additionally, the role of the number of hours spent complying with therapy in ameliorating arterial stiffness and endothelial dysfunction was not evaluated. Finally, other mechanisms involved in increasing AS and causing endothelial dysfunction, which OSAS exacerbates and on which CPAP can have an effect, such as sympathetic hyperactivity, were not considered.

5. Conclusions

Finally, this study confirmed the impact of CPAP therapy in a cohort of elderly patients affected by OSAS and several comorbidities on the improvements of sleep polygraph parameters, renal function and metabolic-inflammatory status and vascular function. CPAP therapy corrected sleep respiratory events and CIH, and the induced pathogenic mechanisms (oxidative stress, systemic inflammation, sympathetic hyperactivation and arousal, activation of RAA system) seemed to have a positive effect on renal function, metabolic parameters and inflammation markers and ameliorate arterial stiffness and endothelial function in elderly patients with OSAS and several comorbidities. In this context, an early diagnosis and treatment with CPAP might also be beneficial to delay or prevent the occurrence of cardiovascular events in these group of patients.

Author Contributions: M.V., V.C., A.P., G.S. (Giandomenico Severini), L.S., C.R., G.A., C.P., V.T.F., F.A., G.S. (Giorgio Sesti), A.C. and A.S. participated in study conceptualization and design. M.V., V.C., G.S. (Giandomenico Severini), G.A., C.P., A.C. and A.S. participated in the methodology. M.V., V.C., G.S. (Giandomenico Severini), G.A., C.P., V.T.F., F.A., G.S. (Giorgio Sesti), A.C. and A.S. participated in writing—original draft preparation. M.V., V.C., G.S. (Giandomenico Severini), G.A., C.P., V.T.F., F.A., G.S. (Giorgio Sesti), A.C. and A.S. participated in writing—review and editing. V.T.F., F.A., G.S. (Giorgio Sesti), A.C. and A.S. participated in study supervision. All authors agreed to be accountable for all aspects of the work in ensuring that questions related to the accuracy or integrity of any part of the work are appropriately investigated and resolved. All authors have read and agreed to the published version of the manuscript.

Funding: This research received no external funding.

Institutional Review Board Statement: The protocol was approved by the Comitato Etico Regione Calabria "Area Centro" (protocol number 2012.63 del 17 October 2012). The procedures used in this study adhere to the tenets of the Declaration of Helsinki.

Informed Consent Statement: Written informed consent has been obtained from the patients.

Data Availability Statement: The raw data supporting the conclusions of this article will be made available by the authors, without undue reservation.

Conflicts of Interest: The authors declare no conflicts of interest.

References

1. Levy, P.R.S.; Oldenburg, O.; Parati, G. Sleep apnoea and the heart. *Eur. Respir. Rev.* **2013**, *22*, 333–335. [CrossRef] [PubMed]
2. Armentaro, G.; Pelaia, C.; Condoleo, V.; Severini, G.; Crudo, G.; De Marco, M.; Pastura, C.A.; Tallarico, V.; Pezzella, R.; Aiello, D.; et al. Effect of SGLT2-Inhibitors on Polygraphic Parameters in Elderly Patients Affected by Heart Failure, Type 2 Diabetes Mellitus, and Sleep Apnea. *Biomedicines* **2024**, *12*, 937. [CrossRef] [PubMed]
3. Ralls, F.; Cutchen, L. A contemporary review of obstructive sleep apnea. *Curr. Opin. Pulm. Med.* **2019**, *25*, 578–593. [CrossRef] [PubMed]
4. Tietjens, J.R.; Claman, D.; Kezirian, E.J.; De Marco, T.; Mirzayan, A.; Sadroonri, B.; Goldberg, A.N.; Long, C.; Gerstenfeld, E.P.; Yeghiazarians, Y. Obstructive Sleep Apnea in Cardiovascular Disease: A Review of the Literature and Proposed Multidisciplinary Clinical Management Strategy. *J. Am. Hear. Assoc.* **2019**, *8*, e010440. [CrossRef] [PubMed]
5. Pelaia, C.; Armentaro, G.; Volpentesta, M.; Mancuso, L.; Miceli, S.; Caroleo, B.; Perticone, M.; Maio, R.; Arturi, F.; Imbalzano, E.; et al. Effects of Sacubitril-Valsartan on Clinical, Echocardiographic, and Polygraphic Parameters in Patients Affected by Heart Failure With Reduced Ejection Fraction and Sleep Apnea. *Front. Cardiovasc. Med.* **2022**, *9*, 861663. [CrossRef]
6. Doonan, R.J.; Scheffler, P.; Lalli, M.; Kimoff, R.J.; Petridou, E.T.; Daskalopoulos, M.E.; Daskalopoulou, S.S. Increased arterial stiffness in obstructive sleep apnea: A systematic review. *Hypertens. Res.* **2010**, *34*, 23–32. [CrossRef]
7. Chalegre, S.T.; Lins-Filho, O.L.; Lustosa, T.C.; França, M.V.; Couto, T.L.G.; Drager, L.F.; Lorenzi-Filho, G.; Bittencourt, M.S.; Pedrosa, R.P. Impact of CPAP on arterial stiffness in patients with obstructive sleep apnea: A meta-analysis of randomized trials. *Sleep. Breath.* **2021**, *25*, 1195–1202. [CrossRef]
8. Shiina, K.; Tomiyama, H.; Takata, Y.; Yoshida, M.; Kato, K.; Saruhara, H.; Hashimura, Y.; Matsumoto, C.; Asano, K.; Usui, Y.; et al. Effects of CPAP therapy on the sympathovagal balance and arterial stiffness in obstructive sleep apnea. *Respir. Med.* **2010**, *104*, 911–916. [CrossRef]
9. Nieto, F.J.; Herrington, D.M.; Redline, S.; Benjamin, E.J.; Robbins, J.A. Sleep apnea and markers of vascular endothelial function in a large community sample of older adults. *Am. J. Respir. Crit. Care Med.* **2004**, *169*, 354–360. [CrossRef]
10. Oyama, J.Y.H.; Maeda, T.; Ito, A.; Node, K.; Makino, N. Continuous positive airway pressure therapy improves vascular dysfunction and decreases oxidative stress in patients with the metabolic syndrome and obstructive sleep apnea syndrome. *Clin. Cardiol.* **2012**, *35*, 231–236. [CrossRef]
11. Levey, A.S. CKD-EPI (Chronic Kidney Disease Epidemiology Collaboration). A new equation to estimate glomerular filtration rate. *Ann. Intern. Med.* **2009**, *150*, 604–612. [CrossRef] [PubMed]
12. Matthews, D.R.H.J.; Rudenski, A.S.; Naylor, B.A.; Treacher, D.F.; Turner, R.C. Homeostasis model assessment: Insulin resistance and beta-cell function from fasting plasma glucose and insulin concentrations in man. *Diabetologia* **1985**, *28*, 412–419. [CrossRef]
13. Kapur, V.K.; Auckley, D.H.; Chowdhuri, S.; Kuhlmann, D.C.; Mehra, R.; Ramar, K.; Harrod, C.G. Clinical Practice Guideline for Diagnostic Testing for Adult Obstructive Sleep Apnea: An American Academy of Sleep Medicine Clinical Practice Guideline. *J. Clin. Sleep. Med.* **2017**, *13*, 479–504. [CrossRef] [PubMed]
14. Chen, C.H.; Ting, C.T.; Nussbacher, A.; Nevo, E.; Kass, D.A.; Pak, P.; Wang, S.-P.; Chang, M.-S.; Yin, F.C.P. Validation of carotid artery tonometry as a means of estimating augmentation index of ascending aortic pressure. *Hypertension* **1996**, *27*, 168–175. [CrossRef]
15. Corretti, M.C.; Anderson, T.J.; Benjamin, E.J.; Celermajer, D.; Charbonneau, F.; Creager, M.A.; Deanfield, J.; Drexler, H.; Gerhard-Herman, M.; Herrington, D.; et al. Guidelines for the ultrasound assessment of endothelial-dependent flow-mediated vasodilation of the brachial artery: A report of the international brachial artery reactivity task force. *J. Am. Coll. Cardiol.* **2002**, *39*, 257–265. [CrossRef]
16. Iftikhar, I.H.K.M.; Das, A.; Magalang, U.J. Meta-analysis: Continuous positive airway pressure improves insulin resistance in patients with sleep apnea without diabetes. *Ann. Am. Thorac. Soc.* **2013**, *10*, 115–120. [CrossRef]
17. Xie, X.P.L.; Ren, D.; Du, C.; Guo, Y. Effects of continuous positive airway pressure therapy on systemic inflammation in obstructive sleep apnea: A meta-analysis. *Sleep. Med.* **2013**, *14*, 1139–1150. [CrossRef]
18. Nagano, M.; Nakamura, M.; Sato, K.; Tanaka, F.; Segawa, T.; Hiramori, K. Association between serum C-reactive protein levels and pulse wave velocity: A population-based cross-sectional study in a general population. *Atherosclerosis* **2005**, *180*, 189–195. [CrossRef]
19. Nagano, S.; Takahashi, M.; Miyai, N.; Oka, M.; Utsumi, M.; Shiba, M.; Mure, K.; Takeshita, T.; Arita, M. Association of serum uric acid with subsequent arterial stiffness and renal function in normotensive subjects. *Hypertens. Res.* **2017**, *40*, 620–624. [CrossRef]
20. Condoleo, V.; Bonfrate, L.; Armentaro, G.; Pelaia, C.; Cassano, V.; De Marco, M.; Severini, G.; Pastura, C.A.; Miceli, S.; Maio, R.; et al. Effects of continuous positive airway pressure on comprehensive geriatric assessment and cognitive function in elderly patients with obstructive sleep apnea syndrome. *Intern. Emerg. Med.* **2023**, *18*, 769–779. [CrossRef]
21. Armentaro, G.; Pelaia, C.; Cassano, V.; Miceli, S.; Maio, R.; Perticone, M.; Pastori, D.; Pignatelli, P.; Andreozzi, F.; Violi, F.; et al. Association between right ventricular dysfunction and adverse cardiac events in mild COPD patients. *Eur. J. Clin. Investig.* **2023**, *53*, e13887. [CrossRef] [PubMed]
22. Pelaia, C.; Armentaro, G.; Miceli, S.; Perticone, M.; Toscani, A.F.; Condoleo, V.; Spinali, M.; Cassano, V.; Maio, R.; Caroleo, B.; et al. Association Between Sleep Apnea and Valvular Heart Diseases. *Front. Med.* **2021**, *8*, 667522. [CrossRef] [PubMed]
23. Kanbay, A.; Buyukoglan, H.; Ozdogan, N.; Kaya, E.; Oymak, F.S.; Gulmez, I.; Demir, R.; Kokturk, O.; Covic, A. Obstructive sleep apnea syndrome is related to the progression of chronic kidney disease. *Int. Urol. Nephrol.* **2011**, *44*, 535–539. [CrossRef]

24. Lavie, L. Oxidative stress-a unifying paradigm in obstructive sleep apnea and comorbidities. *Prog. Cardiovasc. Dis.* **2009**, *51*, 303–312. [CrossRef] [PubMed]
25. Yamauchi, M.K.H. Oxidative stress in obstructive sleep apnea: Putative pathways to the cardiovascular complications. *Antioxid. Redox Signal* **2008**, *10*, 755–768. [CrossRef] [PubMed]
26. Georgianos, P.I.P.M.; Liakopoulos, V.; Balaskas, E.V.; Zebekakis, P.E. Arterial stiffness in end-stage renal disease- pathogenesis, clinical epidemiology, and therapeutic potentials. *Hypertens. Res.* **2018**, *41*, 309–319. [CrossRef] [PubMed]
27. Lal, C.; Weaver, T.E.; Bae, C.J.; Strohl, K.P. Excessive Daytime Sleepiness in Obstructive Sleep Apnea. Mechanisms and Clinical Management. *Ann. Am. Thorac. Soc.* **2021**, *18*, 757–768. [CrossRef]
28. Atkeson, A.; Yeh, S.Y.; Malhotra, A.; Jelic, S. Endothelial Function in Obstructive Sleep Apnea. *Prog. Cardiovasc. Dis.* **2009**, *51*, 351–362. [CrossRef]
29. Mineiro, M.A.; Silva, P.M.D.; Alves, M.; Papoila, A.L.; Marques Gomes, M.J.; Cardoso, J. The Role of Sleepiness on Arterial Stiffness Im-provement after CPAP Therapy in Males with Obstructive Sleep Apnea: A Prospective Cohort Study. *BMC Pulm. Med.* **2017**, *17*, 182. [CrossRef]

Disclaimer/Publisher's Note: The statements, opinions and data contained in all publications are solely those of the individual author(s) and contributor(s) and not of MDPI and/or the editor(s). MDPI and/or the editor(s) disclaim responsibility for any injury to people or property resulting from any ideas, methods, instructions or products referred to in the content.

biomedicines

MDPI

Review

Zebrafish as a Model for Cardiovascular and Metabolic Disease: The Future of Precision Medicine

Ramcharan Singh Angom * and Naga Malleswara Rao Nakka

Department of Biochemistry and Molecular Biology, Mayo Clinic College of Medicine and Science, 4500 San Pablo Road South, Jacksonville, FL 32224, USA; nakka.naga@mayo.edu
* Correspondence: angom.ramcharan@mayo.edu

Abstract: The zebrafish (*Danio rerio*) has emerged as an appreciated and versatile model organism for studying cardiovascular and metabolic diseases, offering unique advantages for both basic research and drug discovery. The genetic conservation between zebrafish and humans and their high fecundity and transparent embryos allow for efficient large-scale genetic and drug-oriented screening studies. Zebrafish possess a simplified cardiovascular system that shares similarities with mammals, making them particularly suitable for modeling various aspects of heart development, function, and disease. The transparency of zebrafish embryos enables the real-time visualization of cardiovascular dynamics, offering insights into early embryonic events and facilitating the study of heart-related anomalies. In metabolic research, zebrafish provide a cost-effective platform for modeling obesity, type 2 diabetes, hyperlipidemia, and other metabolic disorders. Their high reproductive rate allows for the generation of large cohorts for robust statistical analyses, while advanced genetic tools, such as CRISPR/Cas9, enable precise gene editing with which to model specific genetic mutations associated with human diseases. Zebrafish metabolic models have been instrumental in elucidating the molecular mechanisms underlying metabolic diseases, studying the effects of environmental factors, and identifying potential therapeutic targets. Additionally, the permeability of zebrafish embryos to small molecules facilitates drug discovery and screening, offering a rapid and economical approach to identifying compounds with therapeutic potential. In conclusion, zebrafish cardiovascular and metabolic disease models continue to contribute significantly to our perception of disease pathogenesis, providing a platform for translational research and developing novel therapeutic interventions. The versatility, scalability, and genetic manipulability of zebrafish position them as an invaluable asset in unraveling the complexities of cardiovascular and metabolic diseases. This review presents an overview of the zebrafish model's key features and contributions to investigating cardiovascular and metabolic disorders. We discuss the benefits and drawbacks of using zebrafish models to study human disease and the critical findings revealed by the progress in this endeavor to date.

Keywords: cardiovascular disease; metabolic disease; transgenesis; zebrafish; gene editing; CRISPR; TALEN

1. Introduction

The Zebrafish was introduced as an animal model for use in genetic investigations, by Streisinger and colleagues [1]. Large-scale phenotypic screening using N-ethyl-N-nitrosourea (ENU) mutagenesis has identified several mutants [2–4]. Nevertheless, following forward genetic screening, the positional cloning of every ENU mutation required much time and effort [5]. Advanced gene-targeting techniques using zinc-finger nucleases (ZFNs), transcription activator-like effector nucleases (TALENs), and clustered regularly interspaced short palindromic repeats/CRISPR associated protein 9 (CRISPR/Cas9) have surmounted difficulties in producing targeted gene knockout alterations. CRISPR/Cas9 provides knockout animals for zebrafish researchers through a practical reverse genetic approach [6–12].

Furthermore, the use of zebrafish for understanding human genetic illnesses has been made easier by the high degree of genome structural similarity shared between humans and zebrafish (~70% of human genes have at least one evident zebrafish ortholog, while this value is 80% of human genes with respect to mouse orthologs) [13–15]. Zebrafish are increasingly being used to uncover the underlying links between the genotypes and phenotypes of numerous human diseases (Figure 1) thanks to recent developments in next-generation sequencing (NGS) and the need for tailored therapy. Zebrafish also have several advantages, including their amenability to imaging of their developing embryos at the organ level due to optical clarity and the fact that they contain hundreds of embryos in a single cluster [16,17]. Additionally, it is easier to create tissue-specific transgenic animals using a variety of well-chosen gene promoters. Through linking with regulatory components like GAL4/UAS or Cre/LoxP, the Tol2-based transgenic system in zebrafish has recently improved, allowing for the spatiotemporal regulation of gene expression [17–19]. These advantages make it possible to watch cellular dynamics in vivo and image cells in real-time, which helps us to study the underlying molecular mechanisms of different developing organs and explore the disease in vertebrates.

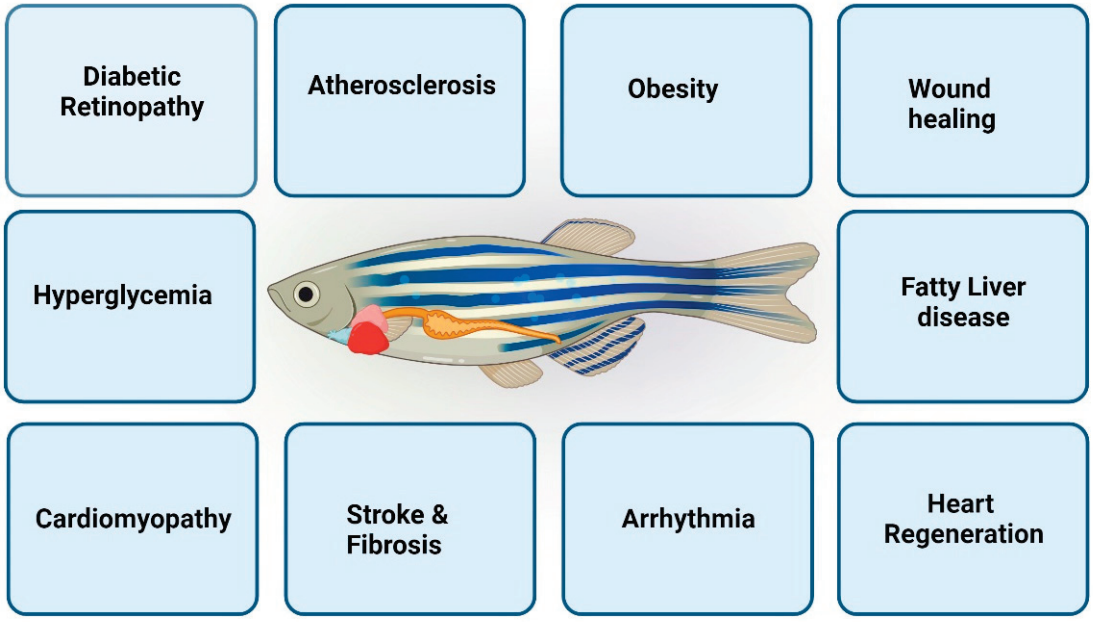


Figure 1. Outline showing various applications of zebrafish in the field of cardiovascular disease and metabolic disease.

2. Genetic Studies Using Zebrafish

Forward and reverse genetic techniques have been effectively applied to zebrafish to discover new signaling pathways and investigate gene functions. Two extensive forward genetic screens have found hundreds of mutant phenotypes related to different facets of development and embryogenesis [4,20]. Without prior knowledge of the underlying genes, such mutants have offered fresh perspectives on a wide range of intricate biological processes. Characterizing these mutants and discovering the mutated genes that produced them helped clarify the cellular and molecular causes of several human diseases since many zebrafish mutant phenotypes are like human hereditary diseases. In another landmark development, more than 50 mutant lines related to cardiac development or function were identified in early screens [21,22]. Multiple genetic regulators of the signaling cascade that are crucial for cardiovascular development were identified in these screens. Since then, several transgenic-assisted screens have been conducted [23], with a focus on certain phases of cardiac morphogenesis.

3. Methods

In order to obtain unbiased and comprehensive information, Scopus, PubMed, and Google Scholar were used as search engines to retrieve published data. The keywords used for this search include "zebrafish model of cardiovascular disease, a zebrafish model of metabolic disease". A total of 250 articles were obtained (published between 2000 and December 2023), out of which only 212 were selected based on the inclusion and exclusion criteria below.

A. Inclusion criteria:
   - A.1. Research articles that report on genetic or non-genetic models of cardiovascular and metabolic disease.
   - A.2. Research articles that involve the keywords heart failure, cardiomyopathy, hypertrophy, arrhythmia, regeneration, drug screen, obesity, diabetes, and atherosclerosis.
   - A.3. Research articles that report the genetic tools used in zebrafish to investigate cardiovascular and metabolic diseases.

B. The exclusion criteria were set to exclude the following articles:
   - B.1. Articles that report on other animal models apart from zebrafish.
   - B.2. Articles that report on zebrafish models of other vascular diseases or other diseases.
   - B.3. Articles that report on aging-related disorders.
   - B.4. Article published in languages other than English.

4. Zebrafish as Cardiovascular Disease Models

The zebrafish (*Danio rerio*) has surfaced as a valuable model organism for cardiovascular disease (CVD) research [24–26], offering unique advantages for exploring the intricacies of cardiovascular development, function, and pathology (Figure 1). This section of our review delves into the strengths and limitations of the zebrafish cardiovascular disease model, shedding light on its contributions to advancing our understanding of cardiovascular disorders. In the last decade, the zebrafish has been increasingly used for various human-disease-related studies [27,28]. For decades, mice have been predominantly used as excellent models for investigating human cardiac diseases. Although mouse models have provided valuable insight into diseased cardiac states, they also have limitations in their application, as their electrophysiological characteristics and basal heart rate are highly different compared to those of humans. Also, in vivo, the investigation of mouse models often requires invasive imaging and monitoring techniques, which requires sacrificing the animal.

Furthermore, generating and maintaining mouse lines are time consuming and expensive. As an alternative model, zebrafish can complement these bottlenecks and allow for the easy study of heart development, heart rate analysis (electrophysiology), and phenotypic characterization [21,29–31]. Zebrafish provide an alternative solution to the study of early mutations affecting the formation and function of the heart (Table 1). This section also presents an overview of some major cardiac disorders modeled using zebrafish (Table 2). These models have been developed to potentially unearth the major genes and molecular pathways that are involved in CVD pathophysiology. Numerous aspects of heart development, function, and illness have been modeled using zebrafish.

Table 1. Characteristic features of zebrafish.

Genetic Conservation and Transparency:	References
Zebrafish display a high degree of genetic similarity with humans regarding cardiovascular development and function. Their transparency during early development allows for real-time visualization of the developing heart and blood vessels, providing unparalleled insights into the molecular and cellular processes involved in cardiovascular diseases.	[13–15]
High Reproductive Output:	
The prolific reproduction of zebrafish facilitates large-scale genetic and drug-related screening studies. Their ability to generate many embryos enables researchers to investigate various genetic and environmental factors influencing cardiovascular health, promoting the identification of novel therapeutic targets.	[16,17]
Conserved Cardiovascular Physiology:	
Zebrafish possess a cardiovascular system with remarkable similarities to mammals. Their two-chambered heart, like the human heart during early development, allows for investigating basic cardiovascular processes, including heart development, contractility, and blood vessel formation, in a simplified yet biologically relevant context.	[21,26–28]
Ease of Genetic Manipulation:	
The advent of advanced genetic tools, such as ZFN, TALEN, CRISPR/Cas9, has made targeted genetic modifications in zebrafish relatively straightforward. This ease of genetic manipulation enables researchers to model specific cardiovascular diseases, study the effects of gene mutations, and identify potential therapeutic targets.	[6,7,11,12]
Drug Discovery and Toxicity Screening:	
Zebrafish's permeability to small molecules makes them amenable to drug delivery. This characteristic, coupled with the ease of monitoring their cardiac function, allows for efficient drug discovery and toxicity screening. Zebrafish models contribute to the preclinical evaluation of drug candidates for cardiovascular diseases.	[32–35]

Table 2. List of selected zebrafish models of cardiac disease.

Zebrafish Gene	*Human Orthologue*	Model	Phenotype	Reference
amhc	*MYH6*	Mutant line	Hypoplastic atrium/enlarged ventricle/ CM hyperplasia	[32]
bag3	*BAG3*	Mutant line	Ventricle hypertrophy, Trabecular density, Myofibril degeneration, Apoptosis	[36]
scl4a1a		Mutant line	Cardiomyopathy, myofibril degeneration, apoptosis, CM hypertrophy and hyperplasia	[37]
cmlc1	*MYL4*	Mutant line	Atrium enlargement, Disrupted sarcomeric structure	[38]
vmhcl	*MYH7*	Mutant line	Disrupted sarcomeric structure, Trabecular density, Enlarged ventricle	[39,40]
gja3	*GJA3, CX46*	Mutant line	Pericardial edema	[41]
gtpbp3	*GTBP3*	Mutant line	CM hypertrophy, Abnormal mitochondrial morphology, Disrupted sarcomeric structure	[42]
vclb	*VCL*	Gene trap line	Disorganized coronary development, Fibrosis, Epicardial/myocardial hyperplasia	[43]
jupa	*JUP*	Mutant lines	Cardiomegaly, Thin atrial/ventricular walls, Disrupted sarcomeric structure	[44]
plcg1	*PLCG1*		Normal myocardial ultrastructure	[45]
jag2b	*JAG2*	Ablation NC-derived CMs	Enlarged ventricle, CM hypertrophy	[46]
		Mutant line	Hypertrophic ventricle	
tnnt2a	*TNNT*	Mutant line	Abnormal sarcomeric assembly	[47]

Along with the genetic and experimental strategies used to produce and examine these models, zebrafish have contributed significantly to our understanding of heart abnormalities. Zebrafish are also helpful in identifying potential genes for congenital cardiac abnormalities. Table 2 lists some established zebrafish-based cardiovascular disease models [32,36–47].

4.1. Heart Regeneration

Zebrafish have shown great promise in the study of heart failure. Different species experience cardiac regeneration, which is an intriguing biological process, at different rates. Although cardiac tissue can regenerate in newborn mice, this ability disappears seven days after birth, and fibrotic scar formation replaces the damaged myocardium [48]. Zebrafish, among other vertebrates, have an innate capacity for cardiac regeneration after severe myocardial damage and, therefore, are now a great model for investigating the molecular pathways involved in the regeneration process [46,49]. Zebrafish also have a remarkable scope for cardiac muscle regeneration after sustaining a considerable injury and are widely used as models for regenerative studies, showing real promise in heart failure research, as compared to higher vertebrates, including mammals, adult zebrafish exhibit extraordinary regenerative potential and can regenerate many organs and tissues, including the retina [50], brain tissues [51], spinal cord [52], and heart [46,53–55]. Applying zebrafish to study cardiac tissue regeneration seems to be a practical step toward regenerative medicine. In the zebrafish heart, when 20% of the myocardium is removed, new cells differentiate from cardiac progenitor cells in a process determined by the epicardium, which appears to recapitulate many elements of embryonic cardiac development [43].

Similarly, zebrafish have also been shown to exhibit improved recovery after experimental myocardial infarction when combined with p38 MAP kinase inhibition [55]. Primary cardiomyocytes from adult zebrafish hearts can be easily isolated and cultured for up to 4 weeks and used as an alternative to in vivo experiments [56]. Several studies have focused on hypoxia's effect on zebrafish's regenerative capacity [57,58]. These studies on zebrafish have demonstrated the functions/effects of nerve growth factors in regard to stimulating cardiac regenerative processes in a failing heart by mediating cardiomyocyte proliferation [59].

Cryoinjuries (CIs) have been induced in zebrafish to model and study the mechanisms of heart regeneration and scar removal post-myocardial infarction [60]. A CI is an invasive procedure that more closely models the pathophysiological processes of human myocardial infarction [61]. A zebrafish model mimicking hypoxia-induced ischemic injury in the mammalian heart was developed to assess regenerative capacity [58]. Zebrafish exposed to hypoxia/reoxygenation (H/R) exhibited cardiomyocyte apoptosis and necrosis. However, cardiomyocyte proliferation was apparent 18–24 h after H/R; 2D-echocardiography was used to measure cardiac function, and the compromised ventricular function recovered to the baseline level. Thus, it is feasible to study reperfusion injury in zebrafish.

Further, in zebrafish, cardiac regeneration following myocardial infarction (MI) is a collective outcome involving multiple cell types. Various processes, including the infiltration of inflammatory cells, the development of fibrosis, the regeneration of cardiomyocytes, the regression of scar tissue, and the restoration of cardiac function, are orchestrated by endocardial, epicardial, fibroblast, and cardiomyocyte cells, among others [62]. In zebrafish, research has revealed that the epicardium supports myocardial regeneration in a cryoinjured heart. Cells derived from the epicardium (namely, EPDCs) migrate to the damaged myocardium after injury and differentiate into myofibroblasts and perivascular fibroblasts, which promote new angiogenesis through paracrine signaling [63]. In addition to the epicardium, the endocardium also plays a role in cardiac regeneration by providing soluble signals to cardiomyocytes and activating genes necessary for cardiac structure development and maintenance, such as hand2 and stat5b [64,65]. A recent study reported a single-cell transcriptomic analysis of non-CMs during cardiac regeneration in zebrafish. It provides an outline for questioning this process's molecular and cellular basis [66].

4.2. Zebrafish Cardiomyopathy Models

Characterizing the key genetic basis and molecular mechanisms underlying human dilated cardiomyopathies (DCM) faces major bottlenecks, and zebrafish models of DCM provide a beneficial resource in the systematic dissection of genetic pathways and the development of better therapeutic strategies [26,67–71]. Titin molecules play a role in sarcomeric assembly in the heart and are crucial for maintaining myofibrillar elasticity and integrity. A mutation in the titin gene is associated with DCM in both humans and zebrafish [72,73]. The Titin gene encodes giant-muscle filament titin (TTN) and causes autosomal-dominant DCM linked to chromosome 2q31. Zebrafish has two titin orthologs, *ttna* and *ttnb*, of which *ttna* is required for group Z-discs and A-bands in the sarcomere and for cardiac contractility. Different titin isoforms have distinct functions, and their disruption leads to variable phenotypes in DCM [72]. Zebrafish runzel mutants have been linked to one of the titin loci and are homozygous lethal with a muscular dystrophy phenotype [73].

Gene mutations in zebrafish laminin alpha4 and integrin-linked kinase were reported in a forward mutagenesis screen. Similar mutations were over-represented in a human cohort with DCM [74,75]. A knockdown of the zebrafish transcriptional co-activator eyes absent homolog 4 (EYA4) was found to recapitulate the phenotypes of impaired cardiac contraction and heart failure seen in human patients [76]. A novel Z-disk protein nexilin (encoded by NEXN) was identified in zebrafish and has been linked to DCM in humans and zebrafish [77]. Zebrafish are suitable for modeling candidate mutations and variants. Several zebrafish DCM genes have a human ortholog, and a human TNNT2 mutation that causes hypertrophic cardiomyopathy (HCM) was modeled in an embryonic zebrafish [67]. Thus, the zebrafish model provides an opportunity to explore the genetic interactions and molecular mechanisms underlying DCM. Further, zebrafish cardiomyopathy models have been utilized to explore the therapeutic potential of Wnt/β-catenin signaling in cardiac hyperplasia. An anemia-induced zebrafish model of cardiomyopathy (tr265) was used and crossed with heat-shock-inducible transgenic fish to modulate the Wnt/β-catenin pathway. Increased activity of the Wnt/β-catenin pathway improved fish survival, probably providing a cardio-protective function via increasing cardiomyocyte hyperplasia [67]. Mutations in zebrafish cardiac troponin C (cTnC) were induced using the conditional expression of antisense RNA and phenotypes wherein cardiac chambers increased in size, and a lower ventricular ejection fraction was observed when compared to the control embryos [78]. Xr1 is a fragile X-related (FXR) gene family member that is expressed in striated and cardiac muscle. The knockdown of fxr1 using antisense morpholino revealed defect reduction in cardiac function as measured via high-speed video microscopy and showed a looping defect of the atrium [79]. A study by Dhandapani PS et al. discovered functional rare RAF1 mutations in the cohorts of South Indian, North Indian, and Japanese populations with a 9% prevalence of childhood-onset DCM cases. This group modeled these mutations in zebrafish and found that due to the altered kinase activity of the RAF1 mutation, the fish embryos showed a heart failure phenotype induced by AKT hyperactivation and rescued by rapamycin [80].

Zebrafish have also been used as models for studying a disease associated with changes in the cardiac thick filaments [81]. Cardiac thick filaments were isolated from zebrafish cardiac muscle, and the structural components were analyzed and reconstructed using electron microscopy. The rebuilt structure showed similarities to mammalian cardiac filaments, thus providing a model for understanding the roles of proteins such as cardiac myosin binding protein-C or titin that form these filaments. The Pkd2 mutant zebrafish showed low cardiac output and atrioventricular block, and mutant hearts displayed disturbed intracellular calcium cycling, contributing to heart failure [82]. Transcriptome analysis of zebrafish hearts identified the corresponding ortholog for the most-known genes for human DCM [70]. The application of forward genetics to zebrafish has identified many mutated genes that impact cardiac contractile function [21,22,83].

4.3. Arteriogenesis

Arteriogenesis has been studied in several models, including mice, but these models are limited by technical difficulties, as visualizing collateral vessel development in vivo is laborious [83]. The availability of mutants with arterial defects or permanently occluded aortas would provide better insight into developing a vessel. As models for understanding arteriogenesis, zebrafish fill this gap as they share the mechanisms of artery development found in mammals [84–86]. The role of ischemia in arteriogenesis is disputed, and mouse models have failed to resolve this question. A zebrafish arteriogenesis model was developed because a zebrafish embryo gains sufficient oxygenation via diffusion to prevent ischemia in response to arterial occlusion [84]. A laser induced aortic occlusion, in zebrafish showed collateral vessel development in the absence of ischemia.

Zebrafish have been used to study the role of N-ras signaling during endothelial differentiation in vertebrates. The zebrafish lmo2 promoter was used to express a constitutively active version of human N-Ras, specifically in endothelial and hematopoietic cells. Activated N-Ras signaling disrupted the balance of arterial–venous specification. This model effectively provides new insights into the pathogenesis of congenital human vascular disease and tumorigenic angiogenesis [87,88]. The availability of zebrafish mutants with arterial defects or permanently occluded aorta would help us understand arteriogenesis, as they share the mechanisms of artery development found in mammals [88]. One such mutant is the zebrafish gridlock mutant. This mutant displayed an incompletely formed lateral aorta and is deficient in circulation. ERK signaling is important to arteriogenesis in zebrafish. Activation of ERK1/2 in gridlock mutants by partially inhibiting PI3K activity restores the distal arterial circulation [89].

Further, the role of ischemia in arteriogenesis is disputed, and mouse models have failed to resolve this question. A zebrafish arteriogenesis model is feasible because the embryo gains sufficient oxygenation via diffusion to prevent ischemia in response to arterial occlusion [84]. It was found that collateral vessels could develop in the absence of ischemia. This study underscores zebrafish's utility as a collateral vessel development model, allowing a novel approach to the study of arteriogenesis.

4.4. Thrombosis

Platelets play a crucial role in primary homeostasis and facilitate thrombus formation; thus, they are a primary pharmaceutical target, as decreasing thrombus formation can minimize the incidence of myocardial infarction and stroke. Understanding the mechanisms involved in platelet function and thrombus formation is imperative to identify drug targets for vascular disease management. Though mouse knockout models have provided insights into characterizing individual genes, their use is limited by requirements for substantial investments and manpower and the possibility of being unable to guarantee a relevant phenotype. In this scenario, the zebrafish (*Danio rerio*) is being explored as a model for studying thrombosis [90–95]. The zebrafish thrombocyte is the functional equivalent of the mammalian platelet. The ability to induce localized thrombosis by targeted laser injury [92], along with the transparency of the zebrafish embryo, enables real-time observation of arterial or venous thrombus formation after an endothelial injury. Forward genetic studies are underway to identify genes determining the thrombotic response to such arterial injuries [92]. Liu Yang et al. generated a zebrafish model of anti-thrombin III (AT3) deficiency by adopting a reverse genetics approach using zinc-finger nucleases [93]. Homozygous at3 zebrafish mutants showed intra-cardiac thrombosis between 2 and 7 months of age. This study uncovered the mechanism behind the at3 mutant phenotypes and suggested a conserved role of the At3 function in zebrafish.

In vivo reverse genetics functional screening of new platelet genes in zebrafish is easy. A comparative transcript study of platelets and their precursor cells, megakaryocytes, nucleated blood cell elements, endothelial cells, and erythroblasts revealed several unique platelet membrane proteins with unknown roles in thrombus formation. Reverse genetics was used to study five genes in a laser-induced arterial thrombosis model. BMP, BAMBI,

and LRRC32 may promote thrombus development. Many large-scale screening programs and genome-wide association and "omics" studies have found genes and loci involved in platelet production and physiology under normal and pathologic settings. Such a resource requires enhanced model systems for in vivo gene functional assessment and the validation of new anti-thrombotic advances [94–99]. Zebrafish models have the potential to facilitate these gene discovery advancements and thus can be utilized for functional validation and in therapy-based studies to address thrombus formation.

Understanding the mechanisms involved in platelet function and thrombus formation is imperative to identify drug targets for vascular disease management. Though mouse knockout models have provided insights into characterizing individual genes, their use is limited by requirements for substantial investments and manpower and the possibility of being unable to guarantee a relevant phenotype. In this scenario, the zebrafish (*Danio rerio*) is being explored as a model for studying thrombosis [99–102]. The zebrafish thrombocyte is the functional equivalent of the mammalian platelet. Thrombocyte proliferation and maturation during zebrafish embryogenesis can be easily tracked using the integrin CD41/CD61 subunit, a platelet-specific marker [100]. The ability to induce localized thrombosis via targeted laser injury [95], paired with the transparency of the zebrafish embryo, enables the real-time observation of arterial or venous thrombus formation after an endothelial injury. Forward genetic studies are underway to identify genes determining the thrombotic response to such arterial injuries [103].

The zebrafish is amenable to the functional screening of novel platelet genes. For example, the function of five of these genes was studied in a laser-induced arterial thrombosis model using a reverse genetics approach, as reviewed by Gut et al. 2017 [104]. Putative roles of BMP, activin membrane-bound inhibitor homolog (BAMBI), and Leucine-rich repeat-containing protein 32 (LRRC32) in promoting thrombus formation were identified. It was found that Discoidin, CUB, and LCCL domain-containing protein 2 (DCBLD2) and endothelial cell adhesion molecule (ESAM) serve to inhibit thrombus formation. Such information on molecules and genes that either support or inhibit platelet-led thrombus formation is essential for designing targets for therapeutic intervention for thrombosis management. In a separate study, Zhu et al. utilized zebrafish to assess anti-thrombotic drugs. This study tested six human antithrombotic drugs (aspirin, clopidogrel, diltiazem hydrochloride, xuanshuantong, salvianolate, and astragalus) in a zebrafish thrombosis model. A larval zebrafish thrombosis model was designed and validated for in vivo studies for quick antithrombotic medication screening and efficacy assessment [103]. Several large-scale screening programs and genome-wide association and "omics" studies have discovered genes and loci associated with the formation or physiology of platelets under normal and pathologic conditions. Such a resource necessitates the availability of improved model systems that permit in vivo functional assessment of these genes and the validation of recent innovations in anti-thrombotic [99,100]. The Zebrafish model has the potential to facilitate these gene discovery advancements and thus can be utilized for functional validation and therapy-based studies to address thrombus formation. Recently, Zhu et al. have shown that Wuliangye prevents and reduces thrombosis via changing metabolic and signaling pathways associated with platelet aggregation and adhesion, oxidative stress, and the inflammatory response [105].

4.5. Modeling Cardiac Rhythm Disorders in Zebrafish

Zebrafish have been widely employed in arrhythmia research [31,106–110] owing to the success of multiple genetic screens, resulting in mutants resembling arrhythmic conditions [21]. The classic genome-wide screening techniques that have been used make genetic models of organisms such as yeast, nematode, or drosophila, powerful tools in the dissection of cell signaling and other phenotypes, have not proven feasible for many physiologic traits, including cardiac electrophysiology [111–114]. Zebrafish models have facilitated the rigorous exploration of arrhythmia mechanisms and allowed systematic approaches to discovering and testing novel drugs or other interventions [113–117]. The earliest electro-

physiological phenomena in cardiac development are accessible in zebrafish. Calcium and voltage transients can be easily recorded in the cardiac primordia before midline migration and fusion into the primitive heart tube [116]. The physiological events in zebrafish are tied closely with cardiac development and can be visualized in vivo (Table 3) [113]. Zebrafish embryonic and adult heart rates and AP and ECG morphology closely resemble those of humans [112–115]. Thus, the zebrafish is a relevant research model for investigating ion channel disorders associated with abnormal repolarization or Ca^{2+}-modulated arrhythmias [31]. Humans frequently experience atrial fibrillation (AF). Sequencing of AF patients revealed a mutation in the BMP antagonist gremlin-2 (GREM2). Zebrafish functional modeling showed that GREM2 regulates BMP signaling to influence cardiac laterality and atrial development. Live heart imaging of zebrafish embryos overexpressing wild-type or mutant GREM2 showed decreased atrial cardiomyocyte contraction rates. Zebrafish can be utilized to study the etiology of human AF and identify novel regulators [113,118]. Many zebrafish lines with ion channel mutations are being exploited as vertebrate models for long- or short-QT syndrome [35]. For this, a transgenic zebrafish arrhythmia model with the human SCN5A-D1275N mutation was developed. Mutations in the cardiac sodium channel SCN5A-D1275N in humans and mice cause atrial and ventricular arrhythmias. SCN5A-D1275N transgenic zebrafish exhibited bradycardia, conduction-system defects, and early death. ECG measures for embryonic and larval zebrafish have been refined to assess QT-prolonging medications, including terfenadine, verapamil, and haloperidol. ECG recording may be used to investigate drugs for cardiac cycle abnormalities and downstream effects, including heart block and arrhythmias in zebrafish larvae and adult [33,34]. The lack of high-throughput functional assays hinders long-QT syndrome genetic testing for determining gene variant pathogenicity correctly. Zebrafish assays have been established to investigate the capacity of known long-QT syndrome hERG1 (KCNH2) mutations and polymorphisms to achieve proper repolarization in kcnh2-knockdown embryonic zebrafish. Genetic modeling and the molecular dissection of human rhythm disorders, as well as the study of electrophysiological features and screens to identify key molecules and pharmacological targets, can be easily achieved in zebrafish models.

Table 3. Zebrafish and Human Electrophysiology.

SL	Resemblances in Electrophysiology between Zebrafish and Humans	Reference
1	Similar long plateau phase	[112]
2	Presence of 0–4 phases	[112,113]
3	Ventricular AP has similar duration. The duration of zebrafish ventricular AP at 19 °C is like human ventricular AP at 37 °C	[114]
4	IK1 is present in atrial and ventricular myocytes	[112,114]
5	IK1 and IKr are the major repolarizing currents in both hearts	[115]
6	Similar fundamental current systems (INa, ICaL, and IK) are present in atrial and ventricular myocytes	[113,114]
7	Atrial and ventricular myocytes of the zebrafish heart have both T-type (ICaT) and L-type (ICaL) Ca^{2+} currents	[112–114]
8	The distinct QT intervals in ECG are similar in both	[112,114]
9	P, QRS, and T waves are clearly distinguishable in a zebrafish ECG	[112,114]

The human and two-chamber zebrafish hearts have similar baseline electrocardiograms despite their anatomical differences. Their P, QRS, and T waves; QT interval duration; and sluggish heart rate were like those of humans (Figure 2). Like human QT duration, zebrafish QT duration is heavily dependent on cardiac frequency and must be corrected for heart rate (QTc) [35]. Many pathological ECG abnormalities in human hearts can be repli-

cated in zebrafish. The sequencing of atrial fibrillation (AF) patients revealed a variance in the BMP antagonist gremlin 2. Functional modeling of GREM2 in zebrafish revealed that it affects cardiac laterality and atrial differentiation by regulating BMP signaling. Using live heart imaging of zebrafish embryos that over-expressed wild-type or variant GREM2, slower cardiac contraction rates were recorded, specifically in atrial cardiomyocytes. The implications of BMP signaling in human AF were uncovered, demonstrating that zebrafish can be used to investigate mechanistic insights into the pathogenesis of this disease and that novel regulators can be identified [118]. Several zebrafish lines with ion channel mutations are now being used as vertebrate models for understanding long- or short-QT syndrome [105].

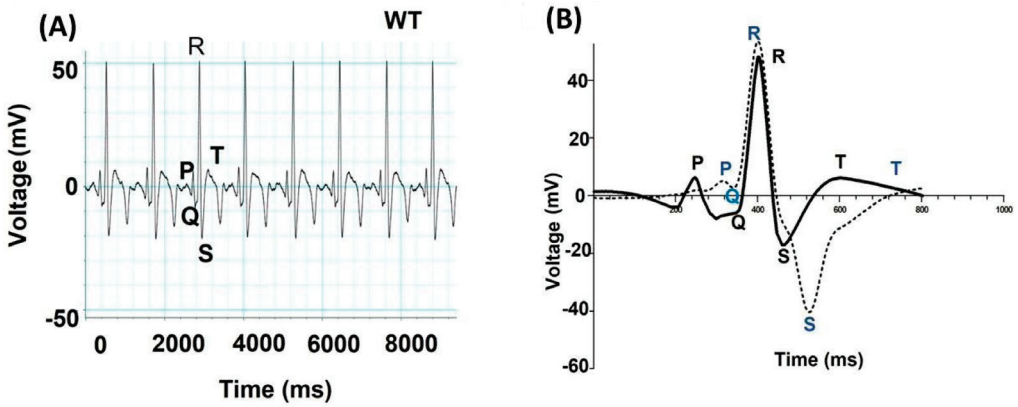


Figure 2. Adult zebrafish electrocardiogram (**A**) Electrocardiogram recordings of wild-type ($bh^{+/+}$) zebrafish. X-axis represents time in milliseconds (ms), and Y-axis represents voltage in millivolts (mV). (**B**) Graph showing an overlay of wild type and $bh^{-/-}$ mutant ECG recordings (Regular line and dashed line represents the ECG profiles of wild type and $bh^{-/-}$ fish, respectively). P, Q, R, S & T represent regular ECG waves. The image in the figure were adapted from the author's publication [119].

Towards this end, a transgenic zebrafish arrhythmia model with the human SCN5A-D1275N (cardiac sodium channel) mutation was created. The mutations in SCN5A-D1275N are associated with various cardiac phenotypes, including atrial and ventricular arrhythmias in humans and mice. Transgenic zebrafish expressing the SCN5A-D1275N mutation exhibit bradycardia, conduction-system abnormalities, and premature death. These phenotypes could be rescued using both human and zebrafish mRNA, suggesting a conserved role of SCN5A in vertebrate heart rhythms. Thus, zebrafish in vivo models for human genetic variants offer a functional assessment of cardiac ion channel genes and the mechanisms involved [35].

ECG measurements have been optimized for embryonic and larval zebrafish to quantify the effect of QT-prolonging drugs such as terfenadine, verapamil, and haloperidol. This circumvents the usage of mammals in ECG-based preliminary screening to detect cardiac dysfunction [34]. A significant problem with genetic testing for long-QT syndrome is the lack of robust functional assays with which to accurately decipher the pathogenicity of identified gene variants in a high-throughput manner. To address this problem, a zebrafish assay was developed to test the ability of known long-QT syndrome hERG1 (KCNH2) mutations and polymorphisms to attain normal repolarization in a kcnh2-knockdown embryonic zebrafish. Kcnh2 is the only repolarizing ion channel in the embryonic zebrafish ventricle. This assay could correctly distinguish a benign variant from a disease-causing variant. The cited study demonstrated the utility of zebrafish in designing cardiac assays that can serve as additional tools for testing the pathogenicity of gene variants in cardiac disorders. Another group developed a larval zebrafish model to quantify chronotropic, inotropic, and arrhythmic effects together with blood flow and vessel diameter. Cardio stimulants (adrenaline and theophylline) and negative chrono/inotropes (cisapride, haloperidol, terfenadine, and verapamil) were evaluated in zebrafish, and cardiac chamber

beat frequencies were recorded. Such a model thus has implications for higher-throughput drug safety and efficacy applications [120]. Therefore, genetic modeling and molecular dissection of human rhythm disorders, the study of electrophysiological features, and screens to identify key molecules and pharmacological targets can be easily achieved in the zebrafish model. APs from adult zebrafish ventricular myocytes were recorded for the first time by Brette et al. [117] and further characterized by Nemtsas et al. (2010) [115]. These pioneering works showed that the resting membrane potential and AP amplitude were similar in ventricular myocytes isolated from humans and zebrafish. Like humans, the zebrafish AP had a plateau rather than a spike or phase 1. Zebrafish have a shorter action potential duration (APD) than humans due to their higher resting heart rate. Like humans and other bigger mammals, APD shortens as stimulus frequency increases due to a shorter plateau phase. Thus, zebrafish ventricular APs mirror those of big mammals, including humans, unlike mice and rats' triangular and nearly rate-independent APs.

4.6. Limitations of Zebrafish as a Cardiovascular Disease Model

4.6.1. Simplified Cardiovascular Anatomy

The zebrafish cardiovascular system is simpler than that of mammals, lacking certain structures such as a coronary circulation system. While it allows for studying basic cardiovascular processes, some aspects of human cardiovascular diseases may not be fully recapitulated in zebrafish models.

4.6.2. Limited Behavioral Studies

The behavioral aspects of cardiovascular diseases, including exercise tolerance and complex cardiovascular responses to stress, are challenging to study in zebrafish. This limitation underscores the need for complementary studies using mammalian models to capture the full spectrum of cardiovascular disease manifestations.

4.6.3. Temperature Sensitivity

Zebrafish are ectothermic, and their physiological processes are influenced by temperature. This temperature sensitivity can pose challenges when attempting to model certain aspects of cardiovascular diseases that are temperature-dependent.

5. Summary

Since their introduction, Zebrafish have been used extensively to investigate the circulatory system. In recent decades, zebrafish have become an essential model for heart development, illness, and regeneration. The zebrafish is a great model for disease causes and potential treatments due to its transgenic availability and amenability to genetic manipulation and in vivo chemical and genetic screening. With its unique ability to regenerate, the zebrafish heart offers a great chance to learn how to battle fibrosis and cardiomyocyte loss with a natural origin. Finding the molecular mechanisms governing these activities will lead to HF and other heart disease treatments. Recent instances show that this animal model can be used to find new cardiomyopathy susceptibility genes and intriguing treatment targets despite technical obstacles. In the coming years, gene-editing tools will improve, allowing those involved in precision medicine to understand this disease's biology and find cures.

6. Metabolic Disease Models

Zebrafish represent an intriguing animal model for comprehending the pathophysiology of metabolic disorders in humans and pinpointing prospective treatment avenues [121] (Figure 1). The metabolic features of zebrafish are comparable to those of humans, so they can be used to supplement information derived from other model organisms, such as rats. This possibility has been amply demonstrated by recent research [122–125] that found that medications licensed for treating human metabolic disorders also worked well in a zebrafish model. Numerous potential human disease genes and loci linked to metabolic

disease have been found thanks to genome-wide association studies (GWAS) and, more recently, whole-exome and whole-genome sequencing [126]. How these genes work and how their malfunction impacts pathophysiology are the current problems in this regard. Zebrafish have been used to effectively examine variant function in vivo at a reasonably high throughput in various disease areas. In recent work, platelet production, which has implications for hematological disease, was discussed [127]. These advantages of zebrafish can be used to make comparable advancements in the field of metabolism. In this section of our review, we focus on the use of zebrafish as an animal model for metabolic disease and their pros and cons in this application. We also examine the latest developments in modeling the associated disorders of metabolic syndrome—obesity, diabetes, fatty liver disease, and atherosclerosis—using zebrafish.

Recently, zebrafish have become popular models for metabolic disorders [128]. This review aims to provide an overview of the strengths and limitations of the zebrafish metabolic disease model, highlighting its contributions to our understanding of metabolic disorders. Though more research is required, evidence supports the idea that zebrafish have similar control mechanisms due to similarities in the peripheral nervous system's development and the way drugs that affect the serotonergic or adrenergic systems can modify glucose metabolism [129,130]. Zebrafish metabolism research has advanced slowly compared to the cardiovascular discipline due to these and other factors. Table 4 presents some of the established metabolic disorder models: acute hyperglycemia [131–134], chronic hyperglycemia [133–138], genetically induced [139–141], and obesity [142–144]. We discuss select zebrafish-based metabolic disease models below.

Table 4. Zebrafish metabolic disease models.

Disease	Method of Induction	References
Acute Hyperglycemia	Induced by intraperitoneal injection of D-glucose	[132,133]
	Chronic Hyperglycemia	
1	Induced by the destruction of pancreatic cells	[134–136]
2	The induction of chronic hyperglycemia by dissolving D-glucose in fish water	[137]
3	Genetic induction	[138–140]
Obesity	Overfeeding models	[141–143]

6.1. Obesity

Over time, accumulating significant quantities of dietary triglycerides in adipose tissue leads to obesity. While obesity is increasingly being recognized as a disease in and of itself, a person's genetic history, gender, and lifestyle and environmental factors all have a significant impact on their likelihood of developing diabetes. For instance, certain people who are extremely fat but deemed healthy in terms of blood lipid profiles and insulin resistance, glucose regulation, and cardiovascular parameters are known as "healthy obese" people. It is believed that a significant factor in preventing difficulties linked to obesity is a strong ability to store neutral lipids and prevent systemic inflammation instead of exposing peripheral tissues to triglycerides, cholesterol, and fatty acids [145–147]. Zebrafish are used to study genetic and dietary factors that control the growth and plasticity of adipose tissues, as well as mechanisms of lipid absorption, packing, transport, and inflammatory responses to aggressive lipid moieties [148,149]. The underlying principles of adipose formation in zebrafish are like those in humans. Adipocytes are first seen in larvae soaked in the neutral lipid dye nile red approximately 7 days after they start feeding, whereas no adipocytes form in animals that are denied nourishment [150]. During the first four days of development, the yolk sac stores and synthesizes lipids [151], but its anatomical shape and energy substrate packing are not much like those of human adipose tissue. At around

30 dpf, when the energy is no longer entirely used for somatic growth, subcutaneous and visceral fat pads anatomically resembling human adipose tissue first develop [150,152,153].

Studies on genetic gain and loss of function have shown that numerous genetic mechanisms influencing adiposity in zebrafish are like those in mammals [154,155]. Nevertheless, deleting leptin signaling, one of the most researched signaling pathways that controls body fat mass, does not demonstrate a conserved function. When compared to healthy individuals, human patients with mutations impacting leptin signaling exhibit excessive eating tendencies, are morbidly obese, and have lower fertility. Similar behaviors are observed in mouse models; after eating, insulin stimulates the release of leptin, which is strongly expressed in mammalian adipocytes [156]. Zebrafish lacking the leptin receptor lepr, on the other hand, exhibit normal growth, fat accumulation, eating patterns, and fertility [157]. Zebrafish fat virtually never expresses the lep gene, but their liver experiences a rise in mRNA levels when they fast.

Zebrafish research has yielded genuinely innovative discoveries in the field of obesity [158,159]. Recent research, for instance, has uncovered a mechanism of PLXND1, a gene linked in population genetics studies to variations in the distribution of fat between the hips and waists in humans and an elevated risk for type 2 diabetes mellitus (T2DM) [160]. While Plexin D1 deletion in mice results in embryonic death before the development of visceral fat [161], Plexin D1/zebrafish is accessible for investigation. Interestingly, visceral fat depots in the zebrafish mutant are hyperplastic, with a reduced capacity to store lipids [161]. As visceral fat tissue could not grow under high-fat diet (HFD) conditions, surplus lipids had to be redistributed to subcutaneous depots. It was demonstrated that modifying the extracellular matrix surrounding the cell is the fundamental mechanism behind this process. This work offers an intriguing set of in vivo and ex vivo adipose tissue-imaging techniques that could be of great value for similar investigations in the future, in addition to revealing novel activities of plxnd1 [161,162].

Though adipose tissue is absent in the early stages of embryonic and larval zebrafish development, other aspects of lipid metabolism can be studied; for instance, the zebrafish gastrointestinal system is anatomically and functionally similar to the mammalian system [163,164]. One way to see lipid uptake and processing in enterocytes is to feed fluorescently tagged lipid moieties to zebrafish larvae. Using this technique, forward genetic search revealed a fat-free mutant, whose reduced processing of cholesterol and phospholipids was accompanied by unchanged intestinal morphology [164]. Later research revealed that this fat-free mutant is responsible for expressing Ang2, a conserved member of the Golgi-associated retrograde protein (GARP) complex, which controls autophagy, endosomal cholesterol trafficking, and lysosomal enzyme sorting [165,166].

6.2. Non-Alcoholic Fatty Liver Disease

Regardless of alcohol intake, nonalcoholic fatty liver disease (NAFLD) is the most common lipid storage disease of the liver and is mainly caused by high-fat diets and foods high in carbohydrates [167]. It is regarded as a consequence of obesity and affects more than 30% of the general population, as well as an even higher percentage of obese people. It is treatable via diet, but if left unchecked, it puts the body at risk for developing cirrhosis, hepatocellular carcinoma, and non-alcoholic steatohepatitis (NASH) [168]. It is unclear which hereditary variables cause benign nonalcoholic fatty liver disease (NALFD) to develop into inflammation, fibrosis, and, ultimately, malignant liver cancer [169]. The benefit of studying NAFLD in zebrafish is that whole-mount Oil Red O staining for neutral lipids allows for the visualization of steatosis in larvae [170,171]. Zebrafish can be fed lipid-rich meals, such as an egg yolk emulsion [172] or Artemia brine shrimp, after feeding begins at 4 dpf. As an alternative, steatosis has been induced via fructose-based or ketogenic diets [173]. Because the larval liver is large enough to be dissected easily, samples can be used for transcriptome, histological, and biochemical investigations [172]. Further, several transgenic lines are available for observing hepatic cell types, such as hepatocytes, biliary cells, endothelial cells, and stellate cells [174,175]. Adult zebrafish can be fed certain

diets for an extended period, and the lipid content of their livers can be assessed using metabolomics or traditional enzymatic techniques [173,176].

Large-scale forward genetics screens once more yielded the first zebrafish models of NAFLD, indicating that significant insights into disease mechanisms can be attained by methodically searching for mutations that cause NAFLD and examining their involvement in this illness's course [176–178]. An ENU mutagenesis screen revealed 19 novel hepatomegaly-characterized mutant lines, most of which showed neutral solid lipid staining. Numerous mutants have distinct histological pathological characteristics, varying from mild cases of micro- or macrovesicular steatosis to severe indications of nonalcoholic steatosis, which include hepatocyte necrosis and ballooning [179]. Cloning the genes impacted by these mutations will probably provide crucial information on how chronic liver disease develops.

6.3. Atherosclerosis

Zebrafish possess features that aid in the study of atherosclerosis, such as the ability to detect lipid deposits inside blood vessels in vivo. According to a series of landmark investigations by Miller's team, wild-type zebrafish continuously fed high-cholesterol diets are more likely to develop histological alterations resembling human atherosclerosis than rodents [164,180]. Therefore, research on murine atherosclerosis relies on a sensitive background, like ApoE/E animals [181]. The fact that the ortholog of the human cholesteryl ester transfer protein (CETP) remains preserved in zebrafish but has vanished from rat genomes provides an evolutionary explanation for this anomaly. Hence, zebrafish experience atherogenic events more frequently than humans because cholesteryl esters in fish are redirected from protective HDL cholesterol particles to "bad" LDL. Miller's group also demonstrated that single-chain monoclonal antibodies coupled with GFP can be used to visualize the oxidation of LDL by malondialdehyde, thereby exploiting zebrafish's advantages for in vivo imaging [180]. Moreover, tracking and measuring the recruitment of macrophages to vascular lesions can be used to develop novel treatment approaches.

Interestingly, the human liver X receptor (encoded by LXRA and LXRB) has functionally conserved activities in zebrafish [182]. In contrast to mice, zebrafish have a single lxr ortholog (encoded by lxra/nr1h3), making it possible to determine its physiological roles through comparatively simple gain- and loss-of-function tests. Zebrafish with the lxra// knockout allele remain alive. However, they exhibit high blood and liver cholesterol levels following prolonged adherence to a high-fat diet (HFD), like the cholesterol intolerance shown in Lxra// and Lxrb// double knockout mice. The authors also showed through overexpression experiments that increased Lxr function, particularly in enterocytes, could have the opposite impact, i.e., a significant slowdown in the accumulation of cholesterol in the blood and liver in response to HFD [183]. From a mechanical perspective, it was discovered that Lxr triggers an acyl-CoA synthetase (encoded by acsl3a) that breaks down ingested lipids and directs them toward lipid droplets for storage rather than rapid release into the bloodstream. This finding has significant clinical implications because multiple studies suggest that postprandial elevations in cholesterol are the primary cause of atherosclerosis. Statins, which prevent the liver's de novo manufacture of cholesterol, do not, however, mainly successfully regulate the postprandial dynamics of cholesterol.

6.4. Diabetes

The Zebrafish has been explored as a suitable model for diabetic research [184,185]. Zhang et al. demonstrated that a new diet-induced obesity (DIO) zebrafish has been shown to display higher blood glucose levels after fasting than normally fed ones. This hyperglycemic zebrafish is a helpful model for T2DM, measuring glucose tolerance, insulin production, and glycaemia responsiveness to human anti-diabetic medications. In addition, liver–pancreas RNA-seq research shows that T2DM zebrafish share human pathogenic pathways [185]. When responding to damage and metabolic stresses, a zebrafish's beta cell mass is remarkably malleable [135,186]. Zebrafish research has primarily focused on

the dissection of the genetic cues that govern the formation, maturation, and flexibility of functioning beta cells. This work is beginning to yield significant insights for therapies for replacing and regenerating beta cells. In this context, several different strategies are being investigated, ranging from the in vitro differentiation of mature beta cells from induced pluripotent stem cells to the in vivo restoration of sufficient numbers of functional beta cells through progenitor pools, non-beta cells, or remaining beta cells [186–188]. Because each progenitor and cell type within the islet can be seen and tracked over time in vivo using fluorescent reporter proteins until the formation of a mature pancreas throughout the embryonic, larval, juvenile, and adult stages, zebrafish are anatomically well suited for this purpose [189–201]. Zebrafish have a single primary islet located in the pancreas's head in addition to numerous minor islets spread throughout this organ [191,192]. Once again, forward genetic screens provided the first research indicating that zebrafish may be used to analyze the genetic network controlling endocrine pancreas development [194]. A line with a mutation in the homeobox gene vhnf1, which prevents normal expression of pdx1, a transcription factor gene required for the induction of the insulin gene, was found in an insertional mutagenesis screen [140]. Lesions in these genes are known to induce a subtype of monogenic diabetes called mature-onset diabetes of the young (MODY) type V for VHNF1 and type IV for PDX1.

Hence, the significance of these findings with respect to this condition became evident. It was subsequently demonstrated that pdx1 deletion in zebrafish results in a drop in insulin levels, a disruption of glucose homeostasis, and a reduction in beta cell numbers [141]. These days, drug screens are performed to identify small compounds that stimulate or obstruct distinct stages of endocrine lineage maturation and specification. Ultimately, these chemicals may be employed to boost the yield of mature beta cells from iPS cells in vitro or stimulate precursor populations that can produce new beta cells in vivo [194]. Using the double transgenic lines Tg(Tp1:hmgb1-mCherry) and Tg(pax6b:GFP), a screen demonstrated that this method was able to identify pax6b-positive progenitor cells inside the intrapancreatic duct [194]. The intrapancreatic duct cells were marked by a Notch activity reporter carried by Tg(Tp1:hmgb1-mCherry) animals. When Notch signaling is suppressed, these progenitor cells are activated, becoming beta cells.

6.5. Limitations of Zebrafish as a Metabolic Disease Model

Researching zebrafish energy metabolism uncovers additional technological difficulties. For instance, zebrafish find it challenging to perform standard tests for humans, such as hormone and glucose tolerance and insulin test. Because the macro- and micronutrient requirements of humans and zebrafish differ significantly, it is challenging to convert dietary data from interventions for zebrafish into human diet guidelines. Monitoring a zebrafish's food intake in a tank is challenging, yet food intake is strongly correlated with growth rate, affecting adipocyte production. This is because zebrafish, throughout young adulthood, prefer somatic growth over body fat deposition. When raising a family of wild-type siblings, this issue becomes apparent since there can be significant variations in growth rates and adiposity due to competition for food, genetic background variances, and other variables. In this poikilothermic mammal, temperature also influences development, metabolic rate, and body fat composition.

Additionally, the microbiome may have an impact on metabolism, which is not taken into account in zebrafish facilities. In contrast to traditional or even specialist germ-free (SPF) mouse housing, water circulation carries the risk of many more possible pathogens. Zebrafish have been shown to have a core microbiome. Currently, several groups are investigating how alterations in the microbiota of the zebrafish gut, either those naturally occurring or caused by infections, affect lipid and glucose homeostasis, an idea that is gaining much attention with respect to mammals. The regulation of systemic metabolism in zebrafish through the innervation of glands such as the thyroid, chromaffin cells, and pancreas, or that of metabolic organs such as enterocytes, the liver, and adipose tissue by sympathetic and parasympathetic inputs, is another aspect that is still mainly unknown.

6.6. Mammalian-Specific Aspects

While zebrafish share many genetic similarities with humans, they lack certain mammalian-specific aspects of metabolism. Therefore, findings from zebrafish studies need to be validated in mammalian models and, ultimately, in human clinical trials to ensure the relevance of the results.

6.7. Limited Tissue Complexity

Zebrafish organs are less complex than those of their mammalian counterparts. This limitation may restrict zebrafish models' ability to fully capture the intricacies of certain metabolic diseases, especially those involving highly specialized tissues or organs.

6.8. Limited Behavioral Studies

Behavioral aspects of metabolic diseases, such as diet-induced behaviors and complex feeding patterns, are challenging to study in zebrafish. This limitation may impede a comprehensive understanding of the behavioral aspects associated with metabolic disorders.

7. Summary

Many metabolic diseases have been modeled in zebrafish. Despite its limitations, the zebrafish model has been successfully used to visualize dynamic cell processes and conduct high-throughput small-molecule screens for illnesses impacting β-cell function. The zebrafish models for obesity, NAFLD, and atherosclerosis are poised to exploit this model system's benefits and replicate diabetes developments. The zebrafish model could attain its full potential in metabolism research via the creation of fluorescence reporter lines for adipose tissue and hypothalamus cell types and enhanced insulin-signaling techniques. Zebrafish-based metabolic disease models provide several fascinating possibilities. We hope the zebrafish system will help us understand metabolic disease development and progression and find new therapy options.

8. Conclusions

In the last two decades, the zebrafish model has emerged as a powerful model system for studying cardiac development, cardiac functions, and human heart disorders. Several zebrafish genetic screens have yielded a collection of cardiac mutants affecting several processes during early heart development and chamber morphogenesis. It is easier to follow the details of cardiac development by combining this cardiac mutant with high-resolution and advanced (3D and 4D) imaging tools. Moving forward from development to function, there has been a paramount development in the genome-editing tools in zebrafish biology. Specifically, targeted gene mutations can be easily created in zebrafish germlines by applying zinc-finger nucleases (ZFNs) and recently developed TALENS and CRISPR technologies. These tools have overcome the limitation of being unable to perform site-directed mutagenesis in zebrafish. The progress in gene-editing and targeting technologies has provided a scope for the functional studies of genes and variations implicated in CVD in zebrafish. This fish model is being utilized for investigating adult cardiac disorders as it provides the advantage of enabling the study of adult heterozygous fish to obtain insights into the progression of cardiac disease and its pathogenesis.

Further, zebrafish have provided significant contributions in the field of drug discovery, and it is expected that these efforts will soon generate a library of compounds with cardiovascular disease-monitoring properties. This is strongly supported by pharmacological screens that have yielded compounds beneficial for managing or treating cardiovascular disorders. Altogether, zebrafish cardiovascular research has provided evidence filling the knowledge gap in understanding human and other mammalian cardiac development and disorders. The current review provides an overview of the existing tools and resources available in zebrafish research and discusses the various advancements in this field.

The zebrafish cardiovascular disease model has proven to be an asset in cardiovascular research, offering unique advantages in terms of genetic conservation, transparency,

and ease of genetic manipulation. While this model has its limitations, particularly in reproducing the complexity of the mammalian cardiovascular system, its contributions to understanding basic cardiovascular processes and facilitating drug discovery are undeniable. As technology continues to evolve, the zebrafish model will continue to be a powerful tool for exploring the causes of cardiovascular diseases and developing innovative therapeutic strategies. On the other hand, the zebrafish metabolic disease model offers a powerful platform for investigating the genetic and molecular mechanisms underlying metabolic disorders. Its genetic similarity, transparency, reproductive rate, and cost-effectiveness advantages make it a valuable tool for high-throughput screening and large-scale studies. However, researchers should be mindful of this model's limitations, emphasizing the need for complementary studies in mammalian models and clinical settings to validate and translate findings into human therapeutic applications. As technology advances and researchers refine their approaches, the zebrafish model will likely continue playing a fundamental role in evolving our understanding of metabolic diseases.

9. Future Directions

The future of zebrafish research in cardiovascular and metabolic studies offers exciting possibilities, driven by technological advancements, interdisciplinary approaches, and the ongoing expansion of our understanding of these complex biological processes. Below, we provide some potential future directions for zebrafish research in cardiovascular and metabolic research.

9.1. Precision Medicine and Personalized Therapies

Leverage zebrafish models for understanding the genetic basis of individual variation in cardiovascular and metabolic responses. Explore personalized therapeutic interventions based on genetic and molecular profiles.

9.2. Functional Genomics and Systems Biology

Combine high-throughput genetic screens with advanced imaging technologies to uncover novel regulators of cardiovascular and metabolic pathways. Apply systems biology approaches to integrate multi-omics data to understand biological networks comprehensively.

9.3. Single-Cell Analysis

Adopt single-cell RNA sequencing and other single-cell technologies to dissect cellular heterogeneity within the heart and metabolic tissues. Investigate how individual cell types contribute to disease progression and response to therapies.

9.4. Live Imaging and 3D Models

Enhance real-time imaging techniques to capture dynamic processes in cardiovascular and metabolic tissues at cellular and subcellular resolutions. Develop advanced 3D culture systems that better mimic in vivo conditions for studying tissue-specific responses.

9.5. Integrative Models for Disease Complexities

Create multifactorial zebrafish models that better incorporate genetic, environmental, and lifestyle factors to represent the complexities of cardiovascular and metabolic diseases. Study comorbidities and interactions between different organ systems in the context of metabolic disorders.

9.6. Non-Coding RNA Biology

Explore the role of non-coding RNAs in regulating cardiovascular and metabolic processes. Explore the therapeutic potential of manipulating non-coding RNAs for disease intervention.

9.7. Environmental Influences and Nutritional Studies

Investigate the impact of environmental pollutants, diet, and lifestyle on cardiovascular and metabolic health using zebrafish models. Investigate the correlation between genetic susceptibility and environmental influences.

9.8. Drug Discovery and Screening

Continue to use zebrafish for high-throughput drug screening to identify novel therapeutic compounds for cardiovascular and metabolic diseases. Optimize preclinical drug testing by integrating zebrafish models into the drug discovery pipeline.

9.9. Functional Validation in Mammalian Models

Validate findings from zebrafish studies in mammalian models to bridge the translational gap and enhance the clinical relevance of discoveries.

9.10. Innovations in Genome Editing

Implement emerging genome-editing technologies to refine and enhance genetic manipulation's precision in zebrafish models. Explore using base and prime editing for more targeted and controlled genetic modifications. These future directions underscore the potential of zebrafish research to contribute significantly to our understanding of cardiovascular and metabolic diseases, offering valuable insights and innovative solutions for improving human health.

9.11. Genomics in Cardiovascular Disease

Identification of Genetic Risk Factors: Genome-wide association studies (GWAS) leverage genomics to identify genetic variants associated with increased susceptibility to cardiovascular diseases. Precision Medicine: Genomic data enable the identification of individual genetic profiles, facilitating personalized treatment strategies based on genetic susceptibility and drug response.

9.12. Transcriptomics in Cardiovascular Disease

Gene Expression Profiling: Transcriptomics reveals gene expression patterns associated with various cardiovascular conditions, aiding in discovering prospective biomarkers and therapeutic targets. Alternative Splicing and Isoform Analysis: Examining alternative splicing events provides insights into the diversity of gene products and their relevance to cardiovascular health.

9.13. Proteomics in Cardiovascular Disease

Protein Profiling: Proteomics helps identify changes in protein expression, post-translational modifications, and protein–protein interactions associated with cardiovascular diseases. Biomarker Discovery: Identification of circulating protein biomarkers aids in the early diagnosis, risk stratification, and monitoring of cardiovascular diseases.

9.14. Metabolomics in Cardiovascular Disease

Metabolic Profiling: Metabolomics explores alterations in metabolite levels, providing insights into metabolic pathways associated with cardiovascular health and disease. Biomarker Identification: Metabolomic signatures are potential cardiovascular risk assessment and treatment-response-monitoring biomarkers.

9.15. Epigenomics in Cardiovascular Disease

DNA Methylation and Histone Modification Studies: Epigenomics involves investigating alterations in DNA methylation and histone modifications, shedding light on the epigenetic regulation of genes associated with cardiovascular diseases. Epi-transcriptomics: Studying RNA modifications enhances our understanding of the role of post-transcriptional regulation in cardiovascular health.

9.16. Integrated OMICS Approaches

Systems Biology: Integrating data from multiple OMICS platforms enables a holistic systems biology approach to unravelling complex connections linking genes, proteins, metabolites, and other molecular entities in cardiovascular diseases. Network Analysis: The construction of molecular interaction networks aids in identifying key nodes and pathways implicated in cardiovascular pathophysiology. Lastly, OMICS technologies, encompassing genomics, transcriptomics, proteomics, metabolomics, and other high-throughput approaches, are crucial in advancing our understanding of cardiovascular diseases (CVDs). These technologies provide comprehensive insights into the molecular mechanisms, genetic factors, and systemic changes associated with cardiovascular conditions.

Individualized Treatment: Pharmacogenomic studies explore genetic variations influencing drug metabolism and response, facilitating the development of personalized cardiovascular therapies. Adverse Drug Reaction Prediction: Genomic data help in predicting individual susceptibility to adverse drug reactions, enhancing drug safety in cardiovascular patients. Integrating OMICS technologies into cardiovascular disease research accelerates the discovery of molecular mechanisms, aids in identifying novel therapeutic targets, and contributes to developing personalized approaches for diagnosis and treatment in cardiovascular medicine.

Funding: The authors declare that financial support was received for the research and authorship. RA was supported by the National Heart, Lung, and Blood Institute, grant numbers HL140411 and R56HL160545, and Ted and Loretta Rogers' Cardiovascular Career Development Award 2023.

Conflicts of Interest: The authors declare no conflicts of interest.

References

1. Streisinger, G.; Walker, C.; Dower, N.; Knauber, D.; Singer, F. Production of clones of homozygous diploid zebra fish (*Brachydanio rerio*). *Nature* **1981**, *291*, 293–296. [CrossRef]
2. Grunwald, D.J.; Streisinger, G. Induction of recessive lethal and specific locus mutations in the zebrafish with ethyl nitrosourea. *Genet. Res.* **1992**, *59*, 103–116. [CrossRef]
3. Kimmel, C.B. Genetics and early development of zebrafish. *Trends Genet.* **1989**, *5*, 283–288. [CrossRef] [PubMed]
4. Haffter, P.; Granato, M.; Brand, M.; Mullins, M.C.; Hammerschmidt, M.; Kane, D.A.; Odenthal, J.; van Eeden, F.J.; Jiang, Y.J.; Heisenberg, C.P.; et al. The identification of genes with unique and essential functions in the development of the zebrafish, *Danio rerio*. *Development* **1996**, *123*, 1–36. [CrossRef]
5. Kim, C.H.; Oda, T.; Itoh, M.; Jiang, D.; Artinger, K.B.; Chandrasekharappa, S.C.; Driever, W.; Chitnis, A.B. Repressor activity of Headless/Tcf3 is essential for vertebrate head formation. *Nature* **2000**, *407*, 913–916. [CrossRef] [PubMed]
6. Doyon, Y.; McCammon, J.M.; Miller, J.C.; Faraji, F.; Ngo, C.; Katibah, G.E.; Amora, R.; Hocking, T.D.; Zhang, L.; Rebar, E.J.; et al. Heritable targeted gene disruption in zebrafish using designed zinc-finger nucleases. *Nat. Biotechnol.* **2008**, *26*, 702–708. [CrossRef]
7. Meng, X.; Noyes, M.B.; Zhu, L.J.; Lawson, N.D.; Wolfe, S.A. Targeted gene inactivation in zebrafish using engineered zinc-finger nucleases. *Nat. Biotechnol.* **2008**, *26*, 695–701. [CrossRef]
8. Bedell, V.M.; Wang, Y.; Campbell, J.M.; Poshusta, T.L.; Starker, C.G.; Krug, R.G., 2nd; Tan, W.; Penheiter, S.G.; Ma, A.C.; Leung, A.Y.; et al. In vivo genome editing using a high-efficiency TALEN system. *Nature* **2012**, *491*, 114–118. [CrossRef] [PubMed]
9. Hsu, P.D.; Lander, E.S.; Zhang, F. Development and applications of CRISPR-Cas9 for genome engineering. *Cell* **2014**, *157*, 1262–1278. [CrossRef]
10. Jinek, M.; Chylinski, K.; Fonfara, I.; Hauer, M.; Doudna, J.A.; Charpentier, E. A programmable dual-RNA-guided DNA endonuclease in adaptive bacterial immunity. *Science* **2012**, *337*, 816–821. [CrossRef] [PubMed]
11. Varshney, G.K.; Sood, R.; Burgess, S.M. Understanding and Editing the Zebrafish Genome. *Adv. Genet.* **2015**, *92*, 1–52. [CrossRef]
12. Sung, Y.H.; Kim, J.M.; Kim, H.T.; Lee, J.; Jeon, J.; Jin, Y.; Choi, J.H.; Ban, Y.H.; Ha, S.J.; Kim, C.H.; et al. Highly efficient gene knockout in mice and zebrafish with RNA-guided endonucleases. *Genome Res.* **2014**, *24*, 125–131. [CrossRef]
13. Postlethwait, J.H.; Yan, Y.L.; Gates, M.A.; Horne, S.; Amores, A.; Brownlie, A.; Donovan, A.; Egan, E.S.; Force, A.; Gong, Z.; et al. Vertebrate genome evolution and the zebrafish gene map. *Nat. Genet.* **1998**, *18*, 345–349. [CrossRef]
14. Howe, K.; Clark, M.D.; Torroja, C.F.; Torrance, J.; Berthelot, C.; Muffato, M.; Collins, J.E.; Humphray, S.; McLaren, K.; Matthews, L.; et al. The zebrafish reference genome sequence and its relationship to the human genome. *Nature* **2013**, *496*, 498–503. [CrossRef]
15. Barbazuk, W.B.; Korf, I.; Kadavi, C.; Heyen, J.; Tate, S.; Wun, E.; Bedell, J.A.; McPherson, J.D.; Johnson, S.L. The syntenic relationship of the zebrafish and human genomes. *Genome Res.* **2000**, *10*, 1351–1358. [CrossRef] [PubMed]

16. Shin, J.T.; Fishman, M.C. From Zebrafish to human: Modular medical models. *Annu. Rev. Genom. Hum. Genet.* **2002**, *3*, 311–340. [CrossRef] [PubMed]
17. Lieschke, G.J.; Currie, P.D. Animal models of human disease: Zebrafish swim into view. *Nat. Rev. Genet.* **2007**, *8*, 353–367. [CrossRef] [PubMed]
18. Halpern, M.E.; Rhee, J.; Goll, M.G.; Akitake, C.M.; Parsons, M.; Leach, S.D. Gal4/UAS transgenic tools and their application to zebrafish. *Zebrafish* **2008**, *5*, 97–110. [CrossRef] [PubMed]
19. Langenau, D.M.; Feng, H.; Berghmans, S.; Kanki, J.P.; Kutok, J.L.; Look, A.T. Cre/lox-regulated transgenic zebrafish model with conditional myc-induced T cell acute lymphoblastic leukemia. *Proc. Natl. Acad. Sci. USA* **2005**, *102*, 6068–6073. [CrossRef]
20. Neuhauss, S.C.; Solnica-Krezel, L.; Schier, A.F.; Zwartkruis, F.; Stemple, D.L.; Malicki, J.; Abdelilah, S.; Stainier, D.Y.; Driever, W. Mutations affecting craniofacial development in zebrafish. *Development* **1996**, *123*, 357–367. [CrossRef]
21. Chen, J.-N.; Haffter, P.; Odenthal, J.; Vogelsang, E.; Brand, M.; Eeden, F.J.M.v.; Furutani-Seiki, M.; Granato, M.; Hammerschmidt, M.; Heisenberg, C.-P.; et al. Mutations affecting the cardiovascular system and other internal organs in zebrafish. *Development* **1996**, *123*, 293–302. [CrossRef] [PubMed]
22. Stainier, D.Y.R.; Fouquet, B.; Chen, J.-N.; Warren, K.S.; Weinstein, B.M.; Meiler, S.E.; Mohideen, M.-A.P.K.; Neuhauss, S.C.F.; Solnica-Krezel, L.; Schier, A.F.; et al. Mutations affecting the formation and function of the cardiovascular system in the zebrafish embryo. *Development* **1996**, *123*, 285–292. [CrossRef] [PubMed]
23. Jin, S.W.; Herzog, W.; Santoro, M.M.; Mitchell, T.S.; Frantsve, J.; Jungblut, B.; Beis, D.; Scott, I.C.; D'Amico, L.A.; Ober, E.A.; et al. A transgene-assisted genetic screen identifies essential regulators of vascular development in vertebrate embryos. *Dev. Biol.* **2007**, *307*, 29–42. [CrossRef] [PubMed]
24. Bakkers, J. Zebrafish as a model to study cardiac development and human cardiac disease. *Cardiovasc. Res.* **2011**, *91*, 279–288. [CrossRef]
25. González-Rosa, J.M. Zebrafish Models of Cardiac Disease: From Fortuitous Mutants to Precision Medicine. *Circ. Res.* **2022**, *130*, 1803–1826. [CrossRef]
26. Ding, Y.; Bu, H.; Xu, X. Modeling Inherited Cardiomyopathies in Adult Zebrafish for Precision Medicine. *Front. Physiol.* **2020**, *11*, 599244. [CrossRef]
27. Beis, D.; Stainier, D.Y. In vivo cell biology: Following the zebrafish trend. *Trends Cell Biol.* **2006**, *16*, 105–112. [CrossRef]
28. Bradford, Y.M.; Toro, S.; Ramachandran, S.; Ruzicka, L.; Howe, D.G.; Eagle, A.; Kalita, P.; Martin, R.; Taylor Moxon, S.A.; Schaper, K.; et al. Zebrafish Models of Human Disease: Gaining Insight into Human Disease at ZFIN. *ILAR J.* **2017**, *58*, 4–16. [CrossRef]
29. Kopp, R.; Schwerte, T.; Pelster, B. Cardiac performance in the zebrafish breakdance mutant. *J. Exp. Biol.* **2005**, *208*, 2123–2134. [CrossRef]
30. Hassel, D.; Scholz, E.P.; Trano, N.; Friedrich, O.; Just, S.; Meder, B.; Weiss, D.L.; Zitron, E.; Marquart, S.; Vogel, B.; et al. Deficient zebrafish ether-à-go-go-related gene channel gating causes short-QT syndrome in zebrafish reggae mutants. *Circulation* **2008**, *117*, 866–875. [CrossRef]
31. Verkerk, A.O.; Remme, C.A. Zebrafish: A novel research tool for cardiac (patho)electrophysiology and ion channel disorders. *Front. Physiol.* **2012**, *3*, 255. [CrossRef] [PubMed]
32. Sarantis, P.; Gaitanaki, C.; Beis, D. Ventricular remodeling of single-chambered myh6$^{-/-}$ adult zebrafish hearts occurs via a hyperplastic response and is accompanied by elastin deposition in the atrium. *Cell Tissue Res.* **2019**, *378*, 279–288. [CrossRef] [PubMed]
33. Dhillon, S.S.; Dóró, E.; Magyary, I.; Egginton, S.; Sík, A.; Müller, F. Optimisation of embryonic and larval ECG measurement in zebrafish for quantifying the effect of QT prolonging drugs. *PLoS ONE* **2013**, *8*, e60552. [CrossRef]
34. Milan, D.J.; Jones, I.L.; Ellinor, P.T.; MacRae, C.A. In vivo recording of adult zebrafish electrocardiogram and assessment of drug-induced QT prolongation. *Am. J. Physiol.-Heart Circ. Physiol.* **2006**, *291*, H269–H273. [CrossRef] [PubMed]
35. Huttner, I.G.; Trivedi, G.; Jacoby, A.; Mann, S.A.; Vandenberg, J.I.; Fatkin, D. A transgenic zebrafish model of a human cardiac sodium channel mutation exhibits bradycardia, conduction-system abnormalities and early death. *J. Mol. Cell. Cardiol.* **2013**, *61*, 123–132. [CrossRef]
36. Ding, Y.; Dvornikov, A.V.; Ma, X.; Zhang, H.; Wang, Y.; Lowerison, M.; Packard, R.R.; Wang, L.; Chen, J.; Zhang, Y.; et al. Haploinsufficiency of mechanistic target of rapamycin ameliorates bag3 cardiomyopathy in adult zebrafish. *Dis. Models Mech.* **2019**, *12*, dmm040154. [CrossRef]
37. Sun, X.; Hoage, T.; Bai, P.; Ding, Y.; Chen, Z.; Zhang, R.; Huang, W.; Jahangir, A.; Paw, B.; Li, Y.-G.; et al. Cardiac Hypertrophy Involves Both Myocyte Hypertrophy and Hyperplasia in Anemic Zebrafish. *PLoS ONE* **2009**, *4*, e6596. [CrossRef]
38. Orr, N.; Arnaout, R.; Gula, L.J.; Spears, D.A.; Leong-Sit, P.; Li, Q.; Tarhuni, W.; Reischauer, S.; Chauhan, V.S.; Borkovich, M.; et al. A mutation in the atrial-specific myosin light chain gene (MYL4) causes familial atrial fibrillation. *Nat. Commun.* **2016**, *7*, 11303. [CrossRef]
39. Scheid, L.-M.; Mosqueira, M.; Hein, S.; Kossack, M.; Juergensen, L.; Mueller, M.; Meder, B.; Fink, R.H.A.; Katus, H.A.; Hassel, D. Essential light chain S195 phosphorylation is required for cardiac adaptation under physical stress. *Cardiovasc. Res.* **2016**, *111*, 44–55. [CrossRef] [PubMed]
40. Bu, H.; Ding, Y.; Li, J.; Zhu, P.; Shih, Y.-H.; Wang, M.; Zhang, Y.; Lin, X.; Xu, X. Inhibition of mTOR or MAPK ameliorates vmhcl/myh7 cardiomyopathy in zebrafish. *JCI Insight* **2021**, *6*, e154215. [CrossRef]

41. Chi, N.C.; Bussen, M.; Brand-Arzamendi, K.; Ding, C.; Olgin, J.E.; Shaw, R.M.; Martin, G.R.; Stainier, D.Y.R. Cardiac conduction is required to preserve cardiac chamber morphology. *Proc. Natl. Acad. Sci. USA* **2010**, *107*, 14662–14667. [CrossRef]
42. Chen, D.; Zhang, Z.; Chen, C.; Yao, S.; Yang, Q.; Li, F.; He, X.; Ai, C.; Wang, M.; Guan, M.-X. Deletion of Gtpbp3 in zebrafish revealed the hypertrophic cardiomyopathy manifested by aberrant mitochondrial tRNA metabolism. *Nucleic Acids Res.* **2019**, *47*, 5341–5355. [CrossRef]
43. Cheng, F.; Miao, L.; Wu, Q.; Gong, X.; Xiong, J.; Zhang, J. Vinculin b deficiency causes epicardial hyperplasia and coronary vessel disorganization in zebrafish. *Development* **2016**, *143*, 3522–3531. [CrossRef]
44. Asimaki, A.; Kapoor, S.; Plovie, E.; Karin Arndt, A.; Adams, E.; Liu, Z.; James, C.A.; Judge, D.P.; Calkins, H.; Churko, J.; et al. Identification of a New Modulator of the Intercalated Disc in a Zebrafish Model of Arrhythmogenic Cardiomyopathy. *Sci. Transl. Med.* **2014**, *6*, 240ra274. [CrossRef]
45. Rottbauer, W.; Just, S.; Wessels, G.; Trano, N.; Most, P.; Katus, H.A.; Fishman, M.C. VEGF–PLCγ1 pathway controls cardiac contractility in the embryonic heart. *Genes Dev.* **2005**, *19*, 1624–1634. [CrossRef]
46. Poss, K.D.; Wilson, L.G.; Keating, M.T. Heart Regeneration in Zebrafish. *Science* **2002**, *298*, 2188–2190. [CrossRef] [PubMed]
47. Sehnert, A.J.; Huq, A.; Weinstein, B.M.; Walker, C.; Fishman, M.; Stainier, D.Y.R. Cardiac troponin T is essential in sarcomere assembly and cardiac contractility. *Nat. Genet.* **2002**, *31*, 106–110. [CrossRef] [PubMed]
48. Porrello, E.R.; Mahmoud, A.I.; Simpson, E.; Hill, J.A.; Richardson, J.A.; Olson, E.N.; Sadek, H.A. Transient regenerative potential of the neonatal mouse heart. *Science* **2011**, *331*, 1078–1080. [CrossRef] [PubMed]
49. Zebrowski, D.C.; Becker, R.; Engel, F.B. Towards regenerating the mammalian heart: Challenges in evaluating experimentally induced adult mammalian cardiomyocyte proliferation. *Am. J. Physiol. Heart Circ. Physiol.* **2016**, *310*, H1045–H1054. [CrossRef] [PubMed]
50. Vihtelic, T.S.; Hyde, D.R. Light-induced rod and cone cell death and regeneration in the adult albino zebrafish (*Danio rerio*) retina. *J. Neurobiol.* **2000**, *44*, 289–307. [CrossRef] [PubMed]
51. Kroehne, V.; Freudenreich, D.; Hans, S.; Kaslin, J.; Brand, M. Regeneration of the adult zebrafish brain from neurogenic radial glia-type progenitors. *Development* **2011**, *138*, 4831–4841. [CrossRef] [PubMed]
52. Becker, T.; Wullimann, M.F.; Becker, C.G.; Bernhardt, R.R.; Schachner, M. Axonal regrowth after spinal cord transection in adult zebrafish. *J. Comp. Neurol.* **1997**, *377*, 577–595. [CrossRef]
53. Bise, T.; Sallin, P.; Pfefferli, C.; Jaźwińska, A. Multiple cryoinjuries modulate the efficiency of zebrafish heart regeneration. *Sci. Rep.* **2020**, *10*, 11551. [CrossRef] [PubMed]
54. Wang, J.; Karra, R.; Dickson, A.L.; Poss, K.D. Fibronectin is deposited by injury-activated epicardial cells and is necessary for zebrafish heart regeneration. *Dev. Biol.* **2013**, *382*, 427–435. [CrossRef] [PubMed]
55. Engel, F.B.; Hsieh, P.C.H.; Lee, R.T.; Keating, M.T. FGF1/p38 MAP kinase inhibitor therapy induces cardiomyocyte mitosis, reduces scarring, and rescues function after myocardial infarction. *Proc. Natl. Acad. Sci. USA* **2006**, *103*, 15546–15551. [CrossRef] [PubMed]
56. Sander, V.; Suñe, G.; Jopling, C.; Morera, C.; Izpisua Belmonte, J.C. Isolation and in vitro culture of primary cardiomyocytes from adult zebrafish hearts. *Nat. Protoc.* **2013**, *8*, 800–809. [CrossRef] [PubMed]
57. Jopling, C.; Suñé, G.; Faucherre, A.; Fabregat, C.; Izpisua Belmonte, J.C. Hypoxia induces myocardial regeneration in zebrafish. *Circulation* **2012**, *126*, 3017–3027. [CrossRef]
58. Parente, V.; Balasso, S.; Pompilio, G.; Verduci, L.; Colombo, G.I.; Milano, G.; Guerrini, U.; Squadroni, L.; Cotelli, F.; Pozzoli, O.; et al. Hypoxia/reoxygenation cardiac injury and regeneration in zebrafish adult heart. *PLoS ONE* **2013**, *8*, e53748. [CrossRef]
59. Lam, N.T.; Currie, P.D.; Lieschke, G.J.; Rosenthal, N.A.; Kaye, D.M. Nerve growth factor stimulates cardiac regeneration via cardiomyocyte proliferation in experimental heart failure. *PLoS ONE* **2012**, *7*, e53210. [CrossRef]
60. Chablais, F.; Veit, J.; Rainer, G.; Jaźwińska, A. The zebrafish heart regenerates after cryoinjury-induced myocardial infarction. *BMC Dev. Biol.* **2011**, *11*, 21. [CrossRef]
61. González-Rosa, J.M.; Martín, V.; Peralta, M.; Torres, M.; Mercader, N. Extensive scar formation and regression during heart regeneration after cryoinjury in zebrafish. *Development* **2011**, *138*, 1663–1674. [CrossRef]
62. González-Rosa, J.M.; Burns, C.E.; Burns, C.G. Zebrafish heart regeneration: 15 years of discoveries. *Regeneration* **2017**, *4*, 105–123. [CrossRef]
63. González-Rosa, J.M.; Peralta, M.; Mercader, N. Pan-epicardial lineage tracing reveals that epicardium derived cells give rise to myofibroblasts and perivascular cells during zebrafish heart regeneration. *Dev. Biol.* **2012**, *370*, 173–186. [CrossRef] [PubMed]
64. Schindler, Y.L.; Garske, K.M.; Wang, J.; Firulli, B.A.; Firulli, A.B.; Poss, K.D.; Yelon, D. Hand2 elevates cardiomyocyte production during zebrafish heart development and regeneration. *Development* **2014**, *141*, 3112–3122. [CrossRef] [PubMed]
65. Vaparanta, K.; Jokilammi, A.; Paatero, I.; Merilahti, J.A.; Heliste, J.; Hemanthakumar, K.A.; Kivelä, R.; Alitalo, K.; Taimen, P.; Elenius, K. STAT5b is a key effector of NRG-1/ERBB4-mediated myocardial growth. *EMBO Rep.* **2023**, *24*, e56689. [CrossRef] [PubMed]
66. Ma, H.; Liu, Z.; Yang, Y.; Feng, D.; Dong, Y.; Garbutt, T.A.; Hu, Z.; Wang, L.; Luan, C.; Cooper, C.D.; et al. Functional coordination of non-myocytes plays a key role in adult zebrafish heart regeneration. *EMBO Rep.* **2021**, *22*, e52901. [CrossRef]
67. Hoage, T.; Sun, X.; Xu, X. Functions of the Wnt/β-catenin pathway in an anemia-induced zebrafish model of cardiomyopathy are location dependent. *Biochem. Biophys. Res. Commun.* **2011**, *415*, 490–496. [CrossRef]

68. Ding, Y.; Sun, X.; Redfield, M.; Kushwaha, S.; Xu, X. Target of rapamcyin (TOR)-based therapeutics for cardiomyopathy. *Cell Cycle* **2012**, *11*, 428–429. [CrossRef]
69. Shih, Y.-H.; Zhang, Y.; Ding, Y.; Ross, C.A.; Li, H.; Olson, T.M.; Xu, X. Cardiac Transcriptome and Dilated Cardiomyopathy Genes in Zebrafish. *Circ. Cardiovasc. Genet.* **2015**, *8*, 261–269. [CrossRef]
70. Gerull, B.; Gramlich, M.; Atherton, J.; McNabb, M.; Trombitás, K.; Sasse-Klaassen, S.; Seidman, J.G.; Seidman, C.; Granzier, H.; Labeit, S.; et al. Mutations of TTN, encoding the giant muscle filament titin, cause familial dilated cardiomyopathy. *Nat. Genet.* **2002**, *30*, 201–204. [CrossRef]
71. Xu, X.; Meiler, S.E.; Zhong, T.P.; Mohideen, M.; Crossley, D.A.; Burggren, W.W.; Fishman, M.C. Cardiomyopathy in zebrafish due to mutation in an alternatively spliced exon of titin. *Nat. Genet.* **2002**, *30*, 205–209. [CrossRef]
72. Seeley, M.; Huang, W.; Chen, Z.; Wolff, W.O.; Lin, X.; Xu, X. Depletion of Zebrafish Titin Reduces Cardiac Contractility by Disrupting the Assembly of Z-Discs and A-Bands. *Circ. Res.* **2007**, *100*, 238–245. [CrossRef]
73. Steffen, L.S.; Guyon, J.R.; Vogel, E.D.; Howell, M.H.; Zhou, Y.; Weber, G.J.; Zon, L.I.; Kunkel, L.M. The zebrafish runzel muscular dystrophy is linked to the titin gene. *Dev. Biol.* **2007**, *309*, 180–192. [CrossRef]
74. Knöll, R.; Postel, R.; Wang, J.; Krätzner, R.; Hennecke, G.; Vacaru, A.M.; Vakeel, P.; Schubert, C.; Murthy, K.; Rana, B.K.; et al. Laminin-alpha4 and integrin-linked kinase mutations cause human cardiomyopathy via simultaneous defects in cardiomyocytes and endothelial cells. *Circulation* **2007**, *116*, 515–525. [CrossRef]
75. Schönberger, J.; Levy, H.; Grünig, E.; Sangwatanaroj, S.; Fatkin, D.; MacRae, C.; Stäcker, H.; Halpin, C.; Eavey, R.; Philbin, E.F.; et al. Dilated cardiomyopathy and sensorineural hearing loss: A heritable syndrome that maps to 6q23-24. *Circulation* **2000**, *101*, 1812–1818. [CrossRef] [PubMed]
76. Schönberger, J.; Wang, L.; Shin, J.T.; Kim, S.D.; Depreux, F.F.; Zhu, H.; Zon, L.; Pizard, A.; Kim, J.B.; Macrae, C.A.; et al. Mutation in the transcriptional coactivator EYA4 causes dilated cardiomyopathy and sensorineural hearing loss. *Nat. Genet.* **2005**, *37*, 418–422. [CrossRef] [PubMed]
77. Hassel, D.; Dahme, T.; Erdmann, J.; Meder, B.; Huge, A.; Stoll, M.; Just, S.; Hess, A.; Ehlermann, P.; Weichenhan, D.; et al. Nexilin mutations destabilize cardiac Z-disks and lead to dilated cardiomyopathy. *Nat. Med.* **2009**, *15*, 1281–1288. [CrossRef]
78. Ho, Y.L.; Lin, Y.H.; Tsai, W.Y.; Hsieh, F.J.; Tsai, H.J. Conditional antisense-knockdown of zebrafish cardiac troponin C as a new animal model for dilated cardiomyopathy. *Circ. J.* **2009**, *73*, 1691–1697. [CrossRef]
79. Van't Padje, S.; Chaudhry, B.; Severijnen, L.A.; van der Linde, H.C.; Mientjes, E.J.; Oostra, B.A.; Willemsen, R. Reduction in fragile X related 1 protein causes cardiomyopathy and muscular dystrophy in zebrafish. *J. Exp. Biol.* **2009**, *212*, 2564–2570. [CrossRef]
80. Dhandapany, P.S.; Razzaque, M.A.; Muthusami, U.; Kunnoth, S.; Edwards, J.J.; Mulero-Navarro, S.; Riess, I.; Pardo, S.; Sheng, J.; Rani, D.S.; et al. RAF1 mutations in childhood-onset dilated cardiomyopathy. *Nat. Genet.* **2014**, *46*, 635–639. [CrossRef] [PubMed]
81. González-Solá, M.; Al-Khayat, H.A.; Behra, M.; Kensler, R.W. Zebrafish cardiac muscle thick filaments: Isolation technique and three-dimensional structure. *Biophys. J.* **2014**, *106*, 1671–1680. [CrossRef]
82. Paavola, J.; Schliffke, S.; Rossetti, S.; Kuo, I.Y.T.; Yuan, S.; Sun, Z.; Harris, P.C.; Torres, V.E.; Ehrlich, B.E. Polycystin-2 mutations lead to impaired calcium cycling in the heart and predispose to dilated cardiomyopathy. *J. Mol. Cell. Cardiol.* **2013**, *58*, 199–208. [CrossRef]
83. Lawson, N.D.; Weinstein, B.M. Arteries and veins: Making a difference with zebrafish. *Nat. Rev. Genet.* **2002**, *3*, 674–682. [CrossRef] [PubMed]
84. Gray, C.; Packham, I.M.; Wurmser, F.; Eastley, N.C.; Hellewell, P.G.; Ingham, P.W.; Crossman, D.C.; Chico, T.J.A. Ischemia is not required for arteriogenesis in zebrafish embryos. *Arterioscler. Thromb. Vasc. Biol.* **2007**, *27*, 2135–2141. [CrossRef] [PubMed]
85. Nakajima, H.; Chiba, A.; Fukumoto, M.; Morooka, N.; Mochizuki, N. Zebrafish Vascular Development: General and Tissue-Specific Regulation. *J. Lipid Atheroscler.* **2021**, *10*, 145–159. [CrossRef] [PubMed]
86. Gore, A.V.; Monzo, K.; Cha, Y.R.; Pan, W.; Weinstein, B.M. Vascular development in the zebrafish. *Cold Spring Harb. Perspect. Med.* **2012**, *2*, a006684. [CrossRef] [PubMed]
87. Ren, C.G.; Wang, L.; Jia, X.E.; Liu, Y.J.; Dong, Z.W.; Jin, Y.; Chen, Y.; Deng, M.; Zhou, Y.; Zhou, Y.; et al. Activated N-Ras signaling regulates arterial-venous specification in zebrafish. *J. Hematol. Oncol.* **2013**, *6*, 34. [CrossRef]
88. Herold, J.; Pipp, F.; Fernandez, B.; Xing, Z.; Heil, M.; Tillmanns, H.; Braun-Dullaeus, R.C. Transplantation of monocytes: A novel strategy for in vivo augmentation of collateral vessel growth. *Hum. Gene Ther.* **2004**, *15*, 1–12. [CrossRef] [PubMed]
89. Ren, B.; Deng, Y.; Mukhopadhyay, A.; Lanahan, A.A.; Zhuang, Z.W.; Moodie, K.L.; Mulligan-Kehoe, M.J.; Byzova, T.V.; Peterson, R.T.; Simons, M. ERK1/2-Akt1 crosstalk regulates arteriogenesis in mice and zebrafish. *J. Clin. Investig.* **2010**, *120*, 1217–1228. [CrossRef] [PubMed]
90. Williams, C.M.; Poole, A.W. Using zebrafish (*Danio rerio*) to assess gene function in thrombus formation. *Methods Mol. Biol.* **2012**, *788*, 305–319. [CrossRef]
91. Jagadeeswaran, P.; Rao, P. Role of KIAA0472, a Novel Ser/Thr Kinase in zebrafish thrombosis. In Proceedings of the International Conference on Zebrafish Development and Genetics, Madison, WI, USA, 14–18 June 2006.
92. Gregory, M.; Hanumanthaiah, R.; Jagadeeswaran, P. Genetic analysis of hemostasis and thrombosis using vascular occlusion. *Blood Cells Mol. Dis.* **2002**, *29*, 286–295. [CrossRef] [PubMed]
93. Liu, Y.; Kretz, C.A.; Maeder, M.L.; Huarng, M.C.; Richter, C.E.; Vo, A.H.; Tsao, P.; Swaroop, A.; Joung, J.K.; Shavit, J.A. A Zebrafish Model Of Antithrombin III Deficiency Displays Bleeding and Thrombosis Secondary To Disseminated Intravascular Coagulation. *Blood* **2013**, *122*, 200. [CrossRef]

94. Genome-wide association study of 14,000 cases of seven common diseases and 3000 shared controls. *Nature* **2007**, *447*, 661–678. [CrossRef] [PubMed]
95. Soranzo, N.; Spector, T.D.; Mangino, M.; Kühnel, B.; Rendon, A.; Teumer, A.; Willenborg, C.; Wright, B.; Chen, L.; Li, M.; et al. A genome-wide meta-analysis identifies 22 loci associated with eight hematological parameters in the HaemGen consortium. *Nat. Genet.* **2009**, *41*, 1182–1190. [CrossRef] [PubMed]
96. Samani, N.J.; Erdmann, J.; Hall, A.S.; Hengstenberg, C.; Mangino, M.; Mayer, B.; Dixon, R.J.; Meitinger, T.; Braund, P.; Wichmann, H.E.; et al. Genomewide association analysis of coronary artery disease. *N. Engl. J. Med.* **2007**, *357*, 443–453. [CrossRef]
97. Macaulay, I.C.; Tijssen, M.R.; Thijssen-Timmer, D.C.; Gusnanto, A.; Steward, M.; Burns, P.; Langford, C.F.; Ellis, P.D.; Dudbridge, F.; Zwaginga, J.-J.; et al. Comparative gene expression profiling of in vitro differentiated megakaryocytes and erythroblasts identifies novel activatory and inhibitory platelet membrane proteins. *Blood* **2006**, *109*, 3260–3269. [CrossRef] [PubMed]
98. Jagadeeswaran, P.; Sheehan, J.P.; Craig, F.E.; Troyer, D. Identification and characterization of zebrafish thrombocytes. *Br. J. Haematol.* **1999**, *107*, 731–738. [CrossRef]
99. Jagadeeswaran, P.; Gregory, M.; Day, K.; Cykowski, M.; Thattaliyath, B. Zebrafish: A genetic model for hemostasis and thrombosis. *J. Thromb. Haemost.* **2005**, *3*, 46–53. [CrossRef]
100. Lin, H.F.; Traver, D.; Zhu, H.; Dooley, K.; Paw, B.H.; Zon, L.I.; Handin, R.I. Analysis of thrombocyte development in CD41-GFP transgenic zebrafish. *Blood* **2005**, *106*, 3803–3810. [CrossRef]
101. Schurgers, E.; Moorlag, M.; Hemker, C.; Lindhout, T.; Kelchtermans, H.; de Laat, B. Thrombin Generation in Zebrafish Blood. *PLoS ONE* **2016**, *11*, e0149135. [CrossRef]
102. Tournoij, E.; Weber, G.J.; Akkerman, J.W.N.; De Groot, P.G.; Zon, L.I.; Moll, F.L.; Schulte-Merker, S. Mlck1a is expressed in zebrafish thrombocytes and is an essential component of thrombus formation. *J. Thromb. Haemost.* **2010**, *8*, 588–595. [CrossRef]
103. Zhu, X.Y.; Liu, H.C.; Guo, S.Y.; Xia, B.; Song, R.S.; Lao, Q.C.; Xuan, Y.X.; Li, C.Q. A Zebrafish Thrombosis Model for Assessing Antithrombotic Drugs. *Zebrafish* **2016**, *13*, 335–344. [CrossRef] [PubMed]
104. Gut, P.; Reischauer, S.; Stainier, D.Y.R.; Arnaout, R. Little Fish, Big Data: Zebrafish as a Model for Cardiovascular and Metabolic Disease. *Physiol. Rev.* **2017**, *97*, 889–938. [CrossRef] [PubMed]
105. Zhu, H.; Lan, C.; Zhao, D.; Wang, N.; Du, D.; Luo, H.; Lu, H.; Peng, Z.; Wang, Y.; Qiao, Z.; et al. Wuliangye Baijiu but not ethanol reduces cardiovascular disease risks in a zebrafish thrombosis model. *Npj Sci. Food* **2022**, *6*, 55. [CrossRef] [PubMed]
106. Gauvrit, S.; Bossaer, J.; Lee, J.; Collins, M.M. Modeling Human Cardiac Arrhythmias: Insights from Zebrafish. *J. Cardiovasc. Dev. Dis.* **2022**, *9*, 13. [CrossRef] [PubMed]
107. Langheinrich, U. Zebrafish: A new model on the pharmaceutical catwalk. *Bioessays* **2003**, *25*, 904–912. [CrossRef] [PubMed]
108. Pott, A.; Rottbauer, W.; Just, S. Functional genomics in zebrafish as a tool to identify novel antiarrhythmic targets. *Curr. Med. Chem.* **2014**, *21*, 1320–1329. [CrossRef] [PubMed]
109. Warren, K.S.; Fishman, M.C. "Physiological genomics": Mutant screens in zebrafish. *Am. J. Physiol.* **1998**, *275*, H1–H7. [CrossRef] [PubMed]
110. Briggs, J.P. The zebrafish: A new model organism for integrative physiology. *Am. J. Physiol. Regul. Integr. Comp. Physiol.* **2002**, *282*, R3–R9. [CrossRef]
111. Jorgensen, E.M.; Mango, S.E. The art and design of genetic screens: Caenorhabditis elegans. *Nat. Rev. Genet.* **2002**, *3*, 356–369. [CrossRef]
112. Créton, R.; Speksnijder, J.E.; Jaffe, L.F. Patterns of free calcium in zebrafish embryos. *J. Cell Sci.* **1998**, *111 Pt 12*, 1613–1622. [CrossRef]
113. Vornanen, M.; Hassinen, M. Zebrafish heart as a model for human cardiac electrophysiology. *Channels* **2016**, *10*, 101–110. [CrossRef]
114. Leong, I.U.; Skinner, J.R.; Shelling, A.N.; Love, D.R. Zebrafish as a model for long QT syndrome: The evidence and the means of manipulating zebrafish gene expression. *Acta Physiol.* **2010**, *199*, 257–276. [CrossRef]
115. Nemtsas, P.; Wettwer, E.; Christ, T.; Weidinger, G.; Ravens, U. Adult zebrafish heart as a model for human heart? An electrophysiological study. *J. Mol. Cell. Cardiol.* **2010**, *48*, 161–171. [CrossRef]
116. Baker, K.; Warren, K.S.; Yellen, G.; Fishman, M.C. Defective "pacemaker" current (Ih) in a zebrafish mutant with a slow heart rate. *Proc. Natl. Acad. Sci. USA* **1997**, *94*, 4554–4559. [CrossRef]
117. Brette, F.; Luxan, G.; Cros, C.; Dixey, H.; Wilson, C.; Shiels, H.A. Characterization of isolated ventricular myocytes from adult zebrafish (Danio rerio). *Biochem. Biophys. Res. Commun.* **2008**, *374*, 143–146. [CrossRef] [PubMed]
118. Müller, I.I.; Melville, D.B.; Tanwar, V.; Rybski, W.M.; Mukherjee, A.; Shoemaker, M.B.; Wang, W.-D.; Schoenhard, J.A.; Roden, D.M.; Darbar, D.; et al. Functional modeling in zebrafish demonstrates that the atrial-fibrillation-associated gene GREM2 regulates cardiac laterality, cardiomyocyte differentiation and atrial rhythm. *Dis. Models Mech.* **2013**, *6*, 332–341. [CrossRef]
119. Angom, R.S.; Joshi, A.; Patowary, A.; Sivadas, A.; Ramasamy, S.; Shamsudheen, K.V.; Kaushik, K.; Sabharwal, A.; Lalwani, M.K.; Subburaj, K.; et al. Forward genetic screen using a gene-breaking trap approach identifies a novel role of grin2bb-associated RNA transcript (grin2bbART) in zebrafish heart function. *Front. Cell Dev. Biol.* **2024**. [CrossRef]
120. Parker, T.; Libourel, P.A.; Hetheridge, M.J.; Cumming, R.I.; Sutcliffe, T.P.; Goonesinghe, A.C.; Ball, J.S.; Owen, S.F.; Chomis, Y.; Winter, M.J. A multi-endpoint in vivo larval zebrafish (*Danio rerio*) model for the assessment of integrated cardiovascular function. *J. Pharmacol. Toxicol. Methods* **2014**, *69*, 30–38. [CrossRef] [PubMed]
121. Santoro, M.M. Zebrafish as a model to explore cell metabolism. *Trends Endocrinol. Metab.* **2014**, *25*, 546–554. [CrossRef] [PubMed]

122. Nakayama, H.; Hata, K.; Matsuoka, I.; Zang, L.; Kim, Y.; Chu, D.; Juneja, L.R.; Nishimura, N.; Shimada, Y. Anti-Obesity Natural Products Tested in Juvenile Zebrafish Obesogenic Tests and Mouse 3T3-L1 Adipogenesis Assays. *Molecules* **2020**, *25*, 5840. [CrossRef]
123. Misselbeck, K.; Parolo, S.; Lorenzini, F.; Savoca, V.; Leonardelli, L.; Bora, P.; Morine, M.J.; Mione, M.C.; Domenici, E.; Priami, C. A network-based approach to identify deregulated pathways and drug effects in metabolic syndrome. *Nat. Commun.* **2019**, *10*, 5215. [CrossRef]
124. Asaoka, Y.; Terai, S.; Sakaida, I.; Nishina, H. The expanding role of fish models in understanding non-alcoholic fatty liver disease. *Dis. Model. Mech.* **2013**, *6*, 905–914. [CrossRef] [PubMed]
125. Nakayama, H.; Shimada, Y.; Zang, L.; Terasawa, M.; Nishiura, K.; Matsuda, K.; Toombs, C.; Langdon, C.; Nishimura, N. Novel Anti-Obesity Properties of Palmaria mollis in Zebrafish and Mouse Models. *Nutrients* **2018**, *10*, 1401. [CrossRef] [PubMed]
126. McCarthy, M.I. Genomics, type 2 diabetes, and obesity. *N. Engl. J. Med.* **2010**, *363*, 2339–2350. [CrossRef] [PubMed]
127. Gieger, C.; Radhakrishnan, A.; Cvejic, A.; Tang, W.; Porcu, E.; Pistis, G.; Serbanovic-Canic, J.; Elling, U.; Goodall, A.H.; Labrune, Y.; et al. New gene functions in megakaryopoiesis and platelet formation. *Nature* **2011**, *480*, 201–208. [CrossRef] [PubMed]
128. Liu, Y.; Liu, S.; Huang, J.; Liu, Y.; Wang, Q.; Chen, J.; Sun, L.; Tu, W. Mitochondrial dysfunction in metabolic disorders induced by per- and polyfluoroalkyl substance mixtures in zebrafish larvae. *Environ. Int.* **2023**, *176*, 107977. [CrossRef]
129. Eisen, J.S.; Weston, J.A. Development of the Neural Crest in the Zebrafish. *Dev. Biol.* **1993**, *159*, 50–59. [CrossRef] [PubMed]
130. Gut, P.; Baeza-Raja, B.; Andersson, O.; Hasenkamp, L.; Hsiao, J.; Hesselson, D.; Akassoglou, K.; Verdin, E.; Hirschey, M.D.; Stainier, D.Y.R. Whole-organism screening for gluconeogenesis identifies activators of fasting metabolism. *Nat. Chem. Biol.* **2013**, *9*, 97–104. [CrossRef]
131. Wang, Q.; Luo, C.; Lu, G.; Chen, Z. Effect of adenosine monophosphate-activated protein kinase-p53-Krüppel-like factor 2a pathway in hyperglycemia-induced cardiac remodeling in adult zebrafish. *J. Diabetes Investig.* **2021**, *12*, 320–333. [CrossRef]
132. Dorsemans, A.C.; Soulé, S.; Weger, M.; Bourdon, E.; Lefebvre d'Hellencourt, C.; Meilhac, O.; Diotel, N. Impaired constitutive and regenerative neurogenesis in adult hyperglycemic zebrafish. *J. Comp. Neurol.* **2017**, *525*, 442–458. [CrossRef]
133. Dorsemans, A.C.; Lefebvre d'Hellencourt, C.; Ait-Arsa, I.; Jestin, E.; Meilhac, O.; Diotel, N. Acute and Chronic Models of Hyperglycemia in Zebrafish: A Method to Assess the Impact of Hyperglycemia on Neurogenesis and the Biodistribution of Radiolabeled Molecules. *J. Vis. Exp.* **2017**, *124*, e55203. [CrossRef]
134. Couret, D.; Bourane, S.; Catan, A.; Nativel, B.; Planesse, C.; Dorsemans, A.C.; Ait-Arsa, I.; Cournot, M.; Rondeau, P.; Patche, J.; et al. A hemorrhagic transformation model of mechanical stroke therapy with acute hyperglycemia in mice. *J. Comp. Neurol.* **2018**, *526*, 1006–1016. [CrossRef]
135. Moss, J.B.; Koustubhan, P.; Greenman, M.; Parsons, M.J.; Walter, I.; Moss, L.G. Regeneration of the pancreas in adult zebrafish. *Diabetes* **2009**, *58*, 1844–1851. [CrossRef] [PubMed]
136. Delaspre, F.; Beer, R.L.; Rovira, M.; Huang, W.; Wang, G.; Gee, S.; Vitery Mdel, C.; Wheelan, S.J.; Parsons, M.J. Centroacinar Cells Are Progenitors That Contribute to Endocrine Pancreas Regeneration. *Diabetes* **2015**, *64*, 3499–3509. [CrossRef] [PubMed]
137. Olsen, A.S.; Sarras, M.P., Jr.; Intine, R.V. Limb regeneration is impaired in an adult zebrafish model of diabetes mellitus. *Wound Repair Regen.* **2010**, *18*, 532–542. [CrossRef] [PubMed]
138. Benchoula, K.; Khatib, A.; Quzwain, F.M.C.; Che Mohamad, C.A.; Wan Sulaiman, W.M.A.; Abdul Wahab, R.; Ahmed, Q.U.; Abdul Ghaffar, M.; Saiman, M.Z.; Alajmi, M.F.; et al. Optimization of Hyperglycemic Induction in Zebrafish and Evaluation of Its Blood Glucose Level and Metabolite Fingerprint Treated with Psychotria malayana Jack Leaf Extract. *Molecules* **2019**, *24*, 1506. [CrossRef] [PubMed]
139. Karanth, S.; Chaurasia, B.; Bowman, F.M.; Tippetts, T.S.; Holland, W.L.; Summers, S.A.; Schlegel, A. FOXN3 controls liver glucose metabolism by regulating gluconeogenic substrate selection. *Physiol. Rep.* **2019**, *7*, e14238. [CrossRef]
140. Kimmel, R.A.; Dobler, S.; Schmitner, N.; Walsen, T.; Freudenblum, J.; Meyer, D. Diabetic pdx1-mutant zebrafish show conserved responses to nutrient overload and anti-glycemic treatment. *Sci. Rep.* **2015**, *5*, 14241. [CrossRef]
141. Maddison, L.A.; Joest, K.E.; Kammeyer, R.M.; Chen, W. Skeletal muscle insulin resistance in zebrafish induces alterations in β-cell number and glucose tolerance in an age- and diet-dependent manner. *Am. J. Physiol. Endocrinol. Metab.* **2015**, *308*, E662–E669. [CrossRef] [PubMed]
142. Oka, T.; Nishimura, Y.; Zang, L.; Hirano, M.; Shimada, Y.; Wang, Z.; Umemoto, N.; Kuroyanagi, J.; Nishimura, N.; Tanaka, T. Diet-induced obesity in zebrafish shares common pathophysiological pathways with mammalian obesity. *BMC Physiol.* **2010**, *10*, 21. [CrossRef]
143. Hasumura, T.; Shimada, Y.; Kuroyanagi, J.; Nishimura, Y.; Meguro, S.; Takema, Y.; Tanaka, T. Green tea extract suppresses adiposity and affects the expression of lipid metabolism genes in diet-induced obese zebrafish. *Nutr. Metab.* **2012**, *9*, 73. [CrossRef]
144. Forn-Cuní, G.; Varela, M.; Fernández-Rodríguez, C.M.; Figueras, A.; Novoa, B. Liver immune responses to inflammatory stimuli in a diet-induced obesity model of zebrafish. *J. Endocrinol.* **2015**, *224*, 159–170. [CrossRef]
145. Jais, A.; Einwallner, E.; Sharif, O.; Gossens, K.; Lu Tess, T.-H.; Soyal Selma, M.; Medgyesi, D.; Neureiter, D.; Paier-Pourani, J.; Dalgaard, K.; et al. Heme Oxygenase-1 Drives Metaflammation and Insulin Resistance in Mouse and Man. *Cell* **2014**, *158*, 25–40. [CrossRef]

146. Lackey, D.E.; Burk, D.H.; Ali, M.R.; Mostaedi, R.; Smith, W.H.; Park, J.; Scherer, P.E.; Seay, S.A.; McCoin, C.S.; Bonaldo, P.; et al. Contributions of adipose tissue architectural and tensile properties toward defining healthy and unhealthy obesity. *Am. J. Physiol. -Endocrinol. Metab.* **2014**, *306*, E233–E246. [CrossRef]
147. Wernstedt Asterholm, I.; Tao, C.; Morley, T.S.; Wang, Q.A.; Delgado-Lopez, F.; Wang, Z.V.; Scherer, P.E. Adipocyte Inflammation Is Essential for Healthy Adipose Tissue Expansion and Remodeling. *Cell Metab.* **2014**, *20*, 103–118. [CrossRef]
148. Seth, A.; Stemple, D.L.; Barroso, I. The emerging use of zebrafish to model metabolic disease. *Dis. Models Mech.* **2013**, *6*, 1080–1088. [CrossRef] [PubMed]
149. Schlegel, A. Studying lipoprotein trafficking in zebrafish, the case of chylomicron retention disease. *J. Mol. Med.* **2015**, *93*, 115–118. [CrossRef] [PubMed]
150. Flynn, E.J.; Trent, C.M.; Rawls, J.F. Ontogeny and nutritional control of adipogenesis in zebrafish (*Danio rerio*). *J. Lipid Res.* **2009**, *50*, 1641–1652. [CrossRef] [PubMed]
151. Fraher, D.; Sanigorski, A.; Mellett, N.A.; Meikle, P.J.; Sinclair, A.J.; Gibert, Y. Zebrafish Embryonic Lipidomic Analysis Reveals that the Yolk Cell Is Metabolically Active in Processing Lipid. *Cell Rep.* **2016**, *14*, 1317–1329. [CrossRef] [PubMed]
152. Imrie, D.; Sadler, K.C. White adipose tissue development in zebrafish is regulated by both developmental time and fish size. *Dev. Dyn.* **2010**, *239*, 3013–3023. [CrossRef]
153. Leibold, S.; Hammerschmidt, M. Long-Term Hyperphagia and Caloric Restriction Caused by Low- or High-Density Husbandry Have Differential Effects on Zebrafish Postembryonic Development, Somatic Growth, Fat Accumulation and Reproduction. *PLoS ONE* **2015**, *10*, e0120776. [CrossRef]
154. McMenamin, S.K.; Minchin, J.E.N.; Gordon, T.N.; Rawls, J.F.; Parichy, D.M. Dwarfism and Increased Adiposity in the gh1 Mutant Zebrafish vizzini. *Endocrinology* **2013**, *154*, 1476–1487. [CrossRef] [PubMed]
155. Chu, C.-Y.; Chen, C.-F.; Rajendran, R.S.; Shen, C.-N.; Chen, T.-H.; Yen, C.-C.; Chuang, C.-K.; Lin, D.-S.; Hsiao, C.-D. Overexpression of Akt1 Enhances Adipogenesis and Leads to Lipoma Formation in Zebrafish. *PLoS ONE* **2012**, *7*, e36474. [CrossRef] [PubMed]
156. Friedman, J.M.; Halaas, J.L. Leptin and the regulation of body weight in mammals. *Nature* **1998**, *395*, 763–770. [CrossRef] [PubMed]
157. Michel, M.; Page-McCaw, P.S.; Chen, W.; Cone, R.D. Leptin signaling regulates glucose homeostasis, but not adipostasis, in the zebrafish. *Proc. Natl. Acad. Sci. USA* **2016**, *113*, 3084–3089. [CrossRef] [PubMed]
158. Zang, L.; Maddison, L.A.; Chen, W. Zebrafish as a Model for Obesity and Diabetes. *Front. Cell Dev. Biol.* **2018**, *6*, 91. [CrossRef] [PubMed]
159. Smolińska, K.; Sobczyński, J.; Szopa, A.; Wnorowski, A.; Tomaszewska, E.; Muszyński, S.; Winiarska-Mieczan, A.; Czernecki, T.; Bielak, A.; Dobrowolska, K.; et al. Innovative high fat diet establishes a novel zebrafish model for the study of visceral obesity. *Sci. Rep.* **2024**, *14*, 3012. [CrossRef] [PubMed]
160. Shungin, D.; Winkler, T.W.; Croteau-Chonka, D.C.; Ferreira, T.; Locke, A.E.; Mägi, R.; Strawbridge, R.J.; Pers, T.H.; Fischer, K.; Justice, A.E.; et al. New genetic loci link adipose and insulin biology to body fat distribution. *Nature* **2015**, *518*, 187–196. [CrossRef]
161. Minchin, J.E.N.; Dahlman, I.; Harvey, C.J.; Mejhert, N.; Singh, M.K.; Epstein, J.A.; Arner, P.; Torres-Vázquez, J.; Rawls, J.F. Plexin D1 determines body fat distribution by regulating the type V collagen microenvironment in visceral adipose tissue. *Proc. Natl. Acad. Sci. USA* **2015**, *112*, 4363–4368. [CrossRef]
162. Minchin, J.E.N.; Rawls, J.F. Chapter 3—In vivo Analysis of White Adipose Tissue in Zebrafish. In *Methods in Cell Biology*; Detrich, H.W., Westerfield, M., Zon, L.I., Eds.; Academic Press: New York, NY, USA, 2011; Volume 105, pp. 63–86.
163. Schlegel, A.; Gut, P. Metabolic insights from zebrafish genetics, physiology, and chemical biology. *Cell. Mol. Life Sci.* **2015**, *72*, 2249–2260. [CrossRef]
164. Farber, S.A.; Pack, M.; Ho, S.-Y.; Johnson, I.D.; Wagner, D.S.; Dosch, R.; Mullins, M.C.; Hendrickson, H.S.; Hendrickson, E.K.; Halpern, M.E. Genetic Analysis of Digestive Physiology Using Fluorescent Phospholipid Reporters. *Science* **2001**, *292*, 1385–1388. [CrossRef]
165. Ho, S.-Y.; Lorent, K.; Pack, M.; Farber, S.A. Zebrafish fat-free is required for intestinal lipid absorption and *Golgi apparatus* structure. *Cell Metab.* **2006**, *3*, 289–300. [CrossRef]
166. Pérez-Victoria, F.J.; Schindler, C.; Magadán, J.G.; Mardones, G.A.; Delevoye, C.; Romao, M.; Raposo, G.; Bonifacino, J.S. Ang2/Fat-Free Is a Conserved Subunit of the Golgi-associated Retrograde Protein Complex. *Mol. Biol. Cell* **2010**, *21*, 3386–3395. [CrossRef] [PubMed]
167. Lim, J.S.; Mietus-Snyder, M.; Valente, A.; Schwarz, J.-M.; Lustig, R.H. The role of fructose in the pathogenesis of NAFLD and the metabolic syndrome. *Nat. Rev. Gastroenterol. Hepatol.* **2010**, *7*, 251–264. [CrossRef] [PubMed]
168. Lorent, K.; Gong, W.; Koo, K.A.; Waisbourd-Zinman, O.; Karjoo, S.; Zhao, X.; Sealy, I.; Kettleborough, R.N.; Stemple, D.L.; Windsor, P.A.; et al. Identification of a plant isoflavonoid that causes biliary atresia. *Sci. Transl. Med.* **2015**, *7*, 286ra267. [CrossRef]
169. Cohen, J.C.; Horton, J.D.; Hobbs, H.H. Human Fatty Liver Disease: Old Questions and New Insights. *Science* **2011**, *332*, 1519–1523. [CrossRef] [PubMed]
170. Schlegel, A. Studying non-alcoholic fatty liver disease with zebrafish: A confluence of optics, genetics, and physiology. *Cell. Mol. Life Sci.* **2012**, *69*, 3953–3961. [CrossRef] [PubMed]
171. Schlegel, A.; Stainier, D.Y.R. Microsomal Triglyceride Transfer Protein Is Required for Yolk Lipid Utilization and Absorption of Dietary Lipids in Zebrafish Larvae. *Biochemistry* **2006**, *45*, 15179–15187. [CrossRef] [PubMed]

172. Li, M.; Page-McCaw, P.; Chen, W. FGF1 Mediates Overnutrition-Induced Compensatory β-Cell Differentiation. *Diabetes* **2015**, *65*, 96–109. [CrossRef]
173. Karanth, S.; Tran, V.M.; Kuberan, B.; Schlegel, A. Polyunsaturated fatty acyl-coenzyme As are inhibitors of cholesterol biosynthesis in zebrafish and mice. *Dis. Models Mech.* **2013**, *6*, 1365–1377. [CrossRef]
174. Sakaguchi, T.F.; Sadler, K.C.; Crosnier, C.; Stainier, D.Y.R. Endothelial Signals Modulate Hepatocyte Apicobasal Polarization in Zebrafish. *Curr. Biol.* **2008**, *18*, 1565–1571. [CrossRef]
175. Schaub, M.; Nussbaum, J.; Verkade, H.; Ober, E.A.; Stainier, D.Y.R.; Sakaguchi, T.F. Mutation of zebrafish Snapc4 is associated with loss of the intrahepatic biliary network. *Dev. Biol.* **2012**, *363*, 128–137. [CrossRef] [PubMed]
176. Hugo, S.E.; Cruz-Garcia, L.; Karanth, S.; Anderson, R.M.; Stainier, D.Y.R.; Schlegel, A. A monocarboxylate transporter required for hepatocyte secretion of ketone bodies during fasting. *Genes Dev.* **2012**, *26*, 282–293. [CrossRef] [PubMed]
177. Matthews, R.P.; Lorent, K.; Mañoral-Mobias, R.; Huang, Y.; Gong, W.; Murray, I.V.J.; Blair, I.A.; Pack, M. TNFα-dependent hepatic steatosis and liver degeneration caused by mutation of zebrafish s-adenosylhomocysteine hydrolase. *Development* **2009**, *136*, 865–875. [CrossRef]
178. Nussbaum, J.M.; Liu, L.J.; Hasan, S.A.; Schaub, M.; McClendon, A.; Stainier, D.Y.R.; Sakaguchi, T.F. Homeostatic generation of reactive oxygen species protects the zebrafish liver from steatosis. *Hepatology* **2013**, *58*, 1326–1338. [CrossRef] [PubMed]
179. Kim, S.-H.; Wu, S.-Y.; Baek, J.-I.; Choi, S.Y.; Su, Y.; Flynn, C.R.; Gamse, J.T.; Ess, K.C.; Hardiman, G.; Lipschutz, J.H.; et al. A Post-Developmental Genetic Screen for Zebrafish Models of Inherited Liver Disease. *PLoS ONE* **2015**, *10*, e0125980. [CrossRef]
180. Fang, L.; Harkewicz, R.; Hartvigsen, K.; Wiesner, P.; Choi, S.-H.; Almazan, F.; Pattison, J.; Deer, E.; Sayaphupha, T.; Dennis, E.A.; et al. Oxidized Cholesteryl Esters and Phospholipids in Zebrafish Larvae Fed a High Cholesterol Diet: Macrophage Binding and Activation. *J. Biol. Chem.* **2010**, *285*, 32343–32351. [CrossRef]
181. Breslow, J.L. Mouse Models of Atherosclerosis. *Science* **1996**, *272*, 685–688. [CrossRef]
182. Bradley, M.N.; Hong, C.; Chen, M.; Joseph, S.B.; Wilpitz, D.C.; Wang, X.; Lusis, A.J.; Collins, A.; Hseuh, W.A.; Collins, J.L.; et al. Ligand activation of LXRβ reverses atherosclerosis and cellular cholesterol overload in mice lacking LXRα and apoE. *J. Clin. Investig.* **2007**, *117*, 2337–2346. [CrossRef]
183. Cruz-Garcia, L.; Schlegel, A. Lxr-driven enterocyte lipid droplet formation delays transport of ingested lipids. *J. Lipid Res.* **2014**, *55*, 1944–1958. [CrossRef]
184. Ferreira, J. New zebrafish transgenic lines to further understand diabetes. *Lab Anim.* **2023**, *52*, 175. [CrossRef]
185. Zang, L.; Shimada, Y.; Nishimura, N. Development of a Novel Zebrafish Model for Type 2 Diabetes Mellitus. *Sci. Rep.* **2017**, *7*, 1461. [CrossRef]
186. Andersson, O.; Adams, B.A.; Yoo, D.; Ellis, G.C.; Gut, P.; Anderson, R.M.; German, M.S.; Stainier, D.Y.R. Adenosine Signaling Promotes Regeneration of Pancreatic β Cells In Vivo. *Cell Metab.* **2012**, *15*, 885–894. [CrossRef] [PubMed]
187. D'Amour, K.A.; Bang, A.G.; Eliazer, S.; Kelly, O.G.; Agulnick, A.D.; Smart, N.G.; Moorman, M.A.; Kroon, E.; Carpenter, M.K.; Baetge, E.E. Production of pancreatic hormone–expressing endocrine cells from human embryonic stem cells. *Nat. Biotechnol.* **2006**, *24*, 1392–1401. [CrossRef]
188. Zhu, S.; Russ, H.A.; Wang, X.; Zhang, M.; Ma, T.; Xu, T.; Tang, S.; Hebrok, M.; Ding, S. Human pancreatic beta-like cells converted from fibroblasts. *Nat. Commun.* **2016**, *7*, 10080. [CrossRef] [PubMed]
189. Dalgin, G.; Prince, V.E. Differential levels of Neurod establish zebrafish endocrine pancreas cell fates. *Dev. Biol.* **2015**, *402*, 81–97. [CrossRef] [PubMed]
190. Dong, P.D.S.; Provost, E.; Leach, S.D.; Stainier, D.Y.R. Graded levels of Ptf1a differentially regulate endocrine and exocrine fates in the developing pancreas. *Genes Dev.* **2008**, *22*, 1445–1450. [CrossRef] [PubMed]
191. Field, H.A.; Dong, P.D.S.; Beis, D.; Stainier, D.Y.R. Formation of the digestive system in zebrafish. ii. pancreas morphogenesis. *Dev. Biol.* **2003**, *261*, 197–208. [CrossRef] [PubMed]
192. Parsons, M.J.; Pisharath, H.; Yusuff, S.; Moore, J.C.; Siekmann, A.F.; Lawson, N.; Leach, S.D. Notch-responsive cells initiate the secondary transition in larval zebrafish pancreas. *Mech. Dev.* **2009**, *126*, 898–912. [CrossRef]
193. Sun, Z.; Hopkins, N. vhnf1, the MODY5 and familial GCKD-associated gene, regulates regional specification of the zebrafish gut, pronephros, and hindbrain. *Genes Dev.* **2001**, *15*, 3217–3229. [CrossRef] [PubMed]
194. Rovira, M.; Huang, W.; Yusuff, S.; Shim, J.S.; Ferrante, A.A.; Liu, J.O.; Parsons, M.J. Chemical screen identifies FDA-approved drugs and target pathways that induce precocious pancreatic endocrine differentiation. *Proc. Natl. Acad. Sci. USA* **2011**, *108*, 19264–19269. [CrossRef] [PubMed]
195. Pack, M.; Solnica-Krezel, L.; Malicki, J.; Neuhauss, S.C.; Schier, A.F.; Stemple, D.L.; Driever, W.; Fishman, M.C. Mutations affecting development of zebrafish digestive organs. *Development* **1996**, *123*, 321–328. [CrossRef] [PubMed]
196. Chung, W.S.; Andersson, O.; Row, R.; Kimelman, D.; Stainier, D.Y. Suppression of Alk8-mediated Bmp signaling cell-autonomously induces pancreatic beta-cells in zebrafish. *Proc. Natl. Acad. Sci. USA* **2010**, *107*, 1142–1147. [CrossRef] [PubMed]
197. Chung, W.S.; Shin, C.H.; Stainier, D.Y. Bmp2 signaling regulates the hepatic versus pancreatic fate decision. *Dev. Cell* **2008**, *15*, 738–748. [CrossRef]
198. Chung, W.S.; Stainier, D.Y. Intra-endodermal interactions are required for pancreatic beta cell induction. *Dev. Cell* **2008**, *14*, 582–593. [CrossRef]

199. Dong, P.D.; Munson, C.A.; Norton, W.; Crosnier, C.; Pan, X.; Gong, Z.; Neumann, C.J.; Stainier, D.Y. Fgf10 regulates hepatopancreatic ductal system patterning and differentiation. *Nat. Genet.* **2007**, *39*, 397–402. [CrossRef]
200. Manfroid, I.; Delporte, F.; Baudhuin, A.; Motte, P.; Neumann, C.J.; Voz, M.L.; Martial, J.A.; Peers, B. Reciprocal endoderm-mesoderm interactions mediated by fgf24 and fgf10 govern pancreas development. *Development* **2007**, *134*, 4011–4021. [CrossRef] [PubMed]
201. Stafford, D.; Prince, V.E. Retinoic acid signaling is required for a critical early step in zebrafish pancreatic development. *Curr. Biol.* **2002**, *12*, 1215–1220. [CrossRef] [PubMed]

Disclaimer/Publisher's Note: The statements, opinions and data contained in all publications are solely those of the individual author(s) and contributor(s) and not of MDPI and/or the editor(s). MDPI and/or the editor(s) disclaim responsibility for any injury to people or property resulting from any ideas, methods, instructions or products referred to in the content.

biomedicines

MDPI

Article

Mitochondrial Dysfunction and Ion Imbalance in a Rat Model of Hemodialysis-Induced Myocardial Stunning

Yuxin Nie [1,2,†], Liyu Lin [1,2,3,4,†], Qiang Yang [1,2], Jiachang Hu [1,2], Minmin Sun [5,6], Fangfang Xiang [1,2], Xuesen Cao [1,2], Jinbo Yu [1,2], Yaqiong Wang [1,2], Jie Teng [1,2,3,4], Xiaoqiang Ding [1,2,3,4], Bo Shen [1,2,*] and Zhen Zhang [1,2,*]

[1] Department of Nephrology, Zhongshan Hospital, Fudan University, No. 180 Fenglin Road, Shanghai 200032, China; nie.yuxin@zs-hospital.sh.cn (Y.N.); lin.liyu@zsxmhospital.com (L.L.); 23111210014@m.fudan.edu.cn (Q.Y.); hu.jiachang@zs-hospital.sh.cn (J.H.); xiang.fangfang@zs-hospital.sh.cn (F.X.); cao.xuesen@zs-hospital.sh.cn (X.C.); yu.jinbo@zs-hospital.sh.cn (J.Y.); wang.yaqiong@zs-hospital.sh.cn (Y.W.); teng.jie@zs-hospital.sh.cn (J.T.); ding.xiaoqiang@zs-hospital.sh.cn (X.D.)
[2] Shanghai Key Laboratory of Kidney and Blood Purification, No. 180 Fenglin Road, Shanghai 200032, China
[3] Department of Nephrology, Zhongshan Hospital (Xiamen), Fudan University, No. 668 Jinhu Road, Xiamen 361015, China
[4] Nephrology Clinical Quality Control Center of Xiamen, No. 668 Jinhu Road, Xiamen 361015, China
[5] Department of Echocardiography, Zhongshan Hospital, Fudan University, No. 180 Fenglin Road, Shanghai 200032, China; sun.minmin@zs-hospital.sh.cn
[6] Shanghai Institute of Cardiovascular Diseases, Shanghai 200032, China
* Correspondence: shen.bo@zs-hospital.sh.cn (B.S.); zhang.zhen1@zs-hospital.sh.cn (Z.Z.)
† These authors contributed equally to this work.

Abstract: Background/Objectives: Hemodialysis-induced myocardial stunning (HIMS) is a frequent complication in patients undergoing maintenance hemodialysis, characterized by transient left ventricular dysfunction due to ischemic episodes. Mitochondrial dysfunction and fluctuations in key ions such as potassium (K^+) and calcium (Ca^{2+}) are implicated in the pathogenesis of HIMS. This study aims to investigate the role of mitochondrial dysfunction and the protective potential of mitochondrial ATP-sensitive potassium channels ($mitoK_{ATP}$) in mitigating HIMS. **Methods**: A 5/6 nephrectomy rat model was established to mimic chronic kidney disease and the subsequent HIMS. The effects of $mitoK_{ATP}$ channel modulators were evaluated by administering diazoxide (DZX), a $mitoK_{ATP}$ opener, and 5-hydroxydecanoate (5-HD), a $mitoK_{ATP}$ blocker, before hemodialysis. Mitochondrial function was assessed by measuring membrane potential, ATP synthase activity, and intramitochondrial Ca^{2+} levels. Myocardial function was evaluated using speckle tracking echocardiography. **Results**: Rats undergoing hemodialysis exhibited significant reductions in left ventricular strain and synchrony. DZX administration significantly improved mitochondrial function and reduced myocardial strain compared to controls. Conversely, 5-HD worsened mitochondrial swelling and disrupted myocardial function. Higher K^+ and Ca^{2+} concentrations in the dialysate were associated with improved mitochondrial energy metabolism and myocardial strain. **Conclusions**: Mitochondrial dysfunction and ion imbalances during hemodialysis are key contributors to HIMS. The activation of $mitoK_{ATP}$ channels provides mitochondrial protection and may serve as a potential therapeutic strategy to mitigate HIMS.

Keywords: myocardial stunning; hemodialysis; mitochondrial dysfunction; chronic kidney disease

1. Introduction

Chronic kidney disease (CKD) is a major global public health challenge that imposes a significant burden on healthcare systems and contributes notably to morbidity and mortality [1]. At its most advanced stage, end-stage renal disease (ESRD), patients must rely on life-sustaining renal replacement therapy (RRT), which includes options such

as kidney transplantation or dialysis—primarily hemodialysis and peritoneal dialysis. Hemodialysis is the most widely used treatment modality globally, yet long-term survival rates remain suboptimal [2].

Cardiovascular diseases (CVDs) are disproportionally prevalent in patients undergoing maintenance hemodialysis (MHD), with significantly higher mortality rates compared to the general population, resulting in extremely undesirable survival outcomes [3–5].

A variety of well-established cardiovascular therapies often show reduced efficacy or inconclusive benefits in individuals with advanced CKD, particularly in those undergoing dialysis [6–9]. Likewise, the clinical utility of some conventional biomarkers for prognosis and risk stratification is compromised in this population [10,11], making the management of CVDs in patients with dialysis especially challenging.

A key factor contributing to this complexity is the presence of kidney-specific risks in addition to traditional cardiovascular risk factors such as hypertension, diabetes, and dyslipidemia. These kidney-specific risks include the accumulation of uremic toxins [12,13], CKD-related mineral and bone disorders (CKD-MBDs) [14], and the non-physiological nature of dialysis [15], all collectively contributing to cardiovascular damage, with one notable manifestation being hemodialysis-induced myocardial stunning (HIMS).

HIMS refers to a condition characterized by transient left ventricular systolic dysfunction resulting from ischemic episodes during hemodialysis sessions. With an incidence of approximately 64%, HIMS is common and represents a serious complication associated with the hemodialysis process, contributing to increased cardiovascular morbidity and mortality in this population [16–18]. Additional studies confirm that frequent occurrences of myocardial stunning during hemodialysis are linked to adverse cardiovascular outcomes and increased mortality [17,19,20].

Evidence strongly suggests that the hemodialysis process itself, particularly when associated with higher ultrafiltration rates, can lead to myocardial injury through various mechanisms. A reduction in myocardial perfusion is thought to play a key role, resulting in ischemia and subsequent myocardial stunning [16,21]. This phenomenon is marked by an increase in biomarkers of myocardial damage, such as cardiac troponin T and cell-free DNA [21–23]. Unfortunately, studies on intra-dialytic intervention are still limited.

Therefore, understanding the pathophysiology of HIMS and developing effective preventive strategies are imperative for improving cardiac function and reducing cardiovascular mortality in patients on MHD.

The myocardium, the most energy-demanding tissue in the body, requires a continuous supply of adenosine triphosphate (ATP) to sustain contractile function. Mitochondria, the principal source of ATP in myocardial cells, are critical to maintaining normal cardiac performance. Mitochondrial dysfunction, characterized by the disruption of ATP synthesis and the opening of mitochondrial permeability transition pores, has been identified as a key contributor to myocardial injury. Consequently, the preservation of mitochondrial integrity is a central focus of cardioprotective strategies [24]. In patients with CKD, mounting evidence indicates that mitochondrial dysfunction is involved in CKD-related cardiovascular complications.

The existence of mitochondrial ATP-sensitive K^+ channels (mitoK_{ATP}) was first reported over two decades ago, sparking significant interest in their role in cellular function [25]. Since then, several mitoK_{ATP} openers, including diazoxide (DZX), nicorandil, BMS191095, and cromakalim, have been identified, and their effects on mitochondrial physiology have been thoroughly explored [26].

It has been established that mitoK_{ATP} play an important role in ischemic preconditioning, positioning them as promising therapeutic targets for cardioprotection during myocardial ischemia. DZX, a mitoK_{ATP} opener with significant selectivity versus the sarcolemmal isoform of the K_{ATP} channel in cardiac myocytes, has been shown to confer protective effects like those of ischemic preconditioning. These protective effects can be blocked by 5-hydroxydecanoate (5-HD), a highly selective K^+ inhibitor of mitoK_{ATP} [27–29]. The activation of mitoK_{ATP} under conditions of ischemia, hypoxia, or energy depletion

may preserve mitochondrial integrity and function through the following mechanisms: preserving mitochondrial structure by maintaining osmotic pressure via modulation of K^+ influx; mitigating Ca^{2+} overload by lowering membrane potential; enhancing mitochondrial respiration [30–32].

Therefore, the present study aimed to investigate the role of mitochondrial dysfunction in the onset of HIMS, with a focus on the impact of mitoK_{ATP}. The findings could offer new insights into therapeutic interventions for managing cardiovascular risks in patients with CKD on hemodialysis.

2. Materials and Methods

2.1. Establishment of Animal Model

A 5/6 nephrectomy was performed in two steps, starting with the surgical excision of the upper and lower poles of the left kidney, followed by uninephrectomy on the contralateral side after one week. Throughout the entire study, the rats were on regular chow and had free access to water.

Serum urea and creatinine levels were measured 2, 4, 8, and 12 weeks after operation. The model was considered successfully established if serum creatinine levels were five times higher than baseline.

2.2. Vascular Access Creation, Extracorporeal Circulation, and Hemodialysis

Rats that successfully underwent the 5/6 nephrectomy were weighed and anesthetized with an intraperitoneal injection of 2% pentobarbital sodium (3 mg/kg).

The designated areas for catheterization were meticulously shaved and disinfected using 10% povidone–iodine solution. A precise midline incision was made along the anterior aspect of the neck, followed by the careful blunt dissection of subcutaneous and muscle tissues using microvascular clamps and forceps. This dissection facilitated the exposure of the left common carotid artery, where the proximal and distal segments were ligated to secure the vessel. An oblique arteriotomy was then performed on the common carotid artery to insert and secure a PE50 catheter, which provided arterial access for hemodialysis. Using a similar surgical approach, a PE50 catheter was introduced into the left femoral vein. The left common carotid artery and the left femoral vein were utilized as the outflow and inflow routes, respectively.

Following the creation of vascular access, systemic anticoagulation was achieved with an intravenous injection of 500 IU/kg heparin through the femoral vein catheter.

A dialyzer specifically designed for small animals (Wego healthcare, Shandong, China, membrane area: 0.02 m^2, blood chamber volume: 1.4 mL) was used. The composition and the dialysate were glucose 11 mmol/L, Na^+ 142 mmol/L, Mg^{2+} 1.5 mmol/L, and HCO_3^- 34 mmol/L, with adjustments in K^+ and Ca^{2+} concentrations tailored to the specific requirements of the experimental protocols.

Blood and dialysate flow rates, along with ultrafiltration rates, were meticulously regulated using a small peristaltic pump. The blood flow rate was maintained between 0.8 and 1.0 mL/min, and the dialysate flow rate was set at 0.4–0.5 mL/min. Prior to initiating the hemodialysis, the extracorporeal circulation was primed. Subsequently, the blood pump was activated to initiate blood withdrawal at a rate of 0.3–0.5 mL/min, gradually increasing to the target rate once steady arterial flow was established. Concurrently, the speeds of the replacement fluid infusion pump and the ultrafiltration pump were adjusted to match the set parameters. Throughout the procedure, vital signs such as respiratory rate, heart rate, and blood pressure were rigorously monitored. The limbs were connected to a synchronized electrocardiogram.

Hemodialysis was conducted over a duration of 2 h, with continuous monitoring under anesthesia and systemic anticoagulation using heparin. Following the treatment, extracorporeal circulation was terminated, and the blood within the circuit was safely reinfused into the rats using an air-driven method (Figure 1).

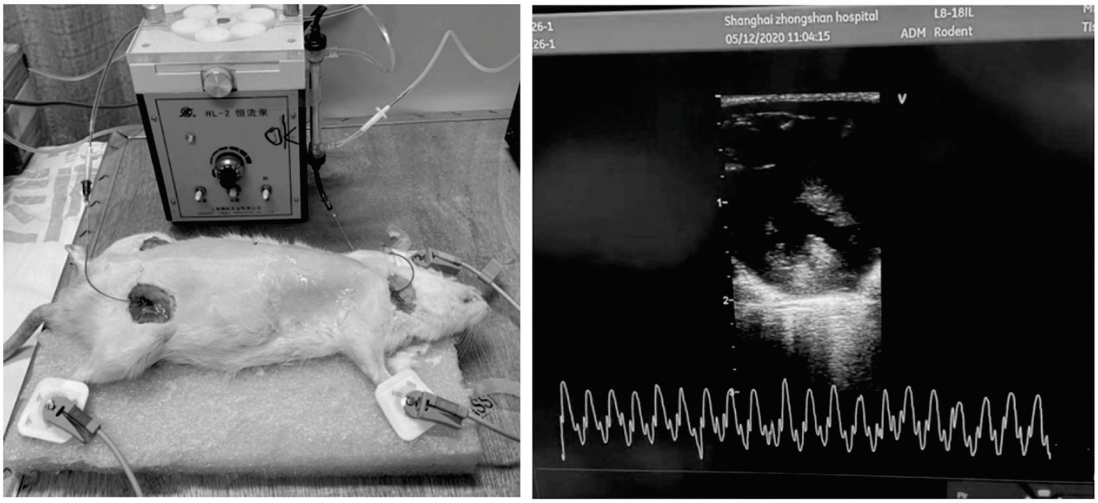


Figure 1. Hemodialysis and echocardiographic monitoring in rats.

2.3. Echocardiography

Echocardiography was performed on the hemodialysis rats prior to dialysis every 30 min during the session and immediately following dialysis, totaling five echocardiographic assessments per session. For these evaluations, rats were positioned supine. Sequential imaging captured three consecutive cardiac cycles across the apical four-chamber, two-chamber, and three-chamber views using a GE Vivid 7 system (GE Medical Systems, Freiburg im Breisgau, Germany). These images were subsequently analyzed offline employing speckle tracking and strain analysis techniques using EchoPAC Clinical Workstation Software (version 113.1, GE, Germany).

2.4. Mitochondrial ATP Channel Intervention

To investigate the cardioprotective effects of mitoK_{ATP} modulators, various agents were administered 10 min prior to dialysis. These included the mitoK_{ATP} opener DZX, (3 mg/kg), the mitoK_{ATP} blocker 5-HD (10 mg/kg), a combination of DZX and 5-HD (DZX 3 mg/kg + 5-HD 5 mg/kg), and the calcium channel blocker nicardipine, which was given via intraperitoneal injection (0.4 mg/kg). This pharmacological regimen was designed to delineate the individual and combined effects of these interventions on cardiac function during the stress of dialysis.

2.5. Sampling and Processing of Experimental Animals

Upon the completion of dialysis, the heart of each rat was excised along the base of the aorta and immediately immersed in ice-cold saline to halt metabolic processes. After removing adherent impurities and excess fat, residual blood was thoroughly rinsed away. Precise dissections of the left ventricle were performed using sharp blades on a chilled slide, and small samples measuring 1 × 1 mm were excised from the left ventricular myocardium. These samples were promptly fixed in 2.5% glutaraldehyde for subsequent electron microscopy analysis. Additionally, 2–3 pieces of 2 × 2 mm from the ventricular muscle were fixed in 10% formaldehyde for histopathological examination. All remaining animal tissues were disposed of following approved bioethical protocols to ensure safety and compliance with regulatory guidelines.

2.6. Grouping of Experimental Animals

Rats were categorized into four groups based on the different K^+ and Ca^{2+} concentrations in the dialysate: K2 Ca1.25, K2 Ca1.5, K3 Ca1.25, and K3 Ca1.5. After 2 h of hemodialysis, mitochondrial-related tests were conducted, including mitochondrial membrane potential with JC-1, mitochondrial ATP synthase activity, and mitochondrial Ca^{2+} overload.

To investigate the impact of mitochondrial ATP channel intervention, rats were categorized into five groups based on the different drugs: control, diazoxide group, 5-HD group, diazoxide + 5-HD group, and calcium channel blocker group.

Each group contained four experimental rats.

2.7. Statistical Analyses

Data are expressed as mean ± standard error. Between-group comparisons were performed using one-way ANOVA followed by Tukey's post hoc test. Statistical significance was set at $p < 0.05$. All statistical analyses and visualization were conducted by Rstudio (RStudio 2023.12.1+402 "Ocean Storm" Release, R version 4.4.0).

3. Results

3.1. Echocardiography

Utilizing speckle tracking echocardiography, changes in cardiac function were detected in a hemodialysis rat model. Specifically, the left ventricular multi-segmental strain value (Figure 2) exhibited a marked decrease after dialysis compared to pre-dialysis measurements. The values of longitudinal and circumferential strain at different time points, including those measured during hemodialysis, are detailed in Section 3.3.

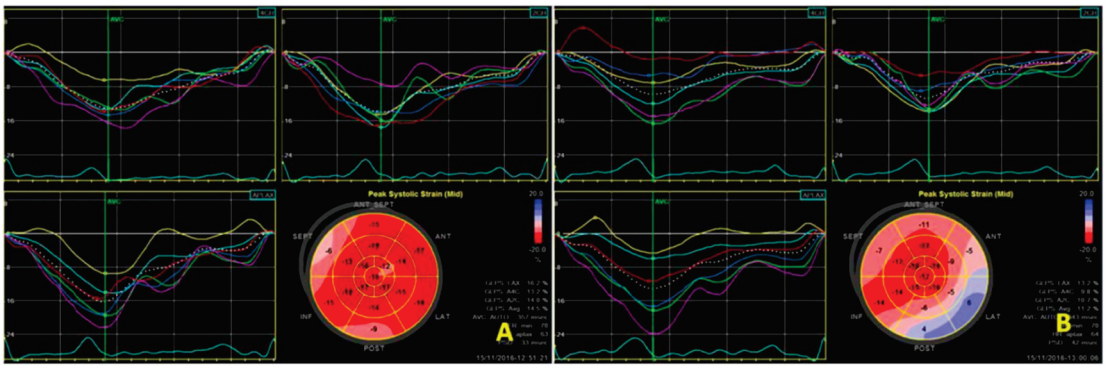


Figure 2. Two-dimensional speckle tracking shows a decrease in left ventricular strain values before (**A**) and immediately after (**B**) dialysis.

3.2. Effects of K^+ and Ca^{2+} Concentrations on Mitochondrial Energy Metabolism and Myocardial Contraction

The animals were stratified into four groups based on the potassium and calcium concentrations: K2 Ca1.25, K2 Ca1.5, K3 Ca1.25, and K3 Ca1.5. After 2 h of hemodialysis, mitochondrial function was assessed through measurements of mitochondrial membrane potential, mitochondrial ATP synthase activity, and mitochondrial Ca^{2+} overload. The findings revealed that the group with the highest ion concentrations ($K_3Ca_{1.5}$) exhibited a trend toward enhanced ATP synthase activity compared to the group with the lowest ion concentrations ($K_2Ca_{1.25}$) ($p = 0.13$). No between-group differences regarding mitochondrial membrane potential, mitochondrial ATP synthase activity, and mitochondrial Ca^{2+} were observed (Figure 3).

3.3. Effects of Mitochondrial ATP Channel Modulators and Calcium Channel Blockers on Mitochondrial Energy Metabolism and Myocardial Stunning

Pre-dialysis interventions were administered 10 min before initiation of hemodialysis: the mitoK$_{ATP}$ channel opener DZX (3 mg/kg), the mitoK$_{ATP}$ channel blocker 5-HD (10 mg/kg), a combination of DZX and 5-HD (DZX 3 mg/kg + 5-HD 5 mg/kg), and the calcium channel blocker nicardipine (intraperitoneal 0.4 mg/kg). Declines in both longitudinal and circumferential myocardial strains were observed as hemodialysis progressed, peaking before the end of the session.

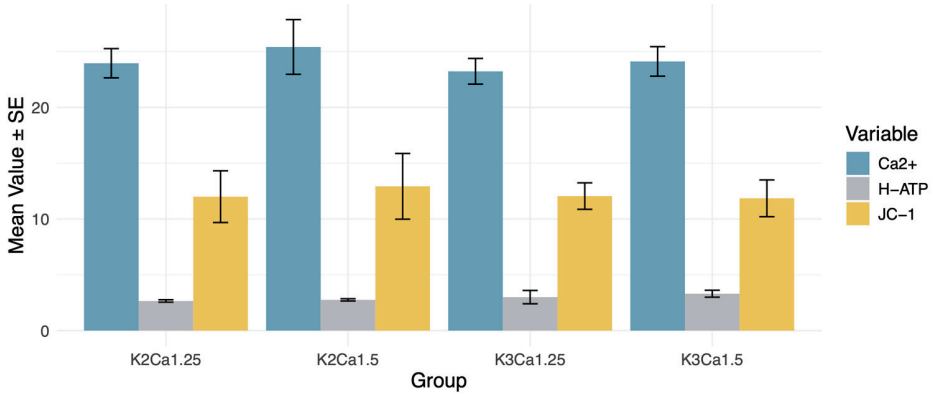


Figure 3. Effects of K^+ and Ca^{2+} concentrations on mitochondrial energy metabolism. DZX (diazoxide), mitoKATP channel opener; 5HD (5-hydroxydecanoate), mitoKATP channel blocker; CCB (nicardipine), calcium channel blocker; JC-1, mitochondrial membrane potential assay; H-ATP, ATP synthase activity; Ca^{2+}, intramitochondrial Ca^{2+} concentration. No between-group differences regarding mitochondrial membrane potential, mitochondrial ATP synthase activity, and mitochondrial Ca^{2+} were observed.

Longitudinal strain (LS) and circumferential strain (CS) of the rat myocardium were analyzed using layer-specific speckle tracking imaging through three-dimensional speckle tracking (Figure 4 and Table 1).

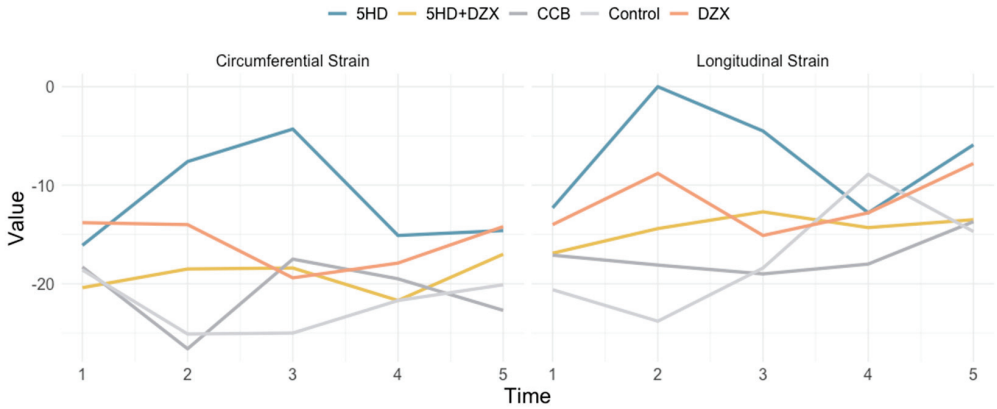


Figure 4. Effects of mitochondrial ATP channel modulators and calcium channel blocking on circumferential strain and longitudinal strain. DZX (diazoxide), mitoKATP channel opener; 5HD (5-hydroxydecanoate), mitoKATP channel blocker; CCB (nicardipine), calcium channel blocker; JC-1, mitochondrial membrane potential assay; H-ATP, ATP synthase activity; Ca^{2+}, intramitochondrial Ca^{2+} concentration.

Table 1. Longitudinal and circumferential strain measurements across experimental groups over time.

Group	Pre-Dialysis		30 Min		60 Min		90 Min		Post-Dialysis	
	CS	LS	CS	LS	CS	LS	CS	LS	CS	LS
DZX	−13.8	−14	−14	−8.8	−19.4	−15.1	−17.9	−12.8	−14.2	−7.8
DZX + 5HD	−20.4	−16.9	−18.5	−14.4	−18.4	−12.7	−21.7	−14.3	−17	−13.5
5HD	−16.1	−12.3	−7.6	0	−4.3	−4.5	−15.1	−12.8	−14.6	−5.9
CCB	−18.3	−17.1	−26.6	−18.1	−17.5	−19	−19.5	−18	−22.7	−13.7
Control	−18.6	−20.6	−25.1	−23.8	−25	−18.4	−21.7	−8.9	−20.1	−14.7

DZX (diazoxide), mitoKATP channel opener; 5HD (5-hydroxydecanoate), mitoKATP channel blocker; CCB (nicardipine), calcium channel blocker; CS, circumferential strain, presented as %; LS, longitudinal strain, presented as %.

A similar trend for the harmful impact of 5-HD was also observed in mitochondrial membrane potential, ATP synthase activity, and intramitochondrial Ca^{2+} concentration (Figure 5). However, no significant between-group difference was observed regarding ATP synthase activity ($p = 0.07$), mitochondrial membrane potential ($p = 0.96$), and Ca^{2+} concentration ($p = 0.44$).

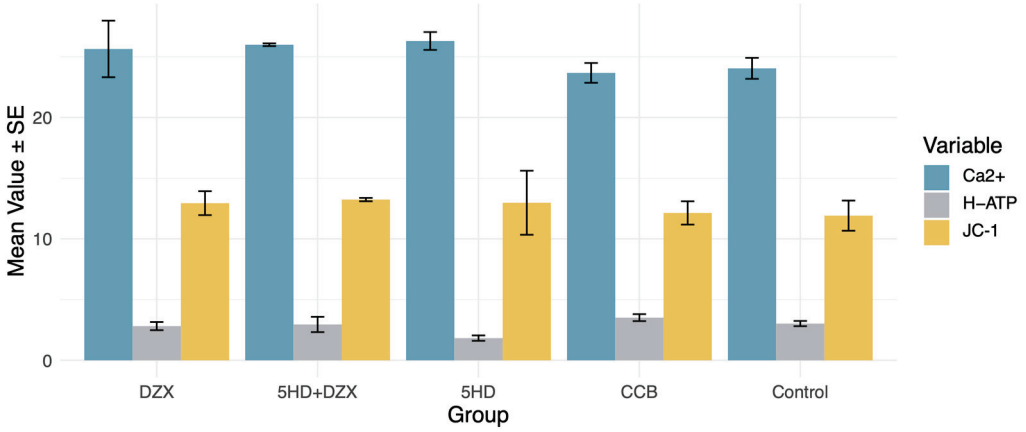


Figure 5. Effects of mitochondrial ATP channel modulators and calcium channel blockers on mitochondrial energy metabolism. DZX (diazoxide), mitoKATP channel opener; 5HD (5-hydroxydecanoate), mitoKATP channel blocker; CCB (nicardipine), calcium channel blocker; JC-1, mitochondrial membrane potential assay; H-ATP, ATP synthase activity; Ca^{2+}, intramitochondrial Ca^{2+} concentration.

Additionally, rats in the 5-HD group exhibited pronounced mitochondrial swelling, variability in size, and partial cristae disruption (Figure 6).

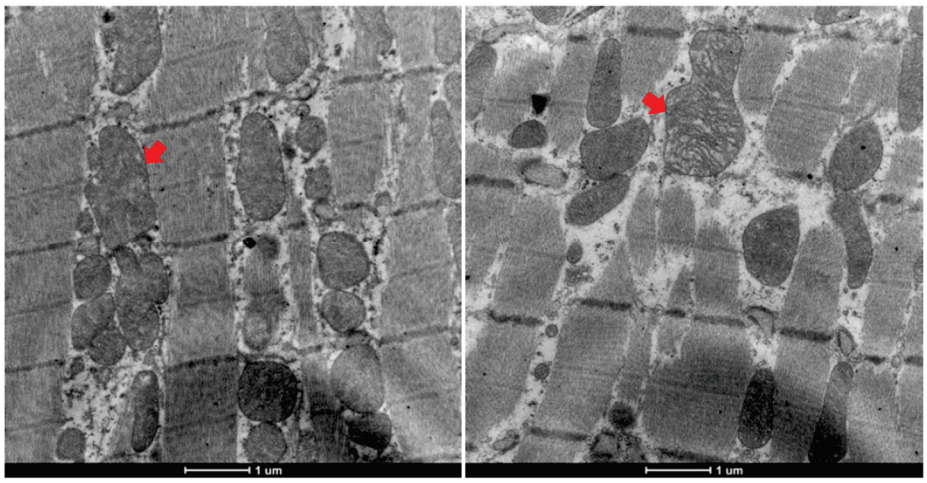


Figure 6. Abnormal mitochondrial morphology in 5-HD-administered rats. (**Left**, mitochondrial swelling; **right**, cristae disruption).

4. Discussion

This study investigated the effects of key ions in the dialysate on mitochondrial function using a 5/6 nephrectomy rat model to simulate the hemodialysis process. Echocardiography showed reductions in both global and segmental contractile functions during and after hemodialysis, accompanied by mitochondrial dysfunction. Intra-dialytic fluctuations in K^+ and Ca^{2+} also contribute to the onset of myocardial stunning. Activation of mitoK$_{ATP}$ channels exerts a potential protective effect on mitochondrial energy metabolism, highlighting a novel therapeutic target for mitigating hemodialysis-induced cardiac dysfunction.

While larger animals such as swine, dogs, or goats are typically favored for hemodialysis research, our study successfully established a rat model for hemodialysis. Despite certain limitations, such as reduced tolerance to high ultrafiltration, this model provides a robust, accessible, and cost-effective platform to investigate the cardiovascular impacts and underlying mechanisms of hemodialysis.

HIMS is a major contributor to the high incidence of CVD in patients on hemodialysis. Recurrent episodes of myocardial stunning not only impair cardiac function but also have detrimental effects on long-term survival. Unlike traditional ischemia–reperfusion-induced myocardial stunning, which is unpredictable and difficult to manage, HIMS can be anticipated and mitigated given the regular and cyclic nature of hemodialysis treatments and is thus a promising target for intervention. This predictability also positions HIMS as an ideal model for investigating myocardial stunning.

Volume removal is a key objective of hemodialysis, which involves extracting accumulated fluid over 48–72 h within a 4 h session. This rapid volume reduction causes significant hemodynamic shifts that can impair cardiac perfusion and induce myocardial stunning. Research indicates that myocardial blood flow decreases during hemodialysis, which correlates with wall motion abnormalities in regions of reduced blood supply [33,34]. Higher ultrafiltration rates are associated with more severe wall motion abnormalities, particularly in regions supplied by a single vessel [6]. In contrast, peritoneal dialysis, which causes less hemodynamic disturbance, rarely leads to myocardial stunning [35].

Mitochondrial energy metabolism disruption, characterized by ATP depletion, is a crucial factor in myocardial ischemic injury [34]. In hemodialysis animal models, HIMS is associated with mitochondrial ultrastructural damage, including swelling and disordered cristae. Thus, mitochondrial dysfunction from rapid volume reduction during hemodialysis may cause abnormal myocardial contraction. Enhancing mitochondrial energy metabolism could offer a potential strategy for preventing or treating HIMS, with significant clinical implications.

Additionally, solute removal is critical during hemodialysis, particularly for maintaining the balance of key ions like K^+ and Ca^{2+}, which are fundamental for myocardial contractility and rhythm stability. Fluctuations in K^+ and Ca^{2+} levels during hemodialysis can cause electrophysiological disturbances such as ectopic excitation and conduction abnormalities [36].

K^+ is essential for maintaining the resting potential of myocardial cells and mitochondria. Our research indicates that the rapid removal of serum K^+ during dialysis prolongs myocardial repolarization time [37], suggesting that K^+ fluctuations can affect potassium channel function. Serum potassium imbalances in either direction are problematic in hemodialysis patients. Hyperkalemia is associated with worsened outcomes [38,39], while post-dialysis hypokalemia is associated with an increased risk of ventricular arrhythmias and mortality [40,41]. A multicenter prospective study found that patients dialyzed with a potassium concentration of 1 mEq/L experienced higher mortality rates compared to those using 2 or 3 mEq/L [42]. These findings suggest that milder changes in serum K^+ concentrations during dialysis may be advantageous.

Drastic intra-dialytic removal of potassium affects cardiac electrophysiology, as the potassium gradient across cell membranes is crucial for repolarization, impacting both resting and action potentials, leading to an increased QT interval, QT dispersion, repolarization heterogeneity, and ultimately arrhythmias [43]. Studies show that profiling potassium levels during dialysis reduces arrhythmic events, with a 36% reduction in premature ventricular complexes observed when profiling is used compared to a constant potassium concentration [44]. Profiling provides smoother potassium clearance than constant low levels, which may decrease arrhythmia risk.

Various potassium channels are present on the inner and outer mitochondrial membranes. During myocardial ischemia, mitochondrial membrane potassium channels open, increasing K^+ influx, reducing mitochondrial membrane potential, causing membrane depolarization, decreasing mitochondrial Ca^{2+} overload, and promoting mitochondrial

respiration. This improves myocardial energy metabolism and protects the ischemic myocardium [45,46]. The rapid decline in serum K^+ during dialysis prolongs myocardial repolarization time, as rapid cardiac repolarization primarily occurs through K^+ efflux. This decline potentially impacts potassium channel function. Our results show that rats dialyzed with a higher K^+ concentration exhibit a trend toward better mitochondrial energy metabolism. We hypothesize that dialysate with a higher K^+ concentration, by creating a smaller K^+ gradient between the dialysate and serum, maintains normal mitochondrial potassium channel function and provides mitochondrial protection. Conversely, a larger gradient between the dialysate and serum K^+ leads to a rapid intra-dialytic decline in serum K^+, weakening myocardial protection, causing mitochondrial Ca^{2+} overload, disrupting myocardial energy metabolism, and leading to myocardial dysfunction, as indicated by abnormal myocardial strain and contraction synchrony.

Ca^{2+} is the trigger for myocardial cell contraction, and the cyclical changes in cytoplasmic Ca^{2+} concentration during myocardial contraction and relaxation are crucial [47,48]. Also, alterations in intracellular Ca^{2+} regulation are associated with arrhythmia. Abnormal handling of Ca^{2+} in the endoplasmic/sarcoplasmic reticulum could lead to intracytoplasmic Ca^{2+} overload and promote arrhythmias such as atrial fibrillation (AF) and ventricular arrhythmias [49]. Intriguingly, the baseline level of sarcoplasmic endoplasmic reticulum calcium ATPase might predict the efficacy of ablative therapy in patients with persistent AF [50].

Hemodialysis patients often suffer from metabolic disorders such as hypocalcemia and hyperphosphatemia, necessitating the use of Ca^{2+}-containing dialysate to correct these imbalances. Whether the dialysate Ca^{2+} concentration is 1.5 mmol/L or 1.75 mmol/L, it is usually higher than the serum free Ca^{2+} concentration, leading to Ca^{2+} transfer from the dialysate into the blood, increasing the body's calcium load. Additionally, chronic malnutrition and hypoalbuminemia in patients on hemodialysis reduce albumin-bound calcium, increasing the proportion of serum free Ca^{2+} and weakening albumin's buffering capacity against the rapid rise in serum Ca^{2+} during dialysis. Thus, serum Ca^{2+} levels often rise rapidly during dialysis. Intracellular Ca^{2+} overload is a classic mechanism of myocardial cell injury. During myocardial ischemic injury, extracellular Ca^{2+} enters and accumulates in the cytoplasm, and mitochondria take up large amounts of Ca^{2+} to alleviate cytoplasmic Ca^{2+} overload. However, this influx of Ca^{2+} into the mitochondria causes swelling, outer membrane rupture, structural damage, disruption of the electron transport chain, interference with ATP synthesis, and energy metabolism disruption. The rapid intra-dialytic rise in serum free Ca^{2+} during dialysis may exacerbate Ca^{2+} overload in the cytoplasm and mitochondria during ischemia, affecting mitochondrial structure and function, and leading to abnormal myocardial energy metabolism. However, in this study, with fixed dialysate K^+ concentrations, there was no significant difference in mitochondrial energy metabolism and myocardial strain among the groups with different ion concentrations. During the relatively short dialysis time (2 h in this study) and low dialysate flow rate, intracellular calcium fluctuations in myocardial cells were not as drastic as expected. It should be noted that calcium channel blocker usage displayed a trend toward cardiac protection. Future studies using larger animals with longer dialysis times and a higher dialysate flow rate may provide more conclusive findings.

In clinical settings, the dialysate Ca^{2+} is a modifiable factor that presents a therapeutic dilemma. Higher dialysate Ca^{2+} levels (1.75 mmol/L) may help manage low PTH and prevent hypercalcemia but may exacerbate vascular calcification and stiffness, contributing to cardiovascular complications. Lower dialysate Ca^{2+} concentrations have been reported to increase QT dispersion and increase the risk of arrythmia [51,52].

HIMS is fundamentally a mild and transient myocardial ischemic injury. Ischemic preconditioning is one of the most effective strategies for preventing ischemic injury [27,53,54]. Previous studies have identified mitoK_{ATP} as critical mediators in ischemic preconditioning. DZX, a specific mitoK_{ATP} opener, has demonstrated protective effects similar to those of ischemic preconditioning [27,28].

In the present study, DZX significantly reduced mitochondrial Ca^{2+} levels compared to the control and 5-HD groups, indicating that DZX alleviates Ca^{2+} overload by promoting mitoK_{ATP} channel opening. This protective effect was reversed by mitoK_{ATP} blockage. Additionally, echocardiographic assessments showed less severe myocardial strain reduction during dialysis in DZX-treated rats. Electron microscopy revealed marked mitochondrial swelling and structural damage in the 5-HD group.

These findings underscore the critical role of mitoK_{ATP} channels in maintaining mitochondrial structure and energy metabolism, with mitoK_{ATP} activation offering potential protection against ischemic myocardial injury. While DZX's cardioprotective effects have been established in ischemia–reperfusion models, the unpredictable nature of traditional myocardial stunning complicates precise prevention. In contrast, the scheduled and cyclical nature of hemodialysis allows for the accurate prediction of HIMS onset, facilitating targeted pharmacological intervention.

Several limitations should be noted. First, this study utilized a rat model, and extending the dialysis duration to a standard 4 h was not feasible due to the physiological constraints of the animal. This limited our ability to fully assess the effects of the routine clinical four-hour hemodialysis. It should also be noted that rapid ultrafiltration is another paramount risk factor for CVD during hemodialysis. But, due to the challenges of ensuring stable extracorporeal circulation in rats, the ultrafiltration was minimal. Validation using large animal models would provide a more comprehensive investigation, taking into consideration both the solutes and fluid removal.

5. Conclusions

Mitochondrial dysfunction induced by myocardial ischemia during hemodialysis is a crucial factor in the development of HIMS, leading to impaired myocardial contractility. Intra-dialytic fluctuations in K^+ and Ca^{2+} also contribute to the onset of myocardial stunning. Activation of mitoK_{ATP} channels exerts a protective effect on mitochondrial energy metabolism, suggesting that exogenous promotion of mitoK_{ATP} channel opening may offer potential therapeutic protection against HIMS.

Author Contributions: Conceptualization, Y.N., X.D. and Z.Z.; data curation, Z.Z.; formal analysis, Y.N.; funding acquisition, Y.N., L.L., J.T. and Z.Z.; investigation, Y.N., L.L., Q.Y., J.H., M.S. and Z.Z.; methodology, Y.N., Q.Y. and J.H.; resources, F.X., X.C., J.Y., Y.W. and B.S.; supervision, X.D.; visualization, Z.Z.; writing—original draft, Y.N., L.L. and Z.Z.; writing—review and editing, J.T. and B.S. All authors have read and agreed to the published version of the manuscript.

Funding: This research was funded by the National Natural Science Foundation of China (81800677 and 82104617), the Natural Science Foundation of Xiamen (3502Z202374020), and the Fujian provincial key clinical specialty of 2023.

Institutional Review Board Statement: The animal study protocol was approved by the Institutional Review Board of Zhongshan Hospital, Fudan University. Approval code: 2019-210, approval date: 20 February 2019.

Data Availability Statement: The data presented in this study are available on request from the corresponding author.

Acknowledgments: During the preparation of this work, the authors used ChatGPT 4 for language editing. After using this tool, the authors reviewed and edited the content as needed and take full responsibility for the content of the publication.

Conflicts of Interest: The authors declare no conflicts of interest.

References

1. GBD Chronic Kidney Disease Collaboration. Global, Regional, and National Burden of Chronic Kidney Disease, 1990–2017: A Systematic Analysis for the Global Burden of Disease Study 2017. *Lancet* **2020**, *395*, 709–733. [CrossRef] [PubMed]
2. Thurlow, J.S.; Joshi, M.; Yan, G.; Norris, K.C.; Agodoa, L.Y.; Yuan, C.M.; Nee, R. Global Epidemiology of End-Stage Kidney Disease and Disparities in Kidney Replacement Therapy. *Am. J. Nephrol.* **2021**, *52*, 98–107. [CrossRef] [PubMed]

3. Zhang, Z.; Wang, Y. Management of Cardiovascular Diseases in Chronic Hemodialysis Patients. *Rev. Cardiovasc. Med.* **2023**, *24*, 185. [CrossRef] [PubMed]
4. Gao, P.; Zou, X.; Sun, X.; Zhang, C. Coronary Artery Disease in CKD-G5D Patients: An Update. *Rev. Cardiovasc. Med.* **2023**, *24*, 227. [CrossRef] [PubMed]
5. Wanner, C.; Amann, K.; Shoji, T. The Heart and Vascular System in Dialysis. *Lancet* **2016**, *388*, 276–284. [CrossRef]
6. Baigent, C.; Landray, M.J.; Reith, C.; Emberson, J.; Wheeler, D.C.; Tomson, C.; Wanner, C.; Krane, V.; Cass, A.; Craig, J.; et al. The Effects of Lowering LDL Cholesterol with Simvastatin plus Ezetimibe in Patients with Chronic Kidney Disease (Study of Heart and Renal Protection): A Randomised Placebo-Controlled Trial. *Lancet* **2011**, *377*, 2181–2192. [CrossRef]
7. Ferro, C.J.; Mark, P.B.; Kanbay, M.; Sarafidis, P.; Heine, G.H.; Rossignol, P.; Massy, Z.A.; Mallamaci, F.; Valdivielso, J.M.; Malyszko, J.; et al. Lipid Management in Patients with Chronic Kidney Disease. *Nat. Rev. Nephrol.* **2018**, *14*, 727–749. [CrossRef]
8. Ethier, J.; Bragg-Gresham, J.L.; Piera, L.; Akizawa, T.; Asano, Y.; Mason, N.; Gillespie, B.W.; Young, E.W. Aspirin Prescription and Outcomes in Hemodialysis Patients: The Dialysis Outcomes and Practice Patterns Study (DOPPS). *Am. J. Kidney Dis.* **2007**, *50*, 602–611. [CrossRef]
9. Calice-Silva, V.; Muenz, D.; Wong, M.M.Y.; McCullough, K.; Charytan, D.; Reichel, H.; Robinson, B.; Stengel, B.; Massy, Z.A.; Pecoits-Filho, R.; et al. International Practice Patterns of Dyslipidemia Management in Patients with Chronic Kidney Disease under Nephrology Care: Is It Time to Review Guideline Recommendations? *Lipids Health Dis.* **2023**, *22*, 67. [CrossRef]
10. Li, H.; Chen, W.; Lin, X.; Chen, W.; Xie, T.; Chen, K.; Hou, S.; Li, H. Influence of Renal Function on the Ability of TyG Index to Predict All-Cause Mortality. *Lipids Health Dis.* **2023**, *22*, 193. [CrossRef]
11. Wang, B.; Jiang, C.; Qu, Y.; Wang, J.; Yan, C.; Zhang, X. Nonlinear Association between Atherogenic Index of Plasma and Chronic Kidney Disease: A Nationwide Cross-Sectional Study. *Lipids Health Dis.* **2024**, *23*, 312. [CrossRef] [PubMed]
12. Tan, X.; Cao, X.; Zou, J.; Shen, B.; Zhang, X.; Liu, Z.; Lv, W.; Teng, J.; Ding, X. Indoxyl Sulfate, a Valuable Biomarker in Chronic Kidney Disease and Dialysis. *Hemodial. Int.* **2017**, *21*, 161–167. [CrossRef] [PubMed]
13. Zhang, P.; Zou, J.-Z.; Chen, J.; Tan, X.; Xiang, F.-F.; Shen, B.; Hu, J.-C.; Wang, J.-L.; Wang, Y.-Q.; Yu, J.-B.; et al. Association of Trimethylamine N-Oxide with Cardiovascular and All-Cause Mortality in Hemodialysis Patients. *Ren. Fail.* **2020**, *42*, 1004–1014. [CrossRef] [PubMed]
14. Zhang, H.; Li, G.; Yu, X.; Yang, J.; Jiang, A.; Cheng, H.; Fu, J.; Liang, X.; Liu, J.; Lou, J.; et al. Progression of Vascular Calcification and Clinical Outcomes in Patients Receiving Maintenance Dialysis. *JAMA Netw. Open* **2023**, *6*, e2310909. [CrossRef]
15. Assimon, M.M.; Wenger, J.B.; Wang, L.; Flythe, J.E. Ultrafiltration Rate and Mortality in Maintenance Hemodialysis Patients. *Am. J. Kidney Dis.* **2016**, *68*, 911–922. [CrossRef]
16. Burton, J.O.; Jefferies, H.J.; Selby, N.M.; McIntyre, C.W. Hemodialysis-Induced Cardiac Injury: Determinants and Associated Outcomes. *Clin. J. Am. Soc. Nephrol.* **2009**, *4*, 914–920. [CrossRef]
17. Assa, S.; Hummel, Y.M.; Voors, A.A.; Kuipers, J.; Westerhuis, R.; de Jong, P.E.; Franssen, C.F.M. Hemodialysis-Induced Regional Left Ventricular Systolic Dysfunction: Prevalence, Patient and Dialysis Treatment-Related Factors, and Prognostic Significance. *Clin. J. Am. Soc. Nephrol.* **2012**, *7*, 1615–1623. [CrossRef]
18. Nie, Y.; Zhang, Z.; Zou, J.; Liang, Y.; Cao, X.; Liu, Z.; Shen, B.; Chen, X.; Ding, X. Hemodialysis-Induced Regional Left Ventricular Systolic Dysfunction: HD-Induced LV Systolic Dysfunction. *Hemodial. Int.* **2016**, *20*, 564–572. [CrossRef]
19. Jefferies, H.J.; Virk, B.; Schiller, B.; Moran, J.; McIntyre, C.W. Frequent Hemodialysis Schedules Are Associated with Reduced Levels of Dialysis-Induced Cardiac Injury (Myocardial Stunning). *Clin. J. Am. Soc. Nephrol.* **2011**, *6*, 1326–1332. [CrossRef]
20. Zuidema, M.Y.; Dellsperger, K.C. Myocardial Stunning with Hemodialysis: Clinical Challenges of the Cardiorenal Patient. *Cardiorenal Med.* **2012**, *2*, 125–133. [CrossRef]
21. Ünlü, S.; Şahinarslan, A.; Sezenöz, B.; Uludağ, O.M.; Gökalp, G.; Seçkin, Ö.; Arınsoy, S.T.; Gülbahar, Ö.; Boyacı, N.B. High-Sensitive Troponin T Increase after Hemodialysis Is Associated with Left Ventricular Global Longitudinal Strain and Ultrafiltration Rate. *Cardiol. J.* **2020**, *27*, 376–383. [CrossRef] [PubMed]
22. Coimbra, S.; Rocha, S.; Nascimento, H.; Valente, M.J.; Catarino, C.; Rocha-Pereira, P.; Sameiro-Faria, M.; Oliveira, J.G.; Madureira, J.; Fernandes, J.C.; et al. Cell-Free DNA as a Marker for the Outcome of End-Stage Renal Disease Patients on Haemodialysis. *Clin. Kidney J.* **2021**, *14*, 1371–1378. [CrossRef] [PubMed]
23. Tovbin, D.; Novack, V.; Wiessman, M.P.; Abd Elkadir, A.; Zlotnik, M.; Douvdevani, A. Circulating Cell-Free DNA in Hemodialysis Patients Predicts Mortality. *Nephrol. Dial. Transpl.* **2012**, *27*, 3929–3935. [CrossRef] [PubMed]
24. Chen, Y.; Liu, J.; Zheng, Y.; Wang, J.; Wang, Z.; Gu, S.; Tan, J.; Jing, Q.; Yang, H. Uncoupling Protein 3 Mediates H_2O_2 Preconditioning-Afforded Cardioprotection through the Inhibition of MPTP Opening. *Cardiovasc. Res.* **2015**, *105*, 192–202. [CrossRef] [PubMed]
25. Inoue, I.; Nagase, H.; Kishi, K.; Higuti, T. ATP-Sensitive K+ Channel in the Mitochondrial Inner Membrane. *Nature* **1991**, *352*, 244–247. [CrossRef]
26. O'Rourke, B. Mitochondrial Ion Channels. *Annu. Rev. Physiol.* **2007**, *69*, 19–49. [CrossRef]
27. Schwartz, L.M.; Reimer, K.A.; Crago, M.S.; Jennings, R.B. Pharmacological Preconditioning with Diazoxide Slows Energy Metabolism during Sustained Ischemia. *Exp. Clin. Cardiol.* **2007**, *12*, 139–147.
28. Maffit, S.K.; Sellitto, A.D.; Al-Dadah, A.S.; Schuessler, R.B.; Damiano, R.J.; Lawton, J.S. Diazoxide Maintains Human Myocyte Volume Homeostasis during Stress. *J. Am. Heart Assoc.* **2012**, *1*, jah3-e000778. [CrossRef]
29. Coetzee, W.A. Multiplicity of Effectors of the Cardioprotective Agent, Diazoxide. *Pharmacol. Ther.* **2013**, *140*, 167–175. [CrossRef]

30. Ishida, H.; Hirota, Y.; Genka, C.; Nakazawa, H.; Nakaya, H.; Sato, T. Opening of Mitochondrial K(ATP) Channels Attenuates the Ouabain-Induced Calcium Overload in Mitochondria. *Circ. Res.* **2001**, *89*, 856–858. [CrossRef]
31. Garlid, K.D.; Paucek, P.; Yarov-Yarovoy, V.; Murray, H.N.; Darbenzio, R.B.; D'Alonzo, A.J.; Lodge, N.J.; Smith, M.A.; Grover, G.J. Cardioprotective Effect of Diazoxide and Its Interaction with Mitochondrial ATP-Sensitive K+ Channels. Possible Mechanism of Cardioprotection. *Circ. Res.* **1997**, *81*, 1072–1082. [CrossRef] [PubMed]
32. Mizutani, S.; Prasad, S.M.; Sellitto, A.D.; Schuessler, R.B.; Damiano, R.J.; Lawton, J.S. Myocyte Volume and Function in Response to Osmotic Stress: Observations in the Presence of an Adenosine Triphosphate-Sensitive Potassium Channel Opener. *Circulation* **2005**, *112*, I219–I223. [CrossRef] [PubMed]
33. Dasselaar, J.J.; Slart, R.H.J.A.; Knip, M.; Pruim, J.; Tio, R.A.; McIntyre, C.W.; de Jong, P.E.; Franssen, C.F.M. Haemodialysis Is Associated with a Pronounced Fall in Myocardial Perfusion. *Nephrol. Dial. Transpl.* **2009**, *24*, 604–610. [CrossRef] [PubMed]
34. Burton, J.O.; Jefferies, H.J.; Selby, N.M.; McIntyre, C.W. Hemodialysis-Induced Repetitive Myocardial Injury Results in Global and Segmental Reduction in Systolic Cardiac Function. *Clin. J. Am. Soc. Nephrol.* **2009**, *4*, 1925–1931. [CrossRef]
35. Selby, N.M.; McIntyre, C.W. Peritoneal Dialysis Is Not Associated with Myocardial Stunning. *Perit. Dial. Int.* **2011**, *31*, 27–33. [CrossRef]
36. Canaud, B.; Kooman, J.P.; Selby, N.M.; Taal, M.W.; Francis, S.; Maierhofer, A.; Kopperschmidt, P.; Collins, A.; Kotanko, P. Dialysis-Induced Cardiovascular and Multiorgan Morbidity. *Kidney Int. Rep.* **2020**, *5*, 1856–1869. [CrossRef]
37. Nie, Y.; Zou, J.; Liang, Y.; Shen, B.; Liu, Z.; Cao, X.; Chen, X.; Ding, X. Electrocardiographic Abnormalities and QTc Interval in Patients Undergoing Hemodialysis. *PLoS ONE* **2016**, *11*, e0155445. [CrossRef]
38. Brunelli, S.M.; Du Mond, C.; Oestreicher, N.; Rakov, V.; Spiegel, D.M. Serum Potassium and Short-Term Clinical Outcomes Among Hemodialysis Patients: Impact of the Long Interdialytic Interval. *Am. J. Kidney Dis.* **2017**, *70*, 21–29. [CrossRef]
39. Yusuf, A.A.; Hu, Y.; Singh, B.; Menoyo, J.A.; Wetmore, J.B. Serum Potassium Levels and Mortality in Hemodialysis Patients: A Retrospective Cohort Study. *Am. J. Nephrol.* **2016**, *44*, 179–186. [CrossRef]
40. Sacher, F.; Jesel, L.; Borni-Duval, C.; De Precigout, V.; Lavainne, F.; Bourdenx, J.-P.; Haddj-Elmrabet, A.; Seigneuric, B.; Keller, A.; Ott, J.; et al. Cardiac Rhythm Disturbances in Hemodialysis Patients: Early Detection Using an Implantable Loop Recorder and Correlation With Biological and Dialysis Parameters. *JACC Clin. Electrophysiol.* **2018**, *4*, 397–408. [CrossRef]
41. Ohnishi, T.; Kimachi, M.; Fukuma, S.; Akizawa, T.; Fukuhara, S. Postdialysis Hypokalemia and All-Cause Mortality in Patients Undergoing Maintenance Hemodialysis. *Clin. J. Am. Soc. Nephrol.* **2019**, *14*, 873–881. [CrossRef] [PubMed]
42. Ferrey, A.; You, A.S.; Kovesdy, C.P.; Nakata, T.; Veliz, M.; Nguyen, D.V.; Kalantar-Zadeh, K.; Rhee, C.M. Dialysate Potassium and Mortality in a Prospective Hemodialysis Cohort. *Am. J. Nephrol.* **2018**, *47*, 415–423. [CrossRef] [PubMed]
43. Santoro, A.; Mancini, E.; London, G.; Mercadal, L.; Fessy, H.; Perrone, B.; Cagnoli, L.; Grandi, E.; Severi, S.; Cavalcanti, S. Patients with Complex Arrhythmias during and after Haemodialysis Suffer from Different Regimens of Potassium Removal. *Nephrol. Dial. Transpl.* **2008**, *23*, 1415–1421. [CrossRef] [PubMed]
44. Redaelli, B.; Locatelli, F.; Limido, D.; Andrulli, S.; Signorini, M.G.; Sforzini, S.; Bonoldi, L.; Vincenti, A.; Cerutti, S.; Orlandini, G. Effect of a New Model of Hemodialysis Potassium Removal on the Control of Ventricular Arrhythmias. *Kidney Int.* **1996**, *50*, 609–617. [CrossRef]
45. Sasaki, N.; Sato, T.; Ohler, A.; O'Rourke, B.; Marbán, E. Activation of Mitochondrial ATP-Dependent Potassium Channels by Nitric Oxide. *Circulation* **2000**, *101*, 439–445. [CrossRef]
46. Xu, W.; Liu, Y.; Wang, S.; McDonald, T.; Van Eyk, J.E.; Sidor, A.; O'Rourke, B. Cytoprotective Role of Ca2+- Activated K+ Channels in the Cardiac Inner Mitochondrial Membrane. *Science* **2002**, *298*, 1029–1033. [CrossRef]
47. Endoh, M. Cardiac Ca2+ Signaling and Ca2+ Sensitizers. *Circ. J.* **2008**, *72*, 1915–1925. [CrossRef]
48. Williams, G.S.B.; Smith, G.D.; Sobie, E.A.; Jafri, M.S. Models of Cardiac Excitation–Contraction Coupling in Ventricular Myocytes. *Math. Biosci.* **2010**, *226*, 1–15. [CrossRef]
49. Santulli, G.; Pagano, G.; Sardu, C.; Xie, W.; Reiken, S.; D'Ascia, S.L.; Cannone, M.; Marziliano, N.; Trimarco, B.; Guise, T.A.; et al. Calcium Release Channel RyR2 Regulates Insulin Release and Glucose Homeostasis. *J. Clin. Investig.* **2015**, *125*, 1968–1978. [CrossRef]
50. Sardu, C.; Santulli, G.; Guerra, G.; Trotta, M.C.; Santamaria, M.; Sacra, C.; Testa, N.; Ducceschi, V.; Gatta, G.; Amico, M.D.; et al. Modulation of SERCA in Patients with Persistent Atrial Fibrillation Treated by Epicardial Thoracoscopic Ablation: The CAMAF Study. *J. Clin. Med.* **2020**, *9*, 544. [CrossRef]
51. Langote, A.; Ahearn, M.; Zimmerman, D. Dialysate Calcium Concentration, Mineral Metabolism Disorders, and Cardiovascular Disease: Deciding the Hemodialysis Bath. *Am. J. Kidney Dis.* **2015**, *66*, 348–358. [CrossRef] [PubMed]
52. van der Sande, F.M.; ter Meulen, K.J.A.; Kotanko, P.; Kooman, J.P. Dialysate Calcium Levels: Do They Matter? *Blood Purif.* **2019**, *47*, 230–235. [CrossRef] [PubMed]
53. Jennings, R.B. Historical Perspective on the Pathology of Myocardial Ischemia/Reperfusion Injury. *Circ. Res.* **2013**, *113*, 428–438. [CrossRef] [PubMed]
54. Jia, P.; Ji, Q.; Zou, Z.; Zeng, Q.; Ren, T.; Chen, W.; Yan, Z.; Shen, D.; Li, Y.; Peng, F.; et al. Effect of Delayed Remote Ischemic Preconditioning on Acute Kidney Injury and Outcomes in Patients Undergoing Cardiac Surgery: A Randomized Clinical Trial. *Circulation* **2024**. [CrossRef]

Disclaimer/Publisher's Note: The statements, opinions and data contained in all publications are solely those of the individual author(s) and contributor(s) and not of MDPI and/or the editor(s). MDPI and/or the editor(s) disclaim responsibility for any injury to people or property resulting from any ideas, methods, instructions or products referred to in the content.

biomedicines

Article

miRNA in the Diagnosis and Treatment of Critical Limb Ischemia

Alexandra Ioana Popescu [1], Andreea Luciana Rață [2,*], Daliborca Vlad [1], Cristian Vlad [1], Roxana Popescu [3], Ramona Roxana Onofrei [4], Marialuisa Morelli [5], Stelian Pantea [2] and Sorin Barac [5]

[1] Pharmacology Department, "Victor Babes" University of Medicine and Pharmacy, 300041 Timisoara, Romania; alexandra.popescu@umft.ro (A.I.P.); vlad.daliborca@umft.ro (D.V.); vlad.cristian@umft.ro (C.V.)
[2] Surgical Emergencies Department, "Victor Babes" University of Medicine and Pharmacy, 300041 Timisoara, Romania; pantea.stelian@umft.ro
[3] Cell and Molecular Biology Department, "Victor Babes" University of Medicine and Pharmacy, 300041 Timisoara, Romania; popescu.roxana@umft.ro
[4] Department of Rehabilitation, Physical Medicine and Rheumatology, Research Center for Assessment of Human Motion, Functionality and Disability, "Victor Babes" University of Medicine and Pharmacy, 300041 Timisoara, Romania; onofrei.roxana@umft.ro
[5] Vascular Surgery Department, "Victor Babes" University of Medicine and Pharmacy, 300041 Timisoara, Romania; isamari1991@gmail.com (M.M.); sorinbarac@gmail.com (S.B.)
* Correspondence: rataandreealuciana@gmail.com; Tel.: +40-736396920

Abstract: Chronic threatening limb ischemia of the inferior limbs (CLTI) is the final stage of peripheral arterial disease (PAD) and is one of the most feared atherosclerotic manifestations because if left untreated, in time, it can lead to amputation. Although there are currently numerous treatment techniques, both open and endovascular, it is a pathology that has no underlying treatment. Therefore, current studies are very much focused on new therapeutic possibilities that can be applied in the early stages of the atherosclerotic process. In numerous studies in the literature, miRNAs have been identified as important markers of atherosclerosis. The present study aims to identify the expression of three miRNAs—*miR-199a, miR-20a, and miR-30c*—in patients with chronic limb-threatening ischemia in the pre- and post-revascularization periods. The aim of the study is to identify whether these three markers play a role in critical ischemia and whether they have the potential for future use in new treatments of this pathology.

Keywords: chronic threatening limb ischemia; microRNA; atherosclerosis

1. Introduction

Chronic lower limb-threatening ischemia (CLTI) is considered the most serious form of peripheral arterial disease (PAD) and is associated with a major risk of amputation, major cardiovascular events, and death [1]. Studies in the literature have reported a mortality rate of 20% in the first 6 months after diagnosis and 50% at 5 years. Clearly, this mortality rate is correlated with other atherosclerotic conditions, including coronary and cerebral pathology [2]. Following the 2019 European Society for Vascular Surgery guidelines for critical ischemia, a clear and concise definition was received, including a heterogeneous group of patients with varying degrees of ischemia that prevents lesion healing and who are at increased risk of amputation. Thus, the diagnosis of critical ischemia now requires the diagnosis of peripheral arterial disease in association with resting pain and tissue loss (ulceration or gangrene) [3].

There is currently a complex array of clinical and paraclinical methods for determining CLTI, but there is very little information about the biomarkers of CLTI [4].

miRNAs have been identified as markers of atherosclerotic disease. miRNAs are short, single-stranded RNA fragments of approximately 22 nucleotides that can modulate gene

expression post-transcriptionally [5]. A recent series of studies demonstrated their utility as biomarkers of CLTI and raised the question about their potential in the treatment of disease [6].

Several miRNAs are being explored as potential markers for predicting and evaluating peripheral arterial disease, but the current data are inconclusive, and more research is needed. There is also a lack of studies on the relationship between circulating miRNAs and clinical parameters in critical limb ischemia. More than 600 miRNAs have now been identified and are thought to regulate more than 50% of human protein-coding genes. miRNAs are, in fact, as functionally important as a transcription factor.

Endothelial cells are one of the most important factors in the health of the vascular tree. There are several miRNAs identified that play an important role in angiogenesis: miR21, the overexpression of which reduces endothelial cell proliferation, reduced actin organization in stress fibers (which may play a role in decreasing cell migration) [7] or miR-126 overexpression, which inhibits leukocyte adhesion to endothelial cells [8].

Other miRNAs have a role in smooth muscle cells: miR-1 overexpression inhibits proliferation, and miR-21 is a proproliferative and antiapoptotic regulator [9].

The aim of this study was to examine the expression of three miRNAs in CLTI patients, both before and after revascularization procedures. The goal is to enhance our understanding of the role of miRNAs in the clinical management of PAD.

2. Materials and Methods

This study was conducted in the Vascular Surgery Department of the "Pius Brînzeu" County Clinical Hospital, Timișoara, Romania. We enrolled 21 patients diagnosed with critical limb-threatening ischemia (CLTI). We collected data 24 h prior to and after the revascularization procedure, with either an open or endovascular one.

The inclusion criteria were as follows: patients above 18 years of age who agreed to participate in the study and confirmed with CLTI according to the current ESVS guidelines. (Ischemic rest pain is usually described as affecting the forefoot and usually aggravated by the decubitus position; for the diagnosis, the pain should be present for more than 2 weeks and associated with one or more abnormal parameters: ankle-brachial index < 0.4, ankle pressure < 50 mmHg in absolute value, hallux pressure under 30 mmHg for the absolute value, a transcutaneous oxygen pressure under 30 mmHg and a flat or weakly pulsating wave curve (equivalent to the third degree of ischemia in the WIfI—Wound, Ischemia, foot Infection classification).The exclusion criteria were patients under 18 years old or who did not give their consent for participation, patients with previous revascularization (no more than 3 months) on the index leg, patients on steroid medication, pregnancy, chronic kidney disease, active neoplasia, chronic liver disease Child–Pugh B minimum, thrombophilia, and other autoimmune diseases that could enhance the microRNA expression.

We also documented all patients' comorbidities, such as coronary disease, hypertension, diabetes mellitus, smoking habits, and medication used pre-admission.

All participants in the study read and signed an informed consent. The data were collected under GDPR (General Data Protection Regulation) laws. The study obtained an agreement from the Hospital Ethics Committee, under the EU GCP Directives, the International Conference of Harmonization of Technical Requirements for Registration of Pharmaceuticals for Human Use (ICH), and the Declaration of Helsinki.

miRNA Collection

Blood samples were meticulously collected in standard vacutainer tubes, each containing EDTA, which acted as an effective anti-coagulant to prevent clotting. We investigated three miRNAs: miR-199a, miR-20a, and miR-30c.

The procedure for miRNA isolation from the collected blood samples was carried out using the MagMax mirVana™ Total RNA Isolation kit, specifically provided by Applied Biosystems and Thermo Fisher Scientific, Baltics UAB (catalog number A27828) (Hillsboro, OR, USA). This kit is known for its efficiency in isolating high-quality total RNA.

Following the isolation process, the quantity of RNA was measured using the Qubit 4 fluorometer, which provides precise quantification. The measurement was performed with the aid of the Qubit™, RNA assay kit, also from Invitrogen by Thermo Fisher Scientific, (Hillsboro, OR, USA) (catalog number Q32880). This kit is well-regarded for its sensitivity and accuracy in RNA quantification. A specific concentration of RNA, measured at 8 ηg/μL, was then converted into complementary DNA (cDNA). This conversion was achieved through the use of the TaqMan™, MicroRNA Reverse Transcription kit, again sourced from Applied Biosystems by Thermo Fisher Scientific, Baltics (catalog number 4366597). This particular kit is designed for the efficient reverse transcription of miRNA into cDNA.

For the purpose of real-time polymerase chain reaction (RT-PCR) amplification, the TaqMan™ Universal Master Mix II, Baltics UAB with UNG was utilized, which was provided by the same manufacturer (catalog number 4440042). This master mix is known for its reliability in various PCR applications.

Additionally, the TaqMan™ miRNA Assay, including specific assays for has-miR-20a, has-miR-30c, and has-miR-199a, was employed to facilitate the amplification of the miRNA of interest. These assays are recognized for their specificity and sensitivity in detecting miRNA.

The cDNA template, prepared from the RNA, was then used in conjunction with the QuantStudio5 Real-Time PCR system, Singapore provided by Applied Biosystems (Waltham, MA, USA) by Thermo Fisher Scientific, to carry out the amplification process. This system is known for its high precision and reproducibility in quantitative PCR.

Each sample underwent testing in duplicate to ensure the accuracy and reliability of the results. This duplication helps in mitigating any potential variability and ensures the robustness of the data.

The relative expression levels of miRNA were determined by calculating the cycle threshold (Ct) values and the delta Ct (ΔCt) values. The ΔCt value is defined as the difference between the Ct value of the housekeeping gene U6 miRNA and the Ct value of the target miRNAs. A low delta Ct value indicates high miRNA expression, suggesting that a small number of fractional cycles were required to reach the amplification threshold for the target miRNAs. Conversely, a high delta Ct value signifies the low expression of target miRNAs, reflecting a greater number of cycles needed to reach the threshold.

For the analysis of the data and statistical validation of the results, GraphPad Prism version 10.2.2 was used, which is widely recognized for its comprehensive statistical analysis capabilities. Paired *t*-tests were performed between pre- and post-treatment differences based on lower limb viability. Differences were considered statistically significant at $p < 0.05$. We also used a ROC (receiver-operating character) curve to determine the predictive performance of miRNAs.

3. Results

Twenty-one patients aged 43–81 years old (mean age 62.50 ± 7.88) were included in the study from the Department of Vascular Surgery. There were five females (23.8%) and sixteen males (76.2%). Patients' demographics, comorbidities, risk factors, and other relevant data are presented in Table 1. One can observe that all the comorbidities are highly specific for patients with chronic limb-threatening ischemia, with the majority of patients having coronary disease, hypertension, and diabetes mellitus.

Table 1. Demographics.

Item	Values
Age	67.9 ± 7.88
Gender (males)	85.72%
Coronary disease	85.71%
Hypertension	95.23%
Smoking	95.23%

Table 1. *Cont.*

Item	Values
Cardiac insufficiency	80.95%
Diabetes mellitus	61.90%
Pre-op medication	
Clopidogrel	42.85%
Asprin	90.47%
Rivaroxaban 2.5 bid	28.57%
Novel anti-coagulants	14.28%
Different associations	37.65%

After the evaluation of the three microRNAs, descriptive statistics on the expression levels of microRNA miRNA30c, miRNA199a, and miRNA20a before and after surgery emerged.

miRNA30c and miRNA20a demonstrate significant changes in expression post-surgery, with miRNA30c showing a reduction and miRNA20a exhibiting a notable shift closer to zero, both indicating their potential as diagnostic markers. miRNA199a, while showing an increase in expression post-surgery, did not achieve the same level of statistical significance (Table 2).

Table 2. miRNAs value before and after surgery.

Descriptive Statistics	ΔCt		
	miR30c	**miR199a**	**miR20a**
Before surgery			
Mean	−5.243	6.152	−7.221
Std. Deviation	1.978	1.076	1.38
Std. Error of Mean	0.4315	0.2348	0.3012
Median	−5.48	6.06	−7.19
After surgery			
Mean	−4.149	6.924	−5.848
Std. Deviation	2.462	1.937	2.038
Std. Error of Mean	0.5372	0.4228	0.4448
Median	−4.75	6.88	−5.72
p-two tailed (Wilcoxon matched-pairs signed rank test)	0.0319	0.0751	0.0078

The ΔCt value is a measure of the expression level of a gene, with lower ΔCt values indicating higher expression. These graphs are useful for visualizing the changes in gene expression levels across different conditions or time points.

Figure 1 shows the miRNA199a expression before and after the revascularization procedure. The mean ΔCt value before surgery is approximately 6.152 with a standard deviation of 1.076, while after surgery, the mean ΔCt value increases to 6.924 with a standard deviation of 1.937. This suggests a slight increase in miR-199a expression after surgery, though the change is not statistically significant—$p = 0.0751$.

For miRNA20a, the mean ΔCt value before surgery is −7.221 with a standard deviation of 1.38. After surgery, the mean ΔCt value increases to −5.848 with a standard deviation of 2.038. The change in miR-20a expression is statistically significant, with a *p*-value of 0.0078, indicating a significant increase in expression post-surgery.

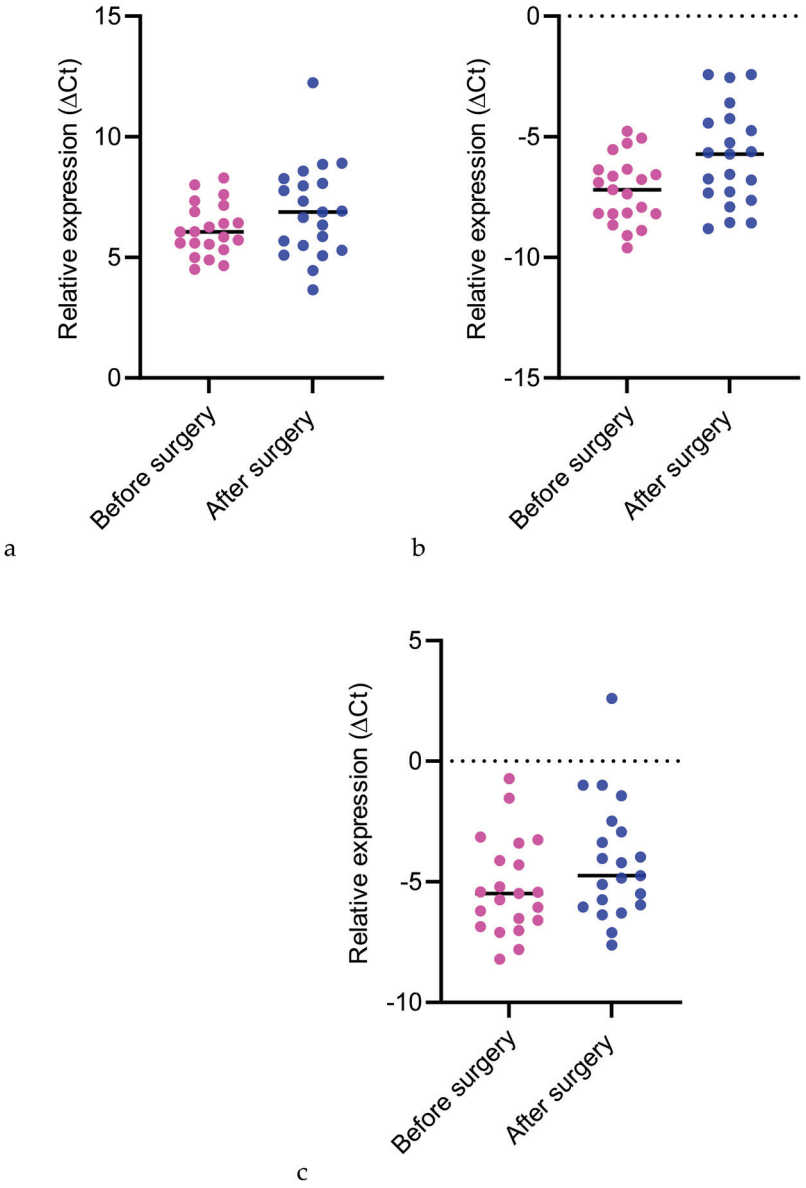
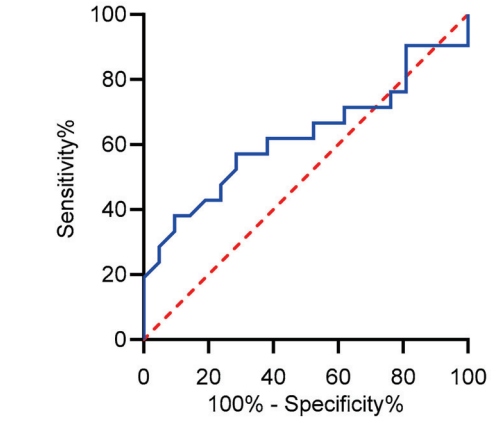


Figure 1. miRNA199a (**a**), miRNA20a (**b**) and miRNA30c (**c**) relative expression graph.

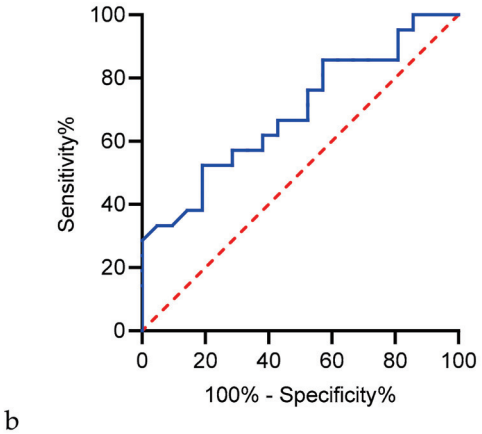
For miRNA30c, the mean ΔCt value before surgery is −5.243 with a standard deviation of 1.978, and after surgery, the mean ΔCt value increases to −4.149 with a standard deviation of 2.462. This change is statistically significant (p = 0.0319), indicating an increase in miR-30c expression after surgery.

Summarizing this, miRNA30c and miRNA20a demonstrate significant changes in expression post-surgery, with miRNA30c showing a reduction and miRNA20a exhibiting a notable shift closer to zero, both indicating their potential as diagnostic markers. miRNA199a, while showing an increase in expression post-surgery, did not achieve the same level of statistical significance. The ROC curves further highlight miRNA30c as the superior diagnostic tool among the three, followed by miRNA20a and miRNA199a. These findings underscore the importance of miRNA expression changes in the context of surgical interventions and their potential utility in diagnostic applications.

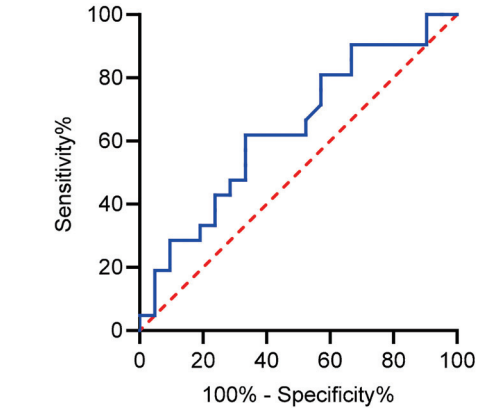
The ROC curve (Figure 2) for the different miRNAs in this study demonstrates the diagnostic performance of this biomarker with specific numerical data and reveals significant insights into the diagnostic efficacy of this particular biomarker.



a



b



c

Figure 2. miRNA199a (**a**), miRNA20a (**b**), and miRNA30c (**c**) ROC curves.

The ROC curve for miRNA199a shows that it performs only slightly better than random guessing, indicating limited diagnostic potential. Its performance, closely resembling that of a random classifier, indicates that miRNA199a is not a robust biomarker for the conditions under investigation; thus, it is crucial to identify biomarkers with a higher AUC and a more significant ability to differentiate between positive and negative cases, ensuring more reliable and effective diagnostic outcomes.

The area under the curve (AUC) appears to be significantly greater than 0.5, suggesting that miRNA 20a has good discriminatory power for the classification task at hand. The curve's overall proximity to the top-left corner, particularly in its initial steep ascent,

indicates robust performance, demonstrating that the classifier achieves high sensitivity with relatively low false-positive rates.

The area under the curve (AUC) appears to be greater than 0.5, indicating that miRNA 30c has some distinguishing power. However, it does not appear to be as strong as it could be (the curve lies near the diagonal baseline), which implies moderate to marginal improvement over random guessing. The curve does not exhibit a rapid ascent toward the top-left corner, which could indicate higher sensitivity at lower false-positive rates.

4. Discussion

The atherosclerotic process is a pathology that develops over many years of life and may be asymptomatic for a long time, but when progression occurs, it becomes one of the major factors in cardiovascular mortality. Atherosclerosis manifests itself in several forms, causing stroke, acute myocardial infarction, and peripheral arterial disease with all its manifestations, both in the limbs and in other peripheral vascular territories. Most often, in the case of the lower limbs, chronic limb-threatening ischemia is caused by the instability of the atheromatous plaque, favoring its rupture, thrombosis formation at its level, and critical ischemia.

Modern research has recently been very much oriented towards developing strategies to identify vulnerable atherosclerotic plaques.

The miR-199 family consists of three members—miR-199a1, miR-199a2, and miR-199b—and functional studies in recent years have shown that they play an important role in maintaining normal homeostasis and regulating disease pathogenesis [10].

MiRNA199a, which has multiple roles in vascular biology, plays a significant role in the context of PAD pathophysiology due to potential therapeutic implications. The effects that can impact the regulation of PAD progression and treatment are as follows: the migration and proliferation of VSMC (vascular smooth muscle cells), which play a crucial role in the formation of atherosclerosis, are regulated by miRNA199a via a control. Thus, when slowing the development of new plaque and stabilizing present plaques, the course of PAD is slowed down. Atherosclerosis, one of the main causes of PAD, is diminished by VSMC [11]. Additionally, miRNA199a aids in the preservation of activity in endothelial cells, which are essential for vascular health. PAD can worsen due to the increased vascular inflammation and plaque formation caused by dysfunctional endothelial cells. miRNA199a promotes healthy endothelium function, and in that way, the risk of vascular problems related to PAD decreases [11]. By regulating the expression of pro-inflammatory cytokines and molecules, miRNA199a has anti-inflammatory effects. One of the main causes of PAD and atherosclerosis is inflammation. Thus, miRNA199a's anti-inflammatory qualities may contribute to reducing the inflammatory load in arteries, leading to better results for PAD patients [12].

The mean ΔCt value for miRNA199a post-surgery increased to 6.924, suggesting an increase in the expression levels of miRNA199a after surgery. The standard deviation increased to 1.937, indicating more variability in post-surgery miRNA199a expression levels. The standard error of the mean rose to 0.4228, reflecting greater variability in the sample's representation of the population mean. The median value after surgery was 6.88, indicating a central tendency towards higher ΔCt values. However, the *p*-value for miRNA199a was 0.0751, which is above the 0.05 threshold, indicating that the changes in miRNA199a expression are not statistically significant. Liu et al. demonstrated the down-regulation of miRNA-199a-5p in smooth muscle cells within the arterial wall in patients with restenosis after vascular procedures. Also, in vivo, the delivery of this microRNA via a lentivirus led to neointimal proliferation after angioplasty procedures, making this miRNA a therapeutic target in these patients [13].

A study led by Qiao et al. demonstrated that miR-199a is a pro-atherogenic miRNA, and its overexpression is positively correlated with the atherosclerotic process, and in particular with endothelial cell damage. In fact, miR-199a induces phenotypic abnormalities in endothelial cells, such as proliferation, migration, and tube formation, by mediating pro-inflammatory axes [14].

MiR-17, miR-18, miR-19a, miR-19b, miR-20a, and miR-92a are the members of the miR-17–92 family [15,16]. The miR-17–92 cluster, which—as mentioned above—includes miRNA20a, is well-known for its role in carcinogenic processes [17]. This cluster is generally considered to be a well-researched miRNA cluster. miRNA20a binds on its target genes more specifically compared to the untranslated regions of the 3′ site (3′ UTR) of the target mRNAs, which are degraded or undergo translational suppression [18].

After surgery, the mean ΔCt value for miRNA20a decreased to −5.848, indicating a reduction in the expression levels of miRNA20a post-surgery. The standard deviation increased to 2.038, suggesting greater variability in miRNA20a expression levels among patients after surgery. The standard error of the mean rose to 0.4448, reflecting a broader range in the sample's representation of the population mean. The median value post-surgery was −5.72, which, although higher than the pre-surgery median, still indicates a negative ΔCt value, reflecting the continued but reduced expression of miRNA20a. The *p*-value associated with the change in inmiRNA20a expression was 0.0078, which is less than the threshold of 0.05, indicating that the observed changes in miRNA20a expression before and after surgery are statistically significant.

Within the miR-17/92 cluster, miR-92a and miR-17 have been particularly studied in cardiovascular pathology, with the overexpression of miR-92a in ischemic cells leading to the inhibition of angiogenesis. Another study on ischemic coronary artery disease demonstrated increased levels of both miR-92a and miR-17 in endothelial cells compared to healthy subjects. Although the expression of miR-20a has not been studied much in the literature, our study places it in a new light, given the statistical significance it demonstrated. Moreover, it can be evaluated as a marker of restenosis post-revascularization procedures, making it an important marker in chronic limb-threatening ischemia [19].

The miR-30 is a miRNA family that consists of six miRNA molecules, which are mature: miR-30a, miR-30b, miR-30c-1, miR-30c-2, miR-30d, and miR-30e. They form a crucial subset of miRNAs with important roles in cardiovascular biology. Encoded by six genes, they are spread over three different regions of chromosomes: 1p34.2 (site of miR-30c and miR-30e), 8q24.22 (site of miR-30b and miR-30d), and finally 6q13 (site of miR-30a). Although they have the same 5′ sequence, they differ at the end of the 3′ sequence, allowing them to carry out a variety of biological tasks [20]. Their involvement in PAD and their importance in preserving vascular health by their regulation of vascular smooth muscle cell behavior and endothelial function tackles the primary underlying cause of PAD, atherosclerosis. They also assist in lowering inflammation and oxidative stress in the vascular system in order to preserve the integrity and function of the arteries [21].

Apart from that, miRNA30c significantly impacts lipid metabolism. One of its main targets,, an essential enzyme involved in the assembly of lipoproteins and secretions, is the "microsomal triglyceride transfer protein" (MTTP). By inhibiting MTTP, which lowers plasma lipid levels, miRNA30c effectively lowers the secretion of triglycerides and very low-density lipoprotein (VLDL). Thus, miRNA30c protects against lipid abnormalities, which are fundamental to atherosclerosis and other CVDs [22,23].

After surgery, the mean ΔCt value for miRNA30c increased to −4.149, indicating a reduction in the expression levels of miR30c post-surgery. The standard deviation also increased to 2.462, suggesting greater variability in miRNA30c expression levels among patients after surgery. The standard error of the mean rose to 0.5372, reflecting a broader range in the sample's representation of the population mean. The median value post-surgery was −4.75, which, although higher than the pre-surgery median, still indicates a negative ΔCt value, reflecting the continued but reduced expression of miRNA30c. The *p*-value associated with a change in miRNA30c expression was 0.0319, which is less than the threshold of 0.05, indicating that the observed changes in miRNA30c expression before and after surgery are statistically significant. A study conducted by Zhang demonstrated that the expression of miR-30C in atherosclerotic vessels is much lower than in normal arteries, and this miRNA inhibits the differentiation of vascular smooth muscle cells from adventitial progenitor cells [24].

An important aspect to be mentioned and studied is the association of these miRNAs with cardiovascular risk factors leading to the development of peripheral arterial disease and its progression to critical ischemia.

There are numerous studies associating miRNA-199a expression with blood pressure. A study conducted by Lynch et al. demonstrated a statistically significant correlation in all 75 patients investigated [25]. Our study sought to determine whether these three miRNA markers play a role in critical lower limb ischemia. One of the limitations of this study is the small number of subjects included. However, we believe that this is an important starting point for assessing the expression of these markers in this pathology and is the basis for larger studies that will highlight miRNA expression in peripheral arterial disease and chronic limb-threatening ischemia in particular.

An important point to take into consideration is the fact that the expression changed after the revascularization procedure. Other studies showed that any changes in the blood flow (only through walking) induced changes in miRNA expression [26].

Ever since their identification, miRNAs have been regarded as having a key role in regulating vascular expression, both under normal and pathological conditions [27].

Their role in atherosclerosis, the leading cause of critical ischemia, comprises the fact that miRNAs are thought to participate either positively or negatively in almost all molecular processes involved in atherosclerosis and arterial remodeling, including endothelial dysfunction, monocyte activation, smooth muscle cell activation, and platelet activation [28,29].

Another important phenomenon to mention is the role of miRNAs in restenosis after revascularization procedures. It is important to note from our study that the miRNAs studied varied pre- and post-revascularization procedures. In fact, any revascularization procedure produces a mechanical vascular injury; first, there is an impairment of the vascular non-endothelium with the destruction of endothelial cells, a reendothelialization process, and the generation of new endothelium. This phenomenon is followed by an inflammatory response, with platelet activation, leukocyte attraction to the injury site, and the release of inflammatory factors and cytokines. This is followed very rapidly by the proliferation of smooth muscle cells and then tissue remodeling in which the smooth muscle cells enter into a hyperactive phase in which they are involved in depositing an extracellular matrix in the intima of the vessels [30].

Thus, basically, the protection of the vascular wall from treatment-induced injury actually leads to neointimal proliferation, vascular remodeling, and restenosis in the vessel.

In view of the above, studies at the level of miRNAs have demonstrated that they are responsible for a whole host of activities at the cellular level, noting here the proliferation of smooth muscle cells, the migration of leukocytes and platelets, and neointima formation.

If we take into account the two aspects mentioned in that miRNA expression changes only after walking exercises in patients with intermittent claudication, or after revascularization procedures, either open or interventional, we can strongly affirm that these markers are extremely important in peripheral arterial disease. Even if most of the current studies in this direction are small, with no control groups or validation cohorts, they still remain a solid basis for further investigations. Of course, uniform conditions, quantifiable and measurable outcomes, multicenter randomized trials, as well as large prospective studies are still needed.

5. Conclusions

The present study demonstrates the importance of microRNAs in chronic limb-threatening ischemia and their potential as biomarkers. Dynamics in their expression in different pre- and post-revascularization situations support the hypothesis that they may also have an important role in the treatment of this pathology when targeting their regulation.

The study of miRNA is a new concern in chronic limb-threatening ischemia. Therefore, different markers are still being identified, and it is necessary to further demonstrate in

larger population-based studies which are the most relevant for diagnosis and which may have potential in treatment.

Author Contributions: Conceptualization, A.I.P. and A.L.R.; methodology, S.B., R.P. and D.V.; software, C.V.; validation, A.L.R., R.R.O., R.P. and D.V.; formal analysis, A.I.P.; investigation, M.M. resources, S.P.; data curation, R.R.O.; writing—original draft preparation, A.I.P. and A.L.R.; writing—review and editing, A.I.P. and A.L.R.; visualization, S.B.; supervision, D.V.; project administration, A.I.P.; funding acquisition, C.V. and S.P. All authors have read and agreed to the published version of the manuscript.

Funding: We would like to acknowledge "Victor Babes", University of Medicine and Pharmacy, Timisoara, for their support in covering the costs of publication for this research paper.

Institutional Review Board Statement: The study was conducted in accordance with the Declaration of Helsinki and approved by the Local Ethics Committee of "Pius Brînzeu" Clinical County Hospital Timișoara, Romania no. 427/13.12.2023.

Informed Consent Statement: Informed consent was obtained from all subjects involved in the study.

Data Availability Statement: The raw data supporting the conclusions of this article will be available upon request.

Conflicts of Interest: The authors declare no conflicts of interest.

References

1. Adam, D.J.; Beard, J.D.; Cleveland, T.; Bell, J.; Bradbury, A.W.; Forbes, J.F.; Fowkes, F.G.; Gillepsie, I.; Ruckley, C.V.; Raab, G.; et al. Bypass versus angioplasty in severe ischaemia of the leg (BASIL): Multicentre, randomised controlled trial. *Lancet* **2005**, *366*, 1925–1934. [CrossRef]
2. Stoyioglou, A.; Jaff, M.R. Medical Treatment of Peripheral Arterial Disease: A Comprehensive Review. *J. Vasc. Interv. Radiol.* **2004**, *15*, 1197–1207. [CrossRef] [PubMed]
3. Conte, M.S.; Bradbury, A.W.; Kolh, P.; White, J.V.; Dick, F.; Fitridge, R.; Mills, J.L.; Ricco, J.-B.; Suresh, K.R.; Murad, M.H.; et al. Global Vascular Guidelines on the Management of Chronic Limb-Threatening Ischemia. *Eur. J. Vasc. Endovasc. Surg.* **2019**, *58*, S1–S109.e33. [CrossRef]
4. Zampetaki, A.; Mayr, M. MicroRNAs in Vascular and Metabolic Disease. *Circ. Res.* **2012**, *110*, 508–522. [CrossRef] [PubMed]
5. Syed, M.H.; Zamzam, A.; Valencia, J.; Khan, H.; Jain, S.; Singh, K.K.; Abdin, R.; Qadura, M. MicroRNA Profile of Patients with Chronic Limb-Threatening Ischemia. *Diagnostics* **2020**, *10*, 230. [CrossRef]
6. Stather, P.W.; Sylvius, N.; Wild, J.B.; Choke, E.; Sayers, R.D.; Bown, M.J. Differential MicroRNA Expression Profiles in Peripheral Arterial Disease. *Circ. Cardiovasc. Genet.* **2013**, *6*, 490–497. [CrossRef]
7. Parikh, V.N.; Jin, R.C.; Rabello, S.; Gulbahce, N.; White, K.; Hale, A.; Cottrill, K.A.; Shaik, R.S.; Waxman, A.B.; Zhang, Y.Y.; et al. MicroRNA-21 Integrates Pathogenic Signaling to Control Pulmonary Hypertension: Results of a Network Bioinformatics Approach. *Circulation* **2012**, *125*, 1520–1532. [CrossRef] [PubMed]
8. Fish, J.E.; Santoro, M.M.; Morton, S.U.; Yu, S.; Yeh, R.-F.; Wythe, J.D.; Ivey, K.N.; Bruneau, B.G.; Stainier, D.Y.R.; Srivastava, D. miR-126 Regulates Angiogenic Signaling and Vascular Integrity. *Dev. Cell* **2008**, *15*, 272–284. [CrossRef]
9. Chen, J.; Yin, H.; Jiang, Y.; Radhakrishnan, S.K.; Huang, Z.-P.; Li, J.; Shi, Z.; Kilsdonk, E.P.; Gui, Y.; Wang, D.-Z.; et al. Induction of MicroRNA-1 by Myocardin in Smooth Muscle Cells Inhibits Cell Proliferation. *Arter. Thromb. Vasc. Biol.* **2011**, *31*, 368–375. [CrossRef]
10. Wang, Q.; Ye, B.; Wang, P.; Yao, F.; Zhang, C.; Yu, G. Overview of microRNA-199a Regulation in Cancer. *Cancer Manag. Res.* **2019**, *11*, 10327–10335. [CrossRef]
11. Sun, X.; Zhang, Y.; Liu, Z.; Li, S.; Wang, L. MicroRNA-199a-3p Exhibits Beneficial Effects in Asymptomatic Atherosclerosis by Inhibiting Vascular Smooth Muscle Cell Proliferation and Migration. *Mol. Biotechnol.* **2021**, *63*, 595–604. [CrossRef] [PubMed]
12. Rane, S.; He, M.; Sayed, D.; Vashistha, H.; Malhotra, A.; Sadoshima, J.; Vatner, D.E.; Vatner, S.F.; Abdellatif, M. Downregulation of MiR-199a Derepresses Hypoxia-Inducible Factor-1α and Sirtuin 1 and Recapitulates Hypoxia Preconditioning in Cardiac Myocytes. *Circ. Res.* **2009**, *104*, 879–886. [CrossRef]
13. Liu, D.; Jing, Y.; Peng, G.; Wei, L.; Zheng, L.; Chang, G.; Wang, M. MiR-199a-5p Deficiency Promotes Artery Restenosis in Peripheral Artery Disease by Regulating ASMCs Function via Targeting HIF-1α and E2F3. *Curr. Vasc. Pharmacol.* **2024**, *22*, 342–354. [CrossRef] [PubMed]
14. Qiao, S.; Wang, X.; Li, H.; Zhang, C.; Wang, A.; Zhang, S. Atherosclerosis-associated endothelial dysfunction is promoted by miR-199a-5p/SIRT1 axis regulated by circHIF1α. *Nutr. Metab. Cardiovasc. Dis.* **2023**, *33*, 1619–1631. [CrossRef] [PubMed]
15. Xiao, Z.; Chen, S.; Feng, S.; Li, Y.; Zou, J.; Ling, H.; Zeng, Y.; Zeng, X. Function and mechanisms of microRNA 20a in colorectal cancer. *Exp. Ther. Med.* **2020**, *19*, 1605–1616. [CrossRef] [PubMed]
16. Mendell, J.T. miRiad Roles for the miR-17-92 Cluster in Development and Disease. *Cell* **2008**, *133*, 217–222. [CrossRef]

17. Guo, L.; Zhao, J.; Qu, Y.; Yin, R.; Gao, Q.; Ding, S.; Zhang, Y.; Wei, J.; Xu, G. microRNA-20a Inhibits Autophagic Process by Targeting ATG7 and ATG16L1 and Favors Mycobacterial Survival in Macrophage Cells. *Front. Cell. Infect. Microbiol.* **2016**, *6*, 134. [CrossRef]
18. Elfaki, I.; Mir, R.; Mir, M.M.; AbuDuhier, F.M.; Babakr, A.T.; Barnawi, J. Potential Impact of MicroRNA Gene Polymorphisms in the Pathogenesis of Diabetes and Atherosclerotic Cardiovascular Disease. *J. Pers. Med.* **2019**, *9*, 51. [CrossRef]
19. Bonauer, A.; Carmona, G.; Iwasaki, M.; Mione, M.; Koyanagi, M.; Fischer, A.; Burchfield, J.; Fox, H.; Doebele, C.; Ohtani, K.; et al. MicroRNA-92a Controls Angiogenesis and Functional Recovery of Ischemic Tissues in Mice. *Science* **2009**, *324*, 1710–1713. [CrossRef]
20. Mir, R.; Elfaki, I.; Khullar, N.; Waza, A.A.; Jha, C.; Mir, M.M.; Nisa, S.; Mohammad, B.; Mir, T.A.; Maqbool, M.; et al. Role of Selected miRNAs as Diagnostic and Prognostic Biomarkers in Cardiovascular Diseases, Including Coronary Artery Disease, Myocardial Infarction and Atherosclerosis. *J. Cardiovasc. Dev. Dis.* **2021**, *8*, 22. [CrossRef]
21. Jadli, A.S.; Parasor, A.; Gomes, K.P.; Shandilya, R.; Patel, V.B. Exosomes in Cardiovascular Diseases: Pathological Potential of Nano-Messenger. *Front. Cardiovasc. Med.* **2021**, *8*, 767488. [CrossRef] [PubMed]
22. Feinberg, M.W.; Moore, K.J. MicroRNA Regulation of Atherosclerosis. *Circ. Res.* **2016**, *118*, 703–720. [CrossRef] [PubMed]
23. Romaine, S.P.R.; Tomaszewski, M.; Condorelli, G.; Samani, N.J. MicroRNAs in cardiovascular disease: An introduction for clinicians. *Heart* **2015**, *101*, 921–928. [CrossRef] [PubMed]
24. Zhang, Q.; Chen, T.; Zhang, Y.; Lyu, L.; Zhang, B.; Huang, C.; Zhou, X.; Wu, Y.; Li, Z. MiR-30c-5p regulates adventitial progenitor cells differentiation to vascular smooth muscle cells through targeting OPG. *Stem Cell Res. Ther.* **2021**, *12*, 67. [CrossRef] [PubMed]
25. Lynch, S.M.; Ward, M.; McNulty, H.; Angel, C.Z.; Horigan, G.; Strain, J.; Purvis, J.; Tackett, M.; McKenna, D.J. Serum levels of miR-199a-5p correlates with blood pressure in premature cardiovascular disease patients homozygous for the *MTHFR* 677C > T polymorphism. *Genomics* **2020**, *112*, 669–676. [CrossRef]
26. Sieland, J.; Niederer, D.; Engeroff, T.; Vogt, L.; Troidl, C.; Schmitz-Rixen, T.; Banzer, W.; Troidl, K. Changes in miRNA expression in patients with peripheral arterial vascular disease during moderate- and vigorous-intensity physical activity. *Eur. J. Appl. Physiol.* **2023**, *123*, 645–654. [CrossRef]
27. Archer, K.; Broskova, Z.; Bayoumi, A.S.; Teoh, J.-P.; Davila, A.; Tang, Y.; Su, H.; Kim, I.-M. Long Non-Coding RNAs as Master Regulators in Cardiovascular Diseases. *Int. J. Mol. Sci.* **2015**, *16*, 23651–23667. [CrossRef]
28. Siasos, G.; Bletsa, E.; Stampouloglou, P.K.; Oikonomou, E.; Tsigkou, V.; Paschou, S.A.; Vlasis, K.; Marinos, G.; Vavuranakis, M.; Stefanadis, C.; et al. MicroRNAs in cardiovascular disease. *Hell. J. Cardiol.* **2020**, *61*, 165–173. [CrossRef]
29. Ramzan, F.; D'souza, R.F.; Durainayagam, B.R.; Milan, A.M.; Markworth, J.F.; Miranda-Soberanis, V.; Sequeira, I.R.; Roy, N.C.; Poppitt, S.D.; Mitchell, C.J.; et al. Circulatory miRNA biomarkers of metabolic syndrome. *Acta Diabetol.* **2019**, *57*, 203–214. [CrossRef]
30. Varela, N.; Lanas, F.; Salazar, L.A.; Zambrano, T. The Current State of MicroRNAs as Restenosis Biomarkers. *Front. Genet.* **2020**, *10*, 1247. [CrossRef]

Disclaimer/Publisher's Note: The statements, opinions and data contained in all publications are solely those of the individual author(s) and contributor(s) and not of MDPI and/or the editor(s). MDPI and/or the editor(s) disclaim responsibility for any injury to people or property resulting from any ideas, methods, instructions or products referred to in the content.

biomedicines

MDPI

Review

The Role of Lipoprotein(a) in Peripheral Artery Disease

Nicholas Pavlatos [1] and Dinesh K. Kalra [2,*]

[1] Department of Internal Medicine, University of Louisville School of Medicine, Louisville, KY 40202, USA; nicholas.pavlatos@louisville.edu
[2] Division of Cardiology, University of Louisville School of Medicine, Louisville, KY 40202, USA
* Correspondence: dinesh.kalra@louisville.edu

Abstract: Lipoprotein(a) is a low-density-lipoprotein-like particle that consists of apolipoprotein(a) bound to apolipoprotein(b). It has emerged as an established causal risk factor for atherosclerotic cardiovascular disease, stroke, and aortic valve stenosis through multifactorial pathogenic mechanisms that include inflammation, atherogenesis, and thrombosis. Despite an estimated 20% of the global population having elevated lipoprotein(a) levels, testing remains underutilized due to poor awareness and a historical lack of effective and safe therapies. Although lipoprotein(a) has a strong association with coronary artery disease and cerebrovascular disease, its relationship with peripheral artery disease is less well established. In this article, we review the epidemiology, biology, and pathogenesis of lipoprotein(a) as it relates to peripheral artery disease. We also discuss emerging treatment options to help mitigate major adverse cardiac and limb events in this population.

Keywords: peripheral artery disease; lipoprotein(a); atherosclerosis; lipids

1. Introduction

Lipoprotein(a) [Lp(a)] is a lipoprotein structurally similar to low-density lipoprotein and is characterized by apolipoprotein(a) [apo(a)] covalently bound to apolipoproteinB-100 (apoB-100). It was first described by Norwegian geneticist Kare Berg and his colleagues in 1963 [1]. He was able to recognize that Lp(a) levels were genetically determined and, by 1974, had suggested that Lp(a) contributes to coronary artery disease (CAD) [2]. Fifty years later, it has been established that Lp(a) is an independent causal risk factor for CAD, cerebrovascular disease (CeVD), and aortic stenosis [3]. The National Lipid Association pooled data from large prospective, population-based studies and found that when compared to patients with Lp(a) < 5 mg/dL, those with Lp(a) Lp(a) $\geq$ 120 mg/dL were at a 5-fold risk of coronary artery stenosis, 3- to 4-fold risk of myocardial infarction, 1.7-fold risk of carotid stenosis, 1.6-fold risk of ischemic stroke, 3-fold risk of aortic stenosis, and 1.6-fold risk of femoral artery stenosis, suggesting CAD likely has a greater association with Lp(a) than PAD and CeVD [4]. Lp(a) levels are 90% genetically determined and not appreciably affected by diet or exercise; therefore, serum levels typically remain stable in individuals over their lifetime [5,6]. Although the consequences of elevated Lp(a) levels are well described, testing remains sparse. Additionally, treatment options are limited as traditional therapies for dyslipidemias appear to be ineffective in the management of elevated Lp(a) levels [7].

Peripheral artery disease (PAD) is a progressive atherosclerotic disorder characterized by narrowing of the arteries other than those that supply the heart or brain, typically affecting the lower extremities [8]. It is estimated that over 200 million people suffer from PAD worldwide, with the majority of patients being asymptomatic [9]. Common symptoms include exertional leg pain, discomfort, and cramping known as claudication but also include more atypical symptoms such as pain at rest. Complications of PAD can be devastating and include infection, critical limb ischemia (CLI), acute limb ischemia (ALI), amputation, and death [10]. Studies have shown that PAD significantly increases mortality

with a 10-year all-cause mortality of 27% for the reference range, 56% for asymptomatic PAD, 63% for intermittent claudication, and 75% for limb ischemia [11]. Additionally, PAD imposes a substantial burden on healthcare spending with an average annual expenditure per PAD patient of USD 11,533 compared to USD 4219 in patients without PAD [12]. Despite data implicating elevated serum Lp(a) levels and the development of PAD, this association remains underrecognized [13]. Major guidelines are lacking in both the diagnosis and management of elevated Lp(a) levels in the setting of PAD.

2. Epidemiology

According to the National Heart Lung and Blood Institute report published in 2018, an estimated 1.43 billion people have Lp(a) levels $\geq$ 50 mg/dL. Although data are lacking in regard to the prevalence of elevated Lp(a) levels in PAD, the Copenhagen General Population study was able to show that elevated Lp(a) levels results in a stepwise increase in PAD. They found that in smokers aged 70–79 years with Lp(a) < 50th and $\geq$99th percentile, the 10-year risk for PAD among females was 8% and 21%, while among males, it was 11% and 29% [14]. The prevalence of elevated Lp(a) varies between continents due to LPA gene remodeling and different migration patterns of people with different sized isoforms of Lp(a) [15]. Studies have shown that South Asians and Blacks of sub-Saharan African descent have higher levels of Lp(a) when compared to Hispanics, East Asians, and Whites [16–18]. The Multi-Ethnic Study of Atherosclerosis (MESA) cohort investigated four ethnic groups and reported median Lp(a) levels among Blacks were 35.1 mg/dL, Whites 12.9 mg/dL, Hispanics 13.1 mg/dL, and Chinese 12.9 mg/dL [19]. Although they did not study South Asians, the Mediators of Atherosclerosis in South Asians Living in America (MASALA) cohort reported a median Lp(a) level of 17.0 mg/dL [20]. Neither study reported the prevalence of PAD in their study populations. Despite Lp(a) being a known independent risk factor for cardiovascular disease and aortic stenosis, testing persists at low rates even in those diagnosed with such conditions. An observational study that reviewed over 5 million patients from 2012 to 2021 at the University of California Health System Warehouse found that only 0.3% of those patients had Lp(a) testing. Additionally, the rate of Lp(a) testing in those with a known diagnosis of PAD was 2.0%. Patients with a history of ischemic heart disease, aortic stenosis, and stroke fared no better as they were tested at similar rates of 2.9%, 3.1%, and 1.8%, respectively [21]. Another observational study analyzing data from 2015 to 2019 of healthcare systems participating in the National Patient-Centered Clinical Research Network found that only 0.06% of patients per year were tested for Lp(a). They also found that out of those diagnosed with atherosclerotic cardiovascular disease, testing was less common in those with PAD compared to ischemic stroke or myocardial infarction (MI) [22]. Poor utilization of Lp(a) testing in the clinical setting is likely a result of low provider awareness, lack of recommendations in major guidelines, limited evidence of benefit in lowering Lp(a), and no currently available approved drugs for this indication.

3. Structure/Genetics

Lp(a) is a low-density-lipoprotein-like molecule made up of two protein-containing moieties, apo(a) and apoB-100, covalently bound by a disulfide bridge (Figure 1) [23]. ApoB-100 is synthesized in the liver and is a key structural component of atherogenic lipoproteins such as low-density lipoprotein, very-low-density lipoprotein, and intermediate-density lipoprotein [24]. The apo(a) chain is structurally similar to plasminogen and is believed to promote inflammation, endothelial dysfunction, and calcification by attracting oxidized phospholipids [25]. Notable components of apo(a) are kringle domains which are triple-looped structures stabilized by three disulfide linkages. These are also present in other coagulation factors, most notably, plasminogen, prothrombin, and urokinase [23,26]. Each apo(a) contains one copy of kringle IV type 1, kringle IV types 3–10, and kringle V domains, and multiple copies of kringle IV type 2 domains, ranging from 1 to over 40 copies. This heterogeneity in the number of kringle IV type 2 repeats makes apo(a) highly polymorphic in size. This is significant as larger apo(a) isoforms are less efficiently secreted by hepato-

cytes, resulting in an inverse relationship between apo(a) isoform size and Lp(a) levels [27]. Plasma Lp(a) levels are highly variable within the same population, ranging from less than 0.1 mg/dL to over 300 mg/dL with up to 80% of variability being attributed to the apo(a) size polymorphisms [28]. The major gene locus for determining apo(a) structure, and therefore Lp(a) concentrations, is LPA which is located on chromosome 6q26-q27 [29]. Genome-wide association studies have identified single-nucleotide polymorphisms at the LPA locus (rs10455872 and rs7452960) that have been proven to increase both serum Lp(a) levels and the development of PAD [30–32].

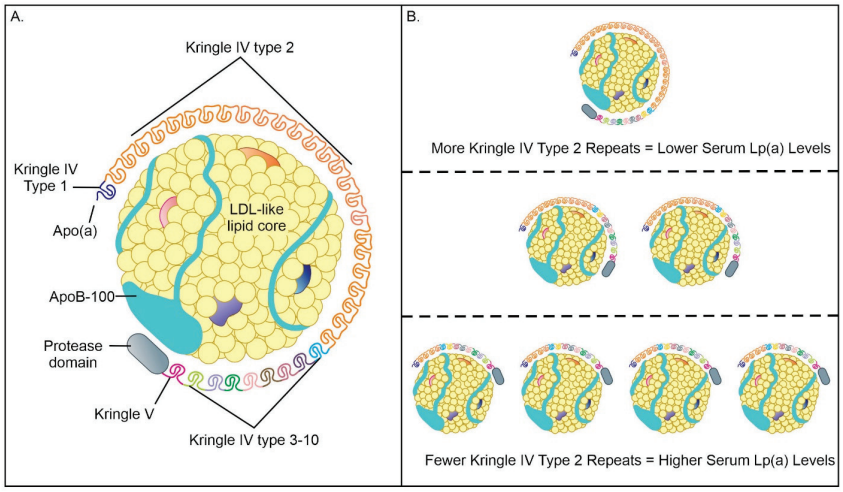


Figure 1. (**A**) Lipoprotein(a) [Lp(a)] structure composed of a low-density-lipoprotein (LDL)-like lipid core containing apolipoprotein B-100 (apoB-100) covalently bound to apolipoprotein(a) [apo(a)] by disulfide bonds. Apo(a) contains single copies of kringle V, kringle IV type 1, kringle IV types 3–10, and a variable number of kringle IV type 2 repeats. (**B**) Serum Lp(a) levels are inversely related to the number of kringle IV type 2 repeats on the apo(a) subunit.

4. Pathogenesis

High levels of Lp(a) are thought to promote atherosclerosis through at least five pathways: (1) attracting leukocytes to the vascular endothelium by increasing the expression of adhesion molecules on vascular endothelial cells and inducing the production of chemotactic agents by them, (2) infiltration of vessel wall and foam cell formation, (3) vascular smooth muscle cell proliferation, (4) endothelial cell dysfunction, and (5) plaque inflammation (Figure 2).

Lp(a) increases the expression of multiple adhesion molecules such as vascular cell adhesion molecule, intercellular cell adhesion molecule, and E-selectin. These surface adhesion molecules allow for corresponding receptors on leukocytes to bind and migrate into the arterial intima [33]. Additionally, Lp(a) induces production of monocyte chemotactic protein in vascular endothelial cells which attracts monocytes and other cytokines, all of which contribute to atherosclerosis [34].

Lp(a) has been detected in the intima and subintima of blood vessels [35]. The proposed mechanism by which this occurs is through the lysine binding site of kringle IV of apo(a) which allows Lp(a) to anchor to the extracellular matrix within the arterial wall [36]. Once inside the arterial wall, Lp(a) undergoes oxidative, lipolytic, and proteolytic changes before uptake by monocytes to form foam cells [37]. Over time, the foam cell's ability to manage extra lipoproteins decreases, resulting in endoplasmic reticulum stress and reactive oxygen species. Eventually, an apoptotic cascade ensues in which foam cells release prothrombotic molecules, cellular proteases, inflammatory cytokines, and oxidized LDL free radicals, all of which act as irritants leading to plaque formation [38].

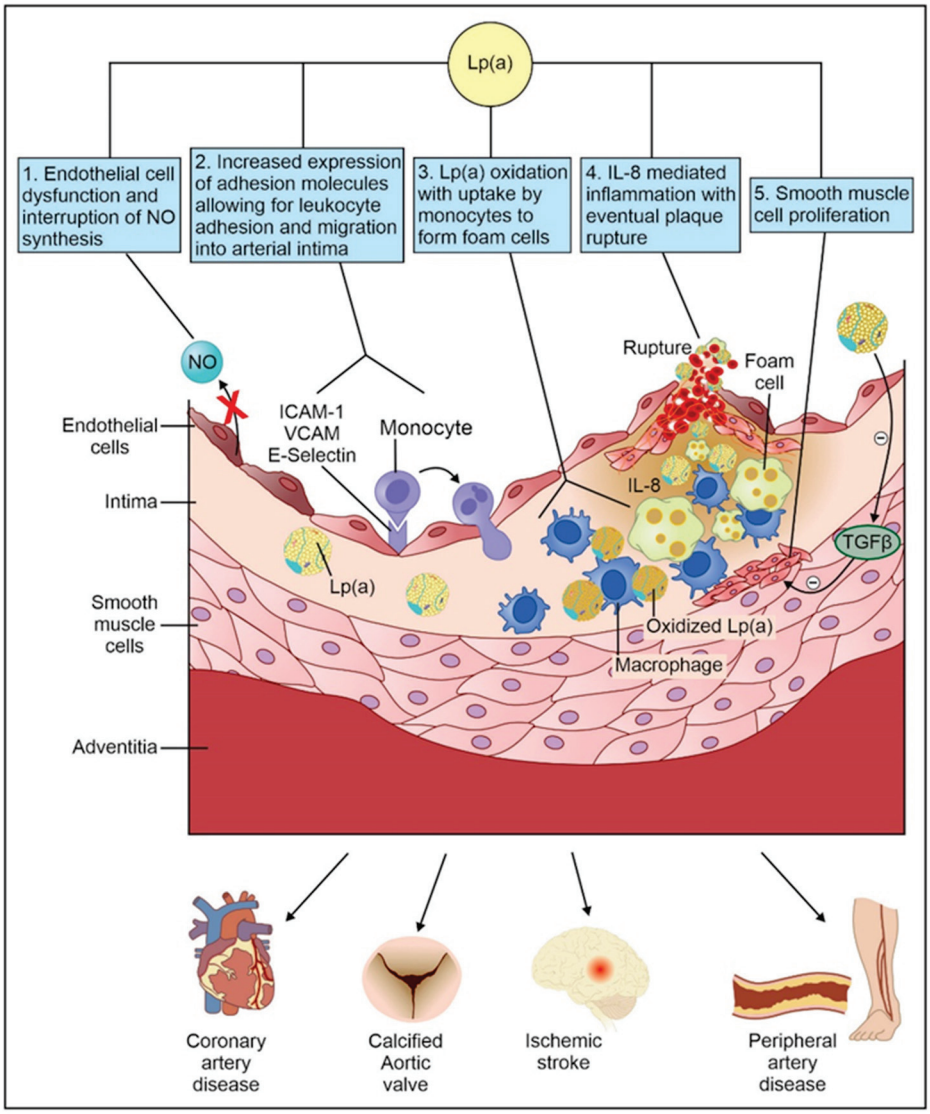


Figure 2. Lp(a) mediated atherogenesis and downstream cardiovascular effects. 1. Lp(a) inhibits nitric oxide synthesis, leading to endothelial cell dysfunction. 2. Lp(a) increases expression of adhesion molecules, allowing for leukocytes to migrate into the arterial intima. 3. Once inside the arterial intima, Lp(a) becomes oxidized and eventually is taken up by monocytes to form foam cells. Once foam cells become overwhelmed by their ability to manage extra lipoproteins, they undergo apoptotic cascade, releasing free radicals, cellular proteases, and inflammatory cytokines. 4. Lp(a) mediates the release of interleukin-8 by macrophages. Interleukin-8 is a key inflammatory cytokine that has chemotactic properties attracting various leukocytes. Interleukin-8 also decreases macrophage expression of metalloproteinases which serve to cleave apo(a), leading to inflammation and plaque rupture. 5. Lp(a) promotes vascular smooth muscle proliferation by indirectly inhibiting transforming factor beta, an inhibitor of smooth muscle cell proliferation. NO: nitric oxide; Lp(a): Lipoprotein(a); ICAM-1: intercellular adhesion molecule-1; VCAM: vascular cell adhesion molecule; IL-8: interleukin-8; TGFβ: Transforming Growth Factor Beta.

Lp(a) promotes vascular smooth muscle proliferation by blocking the conversion of plasminogen to plasmin, thereby preventing plasmin-mediated activation of Transforming Growth Factor Beta, an inhibitor of smooth muscle migration [39].

Elevated levels of Lp(a) inhibit nitric oxide synthesis and thereby promote endothelial cell dysfunction. Nitric oxide has many anti-atherogenic characteristics such as inhibition of platelet activation, smooth muscle proliferation, and reduction in endothelial permeability [37]. Additionally, elevated Lp(a) levels impair endothelium-dependent vasodilation.

This phenomenon has been observed even in the absence of atherosclerosis, indicating a direct inhibitory effect or mechanism at play by which Lp(a) increases vascular permeability and allows direct access of acetylcholine to vascular smooth muscle cells [40].

Elevated levels of Lp(a) also results in plaque inflammation and instability by mediating macrophages to release interleukin-8. Interleukin-8 is an inflammatory cytokine within atherosclerotic plaque and has chemotactic activity towards smooth muscle cells, monocytes, T-cells, and neutrophils [41]. Additionally, interleukin-8 decreases macrophage expression of metalloproteinases which cleave apo(a). Disinhibition of these metalloproteinases leads to plaque inflammation and eventual rupture [42].

Beyond atherosclerosis, Lp(a) is thought to promote thrombosis via the inhibition of plasmin generation, inhibition of Tissue Factor Pathway Inhibitor (TFPI), and increased expression of Plasminogen Activator Inhibitor (Figure 3). Due to apo(a)'s structural similarity to plasminogen, it is theorized that Lp(a) may interfere with fibrinolysis by competitive inhibition of plasmin generation on endothelial cells, monocytes, and platelets. This characteristic of Lp(a) is not well established and may have little clinical relevance [43]. Additionally, Lp(a) inhibits TFP1, an anticoagulant protein that works by inhibiting early phases of procoagulant responses. TFP1 is present on platelets, monocytes, vascular smooth muscle cells, endothelial plaques, and endothelial cells. Lp(a) has been shown to bind and inactivate TFPI, leading to unopposed tissue factor mediated thrombosis [44]. Lastly, Lp(a) causes increased expression of Plasminogen Activator Inhibitor at the endothelial cell surface, thereby inhibiting fibrinolysis [45].

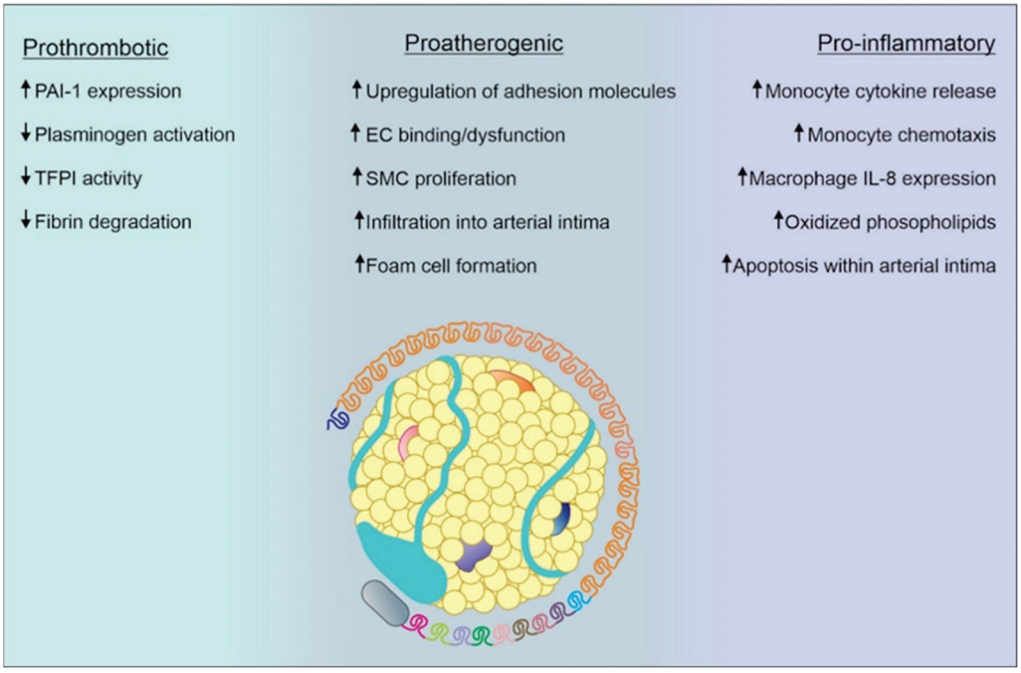


Figure 3. The pathogenicity of Lp(a) is multifactorial and can be classified in three categories: prothrombotic, proatherogenic, and pro-inflammatory. Each of them has its own individual mechanisms. PAI-1: plasminogen activator inhibitor-1; TFPI: tissue factor pathway inhibitor; EC: endothelial cell; SMC: smooth muscle cell; IL-8: interleukin-8.

5. Diagnostic Testing

The measurement of Lp(a) is challenging in that there is a large variation in not only lipid composition of Lp(a) but also in the size of the Apo(a) moiety between individuals. Lp(a) can be measured in molar concentration (nmol/L), mass units (mg/dL), or the seldomly used Lp(a) cholesterol mass [46,47]. Molar concentration by enzyme-linked immunosorbent assay remains the gold standard and is a better predictor of ASCVD than mass units. Although conversions exist between the two units of measure, these are

inaccurate and should be avoided [48]. The European Atherosclerotic Society consensus statement reports that <75 nmol/L or <30 mg/dL is considered normal, 50–125 nmol/L or 30–50 mg/dL is intermediate, and >125 nmol/L or >50 mg/dL is abnormal [49]. The ACC/AHA agree that Lp(a) $\geq$ 125 nmol/L or $\geq$50 mg/dL is considered abnormal and is a risk factor for ASCVD [50].

Serum Lp(a) levels are genetically determined and remain stable over time; therefore, there is little utility in re-checking Lp(a) unless a provider wishes to evaluate the efficacy of treatment. Lp(a) should be checked at steady states as it can be altered by multiple non-genetic factors. Levels are increased during chronic inflammatory conditions, pregnancy, hypothyroidism, kidney disease, and growth hormone therapy. Levels are decreased in severe acute inflammatory conditions, hyperthyroidism, and liver disease [51].

6. Screening

There is a large amount of evidence showing that the majority of PAD remains undetected in clinical practice; therefore, there has been interest in detecting PAD through routine screening. Different guidelines have variable recommendations regarding screening for PAD. In 2018, the United States Preventive Services Task Force concluded that there was insufficient evidence to screen asymptomatic patients for PAD [52]. Although the ESC/ESVS guidelines make no comment on screening of PAD in asymptomatic individuals, they recommend against screening patients with known atherosclerotic disease of other vascular beds as this would likely not change management strategy [53]. In a recent AHA statement, it is recommended to screen for PAD with ABI in high-risk adults such as those $\geq$ 65 years of age and 50–64 years of age with traditional risk factors. Traditional risk factors include smoking, diabetes, hypertension, and dyslipidemia [10]. No major guidelines comment on screening for PAD in the setting of elevated Lp(a) levels.

Given its role as an independent risk factor for ASCVD, many guidelines have published their recommendation on Lp(a) screening. The AHA/ACC state there is a relative indication for checking Lp(a) levels in those with family or personal history of ASCVD that is not explained by another risk factor and in those aged 40–75 without diabetes mellitus who have intermediate risk of ASCVD [50]. The ESC/EAS believe it may be helpful to check Lp(a) once in adults in order to identify those with very high inherited levels of Lp(a). They also state that it is reasonable to check Lp(a) in those who have family history of premature ASCVD and to reclassify on the border of risk categories in order to determine treatment strategies [54]. Other societies such as the National Lipid Association and Canadian Cardiovascular Society take a more aggressive approach in screening, recommending that everyone should obtain an Lp(a) measurement as part of initial lipid screening [55,56]. Just as no major guidelines recommend screening for PAD in the setting of elevated Lp(a) levels, there are conversely no recommendations for screening Lp(a) in the setting of PAD.

7. Lp(a) in PAD

Perhaps the largest study assessing the role of Lp(a) in PAD used samples from the Copenhagen General Population Study, a prospective cohort study in which 108,446 patients aged 20 to 100 years were enrolled between 2003 and 2015. Of the 70,317 individuals who had a measurement of plasma Lp(a), 1162 developed PAD, and 159 had lower-extremity amputation. Individuals with Lp(a) $\geq$ 90th percentile versus <50th percentile were significantly more likely to be diagnosed with PAD in the hospital (HR 2.99, 95% CI 2.09–4.30), experience major adverse limb events (MALE) (2.35, 95% CI 1.04–5.29), and undergo lower-extremity amputation (HR 1.62, 95% CI 1.00–2.62). For the purpose of this study, MALE was defined as revascularization and/or limb amputation. The study also looked into the polymorphisms in Lp(a) structure and found that those with kringle IV type 2 repeats $\leq$ 5th percentile, and thus higher genetically determined Lp(a) levels, were more likely to develop PAD than those with kringle IV type 2 repeats > 50th percentile (1.39, 95% CI 1.17–1.64) [14]. The effects of Lp(a) on MALE were further corroborated by a single-center, retrospective, cohort study consisting of 16,153 hospitalized patients in

France between 2000 and 2020. Serum Lp(a) levels were stratified as normal (<50 mg/dL), high (≥50 mg/dL but <134 mg/dL), and very high (≥134 mg/dL). They found not only a statistically significant stepwise increase in prevalence of PAD between the three groups but also a 5-year cumulative incidence of MALE of 5.44% (95% CI, 3.79%–7.07%) in the very high group, 4.43% (95% CI, 3.68%–5.16%) in the high group, and 3.33% (95% CI, 2.96%–3.70%) in the normal group [57]. These studies indicate that not only is Lp(a) associated with an increase in PAD but also an increase in MALE.

The European Prospective Investigation of Cancer (EPIC)-Norfolk obtained Lp(a) levels of 18,720 participants between the ages of 39 and 79. Of these participants, 596 were diagnosed with PAD. They analyzed Lp(a) logarithmically to examine it as a continuous variable and found the hazard ratio for PAD for a 2.7-fold increase in Lp(a) (equating for 1 standard deviation in Lp[a]) was 1.37 (95% CI 1.25–1.50) [58].

A case–control study which utilized the Linz Peripheral Arterial Disease (LIPAD) data investigated both serum Lp(a) levels and low molecular weight phenotypes of apo(a) in PAD. They measured serum Lp(a) levels and apo(a) phenotypes in 213 patients with symptomatic PAD and compared them to controls matched for age, sex, and presence of diabetes. Low molecular weight phenotypes were defined as apo(a) isoforms with 11–22 kringle IV type 2 repeats, whereas high molecular weight apo(a) isoforms had ≥22 kringle IV type 2 repeats. It was found that those with Lp(a) ≥ 19.5 g/dL were significantly more likely to have PAD (OR 3.73, 95% CI 2.08–6.67). Furthermore, low molecular weight phenotypes of apo(a) were more likely to have PAD (OR 2.21, 95% CI 1.33–3.67) [59].

An Australian study which looked at 1472 people with PAD in the outpatient setting found that patients with Lp(a) ≥ 30 mg/dL were more likely to undergo lower limb revascularization alone (HR 1.33, 95% CI 1.06–1.66) as well as any PAD operation (HR 1.20, 95% CI 1.02–1.41). They did not find an increase in all-cause mortality or major adverse cardiac events (MACEs). Lp(a) levels ≥ 50 mg/dL were also associated with increased risk of lower limb revascularization (HR 1.29, 95% CI 1.00–1.65) but had no association with mortality, MACE, or any PAD operations [60].

The Edinburgh Artery Study evaluated the development of PAD in the general population, taking into account various blood markers including Lp(a). Lp(a) showed a strong independent association in the development of PAD. In order to compare between different hazard ratios, Lp(a) was divided by the inter-tertile range. After adjusting for cardiovascular risk factors and baseline atherosclerotic cardiovascular disease, elevated Lp(a) levels were associated with the development of PAD with a hazard ratio corresponding to an increase equal to the inter-tertile range of 1.22 [61].

The InCHIANTI study studied the association of elevated Lp(a) levels in prevalent and incident cases of PAD in 1002 Italian subjects aged 60–96. After adjusting for confounding variables, they found that participants in the highest quartile of Lp(a) distribution were more likely to have PAD (OR: 1.38, 95% CI 1.01–3.33). This association significantly increased if the diagnostic criteria of PAD was strengthened from ABI < 0.90 to <0.70 (OR: 3.80, 95% CI 1.50–9.61) [62].

FRENA (Factores de Riesgo y Enfermedad Arterial) is a Spanish registry of outpatients with CAD, CeVD, or PAD. Of the 1503 patients recruited, 814 (54%) had Lp(a) levels < 30 mg/dL, 319 (21%) had 30–50 mg/dL, and 370 (25%) had ≥50 mg/dL. It was found that patients with Lp(a) between 30 and 50 mg/dL were at higher risk of limb amputation (HR: 3.18, 95% CI 1.36–7.44), while those with levels ≥ 50 mg/dL were at even higher risk (HR: 22.7, 95% CI 9.38–54.9), suggesting higher Lp(a) levels result in a stepwise increase in PAD [63].

In a retrospective study looking at the association between Lp(a) and PAD in patients who had undergone coronary artery bypass graft and had no history of diabetes were divided into two groups: Lp(a) < 30 mg/dL and Lp(a) ≥ 30 mg/dL. They found that females with Lp(a) > 30 mg/dL had a significant higher risk of developing PAD than those with Lp(a) < 30 mg/dL (OR: 2.589, 95% CI 1.376–4.870). No such association was found in male patients (OR: 0.965, 95% CI 0.628–1.364). Although this study had a limited sample

size, it was the first to suggest a gender deviation in the association between Lp(a) and PAD [64].

In the largest genome-wide association study of PAD which investigated 19 genetic loci in 31,307 individuals with PAD and 211,753 controls, 19 PAD loci were identified. Of the 19 loci, the LPA gene was found to be the most associated with PAD (OR 1.26, 95% CI 1,22–1.30) [32].

Although the majority of the data point toward an association between elevated Lp(a) levels and PAD, not all studies have been able to prove this. In a prospective cohort study assessing 14,916 healthy male physicians aged 40 to 84, novel risk factors for systemic atherosclerosis were obtained including Lp(a). Neither baseline Lp(a) levels nor relative risk of developing future PAD were found to be statistically significant [65]. Another prospective cohort study which evaluated female health professionals > 45 years old found borderline non-significant results for the association of Lp(a) levels and PAD, defined as intermittent claudication and/or peripheral artery surgery (HR 1.6, 95% CI 1.0–2.6; p = 0.07). The lack of statistical significance likely related to a low event rate as only 100 of the 27,935 participants met the primary endpoint of diagnosed PAD [66]. An additional prospective study followed 1222 patients with either intermittent claudication or critical limb ischemia at baseline. They stratified these patients into two cohorts, using two different measurements of serum Lp(a) levels (mg/dL and nmol/L). Lp(a) levels were measured immediately before endovascular repair, and they reported data on cardiovascular mortality during the coming 4.3 and 7.6 years. Despite long follow-ups, they did not find association between Lp(a) levels and cardiovascular death. The endpoint of cardiovascular death was retrospectively collected from the federal death registry. This study had several limitations, including being performed at a single center, measuring Lp(a) in an acute phase, and measuring cardiovascular death as the outcome. It is possible that the investigators missed out on non-fatal cardiovascular events [67].

8. Management

While identifying individuals with elevated Lp(a) levels is a problem in and of itself, the next challenge is how to properly manage this high-risk population. There are very few data on the management of PAD in the setting of elevated Lp(a) levels itself. The AHA/ACC 2016 guidelines have a Class 1A recommendation to initiate HMG-CoA reductase (statin) therapy in all patients diagnosed with PAD [68]. Multiple studies have shown that in patients suffering from PAD, initiation of statin therapy improves MACE and MALE [69–72]. Although no large studies have tested the effects of statin on those suffering from both elevated Lp(a) levels and PAD, the data around statins as a therapeutic option for elevated Lp(a) levels indicate it would likely have little to no effect. While most recent studies indicate that statins do not lower Lp(a) levels [73,74], some suggest that they might actually result in an increase in Lp(a) levels [75–77]. Although one could argue that the use of a statin is warranted even in the absence of hyperlipidemia as it could mitigate the downstream effects of atherosclerosis such as plaque stabilization, some data suggest worse cardiovascular events in patients with elevated Lp(a) levels on statins compared to elevated Lp(a) levels on placebo [78]. Based on current data, it does not appear that statins have a beneficial role in the management of elevated Lp(a) levels in the setting of PAD; however, this has yet to be studied.

Protein convertase subtilisin-kexin type 9 (PCSK9) inhibitors have demonstrated the ability to significantly reduce serum Lp(a) levels. Although commercially available, PCSK9i have not been approved by the United States Food and Drug Administration specifically for the management of elevated Lp(a) levels. The proposed mechanisms by which this occurs are increased LDL receptor expression leading to increased clearance of Lp(a) and possibly direct impact on apoB-100 protein and microsomal triglyceride transfer protein activity [79]. The ODYSSEY OUTCOMES Trial was a multicenter, randomized, double-blind, placebo-controlled trial involving 18,924 patients who had acute coronary syndrome within the preceding year who also had LDL cholesterol of at least 70 mg/dL,

a non-HDL cholesterol of at least 100 mg/dL, or an apoB level of at least 80 mg/dL, and were receiving statin therapy at high-intensity or maximum tolerated dose. Patients were randomly assigned to receive alirocumab subcutaneously every two weeks or a placebo. They were able to prove that in patients who had previous acute coronary syndrome and were receiving high-intensity statin therapy, recurrent ischemic cardiovascular results were lower in the individuals taking alirocumab compared to placebo; however, no data were reported on PAD outcomes [80]. In a prespecified analysis of the trial, investigators studied the role of lowering serum Lp(a) levels with alirocumab and its effect on PAD events including critical limb ischemia, limb revascularization, and amputation for ischemia. They found that alirocumab markedly decreased the number of PAD events compared to placebo (HR 0.69, 95% CI 0.54–0.89, $p = 0.004$). Additionally, they showed greater absolute and relative risk reductions in patients with higher baseline Lp(a) levels. Lastly, they found a decrease in median serum Lp(a) levels by 23.5% [81]. The FOURIER Trial was a multicenter, randomized, double-blind, placebo-controlled trial involving 27,564 patients with known ASCVD who had LDL $\geq$ 70 mg/dL and were on statin therapy. They found that evolocumab on the background of statin therapy significantly reduced the risk of cardiovascular events [82]. A subsequent sub-analysis was able to prove that in patients with PAD, evolocumab reduced the risk of both MACE and MALE [83]. Another sub-analysis showed that evolocumab was able to decrease serum Lp(a) levels by a median of 26.9% [84]. Unlike subsequent analyses of the ODYSSEY OUTCOMES, there was no analysis of Lp(a) in PAD using the FOURIER data. The only adverse event which was statistically significant from placebo in both alirocumab and evolocumab was injection sight reaction which was seen at a rate of 3.8% and 2.1%, respectively [80,82].

Although niacin is well known to raise HDL while lowering LDL and triglycerides, it has also been shown to lower serum Lp(a) levels. Although the mechanism by which this occurs is still unclear, it has been proposed that niacin decreases apo(a) transcription and impairs apoB-100 secretion by inhibiting triglyceride synthesis [85,86]. In the Atherothrombosis Intervention in Metabolic Syndrome with Low HDL/High Triglyceride and Impact on Global Health Outcomes (AIM-HIGH) Trial, patients with known cardiovascular disease with low HDL < 40 mg/dL for men and <50 mg/dL for women, elevated triglycerides 150–400 mg/dL, and LDL < 180 mg/dL were randomized to receive either simvastatin plus placebo or simvastatin, plus extended-release niacin 1500 to 2000 mg/day. Cardiovascular disease was defined as stable CAD, CVD, carotid disease, or PAD. They found that there was no benefit of addition of niacin to statin therapy despite improvement in HDL and triglycerides [87]. A subsequent analysis of the AIM-HIGH study found that the niacin group had reduced Lp(a) levels by 21% (80.2 vs. 63.4 nmol/L) compared to baseline; however, this was not associated with any reduction in cardiovascular events [88]. The Heart Protection Study 2–Treatment of HDL to Reduce the Incidence of Vascular Events (HPS2-THRIVE) studied 25,673 patients 50 to 80 years of age who had MI, CeVD, PAD, or diabetes mellitus with evidence of symptomatic CAD. Patients were given randomized niacin in combination with laropiprant or placebo, on top of simvastatin with or without ezetimibe background therapy. They found that the addition of niacin and laropiprant to simvastatin did not reduce major vascular events. Lp(a) levels were measured in 1999 randomly selected patients one year into the study; however, they found that patients taking niacin and laropiprant had levels 17.8% lower than statin alone (50.7 vs. 60.3 nmol/L) [89]. Although both of these studies were able to show that niacin can significantly reduce serum Lp(a) levels, they did not find a change in cardiovascular outcomes. It should be noted that neither study was prospectively designed for patients with elevated Lp(a) levels, and one could argue that the serum Lp(a) levels in the patients studied did not warrant Lp(a) lowering therapy.

Lipoprotein apheresis is a process in which Lp(a) is removed from circulation via filtration, precipitation, or adsorption. Although a 50–75% decrease in serum Lp(a) levels can be seen, these levels may return to baseline in 8–13 days, requiring patients to undergo weekly or biweekly apheresis. Rarely used in most countries, apheresis is mostly seen in

Germany where it is used in patients with Lp(a) is >60 mg/dL with progressive atherosclerotic disease despite optimization of other risk factors [90]. A study representing ~60% of patients who were receiving lipoprotein apheresis in Germany investigated 170 patients with elevated Lp(a) levels two years before and after receiving apheresis. They found that compared to the two years prior to lipoprotein apheresis, in the two years following the initiation of lipoprotein apheresis, the rate of peripheral arterial events including angioplasty, stenting, or bypass reduced from 30 to 11 [91]. In a small study on 10 patients with isolated elevations in Lp(a) levels who all had PAD and had recently undergone revascularization procedures, they found ankle-brachial-index increased from 0.5 ± 0.2 to 0.9 ± 0.1 ($p < 0.001$). Additionally, the frequency of revascularization procedures was markedly reduced from 35 revascularization within the 12 months prior to initiating apheresis versus 1 revascularization in the 12 months after initiating apheresis [92].

Cholesterol Transfer Protein (CETP) inhibitors mediate the transfer of cholesterol esters from HDL to apoB-100 containing lipoproteins. Four CETP inhibitors have undergone clinical trials and have shown reduction in Lp(a) levels by as much as 36%; however, they were shown to have only mild clinical benefit [93]. A newer CETP inhibitor, obicetrapib has been shown to reduce Lp(a) levels by as much as 56.5% [94]. Phase 3 investigations are currently underway to assess the safety and clinical benefits, including cardiovascular outcomes. There are currently no CETP inhibitors available on the market.

Lomitapide is a microsomal triglyceride transfer protein inhibitor that has been shown to reduce Lp(a) levels by 15–19%. Microsomal triglyceride transfer protein is responsible for transferring triglycerides to apoB in hepatocytes and enterocytes; therefore, inhibition leads to decrease in apoB-containing molecules such as Lp(a). Currently, Lomitapide is only used in patients with homozygous familial hypercholesterolemia [93,95].

There are two RNA-based therapies in clinical development, siRNAs and antisense oligonucleotides (ASOs). Pelacarsen is an ASO that binds to a complementary RNA sequence, triggering the degradation of apo(a) mRNA and consequently lowering Lp(a) levels. In a phase 2 clinical trial involving 286 patients with established ACVD and Lpa levels > 60 mg/dL, various dosages of pelacarsen (20, 40, or 60 mg every four weeks; 20 mg every two weeks; or 20 mg weekly) were administered. The trial revealed that there was a dose-dependent reduction in Lp(a) levels, with an 80% decrease observed in the group receiving 20 mg pelacarsen weekly [96]. Currently, pelacarsen is undergoing a phase 3 trial to investigate whether the reduction in Lp(a) levels translates into clinical benefit. Similar to ASOs, siRNAs are double-stranded RNA molecules that separate within the cell. The antisense strand then binds to its complementary mRNA target, initiating degradation. The antisense strand is both stable and recyclable, allowing for less frequent dosing. In a randomized, double-blind, placebo-controlled phase 2 trial comprising 281 patients with known ASCVD and a median Lp(a) concentration of 67.5 mg/dL, olpasiran was found to significantly reduce Lp(a) levels in a dose-dependent manner. At higher doses, olpasiran can reduce serum Lp(a) levels by over 95% [97]. There is currently a phase 3 trial investigating the role of olpasiran in reducing CAD, MI, and urgent coronary catheterization in patients with Lp(a) > 200 nmol/L. Other RNA targeting therapeutics being investigated to lower Lp(a) levels include zerlasiran and lepodisiran. Although both have been shown to reduce serum Lp(a) levels by up to 99% and 97%, respectively, their role in improving ASCVD outcomes has yet to be studied [98,99]. There are not currently any data regarding the use of RNA-based therapies in patients with both elevated Lp(a) levels and PAD.

Muvalapin is an oral small molecular inhibitor of Lp(a) that works by binding to kringle IV types 7 and 8, thereby preventing apo(a) from binding to apoB-100. In a phase 1 clinical trial, it has recently been shown to reduce serum Lp(a) levels by as much as 65% in healthy participants with Lp(a) $\geq$ 30 mg/dL [100]. It has not yet been studied if this is associated with improved ASCVD outcomes.

9. Conclusions

Although Lp(a) has been classically associated with CAD, CVD, and calcific aortic stenosis, there is a growing body of evidence that implicates Lp(a) as a causal risk factor for PAD as well. Despite this association, current clinical guidelines provide few recommendations in the management of elevated Lp(a) levels in the setting of any of these conditions. Historically, niacin was a therapeutic mainstay as it has been proven to lower serum Lp(a) levels. However, more recent studies have discounted its role as an effective treatment modality as its use has not been associated with improvement in clinical outcomes. Currently, PCSK9 inhibitors remain the only therapeutic option on the market that has been proven to not only lower serum Lp(a) levels but also reduce adverse outcomes associated with PAD. In light of current and emerging data, there has been great interest in developing further treatment modalities that not only empirically lower serum Lp(a) levels but also have proven clinical efficacy in reducing PAD outcomes. As these new therapeutics become commercially available, clinical trials assessing PAD outcomes will need to be conducted to provide direction in the development of clinical guidelines.

Author Contributions: N.P.: Draft manuscript preparation and figure preparation; D.K.K.: Draft manuscript preparation and figure preparation. All authors have read and agreed to the published version of the manuscript.

Funding: This research received no external funding.

Data Availability Statement: Not applicable.

Acknowledgments: Tina Pavlatos, medical illustrator Figures 1–3.

Conflicts of Interest: The authors declare no conflicts of interest.

References

1. Berg, K. A New Serum Type System in Man—The Lp System. *Acta Pathol. Microbiol. Scand.* **1963**, *59*, 369–382. [CrossRef]
2. Berg, K.; Dahlén, G.; Frick, M.H. Lp(a) lipoprotein and pre-beta1-lipoprotein in patients with coronary heart disease. *Clin. Genet.* **1974**, *6*, 230–235. [CrossRef]
3. Maloberti, A.; Fabbri, S.; Colombo, V.; Gualini, E.; Monticelli, M.; Daus, F.; Busti, A.; Galasso, M.; De Censi, L.; Algeri, M.; et al. Lipoprotein(a): Cardiovascular Disease, Aortic Stenosis and New Therapeutic Option. *Int. J. Mol. Sci.* **2022**, *24*, 170. [CrossRef]
4. Wilson, D.P.; Jacobson, T.A.; Jones, P.H.; Koschinsky, M.L.; McNeal, C.J.; Nordestgaard, B.G.; Orringer, C.E. Use of Lipoprotein(a) in clinical practice: A biomarker whose time has come: A scientific statement from the National Lipid Association. *J. Clin. Lipidol.* **2019**, *13*, 374–392. [CrossRef]
5. Raitakari, O.; Kivelä, A.; Pahkala, K.; Rovio, S.; Mykkänen, J.; Ahola-Olli, A.; Loo, B.M.; Lyytikäinen, L.P.; Lehtimäki, T.; Kähönen, M.; et al. Long-term tracking and population characteristics of lipoprotein (a) in the Cardiovascular Risk in Young Finns Study. *Atherosclerosis* **2022**, *356*, 18–27. [CrossRef]
6. Ward, N.C.; Kostner, K.M.; Sullivan, D.R.; Nestel, P.; Watts, G.F. Molecular, Population, and Clinical Aspects of Lipoprotein(a): A Bridge Too Far? *J. Clin. Med.* **2019**, *8*, 2073. [CrossRef]
7. Khan, T.Z.; Bornstein, S.R.; Barbir, M. Lipoprotein(a): The underutilized risk factor for cardiovascular disease. *Glob. Cardiol. Sci. Pract.* **2019**, *2019*, e201911. [CrossRef]
8. Shu, J.; Santulli, G. Update on peripheral artery disease: Epidemiology and evidence-based facts. *Atherosclerosis* **2018**, *275*, 379–381. [CrossRef]
9. Fowkes, F.G.R.; Rudan, D.; Rudan, I.; Aboyans, V.; Denenberg, J.O.; McDermott, M.M.; Norman, P.E.; Sampson, U.K.; Williams, L.J.; Mensah, G.A.; et al. Comparison of global estimates of prevalence and risk factors for peripheral artery disease in 2000 and 2010: A systematic review and analysis. *Lancet* **2013**, *382*, 1329–1340. [CrossRef]
10. Criqui, M.H.; Matsushita, K.; Aboyans, V.; Hess, C.N.; Hicks, C.W.; Kwan, T.W.; McDermott, M.M.; Misra, S.; Ujueta, F.; American Heart Association Council on Epidemiology and Prevention; et al. Lower Extremity Peripheral Artery Disease: Contemporary Epidemiology, Management Gaps, and Future Directions: A Scientific Statement from the American Heart Association. *Circulation* **2021**, *144*, e171–e191. [CrossRef]
11. Sartipy, F.; Sigvant, B.; Lundin, F.; Wahlberg, E. Ten Year Mortality in Different Peripheral Arterial Disease Stages: A Population Based Observational Study on Outcome. *Eur. J. Vasc. Endovasc. Surg.* **2018**, *55*, 529–536. [CrossRef]
12. Scully, R.E.; Arnaoutakis, D.J.; DeBord Smith, A.; Semel, M.; Nguyen, L.L. Estimated annual health care expenditures in individuals with peripheral arterial disease. *J. Vasc. Surg.* **2018**, *67*, 558–567. [CrossRef]
13. Kosmas, C.E.; Silverio, D.; Sourlas, A.; Peralta, R.; Montan, P.D.; Guzman, E.; Garcia, M.J. Role of lipoprotein (a) in peripheral arterial disease. *Ann. Transl. Med.* **2019**, *7* (Suppl. S6), S242. [CrossRef]

14. Thomas, P.E.; Vedel-Krogh, S.; Nielsen, S.F.; Nordestgaard, B.G.; Kamstrup, P.R. Lipoprotein(a) and Risks of Peripheral Artery Disease, Abdominal Aortic Aneurysm, and Major Adverse Limb Events. *J. Am. Coll. Cardiol.* **2023**, *82*, 2265–2276. [CrossRef]
15. Tsimikas, S.; Fazio, S.; Ferdinand, K.C.; Ginsberg, H.N.; Koschinsky, M.L.; Marcovina, S.M.; Moriarty, P.M.; Rader, D.J.; Remaley, A.T.; Reyes-Soffer, G.; et al. NHLBI Working Group Recommendations to Reduce Lipoprotein(a)-Mediated Risk of Cardiovascular Disease and Aortic Stenosis. *J. Am. Coll. Cardiol.* **2018**, *71*, 177–192. [CrossRef]
16. Bilen, O.; Kamal, A.; Virani, S.S. Lipoprotein abnormalities in South Asians and its association with cardiovascular disease: Current state and future directions. *World J. Cardiol.* **2016**, *8*, 247–257. [CrossRef]
17. Paré, G.; Çaku, A.; McQueen, M.; Anand, S.S.; Enas, E.; Clarke, R.; Boffa, M.B.; Koschinsky, M.; Wang, X.; Yusuf, S.; et al. Lipoprotein(a) Levels and the Risk of Myocardial Infarction Among 7 Ethnic Groups. *Circulation* **2019**, *139*, 1472–1482. [CrossRef]
18. Lee, S.R.; Prasad, A.; Choi, Y.S.; Xing, C.; Clopton, P.; Witztum, J.L.; Tsimikas, S. LPA Gene, Ethnicity, and Cardiovascular Events. *Circulation* **2017**, *135*, 251–263. [CrossRef]
19. Guan, W.; Cao, J.; Steffen, B.T.; Post, W.S.; Stein, J.H.; Tattersall, M.C.; Kaufman, J.D.; McConnell, J.P.; Hoefner, D.M.; Warnick, R.; et al. Race is a key variable in assigning lipoprotein(a) cutoff values for coronary heart disease risk assessment: The Multi-Ethnic Study of Atherosclerosis. *Arterioscler. Thromb. Vasc. Biol.* **2015**, *35*, 996–1001. [CrossRef]
20. Makshood, M.; Joshi, P.H.; Kanaya, A.M.; Ayers, C.; Budoff, M.; Tsai, M.Y.; Blaha, M.; Michos, E.D.; Post, W.S. Lipoprotein (a) and aortic valve calcium in South Asians compared to other race/ethnic groups. *Atherosclerosis* **2020**, *313*, 14–19. [CrossRef]
21. Bhatia, H.S.; Hurst, S.; Desai, P.; Zhu, W.; Yeang, C. Lipoprotein(a) Testing Trends in a Large Academic Health System in the United States. *J. Am. Heart Assoc.* **2023**, *12*, e031255. [CrossRef]
22. Kelsey, M.D.; Mulder, H.; Chiswell, K.; Lampron, Z.M.; Nilles, E.; Kulinski, J.P.; Joshi, P.H.; Jones, W.S.; Chamberlain, A.M.; Leucker, T.M.; et al. Contemporary patterns of lipoprotein(a) testing and associated clinical care and outcomes. *Am. J. Prev. Cardiol.* **2023**, *14*, 100478. [CrossRef]
23. Schmidt, K.; Noureen, A.; Kronenberg, F.; Utermann, G. Structure, function, and genetics of lipoprotein (a). *J. Lipid Res.* **2016**, *57*, 1339–1359. [CrossRef]
24. Behbodikhah, J.; Ahmed, S.; Elyasi, A.; Kasselman, L.J.; De Leon, J.; Glass, A.D.; Reiss, A.B. Apolipoprotein B and Cardiovascular Disease: Biomarker and Potential Therapeutic Target. *Metabolites* **2021**, *11*, 690. [CrossRef]
25. Banerjee, R.; Weideman, S.; Fernandez-Vazquez, D.; Banerjee, A.; Hasan, A.; Tsai, S. Role of Lipoprotein A in Lower Extremity Peripheral Artery Disease. *Am. J. Cardiol.* **2023**, *198*, 47–49. [CrossRef]
26. Maranhão, R.C.; Carvalho, P.O.; Strunz, C.C.; Pileggi, F. Lipoprotein (a): Structure, pathophysiology and clinical implications. *Arq. Bras. Cardiol.* **2014**, *103*, 76–84. [CrossRef]
27. Rehberger Likozar, A.; Zavrtanik, M.; Šebeštjen, M. Lipoprotein(a) in atherosclerosis: From pathophysiology to clinical relevance and treatment options. *Ann. Med.* **2020**, *52*, 162–177. [CrossRef]
28. Kronenberg, F. Human Genetics and the Causal Role of Lipoprotein(a) for Various Diseases. *Cardiovasc. Drugs Ther.* **2016**, *30*, 87–100. [CrossRef]
29. Coassin, S.; Kronenberg, F. Lipoprotein(a) beyond the kringle IV repeat polymorphism: The complexity of genetic variation in the LPA gene. *Atherosclerosis* **2022**, *349*, 17–35. [CrossRef]
30. Hopewell, J.C.; Clarke, R.; Parish, S.; Armitage, J.; Lathrop, M.; Hager, J.; Collins, R. Lipoprotein(a) genetic variants associated with coronary and peripheral vascular disease but not with stroke risk in the Heart Protection Study. *Circ. Cardiovasc. Genet.* **2011**, *4*, 68–73. [CrossRef]
31. Clarke, R.; Peden, J.F.; Hopewell, J.C.; Kyriakou, T.; Goel, A.; Heath, S.C.; Parish, S.; Barlera, S.; Franzosi, M.G.; Rust, S.; et al. Genetic variants associated with Lp(a) lipoprotein level and coronary disease. *N. Engl. J. Med.* **2009**, *361*, 2518–2528. [CrossRef]
32. Klarin, D.; Lynch, J.; Aragam, K.; Chaffin, M.; Assimes, T.L.; Huang, J.; Lee, K.M.; Shao, Q.; Huffman, J.E.; Natarajan, P.; et al. Genome-wide association study of peripheral artery disease in the Million Veteran Program. *Nat. Med.* **2019**, *25*, 1274–1279. [CrossRef]
33. Takami, S.; Yamashita, S.; Kihara, S.; Ishigami, M.; Takemura, K.; Kume, N.; Kita, T.; Matsuzawa, Y. Lipoprotein(a) enhances the expression of intercellular adhesion molecule-1 in cultured human umbilical vein endothelial cells. *Circulation* **1998**, *97*, 721–728. [CrossRef]
34. Poon, M.; Zhang, X.; Dunsky, K.G.; Taubman, M.B.; Harpel, P.C. Apolipoprotein(a) induces monocyte chemotactic activity in human vascular endothelial cells. *Circulation* **1997**, *96*, 2514–2519. [CrossRef]
35. Rath, M.; Niendorf, A.; Reblin, T.; Dietel, M.; Krebber, H.J.; Beisiegel, U. Detection and quantification of lipoprotein(a) in the arterial wall of 107 coronary bypass patients. *Arteriosclerosis* **1989**, *9*, 579–592. [CrossRef]
36. Cho, T.; Jung, Y.; Koschinsky, M.L. Apolipoprotein(a), through its strong lysine-binding site in KIV(10'), mediates increased endothelial cell contraction and permeability via a Rho/Rho kinase/MYPT1-dependent pathway. *J. Biol. Chem.* **2008**, *283*, 30503–30512. [CrossRef]
37. Deb, A.; Caplice, N.M. Lipoprotein(a): New insights into mechanisms of atherogenesis and thrombosis. *Clin. Cardiol.* **2004**, *27*, 258–264. [CrossRef]
38. Javadifar, A.; Rastgoo, S.; Banach, M.; Jamialahmadi, T.; Johnston, T.P.; Sahebkar, A. Foam Cells as Therapeutic Targets in Atherosclerosis with a Focus on the Regulatory Roles of Non-Coding RNAs. *Int. J. Mol. Sci.* **2021**, *22*, 2529. [CrossRef]
39. Grainger, D.J.; Kemp, P.R.; Liu, A.C.; Lawn, R.M.; Metcalfe, J.C. Activation of transforming growth factor-beta is inhibited in transgenic apolipoprotein(a) mice. *Nature* **1994**, *370*, 460–462. [CrossRef]

40. Lampsas, S.; Xenou, M.; Oikonomou, E.; Pantelidis, P.; Lysandrou, A.; Sarantos, S.; Goliopoulou, A.; Kalogeras, K.; Tsigkou, V.; Kalpis, A.; et al. Lipoprotein(a) in Atherosclerotic Diseases: From Pathophysiology to Diagnosis and Treatment. *Molecules* **2023**, *28*, 969. [CrossRef]
41. Klezovitch, O.; Edelstein, C.; Scanu, A.M. Stimulation of interleukin-8 production in human THP-1 macrophages by apolipoprotein(a). Evidence for a critical involvement of elements in its C-terminal domain. *J. Biol. Chem.* **2001**, *276*, 46864–46869. [CrossRef]
42. Scipione, C.A.; Sayegh, S.E.; Romagnuolo, R.; Tsimikas, S.; Marcovina, S.M.; Boffa, M.B.; Koschinsky, M.L. Mechanistic insights into Lp(a)-induced IL-8 expression: A role for oxidized phospholipid modification of apo(a). *J. Lipid Res.* **2015**, *56*, 2273–2285. [CrossRef]
43. Loscalzo, J.; Weinfeld, M.; Fless, G.M.; Scanu, A.M. Lipoprotein(a), fibrin binding, and plasminogen activation. *Arteriosclerosis* **1990**, *10*, 240–245. [CrossRef]
44. Ugovšek, S.; Šebeštjen, M. Lipoprotein(a)-The Crossroads of Atherosclerosis, Atherothrombosis and Inflammation. *Biomolecules* **2021**, *12*, 26. [CrossRef]
45. Etingin, O.R.; Hajjar, D.P.; Hajjar, K.A.; Harpel, P.C.; Nachman, R.L. Lipoprotein (a) regulates plasminogen activator inhibitor-1 expression in endothelial cells. A potential mechanism in thrombogenesis. *J. Biol. Chem.* **1991**, *266*, 2459–2465. [CrossRef]
46. Cegla, J.; France, M.; Marcovina, S.M.; Neely, R.D.G. Lp(a): When and how to measure it. *Ann. Clin. Biochem.* **2021**, *58*, 16–21. [CrossRef]
47. Kamstrup, P.R. Lipoprotein(a) and Cardiovascular Disease. *Clin. Chem.* **2021**, *67*, 154–166. [CrossRef]
48. Reyes-Soffer, G.; Ginsberg, H.N.; Berglund, L.; Duell, P.B.; Heffron, S.P.; Kamstrup, P.R.; Lloyd-Jones, D.M.; Marcovina, S.M.; Yeang, C.; Koschinsky, M.L. Lipoprotein(a): A Genetically Determined, Causal, and Prevalent Risk Factor for Atherosclerotic Cardiovascular Disease: A Scientific Statement from the American Heart Association. *Arterioscler. Thromb. Vasc. Biol.* **2022**, *42*, e48–e60. [CrossRef]
49. Kronenberg, F.; Mora, S.; Stroes, E.S.G.; Ference, B.A.; Arsenault, B.J.; Berglund, L.; Dweck, M.R.; Koschinsky, M.; Lambert, G.; Mach, F.; et al. Lipoprotein(a) in atherosclerotic cardiovascular disease and aortic stenosis: A European Atherosclerosis Society consensus statement. *Eur. Heart J.* **2022**, *43*, 3925–3946. [CrossRef]
50. Grundy, S.M.; Stone, N.J.; Bailey, A.L.; Beam, C.; Birtcher, K.K.; Blumenthal, R.S.; Braun, L.T.; de Ferranti, S.; Faiella-Tommasino, J.; Forman, D.E.; et al. 2018 AHA/ACC/AACVPR/AAPA/ABC/ACPM/ADA/AGS/APhA/ASPC/NLA/PCNA Guideline on the Management of Blood Cholesterol: Executive Summary: A Report of the American College of Cardiology/American Heart Association Task Force on Clinical Practice Guidelines. *J. Am. Coll. Cardiol.* **2019**, *73*, 3168–3209. [CrossRef]
51. Enkhmaa, B.; Berglund, L. Non-genetic influences on lipoprotein(a) concentrations. *Atherosclerosis* **2022**, *349*, 53–62. [CrossRef]
52. US Preventive Services Task Force; Curry, S.J.; Krist, A.H.; Owens, D.K.; Barry, M.J.; Caughey, A.B.; Davidson, K.W.; Doubeni, C.A.; Epling, J.W.; Kemper, A.R.; et al. Screening for Peripheral Artery Disease and Cardiovascular Disease Risk Assessment with the Ankle-Brachial Index: US Preventive Services Task Force Recommendation Statement. *JAMA* **2018**, *320*, 177–183. [CrossRef]
53. Aboyans, V.; Ricco, J.B.; Bartelink, M.L.E.L.; Björck, M.; Brodmann, M.; Cohnert, T.; Collet, J.P.; Czerny, M.; De Carlo, M.; Debus, S.; et al. 2017 ESC Guidelines on the Diagnosis and Treatment of Peripheral Arterial Diseases, in collaboration with the European Society for Vascular Surgery (ESVS). *Eur. Heart J.* **2018**, *39*, 763–816. [CrossRef]
54. Mach, F.; Baigent, C.; Catapano, A.L.; Koskinas, K.C.; Casula, M.; Badimon, L.; Chapman, M.J.; De Backer, G.G.; Delgado, V.; Ference, B.A.; et al. 2019 ESC/EAS Guidelines for the management of dyslipidaemias: Lipid modification to reduce cardiovascular risk. *Eur. Heart J.* **2020**, *41*, 111–188. [CrossRef]
55. Pearson, G.J.; Thanassoulis, G.; Anderson, T.J.; Barry, A.R.; Couture, P.; Dayan, N.; Francis, G.A.; Genest, J.; Grégoire, J.; Grover, S.A.; et al. 2021 Canadian Cardiovascular Society Guidelines for the Management of Dyslipidemia for the Prevention of Cardiovascular Disease in Adults. *Can. J. Cardiol.* **2021**, *37*, 1129–1150. [CrossRef]
56. Koschinsky, M.L.; Bajaj, A.; Boffa, M.B.; Dixon, D.L.; Ferdinand, K.C.; Gidding, S.S.; Gill, E.A.; Jacobson, T.A.; Michos, E.D.; Safarova, M.S.; et al. A focused update to the 2019 NLA scientific statement on use of lipoprotein(a) in clinical practice. *J. Clin. Lipidol.* 2024, *in press*. [CrossRef]
57. Guédon, A.F.; De Freminville, J.B.; Mirault, T.; Mohamedi, N.; Rance, B.; Fournier, N.; Paul, J.L.; Messas, E.; Goudot, G. Association of Lipoprotein(a) Levels with Incidence of Major Adverse Limb Events. *JAMA Netw. Open* **2022**, *5*, e2245720. [CrossRef]
58. Gurdasani, D.; Sjouke, B.; Tsimikas, S.; Hovingh, G.K.; Luben, R.N.; Wainwright, N.W.; Pomilla, C.; Wareham, N.J.; Khaw, K.T.; Boekholdt, S.M.; et al. Lipoprotein(a) and risk of coronary, cerebrovascular, and peripheral artery disease: The EPIC-Norfolk prospective population study. *Arterioscler. Thromb. Vasc. Biol.* **2012**, *32*, 3058–3065. [CrossRef]
59. Dieplinger, B.; Lingenhel, A.; Baumgartner, N.; Poelz, W.; Dieplinger, H.; Haltmayer, M.; Kronenberg, F.; Mueller, T. Increased serum lipoprotein(a) concentrations and low molecular weight phenotypes of apolipoprotein(a) are associated with symptomatic peripheral arterial disease. *Clin. Chem.* **2007**, *53*, 1298–1305. [CrossRef]
60. Golledge, J.; Rowbotham, S.; Velu, R.; Quigley, F.; Jenkins, J.; Bourke, M.; Bourke, B.; Thanigaimani, S.; Chan, D.C.; Watts, G.F. Association of Serum Lipoprotein (a) With the Requirement for a Peripheral Artery Operation and the Incidence of Major Adverse Cardiovascular Events in People with Peripheral Artery Disease. *J. Am. Heart Assoc.* **2020**, *9*, e015355. [CrossRef]
61. Tzoulaki, I.; Murray, G.D.; Lee, A.J.; Rumley, A.; Lowe, G.D.O.; Fowkes, F.G.R. Inflammatory, haemostatic, and rheological markers for incident peripheral arterial disease: Edinburgh Artery Study. *Eur. Heart J.* **2007**, *28*, 354–362. [CrossRef]

62. Volpato, S.; Vigna, G.B.; McDermott, M.M.; Cavalieri, M.; Maraldi, C.; Lauretani, F.; Bandinelli, S.; Zuliani, G.; Guralnik, J.M.; Fellin, R.; et al. Lipoprotein(a), inflammation, and peripheral arterial disease in a community-based sample of older men and women (the InCHIANTI study). *Am. J. Cardiol.* **2010**, *105*, 1825–1830. [CrossRef]
63. Sanchez Muñoz-Torrero, J.F.; Rico-Martín, S.; Álvarez, L.R.; Aguilar, E.; Alcalá, J.N.; Monreal, M.; FRENA Investigators. Lipoprotein (a) levels and outcomes in stable outpatients with symptomatic artery disease. *Atherosclerosis* **2018**, *276*, 10–14. [CrossRef]
64. Yi, C.; Junyi, G.; Fengju, L.; Qing, Z.; Jie, C. Association between lipoprotein(a) and peripheral arterial disease in coronary artery bypass grafting patients. *Clin. Cardiol.* **2023**, *46*, 512–520. [CrossRef]
65. Ridker, P.M.; Stampfer, M.J.; Rifai, N. Novel risk factors for systemic atherosclerosis: A comparison of C-reactive protein, fibrinogen, homocysteine, lipoprotein(a), and standard cholesterol screening as predictors of peripheral arterial disease. *JAMA* **2001**, *285*, 2481–2485. [CrossRef]
66. Pradhan, A.D.; Shrivastava, S.; Cook, N.R.; Rifai, N.; Creager, M.A.; Ridker, P.M. Symptomatic peripheral arterial disease in women: Nontraditional biomarkers of elevated risk. *Circulation* **2008**, *117*, 823–831. [CrossRef]
67. Zierfuss, B.; Höbaus, C.; Feldscher, A.; Hannes, A.; Mrak, D.; Koppensteiner, R.; Stangl, H.; Schernthaner, G.H. Lipoprotein (a) and long-term outcome in patients with peripheral artery disease undergoing revascularization. *Atherosclerosis* **2022**, *363*, 94–101. [CrossRef]
68. Gerhard-Herman, M.D.; Gornik, H.L.; Barrett, C.; Barshes, N.R.; Corriere, M.A.; Drachman, D.E.; Fleisher, L.A.; Fowkes, F.G.; Hamburg, N.M.; Kinlay, S.; et al. 2016 AHA/ACC Guideline on the Management of Patients with Lower Extremity Peripheral Artery Disease: Executive Summary: A Report of the American College of Cardiology/American Heart Association Task Force on Clinical Practice Guidelines. *Circulation* **2017**, *135*, e686–e725. [CrossRef]
69. Westin, G.G.; Armstrong, E.J.; Bang, H.; Yeo, K.K.; Anderson, D.; Dawson, D.L.; Pevec, W.C.; Amsterdam, E.A.; Laird, J.R. Association between statin medications and mortality, major adverse cardiovascular event, and amputation-free survival in patients with critical limb ischemia. *J. Am. Coll. Cardiol.* **2014**, *63*, 682–690. [CrossRef]
70. Kumbhani, D.J.; Steg, P.G.; Cannon, C.P.; Eagle, K.A.; Smith, S.C.; Goto, S.; Ohman, E.M.; Elbez, Y.; Sritara, P.; Baumgartner, I.; et al. Statin therapy and long-term adverse limb outcomes in patients with peripheral artery disease: Insights from the REACH registry. *Eur. Heart J.* **2014**, *35*, 2864–2872. [CrossRef]
71. Ramos, R.; García-Gil, M.; Comas-Cufí, M.; Quesada, M.; Marrugat, J.; Elosua, R.; Sala, J.; Grau, M.; Martí, R.; Ponjoan, A.; et al. Statins for Prevention of Cardiovascular Events in a Low-Risk Population with Low Ankle Brachial Index. *J. Am. Coll. Cardiol.* **2016**, *67*, 630–640. [CrossRef]
72. Heart Protection Study Collaborative Group. Randomized trial of the effects of cholesterol-lowering with simvastatin on peripheral vascular and other major vascular outcomes in 20,536 people with peripheral arterial disease and other high-risk conditions. *J. Vasc. Surg.* **2007**, *45*, 645–654; discussion 653–654. [CrossRef]
73. Arsenault, B.J.; Barter, P.; DeMicco, D.A.; Bao, W.; Preston, G.M.; LaRosa, J.C.; Grundy, S.M.; Deedwania, P.; Greten, H.; Wenger, N.K.; et al. Prediction of cardiovascular events in statin-treated stable coronary patients of the treating to new targets randomized controlled trial by lipid and non-lipid biomarkers. *PLoS ONE* **2014**, *9*, e114519. [CrossRef]
74. Khera, A.V.; Everett, B.M.; Caulfield, M.P.; Hantash, F.M.; Wohlgemuth, J.; Ridker, P.M.; Mora, S. Lipoprotein(a) concentrations, rosuvastatin therapy, and residual vascular risk: An analysis from the JUPITER Trial (Justification for the Use of Statins in Prevention: An Intervention Trial Evaluating Rosuvastatin). *Circulation* **2014**, *129*, 635–642. [CrossRef]
75. Fraley, A.E.; Schwartz, G.G.; Olsson, A.G.; Kinlay, S.; Szarek, M.; Rifai, N.; Libby, P.; Ganz, P.; Witztum, J.L.; Tsimikas, S.; et al. Relationship between biomarkers of oxidized low-density lipoprotein, statin therapy, quantitative coronary angiography, and atheroma: Volume observations from the REVERSAL trial. *J. Am. Coll. Cardiol.* **2009**, *53*, 2186–2196. [CrossRef]
76. Choi, S.H.; Chae, A.; Miller, E.; Messig, M.; Ntanios, F.; DeMaria, A.N.; Nissen, S.E.; Witztum, J.L.; Tsimikas, S. Relationship between biomarkers of oxidized low-density lipoprotein, statin therapy, quantitative coronary angiography, and atheroma: Volume observations from the REVERSAL (Reversal of Atherosclerosis with Aggressive Lipid Lowering) study. *J. Am. Coll. Cardiol.* **2008**, *52*, 24–32. [CrossRef]
77. Capoulade, R.; Chan, K.L.; Yeang, C.; Mathieu, P.; Bossé, Y.; Dumesnil, J.G.; Tam, J.W.; Teo, K.K.; Mahmut, A.; Yang, X.; et al. Oxidized Phospholipids, Lipoprotein(a), and Progression of Calcific Aortic Valve Stenosis. *J. Am. Coll. Cardiol.* **2015**, *66*, 1236–1246. [CrossRef]
78. Willeit, P.; Ridker, P.M.; Nestel, P.J.; Simes, J.; Tonkin, A.M.; Pedersen, T.R.; Schwartz, G.G.; Olsson, A.G.; Colhoun, H.M.; Kronenberg, F.; et al. Baseline and on-statin treatment lipoprotein(a) levels for prediction of cardiovascular events: Individual patient-data meta-analysis of statin outcome trials. *Lancet* **2018**, *392*, 1311–1320. [CrossRef]
79. van Capelleveen, J.C.; van der Valk, F.M.; Stroes, E.S.G. Current therapies for lowering lipoprotein (a). *J. Lipid Res.* **2016**, *57*, 1612–1618. [CrossRef]
80. Schwartz, G.G.; Steg, P.G.; Szarek, M.; Bhatt, D.L.; Bittner, V.A.; Diaz, R.; Edelberg, J.M.; Goodman, S.G.; Hanotin, C.; Harrington, R.A.; et al. Alirocumab and Cardiovascular Outcomes after Acute Coronary Syndrome. *N. Engl. J. Med.* **2018**, *379*, 2097–2107. [CrossRef]
81. Schwartz, G.G.; Steg, P.G.; Szarek, M.; Bittner, V.A.; Diaz, R.; Goodman, S.G.; Kim, Y.U.; Jukema, J.W.; Pordy, R.; Roe, M.T.; et al. Peripheral Artery Disease and Venous Thromboembolic Events After Acute Coronary Syndrome: Role of Lipoprotein(a) and

Modification by Alirocumab: Prespecified Analysis of the ODYSSEY OUTCOMES Randomized Clinical Trial. *Circulation* **2020**, *141*, 1608–1617. [CrossRef]
82. Sabatine, M.S.; Giugliano, R.P.; Keech, A.C.; Honarpour, N.; Wiviott, S.D.; Murphy, S.A.; Kuder, J.F.; Wang, H.; Liu, T.; Wasserman, S.M.; et al. Evolocumab and Clinical Outcomes in Patients with Cardiovascular Disease. *N. Engl. J. Med.* **2017**, *376*, 1713–1722. [CrossRef]
83. Bonaca, M.P.; Nault, P.; Giugliano, R.P.; Keech, A.C.; Pineda, A.L.; Kanevsky, E.; Kuder, J.; Murphy, S.A.; Jukema, J.W.; Lewis, B.S.; et al. Low-Density Lipoprotein Cholesterol Lowering with Evolocumab and Outcomes in Patients with Peripheral Artery Disease: Insights from the FOURIER Trial (Further Cardiovascular Outcomes Research With PCSK9 Inhibition in Subjects With Elevated Risk). *Circulation* **2018**, *137*, 338–350. [CrossRef]
84. O'Donoghue, M.L.; Fazio, S.; Giugliano, R.P.; Stroes, E.S.G.; Kanevsky, E.; Gouni-Berthold, I.; Im, K.; Pineda, A.L.; Wasserman, A.M.; Češka, R.; et al. Lipoprotein(a), PCSK9 Inhibition, and Cardiovascular Risk. *Circulation* **2019**, *139*, 1483–1492. [CrossRef]
85. Chennamsetty, I.; Kostner, K.M.; Claudel, T.; Vinod, M.; Frank, S.; Weiss, T.S.; Trauner, M.; Kostner, G.M. Nicotinic acid inhibits hepatic APOA gene expression: Studies in humans and in transgenic mice. *J. Lipid Res.* **2012**, *53*, 2405–2412. [CrossRef]
86. Kamanna, V.S.; Kashyap, M.L. Mechanism of action of niacin. *Am. J. Cardiol.* **2008**, *101*, 20B–26B. [CrossRef]
87. AIM-HIGH Investigators; Boden, W.E.; Probstfield, J.L.; Anderson, T.; Chaitman, B.R.; Desvignes-Nickens, P.; Koprowicz, K.; McBride, R.; Teo, K.; Weintraub, W. Niacin in patients with low HDL cholesterol levels receiving intensive statin therapy. *N. Engl. J. Med.* **2011**, *365*, 2255–2267. [CrossRef]
88. Albers, J.J.; Slee, A.; O'Brien, K.D.; Robinson, J.G.; Kashyap, M.L.; Kwiterovich, P.O.; Xu, P.; Marcovina, S.M. Relationship of apolipoproteins A-1 and B, and lipoprotein(a) to cardiovascular outcomes: The AIM-HIGH trial (Atherothrombosis Intervention in Metabolic Syndrome with Low HDL/High Triglyceride and Impact on Global Health Outcomes). *J. Am. Coll. Cardiol.* **2013**, *62*, 1575–1579. [CrossRef]
89. HPS2-THRIVE Collaborative Group; Landray, M.J.; Haynes, R.; Hopewell, J.C.; Parish, S.; Aung, T.; Tomson, J.; Wallendszus, K.; Craig, M.; Jiang, L.; et al. Effects of extended-release niacin with laropiprant in high-risk patients. *N. Engl. J. Med.* **2014**, *371*, 203–212. [CrossRef]
90. Waldmann, E.; Parhofer, K.G. Lipoprotein apheresis to treat elevated lipoprotein (a). *J. Lipid Res.* **2016**, *57*, 1751–1757. [CrossRef]
91. Leebmann, J.; Roeseler, E.; Julius, U.; Heigl, F.; Spitthoever, R.; Heutling, D.; Breitenberger, P.; Maerz, W.; Lehmacher, W.; Heibges, A.; et al. Lipoprotein apheresis in patients with maximally tolerated lipid-lowering therapy, lipoprotein(a)-hyperlipoproteinemia, and progressive cardiovascular disease: Prospective observational multicenter study. *Circulation* **2013**, *128*, 2567–2576. [CrossRef]
92. Poller, W.C.; Dreger, H.; Morgera, S.; Berger, A.; Flessenkämper, I.; Enke-Melzer, K. Lipoprotein apheresis in patients with peripheral artery disease and hyperlipoproteinemia(a). *Atheroscler. Suppl.* **2015**, *18*, 187–193. [CrossRef]
93. Koutsogianni, A.D.; Liamis, G.; Liberopoulos, E.; Adamidis, P.S.; Florentin, M. Effects of Lipid-Modifying and Other Drugs on Lipoprotein(a) Levels-Potent Clinical Implications. *Pharmaceuticals* **2023**, *16*, 750. [CrossRef]
94. Nicholls, S.J.; Ditmarsch, M.; Kastelein, J.J.; Rigby, S.P.; Kling, D.; Curcio, D.L.; Alp, N.J.; Davidson, M.H. Lipid lowering effects of the CETP inhibitor obicetrapib in combination with high-intensity statins: A randomized phase 2 trial. *Nat. Med.* **2022**, *28*, 1672–1678. [CrossRef]
95. Cuchel, M.; Meagher, E.A.; du Toit Theron, H.; Blom, D.J.; Marais, A.D.; Hegele, R.A.; Averna, M.R.; Sirotri, C.R.; Shah, P.K.; Gaudet, D.; et al. Efficacy and safety of a microsomal triglyceride transfer protein inhibitor in patients with homozygous familial hypercholesterolaemia: A single-arm, open-label, phase 3 study. *Lancet* **2013**, *381*, 40–46. [CrossRef]
96. Tsimikas, S.; Karwatowska-Prokopczuk, E.; Gouni-Berthold, I.; Tardif, J.C.; Baum, S.J.; Steinhagen-Thiessen, E.; Shapiro, M.D.; Stroes, E.S.; Moriarty, P.M.; Nordestgaard, B.G.; et al. Lipoprotein(a) Reduction in Persons with Cardiovascular Disease. *N. Engl. J. Med.* **2020**, *382*, 244–255. [CrossRef]
97. O'Donoghue, M.L.; Rosenson, R.S.; Gencer, B.; López, J.A.G.; Lepor, N.A.; Baum, S.J.; Stout, E.; Gaudet, D.; Knusel, B.; Kuder, J.F.; et al. Small Interfering RNA to Reduce Lipoprotein(a) in Cardiovascular Disease. *N. Engl. J. Med.* **2022**, *387*, 1855–1864. [CrossRef]
98. Nissen, S.E.; Linnebjerg, H.; Shen, X.; Wolski, K.; Ma, X.; Lim, S.; Michael, L.; Ruotolo, G.; Gribble, G.; Navar, A.M.; et al. Lepodisiran, an Extended-Duration Short Interfering RNA Targeting Lipoprotein(a): A Randomized Dose-Ascending Clinical Trial. *JAMA* **2023**, *330*, 2075–2083. [CrossRef]
99. Nissen, S.E.; Wolski, K.; Watts, G.F.; Koren, M.J.; Fok, H.; Nicholls, S.J.; Rider, D.A.; Cho, L.; Romano, S.; Melgaard, C.; et al. Single Ascending and Multiple-Dose Trial of Zerlasiran, a Short Interfering RNA Targeting Lipoprotein(a): A Randomized Clinical Trial. *JAMA* **2024**, *331*, 1534–1543. [CrossRef]
100. Nicholls, S.J.; Nissen, S.E.; Fleming, C.; Urva, S.; Suico, J.; Berg, P.H.; Linnebjerg, H.; Ruotolo, G.; Turner, P.K.; Michael, L.F. Muvalaplin, an Oral Small Molecule Inhibitor of Lipoprotein(a) Formation: A Randomized Clinical Trial. *JAMA* **2023**, *330*, 1042–1053. [CrossRef]

Disclaimer/Publisher's Note: The statements, opinions and data contained in all publications are solely those of the individual author(s) and contributor(s) and not of MDPI and/or the editor(s). MDPI and/or the editor(s) disclaim responsibility for any injury to people or property resulting from any ideas, methods, instructions or products referred to in the content.

biomedicines

MDPI

Review

Cardiometabolic Phenotype in HFpEF: Insights from Murine Models

Ekaterina Ogurtsova [1,2], Tatiana Arefieva [1,2], Anastasiia Filatova [1,3,*], Natalya Radyukhina [1] and Artem Ovchinnikov [3,4]

[1] Laboratory of Cell Immunology, National Medical Research Center of Cardiology Named After Academician E.I. Chazov, Academician Chazov St., 15a, 121552 Moscow, Russia; oghurtsova20@mail.ru (E.O.); tiarefieva@cardio.ru (T.A.); nradukhina@mail.ru (N.R.)
[2] Faculty of Medicine, Lomonosov Moscow State University, Lomonosovsky Prospekt, 27/1, 117192 Moscow, Russia
[3] Laboratory of Myocardial Fibrosis and Heart Failure with Preserved Ejection Fraction, National Medical Research Center of Cardiology Named After Academician E.I. Chazov, Academician Chazov St., 15a, 121552 Moscow, Russia; artcardio@mail.ru
[4] Department of Clinical Functional Diagnostics, A.I. Yevdokimov Moscow State University of Medicine and Dentistry, Delegatskaya St., 20, p. 1, 127473 Moscow, Russia
* Correspondence: anastasia.m088@yandex.ru

Abstract: Heart failure with preserved ejection fraction (HFpEF) remains a significant challenge in modern healthcare. It accounts for the majority of heart failure cases and their number worldwide is steadily increasing. With its high prevalence and substantial clinical impact, therapeutic strategies for HFpEF are still inadequate. This review focuses on the cardiometabolic phenotype of HFpEF which is characterised by such conditions as obesity, type 2 diabetes mellitus, and hypertension. Various murine models that mimic this phenotype are discussed. Each model's pathophysiological aspects, namely inflammation, oxidative stress, endothelial dysfunction, changes in cardiomyocyte protein function, and myocardial metabolism alterations are examined in detail. Understanding these models can provide insight into the mechanisms underlying HFpEF and aid in the development of effective therapeutic interventions.

Keywords: heart failure with preserved ejection; murine models; myocardial fibrosis; diastolic dysfunction; cardiometabolic HFpEF

1. Introduction

Heart failure (HF) with preserved ejection fraction (HFpEF) remains a significant challenge in modern healthcare due to its complex pathophysiology and limited treatment options. It accounts for the majority of all HF cases and the number of cases worldwide is steadily increasing. This rise is attributed to factors like the gradual ageing of the population, the prevalence of a sedentary lifestyle, and the increasing incidence of cardiometabolic conditions, such as obesity, arterial hypertension, and type 2 diabetes mellitus (T2DM) [1]. HFpEF is associated with a priori high morbidity and mortality comparable to HF with reduced ejection fraction (EF) (HFrEF) [2]. According to the US Get With The Guidelines-HF registry, the 5-year mortality rate in hospitalised patients with HFpEF is as high as 75%, similar to that in patients with HFrEF [3].

HFpEF is diagnosed on the basis of HF symptoms, preserved left ventricular (LV) EF (>50%), and evidence of increased LV filling pressure/congestion with elevated brain natriuretic peptide (BNP) levels [4–6]. Despite the enormous clinical and social impact,

therapeutic strategies for HFpEF are rather limited. This is typically a common problem owing to a gap in understanding the mechanisms underlying the development of this condition and the marked heterogeneity of its manifestations [7]. To date, regarding the drugs that have been proven to be effective in HFrEF treatment, sodium–glucose transporter 2 inhibitors and mineralocorticoid receptor antagonists are the only ones that seem to improve the prognosis of patients with HFpEF by preventing HF exacerbations [8–10]. In addition, the majority of pharmacological agents have no potential to improve exercise capacity and quality of life in patients with HFpEF [11]. As most of these patients are elderly with limited functional capacity due to natural age-related changes, there may be a significant problem in their treatment [8]. Moreover, the differences in drug efficacy between the two major forms of HF result from the differences in the disease initiation mechanisms. Cardiomyocyte death for any reason (ischaemic, toxic, infectious, etc.) is the key pathological process in HFrEF as it triggers the entire cascade of subsequent structural and functional myocardial changes. Regarding HFpEF, the main pathophysiological drivers are delayed relaxation and reduced LV compliance in which chronic low-grade myocardial inflammation appears to play a key role [12–14].

Figure 1 shows how HFpEF pathogenesis is linked to metabolic obesity, systemic inflammation, and resulting fibrosis in target organs including the myocardium. A sedentary lifestyle and overeating lead to obesity, impaired glucose and lipid metabolism, activation of the renin-angiotensin-aldosterone system, and arterial hypertension contributing to LV hypertrophy. Adipose tissue releases inflammatory factors, including cytokines and adipokines, causing chronic systemic inflammation indicated by elevated blood concentrations of cytokines and activated immune cells [2]. Oxidative stress and endothelial dysfunction are crucial to metabolic disorders and cardiovascular diseases. Excess reactive oxygen species (ROS) from immune cells activate inflammatory pathways, reducing nitric oxide (NO) availability and impairing endothelial function. Factors like hypertension, hyperglycaemia, dyslipidaemia, and smoking worsen endothelial function which can further exacerbate oxidative stress via inflammation and additional ROS production, creating a vicious cycle that contributes to the progression of cardiovascular disease. The consequences of endothelial dysfunction encompass vasoconstriction due to impaired NO production, increased permeability to inflammatory cells and lipids, and an elevated risk of thrombosis [15]. Oxidative stress-related impairment of NO production by the endothelium results in the dysfunction of the NO-cGMP-PKG signalling pathway in cardiomyocytes. PKG phosphorylates various target proteins, leading to multiple effects: inhibiting L-type calcium channels, enhancing intracellular diastolic calcium reuptake via phospholamban phosphorylation, suppressing prolonged signalling by inhibiting G-protein-coupled receptors and the transient receptor potential canonical channels, inhibiting ischaemia-reperfusion injury through ATP-sensitive potassium channel phosphorylation, and stimulating LV relaxation by phosphorylation of troponin I and titin [16].

Taken together, these mechanisms lead to cardiomyocyte death and fibrosis, which result in impaired myocardial contractility.

Clinical proof of HFpEF' inflammatory nature

Several clinical trials have confirmed the role of inflammation in the development and progression of HFpEF. To describe the main manifestations of HFpEF, their key characteristics are provided below.

High blood levels of inflammatory cytokines. Patients with HFpEF are well known to have significantly higher blood levels of pro-inflammatory and pro-fibrotic markers, lower levels of markers of myocardial damage (high-sensitivity troponin T) and LV wall stress (N-terminal fragment of brain natriuretic hormone precursor, NT-proBNP) compared with patients with HFrEF [17–21]. In addition, elevated blood levels of interleukin(IL)-2

and C-reactive protein are associated with new-onset HFpEF [22,23]. Thus, the intensity of systemic inflammation significantly influences the course and prognosis of HFpEF [22–25].

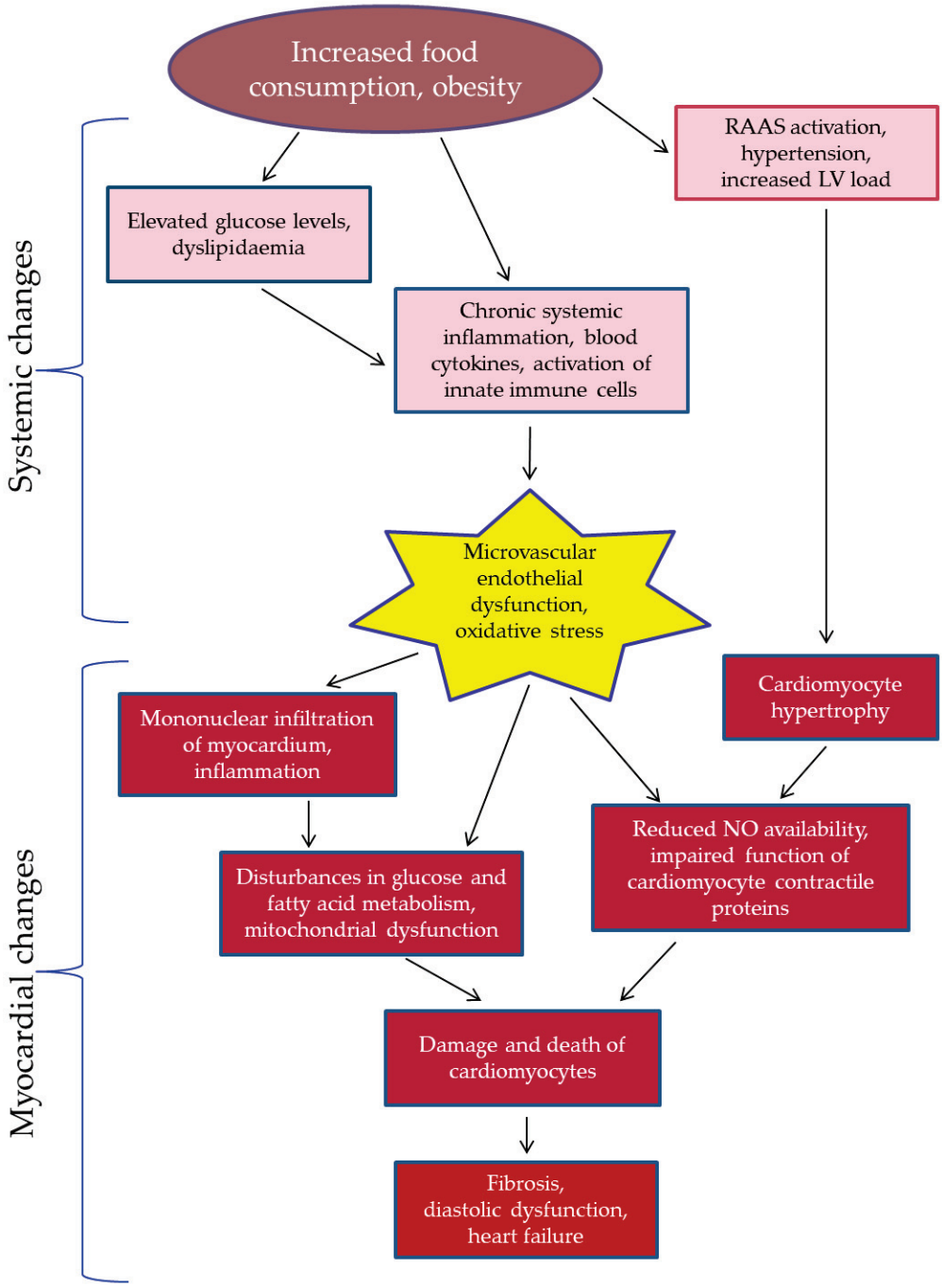


Figure 1. Current understanding of the pathogenesis of HFpEF. NO—nitric oxide; RAAS—renin-angiotensin-aldosterone system.

Activation of endothelial cells. In patients with HFpEF, high levels of endothelial-derived molecules (intercellular adhesion molecule-1, vascular cell adhesion molecule-1, E-selectin) identified in peripheral blood and homogenates of myocardial specimens indicate endothelial cell activation [26–28]. Since circulating pro-inflammatory cytokines primarily affect microvascular endothelial cells, the activity of nicotinamide adenine dinucleotide phosphate oxidase (NOX), the enzyme that leads to the accumulation of ROS in cells, is increased [28]. This leads to uncoupling of endothelial nitric oxide synthase (eNOS) and decreased nitric oxide (NO) bioavailability. The above findings are supported by the low

myocardial nitrite/nitrate concentrations in HFpEF patients [28]. Moreover, the activation of endothelial cells in HFpEF is associated with structural microvascular changes, such as rarefaction and basal membrane thickening of the microvasculature [29,30] which reduce coronary reserve and cause relative myocardial ischaemia.

Activation of circulating monocytes and monocyte infiltration of myocardium. Patients with HFpEF are characterised by an increased content of pro-inflammatory monocytes in the peripheral blood, translating to LV dysfunction [31]. Our recent findings show that myocardial remodelling in HFpEF patients is associated with increased numbers of circulating intermediate monocytes and a decrease in the ratio of regulatory T cells/activated T helper cells [32]. According to other research, stimulation with tumour necrosis factor (TNF) or lipopolysaccharide results in the release of large amounts of pro-inflammatory cytokines by neutrophils from HFpEF patients compared to neutrophils isolated from healthy subjects [26]. In addition, a significant accumulation of activated monocytes/macrophages migrated from the bloodstream is consistently found in myocardial biopsy specimens from patients with HFpEF [27,33,34]. Chemoattractants (mainly monocyte chemotactic protein-1 (MCP-1)) are also required for the migration of monocytes from the bloodstream into the subendothelial space of the myocardium, the initial key step in the inflammatory process. One must note that peripheral chemokine concentration (CCL2/MCP-1, CXCL10/interferon-γ-induced protein 10, CCL17, CCL18) is increased in HFpEF [31]. Notably, the numbers of classic/pro-inflammatory monocytes and alternative/anti-inflammatory circulating monocytes are increased in HFpEF patients. The culture of healthy donor monocytes with HFpEF patient-derived sera leads to M2-macrophage differentiation (as evidenced by the CD206 and IL-10 expression) [31]. According to the data of Bajpai G. et al., CCR2+ macrophage abundance is associated with LV remodelling [35]. In patients with HFpEF, transforming growth factor (TGF)-β-producing macrophages are detected in the myocardium. Moreover, the addition of TGF-β to the culture of fibroblasts obtained from patients with HFpEF is associated with their transformation into myofibroblasts. A positive correlation between cardiac collagen as well as the number of inflammatory cells, and diastolic dysfunction suggests a direct influence of inflammation on fibrosis triggering diastolic dysfunction [27,34].

HFpEF is a heterogeneous disease, mainly with cardiometabolic phenotype

Drug interventions in HFpEF are often ineffective due to the wide variability among patient phenotypes. These phenotypes vary greatly in clinical and haemodynamic features, development mechanisms, prognosis, and response to treatments [36–39]. Such heterogeneity is best assessed using sophisticated approaches (e.g., machine learning techniques). Since 2014, several research groups have applied machine learning to identify multiple clusters/phenotypes of HFpEF. To date, around two dozen phenotypes have been proposed. From study to study, the phenotypes vary, but in most cases, they are reduced to a small number of fairly well-defined phenotypes: cardiometabolic, left atrial myopathy phenotype, natriuretic peptide deficiency phenotype, and pulmonary hypertension/right ventricular dysfunction phenotype [40].

One of the most common HFpEF phenotypes mentioned above is cardiometabolic (or inflammatory-metabolic) [7]. The main risk factors predisposing to the development of HFpEF are pro-inflammatory conditions such as obesity, T2DM, arterial hypertension, chronic kidney disease, hypodynamia, and ageing [37,41–43]. They often combine (especially obesity and T2DM) exacerbating the role of each other [36,38]. As obesity continues to rise, it increases the amount of adipose tissue secreting pro-inflammatory adipokines, which provokes the development of insulin resistance and oxidation processes caused by free radicals, the production of pro-inflammatory cytokines, dysfunctional and reduced microvascular density, increased leukocyte adhesion, macrophage activation, and my-

ocardial fibrosis [2,14,44–46]. Insulin resistance and T2DM are rather common in HFpEF indicating a worse prognosis [47,48]. Irrespectively, T2DM leads to impaired diastolic and systolic LV function with the development of the so-called diabetic cardiomyopathy regardless of other diseases such as arterial hypertension and ischaemic heart disease [49]. Hypertension is also to some extent a pro-inflammatory state. Increased blood levels of the pro-inflammatory cytokines IL-1β, TNF, and interferon-γ have been proven to confirm the risk of arterial hypertension [50]. An increase in the number of T helper 17 cells and in the concentration of cytokines produced by these cells, IL-17 and IL-23, has been reported in the blood of patients with arterial hypertension [51]. One of the key mechanisms implicated in blood pressure increase is the hyper-activation of the renin-angiotensin-aldosterone system. Moreover, angiotensin II, through its type 1 receptors, promotes inflammation in the myocardium by triggering intracellular signalling pathways leading to NF-κB activation and subsequent production of pro-inflammatory cytokines, synthesis of adhesion molecules, and oxidative stress [52,53].

In patients with the cardiometabolic phenotype, the inflammatory-metabolic milieu of obesity and T2DM comorbidities is thought to be a major contributor to the pathophysiology of HFpEF [42]. Interestingly, this phenotype is more common in women, who are more prone to systemic inflammatory diseases than men [5,36,38,54]. Packer M. et al. considered obesity and T2DM to have a greater impact on the woman's heart than the man's heart, HFpEF being clinically more severe. However, the prognosis for women is more favourable than for men [55]. The cardiometabolic phenotype is characterised by pronounced LV hypertrophy and diastolic dysfunction, and a high incidence of adverse outcomes [38–40,55–57]. As the vast majority of HFpEF patients are overweight/obese, this phenotype is to some extent universal [58]. Therapeutic interventions for this phenotype may be useful in the vast majority of patients with HFpEF. In other words, a "one-size-fits-all" approach is being implemented, as to some extent is suggested by the success of sodium–glucose transporter 2 inhibitors in HFpEF [9,58].

Therapies targeting inflammation in HF

The majority of clinical trials assessing the impact of anti-inflammatory therapy in HF have primarily focused on patients with HFrEF and have not demonstrated definitive beneficial outcomes. This is particularly evident in trials involving TNF inhibitors, corticosteroids, xanthine oxidase inhibitors, immunoglobulin G3 (IgG3) immunoadsorption, and methotrexate. To date, canakinumab, a monoclonal antibody targeting IL-1, is the only treatment that has shown a reduction in HF hospitalisation risk among patients with previous myocardial infarction in the CANTOS trial; however, it has not been evaluated in patients with HFpEF [59]. Results from the phase 2 D-HART-2 study in HFpEF patients indicated that IL-1 blockade using anakinra (a recombinant human IL-1 receptor antagonist) did not enhance peak oxygen consumption but was linked to reductions in blood BNP and C-reactive protein levels [60]. The SATELLITE study, which concluded early after randomising 41 patients, established the safety of the myeloperoxidase inhibitor AZD4831 in patients with HF and LV EF of $\geq$40%; it also demonstrated a more than 50% decrease in myeloperoxidase activity from baseline [61]. Our preliminary data suggest that the use of statins in HFpEF was associated with reductions in systemic inflammatory markers (C-reactive protein, MCP-1) and improvements in 6-min walk distance and E/e′ ratio. This supports the previously recognised anti-inflammatory properties of statins and endorses their use in HFpEF management. Currently, the phase 2 clinical trial COLHEART-PRESERVED (NCT06081049) is investigating the efficacy of colchicine in HFpEF. Notably, the ongoing large randomised phase 3 clinical trial, HERMES (NCT05636176), aims to determine the effect of the IL-6 inhibitor ziltirakimab on prognosis in HFpEF.

In summary, despite the established role of inflammation in HFpEF pathophysiology, there is a lack of studies evaluating anti-inflammatory therapies specifically for this condition.

2. HFpEF Animal Models

At present, the availability of suitable animal models of HFpEF throws light on understanding the pathophysiological mechanisms of HFpEF and testing new pharmacological agents. Moreover, pharmacological or surgical approaches, genetic modifications as well as their possible combinations are commonly used in the development of preclinical models of HF [62]. Both small (rodents, guinea pigs) and medium or large (dogs, cats, pigs, monkeys) laboratory animals may be the subject of such manipulation. Yet, a large number of preclinical models that reproduce aspects of HFpEF are also available to researchers [62–64]. For a number of reasons, mice are most commonly used to mimic HFpEF. Firstly, from a practical point of view, mice seem to be optimal animals for carrying out different research: they are cheap to maintain, have a short breeding cycle, develop pathological changes rapidly, and provide easy access to genetic manipulations. Secondly, the mouse genome proves to have sufficient homology with the human genome. However, one of the major challenges of animal models is the fact that none of them are able to fully reproduce the pathophysiological diversity of human HFpEF. Additionally, the heterogeneity of HFpEF manifestations represents another difficulty in creating animal models. Thus, no animal model is suitable for all patients with HFpEF, but for a certain group of patients. In addition, even numerous preclinical models of concentric LV hypertrophy have been a hallmark of HFpEF as they are unable to reproduce the complex myocardial remodelling observed in humans with HFpEF. Usually, the development of animal models of HFpEF has focused on recapitulating the pathology of a single organ (typically the heart) making it difficult to mimic the numerous comorbidities associated with HFpEF [65]. However, the last decade has witnessed the development of innovative multi-component animal models of HFpEF that are able to reproduce the multiple comorbidities and multi-organ involvement typical of HFpEF. Such multi-component models include two-hit models (mimicking two cardiometabolic stresses, that is, arterial hypertension, T2DM or obesity [66–70]). However, three-hit models are also developed including age as an extra risk factor for cardiometabolic stresses [71–75].

As the cardiometabolic phenotype is to some extent a universal phenotype in HFpEF [7], rodent models that recapitulate cardiometabolic stress promise an extra opportunity for the study of HFpEF. In this review, the following murine models that are more or less consistent with the cardiometabolic phenotype of HFpEF are as follows:

(1) Obesity-related HFpEF (leptin-deficient ob/ob and leptin receptor-deficient db/db mutant strains; induced by high-fat diet (HFD));
(2) HFpEF induced by arterial hypertension (chronic subjection to deoxycorticosterone acetate (DOCA), DOCA + angiotensin II infusion, transverse aortic constriction (TAC), chronic subjection to angiotensin II, DOCA infusion + TAC);
(3) Ageing HFpEF (senescence-accelerated mouse strains).

For each of these models, the individual pathophysiological aspects of the cardiometabolic phenotype are characterised below:

(1) Inflammation (production of pro-inflammatory cytokines and activation of inflammatory cells);
(2) Oxidative stress (dysfunction of the antioxidant systems and overproduction of ROS, mitochondrial dysfunction);
(3) Dysfunction of the NO/cyclic guanosine monophosphate (cGMP)/protein kinase G (PKG) pathway (decreased PKG and eNOS activity, activation of inducible NOS (iNOS), decreased cGMP and NO production);

(4) Changes in the level of phosphorylation in cardiomyocyte proteins involved in contraction and regulation of intracellular calcium waves (titin, myosin heavy chain (MHC), sarco-endoplasmic reticulum Ca^{2+}-ATPase (SERCA), phospholamban);
(5) Changes in myocardial metabolism (suppression of glycolysis, increased fatty acid uptake and oxidation, impaired processes of oxidative phosphorylation and ATP synthesis).

2.1. Obesity-Related Models of HFpEF

Given the high prevalence of obesity in patients with HFpEF, its increasing burden contributes to cardiovascular dysfunction.

2.1.1. Diabetic db/db and Obese ob/ob Mice

db/db [BKS-Lepr/db/db/JOrlRj, BKS.Cg-Dock7m+/+Leprdb/J] (Figure 2) and ob/ob [B6.V-Lepob/ob/JRj, B6.Cg-Lepob/J] strains are originally utilised as models of T2DM. Both strains are based on impaired signalling of leptin which represents a small adipokine protein with hormonal properties. As it is synthesised by adipocytes, its level in blood correlates with adipose tissue mass (it is higher in women because they have more excess adipose tissue). The leptin receptor is expressed in various tissues (heart, muscle, lung, small intestine, liver, adipose tissue, central nervous system) and is able to cross the blood-brain barrier and interact with receptors in the hypothalamus to induce a feeling of satiety, thereby regulating appetite. It is worth noting that mutations in the leptin gene or its receptor related to loss of function lead to uncontrollable hunger [76]. There is also a mutation in the db/db mice gene encoding the long isoform of the leptin receptor [77]. In this mouse strain, impaired leptin signalling in the hypothalamus leads to hyperphagia and obesity accompanied by elevated levels of insulin and leptin, hyperglycaemia, and the development of insulin resistance [78–81]. Experimentally, by 6–8 weeks of age, db/db mice suffer from significant hyperinsulinemia, obesity, and hyperglycaemia which worsen thereafter [78,79,82–93].



Figure 2. Twelve-month-old female db/db mouse (weight 63 g). The mouse was sourced from the SPF vivarium of the Institute of Cytology and Genetics, Siberian Branch of the Russian Academy of Sciences.

Another murine strain, ob/ob, has genetic leptin deficiency which can be supplemented externally [94]. Thus, they suffer from obesity, hyperphagia, hyperglycaemia, insulin resistance, and hyperinsulinaemia from an early age [81,95–102]. Impaired glucose tolerance in ob/ob mice occurs at the same age as in db/db mice, at about 6-8 weeks [80].

Both db/db and ob/ob mice demonstrate numerous signs of disturbed lipid metabolism, both models being characterised by hypercholesterolaemia and an increase in plasma fatty acids and triglycerides [78,80,82,84,90,91,98,102,103]. However, these changes are more pronounced in the db/db strain. Moreover, only db/db mice show an increase in plasma ceramide levels [78,91]. Other data report that ob/ob mice have

normal blood triglyceride levels, but liver steatosis can be elevated [100,101]. Db/db mice also demonstrate increased very-low-density lipoprotein and decreased high-density lipoprotein plasma levels [103]. In addition, db/db mice have a reduced activity of hepatic triglyceride lipase which makes them similar to people with T2DM [82]. In db/db mice, a decrease in lipoprotein lipase mRNA content and activity is observed in all tissues [82].

However, there is conflicting evidence regarding metabolic disorders in the myocardium of these murine strains. For example, some authors have described high levels of triglycerides and cholesterol in the myocardium of db/db and ob/ob mice [81], particularly in ob/ob females [101], while no findings have been confirmed by Barouch L.A. et al. [95]. In the myocardium of ob/ob female mice, increased mRNA content of lipoprotein lipase and other proteins involved in lipolysis is found, as well as an increased mRNA level of the insulin-sensitive glucose transporter GLUT-4 and the microsomal triacylglycerol-transport protein which has a protective function in the presence of excess lipids [101]. Increased expression of sodium-glucose cotransporter 1 is also observed in the myocardium of ob/ob mice of both sexes [102].

A decrease in the level of aerobic glucose oxidation and glycolysis in the myocardium is observed in both strains [80], while db/db mice also confirm an increase in the levels of acetyl coenzyme A and succinyl coenzyme A, crucial metabolites in the tricarboxylic acid cycle [78]. All these factors point to a substrate shift in the energy supply of cardiomyocytes, switching from glucose oxidation to beta-oxidation of fatty acids. In addition, there is extra evidence of a disruption in the intracellular insulin signalling pathway in both strains. For example, db/db mice demonstrate an impaired response to insulin stimulation [78] and increased serine residue (307) phosphorylation on insulin receptor substrate-1 (IRS-1) (a protein that plays a pivotal role in insulin signalling) in cardiomyocytes, with subsequent inactivation of the insulin receptor [80]. In addition, these mice have reduced activity of SIRT [silent mating type information regulation 2 homolog 1], which is responsible for the 'beneficial' tyrosine phosphorylation of IRS-1 required for normal insulin receptor function [91]. An increase in the serine-phosphorylated IRS-1 has also been found in ob/ob mice [96]. In general, impaired cardiac metabolism precedes the onset of hyperglycaemia and the development of insulin resistance in both db/db and ob/ob mice [80].

It is also worth mentioning that leptin is important for the maintenance of normal cardiac structure and function as it may have both direct and indirect (via neurohormonal regulation) antihypertrophic effects. Hence, leptin deficiency leads to LV hypertrophy [95,97]. ob/ob mice exhibit LV hypertrophy at 6 months of age, regardless of their weight [95]. Although weight loss by dietary restriction is associated with a reduction in LV hypertrophy, a much greater reduction in LV hypertrophy may be achieved by leptin administration [95]. In ob/ob mice, the cardiac response to beta-adrenergic stimulation was also reduced; administration of leptin partially restored the beta-adrenergic inotropic response [98].

In addition to HFpEF, some comorbidities consistent with those observed in humans are developed in these murine strains, the common comorbidities being the cardiometabolic phenotype of HFpEF which usually occurs in combination with obesity, T2DM and arterial hypertension. For example, in db/db mice, the development of arterial hypertension with age is associated with obesity and T2DM [83,85,88,92]. There is an increase in blood pressure starting at 11 weeks of age, and pronounced arterial hypertension is already present by 14 weeks of age as well. Developing arterial hypertension is associated with increased renin-angiotensin system activity while the baroreflex is not impaired. It is also worth noting that in db/db mice, renin-angiotensin-aldosterone system blockers do not improve metabolism and insulin sensitivity, i.e., they have no effect on hyperglycaemia [83]. Unlike db/db mice, blood pressure is not increased with age and may be even decreased in ob/ob mice [95,101]. Such differences may be related to the fact that the authors of ob/ob mice

studies have measured blood pressure in rather young mice (not older than 10–11 weeks), whereas the authors performing db/db mice studies measured blood pressure in aged mice (10 to 20 weeks). Perhaps, ob/ob mice develop arterial hypertension at a more "mature" age, especially taking into account that all the changes in these mice occurred later and were less pronounced than in db/db mice.

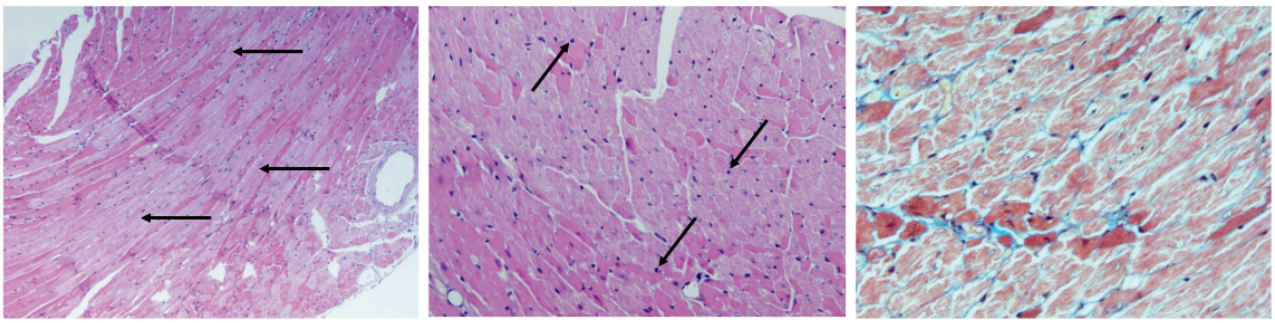
One more critical component of the pathogenesis of HFpEF is chronic low-grade inflammation [12] related to both db/db and ob/ob strains. It is also worth noting that the inflammation can be both systemic and myocardial. For example, the blood levels of the pro-inflammatory cytokines TNF and IL-6 are increased in db/db mice [103] and C-reactive protein—in ob/ob mice [102]. In the myocardium of ob/ob mice, RT-qPCR reveals increased mRNA of IL-1β, IL-6, TNF, NLRP3 and caspase-1 [102], and increased expression of the *TNF* and *MCP-1* genes in db/db mice [87]. According to other data, TNF, MCP-1, IL-1β and IL-6 mRNA content is increased in the adipose tissue but not in the myocardium of db/db mice [78]. However, no findings of any infiltration of the myocardium by macrophages are confirmed by the same authors [78]. In db/db mice, the enhanced NF-κB activity (assessed by the binding activity of free NF-κB p65 in nuclear extracts) and NF-κB p50 expression (determined by RT–qPCR and western blot) in LV tissue is detected. This was associated with increased ROS, superoxide, and peroxynitrite production by mitochondria. The addition of an NF- κB antagonist reduced the production of pro-inflammatory cytokines, protected the heart from oxidative stress, restored mitochondrial integrity, and reduced myocardial dysfunction [103].

Echocardiographic and invasive haemodynamic data confirm the presence of HFpEF characteristic features in both murine strains. In db/db mice, the development of first diastolic (increased early to late mitral inflow (E/A) ratio and early mitral inflow to mitral annulus relaxation velocity (E/e′) ratio, prolonged isovolumic relaxation time (IVRT), decreased tissue Doppler e′/a′ ratio) [78,86,88,89,91–93,104] and subsequently systolic (reduced shortening fraction, EF, velocity of circumferential fibre shortening) LV dysfunction [81,86] is typical. ob/ob mice also exhibit LV diastolic dysfunction (decreased E/A ratio), but there are conflicting data regarding systolic dysfunction [81,96,100–102]. Many studies in db/db mice [78,81,84,86,88,89,92,93,103,104] demonstrate echocardiographic and histological evidence of LV hypertrophy accompanied by the development of myocardial fibrosis (Figure 3). However, no confirmations were found in other studies [87,93]. Additionally, in female mice, myocardial fibrosis is much more pronounced than in male mice [84]. Some studies have reported reduced capillary density in the myocardium [88,93], while others have reported normal or even increased density [87,92]. ob/ob mice also demonstrate the signs of LV hypertrophy (by echocardiography and post-mortem heart weighing) [81,95,98]. However, in contrast to db/db mice, histological data are scarce and ambiguous. For example, according to some sources, ob/ob mice have no or negligible myocardial fibrosis [95,96]; according to other research, myocardial fibrosis is still present [102].

In these murine strains, the presence of LV diastolic dysfunction is confirmed by an increase in plasma BNP level, a biological marker of haemodynamic stress [92,100]. Increased expression of natriuretic peptide estimated by mRNA level has been reported in the myocardium of ob/ob mice [96]. In db/db female mice, there is a significant relative increase in myocardial BNP mRNA content with age which is not confirmed in males [84]. In contrast, another study describes reduced myocardial expression of natriuretic peptide in db/db mice [105].

It should be noted that db/db mice demonstrate sex differences in the development of HFpEF symptoms. Thus, female mice have higher blood pressure levels and greater weight gain than males. Moreover, they have more pronounced LV remodelling processes (more pronounced LV hypertrophy and diastolic dysfunction) [88]. Such differences are

indirectly in line with what is observed in humans where women are more likely to have severe HFpEF than men.



(**A**) (**B**) (**C**)

Figure 3. Histological sections of left ventricular myocardium from 14-month-old db/db mice (unpublished data by the authors). (**A**) Death of cardiomyocytes: areas of necrosis (arrows) appear lighter than living cells. Haematoxylin and eosin stain, 100× magnification. (**B**) Mononuclear leukocyte infiltration: leukocyte nuclei are indicated by arrows. Haematoxylin and eosin stain, 200× magnification. (**C**) Stromal fibrosis: Masson's trichrome stain (collagen is stained blue), 400× magnification.

It is important that an increased cardiomyocyte residual stress induced by altered protein function increases LV myocardial stiffness. The studies report a decreased mRNA and protein content of SERCA2a in the db/db myocardium [78,83,106]. However, other studies confirm the molecular expression of SERCA2a in these mice that does not differ from that in healthy mice [92,93]. In ob/ob mice, the total amount of SERCA2a in the myocardium is not increased, although its decreased activity and increased oxidation are observed. In fact, this is associated with a decreased calcium ion transport from the cytoplasm to the sarcoplasmic reticulum and calcium ion accumulation in the cytoplasm [99] contributing to cardiomyocyte residual stress. A lot of studies [78,92,93] in db/db mice demonstrate that the total amount of the SERCA activity regulator protein phospholamban in the myocardium, as determined by western blotting, is comparable with the control ones, except for one study [106]. Phosphorylation of phospholamban removes its blocking effect on SERCA2a, favouring the fastest possible release of calcium ions into the sarcoplasmic reticulum and accelerating myocardial relaxation. Phosphorylation of phospholamban at serine 16 and threonine 17 has been revealed to be impaired in both db/db and ob/ob mice resulting in delayed calcium efflux, disturbed relaxation and increased LV myocardial stiffness [92,93,96]. In ob/ob mice, leptin administration restores the levels of phosphorylated phospholamban [98]. db/db murine cardiomyocytes are characterised by an impaired response to extracellular calcium and reduced contractility [85,92,106].

Changes in titin molecules which are intracellular spring elements responsible for myocardial stretching during diastole play an important role in increasing myocardial stiffness. In db/db mice, titin changes are mainly due to its hypophosphorylation rather than oxidation or isoform shift from highly extensible N2A molecules to more 'rigid' N2B molecules [89]. In both db/db and ob/ob mice, a change in MHC expression pattern is understood as an isoform shift from a faster α-isoform to a slower β-isoform [80,99]. Such alterations in myocardial MHC isoforms can be detected in 4-week-old mice [80,96]. However, the myocardial levels of MHC-β mRNA in db/db mice are higher in males, while females demonstrate a more pronounced relative increase with age [84]. Simultaneously, another study in db/db mice reports reduced mRNA content of MHC-α and MHC-β [105]. Additionally, in the myocardial tissue of ob/ob mice, the activity of protein kinase A which is responsible for the phosphorylation of titin and other cardiac proteins is reduced [98]. AMP-activated protein kinase levels are also reduced in the myocardium of db/db and ob/ob mice resulting in hypophosphorylation of titin and increased myocardial

stiffness [78,79,87,91,93]. In contrast, no differences in the levels of the phosphorylated cardiac proteins myosin-binding protein C [cMYBP-C] and troponin I are observed in db/db mice [87,92].

Notably, mice of both strains have signs of dysfunction in the NO-cGMP-PKG signalling pathway that plays an essential role in normal myocardial function and has numerous beneficial effects such as accelerating relaxation, reducing cardiomyocyte stiffness, inhibiting pro-hypertrophic signalling, improving mitochondrial function, etc. [107]. Endothelium-dependent vasodilation is mediated by NO which is a potent relaxing factor. In the myocardium of db/db mice, both NO and nitrate levels (reflecting NO content) are reduced in comparison to those of healthy mice [91,92]. In db/db mice, there is a switch from NO-dependent to H_2O_2-dependent vasodilation contributing to impaired microvascular function [108]. The mRNA and protein content of different isoforms of NOS is altered in the myocardium of these mice, which is predominantly manifested by decreased expression of eNOS responsible for NO synthesis [79,105,108] and increased iNOS activity which is responsible for ROS generation [79,108]. Indeed, the decrease of cGMP protein level and cGMP-dependent PKG activity in the myocardium of db/db mice is also observed [89]. An indirect confirmation of the reduced NO bioavailability in db/db mice is confirmed by the disturbed myocardial perfusion observed in ex vivo and in vivo experiments [108].

The evidence of reduced NO bioavailability and impaired signalling through the intracellular NO-cGMP-PKG pathway is also confirmed in ob/ob mice. In particular, they have reduced levels of L-arginine which is a substrate for NOS, and increased levels of the NOS inhibitor asymmetric dimethylarginine [ADMA] in plasma [100]. In addition, ob/ob mice exhibit a reduced nitrate/nitrite ratio in heart homogenates which is a marker of ROS accumulation and reduced NO production [109]. However, other studies demonstrate an increased NO content in the myocardium [97]. A high level of iNOS and a low level of phosphorylated eNOS have been observed in the myocardium of ob/ob mice [97]. Unlike Guo W. et al. [97], these data are not confirmed when assessing eNOS mRNA levels by RT-qPCR. The same study illustrates a decrease in the content of neuronal NOS (nNOS) in the myocardium which can be restored after leptin administration [109].

Moreover, coronary microvascular dysfunction is observed in both ob/ob and db/db mice, most likely as a consequence of vascular tone-impaired regulation induced by reduced NO bioavailability [100]. To date, nitrosative/oxidative stress is a highly evident component of HFpEF pathophysiology [110] and its signs are found in the myocardium of both db/db and ob/ob strains. For example, an increase in NOX activity has been demonstrated in the myocardium of db/db mice. As a result, the binding of NO to superoxide (O_2^-) and subsequent formation of the cytotoxic reactive oxidant peroxynitrite (ONOO-) leads to protein dysfunction [78,103]. On top of that, levels of peroxynitrite are found to be elevated in the myocardium of both mouse strains [97,103]. The amount of protein carbonyls is increased in the myocardium of ob/ob mice indicating protein damage induced by oxidative stress [99]. High levels of the NOX1 and gp91phox (NOX2) subunits of NOX have been demonstrated in the myocardium of db/db mice [98]; however, mRNA content of the NOX2 subunit is higher in females [84]. Moreover, high expression of the membrane NOX subunits p47phox and gp91phox in ob/ob mice is revealed [99], although other studies have not confirmed this at either protein or mRNA level [109]. Nevertheless, increased activity of xanthine oxidoreductase [XOR] which is another likely source of ROS has been observed in ob/ob mice [109].

Furthermore, myocardial levels of the antioxidant glutathione (GSH), attributed to scavenging excess ROS, are reduced in db/db mice [103]. Glutathione is oxidised to glutathione disulfide (GSSG) during peroxide detoxification. A decrease in the GSH/GSSG

ratio indicating high oxidative stress activity is also shown in the myocardium of ob/ob mice [99,109]. In addition, the expression of superoxide dismutase 1 and heme oxygenase 1 which provide protection against oxidative stress is increased in the myocardium of db/db mice [87]. In turn, the activity of catalase which has antioxidant properties, is increased in db/db myocardium [84].

It should be also noted that oxidative stress results in lipid peroxidation. Thus, the levels of malonic dialdehyde, the end product of lipid peroxidation, and non-esterified fatty acids which are markers of oxidative stress are increased in db/db mice [84]. Remarkably, the levels of these substances are higher in female mice indicating that females undergo more oxidative stress than males [84]. Moreover, the increased levels of malonic dialdehyde are also confirmed in the myocardium of ob/ob mice [99].

In accordance with the experiments results, in the myocardium of db/db mice signs of increased endoplasmic reticulum stress are observed in the form of increased expression of phosphorylated protein kinase RNA-like endoplasmic reticulum kinase [PERK], inositol-requiring protein-1α [IRE-1], and eukaryotic initiation factor 2 [eIF2α] [85], or the unfolded protein response in the form of increased protein concentration of GRP78/94, XBP-1, and C/EBP homologous protein [90]. Similarly, signs of endoplasmic reticulum stress and unfolded protein response, i.e., the presence of phosphorylated PERK, eIF2α, and C/EBP homologous protein, are also observed in ob/ob mice [97].

It is well-known that ROS are generated in the mitochondria. In keeping with the above findings, db/db mice demonstrate signs of mitochondrial dysfunction, mainly at the level of complex I, as evidenced by increased levels of H_2O_2 (produced by complex I) and superoxide in mitochondria. Thus, an increased permeability of the mitochondrial membrane contributes to the uncoupling of oxidative phosphorylation and ATP synthesis and leads to the accumulation of ROS in cardiomyocytes [91,103]. There is also evidence of reduced enzymatic activity of complex III of the electron transport chain (the main source of O_2^-) in these mice [103], although this has not been fully confirmed [91].

2.1.2. HFD

Notably, C57BL/6J mice that are maintained on an HFD develop obesity [52,53,77,80,111–123] as glucose tolerance is impaired and insulin resistance results in elevated blood glucose and insulin levels [81,117–121,123,124]. These mice also have elevated blood levels of leptin which allows us to draw some parallels with obese humans [120,122]. Williams T.D. et al. highlight the development of arterial hypertension as one of the underlying conditions of this mouse model [116]. However, some authors have no confirmation of these data [124,125]. Such differences in blood pressure can be explained by the different HFD duration and the age of the mice. In all these studies, mice were switched to an HFD at the same age (5–6 weeks), but were followed for 12–15 weeks in one case [116] and for only 8 weeks in others [124,125]. It is possible that the increase in blood pressure in these mice occurs at a later age and with a longer period of time on a diet.

Yet, it is evident that HFD-fed mice show signs of systemic and local inflammation, the most important pathophysiological mechanism in the development and progression of HFpEF. In particular, they have an increased concentration of IL-6 in plasma [122] and NF-κB content in myocardial tissue [126] as well as increased IL-1β, IL-6, matrix metalloproteinase-9, plasminogen activator inhibitor-1, and adiponectin mRNA levels [120]. In fact, plasminogen activator inhibitor-1 is a key protein secreted by metabolically unhealthy visceral adipose tissue; its activation may contribute to HFpEF via accelerated ageing, inflammation, visceral adiposity, and impaired metabolism [127]. Moreover, histological examination demonstrates inflammatory cell infiltration in the myocardium and liver of these mice [117].

According to echocardiography, magnetic resonance imaging, and invasive haemodynamic studies, HFD mice demonstrate signs of LV diastolic dysfunction (decreased mitral velocity E, E/A and e′/a′ ratios, increased E/e′ ratio, prolonged IVRT) after 8 weeks on an HFD. At the same time, systolic function either is not altered significantly or worsened (reduced shortening fraction and EF) [81,119,121,123,124,126]. In addition to LV diastolic dysfunction, LV hypertrophy is identified according to echocardiography, magnetic resonance imaging, post-mortem weighing and histological examination in HFD-fed mice as well as myocardial fibrosis according to histological examination [119,121,123–126]. Within this concept, some researchers have demonstrated increased content of the pro-fibrotic factors TGF-β and phosphorylated Smad3 in the myocardium and decreased content of the anti-fibrotic factors bone morphogenetic protein-2 and phosphorylated Smad1/5 [120].

In HFD-fed mice, cardiac protein function has not been investigated as extensively as in db/db and ob/ob strains. Nevertheless, similar phenomena can be observed among the three models. For instance, the expression of SERCA2a is not significantly altered in all three models. However, the level of phosphorylated phospholamban which regulates SERCA2a and cardiac troponin T activity in the myocardium is reduced [121].

Furthermore, the signs of altered NO-cGMP-PKG signalling in the myocardium are proved in HFD-fed mice bringing this model closer to the db/db and ob/ob strains. Specifically, the content of nNOS and phosphorylated eNOS (with normal levels of total eNOS) is suppressed in HFD-fed mice [124,126]. Additionally, these mice have impaired endothelium-dependent vasodilation [122,128] and increased myocardial mRNA levels of the endothelial dysfunction markers endothelin-1 and angiotensin II type 1 receptor [120].

In addition to the db/db and ob/ob strains, HFD-fed mice also demonstrate signs of oxidative stress. For instance, they have increased levels of ROS and nitrotyrosine in the cytoplasm and mitochondria of cardiomyocytes, and high content of NOX1, NOX2 and NOX4 in the myocardium [120,122,124,126]. To compensate, myocardial antioxidants such as superoxide dismutase may be accumulated [121]. However, in other studies, superoxide dismutase levels remain unchanged [123,126] although another antioxidant, GSH, is decreased [123].

HFD-fed mice have pathological changes in the structure of cardiomyocyte mitochondria and an increased ratio of intracellular nicotinamide adenine dinucleotide phosphate [NADH] to nicotinamide adenine dinucleotide+ [NAD+] levels in the myocardium. This is indicative of mitochondrial oxidative stress and points to disturbances in the electron transport chain as a major source of ROS in the myocardium [124]. Other research in HFD-fed mice indicates that the permeability of myocardial mitochondrial membranes remains unchanged. The expression of uncoupling protein 3 [UCP3] crucial for electron transport chain disruption and oxidative phosphorylation uncoupling is similar to controls. Additionally, oxygen consumption in isolated cardiac mitochondria is not reduced [121]. Besides the myocardium, aortic protein levels of gp91phox and p47phox, subunits of NOX, are increased in these mice [122].

In obesity, HFD-fed mice exhibit a variety of metabolic disorders: plasma cholesterol, uric acid, triglycerides, and fatty acids; LDL levels are elevated compared to mice fed a healthy diet [117–119,121,122]. Myocardial lipid accumulation and fatty deposits in the liver (signs of steatosis) are also observed in this mouse strain [117–119,121]. Noticeably, activation of pro-apoptotic pathways is a molecular hallmark of HFD-fed mice. In particular, an increased expression of the pro-apoptotic *Bax* and caspase-3 and a decrease in the anti-apoptotic B-cell lymphoma 2 [*Bcl-2*] as well as an increase in pro-apoptotic procaspase-9 and caspase-9 expression are found in the myocardium of these mice [120,121].

2.2. Hypertension-Induced HFpEF Models

It has been established that arterial hypertension is a major risk factor for HFpEF, influencing both its development and prognosis.

2.2.1. DOCA + High Salt Diet + Unilateral Nephrectomy [DOCA]

The DOCA model mimics the development of arterial hypertension as a result of mineralocorticoid excess reproducing only one component of HFpEF pathophysiology, specifically arterial hypertension. Given the simplicity, these mice can be employed to replicate multi-component models of HFpEF when combined with other risk factors.

The DOCA mice subjected to pellet implantation with a gradual release of DOCA and unilateral nephrectomy after being fed a high salt diet develop arterial hypertension within 3–7 days after surgery [129–133]. Simultaneously, it has been observed that male mice exhibit higher blood pressure levels compared to females [134]. Blood pressure elevation is associated with kidney damage [129] being more pronounced in male mice [134]. DOCA mice also demonstrate signs of pulmonary hypertension. This is most likely secondary to heart failure (left-sided pulmonary hypertension) [129]. No differences in body weight are observed in this mouse model [135]. Although initially these mice were used exclusively for hypertension modelling, they now are often considered as one of the relevant HFpEF models. This can be explained by the fact that the heart is a typical target organ of arterial hypertension, and hypertension itself is a major risk factor for the development of HFpEF [136].

Echocardiography and invasive haemodynamic studies show these mice have LV diastolic dysfunction (low e′ velocity, high E/e′ ratio and prolonged IVRT), sometimes with mild systolic dysfunction (low EF) [129,132,133,137]. Additionally, LV hypertrophy being more pronounced in male mice and myocardial fibrosis not being examined in detail in all studies are reported according to echocardiography, post-mortem weighing, and histological examination [129–132,134,138]. Moreover, one study reports higher TGF-β expression in male mice myocardium [134]. Some authors demonstrate lower myocardial capillary density [129], but others fail to confirm this [138].

Previously, the DOCA model considered only mechanical damage caused by volume overload of target organs including the heart. Similar to patients with arterial hypertension, these mice demonstrate signs of myocardial inflammation. For example, pro-inflammatory cytokines mRNA such as IL-1β, IL-6, IL-10, TNF, and MCP-1 (only in male mice) are detected alongside macrophage accumulation in the myocardium [129,130,134]. Furthermore, these mice exhibit signs of vascular inflammation as manifested by increased IL-1β, TNF, and MCP-1 mRNA content in the aortic wall [131].

In addition to the echocardiography and histological data, other signs of HFpEF have been established in this model, in particular, an increased expression of the haemodynamic stress marker atrial natriuretic peptide (ANP) in the myocardium [129,134,139]. Furthermore, male mice show a greater relative increase in ANP than females [134]. One study reported an increase in BNP expression [129], while other studies have not confirmed this [134,139].

Regarding myocardial protein dysfunction, the DOCA model has not been investigated in detail. However, one study has reported a down-regulation of phospholamban phosphorylation [133]. The signs of the NO-cGMP-PKG pathway dysfunction in the myocardium, i.e., decreased NO levels [140] and increased levels of oxidised tetrahydrobiopterin (a cofactor of eNOS) are confirmed in DOCA mice. As such, these alterations promote subsequent substrate uncoupling of eNOS [133] and expression of iNOS [132], and reduced expression of eNOS [140] (although the latter has not been demonstrated in all studies) [132]. Moreover, a low level of eNOS mRNA has also been found in the aorta [131].

As anticipated, DOCA mice demonstrate signs of oxidative stress in the myocardium and vessels. In particular, the levels of superoxide and nitrotyrosine are increased in their myocardium [132,133,140]. However, myocardial mRNA levels of p22phox, gp91phox (NOX2) and NOX4 are not significantly altered distinguishing these mice from the above-described models [138]. Some authors suggest that NOS may be the main source of superoxide in DOCA mice [133]. Thus, in iNOS knockout mice, myocardial relaxation is less impaired, myocardial nitrotyrosine content is lower, and eNOS expression tends to be higher compared to non-knockout mice. Therefore, these findings indirectly support the involvement of iNOS in ROS production [132]. In addition, superoxide levels and the expression of gp91phox and p22phox in the aorta are also increased in this murine model [131,141,142]. Some authors propose that these changes are more pronounced in male mice than in female mice which were similar to the control group in several parameters [134]. This is not exactly in line with what is observed in HFpEF patients where women with the cardiometabolic phenotype are more likely to have a higher incidence and severity of HFpEF compared to men.

This model may better suit the cardiorenal phenotype of HFpEF, characterised by high blood pressure and kidney damage which occurs equally in men and women. However, it is too early to draw any conclusions about the suitability of this model for HFpEF as it has not been well studied as a model for HFpEF. Furthermore, it should be noted that the C57BL/6 mouse strain is quite resistant to the development of arterial hypertension and kidney damage [135]. In this case, the 129/Sv murine strain is most susceptible, with arterial hypertension, LV hypertrophy, and kidney damage being more pronounced than in the C57BL/6 strain [135].

2.2.2. Angiotensin II (Angiotensin II Infusion) [Ang II]

Ang II mice are implanted with an osmotic mini-pump that infuses angiotensin II. The development of arterial hypertension occurs within one week of starting angiotensin II infusion [142,143]. Ang II mice are also not well characterised as a model of arterial hypertension as angiotensin II infusion alone may not be sufficient to mimic arterial hypertension because of the resistance of the C57BL/6 strain to hypertensive organ damage. However, higher levels of blood pressure are observed in the Ang II model compared to the DOCA model as pointed out by some authors [139].

The signs of LV diastolic dysfunction (verified by IVRT prolongation) without systolic dysfunction are described in the Ang II model even with the administration of low doses of angiotensin II insufficient to raise blood pressure [144]. This observation suggests that inflammation and/or metabolic disturbances, rather than mechanical or haemodynamic factors (increase in afterload and preload) are crucial in developing HFpEF. In the above experiment [144], LV filling abnormalities at low doses of angiotensin II infusion may be due to its pro-inflammatory properties.

Consistent with the prior studies, angiotensin II also stimulates NOX in inflammatory cells leading to ROS accumulation. Adoptive transfer of T-cells lacking the angiotensin type I receptor blunts angiotensin II-dependent hypertension and reduces aortic superoxide production [142]. Myocardial infiltration by CD68+ macrophages and increased myocardial protein expression of the pro-inflammatory cytokines TNF and IL-1β is also observed in the Ang II model [143]. This provides further evidence for the involvement of inflammation in the development of HFpEF.

As in other models of HFpEF, histological examination reveals hypertrophy and fibrosis of the LV myocardium [143,144]. Furthermore, fibrosis is more pronounced in the Ang II model than in the DOCA model [140]. In addition, the expression of ANP and BNP and the MHC-α/MHC-β ratio are increased in the myocardium to a greater extent

than in the DOCA mice [139]. These mice also show impaired endothelium-dependent vasodilation and increased ROS production in the aorta [142,143].

2.2.3. DOCA + High Salt Diet + Angiotensin II + Unilateral Nephrectomy [DOCA + Ang II]

The DOCA + Ang II model has been developed in order to overcome the resistance of the C57BL/6 strain to hypertensive organ damage, in particular, kidneys. It has also been understudied and poorly characterised as a model of HFpEF, as are all hypertensive models. Obviously, many abnormalities appear to be more pronounced in the DOCA + Ang II model compared to the DOCA or Ang II models alone [139]. They include high blood pressure, histochemical and laboratory signs of renal damage, severity of LV hypertrophy and fibrosis, increase in myocardial expression of ANP and BNP, and MHC-β/MHC-α ratio [139].

2.2.4. Transverse Aortic Constriction (TAC)

TAC mice undergo ligation of the aortic arch between the bronchopulmonary trunk and the left common carotid artery to induce the development of pressure overload-induced cardiac hypertrophy and HF. The body weight of TAC mice is comparable to that of intact animals [145]. Yet, the TAC model is widely utilised to study arterial hypertension. Moreover, it is actively used as a model for HFpEF demonstrating LV filling abnormalities. The obvious disadvantage of the TAC model as well as other above-mentioned models of HF induced by arterial hypertension is the reproduction of only one clinical aspect of HFpEF, specifically pressure overload. In some hypertensive models, TAC mice show signs of pulmonary oedema, fibrosis, and pulmonary vasculature remodelling (according to the histological study) [146]. These changes are likely to result from LV dysfunction.

Data published indicate that the TAC model typically develops LV diastolic dysfunction shown by a shortened deceleration time of early diastolic mitral flow followed by systolic dysfunction indicated by reduced EF and shortening fraction [132,140–145]. It should be noted that most of these studies did not evaluate the most important diastolic parameters such as the E/A, E/e′, e′/a′ ratios, and IVRT. Moreover, LV hypertrophy is confirmed in TAC mice according to echocardiography, post-mortem weighing and histological examination [138,145–151].

Histological studies also conclude the development of myocardial fibrosis in TAC mice providing an increased expression of TGF-β by myocardial cells [138,145,147,149]. In addition, there is a decrease in the density of capillaries in the myocardium [138]. Increased production of ANP and BNP in the myocardium is another sign of HF [147,149].

Limited data exist on contractile protein expression patterns for the TAC model. In particular, an increase in MHC-β content is found indicating a shift from fast MHC-α to slower MHC-β isoform. It should be noted that these changes have also been observed in other HF models as well [147]. In addition, phosphorylation of ryanodine receptor type 2 [RYR2], the major intracellular calcium release channel in the cardiac sarcoplasmic reticulum, and the calcium transport regulatory protein phospholamban are reduced [151].

The TAC model also demonstrates some evidence of NO-cGMP-PKG pathway dysfunction in the myocardium: although total eNOS and nNOS levels are comparable with the control ones, the phosphorylation of eNOS on Ser114 and nNOS on Ser1412 is reduced [145].

Additionally, this model has evidence of myocardial oxidative stress: increased ROS, decreased nitrate/nitrite ratio (a marker of increased ROS and decreased NO production), activity of the antioxidant enzyme superoxide dismutase, and GSH/GSSG ratio [145,147]. Thus, this evidence suggests a depletion of antioxidant systems [149].

2.2.5. TAC + DOCA

TAC + DOCA mice undergo ligation of the aortic arch followed by the implantation of a DOCA pellet. The development of diastolic dysfunction and increased LV filling pressure,

but preserved systolic function is characteristic of this model [152–154]. Obviously, such changes are more pronounced in TAC + DOCA than in TAC or DOCA models alone [138].

Furthermore, histological studies of the myocardium reveal hypertrophy, fibrosis, and reduced capillary density [138,153,154]. These phenomena occur in patients with HFpEF [155].

It is important to note that TAC + DOCA mice gather reduced exercise tolerance over time [152,154]. In addition, this model also shows signs of oxidative stress in the myocardium manifested by an increase in mRNA levels of p22phox, gp91phox (NOX2) and NOX4 (NOX subunit) [138].

2.3. HFpEF as a Result of Accelerated Ageing (The Senescence-Accelerated Mice)

Ageing is a significant risk factor for heart failure, with HFpEF becoming more common due to age-related conditions.

The SAMP8 murine strain derived from AKR/J mice is known for accelerated senescence, with an average lifespan of 9.7 months [156]. There are over a dozen accelerated ageing lines, but SAMP8 is commonly used. Six-month-old SAMP8 mice exhibit early indicators of ageing [157]. Unlike humans, where age correlates with arterial hypertension and HFpEF risk, blood pressure is not elevated [157]. Therefore, it was initially utilised only to study the ageing process.

Despite the fact that ageing affects the heart, being an independent risk factor for the development of HFpEF, limited information regarding HF pathophysiology is provided in this model. In particular, there are no data on whether myocardial proteins involved in contraction/relaxation and regulation of intracellular calcium turnover are altered.

Following echocardiography and invasive haemodynamic study, LV diastolic dysfunction (decreased E/A and e′/a′ ratios) is developed by 6 months of age in SAMP8 mice, but the systolic function remains preserved [157].

According to post-mortem weight data, LV hypertrophy is proved in this strain [157,158]. Histological examination reveals myocardial fibrosis [157,159], and up-regulation of profibrotic TGF-β is confirmed in heart tissue [157]. In addition, the ANP mRNA content is increased in the myocardium of SAMP8 mice [158].

As stated before, ageing is associated with the development of chronic inflammation. In the SAMP8 mice, signs of inflammation can be detected in the myocardium, in particular, increased mRNA levels of the pro-inflammatory cytokines TNF, IL-1 and IL-6 and increased mRNA and protein levels of the p50 and p52 subunits of NF-κB [159,160]. In contrast, other data have shown that these mice are comparable with control ones in terms of NF-κB activity and expression of TNF and MCP-1 [158].

The SAMP8 strain also demonstrates signs of myocardial NO-cGMP-PKG pathway dysfunction (down-regulation of eNOS, and up-regulation of iNOS) as well as evidence of oxidative damage to cardiomyocyte DNA [159,160]. On the other hand, there is evidence for an elevated expression of myocardial haem oxygenases 1 and 2 which may protect cells from the pathological action of ROS [160].

Senescence-accelerated mice often develop both senescent amyloidosis and secondary AA amyloidosis [161]. They are susceptible to lymphoma, inflammation (colitis, pneumonia, abscesses), and renal failure [161]. The molecular features of the SAMP8 model are a decrease in the anti-apoptotic B-cell lymphoma 2 [*Bcl2*] expression and an increase in the pro-apoptotic Bcl-2 associated X-protein [*BAX*] expression [161] as well as an increase in the activity of the pro-apoptotic caspase 3 [159–161].

Table 1 summarises HFpEF manifestations in mouse models.

Table 1. HFpEF manifestations in mouse models.

	db/db	ob/ob	HFD	DOCA	Ang II	DOCA + Ang II	TAC	TAC + DOCA	SAMP
Systemic inflammation signs	+			no data					
Myocardial inflammation signs	+				+/− (limited data)	no data			+
Myocardial hypertrophy	Described for all models								
Myocardial oxidative stress	+				no data		+/− (limited data)		
Myocardial NO-cGMP-PKG signalling pathway dysfunction	+	+/− (limited data)			no data		+/− (limited data)	no data	+/− (limited data)
Structural and functional alterations in cardiomyocyte contractile proteins	+		+/− (limited data)					no data	
Myocardial fibrosis signs	+	+/− (limited data)	+						
Diastolic dysfunction signs (according to echocardiographic data)	+				+/− (limited data)	no data	+/− (limited data)		
Elevated ANP/BNP in myocardial tissue and/or blood	+		no data	+	+/− (limited data)		+	no data	+/− (limited data)
Gender differences	+ (females show more pronounced changes)	+/− (limited data, females show more pronounced changes)	no data	+/− (limited data, males show more pronounced changes)	no data				

ANP—atrial natriuretic peptide; BNP—brain natriuretic peptide. Murine models: Ang II—angiotensin II infusion; db/db—leptin receptor-deficient strain; DOCA—chronic subjection to deoxycorticosterone acetate; HFD—high-fat diet; ob/ob—leptin-deficient strain; SAMP—senescence-accelerated prone strain; TAC—transverse aortic constriction.

3. Limitations of HFpEF Murine Models

According to data published, the db/db and ob/ob lines most accurately replicate the cardiometabolic characteristics typical of HFpEF among all the murine models. These strains represent the most well-characterised models examined in this review. Consequently, they illustrate sex differences in the onset and progression of HFpEF that closely resemble its clinical course in humans. The db/db strain shows a rapid development of pathological changes. In contrast, people with HFpEF experience a slower progression of these changes. ob/ob mice show slower pathological changes making them more comparable to humans. Another drawback of the db/db and ob/ob strains is their infertility which creates challenges in breeding these models. In the ob/ob strain, this issue can be addressed with leptin administration. The HFD model is simpler and more accessible resembling natural conditions, but it has been studied less extensively than the db/db and ob/ob strains. Furthermore, HFD mice likely do not exhibit sex differences in pathological manifestations and thus, they may not accurately replicate the human clinical progression of HFpEF. Next, DOCA and Ang II models serve as representations of isolated arterial hypertension. Available data indicate that these models primarily involve vascular and renal systems rather than cardiac involvement; however, there are instances where inflammation is observed in the myocardium. The DOCA and Ang II models can be effectively utilised to investigate isolated arterial hypertension as a contributing factor to HFpEF. Further studies are needed to better characterise them. Aortic ligation models are the least characterised murine models for inflammation in HFpEF development. Thus, isolated aortic ligation is seen as a 'mono' model as it is neither 'natural' nor easy to perform. Although the addition of DOCA infusion to aortic ligation may have potential benefits, current data on the TAC + DOCA model are insufficient to assess its appropriateness for studying HFpEF. Finally, accelerated ageing models can study HFpEF's age-related characteristics, but they remain poorly understood. Additionally, 'genetically accelerated' ageing is an artificial process, and these mice do not have T2DM, obesity, or arterial hypertension which are characteristics of patients with HFpEF. It is also noticeable that elderly patients with HFpEF and no cardiometabolic comorbidities are rarely seen in clinical practice.

Table 2 provides a summary of the reasons for the limited use of murine models in the study of HFpEF.

Table 2. Limitations of HFpEF murine models.

	Model Limitations in Data Translation to Humans	**Challenges of Practical Application**
db/db, ob/ob	Rather rapid development of obesity and insulin resistance, which is unlike typical human conditions	Homozygote infertility increases breeding costs
HFD	Possible development of systolic dysfunction	Duration of follow-up
DOCA, Ang II, DOCA + Ang II	Elevated blood pressure is a significant factor in the onset of human damage, including the progression to heart failure	Duration of follow-up (the C57BL/6 strain is fairly resistant to arterial hypertension development and hypertensive damage)
TAC	Primarily hypertensive organ damage, with indication of systolic dysfunction	The need for surgical intervention
TAC + DOCA	Primarily hypertensive organ damage	
SAMP	Early manifestations of inflammatory damage in various organs, neurodegeneration, age-associated lymphoproliferative conditions preceding the development of heart failure	Difficulties in breeding and housing animals due to short fertility period and high mortality rate

Abbreviations are the same as those in Table 1.

In summary, murine models of HFpEF do not fully reflect the cardiometabolic phenotype of HFpEF in humans, as evidenced by discrepancies between clinical trials and experimental data. Currently, research is being conducted on the use of SGLT2 inhibitors

and GLP-1 receptor agonists in the treatment of HFpEF. Randomised clinical trials have shown SGLT2 inhibitors improve cardiovascular outcomes in HFpEF patients [162,163], although experimental results have been inconsistent.

In HFD mice, SGLT2 inhibitors effectively reduce diastolic dysfunction, myocardial hypertrophy and fibrosis, mRNA for inflammatory and fibrosis markers as well as myocardial ROS production [164,165]. In db/db and ob/ob mice, empagliflozin improves LV diastolic function and reduces oxidative stress, mitochondrial dysfunction and ANP and BNP mRNA, although its effect on myocardial hypertrophy and fibrosis is unclear [91,166,167]. However, in TAC mice, empagliflozin shows no impact on LV diastolic dysfunction or myocardial hypertrophy and fibrosis severity [168].

Recent clinical trials show GLP-1 receptor agonists are effective for obesity-related HFpEF [169]. In mice, these drugs are most effective with Ang II and HFD models. Liraglutide partially prevented LV diastolic dysfunction in AngII mice and improved it in HFD mice, also reducing cardiomyocyte hypertrophy and cardiac fibrosis, and enhancing exercise tolerance [170,171]. In accordance with the functional improvements, semaglutide treatment in aged female C57BL6/J mice with HFD and angiotensin II infusion resulted in reduced LV hypertrophy and fibrosis, decreased RNA levels of fibrosis markers, and lower levels of inflammatory markers in the myocardium [172]. However, effects were not reproducible in the db/db model [171].

The presence of this class of drugs in HFD mice, as opposed to their absence in models of genetic obesity, indicates pathophysiological differences in the development of HFpEF between mice and humans. This distinction impacts the translational potential of experimental (mouse) data.

4. Conclusions and Future Perspectives

In conclusion, HFpEF remains a complex and multifaceted condition with significant clinical and social impact. A better understanding of the mechanisms underlying the pathophysiology of HFpEF depends on the quality and comprehensiveness of basic, translational, and clinical research. The murine models described in this review reproduce classic risk factors for the development of HFpEF, such as arterial hypertension, obesity, T2DM and ageing, and will undoubtedly contribute to a better understanding of different aspects of HFpEF and help develop new treatment strategies (Figure 4). However, these models have several disadvantages. First, they do not replicate additional cardiac and non-cardiac impairments found in human HFpEF, such as atrial fibrillation, renal dysfunction, and chronic obstructive pulmonary disease [57]. Second, the lack of extensive characterisation of certain models hinders their potential for further investigation as models for HFpEF. Additionally, several murine models may develop LV systolic dysfunction over time which is more typical of 'mono' models with isolated pressure overload or insulin resistance. It is worth noting that in complex models, LV systolic function typically remains preserved into advanced age [59].

The figure illustrates the key pathophysiological mechanisms involved in the cardiometabolic phenotype of heart failure with preserved ejection fraction (HFpEF). Understanding these mechanisms is crucial for developing targeted therapeutic strategies for HFpEF. Abbreviations are the same as those in Table 1.

Further research should explore these models and their translational potential to bridge the gap between preclinical findings and clinical applications.

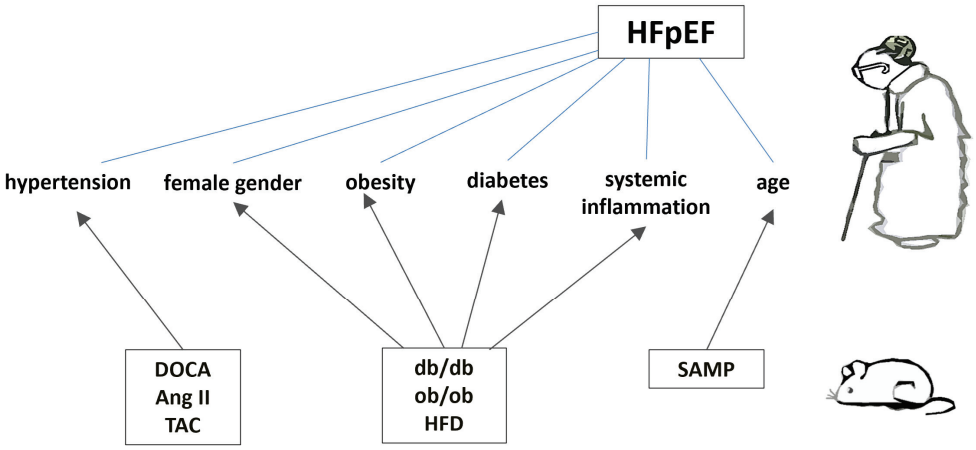


Figure 4. Pathophysiological Mechanisms in Cardiometabolic HFpEF and related murine models.

Author Contributions: Conceptualisation, T.A. and A.O.; literature search, writing—original draft preparation, E.O. and A.F.; writing—review and editing, A.F., N.R., T.A. and A.O.; supervision, T.A. and A.O.; funding acquisition, T.A. and A.O. All authors have read and agreed to the published version of the manuscript.

Funding: This research was funded by the Russian Science Foundation, grant number 24-75-00053.

Acknowledgments: The authors extend their gratitude to Elena Zwaan and Olga Filatova for their assistance with the English editing of the manuscript.

Conflicts of Interest: The authors declare no conflicts of interest.

Abbreviations

The following abbreviations are used in this manuscript:

ADMA	Asymmetric dimethylarginine
ANP	Atrial natriuretic peptide
Bcl-2	anti-apoptotic B-cell lymphoma 2
BNP	Brain natriuretic peptide
cGMP	Cyclic guanosine monophosphate
cMYBP-C	Myosin-binding protein C
DOCA	Deoxycorticosterone acetate
eIF2α	Eukaryotic initiation factor 2
eNOS	Endothelial nitric oxide synthase
GSH	Glutathione
GSSG	Glutathione disulfide
HF	Heart failure
HFD	High-fat diet
HFpEF	Heart failure with preserved ejection fraction
HFrEF	Heart failure with reduced ejection fraction
IL	Interleukin
IRE-1	Inositol-requiring protein-1α
iNOS	Inducible nitric oxide synthase
IRS-1	Insulin receptor substrate-1
IVRT	Isovolumic relaxation time
LV	Left ventricular
MCP-1	Monocyte chemotactic protein-1
MHC	Myosin heavy chain
NAD+	Nicotinamide adenine dinucleotide phosphate
NADH	Nicotinamide adenine dinucleotide phosphate
nNOS	Neuronal nitric oxide synthase

NO	Nitric oxide
NOX	Nicotinamide adenine dinucleotide phosphate oxidase
NT-proBNP	N-terminal fragment of brain natriuretic hormone precursor
PERK	Protein kinase RNA-like endoplasmic reticulum kinase
PKG	Protein kinase G
ROS	Reactive oxygen species
SAMP	Senescence-accelerated prone strain
SERCA	Sarco-endoplasmic reticulum Ca^{2+}-ATPase
SIRT	Silent mating type information regulation 2 homolog 1
T2DM	Type 2 diabetes mellitus
TAC	Transverse aortic constriction
TGF	Transforming growth factor
TNF	Tumour necrosis factor
XOR	Xanthine oxidoreductase

References

1. Vasan, R.S.; Xanthakis, V.; Lyass, A.; Andersson, C.; Tsao, C.; Cheng, S.; Aragam, J.; Benjamin, E.J.; Larson, M.G. Epidemiology of Left Ventricular Systolic Dysfunction and Heart Failure in the Framingham Study: An Echocardiographic Study over 3 Decades. *JACC Cardiovasc. Imaging* **2018**, *11*, 1–11. [CrossRef] [PubMed]
2. Borlaug, B.A.; Jensen, M.D.; Kitzman, D.W.; Lam, C.; Obokata, M.; Rider, O.J. Obesity and heart failure with preserved ejection fraction: New insights and pathophysiological targets. *Cardiovasc. Res.* **2023**, *118*, 3434–3450. [CrossRef]
3. Shah, K.S.; Xu, H.; Matsouaka, R.A.; Bhatt, D.L.; Heidenreich, P.A.; Hernandez, A.F.; Devore, A.D.; Yancy, C.W.; Fonarow, G.C. Heart Failure with Preserved, Borderline, and Reduced Ejection Fraction: 5-Year Outcomes. *J. Am. Coll. Cardiol.* **2017**, *70*, 2476–2486. [CrossRef]
4. Heidenreich, P.A.; Bozkurt, B.; Aguilar, D.; Allen, L.A.; Byun, J.J.; Colvin, M.M.; Deswal, A.; Drazner, M.H.; Dunlay, S.M.; Evers, L.R.; et al. 2022 AHA/ACC/HFSA Guideline for the Management of Heart Failure: Executive Summary: A Report of the American College of Cardiology/American Heart Association Joint Committee on Clinical Practice Guidelines. *Circulation* **2022**, *145*, e876–e894. [CrossRef] [PubMed]
5. McDonagh, T.A.; Metra, M.; Adamo, M.; Gardner, R.S.; Baumbach, A.; Böhm, M.; Burri, H.; Butler, J.; Čelutkienė, J.; Chioncel, O.; et al. ESC Scientific Document Group. 2021 ESC Guidelines for the diagnosis and treatment of acute and chronic heart failure. *Eur. Heart J.* **2021**, *42*, 3599–3726. [CrossRef] [PubMed]
6. Bozkurt, B.; Coats, A.; Tsutsui, H.; Abdelhamid, C.M.; Adamopoulos, S.; Albert, N.; Anker, S.D.; Atherton, J.; Böhm, M.; Butler, J.; et al. Universal definition and classification of heart failure: A report of the Heart Failure Society of America, Heart Failure Association of the European Society of Cardiology, Japanese Heart Failure Society and Writing Committee of the Universal Definition of Heart Failure: Endorsed by the Canadian Heart Failure Society, Heart Failure Association of India, Cardiac Society of Australia and New Zealand, and Chinese Heart Failure Association. *Eur. J. Heart Fail.* **2021**, *23*, 352–380. [CrossRef]
7. Shah, S.J.; Kitzman, D.W.; Borlaug, B.A.; van Heerebeek, L.; Zile, M.R.; Kass, D.A.; Paulus, W.J. Phenotype-Specific Treatment of Heart Failure with Preserved Ejection Fraction: A Multiorgan Roadmap. *Circulation* **2016**, *134*, 73–90. [CrossRef]
8. Anker, S.D.; Butler, J.; Filippatos, G.; Ferreira, J.P.; Bocchi, E.; Böhm, M.; Brunner-La Rocca, H.P.; Choi, D.J.; Chopra, V.; Chuquiure-Valenzuela, E.; et al. Empagliflozin in Heart Failure with a Preserved Ejection Fraction. *N. Engl. J. Med.* **2021**, *385*, 1451–1461. [CrossRef]
9. Solomon, S.D.; McMurray, J.; Claggett, B.; de Boer, R.A.; DeMets, D.; Hernandez, A.F.; Inzucchi, S.E.; Kosiborod, M.N.; Lam, C.; Martinez, F.; et al. Dapagliflozin in Heart Failure with Mildly Reduced or Preserved Ejection Fraction. *N. Engl. J. Med.* **2022**, *387*, 1089–1098. [CrossRef]
10. Solomon, S.D.; McMurray, J.; Vaduganathan, M.; Claggett, B.; Jhund, P.S.; Desai, A.S.; Henderson, A.D.; Lam, C.; Pitt, B.; Senni, M.; et al. Finerenone in Heart Failure with Mildly Reduced or Preserved Ejection Fraction. *N. Engl. J. Med.* **2024**, *391*, 1475–1485. [CrossRef]
11. Redfield, M.M.; Borlaug, B.A. Heart Failure with Preserved Ejection Fraction: A Review. *JAMA* **2023**, *329*, 827–838. [CrossRef] [PubMed]
12. Ovchinnikov, A.G.; Arefieva, T.I.; Potekhina, A.V.; Filatova, A.Y.; Ageev, F.T.; Boytsov, S.A. The Molecular and Cellular Mechanisms Associated with a Microvascular Inflammation in the Pathogenesis of Heart Failure with Preserved Ejection Fraction. *Acta Naturae* **2020**, *12*, 40–51. [CrossRef]
13. Schiattarella, G.G.; Rodolico, D.; Hill, J.A. Metabolic inflammation in heart failure with preserved ejection fraction. *Cardiovasc. Res.* **2021**, *117*, 423–434. [CrossRef]

14. Schiattarella, G.G.; Alcaide, P.; Condorelli, G.; Gilette, T.G.; Heymans, S.; Jones, A.; Kallikourdis, M.; Lichtman, A.; Marelli-Berg, F.; Shah, S.; et al. Immunometabolic mechanisms of heart failure with preserved ejection fraction. *Nat. Cardiovasc. Res.* **2022**, *1*, 211–222. [CrossRef]
15. Higashi, Y. Roles of oxidative stress and inflammation in vascular endothelial dysfunction-related disease. *Antioxidants* **2022**, *11*, 1958. [CrossRef] [PubMed]
16. Kovács, Á.; Alogna, A.; Post, H.; Hamdani, N. Is enhancing cGMP-PKG signalling a promising therapeutic target for heart failure with preserved ejection fraction? *Neth. Heart J.* **2016**, *24*, 268–274. [CrossRef] [PubMed]
17. Putko, B.N.; Wang, Z.; Lo, J.; Anderson, T.; Becher, H.; Dyck, J.; Kassiri, Z.; Oudit, G.Y.; Alberta HEART Investigators. Circulating levels of tumor necrosis factor-alpha receptor 2 are increased in heart failure with preserved ejection fraction relative to heart failure with reduced ejection fraction: Evidence for a divergence in pathophysiology. *PLoS ONE* **2014**, *9*, e99495. [CrossRef]
18. Tromp, J.; Khan, M.; Klip, I.T.; Meyer, S.; de Boer, R.A.; Jaarsma, T.; Hillege, H.; van Veldhuisen, D.J.; van der Meer, P.; Voors, A.A. Biomarker Profiles in Heart Failure Patients with Preserved and Reduced Ejection Fraction. *J. Am. Heart Assoc.* **2017**, *6*, e003989. [CrossRef]
19. Santhanakrishnan, R.; Chong, J.P.; Ng, T.P.; Ling, L.H.; Sim, D.; Leong, K.T.; Yeo, P.S.; Ong, H.Y.; Jaufeerally, F.; Wong, R.; et al. Growth differentiation factor 15, ST2, high-sensitivity troponin T, and N-terminal pro brain natriuretic peptide in heart failure with preserved vs. reduced ejection fraction. *Eur. J. Heart Fail.* **2012**, *14*, 1338–1347. [CrossRef]
20. Sanders-van Wijk, S.; van Empel, V.; Davarzani, N.; Maeder, M.T.; Handschin, R.; Pfisterer, M.E.; Brunner-La Rocca, H.P.; TIME-CHF Investigators. Circulating biomarkers of distinct pathophysiological pathways in heart failure with preserved vs. reduced left ventricular ejection fraction. *Eur. J. Heart Fail.* **2015**, *17*, 1006–1014. [CrossRef]
21. Tromp, J.; Westenbrink, B.D.; Ouwerkerk, W.; van Veldhuisen, D.J.; Samani, N.J.; Ponikowski, P.; Metra, M.; Anker, S.D.; Cleland, J.G.; Dickstein, K.; et al. Identifying Pathophysiological Mechanisms in Heart Failure with Reduced Versus Preserved Ejection Fraction. *J. Am. Coll. Cardiol.* **2018**, *72*, 1081–1090. [CrossRef] [PubMed]
22. Carris, N.W.; Mhaskar, R.; Coughlin, E.; Bracey, E.; Tipparaju, S.M.; Halade, G.V. Novel biomarkers of inflammation in heart failure with preserved ejection fraction: Analysis from a large prospective cohort study. *BMC Cardiovasc. Disord.* **2022**, *22*, 221. [CrossRef] [PubMed]
23. Lakhani, I.; Wong, M.V.; Hung, J.; Gong, M.; Waleed, K.B.; Xia, Y.; Lee, S.; Roever, L.; Liu, T.; Tse, G.; et al. Diagnostic and prognostic value of serum C-reactive protein in heart failure with preserved ejection fraction: A systematic review and meta-analysis. *Heart Fail. Rev.* **2021**, *26*, 1141–1150. [CrossRef]
24. Alogna, A.; Koepp, K.E.; Sabbah, M.; Espindola Netto, J.M.; Jensen, M.D.; Kirkland, J.L.; Lam, C.; Obokata, M.; Petrie, M.C.; Ridker, P.M.; et al. Interleukin-6 in Patients with Heart Failure and Preserved Ejection Fraction. *JACC Heart Fail.* **2023**, *11*, 1549–1561. [CrossRef] [PubMed]
25. Abernethy, A.; Raza, S.; Sun, J.L.; Anstrom, K.J.; Tracy, R.; Steiner, J.; VanBuren, P.; LeWinter, M.M. Pro-inflammatory biomarkers in stable versus acutely decompensated heart failure with preserved ejection fraction. *J. Am. Heart Assoc.* **2018**, *7*, e007385. [CrossRef]
26. Chaar, D.; Dumont, B.L.; Vulesevic, B.; Neagoe, P.-E.; Räkel, A.; White, M.; Sirois, M.G. Neutrophils and Circulating Inflammatory Biomarkers in Diabetes Mellitus and Heart Failure with Preserved Ejection Fraction. *Am. J. Cardiol.* **2022**, *178*, 80–88. [CrossRef]
27. Westermann, D.; Lindner, D.; Kasner, M.; Zietsch, C.; Savvatis, K.; Escher, F.; von Schlippenbach, J.; Skurk, C.; Steendijk, P.; Riad, A.; et al. Cardiac inflammation contributes to changes in the extracellular matrix in patients with heart failure and normal ejection fraction. *Circ. Heart Fail.* **2011**, *4*, 44–52. [CrossRef]
28. Franssen, C.; Chen, S.; Unger, A.; Korkmaz, H.I.; De Keulenaer, G.W.; Tschöpe, C.; Leite-Moreira, A.F.; Musters, R.; Niessen, H.W.; Linke, W.A.; et al. Myocardial Microvascular Inflammatory Endothelial Activation in Heart Failure with Preserved Ejection Fraction. *JACC Heart Fail.* **2016**, *4*, 312–324. [CrossRef]
29. Mohammed, S.F.; Hussain, S.F.; Mirzoev, S.A.; Edwards, W.D.; Maleszewski, J.J.; Redfield, M.M. Coronary microvascular rarefaction and myocardial fibrosis in heart failure with preserved ejection fraction. *Circulation* **2015**, *131*, 550–559. [CrossRef]
30. Srivaratharajah, K.; Coutinho, T.; deKemp, R.; Liu, P.; Haddad, H.; Stadnick, E.; Davies, R.A.; Chih, S.; Dwivedi, G.; Guo, A.; et al. Reduced Myocardial Flow in Heart Failure Patients with Preserved Ejection Fraction. *Circ. Heart Fail.* **2016**, *9*, e002562. [CrossRef]
31. Glezeva, N.; Voon, V.; Watson, C.; Horgan, S.; McDonald, K.; Ledwidge, M.; Baugh, J. Exaggerated inflammation and monocytosis associate with diastolic dysfunction in heart failure with preserved ejection fraction: Evidence of M2 macrophage activation in disease pathogenesis. *J. Card. Fail.* **2015**, *21*, 167–177. [CrossRef] [PubMed]
32. Ovchinnikov, A.; Filatova, A.; Potekhina, A.; Arefieva, T.; Gvozdeva, A.; Ageev, F.; Belyavskiy, E. Blood Immune Cell Alterations in Patients with Hypertensive Left Ventricular Hypertrophy and Heart Failure with Preserved Ejection Fraction. *J. Cardiovasc. Dev. Dis.* **2023**, *10*, 310. [CrossRef]
33. Hahn, V.S.; Yanek, L.R.; Vaishnav, J.; Ying, W.; Vaidya, D.; Zhen Joan Lee, Y.; Riley, S.J.; Subramanya, V.; Brown, E.; Danielle Hopkins, C.; et al. Endomyocardial Biopsy Characterization of Heart Failure with Preserved Ejection Fraction and Prevalence of Cardiac Amyloidosis. *JACC Heart Fail.* **2020**, *8*, 712–724. [CrossRef] [PubMed]

34. Hulsmans, M.; Sager, H.B.; Roh, J.D.; Valero-Muñoz, M.; Houstis, N.E.; Iwamoto, Y.; Sun, Y.; Wilson, R.M.; Wojtkiewicz, G.; Tricot, B.; et al. Cardiac macrophages promote diastolic dysfunction. *J. Exp. Med.* **2018**, *215*, 423–440. [CrossRef]
35. Bajpai, G.; Schneider, C.; Wong, N.; Bredemeyer, A.; Hulsmans, M.; Nahrendorf, M.; Epelman, S.; Kreisel, D.; Liu, Y.; Itoh, A.; et al. The human heart contains distinct macrophage subsets with divergent origins and functions. *Nat. Med.* **2018**, *24*, 1234–1245. [CrossRef]
36. Shah, S.J.; Katz, D.H.; Selvaraj, S.; Burke, M.A.; Yancy, C.W.; Cheorghiade, M.; Bonow, R.O.; Huang, C.-C.; Deo, R.C. Phenomapping for Novel Classification of Heart Failure with Preserved Ejection Fraction. *Circulation* **2015**, *131*, 269–279. [CrossRef]
37. Shah, S.J.; Katz, D.H.; Deo, R.C. Phenotypic Spectrum of Heart Failure with Preserved Ejection Fraction. *Heart Fail. Clin.* **2014**, *10*, 407–418. [CrossRef]
38. Teramoto, K.; Katherine Teng, T.-H.; Chandramouli, C.; Tromp, J.; Sakata, Y.; Lam, C.S. Epidemiology and Clinical Features of Heart Failure with Preserved Ejection Fraction. *Card. Fail. Rev.* **2022**, *8*, e27. [CrossRef] [PubMed]
39. Cohen, J.B.; Schrauben, S.J.; Zhao, L.; Basso, M.D.; Cvijic, M.E.; Li, Z.; Yarde, M.; Wang, Z.; Bhattacharya, P.T.; Chirinos, D.A.; et al. Clinical Phenogroups in Heart Failure with Preserved Ejection Fraction: Detailed Phenotypes, Prognosis, and Response to Spironolactone. *JACC Heart Fail.* **2020**, *8*, 172–184. [CrossRef]
40. Galli, E.; Bourg, C.; Kosmala, W.; Oger, E.; Donal, E. Phenomapping Heart Failure with Preserved Ejection Fraction Using Machine Learning Cluster Analysis: Prognostic and Therapeutic Implications. *Heart Fail. Clin.* **2021**, *17*, 499–518. [CrossRef]
41. Bronzwaer, J.; Paulus, W.J. Diastolic and systolic heart failure: Different stages or distinct phenotypes of the heart failure syndrome? *Curr. Heart Fail. Rep.* **2009**, *6*, 281–286. [CrossRef]
42. Paulus, W.J.; Tschöpe, C. A Novel Paradigm for Heart Failure with Preserved Ejection Fraction. *J. Am. Coll. Cardiol.* **2013**, *62*, 263–271. [CrossRef]
43. Kao, D.P.; Lewsey, J.D.; Anand, I.S.; Massie, B.M.; Zile, M.R.; Carson, P.E.; McKelvie, R.S.; Komajda, M.; McMurray, J.; Lindenfels, J. Characterization of subgroups of heart failure patients with preserved ejection fraction with possible implications for prognosis and treatment response. *Eur. J. Heart Fail.* **2015**, *17*, 925–935. [CrossRef] [PubMed]
44. Mancuso, P. The role of adipokines in chronic inflammation. *Immunotargets Ther.* **2016**, *5*, 47–56. [CrossRef] [PubMed]
45. Lam, C.S. Diabetic cardiomyopathy: An expression of stage B heart failure with preserved ejection fraction. *Diab Vasc. Dis. Res.* **2015**, *12*, 234–238. [CrossRef] [PubMed]
46. Ritchie, R.H.; Abel, E.D. Basic Mechanisms of Diabetic Heart Disease. *Circ. Res.* **2020**, *126*, 1501–1525. [CrossRef]
47. Jackson, A.M.; Rørth, R.; Liu, J.; Kristensen, S.L.; Anand, I.S.; Claggett, B.L.; Cleland, J.; Chopra, V.K.; Desai, A.S.; Ge, J.; et al. Diabetes and pre-diabetes in patients with heart failure and preserved ejection fraction. *Eur. J. Heart Fail.* **2022**, *24*, 497–509. [CrossRef]
48. Lehrke, M.; Marx, N. Diabetes Mellitus and Heart Failure. *Am. J. Med.* **2017**, *130*, S40–S50. [CrossRef]
49. van Heerebeek, L.; Hamdani, N.; Handoko, M.L.; Falcao-Pires, I.; Musters, R.J.; Kupreishvili, K.; Ijsselmuiden, A.; Schalkwijk, C.G.; Bronzwaer, J.; Diamant, M.; et al. Diastolic stiffness of the failing diabetic heart: Importance of fibrosis, advanced glycation end products, and myocyte resting tension. *Circulation* **2008**, *117*, 43–51. [CrossRef]
50. Plante, T.B.; Juraschek, S.P.; Howard, G.; Howard, V.J.; Tracy, R.P.; Olson, N.C.; Judd, S.E.; Mukaz, D.K.; Zakai, N.A.; Long, D.L.; et al. Cytokines, C-Reactive Protein, and Risk of Incident Hypertension in the REGARDS Study. *Hypertension* **2024**, *81*, 1244–1253. [CrossRef]
51. Wang, Z.; Wang, J.; Yang, P.; Song, X.; Li, Y. Elevated Th17 cell proportion, related cytokines and mRNA expression level in patients with hypertension-mediated organ damage: A case control study. *BMC Cardiovasc. Disord.* **2022**, *22*, 257. [CrossRef] [PubMed]
52. Cantero-Navarro, E.; Fernández-Fernández, B.; Ramos, A.M.; Rayego-Mateos, S.; Rodrigues-Diez, R.R.; Sánchez-Niño, M.D.; Sanz, A.B.; Ruiz-Ortega, M.; Ortiz, A. Renin-angiotensin system and inflammation update. *Mol. Cell Endocrinol.* **2021**, *529*, 111254. [CrossRef] [PubMed]
53. Xiao, L.; Harrison, D.G. Inflammation in Hypertension. *Can. J. Cardiol.* **2020**, *36*, 635–647. [CrossRef] [PubMed]
54. Lam, C.; Donal, E.; Kraigher-Krainer, E.; Vasan, R.S. Epidemiology and clinical course of heart failure with preserved ejection fraction. *Eur. J. Heart Fail.* **2011**, *13*, 18–28. [CrossRef]
55. Packer, M.; Lam, C.; Lund, L.H.; Maurer, M.S.; Borlaug, B.A. Characterization of the inflammatory-metabolic phenotype of heart failure with a preserved ejection fraction: A hypothesis to explain influence of sex on the evolution and potential treatment of the disease. *Eur. J. Heart Fail.* **2020**, *22*, 1551–1567. [CrossRef]
56. Segar, M.W.; Patel, K.V.; Ayers, C.; Basit, M.; Tang, W.; Willett, D.; Berry, J.; Grodin, J.L.; Pandey, A. Phenomapping of patients with heart failure with preserved ejection fraction using machine learning-based unsupervised cluster analysis. *Eur. J. Heart Fail.* **2020**, *22*, 148–158. [CrossRef]
57. Woolley, R.J.; Ceelen, D.; Ouwerkerk, W.; Tromp, J.; Figarska, S.M.; Anker, S.D.; Dickstein, K.; Filippatos, G.; Zannad, F.; Metra, M.; et al. Machine learning based on biomarker profiles identifies distinct subgroups of heart failure with preserved ejection fraction. *Eur. J. Heart Fail.* **2021**, *23*, 983–991. [CrossRef]

58. Anker, S.D.; Butler, J.; Filippatos, G.; Shahzeb Khan, M.; Ferreira, J.P.; Bocchi, E.; Böhm, M.; Brunner-La Rocca, H.P.; Choi, D.J.; Chopra, V.; et al. Baseline characteristics of patients with heart failure with preserved ejection fraction in the EMPEROR-Preserved trial. *Eur. J. Heart Fail.* **2020**, *22*, 2383–2392. [CrossRef]
59. Ridker, P.M.; Everett, B.M.; Thuren, T.; MacFadyen, J.G.; Chang, W.H.; Ballantyne, C.; Fonseca, F.; Nicolau, J.; Koenig, W.; Anker, S.D.; et al. Antiinflammatory therapy with Canakinumab for atherosclerotic disease. *N. Engl. J. Med.* **2017**, *377*, 1119–1131. [CrossRef]
60. Van Tassell, B.W.; Buckley, L.F.; Carbone, S.; Trankle, C.R.; Canada, J.M.; Dixon, D.L.; Abouzaki, N.; Oddi-Erdle, C.; Biondi-Zoccai, G.; Arena, R.; et al. Interleukin-1 blockade in heart failure with preserved ejection fraction: Rationale and design of the Diastolic Heart Failure Anakinra Response Trial 2 (D-HART2). *Clin. Cardiol.* **2017**, *40*, 626–632. [CrossRef]
61. Lam, C.; Lund, L.; Shah, S.; Voors, A.A.; Erlinge, D.; Saraste, A.; Pirazzi, C.; Grove, E.L.; Barasa, A.; Schou, M.; et al. Myeloperoxidase inhibition in heart failure with preserved or mildly reduced ejection fraction: SATELLITE trial results. *J. Card. Fail.* **2024**, *30*, 104–110. [CrossRef] [PubMed]
62. Riehle, C.; Bauersachs, J. Small animal models of heart failure. *Cardiovasc. Res.* **2019**, *115*, 1838–1849. [CrossRef]
63. Miyagi, C.; Miyamoto, T.; Kuroda, T.; Karimov, J.H.; Starling, R.C.; Fukamachi, K. Large animal models of heart failure with preserved ejection fraction. *Heart Fail. Rev.* **2022**, *27*, 595–608. [CrossRef]
64. Gao, S.; Liu, X.P.; Li, T.T.; Chen, L.; Feng, Y.P.; Wang, Y.K.; Yin, Y.J.; Little, P.J.; Wu, X.Q.; Xu, S.W.; et al. Animal models of heart failure with preserved ejection fraction (HFpEF): From metabolic pathobiology to drug discovery. *Acta Pharmacol. Sin.* **2024**, *45*, 23–35. [CrossRef] [PubMed]
65. Lourenço, A.P.; Leite-Moreira, A.F.; Balligand, J.L.; Bauersachs, J.; Dawson, D.; de Boer, R.A.; de Windt, L.J.; Falcão-Pires, I.; Fontes-Carvalho, R.; Franz, S.; et al. An integrative translational approach to study heart failure with preserved ejection fraction: A position paper from the Working Group on Myocardial Function of the European Society of Cardiology. *Eur. J. Heart Fail.* **2018**, *20*, 216–227. [CrossRef]
66. Schauer, A.; Draskowski, R.; Jannasch, A.; Kirchhoff, V.; Goto, K.; Männel, A.; Barthel, P.; Augstein, A.; Winzer, E.; Tugtekin, M.; et al. ZSF1 rat as animal model for HFpEF: Development of reduced diastolic function and skeletal muscle dysfunction. *ESC Heart Fail.* **2020**, *7*, 2123–2134. [CrossRef] [PubMed]
67. Murase, T.; Hattori, T.; Ohtake, M.; Abe, M.; Amakusa, Y.; Takatsu, M.; Murohara, T.; Nagata, K. Cardiac remodeling and diastolic dysfunction in DahlS.Z-Lepr(fa)/Lepr(fa) rats: A new animal model of metabolic syndrome. *Hypertens. Res.* **2012**, *35*, 186–193. [CrossRef]
68. Schwarzl, M.; Hamdani, N.; Seiler, S.; Alogna, A.; Manninger, M.; Reilly, S.; Zirngast, B.; Kirsch, A.; Steendijk, P.; Verderber, J.; et al. A porcine model of hypertensive cardiomyopathy: Implications for heart failure with preserved ejection fraction. *Am. J. Physiol. Heart Circ. Physiol.* **2015**, *309*, H1407–H1418. [CrossRef]
69. Sharp, T.E., 3rd; Scarborough, A.L.; Li, Z.; Polhemus, D.J.; Hidalgo, H.A.; Schumacher, J.D.; Matsuura, T.R.; Jenkins, J.S.; Kelly, D.P.; Goodchild, T.T.; et al. Novel Göttingen Miniswine Model of Heart Failure with Preserved Ejection Fraction Integrating Multiple Comorbidities. *JACC Basic. Transl. Sci.* **2021**, *6*, 154–170. [CrossRef]
70. Wang, L.; Halliday, G.; Huot, J.R.; Satoh, T.; Baust, J.J.; Fisher, A.; Cook, T.; Hu, J.; Avolio, T.; Goncharov, D.A.; et al. Treatment with Treprostinil and Metformin Normalizes Hyperglycemia and Improves Cardiac Function in Pulmonary Hypertension Associated with Heart Failure with Preserved Ejection Fraction. *Arterioscler. Thromb. Vasc. Biol.* **2020**, *40*, 1543–1558. [CrossRef]
71. Deng, Y.; Xie, M.; Li, Q.; Xu, X.; Ou, W.; Zhang, Y.; Xiao, H.; Yu, H.; Zheng, Y.; Liang, Y.; et al. Targeting Mitochondria-Inflammation Circuit by β-Hydroxybutyrate Mitigates HFpEF. *Circ. Res.* **2021**, *128*, 232–245. [CrossRef] [PubMed]
72. Withaar, C.; Meems, L.; Markousis-Mavrogenis, G.; Boogerd, C.J.; Silljé, H.; Schouten, E.M.; Dokter, M.M.; Voors, A.A.; Westenbrink, B.D.; Lam, C.; et al. The effects of liraglutide and dapagliflozin on cardiac function and structure in a multi-hit mouse model of heart failure with preserved ejection fraction. *Cardiovasc. Res.* **2021**, *117*, 2108–2124. [CrossRef]
73. Gevaert, A.B.; Shakeri, H.; Leloup, A.J.; Van Hove, C.E.; De Meyer, G.; Vrints, C.J.; Lemmens, K.; Van Craenenbroeck, E.M. Endothelial Senescence Contributes to Heart Failure with Preserved Ejection Fraction in an Aging Mouse Model. *Circ. Heart Fail.* **2017**, *10*, e003806. [CrossRef]
74. Li, Y.; Kubo, H.; Yu, D.; Yang, Y.; Johnson, J.P.; Eaton, D.M.; Berretta, R.M.; Foster, M.; McKinsey, T.A.; Yu, J.; et al. Combining three independent pathological stressors induces a heart failure with preserved ejection fraction phenotype. *Am. J. Physiol. Heart Circ. Physiol.* **2023**, *324*, H443–H460. [CrossRef] [PubMed]
75. Kelley, R.C.; Betancourt, L.; Noriega, A.M.; Brinson, S.C.; Curbelo-Bermudez, N.; Hahn, D.; Kumar, R.A.; Balazic, E.; Muscato, D.R.; Ryan, T.E.; et al. Skeletal myopathy in a rat model of postmenopausal heart failure with preserved ejection fraction. *J. Appl. Physiol.* **2022**, *132*, 106–125. [CrossRef]
76. Vilariño-García, T.; Polonio-González, M.L.; Pérez-Pérez, A.; Ribalta, J.; Arrieta, F.; Aguilar, M.; Obaya, J.C.; Gimeno-Orna, J.A.; Iglesias, P.; Navarro, J.; et al. Role of Leptin in Obesity, Cardiovascular Disease, and Type 2 Diabetes. *Int. J. Mol. Sci.* **2024**, *25*, 2338. [CrossRef] [PubMed]

77. Chen, H.; Charlat, O.; Tartaglia, L.A.; Woolf, E.A.; Weng, X.; Ellis, S.J.; Lakey, N.D.; Culpepper, J.; Moore, K.J.; Breitbart, R.E.; et al. Evidence That the Diabetes Gene Encodes the Leptin Receptor: Identification of a Mutation in the Leptin Receptor Gene in db/db Mice. *Cell* **1996**, *84*, 491–495. [CrossRef]
78. Mori, J.; Patel, V.B.; Alrob, O.A.; Basu, R.; Altamimi, T.; Desaulniers, J.; Wagg, C.S.; Zamaneh, K.; Lopaschuk, G.D.; Oudit, G.Y. Angiotensin 1-7 ameliorates diabetic cardiomyopathy and diastolic dysfunction in db/db mice by reducing lipotoxicity and inflammation. *Circ. Heart Fail.* **2014**, *7*, 327–339. [CrossRef]
79. Vecoli, C.; Cao, J.; Neglia, D.; Inoue, K.; Sodhi, K.; Vanells, L.; Gabrielson, K.K.; Bedja, D.; Paolocci, N.; L'abbate, A.; et al. Apolipoprotein A-I mimetic peptide L-4F prevents myocardial and coronary dysfunction in diabetic mice. *J. Cell Biochem.* **2011**, *112*, 2616–2626. [CrossRef]
80. Buchanan, J.; Mazumder, P.K.; Hu, P.; Chakrabarti, G.; Roberts, M.W.; Jeong Yun, U.; Cooksey, R.C.; Litwin, S.E.; Dale Abel, E. Reduced Cardiac Efficiency and Altered Substrate Metabolism Precedes the Onset of Hyperglycemia and Contractile Dysfunction in Two Mouse Models of Insulin Resistance and Obesity. *Endocrinology* **2005**, *146*, 5341–5349. [CrossRef]
81. Ge, F.; Hu, C.; Hyodo, E.; Arai, K.; Zhou, S.; Lobdell, H., 4th; Walewski, J.L.; Homma, S.; Berk, P.D. Cardiomyocyte Triglyceride Accumulation and Reduced Ventricular Function in Mice with Obesity Reflect Increased Long Chain Fatty Acid Uptake and *De Novo* Fatty Acid Synthesis. *J. Obes.* **2012**, *2012*, 205648. [CrossRef] [PubMed]
82. Kobayashi, K.; Forte, T.M.; Taniguchi, S.; Ishida, B.Y.; Oka, K.; Chan, L. The db/db mouse, a model for diabetic dyslipidemia: Molecular characterization and effects of western diet feeding. *Metabolism* **2000**, *49*, 22–31. [CrossRef]
83. Senador, D.; Kanakamedala, K.; Irigoyen, M.C.; Morris, M.; Elased, K.M. Cardiovascular and autonomic phenotype of *db/db* diabetic mice. *Exp. Physiol.* **2009**, *94*, 648–658. [CrossRef] [PubMed]
84. Bowden, M.A.; Tesch, G.H.; Julius, T.; Rosli, S.; Love, J.E.; Ritchie, R.H. Earlier onset of diabesity-Induced adverse cardiac remodeling in female compared to male mice. *Obesity (Silver Spring)* **2015**, *23*, 1166–1177. [CrossRef] [PubMed]
85. Dong, F.; Ren, J. Adiponectin improves cardiomyocyte contractile function in db/db diabetic obese mice. *Obesity (Silver Spring)* **2009**, *17*, 262–268. [CrossRef]
86. Semeniuk, L.M.; Kryski, A.J.; Severson, D.L. Echocardiographic assessment of cardiac function in diabetic *db/db* and transgenic *db/db*-hGLUT4 mice. *Am. J. Physiol. Heart Circ. Physiol.* **2002**, *283*, H976–H982. [CrossRef]
87. Daniels, A.; van Bilsen, M.; Janssen, B.; Brouns, A.E.; Cleutjens, J.; Roemen, T.; Schaart, G.; van der Velden, J.; van der Vusse, G.J.; van Nieuwenhoven, F.A. Impaired cardiac functional reserve in type 2 diabetic db/db mice is associated with metabolic, but not structural, remodelling. *Acta Physiologica.* **2010**, *200*, 11–22. [CrossRef]
88. Alex, L.; Russo, I.; Holoborodko, V.; Frangogiannis, N.G. Characterization of a mouse model of obesity-related fibrotic cardiomyopathy that recapitulates features of human heart failure with preserved ejection fraction. *Am. J. Physiol. Heart Circ. Physiol.* **2018**, *315*, H934–H949. [CrossRef]
89. Hamdani, N.; Hervent, A.-S.; Vandekerckhove, L.; Matheeussen, V.; Demolder, M.; Baerts, L.; De Meester, I.; Linke, W.A.; Paulus, W.J.; Keulenaer, G. Left ventricular diastolic dysfunction and myocardial stiffness in diabetic mice is attenuated by inhibition of dipeptidyl peptidase 4. *Cardiovasc. Res.* **2014**, *104*, 423–431. [CrossRef]
90. Zhao, R.; Xie, X.; Le, K.; Li, W.; Moghadasian, M.H.; Beta, T.; Shen, G.X. Endoplasmic reticulum stress in diabetic mouse or glycated LDL-treated endothelial cells: Protective effect of Saskatoon berry powder and cyanidin glycans. *J. Nutr. Biochem.* **2015**, *26*, 1248–1253. [CrossRef]
91. Koka, S.; Aluri, H.S.; Xi, L.; Lesnefsky, E.; Kukreja, R.C. Chronic inhibition of phosphodiesterase 5 with tadalafil attenuates mitochondrial dysfunction in type 2 diabetic hearts: Potential role of NO/SIRT1/PGC-1α signaling. *Am. J. Physiol. Heart Circ. Physiol.* **2014**, *306*, H1558–H1568. [CrossRef] [PubMed]
92. Monma, Y.; Shindo, T.; Eguchi, K.; Kurosawa, R.; Kagaya, Y.; Ikumi, Y.; Ichijo, S.; Nakata, T.; Miyata, S.; Matsumoto, A.; et al. Low-intensity pulsed ultrasound ameliorates cardiac diastolic dysfunction in mice: A possible novel therapy for heart failure with preserved left ventricular ejection fraction. *Cardiovasc. Res.* **2021**, *117*, 1325–1338. [CrossRef] [PubMed]
93. Reil, J.-C.; Honl, M.; Reil, G.-H.; Granzier, H.L.; Kratz, M.T.; Kazakov, A.; Fries, P.; Müller, A.; Lenski, M.; Custodis, F.; et al. Heart rate reduction by If-inhibition improves vascular stiffness and left ventricular systolic and diastolic function in a mouse model of heart failure with preserved ejection fraction. *Eur. Heart J.* **2013**, *34*, 2839–2849. [CrossRef] [PubMed]
94. Ingalls, A.M.; Dickie, M.M.; Snell, G.D. Obese, a new mutation in the house mouse. *J. Hered.* **1950**, *41*, 317–318. [CrossRef]
95. Barouch, L.A.; Berkowitz, D.E.; Harrison, R.W.; O'Donell, C.P.; Hare, J.M. Disruption of leptin signaling contributes to cardiac hypertrophy independently of body weight in mice. *Circulation* **2003**, *108*, 754–759. [CrossRef]
96. Hammoudi, N.; Jeong, D.; Singh, R.; Farhat, A.; Komajda, M.; Mayoux, E.; Hajjar, R.; Lebeche, D. Empagliflozin Improves Left Ventricular Diastolic Dysfunction in a Genetic Model of Type 2 Diabetes. *Cardiovasc. Drugs Ther.* **2017**, *31*, 233–246. [CrossRef]
97. Guo, W.; Jiang, T.; Lian, C.; Wang, H.; Zheng, Q.; Ma, H. QKI deficiency promotes FoxO1 mediated nitrosative stress and endoplasmic reticulum stress contributing to increased vulnerability to ischemic injury in diabetic heart. *J. Mol. Cell Cardiol.* **2014**, *75*, 131–140. [CrossRef]

98. Minhas, K.M.; Khan, S.A.; Raju, S.; Phan, A.C.; Gonzalez, D.R.; Skaf, M.W.; Lee, K.; Tejani, A.D.; Saliaris, A.P.; Barouch, L.A.; et al. Leptin repletion restores depressed {beta}-adrenergic contractility in ob/ob mice independently of cardiac hypertrophy. *J. Physiol.* **2005**, *565*, 463–474. [CrossRef]
99. Li, S.-Y.; Yang, X.; Ceylan-Isik, A.F.; Du, M.; Sreejayan, N.; Ren, J. Cardiac contractile dysfunction in Lep/Lep obesity is accompanied by NADPH oxidase activation, oxidative modification of sarco(endo)plasmic reticulum Ca2+-ATPase and myosin heavy chain isozyme switch. *Diabetologia* **2006**, *49*, 1434–1446. [CrossRef]
100. Adingupu, D.D.; Göpel, S.O.; Grönros, J.; Behrendt, M.; Sotak, M.; Miliotis, T.; Dahlqvist, U.; Gan, L.-M.; Jönsson-Rylander, A.-C. SGLT2 inhibition with empagliflozin improves coronary microvascular function and cardiac contractility in prediabetic ob/ob-/- mice. *Cardiovasc. Diabetol.* **2019**, *18*, 16. [CrossRef]
101. Christoffersen, C.; Bollano, E.; Lindegaard, M.; Bartels, E.D.; Goetze, J.P.; Andersen, C.B.; Nielsen, L.B. Cardiac lipid accumulation associated with diastolic dysfunction in obese mice. *Endocrinology* **2003**, *144*, 3483–3490. [CrossRef]
102. Ye, Y.; Bajaj, M.; Yang, H.-C.; Perez-Polo, J.R.; Birnbaum, Y. SGLT-2 Inhibition with Dapagliflozin Reduces the Activation of the Nlrp3/ASC Inflammasome and Attenuates the Development of Diabetic Cardiomyopathy in Mice with Type 2 Diabetes. Further Augmentation of the Effects with Saxagliptin, a DPP4 Inhibitor. *Cardiovasc. Drugs Ther.* **2017**, *31*, 119–132. [CrossRef]
103. Mariappan, N.; Elks, C.M.; Sriramula, S.; Guggilam, A.; Liu, Z.; Borkhsenious, O.; Francis, J. NF-kappaB-induced oxidative stress contributes to mitochondrial and cardiac dysfunction in type II diabetes. *Cardiovasc. Res.* **2010**, *85*, 473–483. [CrossRef] [PubMed]
104. Methawasin, M.; Strom, J.; Borkowski, T.; Hourani, Z.; Runyan, R.; Smith, J.E., 3rd; Granzier, H. Phosphodiesterase 9a Inhibition in Mouse Models of Diastolic Dysfunction. *Circ. Heart Fail.* **2020**, *13*, e006609. [CrossRef] [PubMed]
105. Broderick, T.L.; Parrott, C.R.; Wang, D.; Jankowski, M.; Gutkowska, J. Expression of cardiac GATA4 and downstream genes after exercise training in the db/db mouse. *Pathophysiology* **2012**, *19*, 193–203. [CrossRef]
106. Belke, D.D.; Swanson, E.A.; Dillmann, W.H. Decreased sarcoplasmic reticulum activity and contractility in diabetic db/db mouse heart. *Diabetes* **2004**, *53*, 3201–3208. [CrossRef]
107. Lugnier, C.; Meyer, A.; Charloux, A.; Andrès, E.; Gény, B.; Talha, S. The Endocrine Function of the Heart: Physiology and Involvements of Natriuretic Peptides and Cyclic Nucleotide Phosphodiesterases in Heart Failure. *J. Clin. Med.* **2019**, *8*, 1746. [CrossRef]
108. Juguilon, C.; Wang, Z.; Wang, Y.; Enrick, M.; Jamaiyar, A.; Xu, Y.; Gadd, J.; Chen, C.-L.W.; Pu, A.; Kolz, C.; et al. Mechanism of the switch from NO to H_2O_2 in endothelium-dependent vasodilation in diabetes. *Basic. Res. Cardiol.* **2022**, *117*, 2. [CrossRef] [PubMed]
109. Saraiva, R.M.; Minhas, K.M.; Zheng, M.; Pitz, E.; Treuer, A.; Gonzalez, D.; Schuleri, K.H.; Vandegaer, K.M.; Barouch, L.A.; Hare, J.M. Reduced neuronal nitric oxide synthase expression contributes to cardiac oxidative stress and nitroso-redox imbalance in ob/ob mice. *Nitric Oxide* **2007**, *16*, 331–338. [CrossRef]
110. Schiattarella, G.G.; Altamirano, F.; Tong, D.; French, K.M.; Villalobos, E.; Kim, S.Y.; Luo, X.; Jiang, N.; May, H.I.; Wang, Z.V.; et al. Nitrosative stress drives heart failure with preserved ejection fraction. *Nature* **2019**, *568*, 351–356. [CrossRef]
111. van Heerebeek, L.; Borbély, A.; Niessen, H.; Bronzwaer, J.; van der Velden, J.; Stienen, G.; Linke, W.A.; Laarman, G.J.; Paulus, W.J. Myocardial Structure and Function Differ in Systolic and Diastolic Heart Failure. *Circulation* **2006**, *113*, 1966–1973. [CrossRef]
112. Linke, W.A.; Hamdani, N. Gigantic Business: Titin properties and function through thick and thin. *Circ. Res.* **2014**, *114*, 1052–1068. [CrossRef] [PubMed]
113. Greene, S.J.; Gheorghiade, M.; Borlaug, B.A.; Pieske, B.; Vaduganathan, M.; Burnett, J.C., Jr.; Roessig, L.; Stasch, J.-P.; Solomon, S.D.; Paulus, W.J.; et al. The cGMP Signaling Pathway as a Therapeutic Target in Heart Failure with Preserved Ejection Fraction. *J. Am. Heart Assoc.* **2013**, *2*, e000536. [CrossRef]
114. Münzel, T.; Gori, T.; Keaney, J.F., Jr.; Maack, C.; Daiber, A. Pathophysiological role of oxidative stress in systolic and diastolic heart failure and its therapeutic implications. *Eur. Heart J.* **2015**, *36*, 2555–2564. [CrossRef] [PubMed]
115. van Heerebeek, L.; Hamdani, N.; Falcão-Pires, I.; Leite-Moreira, A.F.; Begieneman, M.; Bronzwaer, J.; van der Velden, J.; Stienen, G.; Laarman, G.J.; Somsen, A.; et al. Low myocardial protein kinase G activity in heart failure with preserved ejection fraction. *Circulation* **2012**, *126*, 830–839. [CrossRef]
116. Williams, T.D.; Chambers, J.B.; Roberts, L.M.; Henderson, R.P.; Overton, J.M. Diet-induced obesity and cardiovascular regulation in C57BL/6J mice. *Clin. Exp. Pharmacol. Physiol.* **2003**, *30*, 769–778. [CrossRef]
117. Basheer, S.; Malik, I.R.; Awan, F.R.; Sughra, K.; Roshan, S.; Khalil, A.; Iqbal, M.J.; Parveen, Z. Histological and Microscopic Analysis of Fats in Heart, Liver Tissue, and Blood Parameters in Experimental Mice. *Genes* **2023**, *14*, 515. [CrossRef]
118. Benetti, E.; Mastrocola, R.; Vitarelli, G.; Cutrin, J.C.; Nigro, D.; Chiazza, F.; Mayoux, E.; Collino, M.; Fantozzi, R. Empagliflozin Protects against Diet-Induced NLRP-3 Inflammasome Activation and Lipid Accumulation. *J. Pharmacol. Exp. Ther.* **2016**, *359*, 45–53. [CrossRef]
119. Zhou, X.; Li, Z.; Qi, M.; Zhao, P.; Duan, Y.; Yang, G.; Yuan, L. Brown adipose tissue-derived exosomes mitigate the metabolic syndrome in high fat diet mice. *Theranostics* **2020**, *10*, 8197–8210. [CrossRef]

120. Wang, H.-T.; Liu, C.-F.; Tsai, T.-H.; Chen, Y.-L.; Chang, H.-W.; Tsai, C.-Y.; Leu, S.; Zhen, Y.-Y.; Chai, H.-T.; Chung, S.-Y.; et al. Effect of obesity reduction on preservation of heart function and attenuation of left ventricular remodeling, oxidative stress and inflammation in obese mice. *J. Transl. Med.* **2012**, *10*, 145. [CrossRef]
121. Abdurrachim, D.; Ciapaite, J.; Wessels, B.; Nabben, M.; Luiken, J.; Nicolay, K.; Prompers, J.J. Cardiac diastolic dysfunction in high-fat diet fed mice is associated with lipotoxicity without impairment of cardiac energetics in vivo. *Biochim. Biophys. Acta* **2014**, *1842*, 1525–1537. [CrossRef] [PubMed]
122. Steven, S.; Dib, M.; Hausding, M.; Kashani, F.; Oelze, M.; Kröller-Schön, S.; Hanf, A.; Daub, S.; Roohani, S.; Gramlich, Y.; et al. CD40L controls obesity-associated vascular inflammation, oxidative stress, and endothelial dysfunction in high fat diet-treated and db/db mice. *Cardiovasc. Res.* **2018**, *114*, 312–323. [CrossRef]
123. Li, W.; Tang, R.; Ouyang, S.; Ma, F.; Liu, Z.; Wu, J. Folic acid prevents cardiac dysfunction and reduces myocardial fibrosis in a mouse model of high-fat diet-induced obesity. *Nutr. Metab.* **2017**, *14*, 68. [CrossRef] [PubMed]
124. Jeong, E.; Chung, J.; Liu, H.; Go, Y.; Gladstein, S.; Farzaneh-Far, A.; Lewandowski, E.D.; Dudley, S.C., Jr. Role of Mitochondrial Oxidative Stress in Glucose Tolerance, Insulin Resistance, and Cardiac Diastolic Dysfunction. *J. Am. Heart Assoc.* **2016**, *5*, e003046. [CrossRef]
125. Carbone, S.; Mauro, A.G.; Mezzaroma, E.; Kraskauskas, D.; Marchetti, C.; Buzzetti, R.; Van Tassell, B.W.; Abbate, A.; Toldo, S. A high-sugar and high-fat diet impairs cardiac systolic and diastolic function in mice. *Int. J. Cardiol.* **2015**, *198*, 66–69. [CrossRef]
126. Roche, C.; Besnier, M.; Cassel, R.; Harouki, N.; Coquerel, D.; Guerrot, D.; Nicol, L.; Loizon, E.; Remy-Jouet, I.; Morisseau, C.; et al. Soluble epoxide hydrolase inhibition improves coronary endothelial function and prevents the development of cardiac alterations in obese insulin-resistant mice. *Am. J. Physiol. Heart Circ. Physiol.* **2015**, *308*, H1020–H1029. [CrossRef]
127. Heinzel, F.R.; Shah, S.J. The future of heart failure with preserved ejection fraction: Deep phenotyping for targeted therapeutics. *Herz* **2022**, *47*, 308–323. [CrossRef]
128. Xia, N.; Weisenburger, S.; Koch, E.; Burkart, M.; Reifenberg, G.; Förstermann, U.; Li, H. Restoration of perivascular adipose tissue function in diet-induced obese mice without changing bodyweight. *Br. J. Pharmacol.* **2017**, *174*, 3443–3453. [CrossRef]
129. Smart, C.D.; Fehrenbach, D.J.; Wassenaar, J.W.; Agrawal, V.; Fortune, N.L.; Dixon, D.D.; Cottam, M.A.; Hasty, A.H.; Hemnes, A.R.; Doran, A.C.; et al. Immune profiling of murine cardiac leukocytes identifies triggering receptor expressed on myeloid cells 2 as a novel mediator of hyper-tensive heart failure. *Cardiovasc. Res.* **2023**, *119*, 2312–2328. [CrossRef]
130. Yan, W.; Bi, H.-L.; Liu, L.-X.; Li, N.-N.; Liu, Y.; Du, J.; Wang, H.-Z.; Li, H.-H. Knockout of immunoproteasome subunit β2i ameliorates cardiac fibrosis and inflammation in DOCA/Salt hypertensive mice. *Biochem. Biophys. Res. Commun.* **2017**, *490*, 84–90. [CrossRef]
131. Cai, R.; Hao, Y.; Liu, Y.-Y.; Huang, L.; Yao, Y.; Zhou, M.-S. Tumor Necrosis Factor Alpha Deficiency Improves Endothelial Function and Cardiovascular Injury in Deoxycorticosterone Acetate/Salt-Hypertensive Mice. *Biomed. Res. Int.* **2020**, *2020*, 3921074. [CrossRef] [PubMed]
132. Sun, Y.; Carretero, O.A.; Xu, J.; Rhaleb, N.-E.; Wang, F.; Lin, C.; Yang, J.J.; Pagano, P.J.; Yang, X.-P. Lack of inducible NO synthase reduces oxidative stress and enhances cardiac response to isoproterenol in mice with deoxycorticosterone acetate-salt hypertension. *Hypertension* **2005**, *46*, 1355–1361. [CrossRef]
133. Silberman, G.A.; Fan, T.-H.M.; Liu, H.; Jiao, Z.; Xiao, H.D.; Lovelock, J.D.; Boulden, B.M.; Widder, J.; Fredd, S.; Bernstein, K.E.; et al. Uncoupled cardiac nitric oxide synthase mediates diastolic dysfunction. *Circulation* **2010**, *121*, 519–528. [CrossRef]
134. Karatas, A.; Hegner, B.; Windt, L.J.; Luft, F.C.; Schubert, C.; Gross, V.; Akashi, Y.J.; Gürgen, D.; Kintscher, U.; da Costa Goncalves, A.C.; et al. Deoxycorticosterone acetate-salt mice exhibit blood pressure-independent sexual dimorphism. *Hypertension* **2008**, *51*, 1177–1183. [CrossRef]
135. Hartner, A.; Cordasic, N.; Klanke, B.; Veelken, R.; Hilgers, K.F. Strain differences in the development of hypertension and glomerular lesions induced by deoxycorticosterone acetate salt in mice. *Nephrol. Dial. Transpl.* **2003**, *18*, 1999–2004. [CrossRef]
136. Lin, Y.; Fu, S.; Yao, Y.; Li, Y.; Zhao, Y.; Luo, L. Heart failure with preserved ejection fraction based on aging and comorbidities. *J. Transl. Med.* **2021**, *19*, 291. [CrossRef]
137. Schnelle, M.; Catibog, N.; Zhang, M.; Nabeebaccus, A.A.; Anderson, G.; Richards, D.A.; Sawyer, G.; Zhang, X.; Toischer, K.; Hasenfuss, G.; et al. Echocardiographic evaluation of diastolic function in mouse models of heart disease. *J. Mol. Cell Cardiol.* **2018**, *114*, 20–28. [CrossRef] [PubMed]
138. Mohammed, S.F.; Ohtani, T.; Korinek, J.; Lam, C.; Larsen, K.; Simari, R.D.; Valenchik, M.L.; Burnett, J.C., Jr.; Redfiled, M.M. Mineralocorticoid accelerates transition to heart failure with preserved ejection fraction via "nongenomic effects". *Circulation* **2010**, *122*, 370–378. [CrossRef]
139. Kirchhoff, F.; Krebs, C.; Abdulhag, U.N.; Meyer-Schwesinger, C.; Maas, R.; Helmchen, U.; Hilgers, K.F.; Wolf, G.; Stahl, R.; Wenzel, U. Rapid development of severe end-organ damage in C57BL/6 mice by combining DOCA salt and angiotensin II. *Kidney Int.* **2008**, *73*, 643–650. [CrossRef]

140. Wang, Q.; Euy-Myoung, J.; Liu, H.; Gu, L.; Dudley, S.C.; Yu, J. Astragaloside IV improves left ventricular diastolic dysfunction in hypertensive mice by increasing the phosphorylation of endothelial nitric oxide synthase. *J. Hypertens.* **2016**, *34*, e48–e49. [CrossRef]
141. Landmesser, U.; Dikalov, S.; Price, S.R.; McCann, L.; Fukai, T.; Holland, S.M.; Mitch, W.E.; Harrison, D.G. Oxidation of tetrahydrobiopterin leads to uncoupling of endothelial cell nitric oxide synthase in hypertension. *J. Clin. Investig.* **2003**, *111*, 1201–1209. [CrossRef] [PubMed]
142. Guzik, T.J.; Hoch, N.E.; Brown, K.A.; McCann, L.A.; Rahman, A.; Dikalov, S.; Goronzy, J.; Weyand, C.; Harrison, D.G. Role of the T cell in the genesis of angiotensin II induced hypertension and vascular dysfunction. *J. Exp. Med.* **2007**, *204*, 2449–2460. [CrossRef] [PubMed]
143. Tian, Y.; Luo, J.; Xu, Q.; Liu, Y.; Cai, R.; Zhou, M.-S. Macrophage depletion protects against endothelial dysfunction and cardiac remodeling in angiotensin II hypertensive mice. *Clin. Exp. Hypertens.* **2021**, *43*, 699–706. [CrossRef]
144. Regan, J.A.; Mauro, A.G.; Carbone, S.; Marchetti, C.; Gill, R.; Mezzaroma, E.; Raleigh, J.V.; Salloum, F.N.; Van Tassel, B.W.; Abbate, A.; et al. A mouse model of heart failure with preserved ejection fraction due to chronic infusion of a low subpressor dose of angiotensin II. *Am. J. Physiol. Heart Circ. Physiol.* **2015**, *309*, H771–H778. [CrossRef]
145. Wang, B.; Xu, M.; Li, W.; Li, X.; Zheng, Q.; Niu, X. Aerobic exercise protects against pressure overload-induced cardiac dysfunction and hypertrophy via β3-AR-nNOS-NO activation. *PLoS ONE* **2017**, *12*, e0179648. [CrossRef]
146. Chen, Y.; Guo, H.; Xu, D.; Xu, X.; Wang, H.; Hu, X.; Lu, Z.; Kwak, D.; Xu, Y.; Gunther, R.; et al. Left ventricular failure produces profound lung remodeling and pulmonary hypertension in mice: Heart failure causes severe lung disease. *Hypertension* **2012**, *59*, 1170–1178. [CrossRef]
147. An, D.; Zeng, Q.; Zhang, P.; Ma, Z.; Zhang, H.; Liu, Z.; Li, J.; Ren, H.; Xu, D. Alpha-ketoglutarate ameliorates pressure overload-induced chronic cardiac dysfunction in mice. *Redox Biol.* **2021**, *46*, 102088. [CrossRef] [PubMed]
148. Tsujita, Y.; Kato, T.; Sussman, M.A. Evaluation of left ventricular function in cardiomyopathic mice by tissue Doppler and color M-mode Doppler echocardiography. *Echocardiography* **2005**, *22*, 245–253. [CrossRef]
149. Lu, Z.; Xu, X.; Hu, X.; Zhu, G.; Zhang, P.; van Deel, E.D.; French, J.P.; Fassett, J.T.; Oury, T.D.; Bache, R.J.; et al. Extracellular superoxide dismutase deficiency exacerbates pressure overload-induced left ventricular hypertrophy and dysfunction. *Hypertension* **2008**, *51*, 19–25. [CrossRef]
150. Zi, M.; Stafford, N.; Prehar, S.; Baudoin, F.; Oceandy, D.; Wang, X.; Bui, T.; Shaheen, M.; Neyses, L.; Cartwright, E.J. Cardiac hypertrophy or failure?—A systematic evaluation of the transverse aortic constriction model in C57BL/6NTac and C57BL/6J substrains. *Curr. Res. Physiol.* **2019**, *1*, 1–10. [CrossRef]
151. Baier, M.J.; Klatt, S.; Hammer, K.P.; Maier, L.S.; Rokita, A.G. Ca2+/calmodulin-dependent protein kinase II is essential in hyperacute pressure overload. *J. Mol. Cell Cardiol.* **2020**, *138*, 212–221. [CrossRef] [PubMed]
152. Slater, R.E.; Strom, J.G.; Methawasin, M.; Liss, M.; Gotthardt, M.; Sweitzer, N.; Granzier, H.L. Metformin improves diastolic function in an HFpEF-like mouse model by increasing titin compliance. *J. Gen. Physiol.* **2019**, *151*, 42–52. [CrossRef]
153. Qiu, Z.; Fan, Y.; Wang, Z.; Huang, F.; Li, Z.; Sun, Z.; Hua, S.; Jin, W.; Chen, Y. Catestatin Protects Against Diastolic Dysfunction by Attenuating Mitochondrial Reactive Oxygen Species Generation. *J. Am. Heart Assoc.* **2023**, *12*, e029470. [CrossRef]
154. Methawasin, M.; Granzier, H. Experimentally Increasing the Compliance of Titin Through RNA Binding Motif-20 (RBM20) Inhibition Improves Diastolic Function in a Mouse Model of Heart Failure with Preserved Ejection Fraction. *Circulation* **2016**, *134*, 1085–1099. [CrossRef]
155. Dimitriadis, K.; Theofilis, P.; Koutsopoulos, G.; Pyrpyris, N.; Beneki, E.; Tatakis, F.; Tsioufis, P.; Chrysohoou, C.; Fragkoulis, C.; Tsioufis, K. The role of coronary microcirculation in heart failure with preserved ejection fraction: An unceasing odyssey. *Heart Fail. Rev.* **2025**, *30*, 75–88. [CrossRef] [PubMed]
156. Marie, A.; Larroze-Chicot, P.; Cosnier-Pucheu, S.; Gonzalez-Gonzalez, S. Senescence-accelerated mouse prone 8 (SAMP8) as a model of age-related hearing loss. *Neurosci. Lett.* **2017**, *656*, 138–143. [CrossRef]
157. Reed, A.L.; Tanaka, A.; Sorescu, D.; Liu, H.; Jeong, E.-M.; Strudy, M.; Walp, E.R.; Dudley, S.C., Jr.; Sutliff, R.L. Diastolic dysfunction is associated with cardiac fibrosis in the senescence-accelerated mouse. *Am. J. Physiol. Heart Circ. Physiol.* **2011**, *301*, H824–H831. [CrossRef]
158. Rodriguez-Calvo, R.; Serrano, L.; Barroso, E.; Coll, T.; Palomer, X.; Camins, A.; Sánchez, R.M.; Alegret, M.; Merlos, M.; Pallàs, M.; et al. Peroxisome Proliferator-Activated Receptor Down-Regulation Is Associated with Enhanced Ceramide Levels in Age-Associated Cardiac Hypertrophy. *J. Gerontol. A Biol. Sci. Med. Sci.* **2007**, *62*, 1326–1336. [CrossRef] [PubMed]
159. Giridharan, V.V.; Karupppagounder, V.; Arumugam, S.; Nakamura, Y.; Guha, A.; Barichello, T.; Quevedo, J.; Watanabe, K.; Konishi, T.; Thandavarayan, R.A. 3,4-Dihydroxybenzalacetone (DBL) Prevents Aging-Induced Myocardial Changes in Senescence-Accelerated Mouse-Prone 8 (SAMP8) Mice. *Cells* **2020**, *9*, 597. [CrossRef]
160. Forman, K.; Vara, E.; García, C.; Kireev, R.; Cuesta, S.; Escames, G.; Tresquerres, J. Effect of a Combined Treatment with Growth Hormone and Melatonin in the Cardiological Aging on Male SAMP8 Mice. *J. Gerontol. A Biol. Sci. Med. Sci.* **2011**, *66A*, 823–834. [CrossRef]

161. Takeda, T.; Matsushita, T.; Kurozumi, M.; Takemura, K.; Higuchi, K.; Hosokawa, M. Pathobiology of the senescence-accelerated mouse (SAM). *Exp. Gerontol.* **1997**, *32*, 117–127. [CrossRef]
162. Zhou, H.; Peng, W.; Li, F.; Wang, Y.; Wang, B.; Ding, Y.; Lin, Q.; Zhao, Y.; Pan, G.; Wang, X. Effect of Sodium-Glucose Cotransporter 2 Inhibitors for Heart Failure with Preserved Ejection Fraction: A Systematic Review and Meta-Analysis of Randomized Clinical Trials. *Front. Cardiovasc. Med.* **2022**, *4*, 875327. [CrossRef] [PubMed]
163. Lin, Y.; Cai, Z.; Yuan, J.; Liu, H.; Pang, X.; Chen, Q.; Tang, X.; Geng, Q.; Dong, S. Effect of pharmacological treatment on outcomes of heart failure with preserved ejection fraction: An updated systematic review and network meta-analysis of randomized controlled trials. *Cardiovasc. Diabetol.* **2022**, *21*, 237. [CrossRef]
164. Croteau, D.; Baka, T.; Young, S.; He, H.; Chambers, J.M.; Qin, F.; Panagia, M.; Pimentel, D.R.; Balschi, J.A.; Colucci, W.S.; et al. SGLT2 inhibitor ertugliflozin decreases elevated intracellular sodium, and improves energetics and contractile function in diabetic cardiomyopathy. *Biomed. Pharmacother.* **2023**, *160*, 114310. [CrossRef] [PubMed]
165. Luo, Y.; Ye, T.; Tian, H.; Song, H.; Kan, C.; Han, F.; Hou, N.; Sun, X.; Zhang, J. Empagliflozin alleviates obesity-related cardiac dysfunction via the activation of SIRT3-mediated autophagosome formation. *Lipids Health Dis.* **2024**, *23*, 308. [CrossRef] [PubMed]
166. Moellmann, J.; Klinkhammer, B.M.; Droste, P.; Kappel, B.; Haj-Yehia, E.; Maxeiner, S.; Artati, A.; Adamski, J.; Boor, P.; Schütt, K.; et al. Empagliflozin improves left ventricular diastolic function of db/db mice. *Biochim. Biophys. Acta Mol. Basis Dis.* **2020**, *1866*, 165807. [CrossRef]
167. Wang, J.; Huang, X.; Liu, H.; Chen, Y.; Li, P.; Liu, L.; Li, J.; Ren, Y.; Huang, J.; Xiong, E.; et al. Empagliflozin Ameliorates Diabetic Cardiomyopathy via Attenuating Oxidative Stress and Improving Mitochondrial Function. *Oxid. Med. Cell Longev.* **2022**, *2022*, 1122494. [CrossRef]
168. Byrne, N.J.; Parajuli, N.; Levasseur, J.L.; Boisvenue, J.; Beker, D.L.; Masson, G.; Fedak, P.W.M.; Verma, S.; Dyck, J.R.B. Empagliflozin Prevents Worsening of Cardiac Function in an Experimental Model of Pressure Overload-Induced Heart Failure. *JACC Basic. Transl. Sci.* **2017**, *2*, 347–354. [CrossRef]
169. Karakasis, P.; Fragakis, N.; Patoulias, D.; Theofilis, P.; Sagris, M.; Koufakis, T.; Vliachakis, P.K.; Rangraze, I.R.; Tanani, M.; Tsioufis, K.; et al. The emerging role of glucagon-like peptide-1 receptor agonists in the management of obesity-related heart failure with preserved ejection fraction: Benefits beyond what scales can measure? *Biomedicines* **2024**, *12*, 2112. [CrossRef]
170. Ni, X.-Y.; Feng, X.-J.; Wang, Z.-H.; Zhang, Y.; Little, P.J.; Cao, Y.; Xu, S.-W.; Tang, L.-Q.; Weng, J.-P. Empagliflozin and liraglutide ameliorate HFpEF in mice via augmenting the Erbb4 signaling pathway. *Acta Pharmacol. Sin.* **2024**, *45*, 1604–1617. [CrossRef]
171. Koike, M.; Saito, H.; Kohno, G.; Takubo, M.; Watanabe, K.; Ishihara, H. Effects of GLP-1RA and SGLT2i, alone or in combination, on mouse models of type 2 diabetes representing different disease stages. *Int. J. Mol. Sci.* **2021**, *22*, 11463. [CrossRef] [PubMed]
172. Withaar, C.; Meems, L.; Nollet, E.E.; Schouten, E.M.; Schroeder, M.A.; Knudsen, L.B.; Niss, K.; Madsen, C.T.; Hoegl, A.; Mazzoni, G.; et al. The cardioprotective effects of semaglutide exceed those of dietary weight loss in mice with HFpEF. *JACC Basic. Transl. Sci.* **2023**, *8*, 1298–1314. [CrossRef] [PubMed]

Disclaimer/Publisher's Note: The statements, opinions and data contained in all publications are solely those of the individual author(s) and contributor(s) and not of MDPI and/or the editor(s). MDPI and/or the editor(s) disclaim responsibility for any injury to people or property resulting from any ideas, methods, instructions or products referred to in the content.

biomedicines

MDPI

Review

Risk Assessment and Personalized Treatment Options in Inherited Dilated Cardiomyopathies: A Narrative Review

Diana-Aurora Arnautu [1,2], Dragos Cozma [3], Ioan-Radu Lala [4], Sergiu-Florin Arnautu [2,*], Mirela-Cleopatra Tomescu [1,2] and Minodora Andor [1,2]

[1] Multidisciplinary Heart Research Center, Victor Babes University of Medicine and Pharmacy, 300041 Timisoara, Romania; aurora.bordejevic@umft.ro (D.-A.A.); tomescu.mirela@umft.ro (M.-C.T.)
[2] Department of Internal Medicine I, Victor Babes University of Medicine and Pharmacy, 300041 Timisoara, Romania
[3] Department of Cardiology, Victor Babes University of Medicine and Pharmacy, 300041 Timisoara, Romania
[4] Department of Cardiology, Western University Vasile Goldis, 310025 Arad, Romania
* Correspondence: arnautu.sergiu@umft.ro

Abstract: Considering the worldwide impact of heart failure, it is crucial to develop approaches that can help us comprehend its root cause and make accurate predictions about its outcome. This is essential for lowering the suffering and death rates connected with this widespread illness. Cardiomyopathies frequently result from genetic factors, and the study of heart failure genetics is advancing quickly. Dilated cardiomyopathy (DCM) is the most prevalent kind of cardiomyopathy, encompassing both genetic and nongenetic abnormalities. It is distinguished by the enlargement of the left ventricle or both ventricles, accompanied by reduced contractility. The discovery of the molecular origins and subsequent awareness of the molecular mechanism is broadening our knowledge of DCM development. Additionally, it emphasizes the complicated nature of DCM and the necessity to formulate several different strategies to address the diverse underlying factors contributing to this disease. Genetic variants that can be transmitted from one generation to another can be a significant contributor to causing family or sporadic hereditary DCM. Genetic variants also play a significant role in determining susceptibility for acquired triggers for DCM. The genetic causes of DCM can have a large range of phenotypic expressions. It is crucial to select patients who are most probable to gain advantages from genetic testing. The purpose of this research is to emphasize the significance of identifying genetic DCM, the relationships between genotype and phenotype, risk assessment, and personalized therapy for both those affected and their relatives. This approach is expected to gain importance once treatment is guided by genotype-specific advice and disease-modifying medications.

Keywords: inherited dilated cardiomyopathy; risk assessment; genotype-specific therapy

1. Introduction

Dilated cardiomyopathy (DCM) affects more than 0.4% of the general population and is the second most frequent cause of heart failure, accounting for around 36% of all heart failure patients, second only to coronary artery disease. The 5-year survival rate following a heart failure diagnosis is just 50%, and mortality might result from arrhythmias or the gradual worsening of heart failure [1]. While there have been some decreases in the occurrence of heart failure due to a decrease in risk factors for cardiovascular disease and more effective therapy, the economic cost associated with HF remains substantial [2]. Approximately 25–30% of individuals diagnosed with DCM are believed to have a hereditary factor that can be identified [3]. The exact prevalence of genetically caused DCM is unknown. It is estimated to vary from 4‰ to 0.4‰. Around 25% of individuals with idiopathic DCM have a family history of the disease. These data are obtained predominantly from European people [3].

Genetic factors that contribute to DCM are not simply caused by individual DNA variants with significant effects, as in a Mendelian model. It is likely that various mutations with unimportant individual outcomes may together contribute to the inherited cardiomyopathy. Even in acquired forms of DCM (such as those induced by alcohol abuse or chemotherapy) one cannot dismiss the possibility of a significant genetic vulnerability to the respective condition [4,5].

Hereditary DCM is classified into syndromic and non-syndromic.

The term "syndromic" is used to describe an illness that is identified by a combination of visible characteristics that either strongly indicate the diagnosis and may be verified by genetic testing or allow for diagnosis even without definitive genetic evidence [6].

Patients with DCM that is neither acquired (secondary) nor syndromic present a non-syndromic hereditary condition [6,7].

The diagnosis of non-syndromic DCM is established when at least two relatives meet the criteria for DCM, or when the patient fulfils the criteria for DCM and has a first-degree family member that died suddenly at an age < 35 years [8]. Non-syndromic DCM is typically anticipated when individuals in the proband's family have a history of heart failure or of premature and unexpected cardiac death without a clearly identifiable reason. If an enlargement of the LV is observed without a significant decrease in LVEF at the evaluation of close relatives, it is advisable to consider a diagnosis of non-syndromic DCM [4,5].

Inherited DCM is frequently met as a sporadic illness in clinical practice, meaning that there is no documented familial history of DCM. The hereditary aspect of DCM, how-ever, is frequently not immediately evident. If a family history is not thoroughly obtained, DCM may be incorrectly labelled as sporadic [9]. Innovative studies conducted by the team at the Mayo Clinic throughout the 1980s and 1990s showed that by systematically screening the family members of individuals with DCM, it was possible to identify familial DCM in around 20–30% of the patients [10,11].

In a recent study, Huggins et al. examined a large dataset from many centers. They found that around 12% of the probands had familial dilated cardiomyopathy (DCM) when just the probands were included. However, when all family members were tested, the estimated frequency of familial DCM was over 30% [12]. The study was a cross-sectional multicenter study that lacked a pre-planned standardized approach and just some of the family members were evaluated. Thus, it is possible to hypothesize that the occurrence of familial DCM may have been greater if all family members at risk of the probands were carefully assessed. Similarly, conducting regular assessments throughout the years would likely result in the detection of a greater proportion of familial DCM cases due to the influence of age on the likelihood of developing the condition. The study con-ducted by Huggins et al. found that the occurrence of familial DCM was somewhat more common in Black probands compared to White probands. This might indicate the impact of mutations that enhance the manifestation of a characteristic. Additionally, it might be indicative of the demographic features of the research population and the statistical methods employed to calculate the frequency of familial DCM. The discovery should be regarded as speculative until it is tested for duplication in separate groups.

In this review, we focus on adult patients with non-syndromic inherited DCM. Our objective is to assist clinicians in comprehending the clinical significance of the hereditary DCM, identifying individuals and their relatives that could benefit from genetic evaluations, acquainting them with frequently conducted genetic tests, guiding them in understanding genetic findings, and informing them about the medical importance of these findings.

2. Defining Hereditary Dilated Cardiomyopathy (DCM)

A cardiomyopathy is defined as a disease of the myocardium that is structurally and functionally abnormal, in the absence of ischemic heart disease, valvular heart disease, hypertension or congenital heart disease [4].

DCM is defined as the presence of LV dilatation and global or regional systolic dysfunction unexplained solely by abnormal loading conditions or coronary artery disease. In early stages, DCM may present with isolated left ventricular dilatation and normal ejection fraction [4]. Right ventricular dilatation and dysfunction may be present but are not necessary for the diagnosis. When dilatation or wall motion abnormalities are predominant to the right ventricle, the possibility of arrhythmogenic right ventricular cardiomyopathy (ARVC) should be considered [4].

Corresponding to the European Society of Cardiology Guidelines for the management of cardiomyopathies [5], left ventricular (LV) dilatation is defined by echocardiography measurements as LV end-diastolic dimensions or volumes that exceed two standard deviations over the average values for the general population, taking into account body size, sex, and/or age. In adults, this refers to an LV end-diastolic diameter of more than 58 mm in men and greater than 52 mm in females, as well as an LV end-diastolic volume index equal to or greater than 75 mL/m^2 in males and equal to or greater than 62 mL/m^2 in females. LV global systolic dysfunction is characterized by a left ventricular ejection fraction (LVEF) that is less than 50%.

LV dilatation and systolic dysfunction are usually assessed from a two-dimensional (2D) echocardiogram or from cardiac magnetic resonance imaging MRI [5]. Another non-invasive methodology is myocardial nuclear research. LV ejection fractions (EFs) can also be measured using an LV angiogram [6].

Once ischemia and nonischemic causes (valvular disease, hypertension, congenital heart disease, tachyarrhythmias, thyroid disease, inflammatory or infectious diseases, radiation, toxins—most common alcohol, chemotherapeutic agents or drugs with idiosyncratic effects) have been eliminated using non-invasive assessment, most often cardiac (MRI), DCM is classified as idiopathic. In rare cases, endomyocardial biopsy is needed [5].

Due to the expanding accessibility of genetic testing, about 20–35% of individuals with presumed idiopathic DCM have been discovered to possess a related genetic mutation [5–7].

3. Diagnosis of Hereditary DCM

3.1. Clinical Picture

The majority of patients diagnosed with DCM are adults, with onset usually occurring in the third or fourth decade of life [9–12]. The first symptoms might be con-fusing and often do not provide enough information to distinguish it from other causes of DCM. The manifestations of illness vary from an absence of symptoms, found only during screening, to severe heart failure or life-threatening arrhythmia and unexpected cardiac death.

Heart failure symptoms involve those of systemic and/or pulmonary congestion (dyspnea, edema), as well as of reduced cardiac output (fatigue) [6].

Palpitations also frequently occur as symptoms due to arrhythmias and/or conduction system disease [6].

Stroke or systemic embolism may develop consequent to left ventricular mural thrombus [6].

Peripartum cardiomyopathy, occurring during or soon after pregnancy, was once considered a rare non-genetic condition, but is now recognized as a form of familial DCM [6]. Current research indicates that up to 15% of individuals with peripartum cardiomyopathy carry pathogenic genetic mutations. For women who have genetic predisposition, pregnancy is believed to act as a trigger by causing higher stress on the circulatory system. This can lead to the manifestation of the disease at an earlier stage than it would typically occur [13,14]. Women with a positive genotype may have a lower likelihood of experiencing a reversal of DCM after pregnancy compared to those who have a negative genotype.

Pointers that suggest a genetic cause include the occurrence of cardiomyopathy or arrhythmia before the age of 35 years, as well as a family history of DCM or sudden cardiac death. Other suggestive conditions are unexplained syncope, the association of cardiomyopathy with arrhythmia, and/or muscle disorders [15]. Ventricular and atrial arrhythmias, as well as conduction disorders, may develop when the left ventricular ejection fraction decreases [16].

Some individuals with inherited DCM have early or obvious abnormalities in their conduction system. When a younger individual experiences conduction disorders, it should raise the possibility of hereditary cardiomyopathy. Electrocardiogram findings may include bradycardia, atrioventricular blocks, axis deviation, or bundle branch blocks [15].

Figure 1 presents the ECG of an adult patient with familial dilated cardiomyopathy at sinus rhythm (A) with cardiac ventricular late potentials (B), while Figure 2 presents an episode of sustained ventricular tachycardia.

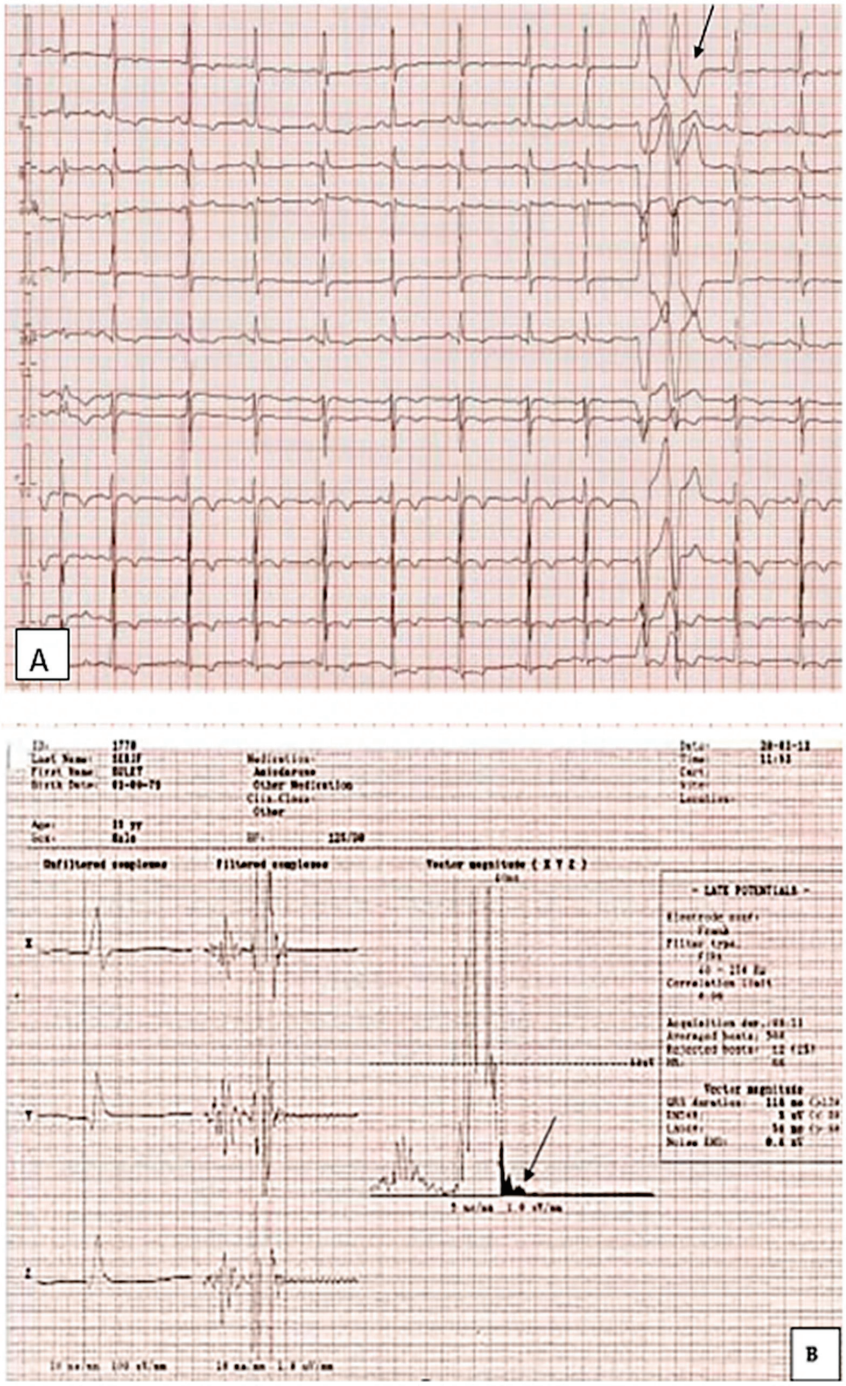


Figure 1. Twelve-lead electrocardiogram in a patient with familial dilated cardiomyopathy. (**A**) Sinus rhythm with recurring premature ventricular beats (arrow). Negative T waves from V1 to V6. (**B**) Ventricular late potentials (arrow).

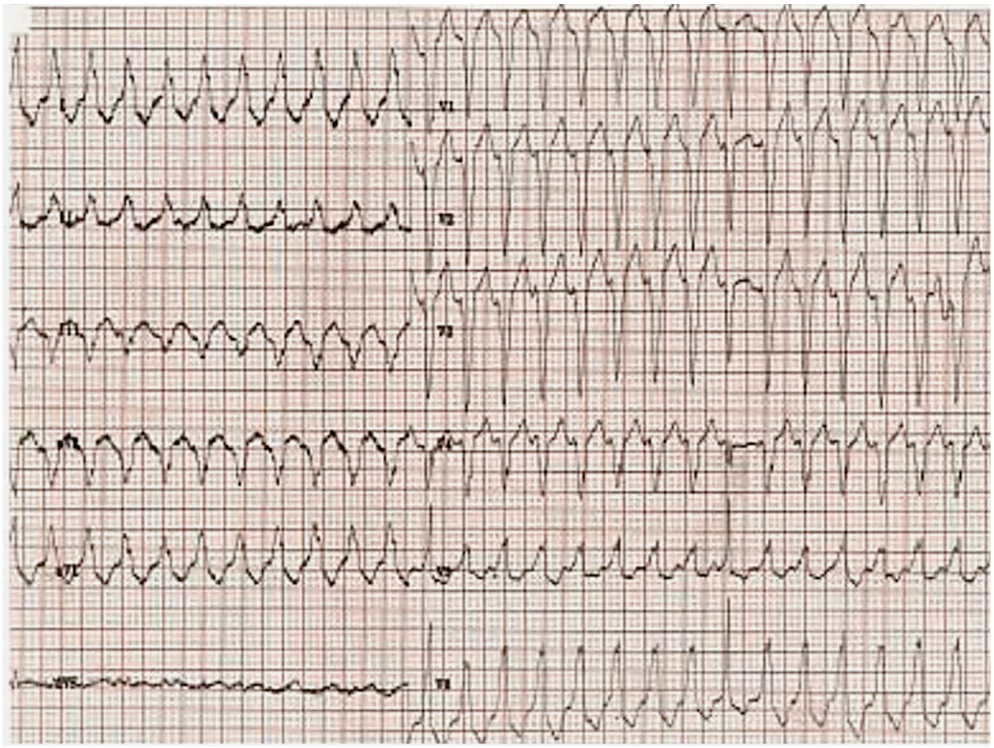


Figure 2. Twelve-lead electrocardiogram. Sustained ventricular tachycardia.

Ventricular late potentials (VLPs) are high-frequency, low-amplitude abnormal electrical signals occurring in the terminal QRS complex or on the ST segment of the electrocardiogram during sinus rhythm. They represent delayed conduction through a diseased myocardium and consist of the presence of electrical activity after the end of the standard QRS. The VLPs are potential substrates for reentry ventricular tachycardia.

The occurrence and intensity of cardiac arrhythmias may not be directly related to the amount of LVEF decrease. The significant similarity in genetics and physical features between arrhythmogenic DCM and arrhythmogenic right ventricular cardiomyopathy (ARVC) with left ventricular involvement has caused a lot of difficulty in diagnosis. As a result, a novel category called "arrhythmogenic cardiomyopathy" has emerged [13].

Unusual but significant warning signs such as atypical skin coloration, muscle weakness, and sensory abnormalities (such as hearing or vision loss) might suggest a particular sort of multisystem illness or a distinct genetic profile to DCM. The presence of these symptoms is sometimes referred to as "red flags" for DCM diagnosis [17]. A significant number of individuals diagnosed with inherited skeletal myopathies, such as Duchenne or Becker, experience the development of DCM as they age [18,19]. DCM can also emerge as part the clinical picture in systemic illnesses such storage or mitochondrial abnormalities [7].

While certain genetic variants may exhibit foreseeable trends, there can be significant variability in the manifestation of diseases, the age at which they appear, and their severity among individuals who possess variants in the same gene [20,21]. This variability can occur both within families and between different families. The penetrance of DCM can be affected by environmental variables, gene modulators, associated medical conditions, and lifestyle choices [20]. These are currently being studied. Genetic diversity may explain the variable individual vulnerability to acquired types of DCM, such as those induced by alcohol abuse or anthracycline cardiotoxicity. This complicates the distinction between hereditary and acquired myocardial diseases [12,21].

3.2. Non-Invasive Imaging Methods

They are essential for diagnosing and monitoring patients with cardiomyopathies. These methods include ultrasound-based techniques, cardiac magnetic resonance (CMR)

imaging, computed tomography (CT), and nuclear techniques including positron emission tomography (PET) and scintigraphy [5].

Regular screening, including clinical evaluation, electrocardiogram (ECG), and transthoracic echocardiography (TTE), should begin in adulthood or earlier if there are treatment implications [22]. The frequency of screening can range from every six months to every five years, depending on the existence or not of high-risk indicators and the usual age at which the illness typically appears in the family [20,22]. LV dilatation on TTE in asymptomatic relatives might indicate subclinical illness, incidental illness, or physiological modifications. It is difficult to differentiate between these conditions, and since there is no dependable method to identify those who may develop obvious illness, regular surveillance is required [23]. Currently, the screening criterion in TTE continues to be the LV size and ejection fraction. However, continuing research is being conducted to explore alternative preclinical indicators. Recently, researchers have assessed the global longitudinal strain of the LV and observed a decrease in patients who are genotype-positive but phenotype-negative compared to genotype-negative controls. Yet, the exact significance of global longitudinal strain in detecting or monitoring subclinical GDCM has not been determined [5,24].

Myocardial deformation imaging, specifically using speckle tracking or tissue Doppler, is a more sensitive indicator than EF (ejection fraction) for detecting subtle ventricular dysfunction. This is particularly useful in cases such as genotype-positive HCM (hypertrophic cardiomyopathy), DCM, and ARVC (arrhythmogenic right ventricular cardiomyopathy) in family members. It also helps identify specific causes of ventricular hypertrophy, such as amyloidosis, athlete's heart, or HCM. Mechanical dispersion serves as a sign of abnormal contraction and draws attention to subtle structural abnormalities [25–29]. Figure 3 exemplifies a patient with familial DCM examined by two-dimensional (2D) transthoracic conventional echocardiography and by 2D speckle-tracking echography. It shows dilated heart chambers, severe LV dysfunction (LVEF of 30%), and a Bull's eye myocardial deformation pattern with overall low peak ventricular longitudinal strain values.

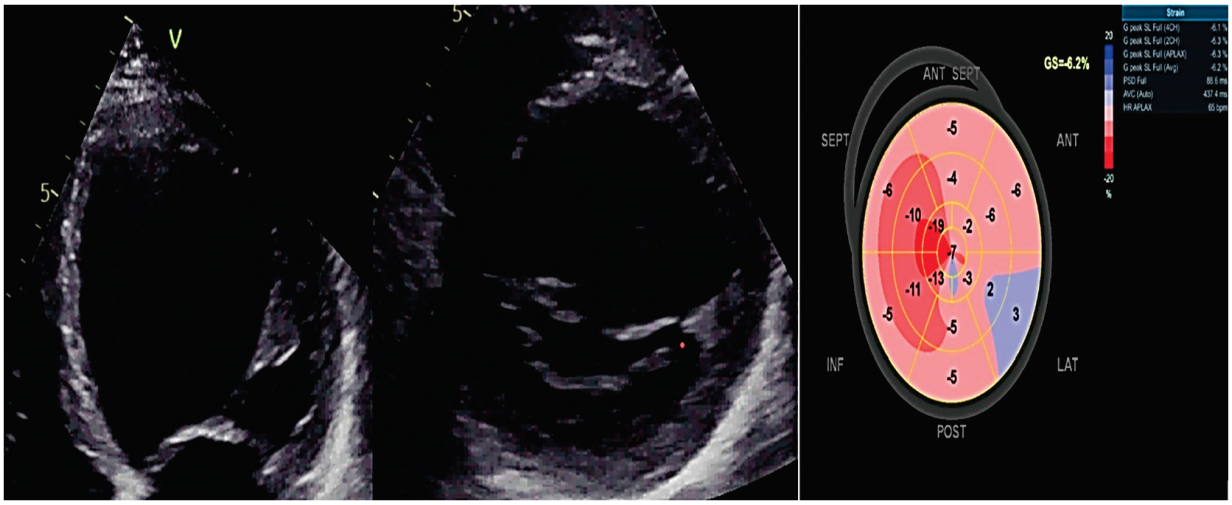


Figure 3. Familial dilated cardiomyopathy. Two-dimensional trans-thoracic conventional echography in apical longitudinal and parasternal short axis vi ews. Bull's eye myocardial deformation with diffuse reduced left ventricular longitudinal peak strain patterns.

Three-dimensional echocardiography measures, with high accuracy, the volumes of heart chambers, but it needs an adequate acoustic window. Contrast agents may be used to enhance the visibility of endocardium in order to show the existence of excessive muscle trabeculation, a condition known as hyper-trabeculation. Additionally, contrast agents can help rule out the presence of intracardiac thrombus [5].

CMR imaging has become the most reliable method for evaluating the size and function of the ventricles [5,24]. It should be performed in all patients recently diagnosed with cardiomyopathy. CMR can offer comprehensive anatomical and physiological data that surpass that of TTE. Additionally, CMR can provide insights into cardiac tissue features, including inflammation and fibrosis, through the use of late gadolinium enhancement (LGE).

CMR has the benefits of being non-invasive and not requiring an acoustic window while also allowing for the analysis of tissue characteristics. The latter benefit is especially crucial in diagnosing non-compaction LV cardiomyopathy (Figure 4), ARVC, myocarditis, amyloidosis, sarcoidosis, and other types of inflammatory diseases, as well as haemochromatosis [29,30]. Standard initial examination should regularly include cine imaging sequences, T2-weighted sequences, pre- and post-contrast T1 mapping, and LGE. These findings should be evaluated alongside genetic results and other clinical features by experienced professionals in cardiac imaging and heart muscle disease assessment [31].

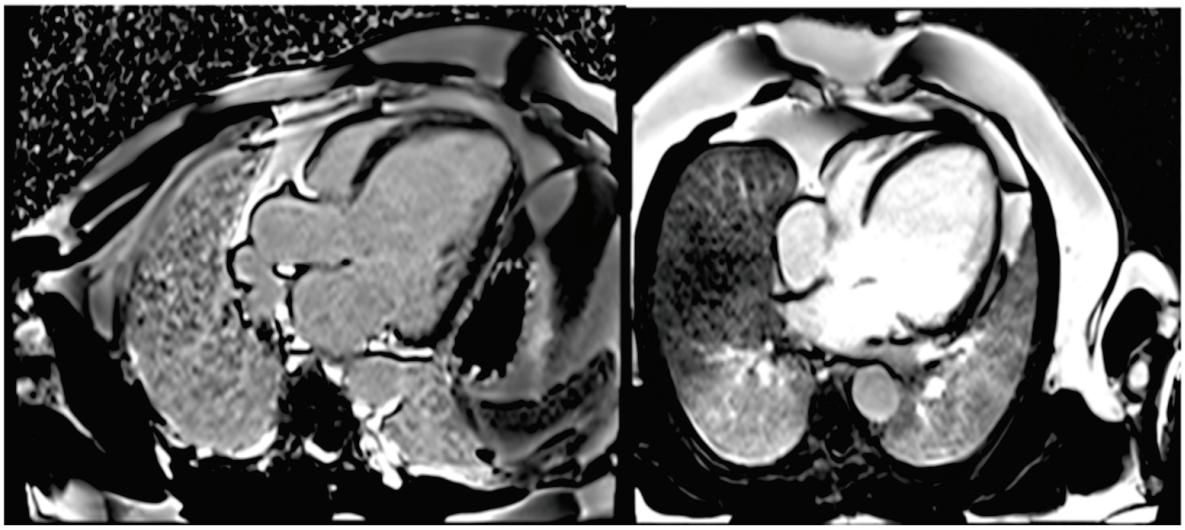


Figure 4. Cardiac magnetic resonance images, 4-chamber (horizontal long axis) and 2-chamber (vertical long axis). Dilated left ventricle with hyper-trabeculations of the antero-lateral wall; late gadolinium enhancement shows septal mid-wall fibrosis, suggestive of idiopathic dilative cardiomyopathy with left ventricular non-compaction.

Regular follow-up CMR should be conducted every 2–5 years, depending on the initial severity and clinical course of the disease. This can help assess the progression of the disease and the effectiveness of therapy [5]. The existence of LGE is linked to the possibility for arrhythmias and more severe illness [23]. Diseases connected to DSP and FLNC frequently exhibit a fibrosis pattern resembling a ring around the outer layer of the heart, known as subepicardial fibrosis [30]. This observation may suggest the need for considering the installation of an implantable cardioverter defibrillator (ICD) [31]. CMR has the capability to identify illness in persons who do not show any symptoms and may also be used to track the progression of the disease [29].

The existence of LGE is linked to the possibility for arrhythmias and more severe illness. Diseases connected to DSP and FLNC frequently exhibit a fibrosis pattern resembling a ring around the outer layer of the heart, known as subepicardial fibrosis, as presented in Figure 5. This observation may suggest the need for considering the installation of an implantable cardioverter defibrillator (ICD). CMR has the capability to identify illness in persons who do not show any symptoms and may also be used to track the progression of the disease [29].

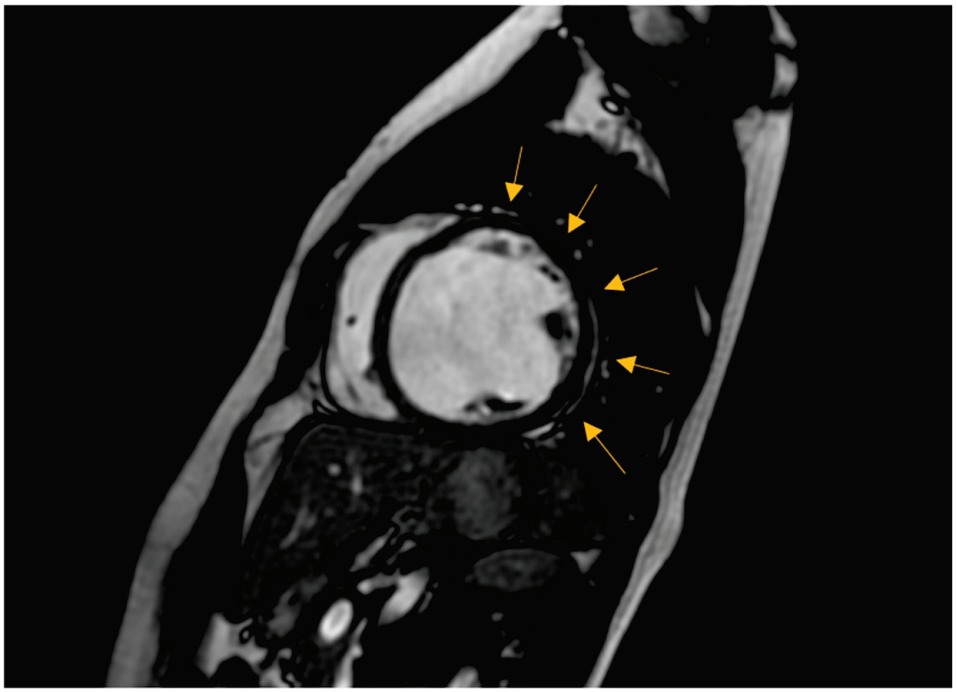


Figure 5. Cardiac magnetic resonance image, short axis. Dilated left ventricle with thin walls; late gadolinium enhancement highlights circumferential "ring-shape" mid wall fibrosis suggestive of desmoplakin cardiomyopathy (arrows).

Computed tomography-based imaging is mostly employed in patients suspected of having cardiomyopathy to exclude coronary artery disease (CAD), either as an alternative diagnosis or as a comorbidity that impacts clinical symptoms and progression [32].

Additional functional testing and imaging may be necessary on a case-by-case basis during the evaluation process.

3.3. Endomyocardial Biopsy

This invasive method is a topic of debate and is not currently included in the usual diagnostic process for most individuals with DCM [20].

3.4. Laboratory Assessment

Currently, there are no established disease-specific biomarkers for DCM [5]. However, researchers are actively investigating this area. Despite the lack of acute myocardial ischemia, high-sensitivity blood troponins frequently show aberrant levels in both acute and chronic heart failure [33]. While troponin testing may offer some risk assessment in cases of cardiomyopathy, it has a small role in the evaluation of suspected DCM [34].

Consistently high levels of serum creatinine kinase (CK) can indicate the presence of myopathies or neuromuscular illnesses such as dystrophinopathies (such as X-linked DCM or Becker muscular dystrophy), laminopathies, desminopathies, or, to a lesser extent, myofibrillar myopathy [29]. Patients with arrhythmogenic right ventricular cardiomyopathy and non-dilated LV cardiomyopathy may exhibit elevated levels of C-reactive protein, especially during bouts resembling myocarditis [35]. Increased concentrations of iron and ferritin in the blood, together with high transferrin saturation, may indicate a potential diagnosis of haemochromatosis. This should prompt additional investigation into the underlying cause (primary or secondary) by genetic testing. Leucocytopenia, lactic acidosis, and myoglobinuria may point towards the presence of mitochondrial disorders [5].

4. History Taking of the Initial Patient with Recently Diagnosed DCM and Family Screening

A comprehensive history taking is necessary for all patients recently diagnosed with DCM. This evaluation is crucial to ensure that any potentially curable or reversible causes are not overlooked. Nevertheless, the presence of a visible immediate factor such as alcohol abuse or chemotherapy does not rule out the possibility of a hereditary element in cardiomyopathy [5]. Women who have a genetic predisposition to peripartum cardiomyopathy may experience a faster beginning of the disease and show symptoms at a younger age compared to other members of their family [14,36]. The family's medical history at the time of diagnosis may show no signs of illness. Regularly reviewing the family history is crucial, since it may evolve to become positive over time [7]. reference

Hereditary DCM is recognized clinically when it develops in two or more closely related individuals, after ruling out other potential causes. An exhaustive family history should encompass a three-generation genealogy [24] that investigates any instances of heart failure, arrhythmia, unexplained mortality, or other cardiac symptoms, especially if they arose at an age younger than expected. An awareness of other symptoms, such as muscular disorders, is also necessary.

The symptoms of the family member do not necessarily have to match those of the reference patient. There are several difficulties in establishing a satisfactory heritage. The variety of illness onset and penetrance of the genetic anomaly, as well as the long period of time it takes for the disease to develop, might complicate the screening process for those who are willing to undergo it. Certain family members manifest hesitation or incapacity to undergo evaluation, while in other cases, families are limited in size and possess insufficient data. Although there are difficulties, it is crucial to create a pedigree as it aids in determining the likelihood of a genetic test being positive [24].

It is worth mentioning that around 25% of individuals with sporadic DCM are later identified as having familial DCM after a thorough evaluation of both the affected individual and their family members [25].

According to research, there is a 33% chance that a family member develops DCM or a partial phenotype of DCM by the age of 80. A partial phenotype is characterized as having either left ventricular enlargement or solely left ventricular systolic dysfunction [37]. For individuals newly diagnosed with DCM, it is recommended that their first-degree relatives have a medical assessment. This evaluation should include clinical cardiovascular screening and genetic testing. These recommendations are supported by guidelines [16,37–40]. Cardiovascular screening, which encompasses cardiovascular history, clinical examination, electrocardiogram, and cardiac imaging, serves to detect the early signs of cardiomyopathy, including asymptomatic or partial DCM phenotype cases [12]. This allows for individualized monitoring or medical treatment prior to the appearance of symptoms, with the objective of preventing the progression of DCM or premature sudden death.

It is advisable to carry out clinical screening for all unaffected first-degree relatives of any person with a genetic anomaly linked to proven or suspected familial DCM [16,41]. The screening of family members not only helps diagnose the primary case, but also often leads to the detection of the disease in persons showing no symptoms who might benefit from clinical examination. Genealogy assessment also aids in the identification of family members exhibiting pertinent phenotypic characteristics, such as isolated arrhythmias or conduction anomalies, and it allows for earlier treatment and perhaps better outcomes [42]. Additionally, it can aid in the process of family planning [43].

A practical flowchart for assessing the risk of genetic DCM in family members of the proband is presented in Figure 6.

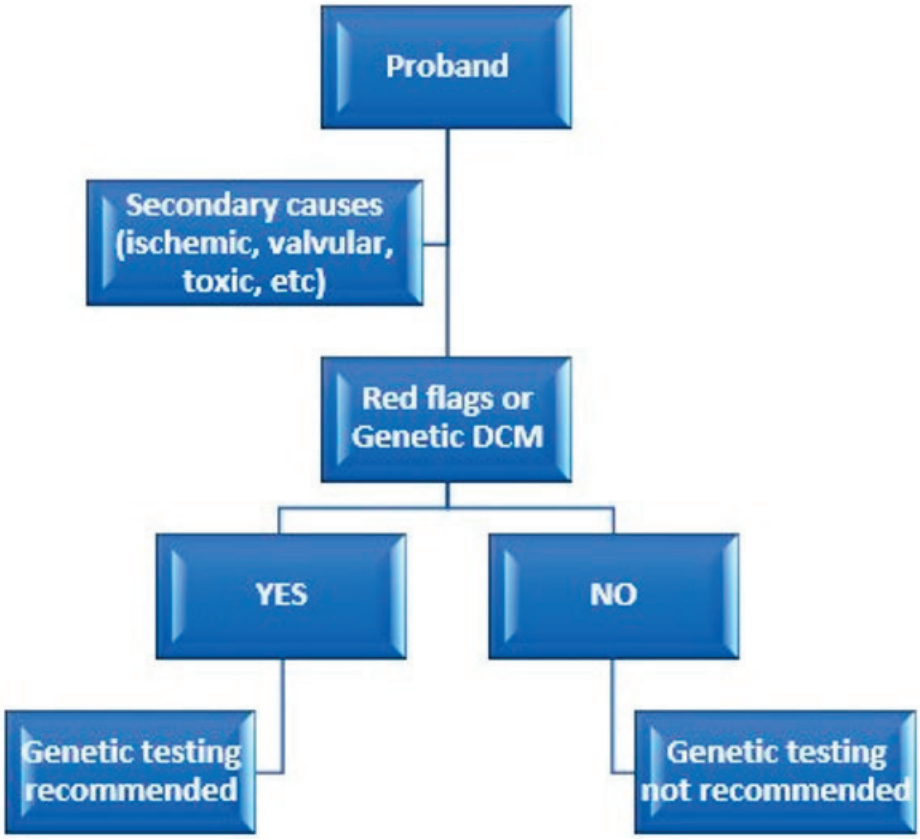


Figure 6. Flow-chart for assessing the risk of genetic dilated cardiomyopathy in family members. Red flags include a strong family history with 2 first-degree relatives having idiopathic dilated cardiomyopathy or sudden cardiac death at age < 35 years.

5. Genetic Testing

Ordering genetic testing has become fairly simple, but interpreting the results can be complicated. It is recommended to undergo such testing in a specialized clinic with multidisciplinary input given the challenges in interpreting genetic variants in the absence of a con-firmed phenotypic diagnosis [23,43]. Recently, clinicians have developed techniques to assist in determining whether genetic testing should be pursued in patients with suspected genetic dilated cardiomyopathy. The Madrid Genotype Score assesses the likelihood of obtaining a meaningful genetic test outcome based on five factors: existing family history of DCM, low voltage on ECG, evidence of skeletal myopathy, lack of hypertension, and lack of left bundle branch block. When four or more of these criteria were fulfilled, a pathogenic or potentially pathogenic variation was detected in 79% of the patients [44].

Genetic testing is valuable for both the proband and their family members since it provides crucial information about the likelihood of DCM recurring or being transmitted [3,23,43]. A systematic methodology for the genetic assessment of FDCM is presented in Figure 7.

Family History. The initial stage in the genetic assessment of individuals suspected of having genetic DCM involves the identification of the proband and obtaining a comprehensive family history. Providers should construct a genealogical chart spanning at least three generations in order to determine the pattern of genetic inheritance, such as autosomal dominant/recessive or X-linked [40]. It is important to document the cause and details surrounding the death of any family member who passed away before the age of 50. An elaborate genealogical chart aids in assessing the first likelihood of genetic testing and identifying other relatives who may be susceptible to the condition. Prior to undergoing genetic testing, it is crucial to engage in genetic counselling.



Figure 7. A practical approach for genetic testing in hereditary dilated cardiomyopathies.

Genetic counselling is assisting patients in comprehending the physical, psychological, and familial consequences of genetic abnormalities. Genetic counselling is often categorized into pre-genetic and post-genetic testing considerations [39].

Prior to conducting a genetic test, it is crucial for healthcare practitioners to engage in pretest counselling with patients. During this counselling session, physicians should thoroughly explain the procedure, advantages, and limits of genetic testing, as well as the expected results [33]. Other factors to consider before conducting the test include selecting the suitable genetic test and determining the most suitable individual to be tested.

Post-test counselling is crucial for ensuring precise result interpretation, which includes clarifying variants of uncertain significance (VUS) and any unexpected findings [40]. The effort to determine a relationship between gene variants of unknown significance and a phenotype of the disease is important not only for cardiovascular research but also for the clinical genetics of patients and their families. Combined variants in previously unreported genes related to cardiomyopathy might also play a significant role in affecting clinical, morphometrics, or myocardial mechanics parameters [45].

Additionally, after the test, it is crucial to start cascade screening of family members if necessary and offer psychosocial assistance to patients and families as required. Providers must possess a high level of skill in genetic interpretation, since it is a complex task. This is due to the fact that genetic tests do not have a simple "yes" or "no" result, and assessing pathogenicity is particularly problematic. This difficulty arises from the variability in how genes are expressed and the inadequate manifestation of hereditary traits [39]. A negative genetic test does not provide certainty that the condition is not hereditary, but rather indicates that no mutation was identified by the test [39]. A variant of uncertain significance (VUS) likewise has a broad range of confidence on its possibility of being pathogenic, ranging from 10% to 90% [34]. Hence, it is crucial for cardio-vascular genetic specialists to reassess outcomes, particularly those classified as VUS, in light of the patient's clinical circumstances. This is especially important if the patient be-longs to a racial or

ethnic group that is not well-represented in existing genomic data-bases, or if there is strong suspicion that a variant may cause a malfunction in the protein. Moreover, genetic testing frequently results in the discovery of incidental findings that are unrelated to the original reason for ordering the genetic test [46,47]. This phenomenon is more prevalent in genetic testing methods that are not specifically focused on a particular target. These methods include whole-genome or exome sequencing, as well as genetic panel testing. The challenges arise from the ethical considerations surrounding the dis-closure of incidental results, particularly when a significant number of these findings do not have practical implications for clinical management. The American College of Medical Genetics and Genomics issued clarifications in 2021 on whether incidental discoveries have actionable outcomes and hence should be addressed during genetic counselling sessions before and after genetic testing [46,47]. The mentioned genes associated with DCM include LMNA, filamin C (FLNC), PAG3, desmin, and RBM20 [48–51].

5.1. Benefits of Genetic Testing

Genetic testing is mostly valuable for identifying family members who are at risk and does not directly benefit the individual being tested (proband), but it can assist in deter-mining the cause of the disease [52]. Hence, the main advantage of genetic testing is the ability to conduct cascade screening of family members, which has the potential to detect subclinical illness [40,53]. Additional advantages encompass distinguishing illnesses that exhibit comparable phenotypic and morphological characteristics, making predictions about disease outcomes, classifying individuals based on their phenotypic risk, enabling early intervention, and providing personalized advice [39,53–55].

The use of genetic testing in DCM is anticipated to expand with increasing knowledge.

5.2. Genetic Testing on the Proband

Conducting genetic tests on the reference patient who is the most probable person affected provides the greatest likelihood of identifying a pathogenic genetic mutation [3]. Choosing the appropriate array for a certain patient is crucial due to subtle variants.

Genetic panel testing is the predominant technique of testing [39]. Due to recent progress in sequencing technology, the process of including genes into these panels has be-come more convenient and cost-effective while maintaining the accuracy and precision of the results [19]. Genetic panel testing is highly beneficial in cases with DCM due to the presence of genetic diversity and the involvement of numerous potential genes [55]. Regular updates to genetic panels are crucial to ensure the inclusion of the latest medically actionable variants [46,47]. The introduction of next-generation sequencing has greatly reduced the expenses associated with whole-genome sequencing or whole-exome sequencing, making them viable options in clinical environments [5].

Whole-genome sequencing is considered the most reliable method for sequencing the entire genome. It provides comprehensive information about several forms of genetic variants, such as single nucleotide polymorphisms (SNPs), insertions–deletions (indels), splice-site variants, and genomic rearrangements [54]. Whole-genome sequencing is especially advantageous in the setting of dilated cardiomyopathy because it can identify dis-ease-causing genetic variants that may be located outside of the exon regions [55]. Thus, whole-genome sequencing can be valuable in cases when genetic panel testing fails to provide answers and there is a strong clinical suspicion of inherited DCM.

Genetic testing on patients with suspected hereditary DCM is usually performed using commercially available next-generation sequencing arrays that are efficient in detecting polygenic diseases. Inherited DCM is characterized by its diversity, with over 100 genes being involved [5]. The presence of genetic diversity in DCM has led to the development of a concept known as the "final common pathway." This hypothesis suggests that many genetic variants impact diverse processes, which ultimately contribute to a shared final phenotype [56–58]. Typically, a genetic mutation alone is insufficient to trigger a DCM phenotype unless there is a second insult, such as hemodynamic, toxic, or stress factors.

This concept is known as the "two-hit" theory [58]. It is crucial to acknowledge that several genetic variants linked to DCM exhibit substantial similarities with other cardiac disorders, such as arrhythmogenic ventricular cardiomyopathy (AVC) and arrhythmogenic right ventricular cardiomyopathy (ARVC). The presence of heterogeneity leads to a decrease in the success rate of genetic testing, which has been previously reported to be 16% in individuals with familial DCM [59]. Nevertheless, as the use of next-generation sequencing has grown, the effectiveness of genetic screening in identifying diagnoses has expanded, presently including a range of 16 to 46% [48,55,58–61].

5.3. Prenatal Genetic Testing

Identifying a disease-causing mutation in a potential parent can also be utilized to provide information for prenatal genetics, specifically pre-implantation genetic diagnosis. The process involves in vitro fertilization with the selection or modification of embryos [62]. This is a highly invasive procedure that involves many stages, including oocyte retrieval, in vitro fertilization, genetic testing of embryos, and implantation of embryos that do not have pathogenic variants. It is important for all patients who have a strong diagnosis with a clearly identified disease-causing or potentially disease-causing genetic mutation to be informed about this possibility. Chorionic villus sampling and amniocentesis are alternative methods used for prenatal genetic diagnosis. Given the multitude of choices available, it is imperative that patients receive comprehensive pre-test genetic counselling to guarantee they possess the necessary knowledge and assistance to make a well-informed choice. This encompasses the ability to comprehend the possible consequences of test results, examine the decision-making process in relation to the results, and facilitate communication with other family members who may be at risk [43].

5.4. Genetic Testing on the Relatives of the Proband

If a disease-causing genetic mutation is identified in the patient of interest, it is advisable to perform cascade genetic testing on the relatives [16].

Relatives who present the inherited DCM undergo investigations to stratify their risk and to establish the strategy of management.

Relatives who are negative for the illness but have a detected disease-causing or possibly disease-causing genetic mutation should have regular and frequent screenings. Unaffected carriers should receive counselling on the symptoms and signs of early-stage DCM. They should also undergo more frequent clinical surveillance, with check-ups scheduled every 1–3 years as recommended by the European Society of Cardiology guide-lines [5] or every 3–5 years according to the American Heart Association guidelines [16].

Relatives without an identified pathogenic variant still regarded susceptible to the disease, however, are recommended to take part in clinical screening. Typically, it is advised to undergo this procedure every two years; however, the frequency may be modified according on factors such as age and risk level [43]. The lack of an identifiable genetic mutation does not automatically indicate the absence of a genetic cause for DCM. The potential explanations are as follows: (a) a gene associated with DCM that is not included in the gene panel used for testing, which could be due to recently discovered disease genes or the absence of gene identification; (b) DCM may not have a purely monogenic cause; there may be a pattern of polygenic disease within families [44]. In addition, advancements in genetic knowledge might require families to undergo genetic re-evaluation in order to identify new pathogenic variants [63].

Family members who do not carry the disease-causing genetic mutation and are not regarded susceptible to the disease might be given reassurance and released from further screening [64].

6. Genes Strongly Associated with DCM and Potential Therapeutic Implications

The area of genetic testing has made significant progress in recent decades. During these years, several variants in more than 60 potential disease genes have been documented.

However, this wide-ranging list has been narrowed down to 12 genes that have strong evidence linking them to the etiology of DCM, as determined by systematic analysis [3–5].

DCM exhibits genetic heterogeneity with a substantial number of cases manifesting as monogenic disorders, while a more complex genetic architecture is present in a number of cases. The majority of monogenic types of NSDCM have an autosomal dominant pat-tern of inheritance. The genes linked to GDCM are involved in several biological processes, such as sarcomere components, cytoskeletal and desmosomal proteins, and mitochondrial proteins, among others, as shown in Figure 8. The genetic etiology of other cardiomyopathies, such as hypertrophic cardiomyopathy, is less diverse compared to this. This indicates that NSDCM might be a common endpoint for multiple pathways [5].

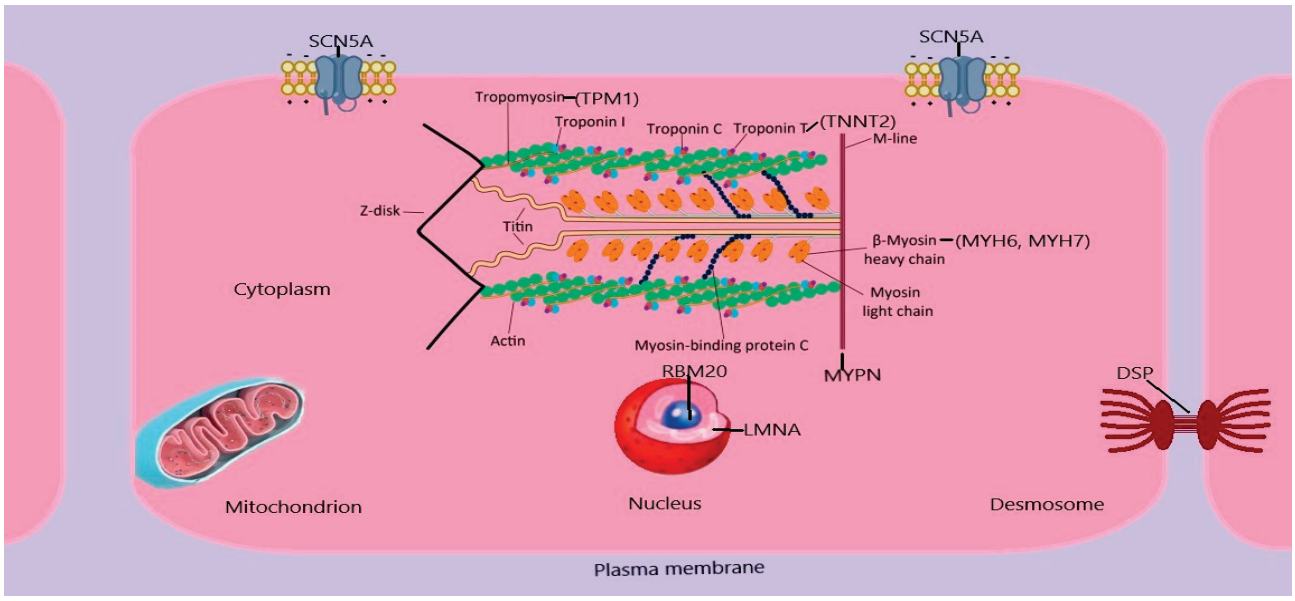


Figure 8. Cellular proteins linked to DCM. Abbreviations: DSP, desmoplakin; LMNA, lamin A/C; MYHN, myosin heavy chain; MYPN, myopalladin; RBM20, RNA binding protein 20; TNNT, cardiac muscle troponin T2; TPM1, α-tropomyosin 1; SCN5A, sodium channel protein type 5.

Furthermore, there is a notable allelic heterogeneity, where several mutations within the same gene might result in a comparable phenotype. It is also important to mention that multiple variants of the same gene can induce different morphological characteristics [44].

Several genetic variants in DCM demonstrate partial and age-related penetrance, as well as heterogenous expressivity. Penetrance refers to the percentage of individuals with a certain genetic variant who exhibit the illness. Incomplete penetrance indicates that not all individuals with the genetic variant have the disease. Penetrance in GDCM is generally age-dependent. This means that an individual inherits the genetic mutation responsible for DCM from birth, but the symptoms of DCM usually do not appear until middle age (over 40 years old) or may not appear at all [3,7].

The level of penetrance for various genetic DCM variants is still unclear and is being actively researched. Heterogeneous expressivity means the presence of differences in both the severity and spectrum of clinical characteristics that are observed in individuals with a certain genetic condition. For instance, if we take into account two subjects from the same family who have the exact same genetic variation, one of them may experience severe DCM, which is indicative of heart transplantation, while the other one may only exhibit minimal symptoms. This suggests that there is a potential for other genetic, epigenetic, or external factors to contribute to the observed characteristics [39,63].

It is increasingly apparent that several genes can be linked to certain characteristics, such as arrhythmic forms of familial DCM, with a high risk of sudden cardiac death. Iden-

tifying these alarming phenotypes is crucial and should prompt immediate consideration of genetic testing [5].

Pathogen mutations can occur in genes that code for a miscellaneous proteins found in the cardiomyocyte sarcomere, cytoskeleton, and nucleus. Autosomal recessive, mitochondrial, and X-linked inheritance have also been documented [64,65].

Genes mutations strongly associated with non-syndromic DCM are described further.

6.1. TTN

The main genetic cause of familial DCM is represented by dividing mutations in the TTN gene which encodes the titin protein. These mutations are present in 15–20% of instances [6]. The mode of inheritance is autosomal dominant. Titin has a significant role in the structure and function of the sarcomeres of the adult myocardium [15,16]. Titin proteins have several functions, such as affording structural and regulatory support. They also have a crucial role in the contractility of skeletal muscles [66]. Truncation mutations in the TTN gene (TTNtv) are highly common in DCM, accounting for around 25% of familial and 18% of sporadic DCM cases [36,57,67]. TTNtv is distinguished by frequent occurrences of arrhythmias, particularly atrial fibrillation and ventricular arrhythmias [68,69].

Those diagnosed with dilated cardiomyopathy (DCM) and with a positive TTNtv (titin truncating variant) status are at a considerably increased risk of experiencing persistent ventricular tachycardia in comparison to those with a negative TTNtv status [70]. Research indicates that in a certain proportion of patients, TTNtv may have a synergistic interaction with other variables such as cardiotoxic chemotherapy or pregnancy. This suggests that addressing these aggravating factors might potentially result in significant improvement [71].

As our comprehension of gene mutations advances, the possibility of using genetic engineering for therapeutic purposes becomes evident.

Promising treatment options might arise from techniques such as reverse-mediated exon skipping, targeted therapy, and genome-editing technologies [72–74].

6.2. LMNA

The second most prevalent reason for hereditary DCM and possibly the most severe one consists in alterations in the LMNA gene, which encrypts proteins Lamins A and C of the nuclear envelope [3]. The prevalence of Lamin A/C variants in individuals diagnosed with DCM is around 6%, and the mode of inheritance is autosomal dominant [6,75,76].

Individuals with pathogenic LMNA mutations have a significantly increased risk of experiencing sudden cardiac death as a result of malignant arrhythmias. Additionally, their overall prognosis is unfavorable [49,77]. Laminopathy frequently involves frameshift mutations that are commonly linked to heart disease. Splice site mutations, on the other hand, are an autonomous risk factor for sudden cardiac death. Non-missense mutations, such as deletions, mutations affecting splicing or truncations are significant risk factors for malignant ventricular arrhythmias. A precise mechanism by which DCM is induced by LMNA mutation is still not fully understood. However, three theories, including mechanical, gene expression, and cytotoxicity, have been suggested to elucidate the myocardial dysfunction related with it [5,6,49,77].

The gene expression theory suggests that faulty Lamins hinder the process of signal transduction and the organisation of chromatin, thereby affecting signal transduction, which is a crucial factor in the development of LMNA-associated dilated cardiomyopathy. This immediately impacts and interrupts the process of gene transcription and other internal signalling pathways, resulting in a notable increase in myocardial fibrosis. This, in turn, causes LV dysfunction and ultimately heart insufficiency [78,79].

Because there is a connection between heart block, bradycardia, and the risk of sudden cardiac mortality in LMNA-related DCM, it is suggested to use Implantable Cardioverter Defibrillators (ICDs) [80].

Additional pathways associated with the LMNA gene have been investigated as potential therapeutic targets. These include the use of rapamycin/rapalog to block mTOR and MEK1/2 kinase pathways, inhibiting the activation of brominated domain protein 4 (BRD4), and targeting the destruction of LINC complex protein SUN1 to counteract LMNA mutations [81–85].

Currently, there is no particular and efficacious therapy available.

6.3. MYH7

The MYH7 protein is essential for supplying energy to cardiomyocytes and regulating the levels of Ca2+ both within and outside these cells [85,86]. MYH7 mutations are responsible for 1% to 5.3% of inherited DCM [87]. The mutations mostly consist of missense variants, which are transmitted in a dominant pattern on the chromosomes. These mutations have a high penetrance in families [86,88]. Genetic mutations in the MYH7 gene can impair the structural and functional integrity of the sarcomere, leading to abnormalities in the contraction of the myocardium [86]. Atrial fibrillation and atrial fibrosis are recognized as first clinical signs of MYH7-related cardiomyopathy, offering significant knowledge for disease identification [87–89]. It has been documented that the combination of mutations in MYH7 and TNNT2, MYH7 and LAMA4, or MYH7 and TPM1 can lead to the development of severe DCM [90–92].

These findings emphasize the need of conducting thorough screening of genes associated with dilated cardiomyopathy (DCM), even after discovering a single mutation that causes the condition. Research has demonstrated that the length of telomeres in mice can provide defence against heart disease in people. Genetic alterations in proteins that play a crucial role in the functioning of cardiomyocytes, such as MYH7, TTN, and MYBPC3, result in the reduction in telomere length. Therefore, substantial reduction in telomere length can be used as a biomarker to indicate accelerated ageing of cardiomyocytes in hereditary hypertrophic cardiomyopathy and DCM [93,94].

TRF2, also known as Telomere Repeat Binding Factor 2, has been shown to inhibit the erosion of telomeres, leading to the enhancement of cellular morphology, suppression of DNA damage response, and prevention of premature cell death [95].

6.4. BAG3

Bcl2-associated athanogene 3 (BAG3) encodes for a protein that prevents cell death and is found on the Z disc of myotomes. BAG3, a member of the anti-apoptotic BAG protein family, is highly expressed in the heart [96,97].

BAG3 is crucial in preventing cell death, maintaining the balance of proteins, regulating the integrity of mitochondria, controlling cardiac contraction, and reducing the occurrence of arrhythmias [98,99]. These mutations of BAG3 are present in about 3% of hereditary DCM and the mode of inheritance is autosomal dominant [6].

Research suggests that every identified or likely harmful genetic variants affect either the WW domain, the Ile-Pro-Val (IPV) domain, or the BAG domain. The three protein domains have important functions in BAG3 action in the heart [99,100].

Research indicates that DCM caused by BAG3 mutations is often observed at an early age in the majority of patients. There is a significant likelihood of the condition advancing to end-stage heart failure, and men generally have a poorer prognosis [101].

BAG3, functioning as a cochaperone protein, forms interactions with high-molecular-weight heat shock proteins that are ATP-dependent, as well as small heat shock proteins (sHSPs) that are ATP-independent. These interactions occur within huge multichaperone protein complexes that have diverse functions. Once BAG3 is eliminated, the levels of impacted sHSPs decrease as a result of protein instability [102,103].

The recruitment of macrophages controlled by BAG3 can help maintain protein homeostasis. However, in hearts lacking BAG3, the process of autophagic flux is reduced, potentially leading to the formation of misfolded protein aggregates [104]. As a result, there is a rise in the amount of proteins that cannot dissolve in a liquid, which speeds up

the ageing of cells. MicroRNAs, also known as miRNAs, are short non-coding RNAs that play a role in regulating the development and functionality of the cardiovascular system through epigenetic mechanisms. They are typically composed of 20–25 nucleotides.

The misregulation of their expression is closely linked to the pathogenesis of several cardiovascular disorders [104,105].

Research shows that the simultaneous presence of miR-154-5p and miR-182-5p has diagnostic significance in dilated cardiomyopathy (DCM) in individuals with BAG3 gene mutations [106]. Genetic compensation, which refers to the transcriptional adaptation of gene expression in response to deleterious gene mutations, has been found in zebrafish lacking the BAG3 gene. This compensatory mechanism serves to safeguard the heart and skeletal muscles from injury. This biological phenomenon may also be present in certain individuals with BAG3 mutations [107]. Additional exploration of the pertinent molecular pathways may provide novel perspectives for the advancement of therapeutic approaches.

6.5. RBM20

The main role of the RNA-binding motif protein 20 (RBM20) is to regulate splicing. It is mainly found in the heart and skeletal muscle, where it controls both constitutive splicing and alternative splicing of pre-messenger RNA. RBM20 gene mutations, primarily characterized by missense mutations that modify conserved residues, are a major contributor to DCM [108,109].

These mutations are responsible for around 3% of all occurrences of dilated cardiomyopathy and transmitted in an autosomal dominant mode [110].

The pathophysiology of these RBM20 mutations arises from a mix of functional loss and harmful functional increase [111]. The TTN gene is the most important among those controlled by RBM20 [112,113]. Reduced RBM20 activity also leads to changes in the expression of protein subtypes that support muscle shape and cardiac function, including CAMKIIδ, LDB3, and CACNA1C. These modifications have the potential to cause variations in the biomechanics, electrical activity, and signal transduction processes, which can ultimately result in cardiomyopathy, fibrosis, arrhythmia, and sudden death [113,114].

Individuals diagnosed with dilated cardiomyopathy (DCM) who possess RBM20 mutations frequently have compromised cardiac function and are prone to experiencing atrial fibrillation, ventricular arrhythmia, and sudden cardiac death [115]. All-trans retinoic acid (ATRA) has been discovered as a possible regulator of RBM20. Research has demonstrated that ATRA has the ability to enhance RBM20 expression and partially re-verse the in vitro dilated cardiomyopathy (DCM) characteristics. Hence, the use of drugs to increase RBM20 expression might be a potentially effective treatment approach for individuals with dilated cardiomyopathy who have RBM20 mutations on one of their gene copies (heterozygous). The majority of RBM20 mutations are concentrated in a region that is rich in arginine/serine, indicating that targeted gene editing techniques such as adenine base editing and primer editing might potentially be used as therapies [115].

6.6. FLNC

The filamin family consists of three isomers: filamin A (FLNA), filamin B (FLNB), and filamin C (FLNC) [116]. FLNC is predominantly found in skeletal and cardiac muscle [117]. FLNC is essential for controlling cellular mechanics, the organization and orientation of Z-disks, and the connections between myofibrils in mammalian hearts [117–123]. Cardiomyocytes lacking FLNC can result in fetal mortality. In addition, adult mice lacking FLNC have fast and severe DCM within a period of two weeks [120]. In adults, mutations in FLNC are found in about 2–4% of DMC and have an autosomal dominant mode of inheritance [6].

These findings emphasize the important function of FLNC in both the development and functioning of heart muscle cells in both young and adult individuals. A truncation mutation in the FLNC gene (FLNCtv) is strongly linked to DCM [121]. Individuals diagnosed with FLNCtv commonly have enlargement of the left ventricle along with impaired

contraction of the heart during systole and the presence of fibrous tissue in the myocardium. Ventricular arrhythmias are common, and families with these mutations have a high occurrence of sudden cardiac death [122–124]. β-catenin (CTNNB1) has been identified as the downstream target of FLNC by use of co-immunoprecipitation and proteomic studies.

FLNC does not have the ability to cause the movement of CTNNB1 into the nucleus. However, this lack of nuclear translocation of CTNNB1 leads to the activation of the platelet-derived growth factor receptor-α (PDGFRA) pathway. Blocking PDGFRA can partially revert the abnormal gene expression pattern of FLNC in patient-specific cardiomyocytes, which is associated with cardiac insufficiency and arrhythmia [124]. Hence, blocking this route might be a promising treatment strategy for FLNC-related cardiomyopathy.

6.7. SCN5A

The sodium channel (SCN) 5A gene, located on human chromosome 3p22, is responsible for producing the α subunit Nav1.5, which forms the pore of the cardiac sodium channel. The SCN5A/Nav1.5 gene is mostly active in the atrial and ventricular muscles of the heart, as well as in the His bundle, bundle branches, and Purkinje fibres [125]. Approximately 2% of individuals with DCM have SCN5A gene mutations, and these have an autosomal dominant mode of inheritance. They can lead to a functional impairment of the sodium channels in the heart [126]. The precise biochemical mechanism by which these mutations lead to ventricular dilatation and dysfunction has not been completely comprehended [127]. SCN5A mutations can disrupt the connection between Nav1.5 and other components of the complex, resulting in structural abnormalities and impairment to contractile function [128].

The voltage-gated ion channel has two mutations (R222Q and R225W) in the voltage sensor domain. These mutations are believed to produce gated hole currents that might potentially be associated with arrhythmia and ventricular dilatation in humans [128]. Occult myocardial damage can occur due to the dysfunctional activity of the mutant SCN5A immune sensor [129]. DCM often displays age-related penetrance, where the characteristics become more noticeable as individuals become older [130]. From a clinical perspective, it frequently presents as severe irregular heart rhythms, such as atrial fibrillation and ventricular tachycardia, as well as conduction block.

Commencing the use of sodium channel blockers can effectively reduce the occurrence of severe illness and death [131].

Studies have also shown that the mRNA stabilizing protein HuR safeguards SCN3A by attaching to the 5′-UTR mRNA, therefore preventing its degradation. To lessen the likelihood of arrhythmia, one can enhance the stability of mRNA in order to maintain de-creased expression of SCN5A [132].

6.8. TNNC1, TNNT2

The TNNC1 gene is responsible for encoding cardiac troponin C (cTnC) in heart tis-sue, while the TNNC2 gene is responsible for encoding cardiac troponin T (cTnT) [133]. The trimer filament Tn complex, which plays a role in muscle contraction, is created by the fusion of cTnT, cTnI, and cTnC [134]. Point mutations in TNNC1 can impact the function of cTnC in two manners: by altering its ability to connect with Ca2+ or by influencing the interaction between cTnC and its binding partner [135]. Approximately 6% of familial DCM cases [136] have troponin complex mutations. The frequency of mutations in the TNNC1 gene is around 1% [137]. The prevalence of TNNT2 mutations in dilated cardiomyopathy (DCM) is around 3% [138]. The mode of inheritance is autosomal dominant. Individuals carrying TNNC1 gene mutations are usually identified at a younger age and have an increased likelihood of encountering life-threatening incidents. These incidents commonly present as severe systolic heart failure at an early stage, requiring the need for heart transplant surgery [127,139]. Studies suggest that a diminished responsiveness of myofilaments to Ca2+ is a crucial factor in the development of filament-associated DCM. Increasing the responsiveness of myofilaments to calcium ions in the first phases of DCM

might potentially be a successful approach for therapy [140]. Xin actin-binding repeat containing proteins (XIRPs) are a set of proteins that are particular to rhabdoms. The XIN protein, which is produced by the XIRP1 gene and is sometimes referred to as HXin-α or CMYA1, is a gene that is particular to the rhabdom and belongs to the XIRP family. In-creased expression of the repetitive isomer XINB can improve the remodelling of DCM caused by TNNT2-ΔK210 mutations in mice. This can partially reverse the enlargement of the heart, impaired contraction of the heart, and the formation of fibrous tissue in the heart. Thus, XIN has the potential to be a therapeutic target [141].

6.9. DES

The major intermediate filament (IF) protein, desmin, is encoded by the DES gene in human heart and skeletal muscle [142]. Desmin functions as a fundamental element of the extramuscular cytoskeleton, creating a complex framework that surrounds the Z disc of the myofibril. This structure serves as a connection between neighbouring myofibrils and the myofibril apparatus to the nucleus, submuscular cytoskeleton, and cytoplasmic organelles including mitochondria [143]. Desmin is the IF protein that is most commonly found in muscle-specific tissues and cardiomyocytes, with a high level of expression [144]. The occurrence of desmin gene mutations in individuals with DCM is below 1.6%. The mode of inheritance is autosomal dominant [145]. The majority of DES variants are missense mutations located in the central domain [146]. Around 74% of individuals with DES mutations experience heart symptoms, and around 50% develop cardiomyopathy, with dilated cardiomyopathy (DCM) being the predominant form [145]. Studies using mice with a deletion of the DES gene have shown that desmin deficiency only affects the anatomy of the heart, but also leads to significant abnormalities in the way the heart processes glucose, fatty acids, and amino acids in its metabolism [146–149]. Hence, it would be wise to avoid medicines that might potentially worsen mitochondrial function in individuals with desmin deficiency [150]. The α-crystallin B-chain, also known as αB-crystallin, is produced by the Desmin and CRYAB genes. It has the ability to potentially interact in a compensatory manner to provide protection for the heart. Increased production of heart-specific αB-crystallin enhances mitochondrial dysfunction in mice models lacking desmin, indicating a promising novel therapeutic strategy [151].

6.10. PLN

Phospholamban (PLN) is a protein located on the membrane of the sarcoplasmic and endoplasmic reticulum (SR/ER) and is in charge for the encoding of a key regulatory protein linked to the cycling of Ca2+. It acts as the main mediator of beta-adrenergic actions, resulting in an increase in cardiac output [152].

Out of all the PLN mutations that have been identified, the PLN-R14DEL mutation is the most common [153,154]. The incidence rate of mutations in the PLN gene as a cause of cardiomyopathy is less than 1%, the inheritance mode is autosomal dominant [155,156].

A comprehensive multicenter investigation with a prolonged period of observation was conducted on individuals carrying the PLN mutation. The study revealed that PLN-R14DEL mutant carriers frequently experienced early ventricular arrhythmia and advanced heart failure, leading to a substantial rise in mortality rates within the cohort [157]. From the viewpoint of a cardiomyocyte, it is acknowledged that PLN R14del has a major impact on its function. Studies have demonstrated that the R14del mutation leads to the accumulation of PLN protein, increase in the unfolded protein response, disruption of calcium control, and impaired contractile and metabolic performance [158]. Although the genetic cause of PLN R14delcardiomyopathy is clearly recognized, the specific molecular process that leads to its development is yet unknown [159]. Low-voltage electrocardiograms are more prevalent in women with PLN mutations, although their prognostic significance is greater in males [160]. Eplerenone medication has been suggested as a potential method to hinder or delay the advancement of the illness in individuals who carry presymptomatic PLN mutations.

Additional multicenter randomized double-blind studies are underway to validate this finding [161]. As our comprehension of the PLN-R14del mutation process advances, precision medicine, which includes gene editing and targeted gene therapy, may emerge as a novel approach for future treatment [159,162,163].

Nevertheless, the majority of ongoing research is still in the animal experimentation stage, and it is uncertain whether these discoveries will be relevant to human subjects [164].

6.11. DSP

The desmoplakin (DSP) gene was determined to be a significant contributor to DCM, not a definite cause (4). Research indicates that DSP mutations are specifically seen in adults with DCM, but the % of DCM caused by pathogenic variants in the gene is unknown. The mode of inheritance is autosomal dominant [165].

Palmoplantar keratoderma can indicate the presence of dilated cardiomyopathy (DCM) linked with a desmoplakin (DSP) mutation at an early stage [166]. Individuals who carry DSP mutations have a greater likelihood of experiencing arrhythmia episodes, comparable to those with LAMA variants, even if they do not have noticeable left ventricular dysfunction or dilatation [167]. Desmoprotein cardiomyopathy has been categorized as an arrhythmic cardiomyopathy caused by mutations in the DSP gene, according to studies. This syndrome is defined by sudden episodes of damage to the heart muscle, the development of fibrosis in the left ventricle before a decrease in its ability to contract, and a high occurrence of abnormal heart rhythms [168,169]. Common electrocardiogram (ECG) abnormalities consist of limb lead QRS depression (peak amplitude less than 0.5 mV) and T-wave inversion in the lateral or inferior leads [168,170]. In arrhythmogenic cardiomyopathy (ACM) resulting from DSP variation, cardiomyocytes secrete a significant quantity of inflammatory cytokines and chemotactic molecules [171].

Examination of left ventricular myocaroma in individuals with DSP has also shown the presence of inflammatory infiltration and scarring [172]. Therefore, inflammation is seen as a crucial characteristic of the condition, and controlling the pathways that trigger inflammation might potentially serve as a novel treatment approach for desmosome-mediated cardiomyopathy.

6.12. Mitofusin (MFN)

Franco et al. conducted a genetic screening of individuals with cardiomyopathy and discovered an uncommon mutation in the mitofusin 2 gene, known as R400Q, which was shown to be more prevalent in this particular population. Mutations in the gene encoding mitofusin 2 have been predominantly associated with nerve damage, but recent studies have demonstrated that interfering with the scheduled degradation of mitochondria can result in the development of dilated cardiomyopathy. When injured, mitochondria are repaired by a process that involves fusing with and exchanging contents with other mitochondria, this process being facilitated by mitofusin proteins. These are valuable findings on the link between mitofusin 2 function and Parkin-mediated mitophagy, showing that a combination of mitophagy and mitochondrial fusion defects can lead to genetic dilated cardiomyopathy [173].

7. Genetic Risk Factors and Prognosis

There is significant interest in using genetic markers to assess prognosis and aid in risk stratification for individuals with DCM, in addition to predicting their likelihood of developing the condition [6]. Genetic testing holds significant potential to enhance precision medicine by providing valuable information for risk assessment and tailored treatment approaches.

Genotype-based classification is becoming more supported as a method for stratifying the risk of individuals with cardiomyopathies as opposed to using phenotype-based classification [174].

For those who have a positive genotype but do not display any physical signs of the condition, there is presently no strong evidence to support a specific approach for managing their condition. Furthermore, there are no treatments available that have been proven to prevent the development of DCM in these individuals [57]. It is crucial to provide genetic counselling and effectively control cardiovascular risk factors in this particular group.

Individuals who possess high-risk genetic variants such as LMNA, FLNC, desmoplakin (DSP), and plakophilin-2 are at risk for malignant ventricular arrhythmias and sudden cardiac death, and should be evaluated for implantable cardioverter defibrillator (ICD) placement, regardless of their physical characteristics or left ventricular dilatation and systolic performance [175,176]. At present, the Heart Failure Society of America recommends considering the use of an implantable cardioverter defibrillator (ICD) for patients who have a left ventricular ejection fraction (LVEF) greater than 35% and also have an LMNA mutation [16]. The Heart Rhythm Society includes the possibility of using an implantable cardioverter defibrillator (ICD) in individuals with a left ventricular ejection fraction (LVEF) of less than 45% [121]. In the 2022 European Society of Cardiology guidelines for prevention of sudden cardiac death, it is recommended that patients with dilated cardiomyopathy (DCM) and a left ventricular ejection fraction (LVEF) of less than 50% receive primary prevention implantable cardioverter defibrillators (ICDs) if they have two or more of the following risk factors: syncope, late gadolinium enhancement on cardiac magnetic resonance imaging (MRI), inducible sustained monomorphic ventricular tachycardia during programmed electrical stimulation, and pathogenic variants in the LMNA, PLN, FLNC, and RBM20 genes [49].

Familial DCM can be a progressive condition, with a substantial number of individuals advancing to end-stage heart failure and needing cardiac transplantation [1,5,20,40,171–185]. Single nucleotide polymorphisms (SNPs) can provide valuable information for the categorization of this risk. In a large-scale genome-wide association study (GWAS), researchers found that a single nucleotide polymorphism (SNP) located on chromosomal band 5q22 was associated with a 36% higher risk of mortality in individuals diagnosed with heart failure [177].

Nevertheless, further data are needed to support the regular use of genetic testing for predicting outcomes in hereditary DCM.

8. Management

8.1. Non-Specific Therapy

There are no specific clinical studies focused on pharmacological treatment for heart failure in inherited DCM, but all the significant trials on heart failure with decreased ejection fraction did involve patients with non-ischemic cardiomyopathy, and it is likely that some of these patients had genetic causes for their condition.

Familial DCM is an important cause of severe heart failure [1,4,5]. Although the reported death rate at 5 years is of 50%, the general prognosis is improving. This can be attributed to improved management of cardiovascular risk factors, earlier detection of the condition, and advancements in heart failure treatment, including heart transplantation [180,181,184].

The current approach to treating familial DCM involves using guideline-directed medicinal interventions that try to prevent or decelerate the progress of heart failure [4,5]. The drugs consist of the usual combination of beta blockers, angiotensin receptor–neprlysin inhibitors, sodium–glucose contransporter-2 inhibitors, and mineralocorticoid receptor antagonists [40]. Administering this medication to individuals with DCM caused by truncating TTN variants frequently lead to the reversal of pathological left ventricular remodeling [185].

Research has shed light on the effectiveness of neurohormonal blocking in heart failure patients categorized by genetic variants, which has contributed to the implementation of pharmacogenetics. The variation in individual responsiveness to β-blockade is likely due to genetic variants in the gene encoding the β-adrenergic receptor within the population.

Polymorphisms in ADRB1 and GRK5, which encode the downstream G-protein-coupled receptor kinase 5, have an impact on the response to β-blockade [183]. Additional results indicate that amino acid changes in the β-adrenergic receptor, such as Arg389Gly, might potentially impact the response to β-blockade. This effect can be explained by the reduction of the renin–angiotensin–aldosterone pathway. Nevertheless, this polymorphism has not been linked to any change in morbidity or death in the sub-studies of the WOSCOPS trial [185] or the MERIT-HF trial [186].

Genes that encode angiotensin II and its accompanying receptors have a role in the development of heart failure and are targeted by antagonistic medication according to medical guidelines. These genes have polymorphisms that result in different responses to treatment. Evidence indicates that individuals with a homozygous DD genotype for the ACE gene, which increases angiotensin II levels, along with a polymorphism in AGTR1 (which encodes the type 1 angiotensin II receptor), may experience higher activation of the renin–angiotensin–aldosterone system and a poorer prognosis, even when treated with ACE inhibitors [187]. Research was conducted to observe individuals with congestive heart failure. It was shown that having at least one D allele of the ACE gene was linked to decreased survival rates, particularly for patients who were not receiving β-blocker medication. However, in another experiment where patients were categorized based on the existence of previously recognized pathogenic changes in AGTR1, no disparities in long-term mortality were found [188].

While the impact magnitude may not be significant, certain single nucleotide polymorphisms (SNPs) have been discovered that elevate the risk of angio-oedema produced by ACE inhibitors [183,188]. In the clinical arena, routine testing for SNPs that are linked to variable responses to neuro-hormonal blocking is not commonly performed since there is a lack of clinical validity and usefulness.

The interplay between environmental variables and an individual's genetic composition is of utmost significance. Environmental variables and triggers have the potential to influence the observable characteristics of DCM in a patient who already has a genetic susceptibility to the condition. Peripartum cardiomyopathy has been linked to both genetic susceptibility and the interaction between an underlying pathogenic variation and the physiological stress of pregnancy [14,189]. Furthermore, the cardiotoxicity of anthracyclines and other antineoplastic drugs may be influenced by genetic predisposition [190]. Upon thorough evaluation, it is evident that environmental triggers may be linked to a poorer prognosis if there is an existing genetic susceptibility to the illness [191]. Crucially, it is vital for both DCM patients and their families to focus on addressing changeable variables that contribute to cardiovascular disease and overall health. The conventional approach to managing hypertension, quitting smoking, preventing diabetes, addressing obesity, and moderating alcohol intake continues to be essential, since additional pathogenic factors affecting the heart are linked to poor outcomes [187]. A primary care setting handles the management of many of these concerns.

8.2. Specific Therapy

In general, pharmacological therapies in inherited DCM are not disease-modifying, with some exceptions.

A notable exception to this is the p.R222Q SCN5A mutation, which allows for the possibility of tailored treatment based on particular mechanisms [192]. This genetic mutation leads to the development of multifocal ectopic Purkinje-related premature contractions (MEPPC), atrial arrhythmias, and DCM as a result of increased activity in the heart sodium channels. The symptoms mentioned can be efficiently managed by using a sodium channel antagonist, such as flecainide. This type of treatment is considered a gene-specific therapy and is a significant example of precision medicine in familial DCM.

Additional gene-specific medicines that are currently being studied but have not yet been used in clinical practice include myosin activator medications (such as omecamtiv

mecarbil) and the suppression of the mitogen-activated protein kinase signaling pathway in laminopathies [5].

Implantable cardiac defibrillator (ICD) treatment can be utilized as either primary or secondary prevention after experiencing life-threatening arrhythmia. Current guidelines employ genetic variants such as LMNA, FLNC, and PLN to categorize individuals based on their risk for malignant arrhythmias. These guidelines suggest the use of primary prevention ICDs for patients with a higher risk, even if their left ventricular ejection fraction (LVEF) is over the usual criterion of 35% [183].

Determining a genetic anomaly is also crucial in making judgements on the appropriate timing for heart transplantation. Patients with pathogenic or possibly pathogenic LMNA mutations frequently experience a swiftly deteriorating clinical condition and re-quire early consideration of cardiac transplantation.

Certain pathogenic variants have stricter guidelines. For instance, individuals with LMNA-associated DCM should avoid engaging in intense physical activity since it is linked to a higher risk of deterioration in heart function and death [193]. It is extremely advantageous and important to pay attention to the psychological well-being and receive genetic counselling from specialists who have been trained in this field. This should not be disregarded or underestimated.

The research of Franco [173] regarding the mutations of MSN2 that affect mitochondrial repair and replacement processes highlight future directions for studies into modifiers of genetic cardiomyopathies.

Contraception or pregnancy planning is crucial for pre-menopausal women with DCM. Women who test positive for a certain genotype and become pregnant should have thorough echocardiographic surveillance both during and after pregnancy to identify any indications of worsening after childbirth. Peripartum cardiomyopathy has the potential to reoccur earlier and with greater severity in subsequent pregnancies. Indeed, for certain women with confirmed DCM, pregnancy may be advised against due to its exceedingly precarious nature, which poses significant risks to both the mother and the fetus [194]. When it comes to contraception for individuals with cardiomyopathy, it is recommended to use barrier techniques or long-acting contraceptive methods that contain levonorgestrel.

For those who have a positive genotype but do not display any physical signs of the condition, there is presently no strong evidence to support a specific approach for man-aging their condition. Furthermore, there are no treatments available that have been proven to prevent the development of DCM in these individuals [195,196]. It is crucial to pro-vide genetic counselling and effectively control cardiovascular risk factors in this particular group.

9. Unresolved Issues and Future Directions

Over the past decade, there has been significant advancement in understanding and improving our knowledge of the genetic foundation of DCM. The objective for the next decade should be to utilize this information in order to develop specific treatments. There are some unresolved inquiries in our comprehension of the genetics of DCM. An enigma is in the very modest genetic diagnostic success rate, especially in cases of familial DCM. This presumably indicates situations with complex genetic structures that are more challenging to investigate—highly influenced by genetics, but not caused by a single gene. These theories encompass oligogenic and polygenic combinations, in which genetic susceptibility is influenced by the cumulative impact of numerous common genetic variants. This is in contrast to a dominant inheritance pattern driven by a single strong genetic component, as seen in Mendelian inheritance. These extra variants can have either additive effects, where the combined burden of these more frequent variants contributes to the disease, or non-additive interactions, where the more common variants affect the impact of a rare variant. Gene–environment interactions are expected to alter the impact of both uncommon and common variants [195,196].

10. Conclusions

Hereditary DCM remains a highly complex condition with broad phenotypic heterogeneity that includes both arrhythmogenic and non-arrhythmogenic forms. Determining a genetic anomaly is also crucial in making judgements on the appropriate timing for heart transplantation in individuals with heart failure.

The heart failure community must advance in the identification and validation of genetic markers that indicate the risk of DCM, the progression of the disease, and the response to therapy. This progress will ultimately lead to the realization of precision medicine in heart failure, with the potential for improved outcomes for patients and their families.

Author Contributions: Conceptualization, D.-A.A. and M.A.; methodology, D.C.; software, M.-C.T.; validation, D.C. and S.-F.A.; formal analysis, M.A.; investigation, D.-A.A., M.A., I.-R.L. and M.-C.T.; resources, M.-C.T.; data curation, D.-A.A.; writing—original draft preparation, D.-A.A. and M.A.; writing—D.-A.A. and S.-F.A.; review and editing, D.C. and M.-C.T.; visualization, M.-C.T. and S.-F.A.; supervision, M.-C.T.; project administration, I.-R.L. and M.-C.T.; funding acquisition, D.C. All authors have read and agreed to the published version of the manuscript.

Funding: This research was funded by Victor Babes University of Medicine and Pharmacy, Timisoara, Romania.

Institutional Review Board Statement: Not applicable.

Informed Consent Statement: Not applicable.

Acknowledgments: The authors thank the medical staff from the echocardiography and cardiac MRI laboratories for their technical support.

Conflicts of Interest: The authors declare no conflicts of interest.

References

1. Stehlik, J.; Edwards, L.B.; Kucheryavaya, A.Y.; Benden, C.; Christie, J.D.; Dobbels, F.; Kirk, R.; Rahmel, A.O.; Hetrz, M.I. The Registry of the International Society for Heart and Lung Transplantation: Twenty-eighth Adult Heart Transplant Report—2011. *J. Heart Lung Transplant.* **2011**, *30*, 1078–1094. [CrossRef] [PubMed]
2. Heidenreich, P.A.; Albert, N.M.; Allen, L.A.; Bluemke, D.A.; Butler, J.; Fonarow, G.C.; Ikonomidis, J.S.; Khavjou, O.; Konstam, M.A.; Maddox, T.M.; et al. Forecasting the impact of heart failure in the United States a policy statement from the American Heart Association. *Circ. Heart Fail.* **2013**, *6*, 606–619. [CrossRef] [PubMed]
3. Paul, C.; Peters, S.; Perrin, M.; Fatkin, D.; Amerena, J. Non-ischemic dilated cardiomyopathy: Recognizing the genetic links. *Intern. Med. J.* **2023**, *53*, 178–185. [CrossRef] [PubMed]
4. Bui, Q.M.; Ding, J.; Hong, K.N.; Adler, E.A. The Genetic Evaluation of Dilated Cardiomyopathy. *Struct. Heart* **2023**, *7*, 100200. [CrossRef] [PubMed]
5. Arbelo, E.; Protonotarios, A.; Gimeno, J.R.; Arbustini, E.; Barriales-Villa, R.; Basso, C.; Bezzina, C.R.; Biagini, E.; Blom, N.A.; de Boer, R.A.; et al. 2023 ESC Guidelines for the management of cardiomyopathies: Developed by the task force on the management of cardiomyopathies of the European Society of Cardiology (ESC). *Eur. Heart J.* **2023**, *44*, 3503–3626. [CrossRef] [PubMed]
6. Hershberger, R.E.; Jordan, E. Dilated Cardiomyopathy Overview. In *GeneReviews® [Internet]*; Adam, M.P., Feldman, J., Mirzaa, G.M., Pagon, R.A., Wallace, S., Bean, L., Gripp, K.W., Amamiya, A., Eds.; University of Washington: Seattle, WA, USA, 2022.
7. Rosenbaum, A.N.; Agre, K.E.; Pereira, N.L. Genetics of dilated cardiomyopathy: Practical implications for heart failure management. *Nat. Rev. Cardiol.* **2020**, *17*, 286–297. [CrossRef]
8. Sweet, M.E.; Taylor, M.R.; Mestroni, L. Diagnosis, prevalence, and screening of familial dilated cardiomyopathy. *Expert. Opin. Orphan Drugs* **2015**, *3*, 869–876. [CrossRef]
9. Marian, A.J. Sporadic dilated cardiomyopathy is often familial. *Cardiovasc. Res.* **2022**, *118*, e69–e71. [CrossRef]
10. Schmidt, M.A.; Michels, V.V.; Edwards, W.D.; Miller, F.A. Familial dilated cardiomyopathy. *Am. J. Med. Genet.* **1988**, *31*, 135–143. [CrossRef]
11. Michels, V.V.; Moll, P.P.; Miller, F.A.; Tajik, A.J.; Chu, J.S.; Driscoll, D.J.; Burnett, J.C.; Rodeheffer, R.J.; Chesebro, J.H.; Tazelaar, H.D. The frequency of familial dilated cardiomyopathy in a series of patients with idiopathic dilated cardiomyopathy. *N. Engl. J. Med.* **1992**, *326*, 77–82. [CrossRef]
12. Huggins, G.S.; Kinnamon, D.D.; Haas, G.J.; Jordan, E.; Hofmeyer, M.; Kransdorf, E.; Ewald, G.A.; Morris, A.A.; Owens, A.; Lowes, B.; et al. DCM Precision Medicine Study of the DCM Consortium. Prevalence and cumulative risk of familial idiopathic dilated cardiomyopathy. *JAMA* **2022**, *327*, 454–463. [CrossRef] [PubMed]

13. Peters, S.; Kumar, S.; Elliott, P.; Kalman, J.M.; Fatkin, D. Arrhythmic genotypes in familial dilated cardiomyopathy: Implications for genetic testing and clinical management. *Heart Lung Circ.* **2019**, *28*, 31–38. [CrossRef] [PubMed]
14. Ware, J.S.; Li, J.; Mazaika, E.; Yasso, C.M.; DeSouza, T.; Cappola, T.P.; Tsai, E.J.; Hilfiker-Kleiner, D.; Kamiya, C.A.; Mazzarotto, F.; et al. Shared genetic predisposition in peripartum and dilated cardiomyopathies. *N. Engl. J. Med.* **2016**, *374*, 233–241. [CrossRef] [PubMed]
15. Hershberger, R.E.; Morales, A.; Siegfried, J.D. Clinical and genetic issues in dilated cardiomyopathy: A review for genetics pro-fessionals. *Genet. Med.* **2010**, *12*, 655–667. [CrossRef] [PubMed]
16. Hershberger, R.E.; Givertz, M.M.; Ho, C.Y.; Judge, D.P.; Kantor, P.F.; McBride, K.L.; Morales, A.; Taylor, M.R.; Vatta, M.; Ware, S.M. ACMG Professional Practice and Guidelines Committee. *Genetic evaluation of cardiomyopathy: A clinical practice resource of the American College of Medical Genetics and Genomics (ACMG). Genet. Med.* **2018**, *20*, 899.
17. Rapezzi, C.; Arbustini, E.; Caforio, A.L.; Charron, P.; Gimeno-Blanes, J.; Heliö, T.; Linhart, A.; Mogensen, J.; Pinto, Y.; Ristic, A.; et al. Diagnostic work-up in cardiomyopathies: Bridging the gap between clinical phenotypes and final diagnosis. A position statement from the ESC working group on myocardial and pericardial diseases. *Eur. Heart J.* **2013**, *34*, 1448–1458. [CrossRef] [PubMed]
18. Towbin, J.A.; Hejtmancik, J.F.; Brink, P.; Gelb, B.; Zhu, X.M.; Chamberlain, J.S.; McCabe, E.R.; Swift, M. X-linked dilated cardiomyopathy-molecular-genetic evidence of linkage to the Duchenne muscular-dystrophy (dystrophin) gene at the Xp21 locus. *Circulation* **1993**, *87*, 1854–1865. [CrossRef] [PubMed]
19. Bonne, G.; Di Barletta, M.R.; Varnous, S.; Bécane, H.M.; Hammouda, E.H.; Merlini, L.; Muntoni, F.; Greenberg, C.R.; Gary, F.; Urtizberea, J.A.; et al. Mutations in the gene encoding lamin A/C cause autosomal dominant Emery- Dreifuss muscular dystrophy. *Nat. Genet.* **1999**, *21*, 285–288. [CrossRef]
20. Fatkin, D.; Johnson, R.; McGaughran, J.; Weintraub, R.G.; Atherton, J.J. Position statement on the diagnosis and management of familial dilated cardiomyopathy. *Heart Lung Circ.* **2017**, *26*, 1127–1132. [CrossRef]
21. Hershberger, R.E.; Cowan, J.; Jordan, E.; Kinnamon, D.D. The complex and diverse genetic architecture of dilated cardiomyopathy. *Circ. Res.* **2021**, *128*, 1514–1532. [CrossRef]
22. Peters, S.; Johnson, R.; Birch, S.; Zentner, D.; Hershberger, R.E.; Fatkin, D. Familial dilated cardiomyopathy. *Heart Lung Circ.* **2020**, *29*, 566–574. [CrossRef]
23. Eldemire, R.; Mestroni, L.; Taylor, M.R.G. Genetics of Dilated Cardiomyopathy. *Annu. Rev. Med.* **2024**, *7*, 417–426. [CrossRef]
24. Pinamonti, B.; Abate, E.; De Luca, A.; Finocchiaro, G.; Korcova, R. Role of cardiac imaging: Echocardiography. In *Dilated Cardiomyopathy: From Genetics to Clinical Management*; Sinagra, G., Merlo, M., Pinamonti, B., et al., Eds.; Springer: Cham, Switzerland, 2019; Chapter 7. Available online: https://www.ncbi.nlm.nih.gov/books/NBK553855/ (accessed on 23 February 2024).
25. Hudson, L.; Morales, A.; Mauro, A.C.; Whellan, D.; Adams, K.F.; O'Connor, C.M.; Hershberger, R.E. Family history of dilated cardiomyopathy among patients with heart failure from the HF-ACTION genetic ancillary study. *Clin. Transl. Sci.* **2013**, *6*, 179–183. [CrossRef]
26. Haugaa, K.H.; Hasselberg, N.E.; Edvardsen, T. Mechanical dispersion by strain echocardiography: A predictor of ventricular arrhythmias in subjects with lamin A/C mutations. *JACC Cardiovasc. Imaging* **2015**, *8*, 104–106. [CrossRef]
27. Haugaa, K.H.; Goebel, B.; Dahlslett, T.; Meyer, K.; Jung, C.; Lauten, A.; Figulla, H.R.; Poerner, T.C.; Edvardsen, T. Risk assessment of ventricular arrhythmias in patients with nonischemic dilated cardiomyopathy by strain echocardiography. *J. Am. Soc. Echocardiogr.* **2012**, *25*, 667–673. [CrossRef]
28. Leren, I.S.; Saberniak, J.; Haland, T.F.; Edvardsen, T.; Haugaa, K.H. Combination of ECG and echocardiography for identification of arrhythmic events in early ARVC. *JACC Cardiovasc. Imaging* **2017**, *10*, 503–513. [CrossRef] [PubMed]
29. Augusto, J.B.; Eiros, R.; Nakou, E.; MouraFerreira, S.; Treibel, T.A.; Captur, G.; Akhtar, M.M.; Protonotarios, A.; Gossios, T.D.; Savvatis, K.; et al. Dilated cardiomyopathy and arrhythmogenic left ventricular cardiomyopathy: A comprehensive genotype-imaging phenotype study. *Eur. Heart J. Cardiovasc. Imaging* **2020**, *21*, 326–336. [CrossRef] [PubMed]
30. Amin, R.J.; Morris-Rosendahl, D.; Edwards, M.; Tayal, U.; Buchan, R.; Hammersley, D.J.; Jones, R.E.; Gati, S.; Khalique, Z.; Almogheer, B.; et al. The addition of genetic testing and cardiovascular magnetic resonance to routine clinical data for stratification of etiology in dilated cardiomyopathy. *Front. Cardiovasc. Med.* **2022**, *9*, 1017119. [CrossRef]
31. Duboscq-Bidot, L.; Xu, P.; Charron, P.; Neyroud, N.; Dilanian, G.; Millaire, A.; Bors, V.; Komajda, M.; Villard, E. Mutations in the Z- band protein myopalladin gene and idiopathic dilated cardiomyopathy. *Cardiovasc. Res.* **2008**, *77*, 118–125. [CrossRef]
32. Sam, D.; Feger, J.; Machang'a, K. Dilated Cardiomyopathy. Reference Article. Available online: https://radiopaedia.org/articles/dilated-cardiomyopathy?lang=us (accessed on 22 May 2024).
33. Castiglione, V.; Aimo, A.; Vergaro, G.; Saccaro, L.; Passino, C.; Emdin, M. Biomarkers for the diagnosis and management of heart failure. *Heart Fail. Rev.* **2022**, *27*, 625–643. [CrossRef]
34. Shakur, R.; Ochoa, J.P.; Robinson, A.J.; Niroula, R.; Chandran, A.; Rahman, T.; Vihinen, M. Prognostic implications of troponin T variations in inherited cardiomyopathies using systems biology. *npj Genom. Med.* **2021**, *6*, 47. [CrossRef]
35. Bonny, A.; Lellouche, N.; Ditah, I.; Hidden-Lucet, F.; Yitemben, M.T.; Granger, B.; Larrazet, F.; Frank, R.; Fontaine, G. C-reactive protein in arrhythmogenic right ventricular dysplasia/cardiomyopathy and relationship with ventricular tachycardia. *Cardiol. Res. Pract.* **2010**, *2010*, 919783. [CrossRef]
36. Arany, Z. Peripartum Cardiomyopathy. *N. Engl. J. Med.* **2024**, *390*, 154–164. [CrossRef]

37. Ni, H.; Jordan, E.; Kinnamon, D.D.; Cao, J.; Haas, G.J.; Hofmeyer, M.; Ewald, G.A.; Morris, A.A.; Owens, A.; Lowes, B.; et al. Screening for Dilated Cardiomyopathy in At-Risk First-Degree Relatives. *J. Am. Coll. Cardiol.* **2023**, *81*, 2059–2071. [CrossRef]
38. Bozkurt, B.; Colvin, M.; Cook, J.; Cooper, L.T.; Deswal, A.; Fonarow, G.C.; Francis, G.S.; Lenihan, D.; Lewis, E.F.; McNamara, D.M.; et al. Current diagnostic and treatment strategies for specific dilated cardiomyopathies: A scientific statement from the American Heart Association. *Circulation* **2016**, *134*, e579–e646. [CrossRef]
39. Musunuru, K.; Hershberger, R.E.; Day, S.M.; Klinedinst, N.J.; Landstrom, A.P.; Parikh, V.N.; Prakash, S.; Semsarian, C.; Sturm, A.C.; American Heart Association Council on Genomic and Precision Medicine; et al. Genetic Testing for Inherited Cardiovascular Diseases: A Scientific Statement from the American Heart Association. *Circ. Genom. Precis. Med.* **2020**, *13*, e000067. [CrossRef]
40. Heidenreich, P.A.; Bozkurt, B.; Aguilar, D.; Allen, L.A.; Byun, J.; Colvin, M.M.; Deswal, A.; Drazner, M.H.; Dunlay, S.M.; Evers, L.R.; et al. 2022 AHA/ACC/HFSA guideline for the management of heart failure: A report of the American College of Cardiology/American Heart Association Joint Committee on Clinical Practice Guidelines. *J. Am. Coll. Cardiol.* **2022**, *79*, e263–e421. [CrossRef] [PubMed]
41. Paldino, A.; De Angelis, G.; Merlo, M.; Gigli, M.; Dal Ferro, M.; Severini, G.M.; Mestroni, L.; Sinagra, G. Genetics of Dilated Cardiomyopathy: Clinical Implications. *Curr. Cardiol. Rep.* **2018**, *20*, 83. [CrossRef]
42. El-Battrawy, I.; Zhao, Z.; Lan, H.; Li, X.; Yücel, G.; Lang, S.; Sattler, K.; Schünemann, J.D.; Zimmermann, W.H.; Cyganek, L.; et al. Ion Channel dysfunctions in dilated cardiomyopathy in limb-girdle muscular dystrophy. *Circ. Genom. Precis. Med.* **2018**, *11*, e001893. [CrossRef] [PubMed]
43. Tayal, U.; Newsome, S.; Buchan, R.; Whiffin, N.; Halliday, B.; Lota, A.; Roberts, A.; Baksi, A.J.; Voges, I.; Midwinter, W.; et al. Phenotype and clinical outcomes of titin cardiomyopathy. *J. Am. Coll. Cardiol.* **2017**, *70*, 2264–2274. [CrossRef] [PubMed]
44. Escobar-Lopez, L.; Ochoa, J.P.; Royuela, A.; Verdonschot, J.A.J.; Dal Ferro, M.; Espinosa, M.A.; Sabater-Molina, M.; Gallego-Delgado, M.; Larrañaga-Moreira, J.M.; Garcia-Pinilla, J.M.; et al. Clinical risk score to predict pathogenic genotypes in patients with dilated cardiomyopathy. *J. Am. Coll. Cardiol.* **2022**, *80*, 1115–1126. [CrossRef]
45. Mėlinytė-Ankudavičė, K.; Šukys, M.; Kasputytė, G.; Krikštolaitis, R.; Ereminienė, E.; Galnaitienė, G.; Mizarienė, V.; Šakalytė, G.; Krilavičius, T.; Jurkevičius, R. Association of uncertain significance genetic variants with myo-cardial mechanics and morphometrics in patients with nonischemic dilated cardiomyopathy. *BMC Cardiovasc. Disord.* **2024**, *24*, 224. [CrossRef] [PubMed]
46. Miller, D.T.; Lee, K.; Gordon, A.S.; Adelman, K.; Bale, S.J.; Chung, W.K.; Gollob, M.H.; Harrison, S.M.; Herman, G.E.; Hershberger, R.E.; et al. Recommendations for reporting of secondary findings in clinical exome and genome sequencing, 2021 update: A policy statement of the American College of Medical Genetics and Genomics (ACMG). *Genet. Med.* **2021**, *23*, 1391–1398. [CrossRef]
47. Miller, D.T.; Lee, K.; Abul-Husn, N.S.; Brothers, K.; Chung, W.K.; Gollob, M.H.; Gordon, A.S.; Harrison, S.M.; Hershberger, R.E.; Klein, T.E.; et al. ACMG SF v3.1 list for reporting of secondary findings in clinical exome and genome sequencing: A policy statement of the American College of Medical Genetics and Genomics (ACMG). *Genet. Med.* **2022**, *24*, 1407–1414. [CrossRef]
48. Wang, Y.; Dobreva, G. Epigenetics in LMNA-Related Cardiomyopathy. *Cells* **2023**, *12*, 783. [CrossRef]
49. Rosario, K.F.; Karra, R.; Amos, K.; Landstrom, A.P.; Lakda, N.K. LMNA Cardiomyopathy: Important Considerations for the Heart Failure Clinician. *J. Card. Fail.* **2023**, *29*, 1657–1666. [CrossRef] [PubMed]
50. Zeppenfeld, K.; Tfelt-Hansen, J.; de Riva, M.; Winkel, B.G.; Behr, E.R.; Blom, N.A.; Charron, P.; Corrado, D.; Dagres, N.; de Chillou, C.; et al. 2022 ESC guidelines for the management of patients with ventricular ar-rhythmias and the prevention of sudden cardiac death. *Eur. Heart J.* **2022**, *43*, 3997–4126. [CrossRef] [PubMed]
51. Mirelis, J.G.; Escobar-Lopez, L.; Ochoa, J.P.; Espinosa, M.Á.; Villacorta, E.; Navarro, M.; Casas, G.; Mora-Ayestarán, N.; Barriales-Villa, R.; Mogollón-Jiménez, M.V.; et al. Combination of late gadolinium enhancement and genotype improves prediction of prognosis in non-ischaemic dilated cardiomyopathy. *Eur. J. Heart Fail.* **2022**, *24*, 1183–1196. [CrossRef]
52. Musunuru, K.; Hickey, K.T.; Al-Khatib, S.M.; Delles, C.; Fornage, M.; Fox, C.S.; Frazier, L.; Gelb, B.D.; Herrington, D.M.; Lanfear, D.E.; et al. American Heart Association Council on Functional Genomics and Translational Biology, Council on Clinical Cardiology, Council on Cardiovascular Disease in the Young, Council on Cardiovascular and Stroke Nursing, Council on Epidemiology and Prevention, Council on Hypertension, Council on Lifestyle and Cardiometabolic Health, Council on Quality of Care and Outcomes Research, and Stroke Council. Basic concepts and potential applications of genetics and genomics for cardi-ovascular and stroke clinicians: A scientific statement from the American Heart Association. *Circ. Cardiovasc. Genet.* **2015**, *8*, 216–242. [CrossRef]
53. Verdonschot, J.A.J.; Hazebroek, M.R.; Wang, P.; Sanders-van Wijk, S.; Merken, J.J.; Adriaansen, Y.A.; Heymans, S.R. Clinical phenotype and genotype associations with improvement in left ventricular function in dilated cardiomyopathy. *Circ. Heart Fail.* **2018**, *11*, e005220. [CrossRef]
54. Wilson, K.D.; Shen, P.; Fung, E.; Karakikes, I.; Zhang, A.; InanlooRahatloo, K.; Odegaard, J.; Sallam, K.; Davis, R.W.; Lui, G.K.; et al. A rapid, high-quality, cost-effective, comprehensive and expandable targeted next-generation sequencing assay for inherited heart diseases. *Circ. Res.* **2015**, *117*, 603–611. [CrossRef]
55. Verdonschot, J.A.J.; Hazebroek, M.R.; Krapels, I.P.C.; Chen, H.; Haddad, F.; Kitani, T.; Wilson, K.D.; Tian, L.; Shrestha, R.; Wu, H.; et al. Implications of genetic testing in dilated cardiomyopathy. *Circ. Genom. Precis. Med.* **2020**, *13*, 476–487. [CrossRef] [PubMed]
56. Meynert, A.M.; Ansari, M.; FitzPatrick, D.R.; Taylor, M.S. Variant detection sensitivity and biases in whole genome and exome sequencing. *BMC Bioinform.* **2014**, *15*, 247. [CrossRef] [PubMed]

57. Herman, D.S.; Lam, L.; Taylor, M.R.; Wang, L.; Teekakirikul, P.; Christodoulou, D.; Seidman, C.E. Truncations of titin causing dilated cardiomyopathy. *N. Engl. J. Med.* **2012**, *366*, 619–628. [CrossRef]
58. Bowles, N.E.; Bowles, K.R.; Towbin, J.A. The "final common pathway" hypothesis and inherited cardiovascular disease. The role of cytoskeletal proteins in dilated cardiomyopathy. *Herz* **2000**, *25*, 168–175. [CrossRef] [PubMed]
59. Heller, S.A.; Shih, R.; Kalra, R.; Kang, P.B. Emery-Dreifuss muscular dystrophy. *Muscle Nerve.* **2020**, *61*, 436–448. [CrossRef]
60. Hazebroek, M.R.; Krapels, I.; Verdonschot, J.; van den Wijngaard, A.; Vanhoutte, E.; Hoos, M.; Snijders, L.; van Montfort, L.; Witjens, M.; Dennert, R.; et al. Prevalence of pathogenic gene mutations and prognosis do not differ in isolated left ventricular dysfunction compared with dilated cardiomyopathy. *Circ. Heart Fail.* **2018**, *11*, e004682. [CrossRef]
61. Gigli, M.; Stolfo, D.; Graw, S.L.; Merlo, M.; Gregorio, C.; Nee Chen, S.; Dal Ferro, M.; Paldino, M.D.A.; De Angelis, G.; Brun, F.; et al. Phenotypic expression, natural history, and risk stratification of cardiomyopathy caused by filamin C truncating variants. *Circulation* **2021**, *144*, 1600–1611. [CrossRef]
62. Sylvius, N.; Bilinska, Z.T.; Veinot, J.P.; Fidzianska, A.; Bolongo, P.M.; Poon, S.; McKeown, P.; Davies, R.A.; Chan, K.L.; Tang, A.S.; et al. In vivo and in vitro examination of the functional significances of novel lamin gene mutations in heart failure patients. *J. Med. Genet.* **2005**, *42*, 639–647. [CrossRef]
63. Shah, R.A.; Asatryan, B.; Sharaf Dabbagh, G.; Khanji, M.Y.; Lopes, L.R.; van Duijvenboden, S.; Holmes, A.; Muser, D.; Landstrom, A.P.; Lee, A.M.; et al. Frequency, penetrance, and variable expressivity of dilated cardiomyopa-thy-associated putative pathogenic gene variants in UK Biobank Participants. *Circulation* **2022**, *146*, 110–124. [CrossRef]
64. Fatkin, D. Guidelines for the diagnosis and management of familial dilated cardiomyopathy. *Heart Lung Circ.* **2011**, *20*, 691–693. [CrossRef] [PubMed]
65. Jordan, E.; Peterson, L.; Ai, T.; Asatryan, B.; Bronicki, L.; Brown, E.; Celeghin, R.; Edwards, M.; Fan, J.; Ingles, J.; et al. Evidence-based assessment of genes in dilated cardiomyopathy. *Circulation* **2021**, *144*, 7–19. [CrossRef] [PubMed]
66. Eldemire, R.; Tharp, C.A.; Taylor, M.R.G.; Sbaizero, O.; Mestroni, L. The sarcomerice spring protein titin: Biophysical properties, molecular mechanisms, and genetic mutations associated with heart failure and cardiomyopathy. *Curr. Cardiol. Rep.* **2021**, *23*, 121. [CrossRef] [PubMed]
67. Gigli, M.; Begay, R.L.; Morea, G.; Graw, S.L.; Sinagra, G.; Taylor, M.R.; Granzier, H.; Mestroni, L. A review of the giant protein titin in clinical molecular diagnostics of cardiomyopathies. *Front. Cardiovasc. Med.* **2016**, *3*, 21. [CrossRef] [PubMed]
68. Akhtar, M.M.; Lorenzini, M.; Cicerchia, M.; Ochoa, J.P.; Hey, T.M.; Sabater Molina, M.; Restrepo-Cordoba, M.A.; Dal Ferro, M.; Stolfo, D.; Johnson, R.L.; et al. Clinical phenotypes and prognosis of dilated cardiomyopathy caused by truncating variants in the TTN gene. *Circ. Heart Fail.* **2020**, *13*, e006832. [CrossRef] [PubMed]
69. Vissing, C.R.; Rasmussen, T.B.; Dybro, A.M.; Olesen, M.S.; Pedersen, L.N.; Jensen, M.; Bundgaard, H.; Christensen, A.H. Dilated cardiomyopathy caused by truncating titin variants: Long-term outcomes, arrhythmias, response to treatment and sex differences. *J. Med. Genet.* **2021**, *58*, 832–841. [CrossRef] [PubMed]
70. Roberts, A.M.; Ware, J.S.; Herman, D.S.; Schafer, S.; Baksi, J.; Bick, A.G.; Buchan, R.J.; Walsh, R.; John, S.; Wilkinson, S.; et al. Integrated allelic, transcriptional, and phenomic dissection of the cardiac effects of titin truncations in health and disease. *Sci. Transl. Med.* **2015**, *7*, 270ra6. [CrossRef] [PubMed]
71. Ware, J.S.; Cook, S.A. Role of titin in cardiomyopathy: From DNA variants to patient stratification. *Nat. Rev. Cardiol.* **2018**, *15*, 241–252. [CrossRef]
72. McAfee, Q.; Chen, C.Y.; Yang, Y.; Caporizzo, M.A.; Morley, M.; Babu, A.; Jeong, S.; Brandimarto, J.; Bedi, K.C., Jr.; Flam, E.; et al. Truncated titin proteins in dilated cardiomyopathy. *Sci. Transl. Med.* **2021**, *13*, eabd7287. [CrossRef]
73. Gramlich, M.; Pane, L.S.; Zhou, Q.; Chen, Z.; Murgia, M.; Schötterl, S.; Goedel, A.; Metzger, K.; Brade, T.; Parrotta, E.; et al. Antisense-mediated exon skipping: A therapeutic strategy for titin-based dilated cardiomyopathy. *EMBO Mol. Med.* **2015**, *7*, 562–576. [CrossRef]
74. Romano, R.; Ghahremani, S.; Zimmerman, T.; Legere, N.; Thakar, K.; Ladha, F.A.; Pettinato, A.M.; Hinson, J.T. Reading frame repair of TTN truncation variants restores titin quantity and functions. *Circulation* **2022**, *145*, 194–205. [CrossRef]
75. van Rijsingen, I.A.; Arbustini, E.; Elliott, P.M.; Mogensen, J.; Hermans-van Ast, J.F.; van der Kooi, A.J.; van Tintelen, J.P.; van den Berg, M.P.; Pilotto, A.; Pasotti, M.; et al. Risk factors for malignant ventricular arrhythmias in lamin a/c mutation carriers a European cohort study. *J. Am. Coll. Cardiol.* **2012**, *59*, 493–500. [CrossRef]
76. Parks, S.B.; Kushner, J.D.; Nauman, D.; Burgess, D.; Ludwigsen, S.; Peterson, A.; Li, D.; Jakobs, P.; Litt, M.; Porter, C.B.; et al. Lamin A/C mutation analysis in a cohort of 324 unrelated patients with idiopathic or familial dilated cardiomyopathy. *Am. Heart J.* **2008**, *156*, 161–169. [CrossRef]
77. Yamada, S.; Ko, T.; Ito, M.; Sassa, T.; Nomura, S.; Okuma, H.; Sato, M.; Imasaki, T.; Kikkawa, S.; Zhang, B.; et al. TEAD1 trapping by the Q353R-lamin A/C causes dilated cardiomyopathy. *Sci. Adv.* **2023**, *9*, eade7047. [CrossRef] [PubMed]
78. Quarta, G.; Syrris, P.; Ashworth, M.; Jenkins, S.; Zuborne Alapi, K.; Morgan, J.; Muir, A.; Pantazis, A.; McKenna, W.J.; Elliott, P.M. Mutations in the lamin A/C gene mimic ar-rhythmogenic right ventricular cardiomyopathy. *Eur. Heart J.* **2012**, *33*, 1128–1136. [CrossRef] [PubMed]
79. Chatzifrangkeskou, M.; Le Dour, C.; Wu, W.; Morrow, J.P.; Joseph, L.C.; Beuvin, M.; Sera, F.; Homma, S.; Vignier, N.; Mougenot, N.; et al. ERK1/2 Directly acts on CTGF/CCN2 expression to mediate myocardial fibrosis in cardiomyopathy caused by mutations in the lamin A/C gene. *Hum. Mol. Genet.* **2016**, *25*, 2220–2233. [CrossRef] [PubMed]

80. Hershberger, R.E.; Jordan, E. LMNA-Related Dilated Cardiomyopathy. In *GeneReviews® [Internet]*; Adam, M.P., Feldman, J., Mirzaa, G.M., Pagon, R.A., Wallace, S.E., Bean, L.J.H., Gripp, K.W., Amemiya, A., Eds.; University of Washington: Seattle, WA, USA, 2022. [PubMed]
81. Chai, R.J.; Werner, H.; Li, P.Y.; Lee, Y.L.; Nyein, K.T.; Solovei, I.; Luu, T.D.A.; Sharma, B.; Navasankari, R.; Maric, M.; et al. Disrupting the LINC complex by AAV mediated gene transduction prevents progression of lamin induced cardiomyopathy. *Nat. Commun.* **2021**, *2*, 4722. [CrossRef]
82. Ramos, F.J.; Chen, S.C.; Garelick, M.G.; Dai, D.F.; Liao, C.Y.; Schreiber, K.H.; MacKay, V.L.; An, E.H.; Strong, R.; Ladiges, W.C.; et al. Rapamycin reverses elevated mTORC1 signaling in lamin A/C-deficient mice, rescues cardiac and skeletal muscle function, and extends survival. *Sci. Transl. Med.* **2012**, *4*, 144ra03. [CrossRef] [PubMed]
83. Wu, W.; Muchir, A.; Shan, J.; Bonne, G.; Worman, H.J. Mitogen-activated protein kinase inhibitors improve heart function and prevent fibrosis in cardiomyopathy caused by mutation in lamin A/C gene. *Circulation* **2011**, *123*, 53–61. [CrossRef]
84. Auguste, G.; Rouhi, L.; Matkovich, S.J.; Coarfa, C.; Robertson, M.J.; Czernuszewicz, G.; Gurha, P.; Marian, A.J. BET Bromodomain inhibition attenuates cardiac phenotype in myocyte-specific lamin A/C-deficient mice. *J. Clin. Investig.* **2020**, *130*, 4740–4758. [CrossRef]
85. Zheng, K.; Liu, L.; Zhang, Y.Q. Recent research on childhood hypertrophic cardiomyopathy caused by MYH7 gene mutations. *Zhongguo Dang Dai Er Ke Za Zhi* **2023**, *25*, 425–430. [CrossRef] [PubMed]
86. Gao, Y.; Peng, L.; Zhao, C. MYH7 in cardiomyopathy and skeletal muscle myopathy. *Mol. Cell. Biochem.* **2023**, *479*, 393–417. [CrossRef] [PubMed]
87. de Frutos, F.; Ochoa, J.P.; Navarro-Peñalver, M.; Baas, A.; Bjerre, J.V.; Zorio, E.; Méndez, I.; Lorca, R.; Verdonschot, J.A.J.; García-Granja, P.E.; et al. Natural history of MYH7-related dilated cardiomyopathy. *J. Am. Coll. Cardiol.* **2022**, *80*, 1447–1461. [CrossRef] [PubMed]
88. Khan, R.S.; Pahl, E.; Dellefave-Castillo, L.; Rychlik, K.; Ing, A.; Yap, K.L.; Brew, C.; Johnston, J.R.; McNally, E.M.; Webster, G. Genotype and cardiac outcomes in pediatric dilated cardiomyopathy. *J. Am. Heart Assoc.* **2022**, *11*, e022854. [CrossRef] [PubMed]
89. Zhang, S.; Wilson, J.; Madani, M.; Feld, G.; Greenberg, B. Atrial arrhythmias and extensive left atrial fibrosis as the initial presentation of MYH7 gene mutation. *JACC Clin. Electrophysiol.* **2018**, *4*, 1488–1490. [CrossRef]
90. Petropoulou, E.; Soltani, M.; Firoozabadi, A.D.; Namayandeh, S.M.; Crockford, J.; Maroofian, R.; Jamshidi, Y. Digenic inheritance of mutations in the cardiac troponin (TNNT2) and cardiac beta myosin heavy chain (MYH7) as the cause of severe dilated cardiomyopathy. *Eur. J. Med. Genet.* **2017**, *60*, 485–488. [CrossRef] [PubMed]
91. Abdallah, A.M.; Carlus, S.J.; Al-Mazroea, A.H.; Alluqmani, M.; Almohammadi, Y.; Bhuiyan, Z.A.; Al-Harbi, K.M. Digenic inheritance of LAMA4 and MYH7 mutations in patient with infantile dilated cardiomyopathy. *Medicina* **2019**, *55*, 17. [CrossRef] [PubMed]
92. Selvi Rani, D.; Nallari, P.; Dhandapany, P.S.; Rani, J.; Meraj, K.; Ganesan, M.; Narasimhan, C.; Thangaraj, K. Coexistence of digenic mutations in both thin (TPM1) and thick (MYH7) filaments of sarcomeric genes leads to severe hypertrophic cardiomyopathy in a south Indian FHCM. *DNA Cell Biol.* **2015**, *34*, 350–359. [CrossRef]
93. Chang, A.C.Y.; Chang, A.C.H.; Kirillova, A.; Sasagawa, K.; Su, W.; Weber, G.; Termglinchan, V.; Karakikes, I.; Seeger, T.; Dainis, A.M.; et al. Telomere shortening is a hallmark of genetic cardiomyopathies. *Proc. Natl. Acad. Sci. USA* **2018**, *115*, 9276–9281. [CrossRef]
94. Chang, A.C.Y.; Blau, H.M. Short telomeres—A hallmark of heritable cardiomyopathies. *Differentiation* **2018**, *100*, 31–36. [CrossRef]
95. Eguchi, A.; Gonzalez, A.; Torres-Bigio, S.I.; Koleckar, K.; Birnbaum, F.; Zhang, J.Z.; Wang, V.Y.; Wu, J.C.; Artandi, S.E.; Blau, H.M. TRF2 rescues telomere attrition and prolongs cell survival in duchenne muscular dystrophy cardiomyocytes derived from human iPSCs. *Proc. Natl. Acad. Sci. USA* **2023**, *120*, e2209967120. [CrossRef] [PubMed]
96. Brenner, C.M.; Choudhary, M.; McCormick, M.G.; Cheung, D.; Landesberg, G.P.; Wang, J.F.; Song, J.; Martin, T.G.; Cheung, J.Y.; Qu, H.Q.; et al. BAG3: Nature's quintessential multifunctional protein functions as a ubiquitous intra-cellular glue. *Cells* **2023**, *12*, 937. [CrossRef] [PubMed]
97. Kirk, J.A.; Cheung, J.Y.; Feldman, A.M. Therapeutic targeting of BAG3: Considering its complexity in cancer and heart disease. *J. Clin. Investig.* **2021**, *131*, e149415. [CrossRef] [PubMed]
98. Liu, L.; Sun, K.; Zhang, X.; Tang, Y.; Xu, D. Advances in the role and mechanism of BAG3 in dilated cardiomyopathy. *Heart Fail. Rev.* **2021**, *26*, 183–194. [CrossRef] [PubMed]
99. Qu, H.Q.; Feldman, A.M.; Hakonarson, H. Genetics of BAG3: A paradigm for developing precision therapies for dilated cardio-myopathies. *J. Am. Heart Assoc.* **2022**, *11*, e027373. [CrossRef] [PubMed]
100. Mizushima, W.; Sadoshima, J. BAG3 plays a central role in proteostasis in the heart. *J. Clin. Investig.* **2017**, *127*, 2900–2903. [CrossRef] [PubMed]
101. Domínguez, F.; Cuenca, S.; Bilińska, Z.; Toro, R.; Villard, E.; Barriales-Villa, R.; Domínguez, F.; Cuenca, S.; Bilińska, Z.; Toro, R.; et al. Dilated cardiomyopathy due to BLC2-associated athanogene 3 (BAG3) mutations. *J. Am. Coll. Cardiol.* **2018**, *72*, 2471–2481. [CrossRef] [PubMed]
102. Fang, X.; Bogomolovas, J.; Wu, T.; Zhang, W.; Liu, C.; Veevers, J.; Stroud, M.J.; Zhang, Z.; Ma, X.; Mu, Y.; et al. Loss-of function mutations in co-chaperone BAG3 destabilize small HSPs and cause cardiomyopathy. *J. Clin. Investig.* **2017**, *127*, 3189–3200. [CrossRef]

103. Gamerdinger, M.; Hajieva, P.; Kaya, A.M.; Wolfrum, U.; Hartl, F.U.; Behl, C. Protein quality control during aging involves recruitment of the macroautophagy pathway by BAG3. *EMBO J.* **2009**, *28*, 889–901. [CrossRef]
104. Small, E.M.; Olson, E.N. Pervasive roles of microRNAs in cardiovascular biology. *Nature* **2011**, *469*, 336–342. [CrossRef]
105. Kalayinia, S.; Arjmand, F.; Maleki, M.; Malakootian, M.; Singh, C.P. MicroRNAs: Roles in cardiovascular development and disease. *Cardiovasc. Pathol.* **2021**, *50*, 107296. [CrossRef] [PubMed]
106. Zaragoza, C.; Saura, M.; Hernández, I.; Ramirez-Carracedo, R.; García-García, F.; Zamorano, J.L.; Mangas, A.; Toro, R. Differential expression of circulating miRNAs as a novel tool to assess BAG3-associated familial dilated cardiomyopathy. *Biosci. Rep.* **2019**, *39*, BSR20180934. [CrossRef] [PubMed]
107. Diofano, F.; Weinmann, K.; Schneider, I.; Thiessen, K.D.; Rottbauer, W.; Just, S. Genetic compensation prevents myopathy and heart failure in an in vivo model of Bag3 deficiency. *PLoS Genet.* **2020**, *16*, e1009088. [CrossRef] [PubMed]
108. Refaat, M.M.; Lubitz, S.A.; Makino, S.; Islam, Z.; Frangiskakis, J.M.; Mehdi, H.; Gutmann, R.; Zhang, M.L.; Bloom, H.L.; MacRae, C.A.; et al. Genetic variation in the alternative splicing regulator RBM20 is associated with dilated cardiomyopathy. *Heart Rhythm.* **2012**, *9*, 390–396. [CrossRef] [PubMed]
109. Watanabe, T.; Kimura, A.; Kuroyanagi, H. Alternative splicing regulator RBM20 and cardiomyopathy. *Front. Mol. Biosci.* **2018**, *5*, 105. [CrossRef] [PubMed]
110. Brauch, K.M.; Karst, M.L.; Herron, K.J.; de Andrade, M.; Pellikka, P.A.; Rodeheffer, R.J.; Michels, V.V.; Olson, T.M. Mutations in ribonucleic acid binding protein gene cause familial dilated cardiomyopathy. *J. Am. Coll. Cardiol.* **2009**, *54*, 930–941. [CrossRef] [PubMed]
111. Nishiyama, T.; Zhang, Y.; Cui, M.; Li, H.; Sanchez-Ortiz, E.; McAnally, J.R.; Tan, W.; Kim, J.; Chen, K.; Xu, L.; et al. Precise genomic editing of pathogenic mutations in RBM20 rescues dilated cardiomyopathy. *Sci. Transl. Med.* **2022**, *14*, eade1633. [CrossRef]
112. LeWinter, M.M.; Granzier, H.L. Titin is a major human disease gene. *Circulation* **2013**, *127*, 938–944. [CrossRef] [PubMed]
113. Guo, W.; Schafer, S.; Greaser, M.L.; Radke, M.H.; Liss, M.; Govindarajan, T.; Maatz, H.; Schulz, H.; Li, S.; Parrish, A.M.; et al. RBM20, A gene for hereditary cardiomyopathy, regulates titin splicing. *Nat. Med.* **2012**, *18*, 766–773. [CrossRef]
114. Zhang, Y.; Wang, C.; Sun, M.; Jin, Y.; Braz, C.U.; Khatib, H.; Hacker, T.A.; Liss, M.; Gotthardt, M.; Granzier, H.; et al. RBM20 Phosphorylation and its role in nucleocytoplasmic transport and cardiac pathogenesis. *FASEB J.* **2022**, *36*, e22302. [CrossRef]
115. Ihara, K.; Sasano, T.; Hiraoka, Y.; Togo-Ohno, M.; Soejima, Y.; Sawabe, M.; Tsuchiya, M.; Ogawa, H.; Furukawa, T.; Kuroyanagi, H. A missense mutation in the RSRSP stretch of Rbm20 causes dilated cardiomyopathy and atrial fibrillation in mice. *Sci. Rep.* **2020**, *10*, 17894. [CrossRef] [PubMed]
116. Song, S.; Shi, A.; Lian, H.; Hu, S.; Nie, Y. Filamin C in cardiomyopathy: From physiological roles to DNA variants. *Heart Fail. Rev.* **2022**, *27*, 1373–1385. [CrossRef] [PubMed]
117. Mao, Z.; Nakamura, F. Structure and function of filamin C in the muscle Z-disc. *Int. J. Mol. Sci.* **2020**, *21*, 2696. [CrossRef] [PubMed]
118. Noureddine, M.; Gehmlich, K. Structural and signaling proteins in the Z-disk and their role in cardiomyopathies. *Front. Physiol.* **2023**, *14*, 1143858. [CrossRef] [PubMed]
119. Powers, J.D.; Kirkland, N.J.; Liu, C.; Razu, S.S.; Fang, X.; Engler, A.J.; Chen, J.; McCulloch, A.D. Subcellular remodeling in filamin C deficient mouse hearts impairs myocyte tension development during progression of dilated cardiomyopathy. *Int. J. Mol. Sci.* **2022**, *23*, 871. [CrossRef] [PubMed]
120. Zhou, Y.; Chen, Z.; Zhang, L.; Zhu, M.; Tan, C.; Zhou, X.; Evans, S.M.; Fang, X.; Feng, W.; Chen, J. Loss of filamin C is catastrophic for heart function. *Circulation* **2020**, *141*, 869–871. [CrossRef] [PubMed]
121. Begay, R.L.; Graw, S.L.; Sinagra, G.; Asimaki, A.; Rowland, T.J.; Slavov, D.B. Filamin C truncation mutations are associated with arrhythmogenic dilated cardiomyopathy and changes in the cell-cell adhesion structures. *JACC Clin. Electrophysiol.* **2018**, *4*, 504–514. [CrossRef] [PubMed]
122. Ortiz-Genga, M.F.; Cuenca, S.; Dal Ferro, M.; Zorio, E.; Salgado-Aranda, R.; Climent, V.; Padrón-Barthe, L.; Duro-Aguado, I.; Jiménez-Jáimez, J.; Hidalgo-Olivares, V.M.; et al. Truncating FLNC mutations are asso-ciated with high-risk dilated and arrhythmogenic cardiomyopathies. *J. Am. Coll. Cardiol.* **2016**, *68*, 2440–2451. [CrossRef]
123. Celeghin, R.; Cipriani, A.; Bariani, R.; Bueno Marinas, M.; Cason, M.; Bevilacqua, M. Filamin-C variant-associated cardiomyopathy: A pooled analysis of individualpatient data to evaluate the clinical profile and risk of sudden cardiac death. *Heart Rhythm.* **2022**, *19*, 235–243. [CrossRef]
124. Chen, S.N.; Lam, C.K.; Wan, Y.W.; Gao, S.; Malak, O.A.; Zhao, S.R.; Lombardi, R.; Ambardekar, A.V.; Bristow, M.R.; Cleveland, J.; et al. Activation of PDGFRA signaling contributes to filamin C-related arrhythmogenic cardiomyopathy. *Sci. Adv.* **2022**, *8*, eabk0052. [CrossRef]
125. Remme, C.A. SCN5A Channelopathy: Arrhythmia, cardiomyopathy, epilepsy and beyond. *Philos. Trans. R. Soc. Lond. Ser. B Biol. Sci.* **2023**, *378*, 20220164. [CrossRef] [PubMed]
126. Zegkos, T.; Panagiotidis, T.; Parcharidou, D.; Efthimiadis, G. Emerging concepts in arrhythmogenic dilated cardiomyopathy. *Heart Fail. Rev.* **2021**, *26*, 1219–1229. [CrossRef] [PubMed]
127. Li, W.; Yin, L.; Shen, C.; Hu, K.; Ge, J.; Sun, A. SCN5A variants: Association with cardiac disorders. *Front. Physiol.* **2018**, *9*, 1372. [CrossRef] [PubMed]

128. Moreau, A.; Gosselin-Badaroudine, P.; Delemotte, L.; Klein, M.L.; Chahine, M. Gating pore currents are defects in common with two Nav1.5 mutations in patients with mixed arrhythmias and dilated cardiomyopathy. *J. Gen. Physiol.* **2015**, *145*, 93–106. [CrossRef] [PubMed]
129. Poller, W.; Escher, F.; Haas, J.; Heidecker, B.; Schultheiss, H.P.; Attanasio, P.; Skurk, C.; Haghikia, A.; Meder, B.; Klaassen, S. Missense variant E1295K of sodium channel SCN5A associated with recurrent ventricular fibrillation and myocardial inflammation. *JACC Case Rep.* **2022**, *4*, 280–286. [CrossRef] [PubMed]
130. Wilde, A.A.M.; Amin, A.S. Clinical Spectrum of SCN5A mutations: Long QT syndrome, brugada syndrome, and cardiomyopathy. *JACC Clin. Electrophysiol.* **2018**, *4*, 569–579. [CrossRef] [PubMed]
131. Peters, S.; Thompson, B.A.; Perrin, M.; James, P.; Zentner, D.; Kalman, J.M.; Vandenberg, J.I.; Fatkin, D. Arrhythmic phenotypes are a defining feature of dilated cardiomyopathy-associated SCN5A variants: A systematic review. *Circ. Genom. Precis. Med.* **2022**, *15*, e003432. [CrossRef] [PubMed]
132. Zhou, A.; Xie, A.; Kim, T.Y.; Liu, H.; Shi, G.; Kang, G.J.; Jiang, N.; Liu, M.; Jeong, E.M.; Choi, B.R.; et al. HuR-mediated SCN5A messenger RNA stability reduces arrhythmic risk in heart failure. *Heart Rhythm.* **2018**, *15*, 1072–1080. [CrossRef]
133. Li, M.X.; Hwang, P.M. Structure and function of cardiac troponin C (TNNC1): Implications for heart failure, cardiomyopathies, and troponin modulating drugs. *Gene* **2015**, *571*, 153–166. [CrossRef]
134. Keyt, L.K.; Duran, J.M.; Bui, Q.M.; Chen, C.; Miyamoto, M.I.; Silva Enciso, J.; Tardiff, J.C.; Adler, E.D. Thin filament cardiomyopathies: A review of genetics, disease mechanisms, and emerging therapeutics. *Front. Cardiovasc. Med.* **2022**, *9*, 972301. [CrossRef]
135. Kalyva, A.; Parthenakis, F.I.; Marketou, M.E.; Kontaraki, J.E.; Vardas, P.E. Biochemical characterisation of troponin C mutations causing hypertrophic and dilated cardiomyopathies. *J. Muscle Res. Cell Motil.* **2014**, *35*, 161–178. [CrossRef] [PubMed]
136. Mogensen, J.; Murphy, R.T.; Shaw, T.; Bahl, A.; Redwood, C.; Watkins, H.; Burke, M.; Elliott, P.M.; McKenna, W.J. Severe disease expression of cardiac troponin C and T mutations in patients with idiopathic dilated cardiomyopathy. *J. Am. Coll. Cardiol.* **2004**, *44*, 2033–2040. [CrossRef] [PubMed]
137. Hershberger, R.E.; Norton, N.; Morales, A.; Li, D.; Siegfried, J.D.; Gonzalez-Quintana, J. Coding sequence rare variants identified in MYBPC3, MYH6, TPM1, TNNC1, and TNNI3 from 312 patients with familial or idiopathic dilated cardiomyopathy. *Circ. Cardiovasc. Genet.* **2010**, *3*, 155–161. [CrossRef] [PubMed]
138. Hershberger, R.E.; Parks, S.B.; Kushner, J.D.; Li, D.; Ludwigsen, S.; Jakobs, P.; Nauman, D.; Burgess, D.; Partain, J.; Litt, M. Coding sequence mutations identified in MYH7, TNNT2, SCN5A, CSRP3, LBD3,and TCAP from 313 patients with familial or idiopathic dilated cardiomyopathy. *Clin. Transl. Sci.* **2008**, *1*, 21–26. [CrossRef] [PubMed]
139. Tadros, H.J.; Life, C.S.; Garcia, G.; Pirozzi, E.; Jones, E.G.; Datta, S.; Parvatiyar, M.S.; Chase, P.B.; Allen, H.D.; Kim, J.J.; et al. Meta-analysis of cardiomyopathy-associated variants in troponin genes identifies loci and intragenic hot spots that are associated with worse clinical outcomes. *J. Mol. Cell Cardiol.* **2020**, *142*, 118–125. [CrossRef] [PubMed]
140. Alves, M.L.; Warren, C.M.; Simon, J.N.; Gaffin, R.D.; Montminy, E.M.; Wieczorek, D.F.; Solaro, R.J.; Wolska, B.M. Early sensitization of myofilaments to Ca^{2+} prevents genetically linked dilated cardiomyopathy in mice. *Cardiovasc. Res.* **2017**, *113*, 915–925. [CrossRef] [PubMed]
141. Li, B.; Guo, Y.; Zhan, Y.; Zhou, X.; Li, Y.; Zhao, C.; Sun, N.; Xu, C.; Liang, Q. Cardiac overexpression of XIN prevents dilated cardiomyopathy caused by TNNT2 ΔK210 mutation. *Front. Cell Dev. Biol.* **2021**, *9*, 691749. [CrossRef] [PubMed]
142. Gomes, G.; Seixas, M.R.; Azevedo, S.; Audi, K.; Jurberg, A.D.; Mermelstein, C.; Costa, M.L. What does desmin do: A bibliometric assessment of the functions of the muscle intermediate filament. *Exp. Biol. Med.* **2022**, *247*, 538–550. [CrossRef]
143. Schröder, R.; Vrabie, A.; Goebel, H.H. Primary desminopathies. *J. Cell Mol. Med.* **2007**, *11*, 416–426. [CrossRef]
144. Tsikitis, M.; Galata, Z.; Mavroidis, M.; Psarras, S.; Capetanaki, Y. Intermediate filaments in cardiomyopathy. *Biophys. Rev.* **2018**, *10*, 1007–1031. [CrossRef]
145. Tesson, F.; Sylvius, N.; Pilotto, A.; Dubosq-Bidot, L.; Peuchmaurd, M.; Bouchier, C.; Benaiche, A.; Mangin, L.; Charron, P.; Gavazzi, A.; et al. Epidemiology of desmin and cardiac actin gene mutations in a European population of dilated cardiomyopathy. *Eur. Heart J.* **2000**, *21*, 1872–1876. [CrossRef] [PubMed]
146. Schirmer, I.; Dieding, M.; Klauke, B.; Brodehl, A.; Gaertner-Rommel, A.; Walhorn, V.; Gummert, J.; Schulz, U.; Paluszkiewicz, L.; Anselmetti, D.; et al. A novel desmin (DES) indel mutation causes severe atypical cardiomyopathy in combination with atrio-ventricular block and skeletal myopathy. *Mol. Genet. Genom. Med.* **2018**, *6*, 288–293. [CrossRef] [PubMed]
147. van Spaendonck-Zwarts, K.Y.; van Hessem, L.; Jongbloed, J.D.; de Walle, H.E.; Capetanaki, Y.; van der Kooi, A.J.; van Langen, I.M.; van den Berg, M.P.; van Tintelen, J.P. Desmin-related myopathy. *Clin. Genet.* **2011**, *80*, 354–366. [CrossRef] [PubMed]
148. Elsnicova, B.; Hornikova, D.; Tibenska, V.; Kolar, D.; Tlapakova, T.; Schmid, B.; Mallek, M.; Eggers, B.; Schlötzer-Schrehardt, U.; Peeva, V.; et al. Desmin knock-out cardiomyopathy: A heart on the verge of metabolic crisis. *Int. J. Mol. Sci.* **2022**, *23*, 12020. [CrossRef] [PubMed]
149. Diermeier, S.; Iberl, J.; Vetter, K.; Haug, M.; Pollmann, C.; Reischl, B.; Buttgereit, A.; Schürmann, S.; Spörrer, M.; Goldmann, W.H.; et al. Early signs of architectural and biomechanical failure in isolated myofibers and immortalized myoblasts from desmin-mutant knock-in mice. *Sci. Rep.* **2017**, *7*, 1391. [CrossRef] [PubMed]
150. Koopman, W.J.; Willems, P.H.; Smeitink, J.A. Monogenic mitochondrial disorders. *N. Engl. J. Med.* **2012**, *366*, 1132–1141. [CrossRef]

151. Diokmetzidou, A.; Soumaka, E.; Kloukina, I.; Tsikitis, M.; Makridakis, M.; Varela, A.; Davos, C.H.; Georgopoulos, S.; Anesti, V.; Vlahou, A.; et al. Desmin and αB-crystallin interplay in the maintenance of mitochondrial homeostasis and cardiomyocyte survival. *J. Cell Sci.* **2016**, *129*, 3705–3720. [CrossRef] [PubMed]
152. Feyen, D.A.M.; Perea-Gil, I.; Maas, R.G.C.; Harakalova, M.; Gavidia, A.A.; Arthur Ataam, J.; Wu, T.H.; Vink, A.; Pei, J.; Vadgama, N.; et al. Unfolded protein response as a compensatory mechanism and potential therapeutic target in PLN R14del cardiomyopathy. *Circulation* **2021**, *144*, 382–392. [CrossRef] [PubMed]
153. Hof, I.E.; van der Heijden, J.F.; Kranias, E.G.; Sanoudou, D.; de Boer, R.A.; van Tintelen, J.P.; van der Zwaag, P.A.; Doevendans, P.A. Prevalence and cardiac phenotype of patients with a phospholamban mutation. *Neth. Heart J.* **2019**, *27*, 64–69. [CrossRef]
154. van der Zwaag, P.A.; van Rijsingen, I.A.; Asimaki, A.; Jongbloed, J.D.; van Veldhuisen, D.J.; Wiesfeld, A.C.; Cox, M.G.; van Lochem, L.T.; de Boer, R.A.; Hofstra, R.M.; et al. Phospholamban R14del mutation in patients diagnosed with dilated cardiomyopathy or arrhythmogenic right ventricular cardiomyopathy evidence supporting the concept of arrhythmogenic cardiomyopathy. *Eur. J. Heart Fail.* **2012**, *14*, 1199–1207. [CrossRef]
155. Medin, M.; Hermida-Prieto, M.; Monserrat, L.; Laredo, R.; Rodriguez-Rey, J.C.; Fernandez, X.; Castro-Beiras, A. Mutational screening of phos-pholamban gene in hypertrophic and idiopathic dilated cardiomyopathy and functional study of the PLN-42 C>G mutation. *Eur. J. Heart Fail.* **2007**, *9*, 37–43. [CrossRef] [PubMed]
156. Villard, E.; Duboscq-Bidot, L.; Charron, P.; Benaiche, A.; Conraads, V.; Sylvius, N.; Komajda, M. Mutation screening in dilated cardiomyo-pathy: Prominent role of the beta myosin heavy chain gene. *Eur. Heart J.* **2005**, *26*, 794–803. [CrossRef]
157. van Rijsingen, I.A.; van der Zwaag, P.A.; Groeneweg, J.A.; Nannenberg, E.A.; Jongbloed, J.D.; Zwinderman, A.H.; Pinto, Y.M.; Dit Deprez, R.H.; Post, J.G.; Tan, H.L.; et al. Outcome in phospholamban R14del carriers: Results of a large multicentre cohort study. *Circ. Cardiovasc. Genet.* **2014**, *7*, 455–465. [CrossRef] [PubMed]
158. Deiman, F.E.; Bomer, N.; van der Meer, P.; Grote Beverborg, N. Review: Precision medicine approaches for genetic cardiomyopathy: Targeting phospholamban R14del. *Curr. Heart Fail. Rep.* **2022**, *19*, 170–179. [CrossRef] [PubMed]
159. Doevendans, P.A.; Glijnis, P.C.; Kranias, E.G. Leducq transatlantic network of excellence to cure phospholamban-induced car-diomyopathy (CURE-PLaN). *Circ. Res.* **2019**, *125*, 720–724. [CrossRef] [PubMed]
160. de Brouwer, R.; Meems, L.M.G.; Verstraelen, T.E.; Mahmoud, B.; Proost, V.; Wilde, A.A.M.; Bosman, L.P.; van Drie, E.; van der Zwaag, P.A.; van Tintelen, J.P.; et al. Sex-specific aspects of phospholamban cardiomyopathy: The importance and prognostic value of low-voltage electrocardiograms. *Heart Rhythm.* **2022**, *19*, 427–434. [CrossRef] [PubMed]
161. Te Rijdt, W.P.; Hoorntje, E.T.; de Brouwer, R.; Oomen, A.; Amin, A.; van der Heijden, J.F.; Karper, J.C.; Westenbrink, B.D.; Silljé, H.H.W.; Te Riele, S.J.M.; et al. Rationale and design of the PHOs-pholamban RElated Cardiomyopathy intervention STudy (i-PHORECAST). *Neth. Heart J.* **2022**, *30*, 84–95. [CrossRef]
162. Grote Beverborg, N.; Später, D.; Knöll, R.; Hidalgo, A.; Yeh, S.T.; Elbeck, Z.; Silljé, H.H.W.; Eijgenraam, T.R.; Siga, H.; Zurek, M.; et al. Phospholamban antisense oligonucleotides improve cardiac function in murine cardiomyopathy. *Nat. Commun.* **2021**, *12*, 5180. [CrossRef] [PubMed]
163. Dave, J.; Raad, N.; Mittal, N.; Zhang, L.; Fargnoli, A.; Oh, J.G.; Savoia, M.E.; Hansen, J.; Fava, M.; Yin, X.; et al. Gene editing reverses arrhythmia susceptibility in humanized PLN-R14del mice: Modelling a European cardiomyopathy with global impact. *Cardiovasc. Res.* **2022**, *118*, 3140–3150. [CrossRef]
164. Vafiadaki, E.; Glijnis, P.C.; Doevendans, P.A.; Kranias, E.G.; Sanoudou, D. Phospholamban R14del disease: The past, the present and the future. *Front. Cardiovasc. Med.* **2023**, *10*, 1162205. [CrossRef]
165. Pugh, T.J.; Kelly, M.A.; Gowrisankar, S.; Hynes, E.; Seidman, M.A.; Baxter, S.M.; Bowser, M.; Harrison, B.; Aaron, D.; Mahanta, L.M.; et al. The landscape of genetic variation in dilated cardiomyopathy as surveyed by clinical DNA sequencing. *Genet. Med.* **2014**, *16*, 601–608. [CrossRef]
166. Karvonen, V.; Harjama, L.; Heliö, K.; Kettunen, K.; Elomaa, O.; Koskenvuo, J.W.; Kere, J.; Weckström, S.; Holmström, M.; Saarela, J.; et al. A novel desmoplakin mutation causes dilated cardiomyopathy with palmoplantar keratoderma as an early clinical sign. *J. Eur. Acad. Dermatol. Venereol.* **2022**, *36*, 1349–1358. [CrossRef] [PubMed]
167. Gigli, M.; Merlo, M.; Graw, S.L.; Barbati, G.; Rowland, T.J.; Slavov, D.B.; Stolfo, D.; Haywood, M.E.; Dal Ferro, M.; Altinier, A.; et al. Genetic risk of arrhythmic phenotypes in patients with dilated cardiomyopathy. *J. Am. Coll. Cardiol.* **2019**, *74*, 1480–1490. [CrossRef] [PubMed]
168. Brandão, M.; Bariani, R.; Rigato, I.; Bauce, B. Desmoplakin cardiomyopathy: Comprehensive review of an increasingly recognized entity. *J. Clin. Med.* **2023**, *12*, 2660. [CrossRef]
169. Smith, E.D.; Lakdawala, N.K.; Papoutsidakis, N.; Aubert, G.; Mazzanti, A.; McCanta, A.C.; Agarwal, P.P.; Arscott, P.; Dellefave-Castillo, L.M.; Vorovich, E.E.; et al. Desmoplakin cardiomyopathy, a fibrotic and inflammatory form of cardiomyopathy distinct from typical dilated or arrhythmogenic right ventricular cardiomyopathy. *Circulation* **2020**, *141*, 1872–1884. [CrossRef] [PubMed]
170. Bariani, R.; Cason, M.; Rigato, I.; Cipriani, A.; Celeghin, R.; De Gaspari, M.; Bueno Marinas, M.; Mattesi, G.; Pergola, V.; Rizzo, S.; et al. Clinical profile and long-term follow-up of a cohort of patients with desmoplakin cardiomyopathy. *Heart Rhythm.* **2022**, *19*, 1315–1324. [CrossRef] [PubMed]
171. Chelko, S.P.; Asimaki, A.; Lowenthal, J.; Bueno-Beti, C.; Bedja, D.; Scalco, A.; Amat-Alarcon, N.; Andersen, P.; Judge, D.P.; Tung, L.; et al. Therapeutic modulation of the immune response in arrhythmogenic cardiomyopathy. *Circulation* **2019**, *140*, 1491–1505. [CrossRef] [PubMed]

172. Bauce, B.; Basso, C.; Rampazzo, A.; Beffagna, G.; Daliento, L.; Frigo, G.; Malagrida, S.; Settimo, L.; Danieli, G.A.; Thiene, G.; et al. Clinical profile of four families with arrhythmogenic right ventricular cardiomyopathy caused by dominant desmoplakin mutations. *Eur. Heart J.* **2005**, *26*, 1666–1675. [CrossRef]
173. Franco, A.; Li, J.; Kelly, D.P.; Hershberger, R.E.; Marian, A.J.; Lewis, R.M.; Song, M.; Dang, X.; Schmidt, A.D.; Mathyer, M.E.; et al. A human mitofusin 2 mutation can cause mitophagic cardiomyopathy. *eLife* **2023**, *12*, e84235. [CrossRef]
174. Paldino, A.; Dal Ferro, M.; Stolfo, D.; Gandin, I.; Medo, K.; Graw, S.; Gigli, M.; Gagno, G.; Zaffalon, D.; Castrichini, M.; et al. Prognostic prediction of genotype vs phenotype in genetic cardiomyopathies. *J. Am. Coll. Cardiol.* **2022**, *80*, 1981–1994. [CrossRef]
175. Meune, C.; Van Berlo, J.H.; Anselme, F.; Bonne, G.; Pinto, Y.M.; Duboc, D. Primary prevention of sudden death in patients with lamin A/C gene mutations. *N. Engl. J. Med.* **2006**, *354*, 209–210. [CrossRef] [PubMed]
176. Towbin, J.A.; McKenna, W.J.; Abrams, D.J.; Ackerman, M.J.; Calkins, H.; Darrieux, F.C.C.; Daubert, J.P.; de Chillou, C.; DePasquale, E.C.; Desai, M.Y.; et al. 2019 HRS expert consensus statement on evaluation, risk stratification, and management of arrhythmogenic cardiomyopathy. *Heart Rhythm.* **2019**, *16*, e301–e372. [CrossRef] [PubMed]
177. Ichida, F.; Tsubata, S.; Bowles, K.R.; Haneda, N.; Uese, K.; Miyawaki, T.; Dreyer, W.J.; Messina, J.; Li, H.; Bowles, N.E.; et al. Novel gene mutations in patients with left ventricular noncompaction or Barth syndrome. *Circulation* **2001**, *103*, 1256–1263. [CrossRef] [PubMed]
178. Smith, J.G.; Felix, J.F.; Morrison, A.C.; Kalogeropoulos, A.; Trompet, S.; Wilk, J.B.; Gidlöf, O.; Wang, X.; Morley, M.; Mendelson, M.; et al. Discovery of genetic variation on chromosome 5q22 associated with mortality in heart failure. *PLOS Genet.* **2016**, *12*, e1006034. [CrossRef]
179. Merlo, M.; Cannatà, A.; Pio Loco, C.; Stolfo, D.; Barbati, G.; Artico, J.; Gentile, P.; De Paris, V.; Ramani, F.; Zecchin, M.; et al. Contemporary survival trends and aetiological characterization in non-ischaemic dilated cardiomyopathy. *Eur. J. Heart Fail.* **2020**, *22*, 1111–1121. [CrossRef]
180. Heidenreich, P.A.; Bozkurt, B.; Aguilar, D.; Allen, L.A.; Byun, J.J.; Colvin, M.M.; Deswal, A.; Drazner, M.H.; Dunlay, S.M.; Evers, L.R.; et al. 2022 AHA/ACC/HFSA guideline for the management of heart failure. *J. Card. Fail.* **2022**, *28*, e1–e167. [CrossRef]
181. Cresci, S.; Kelly, R.J.; Cappola, T.P.; Diwan, A.; Dries, D.; Kardia, S.L.; Dorn, G.W., 2nd. Clinical and genetic modifiers of long-term survival in heart failure. *J. Am. Coll. Cardiol.* **2009**, *54*, 432–444. [CrossRef] [PubMed]
182. Gaertner, A.; Bloebaum, J.; Brodehl, A.; Klauke, B.; Sielemann, K.; Kassner, A.; Fox, H.; Morshuis, M.; Tiesmeier, J.; Schulz, U.; et al. The Combined Human Genotype of Truncating TTN and RBM20 Mutations Is Associated with Severe and Early Onset of Dilated Cardiomyopathy. *Genes* **2021**, *12*, 883. [CrossRef]
183. Owens, A.T.; Day, S.M. Reappraising Genes for Dilated Cardiomyopathy: Stepping Back to Move Forward. *Circulation* **2021**, *144*, 20–22. [CrossRef] [PubMed]
184. Wilde, A.A.M.; Semsarian, C.; Márquez, M.F.; Shamloo, A.S.; Ackerman, M.J.; Ashley, E.A.; Sternick, E.B.; Barajas-Martinez, H.; Behr, E.R.; Bezzina, C.R.; et al. European Heart Rhythm Association (EHRA)/Heart Rhythm Society (HRS)/Asia Pacific Heart Rhythm Society (APHRS)/Latin American Heart Rhythm Society (LAHRS) Expert Consensus Statement on the State of Genetic Testing for Cardiac Diseases. *Heart Rhythm.* **2022**, *19*, 623–629. [CrossRef]
185. White, H.; Maqbool, A.; McMahon, A.D.; Yates, L.; Ball, S.G.; Hall, A.S.; Balmforth, A.J. An evaluation of the β1 adrenergic receptor Arg389Gly polymorphism in individuals at risk of coronary events: A WOSCOPS substudy. *Eur. Heart J.* **2002**, *23*, 1087–1092. [CrossRef] [PubMed]
186. White, H.L.; de Boer, R.A.; Maqbool, A.; Greenwood, D.; van Veldhuisen, D.J.; Cuthbert, R.; Ball, S.G.; Hall, A.S.; Balmforth, A.J. An evaluation of the β1 adrenergic receptor Arg389Gly polymorphism in individuals with heart failure: A MERIT-HF sub-study. *Eur. J. Heart Fail.* **2003**, *5*, 463–468. [PubMed]
187. Pare, G.; Kubo, M.; Byrd, J.B.; McCarty, C.A.; Woodard-Grice, A.; Teo, K.K.; Anand, S.S.; Zuvich, R.L.; Bradford, Y.; Ross, S.; et al. Genetic variants associated with angiotensin- converting enzyme inhibitor- associated angioedema. Pharmacogenet. *Genomics* **2013**, *23*, 470–478.
188. Nelveg-Kristensen, K.E.; Busk Madsen, M.; Torp-Pedersen, C.; Køber, L.; Egfjord, M.; Berg Rasmussen, H.; Riis Hansen, P. Pharmacogenetic risk stratification in angiotensin-converting enzyme inhibitor- treated patients with congestive heart failure: A retrospective cohort study. *PLoS ONE* **2015**, *10*, e0144195. [CrossRef] [PubMed]
189. Van Spaendonck-Zwarts, K.Y.; van Tintelen, J.P.; van Veldhuisen, D.J.; van der Werf, R.; Jongbloed, J.D.; Paulus, W.J.; Dooijes, D.; van den Berg, M.P. Peripartum cardiomyopathy as a part of familial dilated cardiomyopathy. *Circulation* **2010**, *121*, 2169–2175. [CrossRef] [PubMed]
190. Scott, E.; Hasbullah, J.S.; Ross, C.J.; Carleton, B.C. Reducing anthracycline-induced cardiotoxicity through pharmacogenetics. *Pharmacogenomics* **2018**, *19*, 1147–1150. [CrossRef] [PubMed]
191. Hazebroek, M.R.; Moors, S.; Dennert, R.; van den Wijngaard, A.; Krapels, I.; Hoos, M.; Verdonschot, J.; Merken, J.J.; de Vries, B.; Wolffs, P.F.; et al. Prognostic relevance of gene-environment interactions in patients with dilated cardiomyopathy: Applying the MOGE(S) classification. *J. Am. Coll. Cardiol.* **2015**, *66*, 1313–1323. [CrossRef]
192. Mann, S.A.; Castro, M.L.; Ohanian, M.; Guo, G.; Zodgekar, P.; Sheu, A.; Stockhammer, K.; Thompson, T.; Playford, D.; Subbiah, R.; et al. R222Q SCN5A mutation is associated with reversible ventricular ectopy and dilated cardiomyopathy. *J. Am. Coll. Cardiol.* **2012**, *60*, 1566–1573. [CrossRef] [PubMed]

193. Skjølsvik, E.T.; Hasselberg, N.E.; Dejgaard, L.A.; Lie, Ø.H.; Andersen, K.; Holm, T.; Edvardsen, T.; Haugaa, K.H. Exercise is associated with impaired left ventricular systolic function in patients with Lamin A/C genotype. *J. Am. Heart Assoc.* **2020**, *9*, e012937. [CrossRef]
194. Regitz-Zagrosek, V.; Roos-Hesselink, J.W.; Bauersachs, J.; Blomström-Lundqvist, C.; Cífkova, R.; De Bonis, M.; Iung, B.; Johnson, M.R.; Kintscher, U.; Kranke, P.; et al. 2018 ESC guidelines for the management of cardiovascular diseases during pregnancy: The Task Force for the Management of Cardi-ovascular Diseases during pregnancy of the European Society of Cardiology (ESC). *Eur. Heart J.* **2018**, *39*, 3165–3241. [CrossRef]
195. De Boer, R.A.; Heymans, S.; Backs, J.; Carrier, L.; Coats, A.J.S.; Dimmeler, S.; Eschenhagen, T.; Filippatos, G.; Gepstein, L.; Hulot, J.S.; et al. Targeted therapies in genetic dilated and hypertrophic cardiomyopathies: From molecular mechanisms to therapeutic targets. A position paper from the Heart Failure Association (HFA) and the Working Group on Myocardial Function of the European Society of Cardiology (ESC). *Eur. J. Heart Fail.* **2022**, *24*, 406–420. [PubMed]
196. Pinto, Y.M.; Elliott, P.M.; Arbustini, E.; Adler, Y.; Anastasakis, A.; Böhm, M.; Duboc, D.; Gimeno, J.; de Groote, P.; Imazio, M.; et al. Proposal for a revised definition of dilated cardiomyopathy, hypokinetic non-dilated cardiomyopathy, and its implications for clinical practice: A position statement of the ESC working group on myocardial and pericardial diseases. *Eur. Heart J.* **2016**, *37*, 1850–1858. [CrossRef] [PubMed]

Disclaimer/Publisher's Note: The statements, opinions and data contained in all publications are solely those of the individual author(s) and contributor(s) and not of MDPI and/or the editor(s). MDPI and/or the editor(s) disclaim responsibility for any injury to people or property resulting from any ideas, methods, instructions or products referred to in the content.

biomedicines

MDPI

Review

Sodium–Glucose Cotransporter-2 Inhibitors After Acute Myocardial Infarction

Nicia I. Profili [1], Roberto Castelli [1], Roberto Manetti [1], Marta C. Sircana [1], Michela Pagni [1], Gemma Lisa Sechi [1], Antonio Gidaro [2], Costantino Cossu [3], Francesco Bella [3] and Alessandro P. Delitala [1,*]

[1] Department of Medicine, Surgery, and Pharmacy, University of Sassari, 07100 Sassari, Italy; rmanetti@uniss.it (R.M.); m.pagni@studenti.uniss.it (M.P.)
[2] Department of Biomedical and Clinical Sciences Luigi Sacco, University of Milan, Luigi Sacco Hospital, 20157 Milan, Italy
[3] Azienda Ospedaliero-Universitaria di Sassari, 07100 Sassari, Italy; francesco.bella@aouss.it (F.B.)
* Correspondence: aledelitala@uniss.it; Tel.: +39-0792646641

Abstract: Sodium–glucose cotransporter-2 inhibitors (SGLT2i) are a specific class of drugs originally developed for treating type 2 diabetes mellitus. Subsequently, studies demonstrated that their action was not limited to glycemic control but could also have positive effects on other specific outcomes, particularly at the cardiovascular level. Indeed, due to their diuretic effect, SGLT2i improve the clinical control of chronic heart failure and reduce the risk of rehospitalization. In addition, other studies reported a protective effect on major cardiovascular events and mortality. More recently, it has been suggested that the prescription of SGLT2i after an acute myocardial infarction may have positive effects due to their possible effect on inflammation, arrhythmias, and ventricular remodeling. Here, we reviewed studies focused on SGLT2i after an acute myocardial infarction in patients treated with percutaneous coronary intervention.

Keywords: SGLT2i; sodium–glucose cotransporter-2 inhibitors; acute myocardial infarction; acute heart failure; diabetes; cardiovascular disease

1. Introduction

Acute myocardial infarction (AMI) is defined as cardiomyocyte necrosis in the clinical setting of acute myocardial ischemia [1]. Guidelines suggested the use of the term AMI in the presence of clinical evidence of acute myocardial ischemia and the detection of a rise and/or fall of high-sensitivity cardiac troponin T associated with at least one of the following criteria: symptoms of myocardial ischemia, new electrocardiogram changes consistent with ischemia, the development of pathological Q waves, the detection of intracoronary thrombus, or imaging evidence of the loss of viable myocardium or new regional wall motion abnormalities [1]. AMI can be classified into different types according to clinical, pathological, and prognostic criteria. The choice of treatment is based on a specific algorithm that can be time-dependent in patients with high-risk features. Percutaneous coronary intervention (PCI) is the preferred reperfusion strategy [2]. Pharmacological treatment has a pivotal role soon after PCI. Indeed, oral anti-platelet agents are promptly prescribed to reduce the risk of local thrombotic complications and systemic ischemic events, while angiotensin-converting enzyme (ACE) inhibitors and β-blockers are useful to improve outcomes in post-AMI patients complicated by heart failure, diabetes, and/or hypertension [2].

Sodium–glucose cotransporter-2 inhibitors (SGLT2i) are a specific class of drugs initially used to treat type 2 diabetes mellitus [3]. Thereafter, it has been demonstrated that in addition to their glycosuric effect, SGLT2i also provide several benefits for cardiovascular and kidney diseases [4]. Indeed, the glycosuric effect led to a diuretic effect, which in turn, reduces intravascular volume and arterial pressure. Thanks to these hemodynamic effects, SGLT2i showed efficacy in the treatment of chronic heart failure. Experimental and clinical data also demonstrated additional mechanisms: SGLT2i improved adipose tissue metabolism, reduced systemic inflammation, increased insulin sensitivity [4], and improved kidney function [5].

The glycosuric effect may be also useful in cases of acute decompensated heart failure. Studies showed how the prescription of SGLT2i, in addition to the conventional treatment, can increase the chance of positive outcomes (i.e., improved patient-reported symptoms and reduced hospitalization for heart failure) [6]. More recently, studies suggested that SGLT2i may have a role in the management of patients with AMI. Specifically, SGLT2i seem to reduce the risk of specific negative outcomes that can develop after AMI. To better understand the role of SGLT2i in these patients, we revised the clinical studies focused on SGLT2i prescribed to patients with AMI treated with PCI.

2. Biology of Sodium–Glucose Cotransporter

The sodium–glucose cotransporter (SGLT) plays a critical role in humans due to its activity to drive glucose and sodium ions into cells [7]. SGLTs belong to the solute carrier family 5, which includes 12 different member proteins that mediate the transport of sugars (SGLT1-5), vitamins (SGLT6, SGLT7), myo-inositol (SGLT3 and SGLT11), iodide (SGLT5), choline (SGLT7), and monocarboxylate (SGLT8 e SGLT12) [8].

SGLT1's function is to absorb glucose and galactose, but not fructose or mannose, across the intestinal brush-border membrane. Compared to other channels, the conductance of SGLT1 for urea and water is relatively low, but the high levels of its expression in enterocytes explain its critical role in the control of the transport of water and urea across the intestinal membrane [7]. Indeed, the genetic disease glucose–galactose malabsorption causes severe diarrhea in the presence of glucose or galactose in the diet. SGLT1 also regulate the reabsorption of these sugars in the region S2 and S3 of the proximal tubules, which occurrs with a stoichiometry of two sodium ions for each sugar molecule [9].

SGLT2 channels are located in the proximal renal convoluted tubule and are responsible for reabsorbing approximately 90% of the filtered glucose (Figure 1) [10]. Mutations in the gene encoding SGLT2 are responsible for familial renal glycosuria, a disease characterized by the presence of glycosuria despite normal blood glucose levels [11]. Despite its relatively low affinity, SGLT2 is a high-capacity transporter. The glucose reabsorption is sodium-dependent (1:1 stoichiometry) and, therefore, 4–5% of daily filtered sodium load is reabsorbed [11]. Sodium is pumped out of the epithelial cells into the blood through the sodium/potassium-ATPase. This transepithelial flux generates fluid absorption due to the osmotic gradient. SGLT2 expression in proximal tubes is increased in diabetic patients, but the mechanism of this upregulation has not been fully elucidated [12].

SGLT2i can reduce the renal threshold for glucose excretion from 180 mg/dL to 40 mg/dL, thus increasing glycosuria. This effect, found in diabetics and healthy people, further induces additional effects unrelated to glycemic control: increased diuresis, reduced inflammation, and weight loss [6]. Sodium–glucose cotransporter-2 inhibitors have a different activity on SGLT1 and SGTL2. Indeed, empagliflozin has the selectivity of SGLT2, while canagliflozin has the lowest [13].

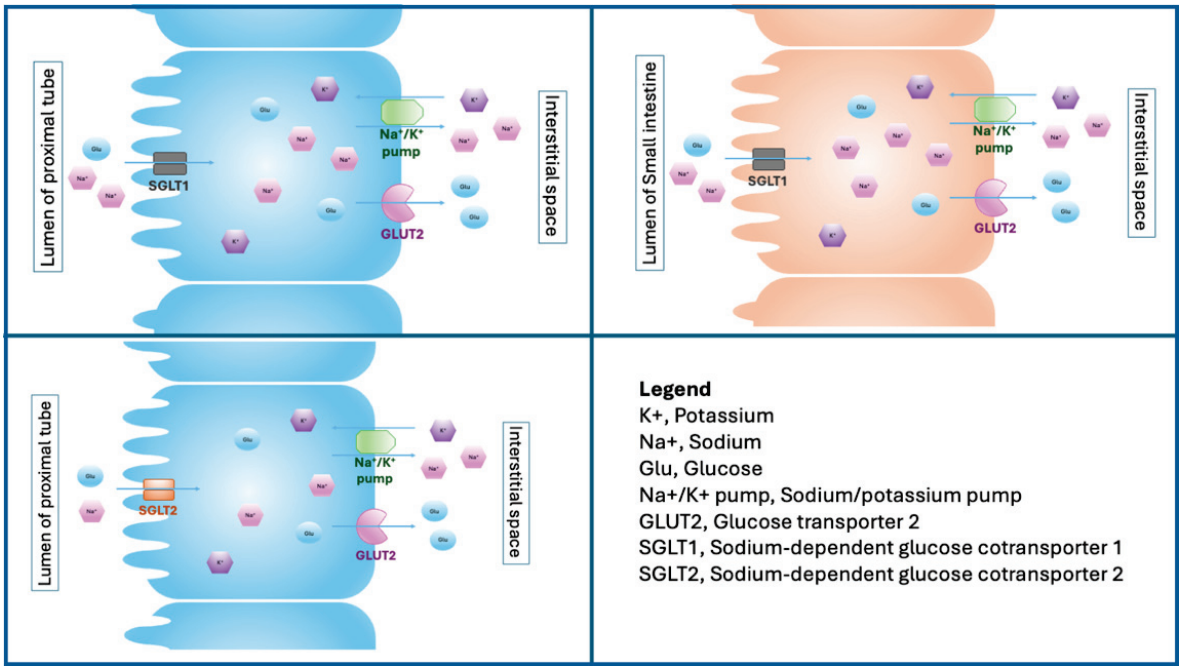


Figure 1. Site and function of SGLT.

3. The Effects of SGLT2i on Inflammatory Biomarkers After AMI

Atherosclerosis is a chronic inflammatory disease of the arterial wall. The exact pathogenesis is unclear, but specific cytokines (interleukin 6, vascular cell adhesion molecule 1, and intercellular adhesion molecule 1) are involved in this process [14]. The role of SGLT2i on inflammatory biomarkers after AMI has been evaluated in two main studies with different results. One study reported the effect of SGLT2i on inflammatory burden and infarct size [15]. This multicenter observational registry included 583 diabetic patients who were admitted with ST-segment elevation myocardial infarction (STEMI) and non-ST-segment elevation myocardial infarction (NSTEMI). The patients who underwent PCI were divided into two groups according to the antidiabetic treatment on admission: SGLT2i users (started at least 3 months before) vs. non-SGLT2i users, including those receiving other antidiabetic drugs. The authors compared inflammatory biomarkers and infarct size between the two groups. They found that baseline treatment with SGLT2i was associated with reduced white blood cell count, neutrophils, and C-reactive protein. In addition, the group of SGLT2i users displayed a smaller infarct size, as evidenced by lower troponin values and lower peaks [15]. On the contrary, a post hoc analysis of the EMMY trial compared the mean change in inflammatory biomarkers (high-sensitivity C-reactive protein, IL-6, neutrophils, leukocytes, and their ratios) after 26 weeks of treatment with either the SGLT2i empagliflozin or placebo in patients with AMI treated with PCI [16]. Authors demonstrated a significant mean reduction, from the baseline to the end of the follow-up, for neutrophils (−20.46%, $p < 0.001$), leukocytes (−10.22%, $p < 0.001$), IL-6 (−57.37%, $p < 0.001$), and high-sensitivity C-reactive protein (26.1%, $p < 0.001$) in patients after AMI. However, treatment with empagliflozin showed no impact on this decline, thus indicating no role in blunted systemic inflammation [16].

4. The Effects of SGLT2i on Cardiac Sympathetic and Parasympathetic Activity

The autonomic nervous system influences most heart functions at multiple levels: sinoatrial node, atrioventricular node, myocardium, and vessels. Abnormalities of both sympathetic and parasympathetic systems can cause different heart manifestations. Heart

rate variability (HRV) represents the physiological phenomenon of beat-to-beat variations in cardiac cycle length. Increased sympathetic or decreased sympathetic activity may lead to an abnormal HRV, which is a strong predictor of mortality and sudden arrythmias in patients with AMI [17]. HRV parameters reflect the autonomic modulation of the heart for a given period and its quantification can be achieved using time–domain, frequency–domain, and nonlinear methods. For the time–domain method, the root mean square of the successive differences (RMSSD) and the standard deviation of the 5 min average NN intervals (SDANN) are the most studied parameters.

RMSSD reflects the beat-to-beat variance in heart rate and is used to estimate the vagally mediated changes reflected in HRV [18], while SDANN shows how far the HRV is from that average at any point in the day. Frequency–domain measurements calculate the amount of signal energy within component bands. The Task Force of the European Society of Cardiology and the North American Society of Pacing and Electrophysiology (1996) divided heart rate oscillations into four frequency bands: ultra low-frequency (ULF), very low-frequency (VLF), low-frequency (LF), and high-frequency (HF) bands [19]. LF and HF are the most commonly used indices, and the latter may reflect the parasympathetic activity of the autonomic nervous system [20].

The EMBODY trial was conceived to evaluate whether the use of SGLT2i was accompanied by an improvement of cardiac nerve activity in patients with AMI and diabetes mellitus [21]. Specifically, the trial assessed the mechanisms by which empagliflozin affected the measurement of HRV, heart rate turbulence (HRT), late potential (LP), and T wave alternans (TWA). The authors randomized 96 diabetic patients to receive either empagliflozin 10 mg/day or placebo (as an add-on to the conventional treatment) 2 weeks after the onset of AMI. After 24 weeks of follow-up, the empagliflozin group showed a significant increase from the baseline SDANN intervals (+11.6 ms, $p = 0.02$) and RMSSD (+6.5 ms, $p = 0.01$). Changes in HF power and sympathovagal balance (LF/HF ratio) were further significant in the treatment group (respectively, +583.1 ms^2, $p = 0.04$, and -0.57, $p = 0.01$). A comparison of HRV parameters between the two groups failed to reach statistical significance. Similarly, although an improvement of HRT from the baseline was found only in patients treated with empagliflozin ($p = 0.01$), the latter was not significant in intergroup comparison. Empagliflozin treatment reduced uric acid levels, systolic blood pressure, and body mass index. The authors concluded that the improvement of cardiac sympathetic and parasympathetic nerve activity could somewhat explain the reduction in cardiovascular deaths, in particular, sudden cardiac death caused by fatal arrhythmias [21].

Three main mechanisms may explain the improvement in HRV and HFT after treatment with SGLT2i. The first mechanism is the hemodynamic effect, which is due to the reduced intravascular volume secondary to the osmotic diuresis and natriuresis. The reduction in intravascular volume led to hemodynamic changes which improved cardiac workout and left ventricular function without modification of heart rate, thus suggesting that SGLT2i reduce the reflex sympathetic nerve hyperactivity. Another mechanism is the possible direct inhibition of the myocardium sodium/hydrogen exchanger which may lead to increased mitochondrial function and reduced oxidative stress, thus potentially reducing the onset of arrythmias [22]. The third possible mechanism is the reduced activity of rostral raphe pallidus (rRPa) [23], which physiologically increases the cardiac sympathetic nerve activity and heart rate [24].

5. Possible Antiarrhythmic Effects of SGLT2i After AMI

Atrial fibrillation is one of the most frequent arrhythmias in adults [25] and specific risks factors have been recognized [26]. Recent data showed that SGLT2i could have possible antiarrhythmic properties [27].

An extensive body of evidence, confirmed by systematic review and meta-analysis, reported an antiarrhythmic effect of the SGLT2i on specific cardiovascular disease [28,29], but the effect of SGLT2i on cardiac arrhythmias post-myocardial infarction has been studied less. The study by Cesaro et al. investigated the onset of arrhythmias in a sample of diabetic patients hospitalized for STEMI or NSTEMI and treated with PCI [30]. The cohort included 646 patients, divided into two groups based on the use of SGLT2i or not. Authors reported 91 cases of new-onset cardiac arrhythmias during the length of hospitalization: 56 were atrial fibrillation and 35 were ventricular tachycardia/fibrillation. Patients treated with SGLT2i had a lower rate of atrial fibrillation and ventricular tachycardia/fibrillation than non-users (4.5% vs. 9.5% and 1.8% vs. 6.2%, $p < 0.05$). In addition, the use of SGLT2i was associated with a reduction of 65% in the risk of new-onset arrhythmias in the multivariate logistic regression [30].

The association between atrial fibrillation and diabetes is complex and not limited to the presence of obesity. Indeed, inadequate glycemic control and longer duration of diabetes dramatically increase the risk of onset of atrial fibrillation. SGTL1 is expressed in cardiac capillaries and cardiomyocytes, which play a role in glucose transport across the membrane. Despite the low expression of SGLT2 in the cardiac cells, SGLT2i may have an antiarrhythmic effect due to direct and indirect mechanisms. Indeed, SGLT2i could decrease the activity of the sympathetic nervous system and significantly reverse cardiac and anatomic remodeling [31,32]. In addition, SGLT2i regulate sodium and calcium channels and reduce the development of calcium-related arrhythmias [33]. SGLT2i may also have indirect beneficial effects through their natriuretic effect, enhanced ketone oxidation, and body weight loss [34].

6. The Effects of SGLT2i on Heart Failure Occurrence After AMI

The SGLT2i have positive effects on all patients with heart failure, independently of left ventricular ejection fraction values [29,35,36]. Further, early treatment helps to delay or reverse cardiac remodeling and prevents progression to symptomatic heart failure [37]. Robust evidence demonstrated that the use of SGLT2i reduced the risk of rehospitalization in patients with chronic heart failure. Indeed, the DELIVER trial showed that dapagliflozin treatment reduced the risk of worsening of heart failure, defined as unplanned hospitalization or emergency visits for heart failure [38]. However, this trial also found that there was no significant difference in cardiovascular mortality between the groups. Thus, a possible bias should be mentioned: the reduction in the risk of the primary composite outcome with Dapagliflozin was primarily attributed to the worsening of heart failure.

The role of SGLT2i on the rate of heart failure rehospitalization after AMI has been recently demonstrated (Table 1). A Chinese study included 961 diabetic patients with AMI treated with PCI during hospitalization [39]. The subjects were stratified into two groups: those who were started on dapagliflozin 10 mg daily and those who were treated with other glucose-lowering drugs. The analysis showed that, after a median follow-up of 540 days, patients treated with SGLT2i had a significantly lower heart failure rate than those treated with other glucose-lowering drugs ($p < 0.001$). In addition, the use of Dapagliflozin reduced the risk of heart failure rehospitalization (HR 0.50, 95%CI 0.30–0.83, $p < 0.001$) [39].

Another study, based on National Health insurance claims data in South Korea, proposed an analysis based on a propensity score matching [40]. The authors revised over 30,000 clinical records and found 938 patients with type 2 diabetes treated PCI for AMI and who received SGLT2i within 14 days after PCI. The patients with or without SGLT2i were matched at a 1:2 ratio. After a median follow-up of 2.1 years, the use of SGLT2i was associated with a lower risk of a composite outcome of hospitalizations for heart failure and all-cause death (7.4% vs. 9.8%, HR 0.68, 95%CI 0.54–0.87, $p = 0.002$) [40].

Similarly, the study by Zhu et al. showed that, during a median of 23 months, patients treated with dapagliflozin had a lower rate of heart failure compared to those treated with

other antidiabetic drugs (2.1% vs. 10.4%, $p < 0.001$) [41]. Interestingly, DAPA administration was significantly associated with a reduced risk of HF ($p = 0.003$), non-fatal myocardial infarction ($p = 0.005$), unplanned repeat revascularization ($p = 0.031$), and the composite outcome of major adverse cardiovascular events ($p = 0.009$), but not non-fatal stroke ($p = 0.072$). However, it should be noted that other studies reported no effect of SGLT2i on rehospitalization for heart failure [41]. Indeed, the study by Adel et al. tested the impact of dapagliflozin 10 mg in a double-blind, randomized, controlled clinical trial in a sample of diabetic patients with acute coronary syndrome treated with PCI [42]. The authors noticed no difference between the two groups, but the small sample limited the statistical power, and no hospitalization for heart failure was noted. Similarly, the EMMY trial, which was a double-blind trial, enrolled 476 patients with AMI [43]. The patients were randomized to 10 mg of empagliflozin or placebo, and the medication was started within 72h of PCI. After 26 weeks of follow-up, both groups experienced a decrease in the N-terminal pro-Brain Natriuretic Peptide (NT-proBNP), which was more pronounced in those treated with SGLT2i. In this group, a greater reduction was observed at 12 weeks. Secondary analysis, however, showed that hospitalization for heart failure did not differ significantly between the two groups, as reported in Table 1 [43]. The timing of SGLT2i prescription has no effect on heart failure hospitalization, as reported in the study by Butler et al. (EMPACT-MI trial) [44]. This randomized, double-blind, placebo-controlled trial included 3260 patients treated with empagliflozin started within 14 days after admission for AMI and 3262 subjects treated with placebo. The primary endpoint (composite of hospitalization for heart failure or death from any cause) occurred at a comparable frequency among the two groups: 8.2% of patients treated with SGLT2i and 9.1% of patients in the control group ($p = 0.21$) [44]. However, additional analysis of the same trial revealed that the risk for first HF hospitalization and total HF hospitalizations was significantly lower in the empagliflozin compared with the control group (3.6% vs. 4.7%, HR 0.77 95%CI 0.60–0.98 $p = 0.031$, and 148 vs. 207 events, HR 0.67 95%CI 0.51–0.89 $p = 0.006$, respectively) [45].

The role of SGLT2i in heart failure hospitalization in patients with AMI and treated with PCI is not clear. Indeed, some reported a reduction in the risk of rehospitalization, but others showed no effect. Methodological issues can in part explain the different results because some studies had a small number of subjects while others, albeit with a wider sample, had a lower frequency of older subjects, thus possibly underestimating the incidence of heart failure hospitalization. However, it should be noted that SGLT2i have a consolidated role in the management of chronic heart failure, as reported in the latest guidelines [46]. Indeed, SGLT2i can increase diuresis thanks to their effect on glycosuria and natriuresis [6]. In addition, they modulate the sympathetic nervous system and the reduction in oxidative stress and inflammation [47].

Table 1. Studies that tested the role of SGLT2i in heart failure rehospitalization after acute myocardial infarction.

Author	Type of SGLT2i	Timing of SGLT2i Initiation	Sample		Follow-Up	Events		Results
			SGLT2i	Controls		SGLT2i	Non-SGLT2i	
Mao [39]	D	N/A	231	231	540 days	13 (5.6%)	35 (15.2%)	SGLT2i reduced the risk of heart failure rehospitalization
Zhu [41]	D	N/A	141	645	23 months	3 (2.1%)	67 (10.4%)	SGLT2i reduced the risk of heart failure rehospitalization

Table 1. *Cont.*

Author	Type of SGLT2i	Timing of SGLT2i Initiation	Sample		Follow-Up	Events		Results
			SGLT2i	Controls		SGLT2i	Non-SGLT2i	
Adel [42]	E	N/A	45	48	6 months	0 (0.0%)	0 (0.0%)	No effect
von Lewinski [43]	E	Within 72 h from PCI	237	239	26 weeks	3 (1.3%)	4 (1.7%)	No effect
Butler [44]	E	Within 14 days	3260	3262	17.9 months	267 (8.2%) *	298 (9.1%) *	No effect on composite outcome (heart failure and death from any cause)
Hernandez [45]	E	Within 14 days	3260	3262	17.9 months	118 (3.6%) [#] 148 (4.5%) [##]	153 (4.7%) [#] 207 (6.3%) [##]	SGLT2i reduced the risk of HF in patients with left ventricular dysfunction or congestion after acute myocardial infarction
Kwon [40]	N/A	Within 14 days	938	1876	2 years	68 (7.4%) [###]	166 (9.8%)	SGLT2i reduced the risk of hospitalizations for heart failure

Abbreviation: D, dapagliflozin; E, empagliflozin; PCI, percutaneous coronary intervention; N/A, not applicable. * Composite outcome (heart failure and death from any cause). [#] First heart failure hospitalization. [##] Total number of heart failure hospitalizations; [###] Composite outcome (all-cause death and hospitalizations for heart failure).

7. The Effects of SGLT2i on Ventricular Remodeling After AMI

Several studies have examined the effect of SGLT2i on specific echocardiographic parameters after AMI, as reported in Table 2. The study by Wan et al. retrospectively included 423 patients with type 2 diabetes mellitus and AMI treated with PCI. The sample was divided into two groups according to the use of SGLT2i [48]. After six months from discharge, patients treated with SGLT2i had a significantly lower left ventricular remodeling index (3.49 ± 19.71 vs. 7.06 ± 15.15, $p < 0.05$), while non-SGLT2i had a higher frequency of left ventricular remodeling >20%, considered pathologic threshold by the authors and calculated as a 20% or greater increase in left ventricular end-diastole volume between baseline and six-month follow-up [48].

The timing of the prescription of SGLT2i after myocardial infarction seems to be critical, even in non-diabetic patients. Indeed, to test this hypothesis, Abdel Dayem et al. performed a double-blind randomized controlled trial of patients with AMI treated with PCI [49]. The patients, free from diabetes mellitus and with echocardiographic evidence of reduced left ventricular ejection fraction <50%, were randomized to receive either placebo or dapagliflozin 10 mg daily. Follow-up visits were set at 4 and 12 weeks. NT-proBNP was assessed at baseline visit and after 12 weeks, while echocardiographic parameters were collected at baseline and in the two follow-up visits. Patients treated with dapagliflozin had a greater decrease in NT-proBNP levels from baseline to 12 weeks compared to the control group (133 ng/L vs. 89 ng/L, $p < 0.05$). Further, at 12 weeks the left ventricular mass index in the treatment group was less than the control group by 11.46% (95%CI: -19.37 to -3.56, $p = 0.029$) [49]. However, it should be noted that other authors found no significant advantages of early administration of SGLT2i. Indeed, the EMMY study evaluated the effect of empagliflozin on cardiovascular parameters (left ventricular function,

left ventricular end-systolic, and end-diastolic diameters) [50]. Specifically, the sample was divided into three groups according to the timing of administration of SGLT2i after PCI: early (<24 h), intermediate (24–48 h), and late (48–72 h). The analysis revealed that SGLT2i treatment, compared to the control group, had a positive effect on the above-mentioned echocardiographic parameters, regardless of the timing of administration [50].

The modification of echocardiographic parameters was also studied with magnetic resonance in the EMPRESS-MI trial [51]. This randomized, double-blind, placebo-controlled, multicenter study enrolled 105 patients with a recent diagnosis of myocardial infarction ($\geq$12 h and <14 days) and left ventricular ejection fraction <45% on magnetic resonance imaging at baseline. The patients, who were randomized to empagliflozin 10 mg daily or placebo, performed a cardiovascular magnetic resonance at baseline and after 24 weeks of treatment. The analysis revealed that treatment with SGLT2i, when compared to placebo, did not significantly reduce the left ventricular end-systolic volume indexed to body surface area (8.3 ± 13.5 mL/m^2 vs. 7.8 ± 16.3 mL/m^2). Similarly, the change in the left ventricular end-diastolic volume indexed to the body surface area (0.6 ± 16.3 mL/m^2 and -0.3 ± 18.7 mL/m^2), the increase in the left ventricular ejection fraction (9.4 ± 7.5% vs. 8.5 ± 7.4%), and the indexed left atrial volume (37.3 mL/m^2 vs. 39.2 mL/m^2) were comparable between the two groups [51].

The effect of SGLT2i on ventricular remodeling in heart failure patients is well known [52], but their impact after AMI is less studied. SGLT2i may contribute to the detrimental effect at the ventricular level after AMI. Different mechanisms have been postulated. Indeed, SGLT2i could reduce inflammation, which is key in ventricular remodeling [53], as demonstrated by the reduction in interleukin-1β secretion and NLRP3 inflammasome activity in macrophages [54,55]. A role in sympathetic nerve activity has been revealed, as previously described. In addition, SGLT2i may also have a positive impact on cardiac fibrosis by reducing fibroblast activation and extracellular matrix remodeling [56].

Table 2. Modification of echocardiographic parameters in patients treated with SGLT2i after acute myocardial infarction.

Author	Sample		Follow-Up	Echocardiographic Parameter	Baseline		Post-Treatment		Results
	SGLT2i	Control			SGLT2i	Control	SGLT2i	Control	
Wan [48]	239	184	6 months	LVEF	53.53 ± 10.20	56.25 ± 9.27	2.17 ± 6.66 *	0.55 ± 9.51 *	SGLT2i protects against LVR
				LVEDV	101.92 ± 30.38	98.17 ± 21.83	1.42±18.10 *	6.36 ± 14.75 *	
				LVESV	49.64 ± 26.62	44.44 ± 19.02	−2.16 ± 14.89 *	2.87 ± 16.02 *	
				LVRI	N/A	N/A	3.49 ± 19.71	7.06 ± 15.15	
Dayem [49]	50	50	12 weeks	LVEF	42.70 ± 7.21	43.29 ± 5.23	50.33 ± 7.49	49.84 ± 8.22	Early SGLT2i administration improves cardiac function
				LVEDd	47.62 ± 0.59	46.28 ± 0.88	47.97 ± 0.82	46.85 ± 0.79	
				LVESd	35.76 ± 0.66	35.56 ± 0.74	35.08 ± 0.73	34.61 ± 0.49	
				LV mass	103.34 ± 18.12	101.47 ± 19.50	93.60 ± 21.58	103.53 ± 17.18	
				ePASP	33.4 ± 9.15	32.90 ± 10.31	31.10 ± 11.54	30.71 ± 10.65	
Carberry [51]	51	53	24 weeks	LVESVI	65.6	62.8	57.2	55	SGLT2i had no effect on cardiac volumes and LVEF
				LVEDVI	97.8	97.6	98.3	97.3	
				LVEF	33.4	36	42.7	44.4	
				LAVI	34.3	36.2	37.3	39.2	
				LVMI	62.2	59.1	52.2	50.4	

Abbreviations: LVEF, left ventricular ejection fraction; LVEDV, left ventricular end-diastolic volume; LVESV, left ventricular end-systolic volume; LVRI, left ventricular remodeling index; LVMI, left ventricular mass index; LAVI, left atrial volume index; LVEDd, left ventricular end-diastolic diameter; LVESd, left ventricular end-systolic diameter; LV mass, left ventricular mass; ePASP, estimated pulmonary artery systolic pressure; LVESVI: left ventricular end-systolic volume; LVEDVI: indexed left ventricular end-diastolic volume; N/A, not applicable. * Difference between echocardiographic parameter at the end of the follow-up and baseline echocardiographic parameter.

8. The Possible Protective Role of SGLT2i on Acute Kidney Injury After AMI

The kidney has a pivotal role in glucose homeostasis due to its capacity to reabsorb the glucose filtered into the glomerular filtrate. In healthy individuals, no glucose is usually present in the urine because all the glucose filtered is reabsorbed in the kidney, and glycosuria occurs when blood glucose exceeds 180 mg/dL [57]. SGLT2 is located in the proximal renal tubule, allowing kidney cells to reabsorb the filtered glucose. Inhibitors of SGLT2 increase glucose excretion in the urine by lowering the renal threshold for glucose excretion independently from insulin.

Recent studies highlighted the importance of SGLT2i after AMI to reduce the risk of acute kidney injury (AKI). Indeed, the administration of iodinated radiocontrast material during PCI increased the risk of developing AKI, which is somewhat modified by additional factors such as age, baseline estimated glomerular filtration rate, and use of contrast agent [58]. This condition may lead to adverse outcomes, such as increased in-hospital and long-term mortality [59]. The study by Cai et al. retrospectively analyzed a cohort of 1839 patients with AMI treated with PCI [60]. The sample was divided into two groups (dapagliflozin users vs. control group), whose baseline characteristics were balanced through a propensity score matching analysis. The primary outcome was the occurrence of AKI 7 days after PCI. The frequency of AKI was lower in the treatment group (15.1% vs. 19.1%), and the multivariate regression analysis, adjusted for confounders, revealed that treatment with SGLT2i was a protective factor for AKI development (OR 0.66, 95%CI 0.44–0.97, $p = 0.036$). Similar results have been obtained in a single-center case–control study, which reported that diabetic patients treated with SGLT2i had a lower risk of developing contrast-induced AKI (OR 0.86, 95%CI 0.76–0.98, $p = 0.028$) [61]. A recent meta-analysis summarized the efficacy of SGLT2i in reducing the risk of AKI (RR 0.46; 95%CI 0.32–0.67, $p < 0.0001$) [62]. Clinical and experimental data have shown that the use of SGLT2i improves kidney function through multiple mechanisms. Indeed, SGLT2i may improve renal oxygenation by activating antifibrotic and anti-inflammatory pathways [63]. Further, dapagliflozin may inhibit hypoxia-inducible factor-1α/human epididymis secretory protein 4/nuclear factor-κB signaling, thus reducing the risk of contrast-induced AKI [64] and reducing oxidative stress, fibrosis, and inflammatory markers [65]. Of course, a clear, direct effect of diuretic osmosis has also been demonstrated. Indeed, the increased diuresis decreases the plasma volume, which activates the tubule-glomerular feedback. The latter may increase sodium reabsorption, cause vasoconstriction of afferent arterioles, and reduce the renin-angiotensin system by decreasing intraglomerular pressure [66].

9. Conclusions

SGLT2i have a critical role in the management of heart failure and are not only related to the presence of diabetes. Current data support the concept that patients improve the clinical control of chronic heart failure and reduce the risk of exacerbation. In this review, we showed that SGLT2i seem to have additional effects in patients with AMI treated with PCI. The overall benefits of early treatment may reduce the risk of the onset of specific complications, such as arrhythmias and ventricular remodeling, which often develop after AMI. However, the benefits for other specific diseases need to be clarified. To address critical knowledge gaps and better understand the mechanisms underlying the beneficial effects of SGLT2i in heart failure, future research should be clearly outlined.

Author Contributions: N.I.P. and A.P.D. wrote the manuscript; R.C., M.C.S., A.G., R.M., M.P., G.L.S., C.C. and F.B. reviewed and edited the manuscript. All authors have read and agreed to the published version of the manuscript.

Funding: The work was supported by grant from Fondazione di Sardegna 2022–2023, Italy.

Data Availability Statement: Not applicable.

Conflicts of Interest: The authors declare no conflicts of interest.

References

1. Thygesen, K.; Alpert, J.S.; Jaffe, A.S.; Chaitman, B.R.; Bax, J.J.; Morrow, D.A.; White, H.D.; ESC Scientific Document Group. Fourth universal definition of myocardial infarction (2018). *Eur. Heart J.* **2019**, *40*, 237–269. [CrossRef] [PubMed]
2. Byrne, R.A.; Rossello, X.; Coughlan, J.J.; Barbato, E.; Berry, C.; Chieffo, A.; Claeys, M.J.; Dan, G.A.; Dweck, M.R.; Galbraith, M.; et al. 2023 ESC Guidelines for the management of acute coronary syndromes. *Eur. Heart J. Acute Cardiovasc. Care* **2024**, *13*, 55–161. [CrossRef]
3. Rosas-Guzman, J.; Rosas-Saucedo, J.; Romero-Garcia, A.R.J. SGLT2 Inhibitors in Diabetes Mellitus Treatment. *Rev. Recent Clin. Trials* **2017**, *12*, 8–18. [CrossRef]
4. Vallon, V.; Verma, S. Effects of SGLT2 Inhibitors on Kidney and Cardiovascular Function. *Annu. Rev. Physiol.* **2021**, *83*, 503–528. [CrossRef]
5. Carvalho, P.E.P.; Veiga, T.M.A.; Simoes, E.S.A.C.; Gewehr, D.M.; Dagostin, C.S.; Fernandes, A.; Nasi, G.; Cardoso, R. Cardiovascular and renal effects of SGLT2 inhibitor initiation in acute heart failure: A meta-analysis of randomized controlled trials. *Clin. Res. Cardiol.* **2023**, *112*, 1044–1055. [CrossRef] [PubMed]
6. Profili, N.I.; Castelli, R.; Gidaro, A.; Manetti, R.; Maioli, M.; Delitala, A.P. Sodium-Glucose Cotransporter-2 Inhibitors in Diabetic Patients with Heart Failure: An Update. *Pharmaceuticals* **2024**, *17*, 1419. [CrossRef]
7. Wright, E.M.; Loo, D.D.; Hirayama, B.A. Biology of human sodium glucose transporters. *Physiol. Rev.* **2011**, *91*, 733–794. [CrossRef] [PubMed]
8. Gyimesi, G.; Pujol-Gimenez, J.; Kanai, Y.; Hediger, M.A. Sodium-coupled glucose transport, the SLC5 family, and therapeutically relevant inhibitors: From molecular discovery to clinical application. *Pflugers Arch.* **2020**, *472*, 1177–1206. [CrossRef]
9. Wright, E.M.; Loo, D.D.; Hirayama, B.A.; Turk, E. Surprising versatility of Na+-glucose cotransporters: SLC5. *Physiology* **2004**, *19*, 370–376. [CrossRef]
10. Salvatore, T.; Carbonara, O.; Cozzolino, D.; Torella, R.; Nasti, R.; Lascar, N.; Sasso, F.C. Kidney in diabetes: From organ damage target to therapeutic target. *Curr. Drug Metab.* **2011**, *12*, 658–666. [CrossRef]
11. Cannizzaro, M.; Jarosova, J.; De Paepe, B. Relevance of solute carrier family 5 transporter defects to inherited and acquired human disease. *J. Appl. Genet.* **2019**, *60*, 305–317. [CrossRef]
12. Novikov, A.; Vallon, V. Sodium glucose cotransporter 2 inhibition in the diabetic kidney: An update. *Curr. Opin. Nephrol. Hypertens.* **2016**, *25*, 50–58. [CrossRef] [PubMed]
13. Mudaliar, S.; Polidori, D.; Zambrowicz, B.; Henry, R.R. Sodium-Glucose Cotransporter Inhibitors: Effects on Renal and Intestinal Glucose Transport: From Bench to Bedside. *Diabetes Care* **2015**, *38*, 2344–2353. [CrossRef] [PubMed]
14. Tedgui, A.; Mallat, Z. Cytokines in atherosclerosis: Pathogenic and regulatory pathways. *Physiol. Rev.* **2006**, *86*, 515–581. [CrossRef]
15. Paolisso, P.; Bergamaschi, L.; Santulli, G.; Gallinoro, E.; Cesaro, A.; Gragnano, F.; Sardu, C.; Mileva, N.; Foa, A.; Armillotta, M.; et al. Infarct size, inflammatory burden, and admission hyperglycemia in diabetic patients with acute myocardial infarction treated with SGLT2-inhibitors: A multicenter international registry. *Cardiovasc. Diabetol.* **2022**, *21*, 77. [CrossRef]
16. Benedikt, M.; Mangge, H.; Aziz, F.; Curcic, P.; Pailer, S.; Herrmann, M.; Kolesnik, E.; Tripolt, N.J.; Pferschy, P.N.; Wallner, M.; et al. Impact of the SGLT2-inhibitor empagliflozin on inflammatory biomarkers after acute myocardial infarction—A post-hoc analysis of the EMMY trial. *Cardiovasc. Diabetol.* **2023**, *22*, 166. [CrossRef] [PubMed]
17. Camm, A.J.; Pratt, C.M.; Schwartz, P.J.; Al-Khalidi, H.R.; Spyt, M.J.; Holroyde, M.J.; Karam, R.; Sonnenblick, E.H.; Brum, J.M.; AzimiLide post Infarct surVival Evaluation, I. Mortality in patients after a recent myocardial infarction: A randomized, placebo-controlled trial of azimilide using heart rate variability for risk stratification. *Circulation* **2004**, *109*, 990–996. [CrossRef]
18. Shaffer, F.; McCraty, R.; Zerr, C.L. A healthy heart is not a metronome: An integrative review of the heart's anatomy and heart rate variability. *Front. Psychol.* **2014**, *5*, 1040. [CrossRef]
19. Task Force of the European Society of Cardiology and the North American Society of Pacing and Electrophysiology. Heart rate variability: Standards of measurement, physiological interpretation and clinical use. *Circulation* **1996**, *93*, 1043–1065. [CrossRef]
20. Sacha, J.; Pluta, W. Different methods of heart rate variability analysis reveal different correlations of heart rate variability spectrum with average heart rate. *J. Electrocardiol.* **2005**, *38*, 47–53. [CrossRef]
21. Shimizu, W.; Kubota, Y.; Hoshika, Y.; Mozawa, K.; Tara, S.; Tokita, Y.; Yodogawa, K.; Iwasaki, Y.K.; Yamamoto, T.; Takano, H.; et al. Effects of empagliflozin versus placebo on cardiac sympathetic activity in acute myocardial infarction patients with type 2 diabetes mellitus: The EMBODY trial. *Cardiovasc. Diabetol.* **2020**, *19*, 148. [CrossRef] [PubMed]
22. Packer, M.; Anker, S.D.; Butler, J.; Filippatos, G.; Zannad, F. Effects of Sodium-Glucose Cotransporter 2 Inhibitors for the Treatment of Patients With Heart Failure: Proposal of a Novel Mechanism of Action. *JAMA Cardiol.* **2017**, *2*, 1025–1029. [CrossRef] [PubMed]

23. Chiba, Y.; Yamada, T.; Tsukita, S.; Takahashi, K.; Munakata, Y.; Shirai, Y.; Kodama, S.; Asai, Y.; Sugisawa, T.; Uno, K.; et al. Dapagliflozin, a Sodium-Glucose Co-Transporter 2 Inhibitor, Acutely Reduces Energy Expenditure in BAT via Neural Signals in Mice. *PLoS ONE* **2016**, *11*, e0150756. [CrossRef] [PubMed]
24. Cao, W.H.; Morrison, S.F. Disinhibition of rostral raphe pallidus neurons increases cardiac sympathetic nerve activity and heart rate. *Brain Res.* **2003**, *980*, 1–10. [CrossRef]
25. Hindricks, G.; Potpara, T.; Dagres, N.; Arbelo, E.; Bax, J.J.; Blomstrom-Lundqvist, C.; Boriani, G.; Castella, M.; Dan, G.A.; Dilaveris, P.E.; et al. 2020 ESC Guidelines for the diagnosis and management of atrial fibrillation developed in collaboration with the European Association for Cardio-Thoracic Surgery (EACTS): The Task Force for the diagnosis and management of atrial fibrillation of the European Society of Cardiology (ESC) Developed with the special contribution of the European Heart Rhythm Association (EHRA) of the ESC. *Eur. Heart J.* **2021**, *42*, 373–498. [CrossRef]
26. Sagris, M.; Vardas, E.P.; Theofilis, P.; Antonopoulos, A.S.; Oikonomou, E.; Tousoulis, D. Atrial Fibrillation: Pathogenesis, Predisposing Factors, and Genetics. *Int. J. Mol. Sci.* **2021**, *23*, 6. [CrossRef]
27. Manolis, A.A.; Manolis, T.A.; Melita, H.; Manolis, A.S. Sodium-glucose cotransporter type 2 inhibitors and cardiac arrhythmias. *Trends Cardiovasc. Med.* **2023**, *33*, 418–428. [CrossRef]
28. Zelniker, T.A.; Bonaca, M.P.; Furtado, R.H.M.; Mosenzon, O.; Kuder, J.F.; Murphy, S.A.; Bhatt, D.L.; Leiter, L.A.; McGuire, D.K.; Wilding, J.P.H.; et al. Effect of Dapagliflozin on Atrial Fibrillation in Patients With Type 2 Diabetes Mellitus: Insights From the DECLARE-TIMI 58 Trial. *Circulation* **2020**, *141*, 1227–1234. [CrossRef]
29. Wang, X.; Zhang, X.; Zhang, W.; Li, J.; Weng, W.; Li, Q. Association of Sodium-Glucose Cotransporter 2 Inhibitors (SGLT2i) with Cardiac Arrhythmias: A Systematic Review and Meta-Analysis of Cardiovascular Outcome Trials. *Rev. Cardiovasc. Med.* **2023**, *24*, 258. [CrossRef]
30. Cesaro, A.; Gragnano, F.; Paolisso, P.; Bergamaschi, L.; Gallinoro, E.; Sardu, C.; Mileva, N.; Foa, A.; Armillotta, M.; Sansonetti, A.; et al. In-hospital arrhythmic burden reduction in diabetic patients with acute myocardial infarction treated with SGLT2-inhibitors: Insights from the SGLT2-I AMI PROTECT study. *Front. Cardiovasc. Med.* **2022**, *9*, 1012220. [CrossRef]
31. Yang, F.; Meng, R.; Zhu, D.L. Cardiovascular effects and mechanisms of sodium-glucose cotransporter-2 inhibitors. *Chronic Dis. Transl. Med.* **2020**, *6*, 239–245. [CrossRef] [PubMed]
32. Zhang, N.; Wang, Y.; Tse, G.; Korantzopoulos, P.; Letsas, K.P.; Zhang, Q.; Li, G.; Lip, G.Y.H.; Liu, T. Effect of sodium-glucose cotransporter-2 inhibitors on cardiac remodelling: A systematic review and meta-analysis. *Eur. J. Prev. Cardiol.* **2022**, *28*, 1961–1973. [CrossRef]
33. Attachaipanich, T.; Chattipakorn, S.C.; Chattipakorn, N. Potential roles of sodium-glucose co-transporter 2 inhibitors in attenuating cardiac arrhythmias in diabetes and heart failure. *J. Cell Physiol.* **2022**, *237*, 2404–2419. [CrossRef] [PubMed]
34. Dyck, J.R.B.; Sossalla, S.; Hamdani, N.; Coronel, R.; Weber, N.C.; Light, P.E.; Zuurbier, C.J. Cardiac mechanisms of the beneficial effects of SGLT2 inhibitors in heart failure: Evidence for potential off-target effects. *J. Mol. Cell Cardiol.* **2022**, *167*, 17–31. [CrossRef]
35. Jhund, P.S.; Kondo, T.; Butt, J.H.; Docherty, K.F.; Claggett, B.L.; Desai, A.S.; Vaduganathan, M.; Gasparyan, S.B.; Bengtsson, O.; Lindholm, D.; et al. Dapagliflozin across the range of ejection fraction in patients with heart failure: A patient-level, pooled meta-analysis of DAPA-HF and DELIVER. *Nat. Med.* **2022**, *28*, 1956–1964. [CrossRef]
36. Ismayl, M.; Abbasi, M.A.; Al-Abcha, A.; El-Am, E.; Lundgren, S.; Goldsweig, A.M.; Anavekar, N.S. Sodium-Glucose Cotransporter-2 Inhibitors in Heart Failure With Mildly Reduced or Preserved Ejection Fraction: A Systematic Review and Meta-Analysis of Randomized Controlled Trials. *Curr. Probl. Cardiol.* **2023**, *48*, 101597. [CrossRef]
37. Usman, M.S.; Januzzi, J.L.; Anker, S.D.; Salman, A.; Parikh, P.B.; Adamo, M.; Filippatos, G.; Khan, M.S.; Lala, A.; Verma, S.; et al. The effect of sodium-glucose cotransporter 2 inhibitors on left cardiac remodelling in heart failure with reduced ejection fraction: Systematic review and meta-analysis. *Eur. J. Heart Fail.* **2024**, *26*, 373–382. [CrossRef]
38. Solomon, S.D.; McMurray, J.J.V.; Claggett, B.; de Boer, R.A.; DeMets, D.; Hernandez, A.F.; Inzucchi, S.E.; Kosiborod, M.N.; Lam, C.S.P.; Martinez, F.; et al. Dapagliflozin in Heart Failure with Mildly Reduced or Preserved Ejection Fraction. *N. Engl. J. Med.* **2022**, *387*, 1089–1098. [CrossRef] [PubMed]
39. Mao, L.; Cai, D.; Chi, B.; Xiao, T.; Zou, A.; Wang, Y.; Chen, Q.; Gu, Q.; Wang, Q.; Ji, Y.; et al. Dapagliflozin reduces risk of heart failure rehospitalization in diabetic acute myocardial infarction patients: A propensity score-matched analysis. *Eur. J. Clin. Pharmacol.* **2023**, *79*, 915–926. [CrossRef]
40. Kwon, O.; Myong, J.P.; Lee, Y.; Choi, Y.J.; Yi, J.E.; Seo, S.M.; Jang, S.W.; Kim, P.J.; Lee, J.M. Sodium-Glucose Cotransporter-2 Inhibitors After Acute Myocardial Infarction in Patients With Type 2 Diabetes: A Population-Based Investigation. *J. Am. Heart Assoc.* **2023**, *12*, e027824. [CrossRef]
41. Zhu, Y.; Zhang, J.L.; Yan, X.J.; Sun, L.; Ji, Y.; Wang, F.F. Effect of dapagliflozin on the prognosis of patients with acute myocardial infarction undergoing percutaneous coronary intervention. *Cardiovasc. Diabetol.* **2022**, *21*, 186. [CrossRef] [PubMed]
42. Adel, S.M.H.; Jorfi, F.; Mombeini, H.; Rashidi, H.; Fazeli, S. Effect of a low dose of empagliflozin on short-term outcomes in type 2 diabetics with acute coronary syndrome after percutaneous coronary intervention. *Saudi Med. J.* **2022**, *43*, 458–464. [CrossRef] [PubMed]

43. von Lewinski, D.; Kolesnik, E.; Tripolt, N.J.; Pferschy, P.N.; Benedikt, M.; Wallner, M.; Alber, H.; Berger, R.; Lichtenauer, M.; Saely, C.H.; et al. Empagliflozin in acute myocardial infarction: The EMMY trial. *Eur. Heart J.* **2022**, *43*, 4421–4432. [CrossRef]
44. Butler, J.; Jones, W.S.; Udell, J.A.; Anker, S.D.; Petrie, M.C.; Harrington, J.; Mattheus, M.; Zwiener, I.; Amir, O.; Bahit, M.C.; et al. Empagliflozin after Acute Myocardial Infarction. *N. Engl. J. Med.* **2024**, *390*, 1455–1466. [CrossRef]
45. Hernandez, A.F.; Udell, J.A.; Jones, W.S.; Anker, S.D.; Petrie, M.C.; Harrington, J.; Mattheus, M.; Seide, S.; Zwiener, I.; Amir, O.; et al. Effect of Empagliflozin on Heart Failure Outcomes After Acute Myocardial Infarction: Insights From the EMPACT-MI Trial. *Circulation* **2024**, *149*, 1627–1638. [CrossRef] [PubMed]
46. McDonagh, T.A.; Metra, M.; Adamo, M.; Gardner, R.S.; Baumbach, A.; Bohm, M.; Burri, H.; Butler, J.; Celutkiene, J.; Chioncel, O.; et al. Corrigendum to: 2021 ESC Guidelines for the diagnosis and treatment of acute and chronic heart failure: Developed by the Task Force for the diagnosis and treatment of acute and chronic heart failure of the European Society of Cardiology (ESC) With the special contribution of the Heart Failure Association (HFA) of the ESC. *Eur. Heart J.* **2021**, *42*, 4901. [CrossRef]
47. Margonato, D.; Galati, G.; Mazzetti, S.; Cannistraci, R.; Perseghin, G.; Margonato, A.; Mortara, A. Renal protection: A leading mechanism for cardiovascular benefit in patients treated with SGLT2 inhibitors. *Heart Fail. Rev.* **2021**, *26*, 337–345. [CrossRef]
48. Wan, J.; Xu, F.; Zuo, H.; Jiang, X.; Wang, Y.; Jiang, Y.; Chen, C.; Yin, C.; Cheng, J.; Li, H. Impact of SGLT2 Inhibitors on Left Ventricular Remodeling in Diabetic Patients with Acute Myocardial Infarction. *J. Cardiovasc. Pharmacol. Ther.* **2024**, *29*, 10742484241301191. [CrossRef]
49. Dayem, K.A.; Younis, O.; Zarif, B.; Attia, S.; AbdelSalam, A. Impact of dapagliflozin on cardiac function following anterior myocardial infarction in non-diabetic patients—DACAMI (a randomized controlled clinical trial). *Int. J. Cardiol.* **2023**, *379*, 9–14. [CrossRef]
50. von Lewinski, D.; Kolesnik, E.; Aziz, F.; Benedikt, M.; Tripolt, N.J.; Wallner, M.; Pferschy, P.N.; von Lewinski, F.; Schwegel, N.; Holman, R.R.; et al. Timing of SGLT2i initiation after acute myocardial infarction. *Cardiovasc. Diabetol.* **2023**, *22*, 269. [CrossRef]
51. Carberry, J.; Petrie, M.C.; Lee, M.M.Y.; Stanley, B.; Brooksbank, K.J.M.; Campbell, R.T.; Good, R.; Jhund, P.S.; Kellman, P.; Lang, N.N.; et al. Empagliflozin to prevent worsening of left ventricular volumes and systolic function after myocardial infarction (EMPRESS-MI). *Eur. J. Heart Fail.* **2024**, *early view*. [CrossRef] [PubMed]
52. Stougiannou, T.M.; Christodoulou, K.C.; Koufakis, T.; Mitropoulos, F.; Mikroulis, D.; Mazer, C.D.; Karangelis, D. Progenitor Cell Function and Cardiovascular Remodelling Induced by SGLT2 Inhibitors. *Front. Biosci.* **2024**, *29*, 145. [CrossRef] [PubMed]
53. Westman, P.C.; Lipinski, M.J.; Luger, D.; Waksman, R.; Bonow, R.O.; Wu, E.; Epstein, S.E. Inflammation as a Driver of Adverse Left Ventricular Remodeling After Acute Myocardial Infarction. *J. Am. Coll. Cardiol.* **2016**, *67*, 2050–2060. [CrossRef] [PubMed]
54. Kim, S.R.; Lee, S.G.; Kim, S.H.; Kim, J.H.; Choi, E.; Cho, W.; Rim, J.H.; Hwang, I.; Lee, C.J.; Lee, M.; et al. SGLT2 inhibition modulates NLRP3 inflammasome activity via ketones and insulin in diabetes with cardiovascular disease. *Nat. Commun.* **2020**, *11*, 2127. [CrossRef]
55. Pirklbauer, M.; Sallaberger, S.; Staudinger, P.; Corazza, U.; Leierer, J.; Mayer, G.; Schramek, H. Empagliflozin Inhibits IL-1beta-Mediated Inflammatory Response in Human Proximal Tubular Cells. *Int. J. Mol. Sci.* **2021**, *22*, 5089. [CrossRef]
56. Kang, S.; Verma, S.; Hassanabad, A.F.; Teng, G.; Belke, D.D.; Dundas, J.A.; Guzzardi, D.G.; Svystonyuk, D.A.; Pattar, S.S.; Park, D.S.J.; et al. Direct Effects of Empagliflozin on Extracellular Matrix Remodelling in Human Cardiac Myofibroblasts: Novel Translational Clues to Explain EMPA-REG OUTCOME Results. *Can. J. Cardiol.* **2020**, *36*, 543–553. [CrossRef]
57. Mather, A.; Pollock, C. Glucose handling by the kidney. *Kidney Int. Suppl.* **2011**, *120*, S1–S6. [CrossRef]
58. Mehran, R.; Owen, R.; Chiarito, M.; Baber, U.; Sartori, S.; Cao, D.; Nicolas, J.; Pivato, C.A.; Nardin, M.; Krishnan, P.; et al. A contemporary simple risk score for prediction of contrast-associated acute kidney injury after percutaneous coronary intervention: Derivation and validation from an observational registry. *Lancet* **2021**, *398*, 1974–1983. [CrossRef]
59. Coca, S.G.; Yusuf, B.; Shlipak, M.G.; Garg, A.X.; Parikh, C.R. Long-term risk of mortality and other adverse outcomes after acute kidney injury: A systematic review and meta-analysis. *Am. J. Kidney Dis.* **2009**, *53*, 961–973. [CrossRef]
60. Cai, D.; Chen, Q.; Mao, L.; Xiao, T.; Wang, Y.; Gu, Q.; Wang, Q.; Ji, Y.; Sun, L. Association of SGLT2 inhibitor dapagliflozin with risks of acute kidney injury and all-cause mortality in acute myocardial infarction patients. *Eur. J. Clin. Pharmacol.* **2024**, *80*, 613–620. [CrossRef]
61. Kultursay, B.; Yilmaz, C.; Guven, B.; Mutlu, D.; Karagoz, A. Potential renoprotective effect of SGLT2 inhibitors against contrast-induced AKI in diabetic STEMI patients undergoing primary PCI. *Kardiol. Pol.* **2024**, *82*, 29–36. [CrossRef] [PubMed]
62. Basutkar, R.S.; Cutinha, R.M.; Sathish, V.; Shahil, A.; Saneen Ck, N. Impact of SGLT2 Inhibitors on Renal Function in Type 2 Diabetic Patients with Coronary Artery Disease Undergoing Percutaneous Intervention: A Systematic Review and Meta-Analysis. *Curr. Diabetes Rev.* **2024**, *21*, e030724231535. [CrossRef]
63. Terami, N.; Ogawa, D.; Tachibana, H.; Hatanaka, T.; Wada, J.; Nakatsuka, A.; Eguchi, J.; Horiguchi, C.S.; Nishii, N.; Yamada, H.; et al. Long-term treatment with the sodium glucose cotransporter 2 inhibitor, dapagliflozin, ameliorates glucose homeostasis and diabetic nephropathy in db/db mice. *PLoS ONE* **2014**, *9*, e100777. [CrossRef] [PubMed]

64. Huang, X.; Guo, X.; Yan, G.; Zhang, Y.; Yao, Y.; Qiao, Y.; Wang, D.; Chen, G.; Zhang, W.; Tang, C.; et al. Dapagliflozin Attenuates Contrast-induced Acute Kidney Injury by Regulating the HIF-1alpha/HE4/NF-kappaB Pathway. *J. Cardiovasc. Pharmacol.* **2022**, *79*, 904–913. [CrossRef] [PubMed]
65. Kawanami, D.; Matoba, K.; Takeda, Y.; Nagai, Y.; Akamine, T.; Yokota, T.; Sango, K.; Utsunomiya, K. SGLT2 Inhibitors as a Therapeutic Option for Diabetic Nephropathy. *Int. J. Mol. Sci.* **2017**, *18*, 1083. [CrossRef]
66. Heerspink, H.J.; Perkins, B.A.; Fitchett, D.H.; Husain, M.; Cherney, D.Z. Sodium Glucose Cotransporter 2 Inhibitors in the Treatment of Diabetes Mellitus: Cardiovascular and Kidney Effects, Potential Mechanisms, and Clinical Applications. *Circulation* **2016**, *134*, 752–772. [CrossRef]

Disclaimer/Publisher's Note: The statements, opinions and data contained in all publications are solely those of the individual author(s) and contributor(s) and not of MDPI and/or the editor(s). MDPI and/or the editor(s) disclaim responsibility for any injury to people or property resulting from any ideas, methods, instructions or products referred to in the content.

biomedicines

MDPI

Review

Weight Loss Therapies and Hypertension Benefits

Vasiliki Katsi, Eleni Manta *, Christos Fragoulis and Konstantinos Tsioufis

First Department of Cardiology, Hippokration General Hospital, National and Kapodistrian University of Athens Medical School, 114 Vasilissis Sofias Avenue, 11527 Athens, Greece; christosfragoulis@yahoo.com (C.F.)
* Correspondence: elenmanta@gmail.com

Abstract: Obesity and hypertension have become an international health issue, with detrimental consequences on patients. Obesity and hypertension share common pathophysiological mechanisms, such as overactivity of the renin–angiotensin–aldosterone and the sympathetic nervous systems, insulin resistance, and disruption of the leptin pathway. Approved therapies for obesity and overweight include phentermine/topiramate, orlistat, naltrexone/bupropion, the glucagon-like peptide-1 receptor agonists liraglutide and semaglutide, tirzepatide, and bariatric surgery. This review gives the clinical data in a thorough manner and explains in detail how each of the previously mentioned therapies affects blood pressure levels.

Keywords: obesity; weight loss therapies; blood pressure; hypertension; phentermine/topiramate; orlistat; naltrexone/bupropion; GLP-1 receptor agonists; tirzepatide; bariatric surgery

1. Introduction

Obesity is defined as the increase in the amount of fat that poses a health concern [1]. The body mass index (BMI) is used for the quantification of body fat, and the somatometric characteristics of the person are taken into account for its calculation. An individual with a BMI over 25 kg/m^2 is classified as overweight, while a BMI over 30 kg/m^2 indicates that a person is obese [2]. Obesity is associated with the occurrence of diseases that serve as cardiovascular risk factors such as type II diabetes mellitus and hyperlipidemia. On top of that, obesity is recognized as an independent risk factor for cardiovascular morbidity and mortality [3]. The prevalence of obesity and overweight in both adults and children is on the rise. The percentage of obese adults increased from 7% to 16% between 1990 and 2022, and at the same time the percentage of obese children and adolescents increased from 2% to 8% worldwide [1].

Arterial hypertension is one of the most significant health issues globally, as it affects 35–40% of adults and is predicted to impact more than 1.5 billion people by 2025 [4]. Hypertension is the greatest avoidable risk factor for cardiovascular disease, as it contributes to 54% of strokes, 30% of end-stage renal disease, and 47% of coronary heart disease, accounting for 0.4 million deaths (or 14.5% of all deaths) and 6.3 million years of disability [5]. Almost half of patients with hypertension are not aware that they suffer from this disease, less than half of those patients do not receive treatment, while only 20% of patients have their blood pressure regulated [6].

This article aims to present the correlation between these two conditions and then to analyze the effect of interventions used to treat obesity on blood pressure levels.

2. The Link between Obesity and Hypertension

There is substantial evidence linking these two health conditions, with obesity being a key risk factor for the development of hypertension. Research indicates that obese individuals have a 3.5 times higher risk of developing hypertension [7]. In fact, in all age groups, the prevalence of hypertension in obese individuals can vary from 60% to 77%, while in people of normal weight this prevalence is around 34% [8].

The fact that arterial hypertension and obesity often coexist is grounded on several causes. First, these two pathological entities are affected by the same environmental factors, such as smoking, increased alcohol and salt intake, and limited physical activity [7]. In addition, overlapping pathophysiological mechanisms have emerged, which are involved in the development of both conditions (Figure 1).

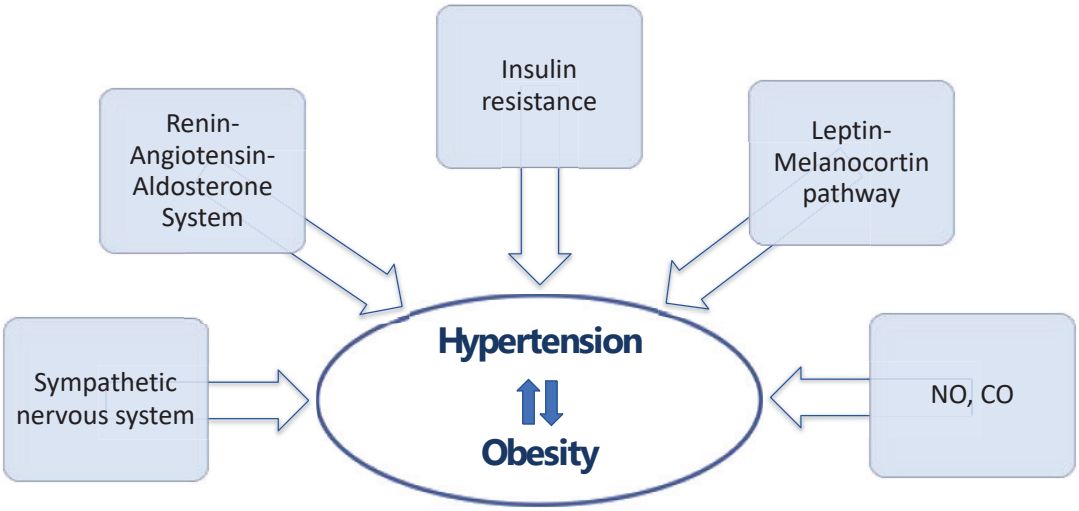


Figure 1. Pathophysiological mechanisms that contribute to the development of arterial hypertension and obesity.

2.1. Sympathetic Nervous System

A key common pathophysiological mechanism of arterial hypertension and obesity is the overactivation of the sympathetic nervous system (SNS). Arterial hypertension is characterized by sympathetic overstimulation, and this activation is initiated by the central nervous system. Further, peripheral factors contribute to chronically elevated blood pressure, such as downregulation of peripheral α1-adrenergic receptors, impaired norepinephrine reuptake from sympathetic nerve endings, impaired reflexes of baroreceptors in the cardiopulmonary region which limit the adrenergic outflow, impaired arterial chemoreceptors, as well as interaction with the renin–angiotensin–aldosterone system [9].

The SNS is also stimulated by obesity. Muscle and renal SNS activity seems to rise with even small weight gains and this rise is greater in people who are both obese and hypertensive [10]. Abnormal adipokine production from adipose tissue, baroreceptor dysfunction, interaction with the renin–angiotensin–aldosterone system, and insulin resistance are among the causative pathways of SNS activation in obesity [10]. The simultaneous occurrence of obesity and hypertension is associated with a higher level of sympathetic activity compared with the sympathetic activity observed in relation to each condition separately. Furthermore, studies have demonstrated that individuals with central fat have higher blood pressure values and stronger sympathetic activation, making the location of fat particularly significant [7].

2.2. Renin–Angiotensin–Aldosterone System

Sympathetic activation in hypertension also depends on the interaction with the renin–angiotensin–aldosterone system, as mentioned above. Circulating angiotensin stimulates the SNS by not only its effect on the brain, but also through its effect on sympathetic nerve endings that facilitate neurotransmission [11]. In addition, renal sympathetic activation facilitates renin release from the paraglomerular apparatus, leading to increased aldosterone levels, sodium and water retention, renal vasoconstriction, and microalbuminuria [12].

Numerous studies showcase that the renin–angiotensin–aldosterone system is also activated in obesity, mainly because of the interaction with the SNS, which leads to the release of renin from the kidneys [10]. Accumulation of fat around the kidney also plays a

role, leading to compression of the kidney, which results in renin secretion [10]. Additionally, adipocytes seem to have their own intrinsic renin–angiotensin–aldosterone system that produces angiotensinogen and angiotensin II [10].

2.3. Insulin Resistance

The adrenergic overstimulation that occurs in hypertension also has a humoral origin, since it is triggered by metabolic alterations such as the hyperinsulinemic state and subsequent insulin resistance, as the stimulating effect of insulin has already been documented [13]. In fact, hyperinsulinemia and subsequent insulin resistance are the main mechanisms leading to sympathetic activation in obesity [9]. It is important to emphasize that, in this as well as in other situations, the SNS often regresses the stimulation it receives, thus forming a vicious circle in which the components involved reinforce each other. In the case of insulin, resistance to it is increased by sympathetic effects on reduced vasoconstriction in skeletal muscle regions, which leads to a further increase in insulin secretion and therefore further sympathetic activation [14]. In addition, insulin promotes sodium reabsorption by the kidneys, while it also appears to affect vasodilation through its effects on the vascular endothelium [7].

2.4. Leptin–Melanocortin Pathway

Another mechanism involved in the occurrence of hypertension and obesity is leptin and the leptin–melanocortin pathway. Leptin is a cytokine that has a role in energy homeostasis, as it negatively affects brain regions related to energy intake by informing the brain about the amount of fat stored in the body. These actions are driven by its binding to melanocortin receptors in the hypothalamus and in sympathetic neurons of the spinal cord [15]. Leptin levels appear elevated in the plasma of hypertensive patients, paralleling the magnitude of adrenergic hyperfunction [9]. In addition, leptin levels are paradoxically elevated in obese individuals, so it has been hypothesized that a state of leptin resistance occurs, suppressing its appetite-modulating effect but not its SNS-stimulating effect [10].

2.5. New Mediators in Hypertension

Nitric oxide (NO) is a signaling molecule that is produced naturally by endothelial cells through the activation of endothelial nitric oxide synthase (eNOS), stimulating the increase in intracellular guanosine 3′,5′-cyclic monophosphate (cGMP) levels in vascular smooth muscle cells (VSMCs) to induce vasodilation. Studies conducted over the last few decades have shown that the reduction in NO production, leading to vasoconstriction and endothelial dysfunction, represents the earliest stages in the development of hypertension [16]. Furthermore, carbon monoxide (CO) has been found to relax blood vessels in various organs. The primary source of CO in the vascular system is heme oxygenase (HO)-2, which is present in both endothelial and vascular smooth muscle cells. Similar to NO, CO's ability to dilate blood vessels occurs through the activation of soluble guanylyl cyclase (sGC), elevation of cGMP, and stimulation of high-conductance Ca^{2+}-activated K^+ channels. The triggering of K^+ channels results in membrane hyperpolarization, which hinders calcium entry from voltage-activated Ca^{2+} channels. Under typical circumstances, CO is generated from the degradation of intracellular heme by heme oxygenase. Subsequently, CO triggers sGC to elevate intracellular cGMP levels, thereby enhancing the activity of K^+ channels to induce vasodilation. CO might also directly influence K^+ channels to boost their activity. The relationship between vascular NO and CO is highly complex. Both gases can activate sGC to elevate cGMP levels and induce vasodilation. Previous research has demonstrated that low levels of CO (0.001 to 0.1 μmol/L) can prompt NO release, while higher levels of CO ($\geq$1 μmol/L) impede eNOS. In instances where CO production is significantly heightened in VSMCs, CO can impede eNOS in endothelial cells, reducing NO production and diminishing NO-mediated increases in cGMP, leading to decreased VSMC relaxation and causing vascular dysfunction [17]. As presented in the obese Zucker rat model of the metabolic syndrome, HO-derived CO production is increased and promotes

hypertension and arteriolar endothelial dysfunction with the mechanisms described above. These results could explain another mechanism that contributes to hypertension in obese patients [18] (Figure 2).

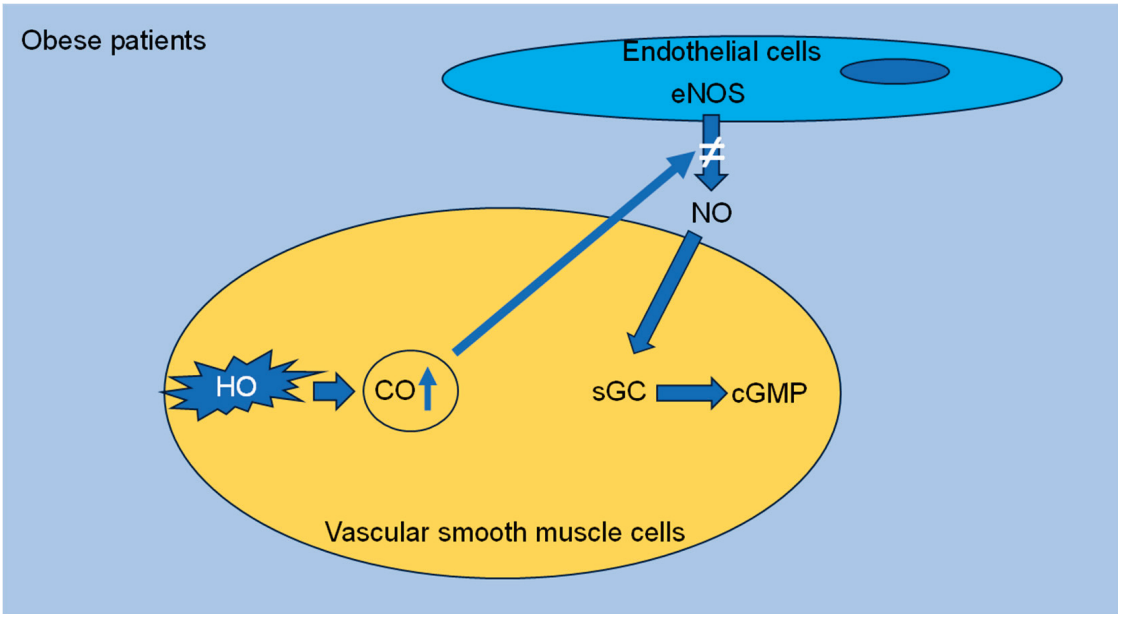


Figure 2. Proposed mechanism of the role of carbon monoxide in obese patients. In obese patients, a hypothesis has developed that HO-derived CO production is increased, resulting in inhibition of eNOS and decreased concentration of NO. This ends up in downregulation of cGMP, vasoconstriction, and endothelial dysfunction, eventually promoting hypertension. cGMP: guanosine 3′,5′-cyclic monophosphate, CO: carbon monoxide, eNOS: endothelial nitric oxide synthase, HO: heme oxygenase, NO: nitric oxide, sGC: soluble guanylyl cyclase.

3. Blood Pressure and Weight Loss

Data from epidemiological studies show that the reduction in body weight leads to a reduction in blood pressure levels. In fact, the relationship between these two variables is linear, as it has been shown that a 1 kg reduction in body weight through lifestyle interventions can lead to a 1 mmHg reduction in systolic blood pressure levels [19,20].

The underlying pathophysiological mechanisms for this association are likely based on adipose tissue. A reduction in adipose tissue appears to reduce induced inflammation, thereby limiting inflammation-induced hardening of the arteries, as well as improving insulin resistance [8]. In addition, the reduction in perirenal fat leads to the reduction in SNS stimulation and the limitation of sodium retention, as these occur in a manner described above [8]. According to the most relevant recent Clinical Consensus of the European Society of Cardiology, it is recommended to maintain a stable BMI within normal limits (20–25 kg/m^2) to reduce both blood pressure levels and cardiovascular risk. In addition, antihypertensive treatment is recommended in patients with obesity and confirmed arterial hypertension (office blood pressure values $\geq$ 140/90 mmHg) or in patients with blood pressure values of 130–139/80–89 mmHg and high cardiovascular risk. Furthermore, the importance of healthy dietary interventions is emphasized as a first step in the treatment of obesity and hypertension, before the initiation of antihypertensive treatment [21].

4. Lifestyle Interventions

Interventions for lifestyle involve dietary adjustments, physical activity, and psychological support. In dietary interventions, the goal is usually to create an energy deficit of 500–750 kcal/day. It is important to customize these interventions based on individual body weight and activity levels. Weight reduction of 5–10% can be attained through different

nutritional and multidisciplinary methods, but sustaining these effects is crucial [21]. The recommendation is to target a stable and healthy BMI (e.g., 20–25 kg/m^2) and waist circumference values (e.g., <94 cm in men and <80 cm in women) to lower the risk of high blood pressure and cardiovascular disease. Embracing a healthy and well-balanced diet, such as the scientifically supported Mediterranean or Dietary Approaches to Stop Hypertension (DASH) diet, is advised [22]. Physical activity interventions generally have modest impacts on weight loss but are essential for maintaining weight loss and decreasing overall cardiovascular risk [21]. It is recommended to engage in moderate-intensity aerobic exercise for ≥150 min/week (≥30 min, 5–7 days/week) or alternatively 75 min of vigorous-intensity aerobic exercise per week over 3 days. This should be supplemented with low- or moderate-intensity dynamic or isometric resistance training (2–3 times/week) to lower the risk of high blood pressure and cardiovascular disease [22]. Lastly, psychological interventions encompass stress and depression management, as well as the adoption and maintenance of the aforementioned healthy behaviors [21]. The average reduction in systolic blood pressure (SBP) due to regular aerobic exercise is 5 mmHg, and the average reduction in diastolic blood pressure (DBP) is 4 mmHg. Adequate reduction in salt (sodium) in the diet results in a similar average reduction in blood pressure. In addition, moderate alcohol consumption can lead to a decrease in SBP by around 4 mmHg and DBP by 2.5 mmHg. For individuals who are overweight or obese, losing 3% to 9% of their weight results in approximately 3 mmHg reductions in both systolic and diastolic blood pressure. Following the DASH diet, which is low in saturated fats and high in fruits and vegetables, can lead to an average reduction of 11 mmHg in SBP and 5.5 mmHg in DBP [23].

5. Pharmacological Therapy for Weight Reduction

The increasing morbidity linked to obesity has prompted the creation of medications designed to effectively treat the condition. The medicinal substances approved by the US Food and Drug Administration (FDA) for chronic weight management are the following: phentermine/topiramate, orlistat, naltrexone/bupropion, the glucagon-like peptide-1 receptor agonists liraglutide and semaglutide, and tirzepatide. The same drugs have been approved by the European Medicines Agency (EMA) for the treatment of obesity in the European Union, except for phentermine/topiramate. The mechanisms by which these medicinal substances lead to a reduction in body weight are analyzed below. Also, the available evidence is analyzed regarding their effects on blood pressure levels, and is schematically illustrated in Figure 3.

Intervention	SBP	DBP
Phentermine / Topiramate	↓	↓
Orlistat	↓	↓
Naltrexone / Bupropion	↑	↑
Liraglutide	↓	↓
Semaglutide	↓	↓
Tirzepatide	↓	↓

Figure 3. Pharmacological therapies for weight reduction and their effect on blood pressure levels.

5.1. Phentermine/Topiramate

5.1.1. Mechanism of Action

Phentermine is a sympathomimetic amine that suppresses appetite by promoting the release of norepinephrine. Topiramate upgrades the action of gamma-aminobutyric acid (GABA) and inhibits carbonic anhydrases, which are excitatory neurotransmitters. Topiramate was initially approved for the treatment of epilepsy, while the mechanisms through which it induces weight loss have not been completely illustrated [24]. The fixed combination of these two substances was created in order to enhance the benefits of both, while concurrently lowering the negative effects that each of the chemicals caused [24]. The FDA has authorized this combination in one formulation for the treatment of obesity; however, the EMA has rejected its use in the European Union due to safety concerns.

5.1.2. Clinical Evidence on Blood Pressure

Several phase III clinical trials examined the safety and effectiveness of phentermine/topiramate in obese participants. In the EQUIP trial, 1267 people with BMI $\geq$ 35 kg/m^2, with or without hypertension, were treated with phentermine/topiramate in low dose (phentermine 3.75 mg/topiramate 23 mg per day) or full dose (phentermine 15 mg/topiramate 92 mg per day) or a placebo for 56 weeks. Individuals who were administered the medication experienced a substantial decrease in both SBP and DBP after 56 weeks of treatment [25]. A similar finding was demonstrated in the CONQUER trial, which concluded that phentermine/topiramate substantially lowered blood pressure in patients who were overweight or obese and had two or more comorbidities. The correlation between weight loss and cardiovascular outcomes was highlighted by the fact that participants who achieved a 10–15% decrease in their baseline weight saw the greatest reduction in blood pressure [26]. In the EQUATE trial, 600 subjects with BMI 30–45 kg/m^2 with or without arterial hypertension were randomized to topiramate 46 mg, topiramate 92 mg, phentermine 7.5 mg, phentermine 15 mg, phentermine/topiramate 7.5/46 mg, phentermine/topiramate 15/92 mg, or a placebo. Subjects who received phentermine/topiramate showed higher reductions in SBP than those who received a placebo, while DBP differences were not statistically significant between the examined groups [27]. The SEQUEL trial was an extension of the CONQUER study for another 52 weeks, where 676 participants of the CONQUER trial continued the assigned drug from the initial randomization. Of the trials mentioned above, this was the only one in which the difference in the reduction in blood pressure between the drug-treated group and the placebo group was not statistically significant [28].

5.1.3. Mechanisms Affecting Blood Pressure

The apparent underlying mechanism by which phentermine/topiramate lowers blood pressure is weight reduction. Additional mechanisms that have been suggested include diuresis induced by carbonic anhydrase inhibition or neurotransmitter inhibition, as mentioned above [24].

5.2. Orlistat

5.2.1. Mechanism of Action

Orlistat is a long-acting gastrointestinal lipase inhibitor. It acts in the lumen of the stomach and the small intestine where it forms a covalent bond with the active serine center of gastric and pancreatic lipases. Thus, the deactivated enzyme is unable to hydrolyze the dietary fat, resulting in a reduction in its absorption by ~30% [29]. Orlistat usage has been linked to comparatively mild weight reduction, and it causes gastrointestinal disturbances that usually lead to its discontinuation by a significant proportion of patients [30].

5.2.2. Clinical Evidence on Blood Pressure

Orlistat's effectiveness in lowering blood pressure has been assessed in a number of clinical trials and meta-analyses. Sahebkar et al. conducted a meta-analysis of 27 randomized controlled trials, with a total of 8150 individuals, in order to compare the effects of

orlistat against placebo on blood pressure. Patients who were overweight or obese and had concomitant conditions including type II diabetes mellitus and hypertension were included in the selected trials. In this meta-analysis, orlistat was found to have a significant effect on lowering SBP by 1.15 mmHg and DBP by 1.07 mmHg, with no significant difference found between subgroups based on dosage (360 mg vs. 180 mg daily) and length of treatment (more vs. less than 12 months) [31]. These findings suggest that orlistat's ability to lower blood pressure is consistent across a range of patient demographics and medication durations.

When paired with dietary changes, orlistat has been demonstrated to dramatically improve blood pressure management in obese people with hypertension. For instance, a meta-analysis conducted in 2002 by Sharma and Golay found that obese individuals with uncontrolled diastolic hypertension or isolated systolic hypertension who were treated with orlistat had higher reduction in blood pressure, both systolic and diastolic, than patients who were given a placebo. In particular, the orlistat group saw a reduction in SBP by 9.4 mmHg and in DBP by 7.7 mmHg. An interesting finding of this particular study is that the greatest drop in blood pressure was observed in patients who lost more than 10% of their body weight [32].

5.2.3. Mechanisms Affecting Blood Pressure

The blood pressure benefit of orlistat has been tested and documented in obese individuals with or without comorbidities such as hypertension or diabetes mellitus. The main mechanism through which orlistat reduces blood pressure is the loss of body weight, which, as previously mentioned, lessens SNS overstimulation. Orlistat also lowers blood pressure in part because of its effects on endothelial function and oxidative stress. Research has indicated that orlistat improves the function of microvascular endothelial cells, potentially by reducing triglyceride and LDL levels, which is essential for preserving normal blood pressure levels [33].

5.3. Naltrexone/Bupropion

5.3.1. Mechanism of Action

Naltrexone is an antagonist of opioid receptors. It mainly inhibits the actions of endogenous opioids, which are recognized for their ability to regulate cardiovascular, reward, and pain responses. Naltrexone may have an impact on food intake and body weight by acting on the melanocortin system of the hypothalamus, which includes opiate neurons [34]. Bupropion is a weak nicotinic acetylcholine receptor antagonist, which also affects the reuptake of catecholamines, specifically dopamine and norepinephrine. Bupropion administration facilitates changes in the concentrations of dopamine and norepinephrine in the brain and may also modify the activity of the neurons that emit these chemicals by preventing their clearance. The melanocortin system is influenced by dopamine and norepinephrine, and a number of characteristics of obesity are associated with a reduction in the hypothalamic dopaminergic tone [34]. The purpose of combining these two ingredients was to maximize their weight reduction benefits through their synergy.

5.3.2. Clinical Evidence on Blood Pressure

The efficacy of this combination in weight regulation was evaluated by four Phase III clinical trials. The CONTRAVE Obesity Research I (COR-I) trial included 1742 patients with a BMI of 30–45 kg/m^2 or a BMI of 27–45 kg/m^2 who also had dyslipidemia or arterial hypertension. The trial compared the effectiveness of naltrexone/bupropion at dosages of 16/360 mg or 32/360 mg to a placebo in treating obesity. The combination therapy caused the mean SBP and DBP to slightly and temporarily rise from baseline [35]. The CONTRAVE Obesity Research II (COR-II) trial examined the effects of the combination naltrexone/bupropion 32/360 mg vs. a placebo in ~1500 individuals with a BMI of 30–45 kg/m^2 or a BMI of 27–45 kg/m^2 who also had dyslipidemia and/or arterial hypertension. Despite the substantial drop in body weight shown in the medication-treated group,

there was no statistically significant difference from the placebo group in the patients' blood pressure values during the follow-up period [36]. The COR Behavior Modification (COR-BMOD) trial included 793 overweight or obese individuals who were already following a balanced diet and physical activity program. Both treatment groups reported a decrease in SBP and DBP, with the placebo group experiencing a greater reduction than the group receiving naltrexone/bupropion 32/360 mg per day [37]. The effectiveness of the combination of naltrexone and bupropion in weight loss has also been demonstrated in overweight or obese patients with type II diabetes mellitus. When the combination was administered to 500 individuals who met these criteria, Hollander and colleagues saw a substantial reduction in body weight when compared with a placebo. The combination in this trial reduced the levels of SBP and DBP, with no statistically significant difference between the individuals who received the medication and the placebo group [38].

The above clinical studies had equivocal results regarding the effect of naltrexone/bupropion on blood pressure levels. The most recent relevant meta-analysis attempted to clarify the picture. Jiang et al. observed that the combination treatment caused a slight rise in both SBP and DBP. More specifically, a small but statistically significant increase in SBP by 1.34 mmHg and DBP by 0.93 mmHg was observed [39].

5.3.3. Mechanisms Affecting Blood Pressure

The chemical processes by which naltrexone and bupropion regulate blood pressure involve interactions with the central nervous system that affect inflammatory processes and neurotransmission pathways. Naltrexone is an opioid receptor antagonist. Thus, it reduces the effects of endogenous opioids. These substances act on receptors in the endothelium of the vessels and in the heart, and cause vasodilation with consequent hypotensive effects. Therefore, naltrexone administration may result in an increase in blood pressure through inhibition of the intrinsic actions of endogenous opioids [40]. Bupropion mainly operates by preventing dopamine and norepinephrine from being reabsorbed, which raises their levels. Because norepinephrine increases SNS activity, blood pressure may also rise as a result. Moreover, bupropion's actions on the neurological system and potentially blood pressure control are attributed to its noncompetitive antagonistic activity at nicotinic acetylcholine receptors [41]. The hypothalamus melanocortin system, which is important for energy balance and cardiovascular control, is also impacted by naltrexone/bupropion combination treatment [34]. The regulation of this route by naltrexone and bupropion may be responsible for the reported cardiovascular effects, as this system's activation can affect blood pressure in the way mentioned above.

5.4. Glucagon-like Peptide-1 Receptor Agonists

5.4.1. Mechanism of Action

Glucagon-like peptide-1 (GLP-1) and gastric inhibitory peptide-1 (GIP) are intestine hormones (also called 'incretins') that are secreted in reaction to stimuli from digested nutrients and have the ability to glucose-dependently trigger the release of insulin from pancreatic cells [42]. The natural GLP-1 hormone has a relatively limited half-life because of its rapid breakdown by the enzyme dipeptidyl peptidase-4 (DPP-4). In order to achieve a longer operation and more enduring therapeutic advantages, GLP-1 receptor agonists were specifically designed to be resistant to degradation by DPP-4 [43].

GLP-1 receptor agonists were initially created to treat type II diabetes mellitus, by amplifying the metabolic effect of the gut hormone GLP-1. GLP-1 delays stomach emptying, increases postprandial insulin secretion, inhibits glucagon release, and suppresses appetite [44]. However, they were also proven to be useful in lowering body weight. Thus, once-daily subcutaneous injection of liraglutide 3.0 mg and once-weekly subcutaneous administration of semaglutide 2.4 mg were studied and approved as anti-obesity medications. GLP-1 receptor agonists lower body weight in a variety of ways, notably by enhancing satiety and reducing appetite, which in turn leads to less calorie consumption [45].

5.4.2. Clinical Evidence on Blood Pressure

Liraglutide

Liraglutide has been licensed as a weight-loss medication for obese individuals with or without type II diabetes mellitus, following phase III clinical studies in the SCALE program, in which subcutaneous administration of liraglutide 3 mg per day resulted in a statistically significant weight reduction compared with a placebo. The trial SCALE Obesity and Prediabetes compared the effects of 3 mg of liraglutide vs. a placebo in 3731 overweight or obese people with treated or untreated hypertension and dyslipidemia, without diabetes. In comparison with the placebo group, the drug-treated group had a statistically significant drop in both SBP (−4.2 mmHg vs. −1.5 mmHg, $p < 0.001$) and DBP (−2.6 mmHg vs. −1.9 mmHg, $p < 0.001$) levels [46]. In the SCALE Diabetes trial, liraglutide 3 mg was found to be statistically significantly superior to liraglutide 1.8 mg and to placebo in lowering SBP, but not DBP, in individuals with type II diabetes mellitus who were overweight or obese [47]. The SCALE Maintenance study examined overweight or obese patients with comorbidities other than diabetes mellitus who had lost at least 5% of their body weight through a low-calorie diet before receiving liraglutide 3 mg or a placebo. Again, liraglutide resulted in a statistically significant reduction in SBP values (estimated treatment difference −2.7 mmHg for liraglutide 3 mg vs. placebo, $p = 0.007$), but not in DBP values (estimated treatment difference −0.3 mmHg for liraglutide 3 mg vs. placebo, $p = 0.64$) [48] (Table 1).

Table 1. Evidence about the impact on blood pressure from clinical trials supporting the approval of liraglutide for the treatment of obesity.

Trial	Total Population, *n*	Hypertension	Anti-Hypertension Therapy	Comparison	Difference in SBP, mmHg	Difference in DBP, mmHg
SCALE Obesity and Prediabetes [46]	3731	mixed	mixed	Liraglutide 3 mg vs. placebo	−4.2 mmHg vs. −1.5 mmHg $p < 0.001$	−2.6 mmHg vs. −1.9 mmHg $p < 0.001$
SCALE Diabetes [47]	846	mixed	mixed	Liraglutide 3 mg vs. Liraglutide 1.8 mg vs. placebo	ETD −2.59 mmHg for liraglutide 3 mg vs. placebo $p = 0.01$	ETD −0.36 mmHg for liraglutide 3 mg vs. placebo $p = 0.59$
SCALE Maintenance [48]	422	mixed	mixed	Liraglutide 3 mg vs. placebo	ETD −2.7 mmHg for liraglutide 3 mg vs. placebo $p = 0.007$	ETD −0.3 mmHg for liraglutide 3 mg vs. placebo $p = 0.64$

DBP, diastolic blood pressure; ETD, estimated treatment difference; mixed, mixed population with or without hypertension, with or without anti-hypertensive therapy; *n*, number of patients; SBP, systolic blood pressure; vs., versus.

Semaglutide

Following the STEP clinical trial program in subjects with and without type II diabetes mellitus, subcutaneous semaglutide 2.4 mg once-weekly was approved for the treatment of obesity, as it displayed a clinically meaningful decrease in body weight and improvement in cardiovascular and metabolic risk indicators. In the STEP 1 trial, semaglutide 2.4 mg was administered to overweight or obese non-diabetic participants, and the results showed a significant decrease in SBP (−6.16 mmHg for the semaglutide group vs. −1.06 mmHg for the placebo group, $p < 0.001$) and DBP values (−2.83 mmHg for the semaglutide group vs. −0.42 mmHg for the placebo group, *p* not reported) when compared with the placebo [49]. The STEP 2 study compared the effect of two different doses of semaglutide, 2.4 mg and 1 mg, with a placebo in diabetic patients. Semaglutide at a dose of 2.4 mg appeared to be superior than at the lower dose, as well as the placebo, in promoting weight loss and in lowering SBP values (estimated treatment difference −3.4 mmHg for semaglutide 2.4 mg vs. placebo, $p = 0.0016$) [50]. In the STEP 3 trial, semaglutide 2.4 mg or a placebo were administered to non-diabetic patients, in combination with behavioral therapy. Administration of semaglutide led to a statistically significant weight loss, as well as a drop

in SBP (−5.6 mmHg for the semaglutide group vs. −1.6 mmHg for the placebo group, $p = 0.001$) and DBP (−3.0 mmHg for the semaglutide group vs. −0.8 mmHg for the placebo group, $p = 0.008$) values [51]. The goal of the STEP 4 study was to test the maintenance of weight loss after the administration of semaglutide 2.4 mg on a weekly basis in non-diabetic overweight or obese subjects. In this context, semaglutide was administered to all subjects for 20 weeks at a progressively rising dose. Those who reached the 2.4 mg semaglutide dose were randomized to continue at that dose or receive a placebo. Participants who continued taking semaglutide continued to lose weight, and they also experienced a statistically significant reduction in SBP values (estimated treatment difference −3.9 mmHg for semaglutide 2.4 mg vs. placebo, $p < 0.001$), but not DBP values (estimated treatment difference −0.6 mmHg for semaglutide 2.4 mg vs. placebo, $p = 0.46$) [52] (Table 2).

Table 2. Evidence about the impact on blood pressure from clinical trials supporting the approval of semaglutide for the treatment of obesity.

Trial	Total Population, *n*	Hypertension	Anti-Hypertension Therapy	Comparison	Difference in SBP, mmHg	Difference in DBP, mmHg
STEP 1 [49]	1961	mixed	mixed	Semaglutide 2.4 mg vs placebo	−6.16 mmHg vs. −1.06 mmHg $p < 0.001$	−2.83 mmHg vs. −0.42 mmHg p NR
STEP 2 [50]	1210	mixed	mixed	Semaglutide 2.4 mg vs. Semaglutide 1 mg vs. placebo	ETD −3.4 mmHg for semaglutide 2.4 mg vs. placebo $p = 0.0016$	ETD −0.7 mmHg for semaglutide 2.4 mg vs. placebo p NR
STEP 3 [51]	611	mixed	mixed	Semaglutide 2.4 mg vs. placebo	−5.6 mmHg vs. −1.6 mmHg $p = 0.001$	−3.0 mmHg vs. −0.8 mmHg $p = 0.008$
STEP 4 [52]	803	mixed	mixed	Semaglutide 2.4 mg vs. placebo	ETD −3.9 mmHg for semaglutide 2.4 mg vs. placebo $p < 0.001$	ETD −0.6 mmHg for semaglutide 2.4 mg vs. placebo $p = 0.46$

DBP, diastolic blood pressure; ETD, estimated treatment difference; mixed, mixed population with or without hypertension, with or without anti-hypertensive therapy; *n*, number of patients; SBP, systolic blood pressure; vs., versus.

5.4.3. Mechanisms Affecting Blood Pressure

It has been shown that GLP-1 receptors are present in many human organs, and therefore GLP-1 receptor agonists exert both their hypotensive and other beneficial effects through several mechanisms apart from weight loss, many of which are still poorly understood. GLP-1 receptor agonists stimulate the secretion of atrial natriuretic peptide from the cardiac atria, which increases sodium excretion and vasodilation, lowering blood pressure [53]. They also cause vasodilation by their direct action on endothelial and smooth muscle cells, leading to the activation of nitric oxide [53]. The interaction between GLP-1 receptor agonists and the renin–angiotensin–aldosterone system is at least partially responsible for the hypotensive effects of those drugs. Specifically, GLP-1 receptor agonists inhibit the activity of angiotensin II by enhancing its inactivation and opposing its effects on target cells such as cardiomyocytes and glomerular endothelial cells. Moreover, GLP-1 receptor agonists appear to briefly reduce circulating aldosterone levels [44]. Finally, GLP-1 receptor agonists also exert a direct effect on the kidneys and lower blood pressure by enhancing natriuresis, while the effect of these substances on the central nervous system has not yet been confirmed [54].

5.5. Tirzepatide

5.5.1. Mechanism of Action

Tirzepatide was first licensed by the FDA and EMA for the treatment of type II diabetes mellitus, and it was granted further permission for the management of obesity in non-diabetic individuals a while ago. Tirzepatide is a novel medication that operates as a dual agonist to the two different types of insulinotropic polypeptide receptors mentioned above,

the GLP-1 and the GIP receptors. Tirzepatide increases insulin secretion, inhibits glucagon release, and aids in weight reduction via activating the GLP-1 and GIP receptors [42].

5.5.2. Clinical Evidence on Blood Pressure

Important information on tirzepatide's effects on blood pressure has been gleaned from a number of significant clinical studies.

SURPASS Trials in Diabetic Patients

The primary goal of the SURPASS trials was to evaluate the medication's effectiveness in helping diabetic patients regulate their blood glucose levels. Secondary outcomes, such as blood pressure changes, were also monitored.

SURPASS-1 was a randomized, double-blind clinical trial that assessed the efficacy of tirzepatide (subcutaneous injections once weekly) in comparison with a placebo in individuals with type II diabetes mellitus not adequately managed with diet and exercise. This study showed that tirzepatide is more effective than the placebo in enhancing glycemic control, reducing body weight, and lowering blood pressure, as the mean SBP drop varied from −4.7 to −5.2 mmHg for the tirzepatide group compared to −2.0 mmHg for the placebo group, while there was no significant difference in DBP between the two groups [55]. In the open-label, phase III SURPASS-2 study, individuals with type II diabetes mellitus were randomly assigned to receive either tirzepatide or semaglutide once a week. Tirzepatide dosage groups of 10 mg and 15 mg showed noticeably higher SBP reductions compared with semaglutide 1 mg [56]. In the SURPASS-3 study, individuals with inadequately managed type II diabetes mellitus were randomized to receive once-weekly tirzepatide or once-daily insulin degludec as an adjuvant to metformin [57]. In the SURPASS-4 study, tirzepatide was compared to insulin glargine in individuals with type II diabetes mellitus and high cardiovascular risk, who were not effectively treated by oral glucose-lowering drugs [58]. Compared with insulin degludec and insulin glargine, all tirzepatide dosages in both trials had favorable effects as regards SBP reduction. In the SURPASS-5 phase III study, subcutaneous tirzepatide was added to titrated insulin glargine, and produced statistically significant improvements in glycemic control among patients with type II diabetes mellitus, as opposed to a placebo. Similarly to the previous studies, this one showcased that all tirzepatide dosages (5, 10, and 15 mg) led to noticeably higher decreases in SBP than the placebo [59] (Table 3).

Table 3. Evidence about the impact on blood pressure from SURPASS trials supporting the approval of tirzepatide for the treatment of type II diabetes mellitus.

Trial	Total Population, *n*	Hypertension	Anti-Hypertension Therapy	Comparison	Difference in SBP, mmHg	Difference in DBP, mmHg
SURPASS-1 [55]	478	mixed	mixed	Tirzepatide 5 mg vs placebo	−4.7 mmHg vs. −2.0 mmHg *p* NR	−2.9 mmHg vs. −1.4 mmHg *p* NR
				Tirzepatide 10 mg vs. placebo	−5.2 mmHg vs. −2.0 mmHg $p < 0.05$	−3.1 mmHg vs. −1.4 mmHg *p* NR
				Tirzepatide 15 mg vs. placebo	−4.7 mmHg vs. −2.0 mmHg *p* NR	−3.4 mmHg vs. −1.4 mmHg *p* NR
SURPASS-2 [56]	1878	mixed	mixed	Tirzepatide 5 mg vs. Semaglutide 1 mg	−4.8 mmHg vs. −3.6 mmHg *p* NR	−1.9 mmHg vs. −1.0 mmHg *p* NR
				Tirzepatide 10 mg vs. Semaglutide 1 mg	−5.3 mmHg vs. −3.6 mmHg $p < 0.05$	−2.5 mmHg vs. −1.0 mmHg *p* NR
				Tirzepatide 15 mg vs. Semaglutide 1 mg	−6.5 mmHg vs. −3.6 mmHg $p < 0.001$	−2.9 mmHg vs. −1.0 mmHg *p* NR

Table 3. *Cont.*

Trial	Total Population, *n*	Hypertension	Anti-Hypertension Therapy	Comparison	Difference in SBP, mmHg	Difference in DBP, mmHg
SURPASS-3 [57]	1444	mixed	mixed	Tirzepatide 5 mg vs. Insulin Degludec	−4.9 mmHg vs. +0.5 mmHg	−2.0 mmHg vs. +0.4 mmHg
				Tirzepatide 10 mg vs. Insulin Degludec	−6.6 mmHg vs. +0.5 mmHg	−2.5 mmHg vs. +0.4 mmHg
				Tirzepatide 15 mg vs. Insulin Degludec	−5.5 mmHg vs. +0.5 mmHg	−1.9 mmHg vs. +0.4 mmHg
SURPASS-4 [58]	2002	mixed	mixed	Tirzepatide 5 mg vs. Insulin Glargine	−2.8 mmHg vs. +1.3 mmHg	−1.0 mmHg vs. + 0.7 mmHg
				Tirzepatide 10 mg vs. Insulin Glargine	−3.7 mmHg vs. +1.3 mmHg	−0.8 mmHg vs. +0.7 mmHg
				Tirzepatide 15 mg vs. Insulin Glargine	−4.8 mmHg vs. +1.3 mmHg	−1.0 mmHg vs. +0.7 mmHg
SURPASS-5 [59]	475	mixed	mixed	Tirzepatide 5 mg + Insulin Glargine vs. Placebo + Insulin Glargine	−6.1 mmHg vs. −1.7 mmHg $p = 0.012$	−2.0 mmHg vs. −2.1 mmHg $p = 0.958$
				Tirzepatide 10 mg + Insulin Glargine vs. Placebo + Insulin Glargine	−8.3 mmHg vs. −1.7 mmHg $p < 0.001$	−3.3 mmHg vs. −2.1 mmHg $p = 0.218$
				Tirzepatide 15 mg + Insulin Glargine vs. Placebo + Insulin Glargine	−12.6 mmHg vs. −1.7 mmHg $p < 0.001$	−4.5 mmHg vs. −2.1 mmHg $p = 0.017$

DBP, diastolic blood pressure; mixed, mixed population with or without hypertension, with or without anti-hypertensive therapy; *n*, number of patients; SBP, systolic blood pressure; vs., versus.

SURMOUNT Trials in Overweight/Obese Individuals

The SURPASS 1–5 trials showed a substantial reduction in weight after tirzepatide treatment; this finding served as the impetus to clinical research on tirzepatide's efficacy in weight control. SURMOUNT-1 examined ~2500 non-diabetic adults with a BMI of 30 kg/m^2 or more, or 27 kg/m^2 or more and at least one comorbidity (cardiovascular disease, arterial hypertension, obstructive sleep apnea, dyslipidemia). Tirzepatide 5 mg, 10 mg, or 15 mg once weekly produced significant and long-lasting dose-dependent reductions in body weight in individuals with a verified diagnosis of obesity when compared to a placebo. Tirzepatide-assisted weight loss in the current trial was associated with statistically greater benefits than a placebo in terms of all assessed cardiovascular risk variables, including SBP and DBP values [60]. The SURMOUNT-1 ABPM Sub-Study examined a selected number of the patients of the aforementioned study, who underwent a 24 h ambulatory blood pressure monitoring. Administration of tirzepatide resulted in a statistically significant reduction in all components of the 24 h blood pressure recording (day, night, and 24 h average blood pressure values) in a manner that was associated with weight loss but not with receiving antihypertensive treatment [61]. The SURMOUNT-2 clinical trial examined both obese and diabetic individuals who were treated with tirzepatide, and showed considerable improvements in glycemic management and weight loss, as well as in blood pressure values, when compared with a placebo [62]. The SURMOUNT-3 study focused on overweight or obese non-diabetic individuals who had achieved a weight loss of $\geq$5% of their body weight via rigorous lifestyle modification. Tirzepatide considerably lowered body weight in these participants, and this was followed by decreases in blood pressure levels [63]. The first randomized controlled trial evaluating tirzepatide's effects on cardiovascular outcomes in overweight/obese non-diabetic people was titled SURMOUNT-4. Its findings imply that tirzepatide does not increase the risk of cardiovascular disease, as it presents

benefits in a number of indicators of cardiovascular health, such as decreased body weight, decreased blood pressure levels, and improvement of the lipid profile [64] (Table 4).

Table 4. Evidence about the impact on blood pressure from SURMOUNT trials supporting the approval of tirzepatide for the treatment of obesity.

Trial	Total Population, *n*	Hypertension	Anti-Hypertension Therapy	Comparison	Difference in SBP, mmHg	Difference in DBP, mmHg
SURMOUNT-1 [60]	2539	mixed	mixed	Tirzepatide 5 mg or 10 mg or 15 mg vs. placebo	Pooled Tirzepatide groups −7.2 mmHg vs. −1.0 mmHg $p < 0.001$	Pooled Tirzepatide groups −4.8 mmHg vs. −0.8 mmHg $p < 0.001$
SURMOUNT-2 [62]	938	mixed	mixed	Tirzepatide 10 or 15 mg vs. placebo	Pooled Tirzepatide groups −6.3 mmHg vs. −1.2 mmHg $p < 0.0001$	Pooled Tirzepatide groups −2.5 mmHg vs. −0.3 mmHg $p = 0.0012$
SURMOUNT-3 [63]	579	mixed	mixed	Tirzepatide 10 or 15 mg vs. placebo	−5.1 mmHg vs. +4.1 mmHg	−3.2 mmHg vs. +2.3 mmHg
SURMOUNT-4 [64]	783	mixed	mixed	Tirzepatide 10 or 15 mg vs. placebo	−9.7 mmHg vs. −2.0 mmHg $p < 0.001$	−5.5 mmHg vs. −1.7 mmHg $p < 0.001$

DBP, diastolic blood pressure; mixed, mixed population with or without hypertension, with or without anti-hypertensive therapy; *n*, number of patients; SBP, systolic blood pressure; vs., versus.

Data from Meta-Analyses

Numerous meta-analyses that examined data from the relevant studies outlined above, as well as a number of smaller ones, have also examined the impact of tirzepatide on blood pressure. Kanbay et al. analyzed data from seven randomized control trials involving 9446 participants. Tirzepatide treatment led to statistically significant reductions in SBP of 4.20 mmHg (95% CI; −5.17 to −3.23) for the 5 mg once-weekly dose, 5.34 mmHg (95% CI; −6.31 to −4.37) for the 10 mg dose, and 5.77 mmHg (95% CI; −6.73 to −4.81) for the 15 mg dose, and in DBP by 2.19 mmHg (95%CI; −2.82 to −1.56) for the 5 mg dose, by 2.53 mmHg (95% CI; −3.16 to −1.90) for the 10 mg dose, and by 2.55 mmHg (95% CI; −3.18 to −1.91) for the 15 mg dose, in comparison with active medications and placebo [65]. Lingvay and colleagues conducted a post hoc analysis of the five SURPASS trials in order to demonstrate the impact of tirzepatide on blood pressure levels and determine if this effect was connected with weight reduction. Tirzepatide caused a higher change in SBP than the other medications used in the trials (tirzepatide 5 mg: −5.1 to −1.3 mmHg, tirzepatide 10 mg: −6.5 to −1.7 mmHg, tirzepatide 15 mg: −11.5 to −3.1 mmHg). The authors claimed that weight reduction was the primary factor mediating changes in SBP, with a modest (r = 0.18–0.22) but significant ($p < 0.001$) association seen between SBP and body weight changes [66]. Lv et al. addressed the effects of tirzepatide in overweight or obese diabetic hypertensive patients in a meta-analysis that reviewed eight studies with 7491 patients. Tirzepatide resulted in a statistically substantial decrease in SBP and DBP levels both when compared with placebo and when compared with GLP-1 receptor agonists [67].

5.5.3. Mechanisms Affecting Blood Pressure

Changes in blood pressure may be caused via a multitude of interrelated routes when tirzepatide is used. First, as mentioned above, it has been shown that reducing body weight decreases blood pressure, and tirzepatide's potent effects on weight loss most likely have a significant influence in that regard [66]. Second, tirzepatide may have an immediate effect on the cardiovascular system. Notably, tirzepatide primarily affects glucose metabolism, although cardiovascular organs also express GIP and GLP-1 receptors. The activation of these receptors may have an effect on the heart rate, fluid balance, and vascular tone—

all of which are crucial for regulating blood pressure [68]. Tirzepatide's dual action as GLP-1 and GIP receptor agonist can also suppress inflammation by lowering the levels of inflammatory markers such as C-reactive protein, intercellular adhesion molecule 1 (ICAM-1), growth differentiation factor 15, and YKL-40 (also known as chitinase-3-like protein-1). As a result, it can improve the endothelial function and lead to consequent blood pressure reduction. Multiple studies have demonstrated these cardiovascular and anti-inflammatory effects and lent credence to this approach [68,69]. Lastly, tirzepatide may indirectly affect blood pressure through its capacity to improve glycemic control. Research on tirzepatide has shown the existence of benefits in glycemic management, which are associated with decreased insulin resistance and improved indicators of endothelial dysfunction [70]. Moreover, hyperglycemia exacerbates endothelial dysfunction and arterial stiffness, both of which can elevate blood pressure. Tirzepatide may lessen these effects by enhancing glycemic management, resulting in blood pressure reduction [71].

6. Bariatric Surgery

6.1. Mechanism of Action

Bariatric surgery appears to play an important role in reducing the risk of cardiovascular disease. Such operations are the adjustable gastric band, sleeve gastrectomy, biliopancreatic diversion, duodenal switch, Roux-en-Y gastric bypass, and one-anastomosis gastric bypass [72,73]. These procedures promote sustained weight loss and improve glycemic control, hypertension, and dyslipidemia in individuals with obesity, hypertension, and type II diabetes mellitus, even several years after the surgery. Studies have demonstrated that metabolic and bariatric surgery is more effective compared to non-surgical treatments in managing important cardiovascular risk factors in the short and mid term [73,74].

6.2. Clinical Evidence on Blood Pressure

A meta-analysis of 19 randomized clinical trials involving 1353 patients revealed that these procedures can significantly lower SBP and DBP and decrease the need for antihypertensive, antidiabetic, and lipid-lowering medications [74]. Wang et al. highlight that Roux-en-Y gastric bypass has the most significant positive impact on blood pressure, serum lipids, and glucose levels. Furthermore, their findings suggest that people with uncontrolled hypertension and diabetes, mild obesity, aged 45 and over, and smaller waist circumference had a more favorable outcome [74]. Finally, a pooled analysis of 18 non-randomized trials, including 1.5 million patients, indicates that bariatric surgery in individuals with obesity who underwent the procedure is linked to lower long-term all-cause and cardiovascular mortality, and smaller occurrence of obesity-related conditions such as new-onset hypertension, high cholesterol, diabetes, and heart disease when compared with controls [75]. According to the type of bariatric surgery, the operation can lead to a reduction of 1.5–5.1 mmHg in SBP and 2.1–5.6 mmHg in DBP [76].

6.3. Mechanisms Affecting Blood Pressure

After undergoing bariatric surgery, individuals with obesity and hypertension observe a decrease in blood pressure as a result of limited calorie intake during recovery. This reduction occurs without any alteration in the mass of visceral adipose tissue. The decrease in leptin levels and the production of reactive oxygen species due to calorie restriction contribute to this effect. Reduced leptin levels lead to a decline in SNS activity, as mentioned above, and subsequently affect blood pressure by diminishing the signals from the central nervous system and carotid body. Moreover, the decrease in reactive oxygen species production enhances vascular endothelial function, further lowering blood pressure. Bariatric surgery speeds up gastrointestinal transit, which increases the release of glucagon-like peptide-1 and peptide YY 3–36 after meals, adding to the blood pressure reduction [73,77].

In the months following bariatric surgery, progressive weight loss is associated with decreased visceral adipose tissue mass, as well as diminished muscle and renal sympathetic nerve activation. This is also linked to reduced activity in the renin–angiotensin–

aldosterone system, insulin resistance, augmented natriuretic peptide blood concentration, systemic inflammation, and arterial stiffness, all of which prevent the reappearance of hypertension [72,77]. Changes in gut microbiota resulting from progressive weight loss may also play a part in preventing the recurrence of hypertension [77]. Additionally, it is widely known that obese individuals with obstructive sleep apnea syndrome endure intermittent episodes of hypoxia and/or hypercapnia, triggering the SNS and the renin–angiotensin–aldosterone system, which significantly contribute to hypertension. Improvements in hypertension after bariatric surgery are also attributed to the resolution of obstructive sleep apnea [73,77].

In the context of type II diabetes mellitus, people who lose a similar amount of weight through calorie restriction experience an increase in insulin sensitivity, which mainly contributes to the enhancement of their glucose profile. Additionally, modifications in gut bacteria, gut hormones, and bile acid signaling also play a crucial role in bringing a substantial improvement in glycemic control. Such alterations typically occur shortly after bariatric surgery. Surgery-induced weight loss leads to a noteworthy improvement in the atherogenic lipid profile, characterized by an elevation in the protective high-density lipoprotein and a reduction in triglycerides, total cholesterol, and low-density lipoprotein cholesterol. Furthermore, it has been shown that surgical interventions alleviate inflammatory conditions associated with obesity, which is evident from a decrease in serum inflammatory markers such as C-reactive protein, leptin, and soluble receptor 1 for tumor necrosis factor. Consequently, patients often observe significant enhancements in their quality of life due to the relief of numerous obesity-related health issues [73].

7. Discussion

Arterial hypertension and obesity are important cardiovascular risk factors with increasing prevalence and ineffective management. Moreover, these two entities are interconnected through a variety of occasionally intricate pathophysiological mechanisms. Weight loss appears to have a significant impact on improving blood pressure levels through various pathways.

The American and European drug regulatory agencies have approved specific classes of drugs for chronic weight management and treatment of non-genetic obesity, with the goal of both losing weight and maintaining that loss for a significant period of time. Numerous clinical trials and meta-analyses have concluded that the aforementioned authorized medication classes result in a reduction in blood pressure levels, either in a weight loss-dependent manner or as a result of additional pleiotropic effects of the drugs. The combination of naltrexone and bupropion is an exception to this rule, as it seems that this medication either raises or does not influence blood pressure levels despite causing weight reduction. Out of all the drug classes detailed in this review, the GLP-1 receptor agonists liraglutide and semaglutide, as well as tirzepatide, have proven to be efficient in the treatment of type II diabetes mellitus in addition to obesity, with beneficial effects on blood pressure observed in both situations.

Apart from pharmaceutical treatment, the basis of obesity treatment must be lifestyle changes by adopting healthy dietary interventions and a physical exercise program. Over and above this, a greater availability of bariatric surgery may contribute to enhancing positive health outcomes for obese individuals, making this field highly compelling from both medical and surgical perspectives. Ultimately, the combination of all the above approaches can lead to a reduction in body weight, the improvement of cardiovascular risk factors such as arterial hypertension, and finally the improvement of the person's quality of life (Figure 4).

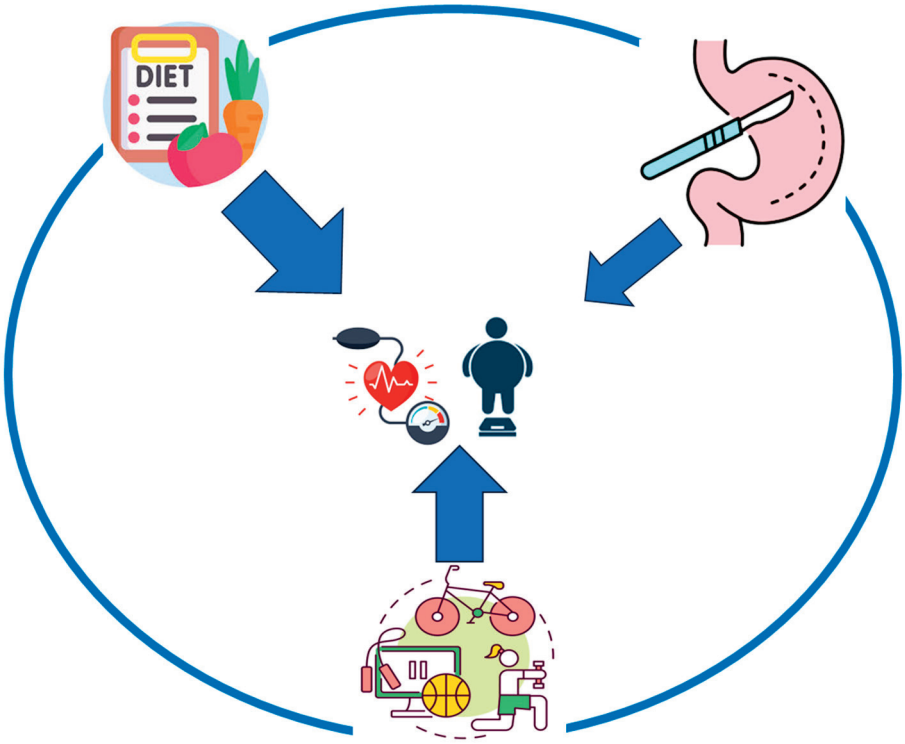


Figure 4. Results of different measures in decrease in blood pressure in obese patients. The image presents the impact of different tools to the decrease in blood pressure. The larger the width of the arrow, the larger the impact. Diet is the tool with the larger impact, followed by physical activity and bariatric surgery.

8. Limitations

Despite the promising results, there are significant constraints to any inferences regarding blood pressure that may be drawn from the trials showing the benefit of licensed anti-obesity medications for weight reduction. To begin with, these studies were not designed to explore the effect of these drugs on blood pressure, so the relevant conclusions drawn are based mainly on observational data. Furthermore, the study population did not have uniformly defined features as regards the existence of diagnosed arterial hypertension, the use of antihypertensive treatment, and, in the presence of the disease, the adequate control of blood pressure. Based on this evidence, therefore, the above interventions that have been approved for controlling body weight cannot also be used to control blood pressure levels. In addition, the extremely high cost and the locally limited availability of the above pharmaceuticals are factors that negatively affect their widespread use.

9. Future Directions

In the treatment of obesity-related hypertension in the future, it is important to implement a more holistic strategy. This would involve personalized lifestyle modification plans, referring patients to specialized dieticians or community/hospital programs that focus on lifestyle education while promoting the use of apps for self-management of blood pressure and weight loss. If these approaches prove ineffective, access to pharmacological weight loss or bariatric surgery should be considered [78]. However, currently available apps have limited functionality, which includes logging blood pressure, giving lifestyle advice, and providing information about hypertension. App development in the future should expand its scope to create a system capable of adapting flexibly to various forms of support, allowing individuals to self-manage their hypertension more effectively [79]. Furthermore, given the importance of obesity treatment in the treatment of arterial hypertension, it is necessary to conduct properly designed clinical studies in the future focusing on the effect

of anti-obesity drugs on blood pressure and, above all, on the benefit of these drugs in hypertensive patients. Such studies should be multicenter and randomized, they should study hypertensive patients and how they respond to weight management drugs, and perhaps they may compare anti-obesity therapies with existing antihypertensive medications.

10. Conclusions

In conclusion, managing excess body weight will have a major positive impact on regulating a number of cardiometabolic risk factors. The development of novel pharmacological therapies has given new weapons in the quiver of health professionals in this direction. Although the aforementioned pharmacological and surgical weight loss treatments are beneficial for blood pressure levels, they cannot be used instead of or in addition to existing hypertension medications that are intended to treat hypertension. Arterial hypertension is a complex disease caused by multifactorial pathophysiological mechanisms, only a portion of which contribute to the development of obesity. The treatment of hypertension has been established by the guidelines of scientific societies, and has been developed via several properly designed clinical trials aimed at determining the best course of action for hypertensive patients. Future research might lead to the development of combined pharmacological interventions targeted at improving many cardiovascular risk factors at once. Physicians dedicated to management of hypertension in collaboration with cardiometabolic and obesity units could initiate anti-obesity treatments in patients with hypertension and obesity, while using modern technology for self-management. This holistic approach should be offered regardless of the existence of diabetes or prediabetes, to reduce overall risk of cardiovascular disease by modifying two of the most important risk factors (hypertension and obesity).

Funding: This research received no external funding.

Conflicts of Interest: The authors declare no conflicts of interest.

References

1. Obesity. Available online: https://www.who.int/health-topics/obesity (accessed on 28 August 2024).
2. National Institutes of Health. Clinical Guidelines on the Identification, Evaluation, and Treatment of Overweight and Obesity in Adults—The Evidence Report. *Obes. Res.* **1998**, *6* (Suppl. S2), 51S–209S.
3. Powell-Wiley, T.M.; Poirier, P.; Burke, L.E.; Després, J.-P.; Gordon-Larsen, P.; Lavie, C.J.; Lear, S.A.; Ndumele, C.E.; Neeland, I.J.; Sanders, P.; et al. Obesity and Cardiovascular Disease: A Scientific Statement from the American Heart Association. *Circulation* **2021**, *143*, e984–e1010. [CrossRef]
4. Williams, B.; Mancia, G.; Spiering, W.; Agabiti Rosei, E.; Azizi, M.; Burnier, M.; Clement, D.; Coca, A.; De Simone, G.; Dominiczak, A.; et al. 2018 Practice Guidelines for the Management of Arterial Hypertension of the European Society of Hypertension and the European Society of Cardiology: ESH/ESC Task Force for the Management of Arterial Hypertension. *J. Hypertens.* **2018**, *36*, 2284–2309. [CrossRef]
5. Olsen, M.H.; Angell, S.Y.; Asma, S.; Boutouyrie, P.; Burger, D.; Chirinos, J.A.; Damasceno, A.; Delles, C.; Gimenez-Roqueplo, A.-P.; Hering, D.; et al. A Call to Action and a Lifecourse Strategy to Address the Global Burden of Raised Blood Pressure on Current and Future Generations: The Lancet Commission on Hypertension. *Lancet* **2016**, *388*, 2665–2712. [CrossRef]
6. Hypertension. Available online: https://www.who.int/news-room/fact-sheets/detail/hypertension (accessed on 28 August 2024).
7. Seravalle, G.; Grassi, G. Obesity and Hypertension. *Pharmacol. Res.* **2017**, *122*, 65–79. [CrossRef]
8. Fantin, F.; Giani, A.; Zoico, E.; Rossi, A.P.; Mazzali, G.; Zamboni, M. Weight Loss and Hypertension in Obese Subjects. *Nutrients* **2019**, *11*, 1667. [CrossRef]
9. Grassi, G. Assessment of Sympathetic Cardiovascular Drive in Human Hypertension: Achievements and Perspectives. *Hypertension* **2009**, *54*, 690–697. [CrossRef]
10. Shariq, O.A.; McKenzie, T.J. Obesity-Related Hypertension: A Review of Pathophysiology, Management, and the Role of Metabolic Surgery. *Gland. Surg.* **2020**, *9*, 80–93. [CrossRef]
11. Reid, I.A. Interactions between ANG II, Sympathetic Nervous System, and Baroreceptor Reflexes in Regulation of Blood Pressure. *Am. J. Physiol.* **1992**, *262*, E763–E778. [CrossRef]

12. Fisher, J.P.; Paton, J.F.R. The Sympathetic Nervous System and Blood Pressure in Humans: Implications for Hypertension. *J. Hum. Hypertens.* **2012**, *26*, 463–475. [CrossRef]
13. Mancia, G.; Grassi, G. The Autonomic Nervous System and Hypertension. *Circ. Res.* **2014**, *114*, 1804–1814. [CrossRef]
14. Mancia, G.; Grassi, G. The Central Sympathetic Nervous System in Hypertension. *Handb. Clin. Neurol.* **2013**, *117*, 329–335. [CrossRef]
15. El Meouchy, P.; Wahoud, M.; Allam, S.; Chedid, R.; Karam, W.; Karam, S. Hypertension Related to Obesity: Pathogenesis, Characteristics and Factors for Control. *Int. J. Mol. Sci.* **2022**, *23*, 12305. [CrossRef]
16. Da Silva, G.; Da Silva, M.; Nascimento, D.; Lima Silva, E.; Gouvêa, F.; De França Lopes, L.; Araújo, A.; Ferraz Pereira, K.; De Queiroz, T. Nitric Oxide as a Central Molecule in Hypertension: Focus on the Vasorelaxant Activity of New Nitric Oxide Donors. *Biology* **2021**, *10*, 1041. [CrossRef]
17. Stec, D.E.; Drummond, H.A.; Vera, T. Role of Carbon Monoxide in Blood Pressure Regulation. *Hypertension* **2008**, *51*, 597–604. [CrossRef]
18. Johnson, F.K.; Johnson, R.A.; Durante, W.; Jackson, K.E.; Stevenson, B.K.; Peyton, K.J. Metabolic Syndrome Increases Endogenous Carbon Monoxide Production to Promote Hypertension and Endothelial Dysfunction in Obese Zucker Rats. *Am. J. Physiol. Regul. Integr. Comp. Physiol.* **2006**, *290*, R601–R608. [CrossRef]
19. Neter, J.E.; Stam, B.E.; Kok, F.J.; Grobbee, D.E.; Geleijnse, J.M. Influence of Weight Reduction on Blood Pressure: A Meta-Analysis of Randomized Controlled Trials. *Hypertension* **2003**, *42*, 878–884. [CrossRef]
20. Aucott, L.; Rothnie, H.; McIntyre, L.; Thapa, M.; Waweru, C.; Gray, D. Long-Term Weight Loss from Lifestyle Intervention Benefits Blood Pressure?: A Systematic Review. *Hypertension* **2009**, *54*, 756–762. [CrossRef]
21. Koskinas, K.C.; Van Craenenbroeck, E.M.; Antoniades, C.; Blüher, M.; Gorter, T.M.; Hanssen, H.; Marx, N.; McDonagh, T.A.; Mingrone, G.; Rosengren, A.; et al. Obesity and Cardiovascular Disease: An ESC Clinical Consensus Statement. *Eur. Heart J.* **2024**, *45*, 4063–4098. [CrossRef]
22. McEvoy, J.W.; McCarthy, C.P.; Bruno, R.M.; Brouwers, S.; Canavan, M.D.; Ceconi, C.; Christodorescu, R.M.; Daskalopoulou, S.S.; Ferro, C.J.; Gerdts, E.; et al. 2024 ESC Guidelines for the Management of Elevated Blood Pressure and Hypertension. *Eur. Heart J.* **2024**, *45*, 3912–4018. [CrossRef]
23. Viera, A.J.; Kshirsagar, A.V.; Hinderliter, A.L. Lifestyle Modifications to Lower or Control High Blood Pressure: Is Advice Associated with Action? The Behavioral Risk Factor Surveillance Survey. *J. Clin. Hypertens.* **2008**, *10*, 105–111. [CrossRef]
24. Engeli, S.; Jordan, J. Novel Metabolic Drugs and Blood Pressure: Implications for the Treatment of Obese Hypertensive Patients? *Curr. Hypertens. Rep.* **2013**, *15*, 470–474. [CrossRef]
25. Allison, D.B.; Gadde, K.M.; Garvey, W.T.; Peterson, C.A.; Schwiers, M.L.; Najarian, T.; Tam, P.Y.; Troupin, B.; Day, W.W. Controlled-Release Phentermine/Topiramate in Severely Obese Adults: A Randomized Controlled Trial (EQUIP). *Obesity* **2012**, *20*, 330–342. [CrossRef]
26. Davidson, M.H.; Tonstad, S.; Oparil, S.; Schwiers, M.; Day, W.W.; Bowden, C.H. Changes in Cardiovascular Risk Associated with Phentermine and Topiramate Extended-Release in Participants With Comorbidities and a Body Mass Index $\geq$27 kg/m^2. *Am. J. Cardiol.* **2013**, *111*, 1131–1138. [CrossRef]
27. Aronne, L.J.; Wadden, T.A.; Peterson, C.; Winslow, D.; Odeh, S.; Gadde, K.M. Evaluation of Phentermine and Topiramate versus Phentermine/Topiramate Extended-release in Obese Adults. *Obesity* **2013**, *21*, 2163–2171. [CrossRef]
28. Garvey, W.T.; Ryan, D.H.; Look, M.; Gadde, K.M.; Allison, D.B.; Peterson, C.A.; Schwiers, M.; Day, W.W.; Bowden, C.H. Two-Year Sustained Weight Loss and Metabolic Benefits with Controlled-Release Phentermine/Topiramate in Obese and Overweight Adults (SEQUEL): A Randomized, Placebo-Controlled, Phase 3 Extension Study. *Am. J. Clin. Nutr.* **2012**, *95*, 297–308. [CrossRef]
29. Blüher, M.; Aras, M.; Aronne, L.J.; Batterham, R.L.; Giorgino, F.; Ji, L.; Pietiläinen, K.H.; Schnell, O.; Tonchevska, E.; Wilding, J.P.H. New Insights into the Treatment of Obesity. *Diabetes Obes. Metab.* **2023**, *25*, 2058–2072. [CrossRef]
30. Cohen, J.B.; Gadde, K.M. Weight Loss Medications in the Treatment of Obesity and Hypertension. *Curr. Hypertens. Rep.* **2019**, *21*, 16. [CrossRef]
31. Sahebkar, A.; Simental-Mendía, L.E.; Kovanen, P.T.; Pedone, C.; Simental-Mendía, M.; Cicero, A.F.G. Effects of Orlistat on Blood Pressure: A Systematic Review and Meta-Analysis of 27 Randomized Controlled Clinical Trials. *J. Am. Soc. Hypertens.* **2018**, *12*, 80–96. [CrossRef]
32. Sharma, A.M.; Golay, A. Effect of Orlistat-Induced Weight Loss on Blood Pressure and Heart Rate in Obese Patients with Hypertension. *J. Hypertens.* **2002**, *20*, 1873–1878. [CrossRef]
33. Al-Tahami, B.A.M.; Ismail, A.A.A.-S.; Bee, Y.T.G.; Awang, S.A.; Salha Wan Abdul Rani, W.R.; Sanip, Z.; Rasool, A.H.G. The Effects of Anti-Obesity Intervention with Orlistat and Sibutramine on Microvascular Endothelial Function. *Clin. Hemorheol. Microcirc.* **2015**, *59*, 323–334. [CrossRef]
34. Billes, S.K.; Sinnayah, P.; Cowley, M.A. Naltrexone/Bupropion for Obesity: An Investigational Combination Pharmacotherapy for Weight Loss. *Pharmacol. Res.* **2014**, *84*, 1–11. [CrossRef]
35. Greenway, F.L.; Fujioka, K.; Plodkowski, R.A.; Mudaliar, S.; Guttadauria, M.; Erickson, J.; Kim, D.D.; Dunayevich, E. Effect of Naltrexone plus Bupropion on Weight Loss in Overweight and Obese Adults (COR-I): A Multicentre, Randomised, Double-Blind, Placebo-Controlled, Phase 3 Trial. *Lancet* **2010**, *376*, 595–605. [CrossRef]

36. Apovian, C.M.; Aronne, L.; Rubino, D.; Still, C.; Wyatt, H.; Burns, C.; Kim, D.; Dunayevich, E.; for the COR-II Study Group. A Randomized, Phase 3 Trial of Naltrexone SR/Bupropion SR on Weight and Obesity-related Risk Factors (COR-II). *Obesity* **2013**, *21*, 935–943. [CrossRef]
37. Wadden, T.A.; Foreyt, J.P.; Foster, G.D.; Hill, J.O.; Klein, S.; O'Neil, P.M.; Perri, M.G.; Pi-Sunyer, F.X.; Rock, C.L.; Erickson, J.S.; et al. Weight Loss With Naltrexone SR/Bupropion SR Combination Therapy as an Adjunct to Behavior Modification: The COR-BMOD Trial. *Obesity* **2011**, *19*, 110–120. [CrossRef]
38. Hollander, P.; Gupta, A.K.; Plodkowski, R.; Greenway, F.; Bays, H.; Burns, C.; Klassen, P.; Fujioka, K.; for the COR-Diabetes Study Group. Effects of Naltrexone Sustained- Release/Bupropion Sustained-Release Combination Therapy on Body Weight and Glycemic Parameters in Overweight and Obese Patients with Type 2 Diabetes. *Diabetes Care* **2013**, *36*, 4022–4029. [CrossRef]
39. Jiang, Q.; Velu, P.; Sohouli, M.H.; Ziamanesh, F.; Shojaie, S.; Fatahi, S.; Li, Q. The Effects of Bupropion Alone and Combined with Naltrexone on Blood Pressure and CRP Concentration: A Systematic Review and Meta-regression Analysis of Randomized Controlled Trials. *Eur. J. Clin. Investig.* **2023**, *54*, e14118. [CrossRef]
40. Cataldi, M.; Cignarelli, A.; Giallauria, F.; Muscogiuri, G.; Barrea, L.; Savastano, S.; Colao, A.; on behalf of Obesity Programs of Nutrition, Education, Research and Assessment (OPERA) Group. Cardiovascular Effects of Antiobesity Drugs: Are the New Medicines All the Same? *Int. J. Obes. Suppl.* **2020**, *10*, 14–26. [CrossRef]
41. Arias, H.R. Is the Inhibition of Nicotinic Acetylcholine Receptors by Bupropion Involved in Its Clinical Actions? *Int. J. Biochem. Cell Biol.* **2009**, *41*, 2098–2108. [CrossRef]
42. Fisman, E.Z.; Tenenbaum, A. The Dual Glucose-Dependent Insulinotropic Polypeptide (GIP) and Glucagon-like Peptide-1 (GLP-1) Receptor Agonist Tirzepatide: A Novel Cardiometabolic Therapeutic Prospect. *Cardiovasc. Diabetol.* **2021**, *20*, 225. [CrossRef]
43. Hu, E.-H.; Tsai, M.-L.; Lin, Y.; Chou, T.-S.; Chen, T.-H. A Review and Meta-Analysis of the Safety and Efficacy of Using Glucagon-like Peptide-1 Receptor Agonists. *Medicina* **2024**, *60*, 357. [CrossRef]
44. Puglisi, S.; Rossini, A.; Poli, R.; Dughera, F.; Pia, A.; Terzolo, M.; Reimondo, G. Effects of SGLT2 Inhibitors and GLP-1 Receptor Agonists on Renin-Angiotensin-Aldosterone System. *Front. Endocrinol.* **2021**, *12*, 738848. [CrossRef]
45. Ard, J.; Fitch, A.; Fruh, S.; Herman, L. Weight Loss and Maintenance Related to the Mechanism of Action of Glucagon-Like Peptide 1 Receptor Agonists. *Adv. Ther.* **2021**, *38*, 2821–2839. [CrossRef]
46. Pi-Sunyer, X.; Astrup, A.; Fujioka, K.; Greenway, F.; Halpern, A.; Krempf, M.; Lau, D.C.W.; Le Roux, C.W.; Violante Ortiz, R.; Jensen, C.B.; et al. A Randomized, Controlled Trial of 3.0 Mg of Liraglutide in Weight Management. *N. Engl. J. Med.* **2015**, *373*, 11–22. [CrossRef]
47. Davies, M.J.; Bergenstal, R.; Bode, B.; Kushner, R.F.; Lewin, A.; Skjøth, T.V.; Andreasen, A.H.; Jensen, C.B.; DeFronzo, R.A.; for the NN8022-1922 Study Group. Efficacy of Liraglutide for Weight Loss Among Patients with Type 2 Diabetes: The SCALE Diabetes Randomized Clinical Trial. *JAMA* **2015**, *314*, 687. [CrossRef]
48. Wadden, T.A.; Hollander, P.; Klein, S.; Niswender, K.; Woo, V.; Hale, P.M.; Aronne, L.; on behalf of the NN8022-1923 Investigators. Weight Maintenance and Additional Weight Loss with Liraglutide after Low-Calorie-Diet-Induced Weight Loss: The SCALE Maintenance Randomized Study. *Int. J. Obes.* **2013**, *37*, 1443–1451. [CrossRef]
49. Wilding, J.P.H.; Batterham, R.L.; Calanna, S.; Davies, M.; Van Gaal, L.F.; Lingvay, I.; McGowan, B.M.; Rosenstock, J.; Tran, M.T.D.; Wadden, T.A.; et al. Once-Weekly Semaglutide in Adults with Overweight or Obesity. *N. Engl. J. Med.* **2021**, *384*, 989–1002. [CrossRef]
50. Davies, M.; Færch, L.; Jeppesen, O.K.; Pakseresht, A.; Pedersen, S.D.; Perreault, L.; Rosenstock, J.; Shimomura, I.; Viljoen, A.; Wadden, T.A.; et al. Semaglutide 2·4 Mg Once a Week in Adults with Overweight or Obesity, and Type 2 Diabetes (STEP 2): A Randomised, Double-Blind, Double-Dummy, Placebo-Controlled, Phase 3 Trial. *Lancet* **2021**, *397*, 971–984. [CrossRef]
51. Wadden, T.A.; Bailey, T.S.; Billings, L.K.; Davies, M.; Frias, J.P.; Koroleva, A.; Lingvay, I.; O'Neil, P.M.; Rubino, D.M.; Skovgaard, D.; et al. Effect of Subcutaneous Semaglutide vs Placebo as an Adjunct to Intensive Behavioral Therapy on Body Weight in Adults with Overweight or Obesity: The STEP 3 Randomized Clinical Trial. *JAMA* **2021**, *325*, 1403. [CrossRef]
52. Rubino, D.; Abrahamsson, N.; Davies, M.; Hesse, D.; Greenway, F.L.; Jensen, C.; Lingvay, I.; Mosenzon, O.; Rosenstock, J.; Rubio, M.A.; et al. Effect of Continued Weekly Subcutaneous Semaglutide vs Placebo on Weight Loss Maintenance in Adults with Overweight or Obesity: The STEP 4 Randomized Clinical Trial. *JAMA* **2021**, *325*, 1414. [CrossRef]
53. Kim, M.; Platt, M.J.; Shibasaki, T.; Quaggin, S.E.; Backx, P.H.; Seino, S.; Simpson, J.A.; Drucker, D.J. GLP-1 Receptor Activation and Epac2 Link Atrial Natriuretic Peptide Secretion to Control of Blood Pressure. *Nat. Med.* **2013**, *19*, 567–575. [CrossRef]
54. Goud, A.; Zhong, J.; Peters, M.; Brook, R.D.; Rajagopalan, S. GLP-1 Agonists and Blood Pressure: A Review of the Evidence. *Curr. Hypertens. Rep.* **2016**, *18*, 16. [CrossRef]
55. Rosenstock, J.; Wysham, C.; Frías, J.P.; Kaneko, S.; Lee, C.J.; Fernández Landó, L.; Mao, H.; Cui, X.; Karanikas, C.A.; Thieu, V.T. Efficacy and Safety of a Novel Dual GIP and GLP-1 Receptor Agonist Tirzepatide in Patients with Type 2 Diabetes (SURPASS-1): A Double-Blind, Randomised, Phase 3 Trial. *Lancet* **2021**, *398*, 143–155. [CrossRef]
56. Frías, J.P.; Davies, M.J.; Rosenstock, J.; Pérez Manghi, F.C.; Fernández Landó, L.; Bergman, B.K.; Liu, B.; Cui, X.; Brown, K. Tirzepatide versus Semaglutide Once Weekly in Patients with Type 2 Diabetes. *N. Engl. J. Med.* **2021**, *385*, 503–515. [CrossRef]

57. Ludvik, B.; Giorgino, F.; Jódar, E.; Frias, J.P.; Fernández Landó, L.; Brown, K.; Bray, R.; Rodríguez, Á. Once-Weekly Tirzepatide versus Once-Daily Insulin Degludec as Add-on to Metformin with or without SGLT2 Inhibitors in Patients with Type 2 Diabetes (SURPASS-3): A Randomised, Open-Label, Parallel-Group, Phase 3 Trial. *Lancet* **2021**, *398*, 583–598. [CrossRef]
58. Del Prato, S.; Kahn, S.E.; Pavo, I.; Weerakkody, G.J.; Yang, Z.; Doupis, J.; Aizenberg, D.; Wynne, A.G.; Riesmeyer, J.S.; Heine, R.J.; et al. Tirzepatide versus Insulin Glargine in Type 2 Diabetes and Increased Cardiovascular Risk (SURPASS-4): A Randomised, Open-Label, Parallel-Group, Multicentre, Phase 3 Trial. *Lancet* **2021**, *398*, 1811–1824. [CrossRef]
59. Dahl, D.; Onishi, Y.; Norwood, P.; Huh, R.; Bray, R.; Patel, H.; Rodríguez, Á. Effect of Subcutaneous Tirzepatide vs Placebo Added to Titrated Insulin Glargine on Glycemic Control in Patients with Type 2 Diabetes: The SURPASS-5 Randomized Clinical Trial. *JAMA* **2022**, *327*, 534. [CrossRef]
60. Jastreboff, A.M.; Aronne, L.J.; Ahmad, N.N.; Wharton, S.; Connery, L.; Alves, B.; Kiyosue, A.; Zhang, S.; Liu, B.; Bunck, M.C.; et al. Tirzepatide Once Weekly for the Treatment of Obesity. *N. Engl. J. Med.* **2022**, *387*, 205–216. [CrossRef]
61. De Lemos, J.A.; Linetzky, B.; Le Roux, C.W.; Laffin, L.J.; Vongpatanasin, W.; Fan, L.; Hemmingway, A.; Ahmad, N.N.; Bunck, M.C.; Stefanski, A. Tirzepatide Reduces 24-Hour Ambulatory Blood Pressure in Adults with Body Mass Index $\geq$27 Kg/m^2: SURMOUNT-1 Ambulatory Blood Pressure Monitoring Substudy. *Hypertension* **2024**, *81*, e41–e43. [CrossRef]
62. Garvey, W.T.; Frias, J.P.; Jastreboff, A.M.; Le Roux, C.W.; Sattar, N.; Aizenberg, D.; Mao, H.; Zhang, S.; Ahmad, N.N.; Bunck, M.C.; et al. Tirzepatide Once Weekly for the Treatment of Obesity in People with Type 2 Diabetes (SURMOUNT-2): A Double-Blind, Randomised, Multicentre, Placebo-Controlled, Phase 3 Trial. *Lancet* **2023**, *402*, 613–626. [CrossRef]
63. Wadden, T.A.; Chao, A.M.; Machineni, S.; Kushner, R.; Ard, J.; Srivastava, G.; Halpern, B.; Zhang, S.; Chen, J.; Bunck, M.C.; et al. Tirzepatide after Intensive Lifestyle Intervention in Adults with Overweight or Obesity: The SURMOUNT-3 Phase 3 Trial. *Nat. Med.* **2023**, *29*, 2909–2918. [CrossRef]
64. Aronne, L.J.; Sattar, N.; Horn, D.B.; Bays, H.E.; Wharton, S.; Lin, W.-Y.; Ahmad, N.N.; Zhang, S.; Liao, R.; Bunck, M.C.; et al. Continued Treatment With Tirzepatide for Maintenance of Weight Reduction in Adults with Obesity: The SURMOUNT-4 Randomized Clinical Trial. *JAMA* **2024**, *331*, 38. [CrossRef]
65. Kanbay, M.; Copur, S.; Siriopol, D.; Yildiz, A.B.; Gaipov, A.; Van Raalte, D.H.; Tuttle, K.R. Effect of Tirzepatide on Blood Pressure and Lipids: A Meta-analysis of Randomized Controlled Trials. *Diabetes Obes. Metab.* **2023**, *25*, 3766–3778. [CrossRef]
66. Lingvay, I.; Mosenzon, O.; Brown, K.; Cui, X.; O'Neill, C.; Fernández Landó, L.; Patel, H. Systolic Blood Pressure Reduction with Tirzepatide in Patients with Type 2 Diabetes: Insights from SURPASS Clinical Program. *Cardiovasc. Diabetol.* **2023**, *22*, 66. [CrossRef]
67. Lv, X.; Wang, H.; Chen, C.; Zhao, Y.; Li, K.; Wang, Y.; Wang, L.; Fu, S.; Liu, J. The Effect of Tirzepatide on Weight, Lipid Metabolism and Blood Pressure in Overweight/Obese Patients with Type 2 Diabetes Mellitus: A Systematic Review and Meta-Analysis. *Diabetes Metab. Syndr. Obes.* **2024**, *17*, 701–714. [CrossRef]
68. Taktaz, F.; Fontanella, R.A.; Scisciola, L.; Pesapane, A.; Basilicata, M.G.; Ghosh, P.; Franzese, M.; Tortorella, G.; Puocci, A.; Vietri, M.T.; et al. Bridging the Gap between GLP1-Receptor Agonists and Cardiovascular Outcomes: Evidence for the Role of Tirzepatide. *Cardiovasc. Diabetol.* **2024**, *23*, 242. [CrossRef]
69. Cho, Y.K.; La Lee, Y.; Jung, C.H. The Cardiovascular Effect of Tirzepatide: A Glucagon-Like Peptide-1 and Glucose-Dependent Insulinotropic Polypeptide Dual Agonist. *J. Lipid Atheroscler.* **2023**, *12*, 213. [CrossRef]
70. Pirro, V.; Roth, K.D.; Lin, Y.; Willency, J.A.; Milligan, P.L.; Wilson, J.M.; Ruotolo, G.; Haupt, A.; Newgard, C.B.; Duffin, K.L. Effects of Tirzepatide, a Dual GIP and GLP-1 RA, on Lipid and Metabolite Profiles in Subjects with Type 2 Diabetes. *J. Clin. Endocrinol. Metab.* **2022**, *107*, 363–378. [CrossRef]
71. Woodman, R.J.; Chew, G.T.; Watts, G.F. Mechanisms, Significance and Treatment of Vascular Dysfunction in Type 2 Diabetes Mellitus: Focus on Lipid-Regulating Therapy. *Drugs* **2005**, *65*, 31–74. [CrossRef]
72. Mancia, G.; Kreutz, R.; Brunström, M.; Burnier, M.; Grassi, G.; Januszewicz, A.; Muiesan, M.L.; Tsioufis, K.; Agabiti-Rosei, E.; Algharably, E.A.E.; et al. 2023 ESH Guidelines for the Management of Arterial Hypertension The Task Force for the Management of Arterial Hypertension of the European Society of Hypertension: Endorsed by the International Society of Hypertension (ISH) and the European Renal Association (ERA). *J. Hypertens.* **2023**, *41*, 1874–2071. [CrossRef]
73. Bottino, R.; Carbone, A.; Formisano, T.; D'Elia, S.; Orlandi, M.; Sperlongano, S.; Molinari, D.; Castaldo, P.; Palladino, A.; Barbareschi, C.; et al. Cardiovascular Effects of Weight Loss in Obese Patients with Diabetes: Is Bariatric Surgery the Additional Arrow in the Quiver? *Life* **2023**, *13*, 1552. [CrossRef]
74. Wang, L.; Lin, M.; Yu, J.; Fan, Z.; Zhang, S.; Lin, Y.; Chen, X.; Peng, F. The Impact of Bariatric Surgery Versus Non-Surgical Treatment on Blood Pressure: Systematic Review and Meta-Analysis. *Obes. Surg.* **2021**, *31*, 4970–4984. [CrossRef]
75. Wiggins, T.; Guidozzi, N.; Welbourn, R.; Ahmed, A.R.; Markar, S.R. Association of Bariatric Surgery with All-Cause Mortality and Incidence of Obesity-Related Disease at a Population Level: A Systematic Review and Meta-Analysis. *PLoS Med.* **2020**, *17*, e1003206. [CrossRef]
76. Hallersund, P.; Sjöström, L.; Olbers, T.; Lönroth, H.; Jacobson, P.; Wallenius, V.; Näslund, I.; Carlsson, L.M.; Fändriks, L. Gastric Bypass Surgery Is Followed by Lowered Blood Pressure and Increased Diuresis—Long Term Results from the Swedish Obese Subjects (SOS) Study. *PLoS ONE* **2012**, *7*, e49696. [CrossRef]
77. Samson, R.; Ayinapudi, K.; Le Jemtel, T.H.; Oparil, S. Obesity, Hypertension, and Bariatric Surgery. *Curr. Hypertens. Rep.* **2020**, *22*, 46. [CrossRef]

78. Antza, C.; Grassi, G.; Weber, T.; Persu, A.; Jordan, J.; Nilsson, P.M.; Redon, J.; Stabouli, S.; Kreutz, R.; Kotsis, V. Assessment and Management of Patients with Obesity and Hypertension in European Society of Hypertension Excellence Centres. A Survey from the ESH Working Group on Diabetes and Metabolic Risk Factors. *Blood Press.* **2024**, *33*, 2317256. [CrossRef]
79. Hui, C.Y.; Creamer, E.; Pinnock, H.; McKinstry, B. Apps to Support Self-Management for People with Hypertension: Content Analysis. *JMIR mHealth uHealth* **2019**, *7*, e13257. [CrossRef]

Disclaimer/Publisher's Note: The statements, opinions and data contained in all publications are solely those of the individual author(s) and contributor(s) and not of MDPI and/or the editor(s). MDPI and/or the editor(s) disclaim responsibility for any injury to people or property resulting from any ideas, methods, instructions or products referred to in the content.

biomedicines

Review

The Role of Ranolazine in the Treatment of Ventricular Tachycardia and Atrial Fibrillation: A Narrative Review of the Clinical Evidence

Kyosuke Murai [1], Amir Vasigh [1], Tamás Alexy [2], Kálmán Tóth [1,3] and László Czopf [1,*]

[1] 1st Department of Medicine, Medical School, University of Pécs, Ifjúság útja 13, H-7624 Pécs, Hungary; toth.kalman@pte.hu (K.T.)
[2] Department of Medicine, Division of Cardiology, University of Minnesota, Minneapolis, MN 55127, USA; alexy001@umn.edu
[3] Szentágothai János Research Centre, Medical School, University of Pécs, Ifjúság útja 20, H-7624 Pécs, Hungary
* Correspondence: czopf.laszlo@pte.hu

Abstract: Cardiac arrhythmias are among the leading causes of morbidity and mortality worldwide. While antiarrhythmic drugs traditionally represent the first-line management strategy, their use is often limited by profound proarrhythmic effects. Several studies, including randomized control trials (RCTs), have demonstrated the antiarrhythmic efficacy of ranolazine, which is registered as an antianginal agent, while also establishing its safety profile. This review compiles clinical evidence investigating the antiarrhythmic properties of ranolazine, focusing primarily on ventricular tachycardia (VT) and atrial fibrillation (AF), as they are common rhythm abnormalities with serious complications. Data from RCTs indicate that ranolazine reduces VT incidence, although this effect is not universal. Therefore, we attempt to better describe the patient population that gains the most benefit from ranolazine due to VT suppression. Additionally, ranolazine is known to enhance the conversion rate of AF to sinus rhythm when combined with other antiarrhythmic drugs such as amiodarone, highlighting its synergistic effect in the atrium without provoking ventricular dysrhythmias. Despite the heterogeneity in the currently available data, ranolazine appears to be an effective and safe option for the management of various arrhythmias.

Keywords: ranolazine; ventricular tachycardia; atrial fibrillation; antiarrhythmic agents

1. Introduction

Cardiac arrhythmias not only represent a serious challenge for the field of cardiovascular medicine worldwide but also significantly contribute to morbidity and mortality. Historically, antiarrhythmic drugs represented the therapeutic mainstay to suppress a wide range of arrhythmias. The Cardiac Arrhythmia Suppression Trial (CAST) and subsequent studies showed that, while these drugs are indeed effective in reducing the incidence of some arrhythmias, they may lead to an increased risk of developing others, as well as to sudden cardiac death. This perceived proarrhythmogenic effect led to an overall decline in their utilization and they are now restricted to a limited range of indications [1–3]. In contrast, ablation therapy has become an increasingly safer procedure; thus, it has become popular in the management of various arrhythmias, including atrial fibrillation (AF) and ventricular tachycardia (VT). Current therapeutic guidelines recommend catheter ablation in patients with symptomatic AF in whom antiarrhythmic drugs have been ineffective, contraindicated, or not tolerated, or when they are not preferred. In selected patients with symptomatic paroxysmal AF, catheter ablation can also be used as first-line therapy [4,5]. Catheter ablation is an important treatment option for ventricular arrhythmia and in situations when antiarrhythmic drugs are ineffective, not tolerated, or not desired by patients [6]. It is important to note, however, that the high success rate of ablation therapy

may be limited to certain clinical scenarios. For instance, it is clearly effective in the management of paroxysmal AF, yet its success rate for the treatment of persistent or permanent AF is lower [7]. Additionally, it is an invasive intervention which carries some risks for complications and requires specialized expertise and costly equipment investments.

In many clinical scenarios, amiodarone remains a frequently used drug. One of the major drawbacks of amiodarone, however, is its long-term side effect profile: it may adversely affect the structure or function of various organ systems, such as the lungs, liver, thyroid, nervous system, and the skin. The delayed onset of action of the oral formulation is another challenge, particularly when an immediate therapeutic effect is desired [8]. On the other hand, administering an intravenous bolus and continuous infusion may provoke hypotension and worsening cardiogenic shock in select patient populations with severely reduced left or right ventricular function.

Considering these challenges, ranolazine, a piperazine derivative, has been proposed as a potential alternative therapy for arrhythmia management, primarily owing to its excellent and well-established safety profile. It was initially approved by the Food and Drug Administration (FDA) in 2006 for the management of chronic stable angina pectoris. Multiple studies have since demonstrated its antiarrhythmic effect, a property that may present a promising future for this drug. This review was prepared to provide a brief summary on the relevant mechanisms of VT and AF and to summarize the limited clinical data available on the use of ranolazine as an antiarrhythmic agent for the management of these rhythm disorders. Figure 1 presents the main mechanism of action of ranolazine.

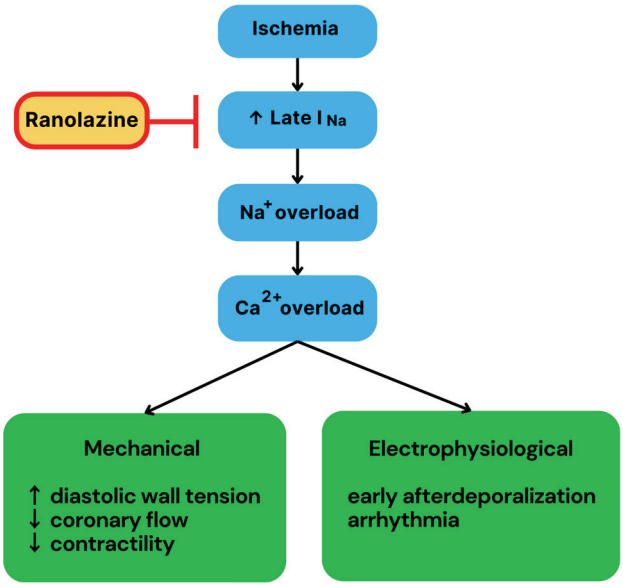


Figure 1. Summary of the most clinically important effects of ranolazine.

VT typically occurs in patients with underlying structural heart disease that most commonly results from myocardial ischemia. However, nonischemic etiologies, such as idiopathic dilated cardiomyopathy, hypertrophic cardiomyopathy, infiltrative diseases including sarcoidosis, congenital and valvular heart disease, may also increase the risk of clinically significant VT. Genetic cardiomyopathies and conduction system disorders, such as long QT and Brugada syndromes, may lead to polymorphic VT in the absence of structural cardiac abnormalities. There are several known mechanisms to induce VT, including triggered activity secondary to early afterdepolarization (EAD) or delayed afterdepolarization (DAD), automaticity, and reentry. EAD occurs during late phase 2 or early phase 3 of the action potential, secondary to its prolonged duration owing to an abnormality in of the following: (1) increased late I_{Na}; (2) inward Ca current; (3) sodium–calcium exchange current; (4) decreased outward potassium current. EAD is the trigger for torsade de pointes (TdP). DAD occurs after complete membrane repolarization and is caused by

intracellular calcium overload. It may develop in the setting of tachycardia, catecholamine excess, and digitalis toxicity. Given their mechanisms, both EAD and DAD are sensitive to non-dihydropyridine calcium channel blockers, late I_{Na} blockers, and sodium–calcium exchange blockers. Triggered activity can be the underlying cause for sustained VT in the setting of ischemic, dilated, and hypertrophic cardiomyopathies, especially when the arrhythmia originates from a well-defined myocardial territory. Automaticity is a less common cause for focal VT. In the acute phase of MI or during transient ischemia, an increased extracellular potassium concentration leads to partial depolarization in the resting phase and may initiate spontaneous activity. Re-entry due to scarring is the most common mechanism of sustained monomorphic VT in patients with ischemic heart disease. Since re-entry typically occurs at fixed anatomical sites, VT ablation is the optimal treatment option in such cases [6,9,10].

There are numerous etiologies of AF, including advanced age, smoking, obesity, alcohol consumption, increased height, hypertension, diabetes mellitus, coronary artery disease, heart failure, valvular disease, and prior cardiac surgery. Other conditions include chronic kidney disease, hyperthyroidism, obstructive sleep apnea, and sepsis owing to the significant catecholamine release or external administration for hypotension management. Genetics may also have an important role. AF often arises from ectopic firing of myocyte sleeves within the pulmonary veins (PVs) draining into of the left atrium. Electrophysiological abnormalities of the PVs are frequently attributed to abnormal shortening of action potential duration and calcium mishandling. A diastolic leak of calcium from sarcoplasmic reticulum enhances inward sodium current via the sodium–calcium exchange, thereby leading to EAD or DAD. The progression of paroxysmal AF to persistent or permanent AF often results from atrial remodeling. Factors contributing to atrial remodeling include stretch-induced fibrosis, hypocontractility, fatty infiltration, inflammation, vascular remodeling, ischemia, ion channel dysfunction, and calcium instability. Aging of the population can shift the primary trigger mechanism for AF, thereby influencing the most appropriate therapeutic interventions. The longer the duration of AF (the greater the AF burden), the more likely its progression to a more permanent form. However, clinical evidence has failed to show a clear association between baseline AF burden and AF-related outcomes such as all-cause mortality and heart failure. Therefore, AF burden cannot be used as a sole factor guiding management [4,5,11,12].

In the ensuing sections, we aimed to answer the following primary question: Does ranolazine administration reduce the prevalence or severity of cardiac rhythm disorders, specifically VT and AF, when compared to placebo or the standard of care among patients with a history of arrhythmias or at risk for developing arrhythmias?

2. Methods

The authors performed a literature search on the PubMed and Embase databases in October 2023, using the following search terms: "ranolazine AND arrhythmia cardiac", or "ranolazine AND heart arrhythmia". All relevant articles published in the English language were carefully examined, specifically those focusing on the primary question detailed above. The scope of this review included observational studies, clinical trials, and randomized controlled studies. Reviews and summaries of molecular studies that did not include human observations were reviewed yet not included when synthesizing and aggregating the data. Additionally, case reports and articles lacking full-text availability were excluded.

3. Results

Following the noted inclusion and exclusion criteria, 11 studies were included in the final synthesized review. Basic study information, the performed interventions, and outcomes are summarized in Tables 1 and 2.

Table 1. Effect of ranolazine on reducing VT burden or severity.

Authors	Population	Intervention/Comparison	Outcome
Scirica (MERLIN-TIMI 36) [13]	Randomized, double-blind study; 6351 patients with NSTEMI or unstable angina randomly assigned to ranolazine (63 ± 11 years, 2093 males) or placebo (63 ± 11 years, 2031 males)	IV ranolazine with 200 mg bolus then 80 mg/h infusion for 12–96 h, then PO 1000 mg ranolazine BID. Continuous ECG monitoring for the first 7 days	The number of VT episodes exceeding 8 beats was significantly reduced in the ranolazine group vs. placebo (166 [5.3%] vs. 265 [8.3%]; $p < 0.001$)
Zareba, Younis (RAID trial) [14,15]	Randomized, double-blind, placebo-controlled, multicenter, intention-to-treat study; 1012 patients with ICD randomly divided into ranolazine (64.3 ± 10.3 years, 410 males) and placebo (64.2 ± 9.9 years, 416 males) groups	Ranolazine 500 mg BID for 1 week, increased to 1000 mg BID if dosage tolerated. Follow-up for mean 28.3 ± 15.8 months	Significantly reduced recurrence of VT/VF requiring ATP or ICD shock in the ranolazine group vs. placebo (433 vs. 650, HR = 0.70 [0.51–0.96]; $p = 0.028$). The benefit of ranolazine was limited to the following subgroups: (1) ranolazine monotherapy (HR = 0.68 [0.55–0.84] vs. HR = 1.33 [0.90–1.96], $p = 0.003$); (2) implanted CRT-D (HR = 0.64 [0.47–0.86] vs. HR = 0.94 [0.74–1.18]; $p = 0.047$); (3) no AF (HR = 0.66 [0.54–0.81] vs. HR = 1.56 [1.02–2.39], $p = 0.003$)

Abbreviations: NSTEMI: non-ST-elevation myocardial infarction; VT: ventricular tachycardia; ICD: implantable cardioverter defibrillator; BID: twice daily; VF: ventricular fibrillation; ATP: anti-tachycardia pacing; CRT-D: cardiac resynchronization therapy–defibrillator; AF: atrial fibrillation; IV: intravenous; PO: per os; HR: hazards ratio; mg: milligram.

Table 2. Effect of ranolazine on AF prevention and on AF conversion to sinus rhythm.

Authors	Population	Intervention/Comparison	Outcome
Scirica (MERLIN-TIMI 36) [13,16]	Randomized, double-blind study; 6351 patients with NSTEMI or unstable angina randomly assigned to ranolazine (63 ± 11 years, 2093 males) or placebo (63 ± 11 years, 2031 males)	IV ranolazine 200 mg bolus followed by 80 mg/h infusion for 12–96 h, then 1000 mg PO BID. Continuous ECG monitoring for the first 7 days, follow-up for 12 months	Trend towards reduced AF occurrence within the first 7 days with ranolazine vs. placebo (55 [1.7%] vs. 75 [2.4%], HR = 0.74 [0.52–1.05]; $p = 0.08$). Reduced clinically significant AF * after 12 months in ranolazine group vs. placebo (2.9% vs. 4.1%, HR = 0.71 [0.55–0.92]; $p = 0.01$)
Koskinas [17]	Randomized, single-blind study; 121 patients with symptomatic AF (<48 h) randomly assigned to amiodarone plus ranolazine (66 ± 11 years, 25 males) or amiodarone-only (64 ± 9 years, 29 males)	Amiodarone: 5 mg/kg IV loading dose in 1 h then 50 mg/h for 24 h or until cardioversion Ranolazine: 1500 mg PO at randomization	Amiodarone plus ranolazine significantly increased AF conversion rate within 24 h (53 [87%] vs. 42 [70%]; $p = 0.024$) and reduced mean time to AF conversion (10.2 ± 3.3 vs.13.3 ± 4.1 h; $p = 0.001$)
Tsanaxidis [18]	Randomized, single-center study; 173 patients with recent-onset AF randomly assigned to amiodarone plus ranolazine (92, 70 ± 10 years, 38 males) and amiodarone-only (81, 67 ± 11 years, 41 males)	Amiodarone: 5 mg/kg IV loading dose, 50 mg/h maintenance infusion. After conversion, 200 mg PO BID for a week and then 200 mg PO daily for a week. Ranolazine: 1000 mg POthen 375 mg BID 6 h after arrhythmia termination	Amiodarone plus ranolazine significantly increased conversion of AF within 24 h (90 [98%] vs. 47 [58%]; $p < 0.001$) and reduced mean time to AF termination (8.6 ± 2.8 h vs. 19.4 ± 4.4 h; $p < 0.0001$) vs. the amiodarone-only group
Simopoulos [19]	Randomized, single-blind study; 511 patients with post-CABG AF randomly assigned to amiodarone plus ranolazine (65.3 ± 9.5 years) or amiodarone-only (65.5 ± 9.6 years)	Amiodarone: 300 mg IV in 30 min, followed by 1125 mg in 36 h Ranolazine: 500 mg PO, 375 mg after 6 h and then 375 mg PO BID	Amiodarone plus ranolazine increased AF conversion to sinus rhythm significantly within 24 h (235 [91.8%] vs. 37 [14.5%]; $p < 0.0001$) and reduced mean time of AF conversion (10.4 ± 4.5 h vs. 24.3 ± 4.6 h; $p < 0.0001$) vs. amiodarone alone
Reiffel (Harmony trial) [20]	Randomized, double-blind, placebo-controlled, intention-to-treat study; 131 patients with paroxysmal AF randomized to (1) placebo (72 ± 8.4 years, 13 males); (2) ranolazine 750 mg (70 ± 10.8 years, 10 males); (3) dronedarone 225 mg (75 ± 7.8 years, 10 males); (4) dronedarone 150 mg plus ranolazine 750 mg (73 ± 9.4 years, 15 males); (5) dronedarone 225 mg plus ranolazine 750 mg (71 ± 7.1 years, 15 males)	Each given BID for 12 weeks	Significantly reduced AF burden ** in group 5 vs. placebo (4.8% vs. 11.1%; $p = 0.008$)

Table 2. *Cont.*

Authors	Population	Intervention/Comparison	Outcome
De Ferrari (Raffaello trial) [21]	Randomized, double-blind, placebo-controlled, multicenter, intention-to-treat study; 238 patients with persistent AF (7 days to 6 months) randomly assigned to: (1) placebo (55, 65.2 ± 9.5 years, 41 males); (2) ranolazine 375 mg (65, 66.9 ± 11.8 years, 46 males); (3) ranolazine 500 mg (60, 65.5 ± 8.5 years, 51 males); (4) ranolazine 750 mg (58, 63.6 ± 11.3 years, 46 males)	Each given BID for 16 weeks after electrical cardioversion	Significantly reduced AF recurrence in group 3 vs. placebo when patients were still in sinus rhythm after 48 h (HR = 0.56, [0.31–1.01]; $p = 0.0495$)
Miles [22]	Retrospective, single-center cohort study; 393 patients after CABG received either amiodarone (211, 64.9 ± 10.9 years, 162 males) or ranolazine (182, 66.7 ± 9.3, 127 males)	Amiodarone: 400 mg daily preoperatively (7 days prior to elective CABG or immediately before urgent CABG), 200 mg BID postoperatively for 10–14 days Ranolazine: 1500 mg on the day prior to elective CABG or on the day of urgent CABG. 1000 mg BID postoperatively for 10–14 days	Ranolazine significantly reduced the incidence of new-onset AF compared to amiodarone (17.5% vs. 26.5%; $p = 0.035$)
Hammond [23]	Retrospective, single-center cohort study; after matched-pair analysis, 114 patients post-CABG or valve surgery received either ranolazine (57, 60.3 ± 11.1 years, 38 males) or placebo (57, 59.6 ± 11.5 years, 38 males)	Preoperative ranolazine 1000 mg on the morning of surgery, 1000 mg BID afterwards for 7 days	Ranolazine significantly reduced the incidence of new-onset AF vs. placebo (10.5% vs. 45.6%; OR = 0.09 [0.021–0.387]; $p < 0.0001$)

Abbreviation: NSTEMI: non-ST-elevation myocardial infarction; BID: twice daily; HR: hazard ratio; CABG: coronary artery bypass graft; OR: odds ratio. * Clinically significant AF as used by the authors includes paroxysmal AF (AF burden between 0.01% and 98%) and predominantly chronic AF (AF burden more than 98%). ** AF burden was calculated as the proportion of recording time (%) in AF.

3.1. Ventricular Tachycardia

The Metabolic Efficiency with Ranolazine for Less Ischemia in Non-ST-Segment Elevation Acute Coronary Syndrome Thrombolysis in Myocardial Infarction 36 (MERLIN-TIMI 36) trial was a randomized, double-blind study in which 6550 patients with NSTEMI were randomly assigned to take either ranolazine or placebo [24]. In a subset analysis, Scirica found ranolazine to significantly reduce the number of VT episodes lasting longer than eight beats during the first 7 days when compared to placebo (166 vs. 265, $p < 0.001$). Continuous ECG monitoring was employed to define arrhythmia burden [13].

Ranolazine in High-Risk Patients with Implanted Cardioverter-Defibrillators (RAID Trial) was another randomized, double-blind, placebo-controlled intention-to-treat study that enrolled 1012 patients with an implantable cardioverter defibrillator (ICD) in situ. Patients were randomly assigned to receive ranolazine or placebo. After a mean of 28.3 months follow-up, ranolazine was found to significantly reduce the incidence of VT and ventricular fibrillation (VF) episodes requiring anti-tachycardia pacing (ATP) or ICD shock, when compared to placebo (433 vs. 650, HR = 0.70 [0.51–0.96]; $p = 0.028$) [14]. In a subset of the RAID trial, Younis observed that the benefits of ranolazine were limited to the following subgroups: (1) patients receiving ranolazine monotherapy (without any concomitant antiarrhythmics); (2) those who have cardiac resynchronization therapy–defibrillator (CRT-D) in place; and (3) patients without atrial fibrillation [15].

3.2. Atrial Fibrillation

Scirica demonstrated in a subset of patients from the MERLIN-TIMI 36 trial that, within the first 7 days after NSTEMI, those in the ranolazine group had a trend towards lower incidence of AF compared to placebo (55 vs. 75, HR = 0.74 [0.52–1.05]; $p = 0.08$) [13]. After one year follow-up, ranolazine led to a substantial decrease in clinically significant AF burden in this population (2.9% vs. 4.1%, HR = 0.71 [0.55–0.92]; $p = 0.01$). Additionally, it reduced the time spent in AF (calculated as proportion of recording time) when compared to placebo (4.4% vs. 16.1%; $p = 0.015$) [16].

Several studies evaluated the potential synergistic effect of ranolazine when used in combination with another antiarrhythmic drug, particularly amiodarone, for the treatment

of AF. Koskinas performed a randomized, single-blind study in which 121 patients with recent-onset symptomatic AF were randomly assigned to a combination of amiodarone plus ranolazine or amiodarone alone. Those in the amiodarone plus ranolazine group not only had a significantly higher conversion rate to sinus rhythm within 24 h (53 vs. 42; $p = 0.024$), but the mean time to AF termination was also significantly shorter (10.2 ± 3.3 h vs. 13.3 ± 4.1 h; $p = 0.001$) [17]. Similarly, Tsanaxidis completed a randomized, single-center study enrolling 173 patients with recent-onset AF. Participants were assigned to amiodarone plus ranolazine or amiodarone alone. Amiodarone plus ranolazine significantly increased the conversion rate of AF within 24 h (90 vs. 47; $p < 0.001$) and reduced the mean time to conversion (8.6 ± 2.8 h vs. 19.4 ± 4.4 h; $p < 0.0001$) [18].

Simopoulos performed a randomized, single-blind study including 511 patients who developed AF following coronary artery bypass graft surgery (CABG). Patients were randomized to receive amiodarone plus ranolazine or amiodarone only. The combination of ranolazine and amiodarone significantly increased the conversion rate of AF within 24 h (235 vs. 37; $p < 0.0001$) and also reduced the mean time needed for AF termination (10.4 ± 4.5 h vs. 24.3 ± 4.6 h; $p < 0.0001$) [19]. In a retrospective single-center cohort study directly comparing the antiarrhythmic effects of amiodarone and ranolazine in 393 post-CABG patients (within 10–14 days), Miles showed that ranolazine was more effective in reducing the incidence of new-onset AF versus amiodarone (17.5% vs. 26.5%; $p = 0.035$). Importantly, there were significant differences in baseline group characteristics, particularly in the proportion of patients with New York Heart Association (NYHA) class IV symptoms and in ejection fraction (EF). This raises an important and valid concern for potential selection bias [22]. Finally, Hammond published a retrospective cohort study with 76 patients who underwent either CABG or valve surgery and received ranolazine or placebo. After matched-pair analysis, ranolazine was found to significantly reduce the incidence of new onset AF after 7 days when compared to placebo (10.5% vs. 45.6%, OR = 0.09 [0.021–0.387]; $p < 0.0001$) [23].

Harmony was a randomized, double-blind, controlled, intention-to-treat study in which 131 patients with paroxysmal AF were randomized into one of five groups: (1) placebo; (2) ranolazine 750 mg; (3) dronedarone 225 mg; (4) dronedarone 150 mg plus ranolazine 750 mg; (5) dronedarone 225 mg plus ranolazine 750 mg. Compared to placebo, the study demonstrated a significantly reduced AF burden when using a combination of dronedarone 225 mg plus ranolazine 750 mg (group 5; 4.8% vs. 11.1%; $p = 0.008$) [20].

The Ranolazine in Atrial Fibrillation Following an Electrical Cardioversion (RAFFAELLO) study was a randomized, double-blind, placebo-controlled, multicenter, intention-to-treat study. It enrolled 238 patients with persistent AF (7 days' to 6 months' duration) who underwent electrical cardioversion. Patients were randomly assigned to one of four groups: (1) placebo; (2) ranolazine 375 mg; (3) ranolazine 500 mg; (4) ranolazine 750 mg. The treatment duration was 16 weeks. AF recurrence was 56.4%, 56.9%, 41.7%, and 39.7% in groups 1–4, respectively. None of the ranolazine doses extended the time until the first AF recurrence. However, 500 mg ranolazine significantly reduced the rate of AF recurrence versus placebo when patients were still in sinus rhythm after 48 h (HR = 0.56 [0.31–1.01]; $p = 0.0495$) [21].

4. Discussion

This narrative review is aimed at compiling existing clinical evidence on the benefits of ranolazine in treating cardiac arrhythmias, specifically VT and AF.

4.1. Brief Mechanism of Action

Ranolazine is a well-established medication acting as an inhibitor of various ion channels, including late I_{Na}, peak I_{Na}, the rapid-activating delayed rectifier I_{Kr}, and, to a clinically lesser extent, L-type I_{Ca} [25]. The mechanisms through which ranolazine acts on late I_{Na} and peak I_{Na} channels are complex and warrant a limited further discussion, because it will aid in understanding the rationale for the studies reviewed here. In brief,

ranolazine is a more effective inhibitor of late I_{Na} channels in ventricular myocytes, whereas it predominantly inhibits peak I_{Na} channels in atrial myocytes [26]. Additionally, I_{Kr} only has a limited role in the atrium. A recent study also demonstrated that ranolazine inhibits TASK-1 potassium channels, which are selectively expressed on the surface of atrial myocytes, although the clinical significance of this inhibition remains limited [27].

4.1.1. Late Sodium Current

Ranolazine functions as an inhibitor of the slowly inactivating domain of the cardiac sodium current, referred to as late I_{Na}. Late I_{Na} is found predominantly on the surface of midmyocardial cells (M cells) and in Purkinje fibers [28]. Under physiologic conditions, the amplitude of the late I_{Na} represents less than 1% of the peak I_{Na} current. However, under various pathological conditions, such as myocardial ischemia or heart failure, there is a significant increase in the number of late I_{Na} channels on the surface of ventricular myocytes. The consequently intensified late I_{Na} current prompts an enhanced sodium influx into the cytoplasm of these cells, raising the intracellular concentration of sodium. In response, a reverse-mode sodium–calcium exchange is activated and prompts a rise in cytosolic calcium concentration. In ventricular myocytes, this can impair mechanical relaxation and induce electrical instability by prolonging the cardiac action potential. In addition, it provokes further spontaneous calcium release from the sarcoplasmic reticulum. These events can lead to two different yet closely related activities in the myocardium: (1) transmural dispersion of repolarization (TDR), as indicated by the time between the peak and the end of T wave, and (2) early afterdepolarization (EAD) or T-wave alternans [29]. All of these can potentially induce ventricular arrhythmias, including torsades de pointes [28]. Ranolazine selectively inhibits the late I_{Na} current in ventricular myocytes, thereby limiting sodium overload and cytosolic calcium accumulation. This leads to a decrease in diastolic wall stress and improved coronary flow, thereby promoting enhanced cardiac function [30].

4.1.2. Peak Sodium Current

Ranolazine exploits the differences in peak sodium current between the atrial and ventricular cells. Burashnikov and others demonstrated that ranolazine exerts an atrium-selective, use-dependent inhibition of the maximum action potential slope and prolongs the effective refractory period in isolated canine coronary-perfused atria and ventricles. These results indicate that ranolazine has the potential to treat AF without unwanted proarrhythmic effects at the ventricular level [31,32].

4.1.3. Transmural Dispersion of Repolarization and Early Afterdepolarization

It is known from the literature that ranolazine does not induce EAD or increase TDR. Antzelevitch elegantly mentioned in his study that "dispersion of repolarization secondary to accentuation of electrical heterogeneities intrinsic to ventricular myocardium as the substrate and EADs as the trigger for the development of TdP". While ranolazine inhibits the I_{Kr} that prolongs the QT interval and would logically trigger TdP, it does not actually lead to TdP, as is the case for other class III antiarrhythmic drugs. Moreover, studies performed on guinea pig and rabbit hearts have shown that ranolazine suppresses TdP induced by selective I_{Kr} blockers.

The electrophysiological effects of ranolazine were studied in detail by Antzelevich. The ventricular myocardium consists of at least three electrophysiologically distinct cell types: epicardial cells, M cells, and endocardial cells. M cells are characterized by an action potential that is heavily prolonged, compared to that of other ventricular myocardial cell types, in response to pathological conditions and when exposed to certain drugs prolonging the QT interval. This emphasizes normal TDR and results in EAD by reducing the repolarization reserve of the ventricular myocytes. In contrast, ranolazine preferentially prolongs action potential duration in the epicardium but shortens it in M cells, thus leading to a reduction in TDR. This is most likely explained by the inhibitory effect of ranolazine on late I_{Na} [25].

4.2. Clinical Benefits of Ranolazine

4.2.1. Ventricular Tachycardia

Two large randomized controlled trials have demonstrated the efficacy of ranolazine in reducing the number of VT episodes. Given that the majority of patients in both of these studies had underlying myocardial ischemia (51.0% of the ranolazine group in MERLIN-TIMI 36 had NSTEMI while 47.1% had unstable angina, and 58% in the RAID trial had ischemic cardiomyopathy), the anti-ischemic effects of ranolazine may have contributed to the reduction in the observed arrhythmia burden. In contrast with these results, Benjamin documented a comparable reduction in the incidence of VT with ranolazine in patients with and without myocardial ischemia in the MERLIN-TIMI 36 trial [13]. Similarly, Younis found in the RAID trial that the reduction in VT events did not differ significantly between patients with ischemic and non-ischemic cardiomyopathy [15]. These findings indicate that ranolazine has direct antiarrhythmic properties.

Our thorough data review suggests that, when used specifically for the management or prevention of VT, certain populations may experience a greater benefit from ranolazine therapy. For example, Younis demonstrated that it was more effective in reducing VT in patients not receiving any other antiarrhythmic agents, individuals without baseline AF, and among those with a CRT-D in situ. These observations are of great importance as, in the RAID trial, 17% of all participants were on an antiarrhythmic agent, with 10% taking amiodarone. Several explanations for these findings may be plausible. Ranolazine may elicit an antiarrhythmic effect similar to that of other agents, and its additional benefit may no further be detectable. Another explanation may be related to its largely rate-independent effect on the ventricle. That is, the antiarrhythmic properties of ranolazine are not enhanced by increased ventricular rates. This suggests that a strong synergistic effect reducing the incidence of VT is highly unlikely to exist between ranolazine and other antiarrhythmic drugs. Interestingly, this is in stark contrast with the results documented in AF, where the combined use of ranolazine and amiodarone demonstrated a strong synergistic effect. Another important observation is that ranolazine appears to have a stronger benefit in patients at low-to-moderate VT risk, and its efficacy is more limited in higher-risk groups (e.g., older individuals, patients with underlying AF, and those already taking antiarrhythmics). Finally, ranolazine was significantly more effective in patients with an implanted CRT-D device compared to those with an ICD. This may be attributed to ranolazine's mechanism of action which involves the inhibition of late I_{Na} in the ventricle. This makes it especially effective in conditions with greater dispersion in transmyocardial repolarization, such as ischemia and heart failure. Likewise, left bundle branch block (LBBB), a common indication for CRT-D, leads to greater dispersion in repolarization. This indicates a potential synergistic effect explaining the benefit of combining ranolazine with CRT-D therapy [15,33]. Importantly, based on a limited number of animal experiments, ranolazine does not appear to alter the defibrillation threshold and, therefore, it does not reduce the safety margin for successful defibrillation [34]. As it is a frequently used anti-ischemic agent, and ischemic cardiomyopathy is a common indication for primary or secondary prevention ICD implantation, the clinical relevance of this finding might be highly significant.

4.2.2. Atrial Fibrillation

Despite a positive trend noted in the MERLIN-TIMI 36 and RAFFAELLO trials, prolonged treatment with ranolazine was not effective in reducing the incidence of new onset and recurrent AF [13,21]. The limited number of studies in this field and their heterogeneity underscore the need for further research in this area.

Several studies have demonstrated that ranolazine, when combined with amiodarone, promoted a more rapid AF termination and conversion to sinus rhythm. This finding aligns with the experimental data demonstrating a favorable synergy between the two agents that is achieved without any undesirable proarrhythmic effects [30,33]. While discussing the clinical significance of the time reduction until AF termination is beyond the scope of this narrative review, such a decrease may potentially lower hospital costs by shortening

inpatient stays. This might ultimately benefit the patients, their caregivers, and society. It is important to emphasize that physicians should always follow their clinical judgment and patient management shall adhere to the most up to date clinical guidelines. Specifically, while the addition of ranolazine to amiodarone favors the maintenance of sinus rhythm, ensuring that no clinically significant myocardial ischemia exists following CABG that would explain arrhythmias is a priority. In addition, optimal medical therapy, including but not limited to aspirin, statins, beta blockers, and a neurohormonal blockade, should be initiated and titrated according to the most recent clinical practice guidelines followed by the addition of amiodarone and ranolazine as necessary [35].

4.3. Safety Profile of Ranolazine

The risk of new-onset or worsening arrhythmias (proarrhythmic effect) and/or toxicity with prolonged exposure limit the use of many antiarrhythmic drugs currently available on the market. However, substantial clinical evidence supports the safety of chronic ranolazine treatment. It does not cause clinically significant bradycardia or hypotension [36,37]. The most common adverse effects associated with ranolazine use include nausea, constipation, dizziness, fatigue and, less frequently, syncope [14,19,21,24,36,37]. Many clinical trials have established that ranolazine does not provoke TdP or sudden cardiac death, despite its modest QT-prolonging effect [17,38]. This is frequently attributed to the fact that ranolazine does not induce EAD or increase TDR.

4.4. Limitations

This narrative review has certain limitations. First, there is considerable heterogeneity among the studies analyzed. Variations in study design, patient populations, interventions, and outcomes across these may limit the ability to directly compare their results. Second, the small number of studies available on each topic limits our possibility to draw a robust conclusion. Third, this review was limited to VT and AF and did not include other arrhythmias, specifically those based on congenital long QT syndrome and supraventricular tachycardias other than AF.

5. Conclusions

Based on available clinical trial data, ranolazine appears to be an effective and safe agent reducing the incidence of VT. However, information regarding its effects on survival is lacking. It may accelerate the conversion of AF into sinus rhythm when used in combination with amiodarone, thus decreasing the time spent in AF and promoting hemodynamic stabilization. The antiarrhythmic properties of ranolazine can provide significant additional clinical benefits to its established anti-ischemic and antianginal effects.

There is a growing number of studies on the use of ranolazine in cardiovascular diseases beyond angina pectoris, including arrhythmias and heart failure. Its mechanism of action is complex and not yet fully understood. Since ranolazine was introduced to the U.S. market in 2006, its long-term safety and efficacy are not yet well-established, which may hinder its use as a first-line agent. Gathering further clinical evidence through clinical trials and observational studies is essential to solidify the information on the beneficial cardiovascular effects of ranolazine.

Although the term "proarrhythmic" is commonly used in the context of antiarrhythmic therapy, whether the full scale of its impact is understood remains unclear. Further biomolecular studies are essential to understand the underlying mechanisms which may, in turn, assist in choosing the most appropriate antiarrhythmic strategy for individual patients.

Author Contributions: Conceptualization, A.V. and K.M.; Methodology, L.C.; Writing—original draft preparation, K.M.; Writing—review and editing, T.A., K.T. and L.C.; Supervision, L.C. All authors have read and agreed to the published version of the manuscript.

Funding: This study was supported by the NKFIH within the framework of the University of Pécs project TKP2021-EGA-17.

Institutional Review Board Statement: Not applicable.

Informed Consent Statement: Not applicable.

Data Availability Statement: Not applicable.

Acknowledgments: We wish to thank Jon Marquette for improving the English grammar and style for this manuscript.

Conflicts of Interest: The authors declare no conflicts of interest.

References

1. Apte, N.; Kalra, D.K. Pharmacotherapy in Ventricular Arrhythmias. *Cardiology* **2023**, *148*, 119–130. [CrossRef] [PubMed]
2. Echt, D.S.; Liebson, P.R.; Mitchell, L.B.; Peters, R.W.; Obias-Manno, D.; Barker, A.H.; Arensberg, D.; Baker, A.; Friedman, L.; Greene, H.L.; et al. Mortality and Morbidity in Patients Receiving Encainide, Flecainide, or Placebo. The Cardiac Arrhythmia Suppression Trial. *N. Engl. J. Med.* **1991**, *324*, 781–788. [CrossRef] [PubMed]
3. Waldo, A.L.; Camm, J.; Deruyter, H.; Friedman, P.L.; Macneil, D.J.; Pauls, J.F.; Pitt, B.; Pratt, C.M.; Schwartz, P.J.; Veltri, E.P. Effect of D-Sotalol on Mortality in Patients with Left Ventricular Dysfunction after Recent and Remote Myocardial Infarction. *Lancet* **1996**, *348*, 7–12. [CrossRef] [PubMed]
4. Hindricks, G.; Potpara, T.; Kirchhof, P.; Kühne, M.; Ahlsson, A.; Balsam, P.; Bauersachs, J.; Benussi, S.; Brandes, A.; Braunschweig, F.; et al. 2020 ESC Guidelines for the Diagnosis and Management of Atrial Fibrillation Developed in Collaboration with the European Association for Cardio-Thoracic Surgery (EACTS). *Eur. Heart J.* **2021**, *42*, 373–498. [CrossRef] [PubMed]
5. Joglar, J.A.; Chung, M.K.; Armbruster, A.L.; Benjamin, E.J.; Chyou, J.Y.; Cronin, E.M.; Deswal, A.; Eckhardt, L.L.; Goldberger, Z.D.; Gopinathannair, R.; et al. 2023 ACC/AHA/ACCP/HRS Guideline for the Diagnosis and Management of Atrial Fibrillation: A Report of the American College of Cardiology/American Heart Association Joint Committee on Clinical Practice Guidelines. *Circulation* **2024**, *149*, e1–e156. [CrossRef] [PubMed]
6. Al-Khatib, S.M.; Stevenson, W.G.; Ackerman, M.J.; Bryant, W.J.; Callans, D.J.; Curtis, A.B.; Deal, B.J.; Dickfeld, T.; Field, M.E.; Fonarow, G.C.; et al. 2017 AHA/ACC/HRS Guideline for Management of Patients with Ventricular Arrhythmias and the Prevention of Sudden Cardiac Death. *Circulation* **2018**, *138*, e272–e391. [CrossRef] [PubMed]
7. Yang, G.; Zheng, L.; Jiang, C.; Fan, J.; Liu, X.; Zhan, X.; Li, J.; Wang, L.; Yang, H.; Zhu, W.; et al. Circumferential Pulmonary Vein Isolation Plus Low-Voltage Area Modification in Persistent Atrial Fibrillation: The STABLE-SR-II Trial. *JACC Clin. Electrophysiol.* **2022**, *8*, 882–891. [CrossRef] [PubMed]
8. Connolly, S.J. Evidence-Based Analysis of Amiodarone Efficacy and Safety. *Circulation* **1999**, *100*, 2025–2034. [CrossRef] [PubMed]
9. Cronin, E.M.; Bogun, F.M.; Maury, P.; Peichl, P.; Chen, M.; Namboodiri, N.; Aguinaga, L.; Leite, L.R.; Al-Khatib, S.M.; Anter, E.; et al. 2019 HRS/EHRA/APHRS/LAHRS Expert Consensus Statement on Catheter Ablation of Ventricular Arrhythmias. *Heart Rhythm.* **2020**, *17*, e2–e154. [CrossRef]
10. John, R.M.; Tedrow, U.B.; A Koplan, B.; Albert, C.M.; Epstein, L.M.; O Sweeney, M.; Miller, A.L.; Michaud, G.F.; Stevenson, W.G. Ventricular Arrhythmias and Sudden Cardiac Death. *Lancet* **2012**, *380*, 1520–1529. [CrossRef]
11. Staerk, L.; Sherer, J.A.; Ko, D.; Benjamin, E.J.; Helm, R.H. Atrial Fibrillation: Epidemiology, Pathophysiology, Clinical Outcomes. *Circ. Res.* **2017**, *120*, 1501–1517. [CrossRef] [PubMed]
12. Brachmann, J.; Sohns, C.; Andresen, D.; Siebels, J.; Sehner, S.; Boersma, L.; Merkely, B.; Pokushalov, E.; Sanders, P.; Schunkert, H.; et al. Atrial Fibrillation Burden and Clinical Outcomes in Heart Failure: The CASTLE-AF Trial. *JACC Clin. Electrophysiol.* **2021**, *7*, 594–603. [CrossRef] [PubMed]
13. Scirica, B.M.; Morrow, D.A.; Hod, H.; Murphy, S.A.; Belardinelli, L.; Hedgepeth, C.M.; Molhoek, P.; Verheugt, F.W.; Gersh, B.J.; McCabe, C.H.; et al. Effect of Ranolazine, an Antianginal Agent with Novel Electrophysiological Properties, on the Incidence of Arrhythmias in Patients with Non–ST-Segment–Elevation Acute Coronary Syndrome: Results from the Metabolic Efficiency with Ranolazine for Less Ischemia in Non-ST-Elevation Acute Coronary Syndrome-Thrombolysis in Myocardial Infarction 36 (MER-LIN-TIMI 36) Randomized Controlled Trial. *Circulation* **2007**, *116*, 1647–1652. [CrossRef]
14. Zareba, W.; Daubert, J.P.; Beck, C.A.; Huang, D.T.; Alexis, J.D.; Brown, M.W.; Pyykkonen, K.; McNitt, S.; Oakes, D.; Feng, C.; et al. Ranolazine in High-Risk Patients with Implanted Cardioverter-Defibrillators: The RAID Trial. *J. Am. Coll. Cardiol.* **2018**, *72*, 636–645. [CrossRef]
15. Younis, A.; Goldenberg, I.; Farooq, S.; Yavin, H.; Daubert, J.; Raitt, M.; Mazur, A.; Huang, D.T.; Mitchell, B.L.; Rashtian, M.R.; et al. Reduction in Ventricular Tachyarrhythmia Burden in Patients Enrolled in the RAID Trial. *JACC Clin. Electrophysiol.* **2022**, *8*, 754–762. [CrossRef] [PubMed]
16. Scirica, B.M.; Belardinelli, L.; Chaitman, B.R.; Waks, J.W.; Volo, S.; Karwatowska-Prokopczuk, E.; Murphy, S.A.; Cheng, M.L.; Braunwald, E.; Morrow, D.A. Effect of Ranolazine on Atrial Fibrillation in Patients with Non-ST Elevation Acute Coronary Syndromes: Observations from the MERLIN-TIMI 36 Trial. *Europeo* **2014**, *17*, 32–37. [CrossRef]
17. Koskinas, K.C.; Fragakis, N.; Katritsis, D.; Skeberis, V.; Vassilikos, V. Ranolazine Enhances the Efficacy of Amiodarone for Conversion of Recent-Onset Atrial Fibrillation. *Europace* **2014**, *16*, 973–979. [CrossRef] [PubMed]

18. Tsanaxidis, N.; Aidonidis, I.; Hatziefthimiou, A.; Daskalopoulou, S.S.; Giamouzis, G.; Triposkiadis, F.; Skoularigis, I. Ranolazine Added to Amiodarone Facilitates Earlier Conversion of Atrial Fibrillation Compared to Amiodarone-Only Therapy. *Pacing Clin. Electrophysiol.* **2017**, *40*, 372–378. [CrossRef]
19. Simopoulos, V.; Hevas, A.; Hatziefthimiou, A.; Dipla, K.; Skoularigis, I.; Tsilimingas, N.; Aidonidis, I. Amiodarone plus Ranolazine for Conversion of Post-Cardiac Surgery Atrial Fibrillation: Enhanced Effectiveness in Reduced Versus Preserved Ejection Fraction Patients. *Cardiovasc. Drugs Ther.* **2018**, *32*, 559–565. [CrossRef]
20. Reiffel, J.A.; Camm, A.J.; Belardinelli, L.; Zeng, D.; Karwatowska-Prokopczuk, E.; Olmsted, A.; Zareba, W.; Rosero, S.; Kowey, P. The HARMONY Trial: Combined Ranolazine and Dronedarone in the Management of Paroxysmal Atrial Fibrillation: Mechanistic and Therapeutic Synergism. *Circ. Arrhythmia Electrophysiol.* **2015**, *8*, 1048–1056. [CrossRef]
21. De Ferrari, G.M.; Maier, L.S.; Mont, L.; Schwartz, P.J.; Simonis, G.; Leschke, M.; Gronda, E.; Boriani, G.; Darius, H.; Torán, L.G.; et al. Ranolazine in the Treatment of Atrial Fibrillation: Results of the Dose-Ranging RAFFAELLO (Ranolazine in Atrial Fibrillation Following An Electrical Cardioversion) study. *Heart Rhythm.* **2015**, *12*, 872–878. [CrossRef] [PubMed]
22. Miles, R.H.; Passman, R.; Murdock, D.K. Comparison of Effectiveness and Safety of Ranolazine Versus Amiodarone for Preventing Atrial Fibrillation After Coronary Artery Bypass Grafting. *Am. J. Cardiol.* **2011**, *108*, 673–676. [CrossRef] [PubMed]
23. Hammond, D.A.; Smotherman, C.; Jankowski, C.A.; Tan, S.; Osian, O.; Kraemer, D.; DeLosSantos, M. Short-Course of Ranolazine Prevents Postoperative Atrial Fibrillation Following Coronary Artery Bypass Grafting and Valve Surgeries. *Clin. Res. Cardiol.* **2015**, *104*, 410–417. [CrossRef] [PubMed]
24. Morrow, D.A.; Scirica, B.M.; Karwatowska-Prokopczuk, E.; Murphy, S.A.; Budaj, A.; Varshavsky, S.; Wolff, A.A.; Skene, A.; McCabe, C.H.; Braunwald, E. Effects of Ranolazine on Recurrent Cardiovascular Events in Patients with Non–ST-Elevation Acute Coronary SyndromesThe MERLIN-TIMI 36 Randomized Trial. *JAMA* **2007**, *297*, 1775–1783. [CrossRef] [PubMed]
25. Antzelevitch, C.; Belardinelli, L.; Wu, L.; Fraser, H.; Zygmunt, A.C.; Burashnikov, A.; Di Diego, J.M.; Fish, J.M.; Cordeiro, J.M.; Goodrow, R.J.; et al. Electrophysiologic Properties and Antiarrhythmic Actions of a Novel Antianginal Agent. *J. Cardiovasc. Pharmacol. Ther.* **2004**, *9*, S65–S83. [CrossRef] [PubMed]
26. Polytarchou, K.; Manolis, A.S. Ranolazine and its Antiarrhythmic Actions. *Cardiovasc. Hematol. Agents Med. Chem.* **2015**, *13*, 31–39. [CrossRef] [PubMed]
27. Ratte, A.; Wiedmann, F.; Kraft, M.; Katus, H.A.; Schmidt, C. Antiarrhythmic Properties of Ranolazine: Inhibition of Atrial Fibrillation Associated TASK-1 Potassium Channels. *Front. Pharmacol.* **2019**, *10*, 1367. [CrossRef] [PubMed]
28. Belardinelli, L.; Antzelevitch, C.; Vos, M.A. Assessing Predictors of Drug-Induced Torsade de Pointes. *Trends Pharmacol. Sci.* **2003**, *24*, 619–625. [CrossRef] [PubMed]
29. Arteyeva, N.V. Dispersion of ventricular repolarization: Temporal and spatial. *World J. Cardiol.* **2020**, *12*, 437–449. [CrossRef]
30. Burashnikov, A.; Di Diego, J.M.; Zygmunt, A.C.; Belardinelli, L.; Antzelevitch, C. Atrium-Selective Sodium Channel Block as a Strategy for Suppression of Atrial Fibrillation: Differences in Sodium Channel Inactivation between Atria and Ventricles and the Role of Ranolazine. *Circulation* **2007**, *116*, 1449–1457. [CrossRef]
31. Antzelevitch, C.; Burashnikov, A.; Sicouri, S.; Belardinelli, L. Electrophysiologic Basis for the Antiarrhythmic Actions of Ranolazine. *Heart Rhythm.* **2011**, *8*, 1281–1290. [CrossRef] [PubMed]
32. Andrade, J.G.; Deyell, M.W. A Role for Ranolazine in the Treatment of Ventricular Arrhythmias? *JACC: Clin. Electrophysiol.* **2022**, *8*, 763–765. [CrossRef] [PubMed]
33. Sicouri, S.; Burashnikov, A.; Belardinelli, L.; Antzelevitch, C. Synergistic Electrophysiologic and Antiarrhythmic Effects of the Combination of Ranolazine and Chronic Amiodarone in Canine Atria. *Circ. Arrhythmia Electrophysiol.* **2010**, *3*, 88–95. [CrossRef] [PubMed]
34. Kumar, K.; Nearing, B.D.; Bartoli, C.R.; Kwaku, K.F.; Belardinelli, L.; Verrier, R.L. Effect of Ranolazine on Ventricular Vulnerability and Defibrillation Threshold in the Intact Porcine Heart. *J. Cardiovasc. Electrophysiol.* **2008**, *19*, 1073–1079. [CrossRef] [PubMed]
35. Levine, G.N.; Bates, E.R.; Bittl, J.A.; Brindis, R.G.; Fihn, S.D.; Fleisher, L.A.; Granger, C.B.; Lange, R.A.; Mack, M.J.; Mauri, L.; et al. 2016 ACC/AHA Guideline Focused Update on Duration of Dual Antiplatelet Therapy in Patients with Coronary Artery Disease: A Report of the American. College of Cardiology/American Heart Association Task Force on Clinical Practice Guidelines. *J. Am. Coll. Cardiol.* **2016**, *68*, 1082–1115. [CrossRef] [PubMed]
36. Chaitman, B.R.; Skettino, S.L.; Parker, J.O.; Hanley, P.; Meluzin, J.; Kuch, J.; Pepine, C.J.; Wang, W.; Nelson, J.J.; Hebert, D.A.; et al. Anti-Ischemic Effects and Long-Term Survival during Ranolazine Monotherapy in Patients with Chronic Severe Angina. *J. Am. Coll Cardiol.* **2004**, *43*, 1375–1382. [CrossRef] [PubMed]
37. Sossalla, S.; Wallisch, N.; Toischer, K.; Sohns, C.; Vollmann, D.; Seegers, J.; Lüthje, L.; Maier, L.S.; Zabel, M. Effects of Ranolazine on Torsades de Pointes Tachycardias in a Healthy Isolated Rabbit Heart Model. *Cardiovasc. Ther.* **2014**, *32*, 170–177. [CrossRef]
38. Karwatowska-Prokopczuk, E.; Wang, W.; Cheng, M.L.; Zeng, D.; Schwartz, P.J.; Belardinelli, L. The Risk of Sudden Cardiac Death in Patients with Non-ST Elevation Acute Coronary Syndrome and Prolonged QTc Interval: Effect of Ranolazine. *Eur.* **2013**, *15*, 429–436. [CrossRef]

Disclaimer/Publisher's Note: The statements, opinions and data contained in all publications are solely those of the individual author(s) and contributor(s) and not of MDPI and/or the editor(s). MDPI and/or the editor(s) disclaim responsibility for any injury to people or property resulting from any ideas, methods, instructions or products referred to in the content.

biomedicines

MDPI

Article

Continuous Monitoring of Advanced Hemodynamic Parameters during Hemodialysis Demonstrated Early Variations in Patients Experiencing Intradialytic Hypotension

Yotam Kolben [1], Ittamar Gork [2], David Peled [3], Shani Amitay [1], Peleg Moshel [1], Nir Goldstein [4], Arik Ben Ishay [4], Meir Fons [4], Michael Tabi [4], Arik Eisenkraft [4,5,*], Yftach Gepner [3,†] and Dean Nachman [1,5,†]

[1] Heart Institute, Hadassah Medical Center, Faculty of Medicine, Hebrew University of Jerusalem, Jerusalem 9112001, Israel; yotam@4kosh.com (Y.K.); shani.amitay@mail.huji.ac.il (S.A.); pelegmoshel@gmail.com (P.M.); deannahman@gmail.com (D.N.)
[2] Department of Nephrology and Hypertension, Hadassah Medical Center, Faculty of Medicine, Hebrew University of Jerusalem, Jerusalem 9112001, Israel; gorkster@gmail.com
[3] Department of Health Promotion, School of Public Health, Faculty of Medicine and Health, Sylvan Adams Sports Institute, Tel Aviv University, Tel Aviv 6997801, Israel; dpeled94@gmail.com (D.P.); gepner@tauex.tau.ac.il (Y.G.)
[4] Biobeat Technologies Ltd., Petah Tikva 4937213, Israel; nirgoldnz@gmail.com (N.G.); arik@bio-beat.com (A.B.I.); meir@bio-beat.com (M.F.); michael@bio-beat.com (M.T.)
[5] Institute for Research in Military Medicine, Faculty of Medicine, The Hebrew University of Jerusalem and the Israel Defense Force Medical Corps, Jerusalem 9112102, Israel
* Correspondence: aizenkra@gmail.com; Tel.: +97-252-921-0896
† These authors contributed equally to this work.

Abstract: Intradialytic hypotension (IDH) is a severe complication of hemodialysis (HD) with a significant impact on morbidity and mortality. In this study, we used a wearable device for the continuous monitoring of hemodynamic vitals to detect hemodynamic changes during HD and attempted to identify IDH. End-stage kidney disease patients were continuously monitored 15 min before starting the session and until 15 min after completion of the session, measuring heart rate (HR), noninvasive cuffless systolic and diastolic blood pressure (SBP and DBP), stroke volume (SV), cardiac output (CO), and systemic vascular resistance (SVR). Data were analyzed retrospectively and included comparing BP measured by the wearable devices (recorded continuously every 5 s) and the cuff-based devices. A total of 98 dialysis sessions were included in the final analysis, and IDH was identified in 22 sessions (22.5%). Both SBP and DBP were highly correlated ($r > 0.62$, $p < 0.001$ for all) between the wearable device and the cuff-based measurements. Based on the continuous monitoring, patients with IDH had earlier and more profound reductions in SBP and DBP during the HD treatment. In addition, nearly all of the advanced vitals differed between groups. Further studies should be conducted in order to fully understand the potential of noninvasive advanced continuous monitoring in the prediction and prevention of IDH events.

Keywords: noninvasive blood pressure; end-stage kidney disease; hemodialysis; intradialytic hypotension; remote patient monitoring; photoplethysmography

1. Introduction

End-stage kidney disease (ESKD) patients undergoing maintenance hemodialysis (HD) treatments suffer from various complications during the treatment [1]. For each dialysis session, the patient's physiological status should be assessed so that the dialysis prescription can be aligned with the goals for the session to achieve the desired rates and total amount of solute and fluid removal, without causing any side effects or complications [2]. Nevertheless, intradialytic hypotension (IDH) is one of the major complications of HD, prevalent in 15–50% of HD sessions, depending on the definition [3]. The Kidney

Disease Outcomes Quality Initiative (KDOQI) and the European Best Practice Guidelines define IDH as the presence of a decrease of at least 20 mmHg in systolic blood pressure (BP) or a reduction in mean arterial pressure (MAP) by 10 mmHg, provided that this decrease is associated with clinical events and the need for nursing interventions [4]. Moreover, IDH is associated with increased morbidity and mortality, with growing evidence of repeated cardiac injury during HD sessions [5,6]. Brain and gut ischemia may also occur [7]. It is assumed to result from a reduction in blood volume when the ultrafiltration rate outpaces the vascular refilling rate from the interstitial space [3].

Nevertheless, it has been suggested that IDH may result from hypovolemia, left ventricular diastolic dysfunction, or a "breakdown" in peripheral resistance [8]. BP reduction, in addition to relevant symptoms, indicates that IDH should be suspected. However, since several intrinsic control mechanisms tightly regulate BP in response to ultrafiltration-induced blood volume reduction, periodic blood pressure measurements during HD are of little use in predicting IDH [9]. The invasive Swan-Ganz pulmonary artery catheterization thermodilution technique is considered as the gold standard for diagnosing IDH. Other invasive and noninvasive methods have been proposed for IDH monitoring in the past, with no wide-scale use so far [9–11].

In this study, we continuously monitored patients undergoing HD treatment using a noninvasive, wireless, wearable photoplethysmography (PPG)-based device (BB-613WP, Biobeat Technologies Ltd., Petach Tikva, Israel; Figure 1). The aims of the study were to determine if the PPG-based device can be used to assess BP accurately during HD and to test whether it is possible to identify IDH in the early stage of the HD session. Furthermore, this study aimed to describe the advanced hemodynamic effects of HD, specifically among IDH patients.

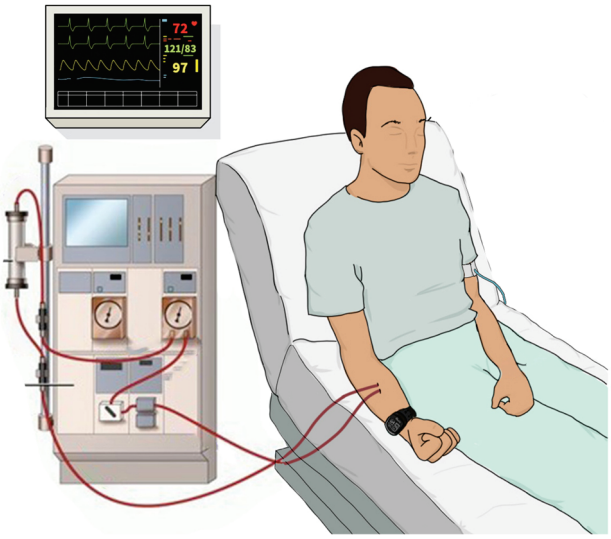


Figure 1. The monitoring sensor is attached to a patient during a dialysis session.

2. Materials and Methods

2.1. Study Design and Overview

This prospective non-interventional study was conducted between 15 January 2021 and 15 February 2022. ESKD patients undergoing chronic intermittent HD treatments in the Hadassah Ein-Kerem medical center were recruited. The study was approved by the Hadassah Ein-Kerem ethics committee (approval number PPGDIA001) and was registered in ClinicalTrials.gov (NCT04680039). Inclusion criteria were patients of both sexes, older than 18 years with ESKD undergoing chronic HD treatments for more than three months, able to adhere to the visit schedule and protocol requirements, and available to complete the study. Exclusion criteria were pregnancy, individuals with a lack of judgment/mental illness, withholding the dialysis session for any reason before initiation, and those employed

by the recruiting center. Each participant signed an informed consent form prior to the beginning of the study. Patients were allowed to participate in more than a single HD session. A screening meeting was held up to seven days prior to the first monitored HD session, and participants were monitored during up to 12 dialysis sessions, with the intervention period lasting 90 days at most (see the study flow chart in Supplemental Figure S1). Hemodialysis sessions occurred during the morning, noon, or evening shifts with session lengths being 3–4 h long. Each patient was attended by the same nurse during the whole HD session. Hemodialysis was performed with NIPRO hemodialysis machines and with the use of ELISIO 19H or EISIO 21H dialyzers and solutions with a potassium concentration of 2.0 mmol/L and calcium of 1.5 mmol/L, with some patients requiring adjustments to a potassium concentration of 3.0 mmol/L and/or calcium concentration of 1.25 mmol/L. In each HD session, the PPG-based monitors were attached to the patients' wrists 15 min before starting the session and until 15 min after completion of the session. The time window before and after each dialysis was used to obtain baseline parameters, to calibrate the PPG device, and to assess the hemodynamic effects after the session termination, respectively. Physiological measurements were recorded continuously every 5 s, and included heart rate (HR), noninvasive cuffless BP, stroke volume (SV), cardiac output (CO), cardiac index (CI), and systemic vascular resistance (SVR). All data were collected and stored during the monitoring period and analyzed retrospectively at the end of the study. At the same time, cuff-based blood pressure measurement devices implemented in the hemodialysis machine were placed on the patients. As the PPG-based device is cuffless, it was placed on the arm with the AV fistula/dialysis venous catheter, so in all cases measurements were taken simultaneously. None of the patients took any medications prior to the beginning of the dialysis session.

2.2. The PPG-Based Monitor

The monitoring devices used in this study (Figure 1) utilize a unique reflective PPG technology, in which part of the transmitted light is reflected from the tissue and detected by a photodiode detector positioned near the light source transmitter. The sensor's high temporal and quantitative resolution allows it to capture changes in tissue reflectance, from which it derives measurements of several hemodynamic parameters using Pulse Wave Transit Time (PWTT) combined with Pulse Wave Analysis (PWA) [12–17]. The device requires a single trimonthly calibration of the HR and BP baseline using an FDA-cleared cuff-based device.

2.3. Data Collection and Statistical Analysis

Data were transmitted and stored in real time in a cloud-based web application used by the healthcare providers, with data being coded and fully de-identified. Unusual events were recorded by the researchers. The dataset was segregated into two distinct groups of IDH status: IDH positive and IDH negative based on a 20 mmHg reduction in SBP or 10 mmHg MAP in cuff-based measurement and clinical parameters. Statistical analyses were performed using built-in functions in MATLAB, where numerical data underwent p-value calculation using the t-test and categorical data underwent analysis using the chi-squared test.

Correlation analyses were conducted to explore associations between the PPG-based device and cuff-based measurements for both systolic and diastolic BP with differentiation between IDH positive and IDH negative. Pearson correlation coefficients were computed using MATLAB. Differences between cuff-based measurements and the PPG-based device measurements were computed for instances where both measurements were available simultaneously (IDH negative = 162, IDH positive = 72). These differences were utilized to generate Bland–Altman plots, distinguishing between systolic and diastolic BP, with the level of agreement estimated using 95% confidence intervals.

Dynamic responses of measured parameters from the PPG-based device system were assessed by normalizing the raw data of each treatment to the treatment duration and

subsequently averaging across all treatments within each section. The data were then divided into 10 subsections, each representing 10% of the treatment duration. Subsequently, a t-test was employed using MATLAB to compare the responses between IDH-positive and IDH-negative subjects for each subsection.

3. Results

In this study, 72 patients were enrolled, among whom 26 patients completed 2 monitored dialysis sessions, resulting in a total of 98 dialysis sessions included in the final analysis. Data were analyzed as per dialysis session, and not per patient. Overall, 22 incidents of IDH occurred. In total, 173,796 measurements of the PPG-based device were collected during an average monitoring period of 3.8 $\pm$ 0.3 h per patient (2447 $\pm$ 418 measurements per patient). Demographic details are provided in Table 1. There were no adverse events or self-reported discomfort from using the device.

Table 1. Basic characteristics of hemodialysis patients. IDH—intradialytic hypotension, ACEi—Angiotensin-Converting Enzyme inhibitors; ARB—Angiotensin Receptor Blockers; MRA—Mineralocorticoid Receptor Antagonist; CCB—Calcium Channel Blockers.

	non-IDH (n = 76)	**IDH (n = 22)**	***p*-Value**
Age (years)	65.5 $\pm$ 9.41	67.0 $\pm$ 13.7	0.13
Female (%)	36.4	32.9	0.76
Medications			
Diuretics (%)	18.2	44.7	0.026
ACEi/ARB/MRA (%)	18.2	23.7	0.022
CCB (%)	40.9	35.5	0.028
β-Blockers (%)	40.9	51.3	0.59
α-Blockers (%)	13.6	34.2	0.64
Medical Background			
Heart failure (%)	36.4	39.5	0.39
Hypertension (%)	95.5	72.4	0.066
Diabetes mellitus (%)	77.3	50.0	0.79
Peripheral vascular disease (%)	59.1	15.8	<0.001
Pulmonary hypertension (%)	45.5	21.1	0.021

As shown in Figure 2, we performed correlation analyses between point measurements taken by cuff-based BP devices during the dialysis sessions and measurements taken using the PPG-based monitoring devices. High correlations were found in IDH and non-IDH patients for systolic blood pressure (SBP) (r = 0.622 and 0.666, respectively; $p < 0.001$) and diastolic blood pressure (DBP) (0.664 and 0.698, respectively; $p < 0.001$). Values are mean $\pm$ SD.

Next, we compared both the cuff-based and the PPG-based cuffless device using a Bland–Altman analysis (Figure 3). The mean bias of the PPG-based cuffless device was very low for the patients without IDH, with 0.2 mmHg for SBP and 1.5 mmHg for DBP. However, for IDH patients, the PPG-based cuffless device overestimated both SBP and DBP (mean bias of 17.7 and 10.7, respectively), indicating strong specificity but less sensitivity.

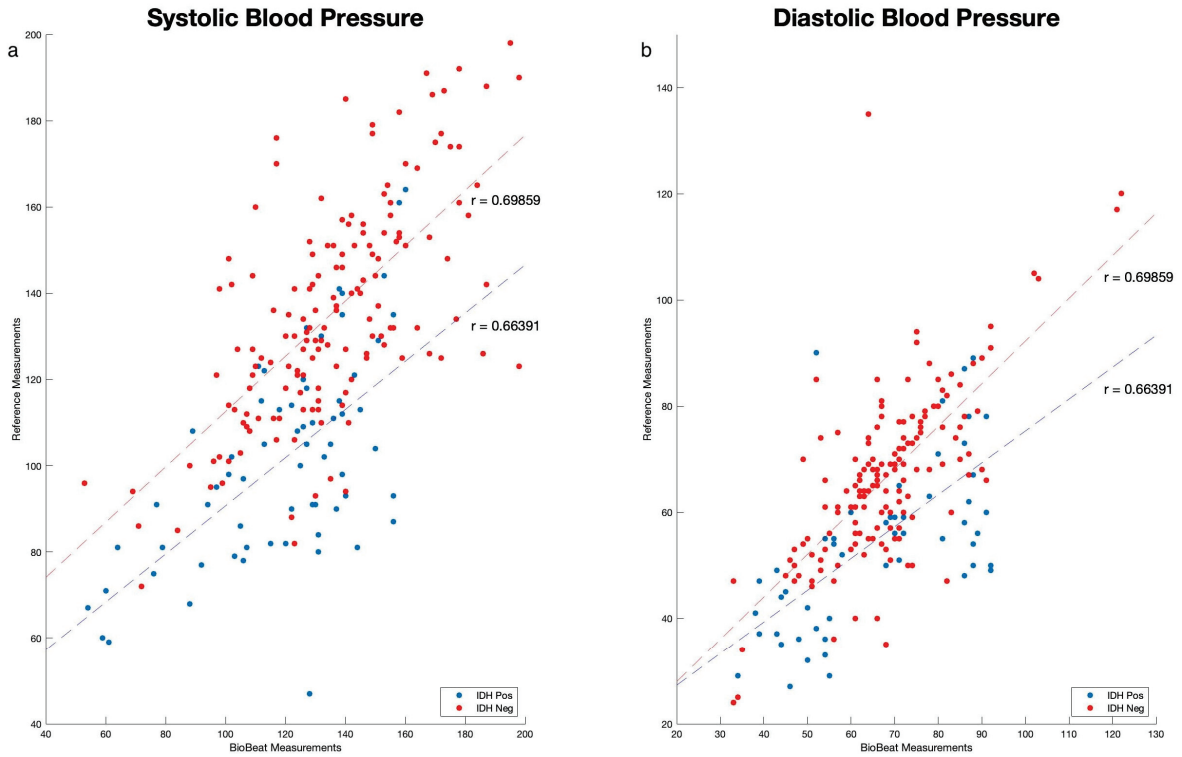


Figure 2. Blood pressure correlation curves between the BP devices: (**a**) systolic blood pressure (SBP) and (**b**) diastolic blood pressure (DBP). Red dots and dashed line are patients that are intradialytic hypotension positive (IDH Pos) and in blue are intradialytic hypotension negative (IDH Neg).

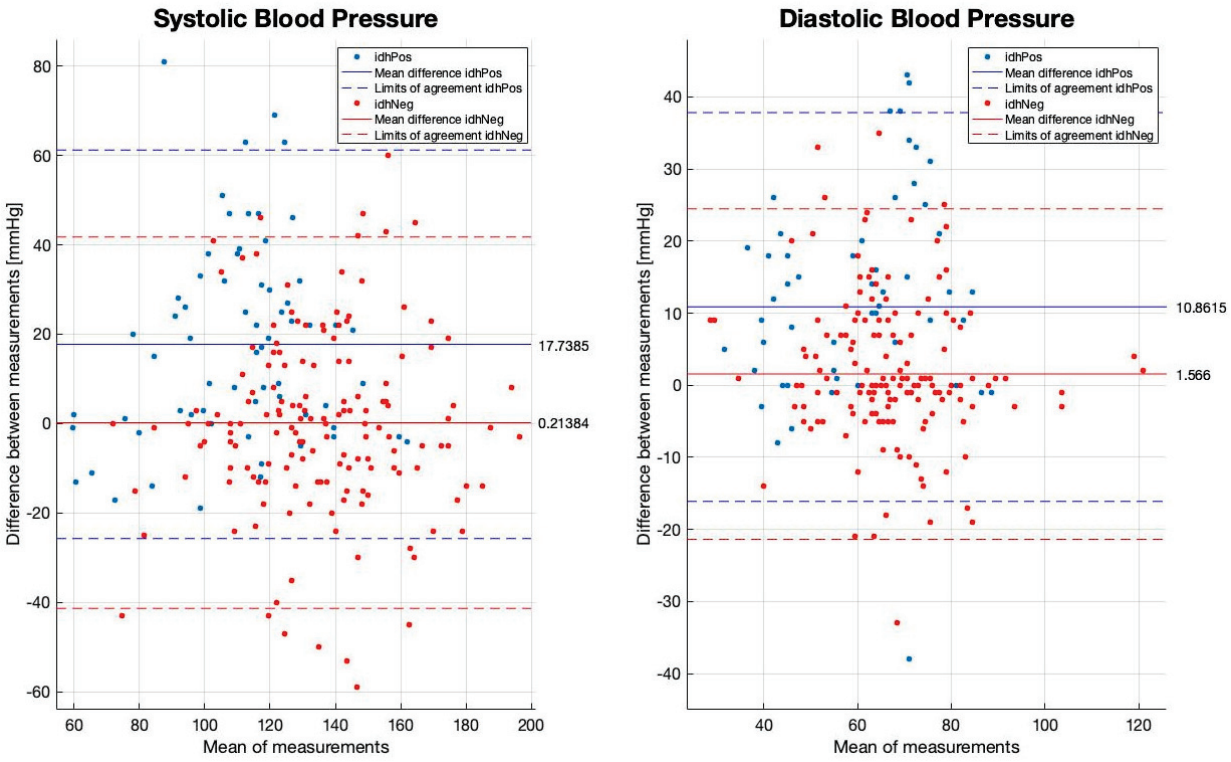


Figure 3. Bland–Altman plots comparing all measurements using the cuff-based and the PPG-based cuffless devices during the dialysis sessions: (**a**) systolic blood pressure; (**b**) diastolic blood pressure. Red dots, IDH positive; blue dots, IDH negative. Dashed line—95% limit of agreement (LOA); continuous line—mean bias.

Next, we compared the mean baseline values of the advanced parameters using the PPG-based cuffless device between IDH and non-IDH sessions. No significant differences were found for any of the vitals (Table 2).

Table 2. Basic mean results of advanced continuous hemodynamic parameters.

	non-IDH (n = 76)	**IDH (n = 22)**	***p*-Value**
Pre-dialysis weight (kg)	96.0 ± 8.02	75.3 ± 12.6	<0.001
Post-dialysis weight (kg)	93.3 ± 7.78	73.7 ± 12.6	<0.001
Weight difference (kg)	−1.71 ± 0.91	−2.12 ± 0.70	0.059
Dialysis duration (hours)	4.10 ± 0.35	3.85 ± 0.31	0.004
Heart rate (beats/min)	87 ± 12	83 ± 14	0.18
Oxygen saturation (%)	98.0 ± 0.7	97.7 ± 1.9	0.59
Respiratory rate (breaths/min)	12 ± 1	12 ± 2	0.39
Temperature (°C)	36.0 ± 0.1	36.0 ± 0.2	0.12
Cardiac Output (L/min)	7.37 ± 1.1	7.22 ± 1.7	0.41
Stroke volume (mL)	85.1 ± 7.8	86.4 ± 9.2	0.56
Systolic blood pressure (mmHg)	123 ± 34	136 ± 32	0.20
Diastolic blood pressure (mmHg)	64 ± 19	67 ± 16	0.34
Mean arterial pressure (mmHg)	84 ± 23	90 ± 20	0.27
Pulse pressure (mmHg)	59 ± 22	69 ± 23	0.20
Systemic vascular resistance ($dyn \cdot s \cdot cm^{-5}$)	947 ± 340	1040 ± 283	0.30

Changes in the SBP, DBP and advanced measured parameters during the dialysis sessions of all patients are shown in Figure 4. During the HD sessions, patients experiencing IDH exhibited earlier and more pronounced reductions in SBP and DBP compared to those without IDH. Specifically, within the first 10% of the dialysis session, both SBP and DBP significantly decreased in the IDH group (which was clinically defined later by the cuff-based measurements) as compared to the non-IDH group. The analysis of the advanced hemodynamic parameters measured by the wearable device revealed significant differences between the IDH and non-IDH sessions. Specifically, SV, CO, SVR, body temperature, SPO_2, RR, PP, and MAP were markedly different between the two groups.

However, there were no significant differences between the groups in terms of risk factors or other hemodynamic parameters identified 15 min prior to the HD session that could predict IDH.

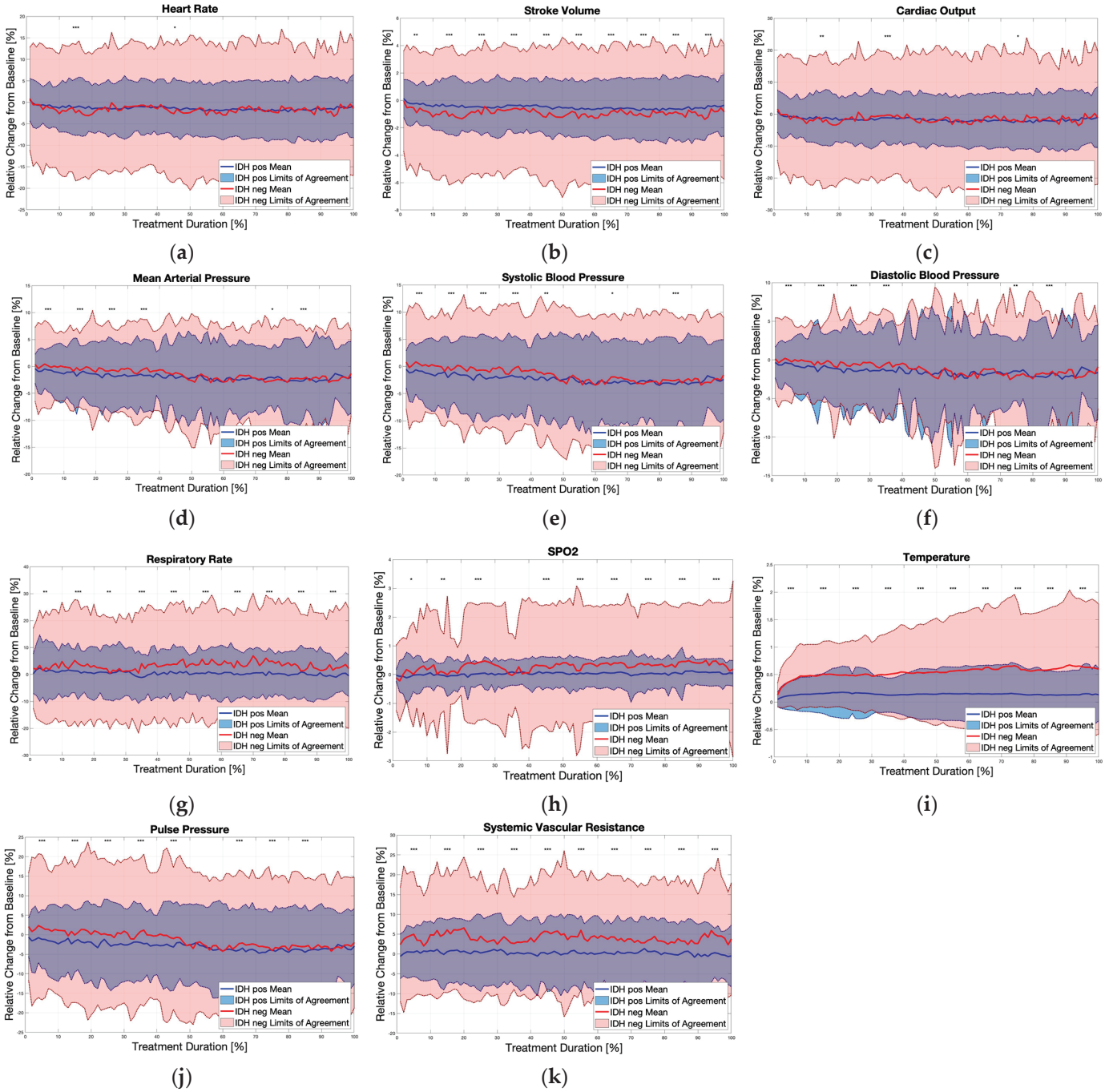


Figure 4. The physiological changes during dialysis in all patients. Baseline measurements were taken as the first 15 min of each dialysis session. Then, changes in each vital were calculated as the relative change during the session (100%) as compared to baseline. A statistical analysis was performed on each 10% separately. An independent sample *t*-test was used to compare the means between IDH and non-IDH for every 10%. The blue (IDH) and the red (non-IDH) lines represent the mean values, and the colored background represent the 95% CI. * $p < 0.05$; ** $p < 0.01$; *** $p < 0.001$.

4. Discussion

In this preliminary study, we have shown that the wearable remote patient monitoring platform can track hemodynamic parameters during dialysis sessions.

Previous studies emphasized that the pathogenesis of IDH is still not completely understood. Yet, it is regarded as multifactorial and is the result of a combination of a decline in blood volume and impaired vascular resistance at a background of a reduced

cardiovascular reserve, in a way that excessive ultrafiltration may decrease the cardiac output. This is especially true when compensatory mechanisms such as HR, myocardial contractility, vascular tone, and splanchnic flow shifts fail to be optimally recruited [18–23]. When diving into the basic characteristics of the patients, an interesting image appears. Many IDH patients also had peripheral vascular disease; this may reflect the vascular contribution to IDH pathogenesis but may also be explained by the technical difficulty in assessing blood pressure in those patients using standard cuff-based measurements. Interestingly, pulmonary hypertension was less common in the IDH group. This finding was not described previously, and its mechanism is obscure. Diuretics were associated with higher rates of IDH. This observation may be explained by intravascular depletion prior to the dialysis, or with the direct vasodilative effect of certain diuretics.

The correlation of the BP measurements between the PPG device and the cuff in both groups is lower than what is accepted in various ISO standards. However, the ISO standard testing is conducted under "sterile" conditions, not allowing the person—among other criteria—to smoke or drink caffeine in the 30 min before BP is taken; they should sit still at least 5 min before measurements are taken, and during measurements the cuffed arm should be kept on a flat surface at the heart level, sitting upright, back straight, feet flat on the floor and not crossed, without movement and no talking. Moreover, this should not be conducted under dynamic circumstances such as hemodialysis. For this reason, we regard the correlation values as good, given the fact they were obtained in a "real-life" scenario that incorporates hemodynamic changes resulting from the shift of fluids. The Bland–Altman analysis revealed a bias in the measurements in the IDH group, but not in the non-IDH group, suggesting suboptimal sensitivity. We could not explain these phenomena, but hemodynamic instability in IDH patients may play a role. Importantly, previous validation studies performed following the ISO standard definitions and under more sterile conditions have shown high correlations between the PPG-based monitor and other devices [24,25].

The early and profound BP reduction in the IDH group is noted at the beginning of the dialysis sessions. Although no hemodynamic parameters helped us significantly predict the IDH events, we assume that a larger cohort may help us with this prediction in the future.

In hypovolemic states, as the CO is reduced due to reduced effective intravascular volume, the main compensatory mechanisms to retain BP are vasoconstriction and SVR elevation [26]. The non-IDH group demonstrated a "classic" reaction to hypovolemia; a reduction in SV and an elevation of SVR. However, the IDH group showed no mean change in SV or SVR. This finding supports the theories that IDH is not a pure hemodynamic response to hypovolemia but a neurohormonal-mediated response, such as a reduction in the sympathetic tone or loss of response to vasopressin [23].

On a general note, as the trend for home dialysis increases, it is important to acknowledge that implementing home dialysis presents several challenges, though the benefits can outweigh these obstacles for many patients [27]. Some challenges are as follows: training requirements of both patients and their caregivers (including learning how to operate the dialysis machine, handle supplies, monitor vital signs, and respond to emergencies); understanding how to troubleshoot common issues that may arise during treatment (e.g., alarms or blood flow problems); adequate space is needed to set up and store equipment and supplies; a reliable source of clean water is required for preparing dialysis fluid; patients performing dialysis at home are at risk of infection, particularly if proper hygiene practices are not followed; social support is often required by patients undergoing home dialysis from family members or caregivers, which may place a strain on relationships and caregiving resources; though home dialysis can be cost effective compared to in-center treatments in the long run, initial setup costs can be significant, and patients must consider the financial implications of ongoing supplies, equipment maintenance, and potential modifications to their home; dialysis can have a significant psychological impact on patients and their families, including feelings of anxiety, isolation, or depression; and patients and caregivers

must be prepared to handle emergencies that may arise during dialysis treatment, such as sudden drops in blood pressure or equipment malfunction. This requires access to emergency support services and the ability to respond quickly and effectively. Despite these challenges, it seems that home dialysis offers many benefits, including greater flexibility, improved quality of life, and the ability to perform treatments in the comfort of one's own home. With proper support, education, and resources, many patients successfully manage home dialysis and experience better health outcomes.

Remote patient monitoring (RPM) can significantly enhance the management of home dialysis by providing real-time and continuous monitoring of relevant patients' vital signs. This enables the early detection of potential complications or changes in health status, allowing for timely interventions and potentially improved patient outcomes [28]. Moreover, RPM can track patients' adherence to their dialysis treatment regimen by monitoring treatment sessions, including the duration and frequency of dialysis sessions. Healthcare providers can identify patients who may be struggling with adherence and provide additional support or education as needed. Another potential advantage would be using the valuable data generated by RPM systems in data-driven decision support. Healthcare providers can analyze these data to identify trends, assess treatment efficacy, and make informed decisions to optimize patient care. Overall, it seems as if RPM could play an important role in enhancing the safety, effectiveness, and convenience of home dialysis by providing continuous support, proactive management, and timely interventions to optimize patient outcomes.

It seems that seeking to identify the optimal intradialytic BP range is vital in driving targeted interventions that clinicians may be able to implement to minimize IDH events and prevent the long-term sequela of IDH. This could include pre-session changes of the dialysis machine setting, adjusting the dialysis settings during the session, and even stopping the session if required. Further investigation should be undertaken to create tools that predict IDH events easily. This, in turn, could allow the early institution of adjustments to the dialysis protocol, preventing IDH from appearing and hopefully avoiding immediate adverse events as well as any long-term sequela.

Regarding this gap in management, the noninvasive system used in this study can serve as an advanced platform and, when integrated with dialysis sessions, provide an early awareness of the risk of IDH. The continuous monitoring may alert the clinician early regarding hemodynamic changes that may represent certain conditions other than IDH, such as acute cardiac events, sepsis, and infusion reaction. Moreover, it might facilitate efforts of moving dialysis sessions into the home, assuring proper hemodynamic monitoring with early notifications and alerts.

Patients were highly compliant with the use of the device, emphasizing the ease of use when compared with cuff-based devices, yet this setting was relatively short in nature. We have previously shown that patients are highly compliant and satisfied with using the device over a longer period, including 24 h and beyond [19,29].

The limitations of this study include its single-center design, which may restrict the generalization of the findings to other populations or settings. Additionally, this study did not specifically address the impact of ethnicity on the detection and management of IDH, which could limit the applicability of the results to different ethnic groups. There may also be unmeasured confounders such as comorbidities, medication use, or other patient-specific factors that could have influenced the results but were not accounted for in the analysis. Though intervention in the case of intradialytic hypotension is highly important, the focus of this study was on the diagnosis and prevention of IDH, and the response of the dialysis unit team was not documented. This should also be looked at in future studies.

Furthermore, the study was limited by its relatively small number of patients. However, even in this small group, the advantages of using such a platform in the early detection of IDH were apparent. Future studies should aim to include larger patient populations to further evaluate the clinical outcomes associated with the use of the wearable platform.

Lastly, we did not collect data on the specific timing of intradialytic hypotension occurrences during the dialysis sessions. Therefore, we were unable to analyze changes in cardiac output, pulse pressure, or stroke volume in relation to the exact timing of IDH events. This should be also looked at in future studies using similar monitoring platforms.

To conclude, this preliminary observational study shows that further studies with larger numbers of participants are required in order to determine whether continuous monitoring using PPG-based devices could serve for the early prediction and prevention of IDH. Interestingly, we show that the pathophysiology of IDH is not explained solely by hypovolemia, but rather another factor that causes a reduction in SVR may play a role.

Supplementary Materials: The following supporting information can be downloaded at: https://www.mdpi.com/article/10.3390/biomedicines12061177/s1, Figure S1: The study flow chart.

Author Contributions: Conceptualization, A.E. and D.N.; methodology, Y.K., A.E. and D.N.; validation, N.G., A.E. and D.N.; formal analysis, Y.K., D.P., S.A., N.G., A.E., Y.G. and D.N.; investigation, Y.K., I.G., S.A., P.M., M.F., M.T., A.E. and D.N.; resources, A.B.I., A.E. and D.N.; data curation, N.G. and A.E.; writing—original draft preparation, Y.K., N.G., A.E., Y.G. and D.N.; writing—review and editing, all authors; visualization, A.E., Y.G. and D.N.; supervision, A.E. and D.N.; project administration, A.E. and D.N.; funding acquisition, A.E. All authors have read and agreed to the published version of the manuscript.

Funding: The PPG monitor was provided by Biobeat Technologies Ltd. with no cost to the researchers. No additional external fundings were provided.

Institutional Review Board Statement: This study was conducted in accordance with the Declaration of Helsinki, was approved by the Institutional Review Board of the Hadassah Ein-Kerem Medical Center, Jerusalem, Israel (protocol code PPGDIA001, December 2020), and was registered in ClinicalTrials.gov (NCT04680039).

Informed Consent Statement: Informed consent was obtained from all subjects involved in the study.

Data Availability Statement: The data presented in this study are available on request from the corresponding author. The data are not publicly available due to privacy and ethical definitions of the Hadassah Medical Center.

Acknowledgments: The authors would like to thank Michal Dranitzki Elhalel, Director of the Department of Nephrology and Hypertension, Hadassah Medical Center, Faculty of Medicine, Hebrew University of Jerusalem, Israel, for her valuable support of this study.

Conflicts of Interest: N.G., A.B.I., M.F., M.T., and A.E. are employees of Biobeat Technologies Ltd. Y.G serves as a member of the advisory board for Biobeat Technologies Ltd. D.N. received advisory fees from Biobeat Technologies Ltd. All other authors declare no conflicts of interest.

References

1. Himmelfarb, J. Hemodialysis complications. *Am. J. Kidney Dis.* **2005**, *45*, 1122–1131. [CrossRef] [PubMed]
2. Himmelfarb, J.; Ikizler, T.A. Hemodialysis. *N. Engl. J. Med.* **2010**, *363*, 1833–1845. [CrossRef] [PubMed]
3. Flythe, J.E.; Xue, H.; Lynch, K.E.; Curhan, G.C.; Brunelli, S.M. Association of mortality risk with various definitions of intradialytic hypotension. *J. Am. Soc. Nephrol.* **2015**, *26*, 724–734. [CrossRef] [PubMed]
4. Kooman, J.; Basci, A.; Pizzarelli, F.; Canaud, B.; Haage, P.; Fouque, D.; Konner, K.; Martin-Malo, A.; Pedrini, L.; Tattersall, J.; et al. EBPG guideline on haemodynamic instability. *Nephrol. Dial. Transplant.* **2007**, *22*, ii22–ii44. [CrossRef] [PubMed]
5. Tislér, A.; Akócsi, K.; Borbás, B.; Fazakas, L.; Ferenczi, S.; Görögh, S.; Kulcsár, I.; Nagy, L.; Sámik, J.; Szegedi, J.; et al. The effect of frequent or occasional dialysis-associated hypotension on survival of patients on maintenance haemodialysis. *Nephrol. Dial. Transplant.* **2003**, *18*, 2601–2605. [CrossRef] [PubMed]
6. McIntyre, C.W.; Odudu, A. Hemodialysis-associated cardiomyopathy: A newly defined disease entity. *Semin. Dial.* **2014**, *27*, 87–97. [CrossRef] [PubMed]
7. McIntyre, C.W.; Burton, J.O.; Selby, N.M.; Leccisotti, L.; Korsheed, S.; Baker, C.S.; Camici, P.G. Hemodialysis-induced cardiac dysfunction is associated with an acute reduction in global and segmental myocardial blood flow. *Clin. J. Am. Soc. Nephrol.* **2008**, *3*, 19–26. [CrossRef] [PubMed]
8. Zucchelli, P.; Santoro, A. Dialysis-induced hypotension: A fresh look at pathophysiology. *Blood Purif.* **1993**, *11*, 85–98. [CrossRef] [PubMed]

9. Germain, M.J.; Joubert, J.; O'Grady, D.; Nathanson, B.H.; Chait, Y.; Levin, N.W. Comparison of stroke volume measurements during hemodialysis using bioimpedance cardiography and echocardiography. *Hemodial. Int.* **2018**, *22*, 201–208. [CrossRef]
10. Lee, A.J.; Cohn, J.H.; Ranasinghe, J.S. Cardiac output assessed by invasive and minimally invasive techniques. *Anesthesiol. Res. Pract.* **2011**, *2011*, 475151. [CrossRef]
11. Levin, N.W.; de Abreu, M.H.F.G.; Borges, L.E.; Tavares Filho, H.A.; Sarwar, R.; Gupta, S.; Hafeez, T.; Lev, S.; Williams, C. Hemodynamic response to fluid removal during hemodialysis: Categorization of causes of intradialytic hypotension. *Nephrol. Dial. Transplant.* **2018**, *33*, 1643–1649. [CrossRef] [PubMed]
12. Nachman, D.; Constantini, K.; Poris, G.; Wagnert-Avraham, L.; Gertz, S.D.; Littman, R.; Kabakov, E.; Eisenkraft, A.; Gepner, Y. Wireless, noninvasive, wearable device for continuous remote monitoring of hemodynamic parameters in a swine model of controlled hemorrhagic shock. *Sci. Rep.* **2020**, *10*, 17684. [CrossRef] [PubMed]
13. Eisenkraft, A.; Maor, Y.; Constantini, K.; Goldstein, N.; Nachman, D.; Levy, R.; Halberthal, M.; Horowitz, N.A.; Golan, R.; Rosenberg, E.; et al. Continuous Remote Patient Monitoring Shows Early Cardiovascular Changes in COVID-19 Patients. *J. Clin. Med.* **2021**, *10*, 4218. [CrossRef]
14. Nachman, D.; Eisenkraft, A.; Kolben, Y.; Carmon, E.; Hazan, E.; Goldstein, N.; Ben Ishay, A.; Hershkovitz, M.; Fons, M.; Merin, R.; et al. Diurnal cardio-respiratory changes in ambulatory individuals deciphered using a multi-parameter wearable device. *Digit. Health* **2023**, *9*, 20552076231218885. [CrossRef] [PubMed]
15. Eisenkraft, A.; Goldstein, N.; Merin, R.; Fons, M.; Ishay, A.B.; Nachman, D.; Gepner, Y. Developing a real-time detection tool and an early warning score using a continuous wearable multi-parameter monitor. *Front. Physiol.* **2023**, *14*, 1138647. [CrossRef] [PubMed]
16. Sharabi, I.; Merin, R.; Gluzman, Y.; Grinshpan, R.; Shtivelman, A.; Eisenkraft, A.; Rubinshtein, R. Assessing the use of a noninvasive monitoring system providing multiple cardio-pulmonary parameters following revascularization in STEMI patients. *Digit. Health* **2023**, *9*, 20552076231179014. [CrossRef] [PubMed]
17. Dagan, M.; Kolben, Y.; Goldstein, N.; Ben Ishay, A.; Fons, M.; Merin, R.; Eisenkraft, A.; Amir, O.; Asleh, R.; Ben-Yehuda, A.; et al. Advanced Hemodynamic Monitoring Allows Recognition of Early Response Patterns to Diuresis in Congestive Heart Failure Patients. *J. Clin. Med.* **2022**, *12*, 45. [CrossRef] [PubMed]
18. Daugirdas, J.T. Dialysis hypotension: A hemodynamic analysis. *Kidney Int.* **1991**, *39*, 233–246. [CrossRef] [PubMed]
19. Reilly, R.F. Attending rounds: A patient with intradialytic hypotension. *Clin. J. Am. Soc. Nephrol.* **2014**, *9*, 798–803. [CrossRef]
20. Chou, J.A.; Kalantar-Zadeh, K.; Mathew, A.T. A brief review of intradialytic hypotension with a focus on survival. *Semin. Dial.* **2017**, *30*, 473–480. [CrossRef]
21. Chou, J.A.; Streja, E.; Nguyen, D.V.; Rhee, C.M.; Obi, Y.; Inrig, J.K.; Amin, A.; Kovesdy, C.P.; Sim, J.J.; Kalantar-Zadeh, K. Intradialytic hypotension, blood pressure changes and mortality risk in incident hemodialysis patients. *Nephrol. Dial. Transplant.* **2018**, *33*, 149–159. [CrossRef] [PubMed]
22. Sars, B.; van der Sande, F.M.; Kooman, J.P. Intradialytic Hypotension: Mechanisms and Outcome. *Blood Purif.* **2020**, *49*, 158–167. [CrossRef] [PubMed]
23. Kanbay, M.; Ertuglu, L.A.; Afsar, B.; Ozdogan, E.; Siriopol, D.; Covic, A.; Basile, C.; Ortiz, A. An update review of intradialytic hypotension: Concept, risk factors, clinical implications and management. *Clin. Kidney J.* **2020**, *13*, 981–993. [CrossRef] [PubMed]
24. Nachman, D.; Gilan, A.; Goldstein, N.; Constantini, K.; Littman, R.; Eisenkraft, A.; Grossman, E.; Gepner, Y. Twenty-Four-Hour Ambulatory Blood Pressure Measurement Using a Novel Noninvasive, Cuffless, Wireless Device. *Am. J. Hypertens.* **2021**, *34*, 1171–1180. [CrossRef] [PubMed]
25. Nachman, D.; Gepner, Y.; Goldstein, N.; Kabakov, E.; Ishay, A.B.; Littman, R.; Azmon, Y.; Jaffe, E.; Eisenkraft, A. Comparing blood pressure measurements between a photoplethysmography-based and a standard cuff-based manometry device. *Sci. Rep.* **2020**, *10*, 16116. [CrossRef]
26. Massaro, A.F. Approach to the Patient with Shock. In *Harrison's Principles of Internal Medicine*, 21st ed.; Loscalzo, J., Fauci, A., Kasper, D., Hauser, S., Longo, D., Jameson, J.L., Eds.; McGraw-Hill Education: New York, NY, USA, 2022; Available online: https://accessmedicine.mhmedical.com/content.aspx?bookid=3095&sectionid=265425332 (accessed on 11 June 2023).
27. United States Renal Data System. 2023 USRDS Annual Data Report: Epidemiology of Kidney Disease in the United States. National Institutes of Health, National Institute of Diabetes and Digestive and Kidney Diseases, Bethesda, MD. 2023. Available online: https://usrds-adr.niddk.nih.gov/2023 (accessed on 19 May 2024).
28. Canaud, B.; Kooman, J.; Davenport, A.; Campo, D.; Carreel, E.; Morena-Carrere, M.; Cristol, J.P. Digital health technology to support care and improve outcomes of chronic kidney disease patients: As a case illustration, the Withings toolkit health sensing tools. *Front. Nephrol.* **2023**, *3*, 1148565. [CrossRef]
29. Hazan, E.; Azarya, I.; Dvir, D.; Gonen, V.; Ekhilevitch, G.; Merin, R.; Eisenkraft, A.; Carmon, E. Assessing Workflow, Satisfaction, and Potential Cost Reduction when Using a Cuffless Ambulatory Blood Pressure Monitor. *J. Fam. Med. Community Health* **2022**, *9*, 1189.

Disclaimer/Publisher's Note: The statements, opinions and data contained in all publications are solely those of the individual author(s) and contributor(s) and not of MDPI and/or the editor(s). MDPI and/or the editor(s) disclaim responsibility for any injury to people or property resulting from any ideas, methods, instructions or products referred to in the content.

biomedicines

MDPI

Article

Electrical Activity Changes and Neurovascular Unit Markers in the Brains of Patients after Cardiac Surgery: Effects of Multi-Task Cognitive Training

Irina Tarasova *, Irina Kukhareva, Darya Kupriyanova, Tatjana Temnikova, Evgenia Gorbatovskaya and Olga Trubnikova

Research Institute for Complex Issues of Cardiovascular Diseases, Academician Barbarash Blvd., 6, 650002 Kemerovo, Russia; kuchin@kemcardio.ru (I.K.); kuprds@kemcardio.ru (D.K.); t.13.ermakova@mail.ru (T.T.); eugenia.tarasowa@yandex.ru (E.G.); truboa@kemcardio.ru (O.T.)
* Correspondence: iriz78@mail.ru

Abstract: Background: There is growing interest in finding methods to enhance cognitive function and comprehend the neurophysiological mechanisms that underlie these improvements. It is assumed that non-pharmacological interventions have better results in cognitive recovery. The aim of this study was to assess the effect of multi-task cognitive training (MTT) on electroencephalographic (EEG) changes and markers of the neurovascular unit in patients undergoing coronary artery bypass grafting (CABG). Methods: This prospective cohort study involved 62 CABG patients aged 45–75 years, 30 of whom underwent a 5–7-day MTT course. The groups of patients were comparable with respect to baseline clinical and anamnestic characteristics. An EEG study was performed before surgery and 11–12 days after CABG. Markers of the neurovascular unit (S100β, NSE, and BDNF) were examined at three time points: before surgery, within the first 24 h after surgery, and 11–12 days after CABG. Results: Patients without training demonstrated higher relative theta power changes compared to the MTT patients. The course of MTT was associated with low plasma S100β concentration but high BDNF levels at the end of the training course. Conclusions: The theta activity changes and the markers of the neurovascular unit (S100β, BDNF) indicated that the severity of brain damage in cardiac surgery patients after a short course of MTT was slightly reduced. Electrical brain activity indicators and vascular markers can be informative for monitoring the process of cognitive rehabilitation in cardiac surgery patients.

Keywords: cognitive training; brain electrical activity; neurovascular unit; S100β; BDNF; coronary surgery

1. Introduction

The development and availability of advanced medical technologies have increased life expectancy. However, age-dependent diseases, including cardiovascular pathology, significantly increase the risk of cognitive impairment and disability [1–3]. Previous studies have shown that successful cognitive functioning depends on adequate cerebral blood flow [4,5]. Cardiovascular diseases independently lead to cerebral blood flow disorders and cognitive impairments, and may require cardiac surgery with artificial blood circulation, which can also cause acute ischemic brain damage [6,7].

The search for methods to enhance cognitive functioning and understand the neurophysiological mechanisms that underlie these improvements is growing. Non-pharmacological interventions are recognized by many experts as the most effective [8–10]. Recent reports indicate that combining physical and cognitive exercises enhances cognitive functions more effectively than either approach alone [11]. The multi-tasking approach, which involves performing motor and cognitive tasks simultaneously, triggers the activation of the different cognitive domains, such as attention, inhibitory control, and executive function [10,12].

Preliminary data showed that multi-task training (MTT) can provide effective cognitive recovery in cardiac surgery patients [10,13].

There is limited research on the impact of multi-tasking on different aspects of cognitive recovery. This is especially true for the recovery of cognitive functions in the postoperative period of cardiac surgery.

Digital electroencephalography (EEG) is widely used for the non-invasive control of brain activity and studying the fundamental mechanisms of brain functioning [14–16]. Unlike MRI and lumbar puncture, EEG is a non-invasive and inexpensive approach, commonly used in describing cognitive disorders of various origins, as it can study high brain functions with maximum time resolution [17,18]. The relevance of theta rhythms of resting EEG for differentiating patients with and without vascular cognitive disorders has been previously identified. High theta rhythm power, mainly in the posterior brain areas, has been shown to be associated with cognitive impairment in cardiac patients [19]. In the study by Deiber et al., the frontal-induced theta response was significantly reduced at baseline in progressive MCI compared to both stable MCI and controls, suggesting altered top-down attentional control [20]. Thus, theta activity changes can be viewed as a marker for impaired attention and executive functions.

Understanding neurophysiological changes associated with rehabilitation remains a burgeoning area of research. Gangemi et al. investigated the neurophysiological effects of cognitive stimulation training in the chronic phase of patients with ischemic stroke. After training, there was a significant increase in both the alpha band power in the occipital areas and the beta band power in the frontal areas, while the theta band power did not show any significant variation [21]. The effects of multi-task executive function training on the features of specific EEG microstates were examined in a study by Santarnecchi and colleagues. The left parietal and occipital regions showed an increase in current density EEG activity after cognitive training, as well as a decrease in density in the right inferior frontal gyrus and insula [22]. The authors concluded that the changes in EEG dynamics associated with successful training suggest the importance of low-level visual computational processes, as well as prefrontal control over parietal dynamics.

Peripheral blood biomarkers for brain damage can provide information about various pathological states [23–25]. The neurovascular unit has already been identified by several indicators, and markers that can measure its functioning are currently being examined. Among these indicators is S-100 calcium-binding protein B (S100β). This protein is mainly expressed in astrocytes, which allows it to be seen as an acute ischemia marker associated with the severity of brain damage [23,26]. In a study by Onatsu et al., it was shown that serum S100β levels are correlated with neurological deficits, infarct size, and significant brain edema during acute stroke [24].

Neuron-specific enolase (NSE) is a glycolytic enzyme that is produced in the cytoplasm of neurons and is precise enough in its ability to detect neuronal damage [27]. Neuron-specific enolase is increased in acute ischemic brain damage [28]. NSE is used as a marker for postoperative cerebral dysfunction in patients who have undergone coronary and carotid artery revascularization, but it is unclear whether it predicts cerebrovascular outcomes [29].

Also, in addition to neurophysiological methods of studying the recovery process in cognitive structures and understanding the mechanisms involved, changes in neurotrophic factors, in particular, brain-derived neurotrophic factor (BDNF), are now of interest to researchers. BDNF is believed to play a key role in brain development and maintenance [30]. Compared to other members of the growth neurotrophic factor family, BDNF is highly expressed in the cerebral cortex and hippocampus [31]. It has been shown that BDNF promotes neuroplasticity and facilitates synaptic transmission, dendritic modification, receptor trade, and long-term potentiation [30]. Moreover, BDNF supports neurogenesis, synaptic growth, and recovery [32]. In longitudinal observational studies of older persons, higher baseline BDNF levels were associated with reduced probability of dementia development [30,33]. It should be noted that BDNF changes demonstrated a close

relationship with changes in the brain under pharmacological and non-pharmacological interventions, including physical and cognitive training. This is one reason why BDNF may be considered one of the most promising biomarkers for the study of the cognitive recovery processes, especially when using multi-task training.

A study by Huang et al. investigated the effects of motor control training on upper limb motor function and neuroplasticity in stroke patients. Significant improvements in overall upper limb function were found after the intervention. BDNF expression levels significantly increased only in the intervention group. The authors proposed that BDNF induction might be affected by a specific type of intervention or rehabilitation program [34].

The advantages of electrophysiological methods and neurotrophic factors suggest that they can be used to identify the key neurophysiological characteristics of successful cognitive recovery in cardiac surgery patients. The current study aimed to investigate the relationship between intervention-associated changes in markers of the neurovascular unit and EEG activity in cardiac surgery patients with and without multi-task training.

2. Materials and Methods

2.1. Patients

This study was approved by the Ethical Committee of the Research Institute for Complex Issues of Cardiovascular Diseases (protocol No. 10 dated 12 October 2020), and was in line with the Helsinki Declaration. The study design is outlined in Figure 1. The study was conducted in a prospective, observational cohort setting. A sample of 60 subjects was chosen from a group of patients who had on-pump coronary artery bypass grafting (CABG) at the Research Institute for Complex Issues of Cardiovascular Diseases clinic. Informed written consent was obtained from all participants included in the study. The inclusion criteria consisted of patients who were aged 45 years or older, had elective CABG, were right-handed to eliminate any influence of laterality on EEG, and had a Montreal Cognitive Assessment (MoCA) score $\geq$ 18. Standardized physical and instrumental examinations were performed on all patients involved. The examiners were not informed about the nature of the patients' participation in the study.

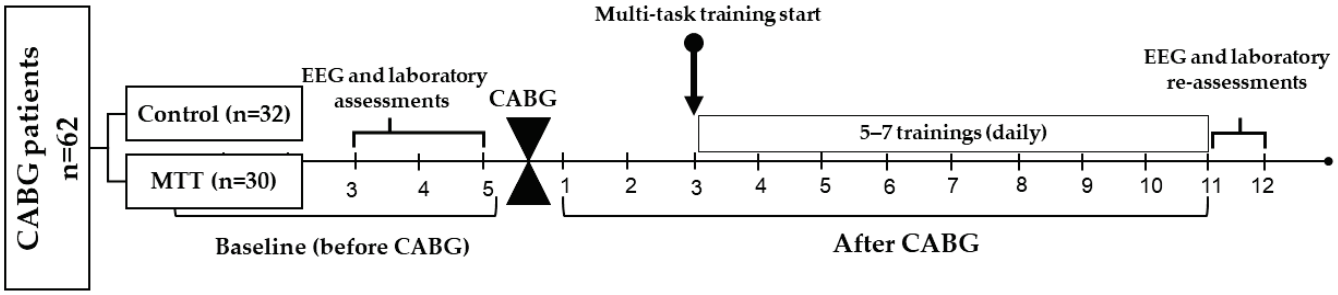


Figure 1. Design of the study. CABG, coronary artery bypass grafting; MTT, multi-task training.

The criteria for the exclusion of patients from the study were as follows:

- Significant pathological changes in the brain, including leukoaraiosis and cysts, as revealed through multi-layered spiral computed tomography;
- Diseases of the central nervous system, including stroke, epilepsy, and neuroimmunological disorders;
- Functional class IV heart failure according to the New York Heart Association (FC NYHA IV) guidelines;
- Life-threatening arrhythmias;
- Malignant pathology;
- Chronic obstructive pulmonary disease with persistent breathing difficulty;
- Depressive symptoms, as identified by the Beck Depression Inventory (BDI-II) (sum scores > 8).

All participants had normal or corrected-to-normal visual acuity, and none reported a history of alcohol or drug abuse. The study did not include patients who were receiving anxiolytic therapy. To avoid any concomitant acute or chronic neurological conditions that could interfere with EEG data, a standard neurological examination was performed. A 1.5 T Exelart Atlas MRI system (Canon Medical Systems, Toshiba, Tokio, Japan) was used to assess the baseline brain state in all patients. Leukoaraiosis, cysts, gliosis, and the enlargement of cerebrospinal fluid spaces were examined. The majority of patients showed grade 1–2 leukoaraiosis, with periventricular and subarachnoid space dilation. These changes are characteristic of the different stages of chronic brain ischemia. Brain cysts were a reason for the exclusion of patients from the study.

The study sample was separated into two groups: multi-task training (MTT) I (n = 30) and control (n = 32). Table 1 presents the preoperative clinical and anamnestic characteristics of the groups. The MTT patients and controls were comparable in terms of age, baseline cognitive status, educational level, and other clinical factors. The treatment protocol and medication did not show any significant differences.

Table 1. The baseline clinical and anamnestic characteristics of the patients.

Variable	Multi-Task Training (n = 30)	Control (n = 32)	p-Value
Age, years, Me (Q25; Q75)	65 (60; 69)	61 (60; 65)	0.11
Male/female, n	6/24	6/26	0.91
MoCA, scores, Me (Q25; Q75)	26 (24; 28)	26 (23; 27)	0.61
Educational level, years, Me (Q25; Q75)	12 (11; 15)	12 (11; 14)	0.23
Functional class of angina, n (%) I–II III	 24 (80) 6 (20)	 24 (75) 8 (25)	0.63
Functional class NYHA, n (%) I–II III	 27 (78) 3 (10)	 30 (78) 2 (6)	0.86
Ejection fraction of left ventricle, %, Me (Q25; Q75)	62 (55; 68)	64 (55; 67)	0.61
Diabetes mellitus type 2, n (%)	9 (30)	15 (47)	0.25
Carotid artery stenoses, n (%)	17 (57)	10 (31)	0.07
Beta-blocker therapy, n (%)	30 (100)	30 (94)	0.31
Antiplatelet therapy, n (%)	30 (100)	32 (100)	-
ACEi therapy, n (%)	16 (53)	21 (66)	0.33
Statin therapy, n (%)	30 (100)	32 (100)	-
Diuretic therapy, n (%)	24 (80)	25 (78)	0.85
Cardiopulmonary bypass time, min, Me (Q25; Q75)	88 (69; 102)	72 (57; 105)	0.24
Surgery time, min, Me (Q25; Q75)	225 (175; 240)	200 (180; 245)	0.69

ACEi, angiotensin-converting enzyme inhibitor; MoCA, Montreal Cognitive Assessment Scale; NYHA, heart failure according to the New York Heart Association.

2.2. Neurophysiological Assessment

To exclude patients with severe cognitive impairment, cognitive screening using modified Russian versions of the Montreal Cognitive Assessment Scale (MoCA) was conducted upon admission to the hospital. Subjects with MoCA scores $\geq$ 18 were excluded from the study.

EEGs were recorded via a 62-channel Quik-cap using a NEUVO-64 system (Compumedics, El Paso, TX, USA) 2–3 days before surgery and 11–12 days after CABG. The EEGs were recorded in the eyes-closed condition in a dimly lit, soundproof, electrically

shielded room, and recording lengths were about 5 min. A modified 10/10 system was used to locate the electrodes on the scalp. The reference and ground electrodes were placed on the tip of the nose and the center of the forehead, respectively. To monitor eye movement artifacts, bipolar eye movement electrodes were placed on the canthus and cheek bone. The amplifier bandwidths were 1.0 to 50.0 Hz, and EEGs were digitized at 1000 Hz. The Neuroscan 4.5 software program (Compumedics, El Paso, TX, USA) was used to analyze the data offline using automatic algorithms. Visual inspection of the eye movements, electromyographic signals, and other artifacts were conducted. Artifact-free EEG fragments were divided into 2 s epochs and underwent Fourier transformation. For each subject, the EEG power values were averaged within the theta range (4–6 Hz). The EEG frequency band selected for the planned analysis was determined based on previous studies and the significance of low-frequency activity in brain damage [19,35]. The data from 56 leads were symmetrically averaged into 5 electrode zones in the left and right hemispheres: frontal (Fp1/2, AF3/4, F1/2, Fp3/4, Fp5/6, F7/8), central (FC1/2, FC3/4, FC5/6, C1/2, C3/4, C5/6), parietal (CP1/2, CP3/4, CP5/6, P1/2, P3/4, P5/6, P7/8), occipital (PO3/4, PO5/6, PO7/8, O1/2) and temporal (FT7/8, T7/8, TP7/8). The midline sites (Fpz, Fz, etc.) were excluded. The indicator of relative change (Δ) was calculated using the following formula: (baseline value–postoperative value)/baseline value) × 100%. The negative values of the indicator showed an increase in the theta power after the surgery compared to baseline, while the positive values showed a decrease.

2.3. Laboratory Data

Measurements were made at three time points in the study period (1–2 days before CABG, within the first 24 h after surgery, and 11–12 days after CABG). After a 12 h fasting period, venipuncture was used to collect whole blood samples from each patient. The procedure for obtaining serum involved allowing whole blood samples to coagulate at room temperature for 30 min, and then, centrifuging them at room temperature for 15 min at 3000 revolutions per minute. The collected serum was stored in polypropylene tubes at −70 °C until assayed. Measurements were taken for S100β, NSE, and BDNF serum parameters. The serum concentrations of S100β and NSE were quantitatively determined by using a commercially available enzyme-linked immunosorbent assay ELISA (FUJIREBIO Diagnostics, Inc., Tokio, Japan). The serum BDNF levels were measured using an ELISA kit (R&D Systems, Minneapolis, MN, USA) on a «Uniplan» tablet reader («PICON», Moscow, Russia). The intra-assay coefficients of variation were <10% for all measurements.

2.4. Multi-Task Training

The training course started 3–4 days after CABG and was conducted daily for 5–7 days. A postural balance task and three cognitive subtasks, including mental arithmetic, verbal fluency, and divergent tasks, were the basis of the original multi-task training protocol. To complete the postural balance exercise, trained patients stood on a balance platform and used visual feedback to keep their center of pressure in the same position. A marker on the monitor screen indicated the subject's pressure center. The patient's goal was to align this marker with the target positioned in the center of the monitor.

At the same time, the patient performed cognitive tasks of various types. The task of mental arithmetic was to subtract 7 from 100 in a sequential manner. The verbal fluency task involved saying as many words as possible that begin with a particular letter within a minute. In the divergent task, the participants were asked to come up with creative ways to use ordinary objects (such as a ruler, glass, and a rope). All tasks were completed one by one, with a short period of rest and breaks from the balance platform [10].

2.5. Statistical Analysis

The analysis of all data was carried out using Statistica 10.0 (StatSoft, Tulsa, OK, USA). The Shapiro–Wilk test was used to test for normal distribution of the data. The majority of the clinical parameters were not distributed in a normal way and were evaluated using

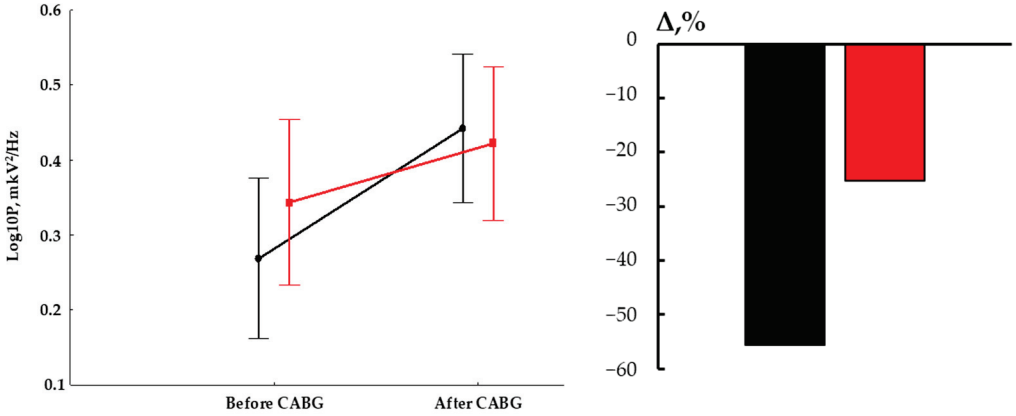
the Mann–Whitney test. To normalize the EEG data, they were transformed using Log10. Further analysis of the EEG data was carried out using a repeated-measures ANOVA. Levene's test was used to verify that the variances for EEG variables were equal. In the ANOVA, statistical significance was corrected using the Greenhouse–Geisser correction. Pairwise comparisons were carried out in groups of patients by using Newman-Keuls multiple comparison tests. The parameters of S100β, NSE, and BDNF after the logarithm transformation were compared with the *t*-test. Indicators within a group were compared using a dependent-samples *t*-test, and differences between groups were evaluated using an independent-samples *t*-test.

3. Results

3.1. Theta Power Data

The repeated measures ANOVA was conducted using GROUP (two levels: MTT/control) as the between-subjects factor and TIME (two levels: before and after surgery), AREA (five levels: frontal, central, parietal, occipital, and temporal), and LATERALITY (two levels: left and right hemispheres) as within-subjects factors.

Statistically significance of the factor TIME ($F_{1,60} = 80.92$, $p < 0.00001$, $\eta = 0.57$) and an interaction of the factors GROUP and TIME ($F_{1,60} = 11.51$, $p = 0.001$, $\eta = 0.16$) were found. Both MMT patients and the controls had higher values of the theta1-rhythm power at 11–12 days after CABG in comparison to the baseline values (Figure 2a). At the same time, the control group had more significant changes, which are also validated by differences in the indicator of relative changes (Δ), $p = 0.001$ (Figure 2b).



(**a**) (**b**)

Figure 2. The theta rhythm power changes in patients with MMT and controls: (**a**) Log10 power values: red line—MTT group, black line—control; (**b**) the indicator of relative change (Δ): red column—MTT group, black column—controls.

The AREA factor and interaction of the factors AREA and LATERALITY ($F_{1,60} = 80.37$, $p < 0.00001$, $\eta = 0.57$ and $F_{1,60} = 8.11$, $p = 0.00003$, $\eta = 0.11$, respectively) were statistically significant. This fact reflected the general patterns in the topographic distribution of theta activity in this sample (see Table 2). It was found that the values of the theta1-rhythm power were significantly higher in the left temporal and occipital areas in comparison to the right ones.

Table 2. The topographic distribution of theta activity in the CABG patients.

Brain Area	Left Hemisphere, Log10P, mkV^2/Hz, M ± SE	Right Hemisphere, Log10P, mkV^2/Hz, M ± SE	*p*-Value
Frontal	0.32 ± 0.038	0.33 ± 0.039	0.31
Central	0.36 ± 0.032	0.37 ± 0.032	0.1
Parietal	0.43 ± 0.030	0.43 ± 0.033	0.83
Occipital	0.47 ± 0.035	0.44 ± 0.036	0.001
Temporal	0.28 ± 0.031	0.24 ± 0.034	0.000009

3.2. Neurovascular Unit Data

In the control group, the S100β serum concentrations increased within the first 24 h after CABG ($p = 0.05$), and then, significantly decreased 11–12 days after cardiac surgery ($p = 0.03$) (see Figure 3). There were no significant differences in the MTT group, but the S100β changes showed the same trend. However, the S100β level was significantly lower in MMT patients than in the controls 11–12 days after cardiac surgery ($p = 0.03$). The changes in serum NSE concentrations were similar; however, the difference did not reach a statistically significant level.

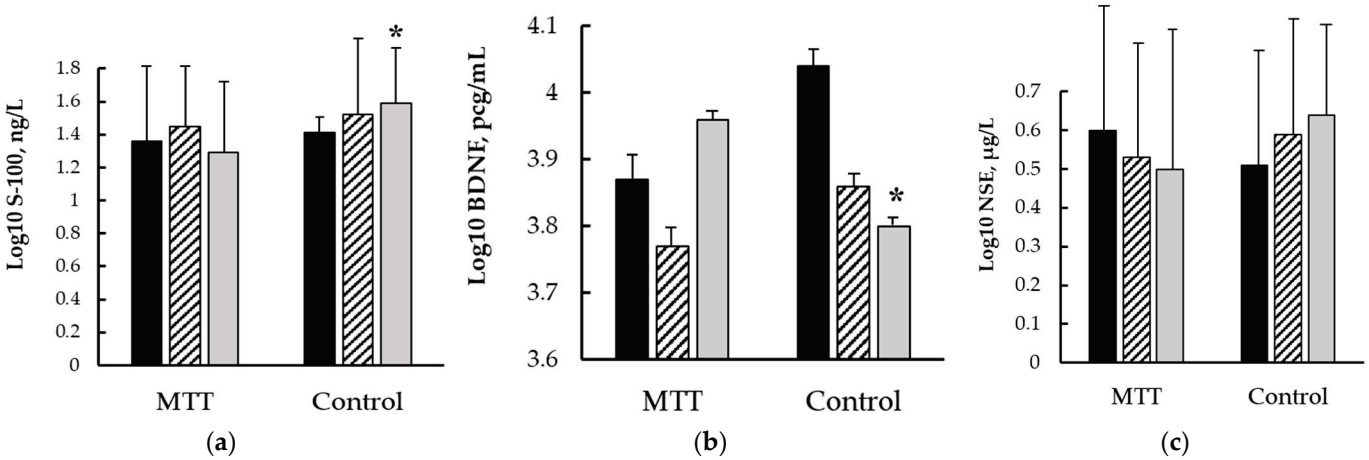


Figure 3. The serum concentrations of (**a**) S100β; (**b**) BDNF; and (**c**) NSE: dark columns—the pre-operative values, dashed columns—the first 24 h after surgery, light columns—the values 11–12 days after CABG, error bars denote SE, *—$p < 0.05$ in *t*-test for independent samples.

The BDNF serum levels decreased within the first 24 h of surgery in both the MTT group and the controls ($p = 0.01$ and $p = 0.02$, respectively). However, 11–12 days after CABG, the MTT group showed higher BDNF levels compared to the pre-operative values ($p = 0.05$). In the control group, the BDNF serum concentration continued to decrease compared to the first 24 h after CABG ($p = 0.03$). Also, the serum concentrations of BDNF were significantly higher in the MMT group than in the control group 10–11 days after CABG ($p = 0.03$).

4. Discussion

The results of this study demonstrate changes in the theta power, S100β, and BDNF serum levels after a short course of MTT in the early postoperative period of on-pump CABG.

It has been previously shown that on-pump surgical interventions such as CABG may lead to ischemic brain damage [36–38]. A magnetic resonance imaging study detected silent brain lesions after CABG in 20.1% of patients [37]. Recent research has indicated that approximately 60–70% of cardiac surgery patients experience postoperative cognitive dysfunction during the early postoperative period [10,37,38].

Event-related theta power is thought to play a role in executive control mechanisms such as conflict detection and response suppression. There have been studies that have shown a reduced theta response in older adults with cognitive decline [39]. An analysis of event-related theta synchronization/desynchronization in cardiac surgery patients found that they exhibited less theta desynchronization in the left frontal–center region compared to patients without cognitive decline [40].

On the other hand, an increase in resting-state theta activity is probably linked to cerebral ischemia during on-pump cardiac surgery. The adverse factors associated with cardiopulmonary bypass (embolism, systemic inflammation, etc.) cause neural dysfunction, tissue atrophy, and damage to neural networks, resulting in the cortical suppression of cortical areas and domination of low-frequency brain activity [38,41]. An increase in resting EEG theta power has been linked to mild cognitive impairment and dementia as diseases progress [42]. It may possibly reflect the vulnerability or resilience of subcortical and thalamocortical loops and the ascending activating systems as additional and supplementary relevant information concerning the progression of cognitive decline.

Previous research has demonstrated that brain electrical activity patterns in patients with brain ischemia have specific characteristics. Al-Qazzaz and colleagues found that the degree of EEG complexity was significantly lower in patients with vascular cognitive impairment compared to healthy subjects [43]. Zappasodi et al. showed that patients with acute unilateral stroke who have an increase in low-frequency activity and decreased hemispheric asymmetry are more likely to have poorer functional outcomes [44].

We demonstrated that the indicator of relative theta power changes was higher in patients without training (55.6%) compared to the MTT patients (25.2%). The impact of cognitive training on the functional organization and compensatory rearrangements of electrical brain activity has been previously demonstrated [22,45]. The activation of local neural networks increased during combined training (physical activity and cognitive load), suggesting the involvement of compensatory brain resources [45]. Thus, a lower decrease in theta power, as seen for the relative change's indicator, probably indicated that the severity of brain damage in cardiac surgery patients after MTT was slightly reduced.

The changes in neurotrophic factors in our study may provide evidence for this assumption. We found an increase in S100β concentrations within the first 24 h after CABG only in the control patients. The MTT group did not show any significant differences, but the S100 changes exhibited the same trend. Although the changes in serum NSE concentrations were similar, the difference did not reach a statistically significant level.

The results of previous studies are consistent with these data. The ability of S100 to identify structural and functional brain damage in cardiac surgery patients was demonstrated by recent studies [29,46]. According to Silva et al., S100 is more closely associated with POCD development than NSE [47].

In addition, we demonstrated that all the patients showed a decrease in BDNF serum levels, regardless of MTT intervention, during the early postoperative period of CABG. This result was confirmed by a recent study [48]. The authors showed that decreased serum levels of BDNF are associated with cognitive decline in patients undergoing CABG surgery. However, we found that the MTT group showed an increase in BDNF levels 11–12 days after CABG when compared to their preoperative values. The serum concentration of BDNF in the control group remained low.

Several studies have demonstrated that BDNF levels increase during physical exercise, including a study of cardiac surgery patients [29,49]. It was indicated that mood and cognitive functions improved in elderly patients with various levels of depression who underwent cognitive training, which was accompanied by an increase in the serum concentration of BDNF [50].

In summary, it can be concluded that on-pump cardiac surgery causes complex, largely unexplored mechanisms of brain damage. The key pathogenic processes are neuroinflammation and ischemia/reperfusion of brain structures caused by cardiopulmonary bypass. The connection between neuroinflammation and BDNF has been demonstrated [51]. On

the other hand, there is evidence that lower levels of BDNF are associated with decreased cognitive function in the postoperative period [52]. Thus, a study by O.H. Miniksar et al. demonstrated associations between BDNF levels and MoCA parameters in patients with CABG [48].

It can be assumed that a short MTT course triggered the processes of neuroplasticity through BDNF expression and reduced ischemic brain damage in the early postoperative CABG period. Thus, the study of the mechanisms underlying postoperative cognitive decline in cardiac surgery patients, with the search for new biomarkers that would have a high diagnostic and predictive ability, as well as reflecting the effectiveness of cognitive recovery procedures, are clinically relevant. Further research is needed to examine the functioning of the neurovascular unit during cardiac surgery.

5. Limitations

It is important to mention some of the limitations of this study. One limitation is the small sample of consecutive patients. Another limitation of the study is the short course of cognitive training. It is our belief that an extended training period would have a more significant impact on the analyzed indicators. Further research should be conducted to address these issues.

6. Conclusions

The theta activity changes and the markers of the neurovascular unit (S100β, BDNF) indicated that the severity of brain damage in cardiac surgery patients after a short course of cognitive training was slightly reduced. Electrical brain activity indicators and vascular markers can be informative for monitoring the process of cognitive rehabilitation in cardiac surgery patients.

Author Contributions: Conceptualization, I.T.; methodology, I.T. and O.T.; validation, I.T.; formal analysis, I.T. and O.T.; investigation, D.K., I.K., T.T. and E.G.; data curation, D.K., I.K., T.T. and E.G.; writing—original draft preparation, I.T.; writing—review and editing, O.T.; project administration, O.T.; funding acquisition, O.T. All authors have read and agreed to the published version of the manuscript.

Funding: This study was supported by the Federal State Ministry of Science and Education of the Russian Federation (Fundamental research topic No. 122012000364-5, dated 20 January 2022).

Institutional Review Board Statement: This study was conducted in accordance with the Declaration of Helsinki and approved by the Institutional Ethics Committee of the Research Institute for Complex Issues of Cardiovascular Diseases (protocol No. 10 dated 12 October 2020). The study was registered on ClinicalTrials.gov (NCT05172362).

Informed Consent Statement: Informed consent was obtained from all subjects involved in this study.

Data Availability Statement: Data are contained within the article.

Conflicts of Interest: The authors declare no conflicts of interest. The funder was not involved in the study design; the collection, analysis, or interpretation of the data; the writing of the article; or the decision to submit the article for publication.

References

1. Deckers, K.; Schievink, S.H.J.; Rodriquez, M.M.F.; van Oostenbrugge, R.J.; van Boxtel, M.P.J.; Verhey, F.R.J.; Köhler, S. Coronary heart disease and risk for cognitive impairment or dementia: Systematic review and meta-analysis. *PLoS ONE* **2017**, *12*, e0184244. [CrossRef] [PubMed]
2. Vishwanath, S.; Qaderi, V.; Steves, C.J.; Reid, C.M.; Hopper, I.; Ryan, J. Cognitive Decline and Risk of Dementia in Individuals With Heart Failure: A Systematic Review and Meta-analysis. *J. Card. Fail.* **2022**, *28*, 1337–1348. [CrossRef]
3. Wee, J.; Sukudom, S.; Bhat, S.; Marklund, M.; Peiris, N.J.; Hoyos, C.M.; Patel, S.; Naismith, S.L.; Dwivedi, G.; Misra, A. The relationship between midlife dyslipidemia and lifetime incidence of dementia: A systematic review and meta-analysis of cohort studies. *Alzheimer's Dement.* **2023**, *15*, e12395. [CrossRef] [PubMed]
4. Catchlove, S.J.; Macpherson, H.; Hughes, M.E.; Chen, Y.; Parrish, T.B.; Pipingas, A. An investigation of cerebral oxygen utilization, blood flow and cognition in healthy aging. *PLoS ONE* **2018**, *13*, e0197055. [CrossRef] [PubMed]

5. MacIntosh, B.J.; Shirzadi, Z.; Atwi, S.; Detre, J.A.; Dolui, S.; Bryan, R.N.; Launer, L.J.; Swardfager, W. Metabolic and vascular risk factors are associated with reduced cerebral blood flow and poorer midlife memory performance. *Hum. Brain Mapping.* **2020**, *41*, 855–864. [CrossRef]
6. Harilall, Y.; Adam, J.K.; Biccard, B.M.; Reddi, A. The effect of optimising cerebral tissue oxygen saturation on markers of neurological injury during coronary artery bypass graft surgery. *Heart Lung Circ.* **2014**, *23*, 68–74. [CrossRef] [PubMed]
7. Kasputytė, G.; Bukauskienė, R.; Širvinskas, E.; Razlevičė, I.; Bukauskas, T.; Lenkutis, T. The effect of relative cerebral hyperperfusion during cardiac surgery with cardiopulmonary bypass to delayed neurocognitive recovery. *Perfusion* **2023**, *38*, 1688–1696. [CrossRef] [PubMed]
8. Stillman, C.M.; Esteban-Cornejo, I.; Brown, B.; Bender, C.M.; Erickson, K.I. Effects of Exercise on Brain and Cognition Across Age Groups and Health States. *Trends Neurosci.* **2020**, *43*, 533–543. [CrossRef] [PubMed]
9. Dhir, S.; Teo, W.P.; Chamberlain, S.R.; Tyler, K.; Yücel, M.; Segrave, R.A. The Effects of Combined Physical and Cognitive Training on Inhibitory Control: A Systematic Review and Meta-Analysis. *Neurosci. Biobehav. Rev.* **2021**, *128*, 735–748. [CrossRef]
10. Tarasova, I.; Trubnikova, O.; Kukhareva, I.; Syrova, I.; Sosnina, A.; Kupriyanova, D.; Barbarash, O.A. Comparison of Two Multi-Tasking Approaches to Cognitive Training in Cardiac Surgery Patients. *Biomedicines* **2023**, *11*, 2823. [CrossRef]
11. Petrigna, L.; Thomas, E.; Gentile, A.; Paoli, A.; Pajaujiene, S.; Palma, A.; Bianco, A. The evaluation of dual-task conditions on static postural control in the older adults: A systematic review and meta-analysis protocol. *Syst. Rev.* **2019**, *8*, 188. [CrossRef] [PubMed]
12. Mack, M.; Stojan, R.; Bock, O.; Voelcker-Rehage, C. Cognitive-motor multitasking in older adults: A randomized controlled study on the effects of individual differences on training success. *BMC Geriatr.* **2022**, *22*, 581. [CrossRef]
13. Syrova, I.D.; Tarasova, I.V.; Trubnikova, O.A.; Kupriyanova, D.S.; Sosnina, A.S.; Temnikova, T.B.; Barbarash, O.L. A multitask approach to prevention of the cognitive decline after coronary artery bypass grafting: A prospective randomized controlled study. *J. Xiangya Med.* **2023**, *8*, 2. [CrossRef]
14. Başar, E.; Düzgün, A. Links of consciousness, perception, and memory by means of delta oscillations of brain. *Front. Psychol.* **2016**, *7*, 275. [CrossRef] [PubMed]
15. Jafari, Z.; Kolb, B.E.; Mohajerani, M.H. Neural oscillations and brain stimulation in Alzheimer's disease. *Prog. Neurobiol.* **2020**, *194*, 101878. [CrossRef] [PubMed]
16. Fernández, A.; Noce, G.; Del Percio, C.; Pinal, D.; Díaz, F.; Lojo-Seoane, C.; Zurrón, M.; Babiloni, C. Resting state electroencephalographic rhythms are affected by immediately preceding memory demands in cognitively unimpaired elderly and patients with mild cognitive impairment. *Front. Aging Neurosci.* **2022**, *14*, 907130. [CrossRef]
17. Abreu, R.; Simões, M.; Castelo-Branco, M. Pushing the Limits of EEG: Estimation of Large-Scale Functional Brain Networks and Their Dynamics Validated by Simultaneous fMRI. *Front. Neurosci.* **2020**, *14*, 323. [CrossRef]
18. Cao, J.; Zhao, Y.; Shan, X.; Blackburn, D.; Wei, J.; Erkoyuncu, J.A.; Chen, L.; Sarrigiannis, P.G. Ultra-high-resolution time-frequency analysis of EEG to characterise brain functional connectivity with the application in Alzheimer's disease. *J. Neural Eng.* **2022**, *19*, 046034. [CrossRef] [PubMed]
19. Tarasova, I.V.; Trubnikova, O.A.; Barbarash, O.L. EEG and Clinical Factors Associated with Mild Cognitive Impairment in Coronary Artery Disease Patients. *Dement. Geriatr. Cogn. Disord.* **2018**, *46*, 275–284. [CrossRef]
20. Deiber, M.P.; Meziane, H.B.; Hasler, R.; Rodriguez, C.; Toma, S.; Ackermann, M.; Herrmann, F.; Giannakopoulos, P. Attention and Working Memory-Related EEG Markers of Subtle Cognitive Deterioration in Healthy Elderly Individuals. *J. Alzheimer's Dis. JAD* **2015**, *47*, 335–349. [CrossRef]
21. Gangemi, A.; De Luca, R.; Fabio, R.A.; Lauria, P.; Rifici, C.; Pollicino, P.; Marra, A.; Olivo, A.; Quartarone, A.; Calabrò, R.S. Effects of Virtual Reality Cognitive Training on Neuroplasticity: A Quasi-Randomized Clinical Trial in Patients with Stroke. *Biomedicines* **2023**, *11*, 3225. [CrossRef] [PubMed]
22. Santarnecchi, E.; Khanna, A.R.; Musaeus, C.S.; Benwell, C.S.Y.; Davila, P.; Farzan, F.; Matham, S.; Pascual-Leone, A.; Shafi, M.M.; Honeywell SHARP Team authors. EEG microstate correlates of fluid intelligence and response to cognitive training. *Brain Topogr.* **2017**, *30*, 502–520. [CrossRef] [PubMed]
23. Du, W.; Li, H.; Sun, J.; Xia, Y.; Zhu, R.; Zhang, X.; Tian, R. The Prognostic Value of Serum Neuron Specific Enolase (NSE) and S100B Level in Patients of Acute Spinal Cord Injury. *Med. Sci. Monit. Int. Med. J. Exp. Clin. Res.* **2018**, *24*, 4510–4515. [CrossRef] [PubMed]
24. Onatsu, J.; Vanninen, R.; JÄkÄlÄ, P.; Mustonen, P.; Pulkki, K.; Korhonen, M.; Hedman, M.; HÖglund, K.; Blennow, K.; Zetterberg, H.; et al. Tau, S100B and NSE as Blood Biomarkers in Acute Cerebrovascular Events. *In Vivo* **2020**, *34*, 2577–2586. [CrossRef] [PubMed]
25. Polyakova, M.; Mueller, K.; Arelin, K.; Lampe, L.; Rodriguez, F.S.; Luck, T.; Kratzsch, J.; Hoffmann, K.T.; Riedel-Heller, S.; Villringer, A.; et al. Increased serum NSE and S100B indicate neuronal and glial alterations in subjects under 71 years with mild neurocognitive disorder/mild cognitive impairment. *Front. Cell. Neurosci.* **2022**, *16*, 788150. [CrossRef] [PubMed]
26. Yilmazer-Hanke, D.; Ouali Alami, N.; Fang, L.; Klotz, S.; Kovacs, G.G.; Pankratz, H.; Weis, J.; Katona, I.; Scheuerle, A.; Streit, W.J.; et al. Differential Glial Chitotriosidase 1 and Chitinase 3-like Protein 1 Expression in the Human Primary Visual Cortex and Cerebellum after Global Hypoxia-Ischemia. *Neuroscience* **2022**, *506*, 91–113. [CrossRef] [PubMed]
27. Barbu, M.; Jónsson, K.; Zetterberg, H.; Blennow, K.; Kolsrud, O.; Ricksten, S.E.; Dellgren, G.; Björk, K.; Jeppsson, A. Serum biomarkers of brain injury after uncomplicated cardiac surgery: Secondary analysis from a randomized trial. *Acta Anaesthesiol. Scand.* **2022**, *66*, 447–453. [CrossRef] [PubMed]

28. Gao, L.; Xie, J.; Zhang, H.; Zheng, H.; Zheng, W.; Pang, C.; Cai, Y.; Deng, B. Neuron-specific enolase in hypertension patients with acute ischemic stroke and its value forecasting long-term functional outcomes. *BMC Geriatr.* **2023**, *23*, 294. [CrossRef] [PubMed]
29. Trubnikova, O.A.; Tarasova, I.V.; Moskin, E.G.; Kupriyanova, D.S.; Argunova, Y.A.; Pomeshkina, S.A.; Gruzdeva, O.V.; Barbarash, O.L. Beneficial Effects of a Short Course of Physical Prehabilitation on Neurophysiological Functioning and Neurovascular Biomarkers in Patients Undergoing Coronary Artery Bypass Grafting. *Front. Aging Neurosci.* **2021**, *13*, 699259. [CrossRef]
30. Nicastri, C.M.; McFeeley, B.M.; Simon, S.S.; Ledreux, A.; Håkansson, K.; Granholm, A.C.; Mohammed, A.H.; Daffner, K.R. BDNF mediates improvement in cognitive performance after computerized cognitive training in healthy older adults. *Alzheimer's Dement.* **2022**, *8*, e12337. [CrossRef]
31. Leger, C.; Quirié, A.; Méloux, A.; Fontanier, E.; Chaney, R.; Basset, C.; Lemaire, S.; Garnier, P.; Prigent-Tessier, A. Impact of Exercise Intensity on Cerebral BDNF Levels: Role of FNDC5/Irisin. *Int. J. Mol. Sci.* **2024**, *25*, 1213. [CrossRef]
32. Shafiee, A.; Beiky, M.; Mohammadi, I.; Rajai, S.; Jafarabady, K.; Moradi, S.; Beikmohamadi, M.; Teixeira, A.L. Effect of smoking on Brain-Derived Neurotrophic Factor (BDNF) blood levels: A systematic review and meta-analysis. *J. Affect. Disord.* **2024**, *349*, 525–533. [CrossRef] [PubMed]
33. Xue, B.; Waseem, S.M.A.; Zhu, Z.; Alshahrani, M.A.; Nazam, N.; Anjum, F.; Habib, A.H.; Rafeeq, M.M.; Nazam, F.; Sharma, M. Brain-Derived Neurotrophic Factor: A Connecting Link Between Nutrition, Lifestyle, and Alzheimer's Disease. *Front. Neurosci.* **2022**, *16*, 925991. [CrossRef] [PubMed]
34. Huang, C.Y.; Chiang, W.C.; Yeh, Y.C.; Fan, S.C.; Yang, W.H.; Kuo, H.C.; Li, P.C. Effects of virtual reality-based motor control training on inflammation, oxidative stress, neuroplasticity and upper limb motor function in patients with chronic stroke: A randomized controlled trial. *BMC Neurol.* **2022**, *22*, 21. [CrossRef]
35. Zhang, J.J.; Sánchez Vidaña, D.I.; Chan, J.N.; Hui, E.S.K.; Lau, K.K.; Wang, X.; Lau, B.W.M.; Fong, K.N.K. Biomarkers for prognostic functional recovery poststroke: A narrative review. *Front. Cell Dev. Biol.* **2023**, *10*, 1062807. [CrossRef]
36. Pierik, R.; Uyttenboogaart, M.; Erasmus, M.E.; Scheeren, T.W.L.; van den Bergh, W.M. Distribution of perioperative stroke in cardiac surgery. *Eur. J. Neurol.* **2019**, *26*, 184–190. [CrossRef] [PubMed]
37. Tachibana, H.; Hiraoka, A.; Saito, K.; Naito, Y.; Chikazawa, G.; Tamura, K.; Totsugawa, T.; Yoshitaka, H.; Sakaguchi, T. Incidence and impact of silent brain lesions after coronary artery bypass grafting. *J. Thorac. Cardiovasc. Surg.* **2021**, *161*, 636–644. [CrossRef]
38. Tarasova, I.; Trubnikova, O.; Kupriyanova, D.; Kukhareva, I.; Syrova, I.; Sosnina, A.; Maleva, O.; Barbarash, O. Effect of carotid stenosis severity on patterns of brain activity in patients after cardiac surgery. *Appl. Sci.* **2023**, *13*, 20. [CrossRef]
39. Lu, J.; Moussard, A.; Guo, S.; Lee, Y.; Bidelman, G.M.; Moreno, S.; Skrotzki, C.; Bugos, J.; Shen, D.; Yao, D.; et al. Music training modulates theta brain oscillations associated with response suppression. *Ann. N. Y. Acad. Sci.* **2022**, *1516*, 212–221. [CrossRef]
40. Tarasova, I.V.; Volf, N.V.; Kupriyanova, D.S.; Trubnikova, O.A.; Barbarash, O.L. Changes in event-related synchronization/desynchronization of brain electric activity in cardiosurgical patients with postoperative cognitive dysfunction. *Sibirskij. Nauchnyj. Medicinskij. Zhurnal.* **2021**, *41*, 12–20. [CrossRef]
41. Daulatzai, M.A. Cerebral hypoperfusion and glucose hypometabolism: Key pathophysiological modulators promote neurodegeneration, cognitive impairment, and Alzheimer's disease. *J. Neurosci. Res.* **2017**, *95*, 943–972. [CrossRef] [PubMed]
42. Babiloni, C.; Arakaki, X.; Azami, H.; Bennys, K.; Blinowska, K.; Bonanni, L.; Bujan, A.; Carrillo, M.C.; Cichocki, A.; de Frutos-Lucas, J.; et al. Measures of resting state EEG rhythms for clinical trials in Alzheimer's disease: Recommendations of an expert panel. *Alzheimers Dement.* **2021**, *17*, 1528–1553. [CrossRef]
43. Al-Qazzaz, N.K.; Ali, S.H.B.M.; Ahmad, S.A.; Islam, M.S.; Escudero, J. Discrimination of stroke-related mild cognitive impairment and vascular dementia using EEG signal analysis. *Med. Biol. Eng. Comput.* **2018**, *56*, 137–157. [CrossRef] [PubMed]
44. Zappasodi, F.; Pasqualetti, P.; Rossini, P.M.; Tecchio, F. Acute phase neuronal activity for the prognosis of stroke recovery. *Neural. Plast.* **2019**, *2019*, 1971875. [CrossRef]
45. Zhavoronkova, L.A.; Maksakova, O.A.; Shevtsova, T.P.; Moraresku, S.I.; Kuptsova, S.V.; Kushnir, E.M.; Iksanova, E.M. Dual tasks as an indicator of the characteristics of cognitive deficit in patients after craniocerebral trauma. *Neurosci. Behav. Phys.* **2020**, *50*, 546–551. [CrossRef]
46. Reis, H.J.; de Oliveira, A.C.; Mukhamedyarov, M.A.; Zefirov, A.L.; Rizvanov, A.A.; Yalvaç, M.E.; Teixeira, A.L.; Janka, Z.; Hussain, A.; Vieira, L.B.; et al. Human cognitive and neuro-psychiatric bio-markers in the cardiac peri-operative patient. *Curr. Mol. Med.* **2014**, *14*, 1155–1163. [CrossRef] [PubMed]
47. Silva, F.P.; Schmidt, A.P.; Valentin, L.S.; Pinto, K.O.; Zeferino, S.P.; Oses, J.P.; Wiener, C.D.; Otsuki, D.A.; Tort, A.B.; Portela, L.V.; et al. S100B protein and neuron-specific enolase as predictors of cognitive dysfunction after coronary artery bypass graft surgery: A prospective observational study. *Eur. J. Anaesthesiol.* **2016**, *33*, 681–689. [CrossRef] [PubMed]
48. Miniksar, Ö.H.; Çiçekçioğlu, F.; Kılıç, M.; Honca, M.; Miniksar, D.Y.; Gocmen, A.Y.; Kaçmaz, O.; Öz, H. Decreased brain-derived neurotrophic factor levels may predict early perioperative neurocognitive disorder in patients undergoing coronary artery bypass surgery: A prospective observational pilot study. *J. Clin. Anesth.* **2021**, *71*, 110235. [CrossRef] [PubMed]
49. Kang, D.; Koh, S.; Kim, T.; Bressel, E.; Kim, D. Circuit training improves the levels of β-Amyloid and brain-derived neurotrophic factor related to cognitive impairment risk factors in obese elderly korean women. *J. Clin. Med.* **2024**, *13*, 799. [CrossRef]
50. Ma, S.L.; Tang, K.T.; Lau, N.C.T.; Chiu, C.L.H.; Lin, C.; Lam, L.C.W.; Lee, A.T.C. Effect of computerized cognitive training on mood, cognition, and serum brain-derived neurotrophic factor level in late-life depression-a pilot randomized controlled trial. *Front. Psychiatry* **2024**, *14*, 1287822. [CrossRef]

51. Hovens, I.B.; van Leeuwen, B.L.; Mariani, M.A.; Kraneveld, A.D.; Schoemaker, R.G. Postoperative cognitive dysfunction and neuroinflammation; Cardiac surgery and abdominal surgery are not the same. *Brain Behav. Immun.* **2016**, *54*, 178–193. [CrossRef]
52. Wyrobek, J.; LaFlam, A.; Max, L.; Tian, J.; Neufeld, K.J.; Kebaish, K.M.; Walston, J.D.; Hogue, C.W.; Riley, L.H.; Everett, A.D.; et al. Association of intraoperative changes in brain-derived neurotrophic factor and postoperative delirium in older adults. *Br. J. Anaesth.* **2017**, *119*, 324–332. [CrossRef]

Disclaimer/Publisher's Note: The statements, opinions and data contained in all publications are solely those of the individual author(s) and contributor(s) and not of MDPI and/or the editor(s). MDPI and/or the editor(s) disclaim responsibility for any injury to people or property resulting from any ideas, methods, instructions or products referred to in the content.

biomedicines

MDPI

Article

Artificial Intelligence Applied to Electrical and Non-Invasive Hemodynamic Markers in Elderly Decompensated Chronic Heart Failure Patients

Gianfranco Piccirillo [1], Federica Moscucci [2,*], Martina Mezzadri [1], Cristina Caltabiano [1], Giovanni Cisaria [1], Guendalina Vizza [1], Valerio De Santis [1], Marco Giuffrè [1], Sara Stefano [1], Claudia Scinicariello [1], Myriam Carnovale [1], Andrea Corrao [1], Ilaria Lospinuso [2], Susanna Sciomer [1] and Pietro Rossi [3]

[1] Department of Internal and Clinical Medicine, Anesthesiology and Cardiovascular Sciences, Policlinico Umberto I, "Sapienza" University of Rome, 00185 Rome, Italy; gianfranco.piccirillo@uniroma1.it (G.P.); martina.mezzadri@uniroma1.it (M.M.); cristina.caltabiano@uniroma1.it (C.C.); giovanni.cisaria@uniroma1.it (G.C.); guendalina.vizza@uniroma1.it (G.V.); valerio.desantis@uniroma1.it (V.D.S.); marcogiuffre25@gmail.com (M.G.); sara.stefano@uniroma1.it (S.S.); claudia.scinicariello@uniroma1.it (C.S.); myriam.carnovale@uniroma1.it (M.C.); andrea.corrao@uniroma1.it (A.C.); susanna.sciomer@uniroma1.it (S.S.)

[2] Department of Internal Medicine and Medical Specialties, Policlinico Umberto I, Viale del Policlinico, 155, 00161 Rome, Italy; lospinuso.i@gmail.com

[3] Arrhythmology Unit, Fatebenefratelli Hospital, Isola Tiberina-Gemelli Isola, 00186 Rome, Italy; rossi.ptr@gmail.com

* Correspondence: federica.moscucci@uniroma1.it; Tel.: +39-06-49970118

Abstract: Objectives: The first aim of this study was to assess the predictive power of Tend interval (Te) and non-invasive hemodynamic markers, based on bioimpedance in decompensated chronic heart failure (CHF). The second one was to verify the possible differences in repolarization and hemodynamic data between CHF patients grouped by level of left ventricular ejection fraction (LVEF). Finally, we wanted to check if repolarization and hemodynamic data changed with clinical improvement or worsening in CHF patients. Methods: Two hundred and forty-three decompensated CHF patients were studied by 5 min ECG recordings to determine the mean and standard deviation (Te_{SD}) of Te (first study). In a subgroup of 129 patients (second study), non-invasive hemodynamic and repolarization data were recorded for further evaluation. Results: Total in-hospital and cardiovascular mortality rates were respectively 19 and 9%. Te was higher in the deceased than in surviving subjects (Te: 120 ± 28 vs. 100 ± 25 ms) and multivariable logistic regression analysis reported that Te was related to an increase of total (χ^2: 35.45, odds ratio: 1.03, 95% confidence limit: 1.02–1.05, $p < 0.001$) and cardiovascular mortality (χ^2: 32.58, odds ratio: 1.04, 95% confidence limit: 1.02–1.06, $p < 0.001$). Subjects with heart failure with reduced ejection fraction (HFrEF) reported higher levels of repolarization and lower non-invasive systolic hemodynamic data in comparison to those with preserved ejection fraction (HFpEF). In the subgroup, patients with the NT-proBNP reduction after therapy showed a lower rate of Te, heart rate, blood pressures, contractility index, and left ventricular ejection time in comparison with the patients without NT-proBNP reduction. Conclusion: Electrical signals from ECG and bioimpedance were capable of monitoring the patients with advanced decompensated CHF. These simple, inexpensive, non-invasive, easily repeatable, and transmissible markers could represent a tool to remotely monitor and to intercept the possible worsening of these patients early by machine learning and artificial intelligence tools.

Keywords: advanced heart failure; bioimpedance cardiography; QT; Tpeak-Tend; QT variability; temporal dispersion of repolarization phase; mortality

1. Introduction

Despite a series of innovative drug therapies (sacubitril, SGLT2 inhibitors, etc.) and medical devices (ICD and CRT), decompensated chronic heart failure (CHF) remains one of the major causes of mortality, morbidity, and rehospitalization especially in developed countries [1–3]. SARS-CoV-2 resulting in coronavirus disease (COVID-19) and other infections requiring medical attention have highlighted the excessive use of hospitalization. To avoid recurrent hospitalizations, it is necessary to introduce non-invasive, simple, inexpensive, transmissible, and early markers of CHF decompensation [4–8], especially since each hospitalization for acute decompensated heart failure increases the risk of worsening clinical conditions and mortality [9–11].

The European Society of Cardiology [12], the American Heart Association, the American College of Cardiology, and the Heart Failure Society of America [13] have introduced a new patient category with CHF, who have heart failure with an intermediate level of ejection fraction (see Methods), to better assess the cardiovascular risk of mortality and possible appropriate new drug therapy. Therefore, the first aim of this study was to evaluate non-invasive ECG repolarization-based markers based on this new classification. In particular, it has been previously observed that an increase in the Tpeak–Tend (Te) interval was a risk factor for total and cardiovascular mortality [14–16]. An increase in this interval and its short-period temporal dispersion was associated with mortality and decompensation in patients with acute CHF [17–23]. Finally, non-invasive hemodynamic parameters were studied based on bioimpedance to assess the possibility of monitoring clinical improvements in these patients [19,24–27]. The final aim of this work is to identify the electrical, bioimpedance, and biohumoral variables which, through artificial intelligence and machine learning devices, will be able to predict the clinical exacerbation of heart failure in the preliminary phases. By intercepting it early, it will be possible to treat the acutely decompensated CHF in the very early stages, trying to avoid hospitalization and the health and non-medical costs that would arise from it.

2. Methods

2.1. Study Subjects and ECG Analysis

We enrolled 243 consecutive patients admitted to our Geriatric Department from January 2019 to October 2023 due to dyspnea or other classic symptoms of decompensated chronic heart failure (CHF) according to the 2021 European Society of Cardiology heart failure guidelines [7] (Figure 1).

Each patient enrolled disclosed medical history and the following assessments were performed: physical examination, standard ECG, transthoracic echocardiogram, and a 5 min of single-lead (II lead) ECG recording. Subsequently, we grouped patients according to left ventricular ejection fraction detected by echocardiography ($LVEF_{Ech}$) [12], decompensated heart failure with reduced ejection fraction (HFrEF) with $LVEF_{Ech} \leq 40\%$, those with mildly reduced ejection fraction (HFmrEF) with $LVEF_{Ech}$ levels of 41–49%, and, finally, those with preserved ejection fraction (HFpEF) with $LVEF_{Ech} \geq 50\%$ [12]. All patients with CHF had stable previous clinical conditions at home with NYHA class II–III and all of them were in the IV NYHA functional class at the time of enrollment. Furthermore, at this time, we collected blood samples for quantifying NT-proBNP levels (Alere Triage Analyzer, Alere, San Diego, CA, USA) and other clinical chemistry analysis. ECG signals were acquired and digitalized with a custom-designed card (National Instruments, Austin, TX, USA) at a sampling frequency of 500 Hz. Measurements used for the ECG segment and interval analysis were detected automatically by a classic adaptive first derivative/threshold algorithm and a template method [28,29]. Our research group designed and produced software for data acquisition, storage, and analysis with the LabView program (National Instruments, Austin, TX, USA). An expert cardiologist (GP) checked the different ECG intervals and segments, automatically marked by the software, and manually corrected the mistakes as needed [28–33].

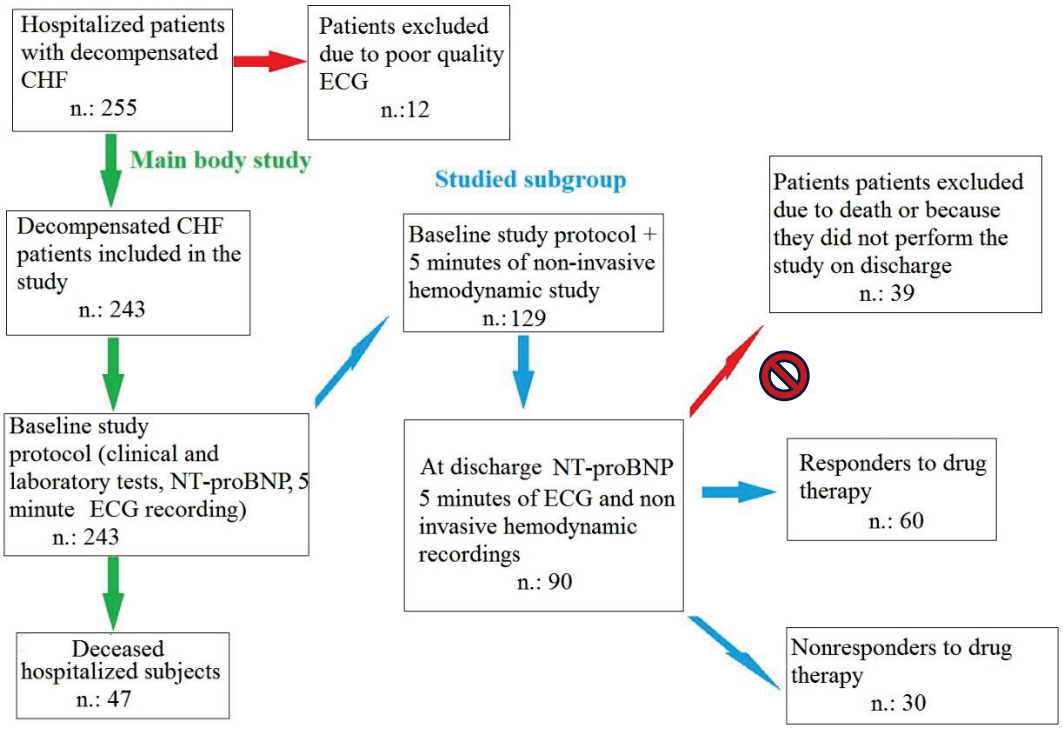


Figure 1. Flowchart of study phases.

The means and standard deviations of QT intervals were obtained, calculated from q to end of T wave (QTe and QTe_{SD}), QTpeak intervals (QTp and QTp_{SD}), and obtained from q to peak of T wave. Finally, we calculated the mean and standard deviation (Te_{SD}) of Te intervals [11,15,16,19,20,23–25,34,35].

One hundred and twenty-nine of the originally enrolled patients underwent non-invasive hemodynamic evaluation by means of bioimpedance cardiography (PhysioFlow; Manatec Biomedical, Poissy, France). This assessment was performed upon hospital admission and discharge (second study) (Figure 1) [19].

Upon patient discharge, a second 5 min ECG for repolarization variables and a second NT-proBNP test were administered. Therefore, the second study evaluated the following data parameters at the beginning of hospitalization and at discharge: hemodynamic, repolarization, and NT-proBNP data. The non-invasive hemodynamic data included the following: heart rate (HR), stroke volume (SV), stroke volume index (SVI), cardiac output (CO), cardiac index (CI), systemic vascular resistance (SVR), systemic vascular resistance index (SVRI), left ventricular ejection fraction ($LVEF_{BIO}$), contractility index (ConI), left ventricular ejection time (LVET), cardiac work index (CWI), left ventricular end-diastolic volume (LVEDV), and early diastolic filling ratio (EDFR) [7,18,19,33,36–42]. Finally, upon hospitalization discharge, both the 5 min ECG and non-invasive hemodynamic recording were repeated.

The study obtained formal approbation by the Ethical Committee of Policlinico Umberto I. The study code was BNP_HRV01 and the protocol number of the approbation document was 282/2023. Moreover, the study was first online registered on ClinicalTrials.gov as NCT04127162.

2.2. Statistical Analysis

All variables with a normal distribution were expressed as mean ± standard deviation, whereas non-normally distributed variables were expressed as a median and inter-quartile range (i.r.), and categorical variables were expressed as frequencies and percentages (%). First, we compared the data obtained from three groups of CHF with different $LVEF_{Ech}$ in the first study. More specifically, categorical variables were analyzed with the χ^2 test.

On the contrary, one-way ANOVA and Bonferroni tests were used to compare data for the normally distributed variables, while the Kruskal–Wallis and Mann–Whitney tests were used to compare non-normally distributed variables (as evaluated by Kolmogorov–Smirnov test).

Secondly, we compared the ECG, non-invasive hemodynamic, and clinical data between deceased and surviving patients and between responders or non-responders to the drug therapy. In the second study, responders were defined as patients with a reduction of NT-proBNP at the end of hospitalization and non-responders were defined as patients without a reduction of NT-proBNP. In particular, a Student's *t*-test and Mann–Whitney test were used respectively for the normally and non-normally distributed variables. Finally, a paired *t*-test and Wilcoxon test were used respectively to compare normally and non-normally distributed data at the beginning and at the end of the study. Multivariable forward (A. Wald) stepwise logistic regression analyses were used to determine the relationship between repolarization variables (covariates) and total or cardiovascular mortality (dependent variables). All data were evaluated by use of the program SPSS-PC+ (SPSS-PC+ Inc., Chicago, IL, USA) and p values of less than or equal to 0.05 were considered statistically significant.

3. Results

Starting from 255 eligible patients with symptoms of decompensated CHF, 12 patients were excluded due to poor-quality ECGs. Consequently, 243 CHF patients were included in the first part of the study. During the hospitalization, a total of 46 patients died (overall mortality rate, 19%): 23 (9.4%) died of bronchopneumonia and respiratory failure (1 patient from COVID-19 pneumonia), 17 died due to terminal heart failure (7%), 3 died of fatal myocardial infarction (1%), 3 died of sudden cardiac death (1%) (2 had sustained ventricular tachycardia and ventricular fibrillation; 1 had acute cor pulmonale secondary to massive embolism). The overall cardiovascular mortality rate was 9.4%.

The general characteristics of HFrEF, HFmrEF, and HFpEF were significantly different based on the echocardiographic data (Table 1).

Table 1. General characteristics of the studied population.

	Heart Failure with Reduced Ejection Fraction	**Heart Failure with Mildly Reduced Ejection Fraction**	**Heart Failure with Preserved Ejection Fraction**	
	N: 112	N: 38	N: 93	*p*
Gender, M/F	65/47	16/22	41/52	>0.5
Age, years	83 ± 10	85 ± 7	83 ± 10	0.497
BMI, kg/m^2	26 ± 5	25 ± 4	26 ± 5	0.536
Heart Rate (radial pulse), beats/m	74 ± 12	73 ± 15	76 ± 13	0.463
Systolic Blood Pressure, mmHg	120 ± 17 **	127 ± 17	130 ± 21 **	<0.001
Diastolic Blood Pressure, mmHg	67 ± 9 **	67 ± 11	73 ± 11 **	<0.001
Left Ventricular Ejection Fraction, %	32 ± 7 **##	45 ± 1 ##§§	52 ± 3 **§§	<0.001
Left Ventricular Mass Index, g/m^2	147 ± 34 **#	129 ± 34 #	123 ± 26 **	<0.001
Left Ventricular End-Diastolic Diameter, mm	57 ± 8 **##	51 ± 5 ##	50 ± 5 **	<0.001
Posterior Wall Thickness, mm	11 ± 2	11 ± 2	11 ± 2	0.691
Interventricular Septum Thickness, mm	12 ± 2	12 ± 1	12 ± 1	0.594
Left Atrial Transversal Diameter, mm	49 ± 8 *#	45 ± 6 #	45 ± 6 *	<0.001
Tricuspid Annular Plane Systolic Excursion, mm	19 ± 3 **	21 ± 5	22 ± 4 **	<0.001
Tricuspid Regurgitation Peak Gradient, mmHg	47 ± 13 #	40 ± 11 #	43 ± 15	0.030
Hemoglobin (g/dL)	11.4 ± 2.1	11.1 ± 1.6	11.4 ± 2.1	0.689
Arterial O_2 Saturation, %	97 ± 3	97 ± 2	97 ± 4	0.655
Fraction of Inspired O_2,%	27 ± 9	26 ± 7	26 ± 8	0.828
PaO_2/FiO_2 ratio	334 ± 103	339 ± 126	329 ± 90	0.884
A-ADO_2, mmHg	39 [51]	35 [49]	33 [41]	0.671
NT-proBNP, pg/mL	6170 [9995] *	2725 [4590]	1660 [3085] *	<0.001
C-ReactiveProtein (mg/dL)	4.0 [9.4]	3.6 [11.7]	5.1 [8.8]	0.926
High-Sensitivity Cardiac Troponin/(pg/L)	62 [98] **##	36 [47] ##	31 [29] **	<0.001
Serum Sodium (mmol/L)	141 ± 6	141 ± 5	141 ± 5	0.957
Serum Potassium (mmol/L)	4.0 ± 0.6	4.1 ± 0.6	4.1 ± 0.6	0.532
Serum Calcium (mmol/L)	2.1 ± 0.2	2.2 ± 0.2	2.2 ± 0.2	0.054
Creatinine Clearance (mL/m)	38 [24] *#	48 [30] #§	50 [38] *§	0.025
Serum Urea (mmol/L)	12.3 [8.3]	10.2 [7.8]	8.3 [5.6]	0.003

Table 1. *Cont.*

	Heart Failure with Reduced Ejection Fraction	Heart Failure with Mildly Reduced Ejection Fraction	Heart Failure with Preserved Ejection Fraction	
Albumin (g/dL)	3.4 ± 0.6	3.4 ± 0.5	3.5 ± 0.6	0.736
Fasting Glucose (mmol/L)	6.8 ± 2.2	6.6 ± 2.7	6.2 ± 2.7	1.131
HbA_{1c} (%)	6.2 ± 1.2	5.9 ± 1.3	5.8 ± 1.0	0.099
Total Cholesterol (mmol/L)	3.6 ± 0.9	3.8 ± 0.9	3.9 ± 1.0	0.444
HDL-Cholesterol (mmol/L)	1.1 ± 0.4	1.1 ± 0.4	1.1 ± 0.4	0.975
LDL-Cholesterol (mmol/L)	1.9 ± 0.8	2.1 ± 0.6	2.1 ± 0.9	0.608
Triglycerides (mmol/L)	1.9 ± 1.6	1.6 ± 0.7	1.5 ± 0.7	0.219
Hypertension, n (%)	80 (71)	32 (84)	77 (41)	0.087
Hypercholesterolemia, n (%)	54 (48)	14 (37)	41 (44)	0.468
Diabetes, n (%)	57 (51)	12 (32)	32 (34)	0.087
Renal Insufficiency, n (%)	67 (60) *	16 (42)	37 (40) *	0.010
Known Myocardial Ischemia History, n (%)	57 (51) **#	8 (21) #	18 (19) **	<0.001
Valve Diseases, n (%)	26 (23)	12 (32)	24 (25)	0.651
Premature Supraventricular Complexes, n (%)	12 (11)	2 (5)	9 (10)	0.609
Premature Ventricular Complexes, n (%)	26 (23)	11 (29)	16 (17)	0.298
Permanent Atrial Fibrillation, n (%)	46 (41)	18 (47)	30 (32)	0.213
Left Bundle Branch Block, n (%)	34 (30) **	10 (26) §§	6 (7) **§§	<0.001
Right Bundle Branch Block, n (%)	18 (16)	4 (11)	13 (14)	0.694
Pacemaker–ICD, n (%)	37 (33) **	10 (26) §§	8 (9) **§§	<0.001
Deceased Hospitalized Patients, n (%)	27 (24)	7 (18)	13 (14)	0.186
β-Blockers, n (%)	82 (73) *	30 (80) §	52 (56) *§	0.008
Furosemide, n (%)	97 (87) **	31 (82)	60 (65) **	0.001
ACE/Sartans	45 (40)	10 (26)	41 (44)	0.165
Aldosterone Antagonists, n (%)	25 (22) *	7 (18)	8 (9) *	0.029
Potassium, n (%)	7 (6)	2 (5)	8 (9)	0.726
Nitrates, n (%)	14 (13)	6 (16)	8 (9)	0.458
Digoxin, n (%)	6 (5)	3 (8)	3 (3)	0.514
Statins, n (%)	36 (32)	8 (21)	26 (28)	0.416
Antiplatelet Drugs, n (%)	47 (42)	9 (24)	35 (38)	0.132
Oral Anticoagulants, n (%)	27 (24)	13 (34)	30 (32)	0.319
Diltiazem or Verapamil, n (%)	1 (1)	1 (3)	6 (7)	0.082
Ivabradine, n	2 (2)	1 (3)	2 (2)	0.948
Dihydropyridine Calcium Channel Blockers, n (%)	8 (7) *	6 (16)	17 (18) *	0.049
Propafenone, n (%)	0 (0)	0 (0)	2 (2)	0.197
Amiodarone, n (%)	11 (10)	1 (3)	7 (8)	0.358
Valsartan/Sacubitril, n (%)	4 (4)	0 (0)	0 (0)	0.093
SGLT-2i, n (%)	1 (1)	0 (0)	0 (0)	0.999

Data are expressed as mean ± SD, or median [interquartile range], or number of patients (%); ** $p < 0.001$ Heart Failure with Reduced Ejection Fraction versus Heart Failure with Preserved Ejection Fraction; * $p < 0.05$ Heart Failure with Reduced Ejection Fraction versus Heart Failure with Preserved Ejection Fraction; ## $p < 0.001$ Heart Failure with Reduced Ejection Fraction versus Heart Failure with Mildly Reduced Ejection Fraction; # $p < 0.05$ Heart Failure with Reduced Ejection Fraction versus Heart Failure with Mildly Reduced Ejection Fraction; §§ $p< 0.001$ Heart Failure with Mildly Reduced Ejection Fraction versus Heart Failure with Preserved Ejection Fraction; § $p < 0.05$ Heart Failure with Mildly Reduced Ejection Fraction versus Heart Failure with Preserved Ejection Fraction.

In fact, the $LVEF_{Ech}$ was significantly lower in HFrEF patients compared to the other two groups ($p < 0.001$) and was lower in HFmrEF than in HFpEF subjects ($p < 0.001$) (Table 1). Left ventricular mass index ($p < 0.001$), left ventricular end-diastolic diameter ($p < 0.001$), and left atrial transversal diameter ($p < 0.05$) were significantly higher in HFrEF in comparison with the other two patient groups (Table 1). Tricuspid annular plane systolic was lower in in HFrEF than HFpEF subjects (Table 1). Finally, tricuspid regurgitation peak gradient was higher in the HFrEF than HFpEF group (Table 1). HFrEF subjects reported a significantly higher blood level of NT-proBNP ($p < 0.05$) in comparison with HFpEF subjects (Table 1) while, on the contrary, the HFrHF group reported a significantly higher troponin level compared to both the other two groups (Table 1). The HFpEF subjects showed a significantly higher creatinine clearance in blood levels of than the other two groups ($p < 0.05$), but the HFmrEF group had a higher creatinine clearance than the HFrEF group (Table 1). Obviously, the HFrEF group included a significantly higher number of subjects with renal insufficiency than the HFpEF group (Table 1). A known history of ischemic heart disease was significantly predominant in subjects with HFrEF compared to the other

two groups (HFmrEF: $p < 0.05$; HFpEF: $p < 0.001$) (Table 1). There were significantly more patients with left bundle branch block or with a pacemaker–ICD in the HFrEF and HFmrEF groups compared to the HFpEF group ($p < 0.001$) (Table 1). There were significantly more patients treated with beta-blockers and furosemide in the HFrEF category than in the HFpEF group. HFmrEF patients were also treated with beta-blockers to a greater extent than HFpHF patients ($p < 0.05$) (Table 1). Additionally, aldosterone antagonist use was significantly more common in patients with HFrEF than in those with HFpEF ($p < 0.05$), and the latter group received more dihydropyridine calcium channel blocker therapy than HfrEF patients (Table 1).

HFrEF patients reported a significant increase in QTe ($p < 0.001$), QTe_{SD} ($p < 0.05$), QTp ($p < 0.05$), Te ($p < 0.001$), and TeSD ($p < 0.001$) compared with HFpHF patients (Table 2). Only TeSD ($p < 0.001$) was significantly higher in HFmrEF ($p < 0.05$) than in HFpEF patients (Table 2).

Table 2. ECG Data of Study Subjects.

	Heart Failure with Reduced Ejection Fraction	Heart Failure with Mildly Reduced Ejection Fraction	Heart Failure with Preserved Ejection Fraction	
Variables	N: 112	N: 38	N: 93	*p*
RR, ms	850 ± 160	864 ± 164	871 ± 174	0.671
QTe, ms	490 ± 87 **	457 ± 94	427 ± 65 **	<0.001
QTe_{SD}, ms	10 [5] *	10 [5]	8 [5] *	0.043
QTp, ms	373 ± 85 *	353 ± 83	332 ± 56 *	0.001
QTp_{SD}, ms	9 [5]	9 [4]	8 [3]	0.216
Te, ms	110 ± 27 **	106 ± 31	94 ± 22 **	<0.001
Te_{SD}, ms	8 [6] **	9 [6] §	6 [4] **§	<0.001

Data are expressed as mean ± SD, or median [interquartile range]; ** $p < 0.001$ Heart Failure with Reduced Ejection Fraction versus Heart Failure with Preserved Ejection Fraction; * $p < 0.05$ Heart Failure with Reduced Ejection Fraction versus Heart Failure with Preserved Ejection Fraction; § $p < 0.05$ Heart Failure with Mildly Reduced Ejection Fraction versus Heart Failure with Preserved Ejection Fraction.

HR ($p < 0.05$) and EDFR ($p < 0.05$) were significantly higher in HFrEF than HfrEF patients (Table 3). On the contrary, SV ($p < 0.05$), SVI ($p < 0.050$), $LVEF_{BIO}$ ($p < 0.001$), and ConI ($p < 0.001$) were significantly lower in subjects with HFpEF (Table 3).

Table 3. Non-invasive Hemodynamic Data of Study Subjects.

	Heart Failure with Reduced Ejection Fraction	Heart Failure with Mildly Reduced Ejection Fraction	Heart Failure with Preserved Ejection Fraction	
Variables	N: 63	N: 20	N: 46	*p*
Heart Rate, b/m	81 ± 23 *	86 ± 30 §	72 ± 13	0.031
Stroke Volume, mL	59 ± 17 *	64 ± 23	71 ± 20 *	0.008
Stroke Volume Index, mL/m^2	33 ± 10 *	37 ± 14	40 ± 10 *	0.004
Cardiac Output, L/m	4.59 ± 1.39	5.04 ± 1.60	4.97 ± 1.16	0.239
Cardiac Index, $L/m/m^2$	2.53 ± 0.75 *	2.95 ± 0.87	2.81 ± 0.74 *	0.047
Systemic Vascular Resistance, $Dyn.s/cm^2$	3390 ± 1440	2901 ± 739	2932 ± 877	0.090
Systemic Vascular Resistance Index, $Dyn.s/cm^2.m^2$	1849 ± 692	1716 ± 458	1639 ± 491	0.188
SBP, mmHg	122 ± 17	124 ± 13	125 ± 13	0.503
MBP, mmHg	71 ± 10	73 ± 9	72 ± 10	0.691
DBP, mmHg	93 ± 12	95 ± 9	95 ± 10	0.563
Left Ventricular Ejection Fraction, %	34 ± 13 **	39 ± 14	46 ± 15 **	<0.001
Contractility Index	61 ± 40 *	78 ± 44	86 ± 53 *	0.031
Left Ventricular Ejection Time, ms	267 ± 77	271 ± 74	291 ± 86	0.271

Table 3. *Cont.*

	Heart Failure with Reduced Ejection Fraction	Heart Failure with Mildly Reduced Ejection Fraction	Heart Failure with Preserved Ejection Fraction	
Left Cardiac Work Index, kg.m/m^2	3.04±	3.63 ± 1.20	3.49 ± 1.04	0.063
Left Ventricular End-Diastolic Volume, mL	194 ± 90	195 ± 134	164 ± 49	0.162
Early Diastolic Filling Ratio	92 ± 35 *	98 ± 57	77 ± 25 *	0.045

Data are expressed as mean ± SD, or median [interquartile range]; ** $p < 0.001$ Heart Failure with Reduced Ejection Fraction versus Heart Failure with Preserved Ejection Fraction; * $p < 0.05$ Heart Failure with Reduced Ejection Fraction versus Heart Failure with Preserved Ejection Fraction; § $p < 0.05$ Heart Failure with Mildly Reduced Ejection Fraction versus Heart Failure with Preserved Ejection Fraction.

Deceased patients reported an increase in some repolarization data, especially the Te and Te_{SD} (Te: 120 ± 28 vs. 100 ± 25 ms, $p < 0.001$; Te_{SD}: 9 vs. 7, p: 0.014). There was no statistical difference between the deceased or the survivors for the non-invasive hemodynamic data.

In the second study, the data were used to compare responders (n.: 60, mean age: 82 ± 7) and non-responders (n.: 30, 81 ± 11) to drug therapies, where the responders reported higher levels of NT-proBNP (4295 i.r. 7528 vs. 2110 i.r. pg/mL, $p < 0.001$) both at baseline and at the discharge (2030 i.r. 3250 vs. 5763 i.r. 7328 pg/mL, $p < 0.001$). In particular, the responders had a 46% reduction of NT-proBNP levels (from 4295 i.r. 7528 to 2030 i.r. 3250 pg/mL, $p < 0.001$). On the contrary, the non-responders had a 58% increase in NT-proBNP levels (from 2110 i.r. 5082 to 5763 i.r. 7328 pg/mL, $p < 0.001$). The repolarization data (Te and Te_{SD}) were similar in both responders and non-responders at baseline (Te: 102 ± 30 vs. 99 ± 27 ms, p: ns; Te_{SD}: 9 i.r. 5 vs. 8 i.r. 3 ms, p: ns) but were higher in the non-responder group at discharge (Te: 96 ± 23 vs. 108 ± 31 ms, $p < 0.05$; Te_{SD}: 6 i.r. 3 vs. 10 i.r. 6 ms, $p < 0.001$) (Figure 2).

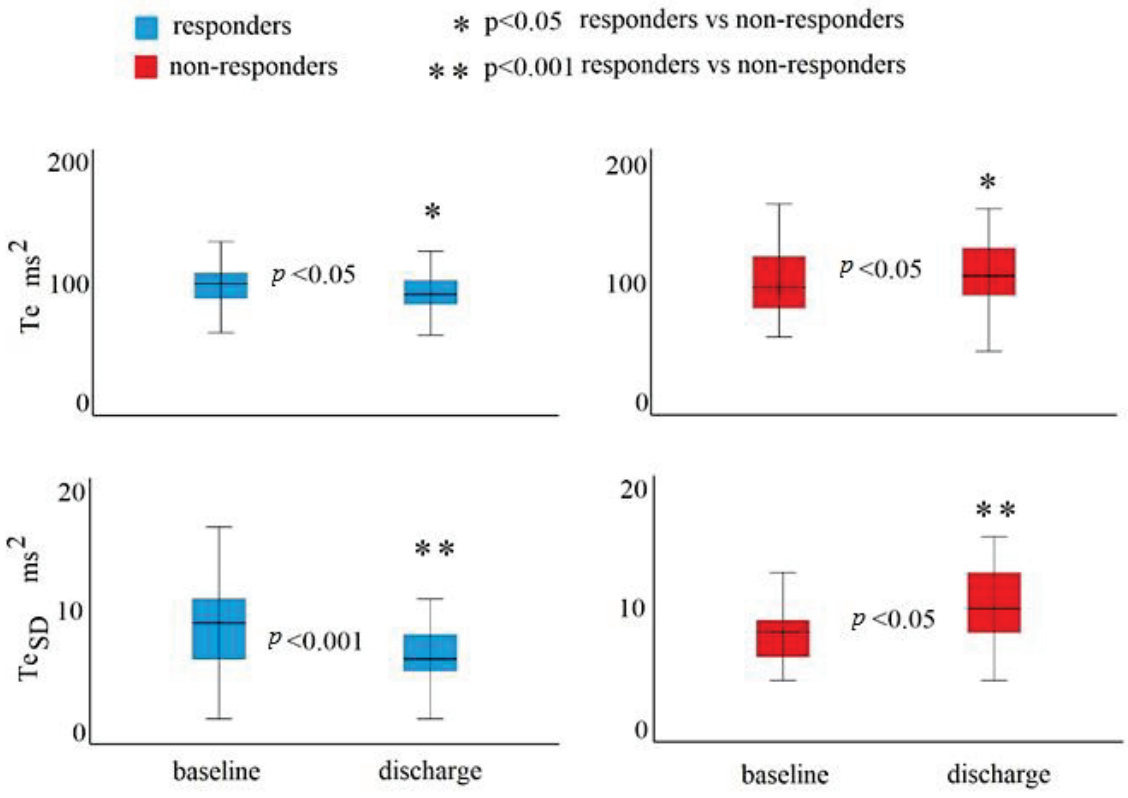


Figure 2. Tpeak−Tend intervals' mean (Te) and standard deviation (TeSD) of a 5 min ECG recording at baseline and discharge.

In the responder group, both Te and Te_{SD} decreased significantly (Te: from 102 ± 30 to 96 ± 23 ms, $p < 0.05$), and both of these values increased in the non-responder group (Te: from 99 ± 27 to 108 ± 31 ms, $p < 0.05$; Te_{SD}: 8 i.r. 3 vs. 10 i.r. 6 ms, p: 0.001) (Figure 2). Regarding the non-invasive hemodynamic data, from baseline to discharge, the responder group had a significant decrease in heart rate ($p < 0.05$) SBP ($p < 0.05$), DBP ($p < 0.05$), and MBP ($p < 0.05$) (Table 4) and increased left ventricular ejection time ($p < 0.05$) (Table 4). The non-responder group did not show any difference in these two study conditions (Table 4). Finally, at the discharge, the responders reported higher levels $LVEF_{BIO}$ ($p < 0.05$) and ConI ($p < 0.05$) than non-responders (Table 4), but the non-responders showed an increase in LVEDV ($p < 0.05$) (Table 4).

Table 4. Clinical, ECG, and Non-invasive Hemodynamic Data of Study Subjects at Baseline and at the Discharge.

	Responders			**Non-Responders**		
	Baseline	**Discharge**		**Baseline**	**Discharge**	
Variables	N: 60	N: 60	*p*	N: 30	N: 30	*p*
Heart Rate, b/m	82 ± 26	74 ± 17	0.020	74 ± 17	77 ± 19	0.308
Stroke Volume, mL	64 ± 20	66 ± 24	0.490	65 ± 15	63 ± 15	0.576
Stroke Volume Index, mL/m^2	36 ± 12	38 ± 14	0.536	35 ± 9	35 ± 10	0.445
Cardiac Output, L/m	4.88 ± 1.48	4.72 ± 1.73	0.558	4.58 ± 1.09	4.60 ± 1.24	0.974
Cardiac Index, L/m/m^2	2.79 ± 0.87	2.69 ± 1.02	0.520	2.53 ± 0.63	2.52 ± 0.62	0.840
Systemic Vascular Resistance, Dyn.s/cm^2	3099 ± 1279	3049 ± 1113	0.868	3221 ± 1048	3307 ± 1166	0.747
Systemic Vascular Resistance Index, Dyn.s/cm^2.m^2	1748 ± 600	1730 ± 619	0.795	1760 ± 506	1852 ± 783	0.532
SBP, mmHg	124 ± 14	119 ± 13	0.025	120 ± 15	123 ± 14	0.190
MBP, mmHg	94 ± 9	90 ± 10	0.006	92 ± 11	94 ± 14	0.297
DBP, mmHg	71 ± 10	68 ± 10	0.016	71 ± 10	72 ± 9	0.693
Left Ventricular Ejection Fraction, %	40 ± 16	41 ± 17 *	0.688	36 ± 14	34 ± 14 *	0.427
Contractility Index	78 ± 56	86 ± 56 *	0.296	67 ± 36	58 ± 29 *	0.108
Left Ventricular Ejection Time, ms	271 ± 98	299 ± 91	0.019	275 ± 60	264 ± 80	0.631
Left Cardiac Work Index, kg.m/m^2	3.39 ± 1.29	3.14 ± 1.44	0.300	3.05 ± 0.97	3.06 ± 0.89	0.459
Left Ventricular End-Diastolic Volume, mL	172 ± 77	171 ± 64 *	0.907	196 ± 71	200 ± 73 *	0.459
Early Diastolic Filling Ratio	91 ± 45	81 ± 25	0.520	88 ± 32	91 ± 47	0.471

Data are expressed as mean ± SD, or median [interquartile range]; * $p < 0.05$ responders versus non-responders.

Multivariable logistic regression analysis reported that Te was related to an increase of total ($p < 0.001$) (Table 5) or cardiovascular mortality ($p < 0.001$) (Table 6).

Table 5. Logistic Regression Between in-Hospital Total Mortality (dependent variable) and ECG Repolarization Data.

Variables	χ^2	**B**	**Univariable Analysis Odds Ratio (95% CI)**	***p* Values**	χ^2	**B**	**Multivariable Analysis Odds Ratio (95% CI)**	***p* Values**
					35.45			
QTe	0.009	0.00	1.00 (1.00–1.00)	0.924		−0.003	1.00 (0.98–1.01)	0.429
QTe_{SD}	2.90	0.04	1.04 (0.99–1.09)	0.096		0.057	1.06 (0.98–1.14)	0.142
QTp	2.82	−0.01	1.00 (0.99–1.00)	0.058		−0.005	1.00 (0.99–1.00)	0.206
QTp_{SD}	0.36	0.02	1.02 (0.95–1.11)	0.542		−0.086	0.92 (0.81–1.05)	0.198
Te	19.49	0.03	1.03 (1.01–1.04)	<0.001		0.032	1.03 (1.01–1.05)	0.001
Te_{SD}	7.92	0.07	1.07 (1.01–1.14)	0.027		0.047	1.05 (0.98–1.12)	0.141

Table 6. Logistic Regression Between in-Hospital Cardiovascular Mortality (dependent variable) and ECG Repolarization Data.

Variables	χ^2	**B**	**Univariable Analysis Odds Ratio (95% CI)**	***p* Values**	χ^2	**B**	**Multivariable Analysis Odds Ratio (95% CI)**	***p* Values**
					32.58			
QTe	0.54	0.00	1.00 (1.00–1.01)	0.454		−0.01	1.00 (0.99–1.01)	0.453
QTe_{SD}	1.97	0.05	1.05 (0.98–1.13)	0.145		0.06	1.07 (0.94–1.21)	0.317

Table 6. *Cont.*

Variables	χ^2	B	Univariable Analysis Odds Ratio (95% CI)	*p* Values	χ^2	B	Multivariable Analysis Odds Ratio (95% CI)	*p* Values
					32.58			
QTp	2.10	−0.00	1.00 (0.99–1.00)	0.153		−0.01	1.00 (0.99–1.00)	0.187
QTp_{SD}	0.67	0.04	1.04 (0.95–1.14)	0.401		−0.09	0.92 (0.77–1.09)	0.317
Te	20.83	0.03	1.03 (1.02–1.05)	<0.001		0.036	1.04 (1.02–1.06)	0.001
Te_{SD}	8.77	0.08	1.08 (1.01–1.16)	0.024		0.052	1.05 (1.98–1.03)	0.160

4. Discussion

The major finding of the present study was confirmation of the association of the Te interval with an increased risk of in-hospital mortality in decompensated patients [17–20,22,23,43]. Secondly, a significant difference was not observed in ECG repolarization and non-invasive hemodynamic data between HFrEF and HFmrEF patients (Tables 2 and 3). However, there was an increase in repolarization data only in HFrEF patients compared to the HFpEF group and only Te_{SD} was higher in the HFmrEF group in comparison with the HFpEF group (Table 2). The non-invasive hemodynamic data showed an obvious significant reduction of systolic function data (HR, SV, SVI, CI, $LVEF_{BIO}$, and ConI) in patients with HFrEF in comparison to the HFpEF group (Table 3). For diastolic function data, we reported a marked reduction in EDFR in HFpEF in comparison with HFrEF patients (Table 3). Thirdly, only the responder patients showed a significant improvement of repolarization and specific hemodynamic data between baseline and discharge. Specifically, the data indicated a decrease in the Te, Te_{SD}, HR, SBP, DBP, and MBP and an increase in the LVET (Figure 2) (Table 4). On the contrary, no variations were observed, between baseline and discharge, in non-responder groups for non-invasive hemodynamic data, but regarding repolarization data, there was an increase in Te and Te_{SD} (Figure 2). Finally, at discharge, responder patients demonstrated higher levels of $LVEF_{BIO}$ and ConI and lower levels of LVEDV, Te, and Te_{SD}. From this set of data, it can be seen that Te remains a useful short-term marker of hospital mortality, but repolarization and non-invasive hemodynamic data were not able to identify the specific categories of CHF based on $LVEF_{ECO}$. However, the low level of agreement between $LVEF_{ECH}$ and $LVEF_{BIO}$ has been previously reported by our group in the same study patients [19]. Conversely, repolarization data and non-invasive hemodynamic data could be used to monitor patients with CHF because this approach allows the use of clinical signs to identify non-responders. In particular, the lack of change in Te, Te_{SD}, heart rate, blood pressure, and LVET, which are a heart-rate-dependent parameters [44], were the best markers of NT-proBNP reduction (Table 4). However, the best results were obtained with repolarization data. The Te and Te_{SD} data showed divergent behavior among non-responders. At the time of discharge, the responders had a significant reduction, while the non-responders had increases in these parameters (Figure 2).

In this study, we discovered the Te and Te_{SD} as specific markers of mortality and CHF decompensation, but the pathophysiological basis of these ECG parameters is still controversial. In fact, in the past, this last part of repolarization was extensively studied as a marker of sudden arrhythmic death both in vivo and in vitro. In particular, some authors hypothesized that the Te interval could represent the transmural dispersion of repolarization and this electrophysiologic condition was related to ventricular malignant arrhythmias [45,46]. This hypothesis has been scrutinized but it is still erroneously reported in studies as the probable electrophysiological basis of the Te [47–49]. However, this hypothesis does not explain how the Te interval is widely associated with an increased risk of total and non-arrhythmic mortality [14–16]. Our data indicate the Te interval was an independent risk factor for total mortality, cardiovascular mortality, and CHF decompensation in a study population with a low level of sudden arrhythmic death. We believe sympathetic hyperactivity and neurohumoral activation could influence the Te

and TeSD. In previous studies, it was reported that sympathetic activation during exercise was able to induce an increase in Te and TeSD in normal subjects [50]. In animal models, we observed an increase in the short-term variability of the Te interval during pacing-induced acute congestive heart failure and experimental acute myocardial ischemia [35,51]. Additionally, the temporal dispersion markers of Te were strongly correlated to the stellate ganglion nerve activity [35,51]. Subsequently, another study reported an increase in the Te interval during left, right, and bilateral stellate ganglion stimulations [52]. Therefore, experimental and clinical studies individuated a relation between sympathetic activity and Te interval. We believe that sympathetic hyperactivity in CHF could affect the last part of repolarization by altering voltage-gated ion channels. We hypothesized that ion channel remodeling in CHF could be capable of increasing both duration and temporal dispersion, expressed as standard deviations of the Te interval. In the last thirty years, experimental and electrophysiological studies have established the deep involvement of sodium channels, potassium channels, calcium handling, and currents in CHF resulting in an increase in the action potential duration [53]. In particular, a delayed inactivation of sodium channels with a prolonged inward of sodium beyond phase 0 was reported [54,55]. Contrarily, a down-regulation of the potassium channels (Ito, IKs, IKr, IK1, and IK2P) [54] represents the most important outward flow of positive ions capable of regulating the action potential duration. Finally, a considerable number of studies indicated impairing of the intracellular myocardial calcium cycle by a multilevel involvement of structures, enzymes, and ion channels resulting in a cytosolic calcium overload, a reduced calcium sarcoplasmic reticulum content, and an increase in action potential duration [56]. On the other hand, in addition, the pathologic myocardial substrate could play a leading role. In fact, myocardial ischemia, necrosis, fibrosis, hypertrophy, and fiber disarray could undoubtedly induce an increase in action potential duration and more specifically Te and Te_{SD}.

The use of artificial intelligence (AI) in the field of clinical cardiology is increasingly promising [57–60]. In particular, in heart failure, the use of knowledge in the pathophysiological and electrocardiographic fields, combined with the possibility of remote monitoring, can play a fundamental role in the lives of patients suffering from this complex clinical condition [61–66]. Thus, machine learning tools are extremely important to acquire deep knowledge and reach specific stratification–prognostic models. The possibility of intercepting clinical alterations in advance, predicted by the electrocardiographic changes of patients suffering from CHF, would allow the cardiologist to modify therapy in time and, hopefully, reduce the possibility of acute heart failure.

Furthermore, the use of machine learning would be of enormous importance in being able to refine the diagnostic capabilities of AI tools with the data collected over time [67,68]. In conclusion, these simple, inexpensive, non-invasive, easily repeatable, and transmissible markers coupled with autonomous decision-making processes based on artificial intelligence algorithms could improve the management and the prognosis of these frail patients.

5. Limitations

The present study is burdened by the smallness of the sample evaluated, albeit calculated a priori.

The small sample size and the advanced age of the enrolled patients influenced the possibility of analyzing the data obtained by correlating them to the dosage of drugs, usually taken by patients for chronic heart failure therapy. In fact, basically faithful to the geriatric medicine principle of "start low and go slow", almost all patients were taking low doses of drugs. Larger studies could allow observation of differences and stratify patients according to drug dosage.

A further limitation was studying hospitalized patients and hypothesizing the use of the data obtained for patients not yet hospitalized. Further studies on outpatient populations are necessary.

Furthermore, another limitation of the study is that just one patient was treated with SGLT2 inhibitors. The sample was in fact largely studied before the recent indications provided by the European Society of Cardiology guidelines on the use in class I evidence A of these drugs in subjects with heart failure and diabetes mellitus [7]. In fact, with the use of these drugs, we expect a lower frequency of hospitalizations for acute cardiac decompensation in CHF patients and, having a fundamentally diuretic effect, even a lower retention of liquids recognizable to bioimpedance. Further enrollment will help fill this gap.

Author Contributions: Conceptualization, G.P., P.R. and F.M.; methodology, G.P., P.R. and F.M; software, G.P.; validation, G.P. and F.M.; formal analysis, G.P.; investigation, F.M., M.M., C.C., G.C., G.V., V.D.S., M.G., S.S. (Sara Stefano), C.S., M.C., A.C., I.L. and S.S. (Susanna Sciomer); data curation F.M., M.M., C.C., G.C., G.V., V.D.S., M.G., S.S. (Sara Stefano), C.S., M.C., A.C., I.L. and S.S. (Susanna Sciomer); writing—original draft preparation, G.P. and F.M.; writing—review and editing, S.S. (Susanna Sciomer) and P.R.; visualization, G.P., F.M., M.M., C.C., G.C., G.V, V.D.S., M.G., S.S. (Sara Stefano), C.S., M.C., A.C., I.L. and S.S. (Susanna Sciomer); supervision, G.P. All authors have read and agreed to the published version of the manuscript.

Funding: This research received no external funding.

Institutional Review Board Statement: Policlinico Umberto I Ethical Committee was informed and approved the study (Prot. 0282/2023).

Informed Consent Statement: All patients at the moment of the test signed an informed consent form, aware that their clinical information could be analyzed anonymously at any time.

Data Availability Statement: All data, materials, and codes used in this study are available upon request from the corresponding author.

Conflicts of Interest: The authors deny personal or financial conflicts of interest regarding this paper.

References

1. Groenewegen, A.; Rutten, F.H.; Mosterd, A.; Hoes, A.W. Epidemiology of heart failure. *Eur. J. Heart Fail.* **2020**, *22*, 1342–1356. [CrossRef] [PubMed]
2. Nabil, S. Comparison of International Guidelines for Managing Chronic Heart Failure with Reduced Ejection Fraction. *Curr. Probl. Cardiol.* **2023**, *48*, 101867. [CrossRef] [PubMed]
3. Rosano, G.M.C.; Seferovic, P.; Savarese, G.; Spoletini, I.; Lopatin, Y.; Gustafsson, F.; Bayes-Genis, A.; Jaarsma, T.; Abdelhamid, M.; Miqueo, A.G.; et al. Impact analysis of heart failure across European countries: An ESC-HFA position paper. *ESC Heart Fail.* **2022**, *9*, 2767–2778. [CrossRef] [PubMed]
4. Ploux, S.; Strik, M.; Ramirez, F.D.; Buliard, S.; Chauvel, R.; Dos Santos, P.; Haïssaguerre, M.; Jobbé-Duval, A.; Picard, F.; Riocreux, C.; et al. Remote management of worsening heart failure to avoid hospitalization in a real-world setting. *ESC Heart Fail.* **2023**, *10*, 3637–3645. [CrossRef] [PubMed]
5. Bäck, M.; von Haehling, S.; Papp, Z.; Piepoli, M.F. A year in heart failure: Updates of clinical and preclinical findings. *ESC Heart Fail.* **2023**, *10*, 2150–2158. [CrossRef] [PubMed]
6. Wenzel, J.P.; Nikorowitsch, J.; Bei der Kellen, R.; Magnussen, C.; Bonin-Schnabel, R.; Westermann, D.; Twerenbold, R.; Kirchhof, P.; Blankenberg, S.; Schrage, B. Heart failure in the general population and impact of the 2021 European Society of Cardiology Heart Failure Guidelines. *ESC Heart Fail.* **2022**, *9*, 2157–2169. [CrossRef]
7. Piccirillo, G.; Moscucci, F.; Sciomer, S.; Magrì, D. Chronic Heart Failure Management: Monitoring Patients and Intercepting Exacerbations. *Rev. Cardiovasc. Med.* **2023**, *24*, 208. [CrossRef]
8. Radhoe, S.P.; Veenis, J.F.; Brugts, J.J. Invasive Devices and Sensors for Remote Care of Heart Failure Patients. *Sensors* **2021**, *21*, 2014. [CrossRef]
9. Setoguchi, S.; Stevenson, L.W.; Schneeweiss, S. Repeated hospitalizations predict mortality in the community population with heart failure. *Am. Heart J.* **2007**, *154*, 260–266. [CrossRef]
10. Gheorghiade, M.; De Luca, L.; Fonarow, G.C.; Filippatos, G.; Metra, M.; Francis, G.S. Pathophysiologic targets in the early phase of acute heart failure syndromes. *Am. J. Cardiol.* **2005**, *96*, 11G–17G. [CrossRef]
11. Reynard, J.T.; Oshodi, O.M.; Lai, J.C.; Lai, R.W.; Bazoukis, G.; Fragakis, N.; Letsas, K.P.; Korantzopoulos, P.; Liu, F.Z.; Liu, T.; et al. Electrocardiographic conduction and repolarization markers associated with sudden cardiac death: Moving along the electrocardiography waveform. *Minerva Cardioangiol.* **2019**, *67*, 131–144. [CrossRef]
12. McDonagh, T.A.; Metra, M.; Adamo, M.; Gardner, R.S.; Baumbach, A.; Böhm, M.; Burri, H.; Butler, J.; Čelutkienė, J.; Chioncel, O.; et al. ESC Scientific Document Group. 2021 ESC Guidelines for the diagnosis and treatment of acute and chronic heart failure. *Eur. Heart J.* **2021**, *42*, 3599–3726. [CrossRef]

13. Heidenreich, P.A.; Bozkurt, B.; Aguilar, D.; Allen, L.A.; Byun, J.J.; Colvin, M.M.; Deswal, A.; Drazner, M.H.; Dunlay, S.M.; Evers, L.R.; et al. 2022 AHA/ACC/HFSA Guideline for the Management of Heart Failure: A Report of the American College of Cardiology/American Heart Association Joint Committee on Clinical Practice Guidelines. *J. Am. Coll. Cardiol.* **2022**, *145*, e895–e1032. [CrossRef]
14. Bachmann, T.N.; Skov, M.W.; Rasmussen, P.V.; Graff, C.; Pietersen, A.; Lind, B.; Struijk, J.J.; Olesen, M.S.; Haunsø, S.; Køber, L.; et al. Electrocardiographic Tpeak-Tend interval and risk of cardiovascular morbidity and mortality: Results from the Copenhagen ECG study. *Heart Rhythm.* **2016**, *13*, 915–924. [CrossRef]
15. Tse, G.; Gong, M.; Wong, W.T.; Georgopoulos, S.; Letsas, K.P.; Vassiliou, V.S.; Chan, Y.S.; Yan, B.P.; Wong, S.H.; Wu, W.K.; et al. The T_{peak}-T_{end} interval as an electrocardiographic risk marker of arrhythmic and mortality outcomes: A systematic review and meta-analysis. *Heart Rhythm.* **2017**, *14*, 1131–1137. [CrossRef]
16. Braun, C.C.; Zink, M.D.; Gozdowsky, S.; Hoffmann, J.M.; Hochhausen, N.; Röhl, A.B.; Beckers, S.K.; Kork, F. A Longer T_{peak}-T_{end} Interval Is Associated with a Higher Risk of Death: A Meta-Analysis. *J. Clin. Med.* **2023**, *12*, 992. [CrossRef]
17. Moscucci, F.; Sciomer, S.; Maffei, S.; Meloni, A.; Lospinuso, I.; Carnovale, M.; Corrao, A.; Di Diego, I.; Caltabiano, C.; Mezzadri, M.; et al. Sex Differences in Repolarization Markers: Telemonitoring for Chronic Heart Failure Patients. *J. Clin. Med.* **2023**, *12*, 4714. [CrossRef] [PubMed]
18. Piccirillo, G.; Moscucci, F.; Mezzadri, M.; Caltabiano, C.; Di Diego, I.; Carnovale, M.; Corrao, A.; Stefano, S.; Scinicariello, C.; Giuffrè, M.; et al. Electrocardiographic and other Noninvasive Hemodynamic Markers in Decompensated CHF Patients. *J. Cardiovasc. Dev. Dis.* **2023**, *10*, 125. [CrossRef] [PubMed]
19. Piccirillo, G.; Moscucci, F.; Corrao, A.; Carnovale, M.; Di Diego, I.; Lospinuso, I.; Caltabiano, C.; Mezzadri, M.; Rossi, P.; Magrì, D. Noninvasive Hemodynamic Monitoring in Advanced Heart Failure Patients: New Approach for Target Treatments. *Biomedicines* **2022**, *10*, 2407. [CrossRef]
20. Piccirillo, G.; Moscucci, F.; Carnovale, M.; Corrao, A.; Di Diego, I.; Lospinuso, I.; Sciomer, S.; Rossi, P.; Magrì, D. Glucose dysregulation and repolarization variability markers are short-term mortality predictors in decompensated heart failure. *Cardiovasc. Endocrinol. Metab.* **2022**, *11*, e0264. [CrossRef]
21. Tse, G.; Yan, B.P. Traditional and novel electrocardiographic conduction and repolarization markers of sudden cardiac death. *Europace* **2017**, *19*, 712–721. [CrossRef]
22. Cullington, D.; Goode, K.M.; Zhang, J.; Cleland, J.G.; Clark, A.L. Is heart rate important for patients with heart failure in atrial fibrillation? *JACC Heart Fail.* **2014**, *2*, 213–220. [CrossRef]
23. Piccirillo, G.; Moscucci, F.; Mariani, M.V.; Di Iorio, C.; Fabietti, M.; Mastropietri, F.; Crapanzano, D.; Bertani, G.; Sabatino, T.; Zaccagnini, G.; et al. Hospital mortality in decompensated heart failure. *A pilot study. J. Electrocardiol.* **2020**, *61*, 147–152. [CrossRef] [PubMed]
24. Venegas-Rodríguez, A.; Pello, A.M.; López-Castillo, M.; Taibo Urquía, M.; Balaguer-Germán, J.; Munté, A.; González-Martín, G.; Carriazo-Julio, S.M.; Martínez-Milla, J.; Kallmeyer, A.; et al. The role of bioimpedance analysis in overweight and obese patients with acute heart failure: A pilot study. *ESC Heart Fail.* **2023**, *10*, 2418–2426. [CrossRef]
25. Senarath, S.; Fernie, G.; Roshan Fekr, A. Influential Factors in Remote Monitoring of Heart Failure Patients: A Review of the Literature and Direction for Future Research. *Sensors* **2021**, *21*, 3575. [CrossRef] [PubMed]
26. Jabbour, S.; Fouhey, D.; Shepard, S.; Valley, T.S.; Kazerooni, E.A.; Banovic, N.; Wiens, J.; Sjoding, M.W. Measuring the Impact of AI in the Diagnosis of Hospitalized Patients: A Randomized Clinical Vignette Survey Study. *JAMA* **2023**, *330*, 2275–2284. [CrossRef]
27. Leto, L.; Testa, M.; Feola, M. The predictive value of plasma biomarkers in discharged heart failure patients: Role of plasma NT-proBNP. *Minerva Cardioangiol.* **2016**, *64*, 157–164.
28. Orini, M.; Al-Amodi, F.; Koelsch, S.; Bailón, R. The Effect of Emotional Valence on Ventricular Repolarization Dynamics Is Mediated by Heart Rate Variability: A Study of QT Variability and Music-Induced Emotions. *Front. Physiol.* **2019**, *10*, 1465. [CrossRef] [PubMed]
29. Saal, D.P.; Thijs, R.D.; van Zwet, E.W.; Bootsma, M.; Brignole, M.; Benditt, D.G.; van Dijk, J.G. Temporal Relationship of Asystole to Onset of Transient Loss of Consciousness in Tilt-Induced Reflex Syncope. *JACC Clin. Electrophysiol.* **2017**, *3*, 1592–1598. [CrossRef]
30. Yamaguchi, K.; Yoshitomi, H.; Ito, S.; Adachi, T.; Sato, H.; Watanabe, N.; Kodani, N.; Sugamori, T.; Endo, A.; Takahashi, N.; et al. Left atrial remodeling and recurrence of congestive heart failure in patients initially diagnosed with heart failure. *Echocardiography* **2014**, *31*, 936–940. [CrossRef]
31. Piccirillo, G.; Magrì, D.; D'Alessandro, G.; Fiorucci, C.; Moscucci, F.; Di Iorio, C.; Mastropietri, F.; Parrotta, I.; Ogawa, M.; Lin, S.F.; et al. Oscillatory behavior of P wave duration and PR interval in experimental congestive heart failure: A preliminary study. *Physiol. Meas.* **2018**, *39*, 035010. [CrossRef]
32. Piccirillo, G.; Moscucci, F.; Magrì, D. Air Pollution Role as Risk Factor of Cardioinhibitory Carotid Hypersensitivity. *Atmosphere* **2022**, *13*, 123. [CrossRef]
33. Piccirillo, G.; Moscucci, F.; Di Diego, I.; Mezzadri, M.; Caltabiano, C.; Carnovale, M.; Corrao, A.; Lospinuso, I.; Stefano, S.; Scinicariello, C.; et al. Effect of Head-Up/-Down Tilt on ECG Segments and Myocardial Temporal Dispersion in Healthy Subjects. *Biology* **2023**, *12*, 960. [CrossRef]
34. Piccirillo, G.; Moscucci, F.; Corrao, A.; Carnovale, M.; Di Diego, I.; Lospinuso, I.; Caltabiano, C.; Mezzadri, M.; Magrì, D. Time and Frequency Repolarization Domains in Elderly Candidates to Transcatheter Aortic Valve Replacement. *La Clin. Ter.* **2023**, *174*, 139–145. [CrossRef]

35. Piccirillo, G.; Moscucci, F.; Pofi, R.; D'Alessandro, G.; Minnetti, M.; Isidori, A.M.; Francomano, D.; Lenzi, A.; Puddu, P.E.; Alexandre, J.; et al. Changes in left ventricular repolarization after short-term testosterone replacement therapy in hypogonadal males. *J. Endocrinol. Investig.* **2019**, *42*, 1051–1065. [CrossRef]
36. Charloux, A.; Lonsdorfer-Wolf, E.; Richard, R.; Lampert, E.; Oswald-Mammosser, M.; Mettauer, B.; Geny, B.; Lonsdorfer, J. A new impedance cardiograph device for the non-invasive evaluation of cardiac output at rest and during exercise: Comparison with the "direct" Fick method. *Eur. J. Appl. Physiol.* **2000**, *82*, 313–320. [CrossRef] [PubMed]
37. Hsu, A.R.; Barnholt, K.E.; Grundmann, N.K.; Lin, J.H.; McCallum, S.W.; Friedlander, A.L. Sildenafil improves cardiac output and exercise performance during acute hypoxia, but not normoxia. *J. Appl. Physiol.* **2006**, *100*, 2031–2040. [CrossRef] [PubMed]
38. Lepretre, P.M.; Koralsztein, J.P.; Billat, V.L. Effect of exercise intensity on relationship between VO2max and cardiac output. *Med. Sci. Sports Exerc.* **2004**, *36*, 1357–1363. [CrossRef]
39. Tonelli, A.R.; Alnuaimat, H.; Li, N.; Carrie, R.; Mubarak, K.K. Value of impedance cardiography in patients studied for pulmonary hypertension. *Lung* **2011**, *189*, 369–375. [CrossRef] [PubMed]
40. Gordon, N.; Abbiss, C.R.; Maiorana, A.J.; Marston, K.J.; Peiffer, J.J. Intrarater reliability and agreement of the physioflow bioimpedance cardiography device during rest, moderate and high-intensity exercise. *Kinesiology* **2018**, *50* (Suppl. 1), 140–149.
41. Leão, R.N.; Da Silva, P.M. Impedance Cardiography in the Evaluation of Patients with Arterial Hypertension. *Int. J. Cardiovasc. Sci.* **2019**, *32*, 61–69. [CrossRef]
42. Anand, G.; Yu, Y.; Lowe, A.; Kalra, A. Bioimpedance analysis as a tool for hemodynamic monitoring: Overview, methods and challenges. *Physiol. Meas.* **2021**, *42*, 03TR01. [CrossRef] [PubMed]
43. Piccirillo, G.; Moscucci, F.; Carnovale, M.; Corrao, A.; Di Diego, I.; Lospinuso, I.; Caltabiano, C.; Mezzadri, M.; Rossi, P.; Magrì, D. Short-Period Temporal Dispersion Repolarization Markers in Elderly Patients with Decompensated Heart Failure. *La Clin. Ter.* **2022**, *173*, 356–361.
44. Alhakak, A.S.; Teerlink, J.R.; Lindenfeld, J.; Böhm, M.; Rosano, G.M.C.; Biering-Sørensen, T. The significance of left ventricular ejection time in heart failure with reduced ejection fraction. *Eur. J. Heart Fail.* **2021**, *23*, 541–551. [CrossRef] [PubMed]
45. Antzelevitch, C. Heterogeneity and cardiac arrhythmias: An overview. *Heart Rhythm.* **2007**, *4*, 964–972. [CrossRef]
46. Antzelevitch, C.; Di Diego, J.M. Tpeak-Tend interval as a marker of arrhythmic risk. *Heart Rhythm.* **2019**, *16*, 954–955. [CrossRef]
47. Opthof, T.; Coronel, R.; Wilms-Schopman, F.J.; Plotnikov, A.N.; Shlapakova, I.N.; Danilo, P.; Rosen, M.R., Jr.; Janse, M.J. Dispersion of repolarization in canine ventricle and the electrocardiographic T wave: Tp-e interval does not reflect transmural dispersion. *Heart Rhythm.* **2007**, *4*, 341–348. [CrossRef]
48. Malik, M.; Huikuri, H.; Lombardi, F.; Schmidt, G.; Zabel, M. e-Rhythm Study Group of EHRA Conundrum of the Tpeak-Tend interval. *J. Cardiovasc. Electrophysiol.* **2018**, *29*, 767–770. [CrossRef]
49. Malik, M.; Huikuri, H.V.; Lombardi, F.; Schmidt, G.; Verrier, R.L.; Zabel, M. e-Rhythm Group of EHRA Is the T_{peak}-T_{end} interval as a measure of repolarization heterogeneity dead or just seriously woded? *Heart Rhythm.* **2019**, *16*, 952–953. [CrossRef]
50. Piccirillo, G.; Moscucci, F.; Iorio, C.D.; Fabietti, M.; Mastropietri, F.; Crapanzano, D.; Bertani, G.; Sabatino, T.; Zaccagnini, G.; Lospinuso, I.; et al. Time- and frequency-domain analysis of repolarization phase during recovery from exercise in healthy subjects. *Pacing Clin. Electrophysiol. PACE* **2020**, *43*, 1096–1103. [CrossRef]
51. Piccirillo, G.; Moscucci, F.; D'Alessandro, G.; Pascucci, M.; Rossi, P.; Han, S.; Chen, L.S.; Lin, S.F.; Chen, P.S.; Magrì, D. Myocardial repolarization dispersion and autonomic nerve activity in a canine experimental acute myocardial infarction model. *Heart Rhythm.* **2014**, *11*, 110–118. [CrossRef]
52. Yagishita, D.; Chui, R.W.; Yamakawa, K.; Rajendran, P.S.; Ajijola, O.A.; Nakamura, K.; So, E.L.; Mahajan, A.; Shivkumar, K.; Vaseghi, M. Sympathetic nerve stimulation, not circulating norepinephrine, modulates T-peak to T-end interval by increasing global dispersion of repolarization. *Circ. Arrhythmia Electrophysiol.* **2015**, *8*, 174–185. [CrossRef]
53. Aiba, T.; Tomaselli, G.F. Electrical remodeling in the failing heart. *Curr. Opin. Cardiol.* **2010**, *25*, 29–36. [CrossRef]
54. Rahm, A.K.; Lugenbiel, P.; Schweizer, P.A.; Katus, H.A.; Thomas, D. Role of ion channels in heart failure and channelopathies. *Biophys. Rev.* **2018**, *10*, 1097–1106. [CrossRef] [PubMed]
55. Remme, C.A.; Bezzina, C.R. Sodium channel (dys)function and cardiac arrhythmias. *Cardiovasc. Ther.* **2010**, *28*, 287–294. [CrossRef] [PubMed]
56. Gorski, P.A.; Ceholski, D.K.; Hajjar, R.J. Altered myocardial calcium cycling and energetics in heart failure—A rational approach for disease treatment. *Cell Metab.* **2015**, *21*, 183–194. [CrossRef] [PubMed]
57. Trayanova, N.A.; Lyon, A.; Shade, J.; Heijman, J. Computational modeling of cardiac electrophysiology and arrhythmogenesis. *Physiol. Rev.* **2023**. Advance online publication. [CrossRef] [PubMed]
58. Ribeiro, A.L.P.; Paixão, G.M.M.; Gomes, P.R.; Ribeiro, M.H.; Ribeiro, A.H.; Canazart, J.A.; Oliveira, D.M.; Ferreira, M.P.; Lima, E.M.; Moraes, J.L.; et al. Tele-electrocardiography and bigdata: The CODE (Clinical Outcomes in Digital Electrocardiography) study. *J. Electrocardiol.* **2019**, *57S*, S75–S78. [CrossRef] [PubMed]
59. Nakasone, K.; Nishimori, M.; Kiuchi, K.; Shinohara, M.; Fukuzawa, K.; Takami, M.; El Hamriti, M.; Sommer, P.; Sakai, J.; Nakamura, T.; et al. Development of a Visualization Deep Learning Model for Classifying Origins of Ventricular Arrhythmias. *Circ. J. Off. J. Jpn. Circ. Soc.* **2022**, *86*, 1273–1280. [CrossRef] [PubMed]
60. Kaur, D.; Hughes, J.W.; Rogers, A.J.; Kang, G.; Narayan, S.M.; Ashley, E.A.; Perez, M.V. Race, Sex, and Age Disparities in the Performance of ECG Deep Learning Models Predicting Heart Failure. *Circ. Heart Fail.* **2024**, *17*, e010879. [CrossRef] [PubMed]

61. Rahman, A.U.; Alsenani, Y.; Zafar, A.; Ullah, K.; Rabie, K.; Shongwe, T. Enhancing heart disease prediction using a self-attention-based transformer model. *Sci. Rep.* **2024**, *14*, 514. [CrossRef]
62. Zhang, C.J.; Tang, F.Q.; Cai, H.P.; Qian, Y.F. Heart failure classification using deep learning to extract spatiotemporal features from ECG. *BMC Med. Inform. Decis. Mak.* **2024**, *24*, 17. [CrossRef] [PubMed]
63. Wu, J.; Biswas, D.; Ryan, M.; Bernstein, B.M.; Rizvi, M.; Fairhurst, N.; Kaye, G.; Baral, R.; Searle, T.; Melikian, N.; et al. Artificial intelligence methods for improved detection of undiagnosed heart failure with preserved ejection fraction. *Eur. J. Heart Fail.* **2023**. Advance online publication. [CrossRef]
64. Ramírez, J.; Monasterio, V.; Mincholé, A.; Llamedo, M.; Lenis, G.; Cygankiewicz, I.; Bayés de Luna, A.; Malik, M.; Martínez, J.P.; Laguna, P.; et al. Automatic SVM classification of sudden cardiac death and pump failure death from autonomic and repolarization ECG markers. *J. Electrocardiol.* **2015**, *48*, 551–557. [CrossRef]
65. Palacios, S.; Cygankiewicz, I.; Bayés de Luna, A.; Pueyo, E.; Martínez, J.P. Periodic repolarization dynamics as predictor of risk for sudden cardiac death in chronic heart failure patients. *Sci. Rep.* **2021**, *11*, 20546. [CrossRef]
66. Barrett, M.; Boyne, J.; Brandts, J.; Brunner-La Rocca, H.P.; De Maesschalck, L.; De Wit, K.; Dixon, L.; Eurlings, C.; Fitzsimons, D.; Golubnitschaja, O.; et al. Artificial intelligence supported patient self-care in chronic heart failure: A paradigm shift from reactive to predictive, preventive and personalised care. *EPMA J.* **2019**, *10*, 445–464. [CrossRef]
67. Pagallo, U.; O'Sullivan, S.; Nevejans, N.; Holzinger, A.; Friebe, M.; Jeanquartier, F.; Jean-Quartier, C.; Miernik, A. The underuse of AI in the health sector: Opportunity costs, success stories, risks and recommendations. *Health Technol.* **2024**, *14*, 1–14. [CrossRef] [PubMed]
68. Croon, P.M.; Selder, J.L.; Allaart, C.P.; Bleijendaal, H.; Chamuleau, S.A.J.; Hofstra, L.; Išgum, I.; Ziesemer, K.A.; Winter, M.M. Current state of artificial intelligence-based algorithms for hospital admission prediction in patients with heart failure: A scoping review. *Eur. Heart J. Digit. Health* **2022**, *3*, 415–425. [CrossRef] [PubMed]

Disclaimer/Publisher's Note: The statements, opinions and data contained in all publications are solely those of the individual author(s) and contributor(s) and not of MDPI and/or the editor(s). MDPI and/or the editor(s) disclaim responsibility for any injury to people or property resulting from any ideas, methods, instructions or products referred to in the content.

biomedicines

MDPI

Systematic Review

Prognostic Value of Lectin-like Oxidized Low-Density Lipoprotein Receptor-1 for Future Cardiovascular Disease Risk and Outcome: A Systematic Review and Meta-Analysis

Amilia Aminuddin [1,*], Nazirah Samah [1], Nur Aishah Che Roos [2], Shawal Faizal Mohamad [3], Boon Cong Beh [3], Adila A. Hamid [1] and Azizah Ugusman [1,*]

[1] Department of Physiology, Faculty of Medicine, Universiti Kebangsaan Malaysia, Jalan Yaacob Latif, Bandar Tun Razak, Cheras, Kuala Lumpur 56000, Malaysia; p124809@siswa.ukm.edu.my (N.S.); adilahamid@ppukm.ukm.edu.my (A.A.H.)
[2] Faculty of Medicine and Defence Health, National Defence University of Malaysia, Kem Sungai Besi, Kuala Lumpur 57000, Malaysia; nuraishah@upnm.edu.my
[3] Department of Cardiology, Universiti Kebangsaan Malaysia, Jalan Yaacob Latif, Bandar Tun Razak, Cheras, Kuala Lumpur 56000, Malaysia; drshawal81.hctm@ukm.edu.my (S.F.M.); dr.behbooncong@ppukm.ukm.edu.my (B.C.B.)
* Correspondence: amilia@hctm.ukm.edu.my (A.A.); dr.azizah@hctm.ukm.edu.my (A.U.)

Abstract: Cardiovascular disease (CVD) remains a leading cause of mortality globally, underscoring the need for robust predictive biomarkers to enhance risk stratification. Soluble lectin-like oxidized low-density lipoprotein receptor-1 (sLOX-1) has emerged as a promising biomarker linked to oxidative stress and endothelial dysfunction, both critical mechanisms in atherogenesis and cardiovascular events. **Objectives**: This study aimed to evaluate the prognostic value of sLOX-1 in predicting major adverse cardiovascular and cerebrovascular events (MACCEs), myocardial infarction (MI), heart failure (HF), and stroke outcomes through a systematic review and meta-analysis. **Methods**: A systematic literature search was conducted across PubMed, Scopus, Web of Science, and Ovid databases for studies published between 2014 and October 2024. Eligible studies assessed the association between sLOX-1 levels and future CVD outcomes in adult populations. Meta-analysis pooled hazard ratios (HRs) were assessed using random- and fixed-effects models. Heterogeneity was evaluated using the I^2 statistic, and study quality was assessed using the Newcastle–Ottawa Scale. **Results**: Fourteen studies were included, encompassing diverse populations with coronary artery disease (CAD), acute coronary syndrome (ACS), or stroke, with follow-up durations ranging from 30 days to 19.5 years. The meta-analysis of three studies on CAD patients demonstrated a significant association between elevated sLOX-1 levels and increased MACCE risk (HR: 2.3, 95% CI: 0.99–5.33, $p = 0.05$), albeit with high heterogeneity ($I^2 = 83\%$). The fixed-effects analysis yielded a more consistent HR of 1.47 (95% CI: 1.19–1.81, $p < 0.01$). **Conclusions**: sLOX-1 shows promising potential as a prognostic biomarker for CVD and is associated with an increased risk of MACCEs in CAD patients. However, the high heterogeneity among the included studies highlights the need for standardized protocols and larger, well-designed prospective studies to validate its clinical utility. The integration of sLOX-1 into risk prediction models could improve CVD management by identifying high-risk individuals for targeted interventions.

Keywords: cardiovascular disease; coronary artery disease; acute coronary syndrome; myocardial infarction; stroke; soluble lectin-like oxidized LDL receptor-1; risk

1. Introduction

Cardiovascular disease (CVD) remains the leading cause of morbidity and mortality worldwide, accounting for an estimated 17.9 million deaths each year, representing 31% of all global deaths [1]. CVD encompasses a broad spectrum of heart and vascular disorders, including coronary artery disease (CAD), stroke, and peripheral artery disease. In Malaysia, the burden of CVD is alarming, with ischemic heart disease identified as the leading cause of death, contributing to 17% of total fatalities in 2020 [2]. The rising prevalence of risk factors such as hypertension, diabetes, obesity, and smoking has further escalated the incidence of CVD in the country [3]. Given the substantial health and economic toll of CVD, enhancing early detection and prevention strategies is imperative. Identifying reliable biomarkers to predict future cardiovascular events is vital for mitigating the impact of CVD on individuals and healthcare systems.

In recent years, the search for reliable biomarkers has become an integral focus of cardiovascular research, aimed at improving the early diagnosis and prognosis of CVD. Biomarkers provide insight into underlying pathophysiological processes and can help identify individuals at high risk for cardiovascular events, even before clinical symptoms manifest [4]. Traditional markers, such as high-sensitivity C-reactive protein (hs-CRP) and troponins, have been widely used, yet their predictive value may be limited in certain populations [5]. This has led to the investigation of novel biomarkers with greater specificity and accuracy. One such promising marker is soluble lectin-like oxidized low-density lipoprotein receptor-1 (sLOX-1), a receptor involved in the binding and uptake of oxidized LDL (oxLDL), which plays a pivotal role in the development and progression of atherosclerosis [6]. Elevated levels of sLOX-1 have been associated with endothelial dysfunction, plaque instability, and an increased risk of acute coronary events, making it a potential candidate for improving CVD risk stratification [7].

sLOX-1 is a truncated, circulating form of the membrane-bound LOX-1 receptor, which is predominantly expressed on endothelial cells, macrophages, and smooth muscle cells within atherosclerotic plaques [8]. Structurally, LOX-1 belongs to the C-type lectin family and consists of four main domains: a short N-terminal cytoplasmic domain, a transmembrane domain, a neck region, and an extracellular C-type lectin-like domain [9]. The extracellular domain is responsible for binding oxLDL, a key driver of atherogenesis. Under conditions of oxidative stress and inflammation, oxLDL accumulates in the vascular endothelium, triggering LOX-1 activation [10]. This binding promotes endothelial dysfunction, foam cell formation, and plaque instability, all of which contribute to atherosclerosis progression.

The soluble form, sLOX-1, is released into circulation upon cleavage of the membrane-bound receptor, with elevated serum levels observed in patients with acute coronary syndrome (ACS) and other cardiovascular disorders. These findings suggest its potential as a non-invasive biomarker for CVD [11–13]. sLOX-1 has been linked to endothelial dysfunction, a critical early event in the development of atherosclerosis, driven by factors such as hypertension, diabetes, and hyperlipidemia [14]. Elevated sLOX-1 levels have also been associated with increased inflammatory markers such as interleukin-6 (IL-6) and tumor necrosis factor-alpha (TNF-α), both of which exacerbate atherogenic processes [15]. Clinical investigations have demonstrated a correlation between sLOX-1 levels and the severity of atherosclerosis in patients with suspected CAD [16], reinforcing its relevance as a predictive biomarker in CVD management.

Beyond its association with acute events, growing evidence suggests that sLOX-1 could be a valuable predictor of future CVD events. Several longitudinal studies have investigated the relationship between baseline sLOX-1 levels and the incidence of cardiovascular outcomes such as myocardial infarction (MI), heart failure (HF), and stroke.

For instance, baseline sLOX-1 concentrations have been shown to predict MI and heart failure in general populations [17]. Among patients with established CAD, higher sLOX-1 levels have been linked to increased long-term mortality and recurrent ischemic events [18]. However, despite the accumulating data, the overall consistency and strength of these associations remain unclear. To address this, a systematic review and meta-analysis were conducted to quantitatively assess the predictive value of sLOX-1 for future CVD events. This meta-analysis aimed to provide a comprehensive and reliable estimate of the association, explore potential sources of heterogeneity across studies, and further clarify sLOX-1's role in cardiovascular risk stratification.

2. Methodology

This review was conducted in accordance with the Preferred Reporting Items for Systematic Reviews and Meta-Analysis (PRISMA) guidelines [19]. The PRISMA checklist is reported in Appendix A (Tables A1 and A2). The review protocol has been registered with the International Platform of Registered Systematic Review Protocols (registration number INPLASY2024120078) [20].

2.1. Research Question and Search Strategy

The research question was formulated using the "PICO" framework. Patients with ACS, CAD, and acute ischemic stroke (AIS) or healthy subjects were identified as the "Population (P)". Low sLOX-1 levels were defined as the "Comparison (C)", while the occurrence of major adverse cardiocerebrovascular events (MACCEs), MI, HF, recurrent stroke, or unfavorable outcomes post stroke constituted the "Outcome (O)". sLOX-1 levels were designated as the "Intervention (I)". Hence, the research question was as follows: are increased sLOX-1 levels predictive of future CVD? A comprehensive literature search was carried out across four databases (Ovid, Scopus, Pubmed, and Google Scholar), focusing on studies published between 2014 and October 2024 (Accessed on 1 November 2024). The search employed the following keywords: ("LOX-1" OR "lectin-like oxidized LDL receptor-1") AND ("Cardiovascular disease" OR "CVD" OR "Coronary artery disease" OR "CAD" OR "Myocardial infarction" OR "Acute coronary syndrome" OR "Atherosclerosis" OR "Peripheral vascular disease" OR "Cerebrovascular accident" OR "Stroke" OR "Major cardiovascular event" OR "MACE" OR "Mortality").

2.2. Study Criteria

Two researchers (NS and AA) independently reviewed each article, ensuring compliance with predefined inclusion and exclusion criteria. The inclusion criteria included the following: (1) full-text peer-reviewed original articles published in English, (2) prospective and retrospective studies investigating the relationship between sLOX-1 and future coronary artery disease (CAD), cardiovascular disease (CVD), or major adverse cardiovascular events (MACEs), and (3) studies involving adult patients diagnosed with ACS, CAD, or AIS or healthy subjects, regardless of gender. The exclusion criteria consisted of (1) articles not published in English, (2) reviews, conference abstracts, editorials, newsletters, books, and book chapters, (3) in vitro studies, and (4) research involving animals.

2.3. Article Selection and Data Extraction

The article selection process comprised three stages. First, articles were screened according to their titles and types, with review or editorial articles excluded. Next, abstracts were examined to remove any articles that were irrelevant to sLOX-1 and CAD, CVD, or MACEs. Finally, the remaining articles underwent a detailed full-text review, and those that did not meet the inclusion criteria were eliminated. The article selection process was conducted independently by two reviewers (A.A. and N.S.). Similarly, data extraction was

performed independently by two reviewers (A.A. and N.S.) using a standardized Excel form. Data extracted included study design, study duration, participant characteristics (e.g., age, gender, CVD diagnosis), methods of sLOX-1 measurement, and the relationship between sLOX-1 and atherosclerosis. Any disagreement was resolved by consensus or consultation with a third reviewer (A.U.) if necessary.

2.4. Risk of Bias Assessment

Two reviewers (N.S. and A.A.) independently assessed the risk of bias in the selected articles using the Newcastle–Ottawa Scale (NOS) [21]. For cohort and cross-sectional studies, the NOS evaluated the selection of study groups (exposed vs. non-exposed), their comparability, and outcome assessment. In contrast, for case–control studies, the NOS evaluated the selection of study groups (cases vs. controls), their comparability, and exposure assessment. Each of the eight NOS items was rated with one or two stars. Studies that received a total score of seven to nine stars were classified as high-quality, those with four to six stars as fair-quality, and those with one to three stars as low-quality.

2.5. Statistical Analysis

A meta-analysis was conducted using Review Manager (RevMan version 5.4 software, The Cochrane Collaboration 2000, Copenhagen, Denmark) [22]. The hazard ratio (HR) or odds ratio (OR), with a 95% confidence interval (CI), derived from multivariate Cox proportional hazard analysis, were used as the effect estimate to evaluate s-LOX-1 as a predictor of MACEs in patients with ACS or AIS. The heterogeneity among studies was assessed using (1) the chi-squared test, with a p-value of less than 0.10 indicating statistical significance, and (2) the Higgin's I^2 statistic [23]. An I^2 value of <25% indicated low heterogeneity, while an I^2 value of $\geq$75% indicated high heterogeneity. Due to the limited number of studies available for meta-analysis and varying study population across studies, the random-effects (RE) model was employed. Statistical significance was set at $p < 0.05$. Subgroup analysis was not performed due to the limited number of studies. In addition, funnel plots or the Egger test for publication bias were not conducted, as fewer than 10 studies were included.

3. Results

The search retrieved a total of 9918 articles from four databases: Ovid (1490), Scopus (7925), Pubmed (500), and Google Scholar (3). Articles were compiled using Mendeley Desktop Version 1.19.8 (Mendeley Ltd., London, UK) and 821 duplicates were removed. Additionally, 4155 reviews, editorials, and non-English-language articles were excluded. Title and abstract screening excluded 4908 articles unrelated to sLOX-1, CAD, or MACEs. The remaining 34 articles were read in full, with only 14 articles meeting the eligibility criteria for inclusion. The study selection process is summarized in Figure 1. The quality assessment of the 14 selected articles using the NOS scale is outlined in Tables 1 and 2. The scores ranged from 6 to 8, reflecting fair to high quality. Specifically, 12 studies were categorized as high-quality [13,17,18,24–32], while 2 studies were classified as fair-quality [33,34]. Altogether, the risk of bias for all included studies in terms of the selection, comparator, and outcome reporting bias was considered low. Therefore, results synthesized using data from the included studies may contribute to a reliable source of information which could be used to inform clinical practice regarding the association between sLOX-1 and future CVD risk.

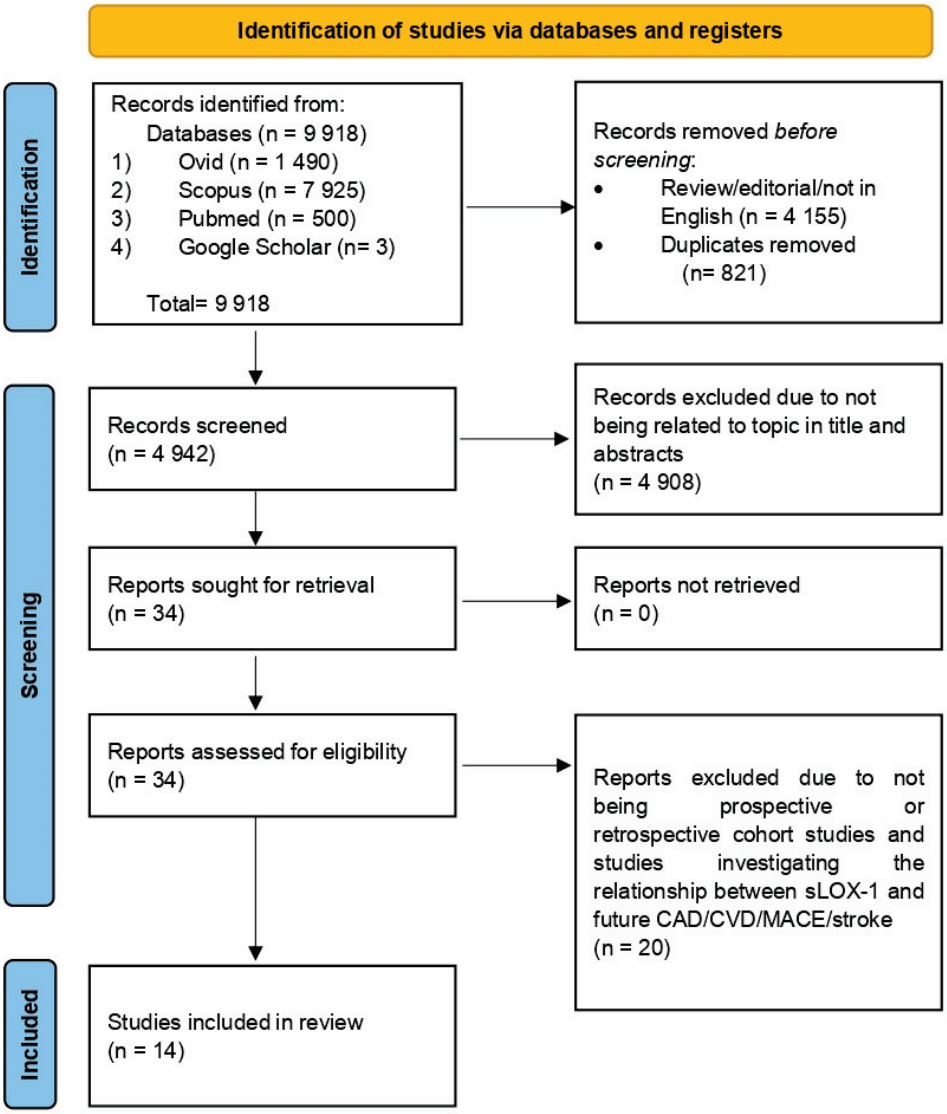


Figure 1. Flow chart illustrating the process of selecting and screening based on PRISMA.

Table 1. The Newcastle–Ottawa Scale (NOS) for assessing the quality of cohort studies (CAD studies).

Author	Type of Study	Selection				Comparability	Outcome			Total Score
		Representatives of Exposed Cohort	Selection of Non-Exposed Cohort	Ascertainment of Exposure	Demonstration that Outcome of Interest Was Not Present at Start of Study	Comparability of Cohorts on the Basis of the Design or Analysis	Assessment of Outcome	Was Follow-Up Long Enough for Outcomes to Occur?	Adequacy of Follow-Up of Cohorts	
		Truly Representative of the Average Community	Drawn from the Same Community as the Exposed Cohort	From Secure Record	Yes	Study Controls for Any Additional Factors	Independent Blind Assessment/Record Linkage	Yes	Complete Follow-Up (All Subjects Accounted for)	
Kraler et al. [24]	Prospective cohort	*	*	*	*	*	*	*		7
Zhao (a) et al. [33]	Prospective	*	*	*	*		*	*		6
Kumar et al. [25]	Prospective	*	*	*	*	*	*	*	*	8
Schiopu et al. [17]	Prospective cohort	*	*	*	*		*	*	*	7
Mashayekhi et al. [18]	Prospective	*	*	*	*		*	*	*	7
Zhao (b) et al. [26]	Prospective	*	*	*	*		*	*	*	7
Higuma et al. [27]	Prospective	*	*	*	*		*	*	*	7

* Indicates one star.

Table 2. The Newcastle–Ottawa Scale (NOS) for assessing the quality of cohort studies (stroke studies).

Author	Type of Study	Selection				Comparability	Outcome			Total Score
		Representatives of Exposed Cohort	Selection of Non-Exposed Cohort	Ascertainment of Exposure	Demonstration that Outcome of Interest Was Not Present at Start of Study	Comparability of Cohorts on the Basis of the Design or Analysis	Assessment of Outcome	Was Follow-Up Long Enough for Outcomes to Occur?	Adequacy of Follow-Up of Cohorts	
		Truly Representative of the Average Community	Drawn from the Same Community as the Exposed Cohort	From Secure Record	Yes	Study Controls for Any Additional Factors	Independent Blind Assessment/Record Linkage	Yes	Complete Follow-Up (All Subjects Accounted for)	
Zheng et al. [34]	Prospective	*	*	*	*		*	*		6
Ren et al. [28]	Retrospective	*	*	*	*		*	*	*	7
Li et al. [13]	Prospective	*	*	*	*		*	*	*	7
Yan et al. [29]	Prospective	*	*	*	*	*	*	*		7
Yang et al. [30]	Prospective	*	*	*	*		*	*	*	7
Wang et al. [31]	Prospective	*	*	*	*	*	*	*		7
Markstad et al. [32]	Cohort	*	*	*	*		*	*	*	7

* Indicates one star.

3.1. General Characteristics of the Included Studies

The 14 studies included in this study were published between 2014 and October 2024. Seven studies focused on the predictive value of sLOX-1 for CAD, while another seven focused on the role of sLOX-1 as predictor for stroke. All studies were prospective, except for the study by Ren et al., 2023 [28], which was retrospective. Two studies involved subjects without CAD or stroke at baseline [17,32], while the remaining studies involved subjects who already had CAD or ACS [18,24–27,33] or stroke [13,19,28–31]. The duration of follow-up ranged from 30 days to 19.5 years. Most of the subjects were male, with ages ranging from middle-aged to elderly. All studies assessed sLOX-1 levels from plasma or serum samples. For CAD or ACS patients, outcome measures included MACCEs, HF, or MI. For stroke patients, outcomes focused on functional recovery post stroke and stroke recurrence. The definition of MACCEs varied among studies. For instance, Zhao (a) et al., 2019 [33] defined MACCEs as all-cause death, readmission for ACS, unplanned repeat revascularization, definite stent thrombosis, and ischemic stroke, while Zhao (b) et al., 2019 [26] defined them as all-cause death, nonfatal acute MI, and readmission for Braunwald's class IIIb unstable angina requiring treatment. In addition, Higuma et al., 2015 [27] defined MACCEs as cardiovascular mortality and recurrent nonfatal MI. Several studies used different cut-off values to define high sLOX-1 levels. For instance, Higuma et al. defined it as >71 pg/mL, while Zhao et al. [33] used $\geq$1.10 ng/mL, and Zhao et al. [26] applied >0.91 ng/mL. For sLOX-1 measurements, the ELISA technique was used in most of the studies [13,18,24–26,29,30,34]. However, there were other methods used, such as the PEA technique [17], sandwich chemiluminescent enzyme immunoassay [27], anti-analyzer [31], and multiplex kit [34].

3.2. Summary of Findings

3.2.1. sLOX-1 and Future MACCEs, MI and HF

For studies investigating the association between sLOX-1 and future MACCEs, MI, or HF, most subjects had ACS or CAD, with only one study involving a non-CAD population [17]. Among CAD or ACS patients, five studies reported a significant positive association (Table 3). For example, Higuma et al., 2015 [27] found that higher sLOX-1 levels predicted a higher risk of MACCEs, with a HR of 2.44 (95% CI: 1.07–5.57), while Zhao (a) and (b) et al. 2019 [26,33] reported HRs of 1.28 (95% CI: 1.02–1.60) and 4.73 (95% CI: 2.17–10.30), respectively. The authors of [24] also reported that elevated sLOX-1 levels were associated with a 2.3-fold increased risk of cardiovascular mortality within one year of follow-up (HR: 2.29, 95% CI: 1.19–5.34; $p = 0.0148$). In another study, sLOX-1 levels were associated with MACCE in ST-elevation MI (STEMI) and unstable angina (UA)/non-STEMI groups (Spearman correlation coefficients: 0.345, $p < 0.001$, and 0.189, $p = 0.017$, respectively) [18]. Among patients with recurrent cases of MI and stroke, the baseline post interventional sLOX-1 levels were higher compared to the non-recurrent cases [25]. In a study of non-CAD subjects, higher sLOX-1 levels were associated with an increased risk of MACCEs (HR: 1.76, 95% CI: 1.40–2.21) [17].

3.2.2. sLOX-1 and Future Functional Outcomes Post Strokes or Recurrent Strokes

Among stroke patients, several studies identified significant associations between baseline sLOX-1 and unfavorable or favorable functional outcomes post strokes [13,29,30,34] (Table 4). Functional outcomes were measured using the Modified Rankin Score (mRS). Additionally, several studies reported a significant association between sLOX-1 levels and higher risk of recurrent stroke among patients with or without prior history of stroke [28,31,32].

Table 3. Association between circulating sLOX-1 and future cardiovascular events among CAD patients and healthy subjects.

Ref.	Study Design	Population Characteristic	sLOX-1 Measurement	Outcomes Assessed	Key Findings	Conclusion
Kraler et al. [24]	Prospective cohort study. Follow-up at 30 days and 1 year	Patients with ACS ($n = 2639$) ACS = 65.7 ± 1.2 years old	Elisa kit (Thermo Scientific™ Pierce™, Waltham, MA, USA)	Mortality post ACS for all causes and CVD at 30 days and 1 year	(1) ACS patients in the highest sLOX-1 tertile displayed a 2.3-fold increased risk of cardiovascular mortality within 1 year of follow-up (HR, 2.29, 95% CI, 1.19–5.34; $p = 0.0148$). (2) Risk of CVD death at 30 days was increased by 281% in the highest tertile (HR, 3.81, 95% CI, 1.62–19.62; $p = 0.0036$). (3) After multivariable adjustment, high sLOX-1 levels (third tertile) were associated with an increased risk of death from any cause at 30 days (T3: fully adjusted HR, 3.11, 95% CI, 1.44–10.61; $p = 0.0055$). (4) High plasma sLOX-1 was an independent predictor of all-cause mortality over 1 year (HR, 2.04, 95% CI, 1.19–3.92, $p = 0.0098$).	Soluble LOX-1 is a novel and independent biomarker for fatal events in patients presenting with ACS.
Zhao (a) et al. [33]	Prospective study. Review at 2 years	984 patients who were treated for primary PCI; 768 patients had ACS (78.05%); Divided into (1) MACCEs: 69 (59–76) years old, 78.14% men; (2) MACCE-free: 67 (59–74) year old, 70.43% men	ELISA kit (USCN, Wuhan, China).	Composite of MACCEs (all-cause death, readmission for ACS, unplanned repeat revascularization, definite stent thrombosis, and ischemic stroke)	Serum sLOX-1 levels at 2 years were associated with MACCEs (HR 1.278, 95% CI 1.019–1.604, $p = 0.034$).	High baseline serum sLOX-1 concentration predicts 2-year MACCEs and shows an additional prognostic value to conventional risk factors in patients after primary PCI.
Kumar et al. [25]	Prospective study. Follow-up at 1 year	Patients undergoing angiography and diagnosed with ACS and stable CAD. Divided into (1) Group I: patients who underwent coronary angiography ($n = 18$) but did not have established CAD; (2) Group II: patients with stable CAD who underwent percutaneous intervention ($n = 50$); (3) Group III: patients with acute coronary syndrome ($n = 64$); (4) Group IV: healthy controls ($n = 28$)	ELISA kit (USCN, Wuhan, China)	Recurrence of MI and stroke	In recurrence cases ($n = 9$), pre-treatment sLOX-1 level was higher than in non-recurrence cases ($n = 123$); however, the difference was not significant ($p = 0.655$). However, the post-interventional sLOX-1 level was significantly different and higher in recurrence cases ($p = 0.027$).	sLOX-1 is a useful biomarker of stable CAD/ACS and has a potential in the risk prediction of a future recurrence of CAD.
Schiopu et al. [17]	Prospective population-based cohort with 19.5 ± 4.9 years follow-up period	4658 apparently healthy subjects. Grouping following event/no event: (1) No MI: 57.2 ± 5.9; (2) MI: 59.8 ± 5.5; (3) No HF: 57.2 ± 5.9; (4) HF: 61.1 ± 5.0	PEA technique using the Proseek Multiplex CVD96x96 reagents kit (Olink Bioscience, Uppsala, Sweden)	MI or HF	Subjects in the highest tertile of sLOX-1 had an increased risk of myocardial infarction (hazard ratio (95% CI) 1.76 (1.40–2.21) as compared with those in the lowest tertile. No association seen for HF.	There is an association between elevated sLOX-1 and the risk of first-time myocardial infarction.
Mashayekhi et al. [18]	Prospective study. Follow-up at 30 days	320 patients with ACS (236 males and 84 females; mean age 57.29 ± 9.7 years)	ELISA kit (Shanghai Crystal Day Biotech Co. Ltd., Shan hai, China)	In-hospital death, heart failure, and recurrent ischemia	sLOX-1 correlated with MACEs in STEMI and UA/NSTEMI groups (Spearman correlation coefficient = 0.345, $p < 0.001$; Spearman correlation coefficient = 0.189, $p = 0.017$, respectively).	Circulating sLOX-1 could be used as a biomarker to predict major adverse cardiac events in patients with ACS and may be clinically useful in the triage and management of these patients.

Table 3. *Cont.*

Ref.	Study Design	Population Characteristic	sLOX-1 Measurement	Outcomes Assessed	Key Findings	Conclusion
Zhao (b) et al. [26]	Prospective study. Follow-up at 2 years	833 patients with stable CAD. Divided into (1) MACE (n = 75), aged 68 (39–84) years old, 72% male; (2) No MACE (n = 758), aged 64 (32–87) years old, 76% male	ELISA kit (USCN, Wuhan, China)	Composite of MACEs, which were identified as all-cause death, nonfatal AMI, and readmission for Braunwald's class IIIb UA requiring treatment	Subjects in the highest tertile of sLOX-1 had an increased risk of MACE (HR: 4.73; 95% CI: 2.17–10.30) as compared with those in the lowest tertile.	Baseline sLOX-1 concentrations correlate with 2-year MACEs in stable CAD patients.
Higuma et al. [27]	Prospective study. Follow-up at 3 years	153 patients with STEMI, mean age 67 ± 12 years old, 75% male	Sandwich chemiluminescent enzyme immunoassay (Shionogi Co., Ltd., Osaka, Japan)	All-cause mortality and the combined endpoint of MACEs, which were defined as cardiovascular mortality and recurrent nonfatal MI	Log plasma sLOX-1 level was associated with all-cause mortality (HR: 3.743; 95% CI: 1.853–7.562, $p < 0.001$) and MACEs (HR: 2.436; 95% CI: 1.066–5.566, $p = 0.035$).	Measurement of plasma sLOX-1 may be useful in identifying patients at high risk for future cardiovascular events.

ACS, acute coronary syndrome; CVD, cardiovascular disease; CAD, coronary artery disease; MI, myocardial infarction; AMI, acute myocardial infarction; HF, heart failure; MACCEs, major adverse cardiac and cerebrovascular events; MACEs, major adverse cardiovascular events; STEMI, ST-elevation myocardial infarction; UA, unstable angina; sLOX-1, soluble lectin-like oxidized low-density lipoprotein receptor-1; HR, hazard ratio; CI, confidence interval; p, p-value; PCI, percutaneous coronary intervention; ELISA, enzyme-linked immunosorbent assay; PEA, proximity extensive assay.

Table 4. Association between circulating s-LOX-1 and future recurrent stroke or unfavorable outcomes post stroke among stroke patients and healthy subjects.

Ref.	Study Design	Population Characteristic	sLOX-1 Measurement	Outcomes Assessed	Key Findings	Conclusion
Zheng et al. [34]	Prospective study: follow-up at 3 months	260 patients with AIS. Divided into (1) recurrent ischemic stroke (n = 101), age 68.0 (58.0–78.0) years old, men 75.2%; (2) first-ever ischemic stroke (n = 165), age 61.0 (55.0–69.0) years old, men 72.7%	ELISA (Solarbio Life Science, Beijing, China)	mRS score at 90 days' follow-up. An mRS score of 0–2 at follow-up was defined as a favorable outcome and 3–6 as an unfavorable outcome	(1) No correlation was found between sLOX-1 levels and mRS score at 3 months in all patients with AIS or with first-ever stroke. (2) After adjusting for age, admission NIHSS score, NLR, and other variables in the binominal multivariate logistic analysis, sLOX-1 levels remained an independent predictor of unfavorable outcomes in patients with recurrent ischemic stroke with an adjusted OR of 1.489 (95% CI: 1.204–1.842, $p < 0.0001$).	Diagnosis and prognosis are different between patients with recurrent stroke and those experiencing a first-ever stroke. Additionally, sLOX-1 levels serve as an independent prognostic marker in patients with recurrent stroke.
Ren et al. [28]	Retrospective study: review at 12 months	199 patients with AIS and TIA. Divided into (1) Non-recurrence group (n = 158): 63.56 ± 12.98 years old, 64.6% male; (2) Recurrence group (n = 41): 67.10 ± 9.96 years old, 78% male	Not mentioned	Stroke recurrence based on imaging (n = 30) or new neurological deficit symptoms (n = 11)	sLOX-1 levels were independent risk factors for stroke recurrence (HR: 1.001, 95% CI: 1.000–1.002, p = 0.002).	sLOX-1 levels can be used as a supplement to HR-MR-VWI to predict stroke recurrence.
Li et al. [13]	Prospective study: review at 1 year	272 patients with AIS aged 63.04 ± 8.92 years old, 176 (64.7%) were men 1 year	ELISA	mRS score: favorable or non-favorable outcome. Scores 3 and above considered poor outcome	sLOX-1 was an independent predictor for unfavorable functional outcomes in stroke cases with an adjusted OR of 2.946 (95% CI: 1.788–4.856, $p < 0.001$).	sLOX-1 could be used to predict the long-term functional outcome of stroke.
Yan et al. [29]	Prospective study: review at 3 months	127 ACI patients (first-ever stroke) (78 males and 49 females). Divided into (1) Healthy: 58.42 ± 8.93 years old; (2) No stenosis: 75.4 ± 11.72 years old; (3) Mild stenosis: 62.08 ± 11.25 years old; (4) Moderate stenosis: 61.4 ± 16.04 years old; (5) Severe stenosis: 66.75 ± 13.53 years old	ELISA	mRS for functional recovery, scores 3 and above considered poor outcome	After adjusting for all confounders, sLOX-1 levels were significantly associated with poor functional outcomes, with an OR of 1.005 (95% CI: 1.002–1.007, $p < 0.001$).	The level of sLOX-1 could serve as a useful biomarker to predict the functional outcome of ACI.

Table 4. *Cont.*

Ref.	Study Design	Population Characteristic	sLOX-1 Measurement	Outcomes Assessed	Key Findings	Conclusion
Yang et al. [30]	Prospective study: follow-up at 3 months	207 patients with small-artery atherosclerotic occlusion cerebral infarction. Divided by age and male sex (1) Tertile 1, sLOX-1 level < 2.24 pg/mL= 67 (63.50, 75.00) years old, male 67%; (2) Tertile 2, sLOX-1 level 2.24 to 2.89 pg/mL = 66 (58.00, 72.00) years old, male 74%; (3) Tertile 3, sLOX-1 level ≥ 2.90 pg/mL = 68 (59.25, 73.00) years old, male 65%	ELISA (RapidBio Laboratory, CA, USA)	mRS score at 90 days, where 0 to 2 (able to look after own affairs without assistance) was defined as a favorable outcome and 3 to 6 (unable to look after own affairs or death) was defined as poor outcome	Patients in the lowest sLOX-1 tertile had a higher likelihood of achieving a favorable functional outcome at 90 days (OR: 3.47, 95% CI: 1.21–9.96).	In patients with acute atherosclerosis-related ischemic stroke, circulating sLOX-1 levels are correlated with favorable functional outcomes at 90 days.
Wang et al. [31]	Prospective study: review at 3, 6 and 12 months	1200 patients with AIS or TIA. Divided into (1) 400 recurrent cases aged 64.00 (55.00–72.00) years old, 66.5% men; (2) 800 controls (age- and sex-matched) aged 64.00 (55.00–73.00) years old, 66.5% men	Anti-analyzers by using 2 monoclonal antihuman LOX-1 antibodies (TS 92) (ILB International GmbH, Hamburg, Germany)	Recurrent stroke (ischemic or hemorrhagic), ischemic stroke, and combined vascular events (including ischemic stroke, hemorrhagic stroke, myocardial infraction, or vascular death)	(1) Higher sLOX-1 levels were associated with increased odds of recurrent stroke within 3 months and 1 year of follow-up. The adjusted ORs for the highest tertile compared to the lowest tertile of sLOX-1 were 2.10 (95% CI: 1.40–3.16; p for trend < 0.0001) and 2.23 (95% CI: 1.61–3.08; p for trend < 0.0001), respectively. (2) Similar findings were observed for ischemic stroke, with an adjusted OR of 1.95 (95% CI: 1.28–2.96), and for combined vascular events, with an adjusted OR of 1.95 (95% CI: 1.28–2.96) within 3 months. At 1 year, the adjusted ORs for combined vascular events were 2.30 (95% CI: 1.66–3.19) and 2.31 (95% CI: 1.64–3.24), respectively. (3) Multivariable-adjusted spline regression models revealed J-shaped associations between sLOX-1 levels and the odds of recurrent stroke, ischemic stroke, and combined vascular events within both 3 months and 1 year.	sLOX-1 levels could independently predict recurrent stroke in patients with AIS or TIA.
Markstad et al. [32]	Cohort study: follow-up for 16.5 ± 3.6 years	4703 subjects with no previous history of stroke	Olink Proseek Multiplex kit (Olink Proteomics AB, Uppsala, Sweden)	Recurrent ischemic stroke	(1) Baseline sLOX-1 was associated with recurrent ischemic stroke after 16.5 years of follow-up. Those in the highest tertile had a hazard ratio of 1.75 (95% CI, 1.28–2.39) compared with those in the lowest tertile after adjustment for age and sex. (2) This association remained significant after further adjustment for factors including current smoking, diabetes mellitus, waist circumference, systolic blood pressure, LDL cholesterol, triglycerides, and CRP, with an adjusted odds ratio of 1.41 (CI: 1.01–1.96, $p < 0.05$).	Circulating sLOX-1 levels correlate with carotid plaque inflammation and risk for ischemic stroke.

AIS, acute ischemic stroke; TIA, transient ischemic stroke; ACI, acute cerebral infarction; ELISA, enzyme-linked immunosorbent assay; mRS, modified rankin score; NIHSS, National Institute of Health stroke scale or score; sLOX-1, soluble lectin-like oxidized low-density lipoprotein receptor-1; HR, hazard ratio; OR, odds ratio; CI, confidence interval; p, p-value; HR-MR-VWI, high-resolution magnetic resonance vessel wall imaging; LDL, low-density lipoprotein; CRP, C-reactive protein.

3.2.3. Meta-Analysis

sLOX-1 and MACCEs

Our meta-analysis of three studies [26,27,33] examined the prognostic value of sLOX-1 for predicting MACCE in CAD patients. Using a random-effects model, it was found that higher sLOX-1 levels were associated with a 2.3-fold increased risk of MACCE (HR: 2.3, 95% CI: 0.99–5.33, $p = 0.05$) (Figure 2). However, the wide confidence interval and high heterogeneity ($I^2 = 83\%$) indicated variability across the studies. To address heterogeneity, a sensitivity analysis using a fixed-effects model was performed (Figure 3). This analysis yielded a more precise HR of 1.47 (95% CI: 1.19–1.81, $p < 0.01$), confirming a consistent and statistically significant association between elevated sLOX-1 levels and increased MACCE risk. There were several potential sources of variability. First, there were differences in study population, such as age and prevalence of comorbidities. Although the mean age of the subjects in the three studies was relatively similar (67–69 years old), the age range were different. For example, one study by Zhao et al. [26] involved subjects with age ranges between 32 and 87 years old, while the other study by Zhao et al. [33] involved subjects with age ranges between 59 and 76 years old. In addition, each study had different distributions of comorbidities. For example, in the study population in Higuma et al. [27], 75% had hypertension, 33% had diabetes, 63% had dyslipidemia, and 54% smoked. In Zhao et al. [33], among those with MACCEs, 50% smoked, 31.3% had diabetes, and 58.26% had hypertension. In the study population in Zhao et al. [26], 72% had hypertension, 45% smoked, and 45% had diabetes. Variations in comorbidities also contributed to variations in the medications used. Most of the populations in the three studies used statins, angiotensin-converting enzyme inhibitors, angiotensin II receptor blockers, and beta blockers; however, the percentages that used them were different [26,27,33]. Another possible contributing factor was the method used for sLOX-1 measurements. The studies by Zhao et al. ([26,33]) used ELISA, while the study by Higuma et al. [27] used a sandwich chemiluminescent enzyme immunoassay. Moreover, the definition of outcome was also differed across the studies, as mentioned above.

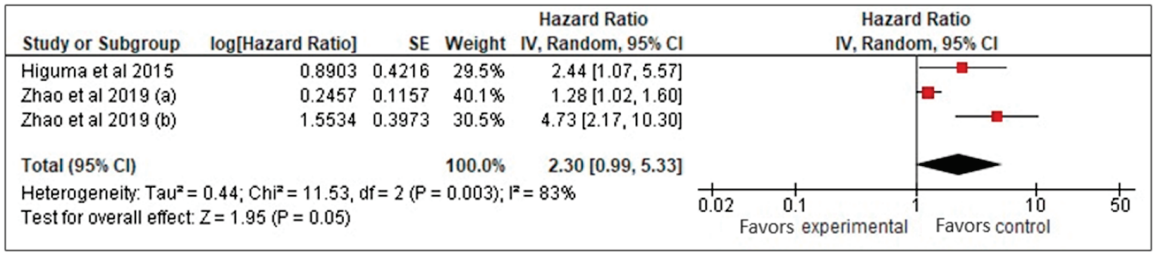


Figure 2. sLOX-1 as a predictor of MACCEs (random-effects model) [26,27,33]. Red box indicates the effect size for individual study which in this model, the size of the boxes are fairly similar indicating equal weight distribution across all included studies. While, the black diamond, which is the visual representation of the pooled effect sizes, is wide with its right tip touches the line of no effect denoting borderline statistical significance with wide 95% CI.

sLOX-1 and Stroke Outcomes

A meta-analysis for sLOX-1 and stroke outcomes could not be conducted due to high variation between the studies. Although there were three studies that investigated the association between baseline s-LOX-1 and functional outcomes post stroke [13,29,34], the patients included were not similar. For example, the study by Yan et al. [29] involved patients with first-ever stroke, while Zheng et al. [34] involved patients with first-ever stroke and recurrent ischemic stroke. In another study, this characteristic was not detailed [13]. In addition, there were differences in patient age, comorbidities, the medications used, and the duration of follow-up between studies. For example, the studies by Zheng et al. [34]

and Yan et al. [29] assessed the patient condition at three months, while the study by Li et al. [13] reviewed the patient condition at one year. Because of these variation, the pooling of data was deemed inappropriate.

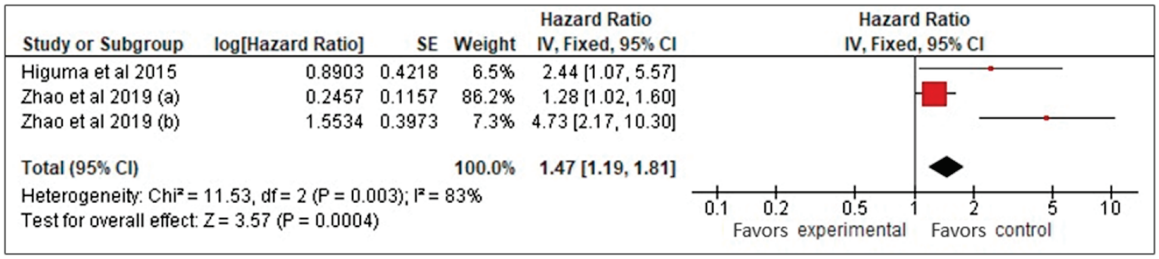


Figure 3. sLOX-1 as a predictor of MACCEs (fixed-effects) [26,27,33]. Red box indicates the effect size for individual study while the black diamond is the visual representation of the pooled effect sizes. In this model, the most weight (86.2%) is allocated to the study with the biggest red square, thus influencing the pooled effect size (black diamond).

4. Discussion

Our meta-analyses involving CAD patients supported the role of sLOX-1 as a prognostic biomarker for MACCE. The stronger association observed in the fixed-effects model suggests that sLOX-1 may have consistent predictive value when study-level variations are accounted for. However, the high heterogeneity observed in both models necessitates caution when interpreting the pooled estimates. Possible contributors to this heterogeneity include differences in study populations (e.g., age, comorbidities, and treatment regimens), sLOX-1 measurement methods and threshold definitions, MACCE definitions, and follow-up durations. The variability in sLOX-1 cut-off values reported across studies may also reflect underlying differences in systemic inflammation, as inflammation is a known contributor to elevated sLOX-1 levels. However, most of the studies included in the meta-analysis did not report data on CRP, limiting our ability to normalize sLOX-1 levels based on inflammation. Despite this limitation, the robust association between sLOX-1 levels and cardiovascular outcomes observed in most of the studies suggests that sLOX-1 remains a valuable biomarker, even without adjustment for inflammatory status.

The integration of sLOX-1 into clinical practice offers several potential pathways to enhance cardiovascular care. As a biomarker associated with oxidative stress and endothelial dysfunction, sLOX-1 could serve as an adjunct to traditional risk scores, such as the Framingham Risk Score or GRACE score, to improve risk stratification, particularly for individuals at intermediate or high risk. Additionally, its role in the early detection of subclinical atherosclerosis or acute vascular events could be pivotal in identifying individuals with ambiguous symptoms or those requiring timely intervention. sLOX-1 levels may also inform personalized treatment decisions, such as guiding the use of statins, antioxidants, or anti-inflammatory therapies, and monitoring these levels could help assess treatment efficacy over time. Furthermore, in acute coronary syndrome patients, sLOX-1 could refine prognostic models, aiding in decisions regarding invasive procedures or extended monitoring during hospital admission and follow-up. Lastly, its utility in specific high-risk populations, such as individuals with diabetes, metabolic syndrome, or chronic inflammatory conditions, could enable targeted screening and earlier intervention to mitigate cardiovascular risk. However, integrating sLOX-1 into routine clinical practice faces several challenges. Firstly, the variability in sLOX-1 measurement techniques, including the use of different ELISA kits and assay methodologies, poses a significant challenge. The use of diverse kits, each employing antibodies with varying specificities and affinities, can substantially influence protein measurement [35]. Additionally, differences in detection limits

and quantification thresholds among kits may lead to the underestimation of low protein concentrations when low-sensitivity kits are used [36]. These inconsistencies complicate result comparability and the establishment of universal reference ranges. Furthermore, there is no consensus on clinically meaningful sLOX-1 cut-off values for risk stratification. Many studies report associations between sLOX-1 levels and outcomes but fail to define threshold categories, such as low, moderate, or high risk [17]. Lastly, integrating sLOX-1 testing into routine clinical workflows requires the development of cost-effective, scalable methods and collaborative efforts between researchers and clinicians to establish a standardized interpretation of sLOX-1 levels for informed clinical decision-making.

Several mechanisms have been implicated in the association between sLOX-1, MACCEs, and post-stroke functional outcomes. First, sLOX-1 is associated with oxidative stress and endothelial dysfunction. Its ligand, oxLDL, disrupts eNOS activity in endothelial cells, reducing nitric oxide (NO) production. Lower NO levels lead to endothelial dysfunction, promoting damage, lipid buildup, and plaque formation [37]. Elevated sLOX-1 levels reflect oxidative stress, impair endothelial function, and contribute to atherosclerosis, plaque rupture, and thrombus formation [10]. High circulating sLOX-1 levels are linked to an increased likelihood of thrombotic events and worse outcomes in acute cardiovascular conditions [8]. Second, sLOX-1 release is associated with the activation of pro-inflammatory pathways, leading to the upregulation of adhesion molecules. Activation of mitogen-activated protein kinase (MAPK) by oxLDL promotes the transcription of adhesion molecules, including monocyte chemoattractant protein-1 (MCP-1), intracellular adhesion molecules-1 (ICAM-1), and vascular cell adhesion molecules (VCAM-1). Elevated MCP-1 attracts monocytes to the endothelium [38–40]. This inflammatory response exacerbates atherosclerosis and predisposes individuals to adverse cardiovascular and cerebrovascular events, impeding poor functional recovery after a stroke. Third, in atherosclerosis, sLOX-1 contributes to vascular remodeling, promoting the migration and proliferation of smooth muscle cells and the production of matrix metalloproteinases (MMPs) [41,42]. The binding of oxLDL to LOX-1 on endothelial cells activates the protein kinase C-beta (PKC-β) signaling cascade. PKC-β increases the expression of MMPs [41]. Excessive MMP activity degrades the extracellular matrix and contributes to endothelial dysfunction, vascular remodeling, and plaque instability. This process increases the vulnerability of plaques to rupture, thereby increasing the risk of acute cardiovascular events, including MI and stroke [41,42]. In stroke, elevated sLOX-1 levels are linked to increased vascular permeability and damage, correlating with poorer functional outcomes and recovery [43]. The detailed mechanisms underlying the role sLOX-1 in CVD pathophysiology have been extensively reviewed in previous studies [10,44].

5. Limitations and Future Directions

The exclusion of gray literature and unpublished data is a limitation of this review. While this decision was made to prioritize the quality and rigor of the evidence, it may have resulted in the omission of relevant studies, potentially introducing publication bias. In addition, a restriction of this meta-analysis lies in the limited number of available studies, which restricts the statistical power and the robustness of the pooled estimates. A small number of studies inherently increases the influence of individual study results on the overall meta-analysis, potentially biasing the conclusions. Furthermore, the wide confidence intervals observed in the random-effects model highlight imprecisions, necessitating caution in interpretation.

High heterogeneity across studies also raises concerns about the consistency and comparability of results. Variations in study design, population characteristics, sLOX-1 assay methodologies, and follow-up durations challenge the generalizability of the findings.

Standardized protocols in future research are needed to address this issue. Publication bias and potential unmeasured confounders within the included studies cannot be excluded, further limiting the reliability of the results. Well-designed prospective studies are urgently needed to confirm the prognostic value of sLOX-1, particularly for MACCEs and functional outcomes post stroke. Such studies should recruit diverse populations to enhance the generalizability of findings across demographic and clinical subgroups. Efforts should also focus on standardizing sLOX-1 measurement protocols, including assay methods, sampling techniques, and risk stratification thresholds. A consensus on these parameters will facilitate the clinical integration of sLOX-1 and allow for meaningful comparisons between studies.

Additionally, further investigations into the biological mechanisms linking sLOX-1 and MACE are critical. Understanding sLOX-1′s role in endothelial dysfunction, inflammation, and plaque instability could validate its clinical relevance and uncover novel therapeutic targets for CVD. Exploring these mechanisms may also clarify sLOX-1′s potential utility in guiding treatment strategies or monitoring disease progression.

6. Conclusions

This systematic review highlights the potential of sLOX-1 as a prognostic biomarker for CVD, particularly in predicting MACCEs. Despite promising findings, limitations such as the small number of studies, wide confidence intervals, and significant heterogeneity across studies underscore the need for cautious interpretation. While sLOX-1 shows promise as a tool for cardiovascular risk stratification, more robust evidence is required before its integration into routine clinical practice. Future studies should focus on standardizing sLOX-1 measurement protocols and definitions of outcomes.

Author Contributions: Conceptualization and methodology, A.A.; methodology and data curation, N.S.; data curation and original-draft, A.A. and A.U.; formal analysis (meta-analysis), N.A.C.R.; writing—review and editing, S.F.M. and B.C.B.; formal analysis (risk bias) and investigation, A.A., N.S. and A.A.H.; writing—review, editing, validation and proofreading, A.A., N.S., A.A.H. and A.U. All authors have read and agreed to the published version of the manuscript.

Funding: This research was funded by a Research University Grant (GUP) with grant number (GUP-2024-030) provided by the Universiti Kebangsaan Malaysia.

Informed Consent Statement: Not applicable.

Data Availability Statement: The original contributions presented in this study are included in the article. Further inquiries can be directed to the corresponding author.

Acknowledgments: All authors would like to thank the Faculty of Medicine, UKM, for the resources used to complete this study.

Conflicts of Interest: The authors have declared no conflicts of interest.

Appendix A

Table A1. PRISMA 2020 item checklist.

Section and Topic	Item	Checklist Item	Location Where Item is Reported
Title	1	Identify the report as a systematic review.	Title, line 3–4
Abstract	2	See the PRISMA 2020 for Abstracts checklist.	Appendix A
		Introduction	
Rationale	3	Describe the rationale for the review in the context of existing knowledge.	Introduction, paragraphs 1–5
Objectives	4	Provide an explicit statement of the objective(s) or question(s) the review addresses.	Introduction, paragraph 5, lines 97–101

Table A1. *Cont.*

Section and Topic	Item	Checklist Item	Location Where Item is Reported
		Methods	
Eligibility criteria	5	Specify the inclusion and exclusion criteria for the review and how studies were grouped for the syntheses.	Methodology, see Section 2.2
Information sources	6	Specify all databases, registers, websites, organisations, reference lists, and other sources searched or consulted to identify studies. Specify the date when each source was last searched or consulted.	Methodology, see Section 2.1, line 118
Search strategy	7	Present the full search strategies for all databases, registers and websites, including any filters and limits used.	Methodology, see Section 2.1
Selection process	8	Specify the methods used to decide whether a study met the inclusion criteria of the review, including how many reviewers screened each record and each report retrieved, whether they worked independently, and if applicable, details of automation tools used in the process.	Methodology, see Section 2.3
Data collection process	9	Specify the methods used to collect data from reports, including how many reviewers collected data from each report, whether they worked independently, any processes for obtaining or confirming data from study investigators, and if applicable, details or automation tools used in the process.	Methodology, see Section 2.3
Data items	10a	List and define all outcomes for which data were sought. Specify whether all results that were compatible with each outcome domain in each study were sought (e.g., for all measures, time points, analyses), and if not, the methods used to decide which results to collect.	Methodology, see Section 2.3, line 144–147
	10b	List and define all other variables for which data were sought (e.g., participant and intervention characteristics, funding sources). Describe any assumptions made about any missing or unclear information.	Not applicable
Study risk of bias assessment	11	Specify the methods used to assess risk of bias in the included studies, including details of the tool(s) used, how many reviewers assessed each study and whether they worked independently, and if applicable, details of automation tools used in the process.	Methodology, see Section 2.4
Effect measures	12	Specify for each outcome the effect measure(s) (e.g., risk ratio, mean difference) used in the synthesis or presentation of results.	Methodology, see Section 2.5, line 161
Synthesis methods	13a	Describe the processes used to decide which studies were eligible for each synthesis (e.g., tabulating the study intervention characteristics and comparing against the planned groups for each synthesis (item #5))	Not applicable
	13b	Describe any methods required to prepare the data for presentation or synthesis, such as handling of missing summary statistics, or data conversions	Articles were exported from databases into Mendeley web as taught by Mrs. Norizam Salamat
	13c	Describe any methods used to tabulate or visually display results of individual studies and syntheses.	Not applicable
	13d	Describe any methods used to synthesise results and provide a rationale for the choice(s). If meta-analysis was performed, describe the model(s), method(s) to identify the presence and extent of statistical heterogeneity, and software package(s) used.	Methodology, see Section 2.5
	13e	Describe any methods used to explore possible causes of heterogeneity among study results (e.g., subgroup analysis, metaregression).	Methodology, see Section 2.5, line 163–166
	13f	Describe any sensitivity analyses conducted to assess robustness of the synthesised results.	Methodology, see Section 2.5, line 168
Reporting bias assessment	14	Describe any methods used to assess risk of bias due to missing results in a synthesis (arising from reporting biases).	Not applicable
Certainty assessment	15	Describe any methods used to assess certainty (or confidence) in the body of evidence for an outcome.	Not applicable

Table A1. *Cont.*

Section and Topic	Item	Checklist Item	Location Where Item is Reported
		Results	
Study selection	16a	Describe the results of the search and selection process, from the number of records identified in the search to the number of studies included in the review, ideally using a flow diagram (see Figure 1).	Results, see Figure 1, Sections 3.1 and 3.2.
	16b	Cite studies that might appear to meet the inclusion criteria, but which were excluded, and explain why they were excluded	Not stated
Study characteristics	17	Cite each included study and present its characteristics.	Results, see Tables 3 and 4
Risk of bias in studies	18	Present assessments of risk of bias for each included study.	Results, see Tables 1 and 2
Results of individual studies	19	For all outcomes, present, for each study: (a) summary statistics for each group (where appropriate) and (b) an effect estimate and its precision (e.g., confidence/credible interval), ideally using structured tables or plots.	Results, see Tables 3 and 4, column "Key findings" and "Conclusion"
Results of syntheses	20a	For each synthesis, briefly summarise the characteristics and risk of bias among contributing studies	Results, see Tables 3 and 4, column "Population characteristic". For risk of bias, see Tables 1 and 2
	20b	Present results of all statistical syntheses conducted. If meta-analysis was done, present for each the summary estimate and its precision (e.g., confidence/credible interval) and measures of statistical heterogeneity. If comparing groups, describe the direction of the effect.	Results, see Section 3.2.3 Meta-analysis
	20c	Present results of all investigations of possible causes of heterogeneity among study results.	Results, see Figure 3
	20d	Present results of all sensitivity analyses conducted to assess the robustness of the synthesised results.	Results, see Figure 2
Reporting biases	21	Present assessments of risk of bias due to missing results (arising from reporting biases) for each synthesis assessed	Not applicable
Certainty of evidence	22	Present assessments of certainty (or confidence) in the body of evidence for each outcome assessed.	Not applicable
Discussion	23a	Provide a general interpretation of the results in the context of other evidence	Discussion, paragraph 1–3
	23b	Discuss any limitations of the evidence included in the review.	Not applicable
	23c	Discuss any limitations of the review processes used.	Limitations and Future Directions
	23d	Discuss implications of the results for practice, policy, and future research.	Conclusion
		Other information	
Registration and protocol	24a	Provide registration information for the review, including register name and registration number, or state that the review was not registered.	See "Protocol Registration"
	24b	Indicate where the review protocol can be accessed, or state that a protocol was not prepared	See "Protocol Registration"
	24c	Describe and explain any amendments to information provided at registration or in the protocol.	Not applicable
Support	25	Describe sources of financial or non-financial support for the review, and the role of the funders or sponsors in the review.	See "Funding"
Competing interests	26	Declare any competing interests of review authors.	See "Conflict of Interest"
Availability of data, code, and other materials	27	Report which of the following are publicly available and where they can be found: template data collection forms; data extracted from included studies; data used for all analyses; analytic code; any other materials used in the review.	See "Data availability statement"

Table A2. PRISMA 2020 for Abstract checklist.

Section and Topic	Item	Checklist Item	Location Where Item is Reported
Title	1	Identify the report as a systematic review.	Abstract, line 22–23
		Background	
Objectives	2	Provide an explicit statement of the main objective (s) or question (s) the review addresses.	Abstract, line 19–22
		Methods	
Eligibility criteria	3	Specify the inclusion and exclusion criteria for the review.	Not stated in abstract
Information sources	4	Specify the information sources (e.g., databases, registers) used to identify studies and the date when each was last searched.	Abstract, line 22–27
Risk of bias	5	Specify the methods used to assess risk of bias in the included studies.	Abstract, line 28
Synthesis of results	6	Specify the methods used to present and synthesise results.	Abstract, line 22–28
		Results	
Included studies	7	Give the total number of included studies and participants and summarise relevant characteristics of studies.	Abstract, line 28
Synthesis of results	8	Present results for main outcomes, preferably indicating the number of included studies and participants for each. If meta-analysis was done, reports the summary estimate and confidence/credible interval. If comparing groups, indicate the direction of the effects (i.e., which group is favoured).	Abstract, line 28–34
		Discussion	
Limitation of evidence	9	Provide a brief summary of the limitations of the evidence included in the review (e.g., study risk of bias, inconsistency and imprecision).	Not stated in abstracts
Interpretation	10	Provide a general interpretation of the results and important implications.	Abstract, line 34–39
		Other	
Funding	11	Specify the primary source of funding for the review.	Not stated in abstract
Registration	12	Provide the register name and registration number	Not stated in abstract

References

1. Timmis, A.; Vardas, P.; Townsend, N.; Torbica, A.; Katus, H.; De Smedt, D.; Gale, C.P.; Maggioni, A.P.; Petersen, S.E.; Huculeci, R.; et al. European Society of Cardiology: Cardiovascular disease statistics 2021. *Eur. Heart J.* **2022**, *43*, 716–799. [CrossRef]
2. Institute of Public Health. National Health and Morbidity Survey. 2020. Available online: https://iku.gov.my/images/IKU/Document/REPORT/2020/report/2_Report_NHMS2020_Vol-2.pdf (accessed on 19 October 2024).
3. Institute of Public Health. National Health and Morbidity Survey. 2023. Available online: https://iku.gov.my/images/nhms2023/fact-sheet-nhms-2023.pdf (accessed on 19 October 2024).
4. Ullah, A.; Sajid, S.; Qureshi, M.; Kamran, M.; Anwaar, M.A.; Naseem, M.A.; Zaman, M.U.; Mahmood, F.; Rehman, A.; Shehryar, A.; et al. Novel biomarkers and the multiple-marker approach in early detection, prognosis, and risk stratification of cardiac diseases: A narrative review. *Cureus* **2023**, *15*, e42081. [CrossRef] [PubMed]
5. Liu, R.; Xu, F.; Ma, Q.; Zhou, Y.; Liu, T. C-Reactive Protein Level Predicts Cardiovascular Risk in Chinese Young Female Population. *Oxidative Med. Cell. Longev.* **2021**, 6538079. [CrossRef] [PubMed]
6. Hofmann, A.; Brunssen, C.; Wolk, S.; Reeps, C.; Morawietz, H. Soluble LOX-1: A novel biomarker in patients with coronary artery disease, stroke, and acute aortic dissection? *J. Am. Heart Assoc.* **2020**, *9*, e013803. [CrossRef] [PubMed]
7. Jin, P.; Cong, S. LOX-1 and atherosclerotic-related diseases. *Clin. Chim. Acta* **2009**, *491*, 24–29. [CrossRef] [PubMed]
8. Barreto, J.; Karathanasis, S.K.; Remaley, A.; Sposito, A.C. Role of LOX-1 (lectin-like oxidized low-density lipoprotein receptor 1) as a cardiovascular risk predictor: Mechanistic insight and potential clinical use. *Arterioscler. Thromb. Vasc. Biol.* **2021**, *41*, 153–166. [CrossRef] [PubMed]
9. Sawamura, T.; Kume, N.; Aoyama, T.; Moriwaki, H.; Hoshikawa, H.; Aiba, Y.; Tanaka, T.; Miwa, S.; Katsura, Y.; Kita, T.; et al. An endothelial receptor for oxidized low-density lipoprotein. *Nature* **1997**, *386*, 73–77. [CrossRef] [PubMed]
10. Kattoor, A.J.; Kanuri, S.H.; Mehta, J.L. Role of Ox-LDL and LOX-1 in Atherogenesis. *Curr. Med. Chem.* **2019**, *26*, 1693–1700. [CrossRef]
11. Hussein, R.A.; Abdul-Rasheed, O.F.; Basheer, M. Evaluation of soluble lectin-like oxidized low-density lipoprotein receptor-1 (sLOX-1) and sLOX-1/oxidized LDL ratio as novel biomarkers of acute coronary syndrome. *Acta Biochim. Pol.* **2022**, *69*, 309–314. [CrossRef] [PubMed]

12. Kume, N.; Mitsuoka, H.; Hayashida, K.; Tanaka, M.; Kominami, G.; Kita, T. Soluble lectin-like oxidized LDL receptor-1 (sLOX-1) as a sensitive and specific biomarker for acute coronary syndrome—Comparison with other biomarkers. *J. Cardiol.* **2010**, *56*, 159–165. [CrossRef] [PubMed]
13. Li, X.-M.; Jin, P.-P.; Xue, J.; Chen, J.; Chen, Q.-F.; Luan, X.-Q.; Zhang, Z.-R.; Yu, T.-E.; Cai, Z.-Y.; Zhao, K.; et al. Role of sLOX-1 in intracranial artery stenosis and in predicting long-term prognosis of acute ischemic stroke. *Brain Behav.* **2018**, *8*, e00879. [CrossRef] [PubMed]
14. Zhao, J.; Zhang, Y.; Huang, Z.; Wu, F.; Li, N.; Liang, C. Association between impaired cutaneous microvascular endothelial function and lectin-like oxidized low-density lipoprotein receptor-1 in patients with coronary slow flow. *Microvasc. Res.* **2020**, *129*, 103984. [CrossRef] [PubMed]
15. Florida, E.M.; Li, H.; Hong, C.G.; Ongstad, E.L.; Gaddipati, R.; Sitaula, S.; Varma, V.; Parel, P.M.; O'Hagan, R.; Chen, M.Y.; et al. Relationship of soluble lectin-like low-density lipoprotein receptor-1 (sLOX-1) with inflammation and coronary plaque progression in psoriasis. *J. Am. Heart Assoc.* **2023**, *12*, e031227. [CrossRef]
16. Kott, K.A.; Genetzakis, E.; Gray, M.P.; Hansen, P.; McGuire, H.M.; Yang, J.Y.; Grieve, S.M.; Vernon, S.T.; Figtree, G.A. Serum soluble lectin-like oxidized low-density lipoprotein receptor-1 (sLOX-1) is associated with atherosclerosis severity in coronary artery disease. *Biomolecules* **2023**, *13*, 1187. [CrossRef] [PubMed]
17. Schiopu, A.; Björkbacka, H.; Narasimhan, G.; Loong, B.J.; Engström, G.; Melander, O.; Orho-Melander, M.; Nilsson, J. Elevated soluble LOX-1 predicts risk of first-time myocardial infarction. *Ann. Med.* **2023**, *55*, 2296552. [CrossRef] [PubMed]
18. Mashayekhi, S.; Ziaee, M.; Garjani, A.; Sarbakhsh, P.; Ghaffari, S. Prognostic value of sLOX-1 level in acute coronary syndromes based on thrombolysis in myocardial infarction risk score and clinical outcome. *J. Emerg. Med.* **2018**, *55*, 390–398. [CrossRef] [PubMed]
19. Page, M.J.; McKenzie, J.E.; Bossuyt, P.M.; Boutron, I.; Hoffmann, T.C.; Mulrow, C.D.; Shamseer, L.; Tetzlaff, J.M.; Akl, E.A.; Brennan, S.E.; et al. The PRISMA 2020 statement: An updated guideline for reporting systematic reviews. *BMJ* **2021**, *372*, 39.
20. Aminuddin, A.; Samah, N.; Che Roos, N.A.; Mohamad, S.F.; Beh, B.C.; Hamid, A.A.; Ugusman, A. Prognostic value of lectin-like oxidized LDL receptor-1 for future CVD risk and outcome: Systematic review and meta-analysis. *INPLASY Protoc.* **2024**, 120078. [CrossRef]
21. Wells, G.A.; Shea, B.; O'Connell, D.; Peterson, J.; Welch, V.; Losos, M.; Tugwell, P. The Newcastle-Ottawa Scale (NOS) for Assessing the Quality of Nonrandomized Studies in Meta-Analyses. OHRI. 2021. Available online: https://www.ohri.ca/programs/clinical_epidemiology/oxford.asp (accessed on 25 October 2024).
22. Cochrane Collaboration. Review Manager (RevMan) [Computer Software]. Cochrane. 2023. Available online: https://revman.cochrane.org/info (accessed on 4 November 2024).
23. Higgins, J.P.; Thompson, S.G.; Deeks, J.J.; Altman, D.G. Measuring inconsistency in meta-analyses. *BMJ* **2003**, *327*, 557–560. [CrossRef] [PubMed]
24. Kraler, S.; Wenzl, F.A.; Georgiopoulos, G.; Obeid, S.; Liberale, L.; von Eckardstein, A.; Muller, O.; Mach, F.; Räber, L.; Losdat, S.; et al. Soluble lectin-like oxidized low-density lipoprotein receptor-1 predicts premature death in acute coronary syndromes. *Eur. Heart J.* **2022**, *43*, 1849–1860. [CrossRef] [PubMed]
25. Kumar, S.; Ali, W.; Mishra, S.; Pradhan, A.; Sethi, R.; Kushwaha, R.; Singh, U.S.; Perrone, M.A. Circulating soluble lectin-like oxidized low-density lipoprotein receptor-1: A diagnostic indicator across the spectrum of acute coronary syndrome. *J. Clin. Med.* **2021**, *10*, 5567. [CrossRef] [PubMed]
26. Zhao, Z.; Xu, Y.; Li, S.; Guo, J.; Sun, J.; Hong, J.; Chen, L. Baseline serum sLOX-1 concentrations are associated with 2-year major adverse cardiovascular and cerebrovascular events in patients after percutaneous coronary intervention. *Dis. Markers* **2019**, 4925767. [CrossRef]
27. Higuma, T.; Abe, N.; Tateyama, S.; Endo, T.; Shibutani, S.; Yokoyama, H.; Hanada, K.; Yamada, M.; Tomita, H.; Hanada, H.; et al. Plasma soluble lectin-like oxidized low-density lipoprotein receptor-1 as a novel prognostic biomarker in patients with ST-segment elevation acute myocardial infarction. *Circ. J.* **2015**, *79*, 641–648. [CrossRef] [PubMed]
28. Ren, K.; Jiang, H.; Li, T.; Qian, C.; Zhu, L.; Wang, T. Correlation of sLOX-1 levels and MR characteristics of culprit plaques in intracranial arteries with stroke recurrence. *Diagnostics* **2023**, *13*, 804. [CrossRef] [PubMed]
29. Yan, P.; Cao, J.; Zhou, Y.; Zhou, X.; Sun, Z.; Zhu, X. Serum levels of sLOX-1 and Lp-PLA2 can predict the prognosis of acute cerebral infarction with high specificity. *Physiol. Rep.* **2022**, *10*, e15160. [CrossRef] [PubMed]
30. Yang, X.; Hou, D.; Liu, J.; Wang, T.; Luo, Y.; Sun, W.; Li, C.; Shen, L.; Liu, W.; Wu, D. Soluble lectin-like oxidized low-density lipoprotein receptor-1 level is related to clinical prognosis in patients with acute atherosclerosis-related ischemic stroke. *Clin. Appl. Thromb./Hemost.* **2021**, *27*, 10760296211059500. [CrossRef] [PubMed]
31. Wang, A.; Tian, X.; Xu, J.; Li, H.; Xu, Q.; Chen, P.; Meng, X.; Wang, Y. Soluble lectin-like oxidized low-density lipoprotein receptor-1 and recurrent stroke: A nested case–control study. *CNS Neurosci. Ther.* **2022**, *28*, 2001–2010. [CrossRef]

32. Markstad, H.; Edsfeldt, A.; Mattison, I.Y.; Bengtsson, E.; Singh, P.; Cavalera, M.; Asciutto, G.; Björkbacka, H.; Fredrikson, G.N.; Dias, N.; et al. High levels of soluble lectin-like oxidized low-density lipoprotein receptor-1 are associated with carotid plaque inflammation and increased risk of ischemic stroke. *J. Am. Heart Assoc.* **2019**, *8*, e009874. [CrossRef]
33. Zhao, Z.; Xu, Y.; Li, S.; Guo, J.; Chen, L. Higher serum lectin-like oxidized low-density lipoprotein receptor-1 in patients with stable coronary artery disease is associated with major adverse cardiovascular events: A multicenter pilot study. *Biochem. Medica* **2019**, *29*, 010705. [CrossRef]
34. Zheng, Y.; Huang, Y.; Li, L.; Wang, P.; Wang, R.; Tao, Z.; Fan, J.; Han, Z.; Li, F.; Zhao, H.; et al. sLOX-1: A molecule for evaluating the prognosis of recurrent ischemic stroke. *Neural Plast.* **2021**, 6718184. [CrossRef] [PubMed]
35. Duncan, M.W. The importance of antibody validation for ELISA: Avoiding errors in biomarker quantification. *J. Immunol. Methods* **2013**, *387*, 1–13.
36. Andreasson, U.; Perret-Liaudet, A.; van Waalwijk van Doorn, L.J.C.; Blennow, K.; Chiasserini, D.; Engelborghs, S.; Fladby, T.; Genc, S.; Kruse, N.; Kuiperij, H.B.; et al. A practical guide to immunoassay method validation. *Front. Neurol.* **2015**, *6*, 179. [CrossRef] [PubMed]
37. Blair, A.; Shaul, P.W.; Yuhanna, I.S.; Conrad, P.A.; Smart, E.J. Oxidized low-density lipoprotein displaces endothelial nitric-oxide synthase (eNOS) from plasmalemmal caveolae and impairs eNOS activation. *J. Boil. Chem.* **1999**, *274*, 32512–32519. [CrossRef] [PubMed]
38. Li, D.; Mehta, J.L. Théroux, Antisense to LOX-1 inhibits oxidized LDL–mediated upregulation of monocyte chemoattractant protein-1 and monocyte adhesion to human coronary artery endothelial cells. *Circulation* **2000**, *101*, 2889–2895. [CrossRef] [PubMed]
39. Aoyama, T.; Sawamura, T.; Furutani, Y.; Matsuoka, R.; Yoshida, M.C.; Fujiwara, H.; Masaki, T. Structure and chromosomal assignment of the human lectin-like oxidized low-density lipoprotein receptor-1 (LOX-1) gene. *Biochem. J.* **1999**, *339*, 177–184. [CrossRef] [PubMed]
40. Singh, R.M.; Chen, H.; Kazzaz, N.; Li, D.; Liu, L.; Mehta, J.L. Oxidized-LDL through LOX-1 increases the expression of angiotensin-converting enzyme in human coronary artery endothelial cells. *Cardiovasc. Res.* **2003**, *57*, 238–243. [CrossRef]
41. Li, D.; Liu, L.; Chen, H.; Sawamura, T.; Ranganathan, S.; Mehta, J.L. LOX-1 mediates oxidized low-density lipoprotein-induced expression of matrix metalloproteinases in human coronary artery endothelial cells. *Circulation* **2003**, *107*, 612–617. [CrossRef] [PubMed]
42. Li, L.; Renier, G. The oral anti-diabetic agent, gliclazide, inhibits oxidized LDL-mediated LOX-1 expression, metalloproteinase-9 secretion, and apoptosis in human aortic endothelial cells. *Atherosclerosis* **2009**, *204*, 40–46. [CrossRef]
43. Xu, F.; Sun, Y.; Chen, Y.; Sun, Y.; Li, R.; Liu, C.; Zhang, C.; Wang, R.; Zhang, Y. Endothelial cell apoptosis is responsible for the formation of coronary thrombotic atherosclerotic plaques. *Tohoku J. Exp. Med.* **2009**, *218*, 25–33. [CrossRef] [PubMed]
44. Sánchez-León, M.E.; Loaeza-Reyes, K.J.; Matias-Cervantes, C.A.; Mayoral-Andrade, G.; Pérez-Campos, E.L.; Pérez-Campos-Mayoral, L.; Hernández-Huerta, M.T.; Zenteno, E.; Pérez-Cervera, Y.; Pina-Canseco, S. LOX-1 in cardiovascular disease: A comprehensive molecular and clinical review. *Int. J. Mol. Sci.* **2024**, *25*, 5276. [CrossRef]

Disclaimer/Publisher's Note: The statements, opinions and data contained in all publications are solely those of the individual author(s) and contributor(s) and not of MDPI and/or the editor(s). MDPI and/or the editor(s) disclaim responsibility for any injury to people or property resulting from any ideas, methods, instructions or products referred to in the content.

biomedicines

MDPI

Systematic Review

Systematic Review of Left Ventricular Remodeling in Response to Hypoglycemic Medications: Assessing Changes in End-Systolic and End-Diastolic Diameters

Bogdan-Flaviu Buz [1,2,3,4], Rodica Anamaria Negrean [5,*], Florina Caruntu [2,3,6], Tudor Parvanescu [2,3,6], Milena Slovenski [2,3,6], Mirela Cleopatra Tomescu [2,3,6] and Diana-Aurora Arnautu [2,3,6]

1 Doctoral School, Victor Babes University of Medicine and Pharmacy, 300041 Timisoara, Romania; flaviu-bogdan.buz@umft.ro
2 Multidisciplinary Heart Research Center, Victor Babes University of Medicine and Pharmacy, 300041 Timisoara, Romania; caruntu.florina@umft.ro (F.C.); parvanescu.tudor@umft.ro (T.P.); milena.slovenski@umft.ro (M.S.); tomescu.mirela@umft.ro (M.C.T.); aurora.bordejevic@umft.ro (D.-A.A.)
3 Department of Internal Medicine, Victor Babes University of Medicine and Pharmacy, 300041 Timisoara, Romania
4 Cardiology Clinic, Institute of Cardiovascular Diseases, 300310 Timisoara, Romania
5 Department of Preclinical Disciplines, Faculty of Medicine and Pharmacy, University of Oradea, 410073 Oradea, Romania
6 Cardiology Clinic, Clinical Municipal Emergency Hospital, 300040 Timisoara, Romania
* Correspondence: rodicanegrean@uoradea.ro

Abstract: Hypoglycemic medications are widely used in managing diabetes mellitus, with emerging evidence suggesting their role in cardiac reverse remodeling. This systematic review aims to quantitatively synthesize data regarding the impact of these medications on left ventricular end-diastolic diameter (LVEDD) and end-systolic diameter (LVESD), and to evaluate the clinical relevance of these changes in promoting favorable cardiac outcomes. We conducted a comprehensive search across PubMed, Scopus, and the Web of Science up to 22 April 2024, selecting studies based on inclusion criteria that focused on the impact of hypoglycemic medications on LVEDD and LVESD in patients with diabetes. Studies were selected through a rigorous process, adhering to PRISMA guidelines, and involving various designs including randomized controlled trials and observational studies. The main outcomes were changes in LVEDD and LVESD measured by validated cardiac imaging techniques. A total of ten studies met the inclusion criteria, involving a total of 1180 patients. Treatment durations ranged from 3 to 24 months. Significant improvements in cardiac dimensions were noted with some medications. For instance, Liraglutide treatment over three months significantly improved LVEF from 47.2% to 57.2% and reduced LVEDD and LVESD from 46.5 mm to 45.2 mm and 35.2 mm to 32.7 mm, respectively. In contrast, other medications like Sitagliptin showed minimal impact over 24 months. On average, hypoglycemic medications reduced LVEDD from 58.2 mm to 55.0 mm and LVESD from 48.3 mm to 44.3 mm, with a mean improvement in LVEF from 38.9% to 43.8%. Hypoglycemic medications contribute variably to cardiac reverse remodeling. Medications such as Liraglutide and Dapagliflozin demonstrate significant potential in improving cardiac dimensions and function, indicating their utility beyond glycemic control. This review highlights the need for tailored treatment approaches to maximize cardiac outcomes in patients with diabetes, suggesting a broader therapeutic role for these agents.

Keywords: cardiology; systematic review; heart failure

1. Introduction

Cardiac reverse remodeling refers to structural and functional improvements in the heart, particularly the left ventricle, observed after targeted medical interventions in conditions like heart failure [1–3]. With heart failure affecting approximately 26 million people

globally, and its prevalence increasing with an aging population, the need for effective treatments is critical [4,5]. Measures of left ventricular end-systolic (LVESD) and end-diastolic diameters (LVEDD) are essential in monitoring these improvements, directly correlating with patient outcomes [6,7].

Hypoglycemic medications, notably those within the SGLT2 inhibitor class, extend beyond glycemic control to potentially influence cardiac outcomes [8,9]. Research suggests these medications might facilitate cardiac structural improvements through mechanisms like reduced cardiac load and enhanced myocardial metabolism [10,11]. Given the convergence of diabetes and heart failure, where approximately 30% of heart failure patients also suffer from diabetes, these findings are particularly significant [12,13].

Speckle tracking echocardiography (STE) is a prominent example, offering a sophisticated approach to evaluate myocardial deformation and function without relying on geometric assumptions about the heart's shape [14]. This technique tracks the natural acoustic markers or 'speckles' within the myocardial tissue throughout the cardiac cycle, allowing for the detailed analysis of left ventricular strain patterns [15]. Furthermore, the advent of three-dimensional echocardiography and cardiac magnetic resonance imaging (MRI) provides even more detailed and accurate assessments of ventricular volumes and function [16].

Based on these measurement methods, recent studies have shown varying degrees of left ventricular remodeling in patients using hypoglycemic medications [17]. For instance, clinical trials involving SGLT2 inhibitors have reported reductions in left ventricular indices, suggesting potential reverse remodeling effects [18]. In the assessment of left ventricular dimensions such as LVESD and LVEDD, advanced imaging techniques have significantly enhanced the precision and reliability of measurements. Therefore, the hypothesis of this systematic review is that hypoglycemic medications contribute to significant cardiac reverse remodeling in patients with diabetes, as evidenced by reductions in LVESD and LVEDD. The objectives were to quantitatively synthesize data on the impact of these medications on left ventricular diameters and to evaluate the clinical relevance of these changes, aiming to pinpoint the most effective agents promoting favorable cardiac outcomes.

2. Materials and Methods

2.1. Eligibility Criteria

This systematic review selected studies for inclusion based on the following criteria: (1) patients diagnosed with diabetes mellitus and treated with hypoglycemic medications, assessing their effects on LVESD and LVEDD; (2) research specifically investigating the cardiac reverse remodeling effects associated with the use of these medications, with a particular focus on changes in LVESD and LVEDD as primary outcomes; (3) a comprehensive range of study designs, including randomized controlled trials, observational studies, cohort studies, case-control studies, and cross-sectional studies; (4) studies employing validated cardiac imaging techniques, such as echocardiography or magnetic resonance imaging, to measure changes in LV dimensions accurately; and (5) only peer-reviewed articles published in English.

The exclusion criteria were the following: (1) studies not involving human participants, such as in vitro or animal studies, except where preclinical data were used to support clinical findings; (2) research not specifically examining the impact of hypoglycemic medications on cardiac dimensions or studies that did not differentiate the effects of these medications from other therapeutic interventions; (3) studies that failed to provide clear, quantifiable outcomes related to changes in LVESD and LVEDD or lacked sufficient detail for a comprehensive assessment; (4) gray literature, including non-peer-reviewed articles, preprints, conference abstracts, general reviews, commentaries, and editorials, to ensure consistency and reliability of the analyzed data; and (5) studies deemed low-quality based on predetermined, quantifiable metrics.

In this study, we prioritized cardiac remodeling, specifically left ventricular dimension changes, as the primary outcome over direct outcomes like mortality and hospitalization. This decision is grounded in established correlations between ventricular remodeling indices and clinical endpoints in heart failure. Reductions in left ventricular end-systolic and end-diastolic diameters are robust predictors of improved survival and reduced morbidity. These parameters not only offer insights into the direct effects of therapeutic interventions on cardiac morphology but also serve as prognostic indicators, allowing for the early assessment of treatment efficacy. Therefore, focusing on cardiac remodeling provides crucial, actionable data on the cardioprotective effects of hypoglycemic medications in patients with coexisting diabetes and heart failure.

2.2. Information Sources

The primary information sources for this systematic review were the electronic databases PubMed, Scopus, and the Web of Science. The literature search specifically targeted publications up to the initial search date, 22 April 2024. The search was designed to encompass a broad spectrum of studies, including those that evaluate clinical outcomes, patient demographics, treatment modalities, and specifically the impact of hypoglycemic medications on cardiac reverse remodeling, focusing on changes in LVESD and LVEDD.

2.3. Search Strategy

The search strategy for this systematic review was meticulously developed using an array of keywords and phrases that are closely aligned with the objectives of the study, which centers on the influence of hypoglycemic medications on cardiac reverse remodeling, particularly the changes in left ventricular end-systolic diameter and end-diastolic diameter. Key search terms included "diabetes mellitus", "type 2 diabetes", "hypoglycemic medications", "antidiabetic drugs", "cardiac reverse remodeling", "cardiac structure changes", "left ventricular dimensions", "LVESD", "LVEDD", " left ventricular end-systolic diameter", " left ventricular end-diastolic diameter", "cardiac function", "heart structure modification", "speckle tracking echocardiography", "3D echocardiography", "cardiac MRI", "clinical outcomes", "SGLT2 inhibitors", "GLP-1 receptor agonists", "DPP-4 inhibitors", and "metabolic effects on heart."

These terms were integrated using Boolean operators (AND, OR, NOT) to construct a comprehensive search string. The search included relevant Medical Subject Headings (MeSH) to ensure the inclusion of all the pertinent literature. The search string was thus formulated: ((("diabetes mellitus" OR "type 2 diabetes") AND ("hypoglycemic medications" OR "SGLT2 inhibitors" OR "GLP-1 receptor agonists" OR "DPP-4 inhibitors") AND ("cardiac reverse remodeling" OR "cardiac function" OR "heart structure modification") AND ("left ventricular dimensions" OR "LVESD" OR "LVEDD") AND ("echocardiography" OR "speckle tracking" OR "3D echocardiography" OR "cardiac MRI") AND ("clinical outcomes" OR "heart failure" OR "cardiovascular effects" OR "metabolic effects"))).

2.4. Selection Process

Consistent with the Preferred Reporting Items for Systematic Reviews and Meta-Analyses (PRISMA) guidelines [19], the selection process for this review was designed to ensure both transparency and methodological rigor. Initially, all retrieved articles were independently screened by two reviewers to confirm their compliance with the pre-established inclusion and exclusion criteria. Discrepancies between reviewers during this preliminary phase were resolved through a consensus discussion or, when necessary, the intervention of a third reviewer. To enhance the credibility and reproducibility of our review process, the entire protocol, including detailed methodologies, was registered and is available on the Open Science Framework (OSF) under the registration code osf.io/tebvq.

2.5. Data Collection Process

The data collection phase began with the removal of duplicate records from the initially retrieved articles. Following this, two independent reviewers undertook a meticulous screening of abstracts and, where required, full texts to determine the eligibility of each study according to the set inclusion and exclusion criteria. During this stage, any disagreements between the reviewers were thoroughly discussed until a consensus was reached. For unresolved discrepancies, a third reviewer was brought in to make the final decision. This structured approach ensured a comprehensive and unbiased selection of studies for inclusion in the systematic review.

2.6. Data Items

For this systematic review, primary data items collected included cardiac measurements such as left ventricular ejection fraction (LVEF), LVEDD, and LVESD. These metrics were used to assess the impact of hypoglycemic medications on cardiac reverse remodeling. Secondary data encompassed study characteristics such as design and quality, geographic location, patient demographics (age, gender, and comorbidities), and specifics of hypoglycemic treatment (medication type and duration). Treatment specifics, including the type of hypoglycemic medication used (GLP-1 receptor agonists, DPP-4 inhibitors, and SGLT-2 inhibitors), and the treatment duration were recorded to evaluate the differential effects of various drug classes on cardiac outcomes. Outcomes were further interpreted in terms of improvement or deterioration in cardiac function, with a specific focus on statistically significant changes observed over the treatment period.

2.7. Risk of Bias and Quality Assessment

The assessment of the methodological quality of observational studies was conducted employing the Newcastle–Ottawa Scale [20]. This scale scrutinizes three fundamental aspects: the selection criteria for the study groups, their comparability, and the determination of exposure or outcome relevant to case-control or cohort studies, respectively. Studies receive stars for performance in these categories, accumulating a total score that categorizes the quality of each study as low, medium, or high.

3. Results

3.1. Study Selection and Study Characteristics

Following an initial literature search, 882 articles were identified. Preliminary screening based on titles and abstracts led to the exclusion of 732 entries deemed irrelevant. A subsequent in-depth examination of the remaining articles resulted in the removal of 81 duplicates and 59 articles that either did not meet the inclusion criteria or lacked essential data. Ultimately, the systematic review included ten studies, conducted between 2015 and 2024, which are systematically presented in Figure 1.

Table 1 outlines the characteristics of the ten studies [21–30] that explored the effects of hypoglycemic medications on cardiac reverse remodeling, specifically measuring changes in LVESD and LVEDD. The research designs included randomized, double-blind, placebo trials [21,26,29], randomized prospective open-label blinded-endpoint trials [22,28,30], and prospective observational studies [23–25,27]. Study quality assessments classified several as high and others as medium. Notably, the studies by Chen et al. [21], Yamada et al. [22], Yamamoto et al. [23], Sardu et al. [24], Otagaki et al. [25], Rau et al. [26], Gamaza-Chulian et al. [27], Reis et al. [28], Fu et al. [29], and Hong et al. [30] represented a significant cross-section of international research, indicating broad global interest and diverse applications of hypoglycemic medications in cardiac care across different patient populations.

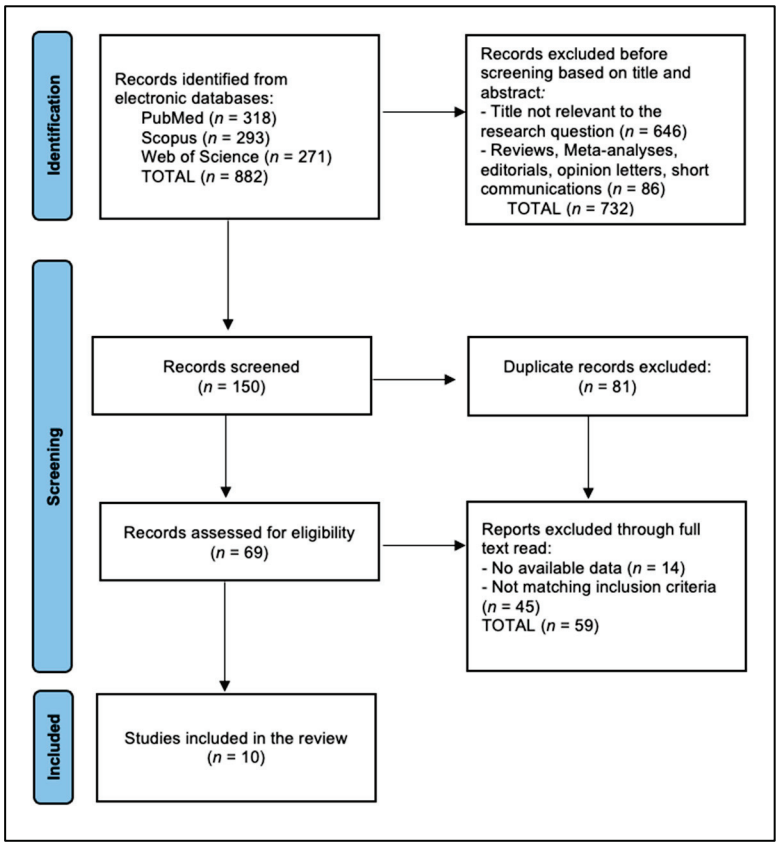


Figure 1. PRISMA flow diagram.

Table 1. Study characteristics.

Number	First Author	Reference	Country	Study Year	Study Design	Study Quality
1	Chen et al.	[21]	China	2015	Randomized, double-blind, placebo trial	High
2	Yamada et al.	[22]	Japan	2017	Randomized, prospective, open-label, blinded-endpoint trial	High
3	Yamamoto et al.	[23]	Japan	2017	Prospective, observational	Medium
4	Sardu et al.	[24]	Italy	2018	Prospective, observational	Medium
5	Otagaki et al.	[25]	Japan	2019	Prospective, observational	Medium
6	Rau et al.	[26]	Germany	2021	Randomized, double-blind, placebo trial	High
7	Gamaza-Chulian et al.	[27]	Spain	2021	Prospective, observational	Medium
8	Reis et al.	[28]	Portugal	2022	Randomized, open-label trial	Medium
9	Fu et al.	[29]	China	2023	Randomized, double-blind, placebo trial	High
10	Hong et al.	[30]	China	2024	Randomized, prospective, open-label, blinded-endpoint trial	Medium

3.2. Results of Individual Studies

Across the ten studies included in the systematic review, a total of 1180 patients were analyzed. The average age of these patients was 69.1 years, while the proportion of male participants was about 70.7%. These studies varied considerably in sample size, ranging from 40 [28] to 559 participants [24], predominantly involving elderly subjects with average ages spanning from 57.7 [21] to 72 years [24]. The medications reviewed included Glucagon-like Peptide-1 Receptor Agonists (GLP-1RA), Dipeptidyl Peptidase-4 Inhibitors (DPP-4I), and Sodium Glucose Cotransporter Type 2 Inhibitors (SGLT-2I), with the patient populations mostly composed of men and the gender proportion varying from 55.8% [27] to 82.5% [28]. Comorbidities across these cohorts included cardiovascular disease (CVD), either alone or combined with Type 2 Diabetes Mellitus (T2DM), highlighting the prevalent cardiovascular risk factors in the studied groups, as presented in Table 2.

Table 2. Characteristics of patients included in the studies.

Number	First Author	Reference	Sample Size	Age (Years)	Treatment	Comorbidities	Gender (Men)
1	Chen et al.	[21]	83	57.7 (11.3)	GLP-1RA	CVD	73.3%
2	Yamada et al.	[22]	115	69 (8)	DPP-4I	T2DM	67.0%
3	Yamamoto et al.	[23]	137	71 (10)	DPP-4I	CVD+T2DM	63.8%
4	Sardu et al.	[24]	559	72 (6)	GLP-1RA	CVD+T2DM	72.1%
5	Otagaki et al.	[25]	42	65 (13.8)	SGLT-2I	T2DM	69.1%
6	Rau et al.	[26]	42	62 (6.8)	SGLT-2I	T2DM	77.2%
7	Gamaza-Chulian et al.	[27]	52	66.8 (8.6)	SGLT-2I	T2DM	55.8%
8	Reis et al.	[28]	40	60.9 (13)	SGLT-2I	CVD	82.5%
9	Fu et al.	[29]	60	70.7 (6.7)	SGLT-2I	CVD+T2DM	71.7%
10	Hong et al.	[30]	50	67 (59.7)	SGLT-2I	CVD	80.0%

NR—not reported; T2DM—Type 2 Diabetes Mellitus; CVD—cardiovascular disease; GLP-1RA—Glucagon-like Peptide-1 Receptor; DPP-4I—Dipeptidyl Peptidase-4 Inhibitor; SGLT-2I—Sodium Glucose Cotransporter Type 2 Inhibitor.

3.3. Results of Synthesis

In a study by Chen et al. [21], Liraglutide showed a notable improvement in LVEF from 47.2% to 57.2% after three months, which was statistically significant compared to the placebo group. Similarly, both LVEDD and LVESD showed reductions, indicating a positive effect on cardiac dimensions and function in patients with Non-ST-Elevation Myocardial Infarction (NSTEMI). Conversely, Yamada et al. [22] reported minimal changes in cardiac measurements after 24 months of Sitagliptin treatment, with no significant impact on cardiac reverse remodeling, except for some improvement in diastolic function markers.

Other studies have demonstrated varied responses depending on the treatment duration and drug type. For example, Sardu et al. [24] found that treatment with GLP-1 RA over 12 months resulted in improvements in all measured cardiac dimensions, alongside a decrease in arrhythmic events and heart failure hospitalizations, highlighting the potential of this treatment in enhancing cardiac outcomes. On the other hand, treatments with Dapagliflozin in studies by Fu et al. [29] and Hong et al. [30] over 12 months not only showed significant improvements in all cardiac dimensions but also demonstrated the efficacy of long-term treatment in promoting beneficial cardiac remodeling, particularly in patients with Heart Failure with reduced ejection fraction (HFrEF) and non-ischemic dilated cardiomyopathy (NIDCM).

The average cardiac measurements showed a significant improvement in LVEF after intervention, from a mean value of 38.9% to 43.8%. Similar significant findings were identified in terms of LVEDD (from a baseline of 58.2 mm to 55.0 mm after intervention), and LVESD (from a baseline of 48.3 mm to 44.3 mm after intervention). These results collectively suggest that while some treatments like Sitagliptin may offer limited cardiac remodeling benefits, others like Liraglutide, Dapagliflozin, and GLP-1 RA appear to significantly enhance both the structural and functional aspects of the heart (Table 3 and Figure 2).

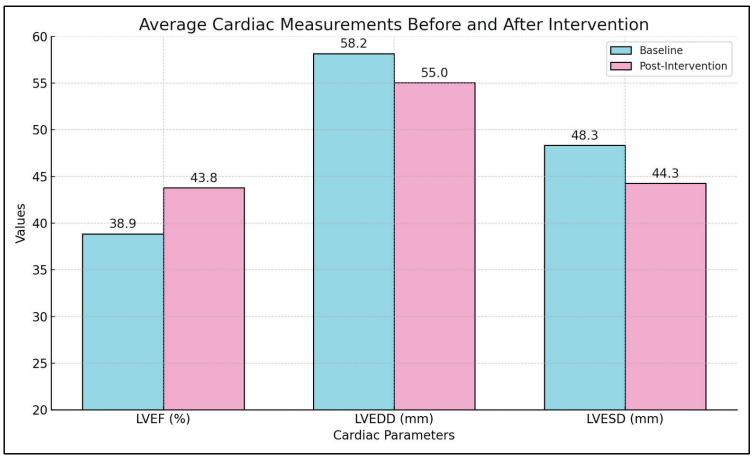


Figure 2. Average cardiac measurements before and after intervention.

Table 3. Cardiac measurements and outcomes.

Number	First Author	Reference	Treatment Scheme	LVEF	LVEDD	LVESD	Outcomes and Interpretation
1	Chen et al.	[21]	Liraglutide for 3 months	Placebo: 47.7% at baseline vs. 52.6% at 3 months. Liraglutide: 47.2% at baseline vs. 57.2% at 3 months *.	Placebo: 46.3 mm at baseline vs. 45.9 mm at 3 months. Liraglutide: 46.5 mm at baseline vs. 45.2 mm at 3 months.	Placebo: 35.1 mm at baseline vs. 33.7 mm at 3 months. Liraglutide: 35.2 mm at baseline vs. 32.7 mm at 3 months *.	Liraglutide could improve left ventricular function in patients with NSTEMI.
2	Yamada et al.	[22]	Sitagliptin for 24 months	Baseline: 63.6%; 24 months: 62.5%	Baseline: 48.5 mm; 24 months: 47.5 mm	Baseline: 31.7 mm; 24 months: 31.5 mm	Except for significant e baseline-adjusted change in E/e′ for 24 months, Sitagliptin treatment was not associated with improvements in cardiac reverse remodeling.
3	Yamamoto et al.	[23]	DPP-4I (not mentioned) for 12 months	Baseline: 45%; 12 months: 50% *	Baseline: 55.7 mm; 12 months: 53.8 mm *	NR	DPP-4i treatment over 1 year showed improvement in LVEF and a decrease in LVEDD, suggesting potential stabilization or improvement in cardiac structure and function in HFpEF patients.
4	Sardu et al.	[24]	GLP-1 RA (not mentioned) for 12 months	Baseline: 27%; 12 months: 32% *	Baseline: 67 mm; 12 months: 66 mm	Baseline: 43 mm; 12 months: 36 mm	CRTd with GLP-1 RA therapy led to improvements in LVEF, reduced LVEDD and LVESD, significant decreases in arrhythmic events and heart failure hospitalizations, and an increase in CRTd responders.
5	Otagaki et al.	[25]	Tofogliflozin for 6 months	Placebo: 61.0% at baseline vs. 63.0% at 6 months. Tofogliflozin: 58.0% at baseline vs. 63.0% at 6 months *.	Placebo: 48.0 mm at baseline vs. 49.0 mm at 6 months. Tofogliflozin: 50 mm at baseline vs. 45 mm at 6 months *.	Placebo: 34 mm at baseline vs. 32 mm at 6 months. Tofogliflozin: 32 mm at baseline vs. 30 mm at 6 months.	Tofogliflozin treatment over 6 months demonstrated significant improvements in LVEF, LVEDD, and E/e', suggesting beneficial effects on both systolic and diastolic functions in T2DM patients.
6	Rau et al.	[26]	Empagliflozin for 3 months	Placebo: 48% at baseline vs. 48% at 3 months. Empagliflozin: 51% at baseline vs. 51% at 3 months.	Placebo: 50 mm at baseline vs. 50 mm at 3 months. Empagliflozin: 49 mm at baseline vs. 48 mm at 3 months.	Placebo: 36 mm at baseline vs. 37 mm at 3 months. Empagliflozin: 34 mm at baseline vs. 33 mm at 3 months.	No significant changes in LVEF, LVEDD, or LVESD were observed over the course of treatment with empagliflozin compared to placebo.

Table 3. *Cont.*

Number	First Author	Reference	Treatment Scheme	LVEF	LVEDD	LVESD	Outcomes and Interpretation
7	Gamaza-Chulian et al.	[27]	SGLT-2I (not mentioned) for 6 months	Baseline: 64.6%; 6 months: 64.4%	Baseline: 44.5 mm; 6 months: 45.0 mm	NR	SGLT2 inhibitors were associated with significant reductions in indexed LVM and improvements in GLS, suggesting beneficial effects on cardiac remodeling and function in T2DM patients, although there was no significant evidence of reverse remodeling in terms of LVEF and LVEDD.
8	Reis et al.	[28]	Dapagliflozin for 6 months	Baseline: 34.5% vs. 6 months: 36.9% (Dapagliflozin) Baseline: 33.5% vs. 6 months: 36.2% (Control)	Baseline: 65.1 mm vs. 6 months: 63.0 mm (Dapagliflozin) Baseline: 67.2 mm vs. 6 months: 65.8 mm (Control)	Baseline: 49.4 mm vs. 6 months: 46.1 mm (Dapagliflozin) Baseline: 46.9 mm vs. 6 months: 41.6 mm (Control)	There were no statistically significant changes in LVEF, LVEDD, or LVESD observed over the course of treatment with Dapagliflozin compared to the control. The study suggested a modest trend towards improved cardiac function and remodeling in the Dapagliflozin group, although changes were not statistically significant.
9	Fu et al.	[29]	Dapagliflozin for 12 months	Baseline: 30.6% vs. 12 months: 36.3% (Dapagliflozin) Baseline: 31.3% vs. 12 months: 33.7% (Placebo)*	Baseline: 59.3 mm vs. 12 months: 53.8 mm (Dapagliflozin) Baseline: 59.9 mm vs. 12 months: 55.5 mm (Placebo) *	Baseline: 50.3 mm vs. 12 months: 46.0 mm (Dapagliflozin) Baseline: 50.7 mm vs. 12 months: 48.3 mm (Placebo) *	Dapagliflozin demonstrated a statistically significant improvement in LVEF, LVEDD, and LVESD over one year, suggesting beneficial effects on cardiac remodeling in patients with type 2 diabetes and HFrEF.
10	Hong et al.	[30]	Dapagliflozin for 12 months	Baseline: 27.87% vs. 12 months: 42.22% (Dapagliflozin) Baseline: 31.99% vs. 12 months: 35.52% (Placebo)*	Baseline: 64.3 mm vs. 12 months: 59.35 mm (Dapagliflozin) Baseline: 68.30 mm vs. 12 months: 66.37 mm (Placebo) *	Baseline: 53.61 mm vs. 12 months: 47.39 mm (Dapagliflozin) Baseline: 57.15 mm vs. 12 months: 54.52 mm (Placebo) *	Dapagliflozin combined with conventional therapy resulted in significant improvements in LVEF, LVEDD, and LVESD compared to placebo, indicating a substantial benefit in cardiac function and remodeling in NIDCM patients.

NR—not reported; LVEF—left ventricle ejection fraction; LVEDD—left ventricle end-diastolic diameter (mm); LVESD—left ventricle end-systolic diameter (mm); *—statistically significant differences; GLP-1RA—Glucagon-like Peptide-1 Receptor; DPP-4I—Dipeptidyl Peptidase-4 Inhibitor; SGLT-2I—Sodium Glucose Cotransporter Type 2 Inhibitor; LVM—Left Ventricular Mass; GLS—Global Longitudinal Strain.

4. Discussion

4.1. Summary of Evidence

This systematic review critically evaluated the impact of hypoglycemic medications on cardiac reverse remodeling, particularly focusing on left ventricular dimensions in patients with diabetes mellitus. Among the notable findings, Liraglutide demonstrated a profound improvement in left ventricular ejection fraction, from 47.2% to 57.2%, and reductions in LVEDD and LVESD within three months of treatment. These results are consistent with prior studies suggesting that GLP-1 receptor agonists, like Liraglutide, may exert significant cardioprotective effects by improving cardiac function and structure, potentially via mechanisms linked to improved metabolic control and direct cardiovascular actions.

Conversely, the minimal changes observed with Sitagliptin over 24 months highlight the variability in the cardiac effects of DPP-4 inhibitors, which have been suggested to have more modest benefits on cardiac remodeling. This discrepancy may stem from differences in the molecular mechanisms of action between GLP-1 receptor agonists and DPP-4 inhibitors, where the former has a more direct role in cardiovascular protection. The differential impact underscores the importance of selecting appropriate hypoglycemic treatments based on individual patient cardiovascular risk profiles and the specific cardiac benefits of each drug class.

The significant improvements observed with Dapagliflozin in both short-term and long-term studies, particularly in patients with heart failure with reduced ejection fraction (HFrEF) and non-ischemic dilated cardiomyopathy (NIDCM), further support the role of SGLT-2 inhibitors in cardiac reverse remodeling. These findings align with the growing body of evidence that SGLT-2 inhibitors not only improve glycemic control but also confer substantial cardiovascular benefits, possibly through effects on cardiac load, metabolic efficiency, and direct myocardial energetics.

The systematic reviews by Huang et al. [17] and Carluccio et al. [18] provide comparative insights into the effects of hypoglycemic agents and SGLT2 inhibitors on cardiac remodeling, although focusing on different cardiac measurements than in our systematic review where the LVEDD and LVESD were the main study outcomes. Huang et al. found that GLP-1RA notably improved left ventricular end-systolic diameter by -0.38 mm and mass index (LVMI) by -1.07 g/m^2, contrasting with DPP-4i, which enhanced diastolic function but reduced left ventricular ejection fraction by -0.89%. SGLT-2i, on the other hand, improved both LVMI by -0.28 g/m^2 and left ventricular end-diastolic volume by -0.72 mL, indicating broad benefits. Carluccio et al. highlighted the efficacy of SGLT2 inhibitors in heart failure patients, showing significant reductions in LVEDV by -10.59 mL, LVESV by -8.80 mL, and an increase in LVEF by +1.98%.

Animal studies such as those by Ting-I Lee et al. [31] and Camila Moreno Rosa et al. [32] explored the cardioprotective effects of SGLT2 inhibitors using streptozotocin-induced diabetic rat models, highlighting similar yet distinct outcomes. Lee et al. reported that empagliflozin treatment led to decreased left ventricular end-diastolic diameters and shorter QT intervals, with significant improvements in the electrophysiological properties of cardiac cells—such as reduced late Na+ current and Na+/hydrogen-exchanger currents. This study detailed cellular-level enhancements, like the reduction in the incidence and frequency of Ca2+ sparks and a decrease in oxidative stress markers. On the other hand, Rosa et al. found that Dapagliflozin not only improved cardiac dimensions but also led to notable systemic effects, including a decrease in blood pressure and glycemia, and an increase in body weight (from 381 $\pm$ 52 g in diabetic rats to 430 $\pm$ 48 g in treated rats). Their study emphasized broader cardiovascular improvements, noting an attenuation in myocardial hydroxyproline concentration and a lower lipid hydroperoxide concentration (304 $\pm$ 40 nmol/g tissue in treated rats versus 385 $\pm$ 54 nmol/g in untreated). While Lee et al. focused more on the stabilization of cardiac function through modulation of ionic currents, Rosa et al. highlighted the reduction of oxidative stress and an overall improvement in cardiac structural function, making both studies complementary in illustrating the multi-faceted benefits of SGLT2 inhibitors in diabetic cardiomyopathy.

Similarly, Ikonomidis et al. [33] demonstrated significant improvements in vascular and myocardial function markers after a 12-month treatment with GLP-1RA and SGLT-2 inhibitors, or their combination. They reported notable reductions in the perfused boundary region (improved by over 10% with combination therapy), pulse wave velocity, and central systolic blood pressure, with the myocardial work index increasing by 12.7% and 17.4% in GLP-1RA and the combined therapy groups, respectively. Conversely, Paiman et al. [34], focusing on South Asian patients in the Netherlands treated with Liraglutide, observed no significant changes in left ventricular diastolic and systolic function, with stroke volume decreasing by 9 mL and heart rate increasing by 10 bpm. These disparities highlight the influence of patient demographic and treatment modality on therapeutic outcomes, where the combination therapy in a diverse European cohort showed superior efficacy compared to monotherapy in a specific ethnic group.

The studies by Santos-Gallego et al. [35] and Akasaka et al. [36] explored the impact of SGLT2 inhibitors on cardiac function, albeit with different patient profiles and endpoints. In the EMPA-TROPISM study by Santos-Gallego et al., empagliflozin significantly improved cardiac structure and function in nondiabetic patients with heart failure and reduced ejection fraction (HFrEF), evidenced by marked reductions in left ventricular end-diastolic volume (−25.1 mL) and end-systolic volume (−26.6 mL), enhancements in ejection fraction (+6.0%), and improvements in functional capacity measures such as the 6 min walk test (+81 m) and peak oxygen consumption (+1.1 mL/min/kg). Contrastingly, Akasaka et al., in the EXCEED study, did not observe significant improvements in diastolic function in diabetic patients with heart failure and preserved ejection fraction (HFpEF) after treatment with ipragliflozin, with minimal changes in E/e' and other diastolic function parameters over 24 weeks. These contrasting outcomes underline the potential of SGLT2 inhibitors like empagliflozin in improving systolic and volumetric parameters in HFrEF, which may not translate similarly to HFpEF patients, particularly those managed with diastolic function as a primary outcome.

4.2. Limitations

This study posits that reverse remodeling improves outcomes; however, this remains a hypothesis in the context of diabetic cardiomyopathy. The lack of definitive evidence supporting this relationship necessitates a cautious interpretation of the findings and the acknowledgment of this as a limitation. Several other limitations that could affect the interpretation and generalizability of the findings are necessary to acknowledge. Primarily, the variability in study designs, patient populations, and treatment durations across the included studies introduced a degree of heterogeneity that may limit the applicability of the results. Additionally, the predominance of older adult participants with comorbid cardiovascular conditions in most studies may not have fully represented outcomes in younger populations or individuals without significant cardiac histories. Furthermore, the mixed quality of the studies, with some classified as medium, indicates potential biases that could impact the robustness and reliability of the synthesized data.

5. Conclusions

In conclusion, this systematic review demonstrates that certain hypoglycemic medications, particularly Liraglutide and Dapagliflozin, can significantly improve cardiac dimensions and functions in patients with diabetes, suggesting their potential utility in managing cardiac comorbidities associated with diabetes. The evidence supports a nuanced approach to prescribing these medications, tailored to the individual patient's cardiovascular risk and existing comorbidities, to maximize both glycemic and cardiac outcomes. Further high-quality, long-term randomized controlled trials are needed to expand upon these findings and better define the mechanisms through which these medications exert their cardioprotective effects.

Author Contributions: Conceptualization, B.-F.B. and R.A.N.; methodology, B.-F.B. and R.A.N.; software, B.-F.B. and R.A.N.; validation, F.C. and T.P.; formal analysis, F.C. and T.P.; investigation, F.C. and T.P.; resources, M.S. and M.C.T.; data curation, M.S. and M.C.T.; writing—original draft preparation, B.-F.B., M.S., and M.C.T.; writing—review and editing, D.-A.A.; visualization, D.-A.A.; supervision, D.-A.A.; project administration, D.-A.A. All authors have read and agreed to the published version of the manuscript.

Funding: The costs of publication were supported by the Victor Babes University of Medicine and Pharmacy Timisoara.

Data Availability Statement: The original contributions presented in the study are included in the article; further inquiries can be directed to the corresponding author.

Conflicts of Interest: The authors declare no conflicts of interest.

References

1. Azevedo, P.S.; Polegato, B.F.; Minicucci, M.F.; Paiva, S.A.; Zornoff, L.A. Cardiac Remodeling: Concepts, Clinical Impact, Pathophysiological Mechanisms and Pharmacologic Treatment. *Arq. Bras. Cardiol.* **2016**, *106*, 62–69. [CrossRef]
2. Kodsi, M.; Makarious, D.; Gan, G.C.H.; Choudhary, P.; Thomas, L. Cardiac reverse remodelling by imaging parameters with recent changes to guideline medical therapy in heart failure. *ESC Heart Fail.* **2023**, *10*, 3258–3275. [CrossRef] [PubMed] [PubMed Central]
3. Leancă, S.A.; Afrăsânie, I.; Crișu, D.; Matei, I.T.; Duca, Ș.T.; Costache, A.D.; Onofrei, V.; Tudorancea, I.; Mitu, O.; Bădescu, M.C.; et al. Cardiac Reverse Remodeling in Ischemic Heart Disease with Novel Therapies for Heart Failure with Reduced Ejection Fraction. *Life* **2023**, *13*, 1000. [CrossRef]
4. Savarese, G.; Lund, L.H. Global Public Health Burden of Heart Failure. *Card. Fail. Rev.* **2017**, *3*, 7–11. [CrossRef] [PubMed] [PubMed Central]
5. Hassannejad, R.; Shafie, D.; Turk-Adawi, K.I.; Hajaj, A.M.; Mehrabani-Zeinabad, K.; Lui, M.; Kopec, J.A.; Abdul Rahim, H.F.; Safiri, S.; Fadhil, I.; et al. Changes in the burden and underlying causes of heart failure in the Eastern Mediterranean Region, 1990-2019: An analysis of the Global Burden of Disease Study 2019. *EClinicalMedicine* **2022**, *56*, 101788. [CrossRef] [PubMed] [PubMed Central]
6. Cheng, L.; Liao, K.; Wang, Y.; Lv, F.; Guo, X.; Zheng, Y.; Qin, J. Study of the Correlation Between the Ratio of Diastolic to Systolic Durations and Echocardiography Measurements and Its Application to the Classification of Heart Failure Phenotypes. *Int. J. Gen. Med.* **2021**, *14*, 5493–5503. [CrossRef] [PubMed] [PubMed Central]
7. Schach, C.; Körtl, T.; Wachter, R.; Maier, L.S.; Sossalla, S. Echocardiographic Evaluation of LV Function in Patients with Tachyarrhythmia and Reduced Left Ventricular Function in Response to Rhythm Restoration. *J. Clin. Med.* **2021**, *10*, 3706. [CrossRef] [PubMed] [PubMed Central]
8. Hasan, I.; Rashid, T.; Jaikaransingh, V.; Heilig, C.; Abdel-Rahman, E.M.; Awad, A.S. SGLT2 inhibitors: Beyond glycemic control. *J. Clin. Transl. Endocrinol.* **2024**, *35*, 100335. [CrossRef] [PubMed] [PubMed Central]
9. Fatima, A.; Rasool, S.; Devi, S.; Talha, M.; Waqar, F.; Nasir, M.; Khan, M.R.; Ibne Ali Jaffari, S.M.; Haider, A.; Shah, S.U.; et al. Exploring the Cardiovascular Benefits of Sodium-Glucose Cotransporter-2 (SGLT2) Inhibitors: Expanding Horizons Beyond Diabetes Management. *Cureus* **2023**, *15*, e46243. [CrossRef] [PubMed] [PubMed Central]
10. Pabel, S.; Hamdani, N.; Luedde, M.; Sossalla, S. SGLT2 Inhibitors and Their Mode of Action in Heart Failure-Has the Mystery Been Unravelled? *Curr. Heart Fail Rep.* **2021**, *18*, 315–328. [CrossRef] [PubMed] [PubMed Central]
11. Yang, F.; Meng, R.; Zhu, D.L. Cardiovascular effects and mechanisms of sodium-glucose cotransporter-2 inhibitors. *Chronic Dis. Transl. Med.* **2020**, *6*, 239–245. [CrossRef] [PubMed] [PubMed Central]
12. Palazzuoli, A.; Iacoviello, M. Diabetes leading to heart failure and heart failure leading to diabetes: Epidemiological and clinical evidence. *Heart Fail. Rev.* **2023**, *28*, 585–596. [CrossRef] [PubMed] [PubMed Central]
13. Elendu, C.; Amaechi, D.C.; Elendu, T.C.; Ashna, M.; Ross-Comptis, J.; Ansong, S.O.; Egbunu, E.O.; Okafor, G.C.; Jingwa, K.A.; Akintunde, A.A.; et al. Heart failure and diabetes: Understanding the bidirectional relationship. *Medicine* **2023**, *102*, e34906. [CrossRef] [PubMed] [PubMed Central]
14. Abduch, M.C.; Alencar, A.M.; Mathias, W., Jr.; Vieira, M.L. Cardiac mechanics evaluated by speckle tracking echocardiography. *Arq. Bras. Cardiol.* **2014**, *102*, 403–412. [CrossRef] [PubMed] [PubMed Central]
15. Al Saikhan, L.; Park, C.; Tillin, T.; Jones, S.; Mayet, J.; Chaturvedi, N.; Hughes, A. Does 3D-speckle tracking echocardiography improve prediction of major cardiovascular events in a multi-ethnic general population? A Southall and Brent Revisited (SABRE) cohort study. *PLoS ONE* **2023**, *18*, e0287173. [CrossRef] [PubMed] [PubMed Central]
16. Guo, F.Q.; Wu, B.L.; Liu, X.W.; Pan, T.; Gao, B.L.; Li, C.Y. Three-Tesla magnetic resonance imaging of left ventricular volume and function in comparison with computed tomography and echocardiography. *Medicine* **2023**, *102*, e33549. [CrossRef] [PubMed] [PubMed Central]

17. Huang, Y.L.; Xu, X.Z.; Liu, J.; Wang, P.Y.; Wang, X.L.; Feng, H.L.; Liu, C.J.; Han, X. Effects of new hypoglycemic drugs on cardiac remodeling: A systematic review and network meta-analysis. *BMC Cardiovasc. Disord.* **2023**, *23*, 293. [CrossRef] [PubMed] [PubMed Central]
18. Carluccio, E.; Biagioli, P.; Reboldi, G.; Mengoni, A.; Lauciello, R.; Zuchi, C.; D'addario, S.; Bardelli, G.; Ambrosio, G. Left ventricular remodeling response to SGLT2 inhibitors in heart failure: An updated meta-analysis of randomized controlled studies. *Cardiovasc. Diabetol.* **2023**, *22*, 235. [CrossRef]
19. Page, M.J.; McKenzie, J.E.; Bossuyt, P.M.; Boutron, I.; Hoffmann, T.C.; Mulrow, C.D.; Shamseer, L.; Tetzlaff, J.M.; Akl, E.A.; Brennan, S.E.; et al. The PRISMA 2020 statement: An updated guideline for reporting systematic reviews. *Syst. Rev.* **2021**, *10*, 89. [CrossRef] [PubMed] [PubMed Central]
20. Stang, A. Critical evaluation of the Newcastle-Ottawa scale for the assessment of the quality of nonrandomized studies in meta-analyses. *Eur. J. Epidemiol.* **2010**, *25*, 603–605. [CrossRef] [PubMed]
21. Chen, W.-R.; Shen, X.-Q.; Zhang, Y.; Chen, Y.-D.; Hu, S.-Y.; Qian, G.; Wang, J.; Yang, J.-J.; Wang, Z.-F.; Tian, F. Effects of liraglutide on left ventricular function in patients with non-ST-segment elevation myocardial infarction. *Endocrine* **2015**, *52*, 516–526. [CrossRef]
22. Yamada, H.; Tanaka, A.; Kusunose, K.; Amano, R.; Matsuhisa, M.; Daida, H.; Ito, M.; Tsutsui, H.; Nanasato, M.; Kamiya, H.; et al. Effect of sitagliptin on the echocardiographic parameters of left ventricular diastolic function in patients with type 2 diabetes: A subgroup analysis of the PROLOGUE study. *Cardiovasc. Diabetol.* **2017**, *16*, 63. [CrossRef] [PubMed]
23. Yamamoto, M.; Seo, Y.; Ishizu, T.; Nishi, I.; Hamada-Harimura, Y.; Machino-Ohtsuka, T.; Sato, K.; Sai, S.; Sugano, A.; Obara, K.; et al. Effect of Dipeptidyl Peptidase-4 Inhibitors on Cardiovascular Outcome and Cardiac Function in Patients with Diabetes and Heart Failure—Insights from the Ibaraki Cardiac Assessment Study-Heart Failure (ICAS-HF) Registry. *Circ. J.* **2017**, *81*, 1662–1669. [CrossRef] [PubMed]
24. Sardu, C.; Paolisso, P.; Sacra, C.; Santamaria, M.; de Lucia, C.; Ruocco, A.; Mauro, C.; Paolisso, G.; Rizzo, M.R.; Barbieri, M.; et al. Cardiac resynchronization therapy with a defibrillator (CRTd) in failing heart patients with type 2 diabetes mellitus and treated by glucagon-like peptide 1 receptor agonists (GLP-1 RA) therapy vs. conventional hypoglycemic drugs: Arrhythmic burden, hospitalizations for heart failure, and CRTd responders rate. *Cardiovasc. Diabetol.* **2018**, *17*, 137. [CrossRef] [PubMed] [PubMed Central]
25. Otagaki, M.; Matsumura, K.; Kin, H.; Fujii, K.; Shibutani, H.; Matsumoto, H.; Takahashi, H.; Park, H.; Yamamoto, Y.; Sugiura, T.; et al. Effect of Tofogliflozin on Systolic and Diastolic Cardiac Function in Type 2 Diabetic Patients. *Cardiovasc. Drugs Ther.* **2019**, *33*, 435–442. [CrossRef] [PubMed]
26. Rau, M.; Thiele, K.; Hartmann, N.-U.K.; Schuh, A.; Altiok, E.; Möllmann, J.; Keszei, A.P.; Böhm, M.; Marx, N.; Lehrke, M. Empagliflozin does not change cardiac index nor systemic vascular resistance but rapidly improves left ventricular filling pressure in patients with type 2 diabetes: A randomized controlled study. *Cardiovasc. Diabetol.* **2021**, *20*, 6. [CrossRef] [PubMed]
27. Gamaza-Chulián, S.; Díaz-Retamino, E.; González-Testón, F.; Gaitero, J.C.; Castillo, M.J.; Alfaro, R.; Rodríguez, E.; González-Caballero, E.; Martín-Santana, A. Effect of sodium-glucose cotransporter 2 (SGLT2) inhibitors on left ventricular remodelling and longitudinal strain: A prospective observational study. *BMC Cardiovasc. Disord.* **2021**, *21*, 456. [CrossRef]
28. Reis, J.; Teixeira, A.R.; Gonçalves, A.V.; Moreira, R.I.; Silva, T.P.; Timóteo, A.T.; Ferreira, R.C. Dapagliflozin Impact on the Exercise Capacity of Non-Diabetic Heart Failure with Reduced Ejection Fraction Patients. *J. Clin. Med.* **2022**, *11*, 2935. [CrossRef] [PubMed]
29. Fu, Q.; Zhou, L.; Fan, Y.; Liu, F.; Fan, Y.; Zhang, X.; Wang, L.; Cheng, L. Effect of SGLT-2 inhibitor, dapagliflozin, on left ventricular remodeling in patients with type 2 diabetes and HFrEF. *BMC Cardiovasc. Disord.* **2023**, *23*, 544. [CrossRef] [PubMed] [PubMed Central]
30. Hong, J.; Huang, L.; Jin, N.; Zhao, X.; Hu, J. Effect of dapagliflozin on left ventricular structure and function in patients with non-ischemic dilated cardiomyopathy: An observational study. *Medicine* **2024**, *103*, e37579. [CrossRef] [PubMed] [PubMed Central]
31. Lee, T.-I.; Chen, Y.-C.; Lin, Y.-K.; Chung, C.-C.; Lu, Y.-Y.; Kao, Y.-H.; Chen, Y.-J. Empagliflozin Attenuates Myocardial Sodium and Calcium Dysregulation and Reverses Cardiac Remodeling in Streptozotocin-Induced Diabetic Rats. *Int. J. Mol. Sci.* **2019**, *20*, 1680. [CrossRef]
32. Rosa, C.M.; Campos, D.H.S.; Reyes, D.R.A.; Damatto, F.C.; Kurosaki, L.Y.; Pagan, L.U.; Gomes, M.J.; Corrêa, C.R.; Fernandes, A.A.H.; Okoshi, M.P.; et al. Effects of the SGLT2 Inhibition on Cardiac Remodeling in Streptozotocin-Induced Diabetic Rats, a Model of Type 1 Diabetes Mellitus. *Antioxidants* **2022**, *11*, 982. [CrossRef] [PubMed]
33. Ikonomidis, I.; Pavlidis, G.; Thymis, J.; Birba, D.; Kalogeris, A.; Kousathana, F.; Kountouri, A.; Balampanis, K.; Parissis, J.; Andreadou, I.; et al. Effects of Glucagon-Like Peptide-1 Receptor Agonists, Sodium-Glucose Cotransporter-2 Inhibitors, and Their Combination on Endothelial Glycocalyx, Arterial Function, and Myocardial Work Index in Patients With Type 2 Diabetes Mellitus After 12-Month Treatment. *J. Am. Heart Assoc.* **2020**, *9*, e015716. [CrossRef] [PubMed] [PubMed Central]
34. Paiman, E.H.M.; van Eyk, H.J.; van Aalst, M.M.A.; Bizino, M.B.; van der Geest, R.J.; Westenberg, J.J.M.; Geelhoed-Duijvestijn, P.H.; Kharagjitsingh, A.V.; Rensen, P.C.N.; Smit, J.W.A.; et al. Effect of Liraglutide on Cardiovascular Function and Myocardial Tissue Characteristics in Type 2 Diabetes Patients of South Asian Descent Living in the Netherlands: A Double-Blind, Randomized, Placebo-Controlled Trial. *J. Magn. Reson. Imag.* **2020**, *51*, 1679–1688. [CrossRef] [PubMed] [PubMed Central]

35. Santos-Gallego, C.G.; Vargas-Delgado, A.P.; Requena-Ibanez, J.A.; Garcia-Ropero, A.; Mancini, D.; Pinney, S.; Macaluso, F.; Sartori, S.; Roque, M.; Sabatel-Perez, F.; et al. Randomized Trial of Empagliflozin in Nondiabetic Patients with Heart Failure and Reduced Ejection Fraction. *J. Am. Coll. Cardiol.* **2021**, *77*, 243–255. [CrossRef] [PubMed]
36. Akasaka, H.; Sugimoto, K.; Shintani, A.; Taniuchi, S.; Yamamoto, K.; Iwakura, K.; Okamura, A.; Takiuchi, S.; Fukuda, M.; Kamide, K.; et al. Effects of ipragliflozin on left ventricular diastolic function in patients with type 2 diabetes and heart failure with preserved ejection fraction: The EXCEED randomized controlled multicenter study. *Geriatr. Gerontol. Int.* **2022**, *22*, 298–304. [CrossRef] [PubMed] [PubMed Central]

Disclaimer/Publisher's Note: The statements, opinions and data contained in all publications are solely those of the individual author(s) and contributor(s) and not of MDPI and/or the editor(s). MDPI and/or the editor(s) disclaim responsibility for any injury to people or property resulting from any ideas, methods, instructions or products referred to in the content.

MDPI AG
Grosspeteranlage 5
4052 Basel
Switzerland
Tel.: +41 61 683 77 34

Biomedicines Editorial Office
E-mail: biomedicines@mdpi.com
www.mdpi.com/journal/biomedicines



Disclaimer/Publisher's Note: The title and front matter of this reprint are at the discretion of the Guest Editor. The publisher is not responsible for their content or any associated concerns. The statements, opinions and data contained in all individual articles are solely those of the individual Editor and contributors and not of MDPI. MDPI disclaims responsibility for any injury to people or property resulting from any ideas, methods, instructions or products referred to in the content.





Academic Open
Access Publishing

mdpi.com

ISBN 978-3-7258-7427-9